NASA Contractor Report 3200

Rotary Balance Data for a Typical Single-Engine General Aviation Design for an Angle-of-Attack Range of 8° to 90°

I - Low-Wing Model C

William J. Mulcay and Robert A. Rose

CONTRACT NAS1-14849
OCTOBER 1980

NASA

NASA Contractor Report 3200

Rotary Balance Data for a Typical Single-Engine General Aviation Design for an Angle-of-Attack Range of 8° to 90°

I - Low-Wing Model C

William J. Mulcay and Robert A. Rose
Bihrle Applied Research, Inc.
Jericho, New York

Prepared for
Langley Research Center
under Contract NAS1-14849

NASA
National Aeronautics
and Space Administration

Scientific and Technical
Information Branch

1980

SUMMARY

Aerodynamic characteristics obtained in a helical flow environment utilizing a rotary balance located in the Langley spin tunnel are presented in plotted form for a 1/6-scale, single-engine, low-wing, general aviation model (model C). The configurations tested included the basic airplane and control deflections, wing leading edge and fuselage modification devices, tail designs and airplane components. Data are presented without analysis for an angle-of-attack range of 8° to 90° and clockwise and counter clockwise rotations covering an $\frac{\Omega b}{2V}$ range from 0 to .9.

INTRODUCTION

The NASA Langley Research Center has a broad general aviation stall/spin research program underway which includes spin-tunnel and free-flight radio control model tests, as well as full-scale flight tests for a number of configurations typical of light, general aviation airplanes. To support this effort, rotary balance wind tunnel force tests covering these same configurations will be conducted to establish a data base for analysis of model and full-scale flight results, and to develop design charts for desirable stall/spin characteristics.

A 1/6-scale, single-engine, general aviation model, referred to as model C, having a low-wing location, was tested in a helical flow environment utilizing a rotary balance located in the Langley spin tunnel. This report presents the data obtained for the basic configuration and control settings, various wing leading-edge and fuselage modifications, tail designs and airplane components. Data for model C having a high-wing location are presented in reference 1.

SYMBOLS

The units for physical quantities used herein are presented in the International System of Units (SI) and U.S. Customary Units. The measurements were made in the U.S. Customary Units; equivalent dimensions were determined by using the conversion factors given in reference 2.

b	wing span, m (ft)
$\bar{c}$	mean aerodynamic chord, cm (in.)
C_N	normal-force coefficient, $\frac{\text{Normal force}}{qS}$
C_A	axial-force coefficient, $\frac{\text{Axial force}}{qS}$
C_Y	side-force coefficient, $\frac{\text{Side force}}{qS}$
C_ℓ	rolling-moment coefficient, $\frac{\text{Rolling moment}}{qSb}$
C_m	pitching-moment coefficient, $\frac{\text{Pitching moment}}{qS\bar{c}}$
C_n	yawing-moment coefficient, $\frac{\text{Yawing moment}}{qSb}$
q	free-stream dynamic pressure, N/m^2 (lb/ft^2)
S	wing area, m^2 (ft^2)
V	free-stream velocity, m/sec (ft/sec)
α	angle of attack, deg
β	angle of sideslip, deg
Ω	angular velocity about spin axis, rad/sec
$\frac{\Omega b}{2V}$	spin coefficient, positive for clockwise spin
δ_a	aileron deflection, positive when right aileron is down $(\delta_{a_{right}} - \delta_{a_{left}})/2$, deg
δ_e	all movable horizontal tail deflection, positive when trailing edge is down, deg
δ_r	rudder deflection, positive when trailing edge is to left, deg

Abbreviations:

cg   center of gravity

LE   leading edge

SR   spin radius

TE   trailing edge

TEST EQUIPMENT

A rotary balance measures the forces and moments acting on an airplane while subjected to rotational flow conditions; the background for this apparatus is discussed in reference 3. A photograph and sketch of the rotary balance apparatus installed in the Langley spin tunnel are shown in figures 1 and 2, respectively. The rotating portion of the balance system, mounted on a horizontal supporting boom which is hinged at the wall, is moved from the wall to the center of the tunnel by cables. The rotary arm of the balance system, which rotates about a vertical axis, is attached to the outer end of the horizontal supporting boom and is driven by a drive shaft through couplings and gears.

A test model is mounted on a strain gauge balance which is affixed to the bottom of the rotary balance apparatus. Controls located outside the tunnel are used to activate motors on the rig which position the model to the desired attitude. The angle-of-attack range of the rig is 8 to 90 degrees and the sideslip angle range is ±15 degrees. The spin radius and the lateral displacement motors allow the operator to position the moment center of the balance on the spin axis or at a specific distance from the spin axis. This is done for each combination of angle of attack and sideslip angle. The general practice is to mount the moment center of the balance at the cg location about which the aerodynamic moments are desired. Electrical current from the balance, and to the motors on the rig, is conducted through

the slip rings located at the rig head. Examples of how the rig is positioned for different angle of attack and sideslip angle are shown in figures 2a and 2b, respectively.

The model can be rotated up to 90 rpm in either direction. By using different rotational speeds and a specific airflow in the tunnel, the motions of a steady spinning airplane can be simulated. The aerodynamic forces and moments can then be measured for values of $\frac{\Omega b}{2V}$, including the case of $\frac{\Omega b}{2V} = 0$, where static aerodynamic forces and moments can be obtained.

A NASA six-component strain gauge balance is mounted inside the model and measures the normal, lateral and longitudinal forces and the yawing, rolling and pitching moments acting about the model body axis. The interactions that exist between the six components are available from balance calibration tests and are accounted for after the balance voltages are converted to forces and moments.

The data acquisition, reduction and presentation system for the rotary balance system is composed of a 12-channel scanner/voltmeter, a mini-computer and a plotter. With this equipment, on-line digital print-out and/or graphical plots of data are possible.

TEST PROCEDURES

Rotary aerodynamic data are obtained in two steps. The first step is to record the inertial forces and moments (tares) acting on the model at different attitudes and rotational speeds. To accomplish this, a covered bird-cage like structure is mounted to the upper rig which encloses the model without touching it. In this manner, the air immediately surrounding the model is rotated with it. As the rig is rotated at the desired attitude and rate, the inertial forces and moments generated by the model are measured and stored on magnetic tape for later use.

The second step in the data-gathering process is to measure aerodynamic and inertial forces at different attitudes and rotational speeds for a selected tunnel velocity with, of course, the cage structure removed. The tares are subtracted from these values, and the remaining aerodynamic forces and moments are then converted to coefficient form and stored on magnetic tape.

MODEL

A 1/6-scale low-wing, single engine, light general aviation model was constructed of fiberglass-epoxy, wood and aluminum. A three-view drawing of this model is shown in figure 3, dimensional characteristics of the basic model are listed in Table I, and a photograph of the model installed on the rotary balance located in the Langley spin tunnel is presented in figure 1.

The various airplane components were removable for component build-up tests, the testing of wing leading edge and fuselage modification devices and tail configurations. The three tail configurations tested involved different vertical and horizontal locations of the horizontal tail as shown in figure 4. The wing leading edge modifications include full-span leading edge droops of moderate and large nose radius and an outboard drooped section of large nose radius (figures 5 and 6). The fuselage modifications tested include a cowl-strake and tail-fillet combination and with addition of either a ventral fin or emergency spin chute installation (figure 7). Also tested were a sharp-edged fuselage bottom and a dorsal fin off configuration (figures 8 and 9).

The model control surfaces could be set at any position prior to the test. The maximum deflections for the control surfaces were:

Rudder, deg	25 right, 25 left
All movable horizontal tail, deg	15 up, 2 down
Aileron, deg	20 up, 10 down

TEST CONDITIONS

The tests were conducted in the spin tunnel at an airstream velocity of 7.62 m/sec (25ft/sec) which corresponds to a Reynolds number of approximately 119,000 based on model wing chord. Unless noted otherwise in Table II, all the configurations were tested through an angle-of-attack range of 8 to 90° at a zero sideslip angle, with the spin axis passing through the full-scale airplane cg location for angles of attack above 30°. For angles of attack below 35°, the spin axis was set 182.9 cm (72 in.) forward of the cg location. Consequently, data was obtained for both 0 and 182.9 cm (72 in.) spin radius at angles of attack of 30 and 35°. For each angle of attack, data were obtained for nominal $\frac{\Omega b}{2V}$ values of .1, .2, .3, .4, .5, .6, .7, .8, and .9 in both clockwise and counter clockwise directions, as well as for $\frac{\Omega b}{2V} = 0$ (static value).

DATA PRESENTATION

Table II identifies the configurations tested and the corresponding appendix figure numbers which present the aerodynamic data. The aerodynamic coefficients vs. $\frac{\Omega b}{2V}$ are presented for each configuration in six sequentially numbered figures in the following order: C_n, C_ℓ, C_m, C_N, C_Y, C_A. Each figure in turn consists of four (seven for the basic configuration) pages which present the subject aerodynamic coefficient vs. $\frac{\Omega b}{2V}$ for the following angles of attack and spin radii, unless noted otherwise in Table II:

a) α = 8, 10, 12, 14, 16 deg SR = 182.9 cm (72 in.)
b) α = 18, 20, 25, 30, 35 deg SR = 182.9 cm (72 in.)
c) α = 30, 35, 40, 45, 50 deg SR = 0
d) α = 55, 60, 70, 80, 90 deg SR = 0

All the moment data are presented for a cg position of $.21\bar{c}$.

Lift coefficient vs. angle of attack for zero rotation rate is presented at the end of the Appendix for several configurations cited in Table II.

REFERENCES

1. Hultberg, Randy S.; Chu, Julio; Dickens, Waldo L.: Rotary Balance Data for a Typical Single-Engine General Aviation Design for an Angle-of-Attack Range of 8° to 90°. II - High-Wing Model C. NASA CR-3201, 1980.

2. Mechtly, E.A.: The International System of Units - Physical Constants and Conversion Factors. NASA SP-7012, 1973.

3. Bihrle, William, Jr.; Hultberg, Randy S.; and Mulcay, William: Rotary Balance Data for a Typical Single-Engine Low-Wing General Aviation Design for an Angle-of-Attack Range of 30° to 90°. NASA CR-2972, 1978.

TABLE I.- DIMENSIONAL CHARACTERISTICS OF THE BASIC MODEL

Overall length, m (ft)	1.31 (4.29)
Wing:	
Span, m (ft)	1.66 (5.46)
Area, m^2 (ft^2)	.38 (4.06)
Root chord, cm (in.)	22.32 (8.79)
Tip chord, cm (in.)	22.32 (8.79)
Mean aerodynamic chord, cm (in.)	22.32 (8.79)
Leading edge of $\bar{c}$, distance rearward of leading edge of root chord, cm (in.)	0.0 (0.0)
Aspect ratio	7.4
Dihedral, deg	6.5
Incidence:	
Root, deg	+3.257
Tip, deg	+1.0
Airfoil Section	NACA 63_2 A415
Horizontal tail:	
Span, m (ft)	0.54 (1.78)
Incidence, deg	0.0
Airfoil section	NACA $63A_1$ 012(modified)
Vertical tail:	
Airfoil section	NACA $63A_1$012
Sweep @ LE, deg	41.0

TABLE II.- CONFIGURATIONS TESTED AND FIGURE INDEX

(Unless noted otherwise, all configurations tested through α=8 to 90^{o} at β=0^{o}.)

FIGURE NO.	CONFIGURATION	δ_e deg	δ_a deg	δ_r deg	REMARKS
[a]A1-A6	Basic	0	0	0	also α=8-60^{o}SR=6"
A7-A12	↓	↓	↓	↓	β=10^{o}
A13-A18		-15		-25	
A19-A24			20 up +10down		
A25-A30	↓	↓	-20up -10down	↓	
[a]A31-A36	Full-span LE wing droop w/moderate nose radius	0	0	0	
[a]A37-A42	↓ w/large nose radius				
A43-A48	↓ ↓ and sharp edge fuselage bottom				
[a]A49-A54	Outboard LE wing droop w/large nose radius having inboard fairing				
[a]A55-A60	Outboard LE wing droop w/large nose radius		↓		
A61-A66					β=10^{o}
A67-A72	↓		20 up +10down		
A73-A78	Sharp-edge fuselage bottom		0		
A79-A84	Basic configuration with cowl strakes, ventral and tail fillets	↓		↓	
A85-A90	Horiz. tail off	off			
A91-A96	Vert. tail off	0		off	
A97-A102	Horiz. and vert. tail off	off	↓	↓	
A103-A108	Body alone	↓	off		
A109-A114	Wing off	0		0	
A115-A120	Wing and horiz. tail off	off		↓	
A121-A126	Wing and vert. tail off	0	↓	off	
A127-A132	Dorsal fin off	↓	o	o	
A133-A138	T Tail			↓	
A139-A144	↓	-15		-25	
A145-A150	#1 Horiz. tail	0		0	
A151-A156	↓	-15		-25	
A157-A162	Basic configuration with cowl strakes, tail fillets and emergency spin chute installation.	0		0	
A163-A168	Basic configuration with cowl strakes and tail fillets	↓	↓	↓	

[a] C_L vs. α presented in figure A169

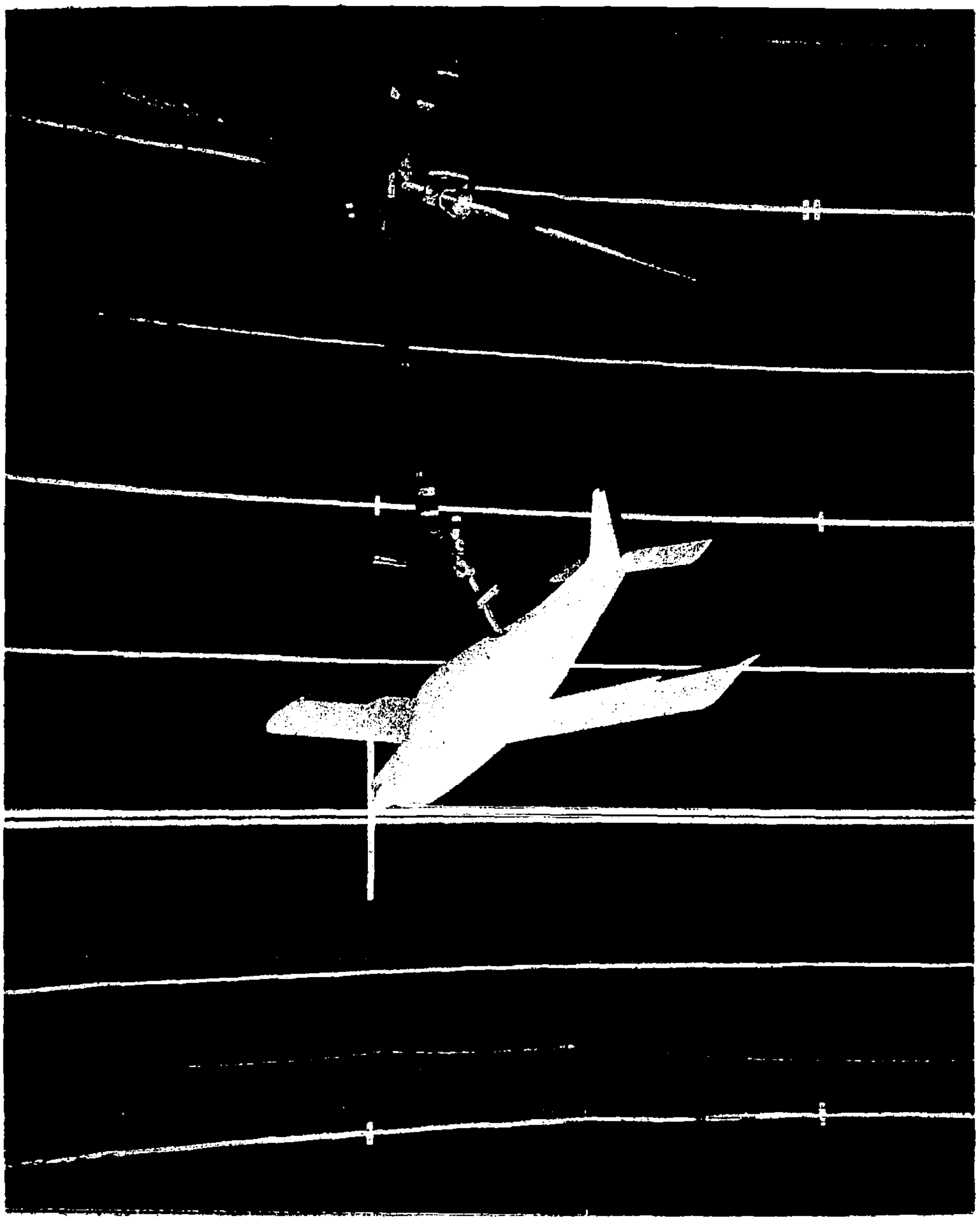

Figure 1. - Photograph of 1/6-scale model installed on rotary balance apparatus.

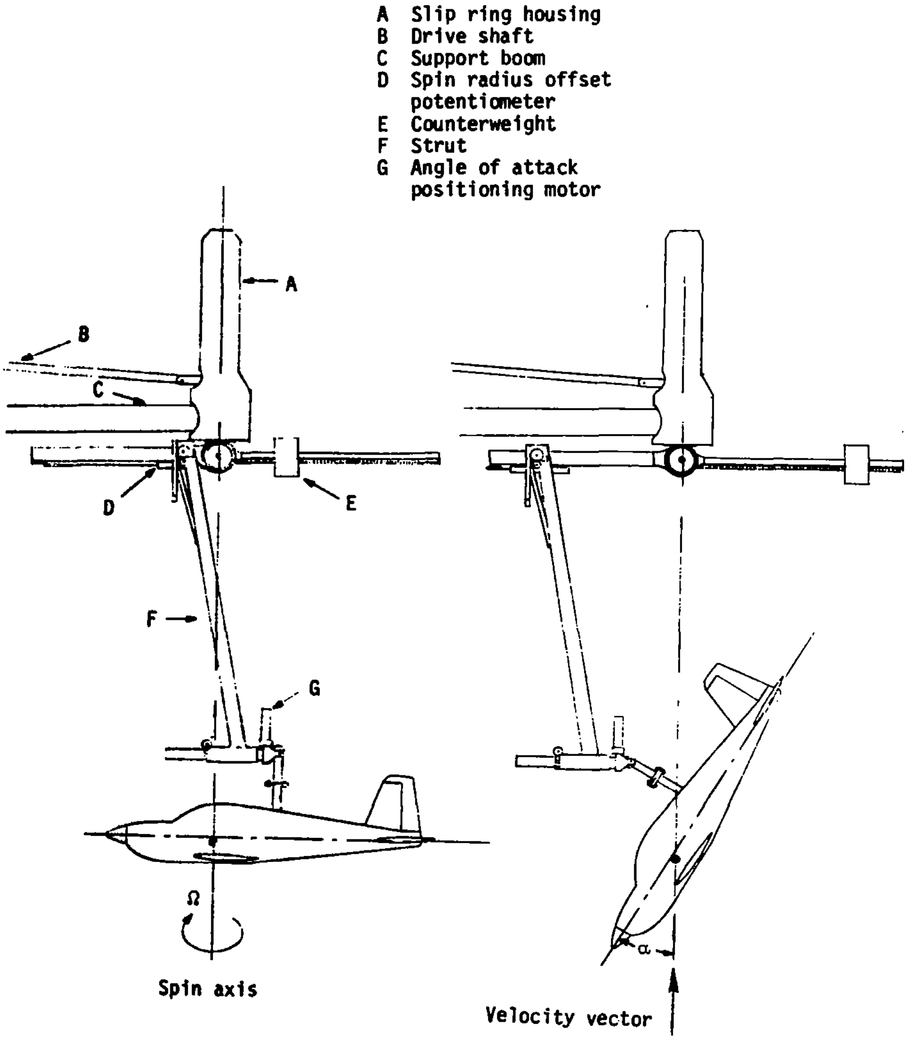

(a) Side view of model.

Figure 2.- Sketch of rotary balance apparatus.

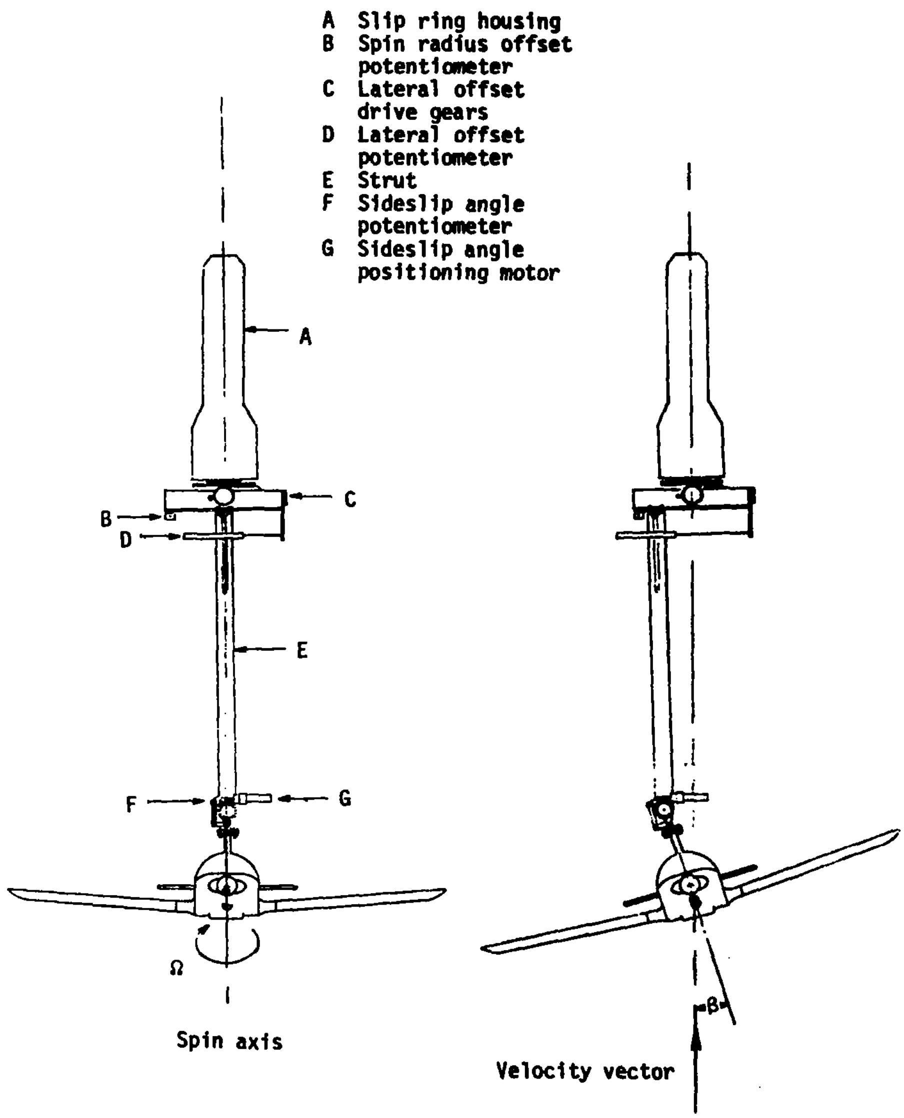

(b) Front view of model.

Figure 2.- Concluded.

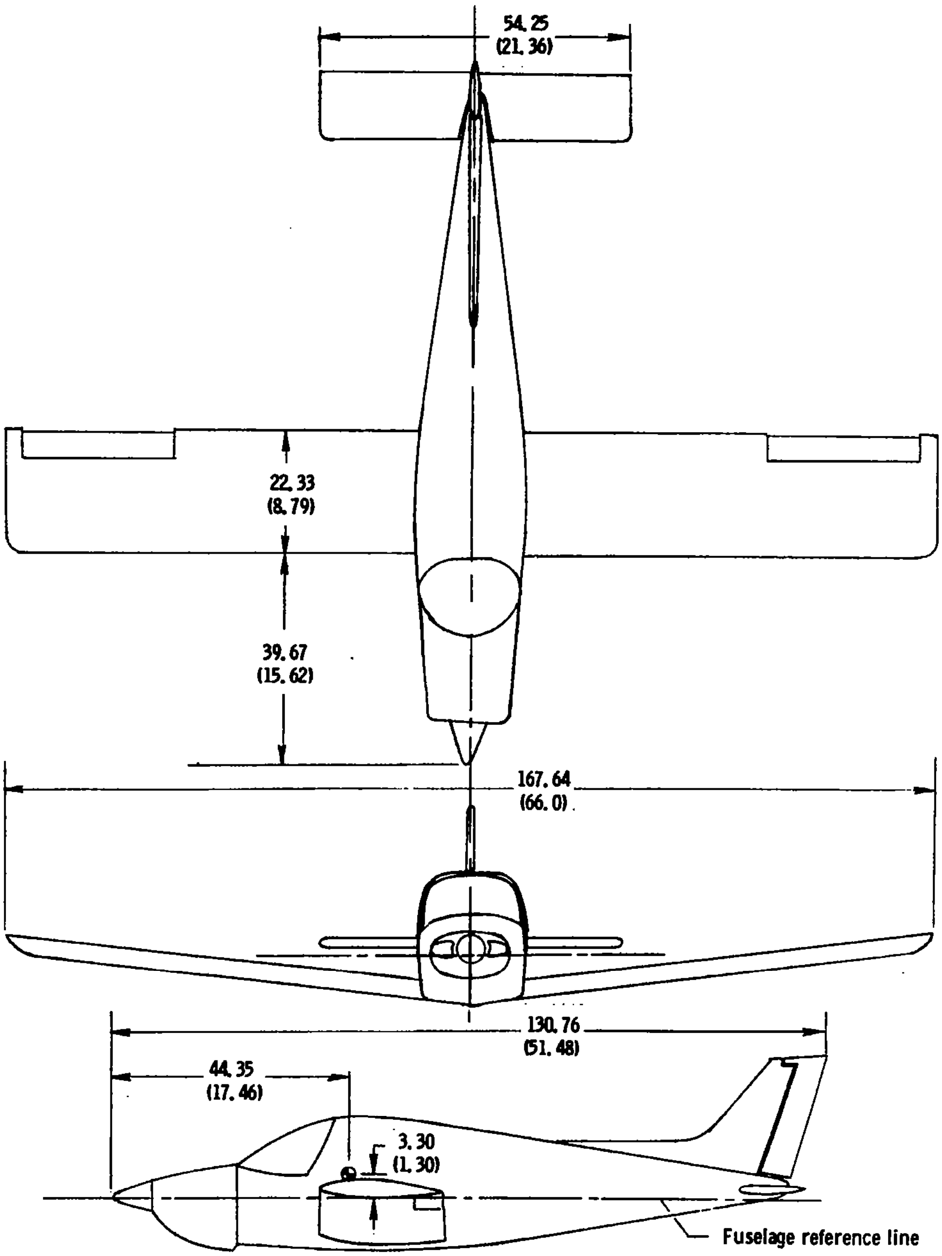

Figure 3. - Three-view drawing of 1/6-scale low-wing general aviation model C. Center-of-gravity positioned at 0.21 $\bar{c}$. Dimensions are given in centimeters(inches), model scale.

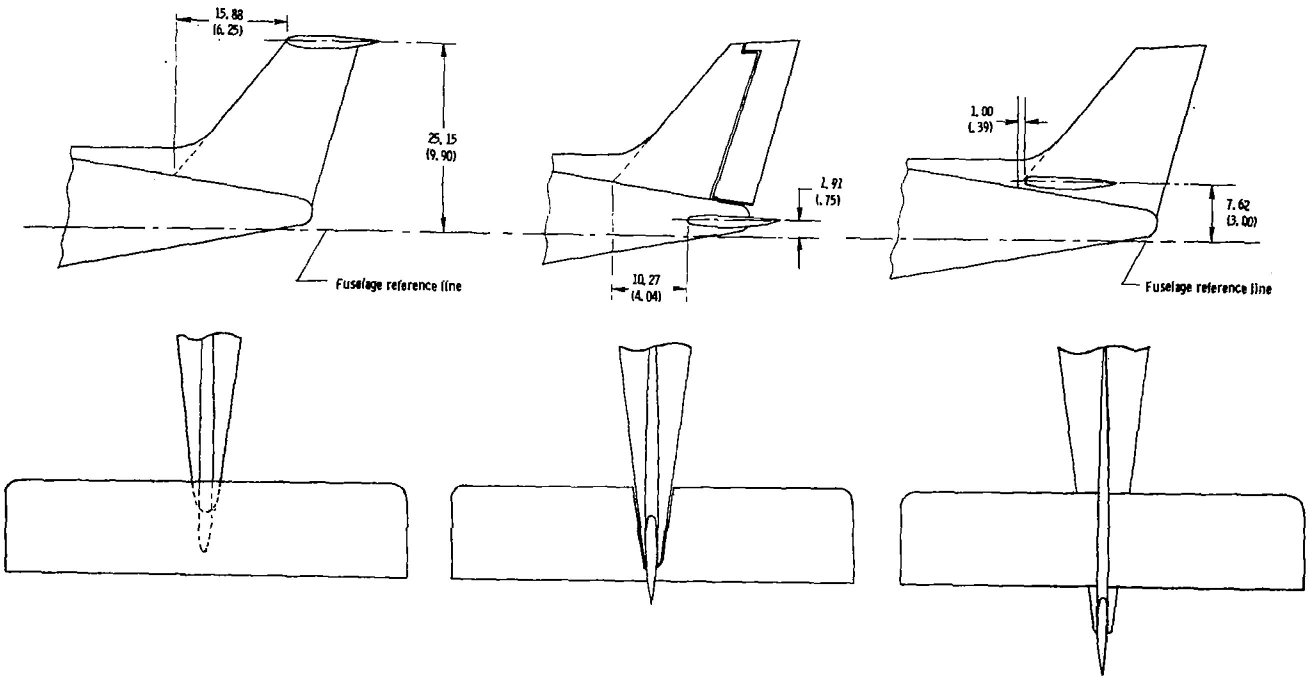

a) T-tail

b) Basic tail

c) Tail 1

Figure 4. - Tail configurations tested on the model. Dimensions are given in centimeters(inches), model scale.

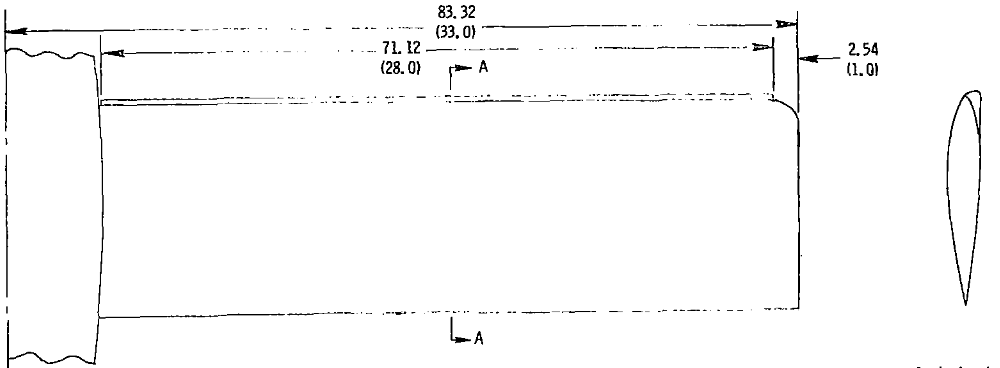

a(Full-span leading edge droop with moderate nose radius.

Sect. A - A

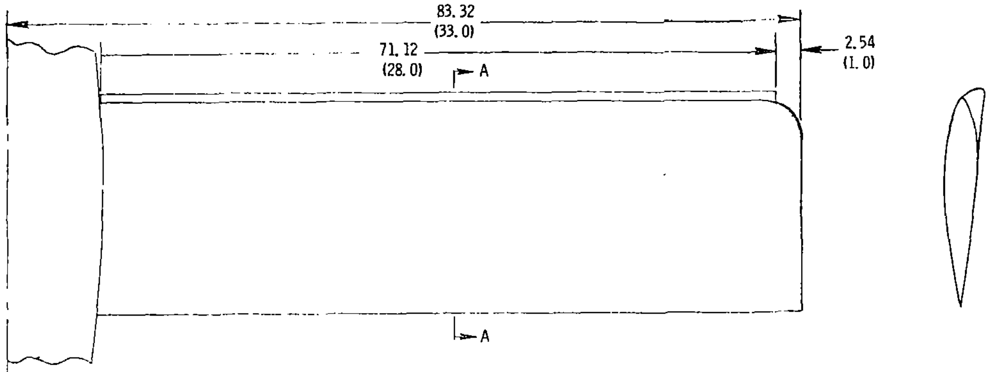

b) Full-span leading edge droop with large nose radius.

Sect. A - A

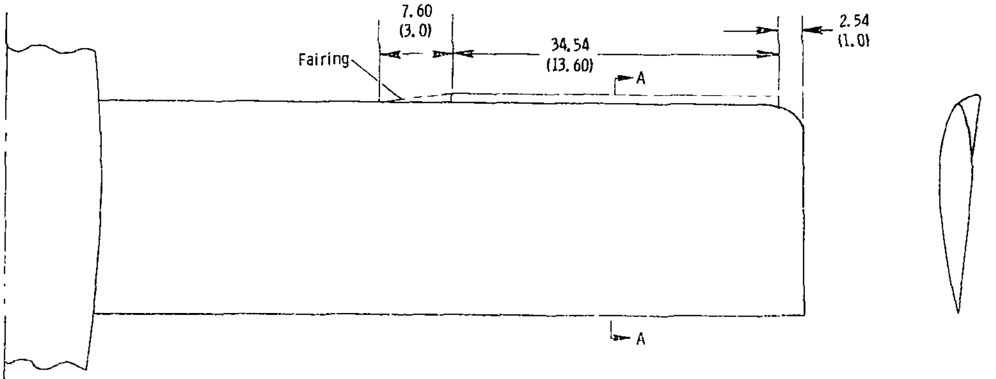

c) Outboard leading edge droop with large nose radius.

Sect. A - A

Figure 5. -Wing leading edge modifications tested on model. Dimensions are given in centimeters(inches), model scale.

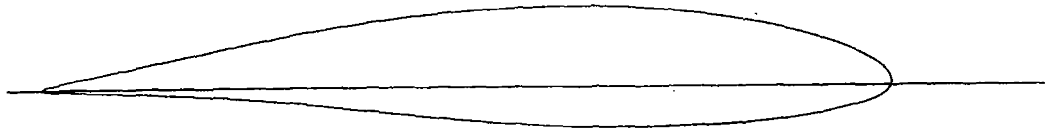

a) Basic airfoil

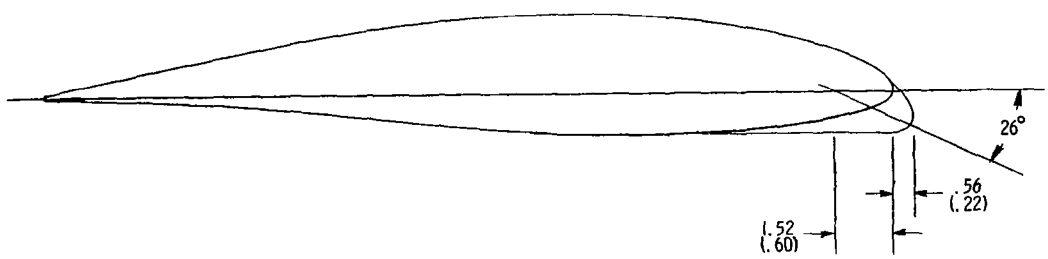

b) Basic airfoil with moderate nose radius

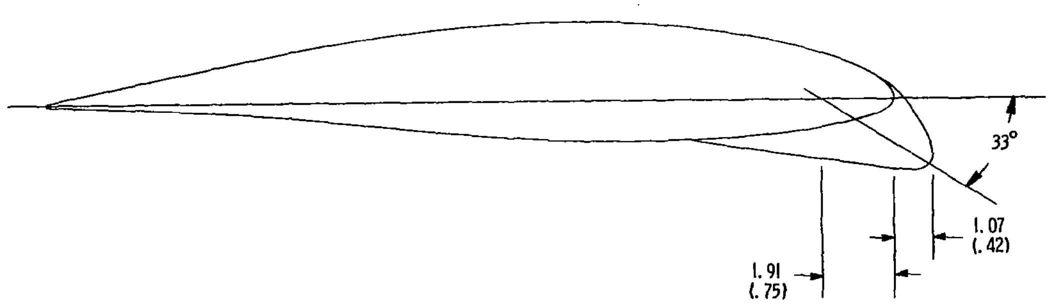

c) Basic airfoil with large nose radius

Figure 6. - Airfoil sections tested on model. Dimensions are given in centimeters (inches) model scale.

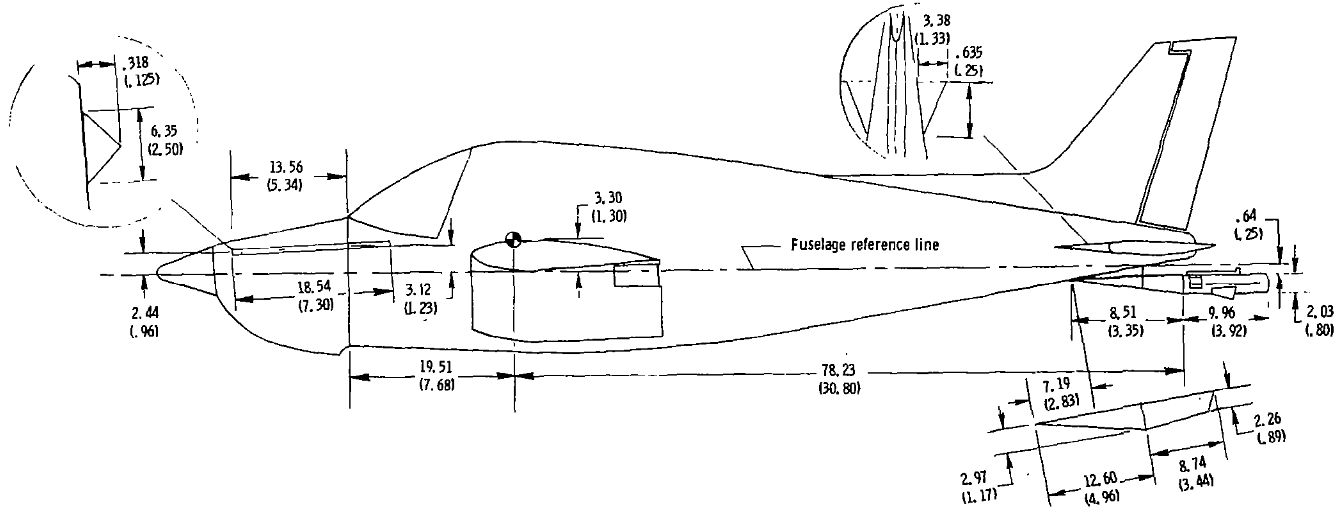

Figure 7. - Fuselage tested with cowl strakes, tail fillets, ventral fin and emergency spin chute installation. Dimensions are given in centimeters(inches), model scale.

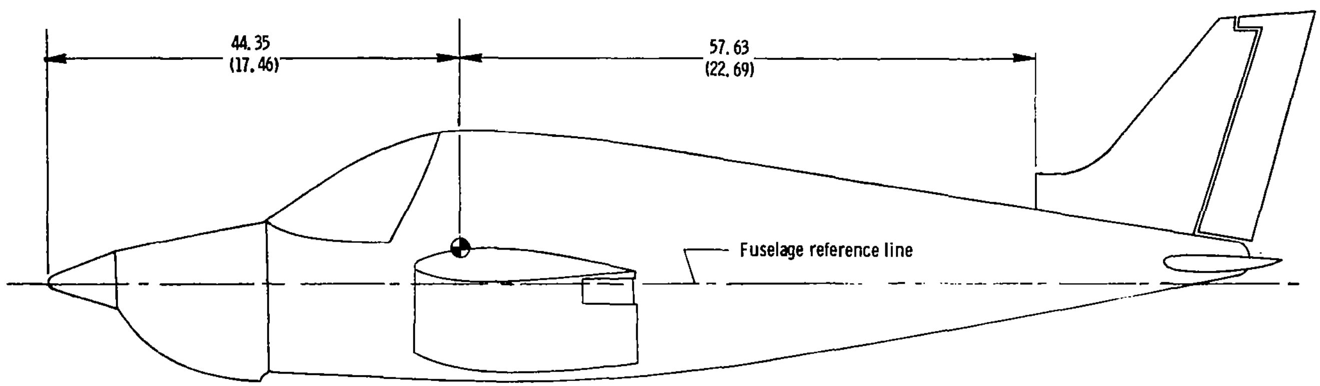

Figure 8. - Dorsal fin off configuration tested on the model. Dimensions are given in centimeters(inches), model scale.

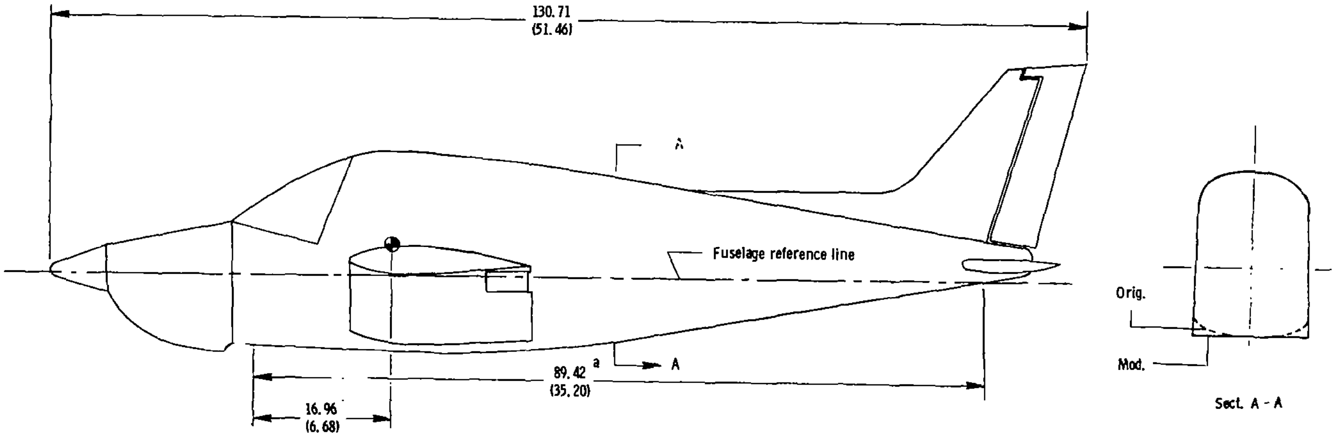

[a] Length of Sharp-edged fuselage bottom.

Figure 9. - Sharp-edged fuselage bottom modification tested on the model. Dimensions are given in centimeters(inches), model scale.

APPENDIX

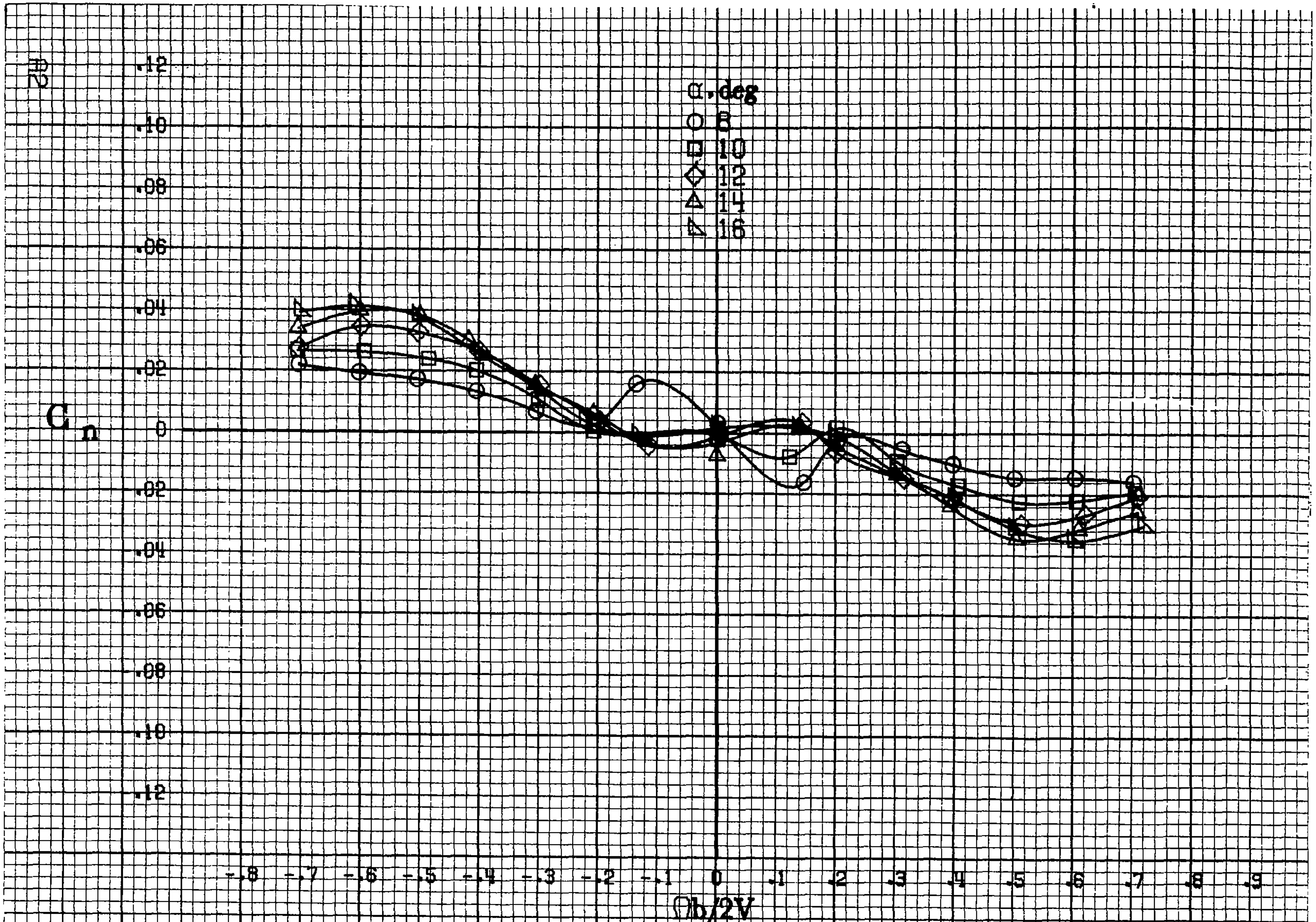

(a) α = 8 to 16 deg, SR = 182.9 cm (72 in).

Figure A1.-Effect of rotation rate and angle of attack on yawing-moment coefficient for basic configuration. $\delta_e = 0°$, $\delta_a = 0°$, $\delta_r = 0°$, $\beta = 0°$.

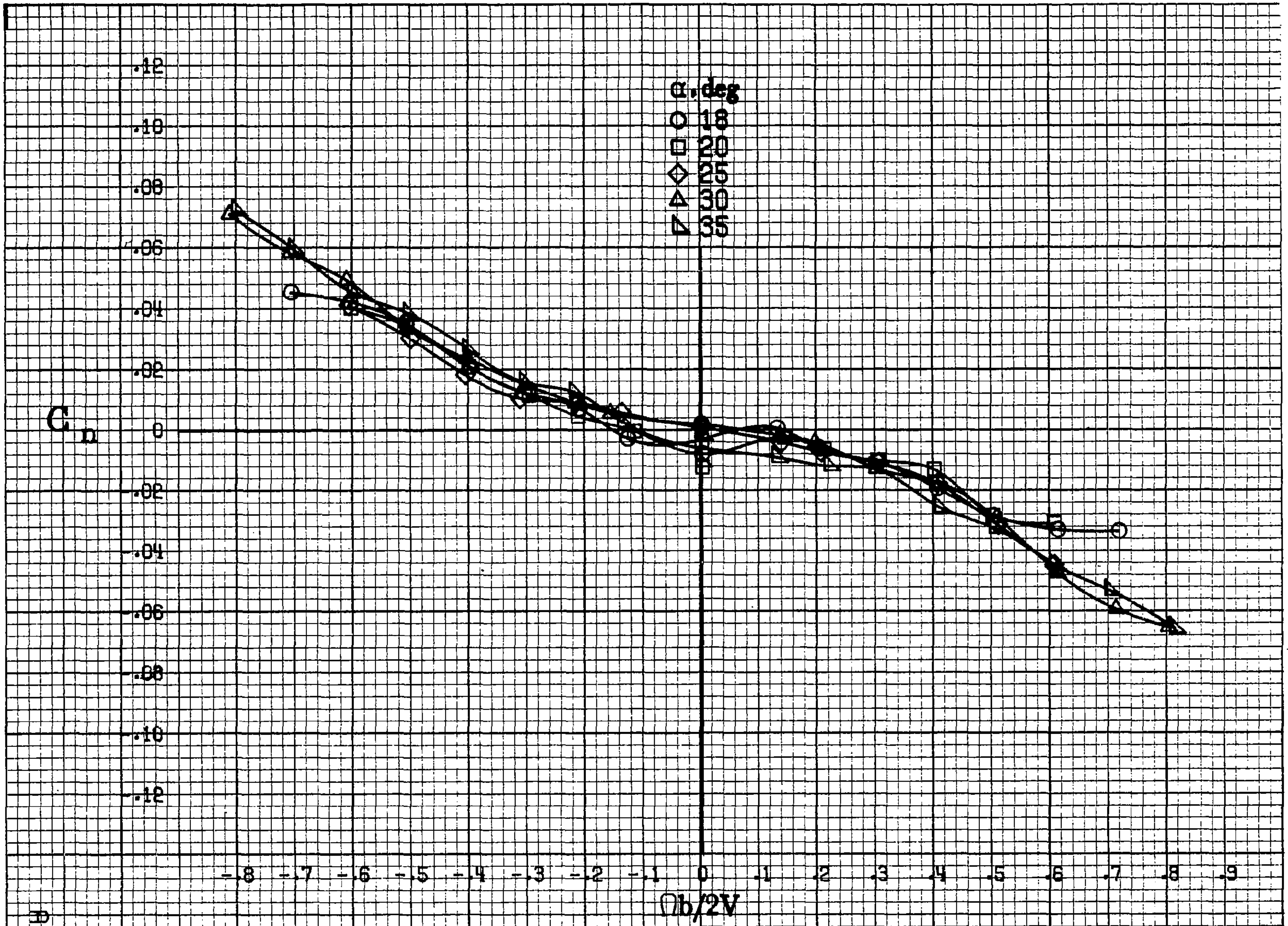

(b) α = 18 to 35 deg, SR = 182.9 cm (72 in).

Figure A1.-Continued.

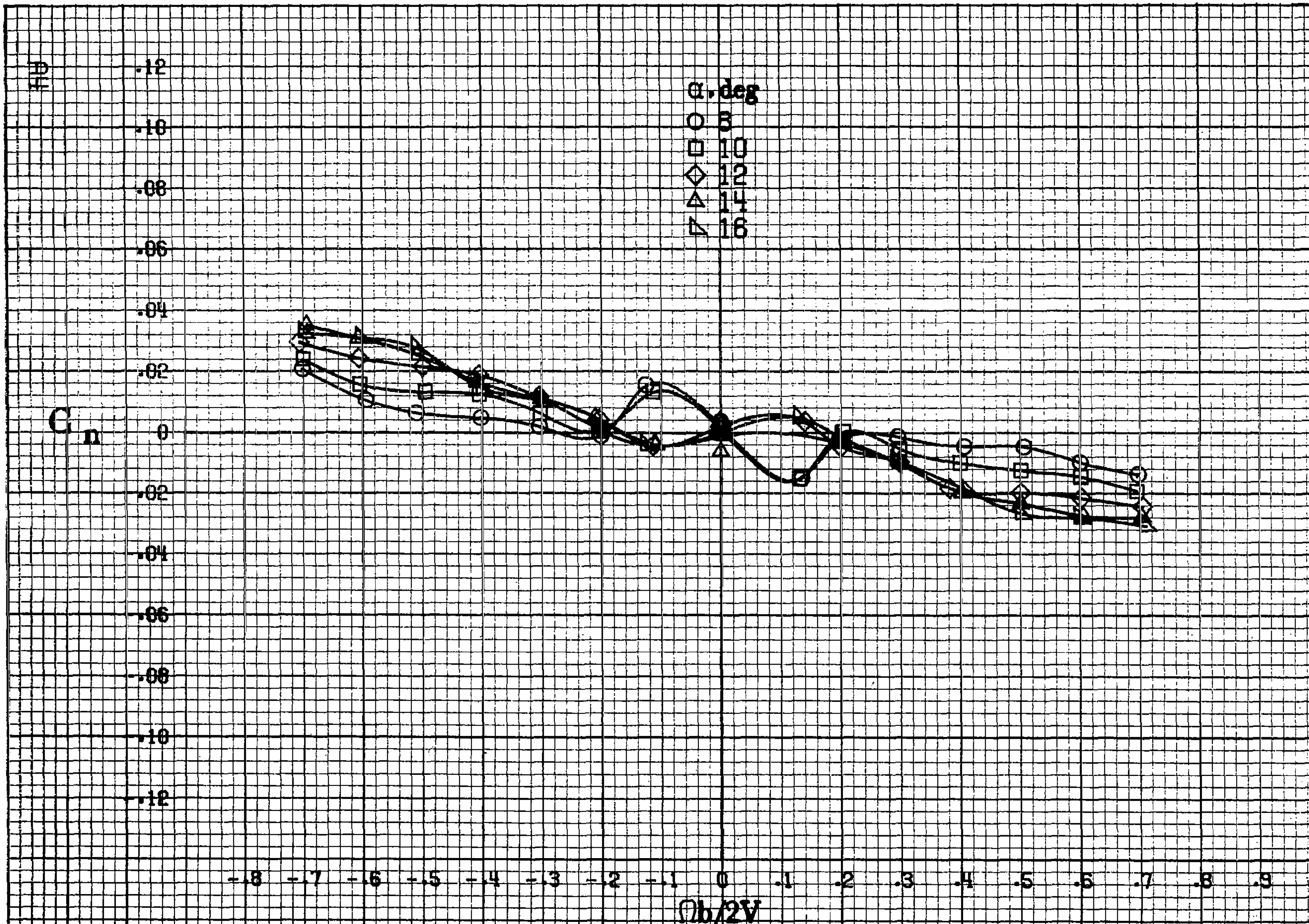

(c) α = 8 to 16 deg, SR = 91.4 cm (36 in).
Figure A1. Continued.

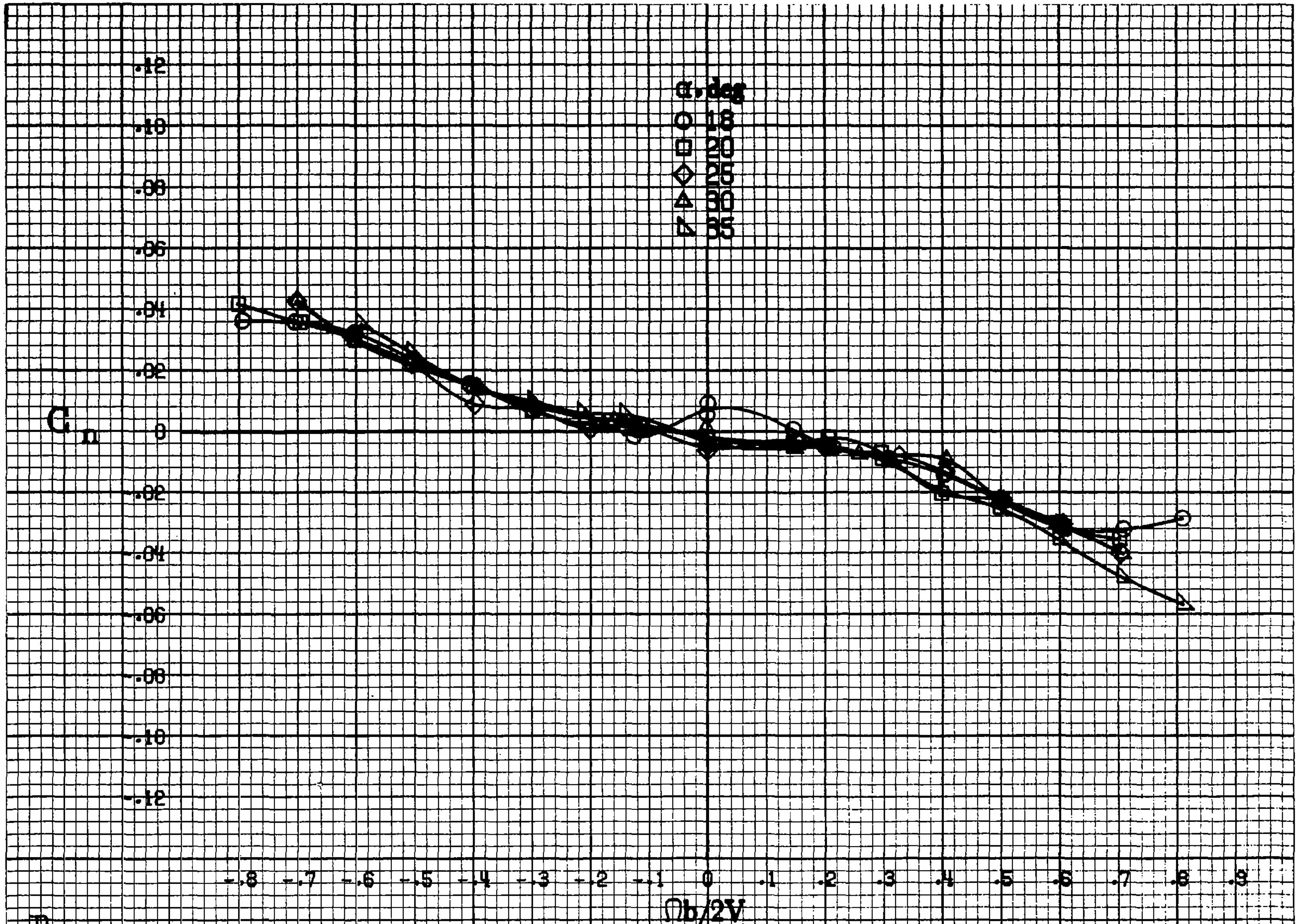

(d) α = 18 to 35 deg, SR = 91.4 cm (36 in).

Figure A1. Continued.

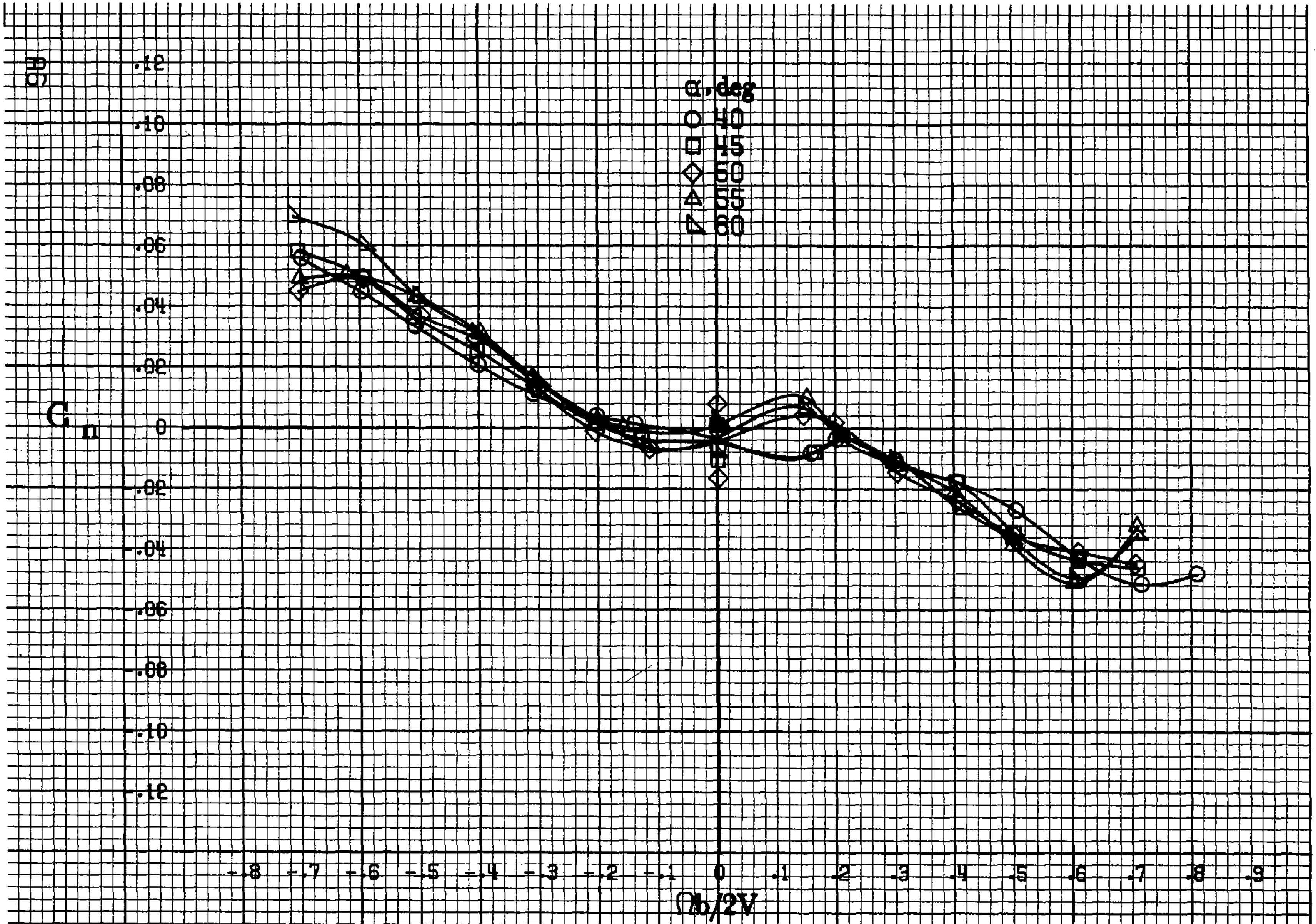

(e) α = 40 to 60 deg, SR = 91.4 cm (36 in).

Figure A1. Continued.

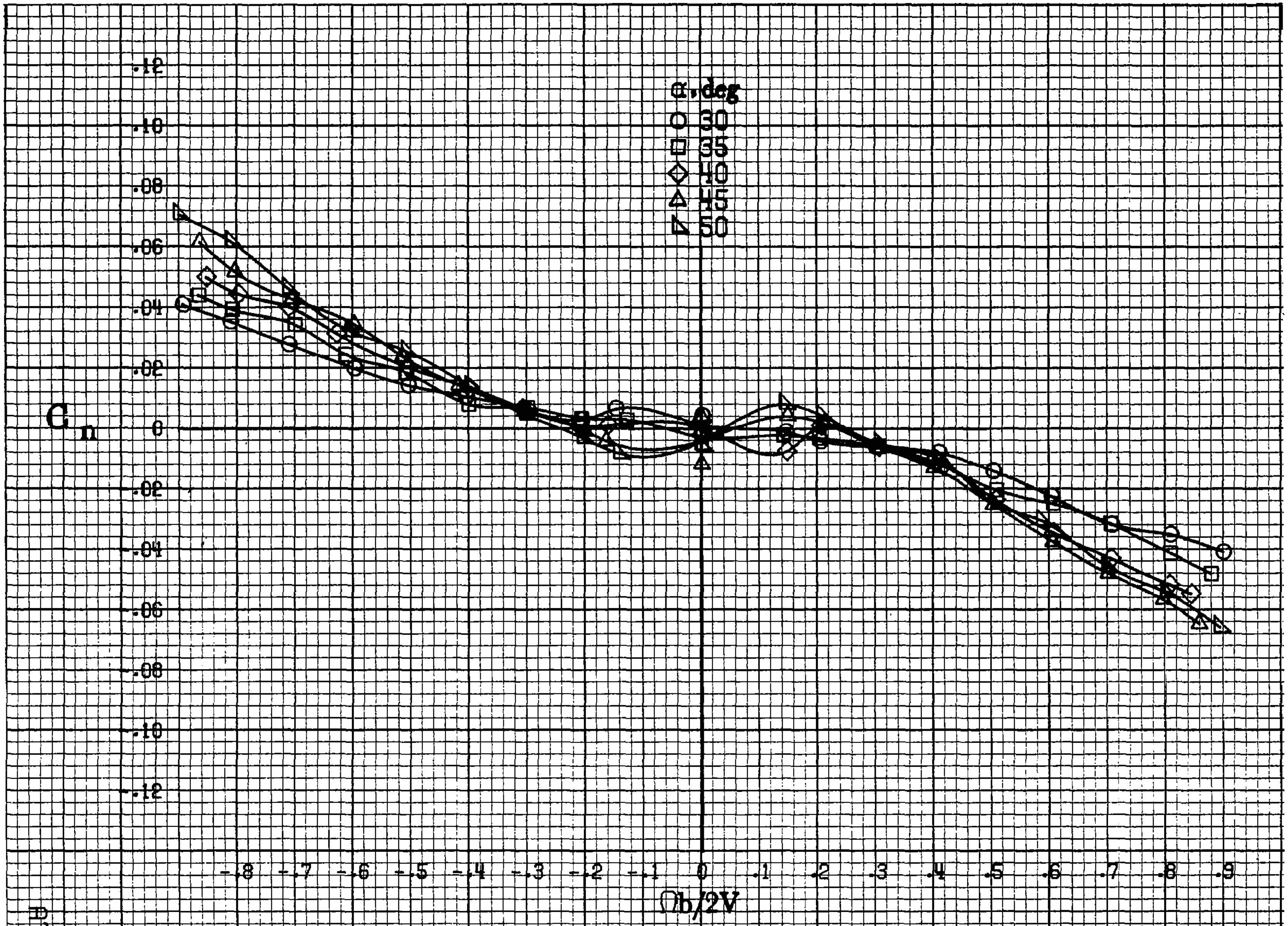

(f) α = 30 to 50 deg, SR = 0.

Figure A1.-Continued.

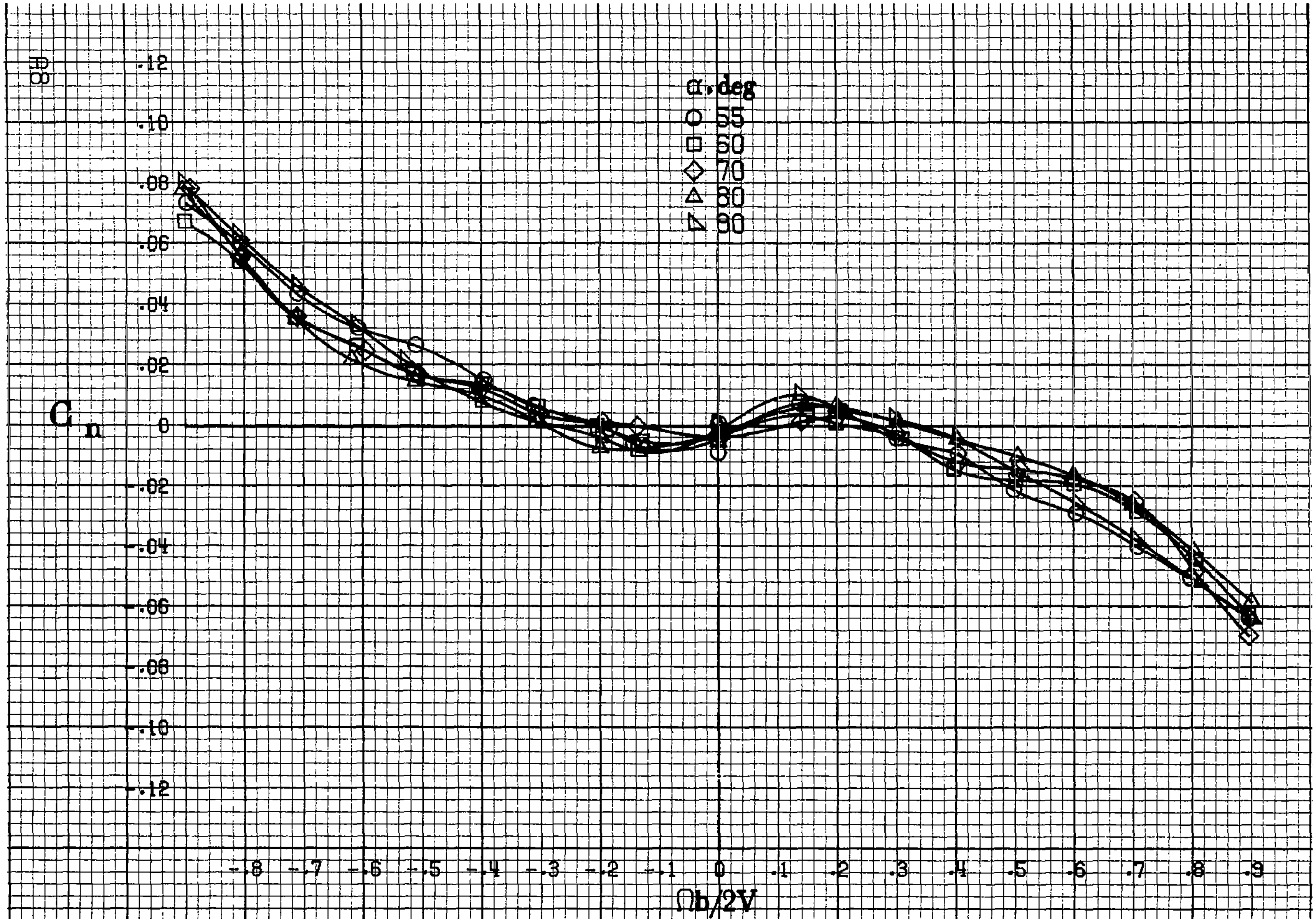

(g) α = 55 to 90 deg, SR = 0.

Figure A1. Concluded.

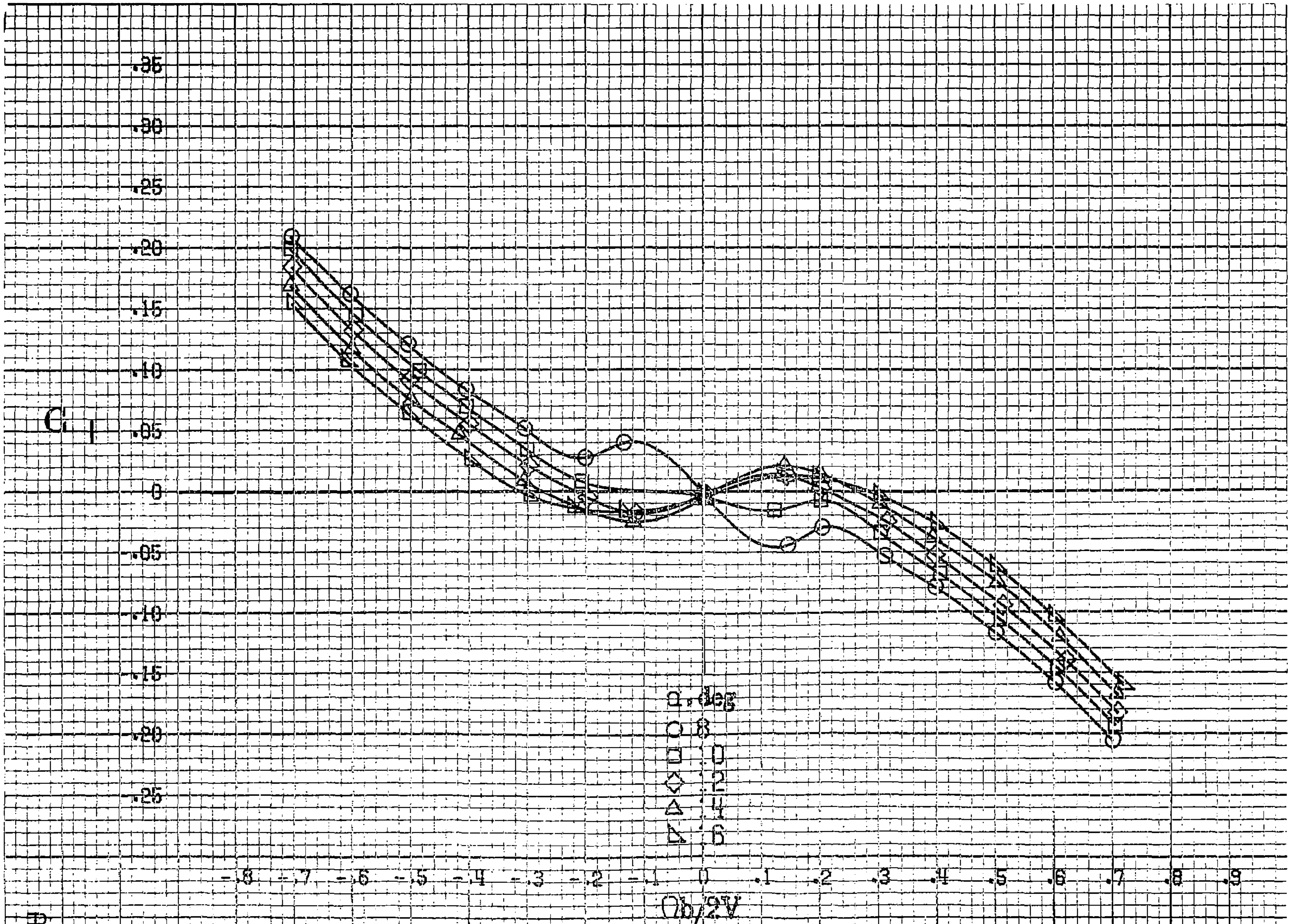

(a) $\alpha = 8$ to 16 deg, SR = 182.9 cm (72 in.).

Figure A2.- Effect of rotation rate and angle of attack on rolling-moment coefficient for basic configuration. $\delta_e = 0°$, $\delta_a = 0°$, $\delta_r = 0°$, $\beta = 0°$.

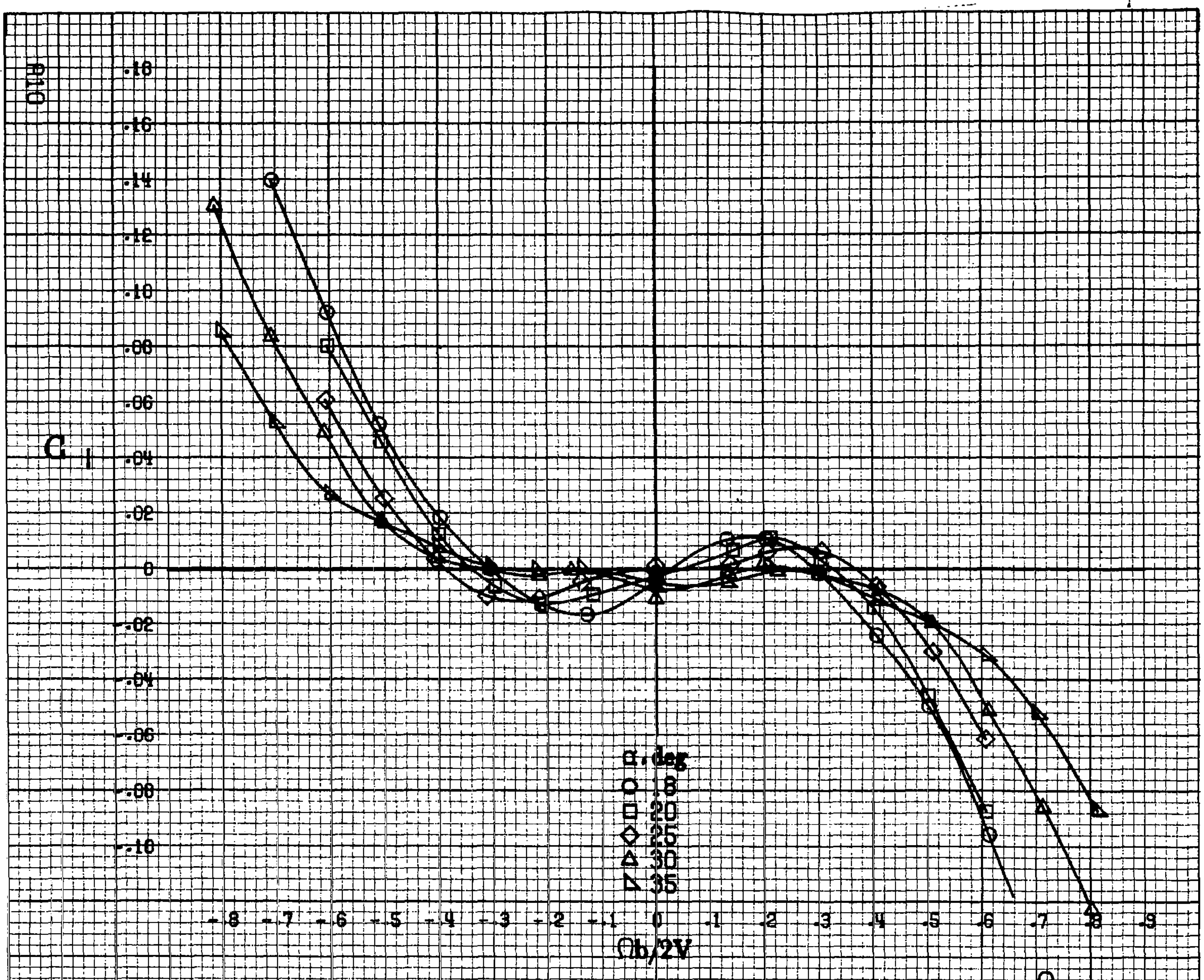

(b) α = 18 to 35 deg, SR = 182.9 cm (72 in).

Figure A2.-Continued.

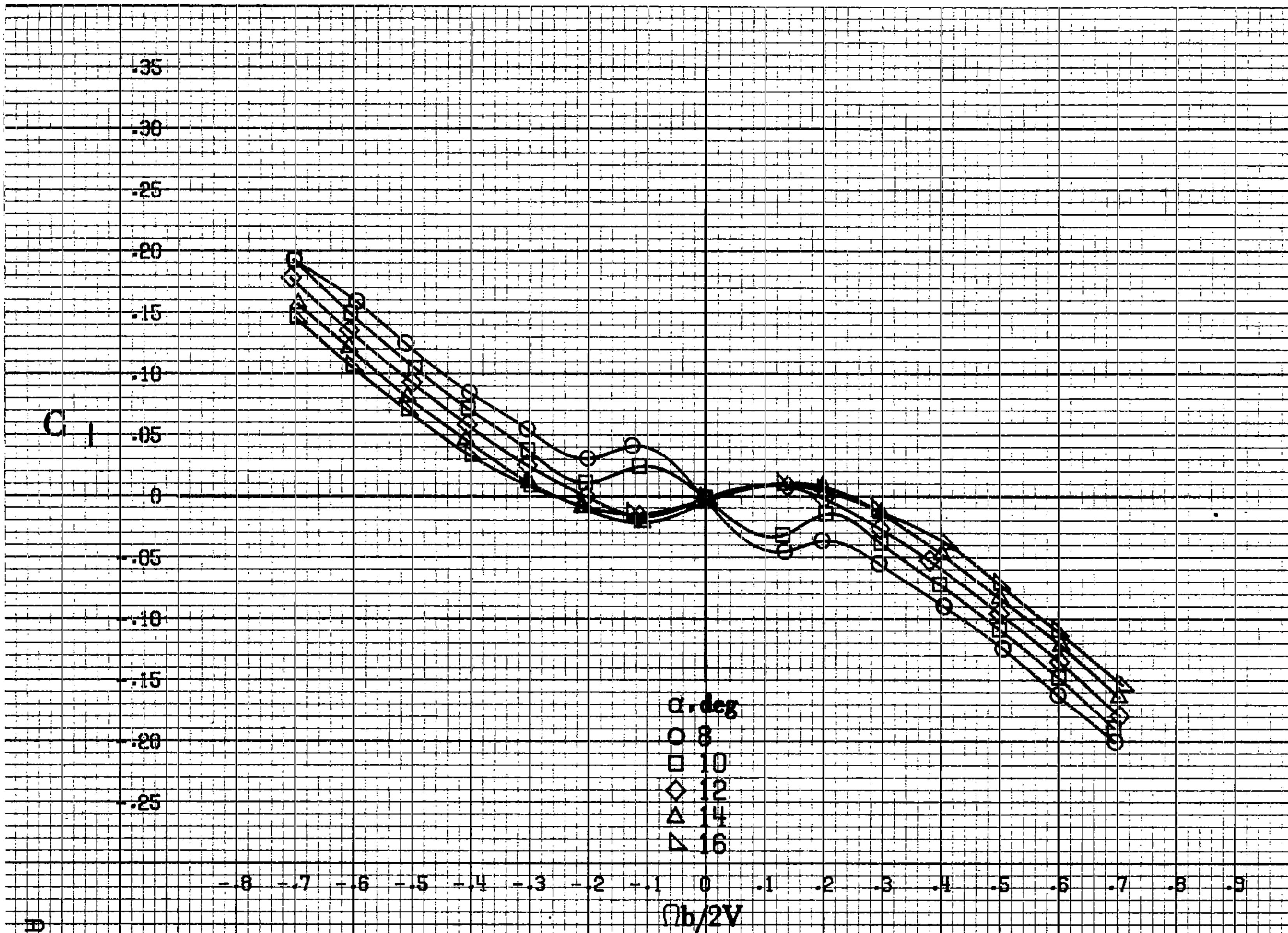

(c) α = 8 to 16 deg, SR = 91.4 cm (36 in).

Figure A2. Continued.

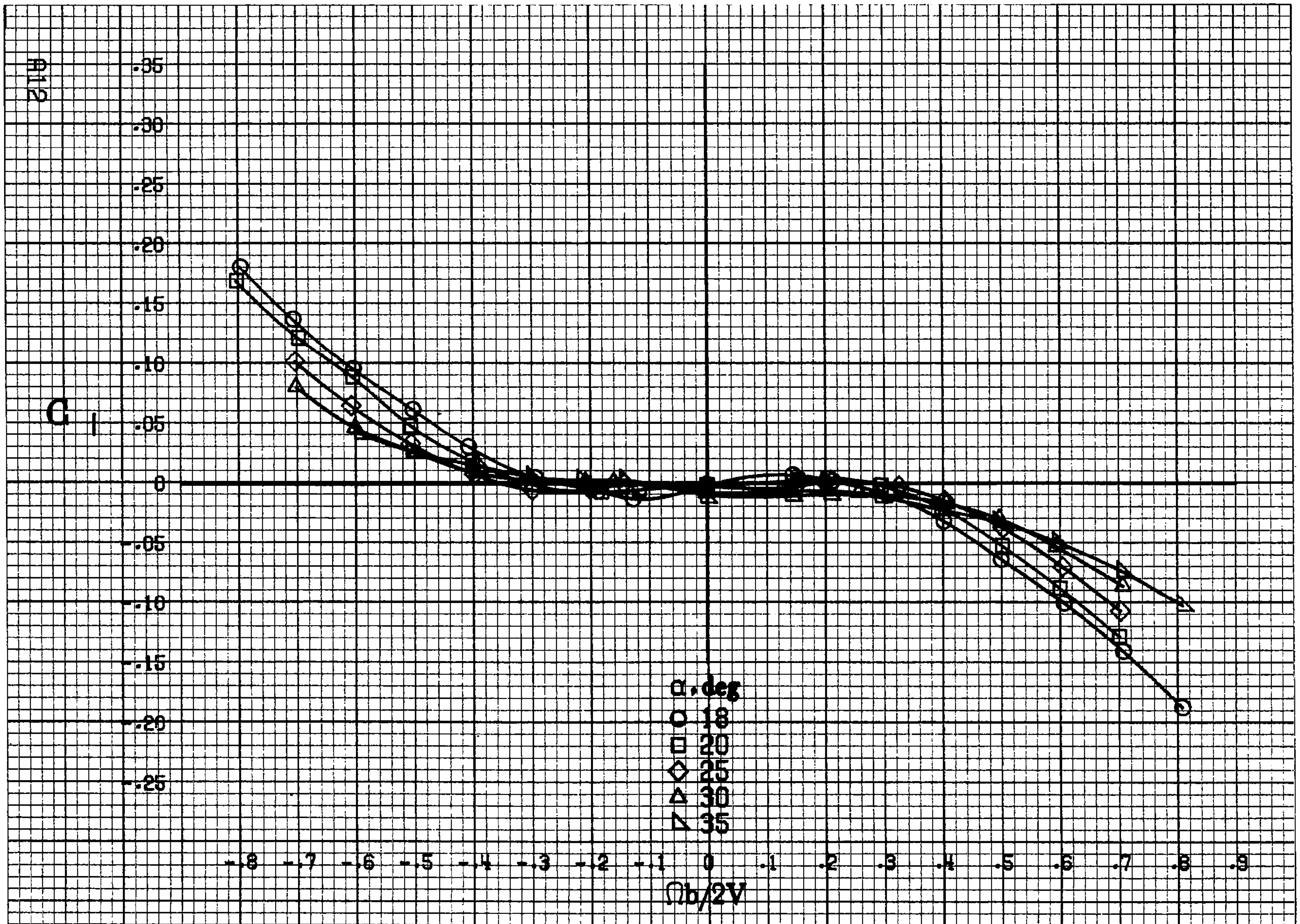

(d) α = 18 to 35 deg, SR = 91.4 cm (36 in).

Figure A2. Continued.

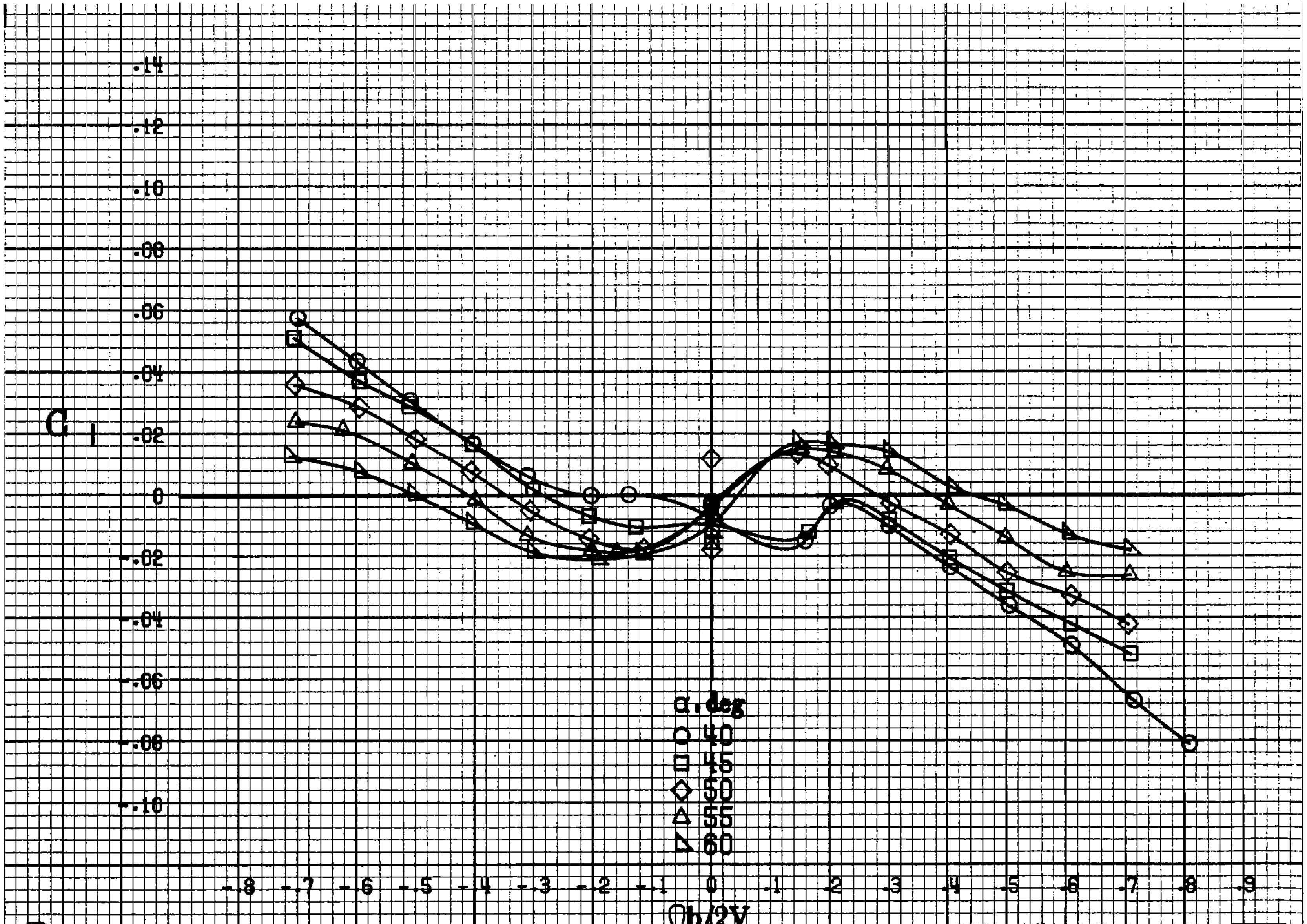

(e) α = 40 to 60 deg, SR = 91.4 cm (36 in).

Figure A2. Continued.

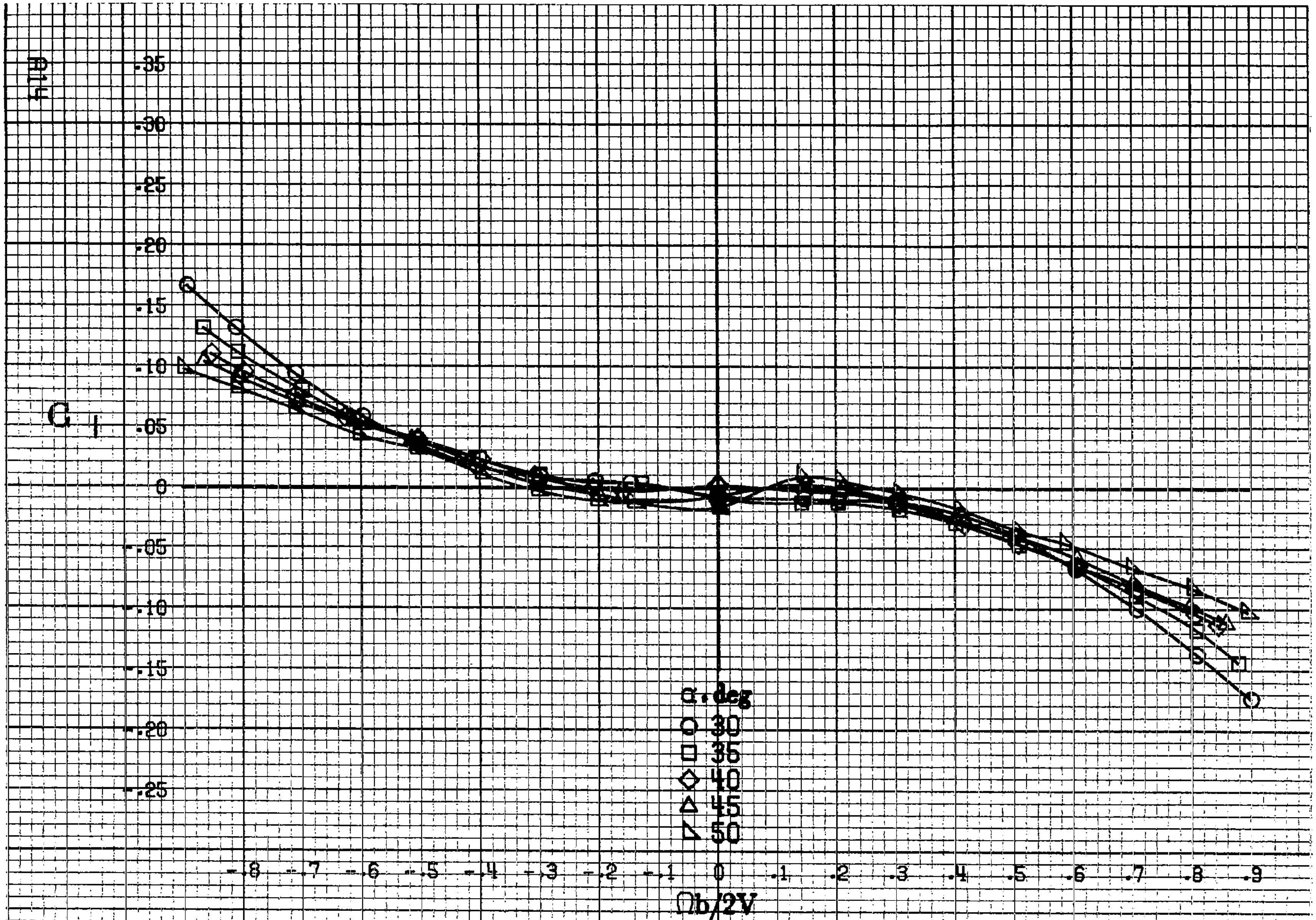

(f) α = 30 to 50 deg, SR = 0.

Figure A2. Continued.

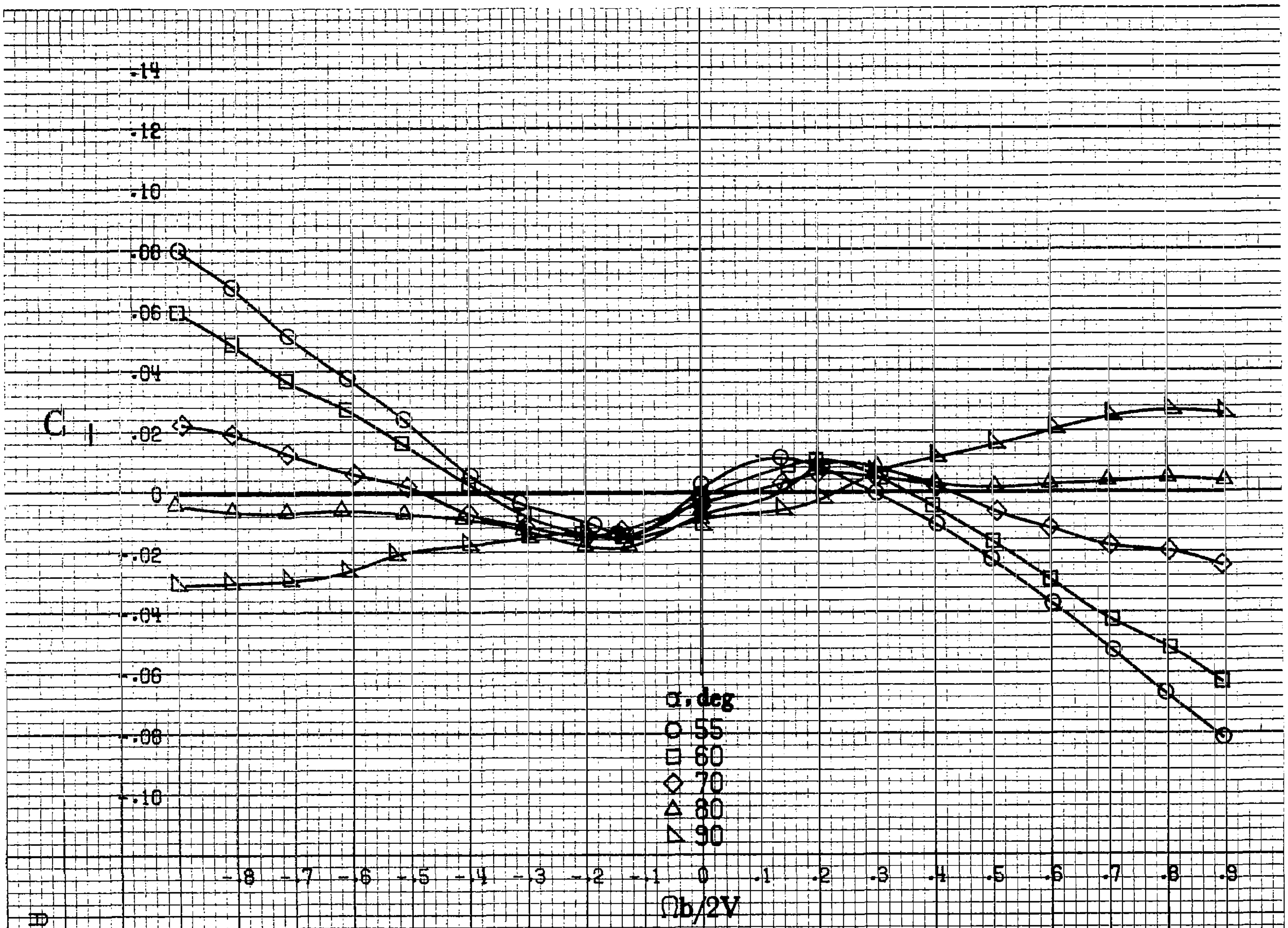

(g) α = 55 to 90 deg, SR = 0.

Figure A2. Concluded.

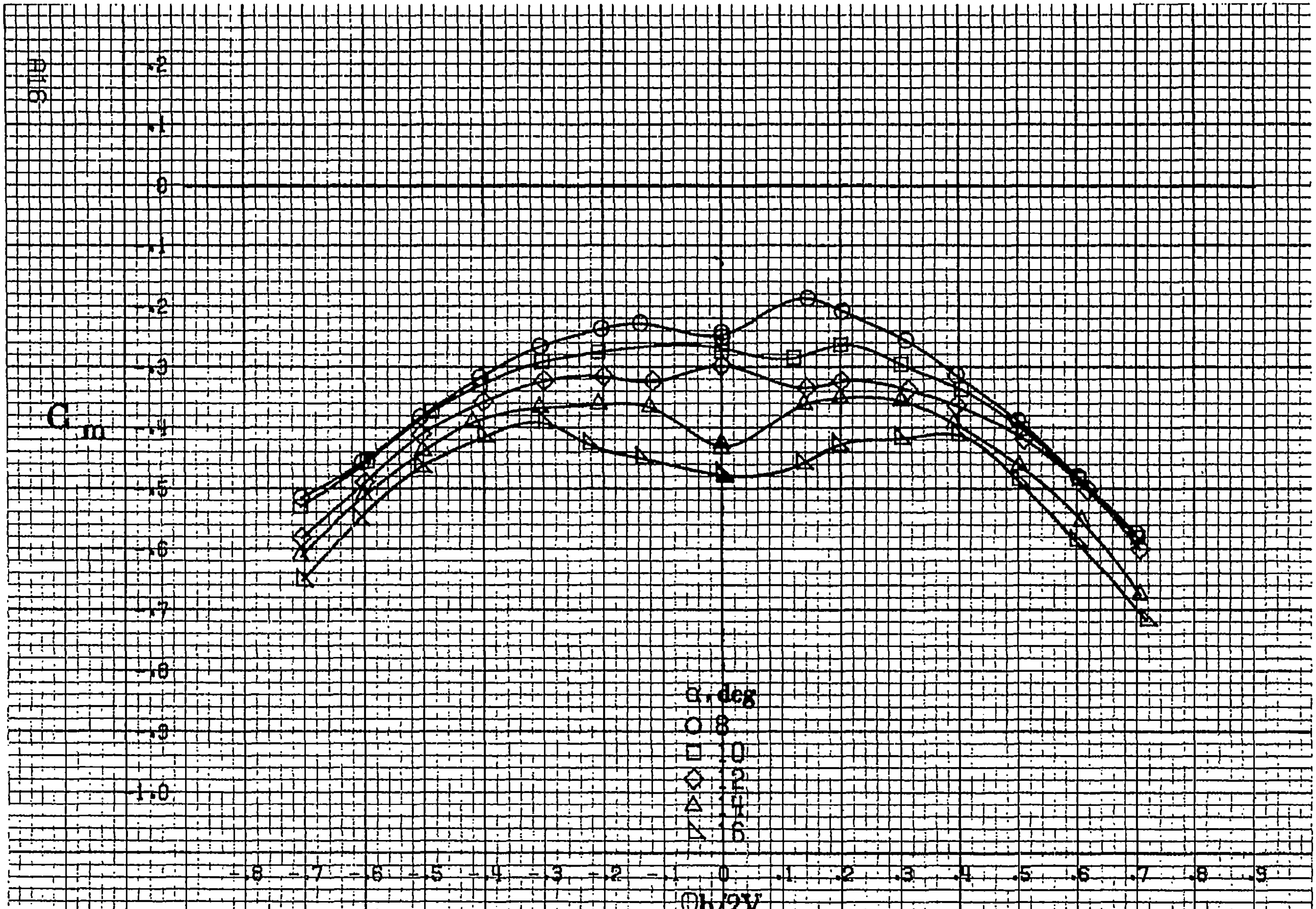

(a) $\alpha = 8$ to 16 deg, SR = 182.9 cm (72 in).

Figure A3.-Effect of rotation rate and angle of attack on pitching-moment coefficient for basic configuration. $\delta_e = 0°$, $\delta_a = 0°$, $\delta_r = 0°$, $\beta = 0°$.

(b) α = 18 to 35 deg, SR = 182.9 cm (72 in).

Figure A3.-Continued.

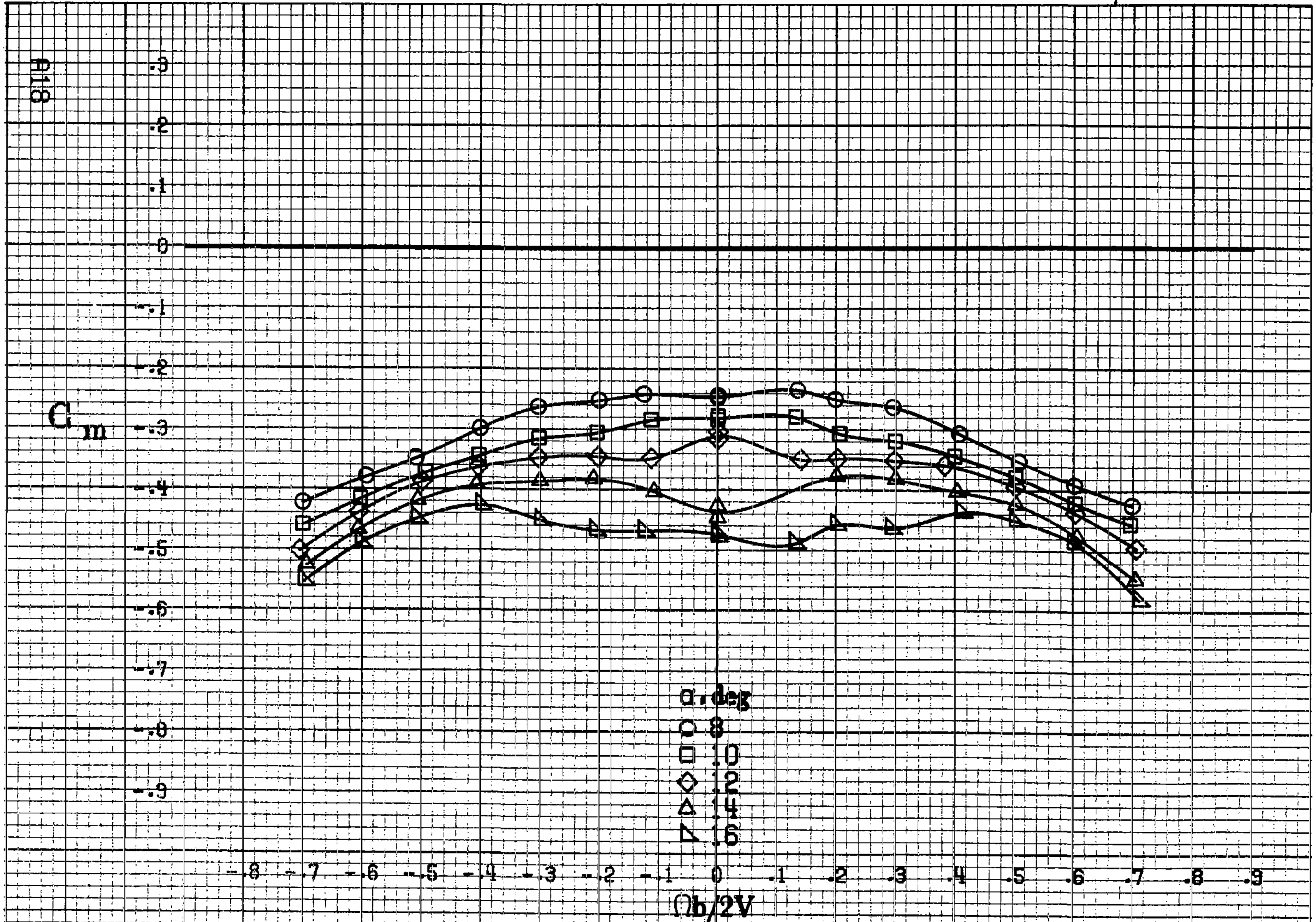

(c) α = 8 to 16 deg, SR = 91.4 cm (36 in).

Figure A3. Continued.

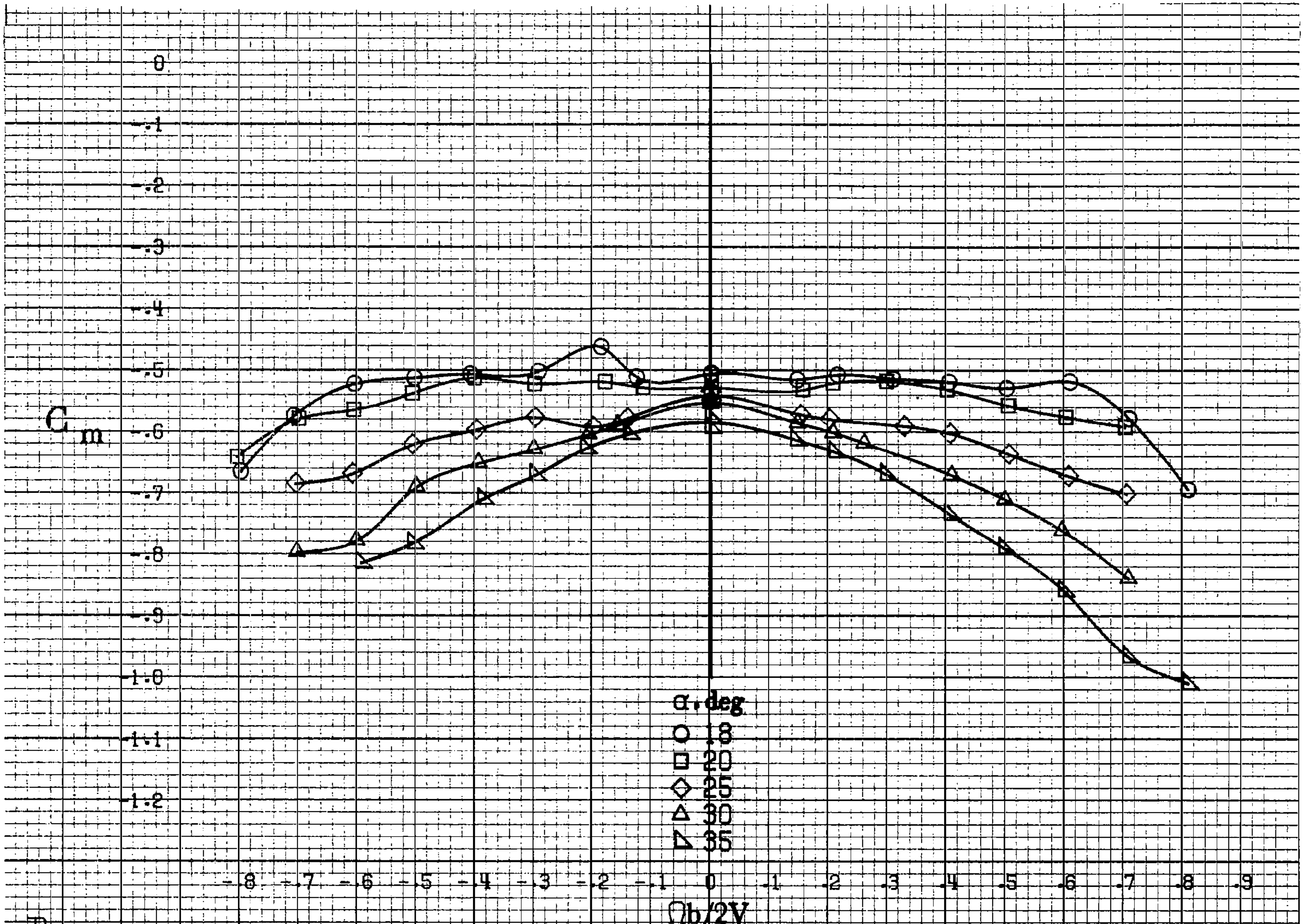

(d) α = 18 to 35 deg, SR = 91.4 cm (36 in).
Figure A8.-Continued.

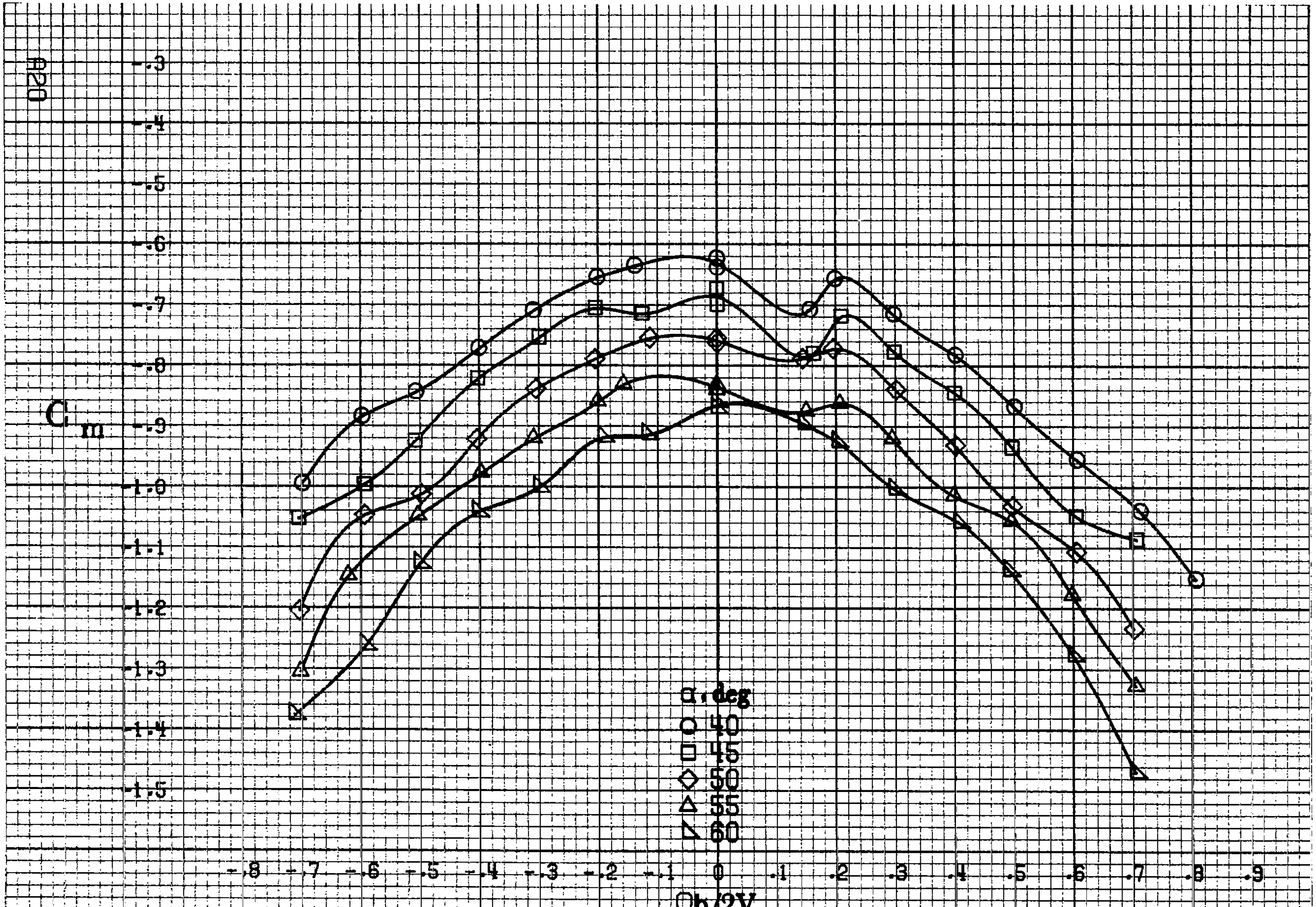

(e) α = 40to60deg, SR = 91.4cm (36in).

Figure A3. Continued.

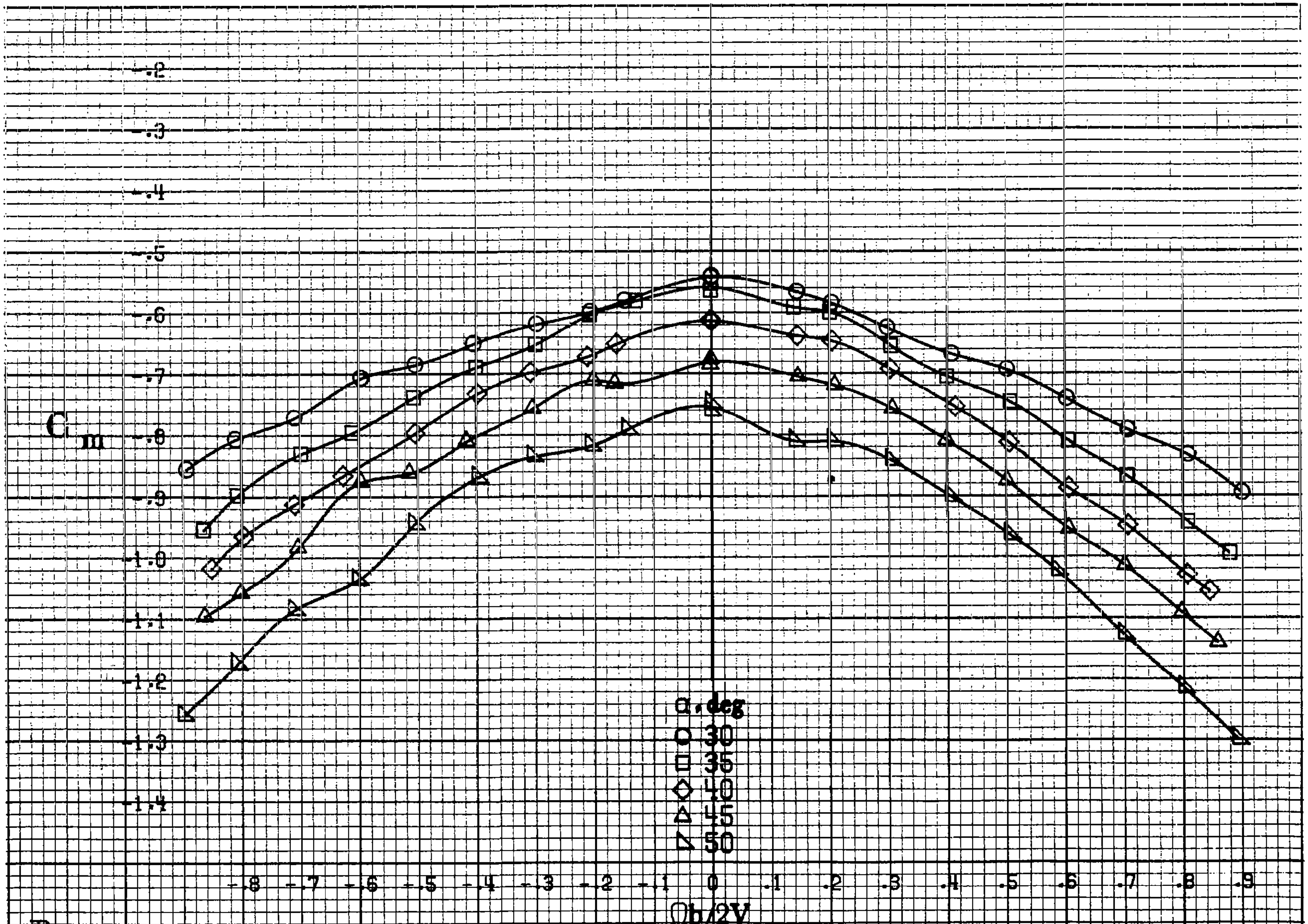

(f) α = 30to50deg, SR = 0.

Figure A3. Continued.

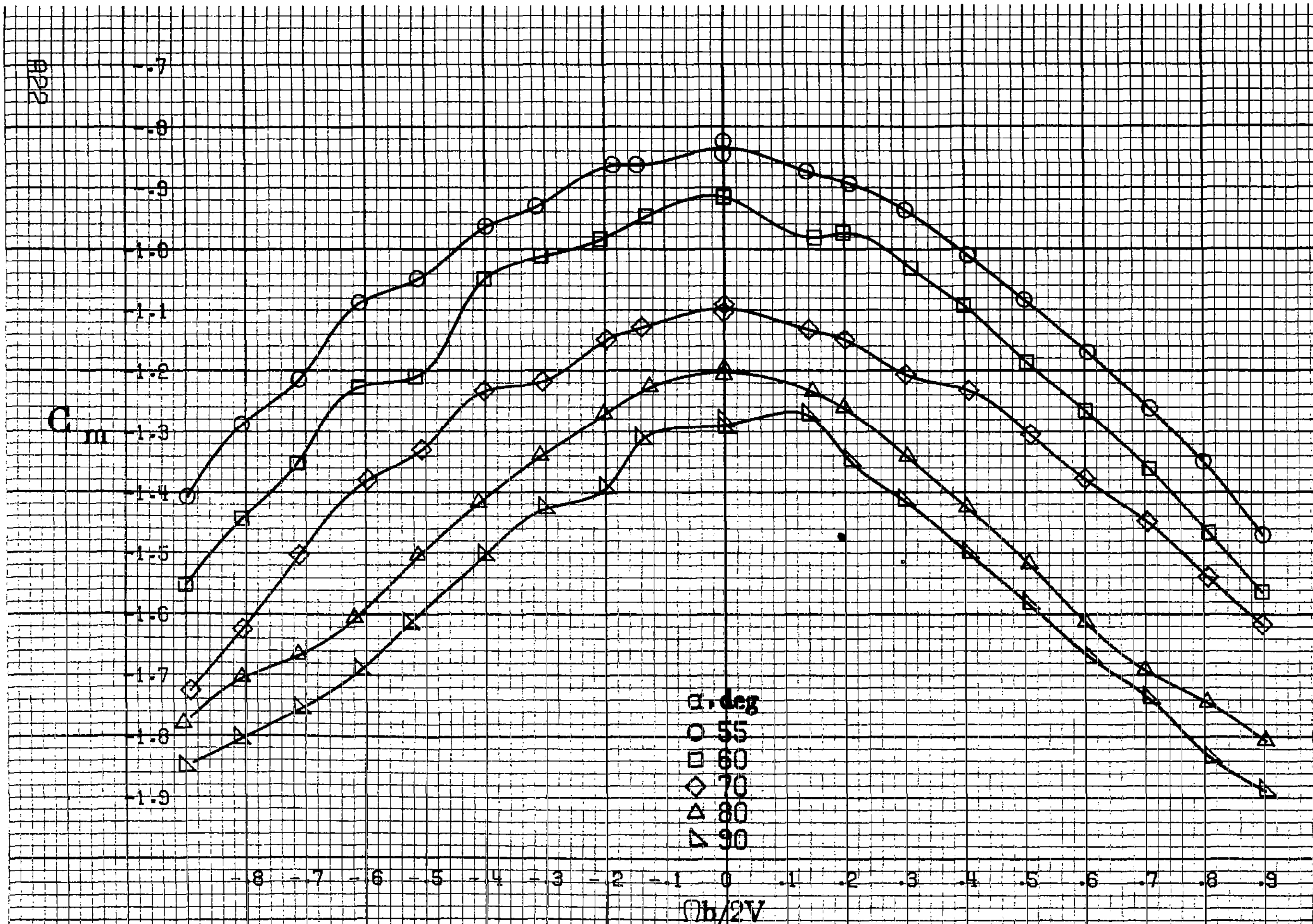

(g) α = 55 to 90 deg, SR = 0.

Figure A8.-Concluded.

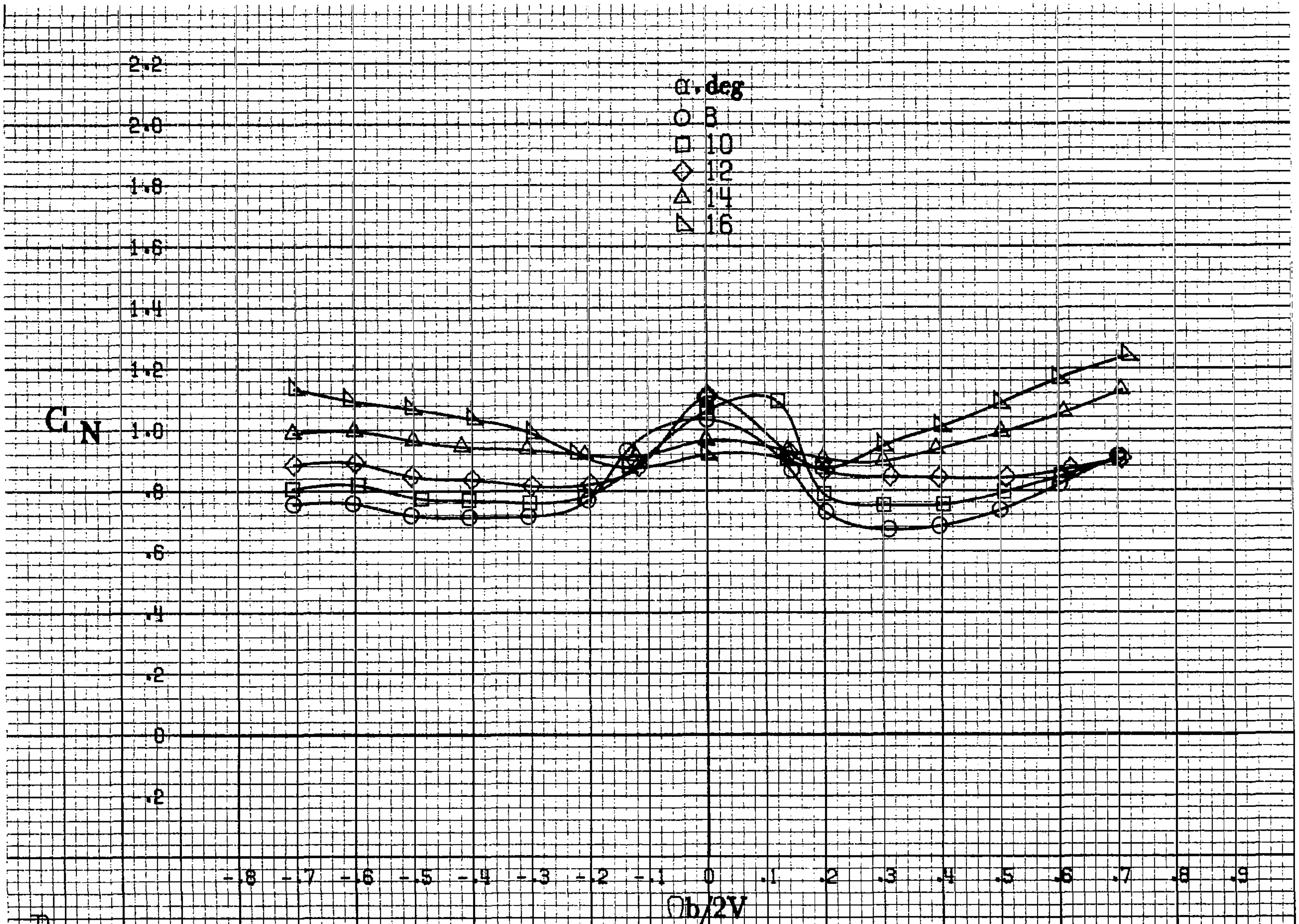

(a) α = 8 to 16 deg, SR = 182.9 cm (72 in).

Figure A4.- Effect of rotation rate and angle of attack on normal-force coefficient for basic configuration. $\delta_e = 0°$, $\delta_a = 0°$, $\delta_r = 0°$, $\beta = 0°$.

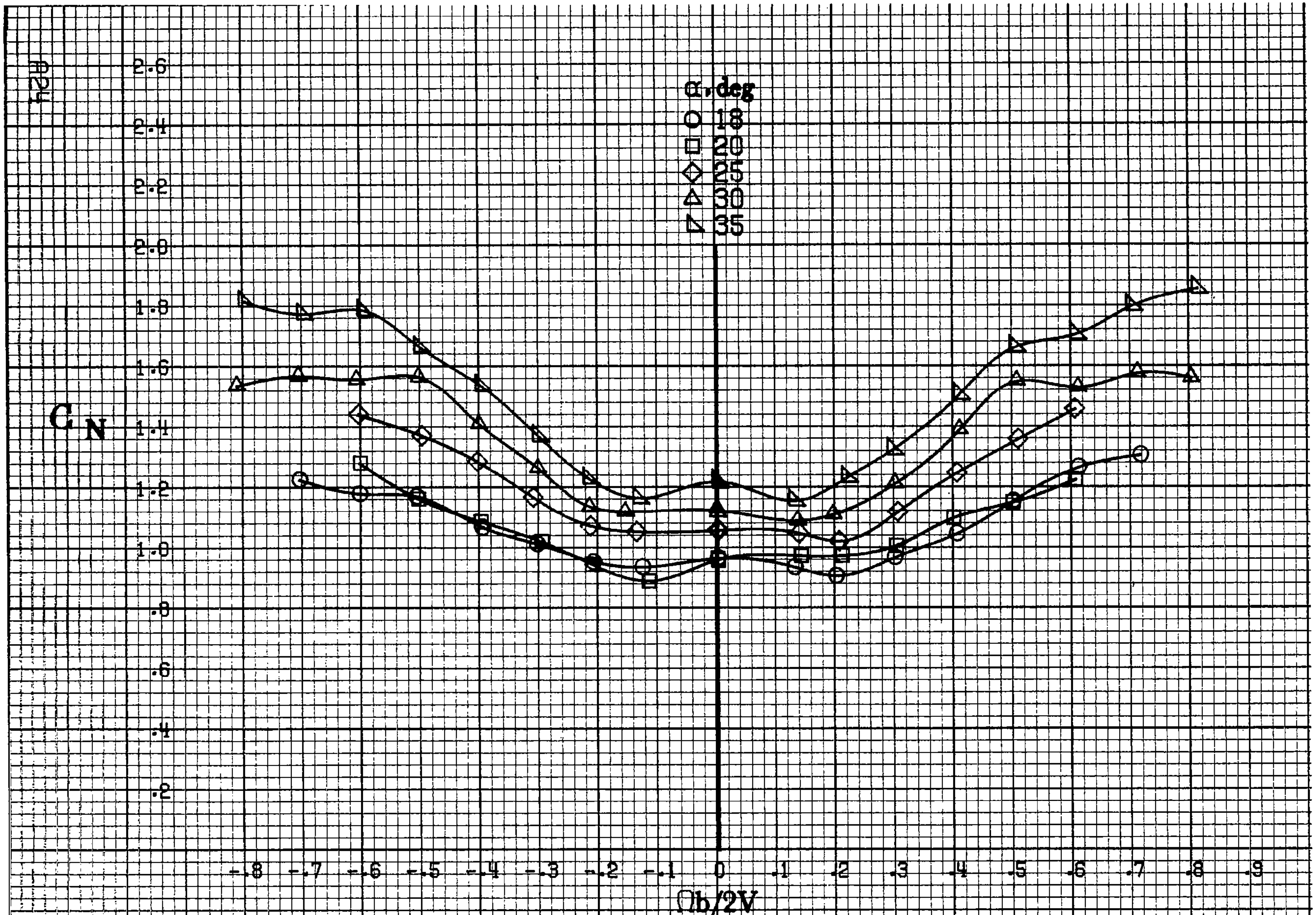

(b) α = 18 to 35 deg, SR = 182.9 cm (72 in).

Figure A4. Continued.

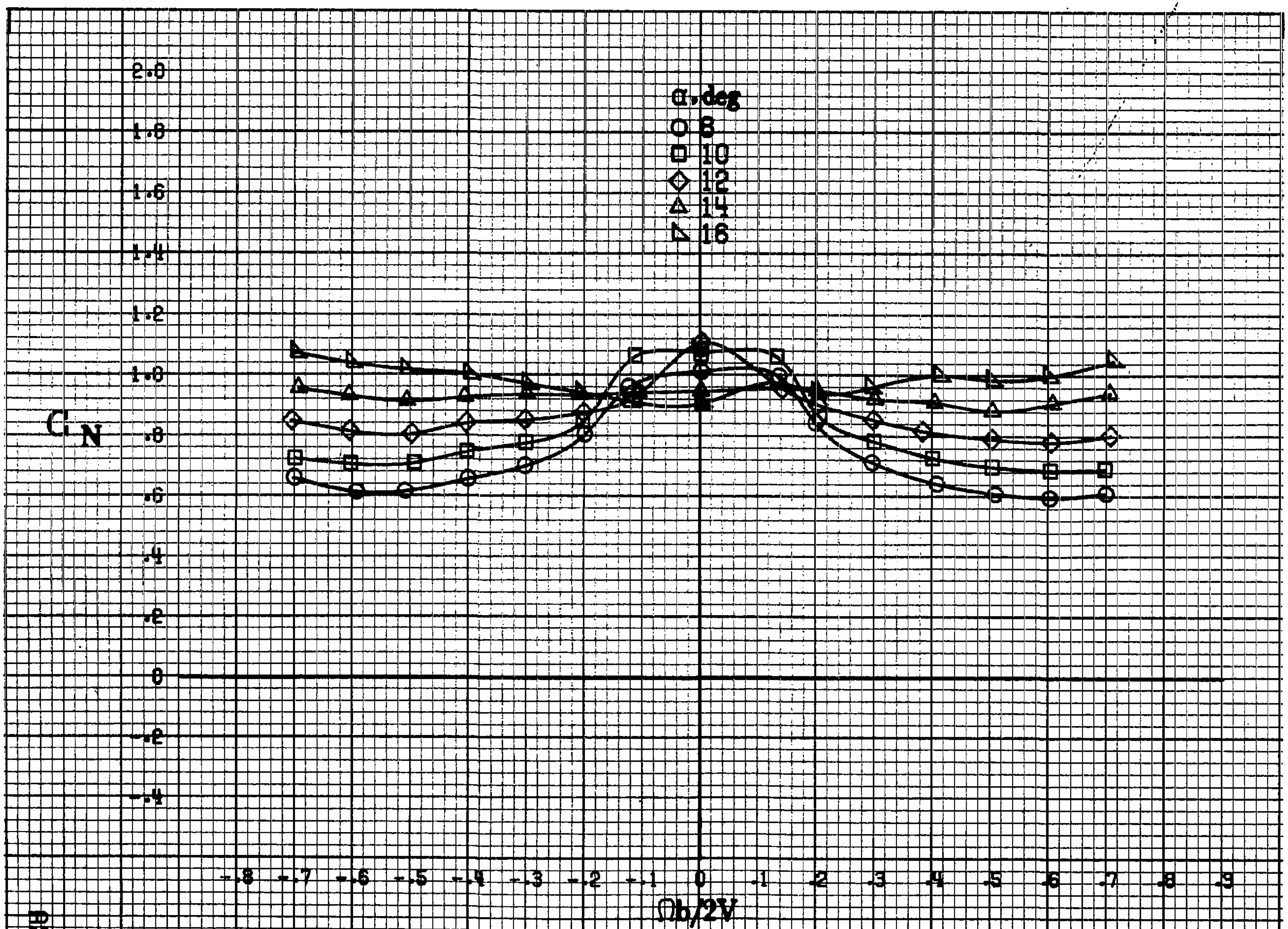

(c) α = 8 to 16 deg, SR = 91.4 cm (36 in).

Figure A4.- Continued.

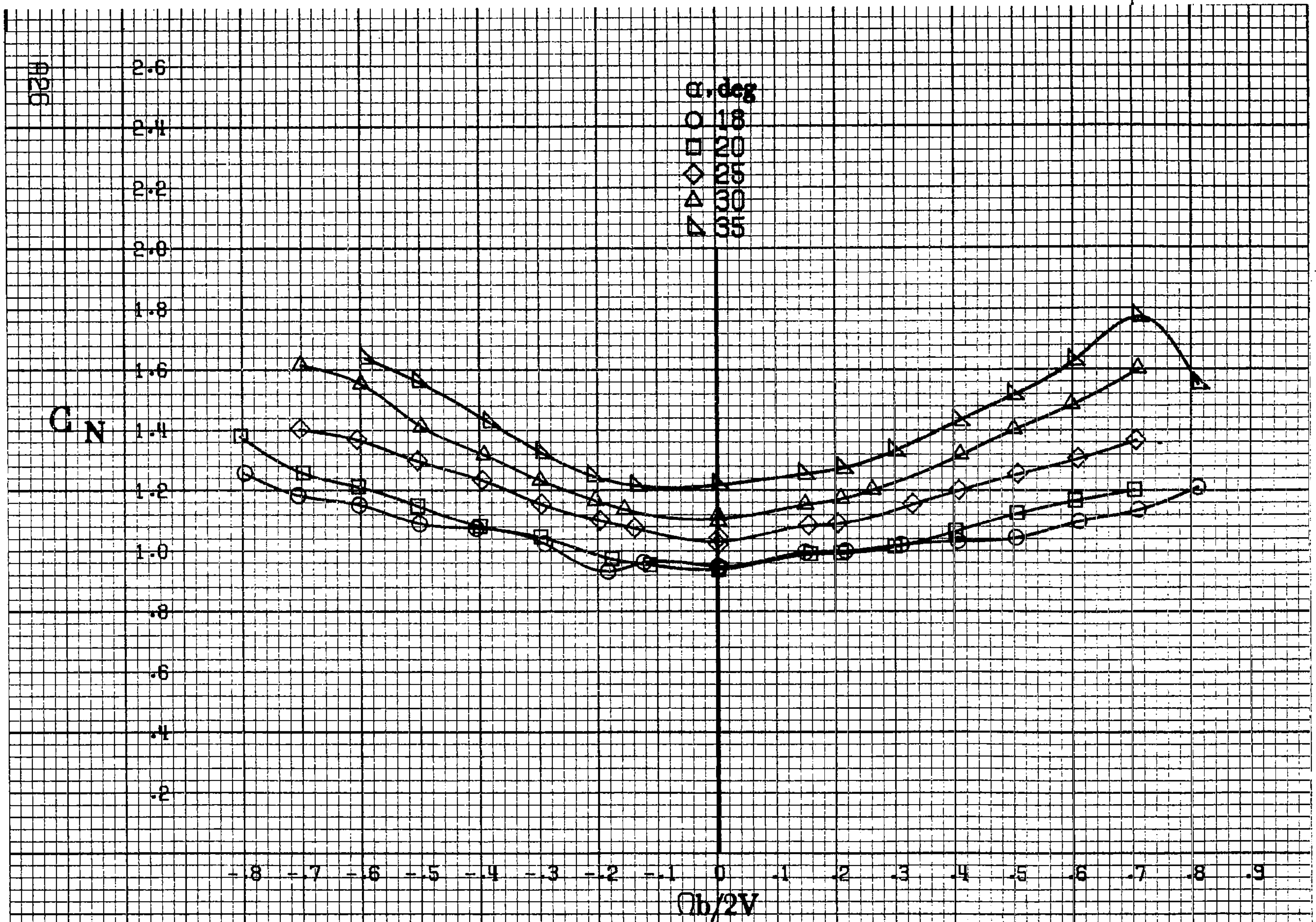

(d) α = 18 to 35 deg, SR = 91.4 cm (36 in).

Figure A4.-Continued.

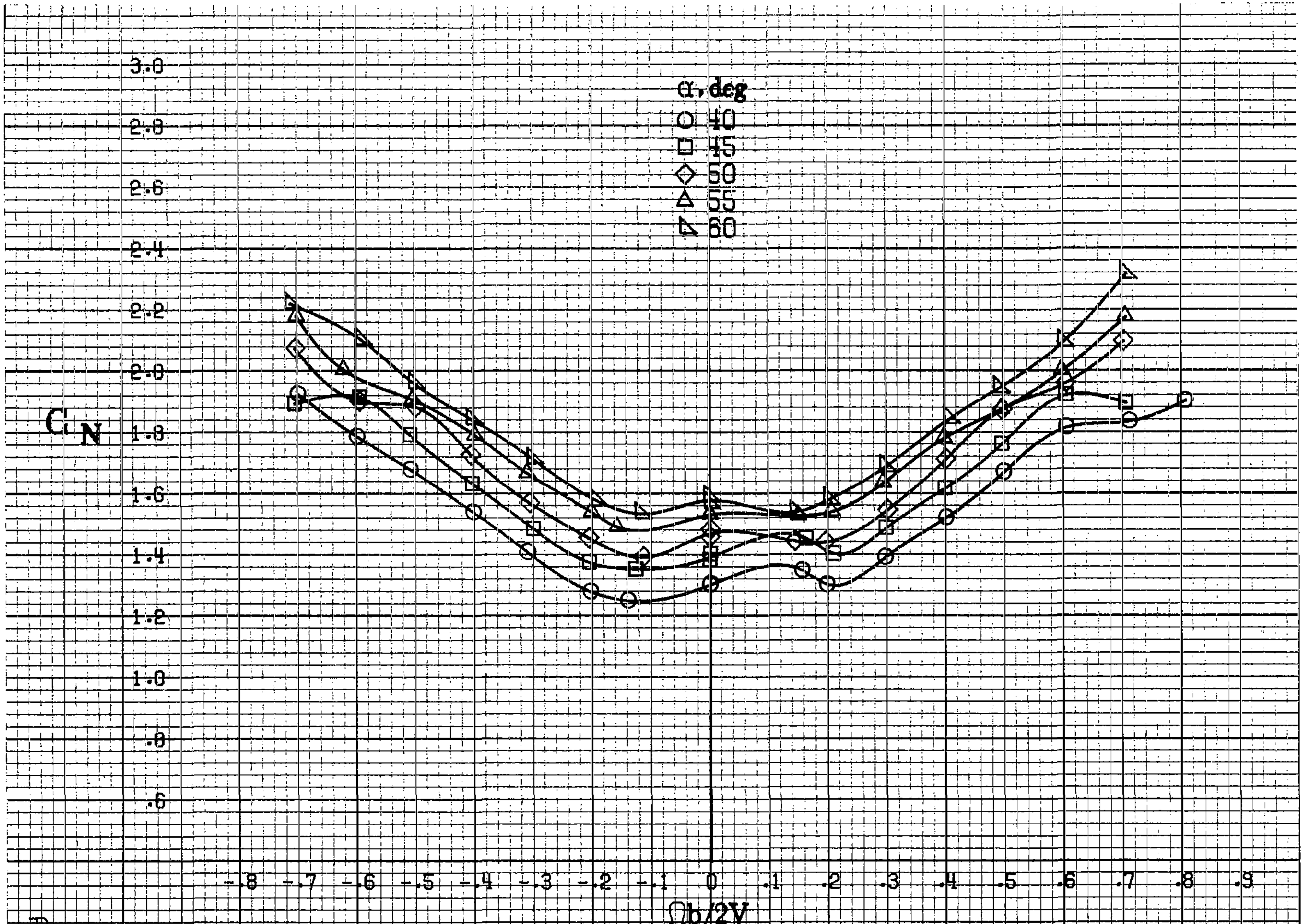

(e) α = 40 to 60 deg, SR = 91.4 cm (36 in).

Figure A4. Continued.

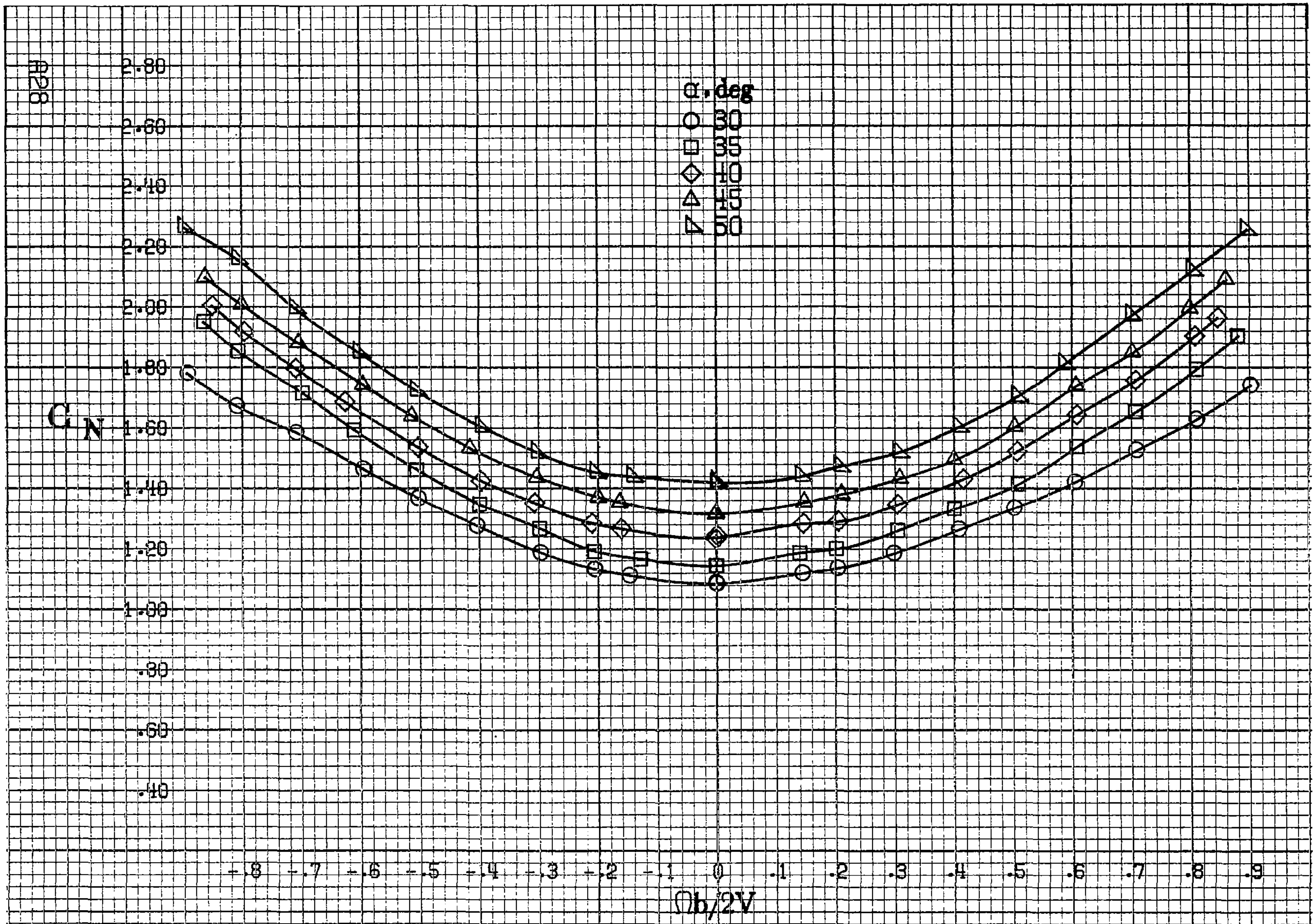

(f) α = 30to50deg, SR = 0.

Figure A4. Continued.

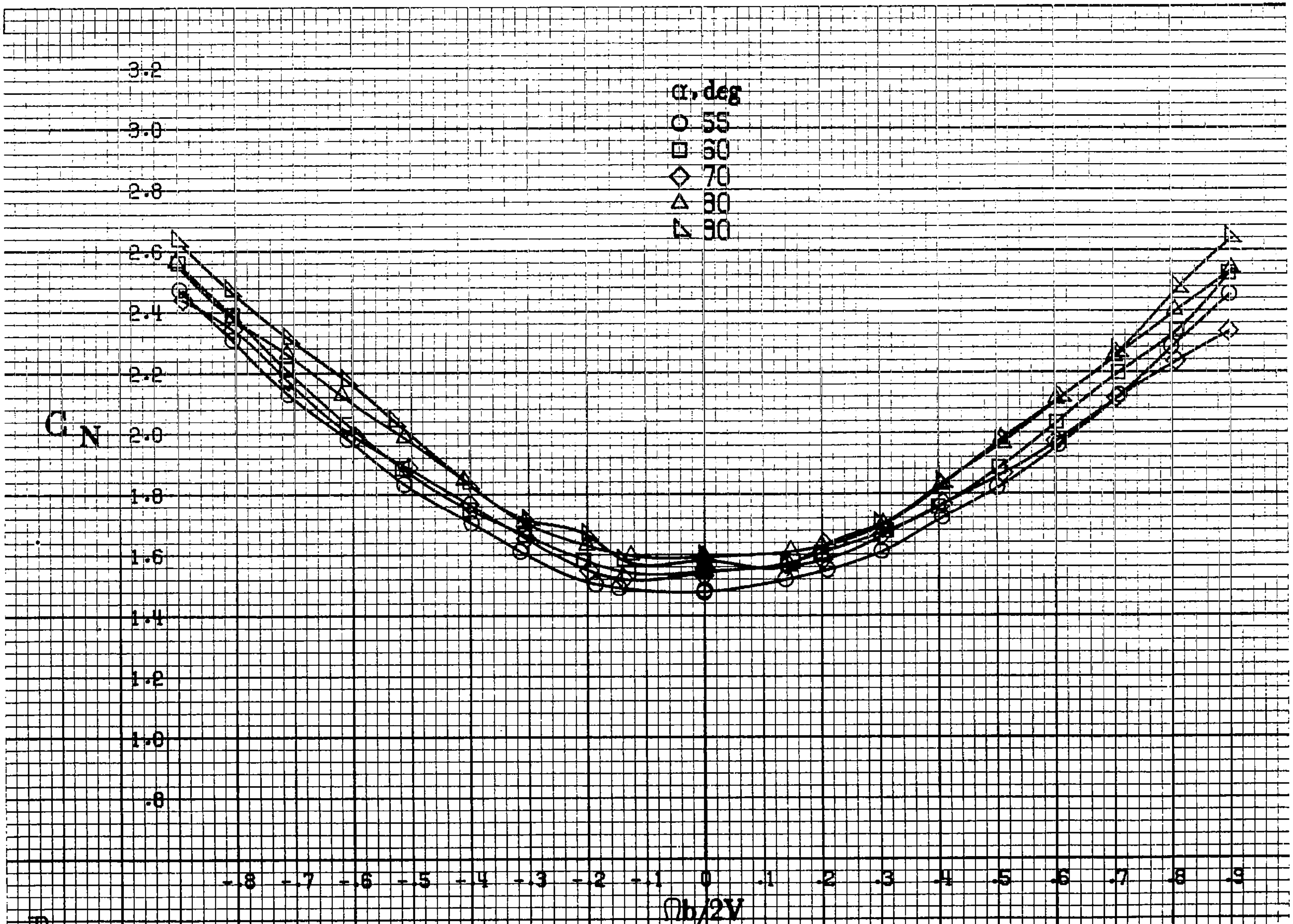

(g) α = 55 to 90 deg, δR = 0.
Figure A4. Concluded.

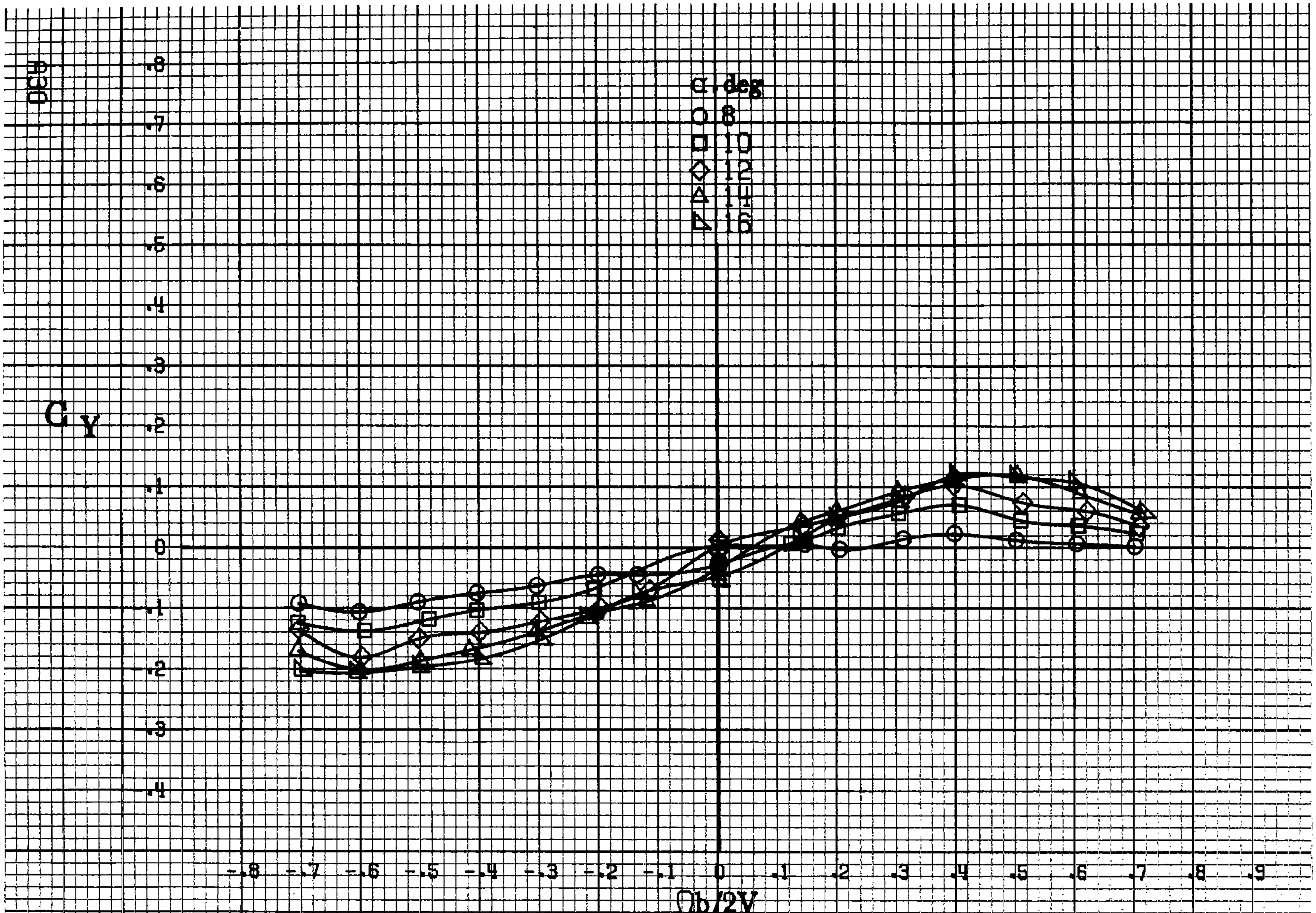

(a) α = 8 to 16 deg, SR = 182.9 cm (72 in).

Figure A5.-Effect of rotation rate and angle of attack on side-force coefficient for basic configuration. $\delta_e = 0°$, $\delta_a = 0°$, $\delta_r = 0°$, $\beta = 0°$.

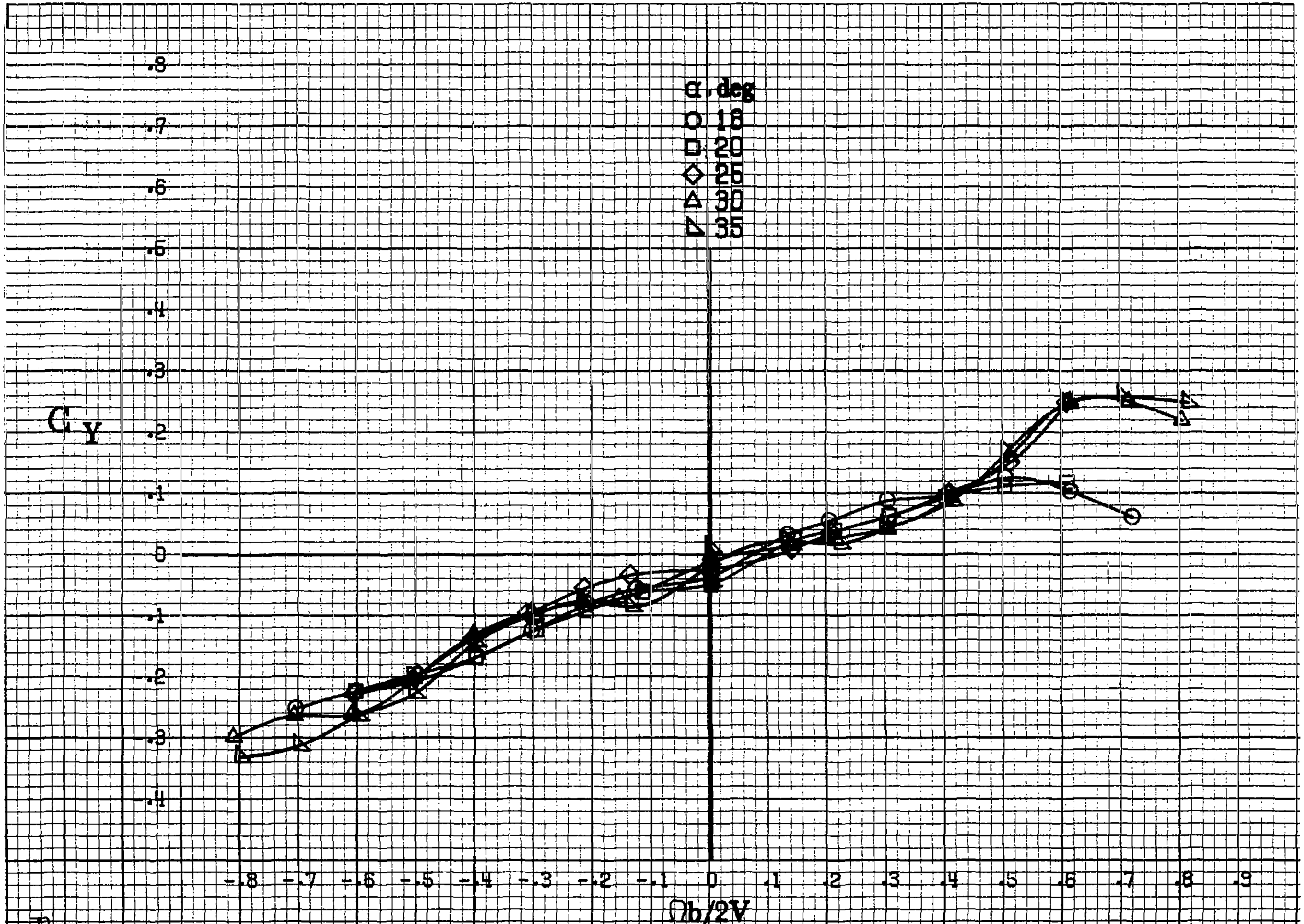

(b) α = 18 to 35 deg, SR = 182.9 cm (72 in).

Figure A5.-Continued.

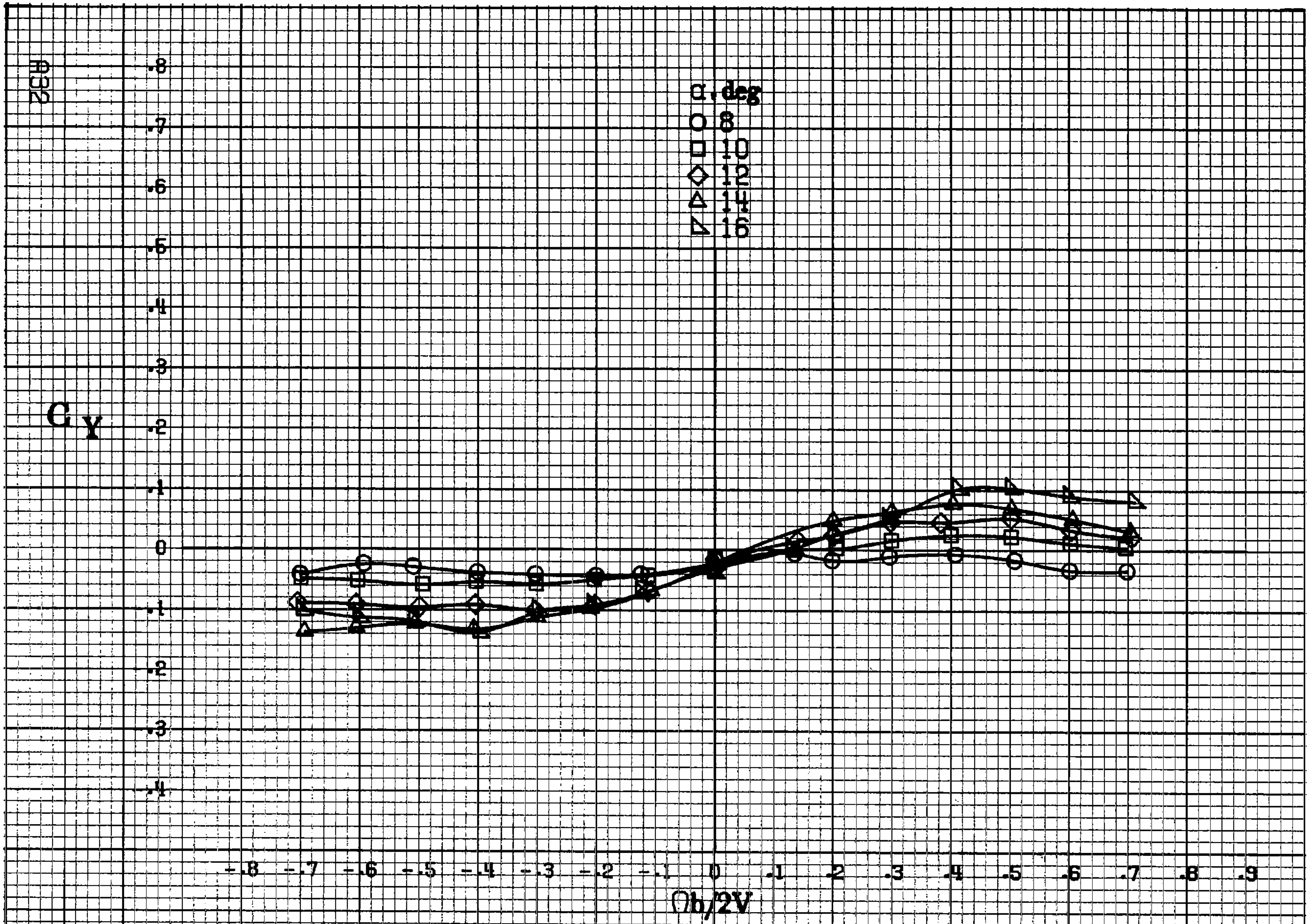

(c) α = 8 to 16 deg, SR = 91.4 cm (36 in).

Figure A5. Continued.

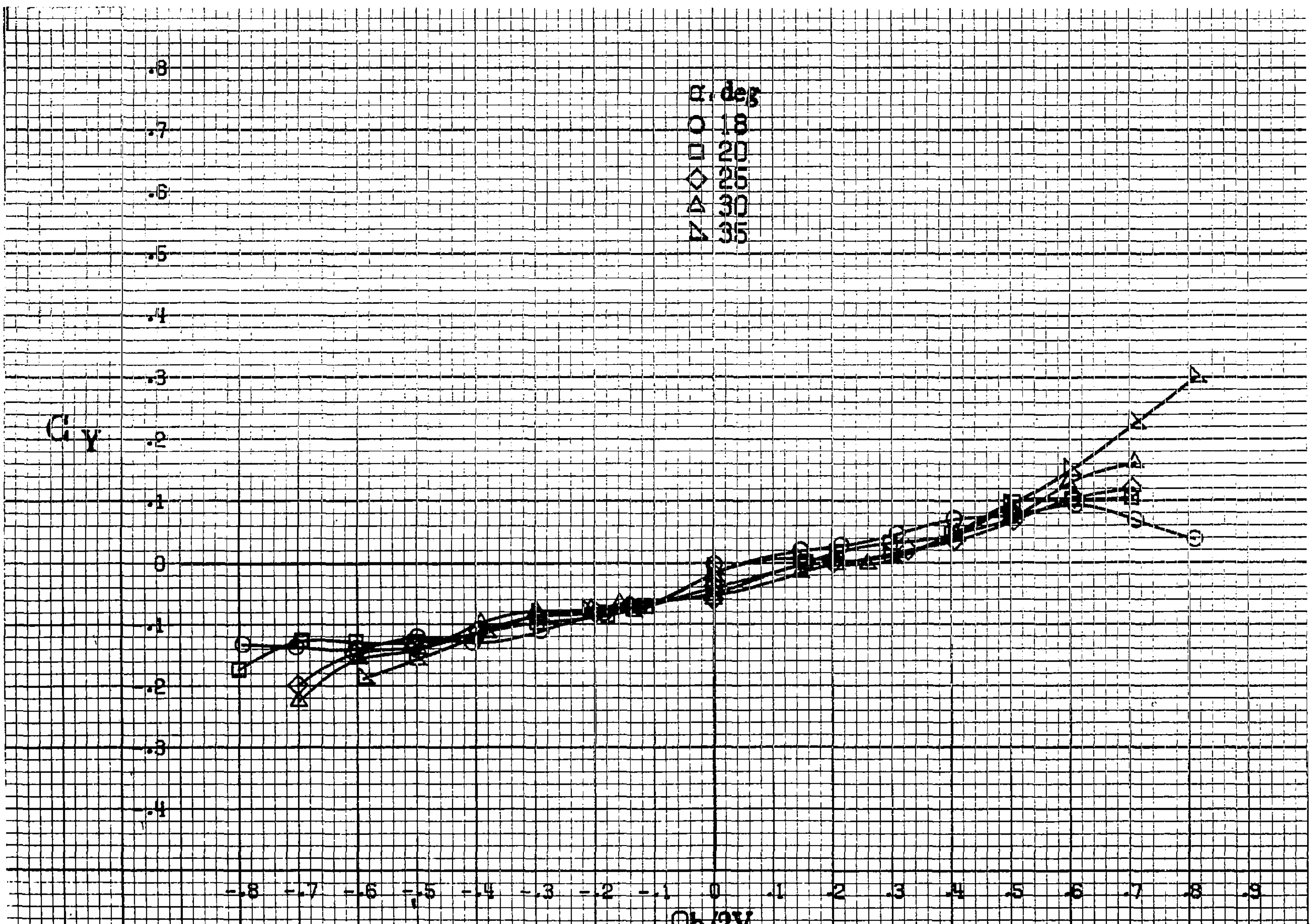

(d) α=18to35deg, SR=91.4cm(36in).

Figure A5.-Continued.

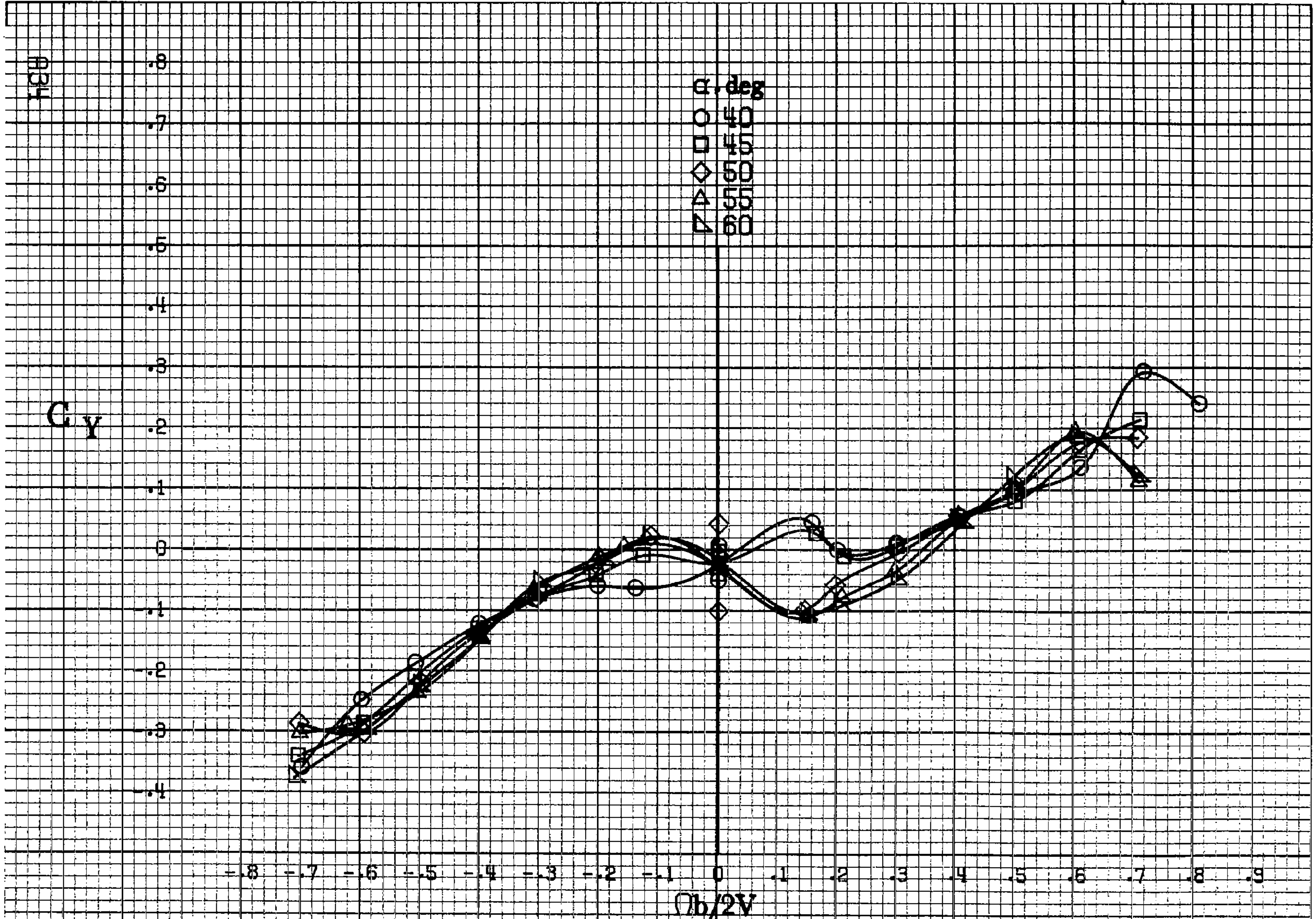

(e) α = 40 to 60 deg, SR = 91.4 cm (36 in).

Figure A5. Continued.

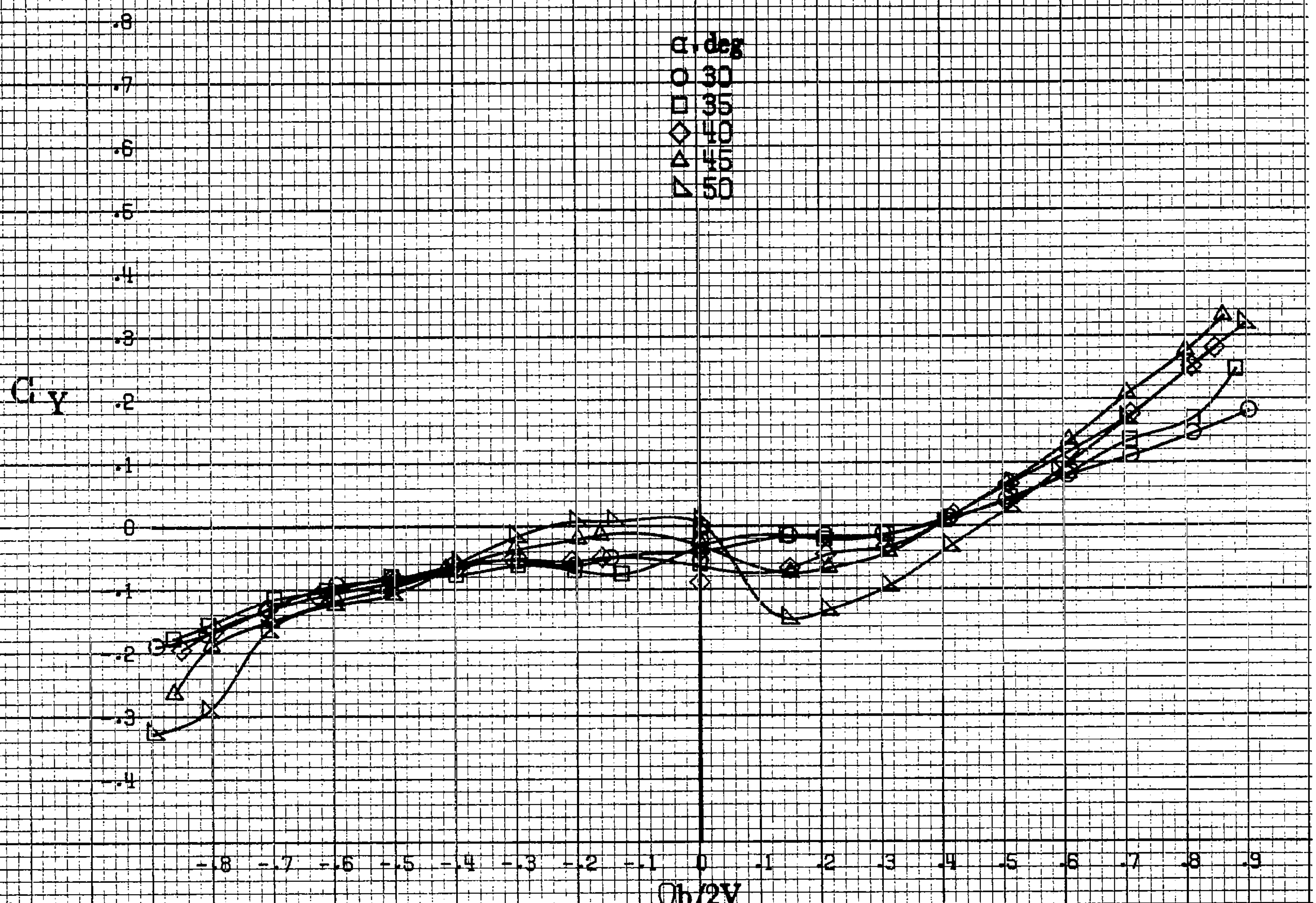

(f) α=30to50deg, SR=0.
Figure A5.-Continued.

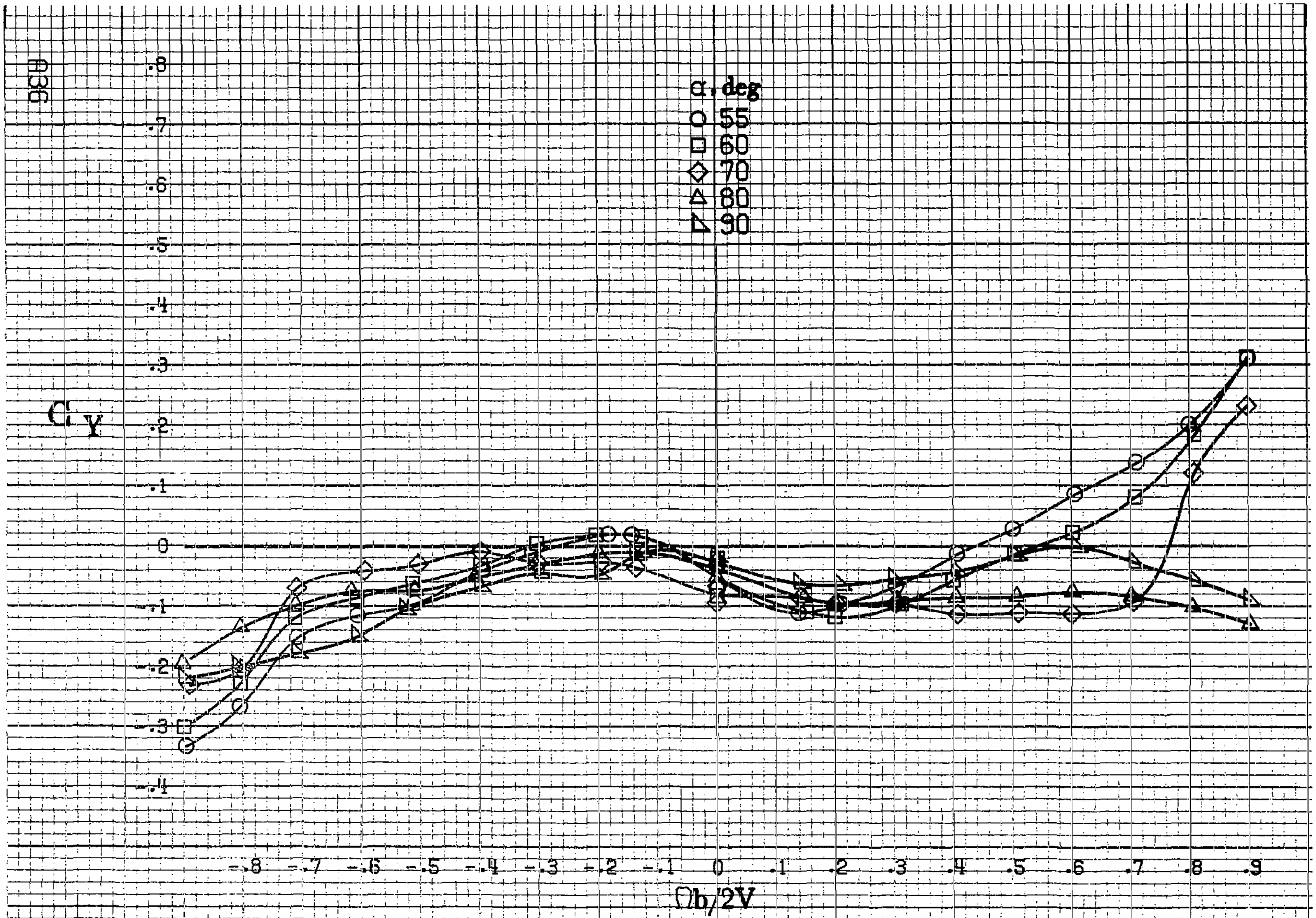

(g) α = 55 to 90 deg, SR = 0.

Figure A5.-Concluded.

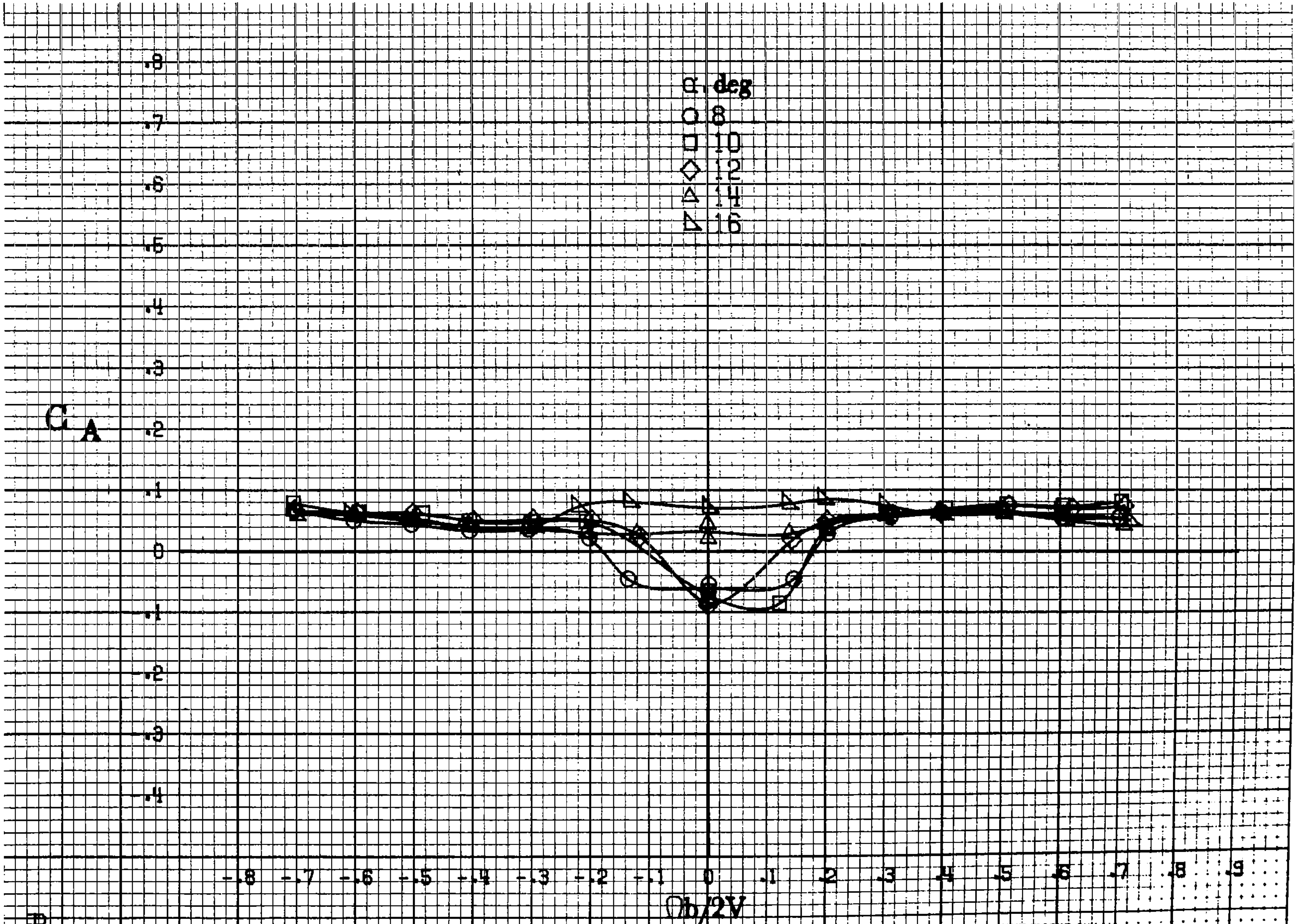

(a) $\alpha = 8$ to 16 deg, SR = 182.9 cm (72 in).

Figure A6.-Effect of rotation rate and angle of attack on axial-force coefficient for basic configuration. $\delta_e = 0°$, $\delta_a = 0°$, $\delta_r = 0°$, $\beta = 0°$.

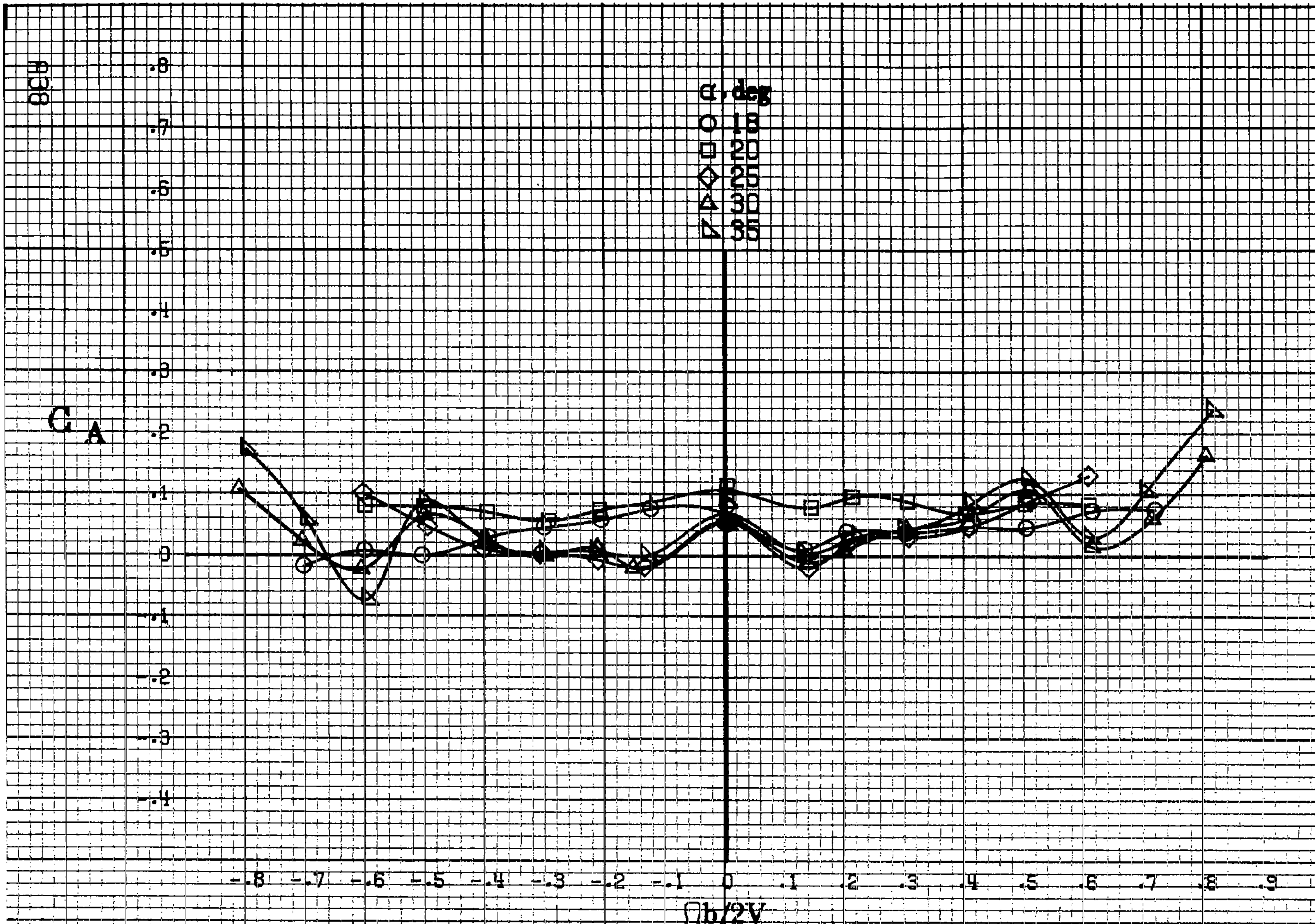

(b) α = 18 to 35 deg, SR = 182.9 cm (72 in).

Figure A6.- Continued.

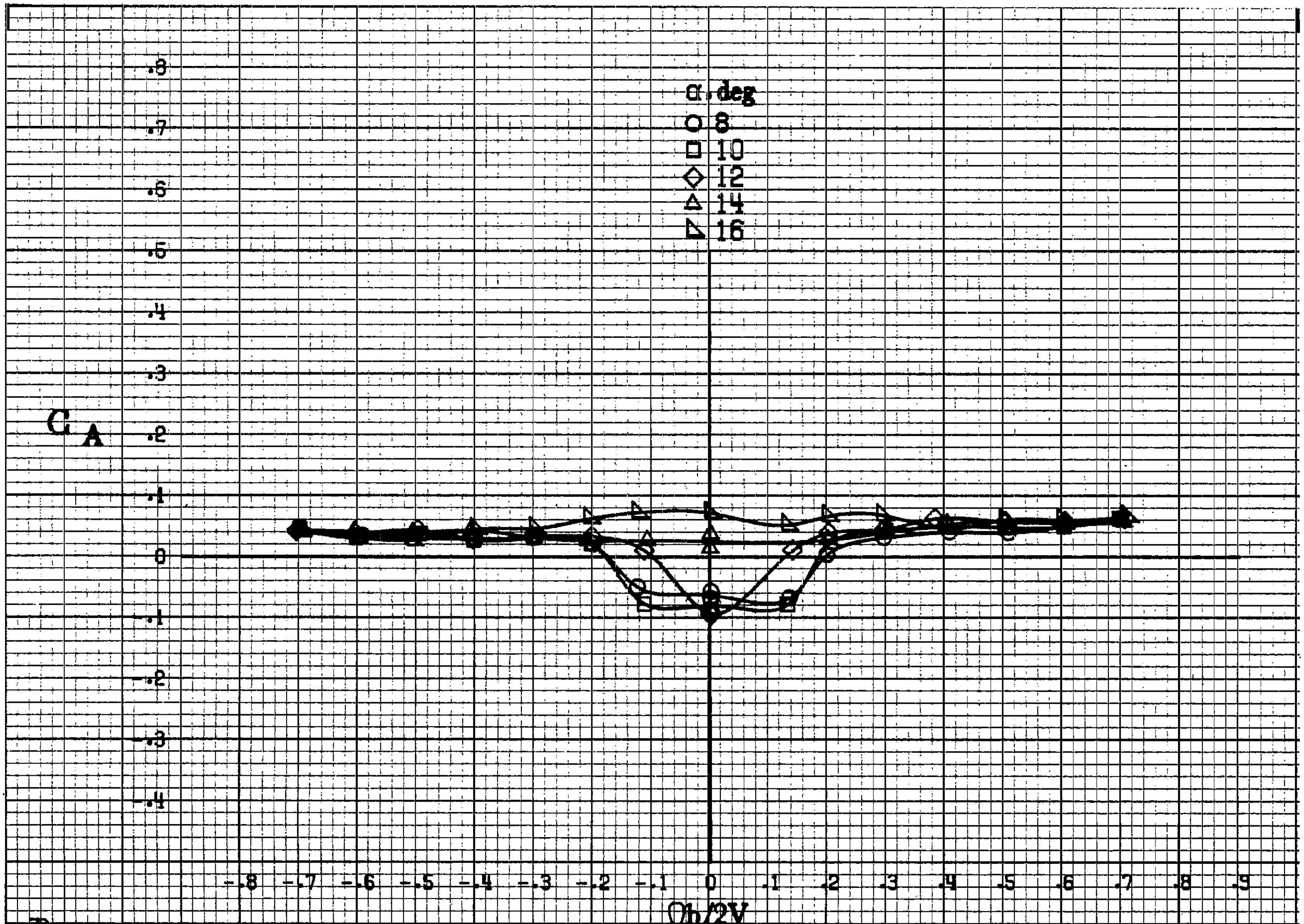

(c) α = 8 to 16 deg, SR = 91.4 cm (36 in).

Figure A6.-Continued.

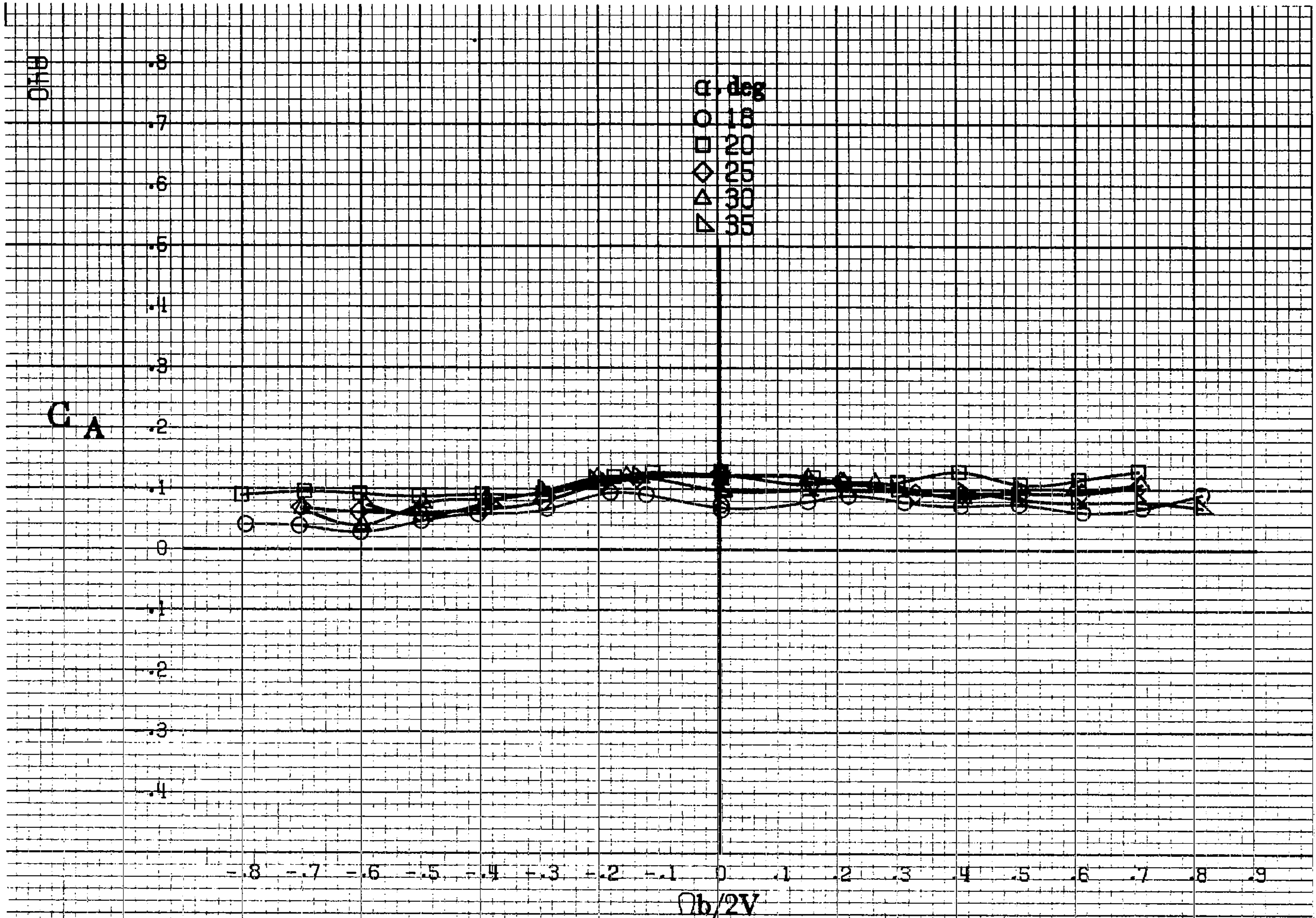

(d) α = 13 to 35 deg, SR = 91.4 cm (36 in).

Figure A6.-Continued.

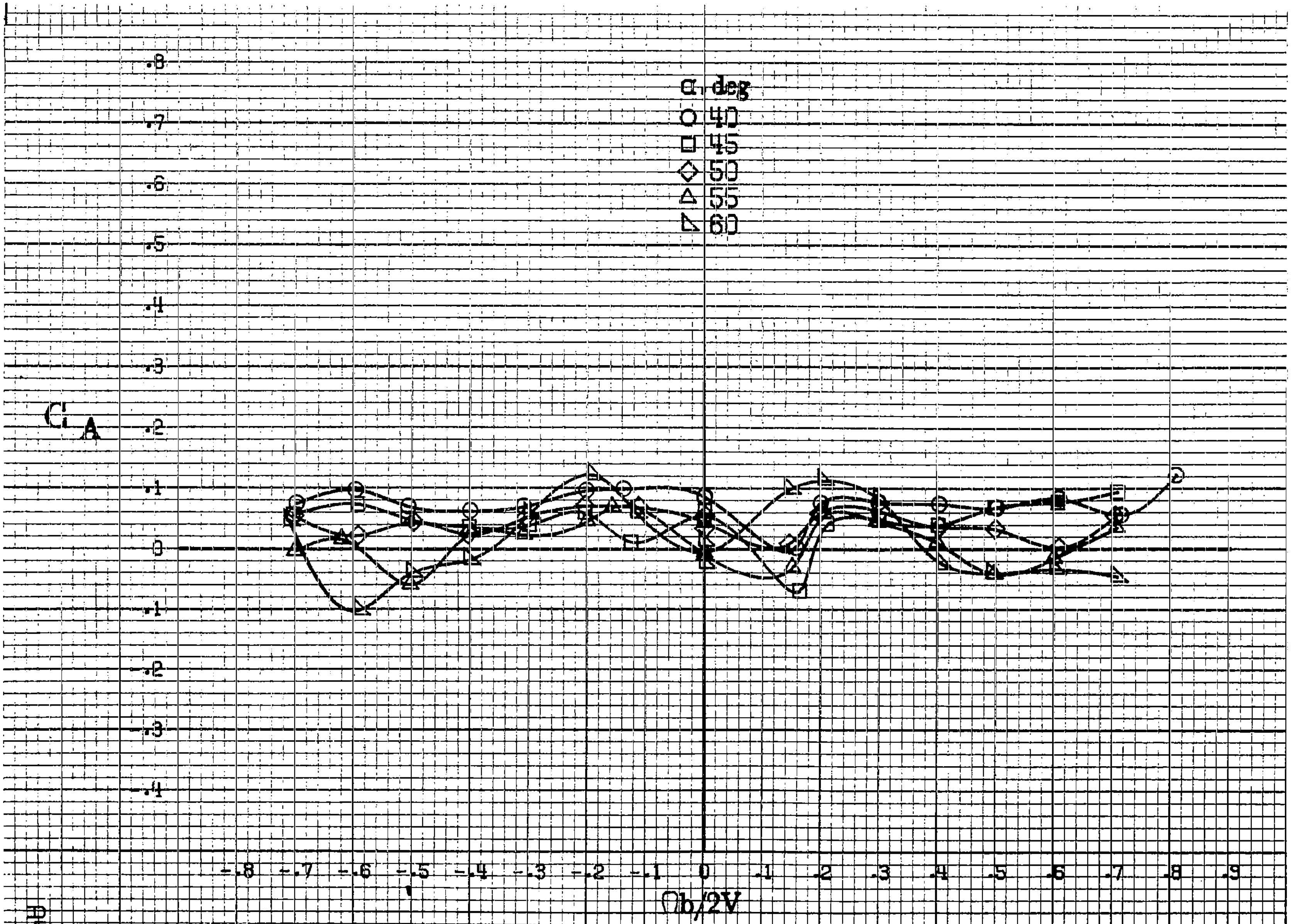

(e) α = 40 to 60 deg, SR = 91.4 cm (36 in).

Figure A6. Continued.

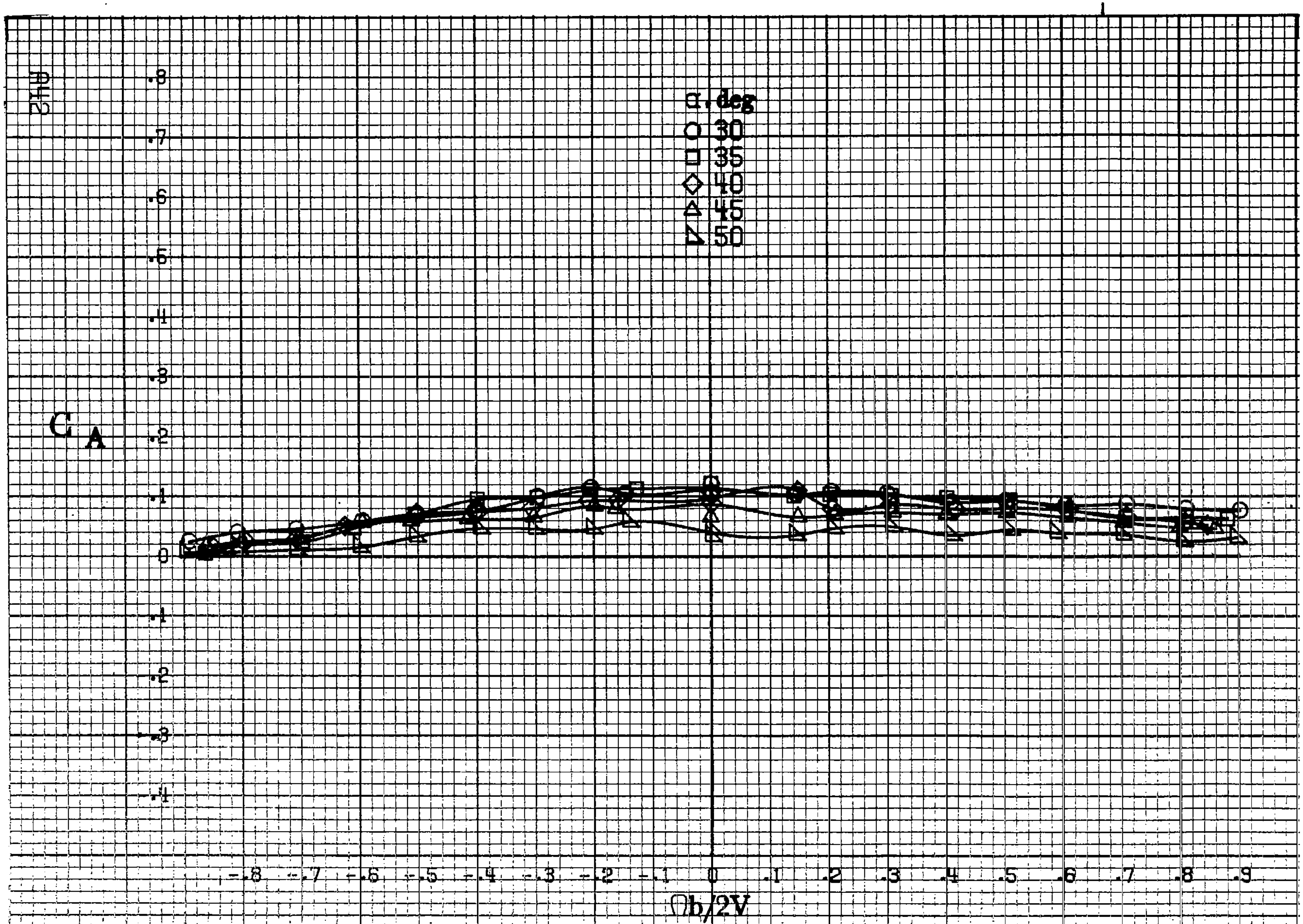

(f) α = 30 to 50 deg, SR = 0.

Figure A6.-Continued.

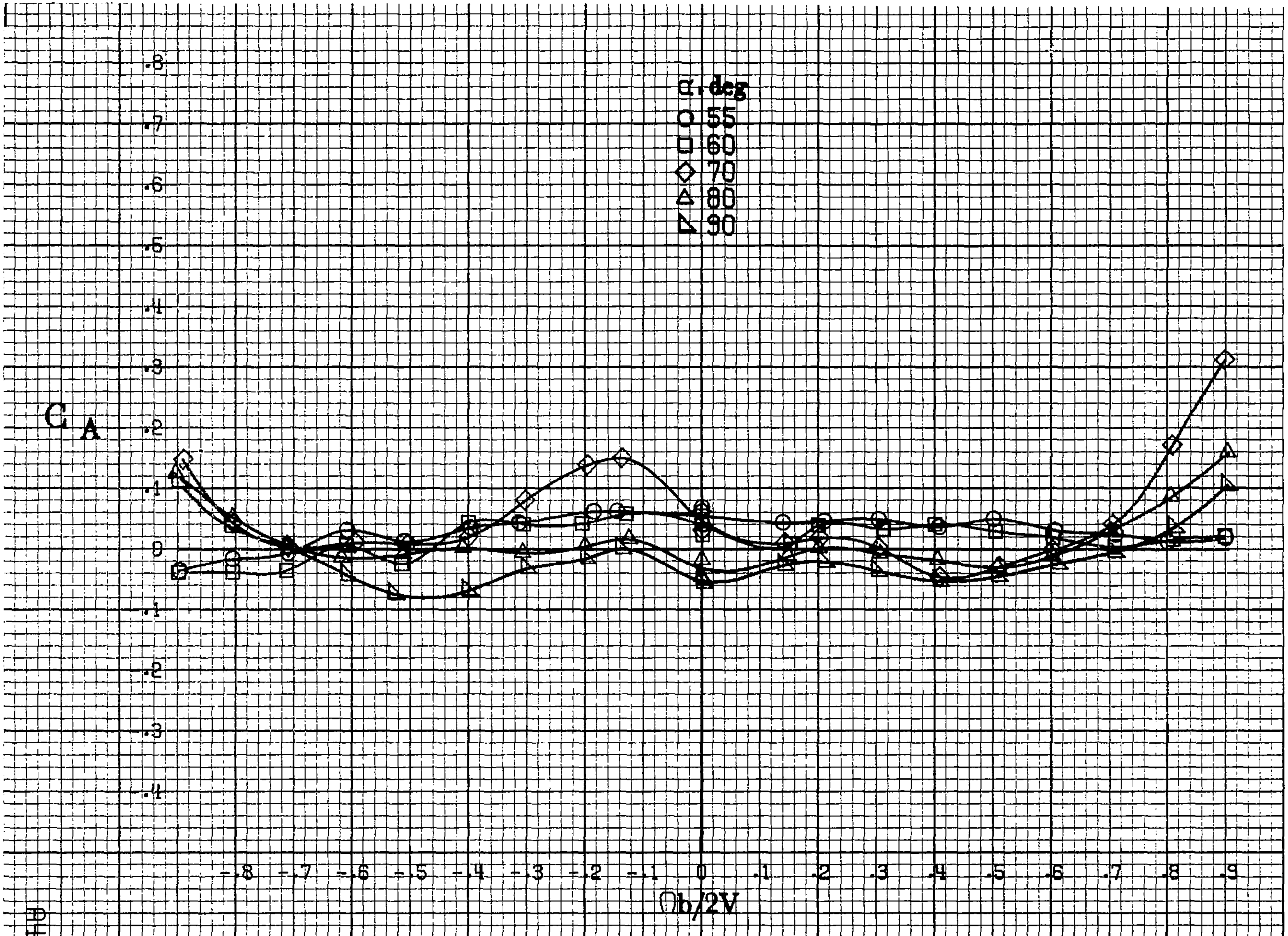

(g) α = 55 to 90 deg, SR = 0.

Figure A6.-Concluded.

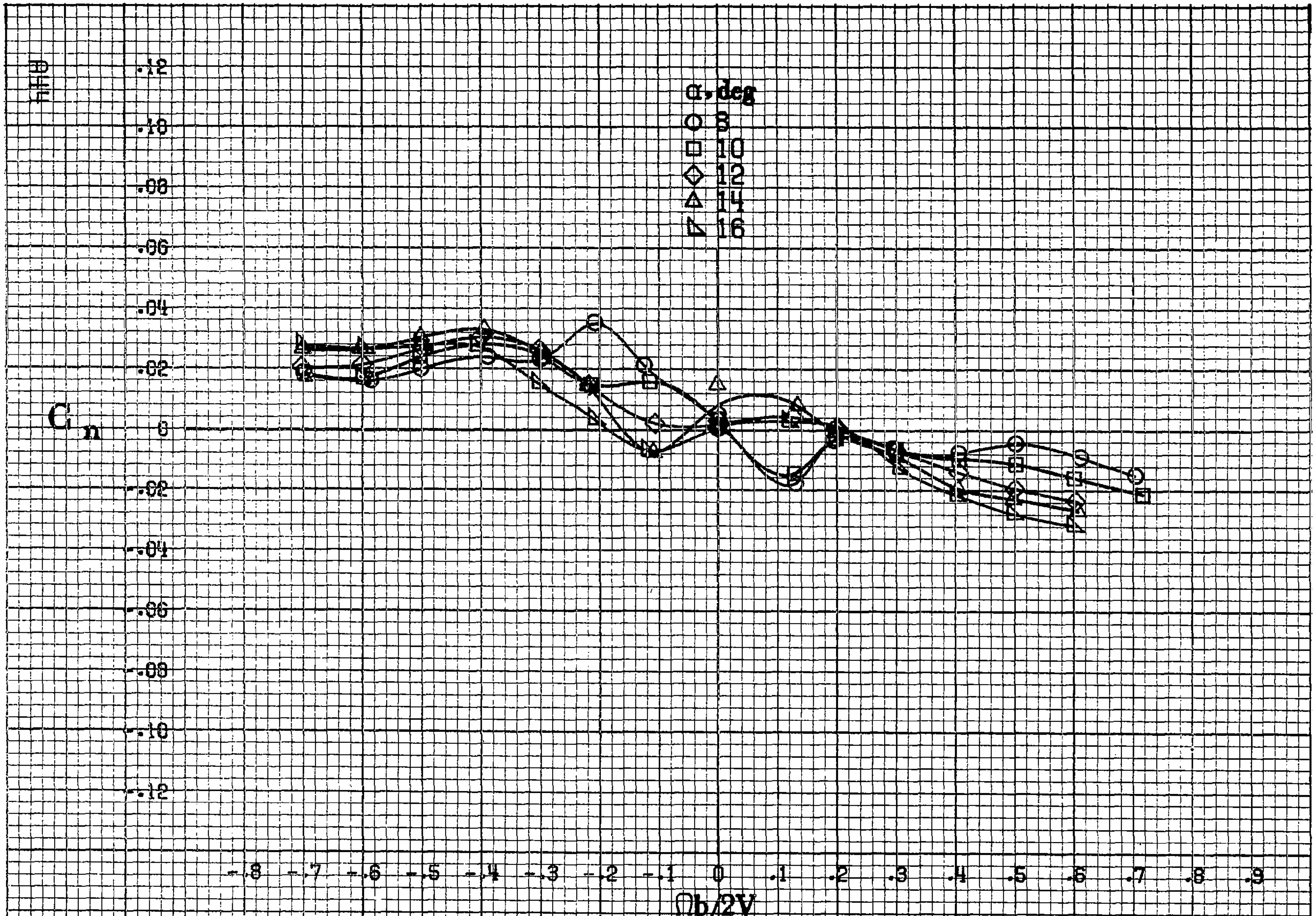

(a) α = 8 to 16 deg, SR = 182.9 cm (72 in).

Figure A7.- Effect of rotation rate and angle of attack on yawing-moment coefficient for basic configuration. $\delta_e = 0^\circ$, $\delta_a = 0^\circ$, $\delta_r = 0^\circ$, $\beta = 10^\circ$.

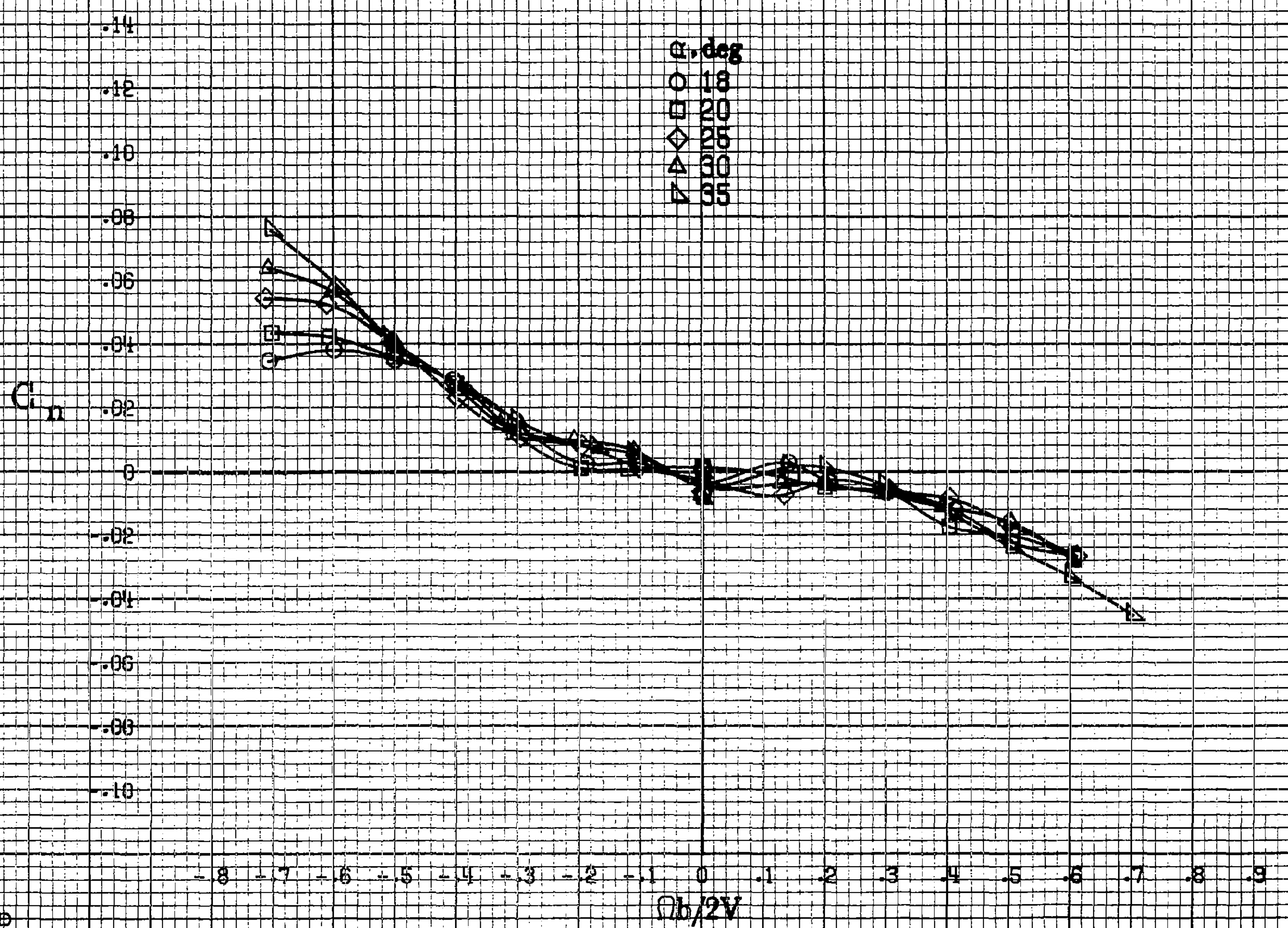

(b) α = 18 to 35 deg, SR = 182.9 cm (72 in).

Figure A7. Continued.

(c) α = 30to50deg, SR = 0.
Figure A7. Continued.

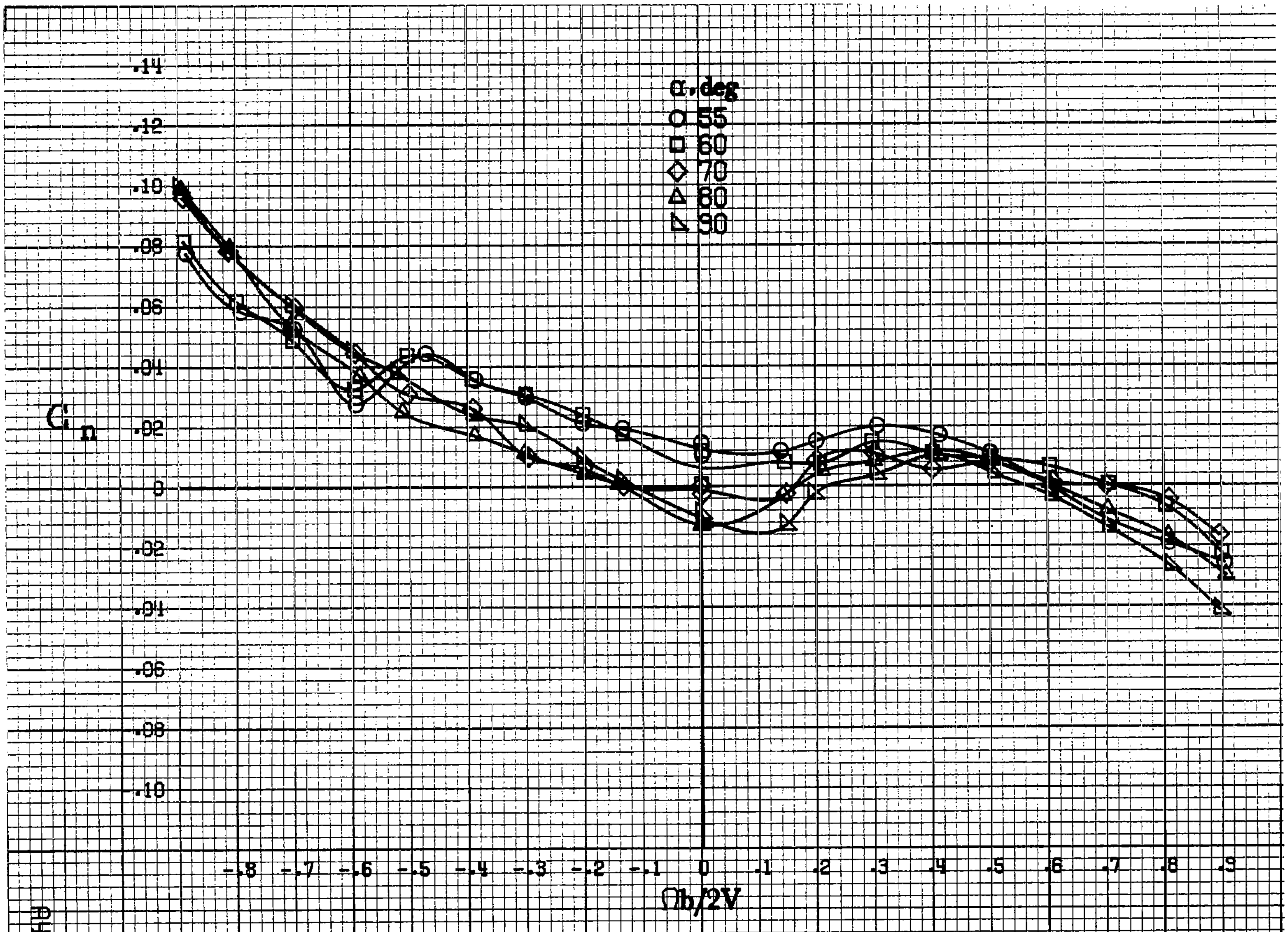

(d) α = 55 to 90 deg, SR = 0.
Figure A7.-Concluded.

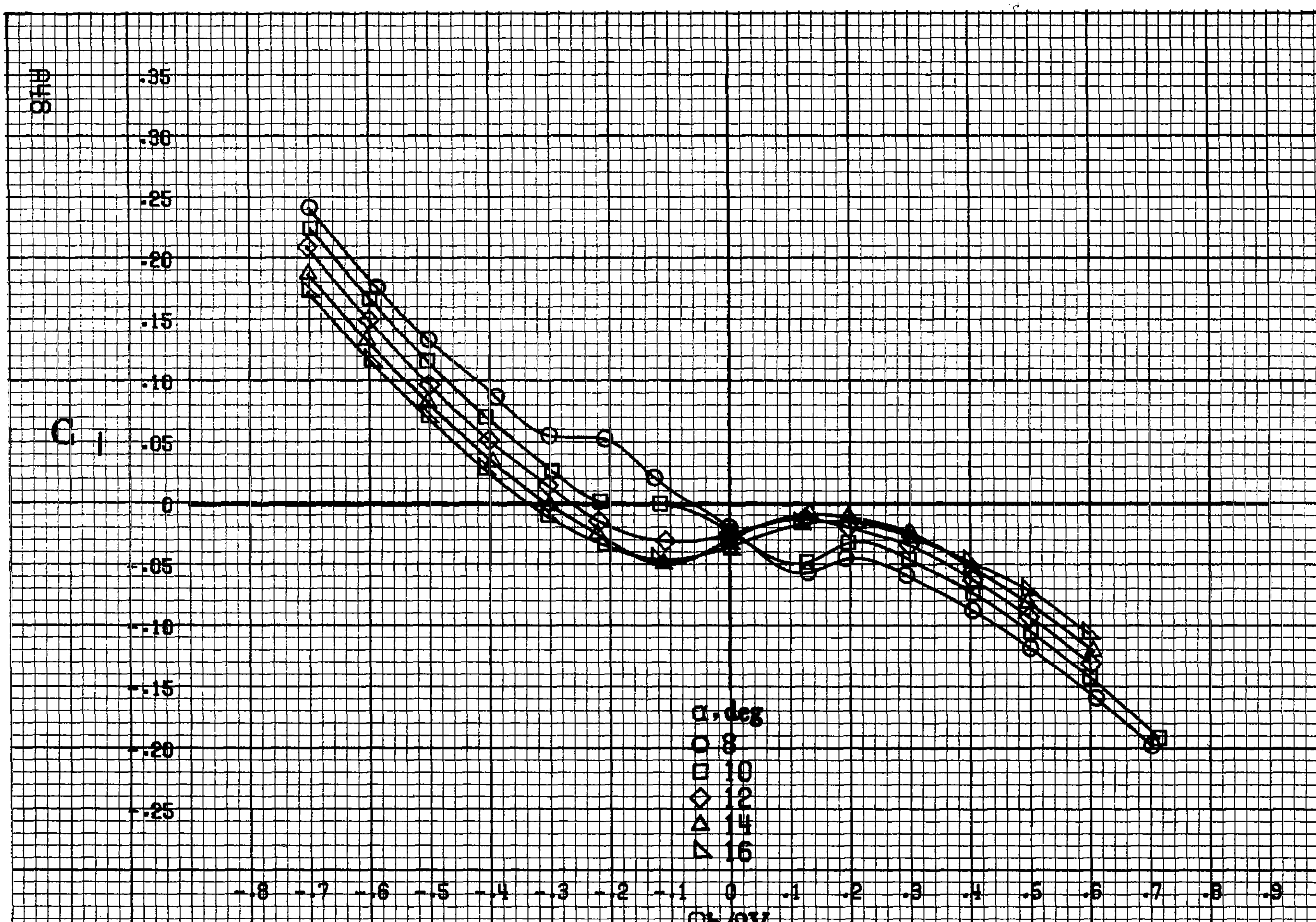

(a) α= 8 to 16 deg, SR = 182.9 cm (72 in).

Figure A8.-Effect of rotation rate and angle of attack on rolling-moment coefficient for basic configuration. $\delta_e = 0°$, $\delta_a = 0°$, $\delta_r = 0°$, $\beta = 10°$.

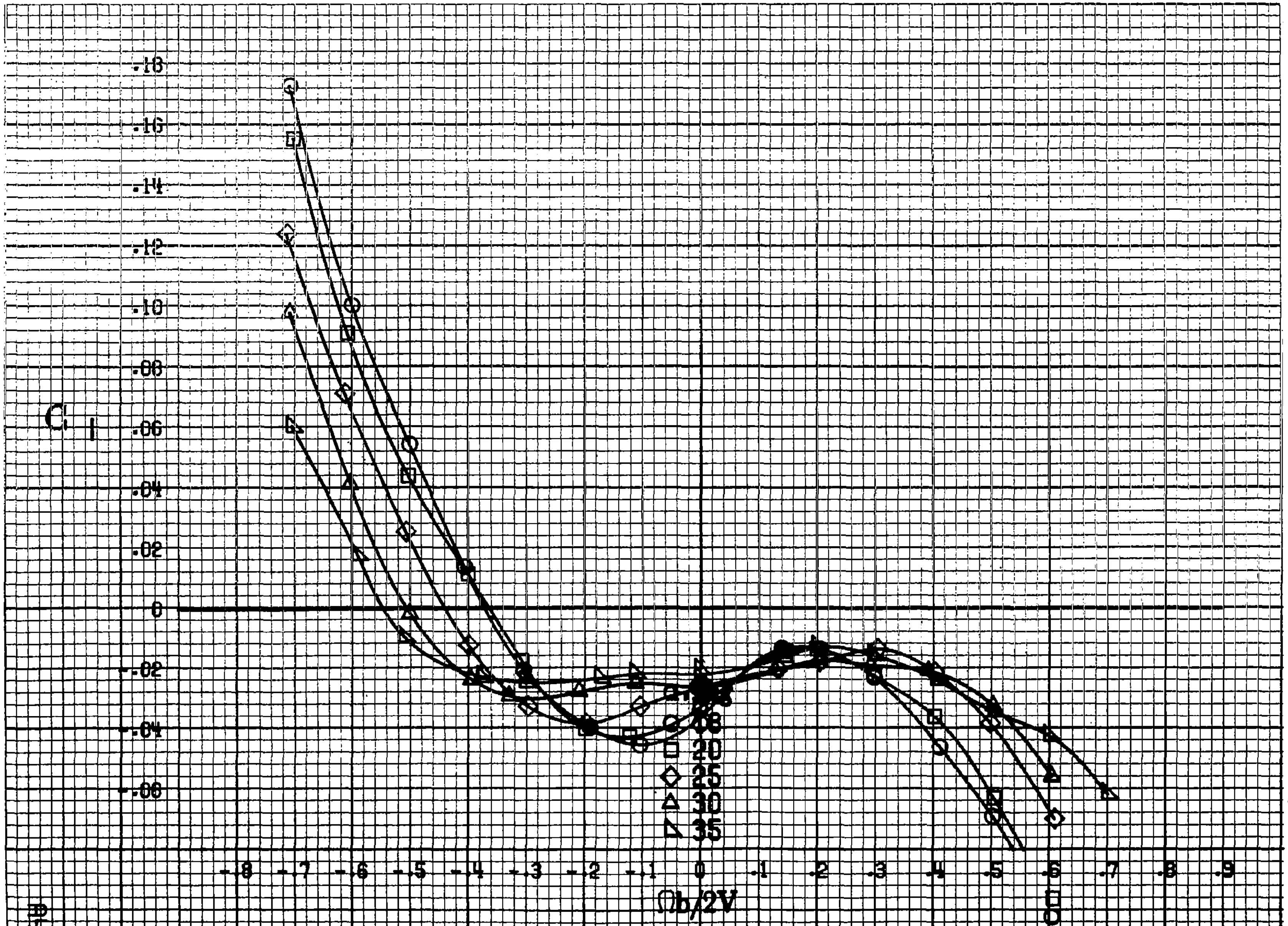

(b) α = 18to35deg, SR = 182.9cm(72in).

Figure A8. Continued.

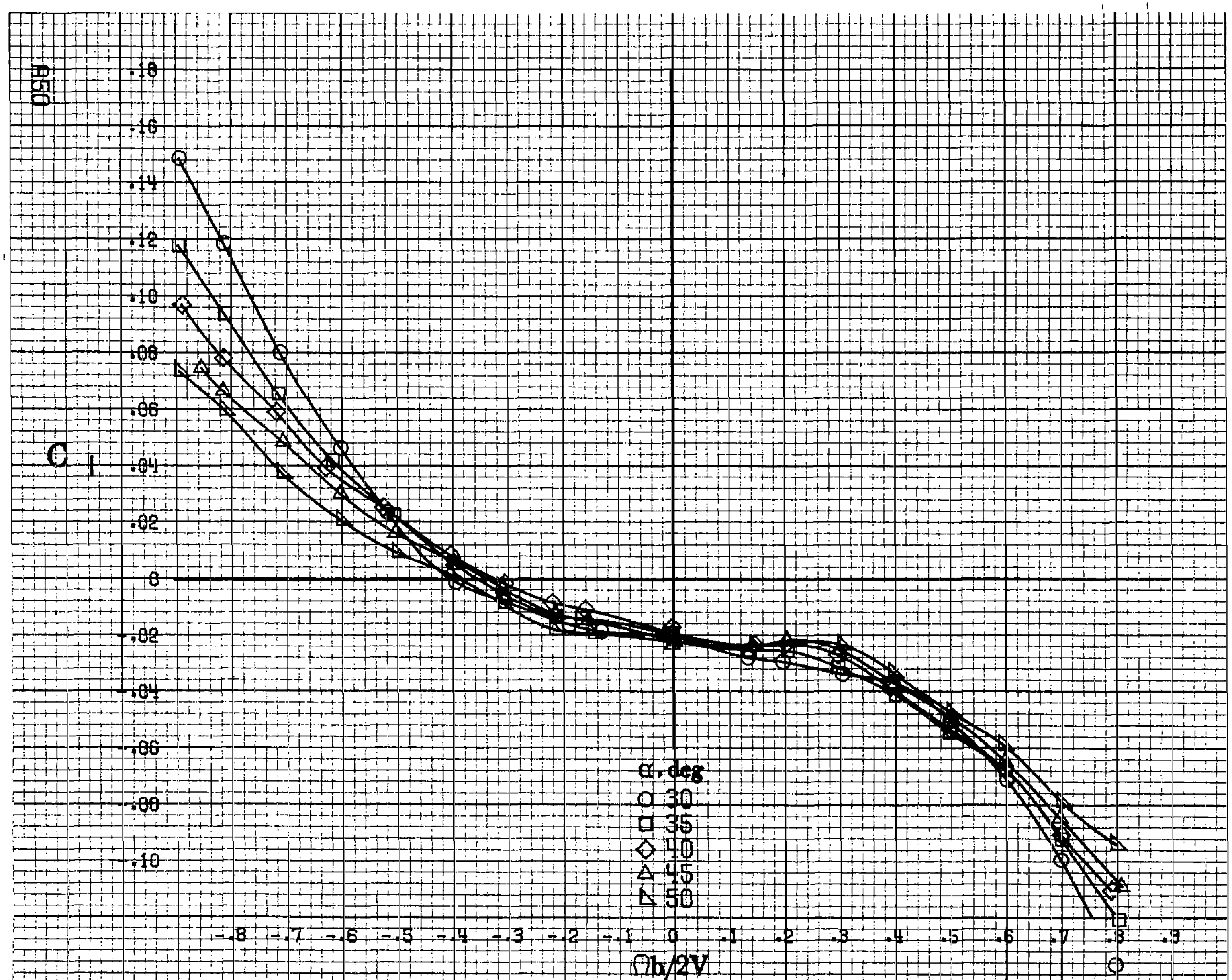

(c) α = 30 to 50 deg, SR = 0.

Figure A8.-Continued.

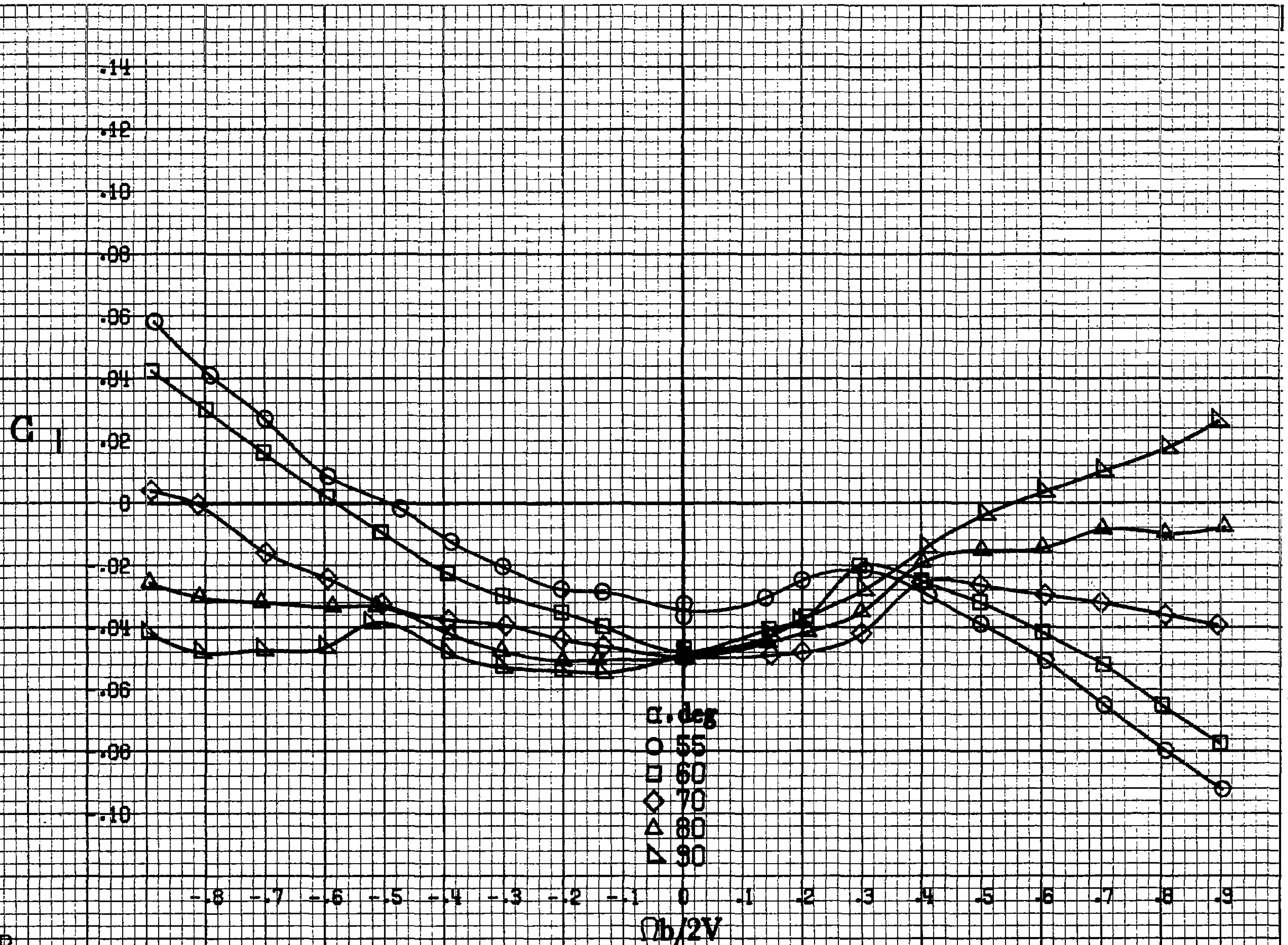

(d) α = 55 to 90 deg, SR = 0.

Figure A8.-Concluded.

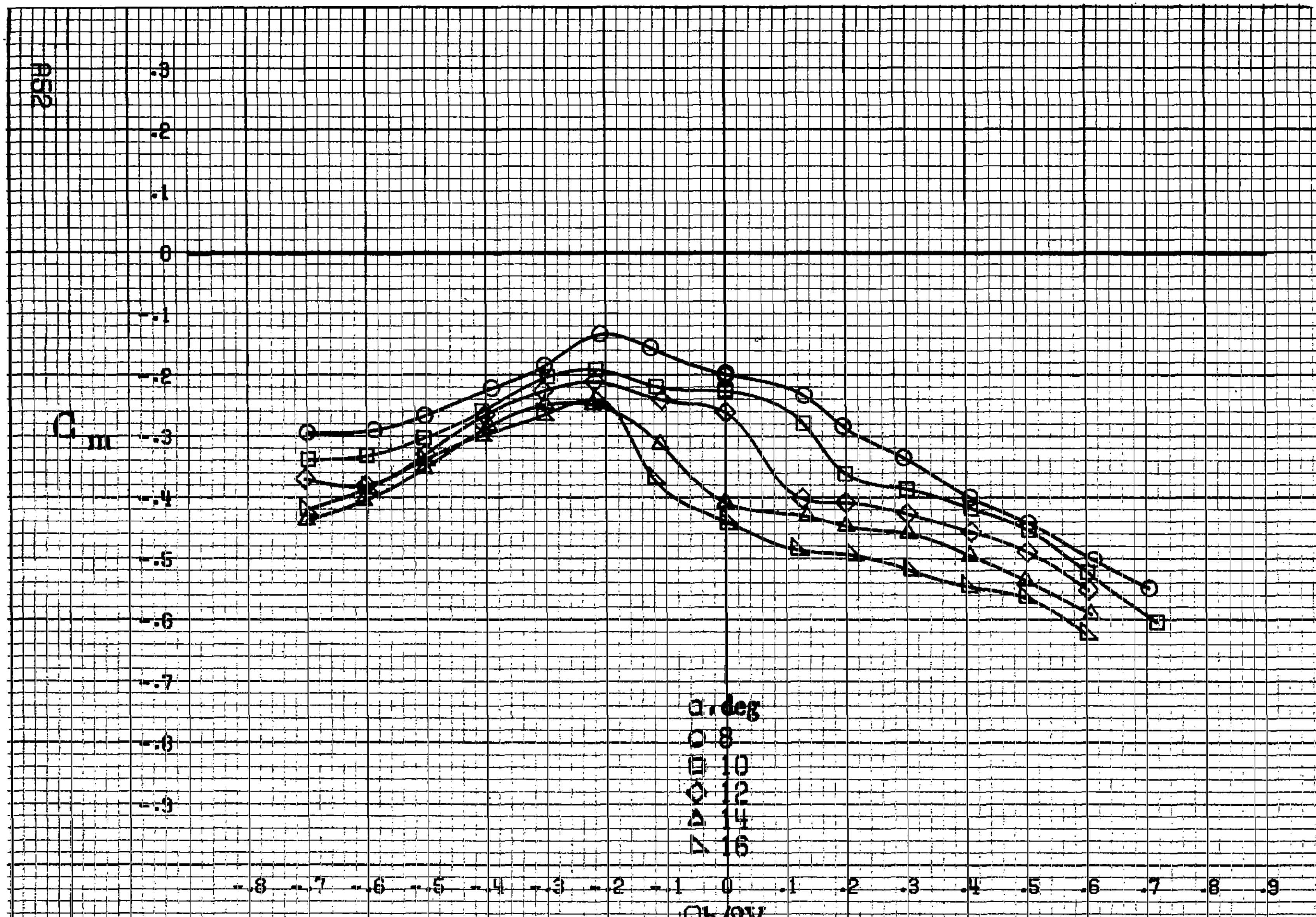

(a) α = 8 to 16 deg, SR = 132.9 cm (72 in).

Figure A9.-Effect of rotation rate and angle of attack on pitching-moment coefficient for basic configuration. $\delta_e = 0°$, $\delta_a = 0°$, $\delta_r = 0°$, $\beta = 10°$.

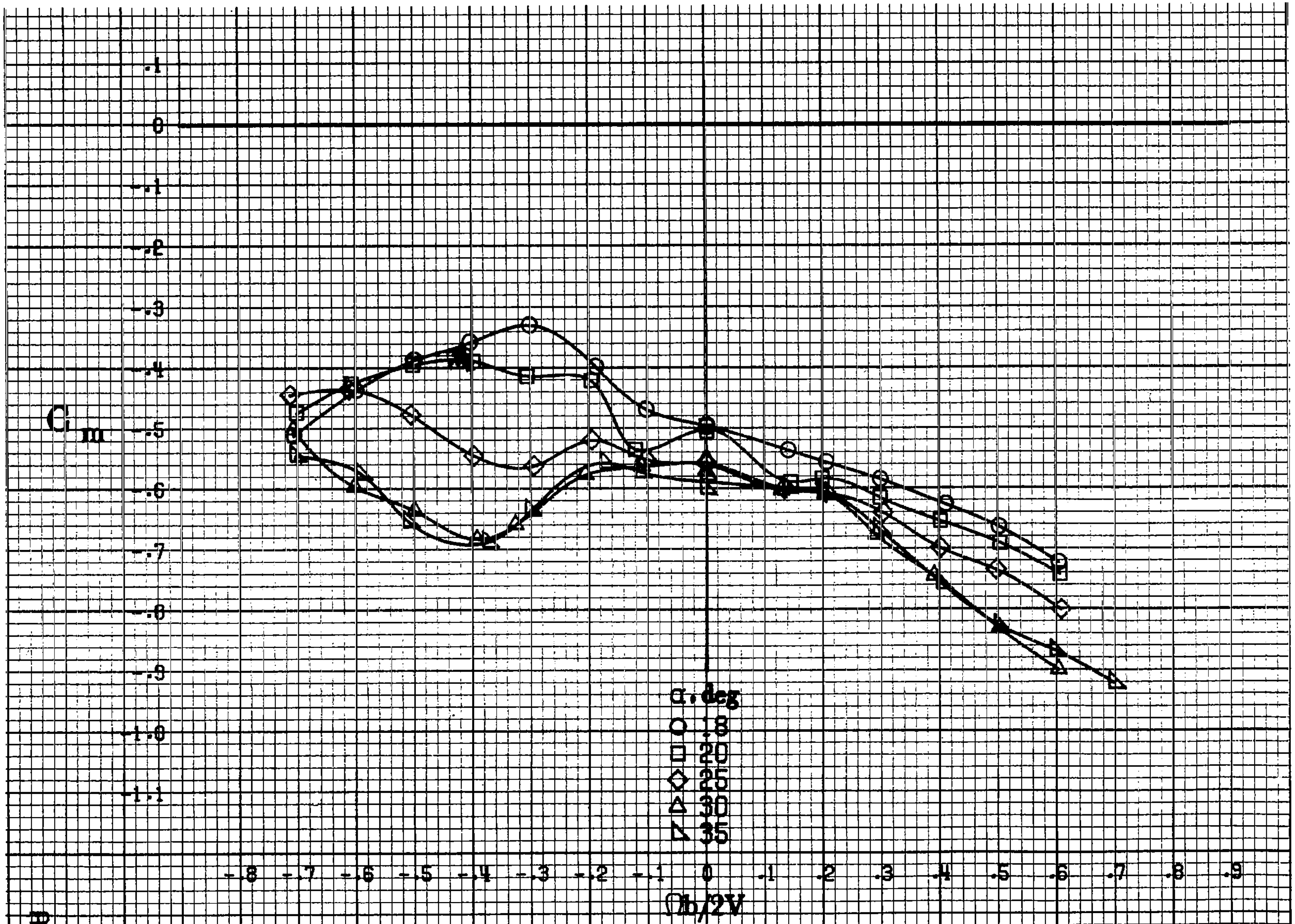

(b) α = 18 to 35 deg, SR = 182.9 cm (72 in).

Figure A9. Continued.

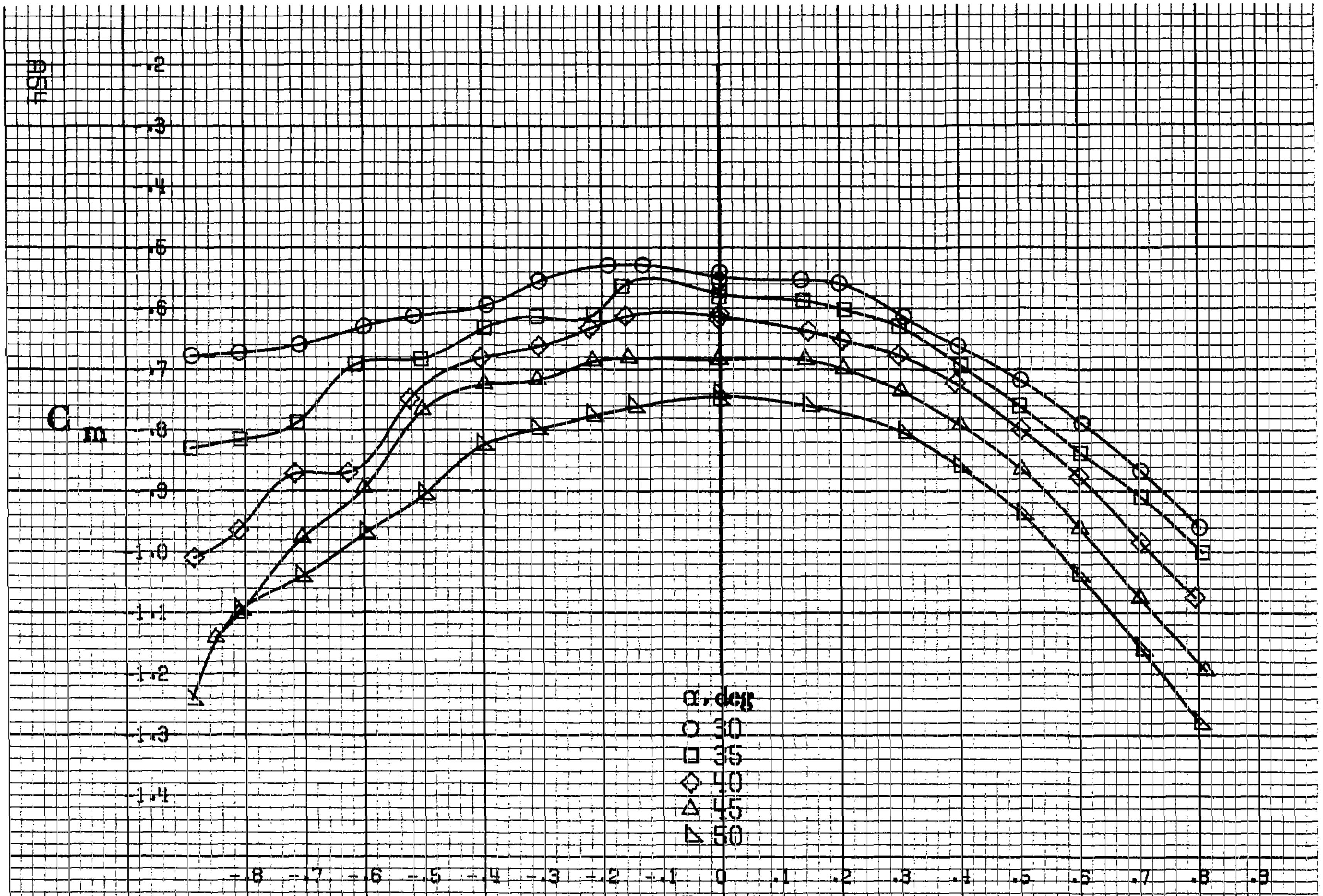

(c) α = 30to50deg, SR = 0.
Figure A9. Continued.

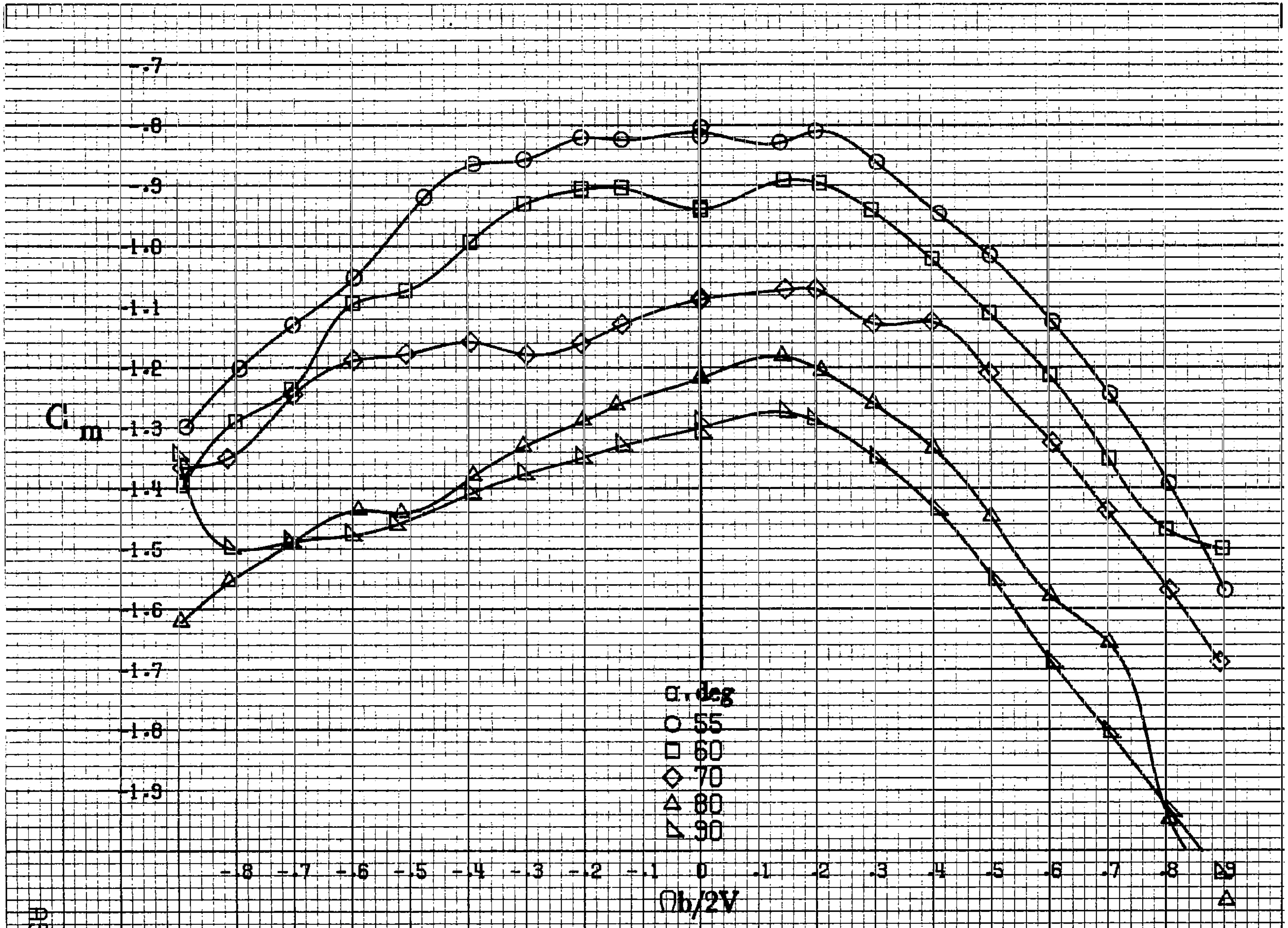

(d) α = 55 to 90 deg, SR = 0.

Figure A9.-Concluded.

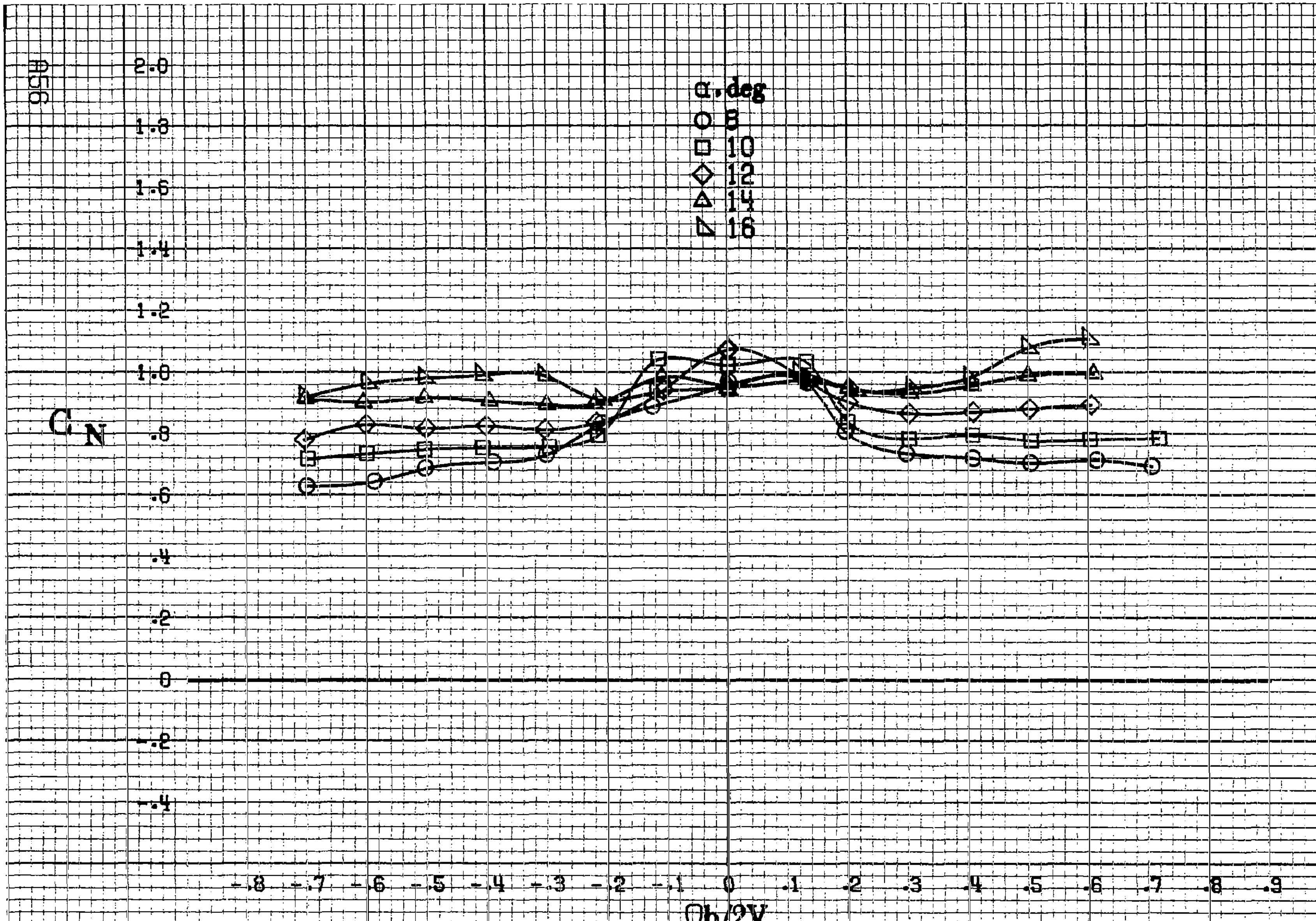

(a) α = 8 to 16 deg, SR = 182.9 cm (72 in).

Figure A10.-Effect of rotation rate and angle of attack on normal-force coefficient for basic configuration. $\delta_e = 0°$, $\delta_a = 0°$, $\delta_r = 0°$, $\beta = 10°$.

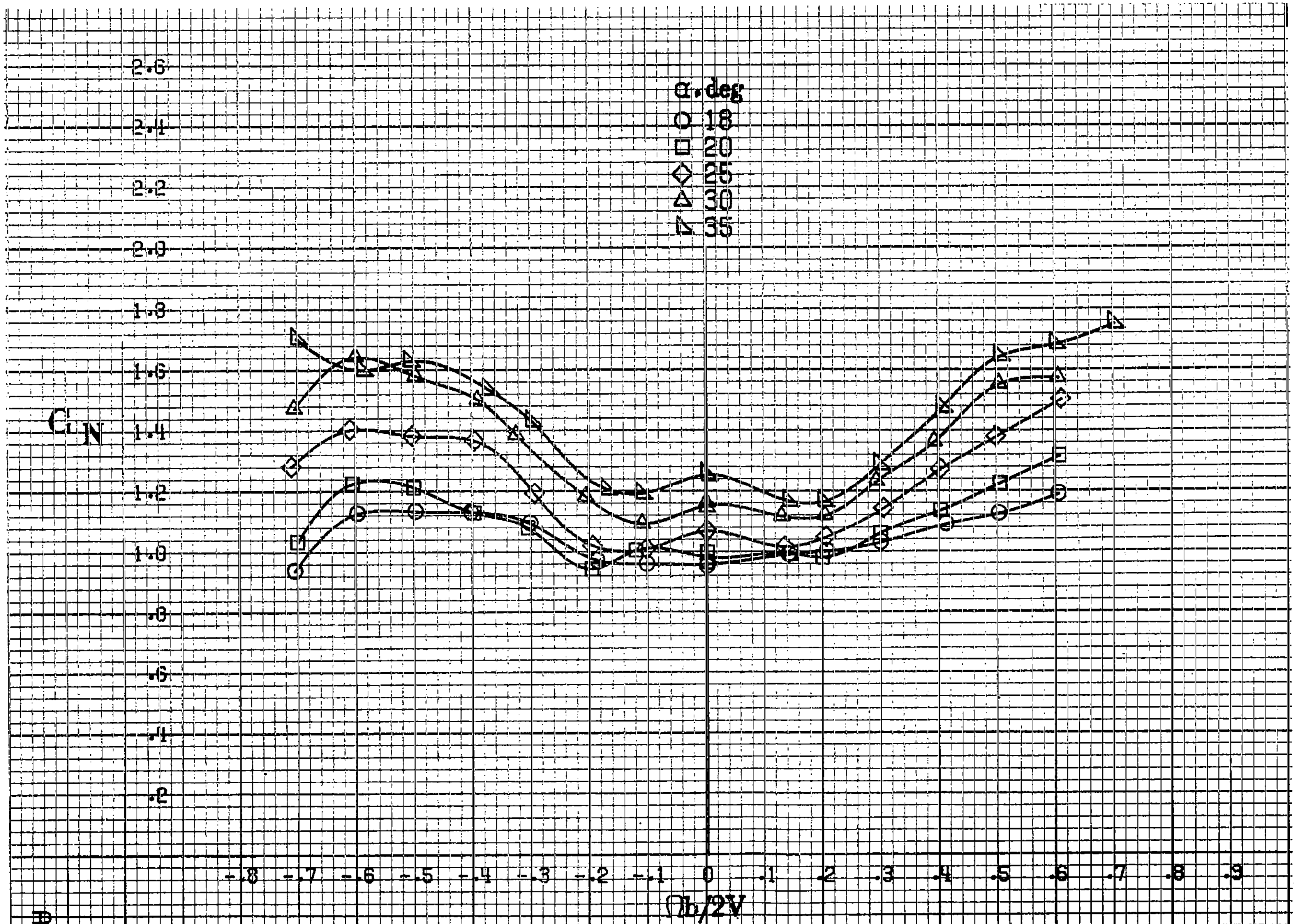

(b) α = 18 to 35 deg, SR = 182.9 cm (72 in).

Figure A10.-Continued.

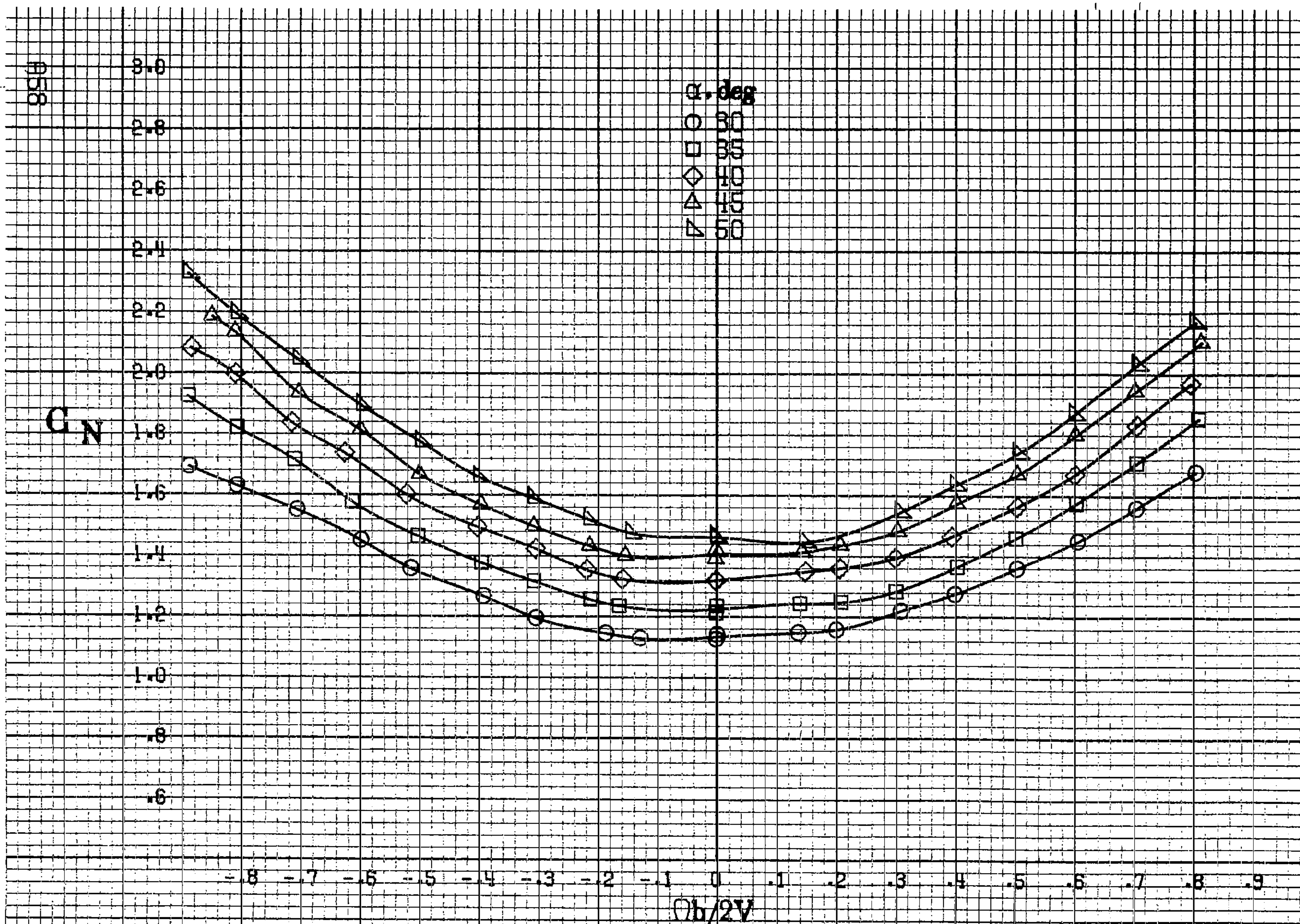

(c) α = 30 to 50 deg, SR = 0.

Figure A10.-Continued.

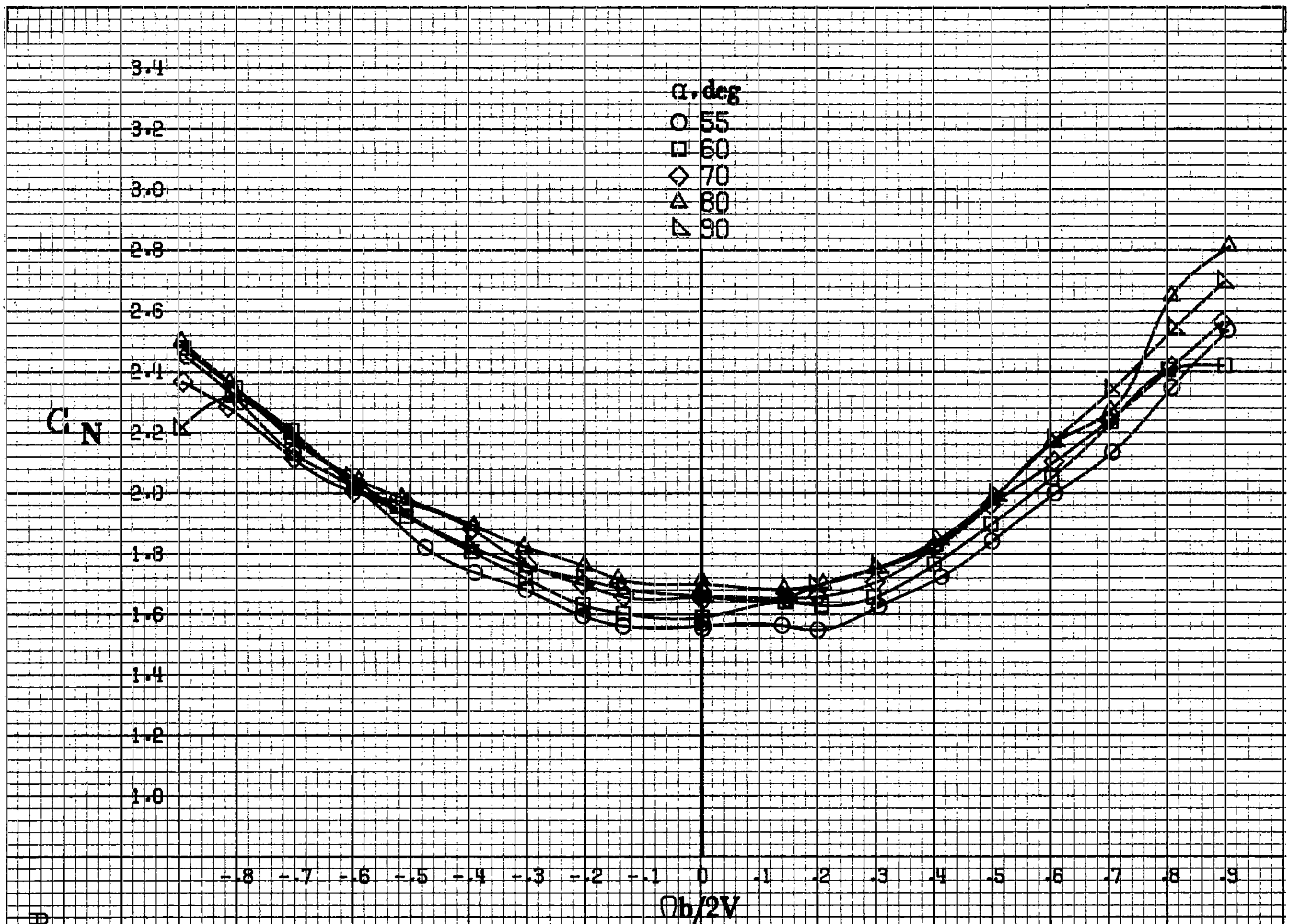

(d) α = 55to90deg, SR = 0.
Figure A10.-Concluded.

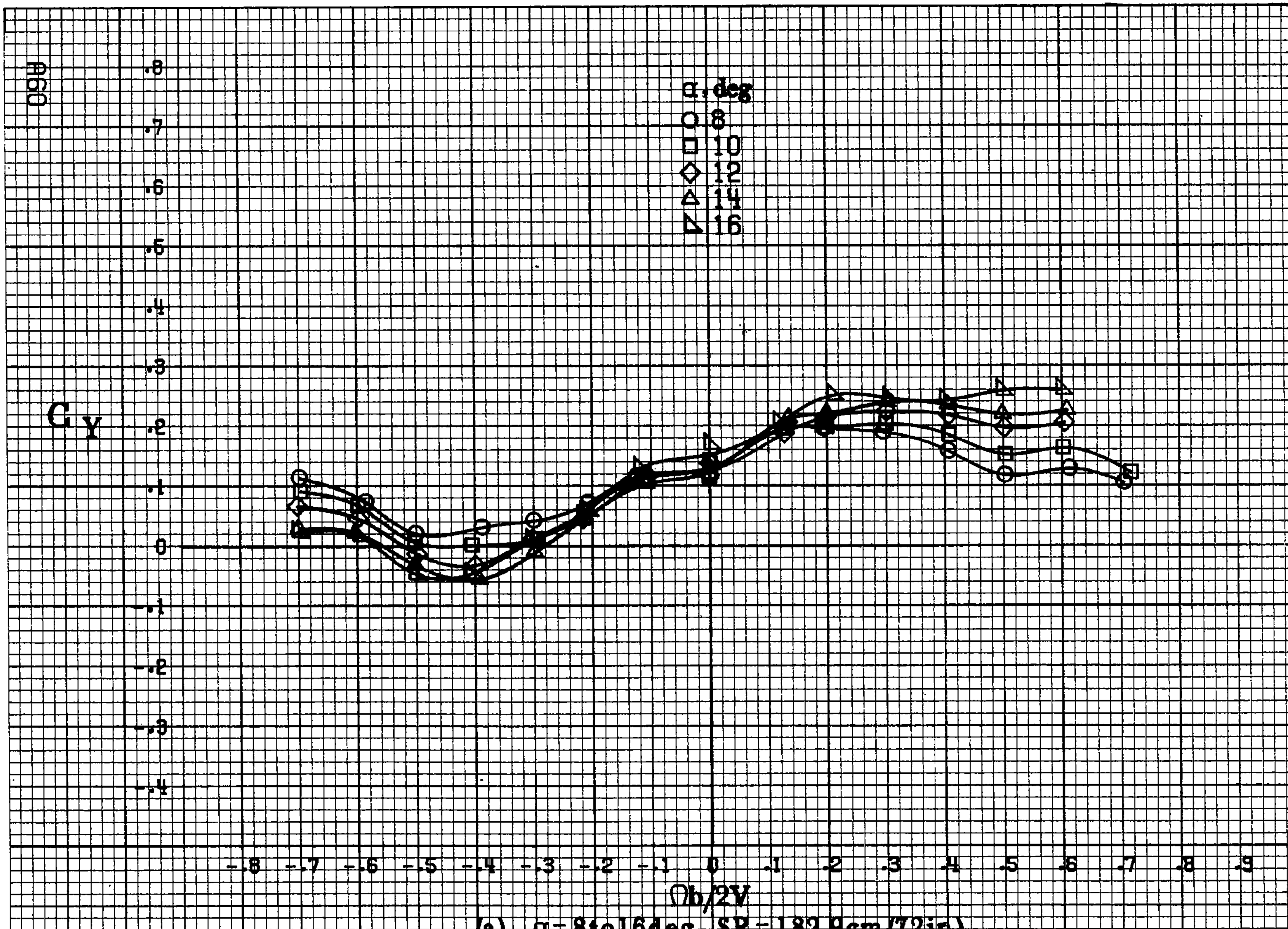

(a) $\alpha = 8$ to 16 deg, SR = 182.9 cm (72 in).

Figure A11.-Effect of rotation rate and angle of attack on side-force coefficient for basic configuration. $\delta_e = 0°$, $\delta_a = 0°$, $\delta_r = 0°$, $\beta = 10°$.

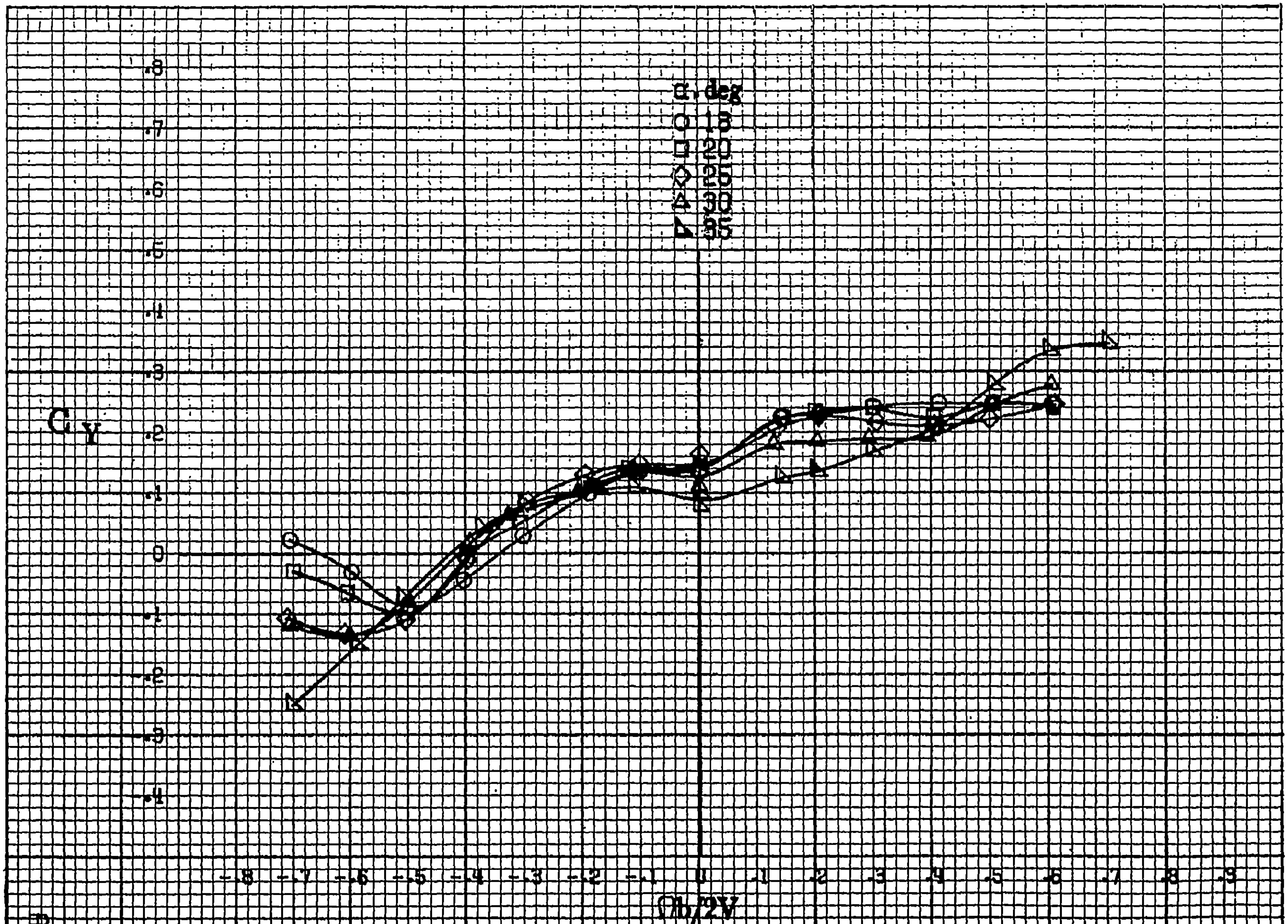

(b) α = 18 to 35 deg, SR = 182.9 cm (72 in).
Figure A11.-Continued.

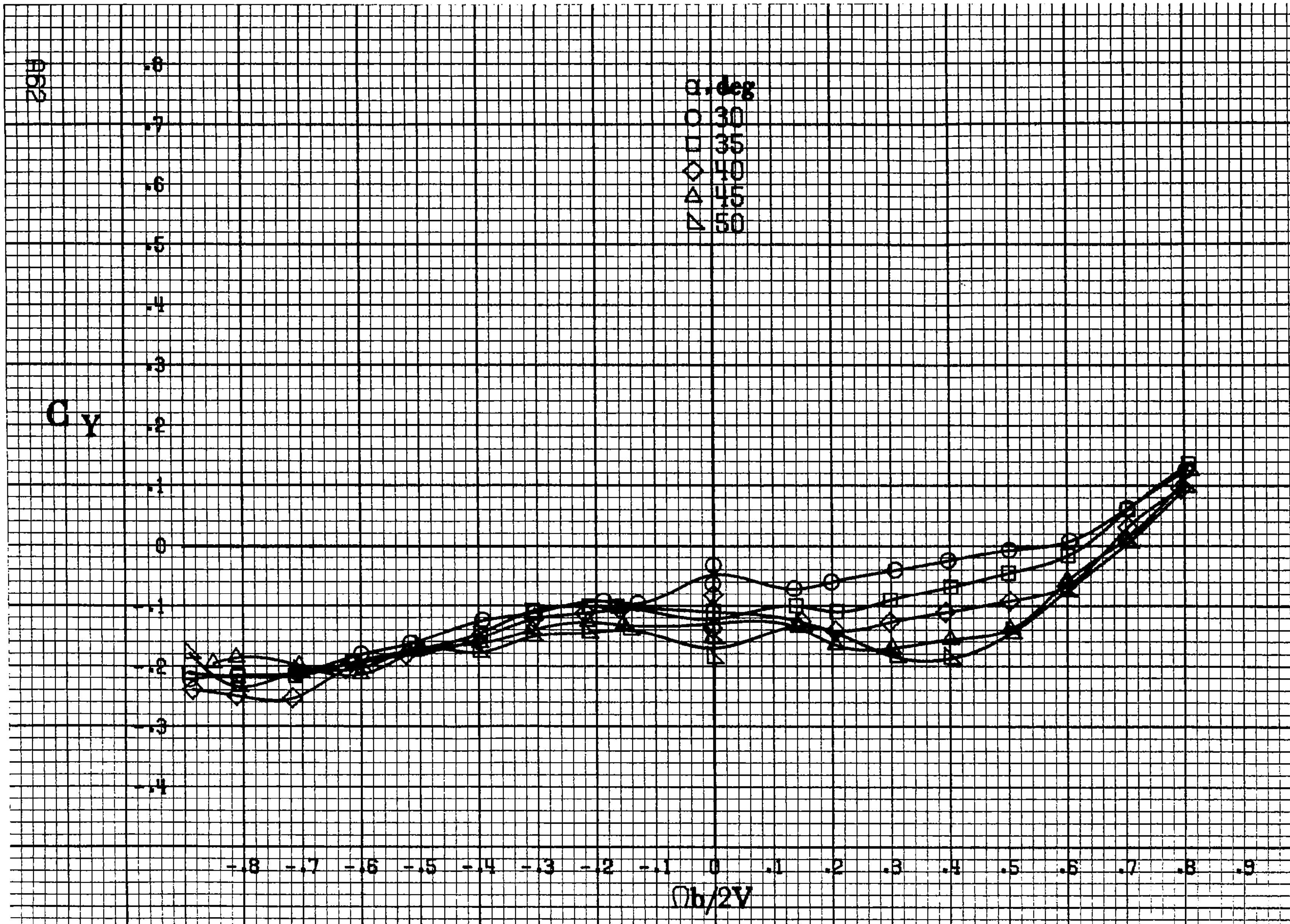

(c) α = 30 to 50 deg, SR = 0.

Figure A11.-Continued.

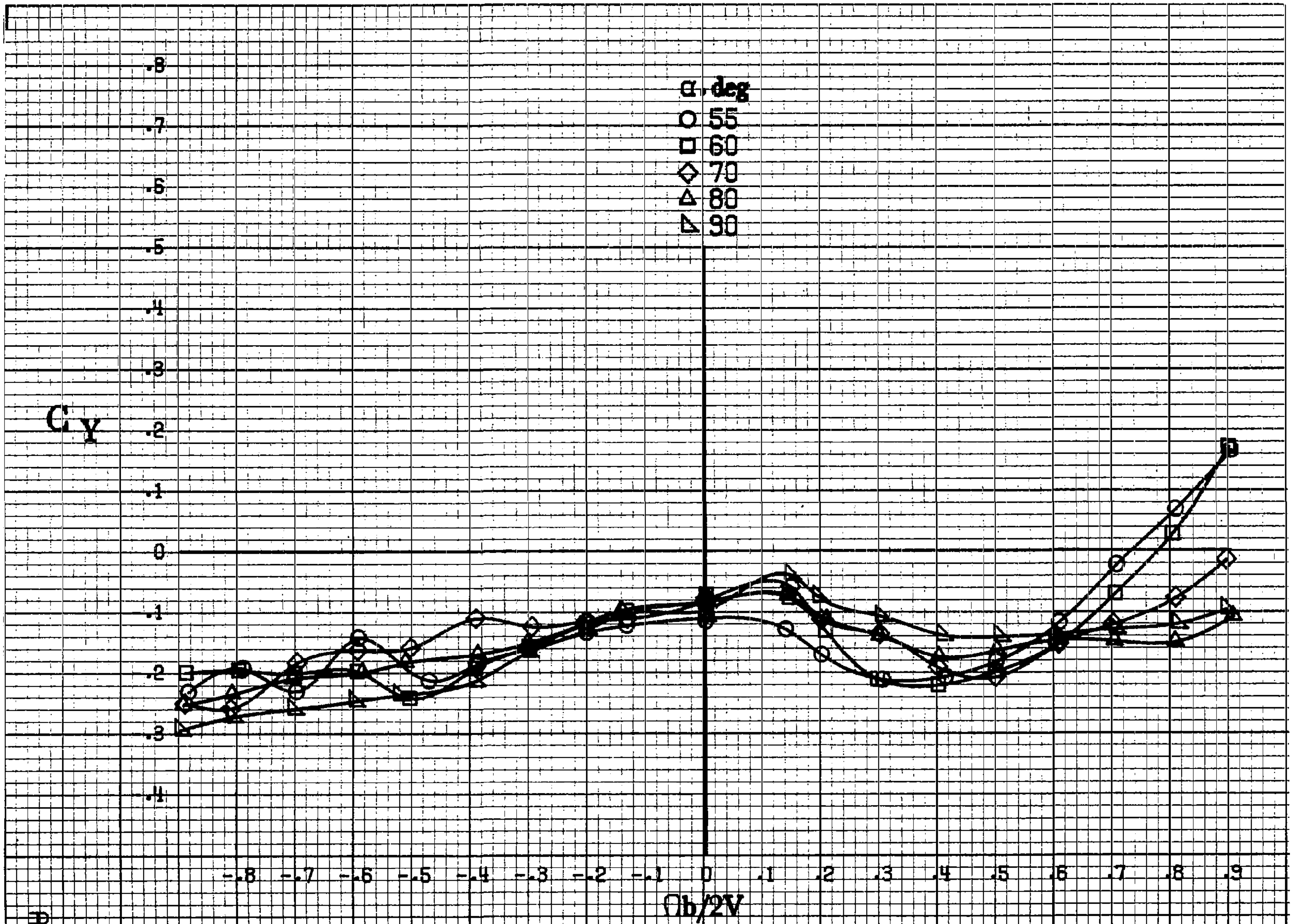

(d) α=55to90deg, SR=0.
Figure A11.-Concluded.

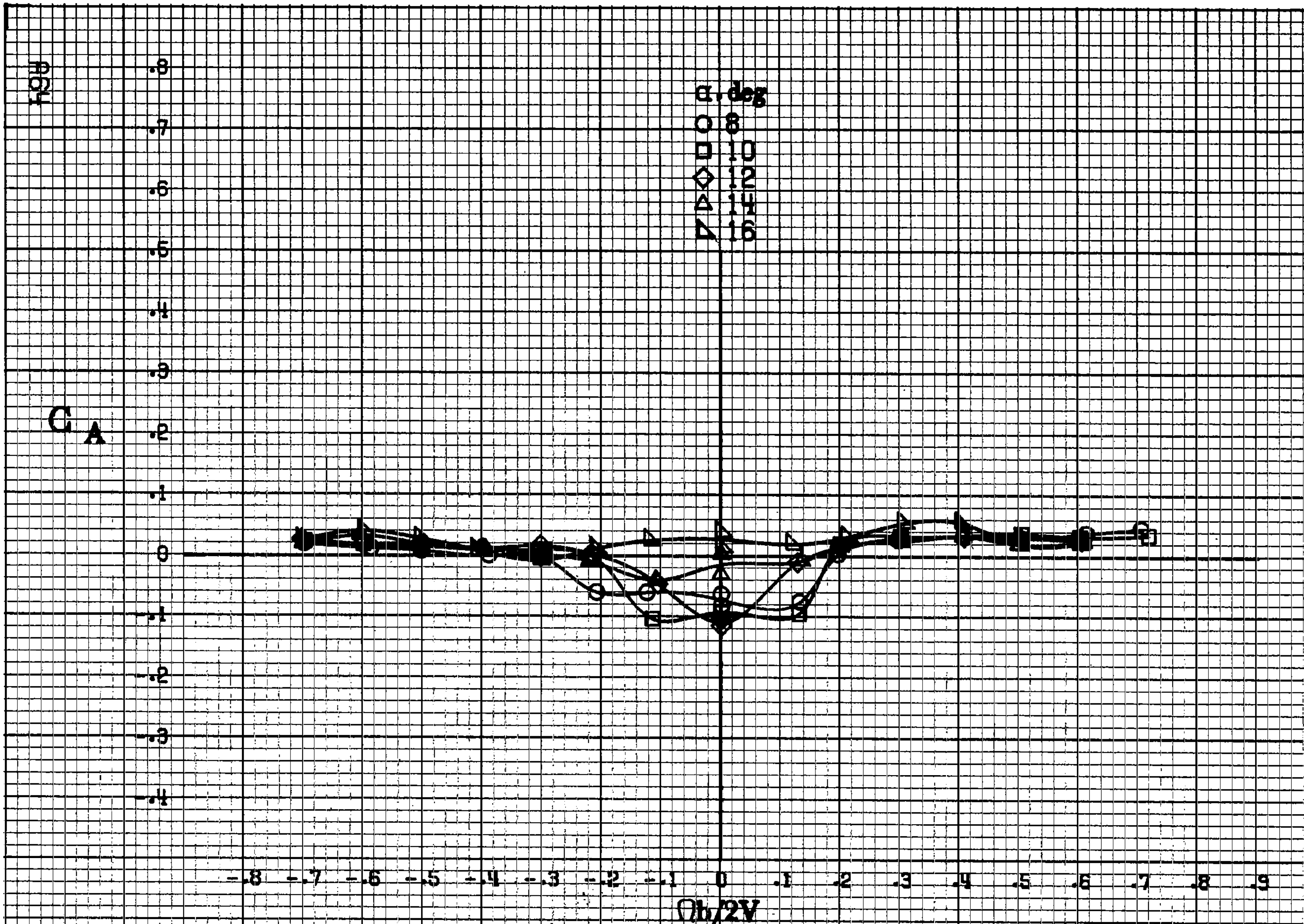

(a) α = 8 to 16 deg, SR = 182.9 cm (72 in).

Figure A12.-Effect of rotation rate and angle of attack on axial-force coefficient for basic configuration. $\delta_e = 0°$, $\delta_a = 0°$, $\delta_r = 0°$, $\beta = 10°$.

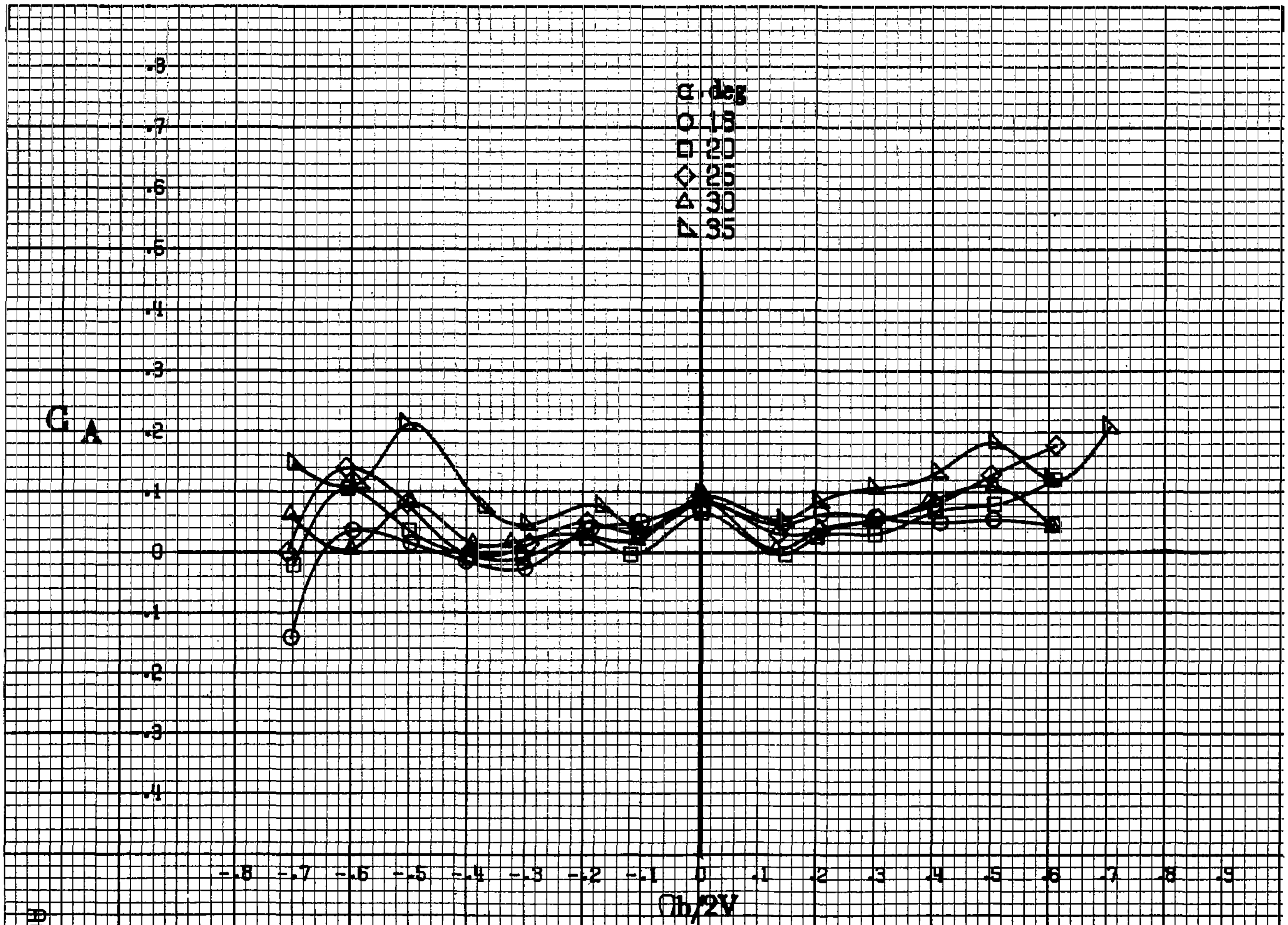

(b) α = 18 to 35 deg, SR = 182.9 cm (72 in).

Figure A12.- Continued.

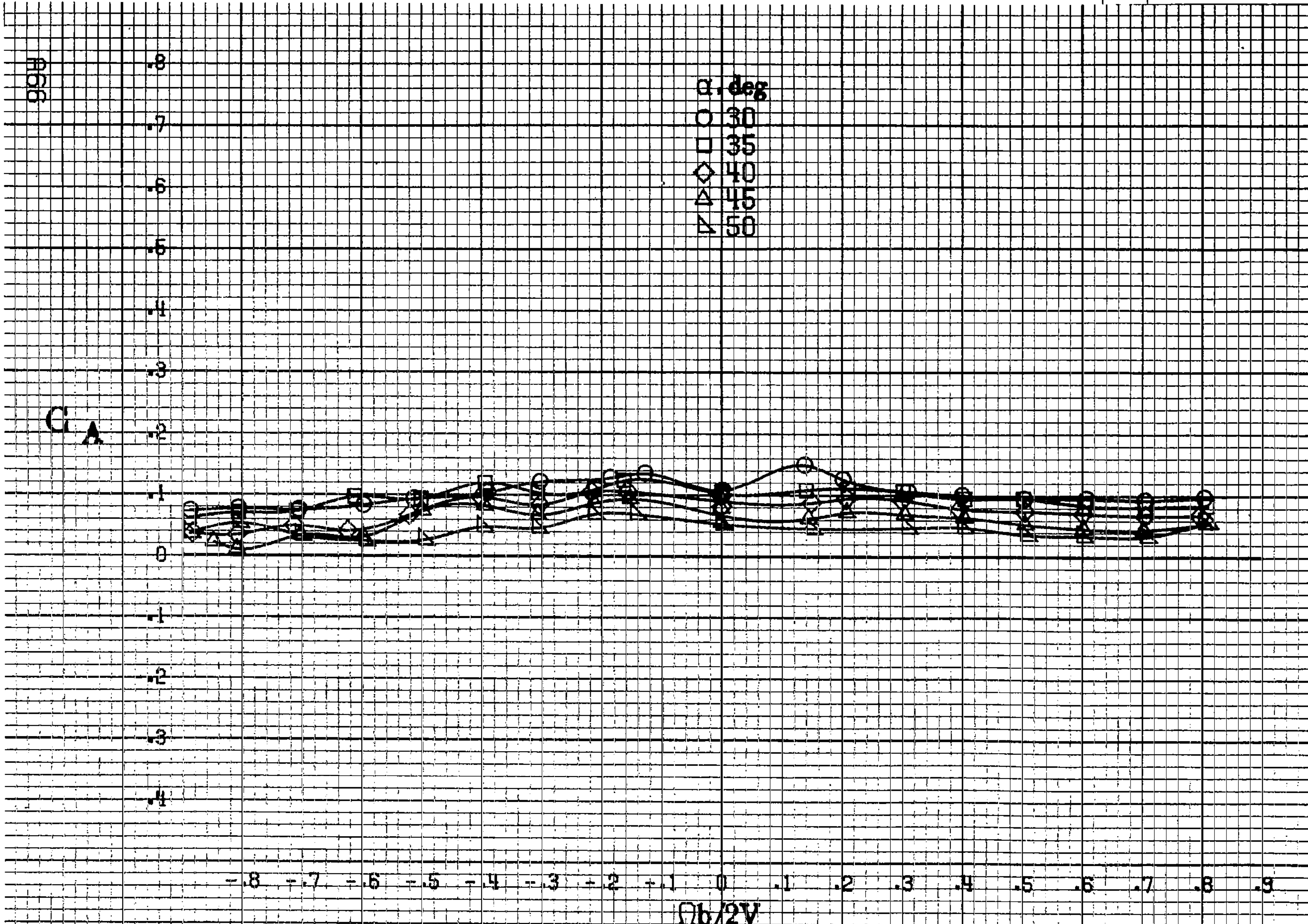

(c) α = 30 to 50 deg, SR = 0.

Figure A12.-Continued.

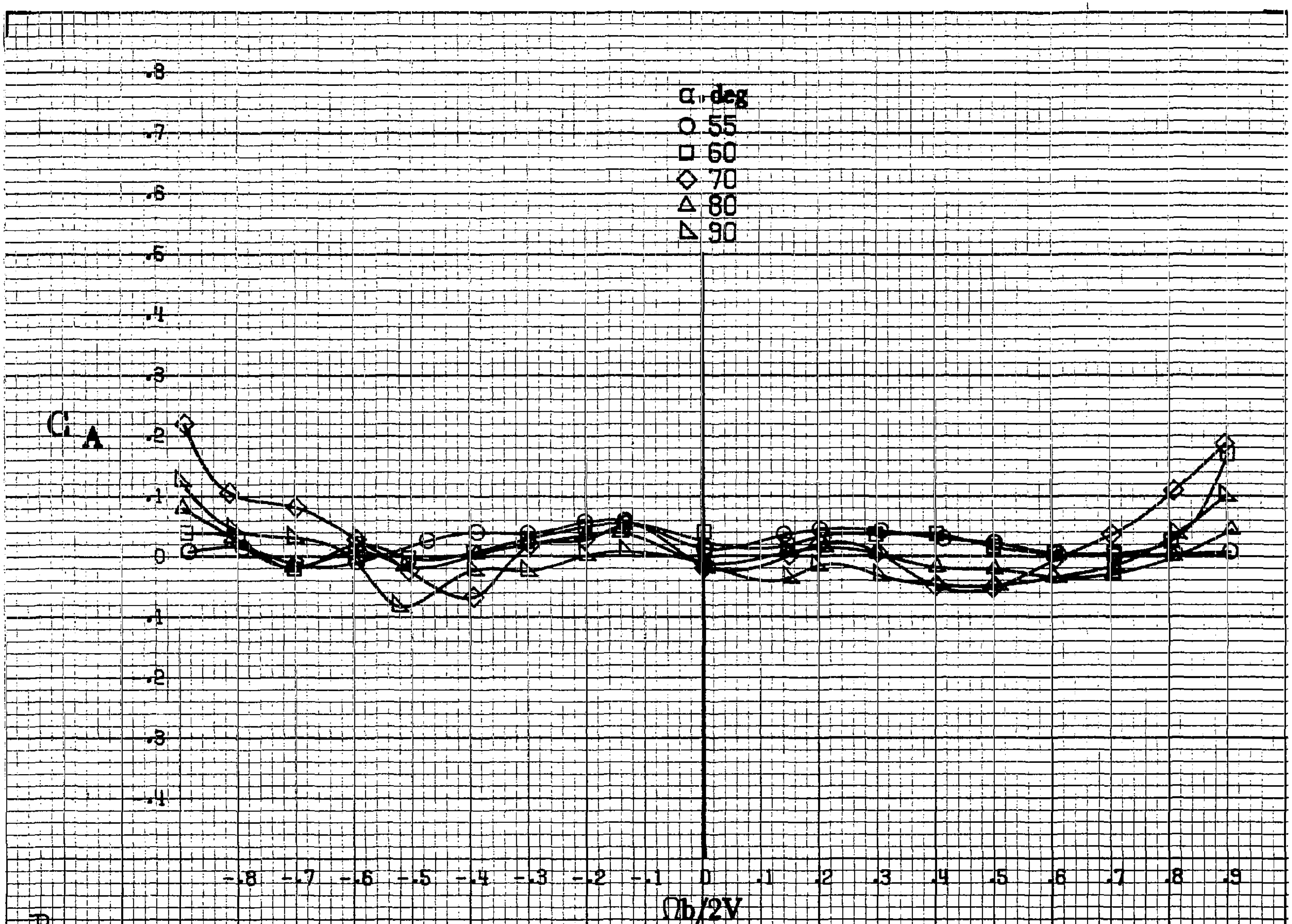

(d) α = 55 to 90 deg, SR = 0.

Figure A12.-Concluded.

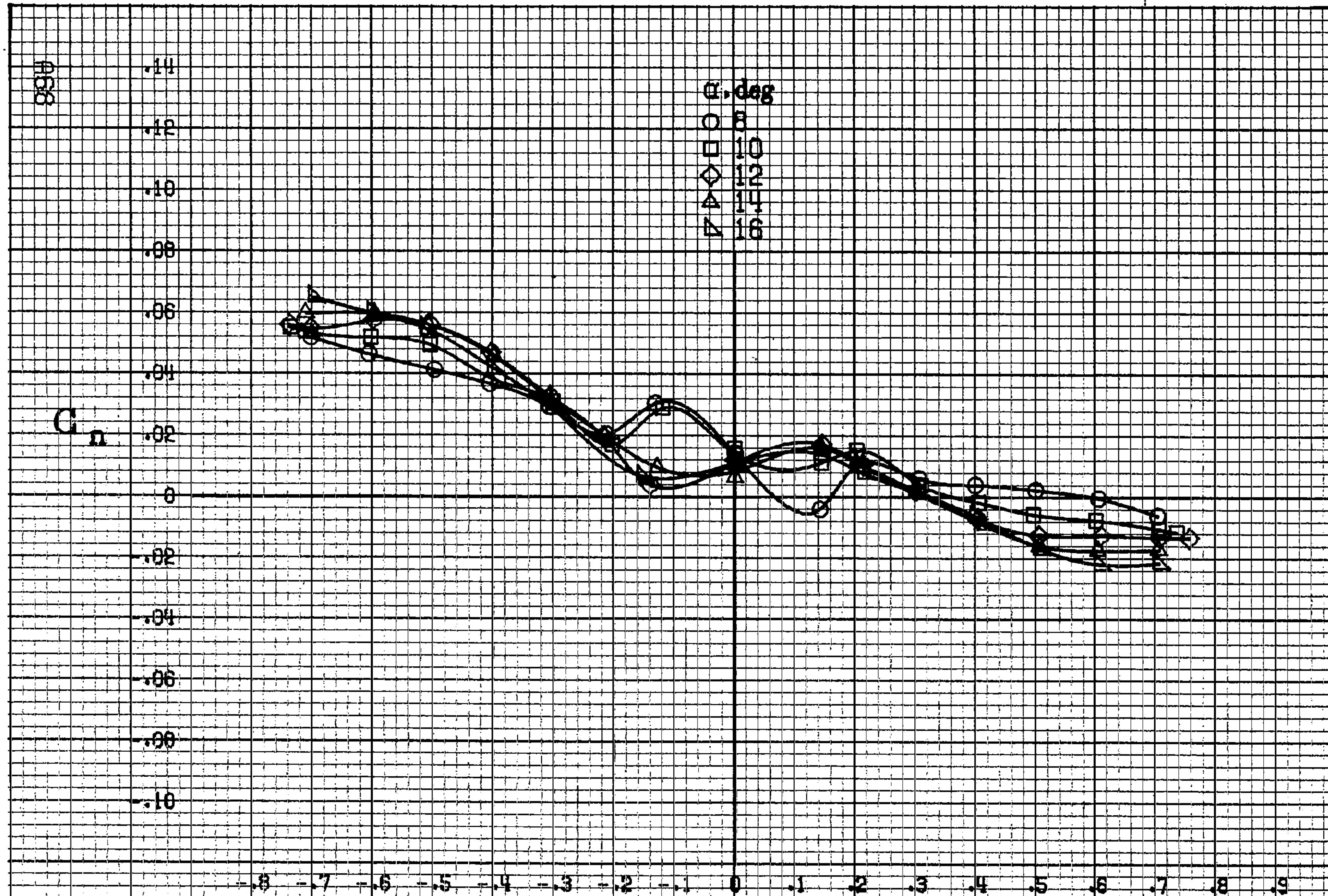

(a) $\alpha = 8$ to 16 deg, SR = 182.9 cm (72 in).

Figure A18.-Effect of rotation rate and angle of attack on yawing-moment coefficient for basic configuration. $\delta_e = -15°$, $\delta_a = 0°$, $\delta_r = -25°$, $\beta = 0°$.

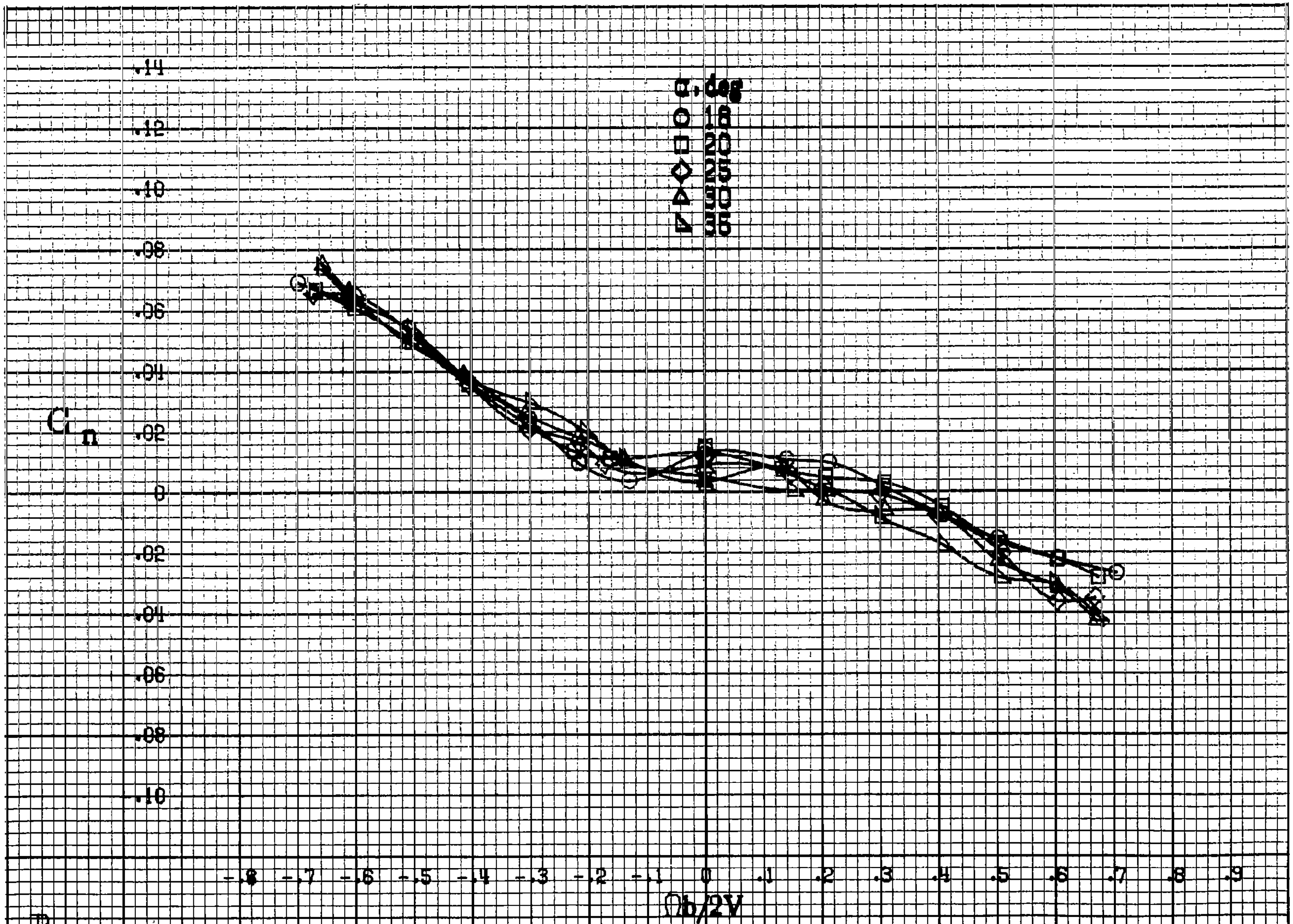

(b) α = 18 to 35 deg, SR = 182.9 cm (72 in).

Figure A18.- Continued.

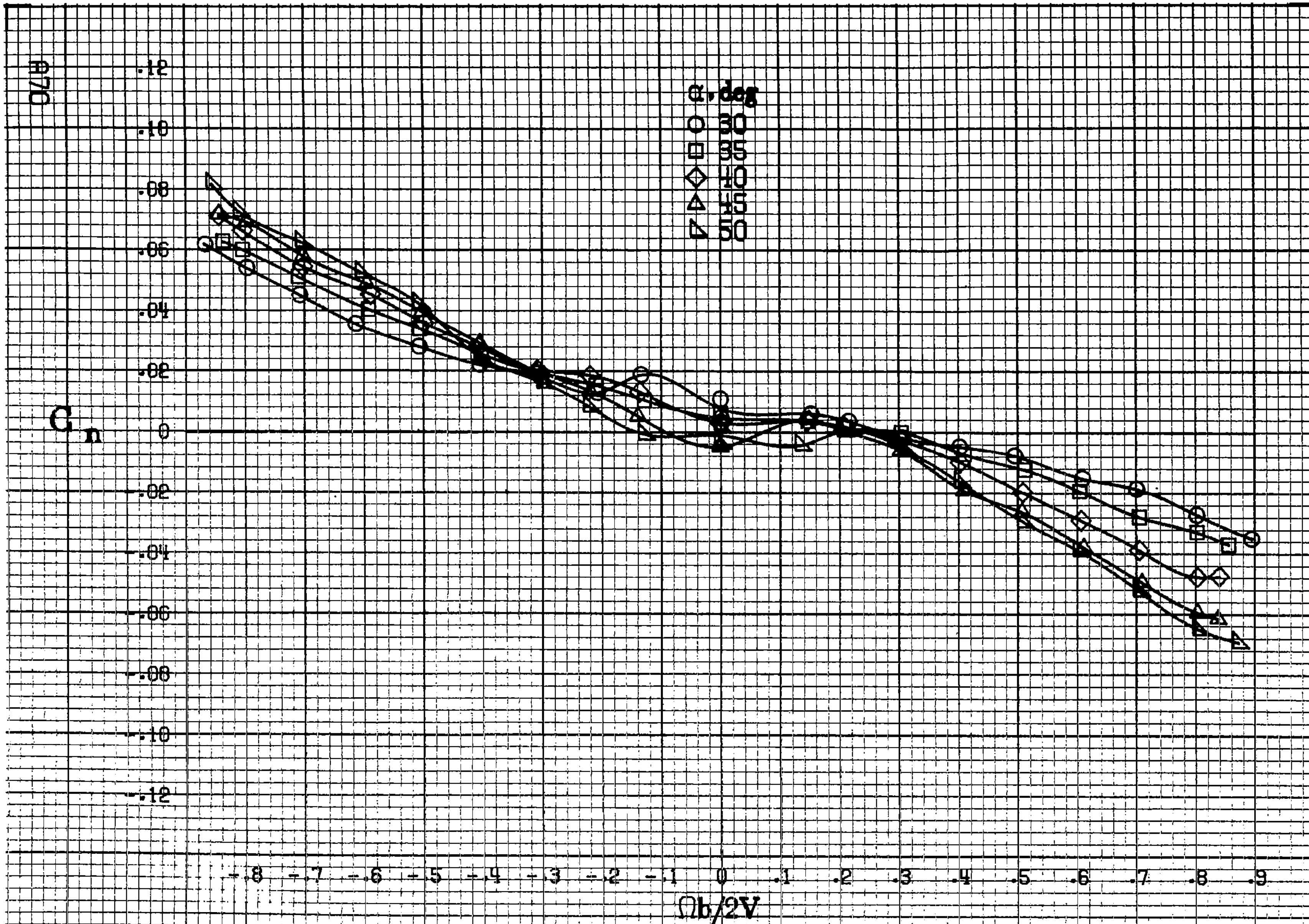

(c) $\alpha = 30$ to 50 deg, SR = 0.

Figure A.18.-Continued.

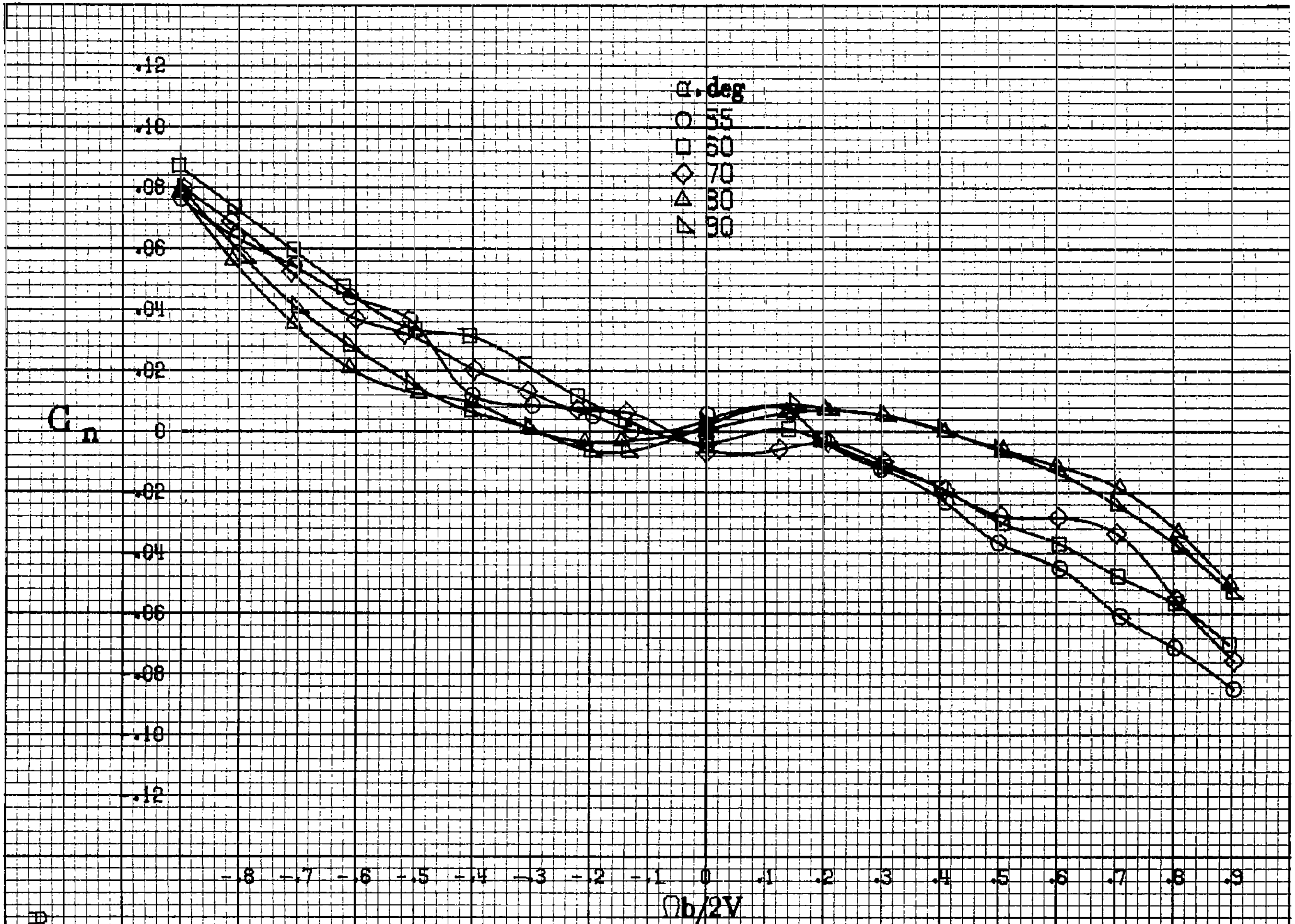

(d) α = 55 to 90 deg, SR = 0.

Figure A18.-Concluded.

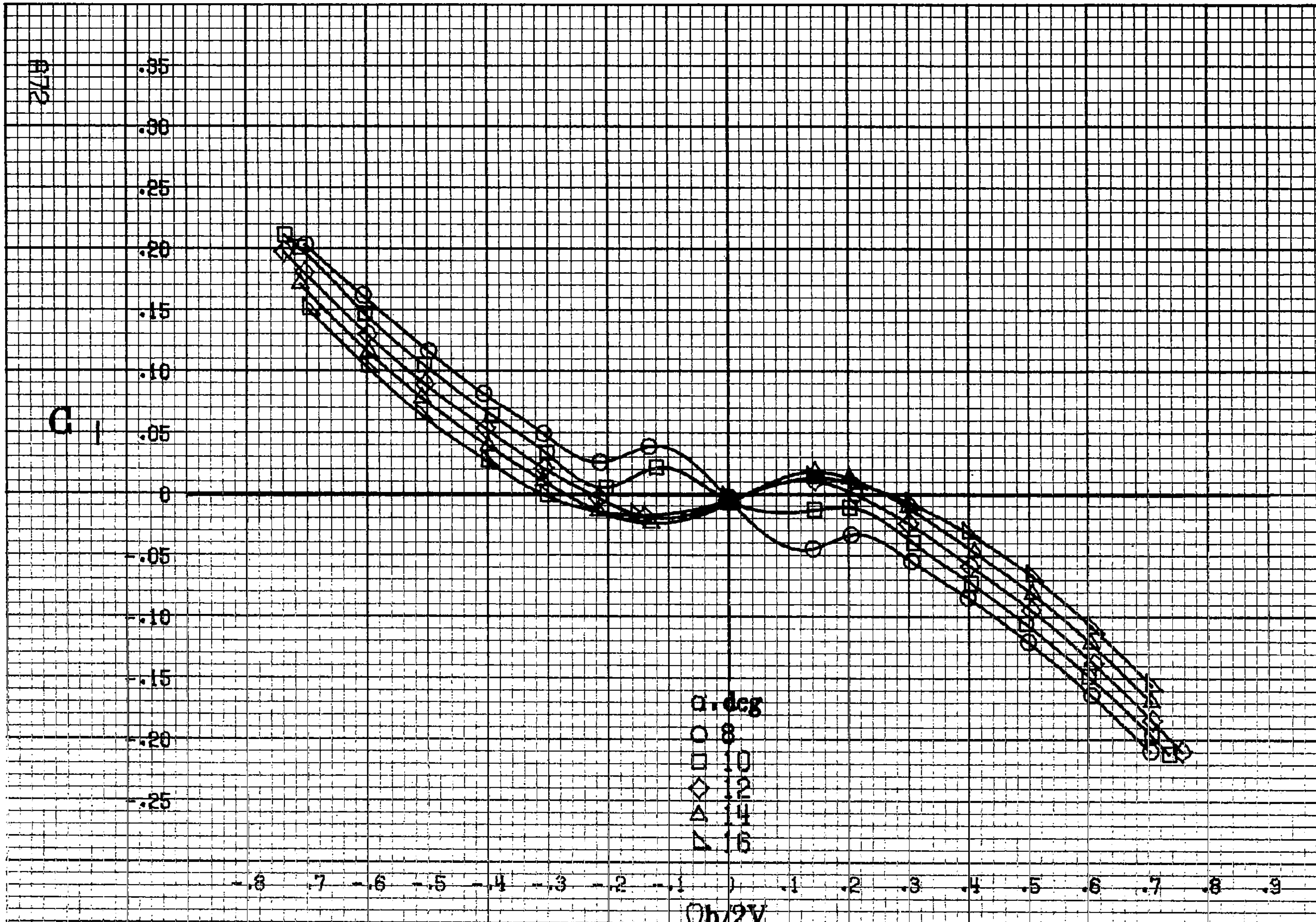

(a) $\alpha = 8$ to 16 deg, SR = 182.9 cm (72 in).

Figure A14.-Effect of rotation rate and angle of attack on rolling-moment coefficient for basic configuration. $\delta_e = -15°$, $\delta_a = 0°$, $\delta_r = -25°$, $\beta = 0°$.

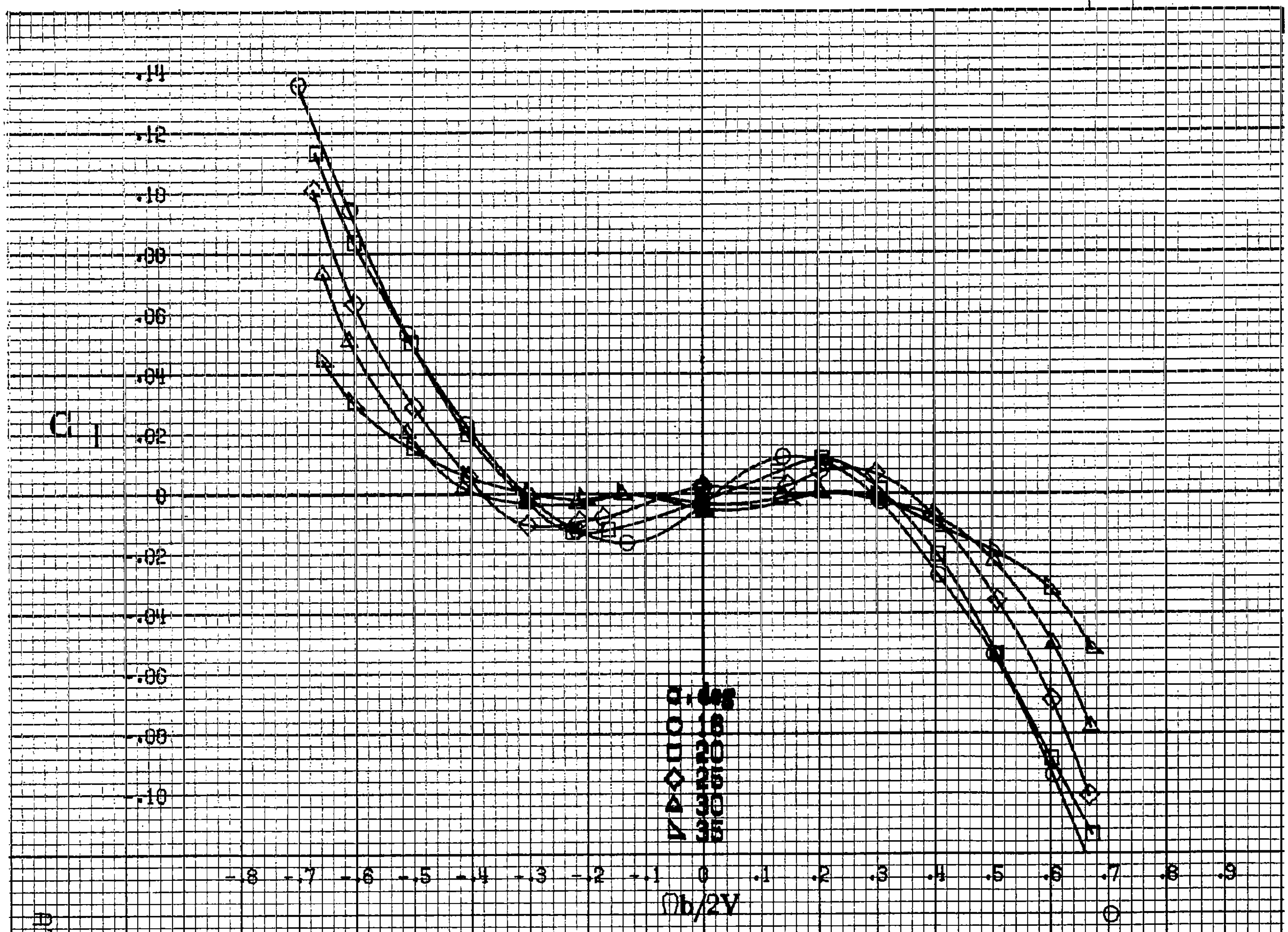

(b) α = 18 to 35 deg, SR = 182.9 cm (72 in).

Figure A14.-Continued.

A74

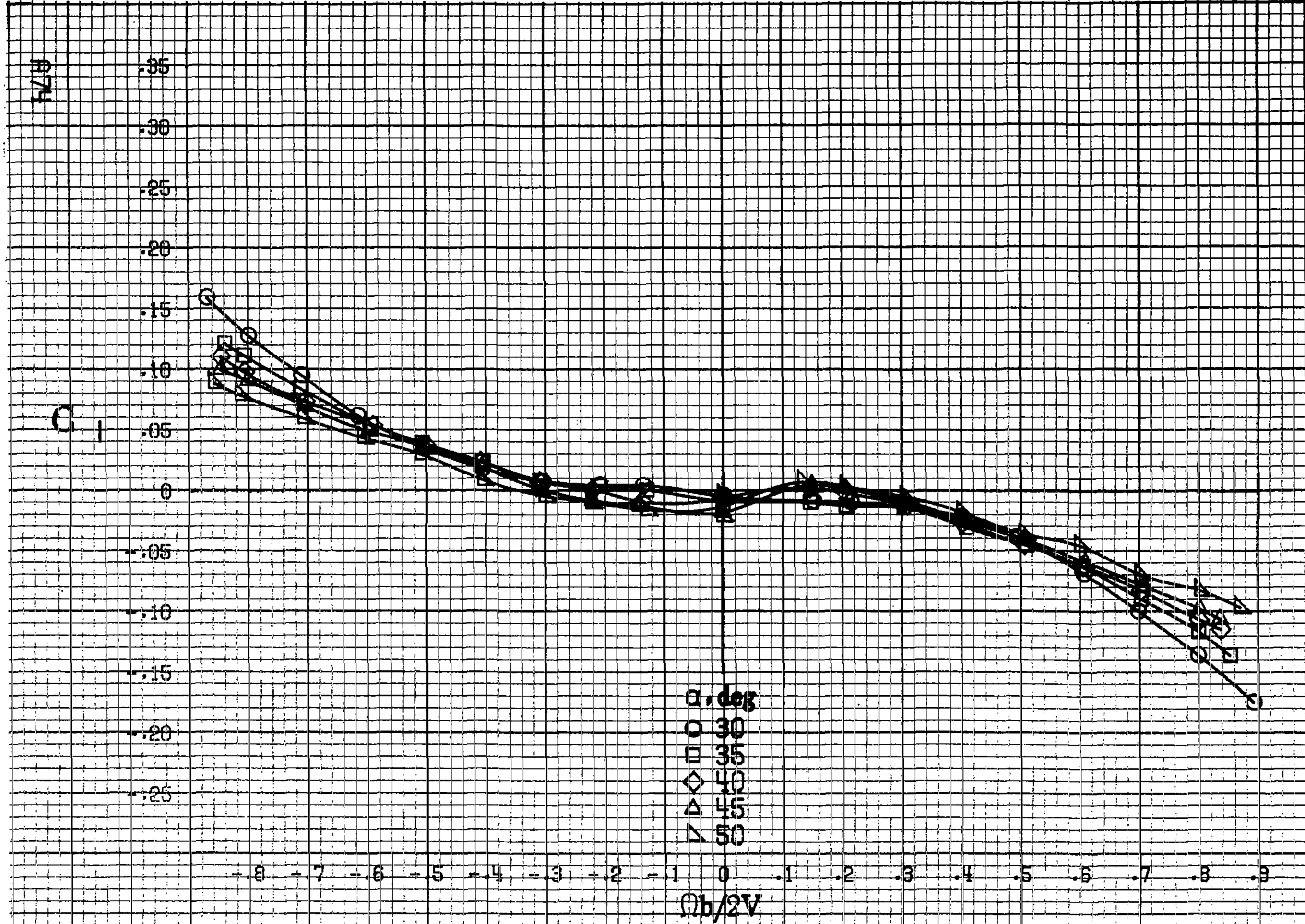

(c) α = 30 to 50 deg, SR = 0.

Figure A14.-Continued.

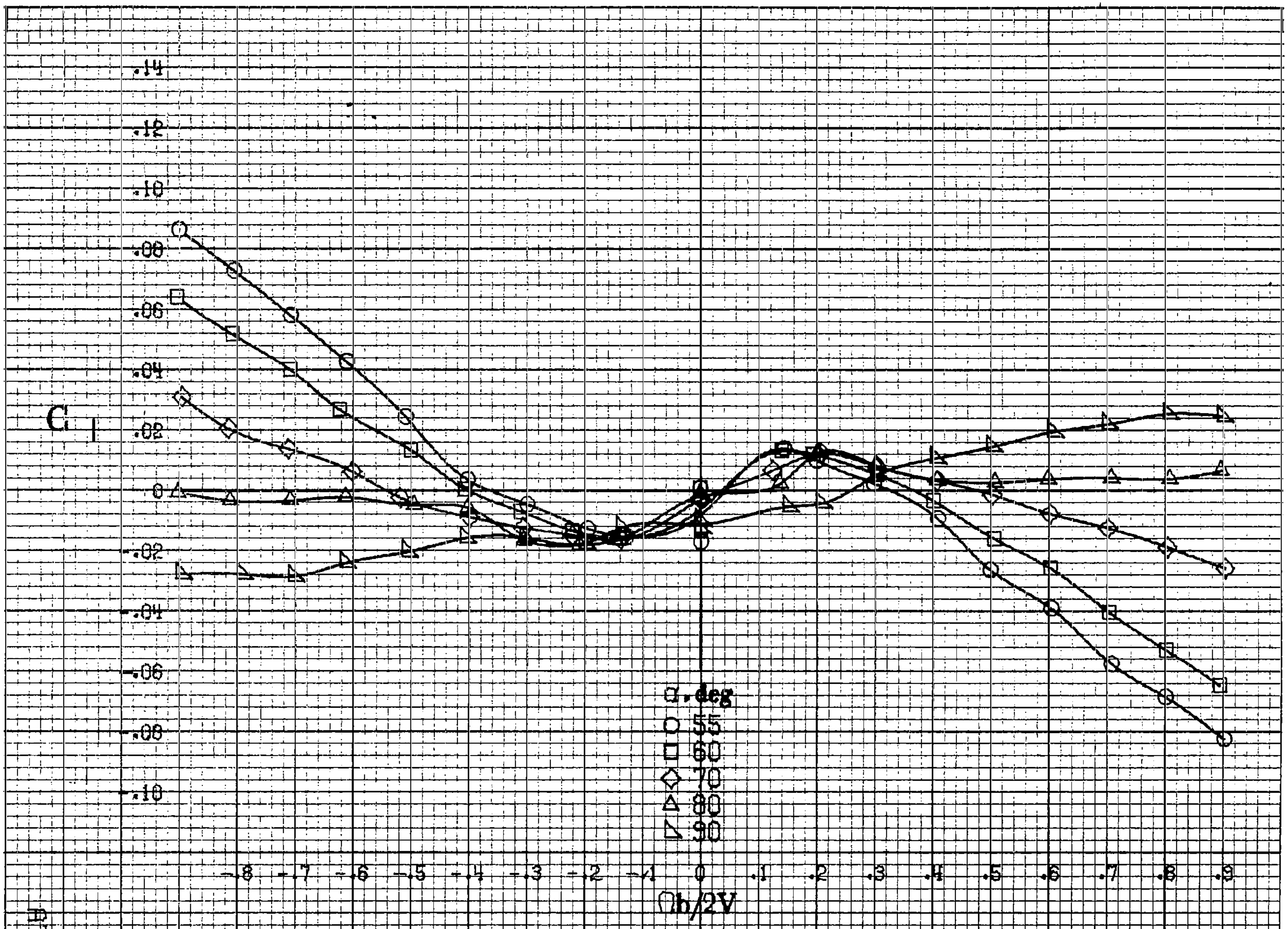

(d) α = 55 to 90 deg, SR = 0.

Figure A14.-Concluded.

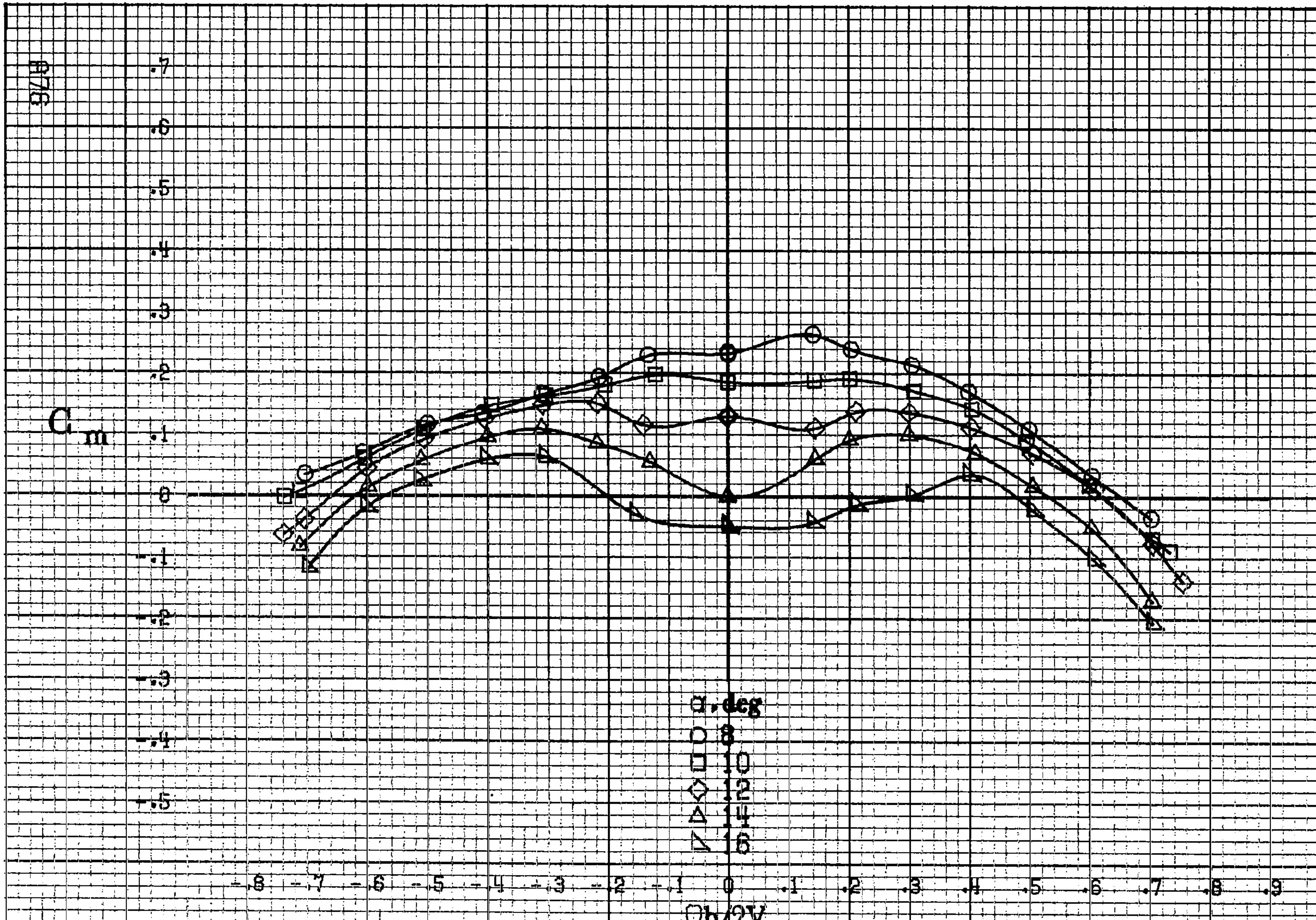

(a) $\alpha = 8$ to 16 deg, SR = 182.9cm (72in).

Figure A15.-Effect of rotation rate and angle of attack on pitching-moment coefficient for basic configuration. $\delta_e = -15°$, $\delta_a = 0°$, $\delta_r = -25°$, $\beta = 0°$.

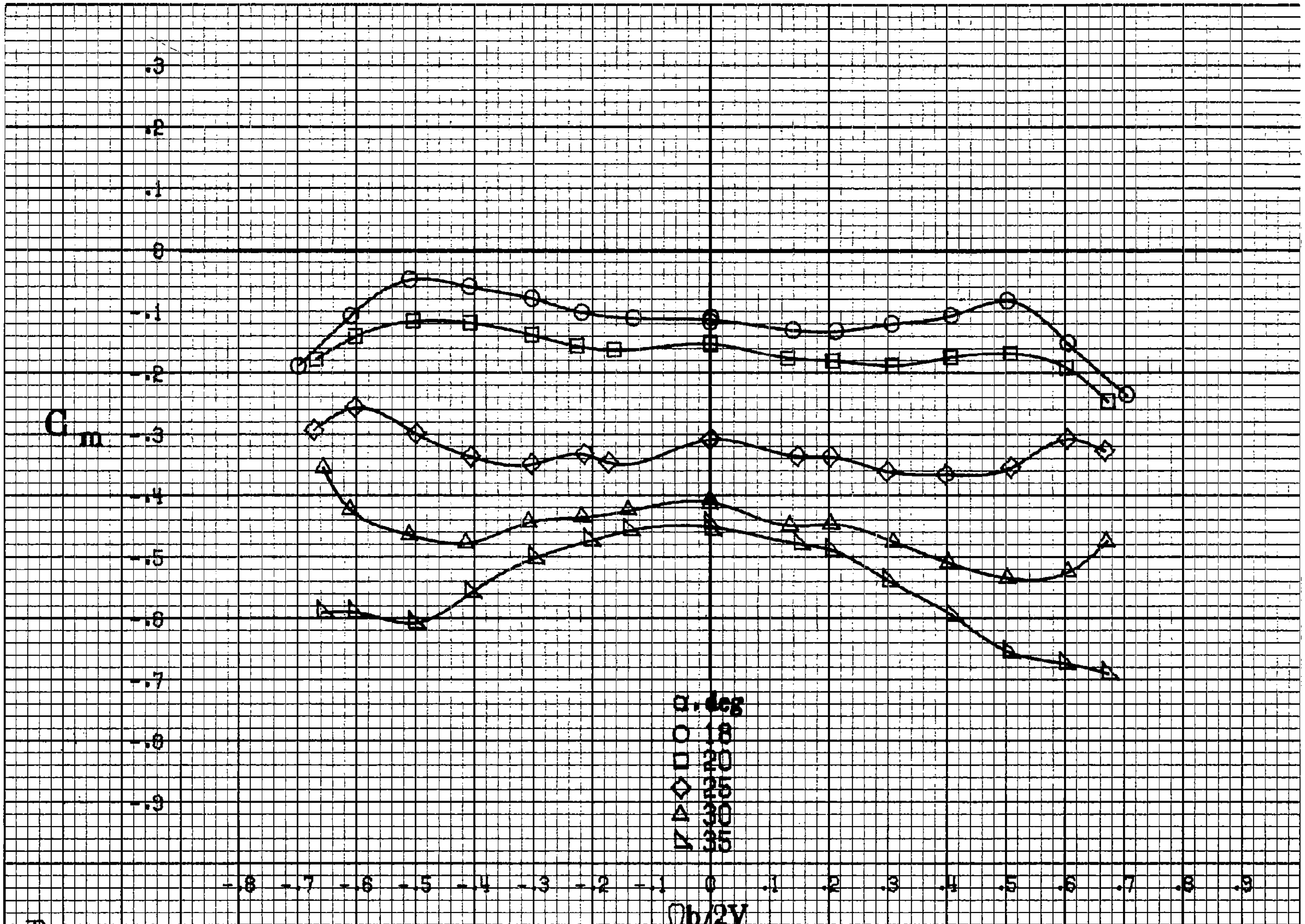

(b) α = 18 to 35 deg, SR = 182.9 cm (72 in).

Figure A15.-Continued.

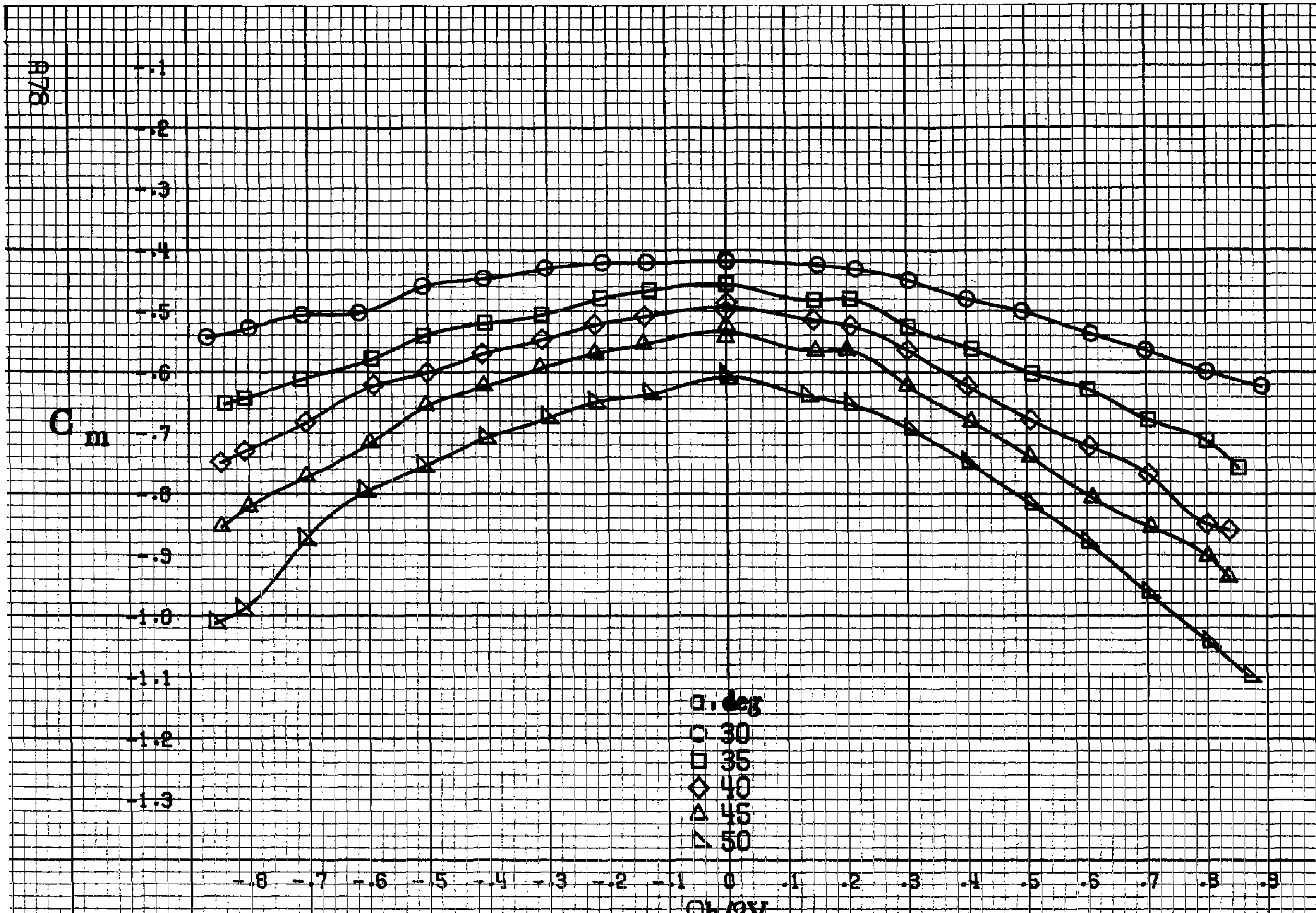

(c) α = 30 to 50 deg, SR = 0.

Figure A15.-Continued.

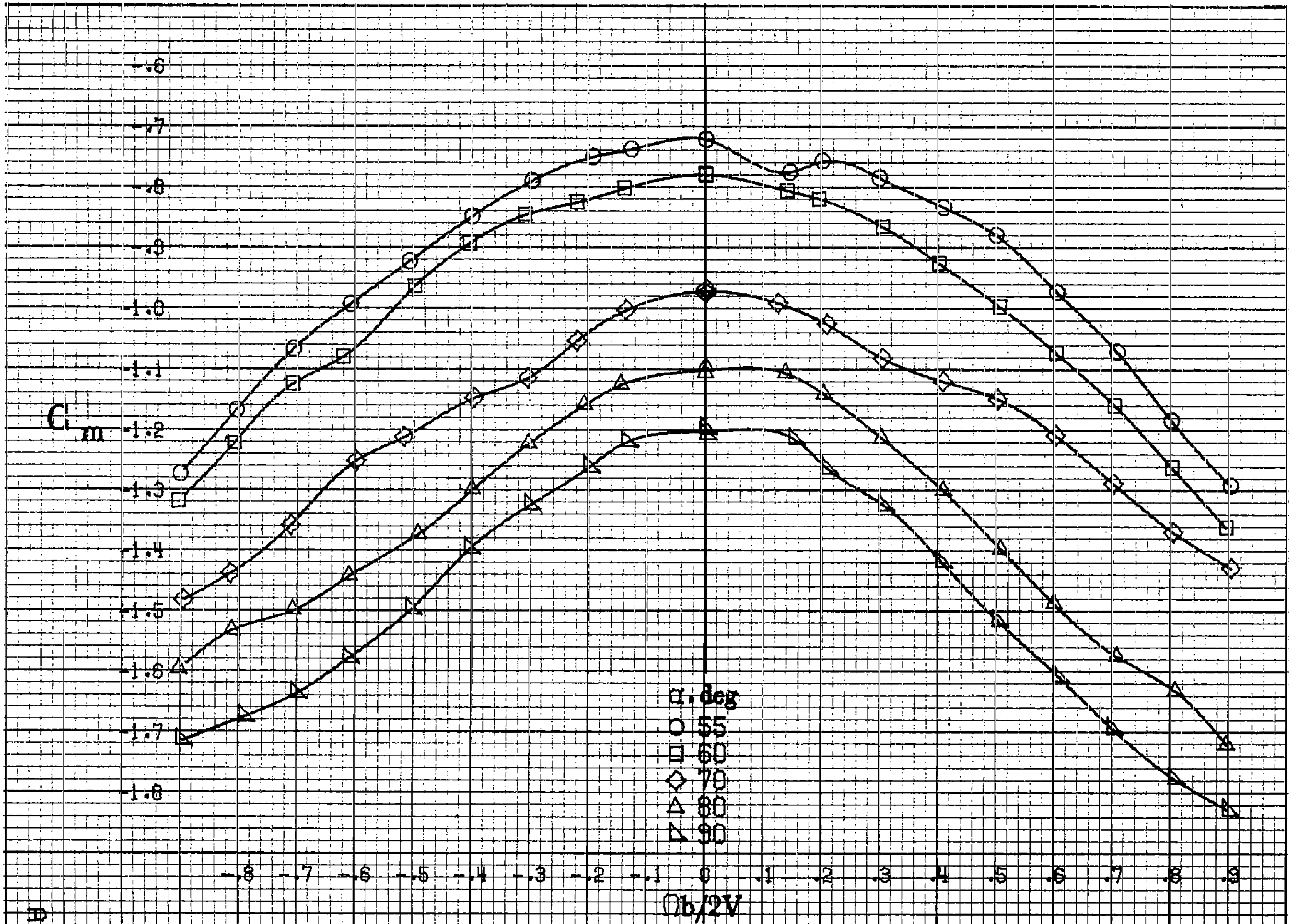

(d) α = 55 to 90 deg, SR = 0.

Figure A15.-Concluded.

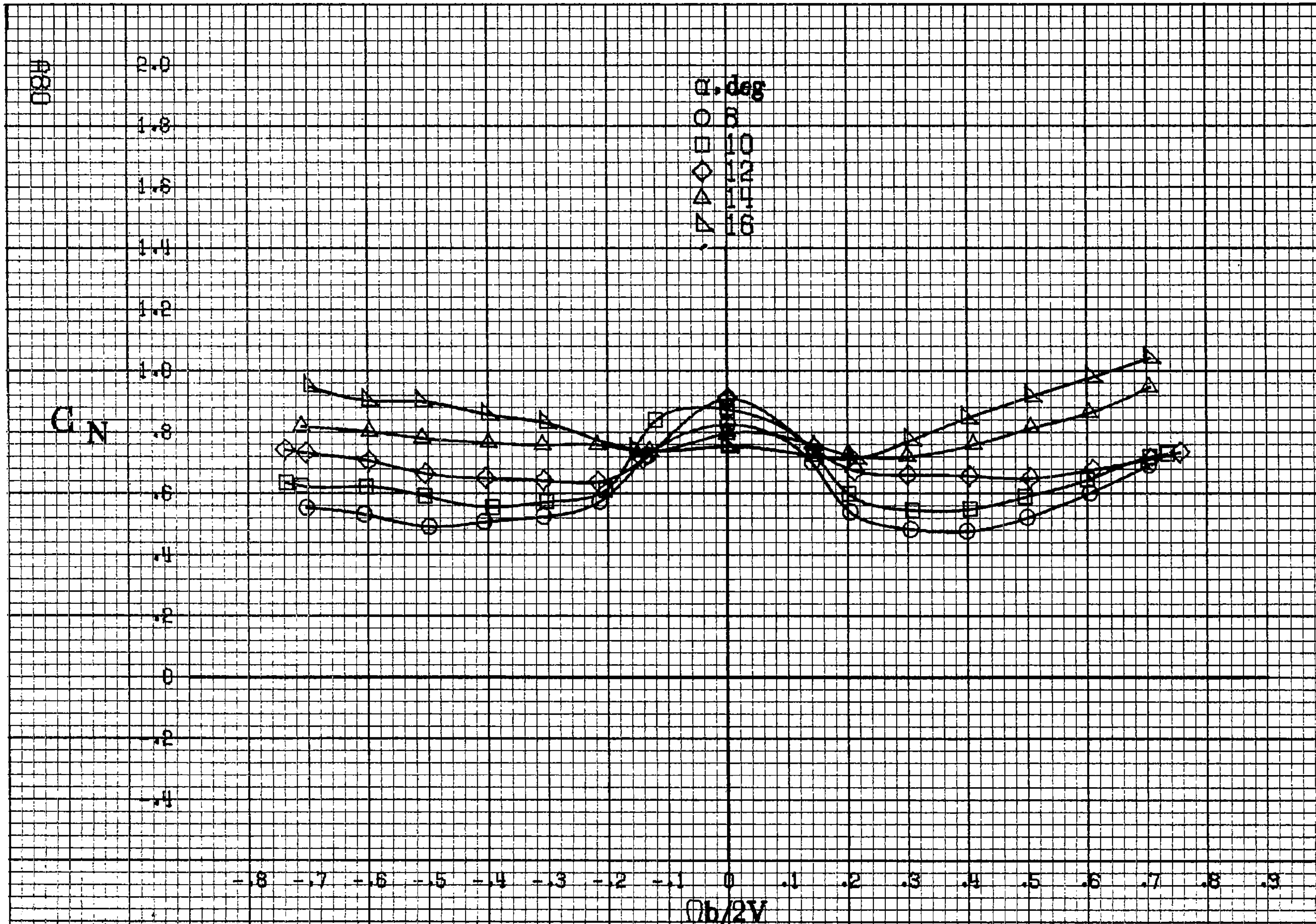

(a) α = 8 to 16 deg, SR = 182.9 cm (72 in).

Figure A16.-Effect of rotation rate and angle of attack on normal-force coefficient for basic configuration. $\delta_e = -15^\circ$, $\delta_a = 0^\circ$, $\delta_r = -25^\circ$, $\beta = 0^\circ$.

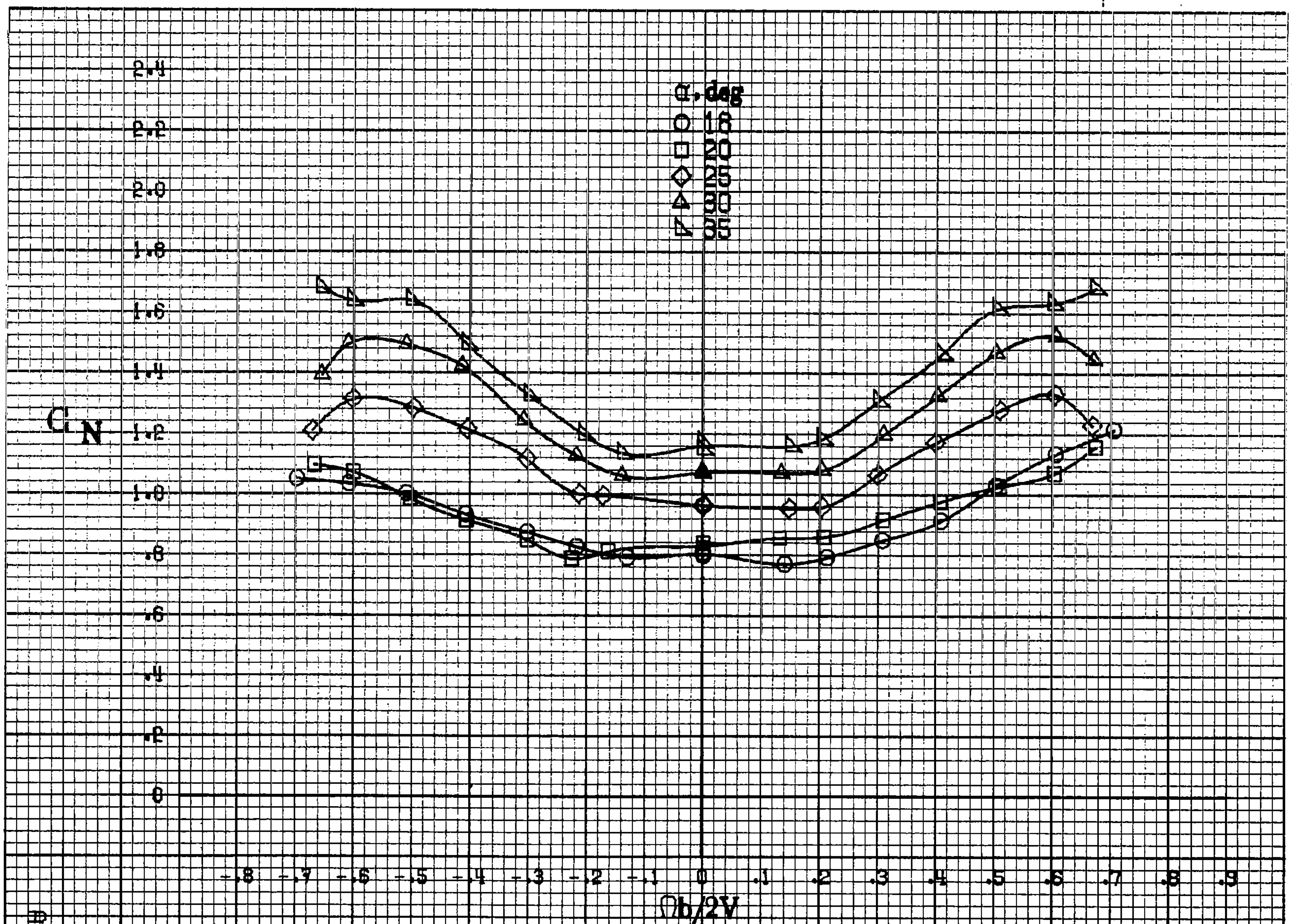

(b) α = 18to35deg, SR = 182.9cm (72in).
Figure A16.-Continued.

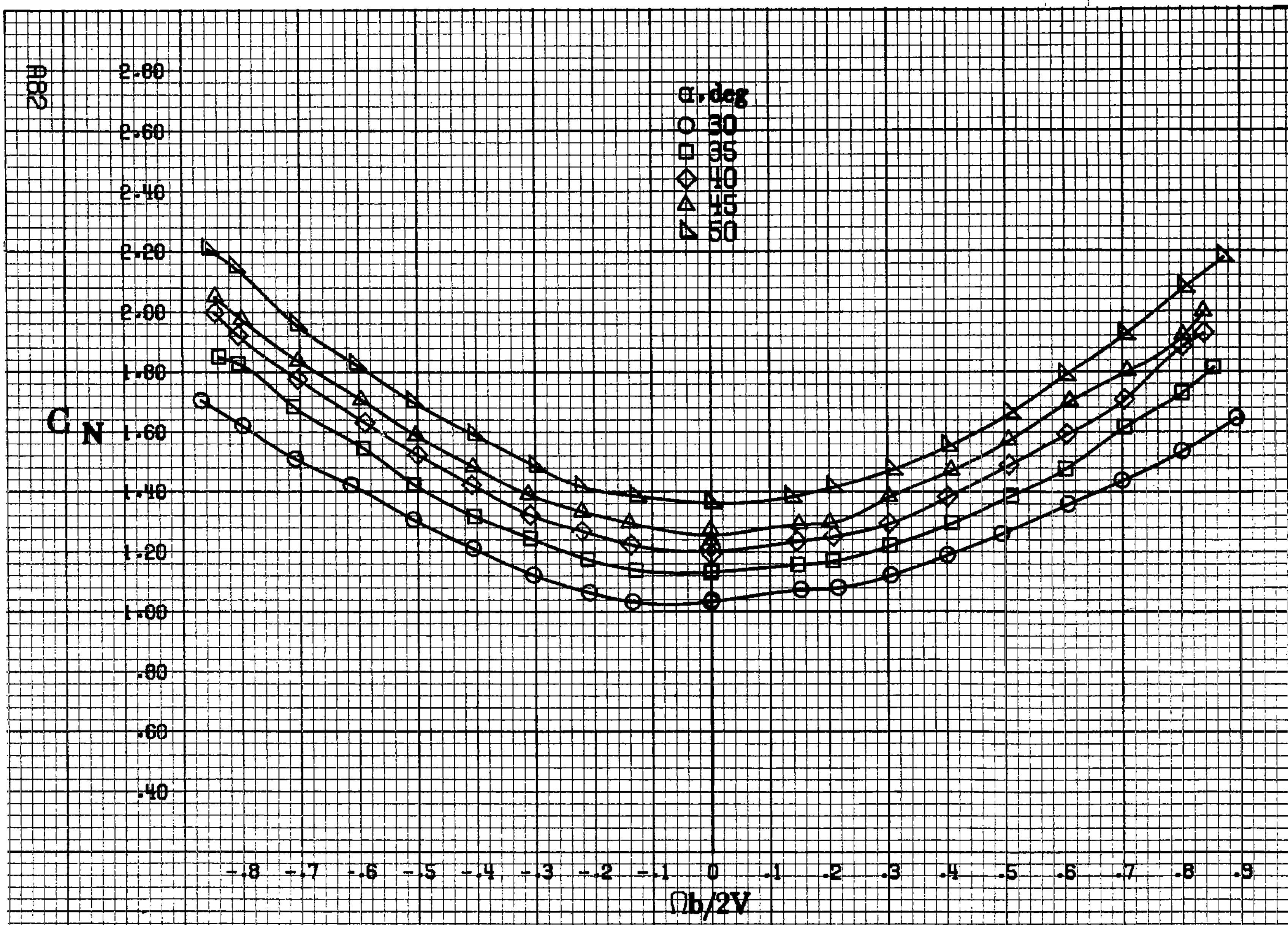

(c) α = 30 to 50 deg, SR = 0.

Figure A16.-Continued.

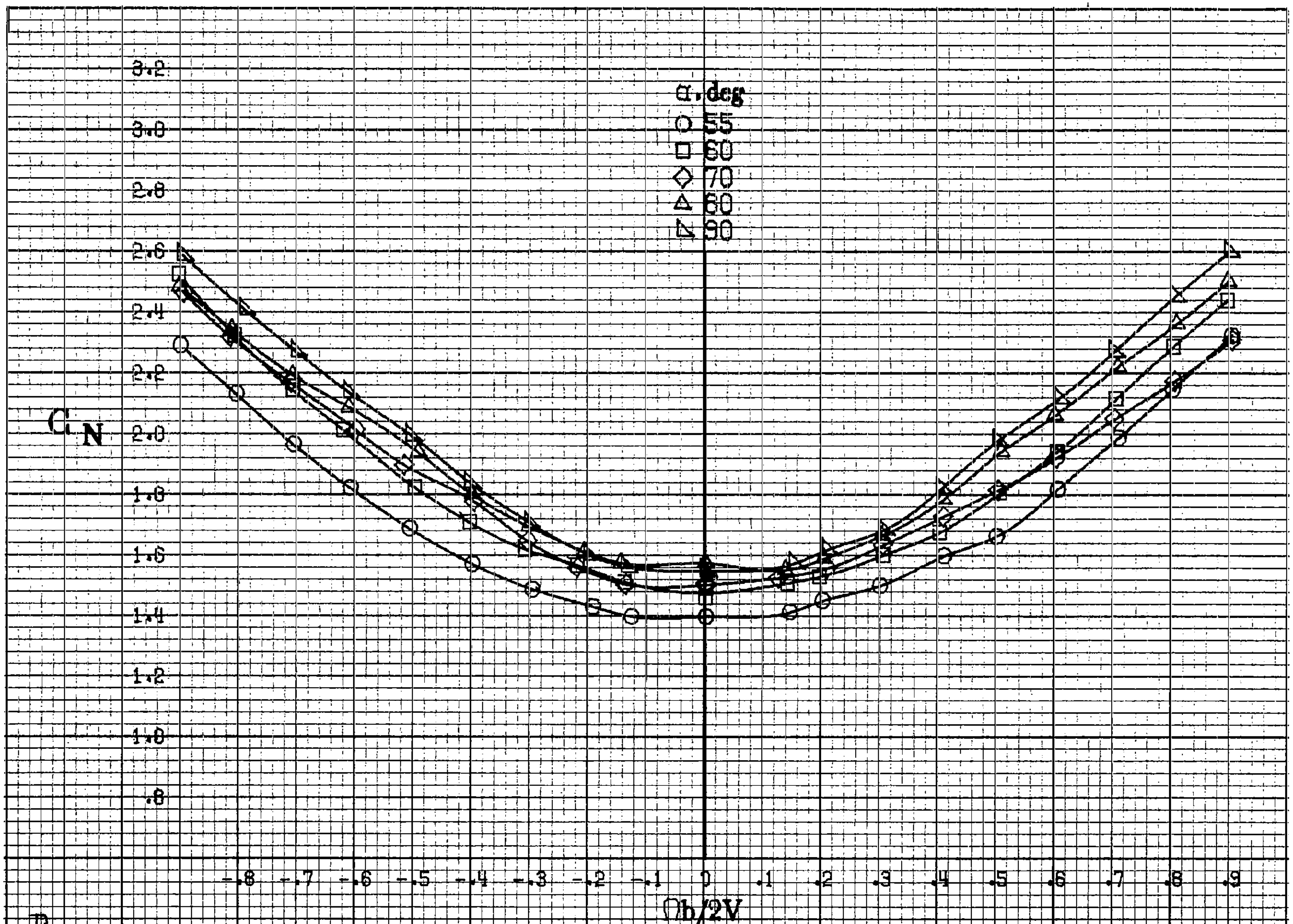

(d) α = 55 to 90 deg, SR = 0.
Figure A16.-Concluded.

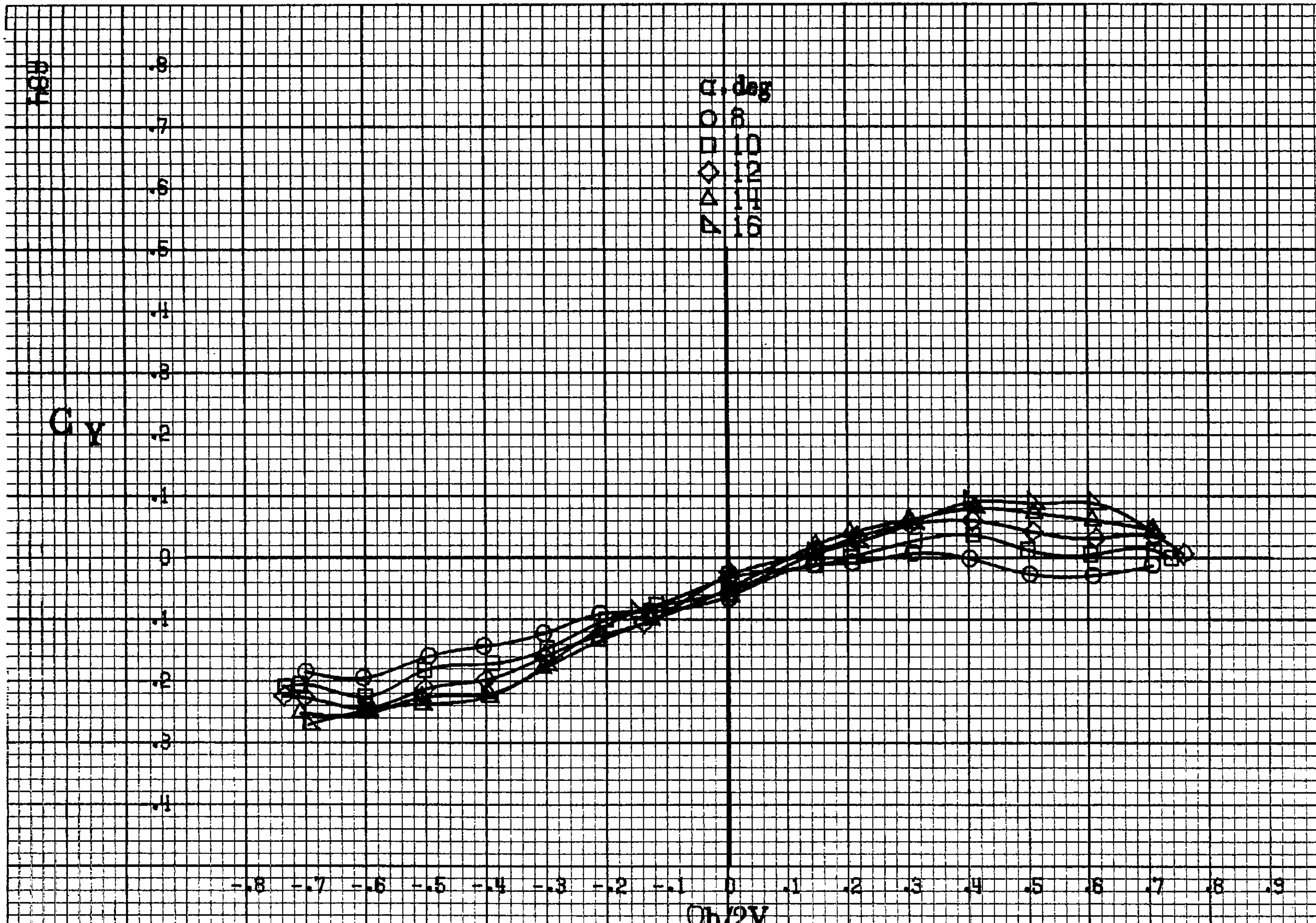

(a) $\alpha = 8$ to 16 deg, SR = 182.9 cm (72 in).

Figure A17.-Effect of rotation rate and angle of attack on side-force coefficient for basic configuration. $\delta_e = -15°$, $\delta_a = 0°$, $\delta_r = -25°$, $\beta = 0°$.

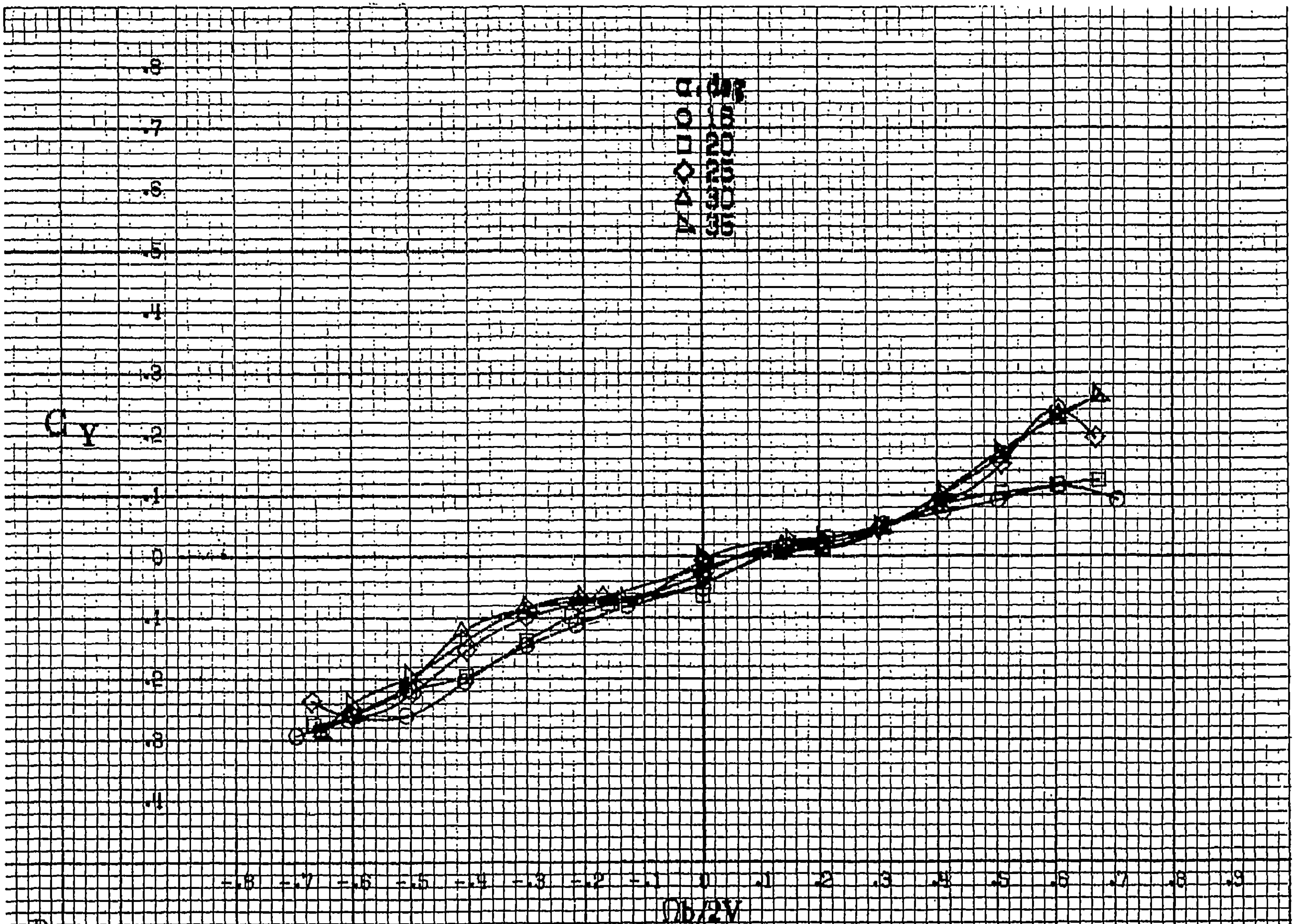

(b) α = 18 to 35 deg, SR = 182.9 cm (72 in).

Figure A17.-Continued.

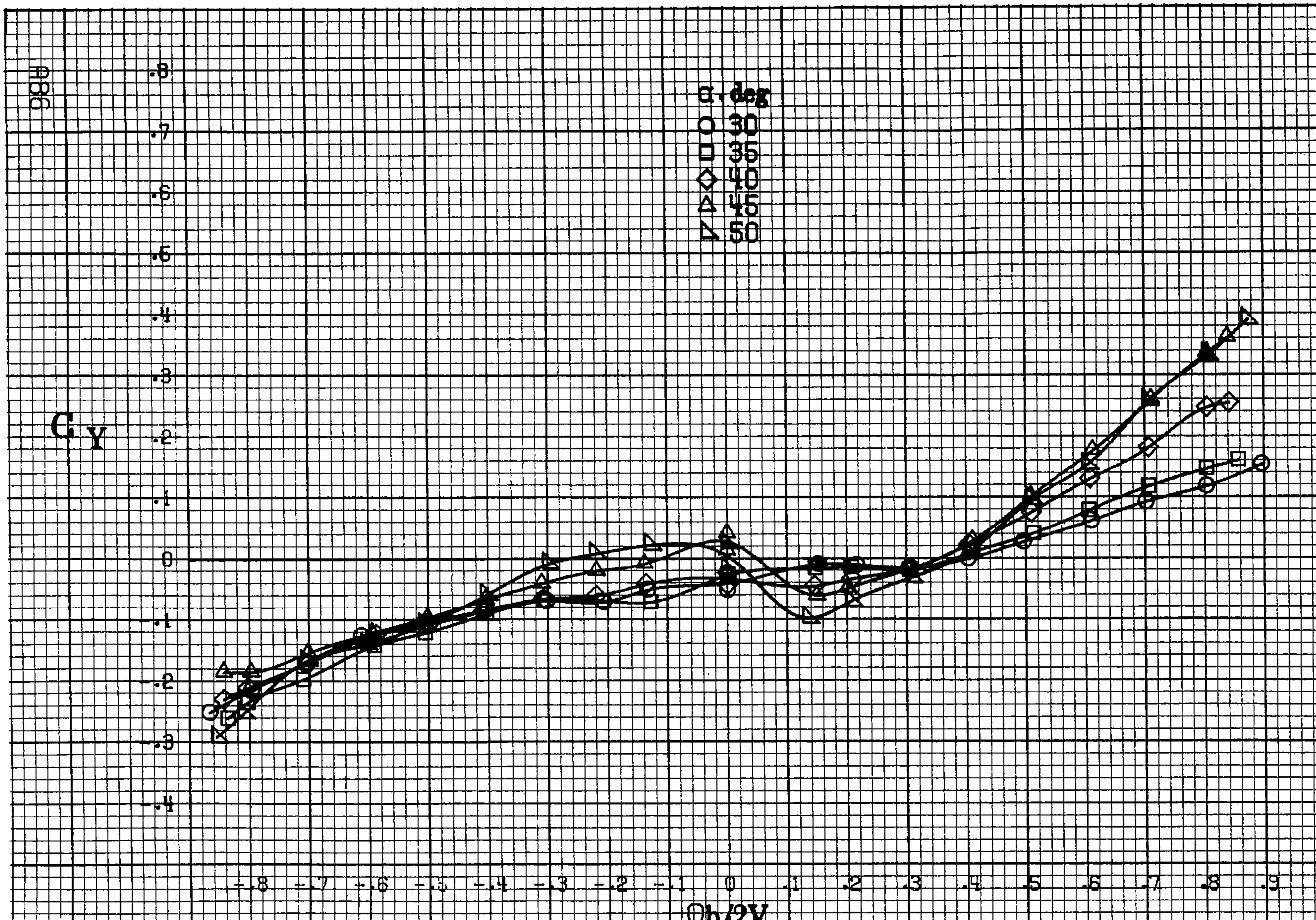

(c) α = 30 to 50 deg, SR = 0.

Figure A17.-Continued.

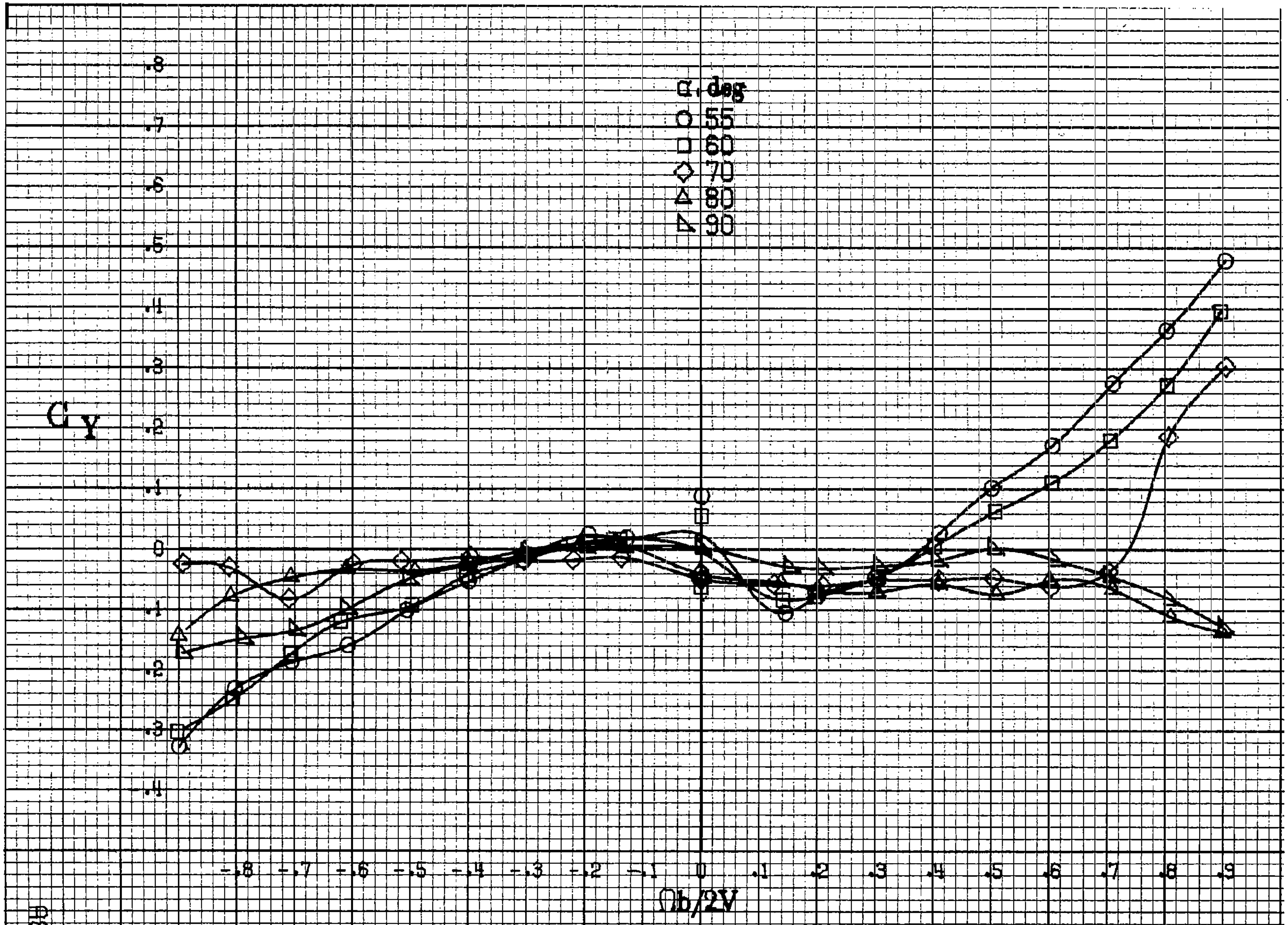

(d) α = 55 to 90 deg, SR = 0.

Figure A17.-Concluded.

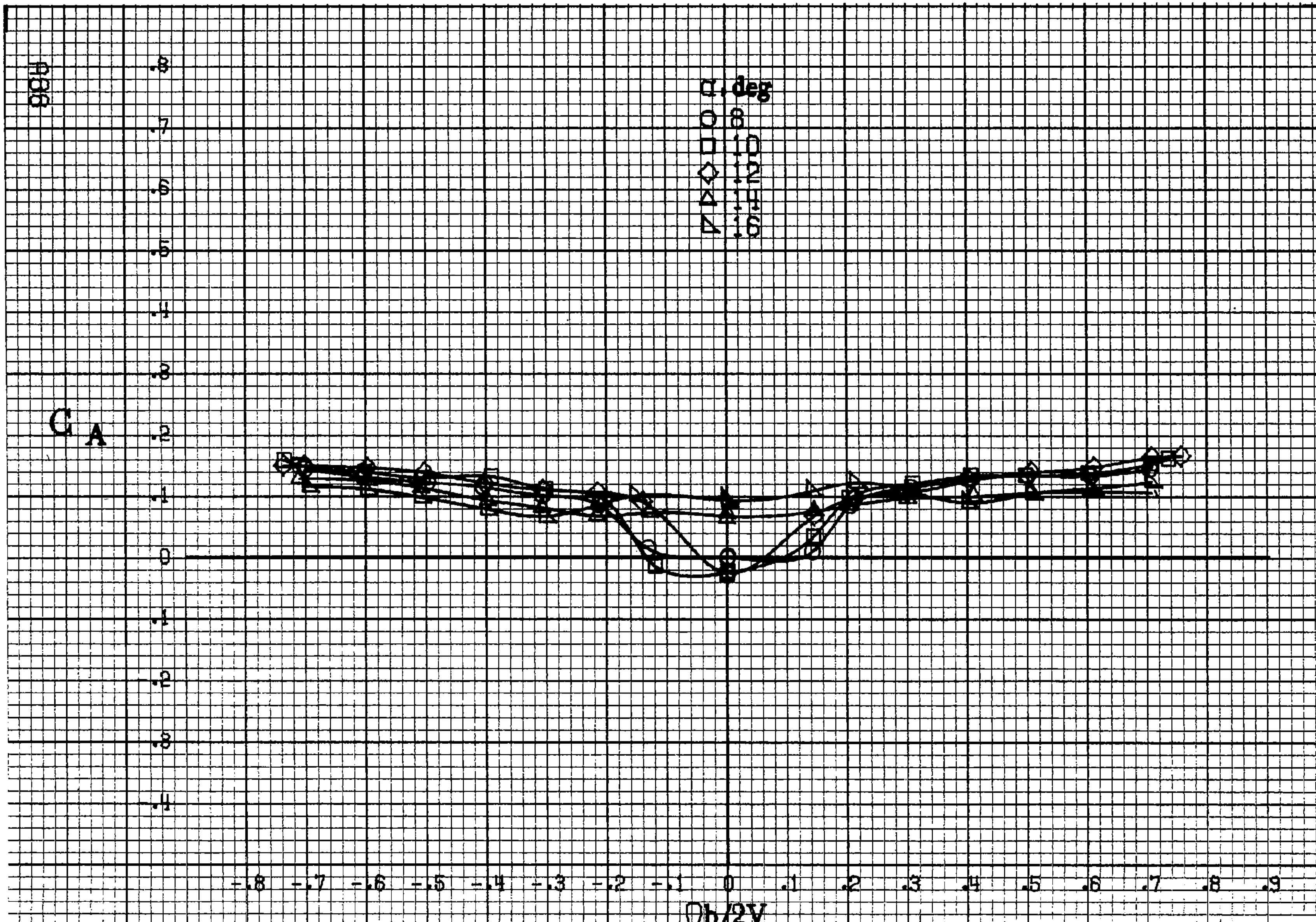

(a) α = 8 to 16 deg, SR = 182.9 cm (72 in).

Figure A18.-Effect of rotation rate and angle of attack on axial-force coefficient for basic configuration. $\delta_e = -15°$, $\delta_a = 0°$, $\delta_r = -25°$, $\beta = 0°$.

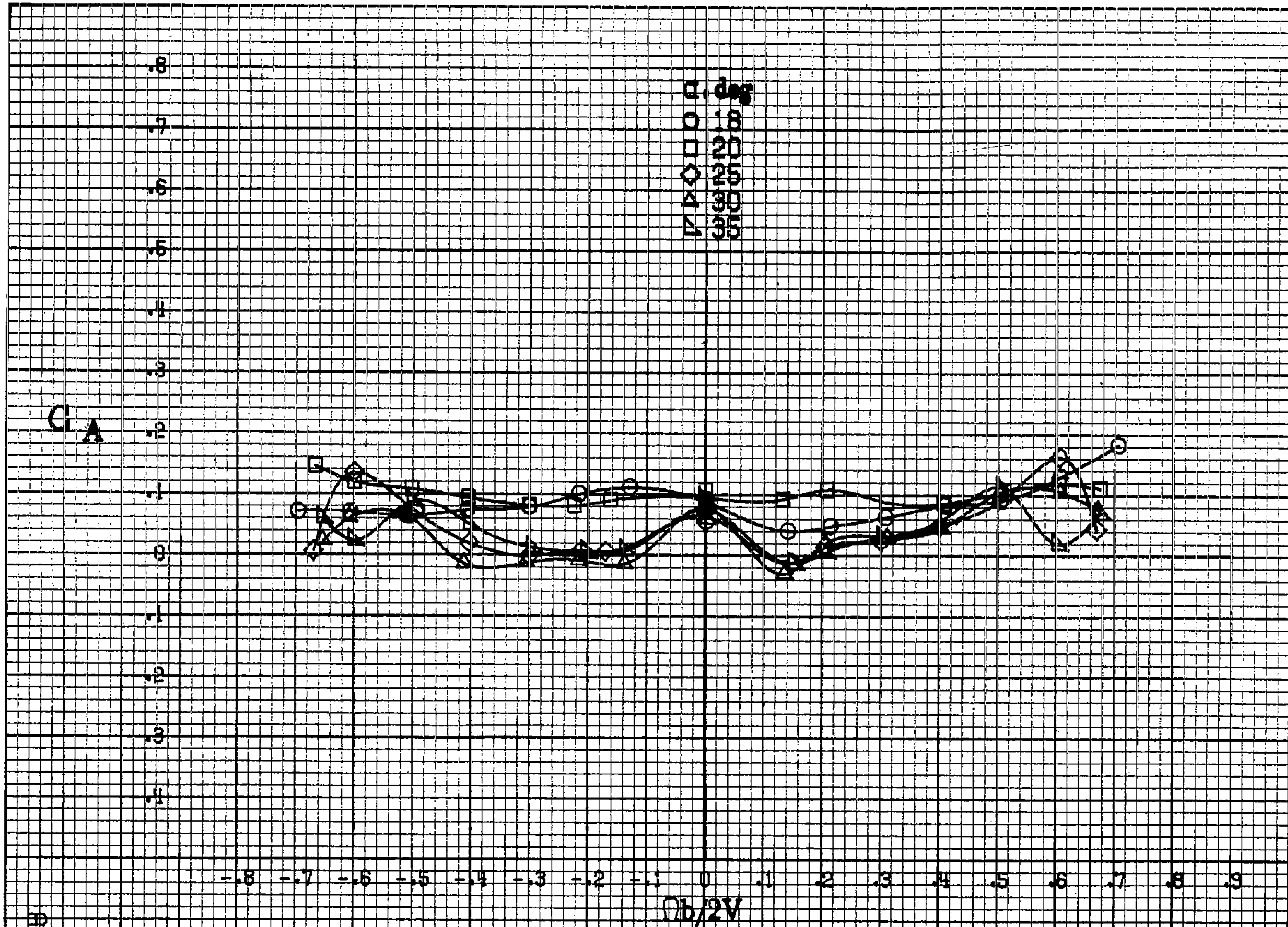

(b) α = 18 to 35 deg, SR = 182.9 cm (72 in).

Figure A18.-Continued.

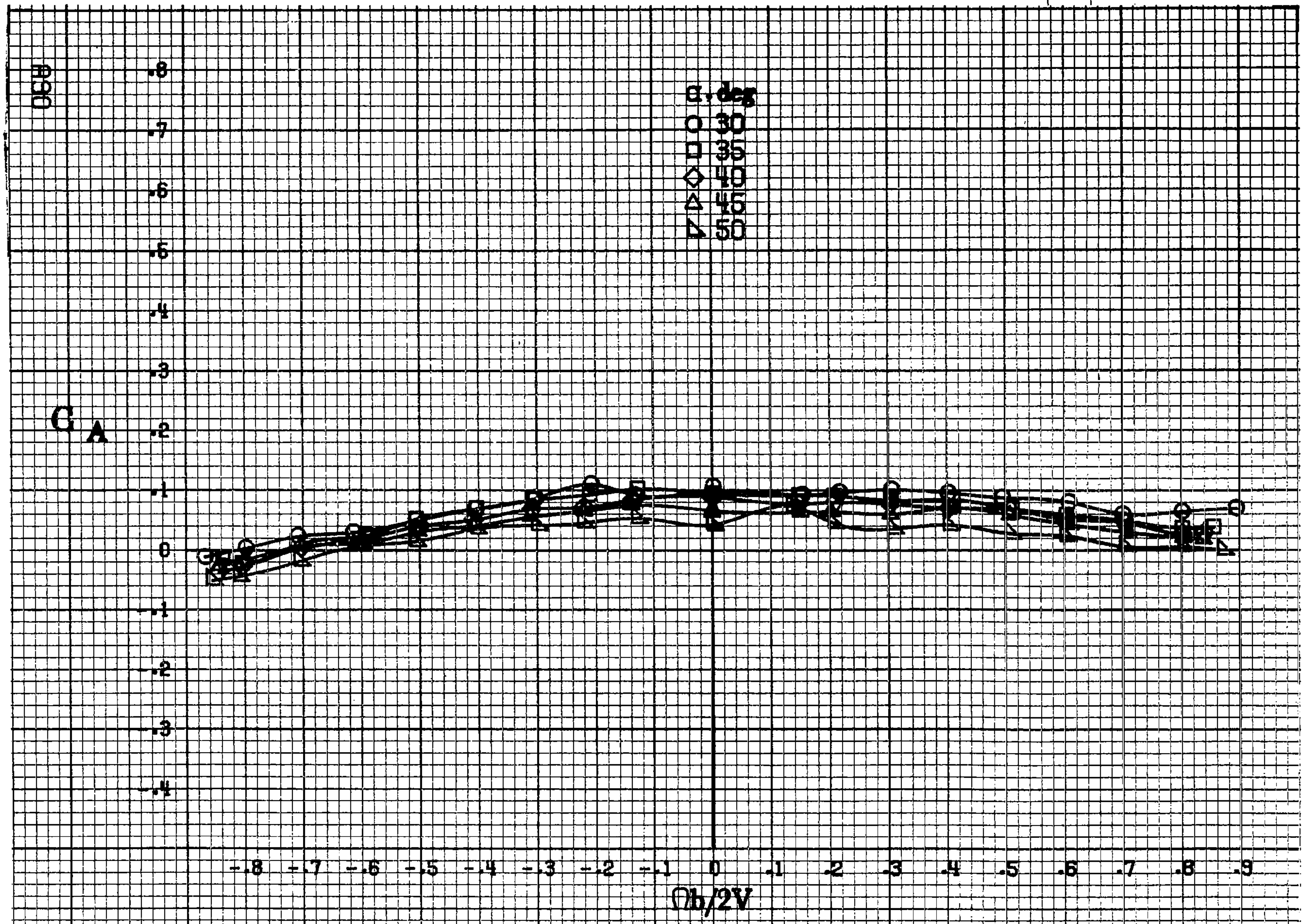

(c) $\alpha = 30$ to 50 deg, SR = 0.

Figure A18.-Continued.

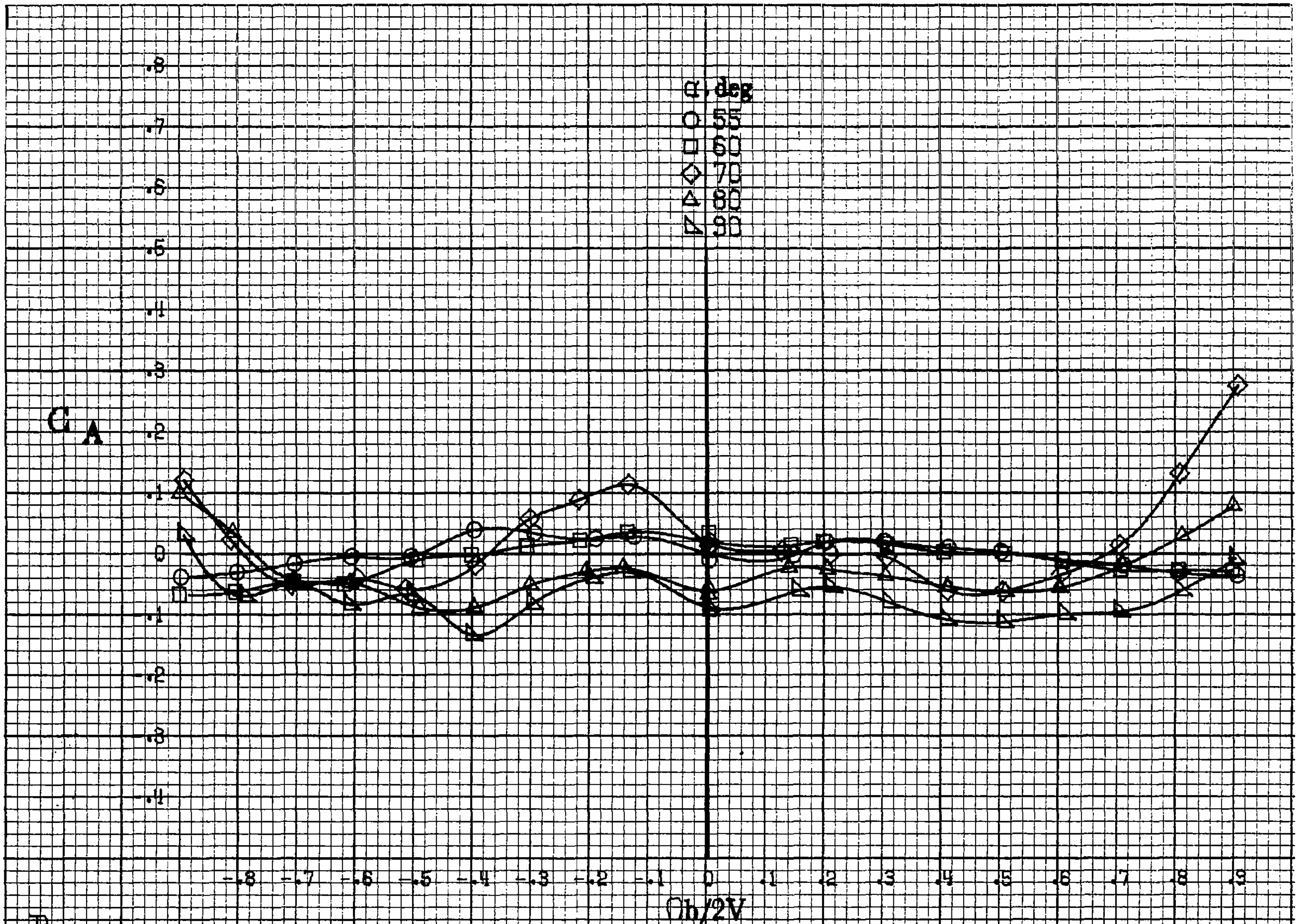

(d) α = 55 to 90 deg, SR = 0.

Figure A18.-Concluded.

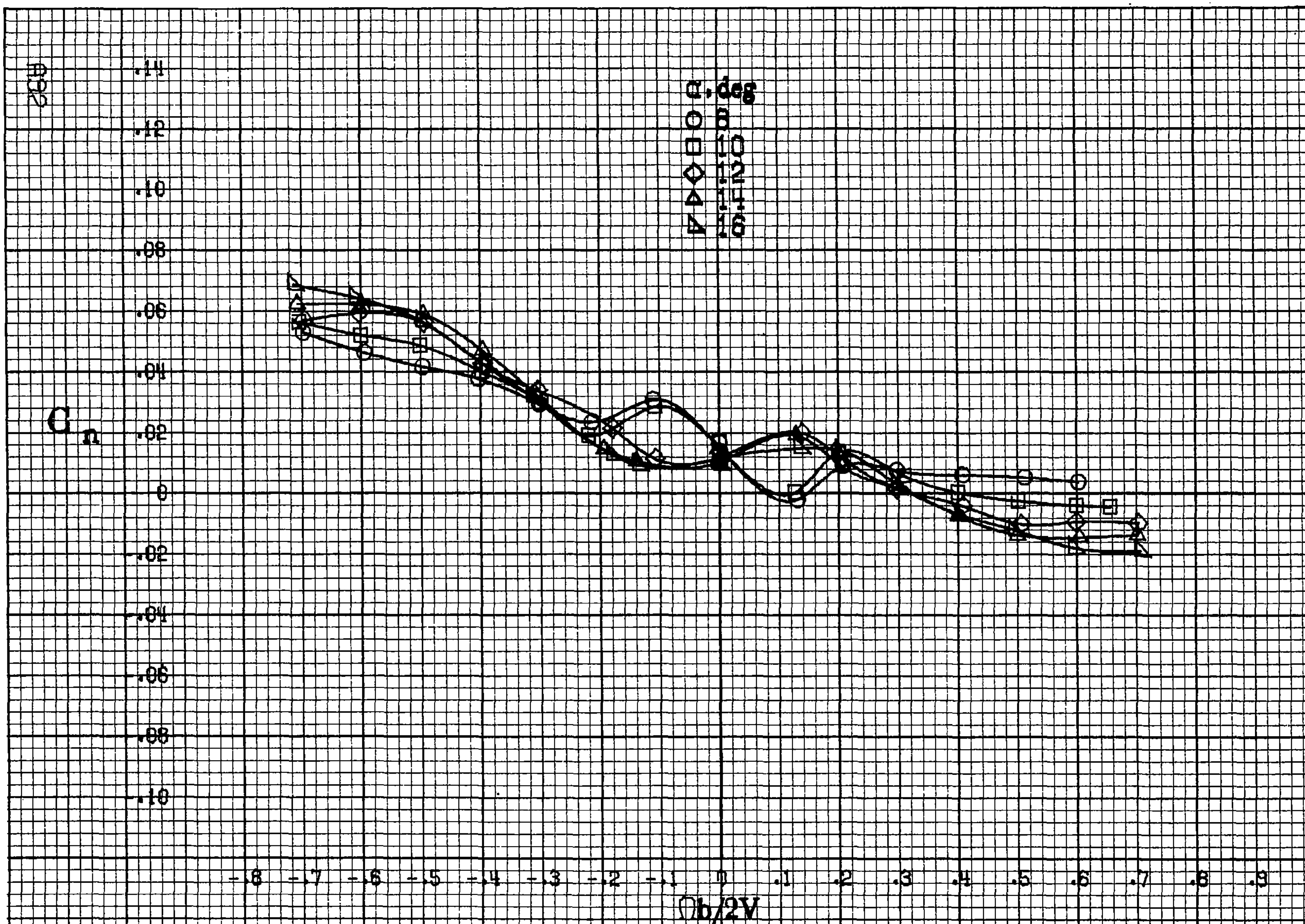

(a) $\alpha = 8$ to 16 deg, SR = 182.9 cm (72 in).

Figure A19.-Effect of rotation rate and angle of attack on yawing-moment coefficient for basic configuration. $\delta_e = -15°$, $\delta_a = 15.0°$, $\delta_r = -25°$, $\beta = 0°$.

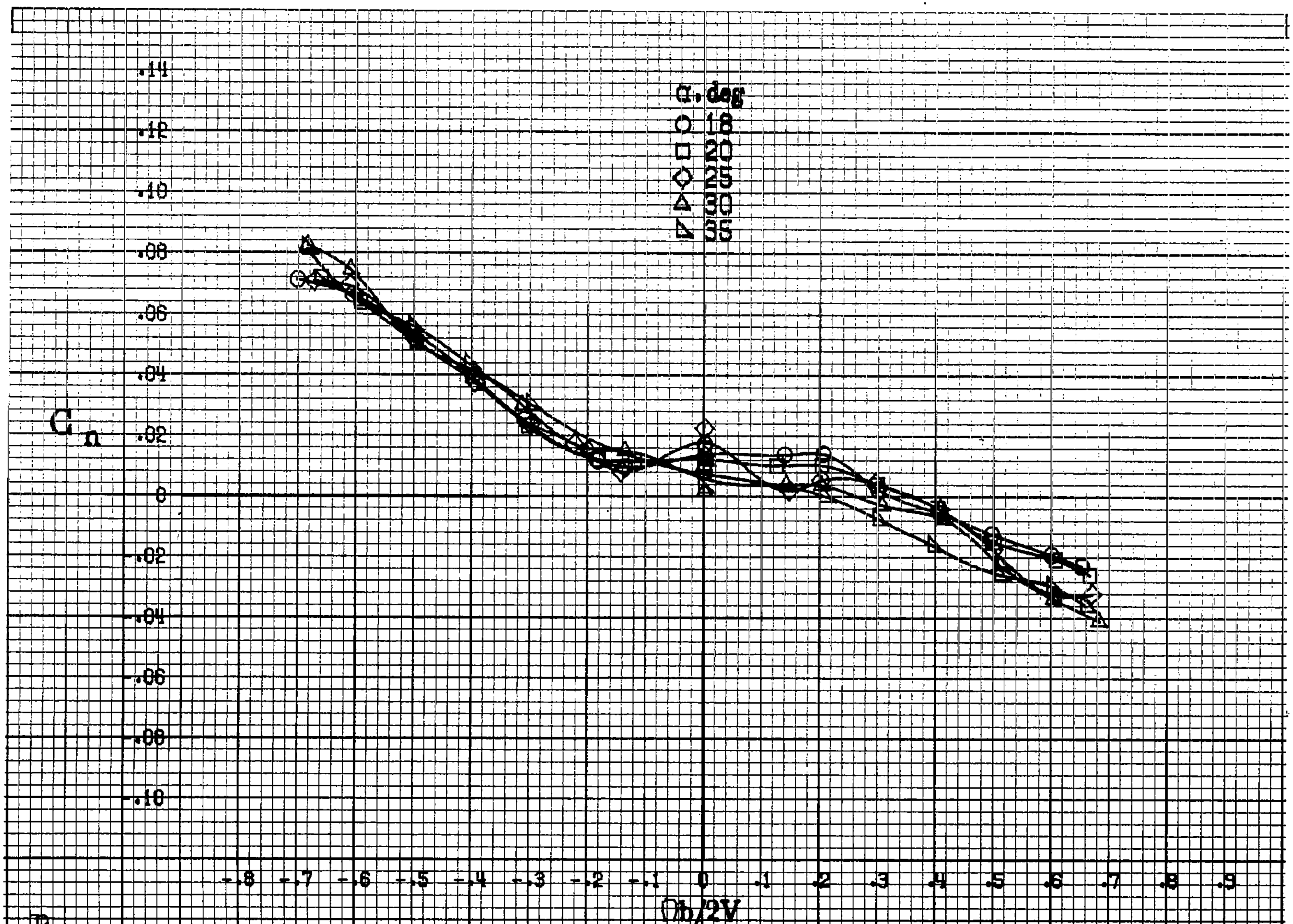

(b) α = 18 to 35 deg, SR = 182.9 cm (72 in).

Figure A19.-Continued.

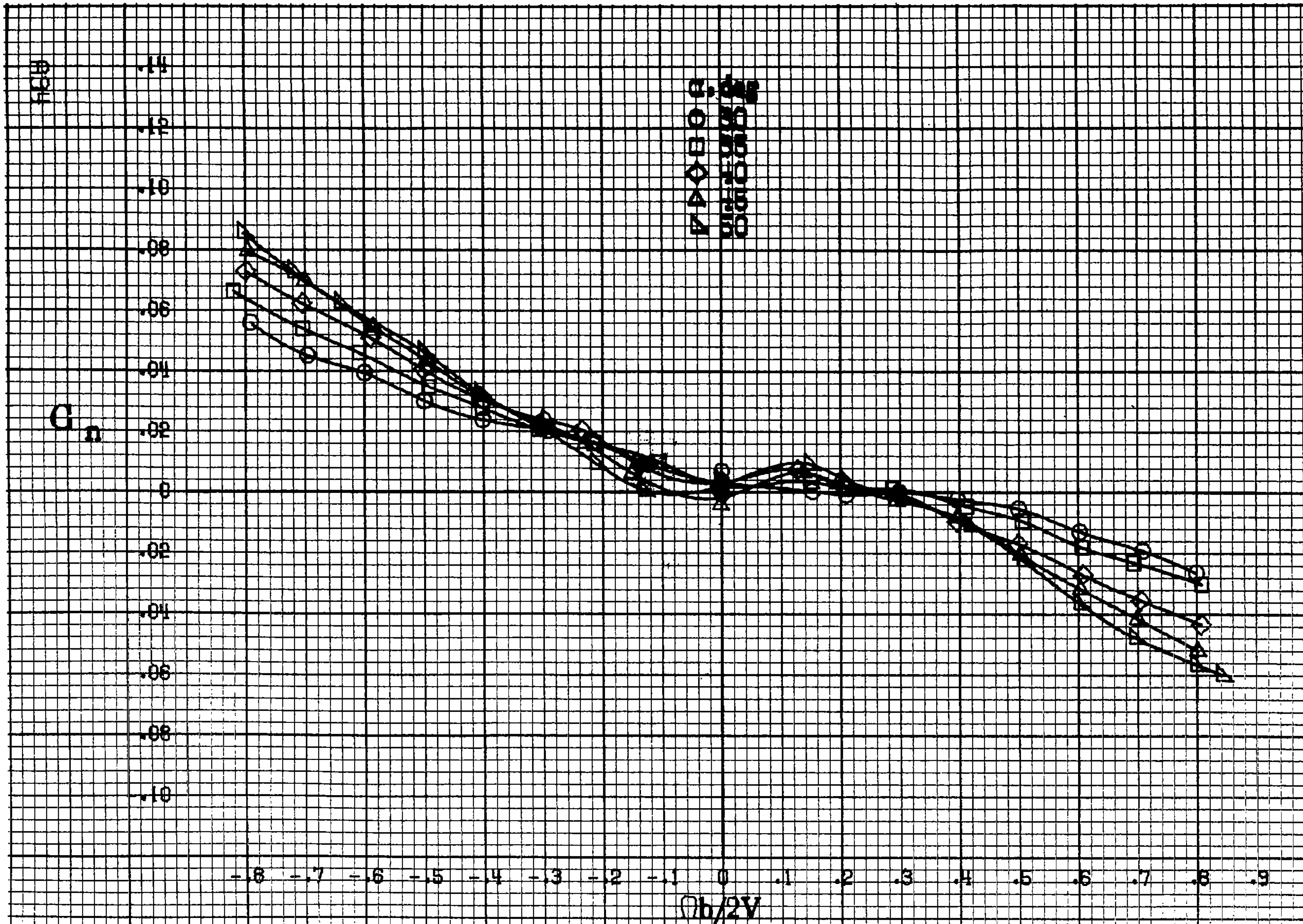

(c) α = 30 to 50 deg, SR = 0.

Figure A19.-Continued.

(d) α = 55 to 90 deg, SR = 0.

Figure A19.-Concluded.

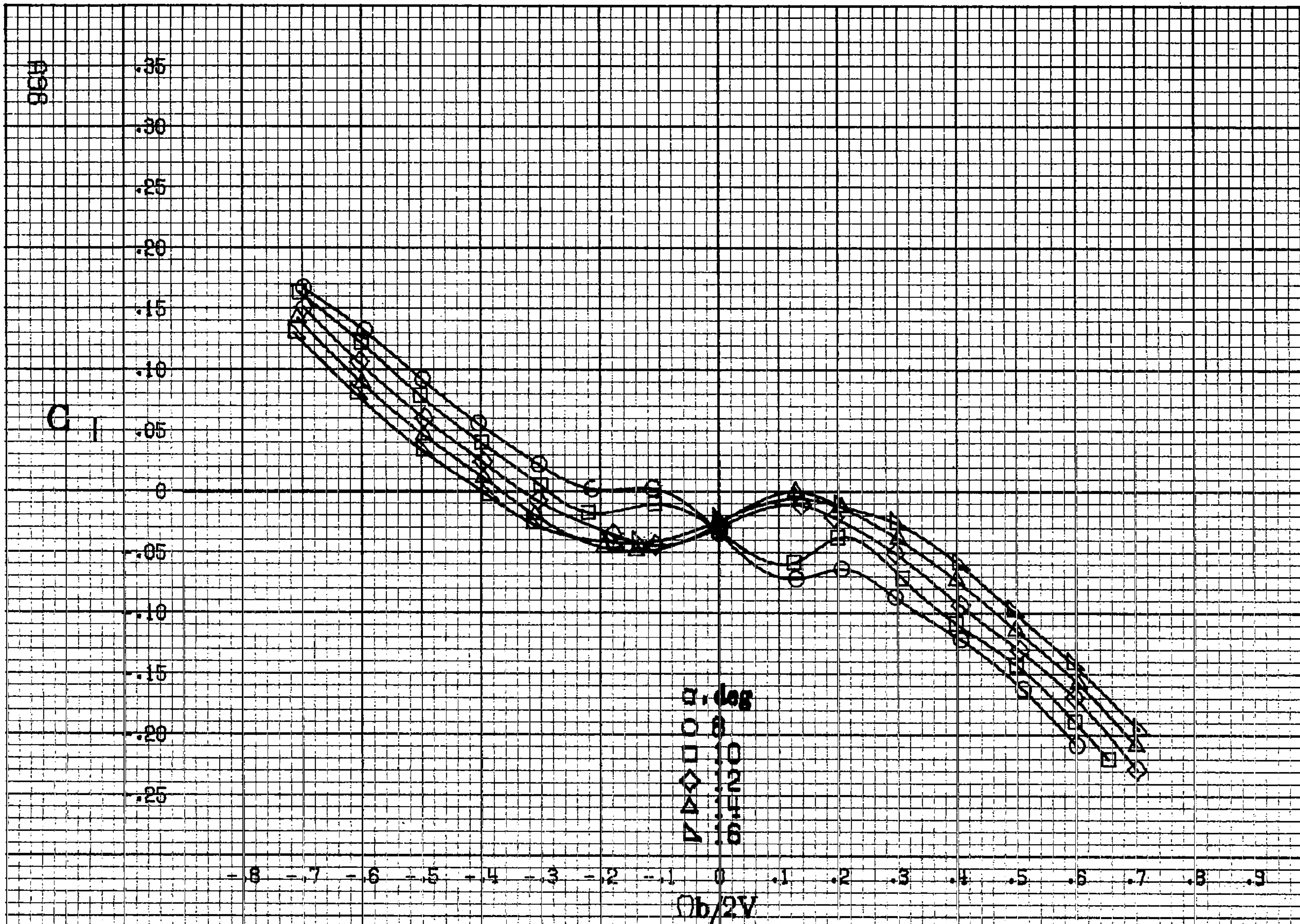

(a) $\alpha = 8$ to 16 deg, SR = 182.9 cm (72 in).

Figure A20.-Effect of rotation rate and angle of attack on rolling-moment coefficient for basic configuration. $\delta_e = -15°$, $\delta_a = 15.0°$, $\delta_r = -25°$, $\beta = 0°$.

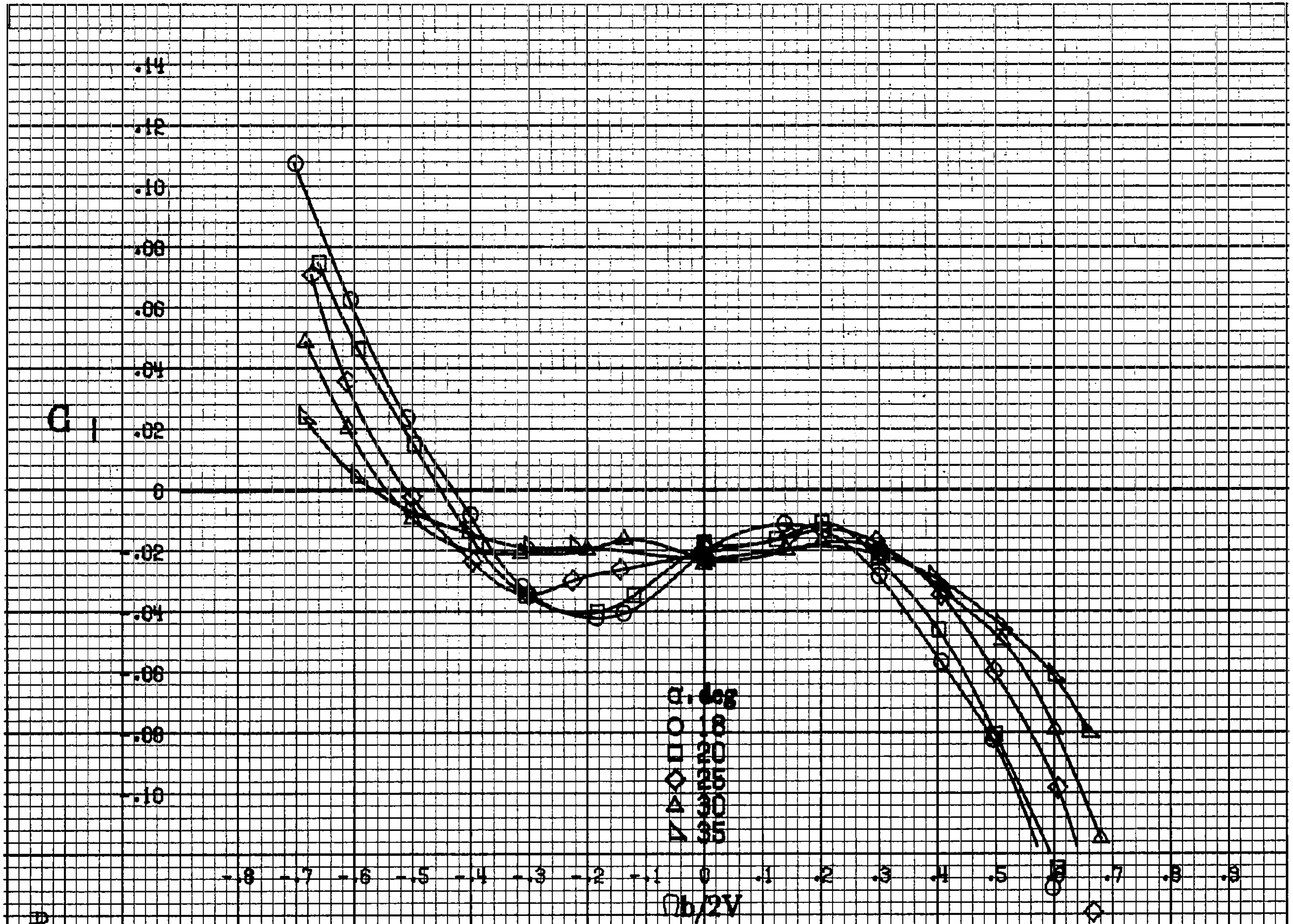

(b) α = 18 to 35 deg, SR = 182.9 cm (72 in).

Figure A20.-Continued.

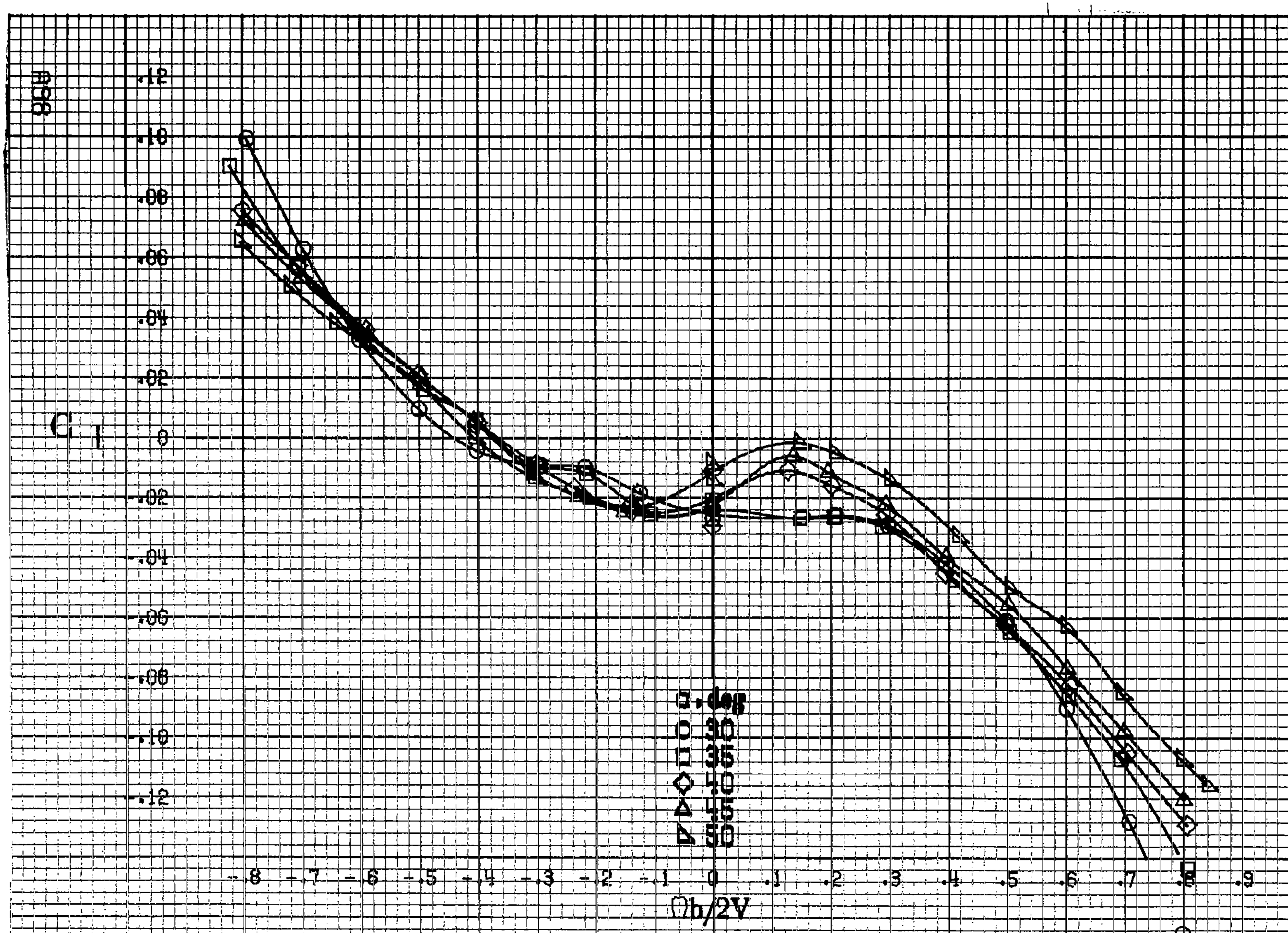

(c) α = 30 to 50 deg, SR = 0.
Figure A20.-Continued.

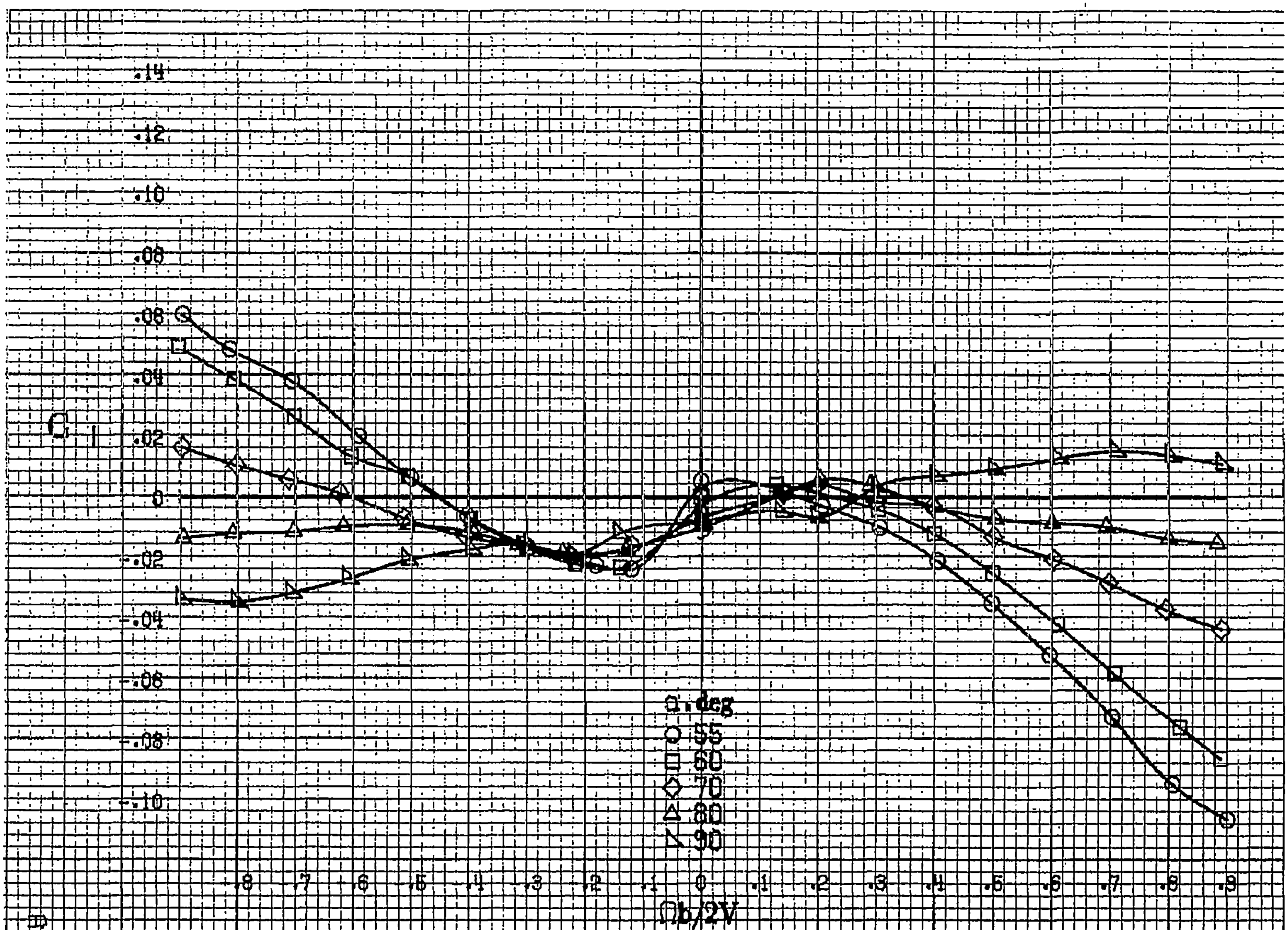

(d) α = 55 to 90 deg, SR = 0.
Figure A20.-Concluded.

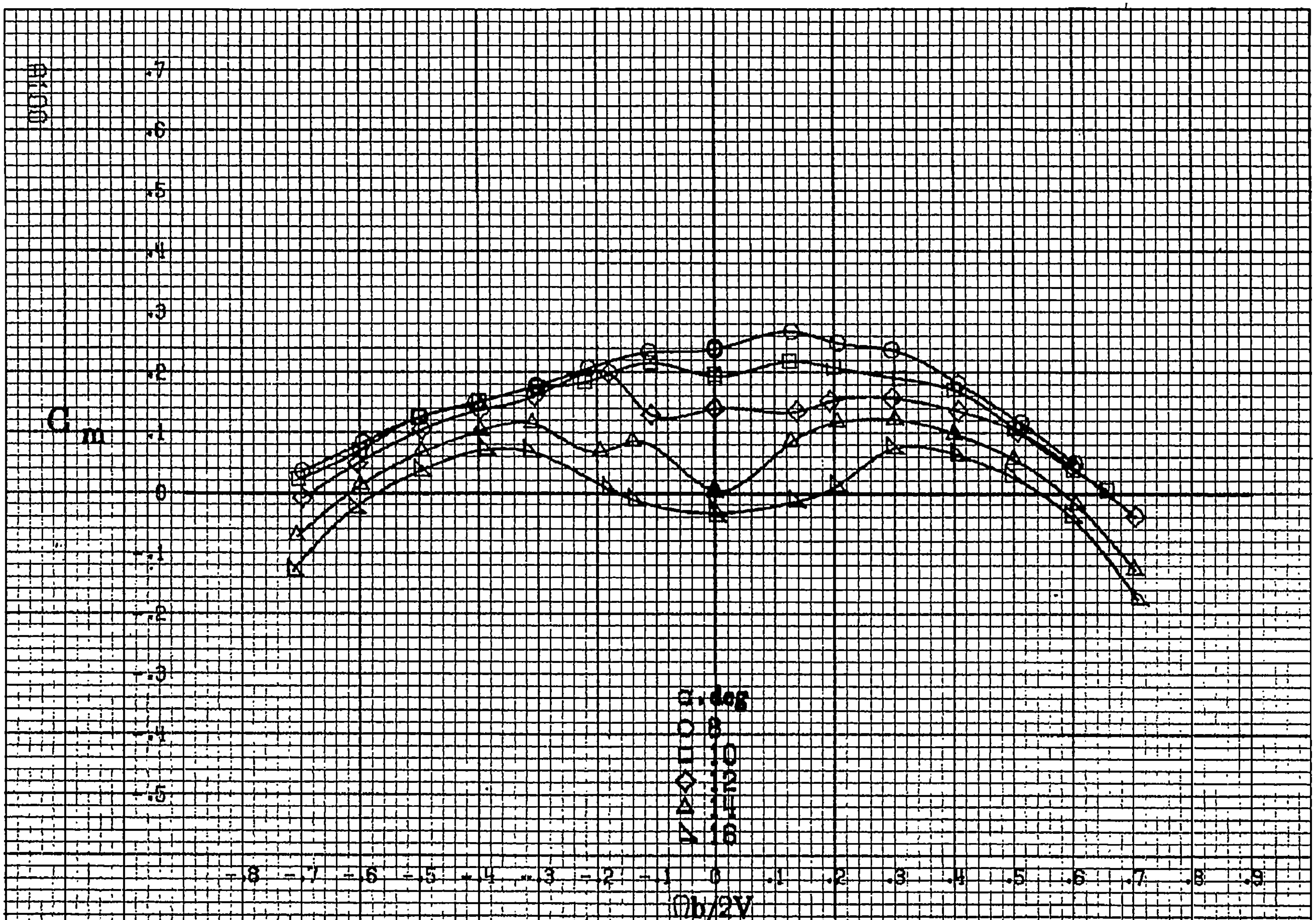

(a) $\alpha = 8$ to 16 deg, SR = 182.9 cm (72 in).

Figure A21.- Effect of rotation rate and angle of attack on pitching-moment coefficient for basic configuration. $\delta = -15^\circ$, $\delta = -15.0^\circ$, $\delta = -25^\circ$, $\beta = 0^\circ$.

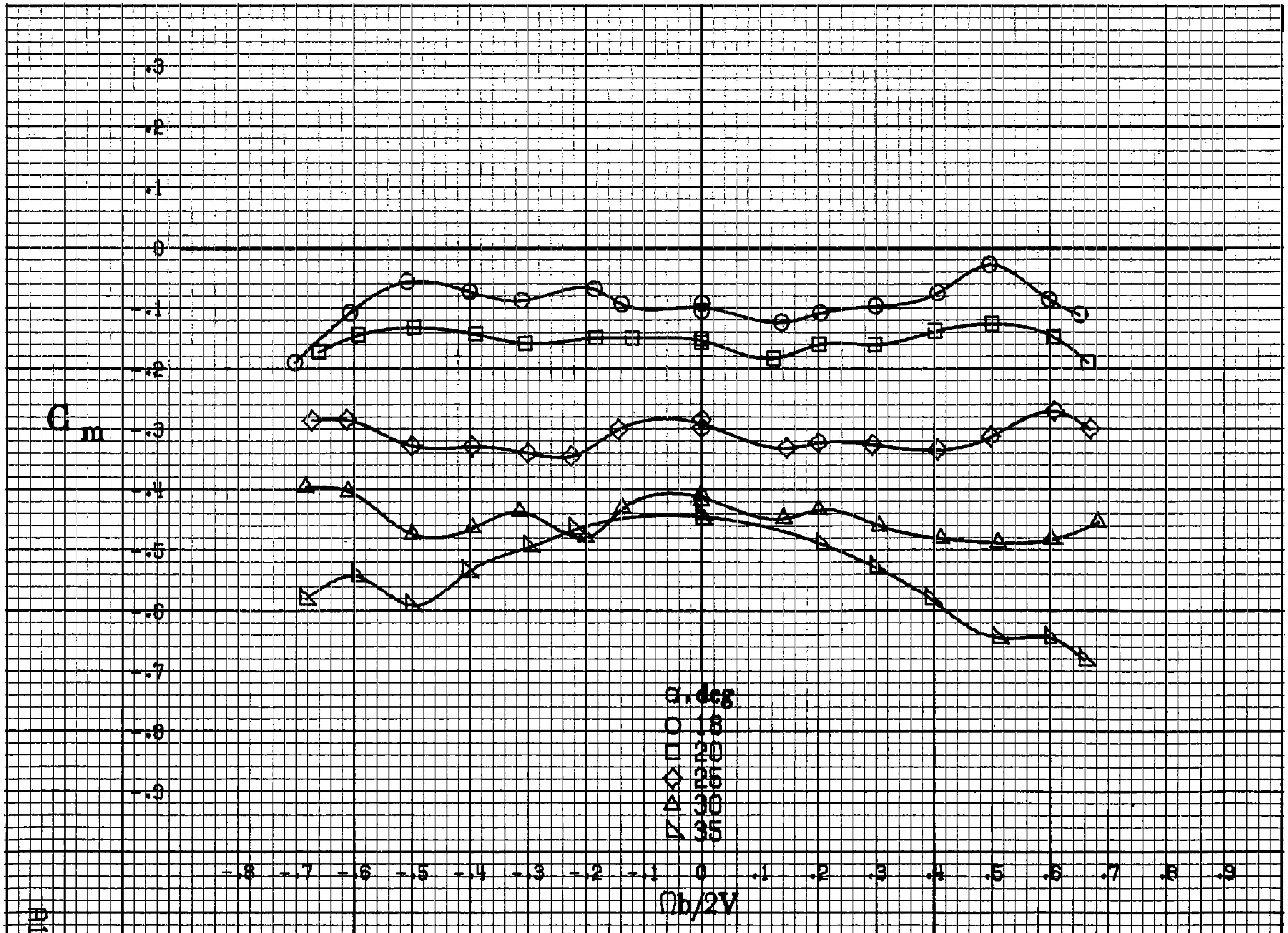

(b) α = 18 to 35 deg, SR = 182.9 cm (72 in).

Figure A21.-Continued.

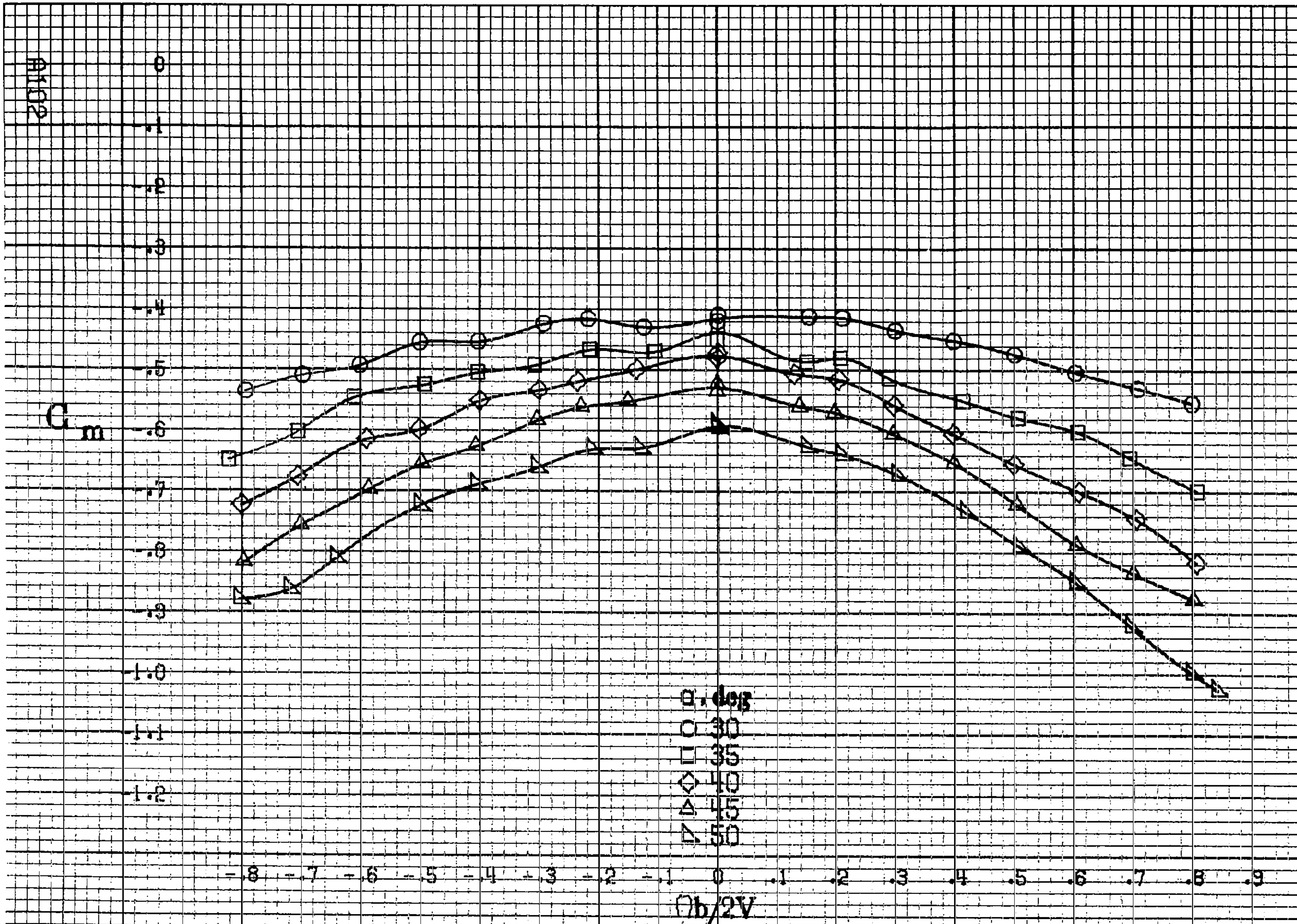

(c) α = 30 to 50 deg, SR = 0.

Figure A21.-Continued.

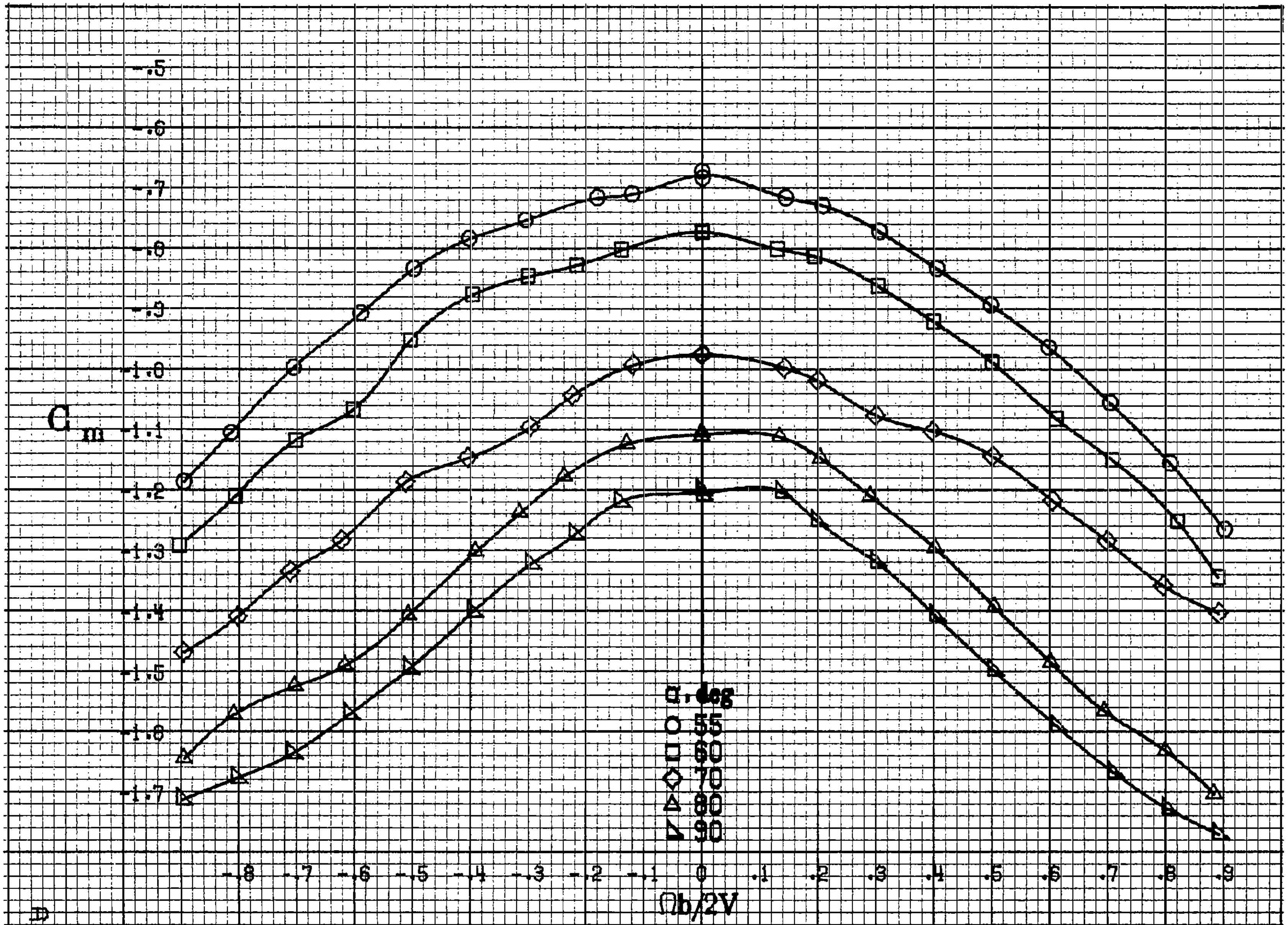

(d) α = 55 to 90 deg, SR = 0.

Figure A21.-Concluded.

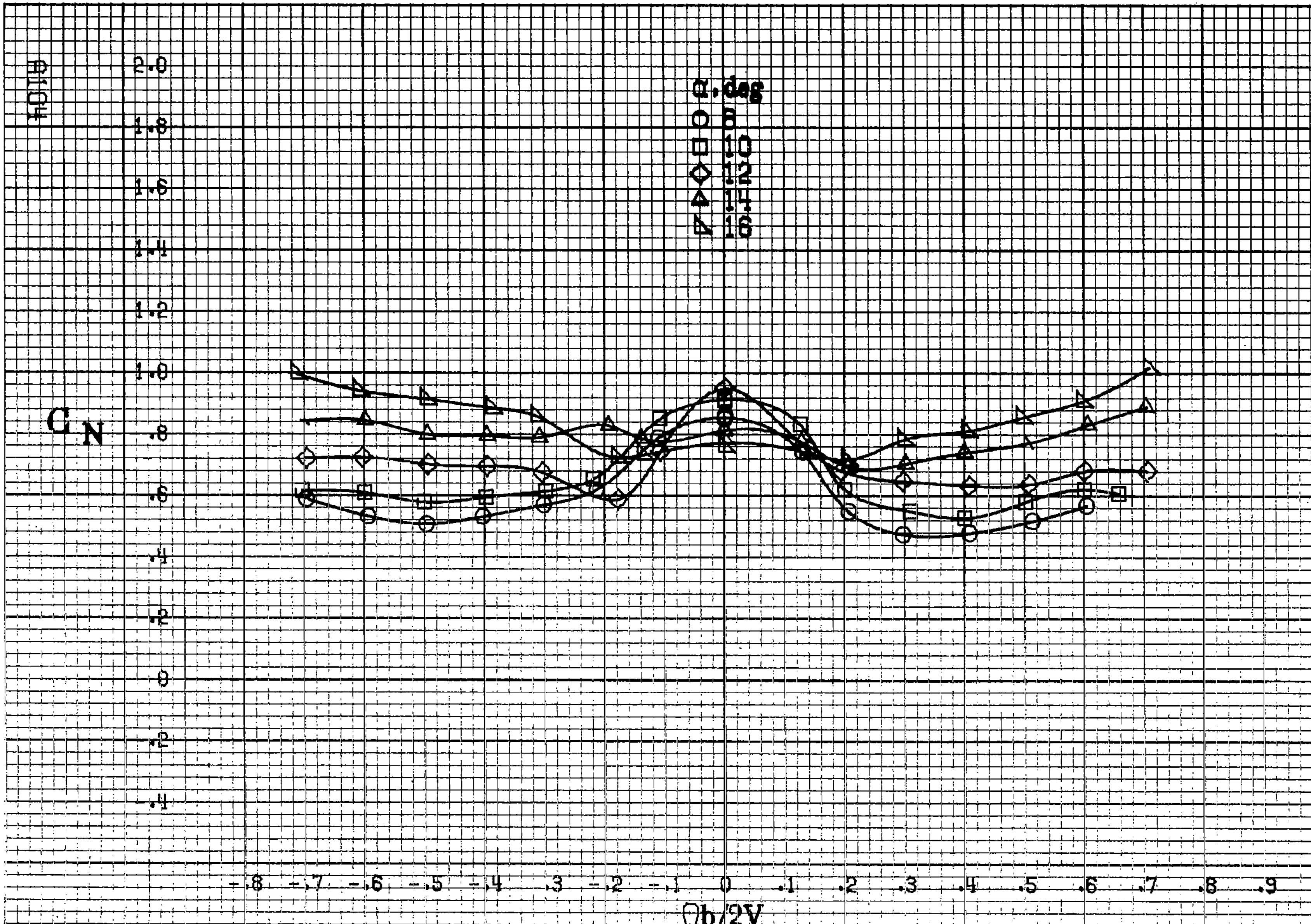

(a) $\alpha = 8$ to 16 deg, SR = 182.9 cm (72 in.).

Figure A22.-Effect of rotation rate and angle of attack on normal-force coefficient for basic configuration. $\delta_e = -15°$, $\delta_a = 15.0°$, $\delta_r = -25°$, $\beta = 0°$.

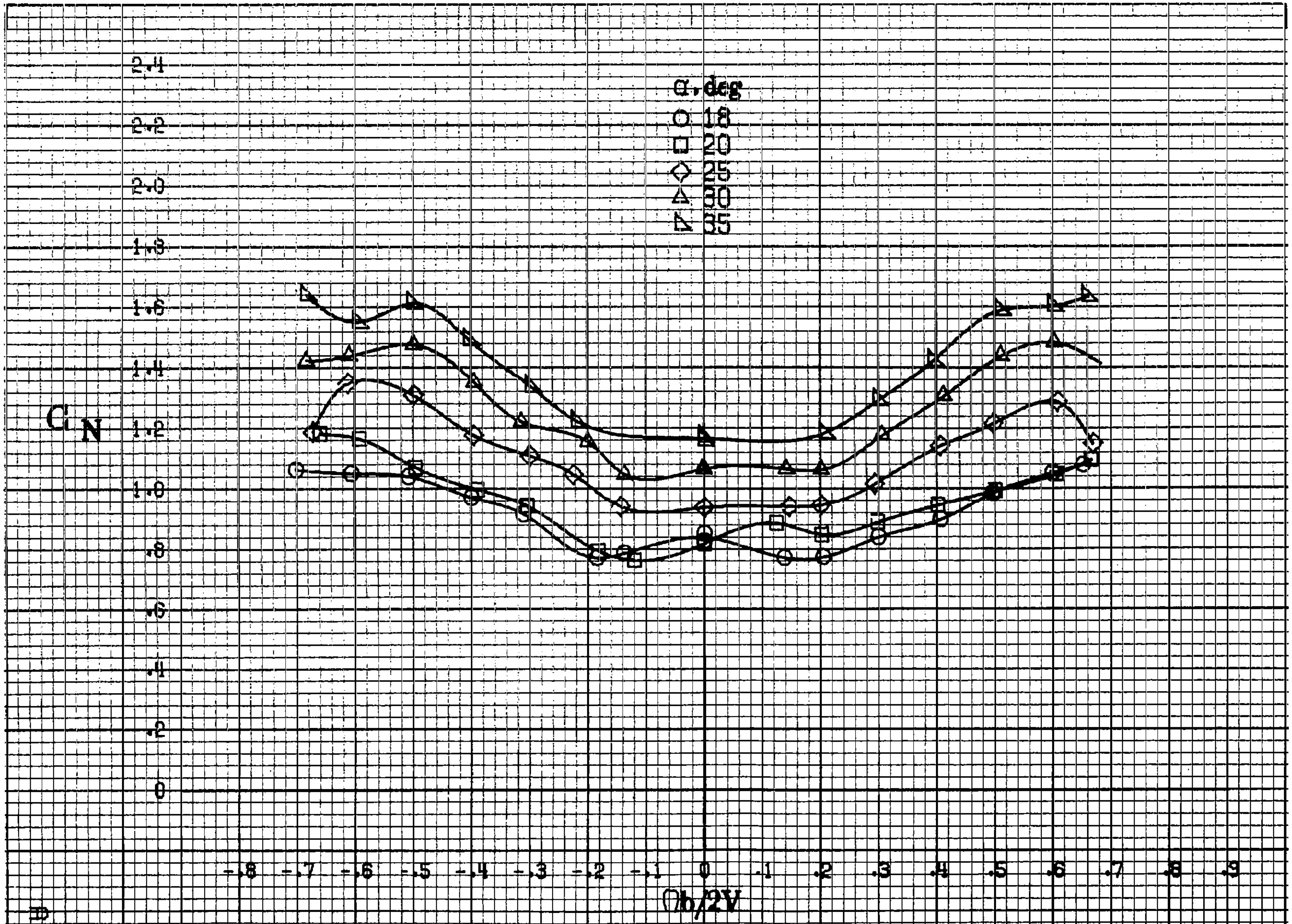

(b) α = 18 to 35 deg, SR = 182.9 cm (72 in).

Figure A22.- Continued.

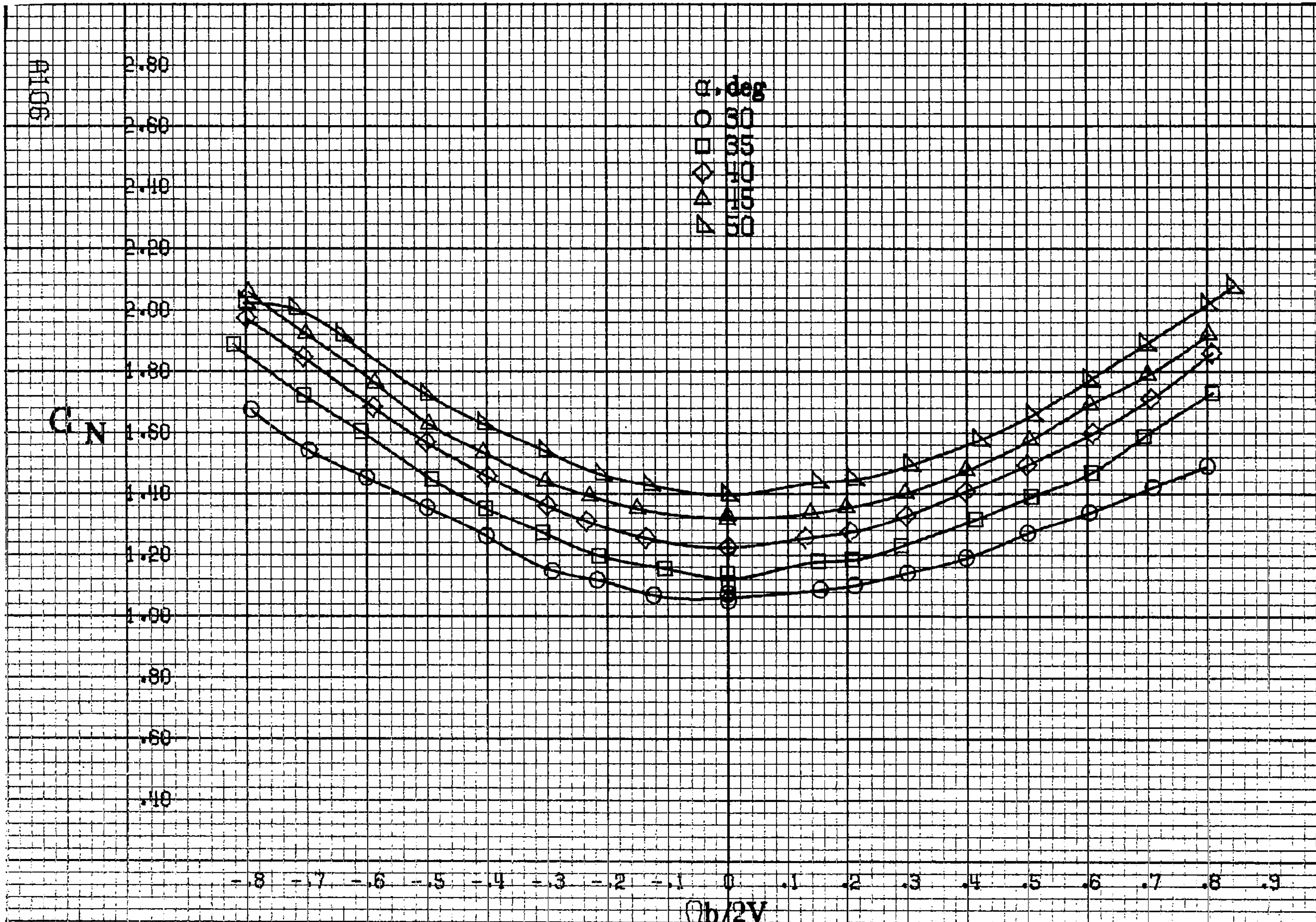

(c) α = 30 to 50 deg, SR = 0.

Figure A22.-Continued.

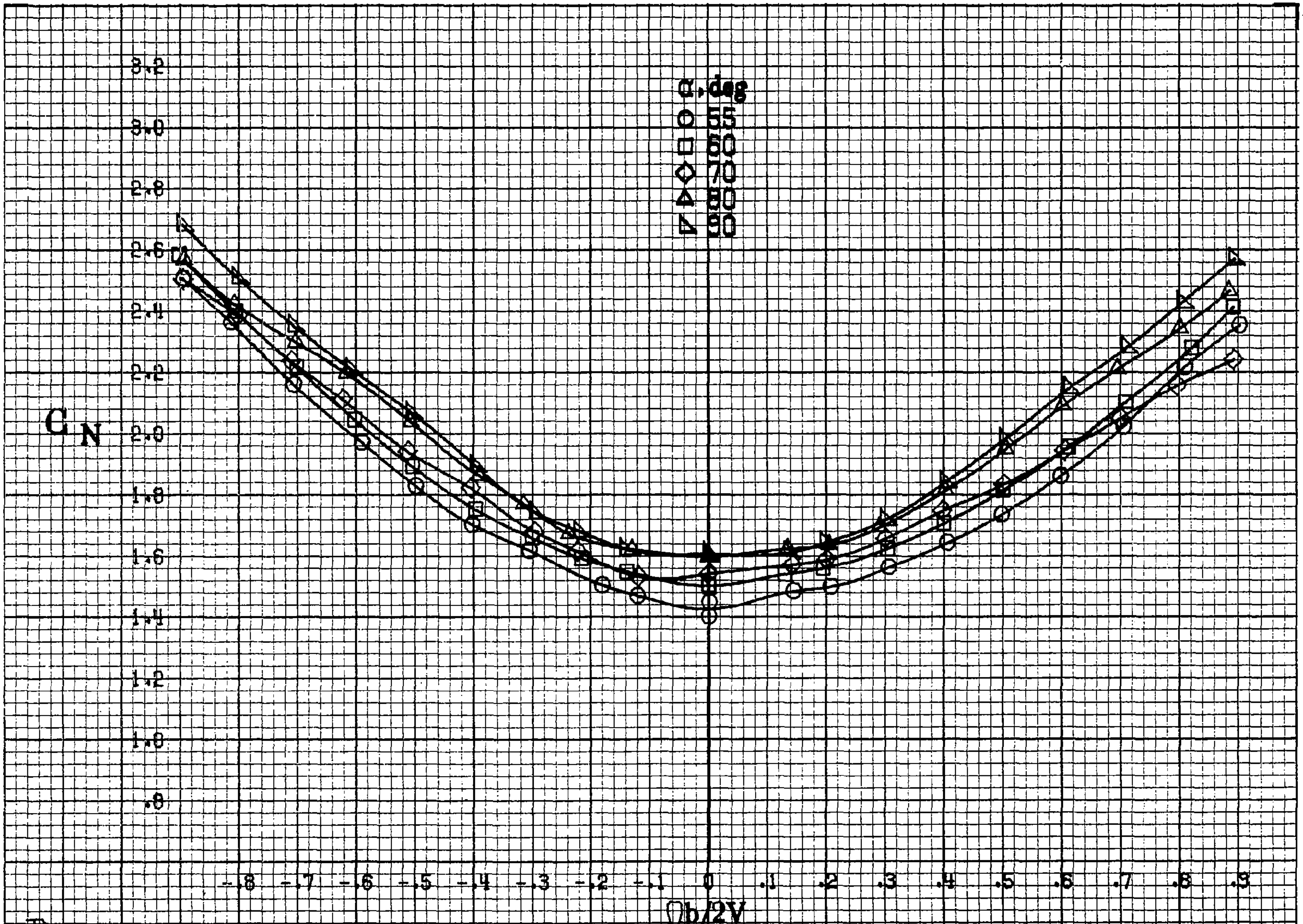

(d) α = 55 to 90 deg, SR = 0.
Figure A22.-Concluded.

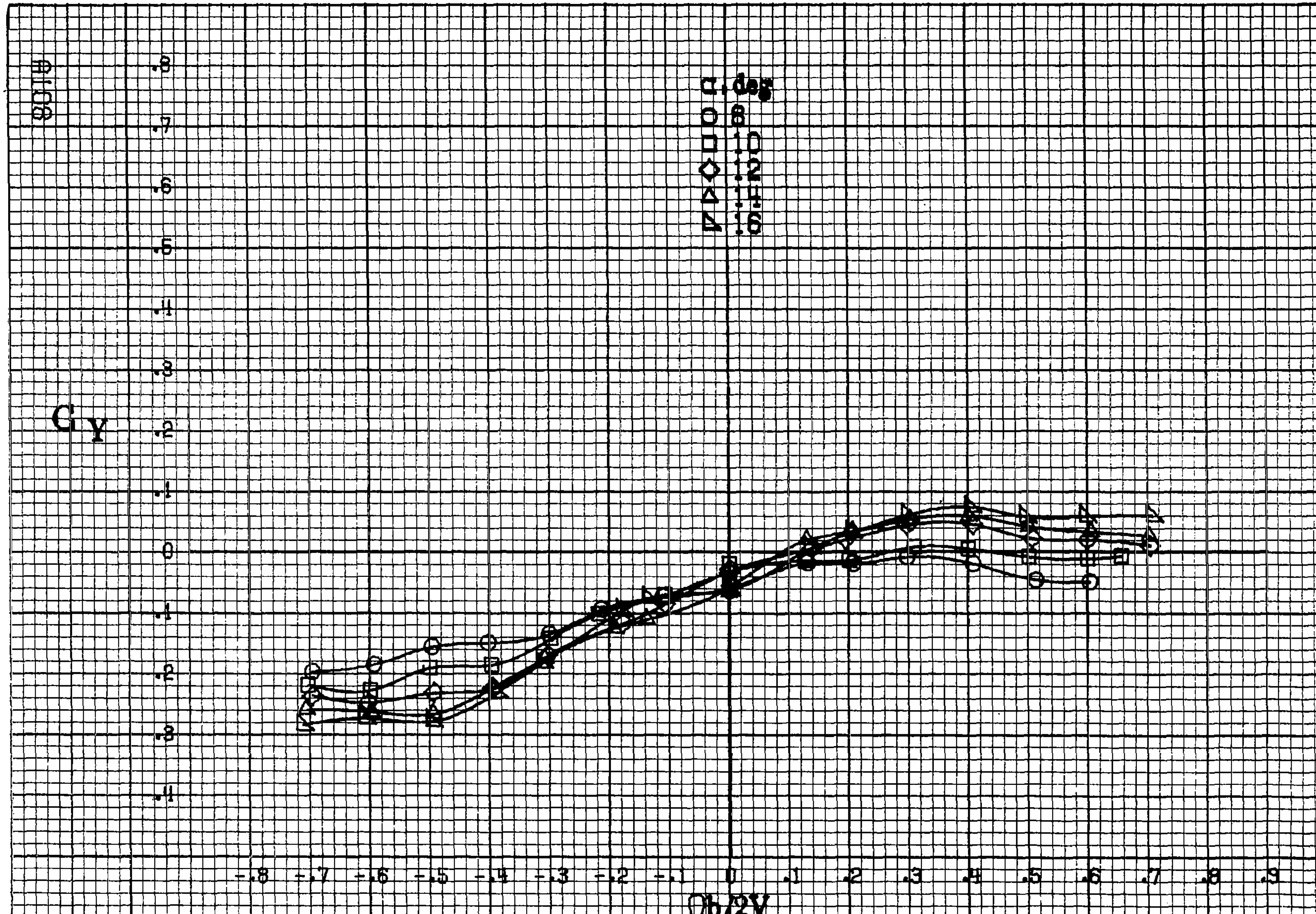

(a) α = 8 to 16 deg, SR = 182.9 cm (72 in).

Figure A23.- Effect of rotation rate and angle of attack on side-force coefficient for basic configuration. $\delta_e = -15^\circ$, $\delta_a = 15.0^\circ$, $\delta_r = -25^\circ$, $\beta = 0^\circ$.

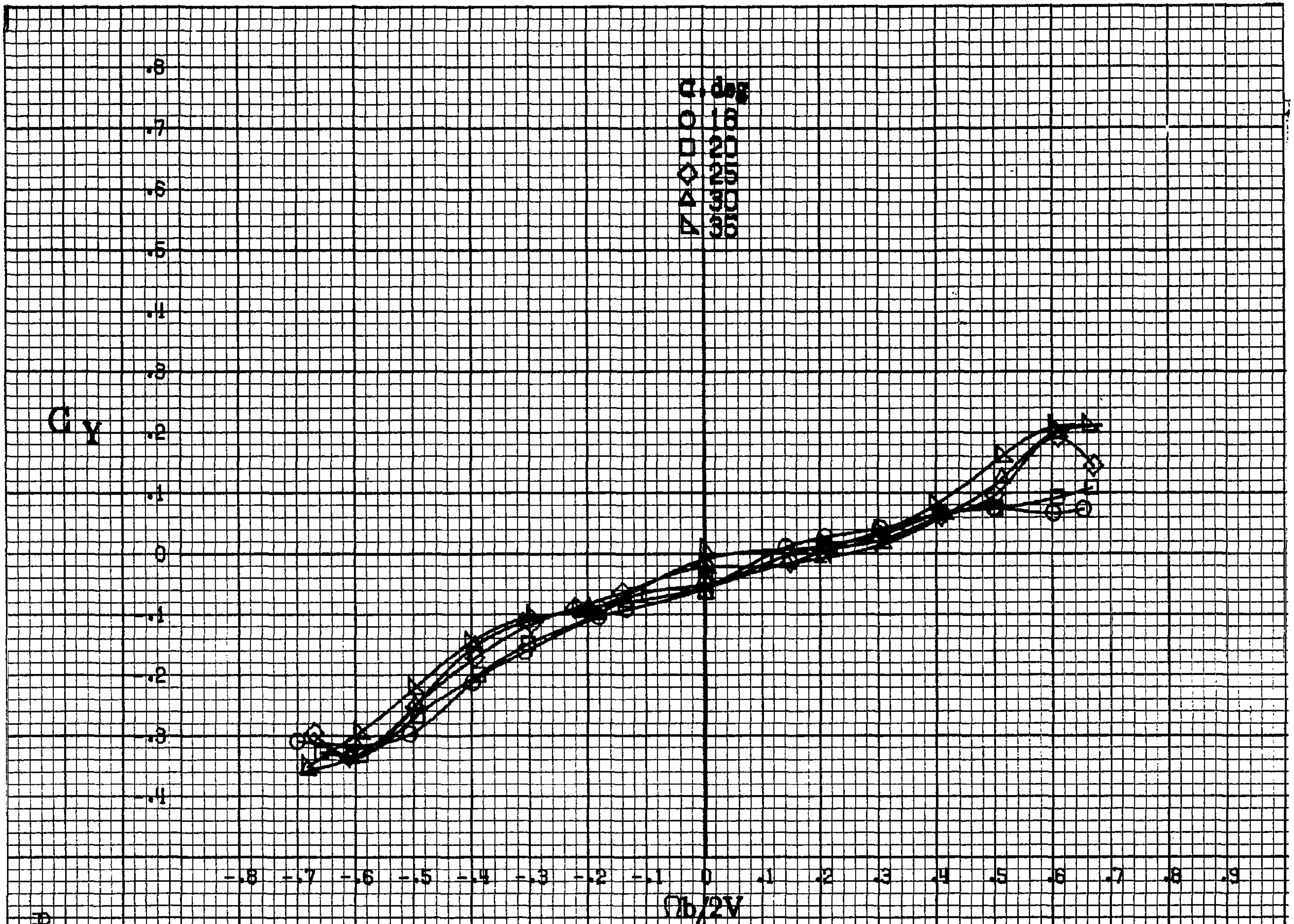

(b) α = 18 to 35 deg, SR = 182.9 cm (72 in).

Figure A28.-Continued.

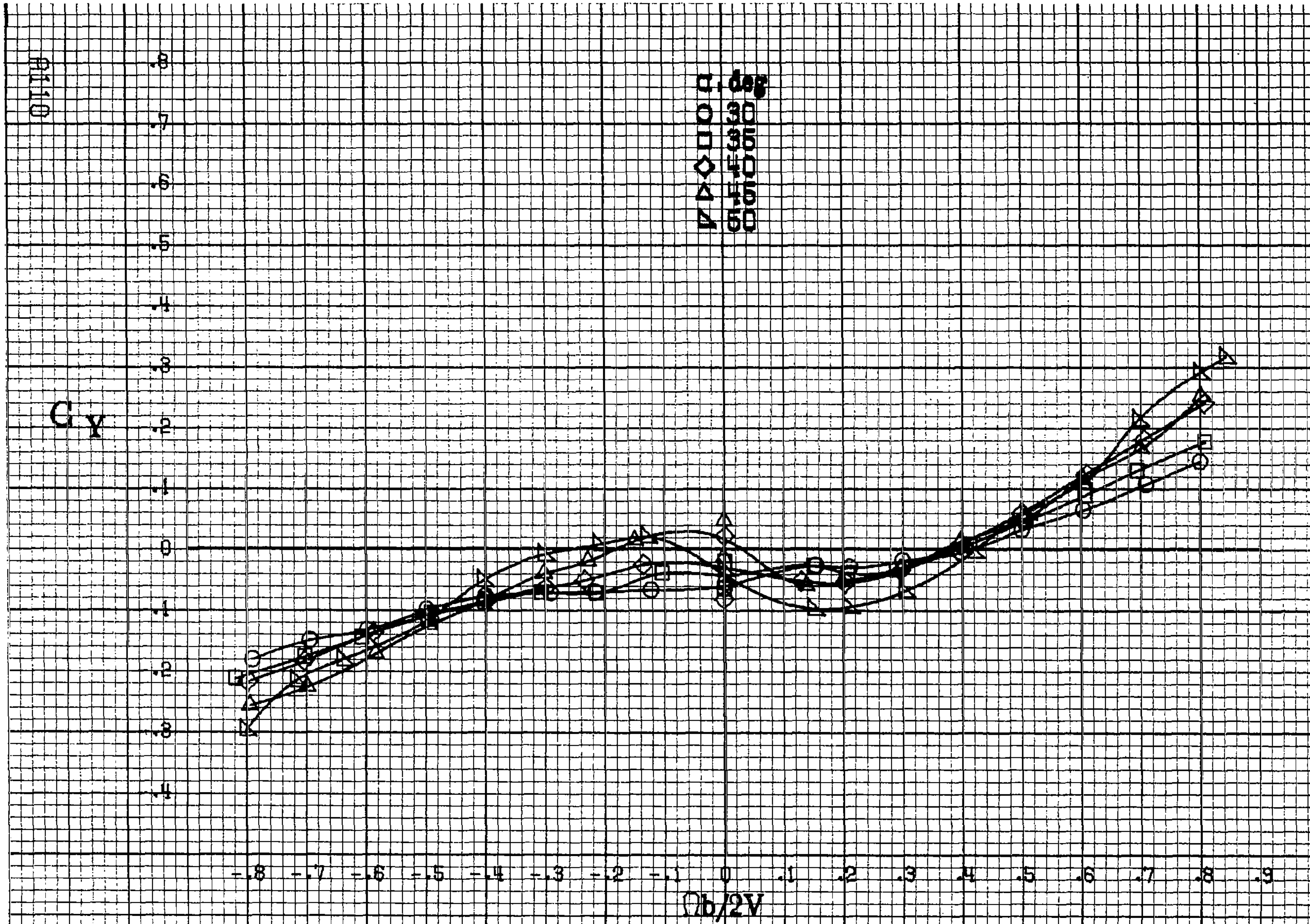

(c) α = 30 to 50 deg, SR = 0.

Figure A28.-Continued.

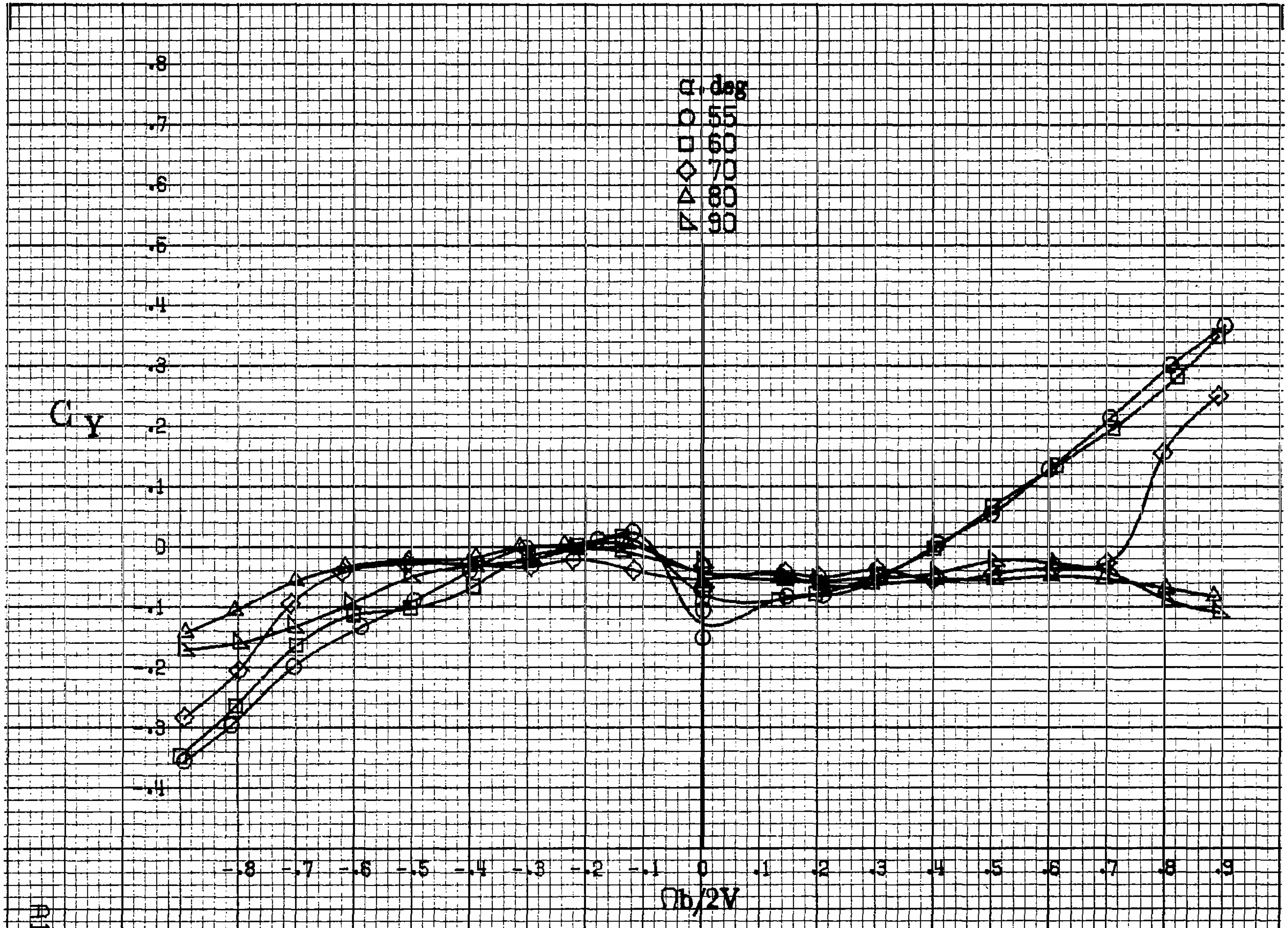

(d) α = 55 to 90 deg, SR = 0.

Figure A23.-Concluded.

A112

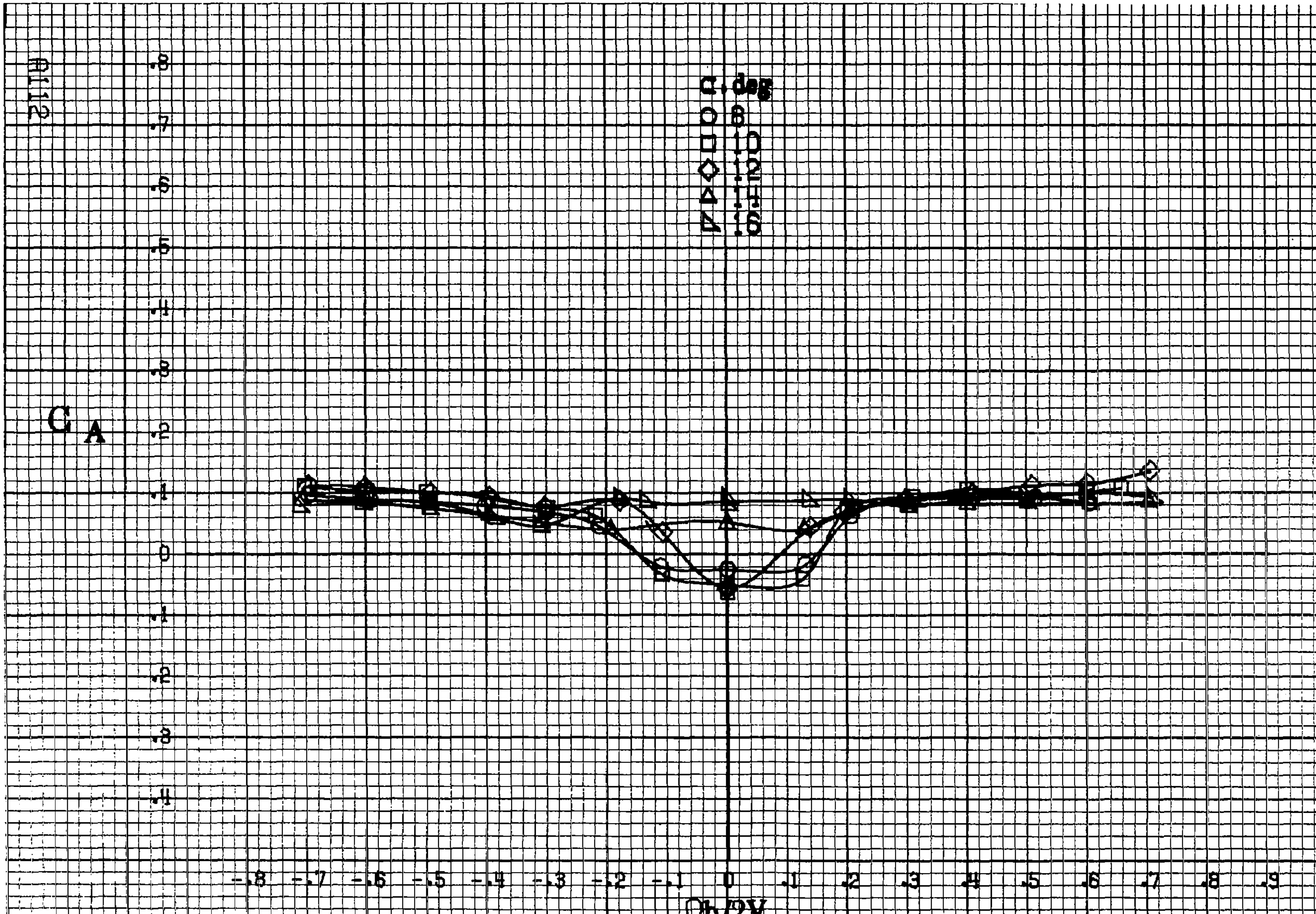

(a) $\alpha = 8$ to 16 deg, $SR = 182.9$ cm (72 in).

Figure A24.-Effect of rotation rate and angle of attack on axial-force coefficient for basic configuration. $\delta_e = -15^\circ$, $\delta_a = 15.0^\circ$, $\delta_r = -25^\circ$, $\beta = 0^\circ$.

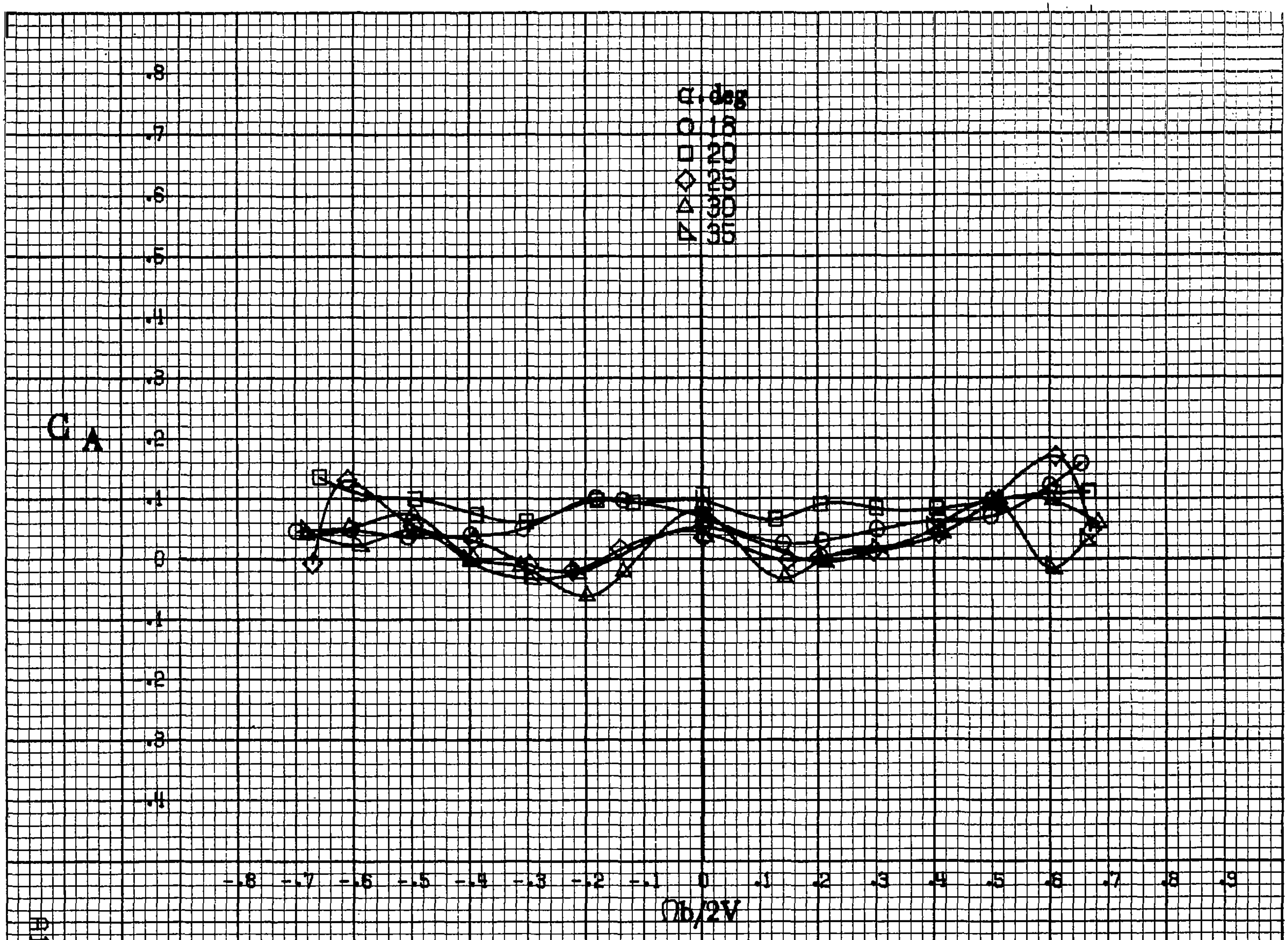

(b) α = 18 to 35 deg, SR = 182.9 cm (72 in).

Figure A24.-Continued.

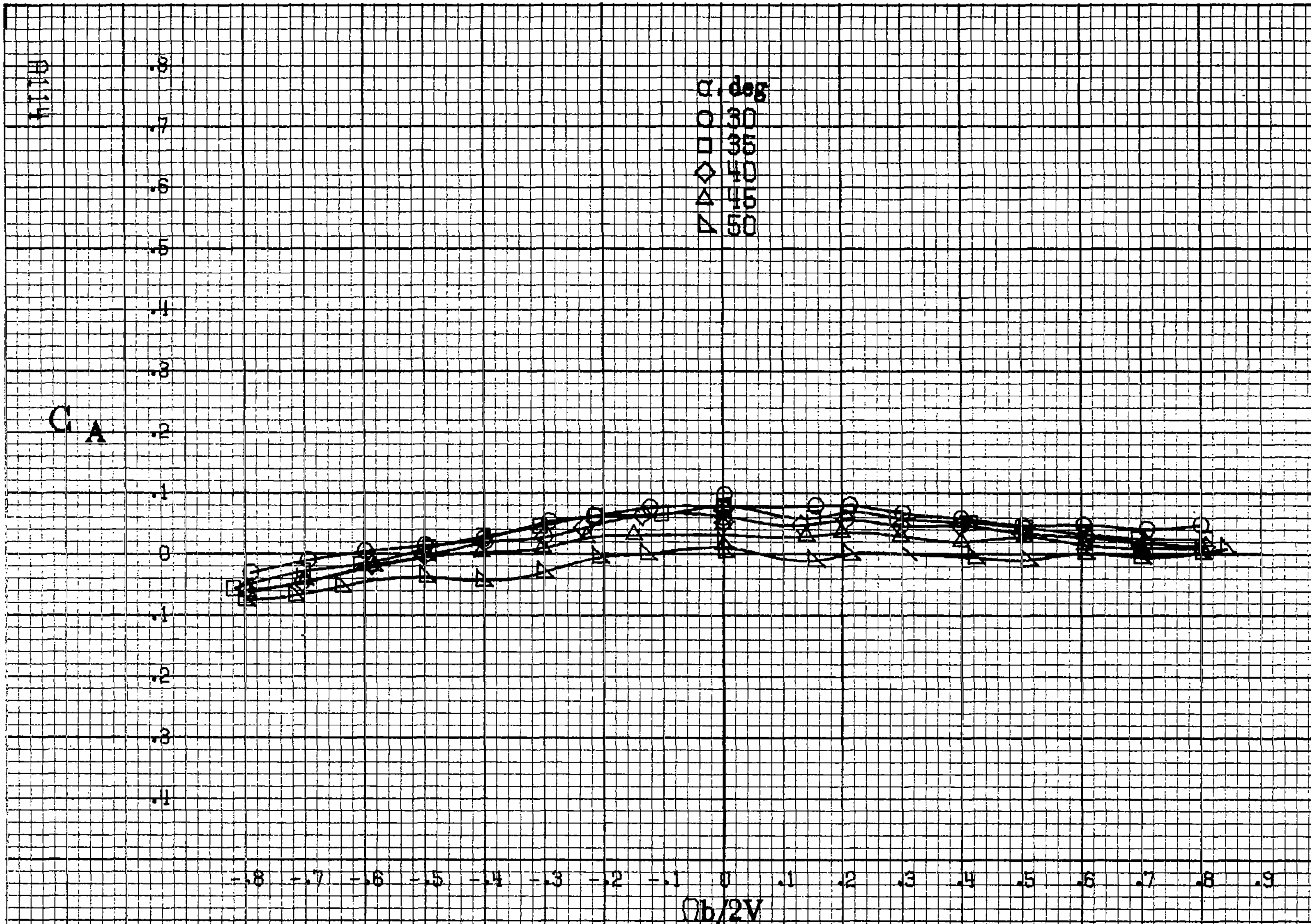

(c) α = 30 to 50 deg, SR = 0.

Figure A24.-Continued.

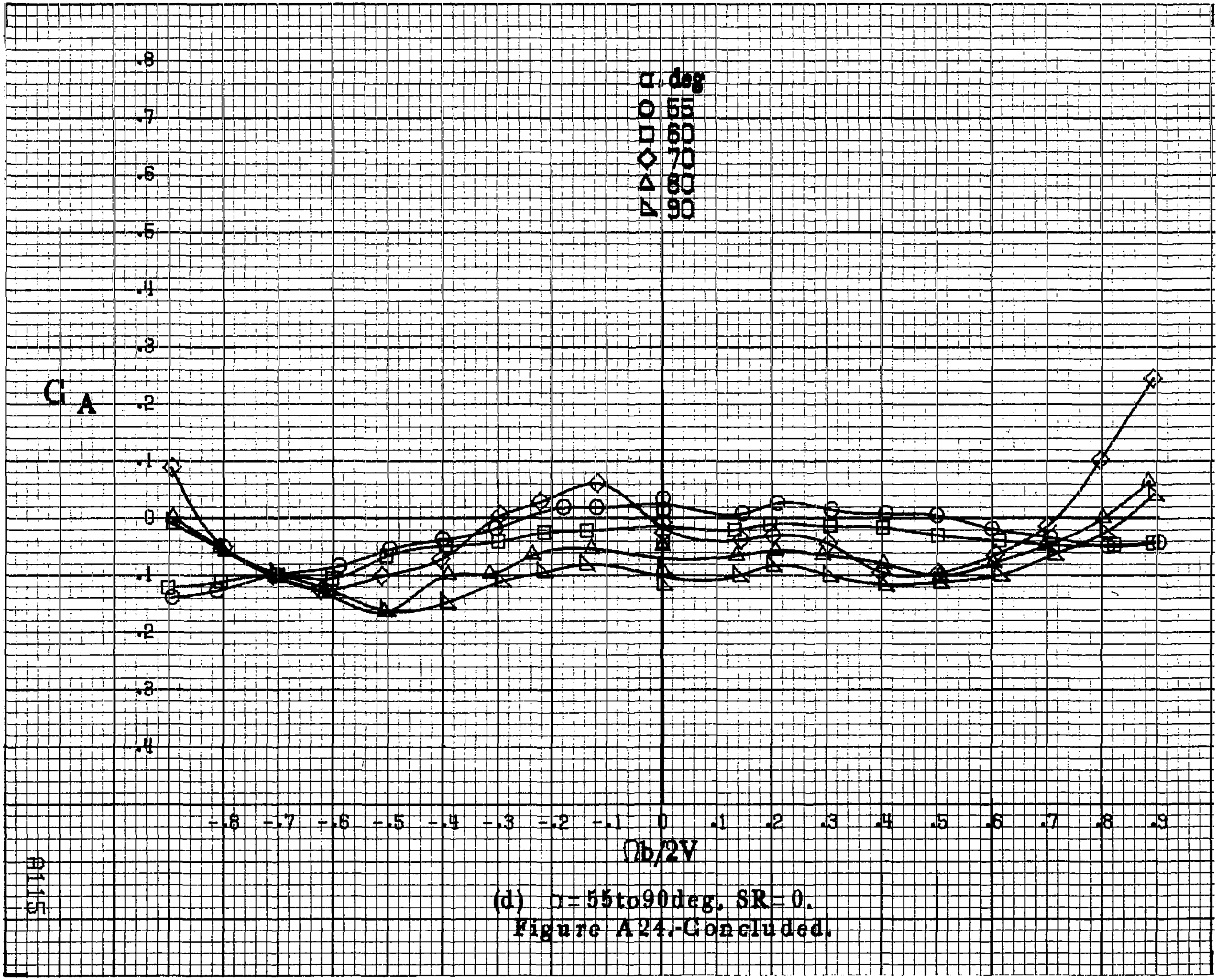

(d) β = 55 to 90 deg, SR = 0.

Figure A24.-Concluded.

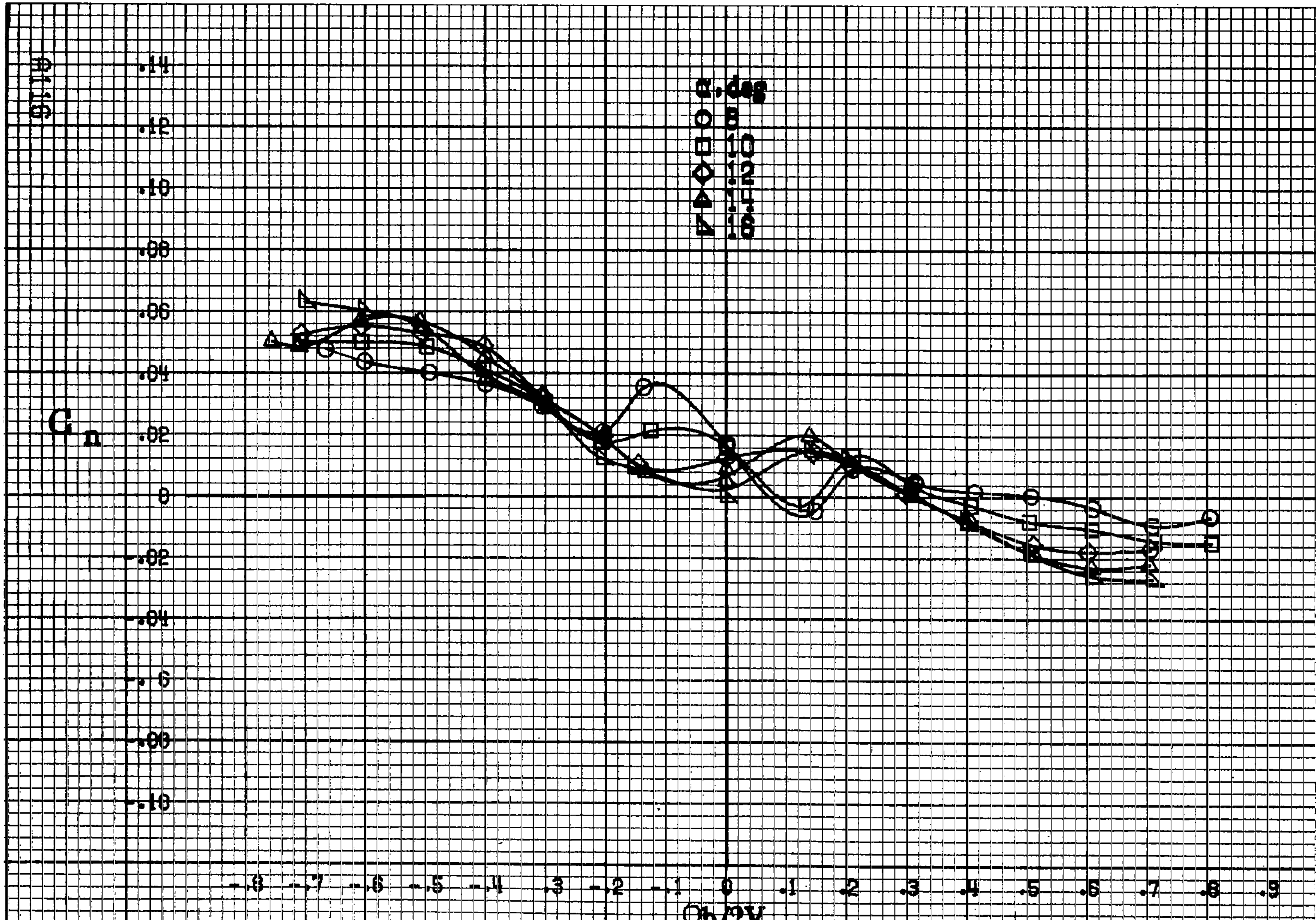

(a) $\alpha = 8$ to 16 deg, SR = 182.9 cm (72 in).

Figure A25.-Effect of rotation rate and angle of attack on yawing-moment coefficient for basic configuration. $\delta_e = -15°$, $\delta_a = -15.0°$, $\delta_r = -25°$. $\beta = 0°$.

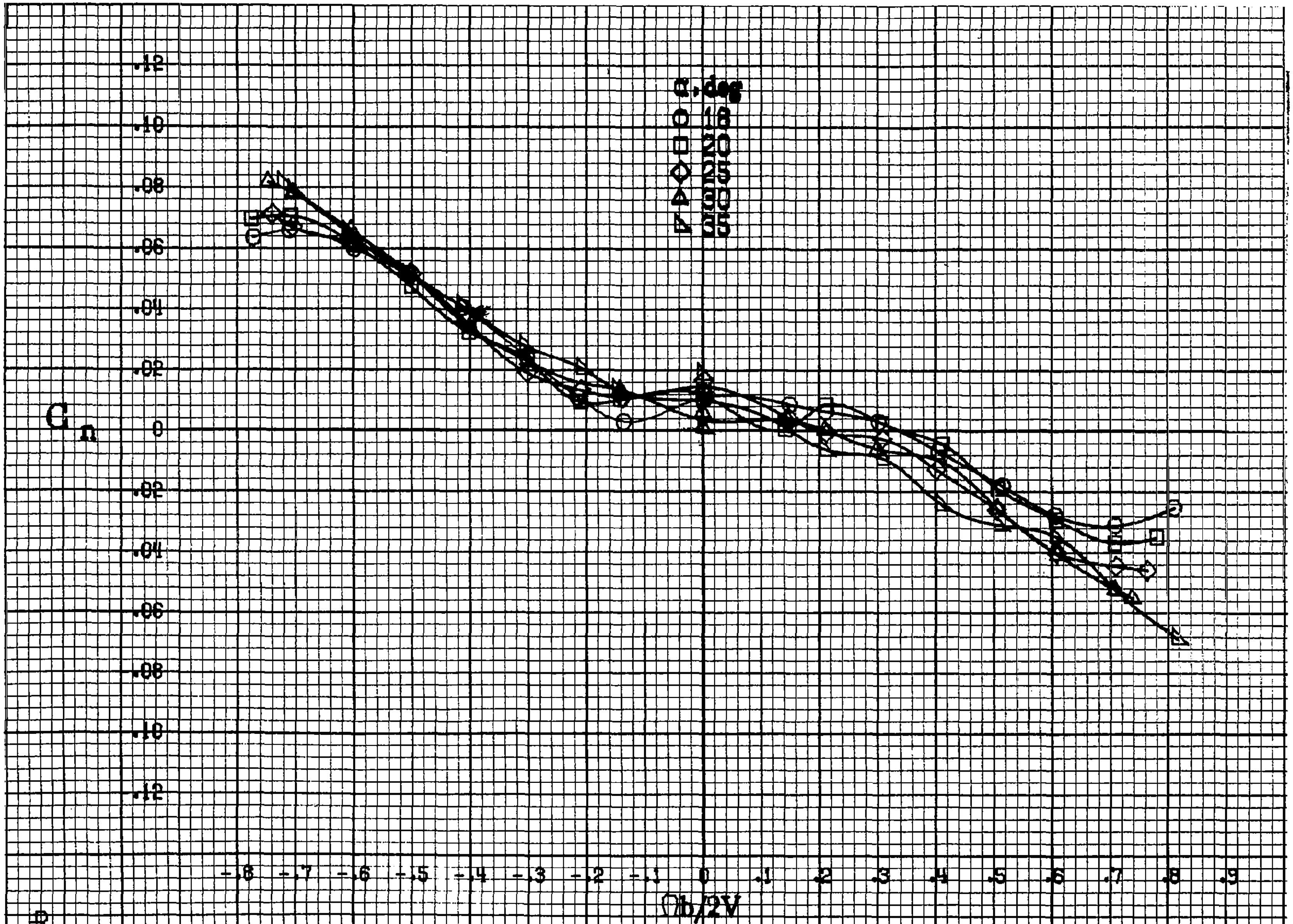

(b) α = 18 to 35 deg, SR = 182.9 cm (72 in).

Figure A25.-Continued.

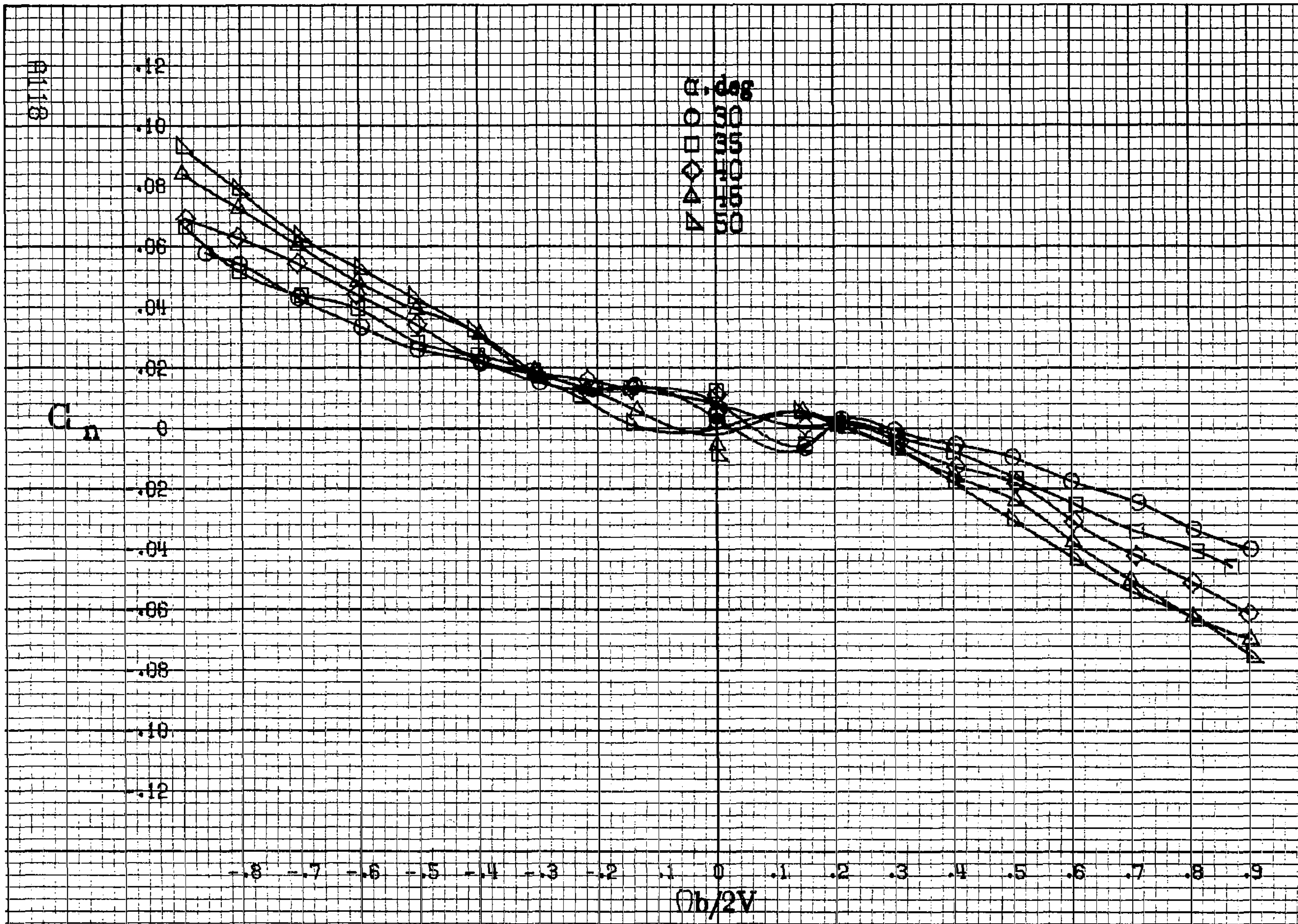

(c) α = 30to50deg, SR = 0.

Figure A25.-Continued.

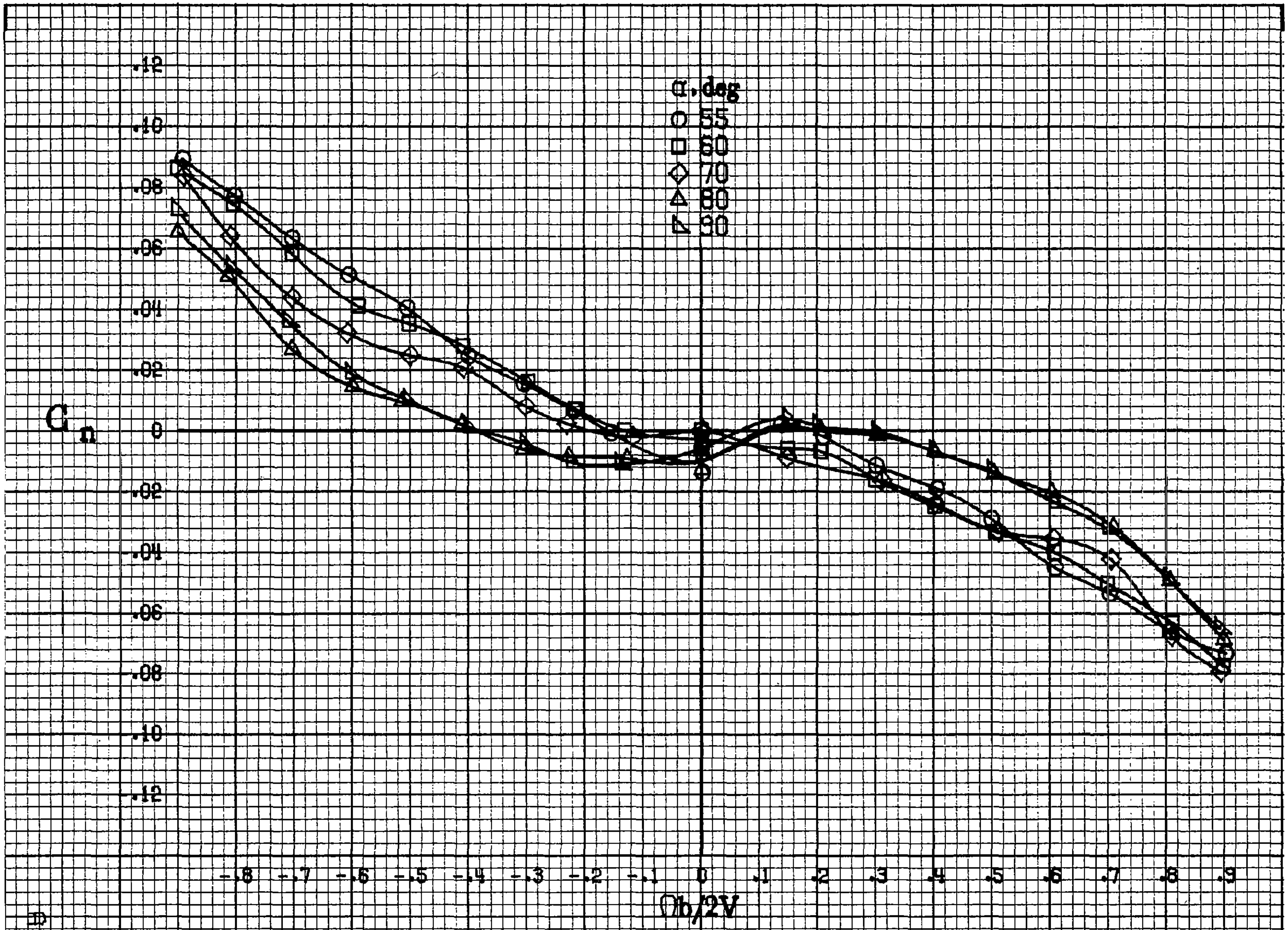

(d) α = 55 to 90 deg, SR = 0.
Figure A25.-Concluded.

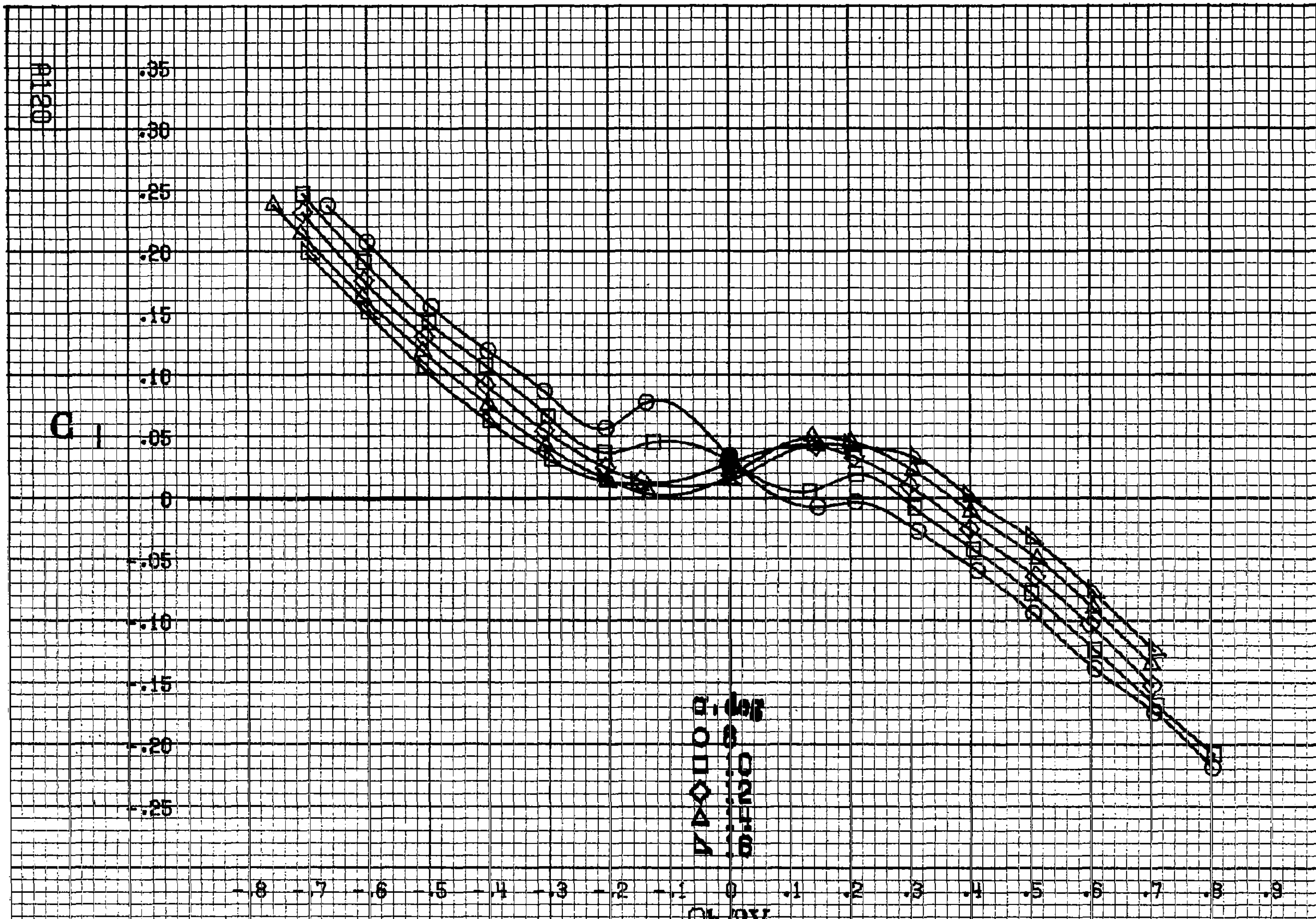

(a) α = 8 to 16 deg, SR = 182.9 cm (72 in).

Figure A26.- Effect of rotation rate and angle of attack on rolling-moment coefficient for basic configuration. $\delta_e = -15^\circ$, $\delta_a = -15.0^\circ$, $\delta_r = -25^\circ$, $\beta = 0^\circ$.

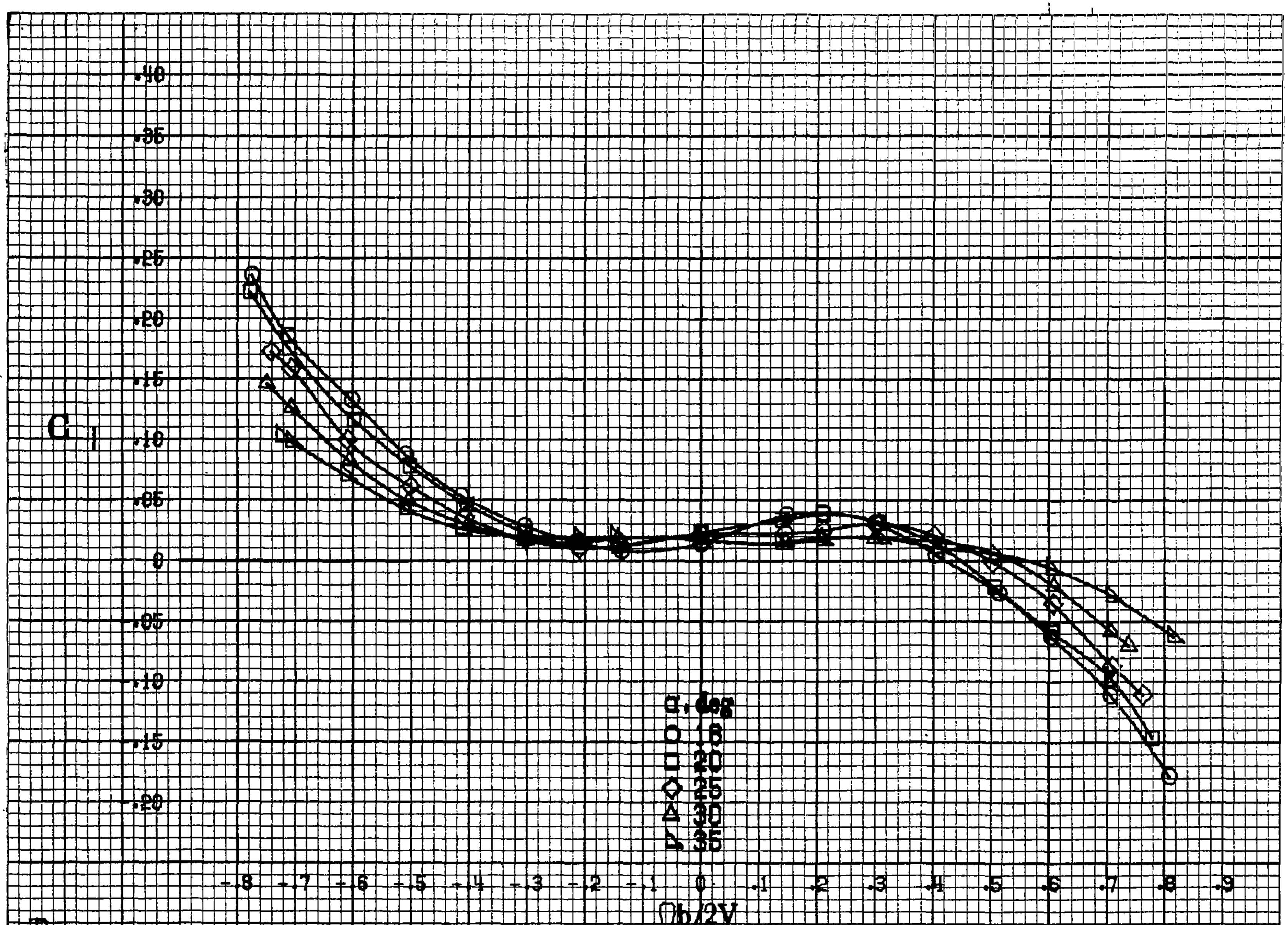

(b) α = 18 to 35 deg, SR = 182.9 cm (72 in).

Figure A26.-Continued.

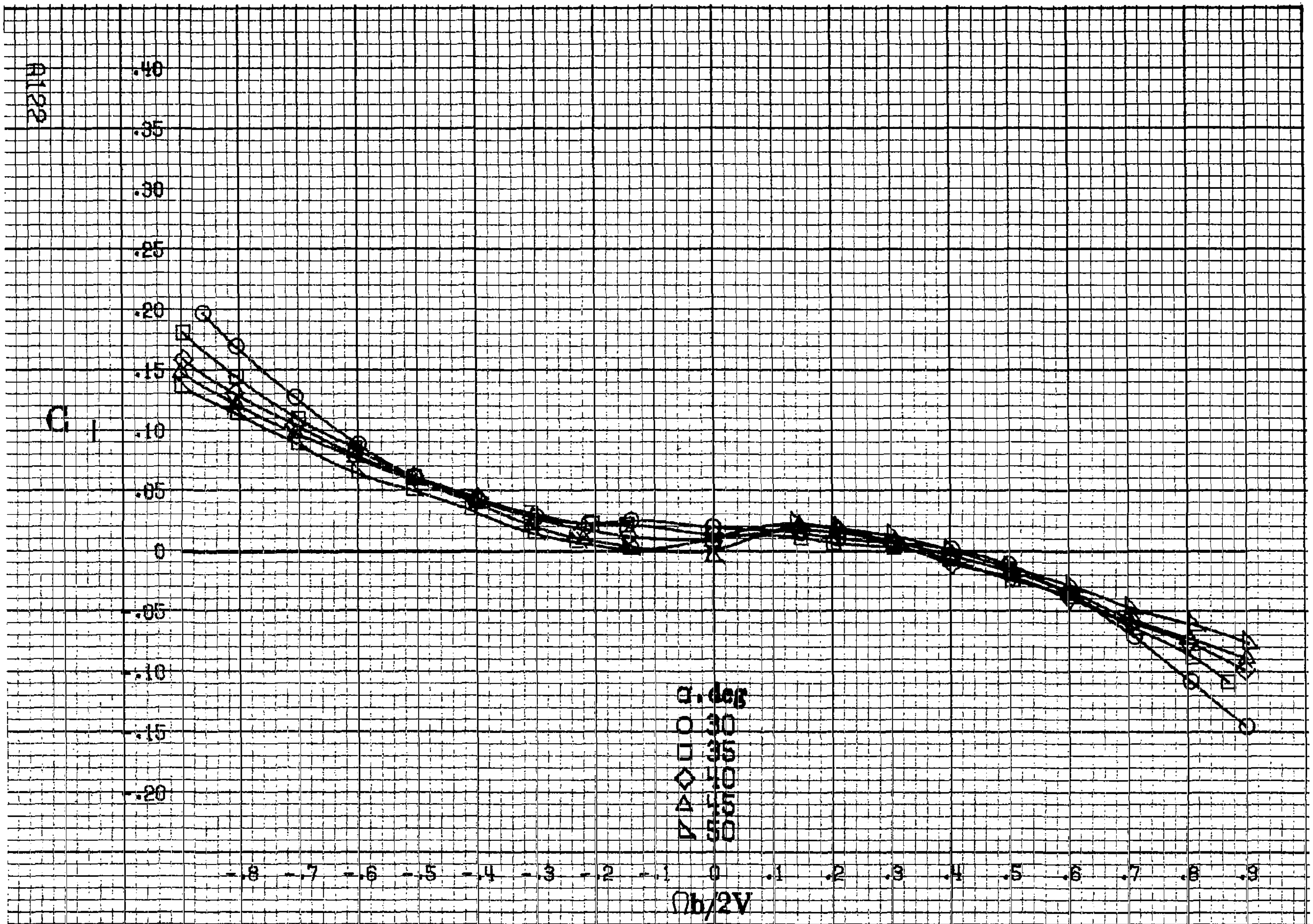

(c) α = 30 to 50 deg, SR = 0.

Figure A26.-Continued.

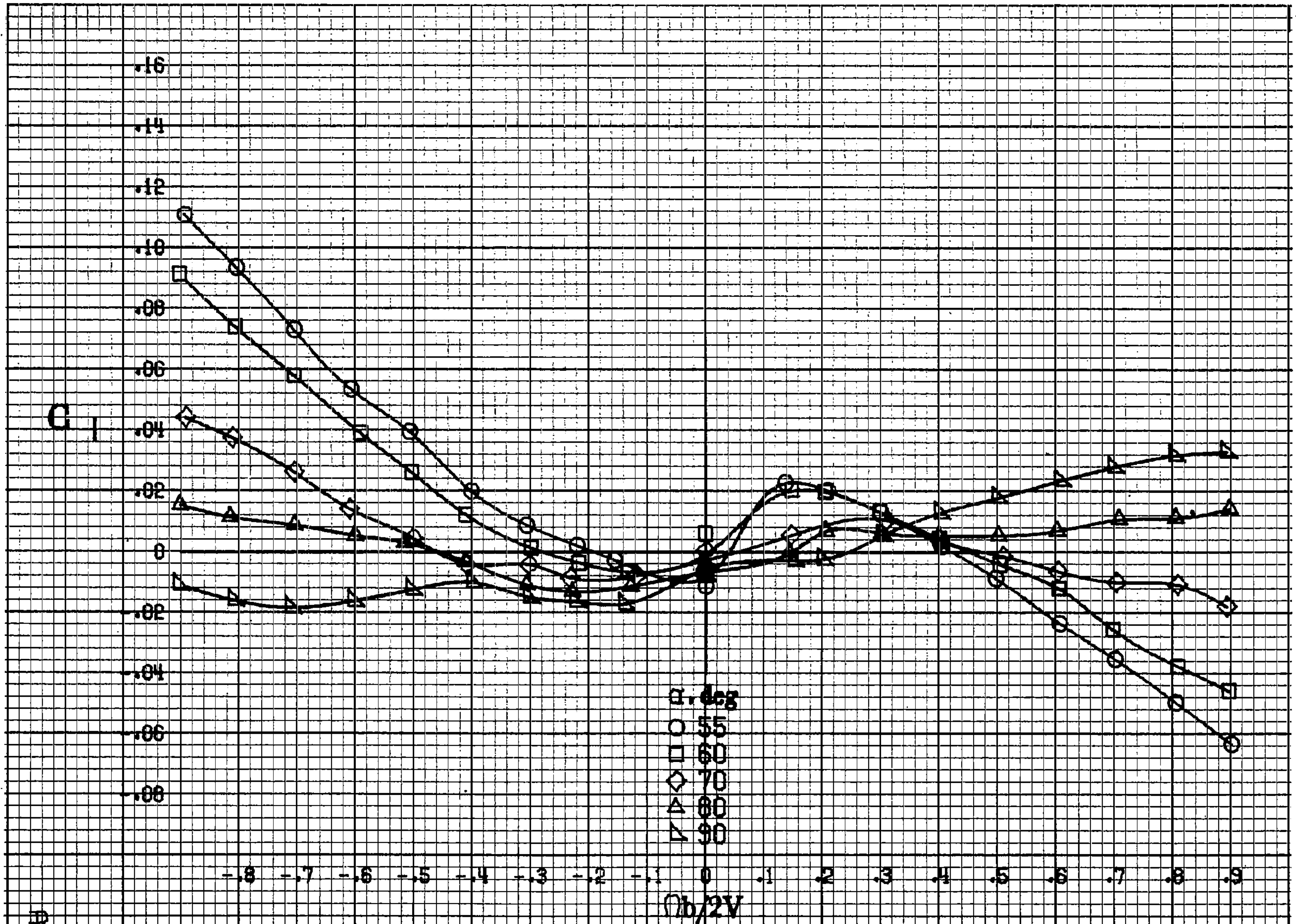

(d) α = 55 to 90 deg, SR = 0.
Figure A26.-Concluded.

A123

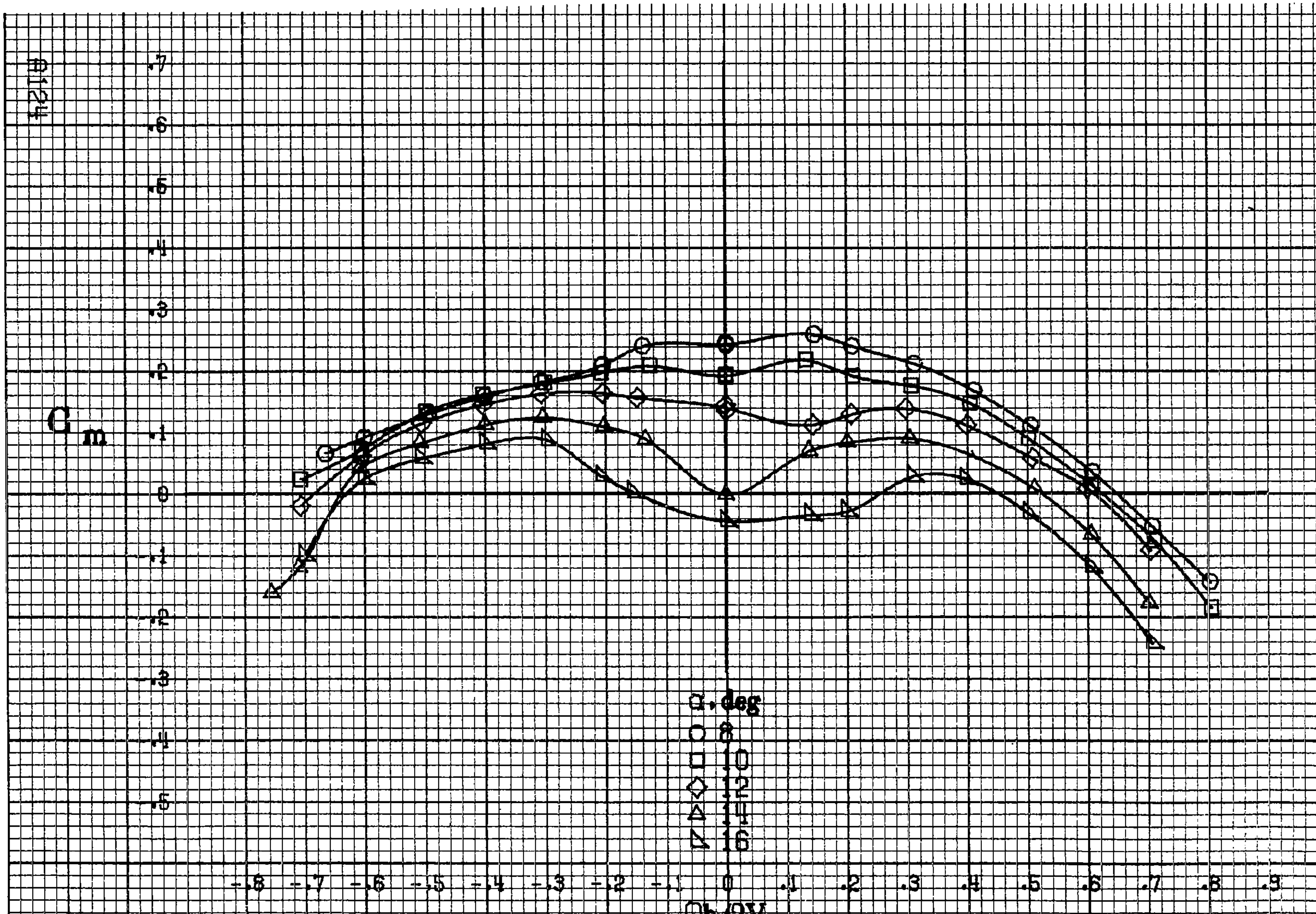

(a) α = 8 to 16 deg, SR = 182.9 cm (72 in).

Figure A27.- Effect of rotation rate and angle of attack on pitching-moment coefficient for basic configuration. $\delta_e = -15°$, $\delta_a = -15.0°$, $\delta_r = -25°$, $\beta = 0°$.

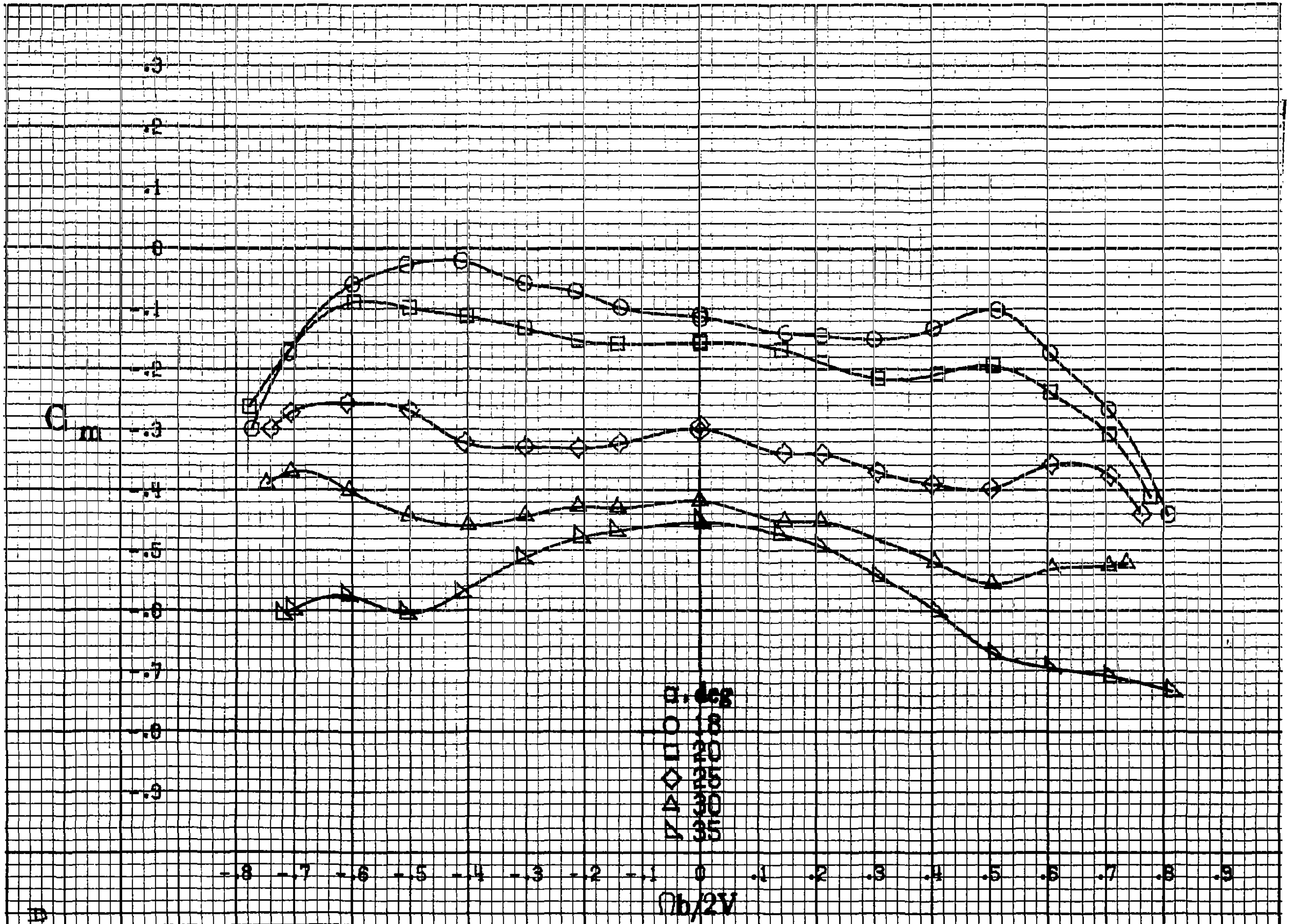

(b) α = 18 to 35 deg, SR = 182.9 cm (72 in).

Figure A27.- Continued.

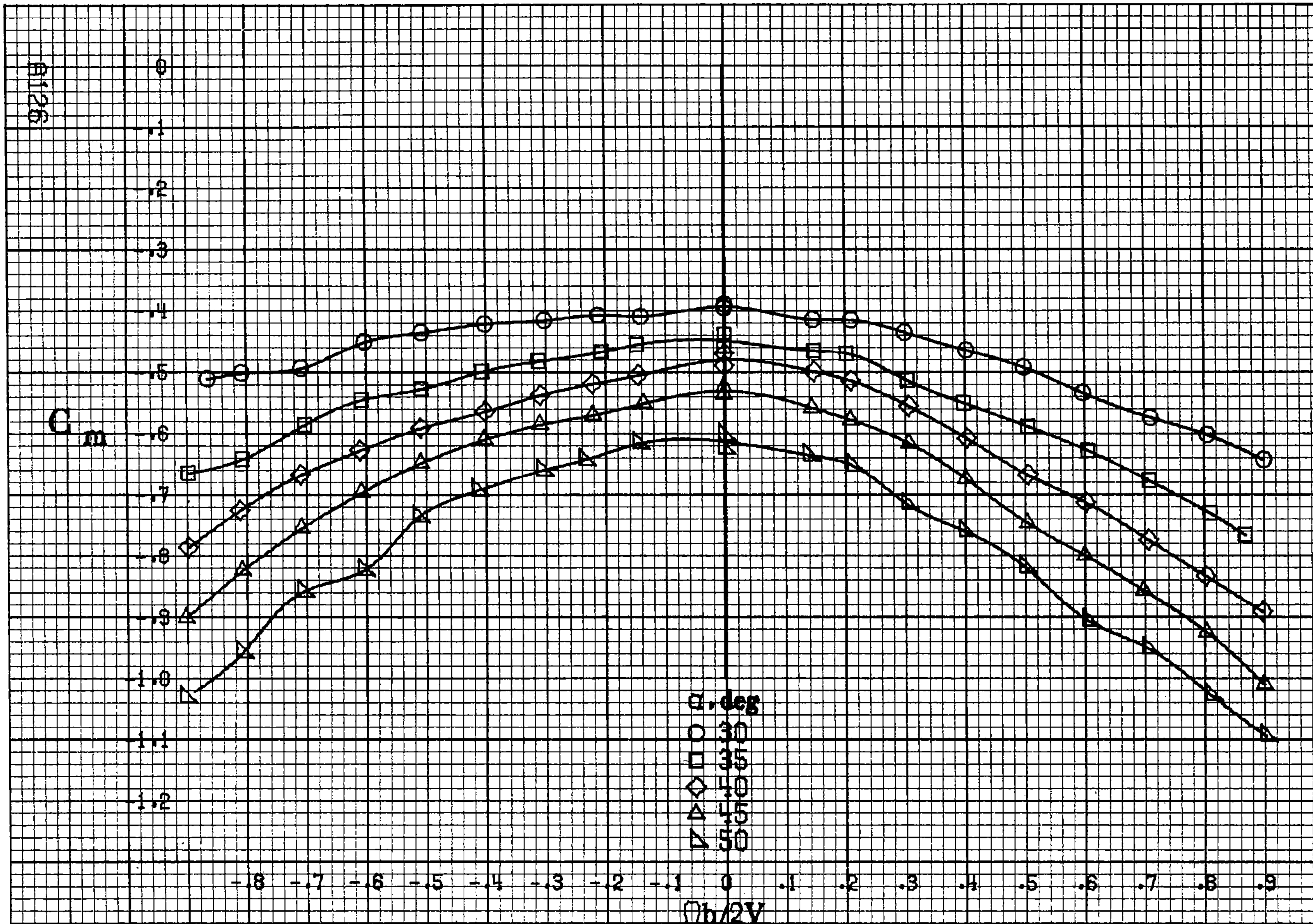

(c) α = 30 to 50 deg, SR = 0.

Figure A27.-Continued.

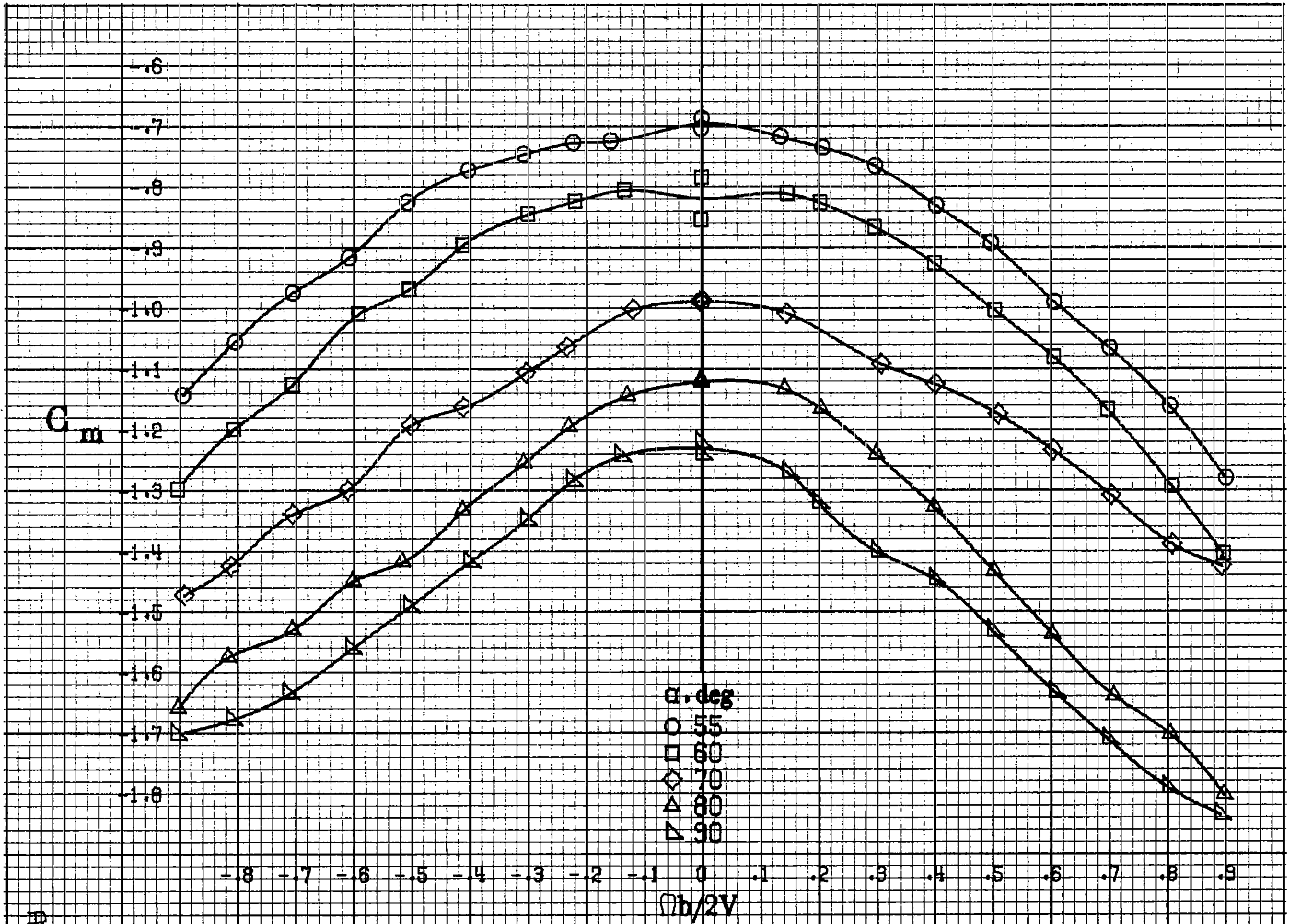

(d) $\alpha = 55$ to 90 deg, SR = 0.

Figure A27.-Concluded.

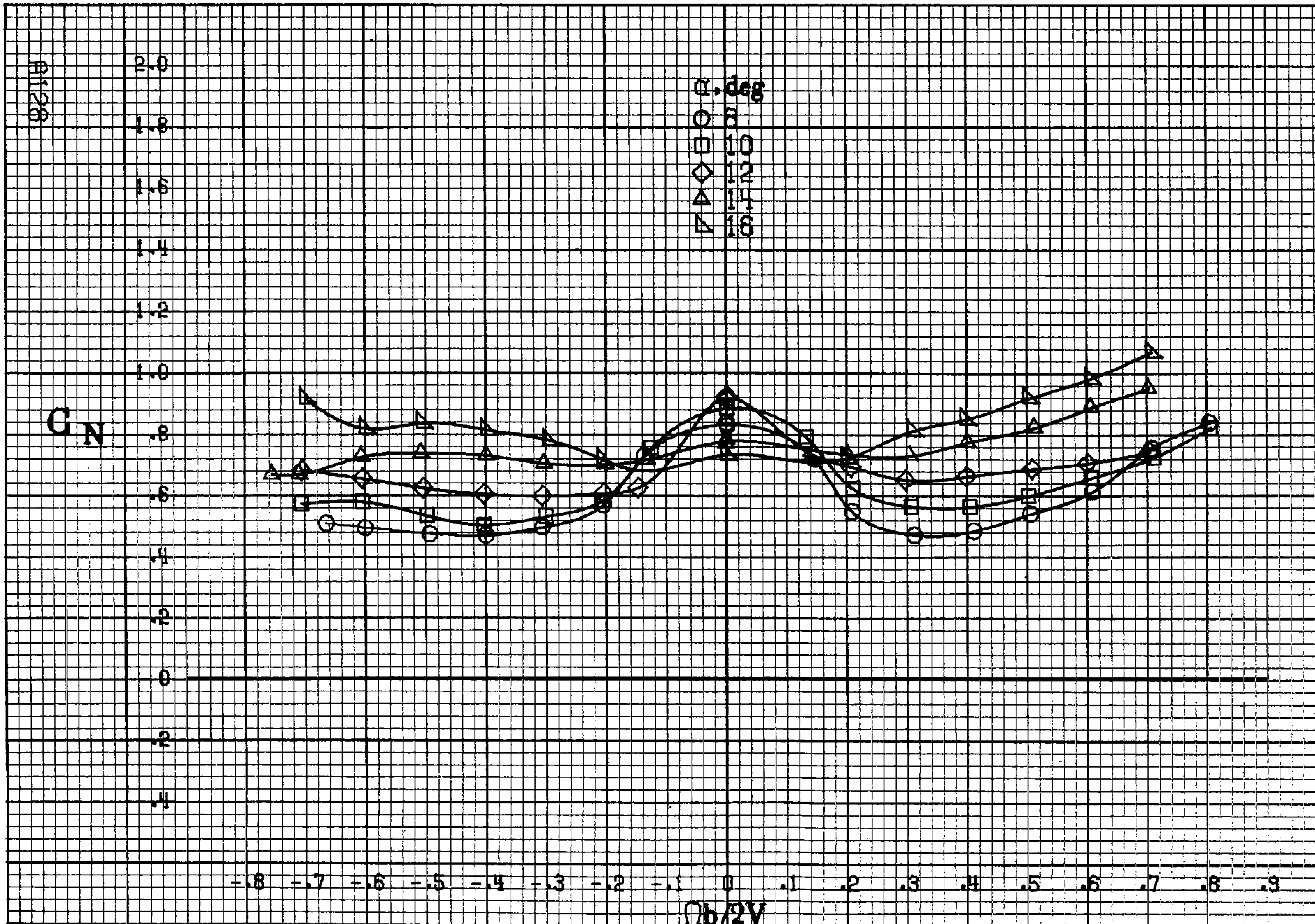

(a) α = 8 to 16 deg, SR = 182.9 cm (72 in.).

Figure A28.- Effect of rotation rate and angle of attack on normal-force coefficient for basic configuration. $\delta_e = -15°$, $\delta_a = -15.0°$, $\delta_r = -25°$, $\beta = 0°$.

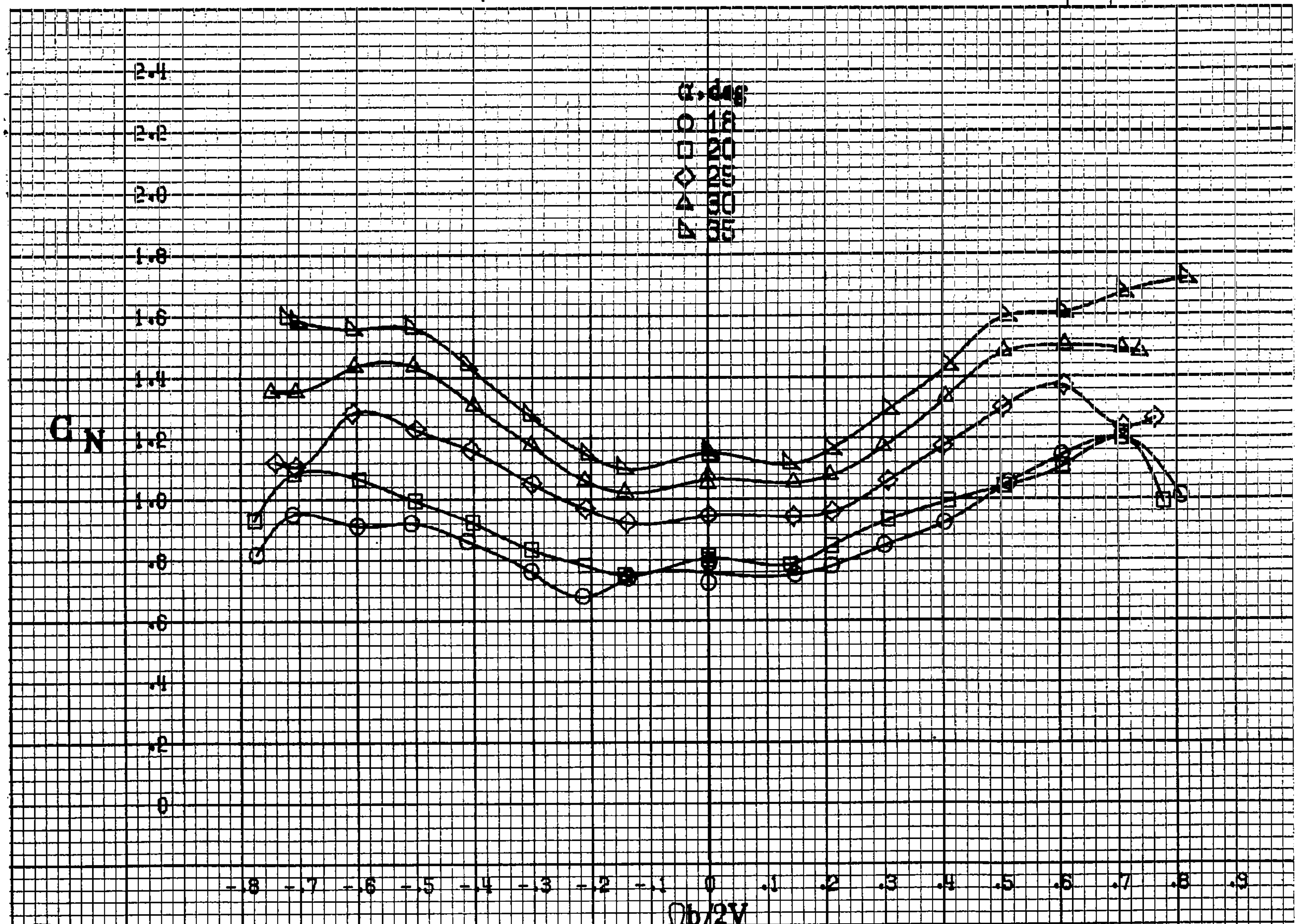

(b) α = 18 to 35 deg, SR = 182.9 cm (72 in).

Figure A28.-Continued.

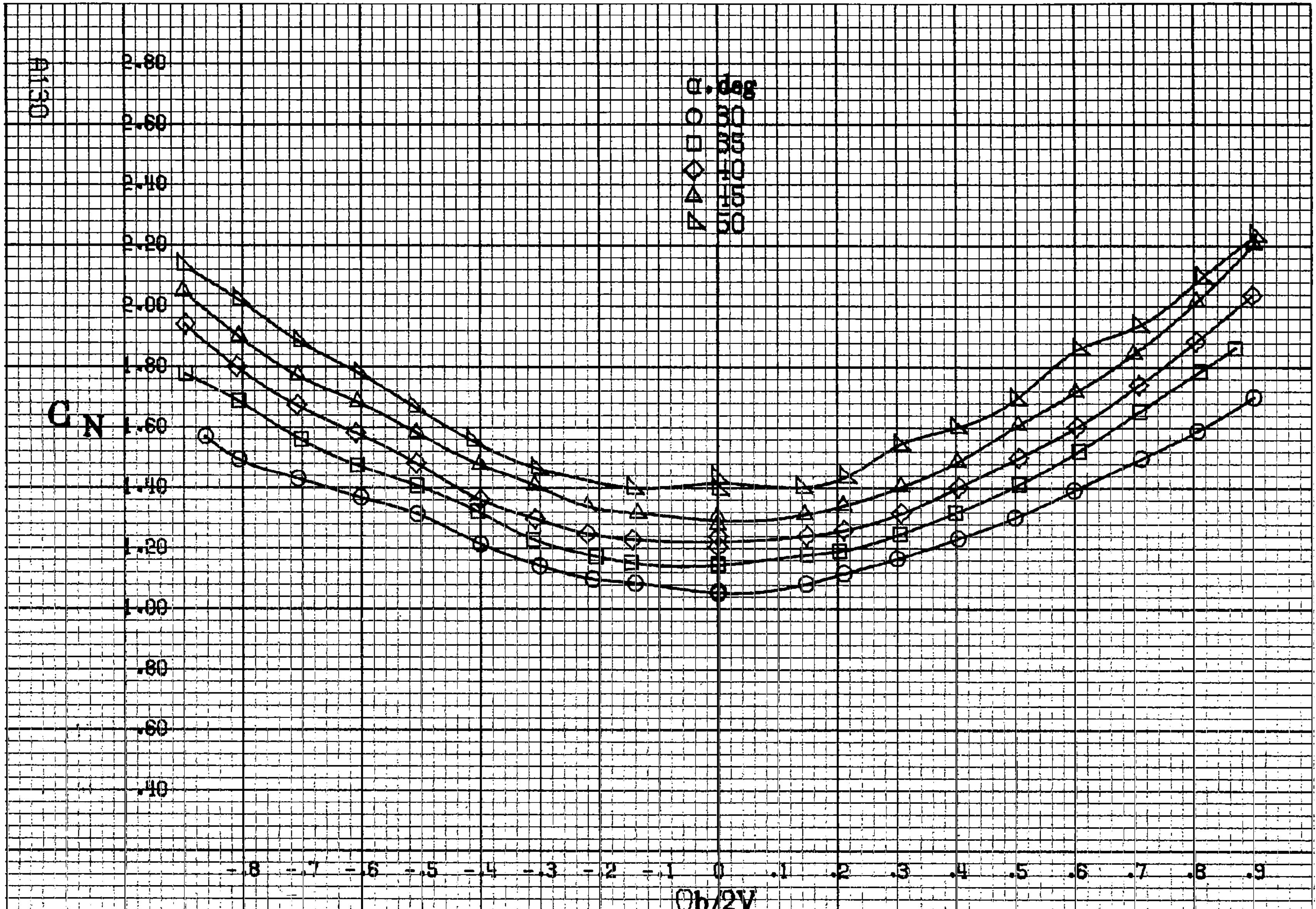

(c) α = 30 to 50 deg, SR = 0.

Figure A28.-Continued.

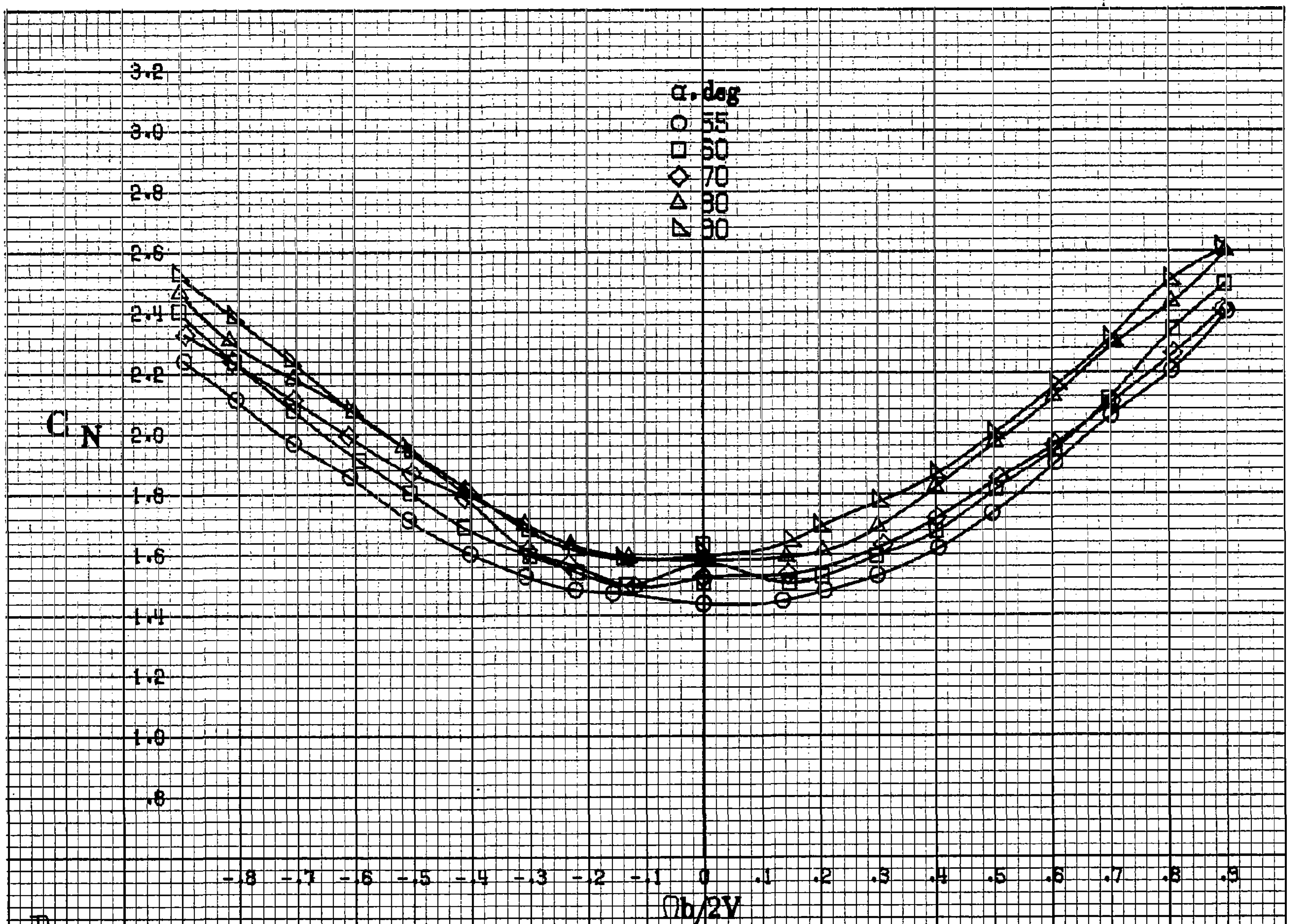

(d) α = 55 to 90 deg, SR = 0.

Figure A28.-Concluded.

A131

A132

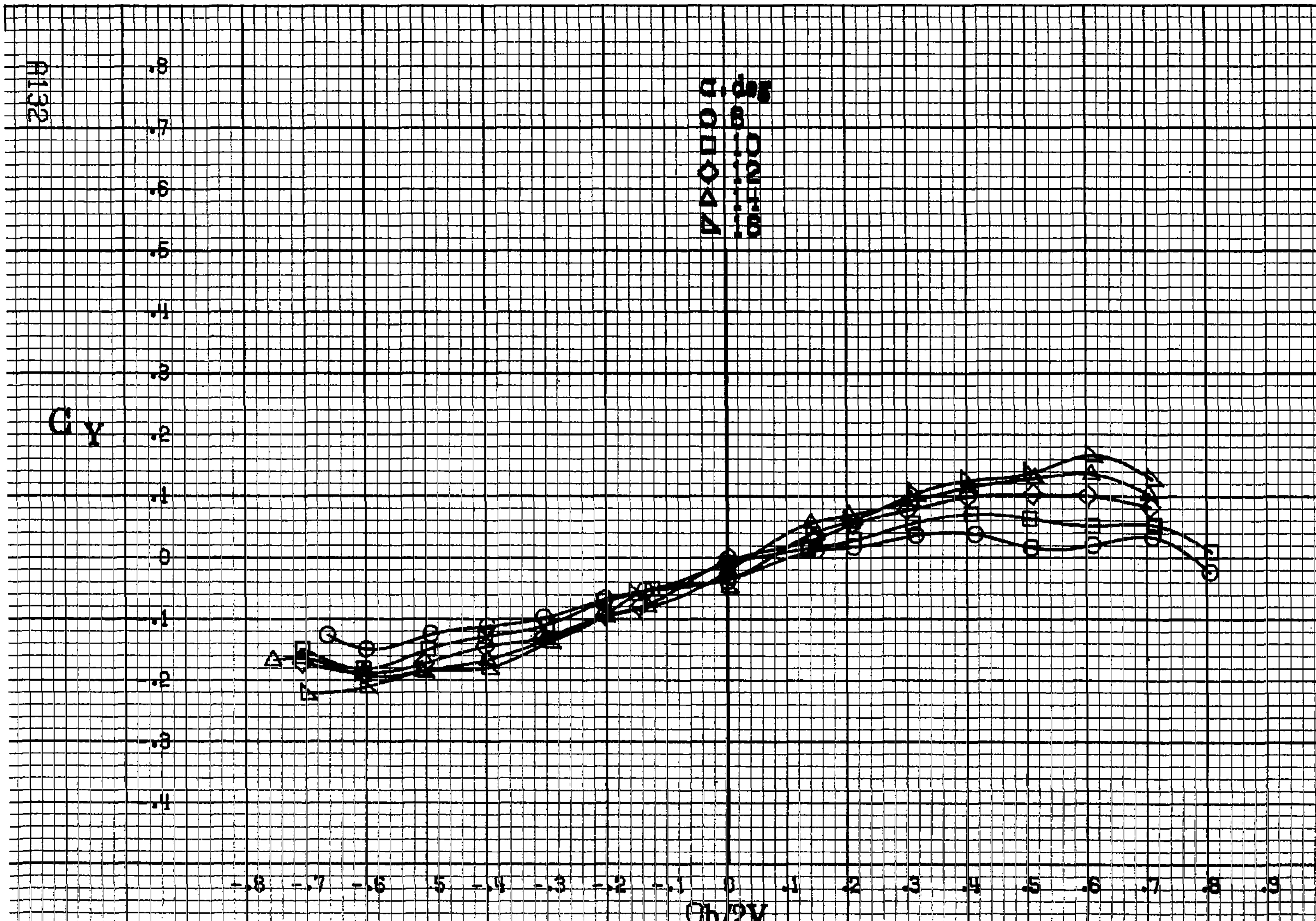

(a) α = 8 to 16 deg, SR = 182.9 cm (72 in).

Figure A28.- Effect of rotation rate and angle of attack on side-force coefficient for basic configuration. δ_e = -15°, δ_a = -15.0°, δ_r = 25°, β = 0°.

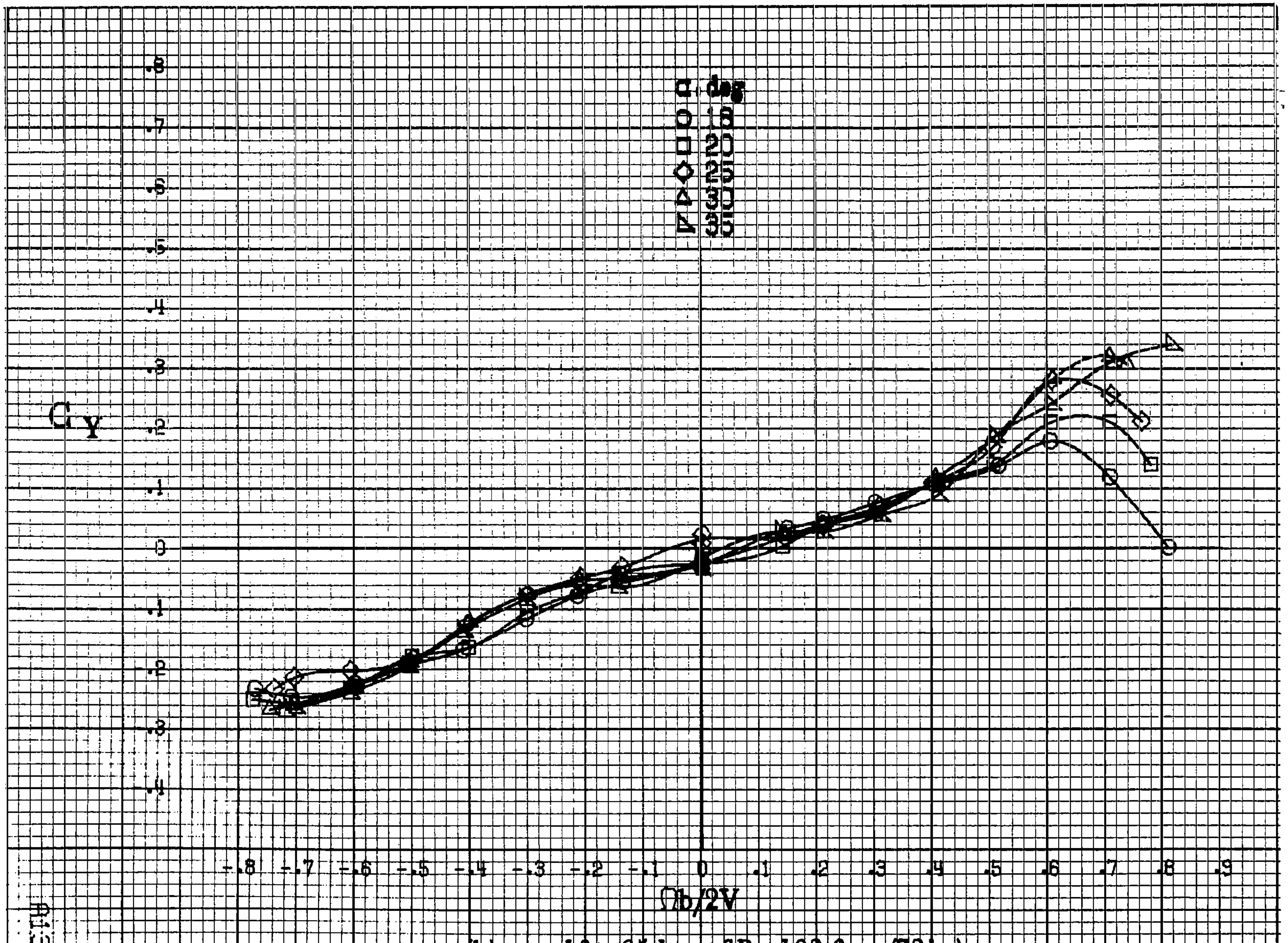

(b) α = 18 to 35 deg, SR = 182.9 cm (72 in).
Figure A29.-Continued.

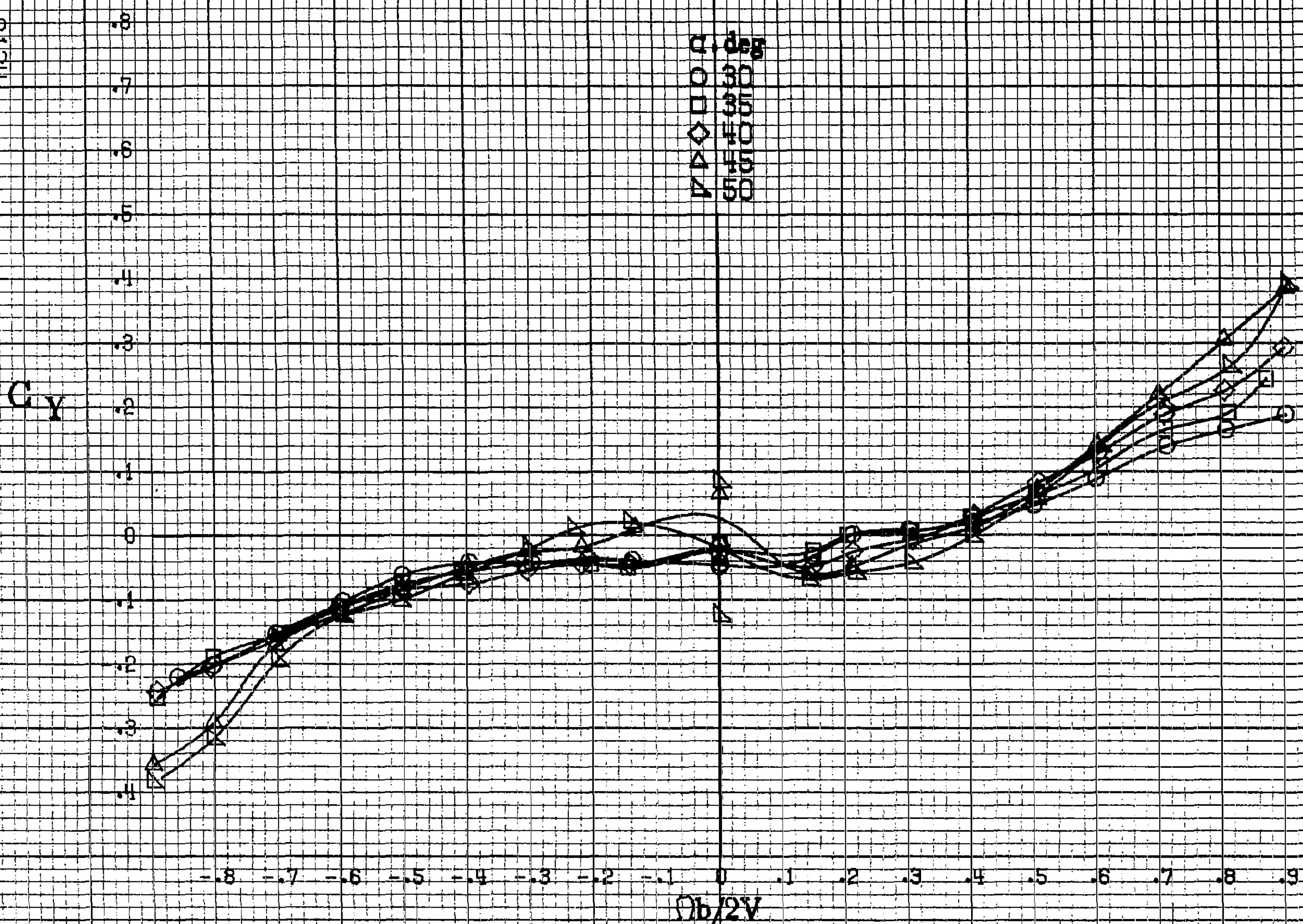

(c) α = 30 to 50 deg, SR = 0.

Figure A29.-Continued.

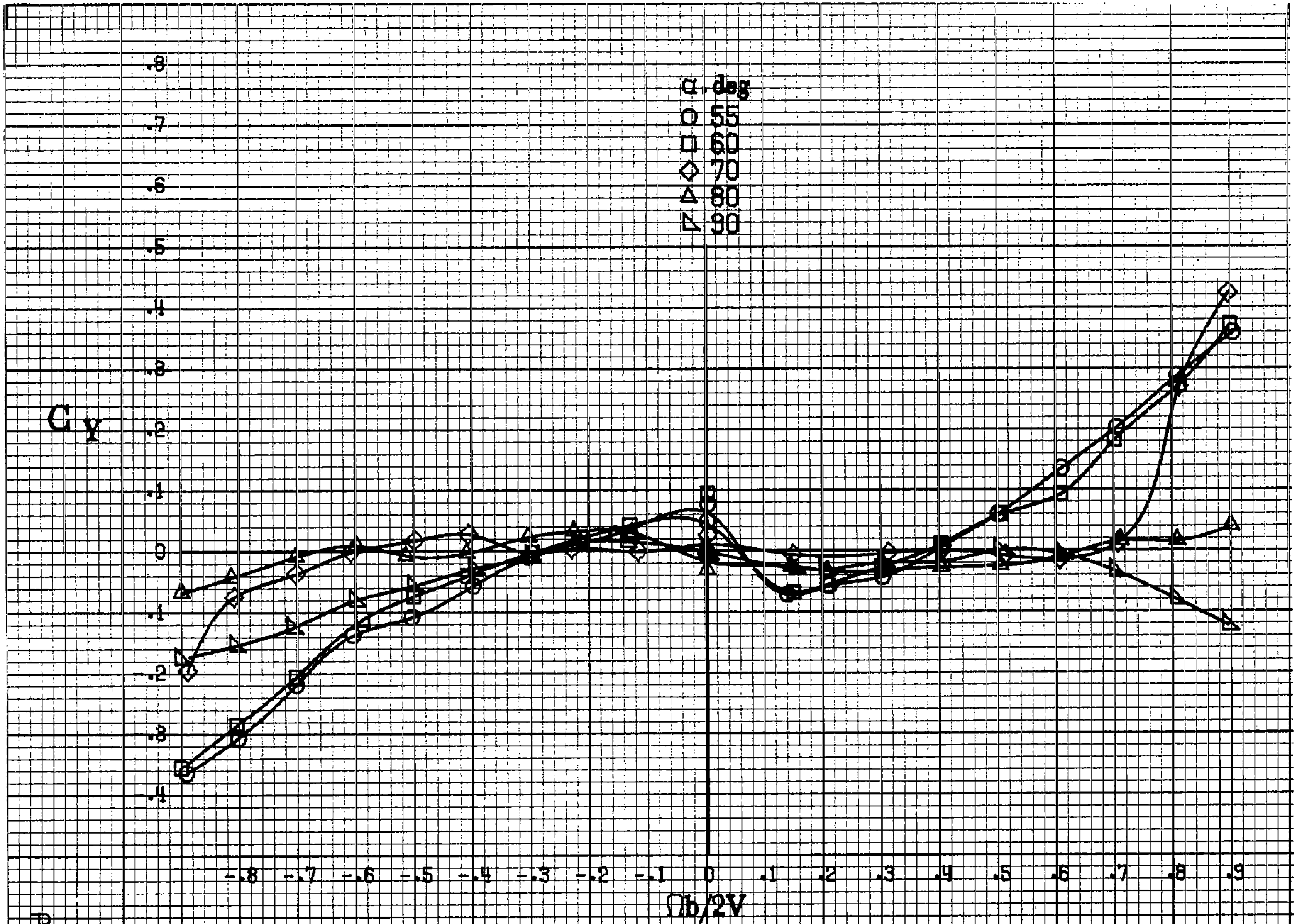

(d) α = 55 to 90 deg, SR = 0.

Figure A29.-Concluded.

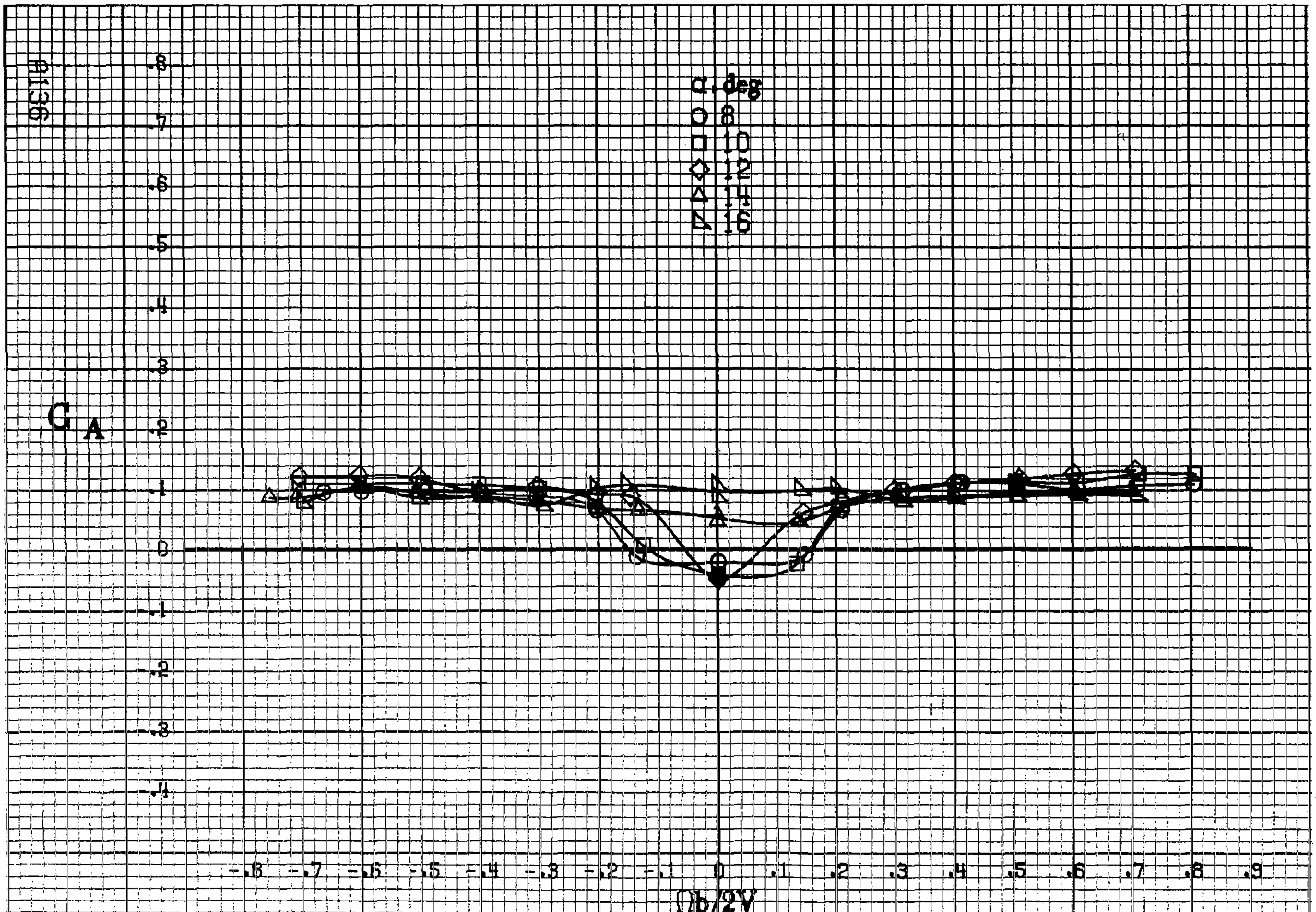

(a) α = 8 to 16 deg, SR = 182.9 cm (72 in).

Figure A30.- Effect of rotation rate and angle of attack on axial-force coefficient for basic configuration. $\delta_e = -15^\circ$, $\delta_a = -15.0^\circ$, $\delta_r = -25^\circ$, $\beta = 0^\circ$.

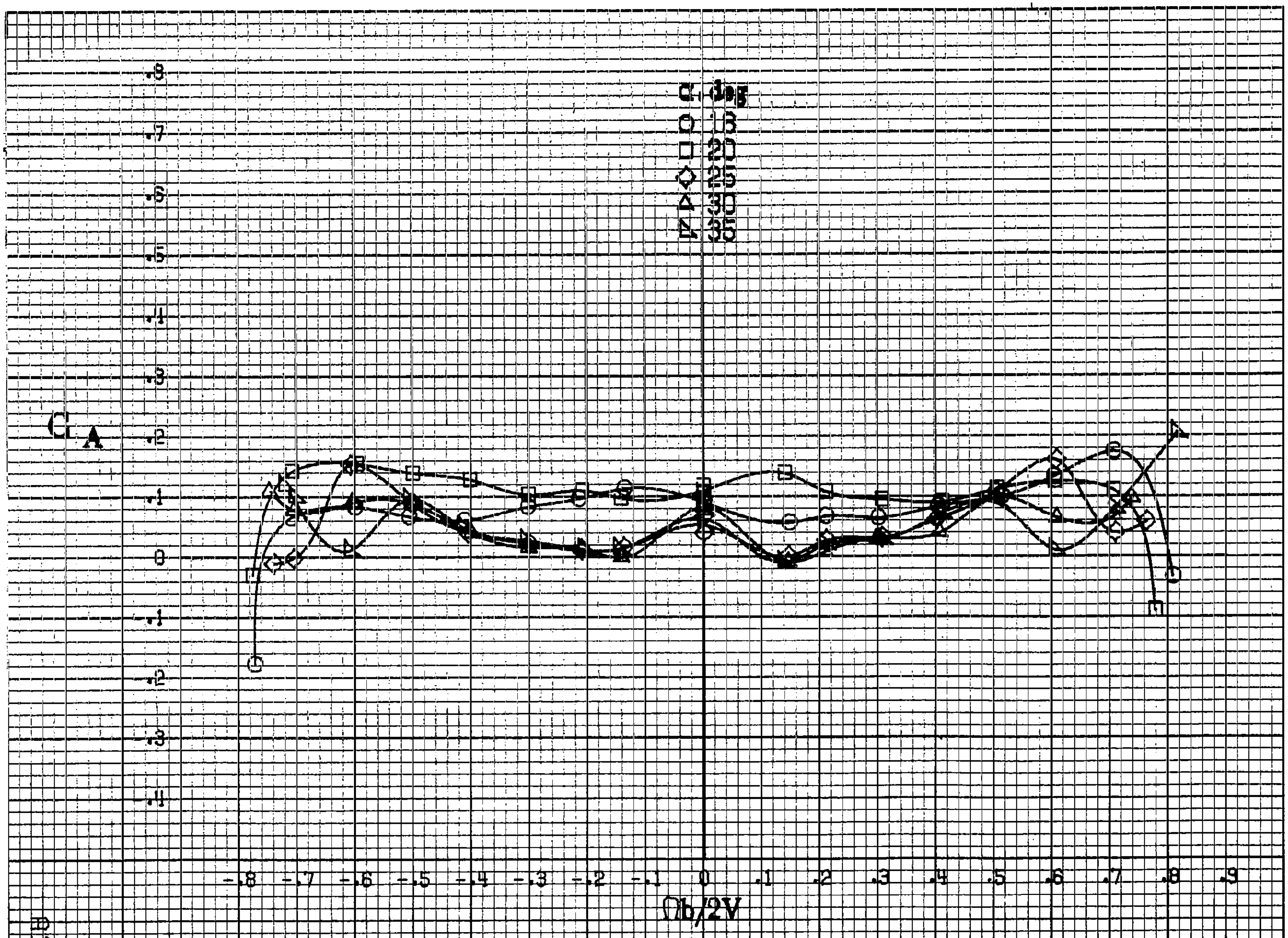

(b) α = 18 to 35 deg, SR = 182.9 cm (72 in).

Figure A80.-Continued.

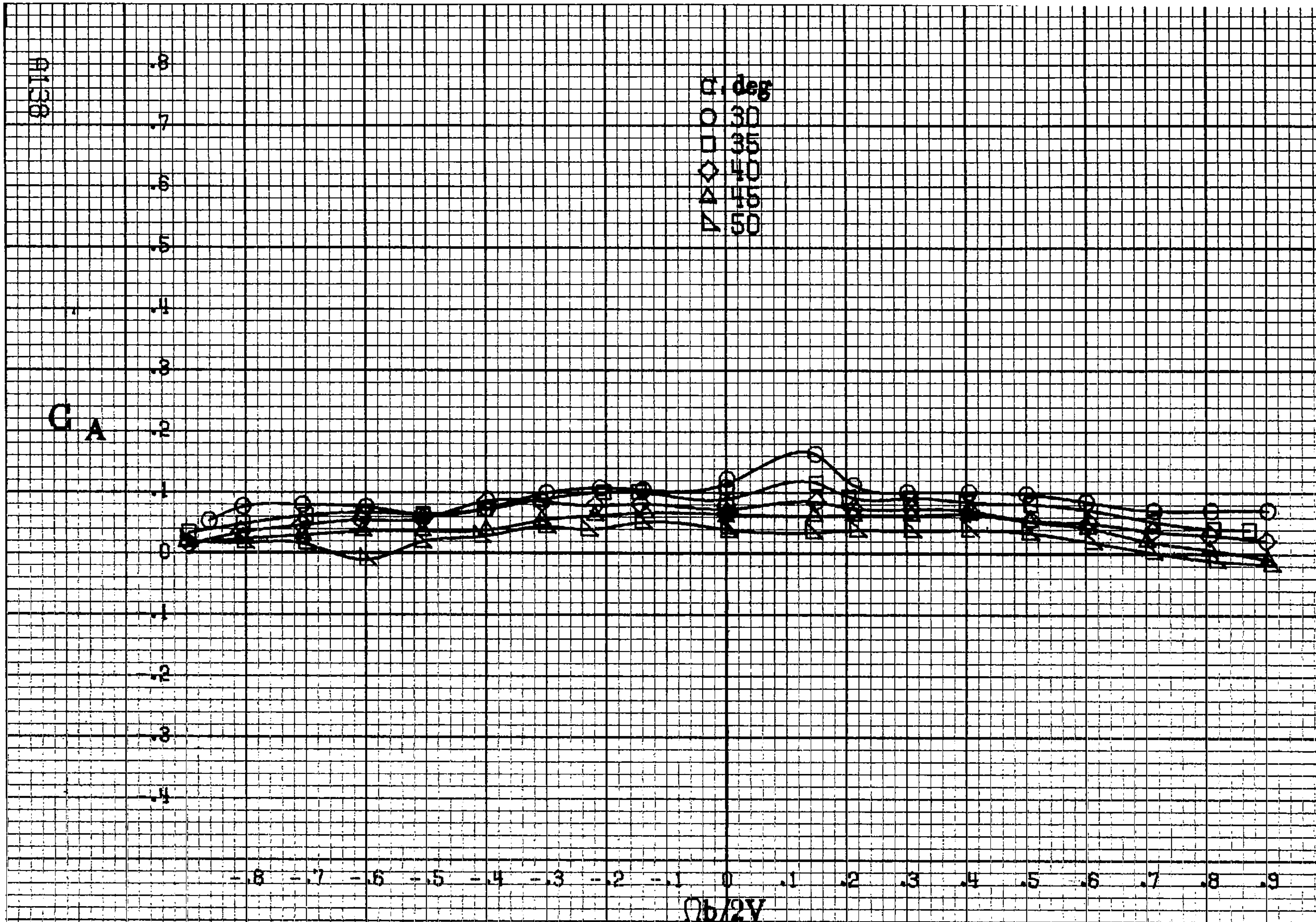

(c) α = 30 to 50 deg, SR = 0.

Figure A80.-Continued.

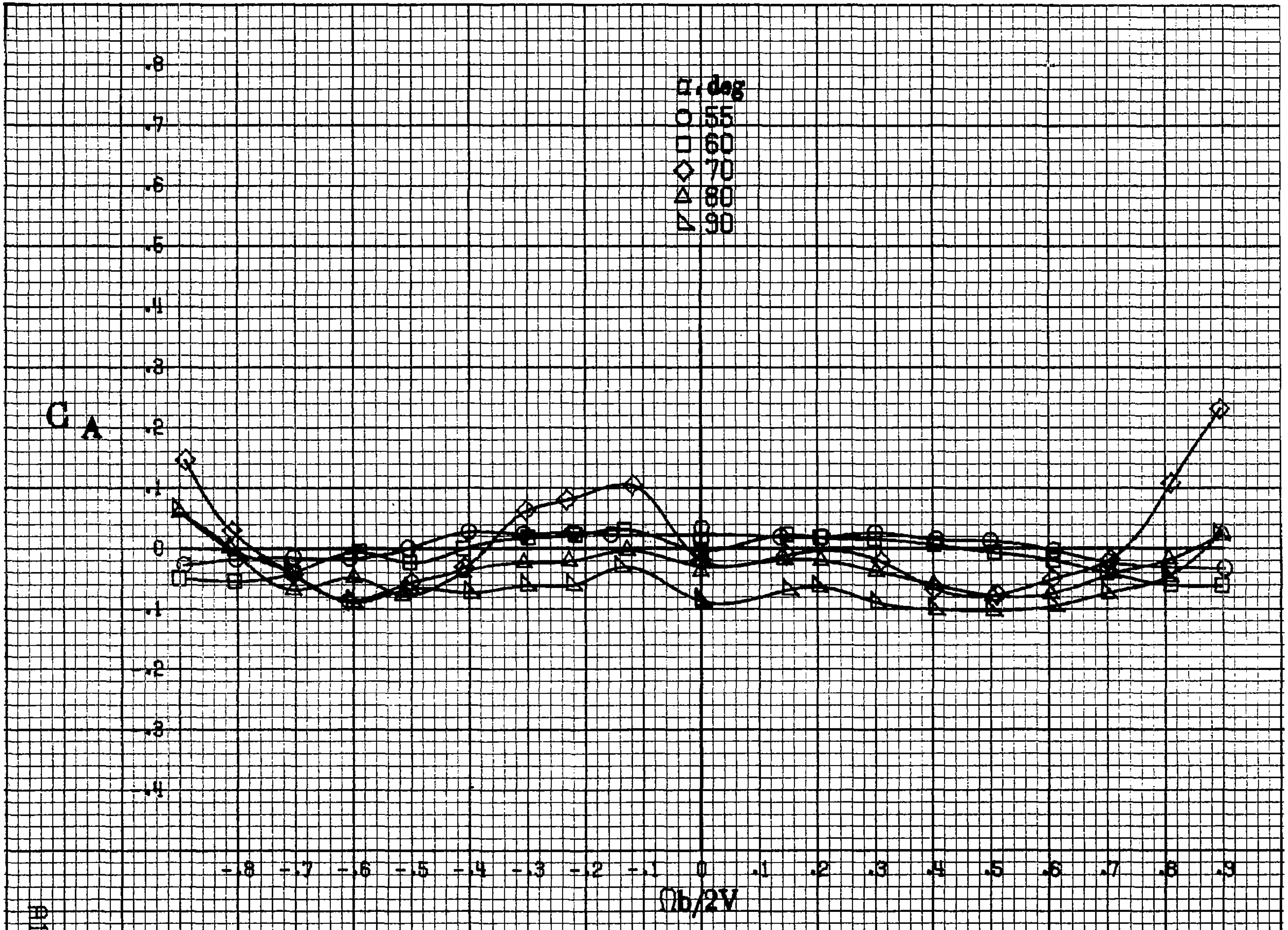

(d) Ω = 55 to 90 deg, SR = 0.

Figure A80.-Concluded.

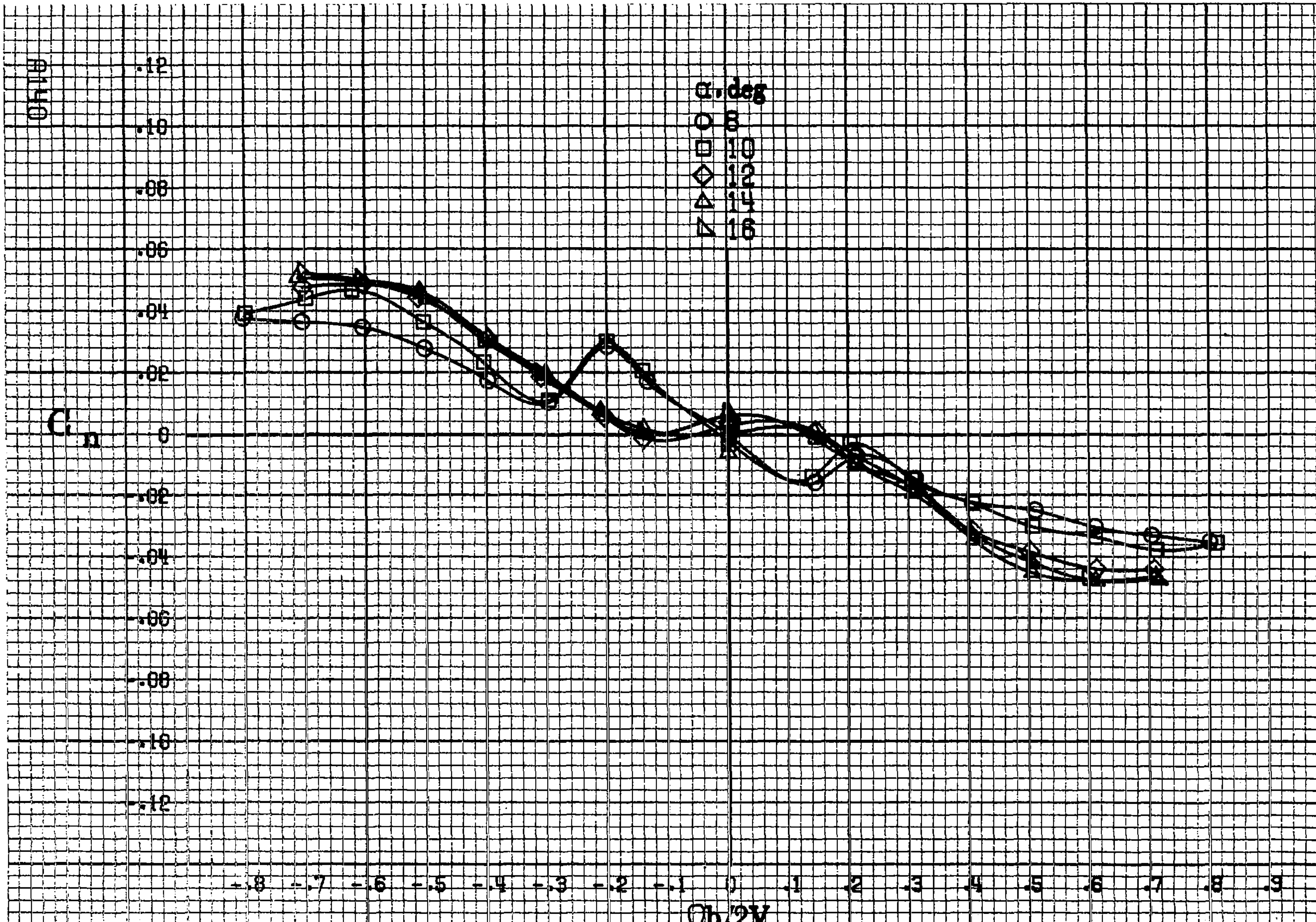

(a) $\alpha = 8$ to 16 deg, SR = 182.9 cm (72 in).

Figure A31.- Effect of rotation rate and angle of attack on yawing-moment coefficient for full-span LE wing droop with moderate nose radius. $\delta_e = 0°$, $\delta_a = 0°$, $\delta_r = 0°$, $\beta = 0°$.

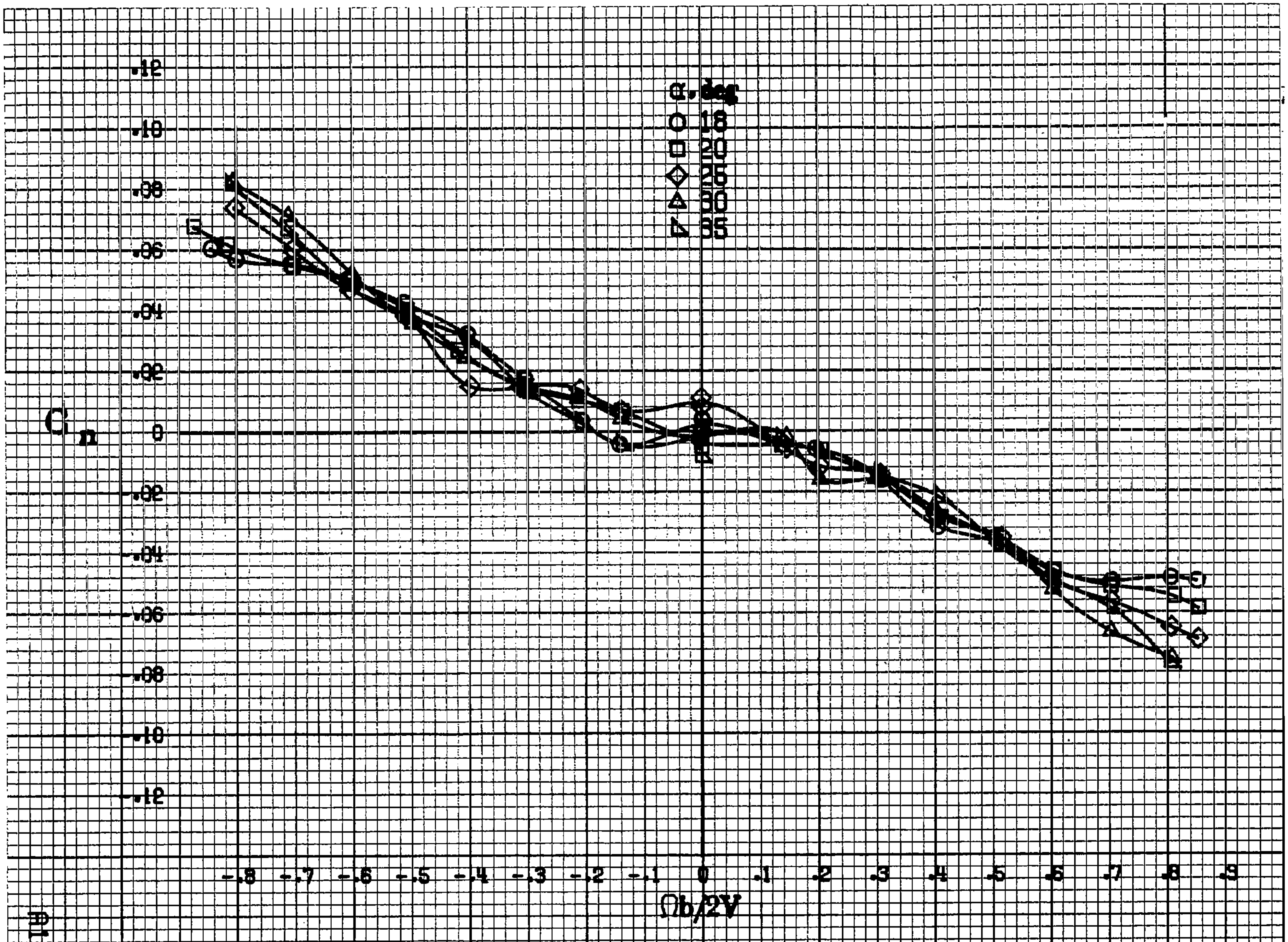

(b) α = 18 to 35 deg, SR = 182.9 cm (72 in).

Figure A81.-Continued.

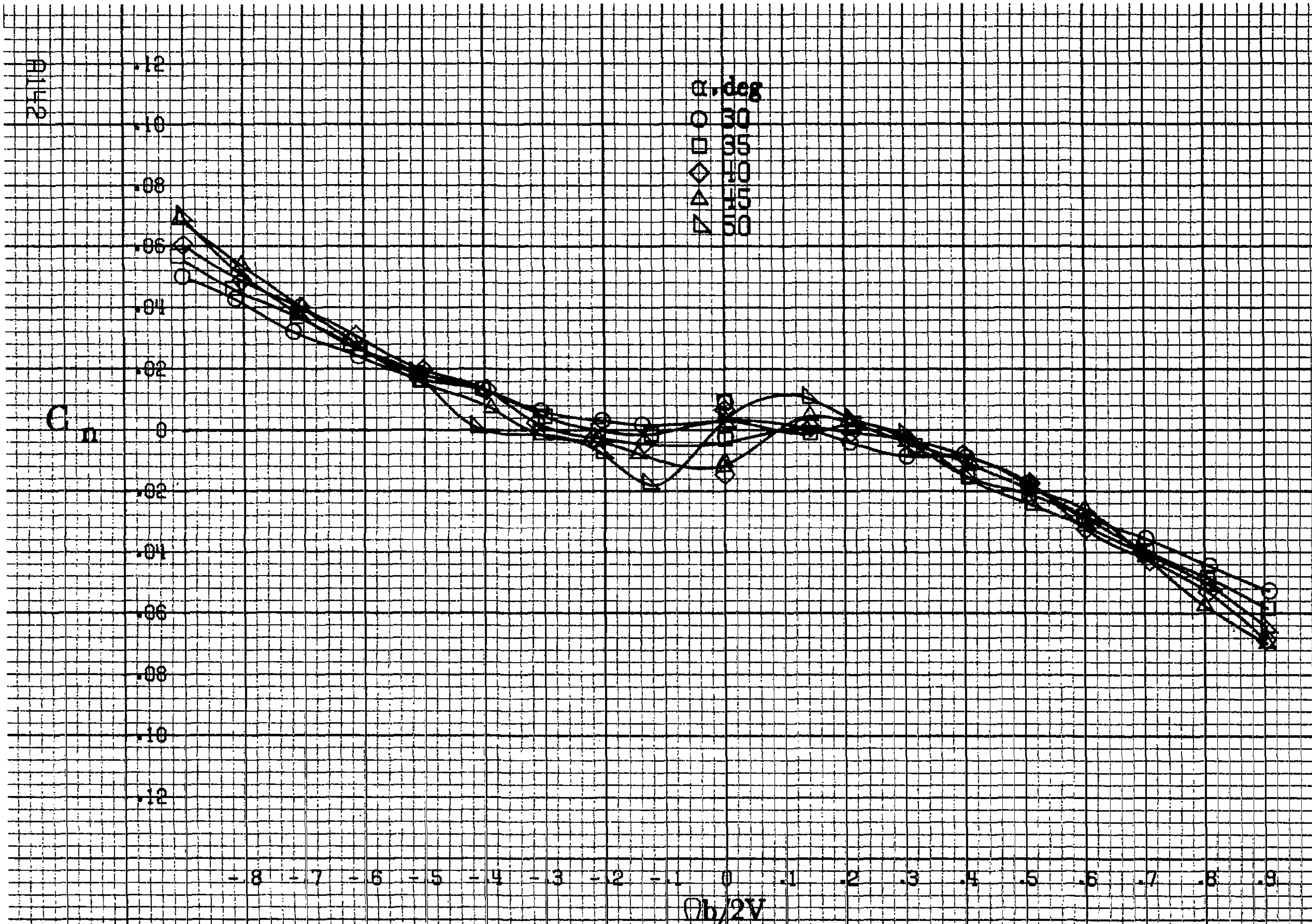

(c) α = 30 to 50 deg, SR = 0.
Figure A81.-Continued.

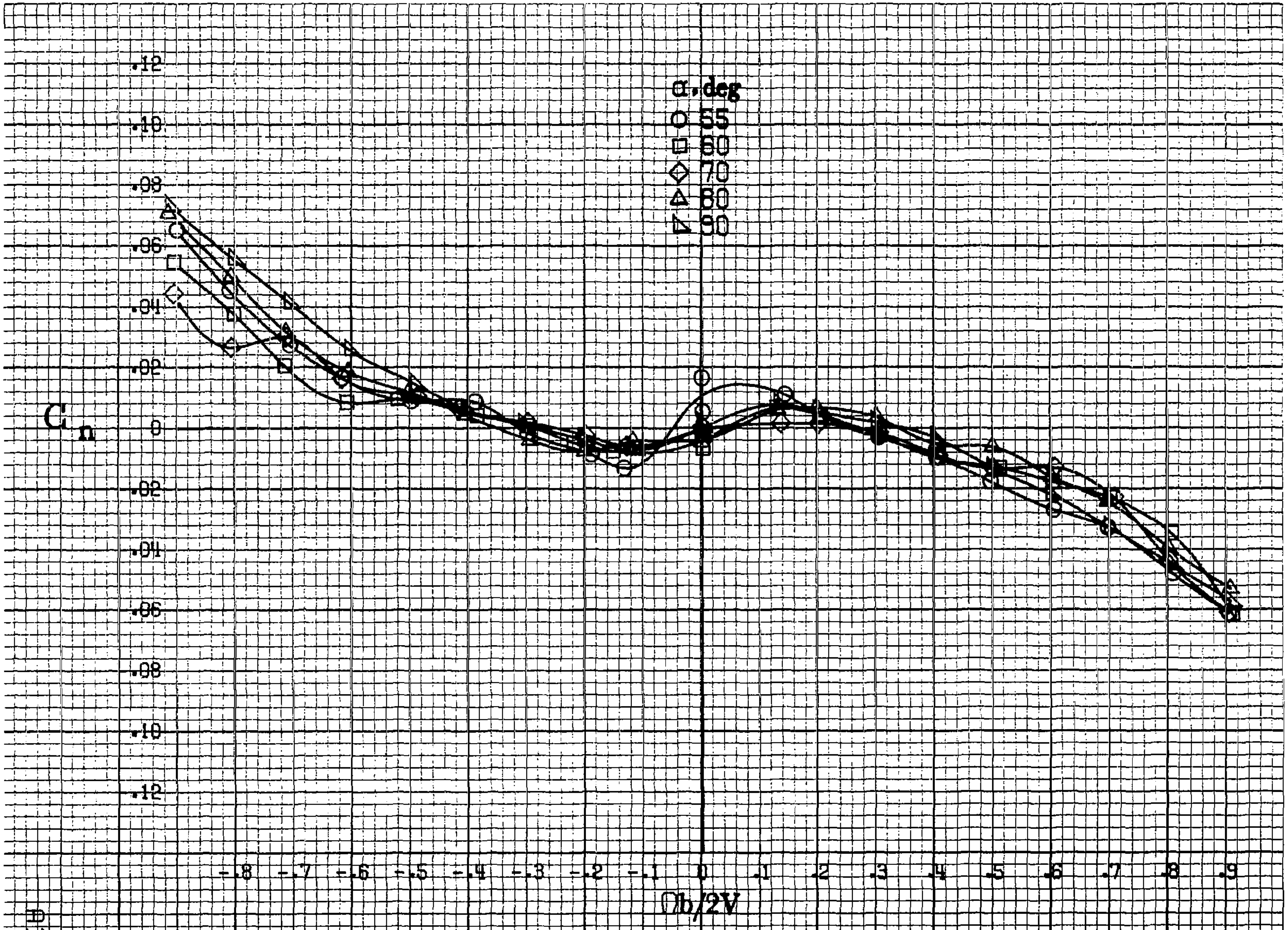

(d) α = 55 to 90 deg, SR = 0.

Figure A31.-Concluded.

A144

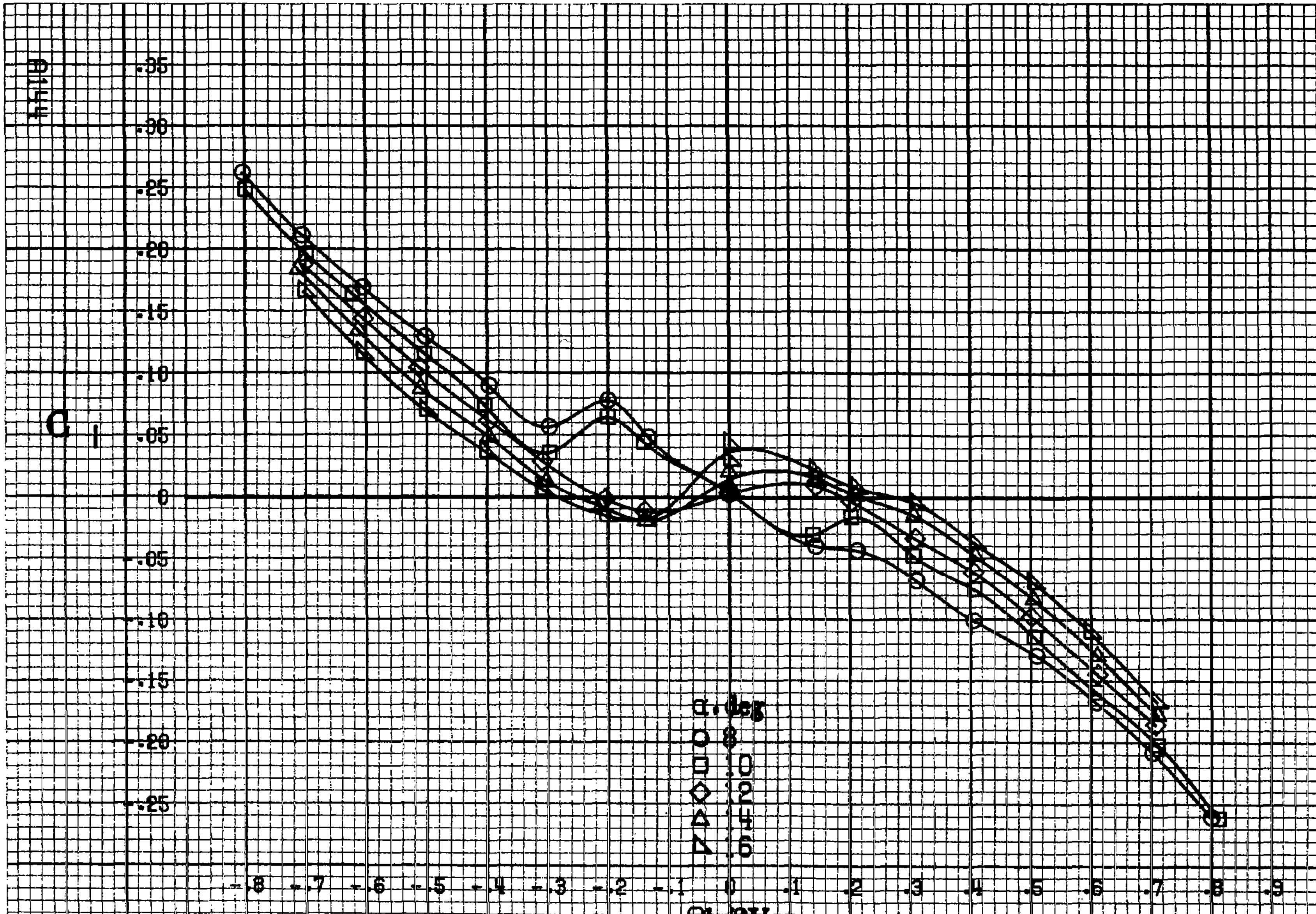

(a) α = 8 to 16 deg, SR = 182.9 cm (72 in.).

Figure A32.- Effect of rotation rate and angle of attack on rolling-moment coefficient for full-span LE wing droop with moderate nose radius. $\delta_r = 0°$, $\delta_a = 0°$, $\delta_e = 0°$, $\beta = 0°$.

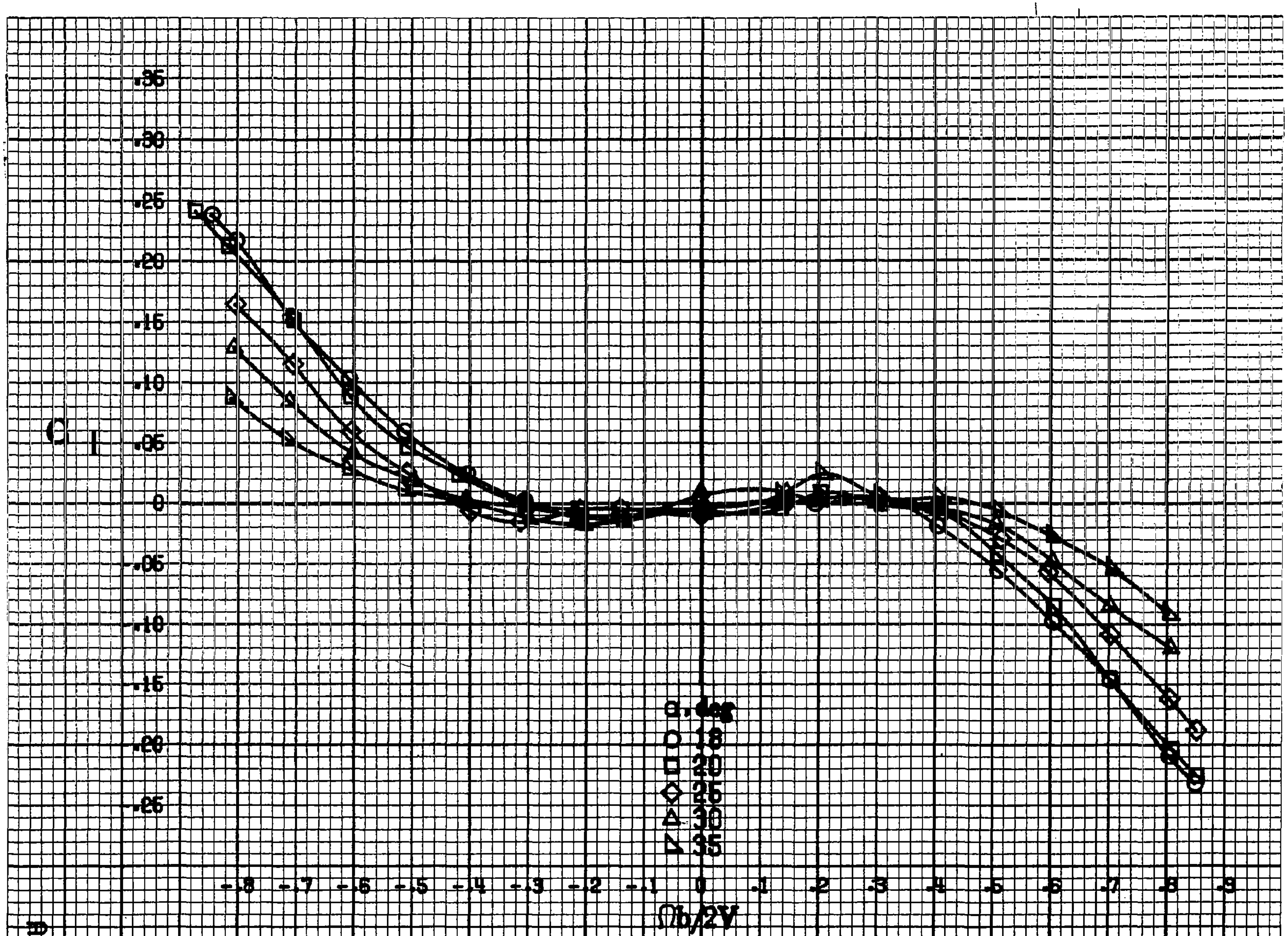

(b) α = 18 to 35 deg, SR = 182.9 cm (72 in).

Figure A32.-Continued.

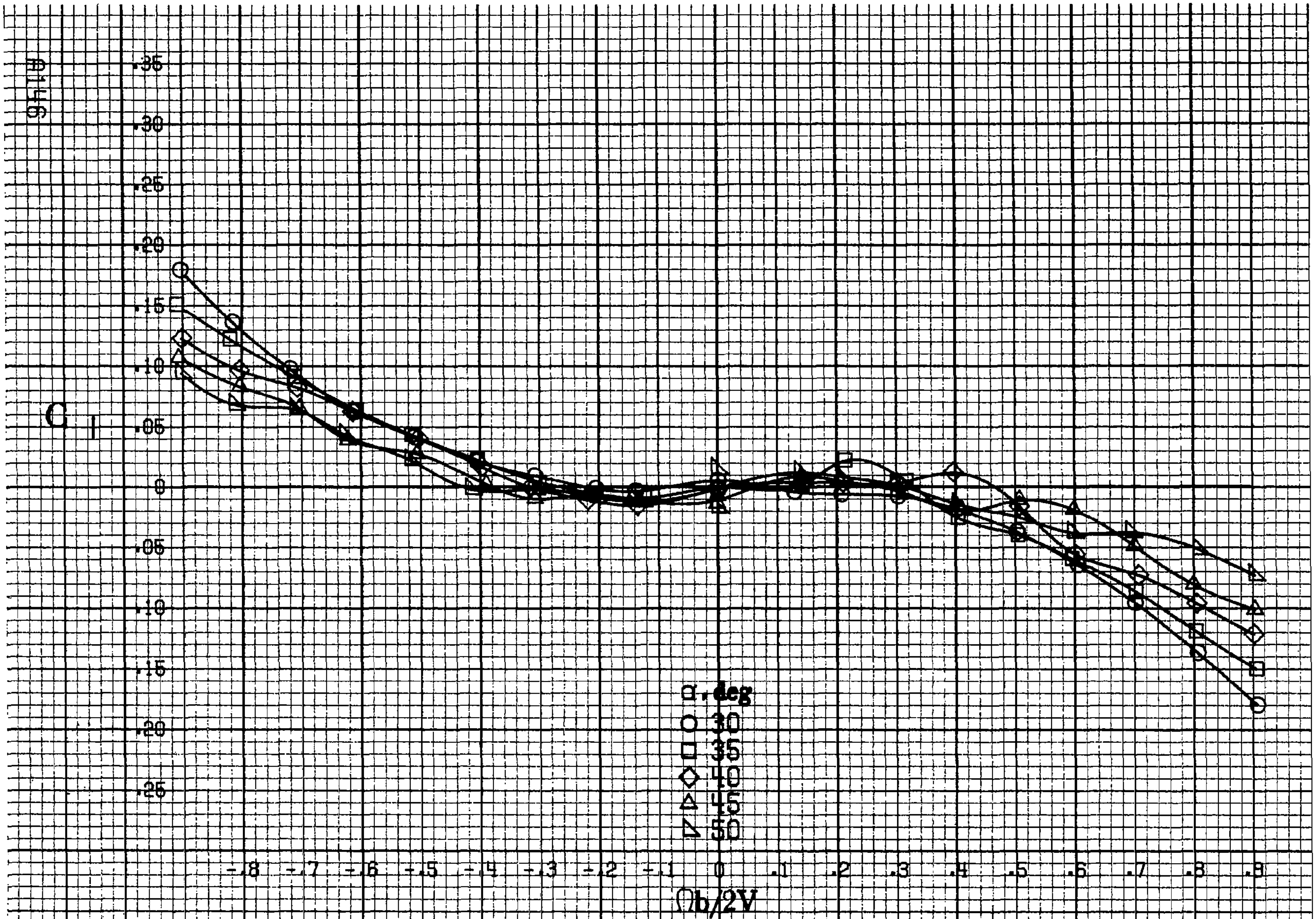

(c) $\alpha = 30$ to 50 deg, SR = 0.

Figure A82.-Continued.

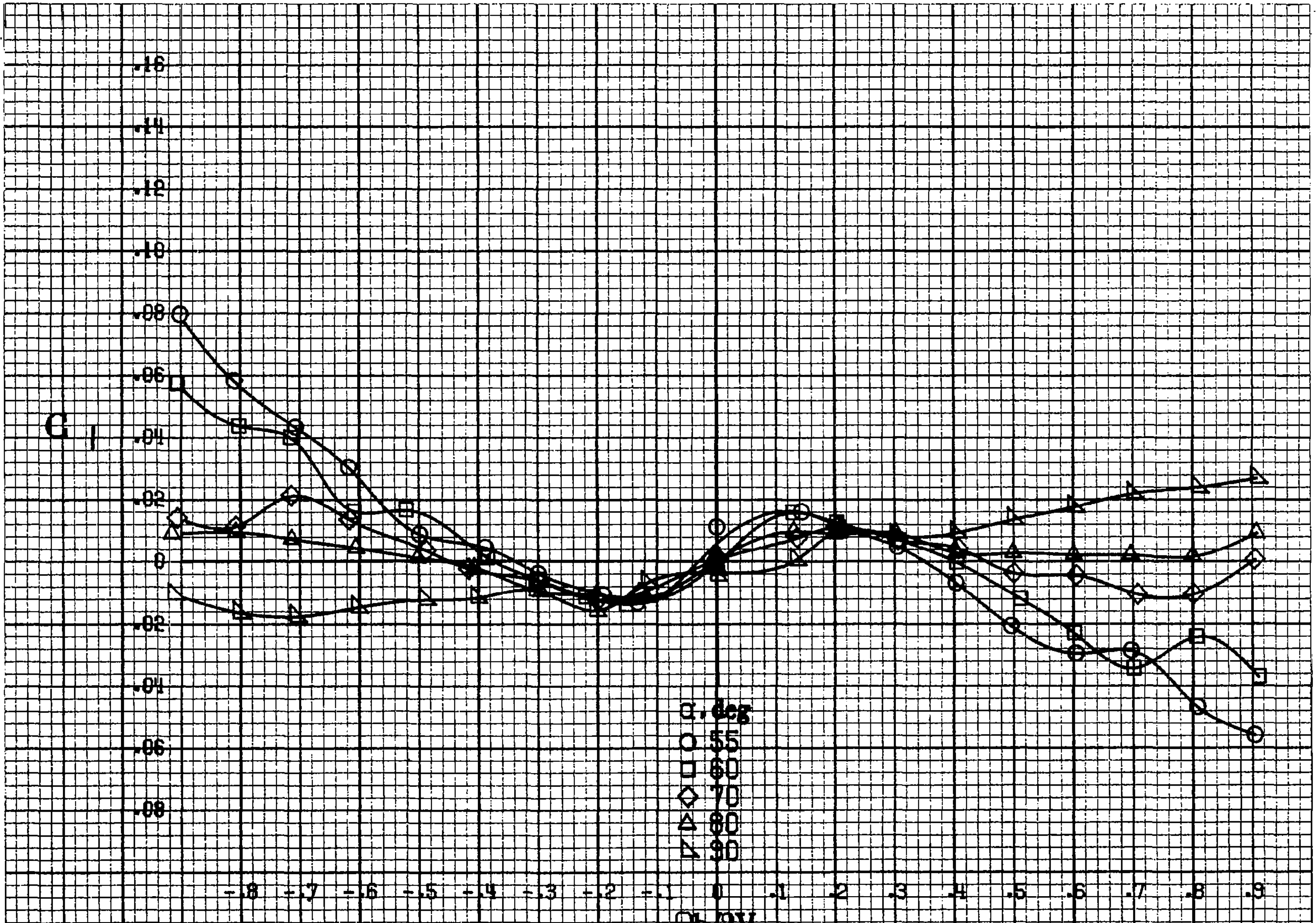

(d) α = 55 to 90 deg, SR = 0.

Figure A82.-Concluded.

A147

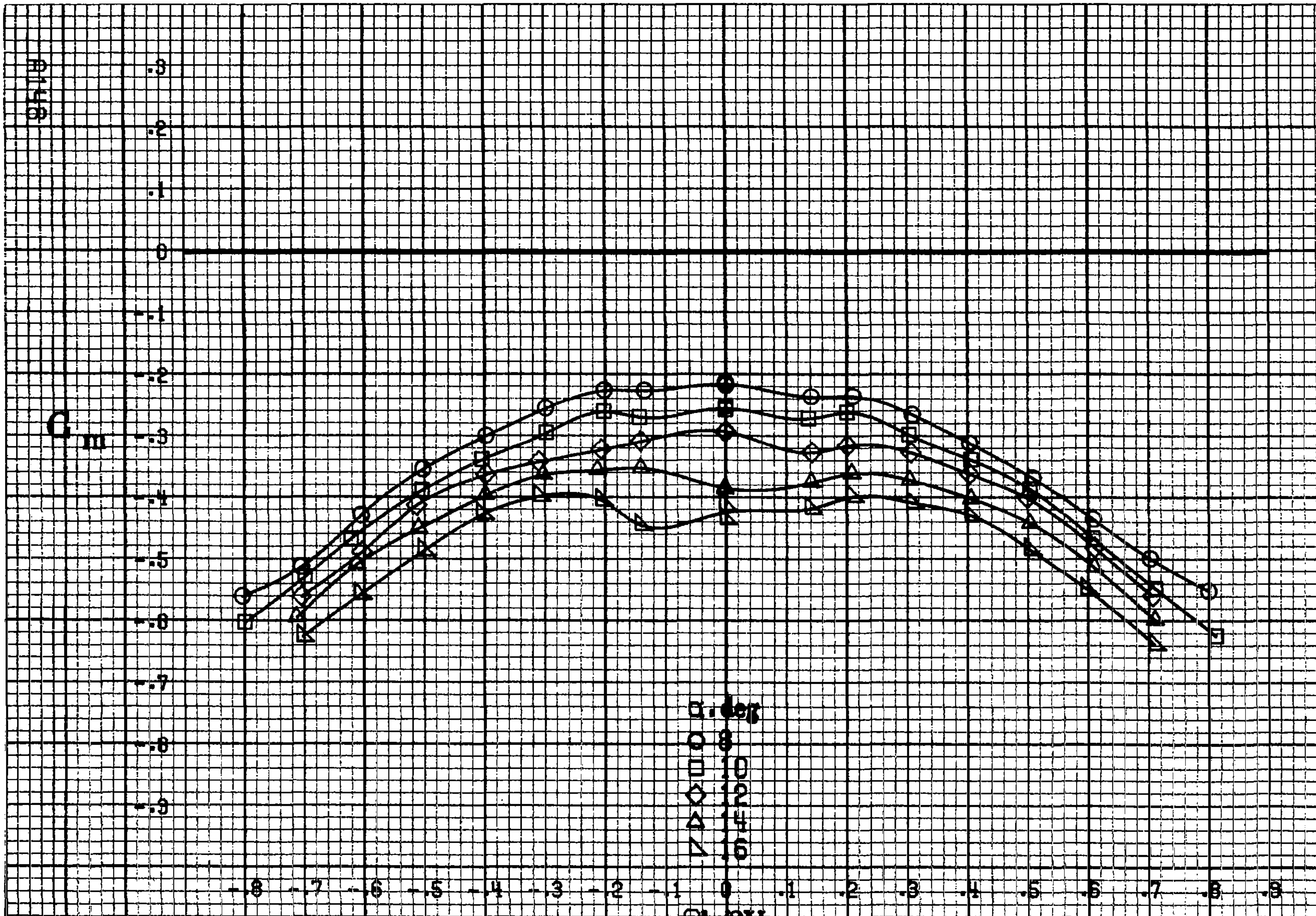

(a) $\alpha = 8$ to 16 deg, SR = 182.9 cm (72 in).

Figure A33.-Effect of rotation rate and angle of attack on pitching-moment coefficient for full-span LE wing droop with moderate nose radius. $\delta_a = 0°$, $\delta_e = 0°$, $\delta_r = 0°$, $\beta = 0°$.

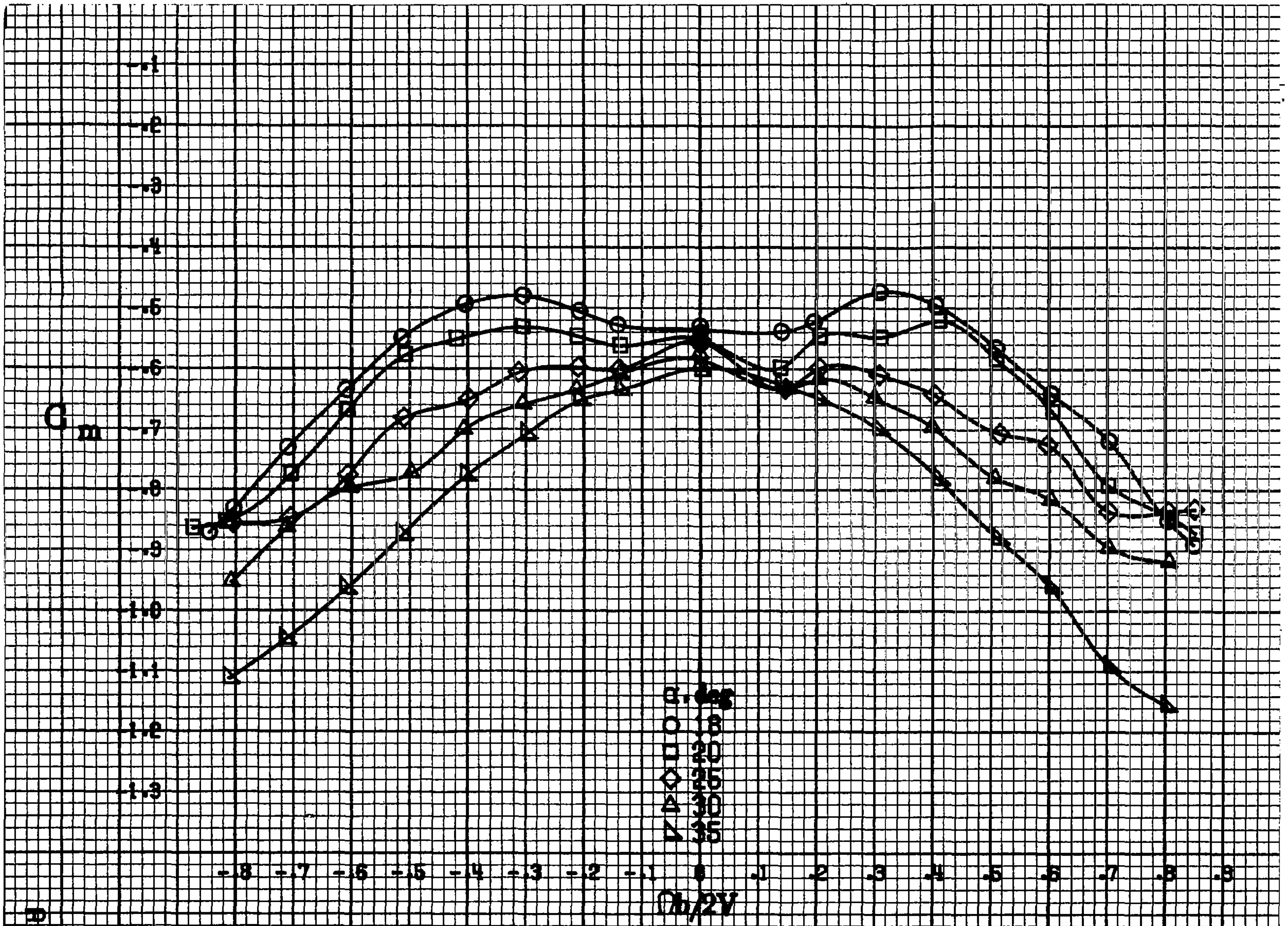

(b) α = 18 to 35 deg, SR = 182.9 cm (72 in).

Figure A38.-Continued.

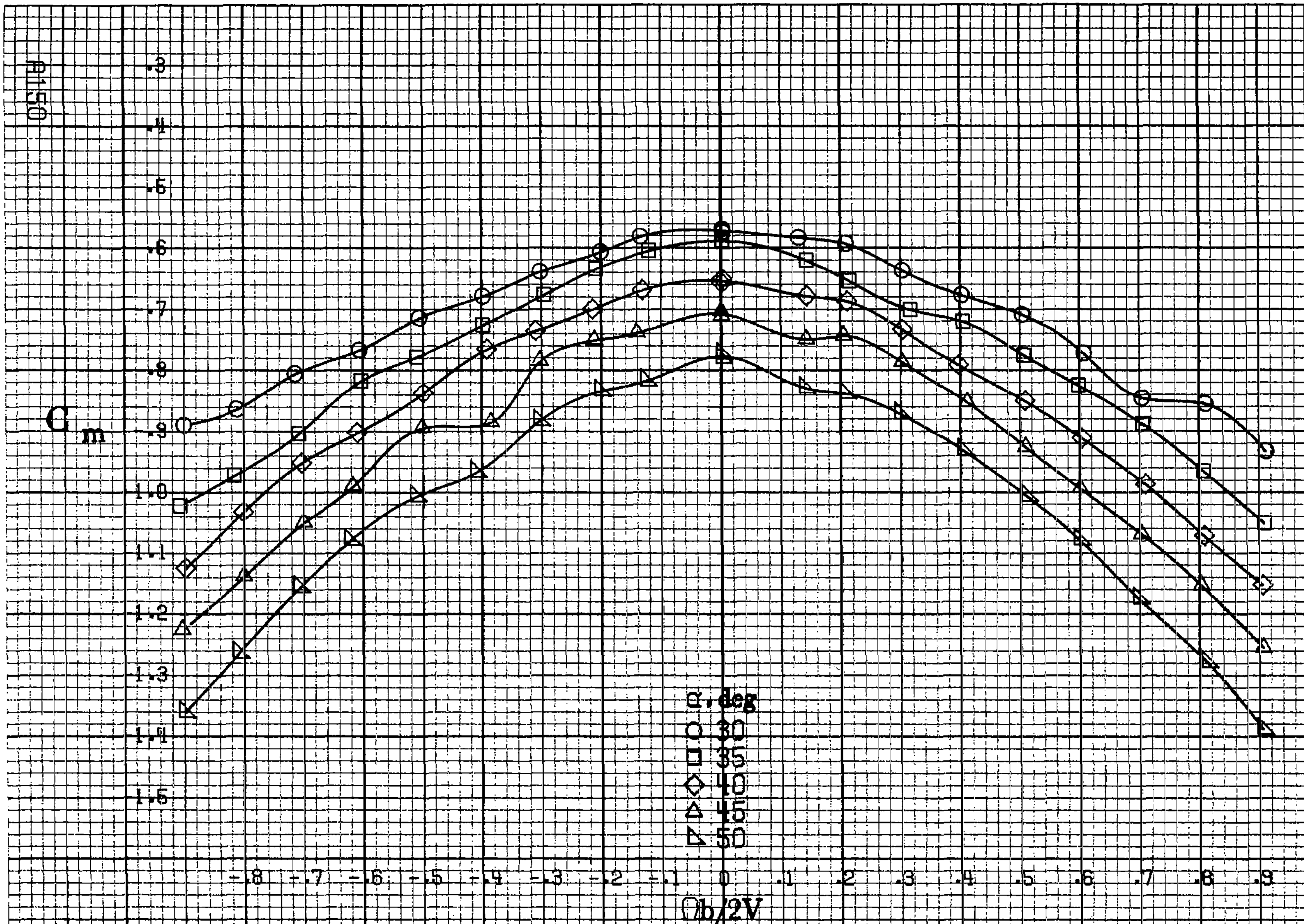

(c) α = 30 to 50 deg, SR = 0.

Figure A33.-Continued.

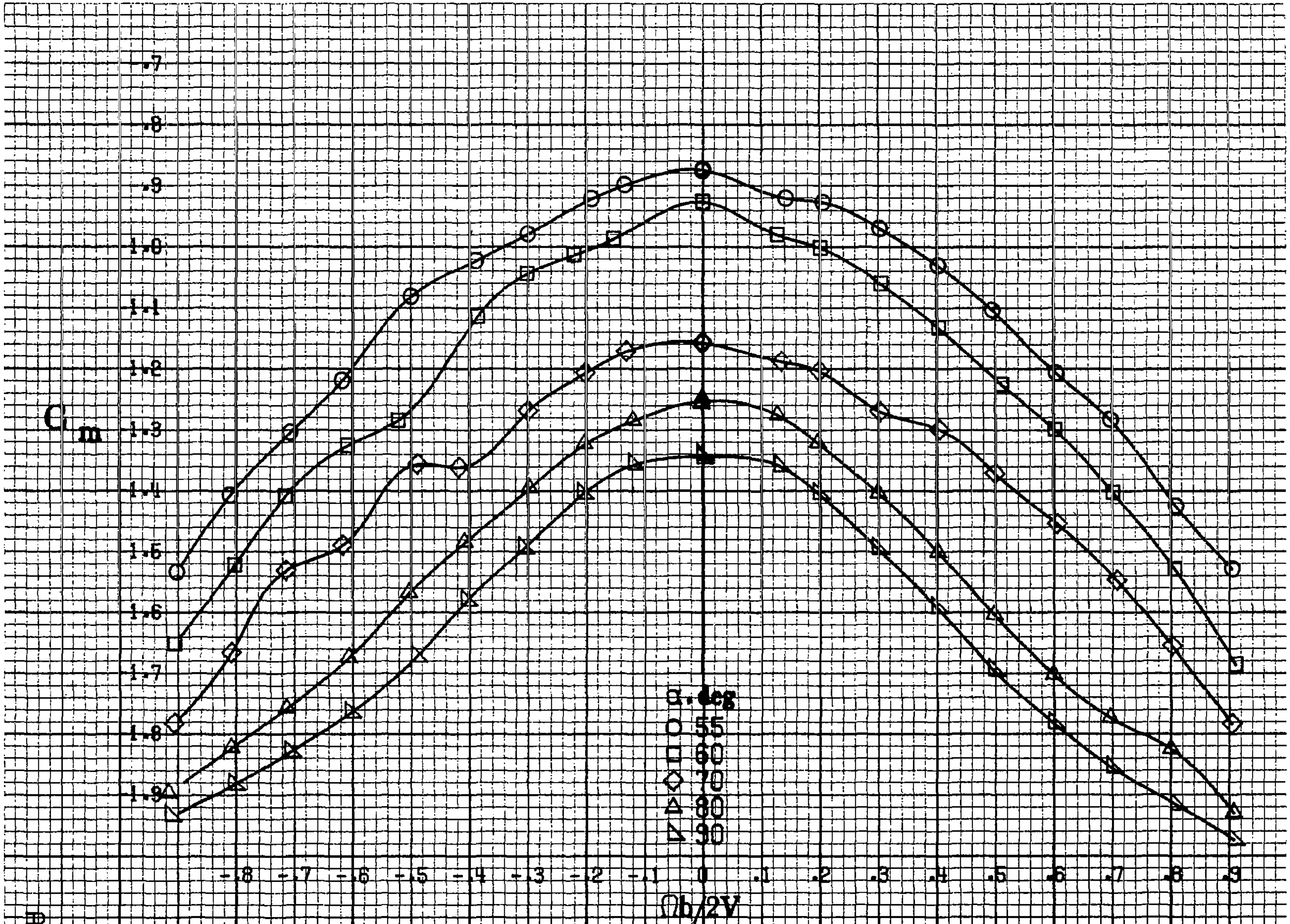

(d) α = 55 to 90 deg, SR = 0.

Figure A38.-Concluded.

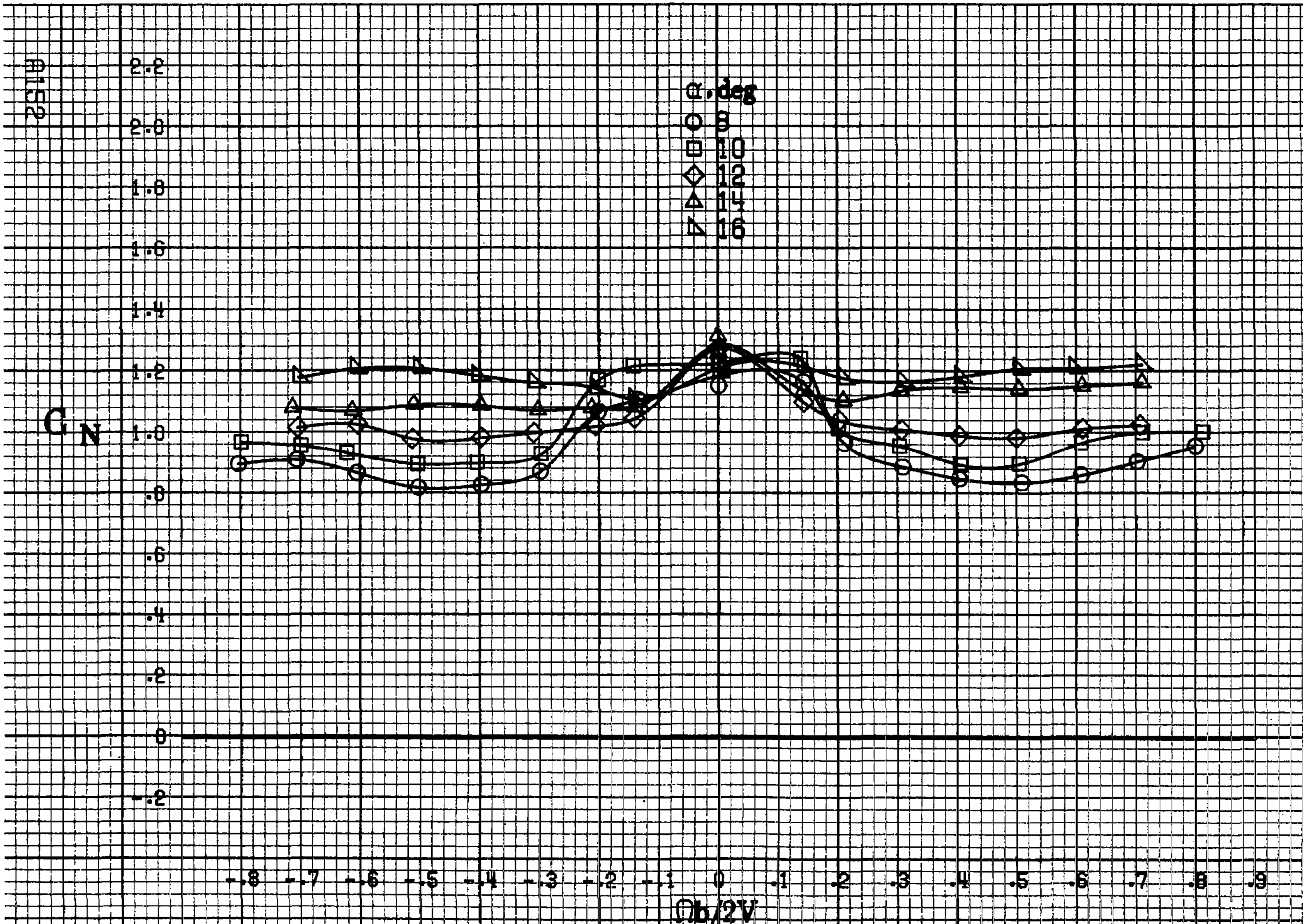

(a) $\alpha = 8$ to 16 deg, SR = 182.9 cm (72 in.).

Figure A34.-Effect of rotation rate and angle of attack on normal-force coefficient for full-span LE wing droop with moderate nose radius. $\delta_e = 0°$, $\delta_a = 0°$, $\delta_r = 0°$, $\beta = 0°$.

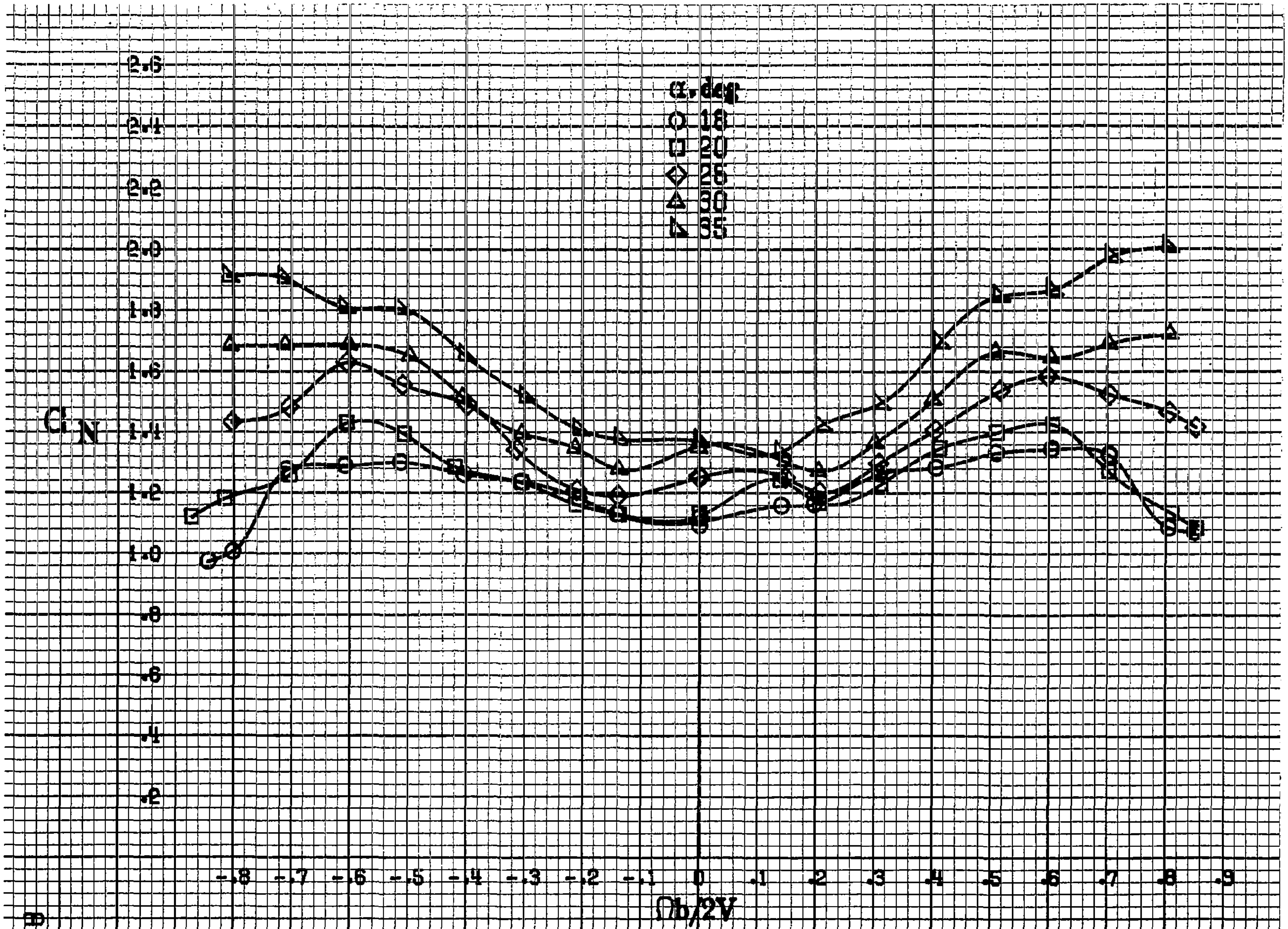

(b) α = 18 to 35 deg, SR = 182.9 cm (72 in).

Figure A84.-Continued.

A154

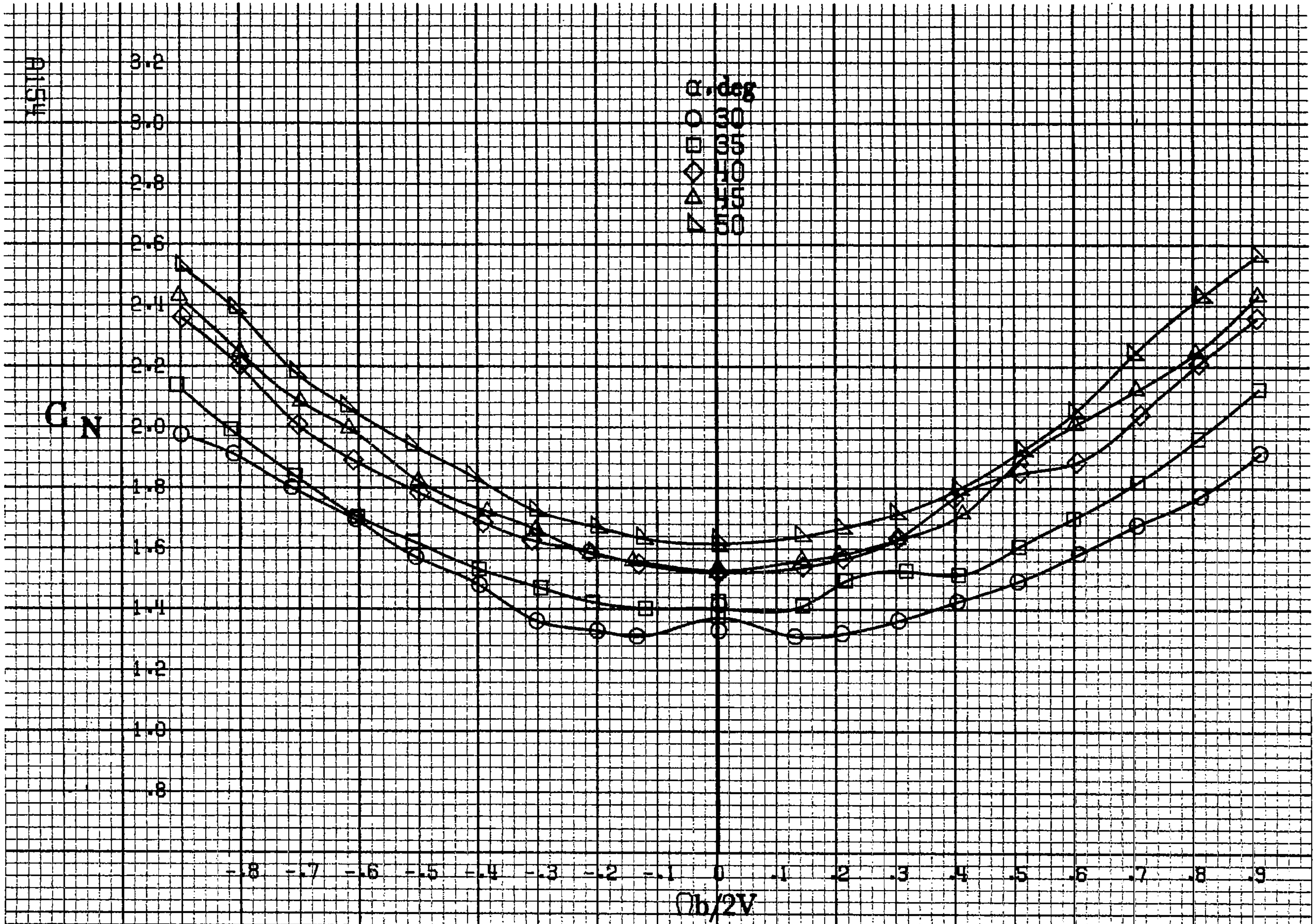

(c) α = 30 to 50 deg, SR = 0.

Figure A34.-Continued.

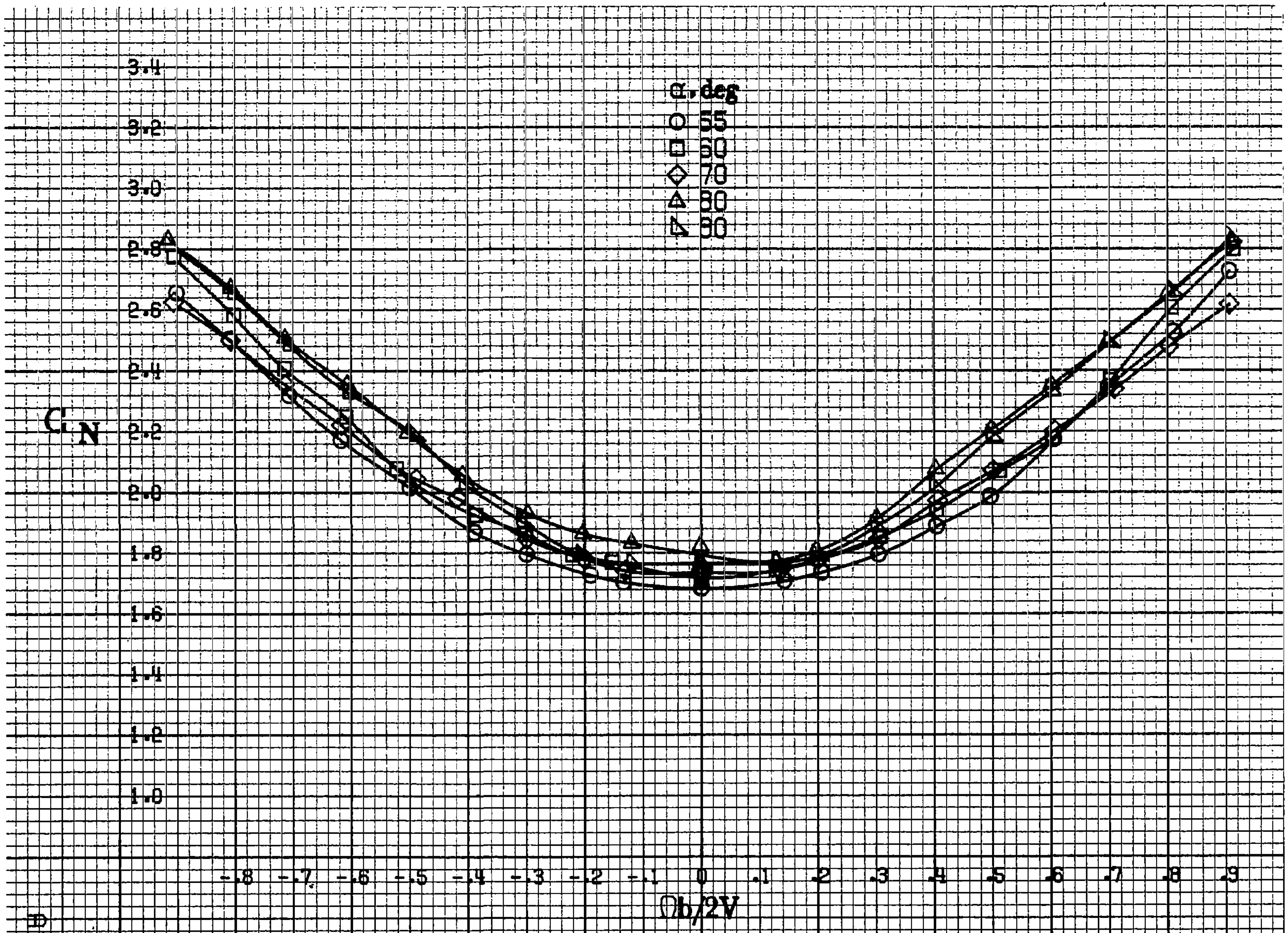

(d) α = 55 to 90 deg, SR = 0.

Figure A84.-Concluded.

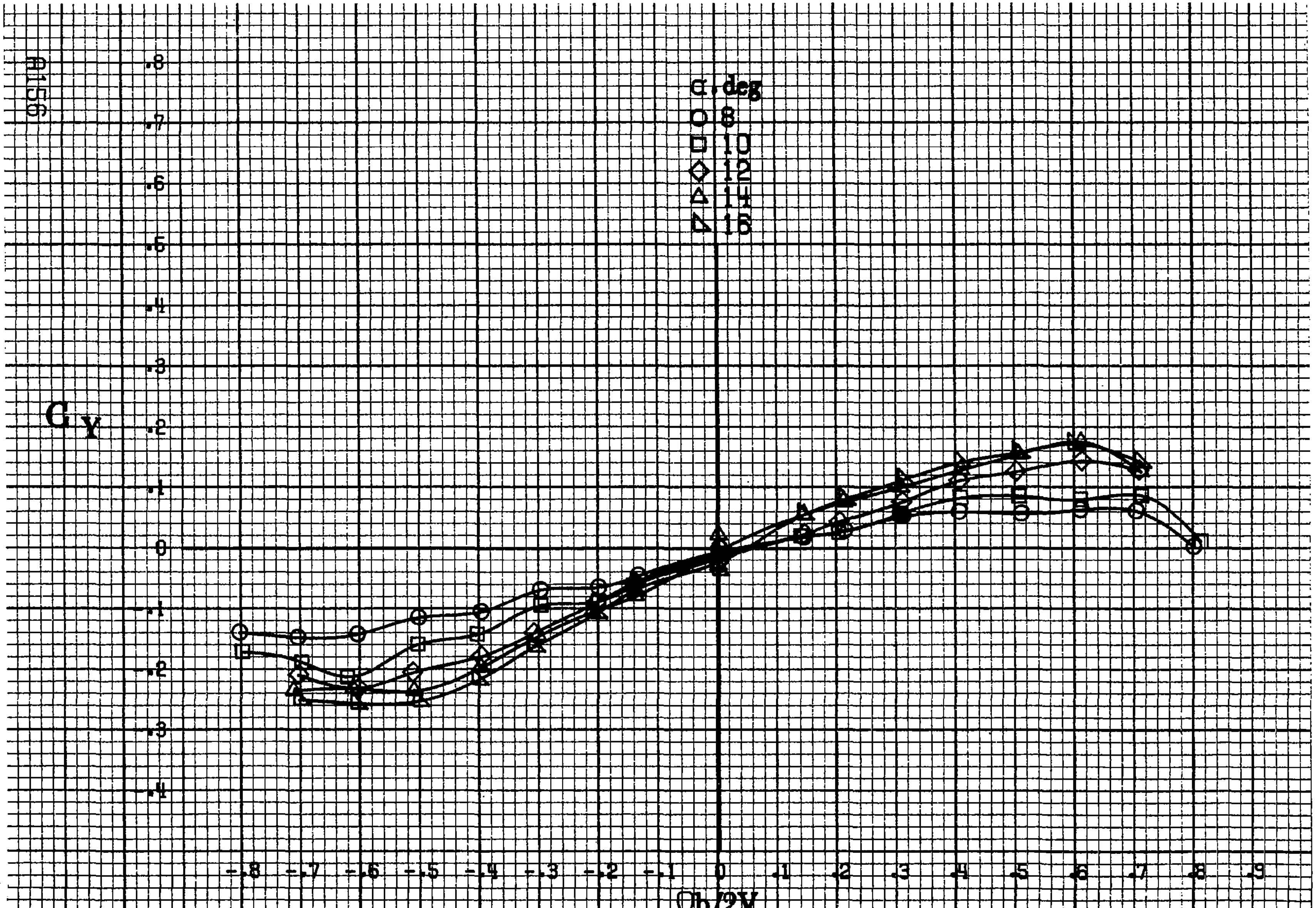

(a) $\alpha = 8$ to 16 deg, SR = 182.9 cm (72 in).

Figure A35.-Effect of rotation rate and angle of attack on side-force coefficient for full-span LE wing droop with moderate nose radius. $\delta_e = 0°$, $\delta_a = 0°$, $\delta_r = 0°$, $\beta = 0°$.

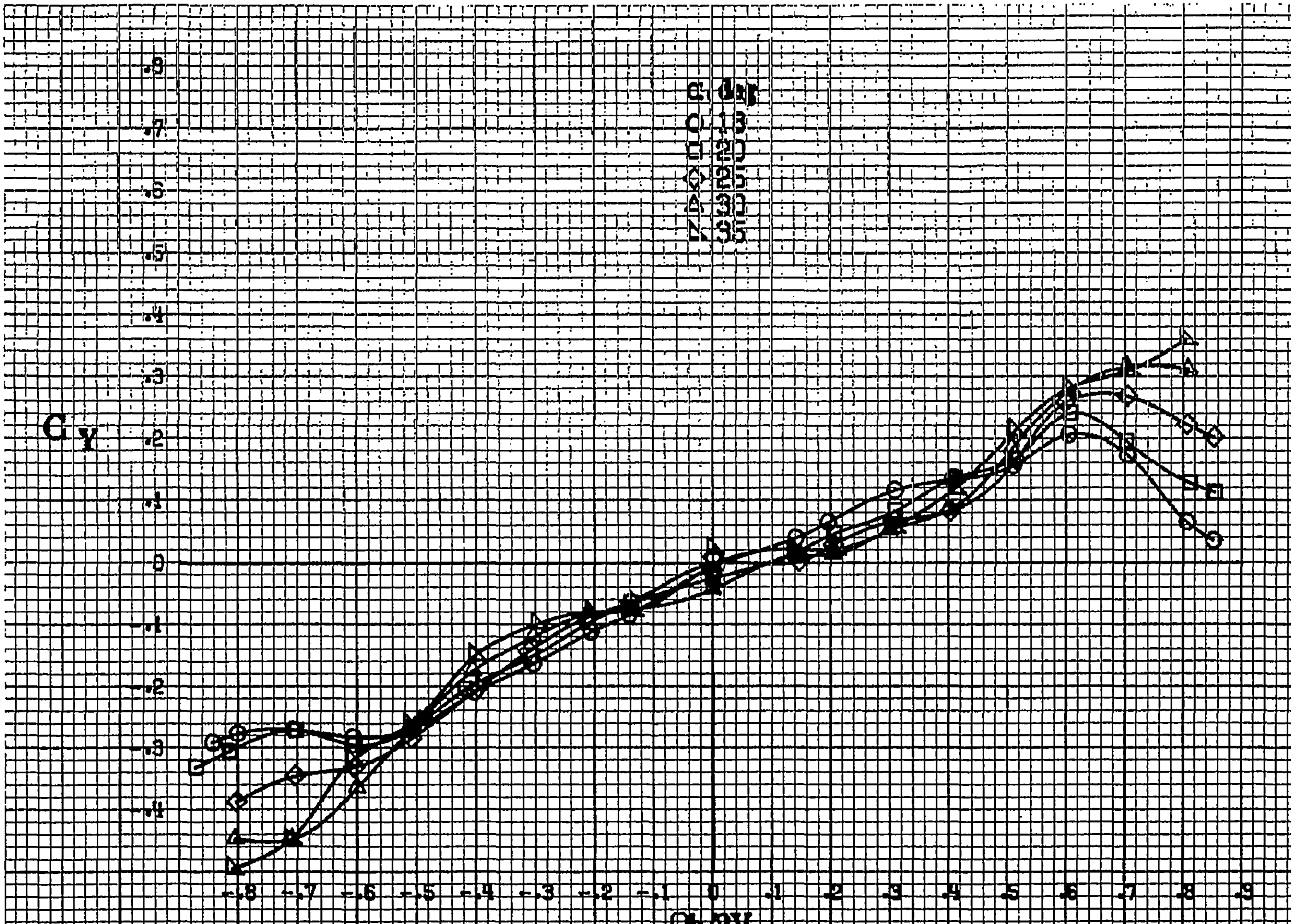

(b) α = 13 to 35 deg, SR = 182.9 cm (72 in).
Figure A35.-Continued.

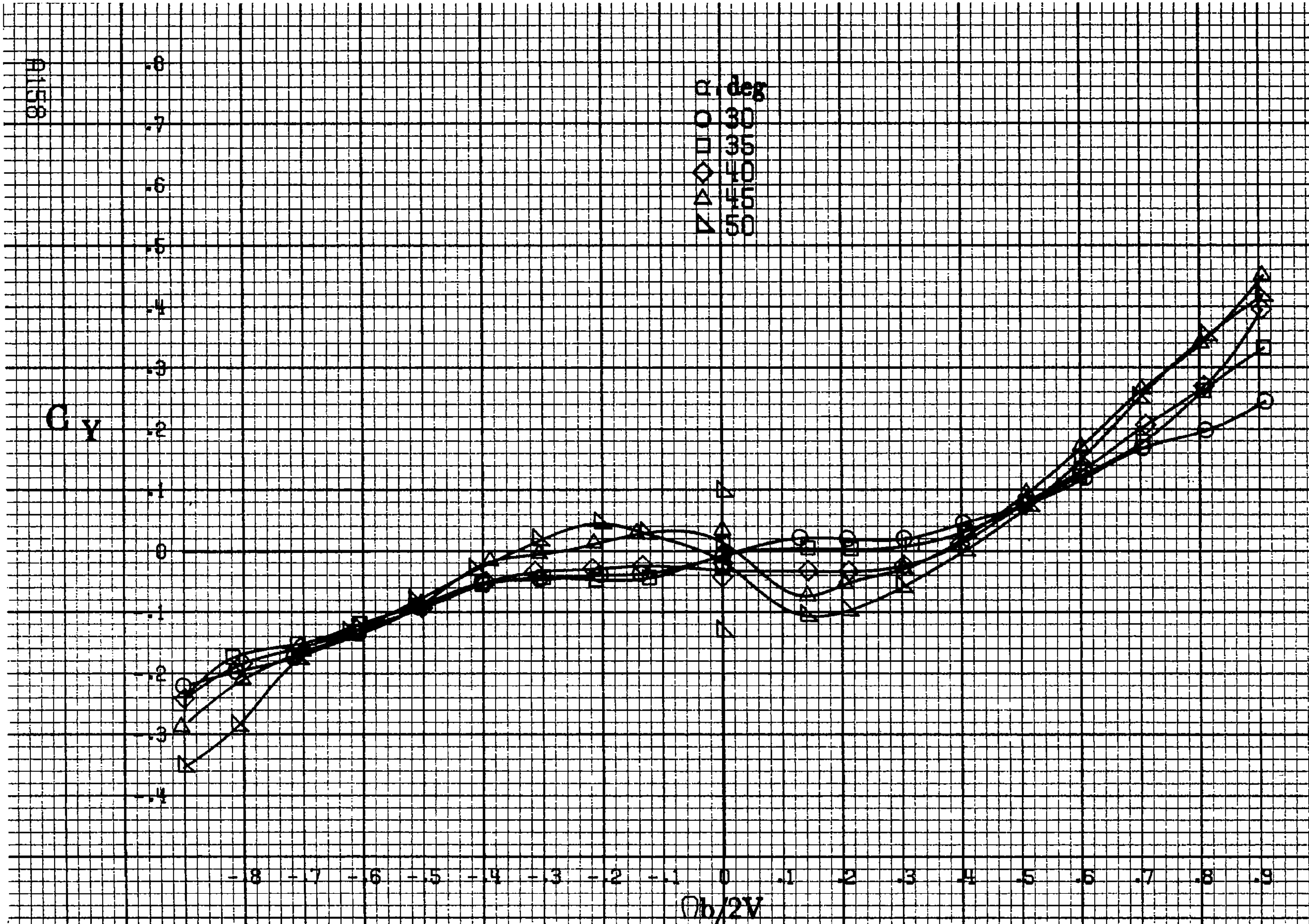

(c) α = 30 to 50 deg, SR = 0.

Figure A35.- Continued.

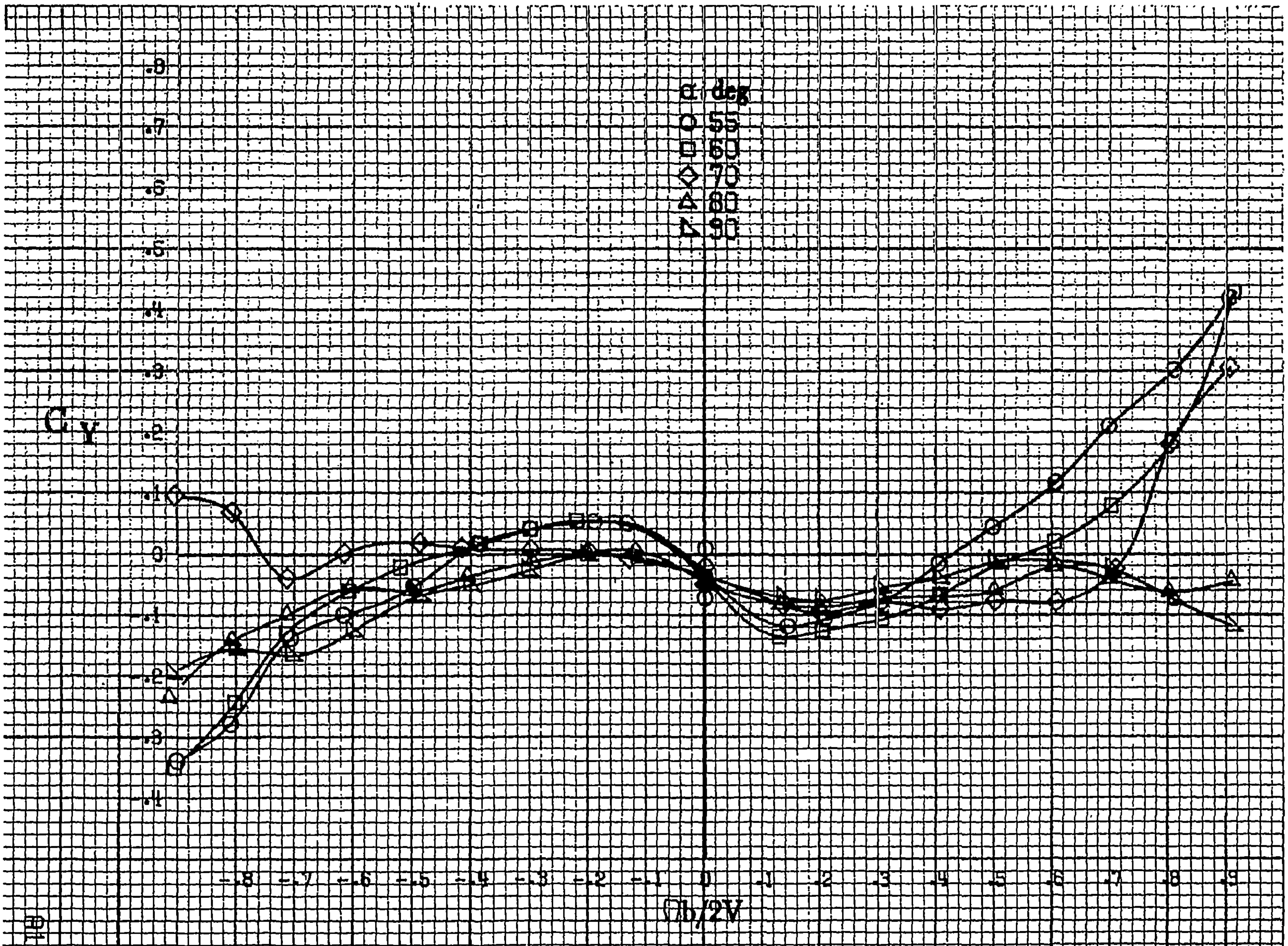

(d) α = 55 to 90 deg, SR = 0.
Figure A35.-Concluded.

A160

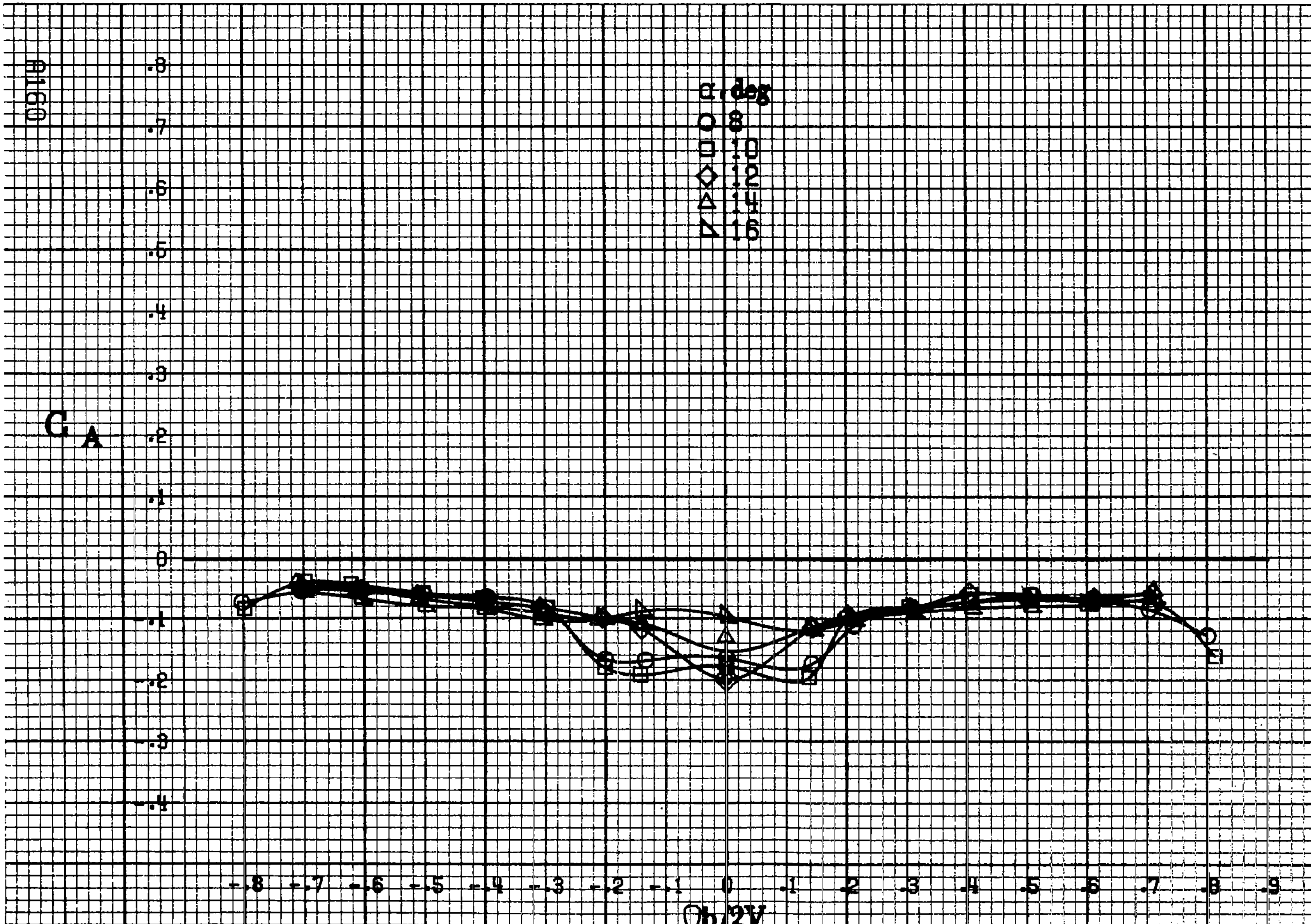

(a) α = 8 to 16 deg, SR = 182.9 cm (72 in.).

Figure A38.- Effect of rotation rate and angle of attack on axial-force coefficient for full-span LE wing droop with moderate nose radius. $\delta_e = 0°$, $\delta_a = 0°$, $\delta_r = 0°$, $\beta = 0°$.

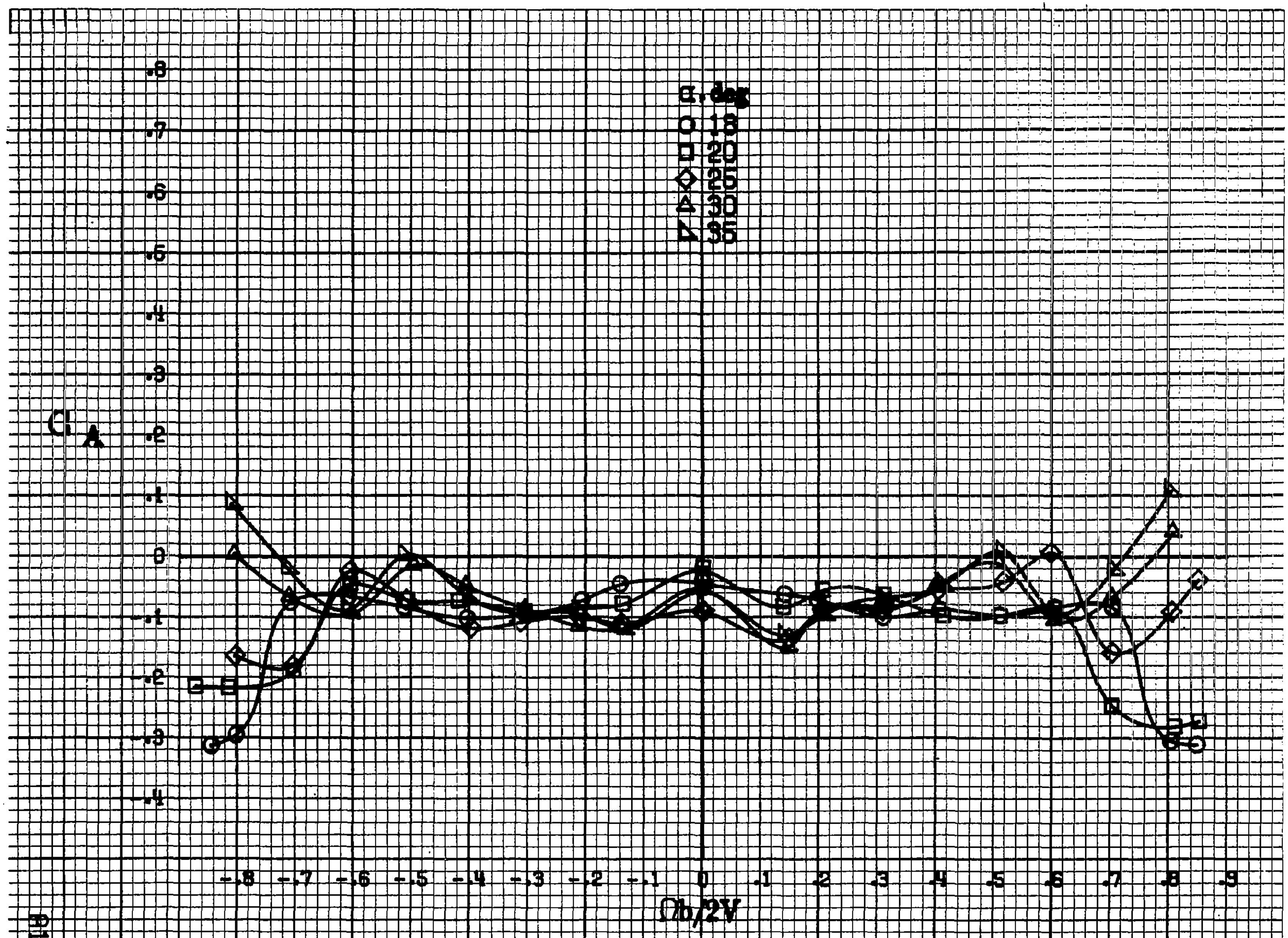

(b) α = 18 to 35 deg, SR = 182.9 cm (72 in).

Figure A36.-Continued.

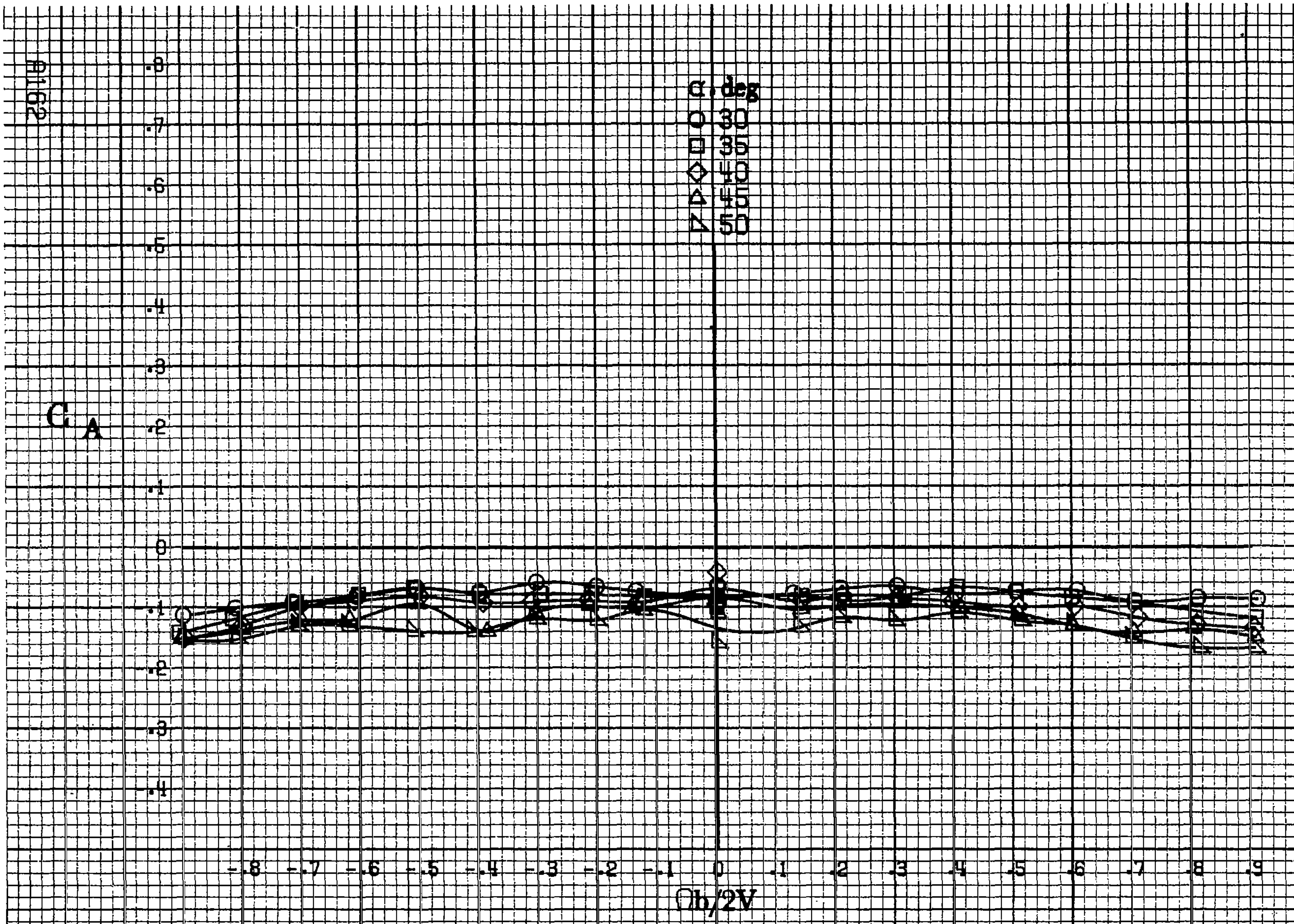

(c) α = 30 to 50 deg, SR = 0.

Figure A36.-Continued.

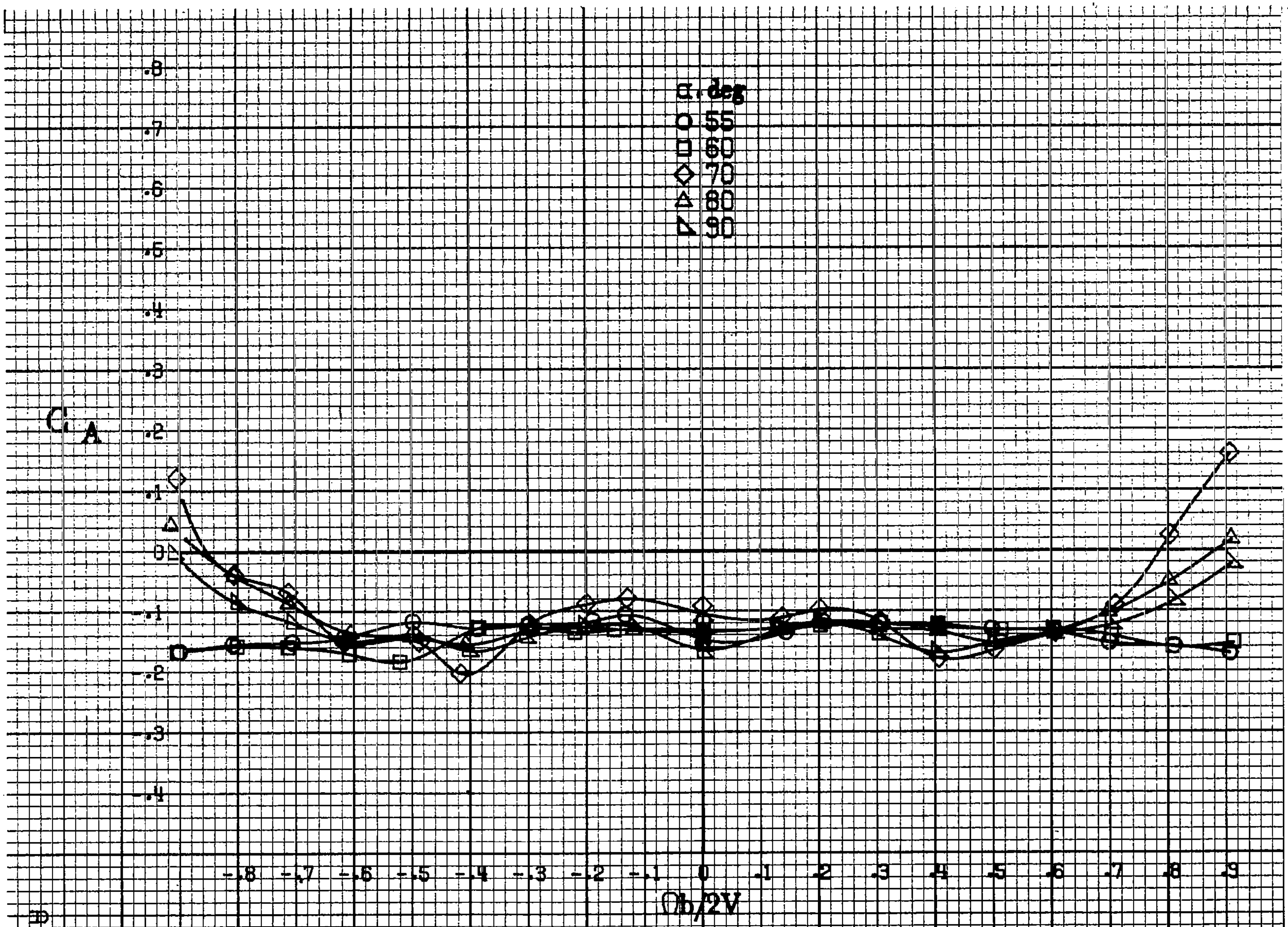

(d) α=55to90deg, SR=0.

Figure A86.-Concluded.

A163

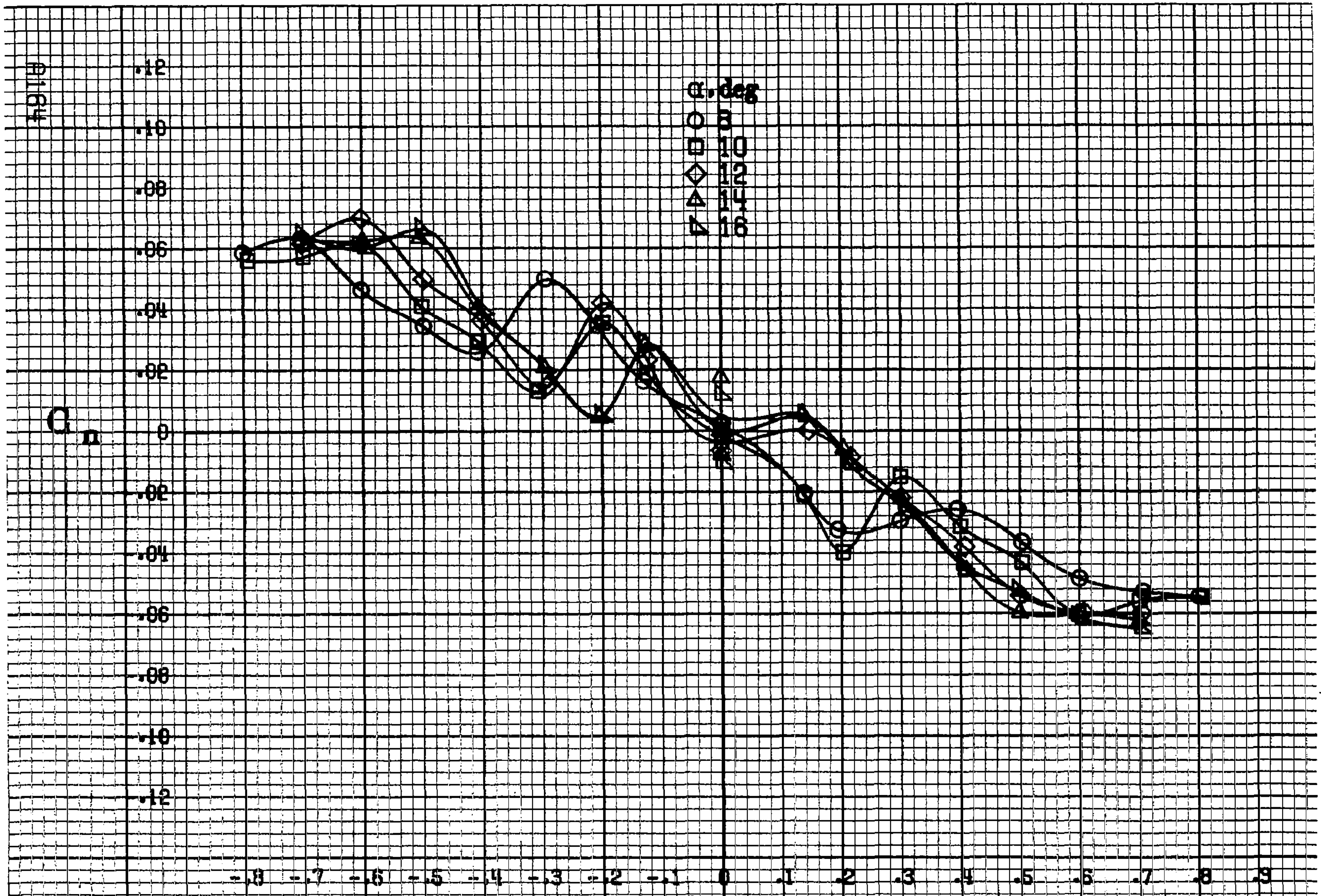

(a) α = 8 to 16 deg, SR = 182.9 cm (72 in).

Figure A37. Effect of rotation rate and angle of attack on yawing-moment coefficient for full-span LE wing droop with large nose radius. $\delta_a = 0°$, $\delta_e = 0°$, $\delta_r = 0°$, $\beta = 0°$.

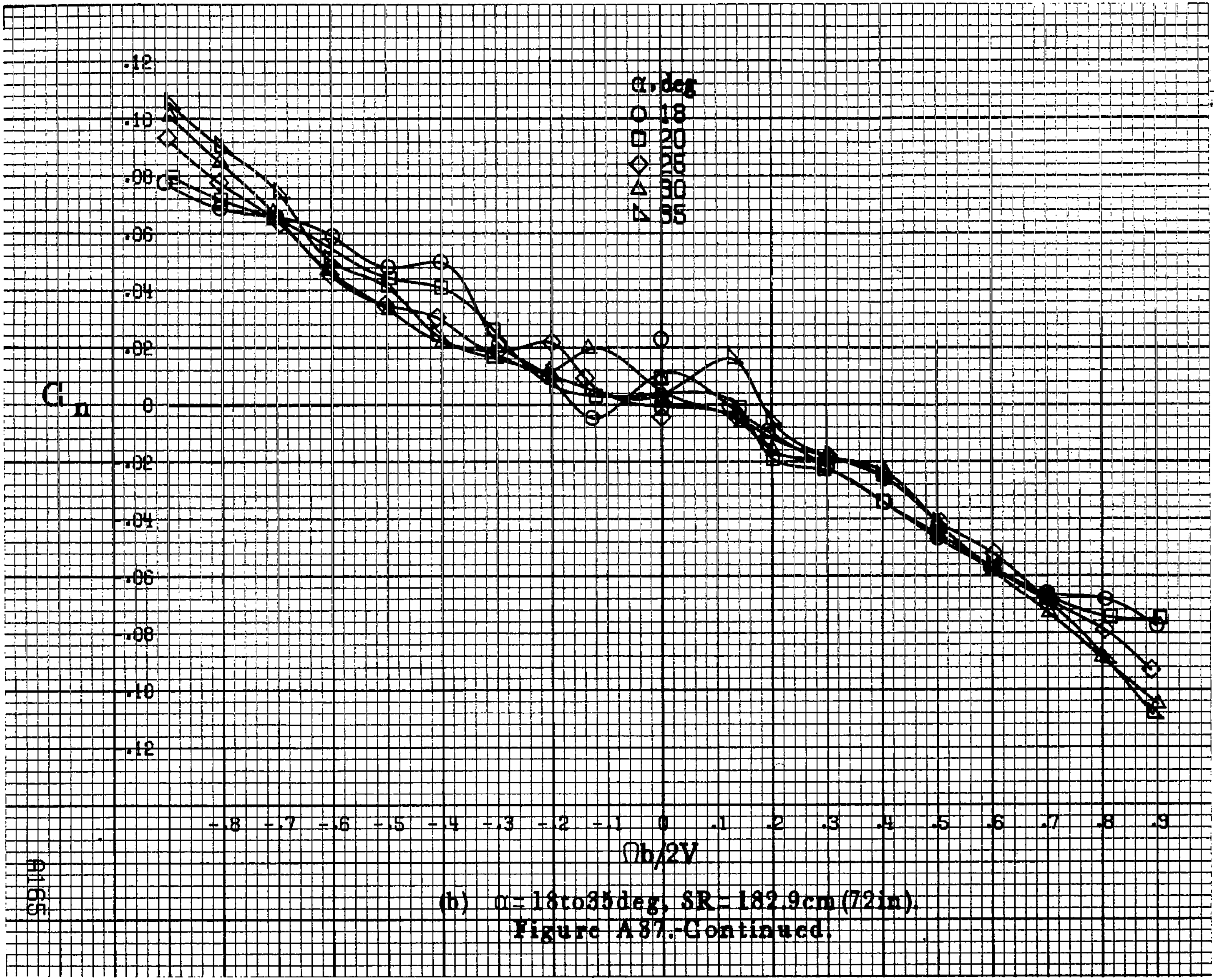

(b) α = 18 to 35 deg, SR = 182.9 cm (72 in).

Figure A87.- Continued.

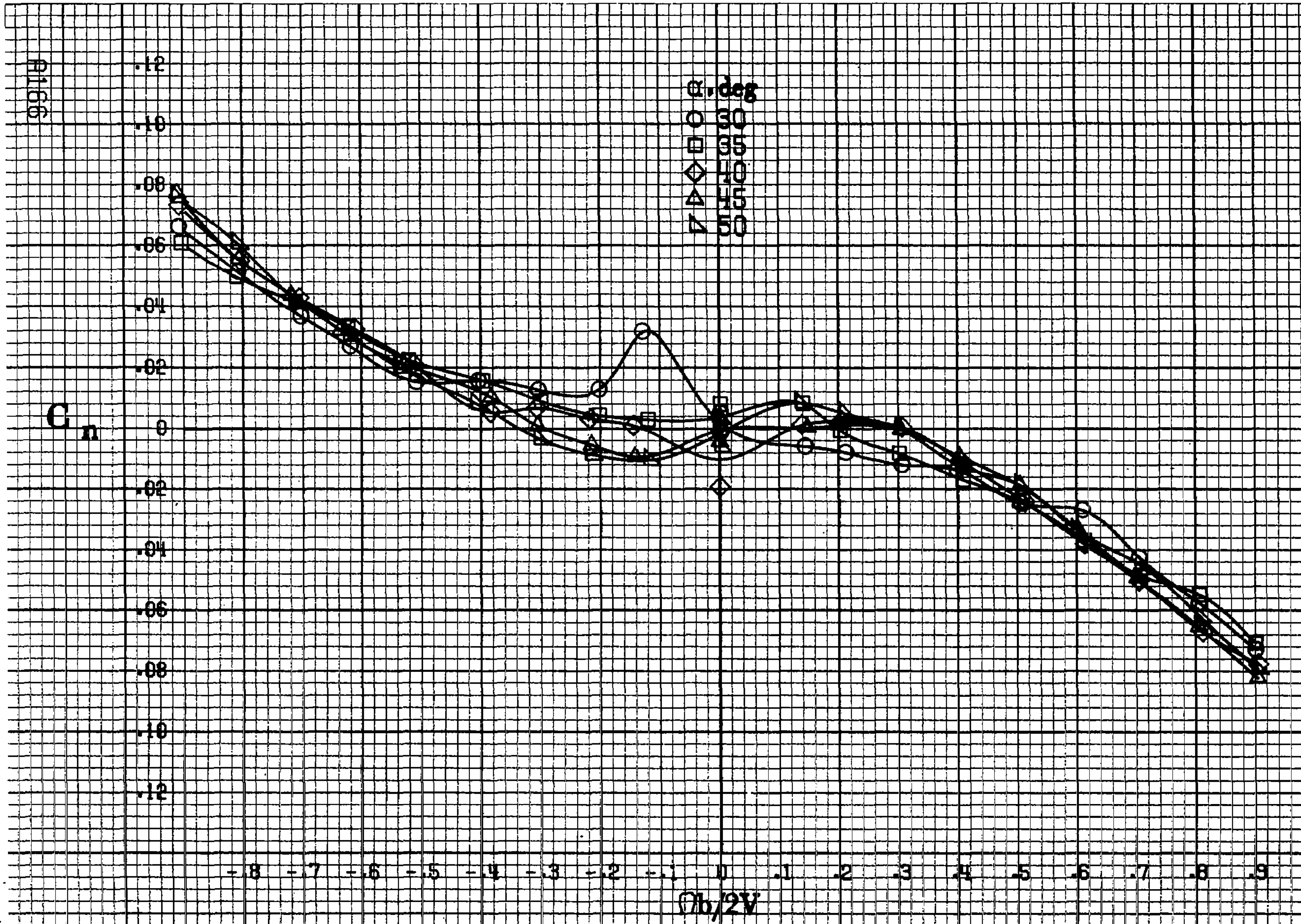

(c) α = 30 to 50 deg, SR = 0.

Figure A37.-Continued.

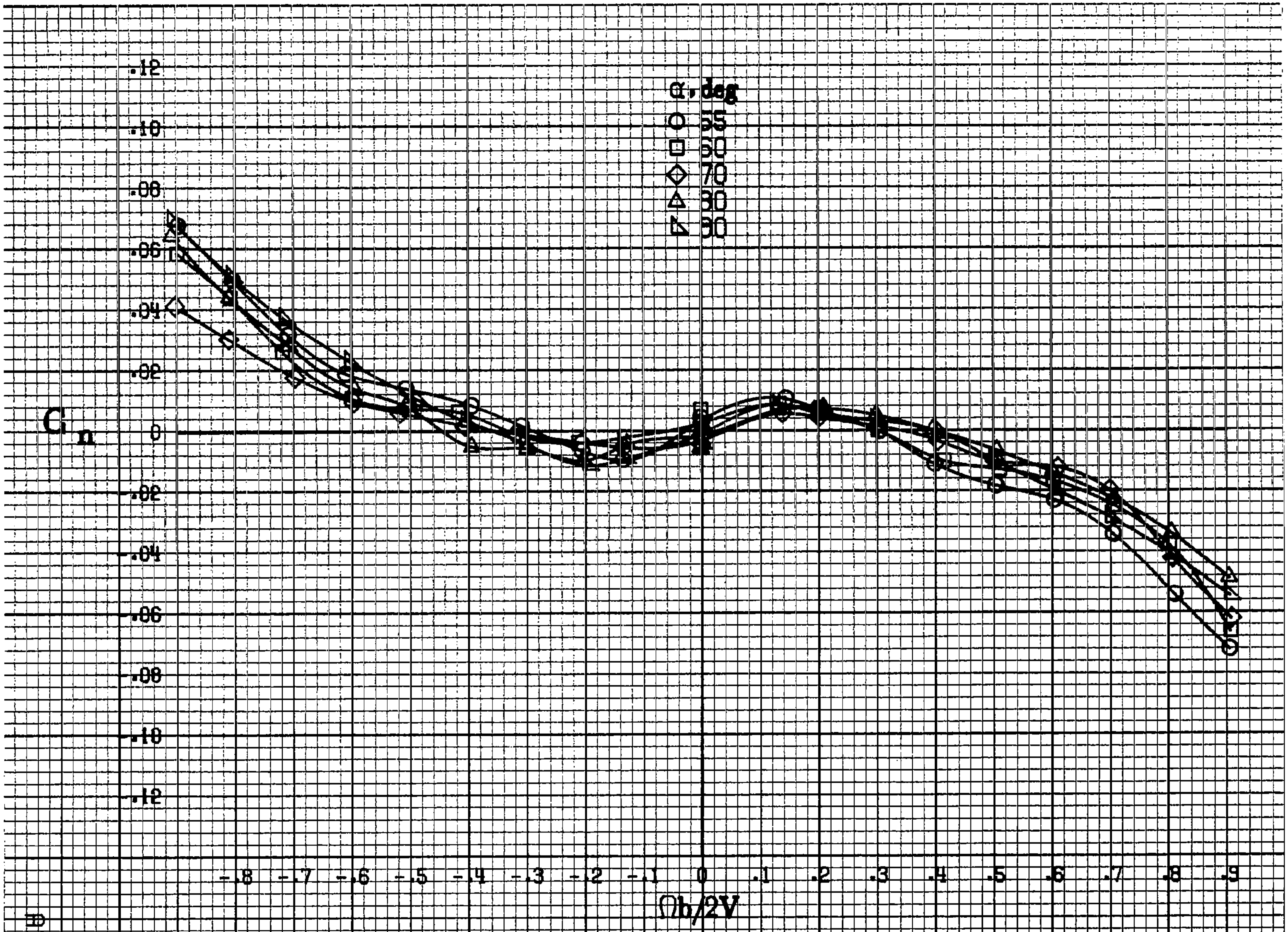

(d) α=55to90deg, SR=0.
Figure A87.-Concluded.

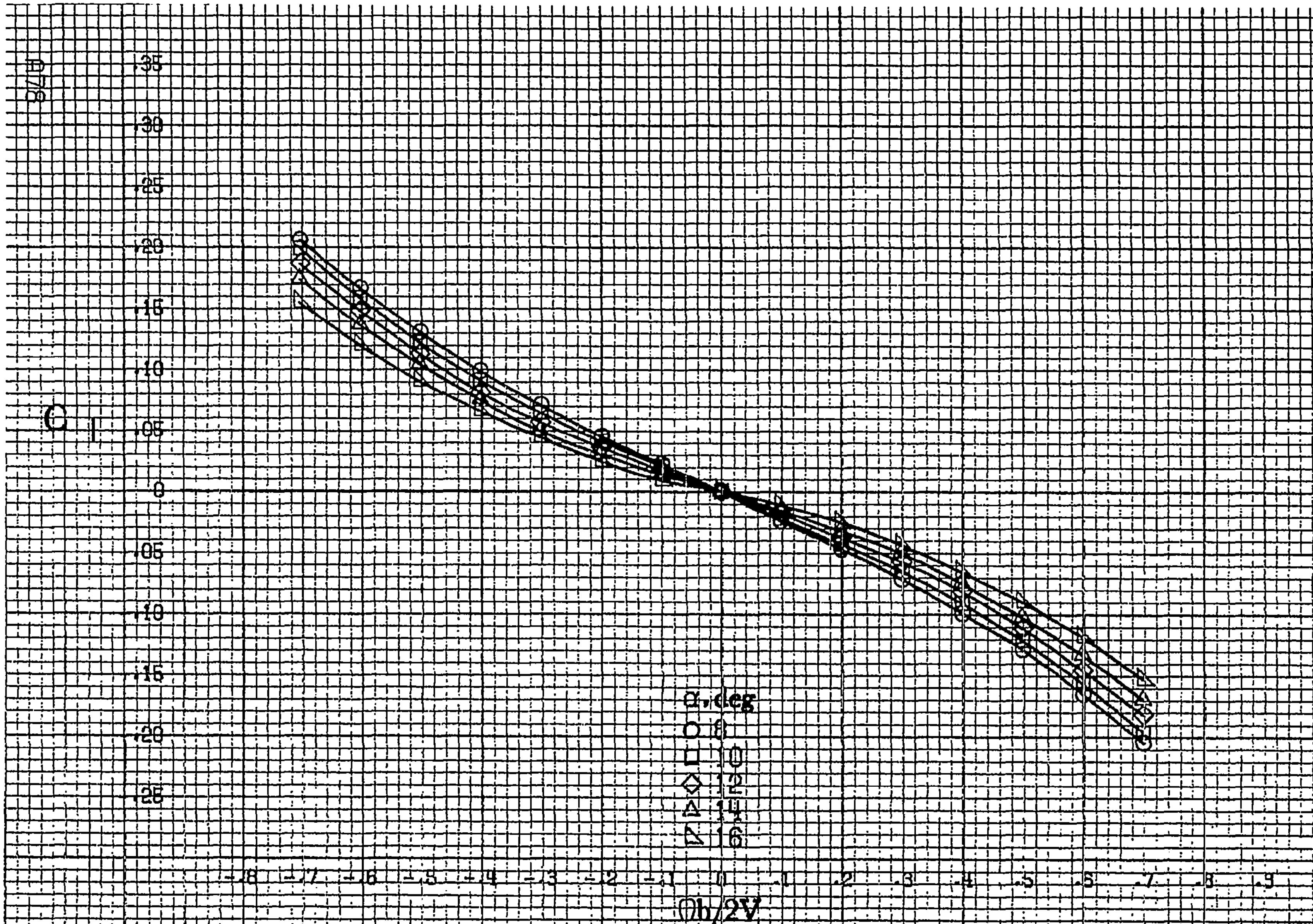

(a) $\alpha = 8$ to 16 deg, SR = 182.9cm (72in).

Figure A20.- Effect of rotation rate and angle of attack on rolling-moment coefficient for body wing horizontal tail configuration. $\delta_e = 0°$, $\delta_a = 0°$, $\delta_r = 0°$, $\beta = 0°$.

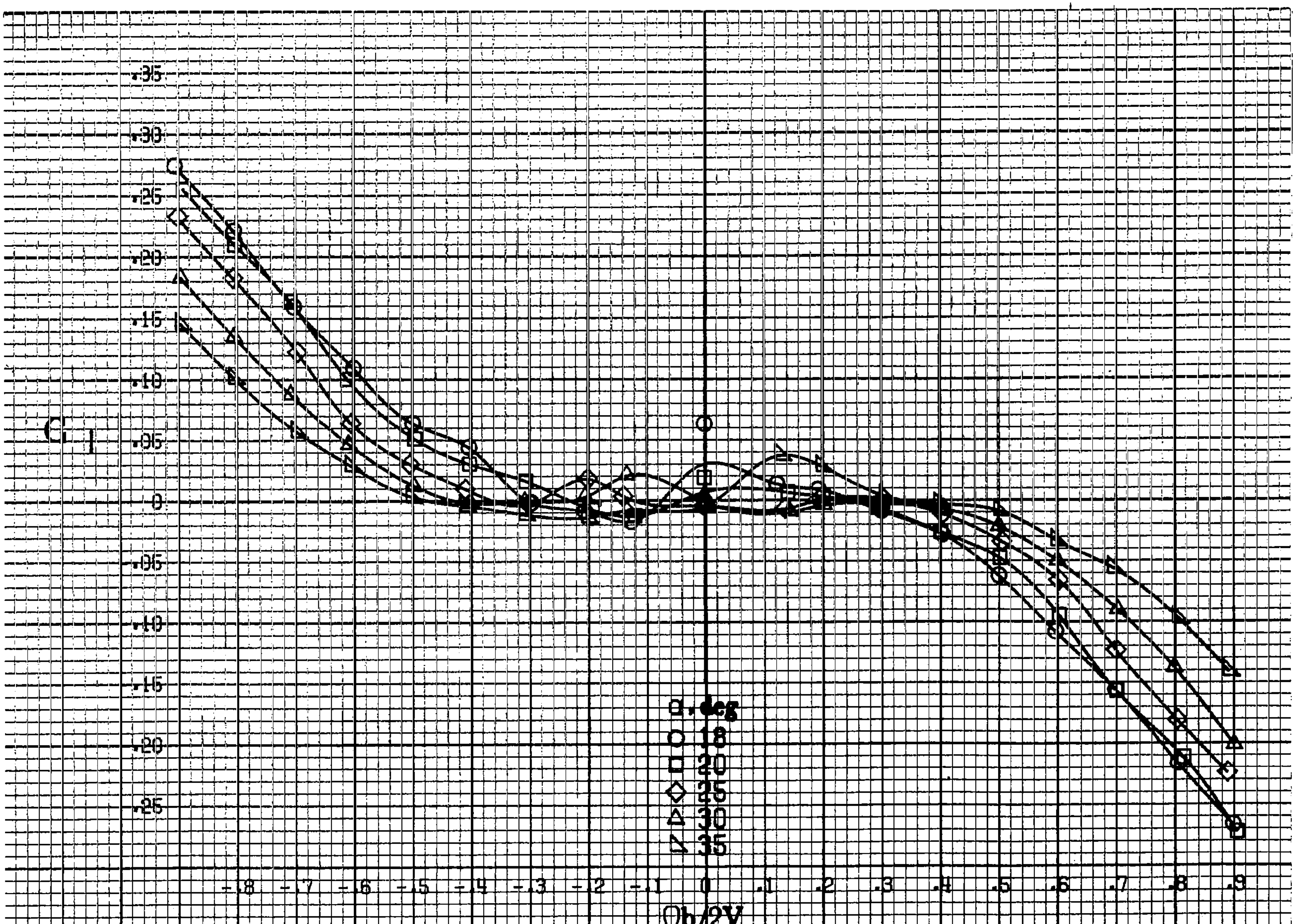

(b) α = 18 to 35 deg, SR = 182.9 cm (72 in).

Figure A88.-Continued.

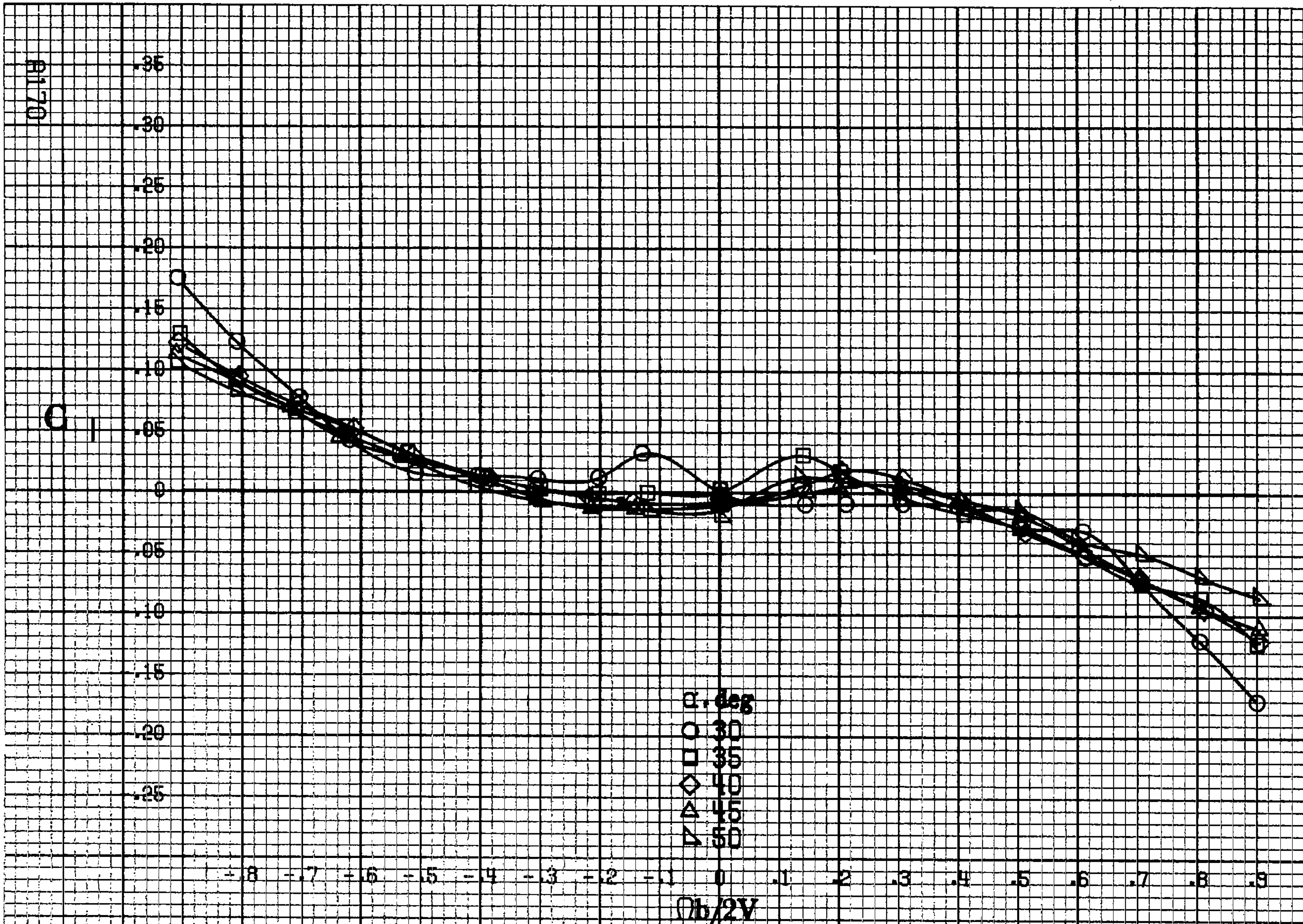

(c) α = 30 to 50 deg, SR = 0.

Figure A88.-Continued.

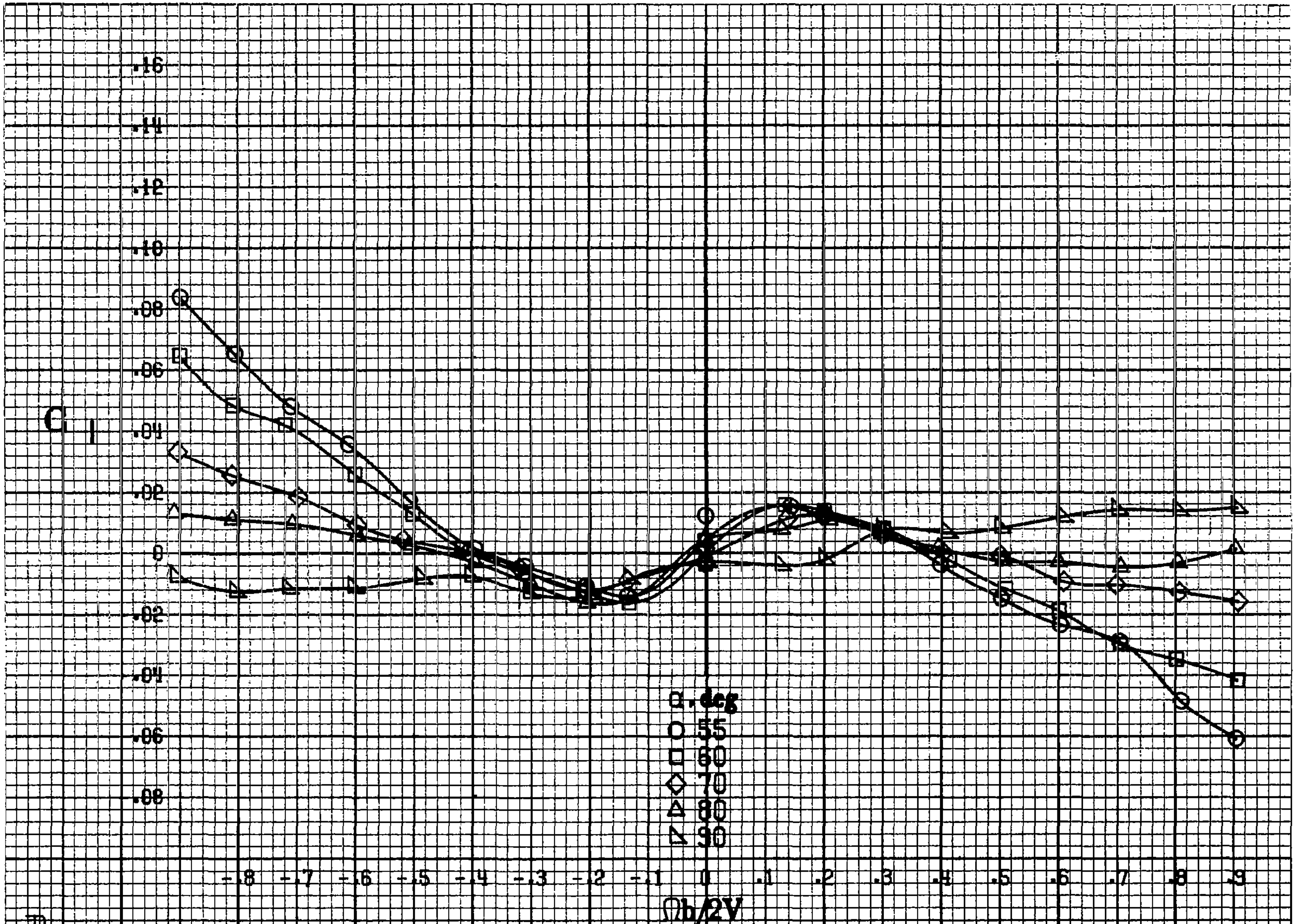

(d) α = 55 to 90 deg, SR = 0.

Figure A38.-Concluded.

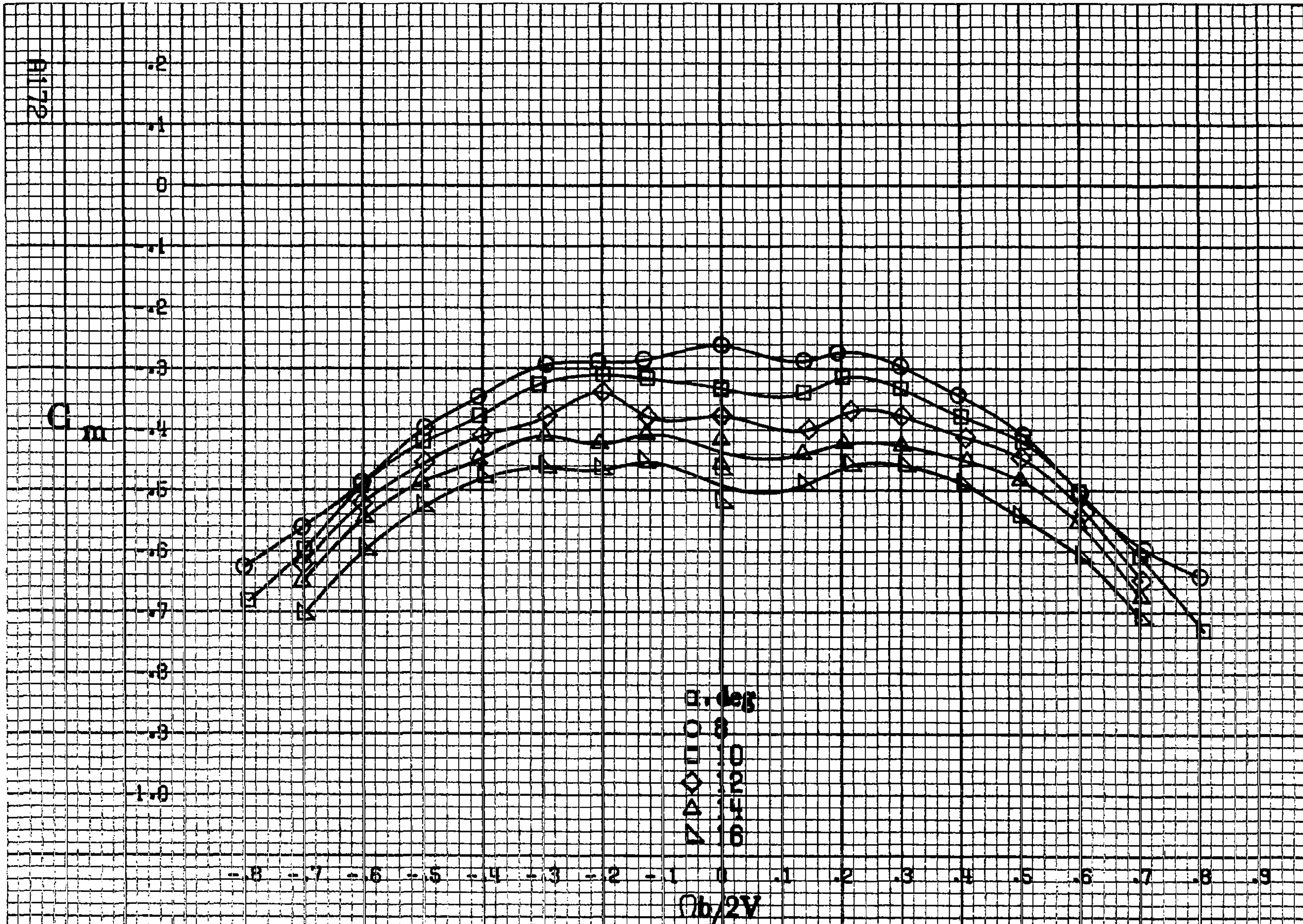

(a) α = 8 to 16 deg, SR = 182.9 cm (72 in).

Figure A39.- Effect of rotation rate and angle of attack on pitching-moment coefficient for full-span LE wing droop with large nose radius. $\delta_e = 0°$, $\delta_a = 0°$, $\delta_r = 0°$, $\beta = 0°$.

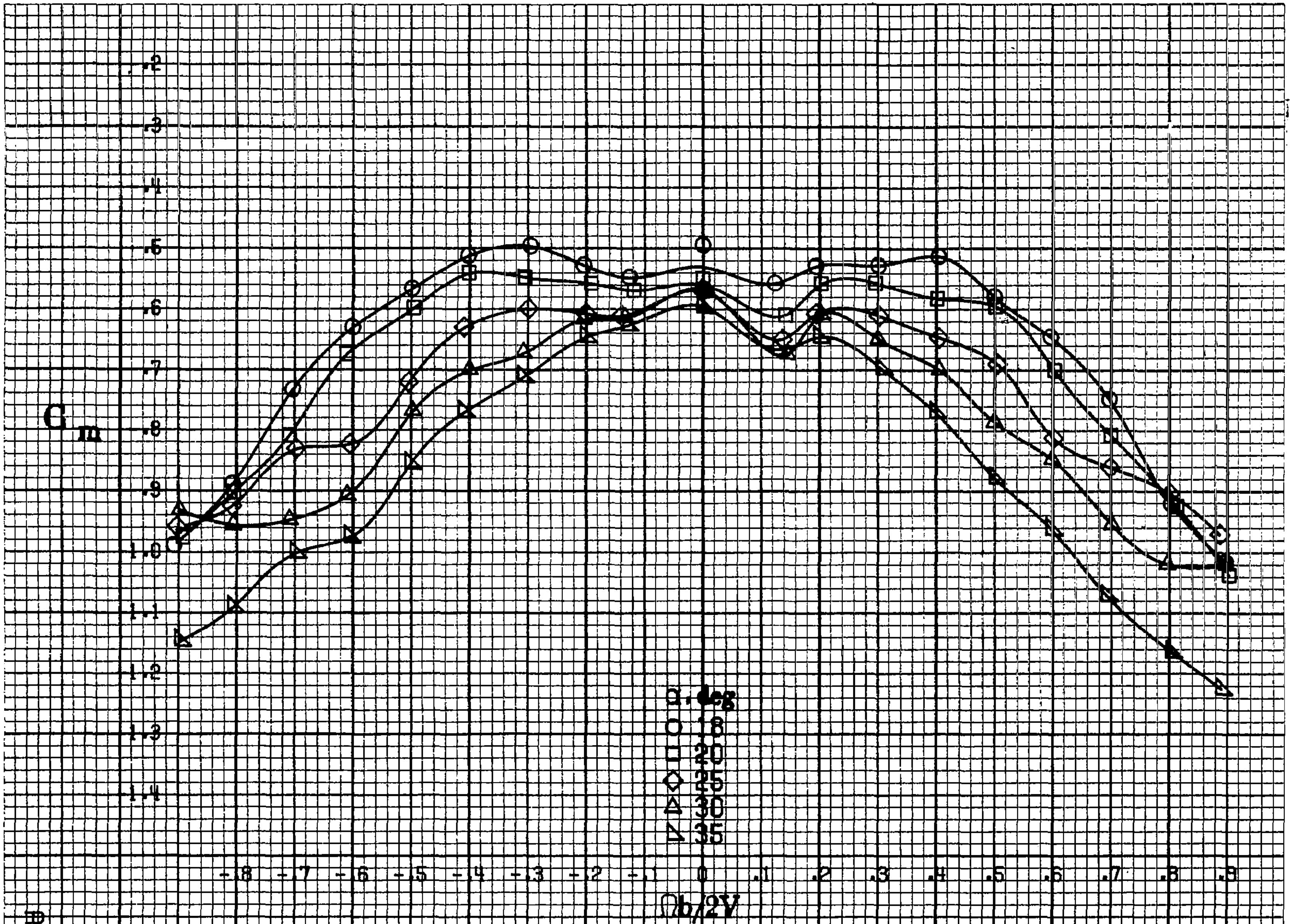

(b) α = 18 to 35 deg, SR = 182.9 cm (72 in).

Figure A39.-Continued.

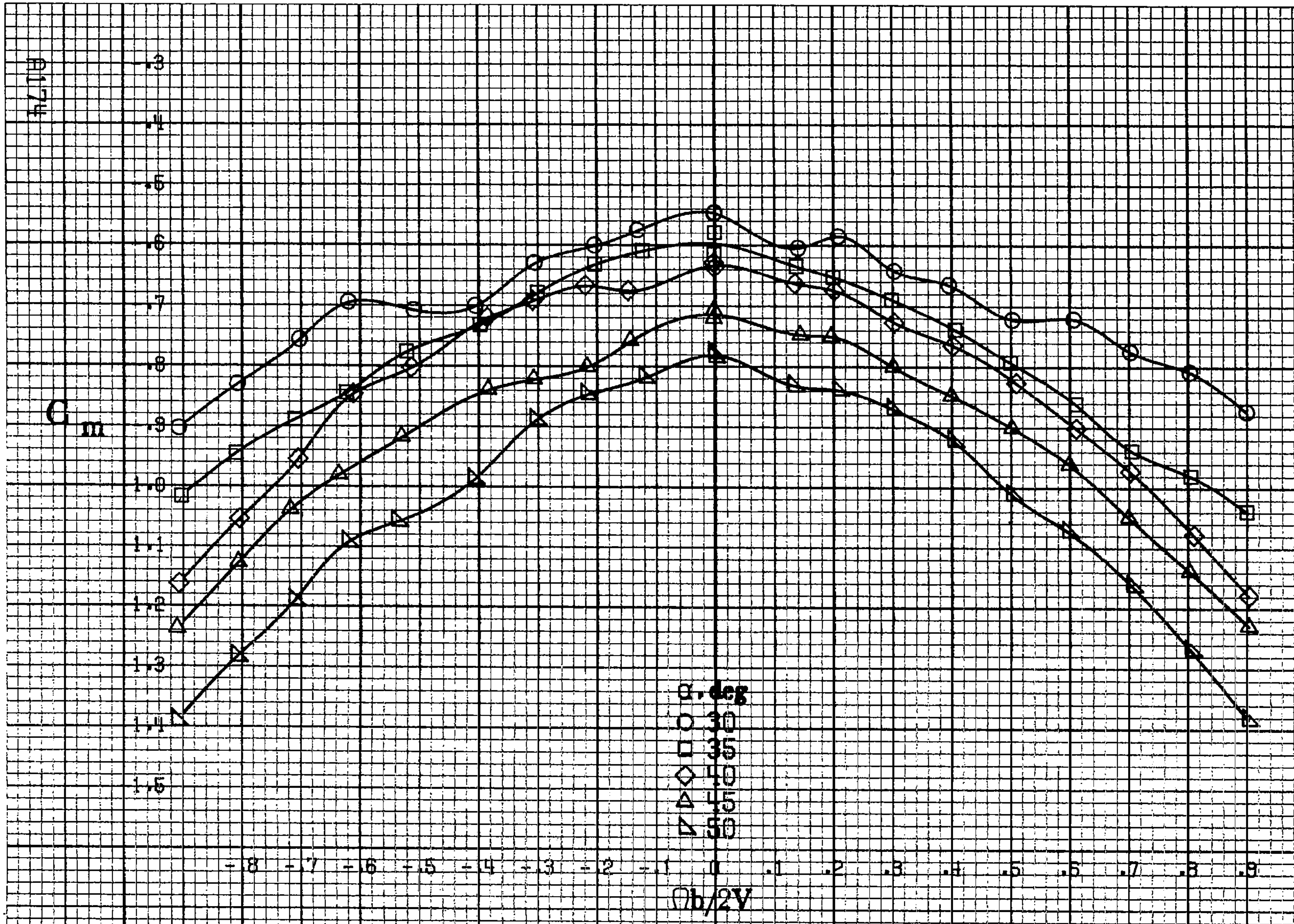

(c) α = 30 to 50 deg, SR = 0.

Figure A89.-Continued.

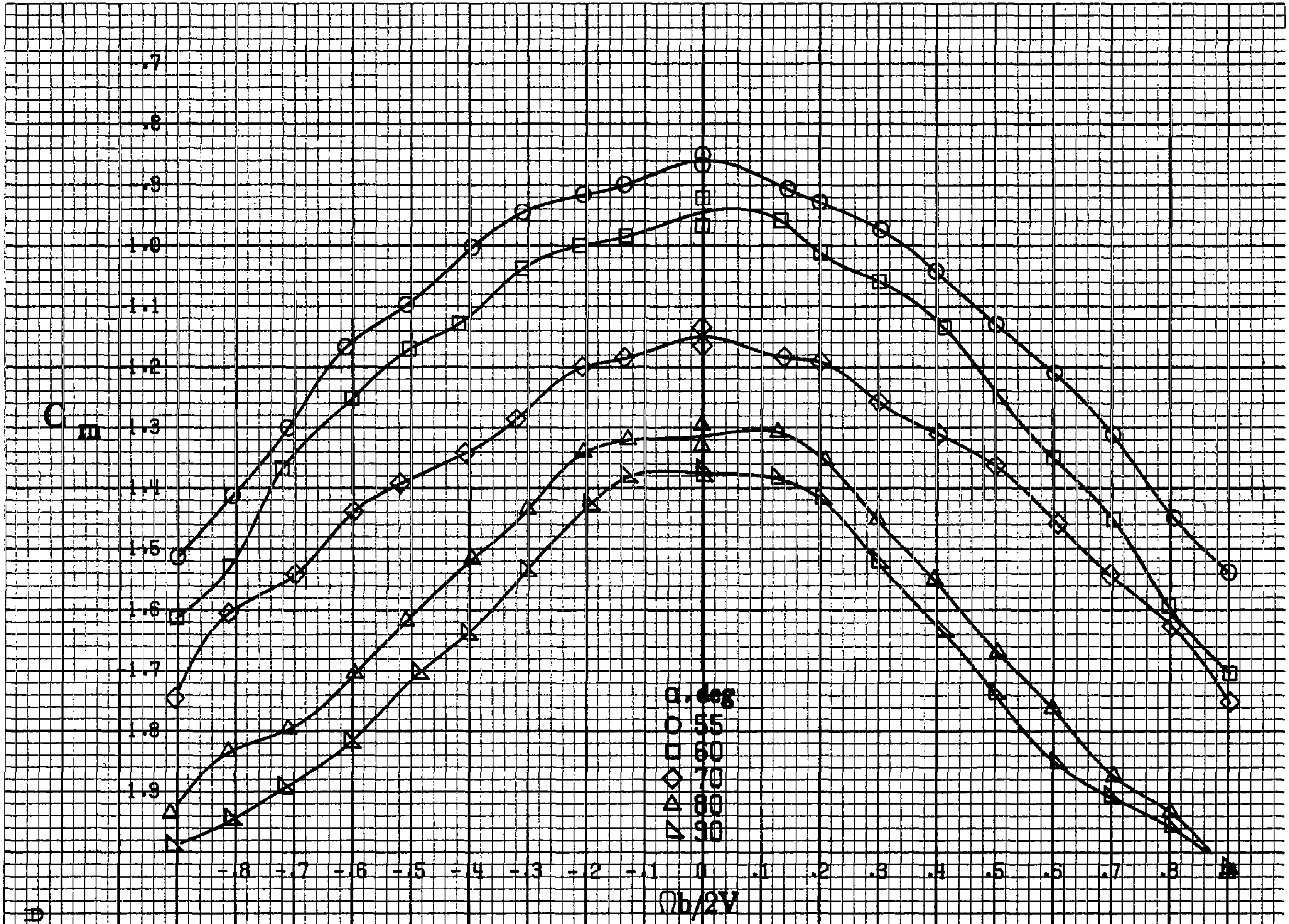

(d) α = 55 to 90 deg, SR = 0.

Figure A89.-Concluded.

A175

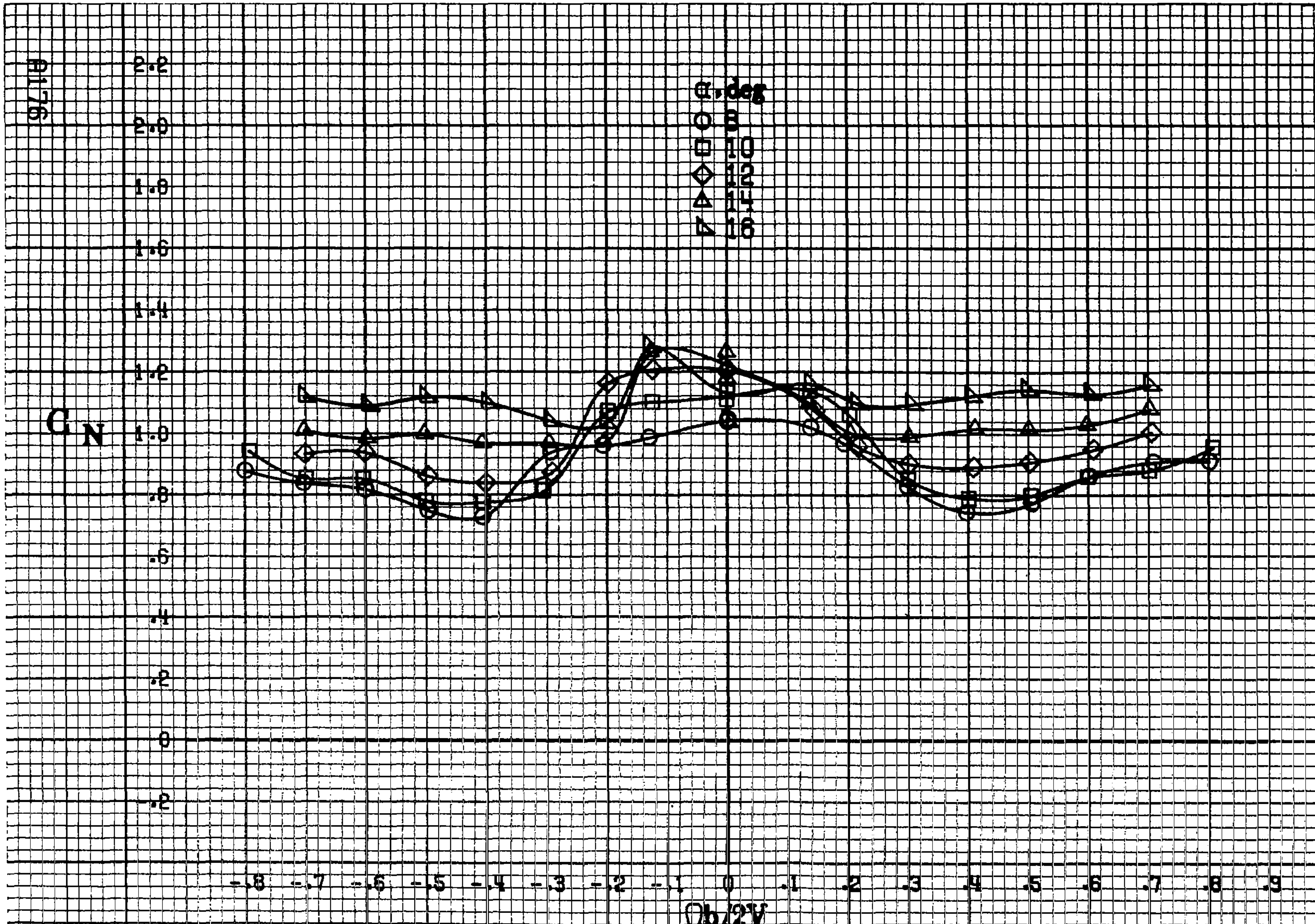

(a) $\alpha = 8$ to 16 deg, SR = 182.9 cm (72 in).

Figure A40.- Effect of rotation rate and angle of attack on normal-force coefficient for full-span LE wing droop with large nose radius. $\delta_e = 0°$. $\delta_a = 0°$. $\delta_r = 0°$. $\beta = 0°$.

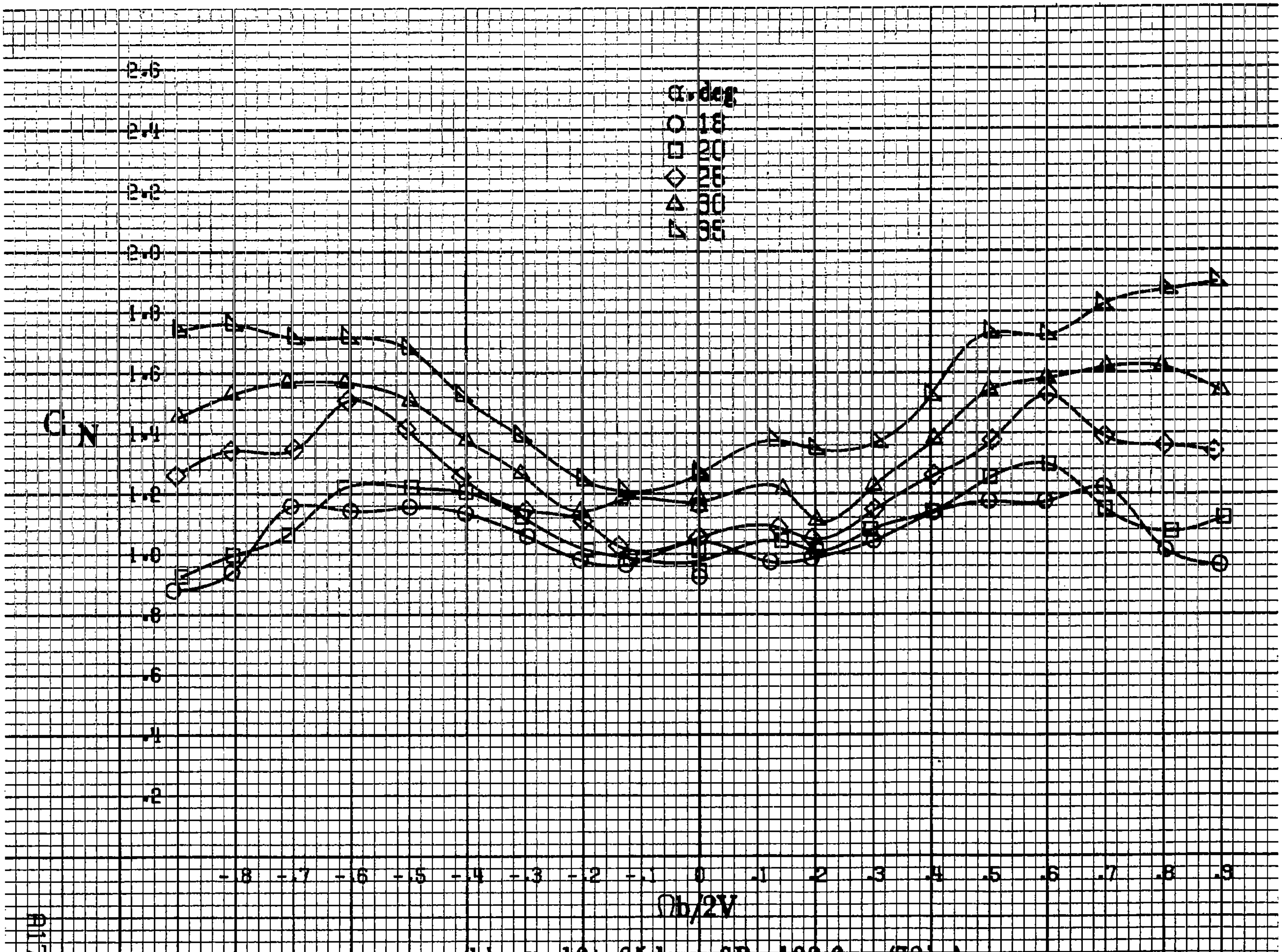

(b) α = 18 to 35 deg, SR = 182.9 cm (72 in).

Figure A 40.-Continued.

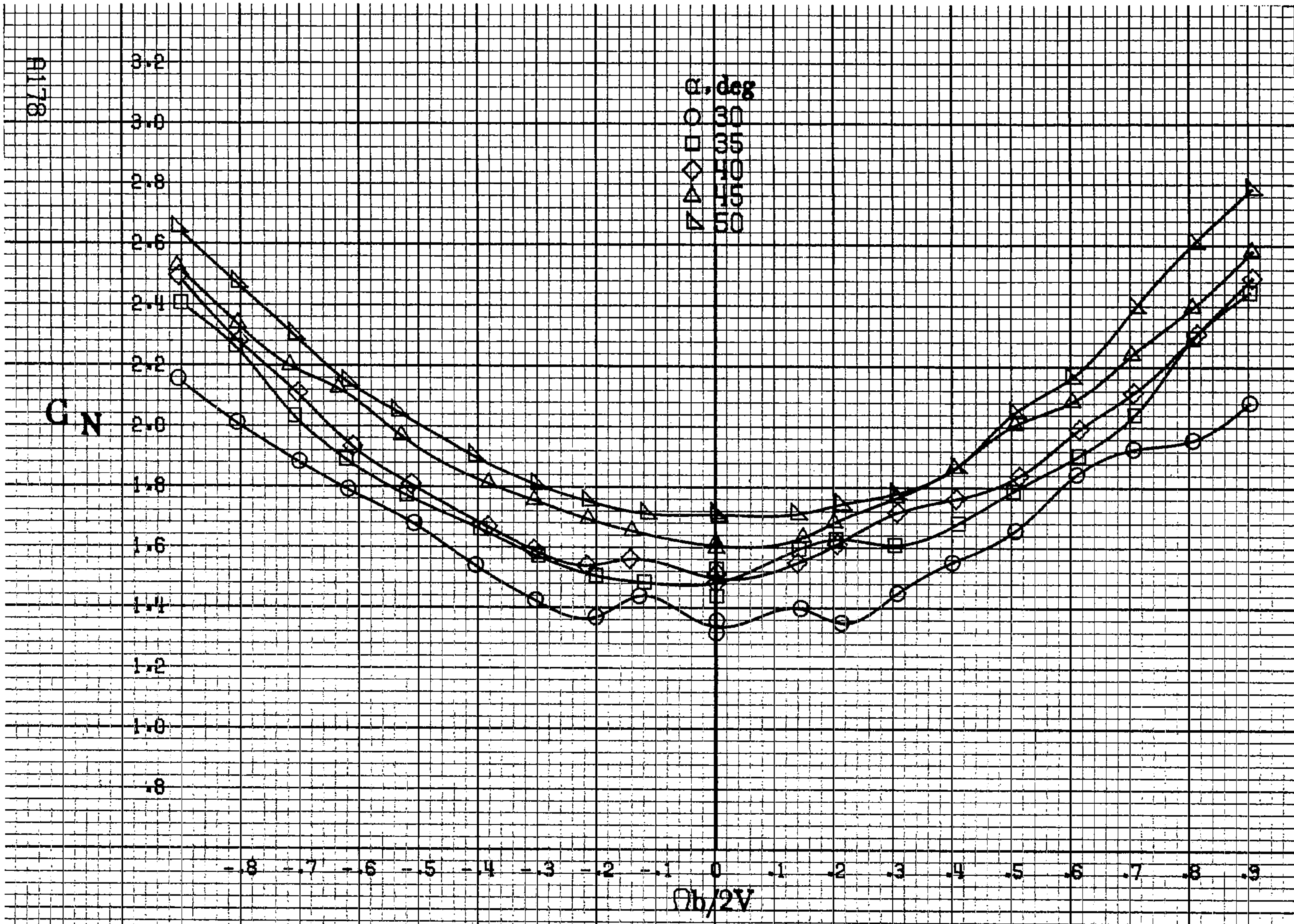

(c) α = 30 to 50 deg, SR = 0.

Figure A40.-Continued.

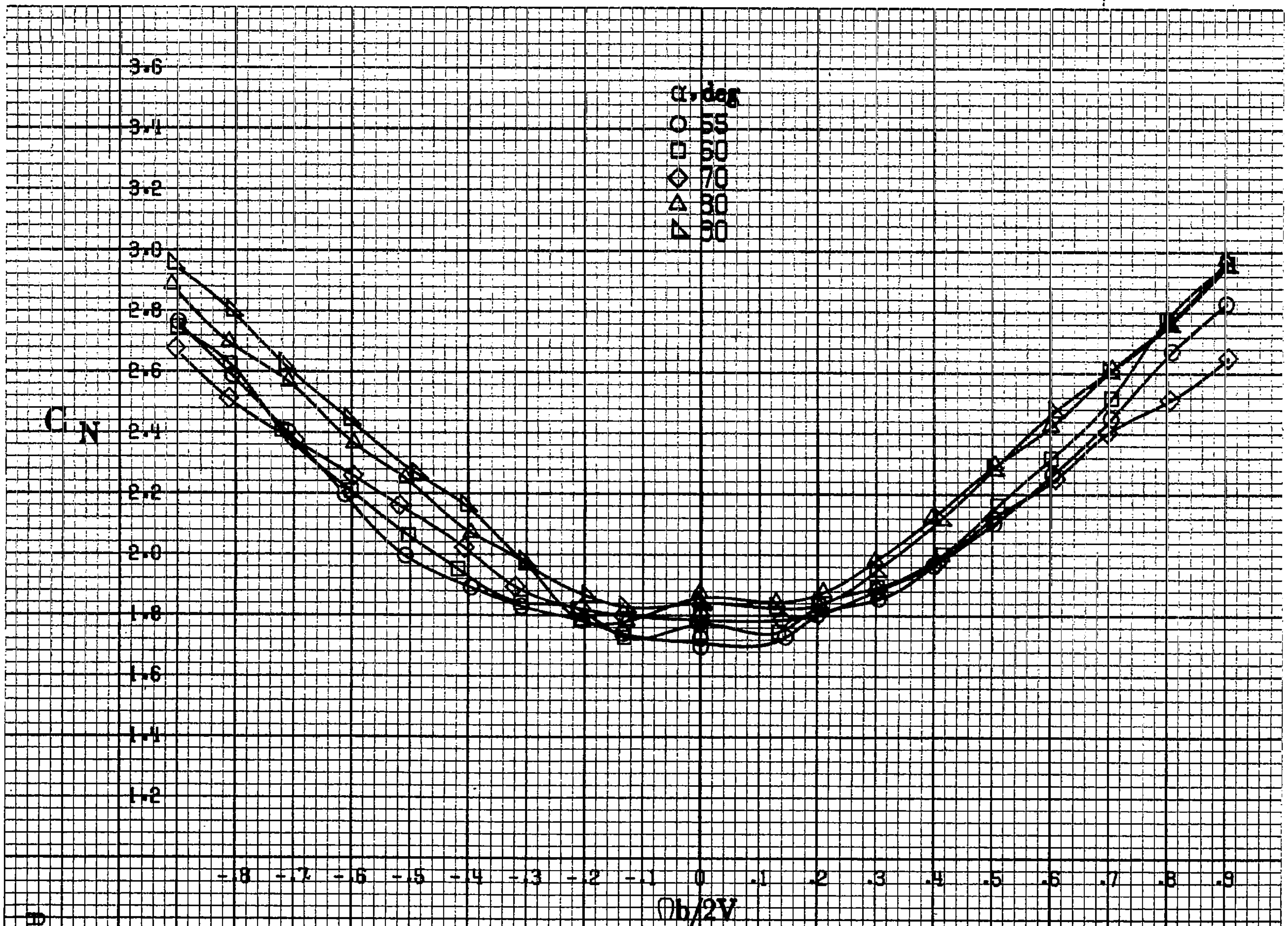

(d) α = 55 to 90 deg, SR = 0.

Figure A 40.-Concluded.

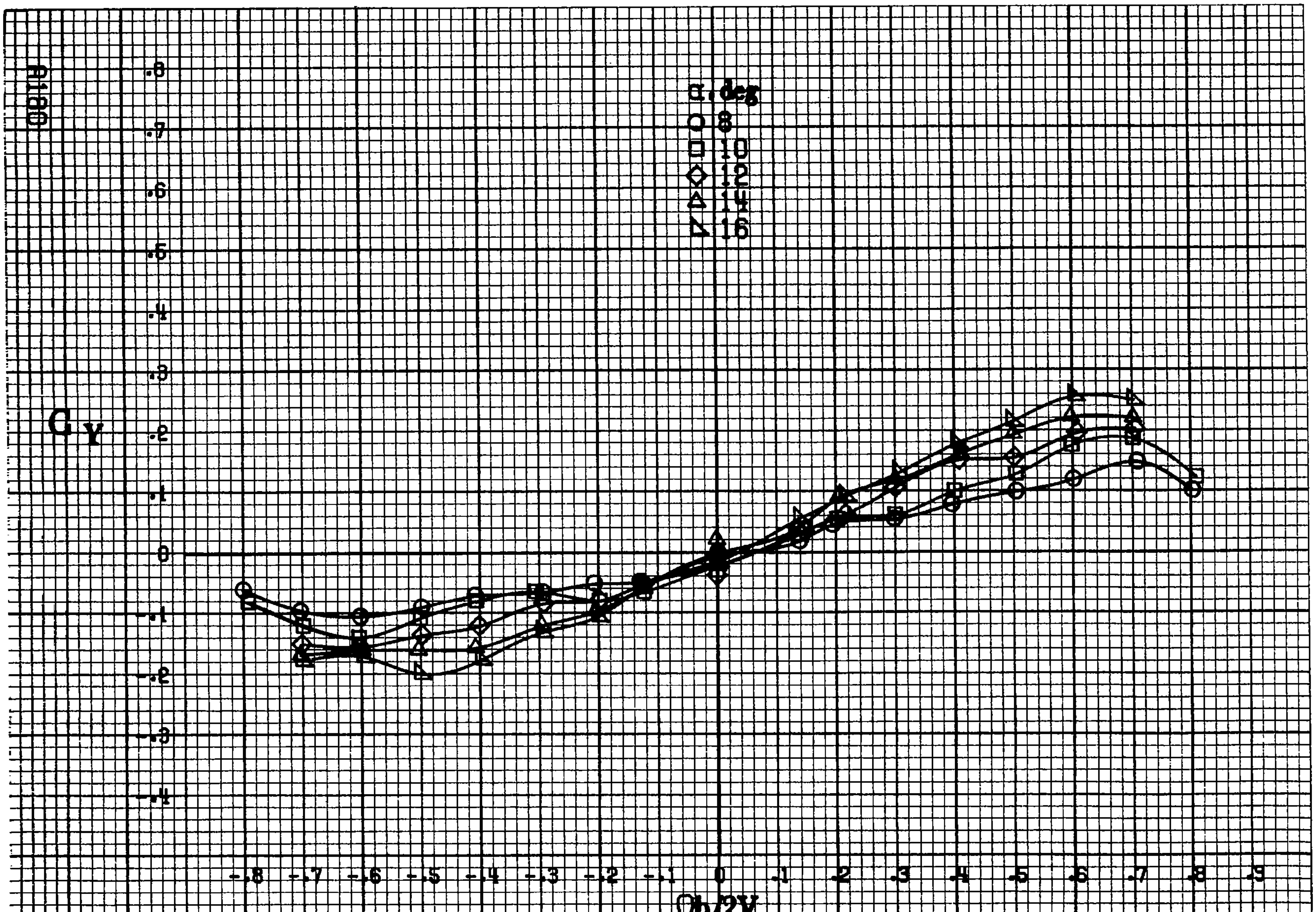

(a) α = 8 to 16 deg, SR = 182.9 cm (72 in).

Figure A41.- Effect of rotation rate and angle of attack on side-force coefficient for full-span LE wing droop with large nose radius. $\delta_e = 0°$, $\delta_a = 0°$, $\delta_r = 0°$, $\beta = 0°$.

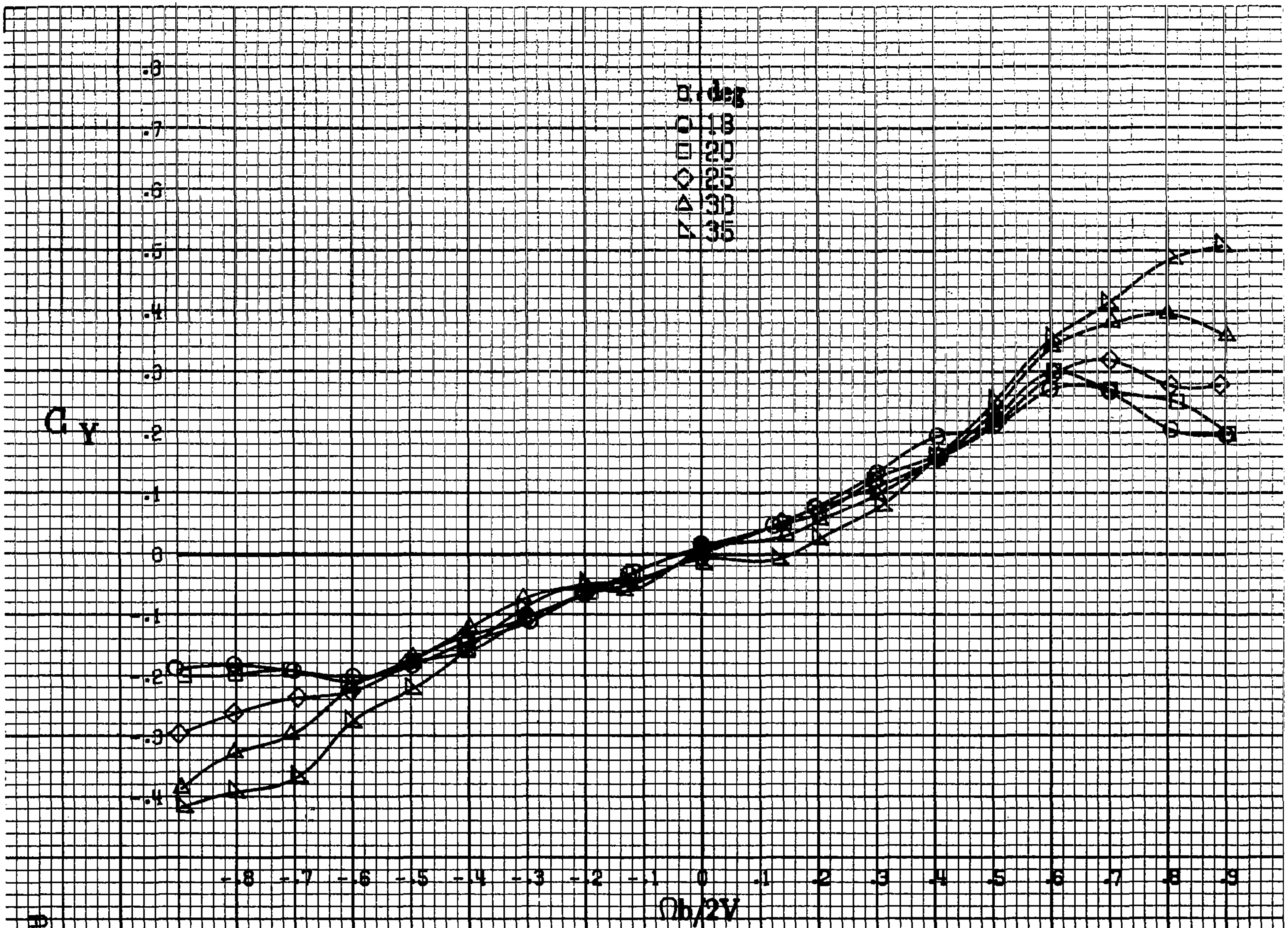

(b) α = 18 to 35 deg, SR = 182.9 cm (72 in).

Figure A41.-Continued.

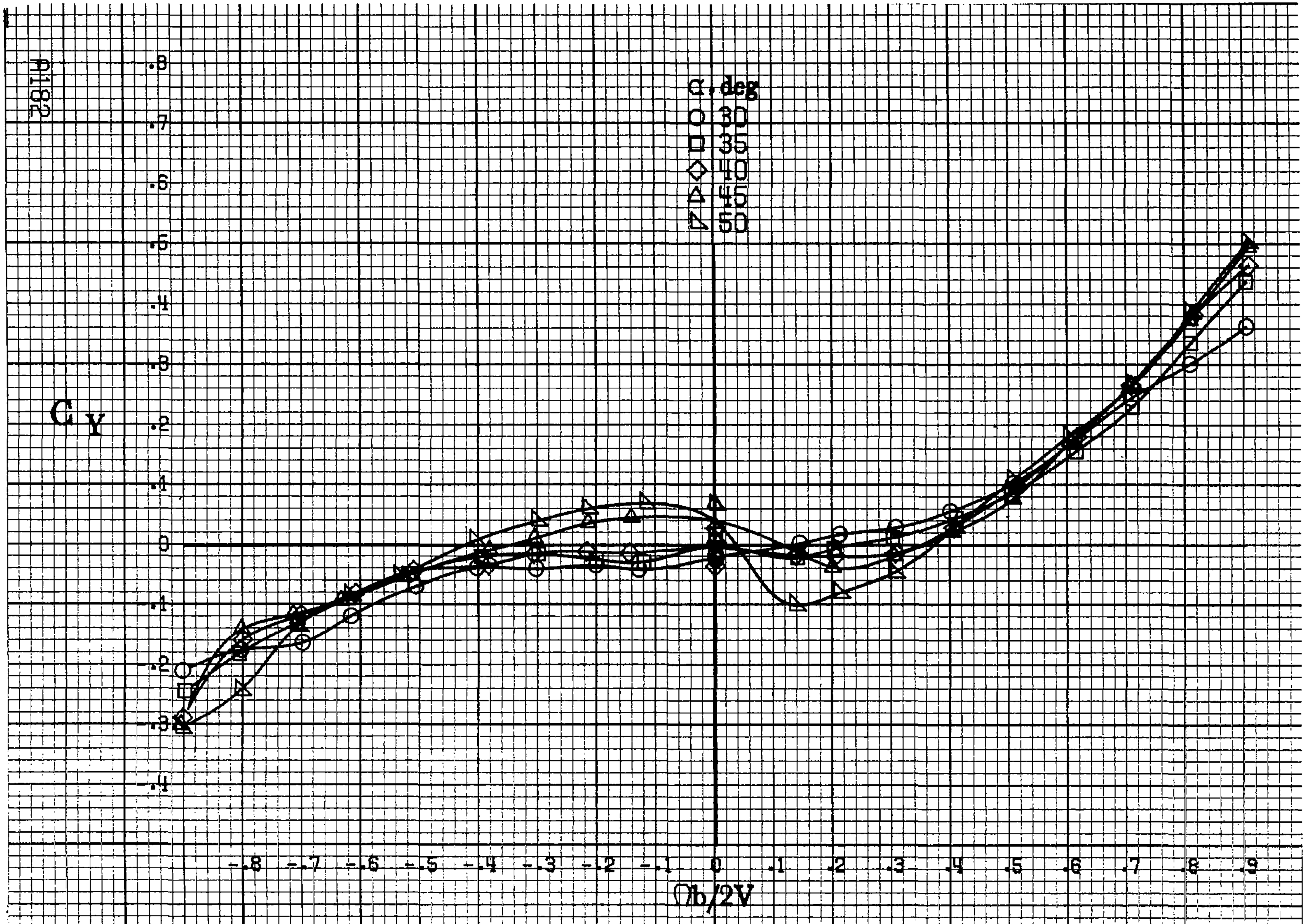

(c) α = 30 to 50 deg, SR = 0.

Figure A41.-Continued.

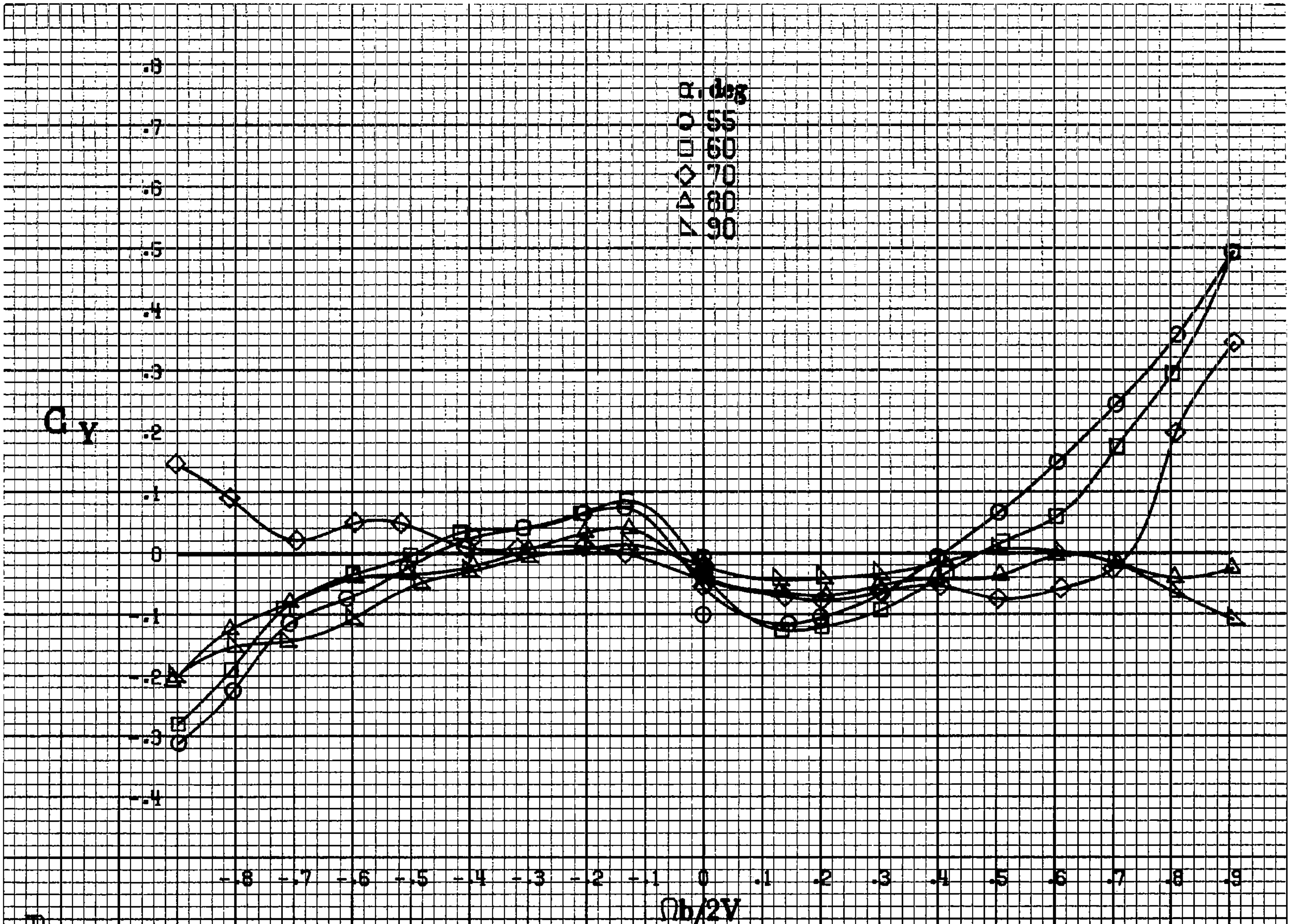

(d) α = 55 to 90 deg, SR = 0.

Figure A41.-Concluded.

A184

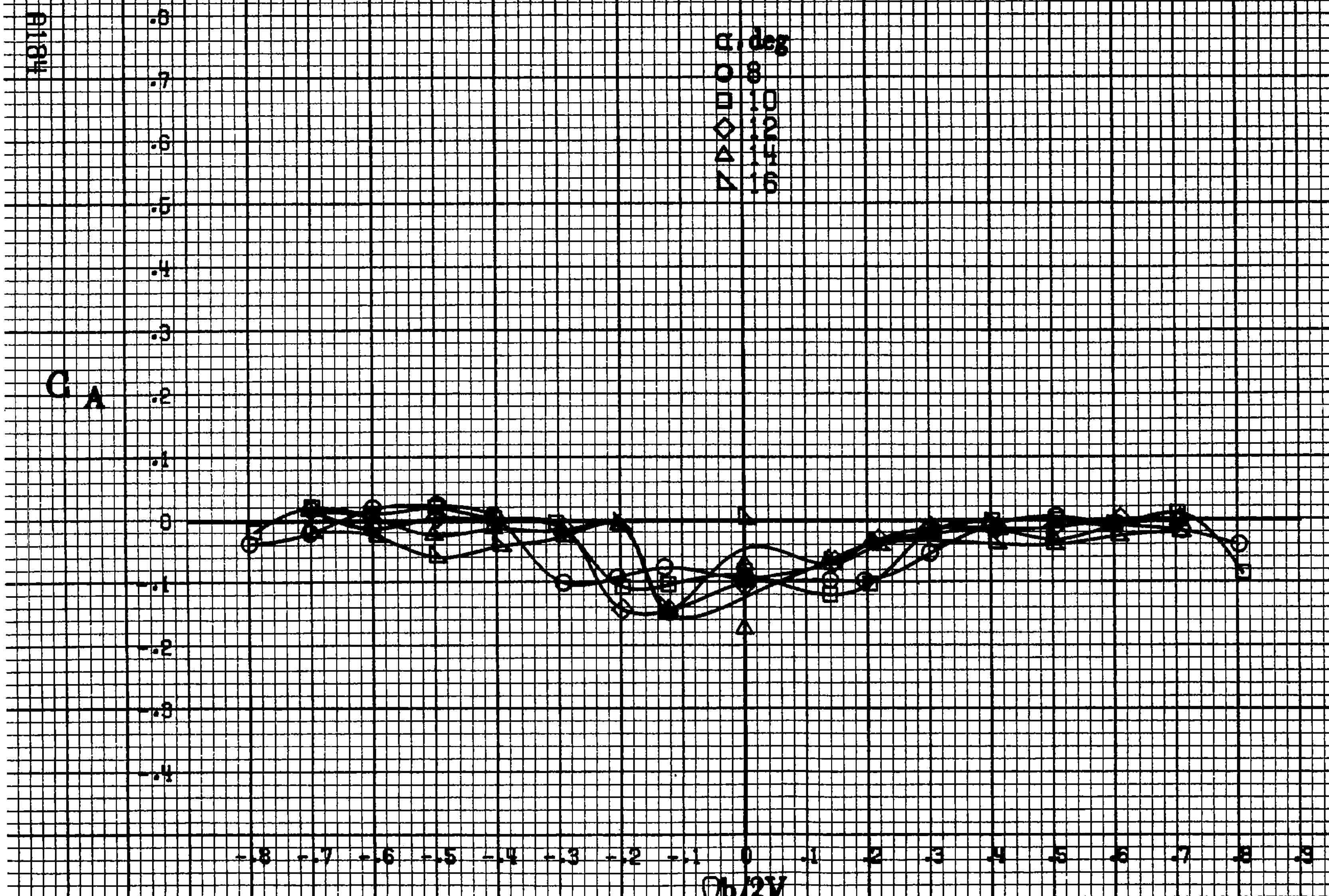

(a) α = 8 to 16 deg, SR = 182.9 cm (72 in).

Figure A42.-Effect of rotation rate and angle of attack on axial-force coefficient for full-span LE wing droop with large nose radius. $\delta_e = 0°$, $\delta_a = 0°$, $\delta_r = 0°$, $\beta = 0°$.

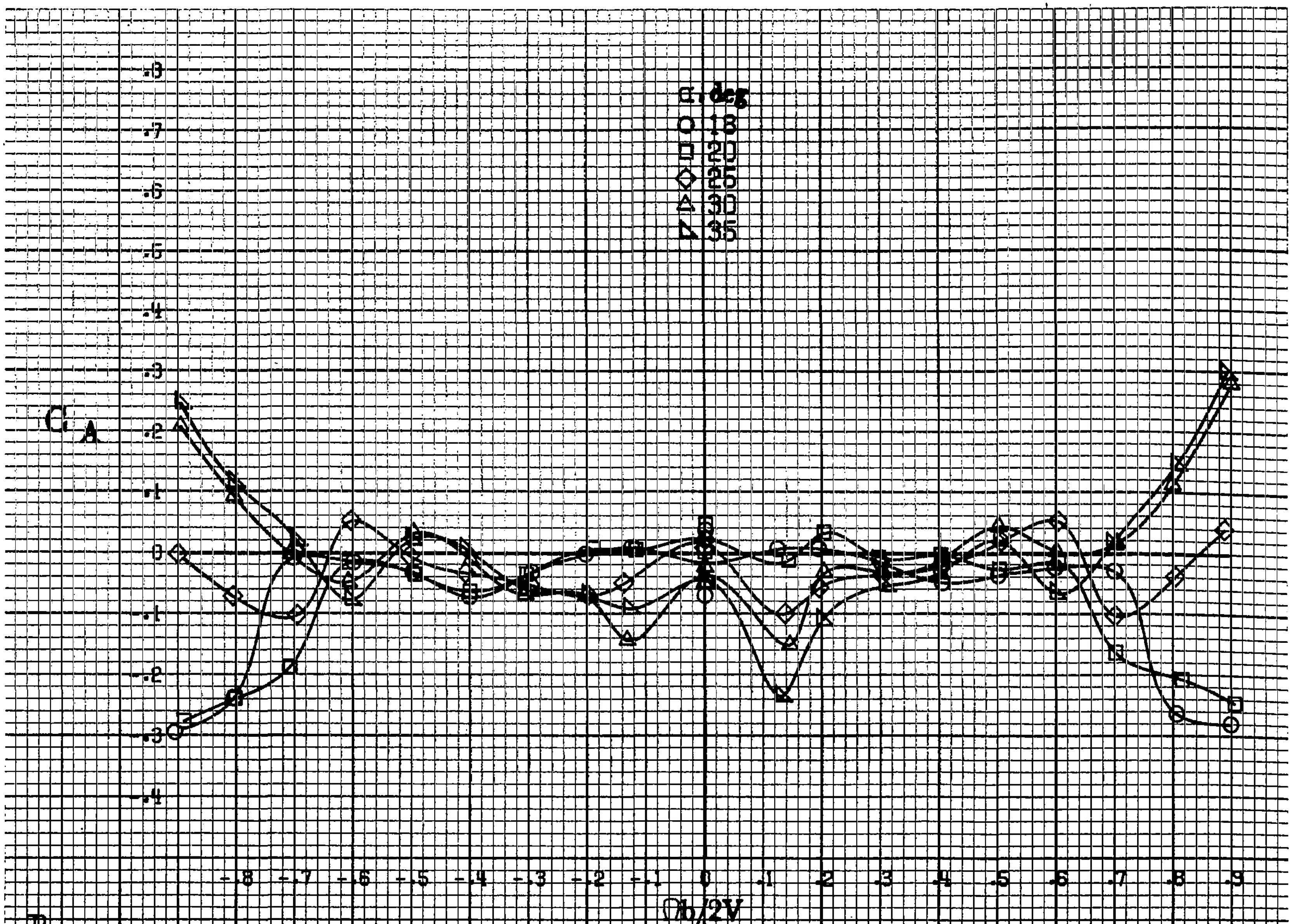

(b) α = 18 to 35 deg, SR = 182.9 cm (72 in).

Figure A42.- Continued.

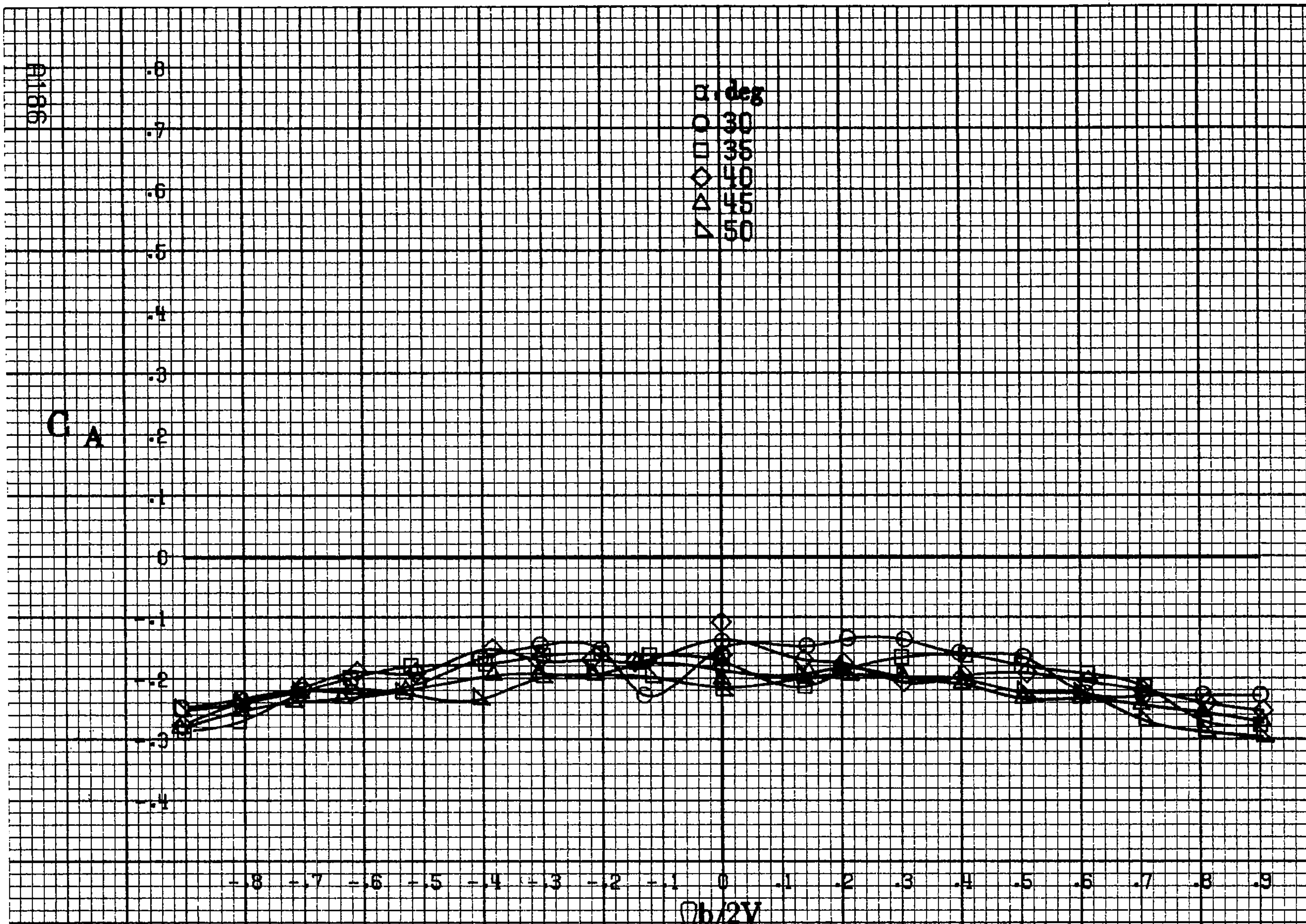

(c) α = 30 to 50 deg, SR = 0.

Figure A42.-Continued.

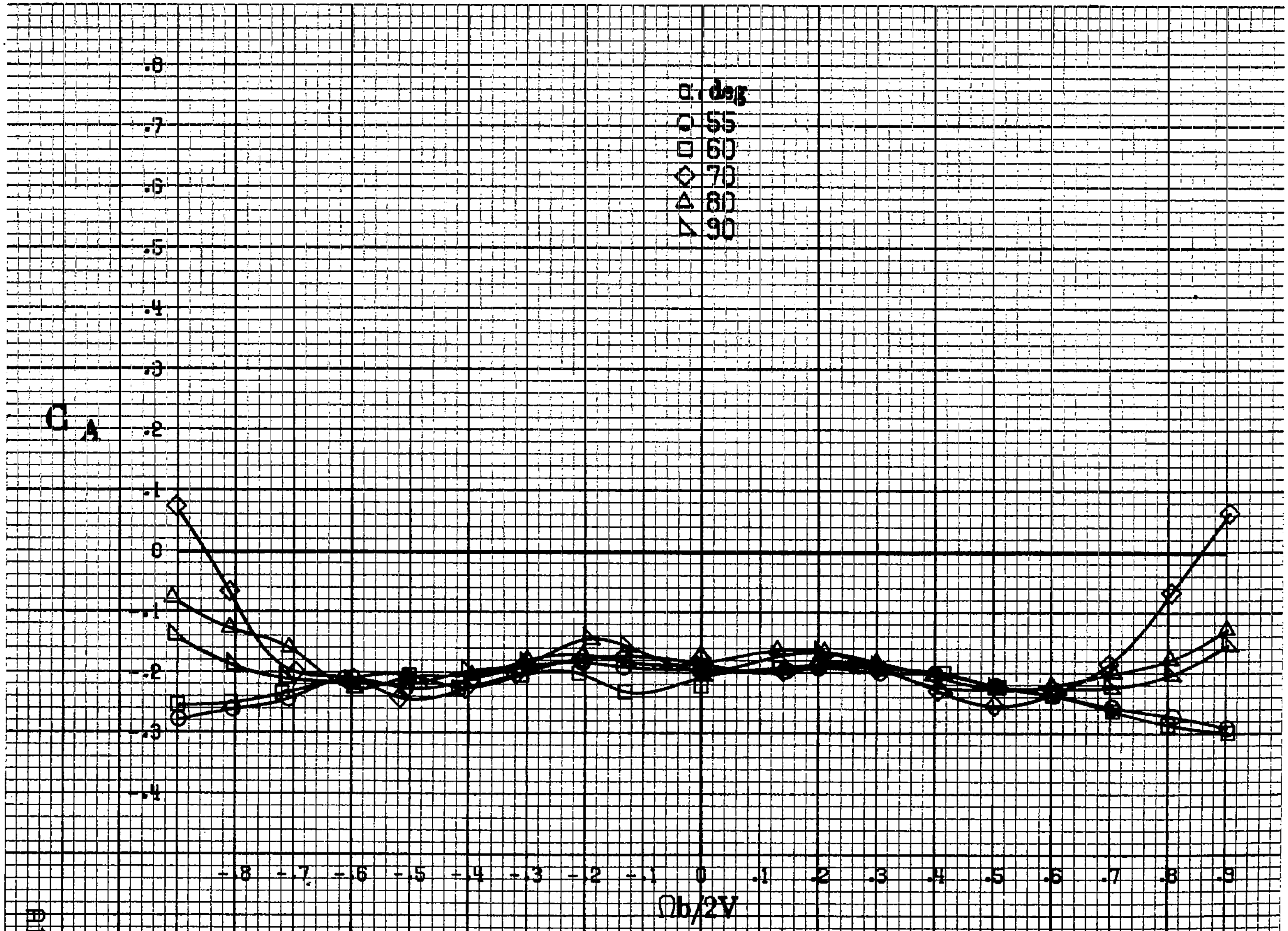

(d) α = 55 to 90 deg, SR = 0.

Figure A42.-Concluded.

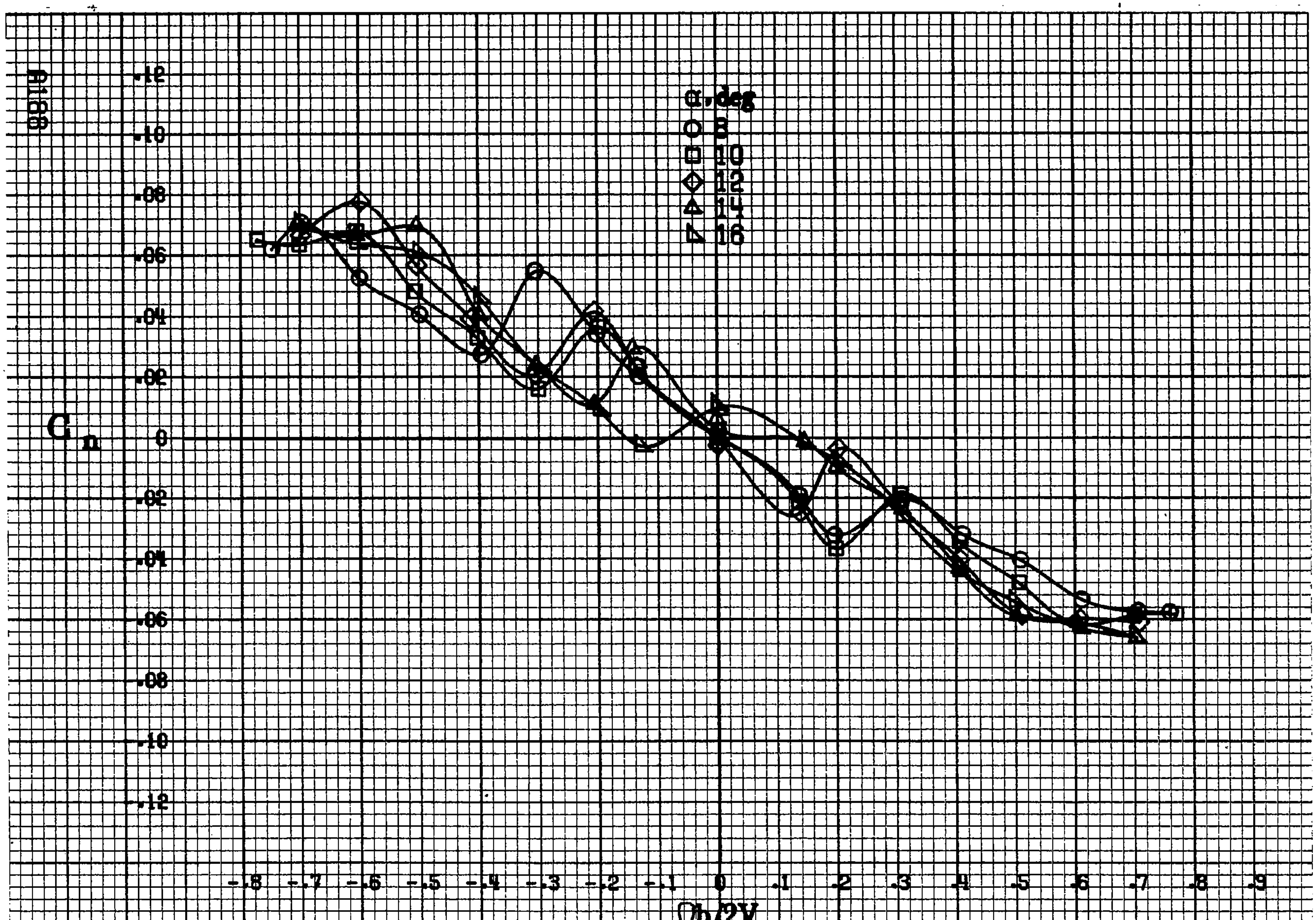

(a) $\alpha = 8$ to 16 deg, SR = 182.9 cm (72 in).

Figure A43.- Effect of rotation rate and angle of attack on yawing-moment coefficient for full-span LE wing droop with large nose radius and sharp-edged fuselage bottom. $\delta_e = 0°$, $\delta_a = 0°$, $\delta_r = 0°$, $\beta = 0°$.

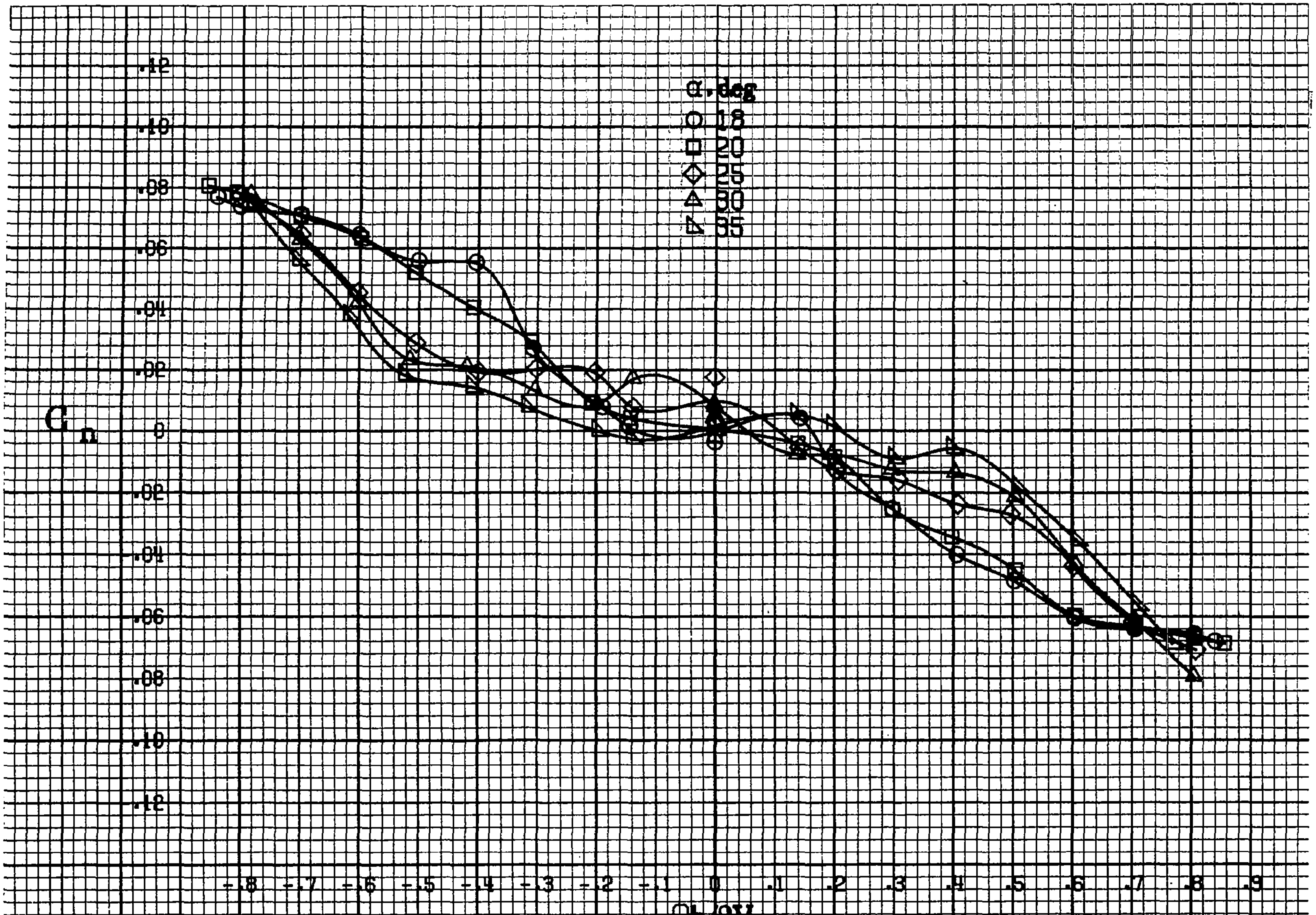

(b) α = 18 to 35 deg, SR = 182.9 cm (72 in).

Figure A43.-Continued.

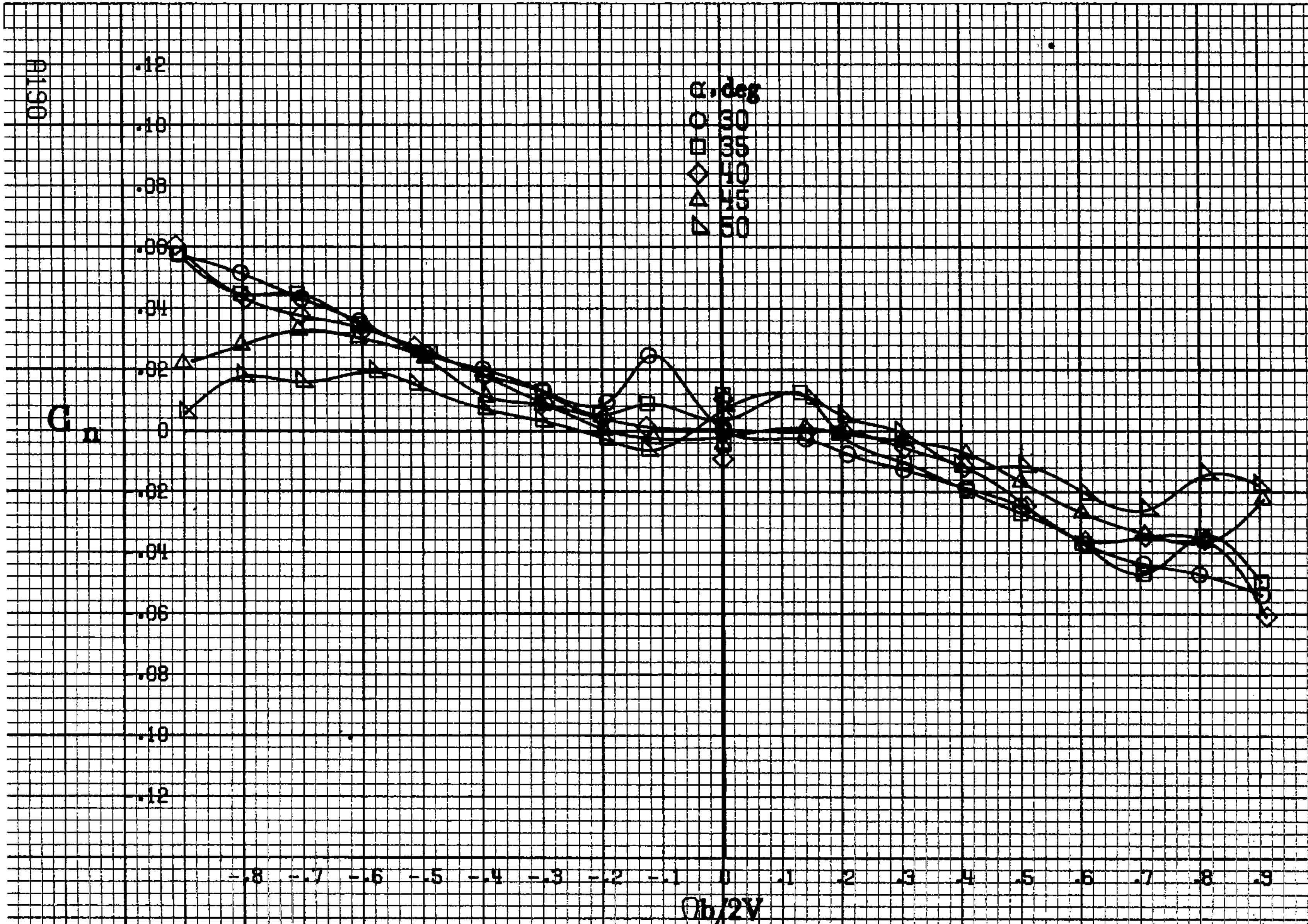

(c) α = 30 to 50 deg, SR = 0.

Figure A48.-Continued.

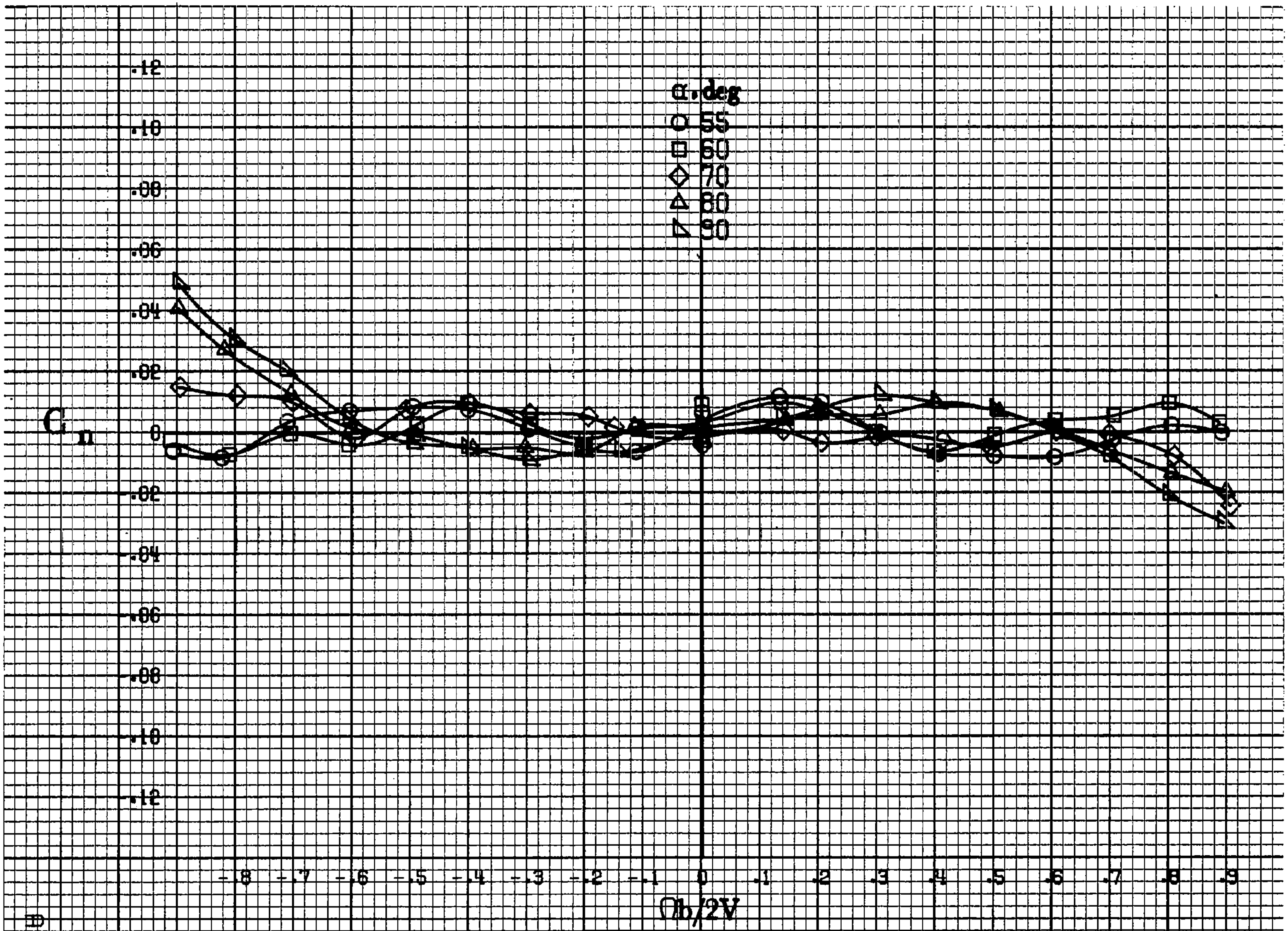

(d) α = 55 to 90 deg, SR = 0.

Figure A43.-Concluded.

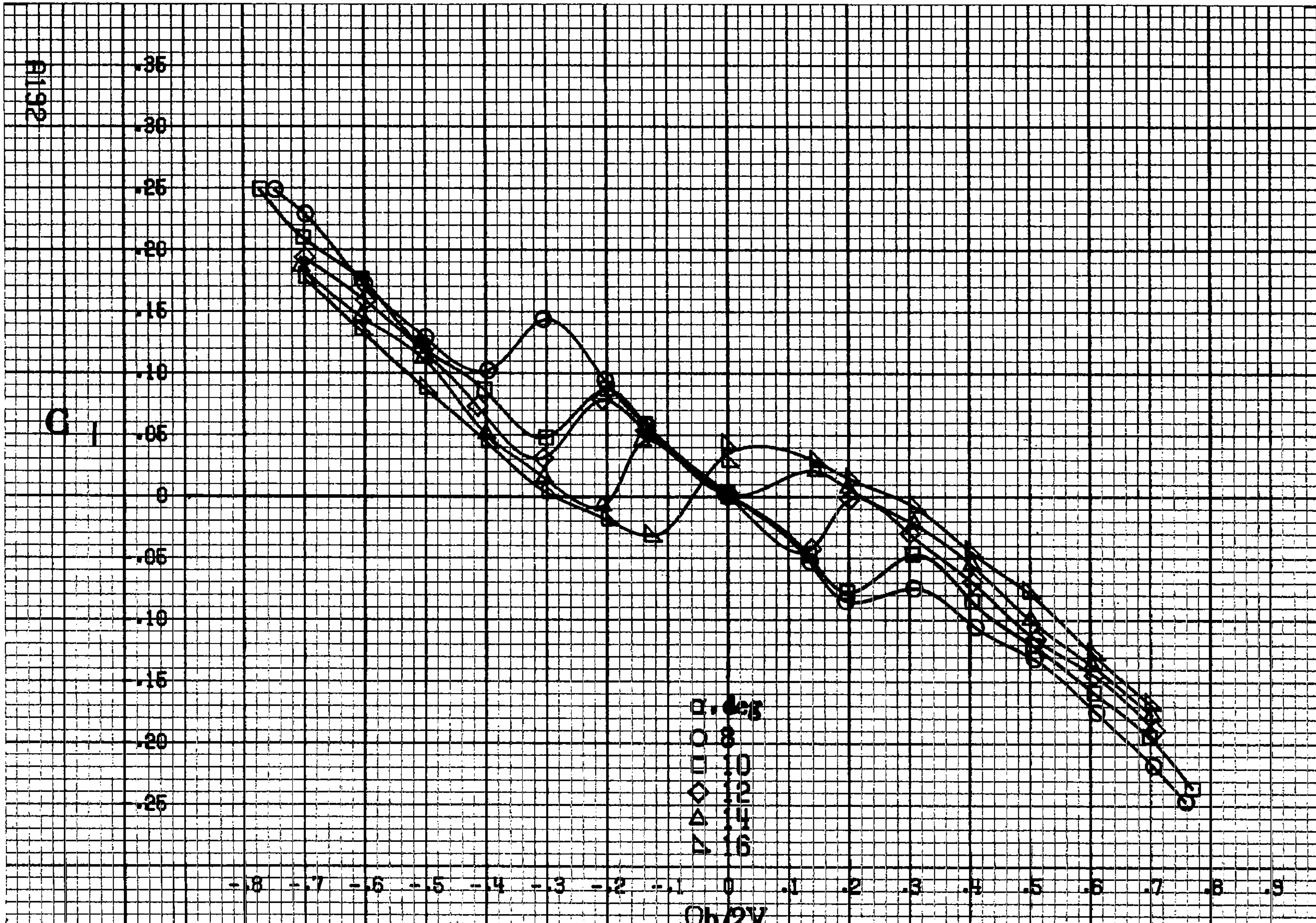

(a) $\alpha = 8$ to 16 deg, SR = 182.9 cm (72 in).

Figure A44.-Effect of rotation rate and angle of attack on rolling-moment coefficient for full-span LE wing droop with large nose radius and sharp-edged fuselage bottom. $\delta_e = 0°$, $\delta_a = 0°$, $\delta_r = 0°$, $\beta = 0°$.

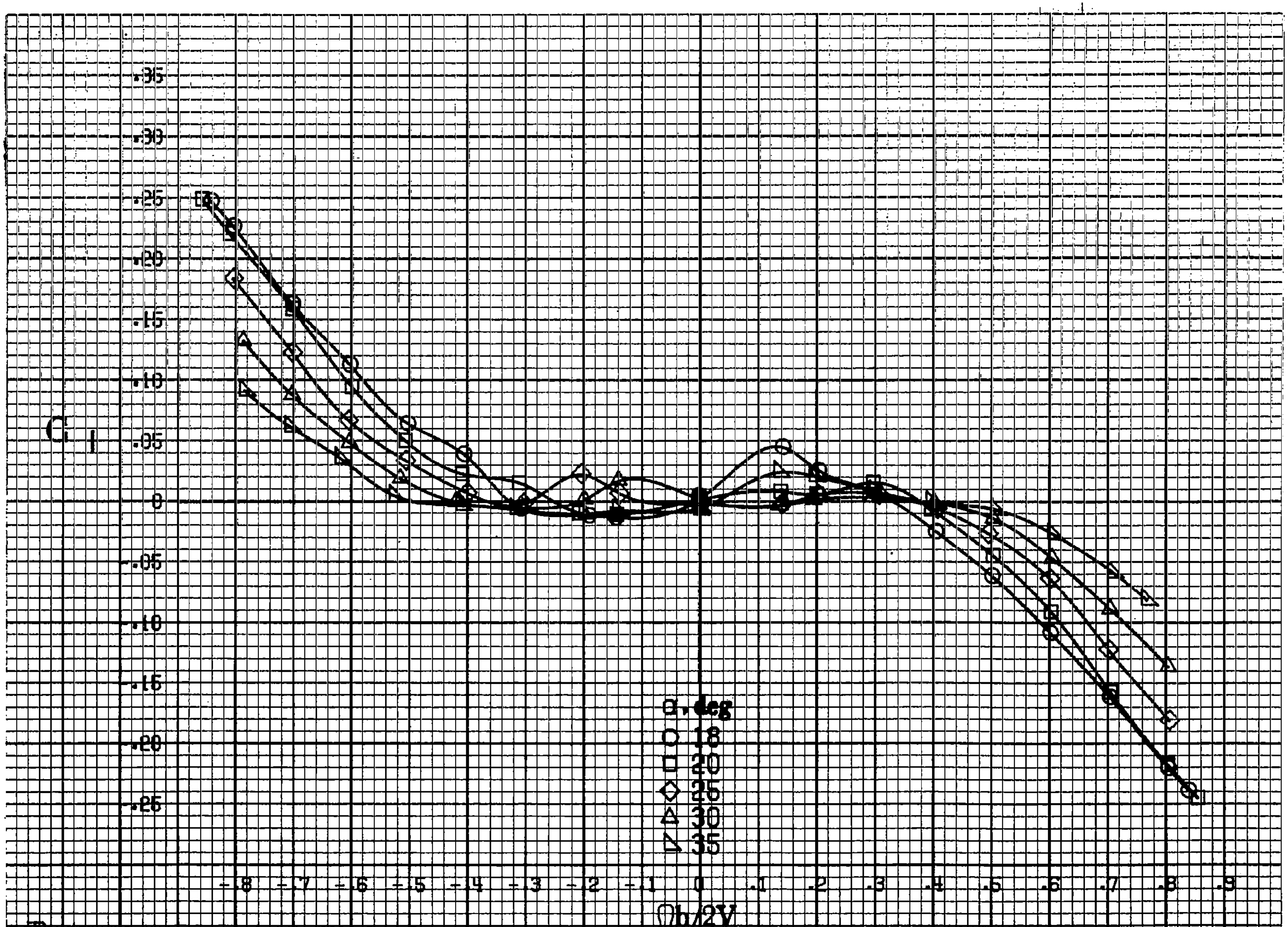

(b) α = 18 to 35 deg, SR = 182.9 cm (72 in).

Figure A44.-Continued.

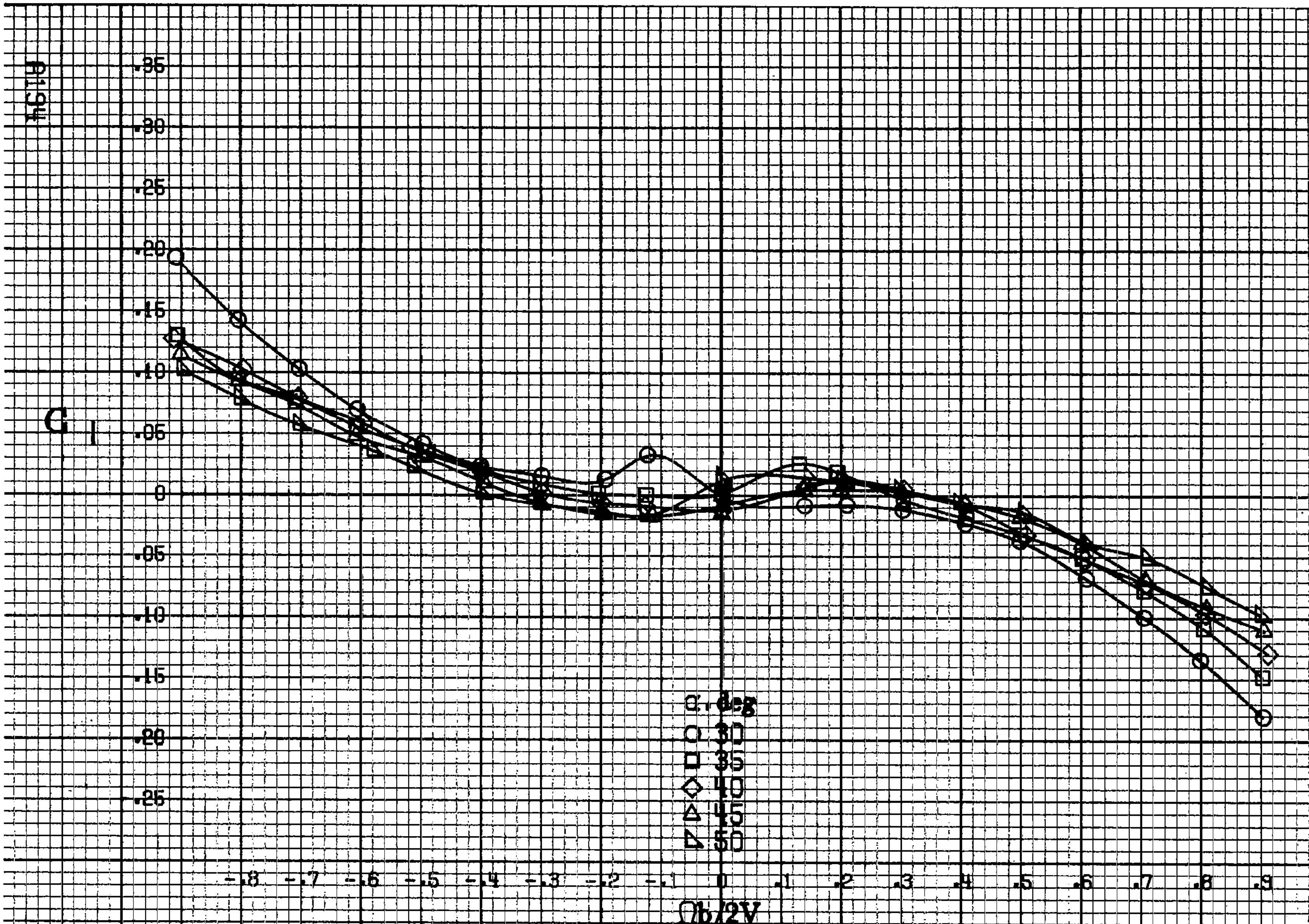

(c) α = 30 to 50 deg, SR = 0.

Figure A 44.-Continued.

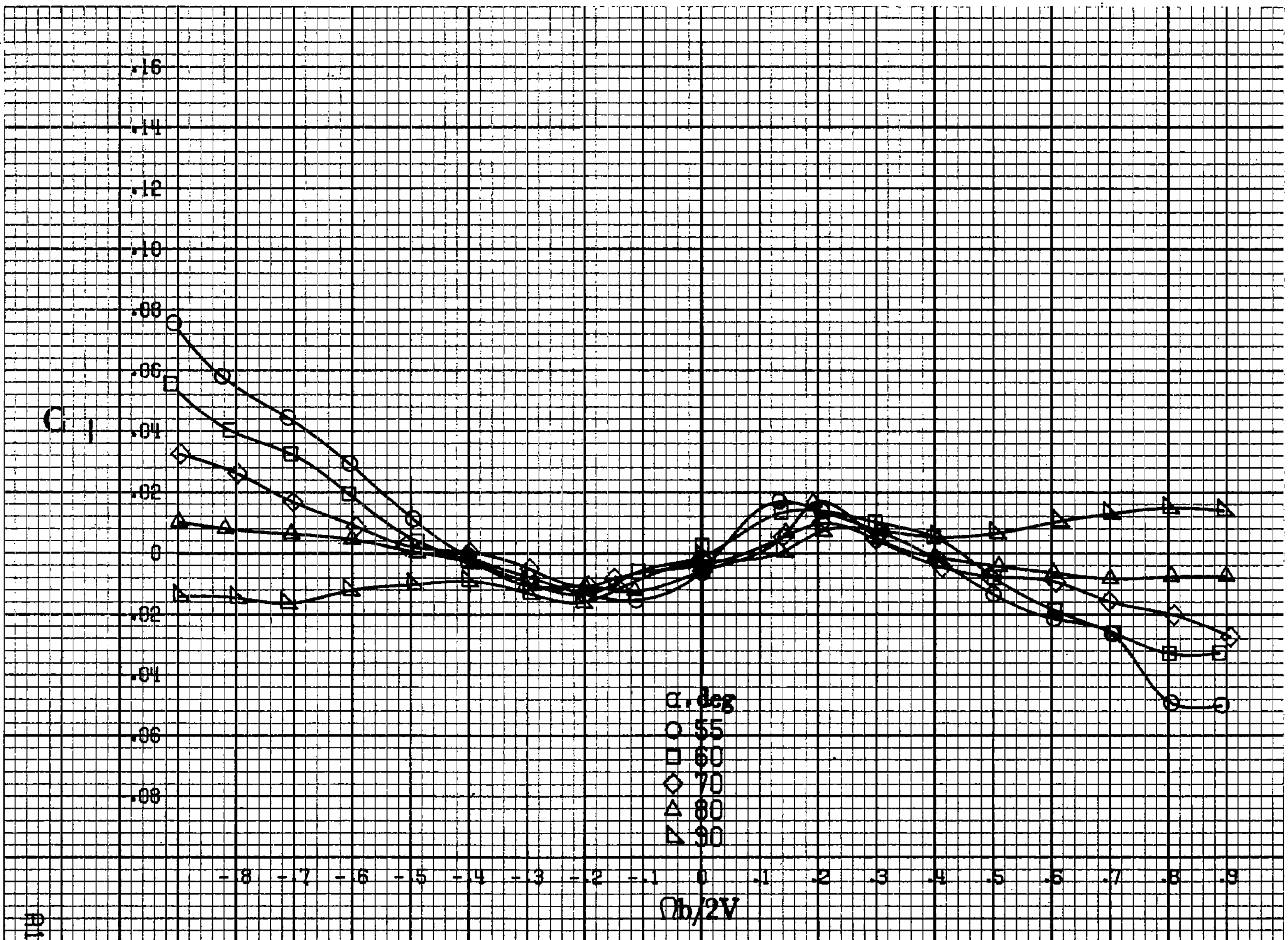

(d) α = 55 to 90 deg, SR = 0.

Figure A44.-Concluded.

A196

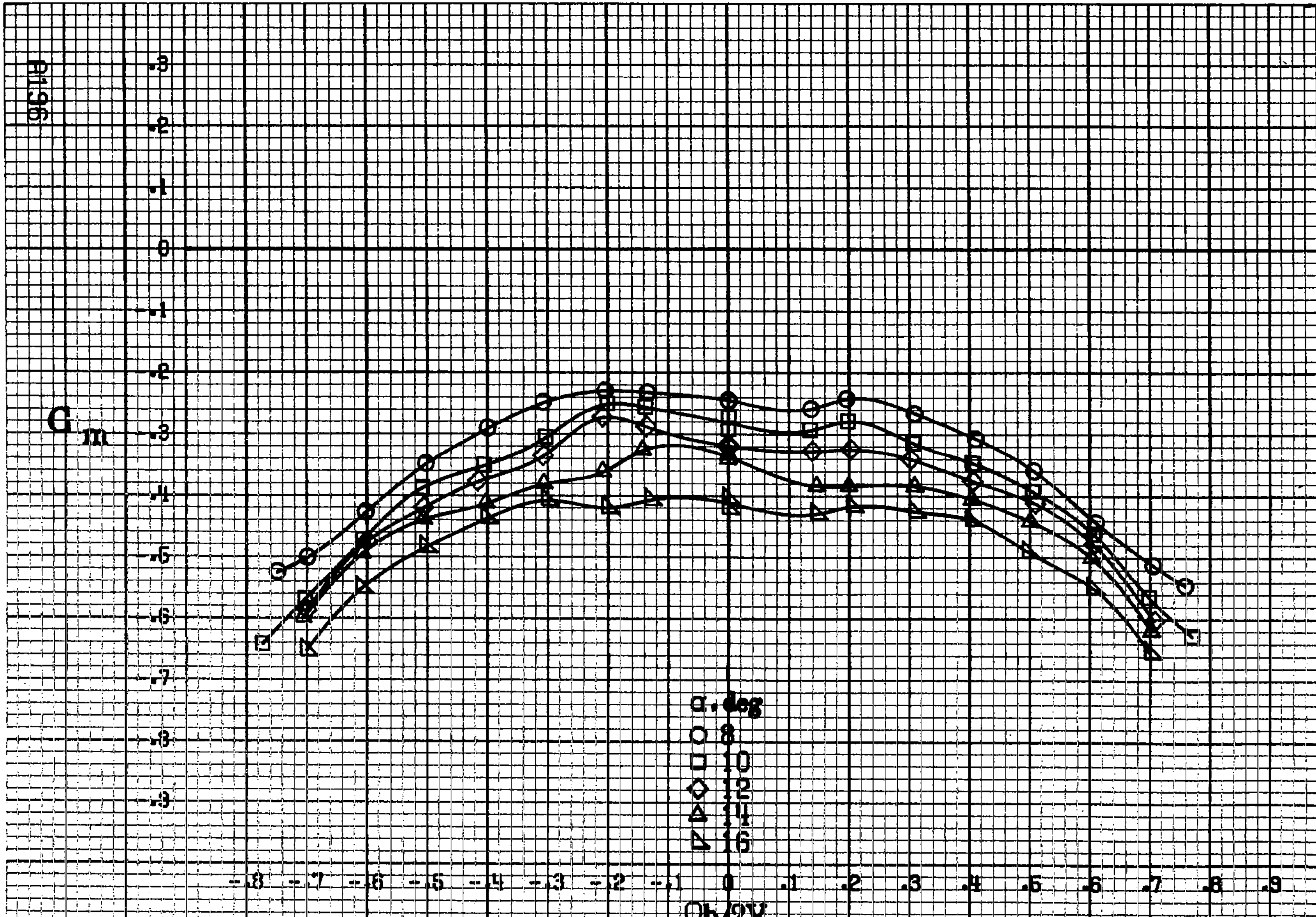

(a) α = 8 to 16 deg, SR = 182.9 cm (72 in.).

Figure A46.- Effect of rotation rate and angle of attack on pitching-moment coefficient for full-span LE wing droop with large nose radius and sharp-edged fuselage bottom. $\delta_e = 0°$, $\delta_a = 0°$, $\delta_r = 0°$, $\beta = 0°$.

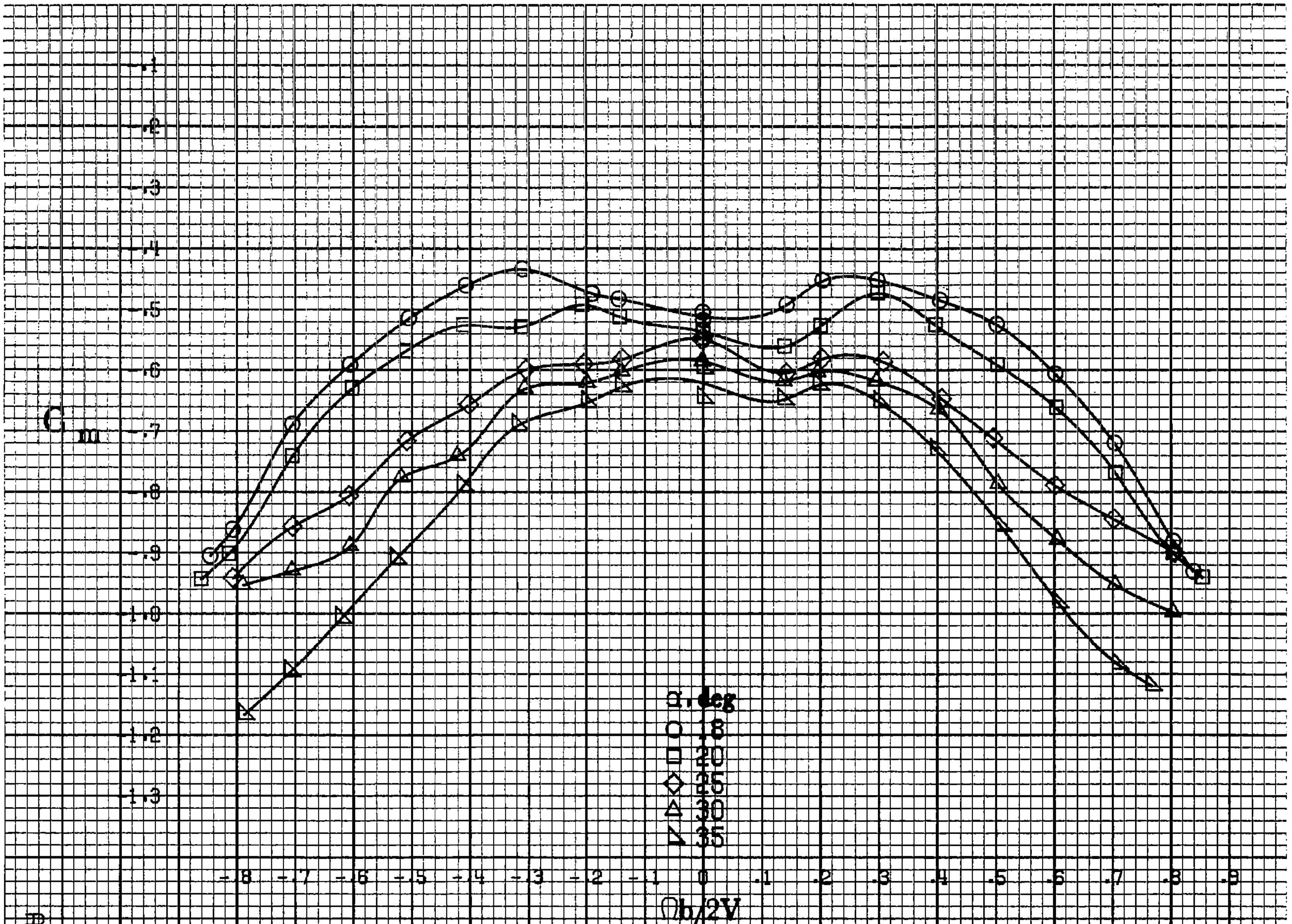

(b) α = 18to35deg, SR = 182.9cm (72in).

Figure A45.-Continued.

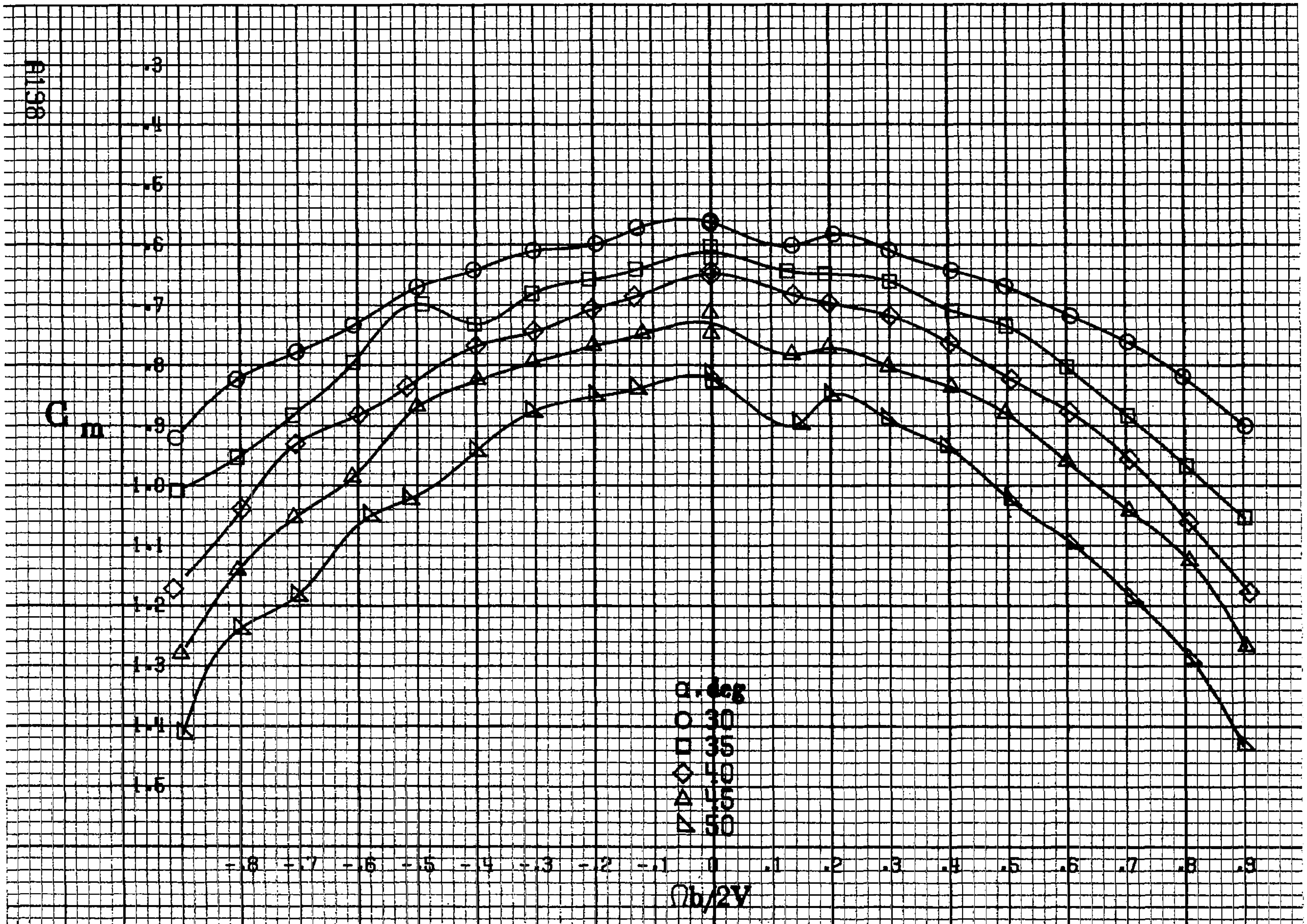

(c) α = 30 to 50 deg, SR = 0.

Figure A45.-Continued.

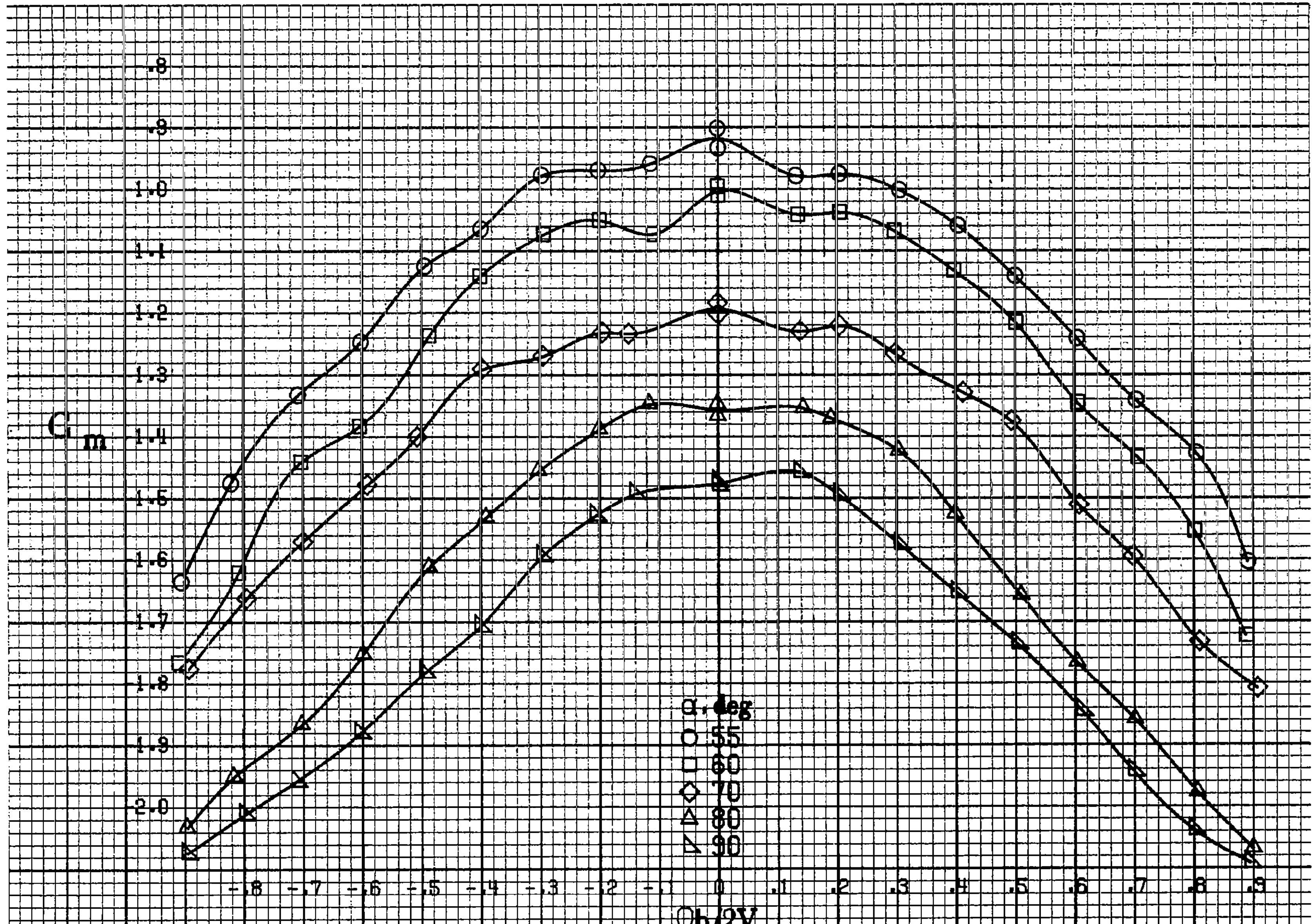

(d) α = 55 to 90 deg, SR = 0.

Figure A45.-Concluded.

A199

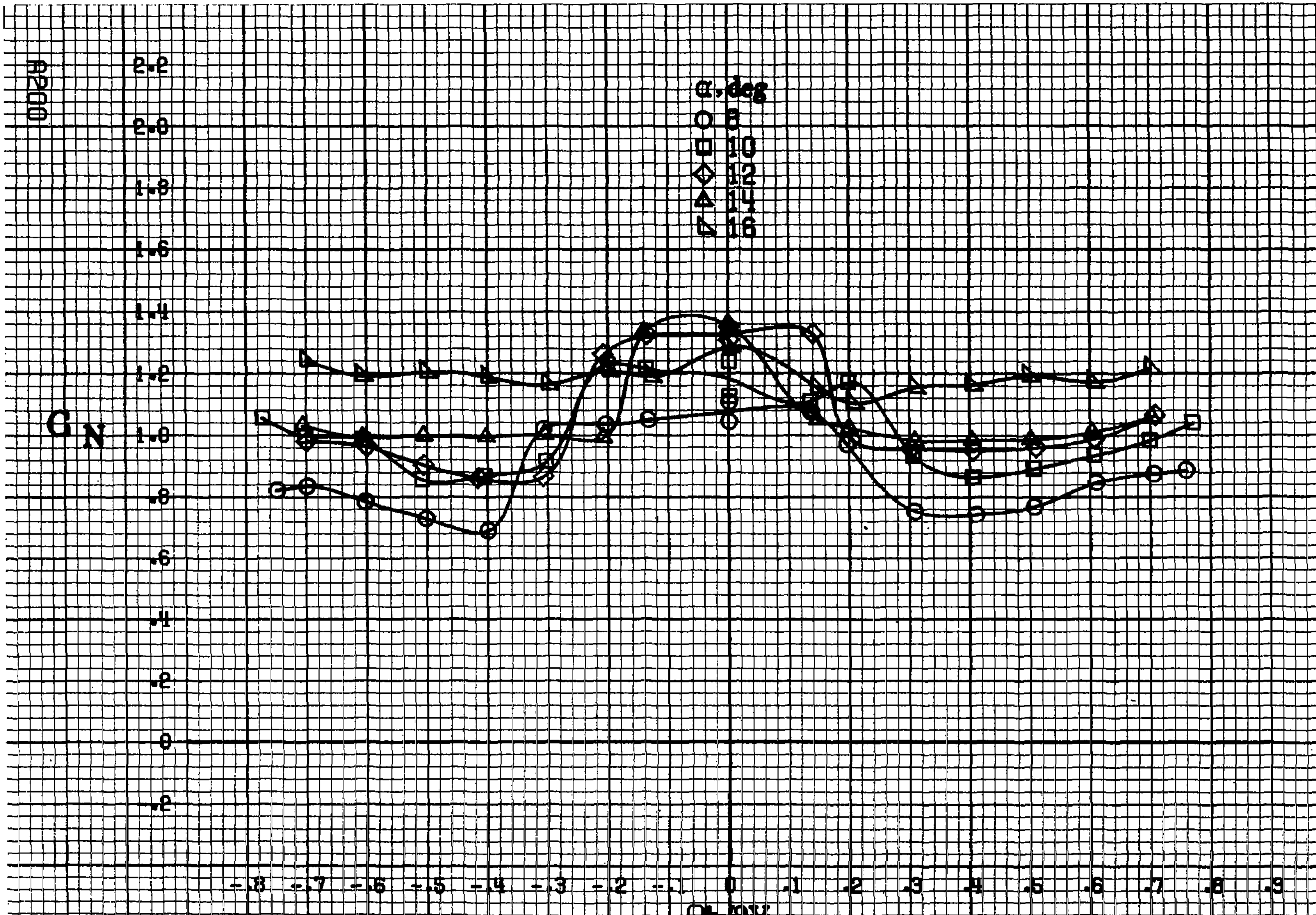

(a) α = 8 to 16 deg, SR = 182.9 cm (72 in).

Figure A46.-Effect of rotation rate and angle of attack on normal-force coefficient for full-span LE wing droop with large nose radius and sharp-edged fuselage bottom. $\delta_e = 0°$, $\delta_a = 0°$, $\delta_r = 0°$, $\beta = 0°$.

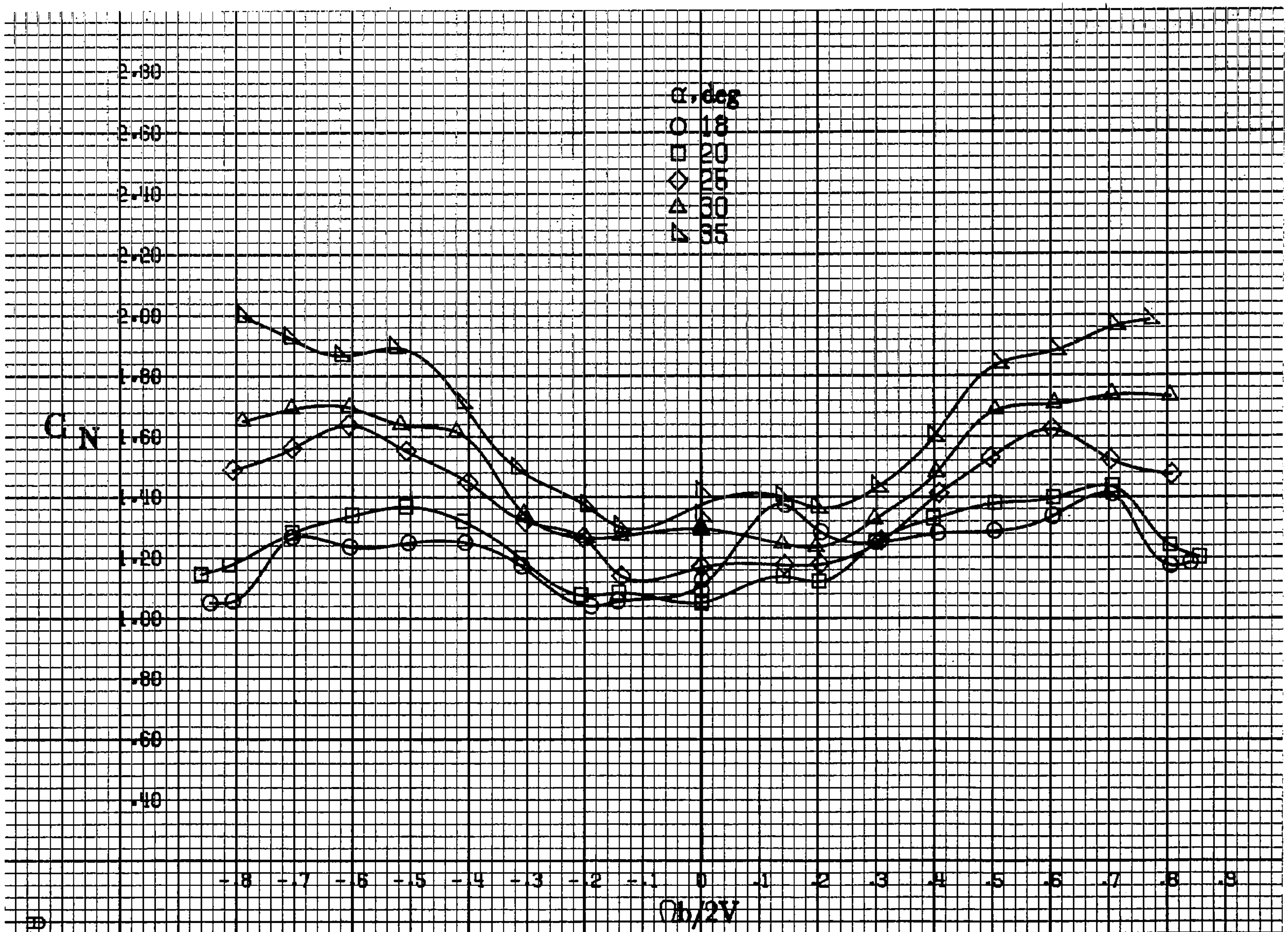

(b) α = 18 to 35 deg, SR = 182.9 cm (72 in).

Figure A46.-Continued.

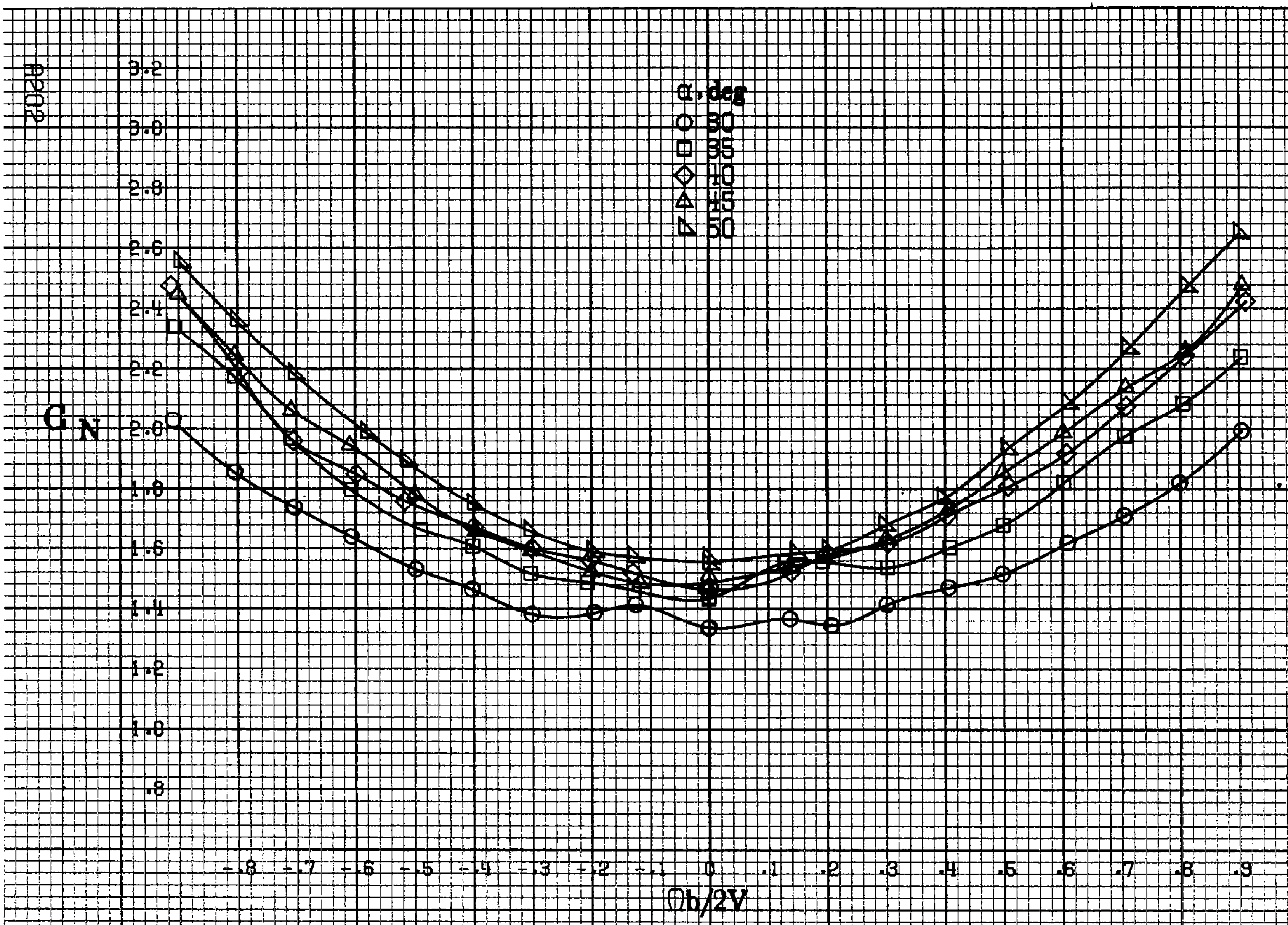

(c) α = 30 to 50 deg, SR = 0.

Figure A46.-Continued.

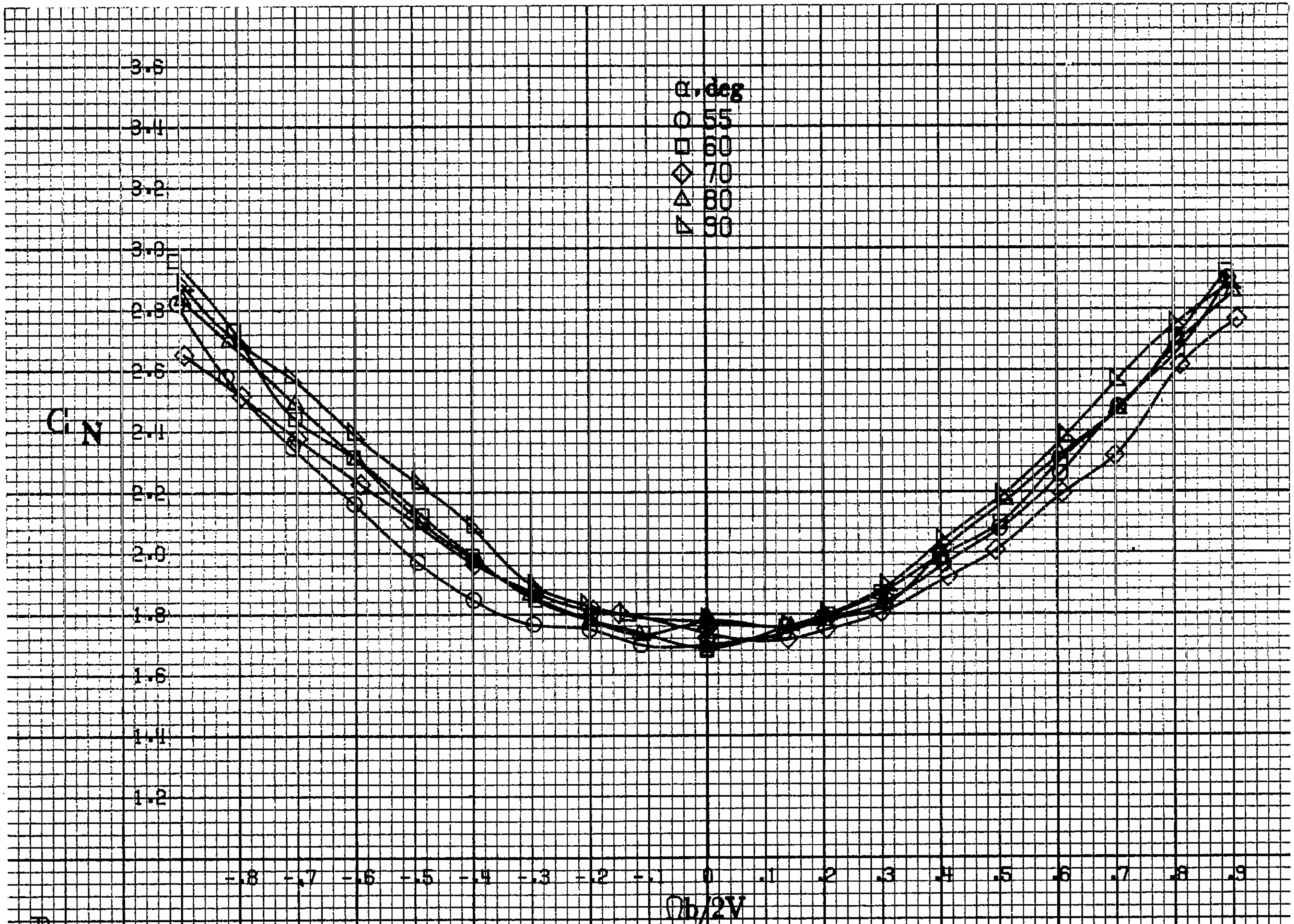

(d) α = 55 to 90 deg, SR = 0.

Figure A46.-Concluded.

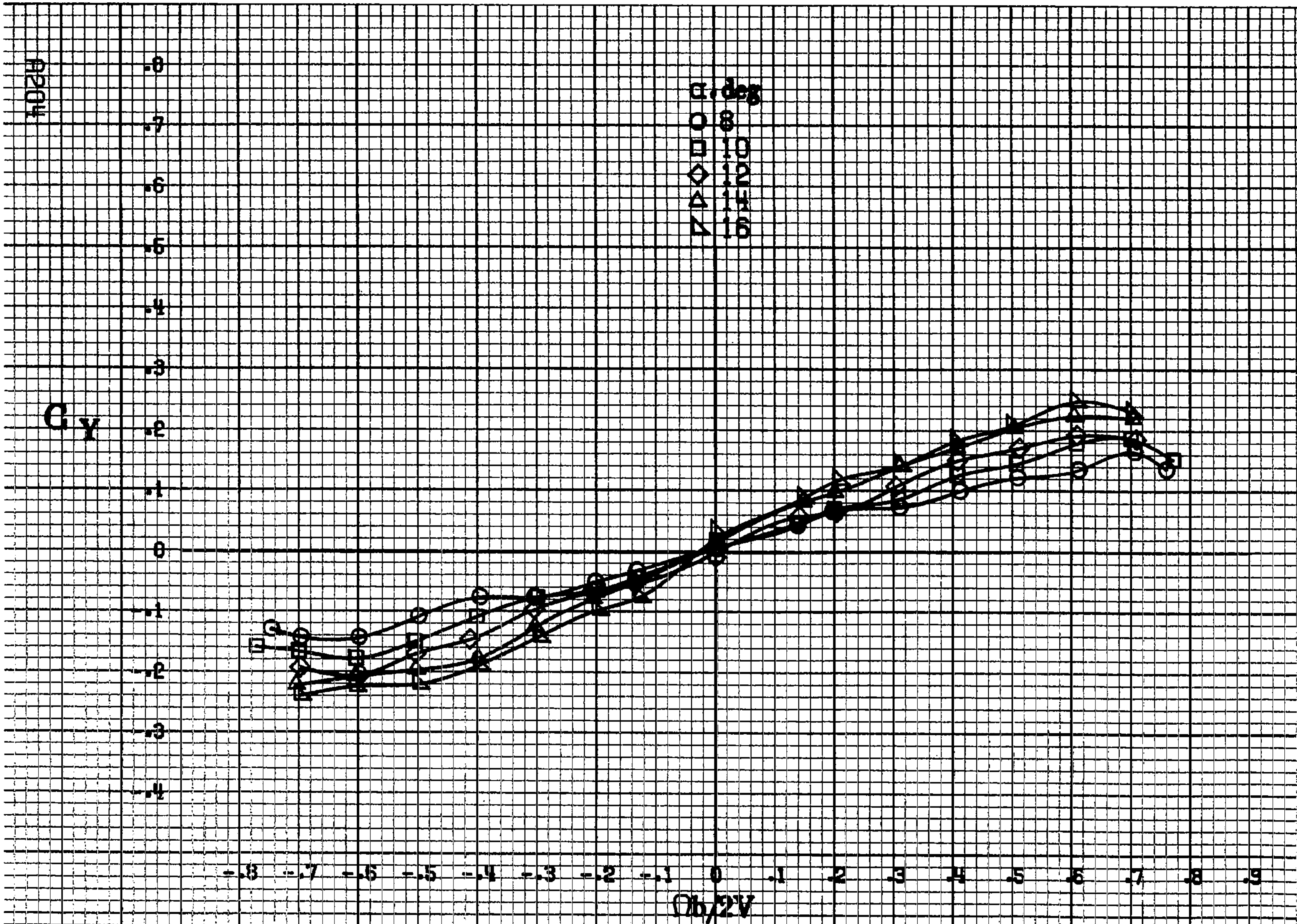

(a) $\alpha = 8$ to 16 deg, SR = 182.9 cm (72 in).

Figure A47.- Effect of rotation rate and angle of attack on side-force coefficient for full-span LE wing droop with large nose radius and sharp-edged fuselage bottom. $\delta_e = 0°$, $\delta_a = 0°$, $\delta_r = 0°$, $\beta = 0°$.

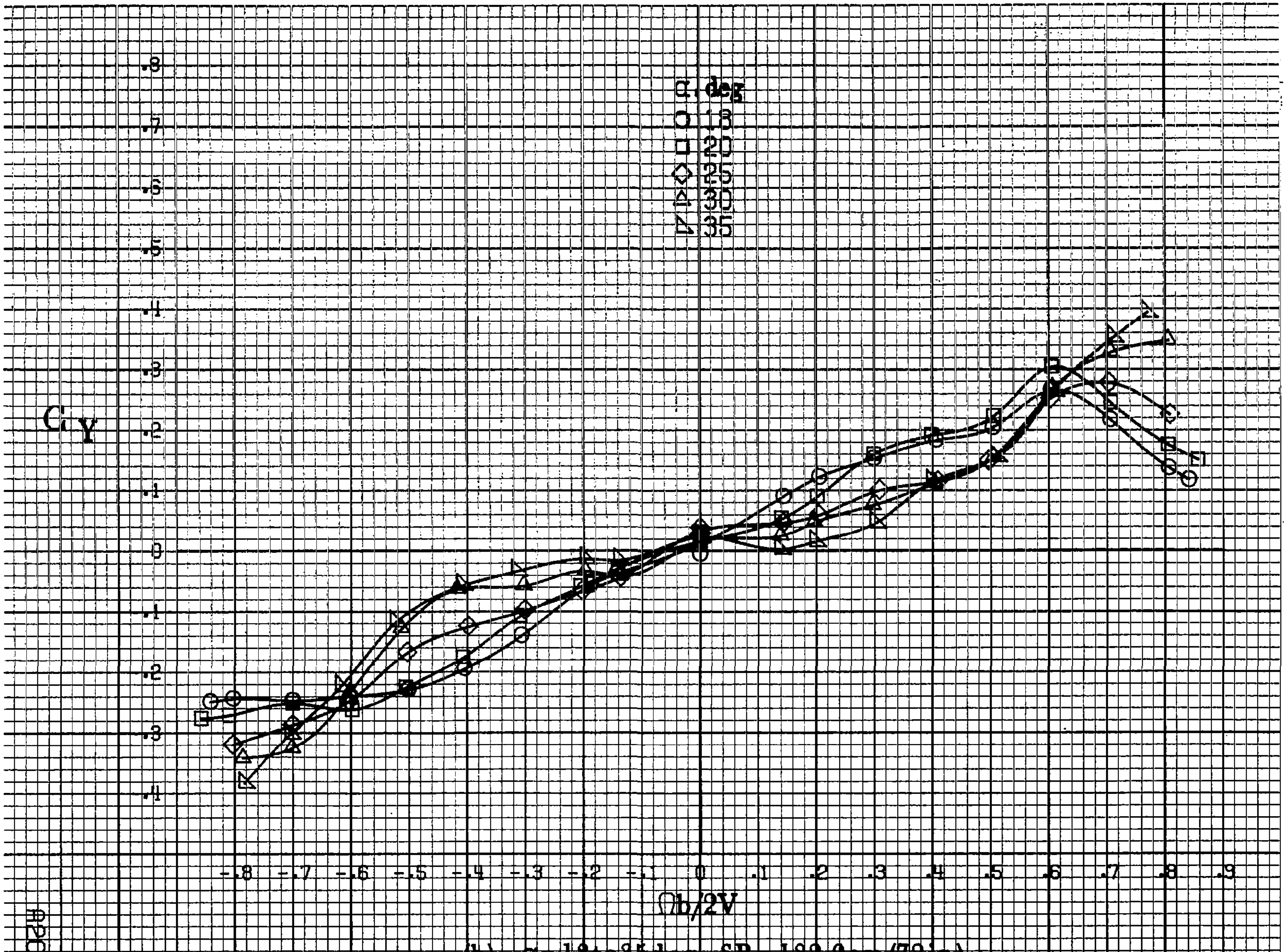

(b) α = 18 to 35 deg, SR = 182.9 cm (72 in).

Figure A47.-Continued.

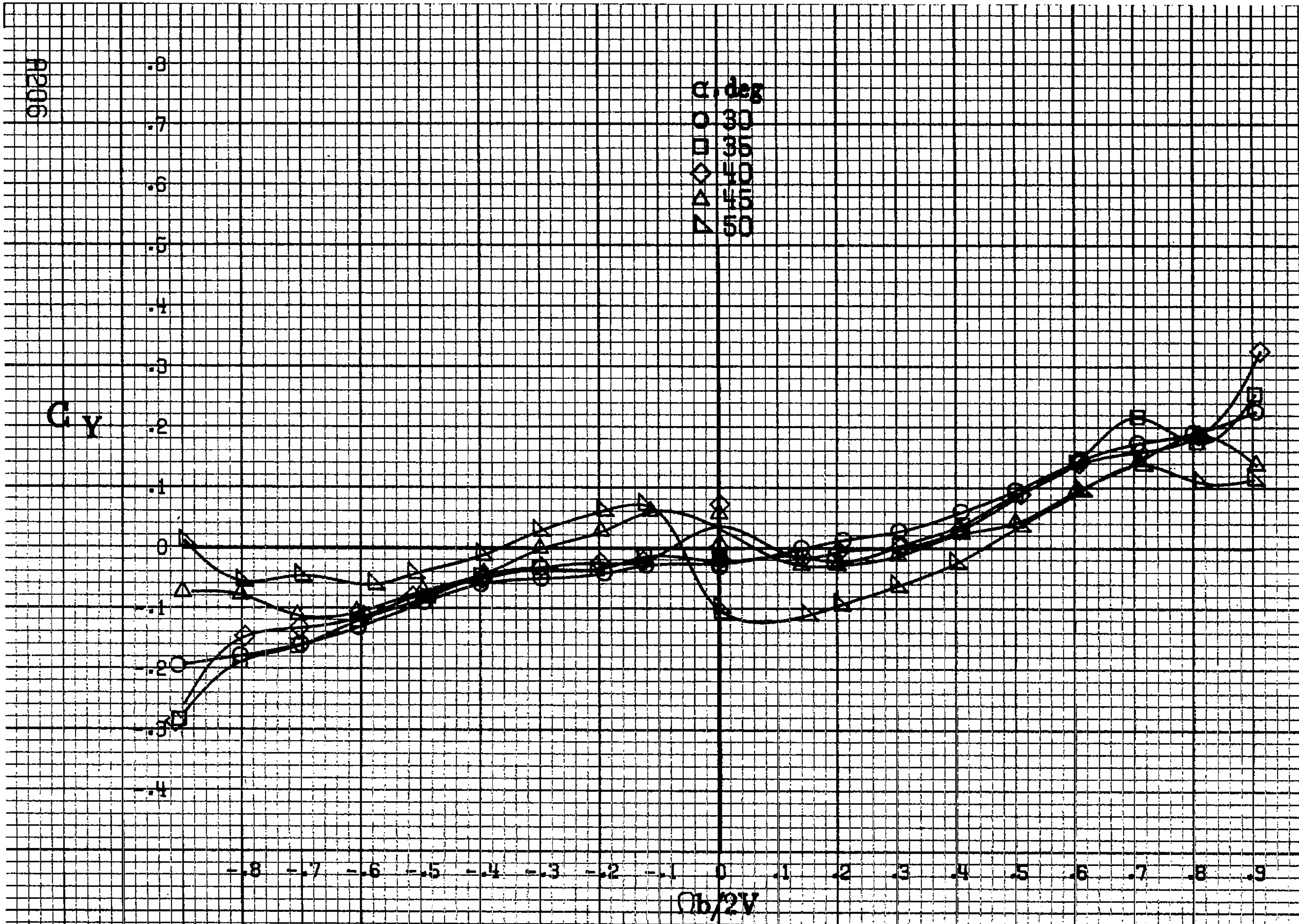

(c) α = 30 to 50 deg, SR = 0.

Figure A47.-Continued.

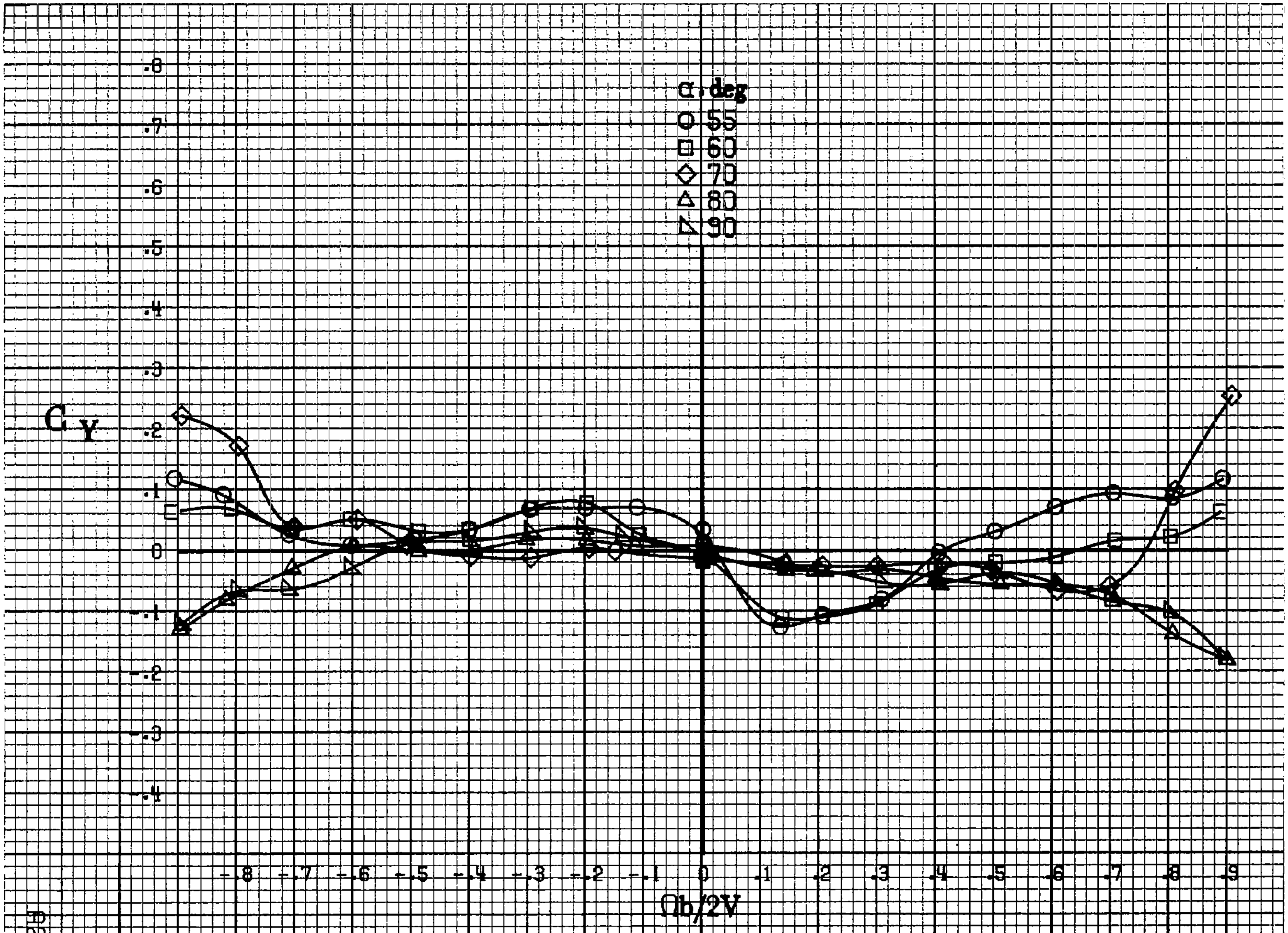

(d) α = 55 to 90 deg, SR = 0.

Figure A47.-Concluded.

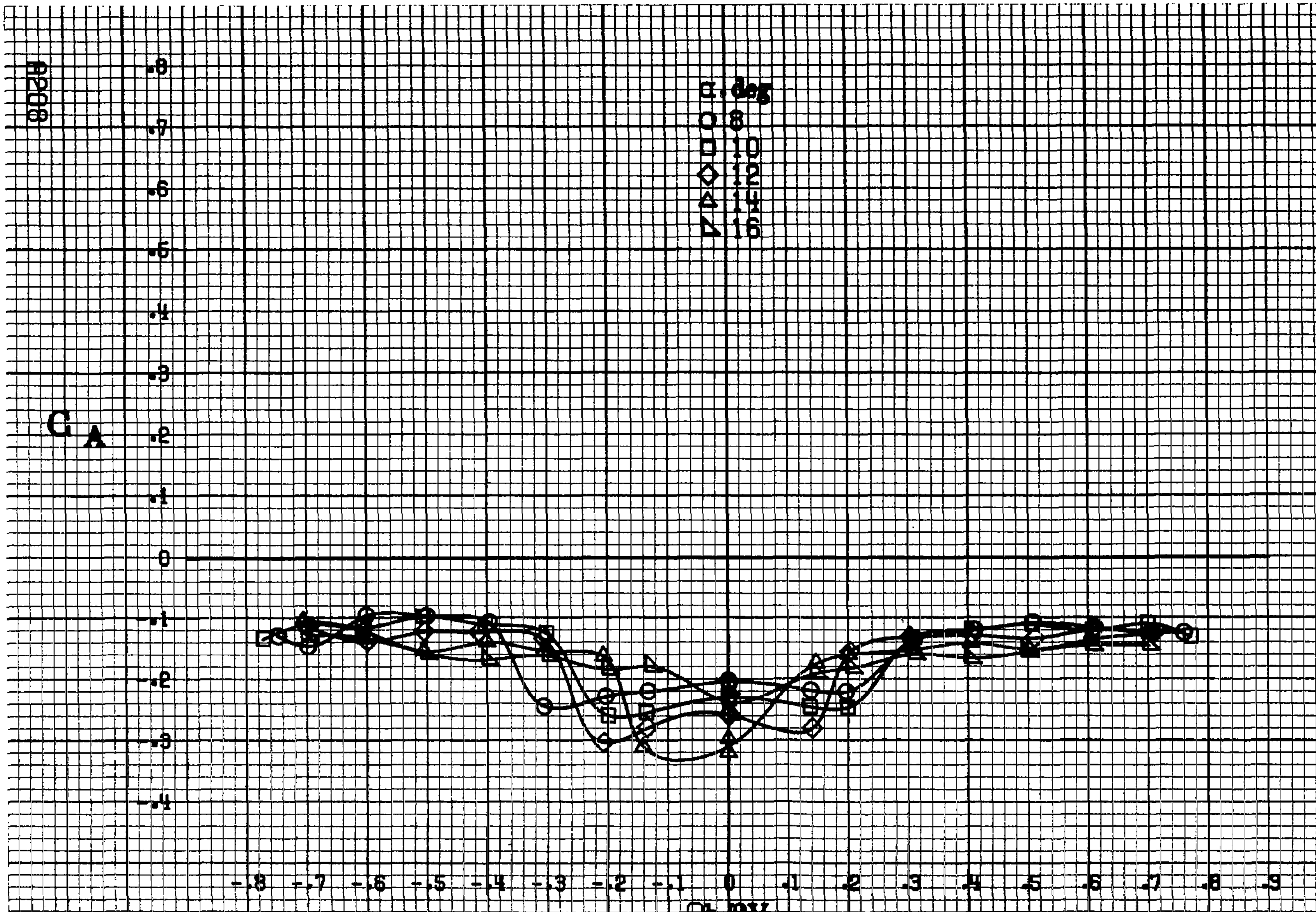

(a) α = 8 to 16 deg, SR = 182.9 cm (72 in).

Figure A48.-Effect of rotation rate and angle of attack on axial-force coefficient for full-span LE wing droop with large nose radius and sharp-edged fuselage bottom. $\delta_e = 0°$, $\delta_a = 0°$, $\delta_r = 0°$, $\beta = 0°$.

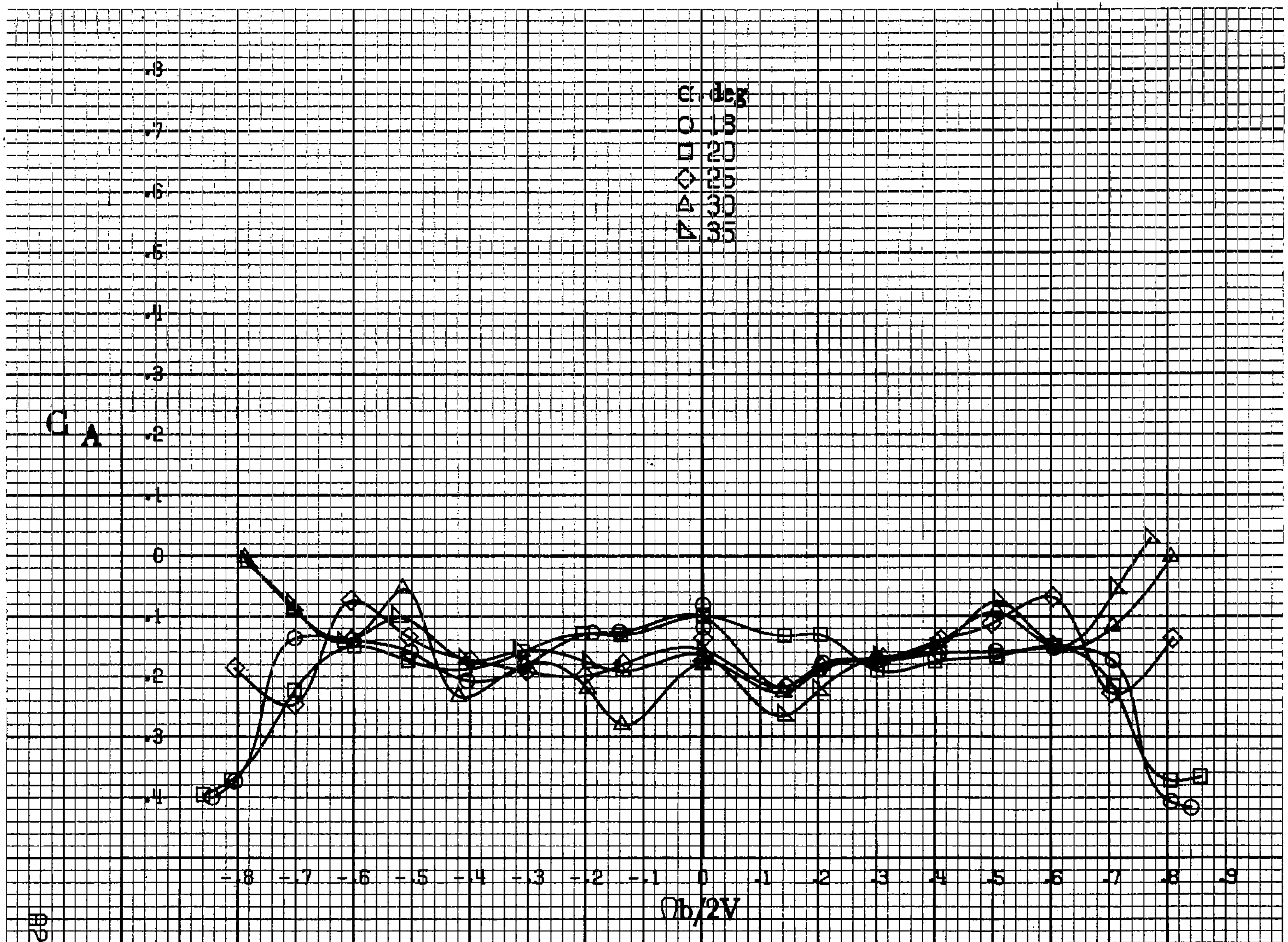

(b) α = 18 to 35 deg, SR = 182.9 cm (72 in).

Figure A48.-Continued.

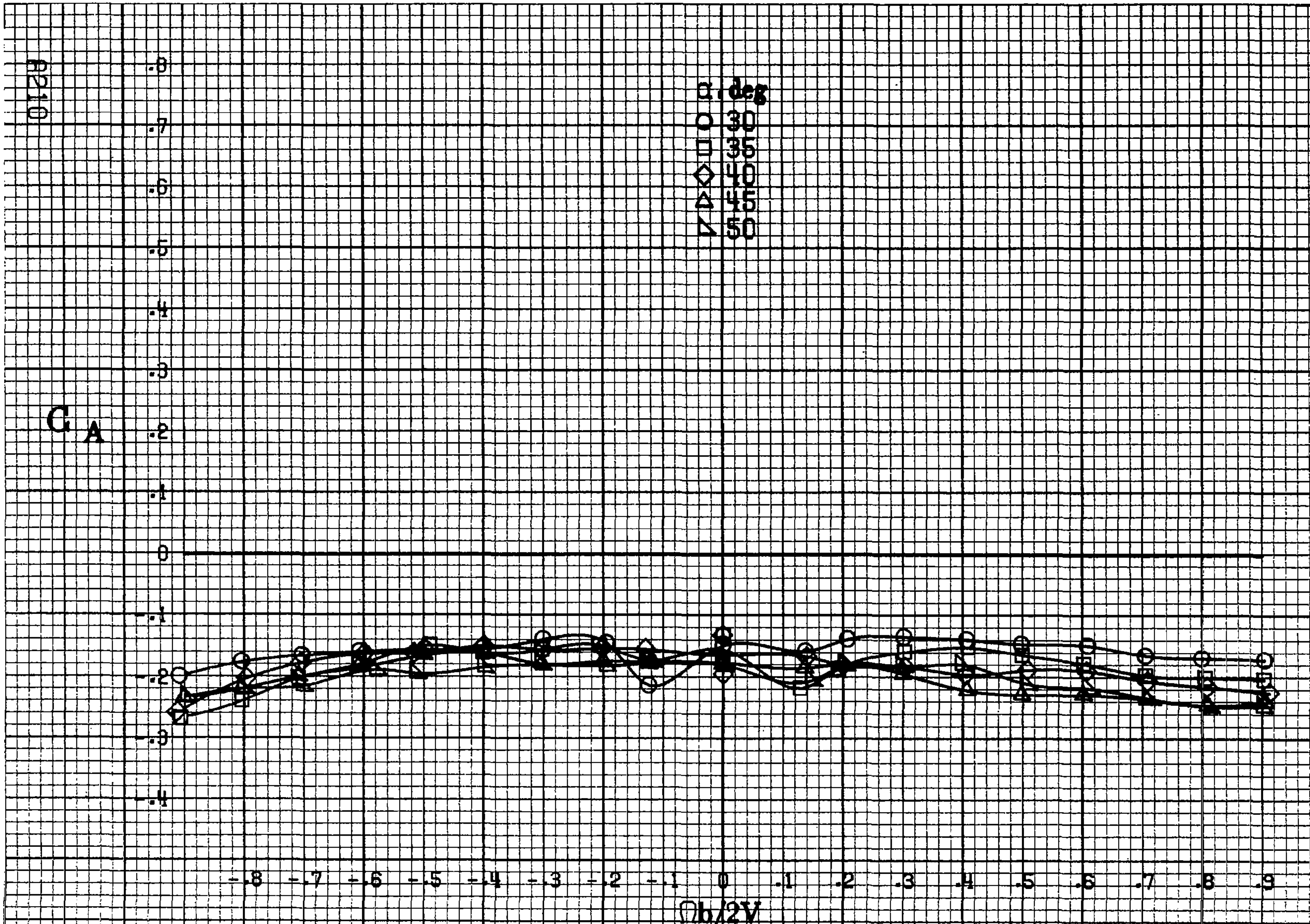

(c) α = 30 to 50 deg, SR = 0.

Figure A48.-Continued.

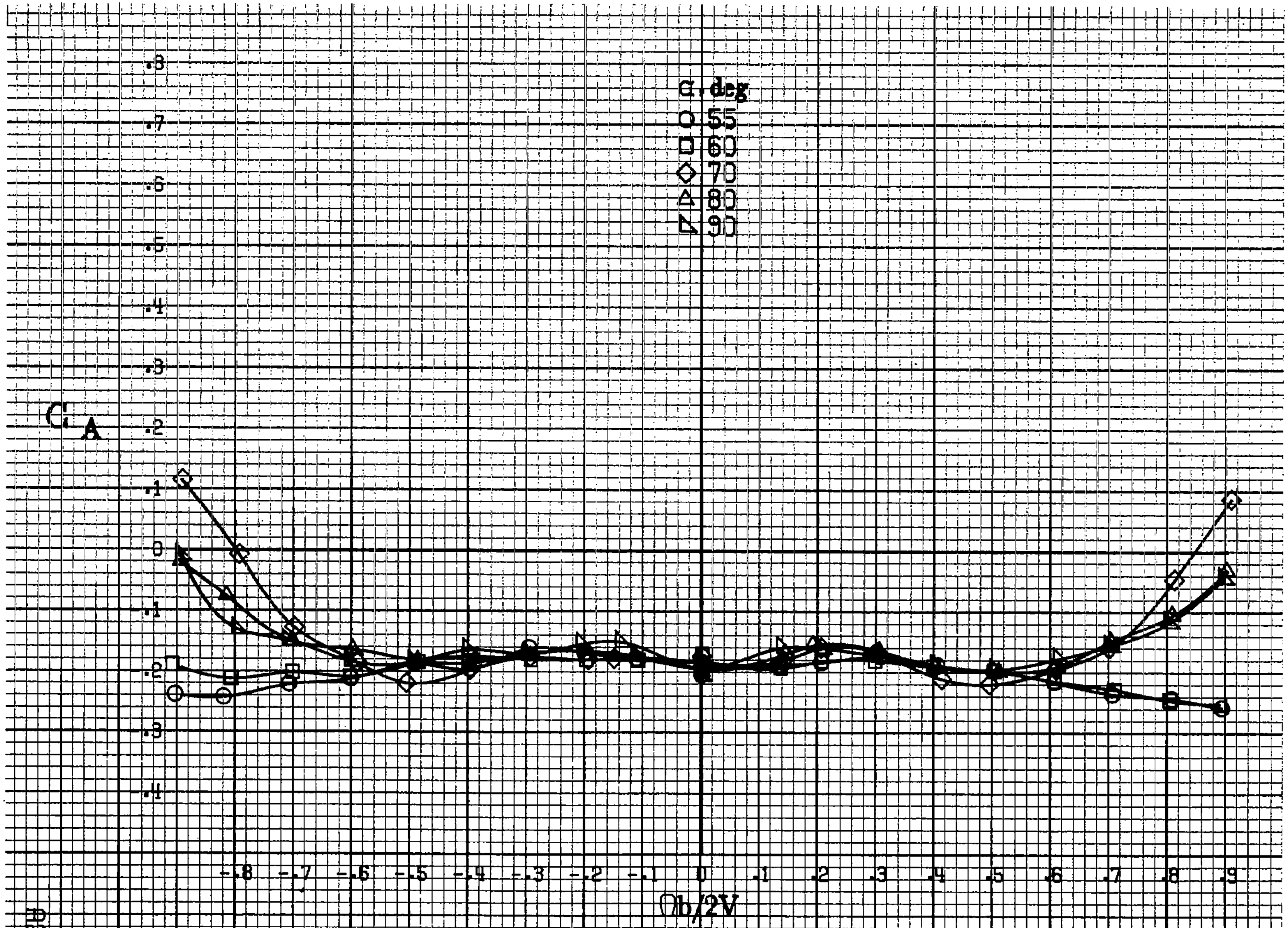

(d) α = 55 to 90 deg, SR = 0.

Figure A48.-Concluded.

(a) α = 8 to 16 deg, SR = 182.9 cm (72 in).

Figure A49.-Effect of rotation rate and angle of attack on yawing-moment coefficient for outboard LE wing droop with large nose radius and inboard fairing. $\delta_e = 0°$, $\delta_a = 0°$, $\delta_r = 0°$, $\beta = 0°$.

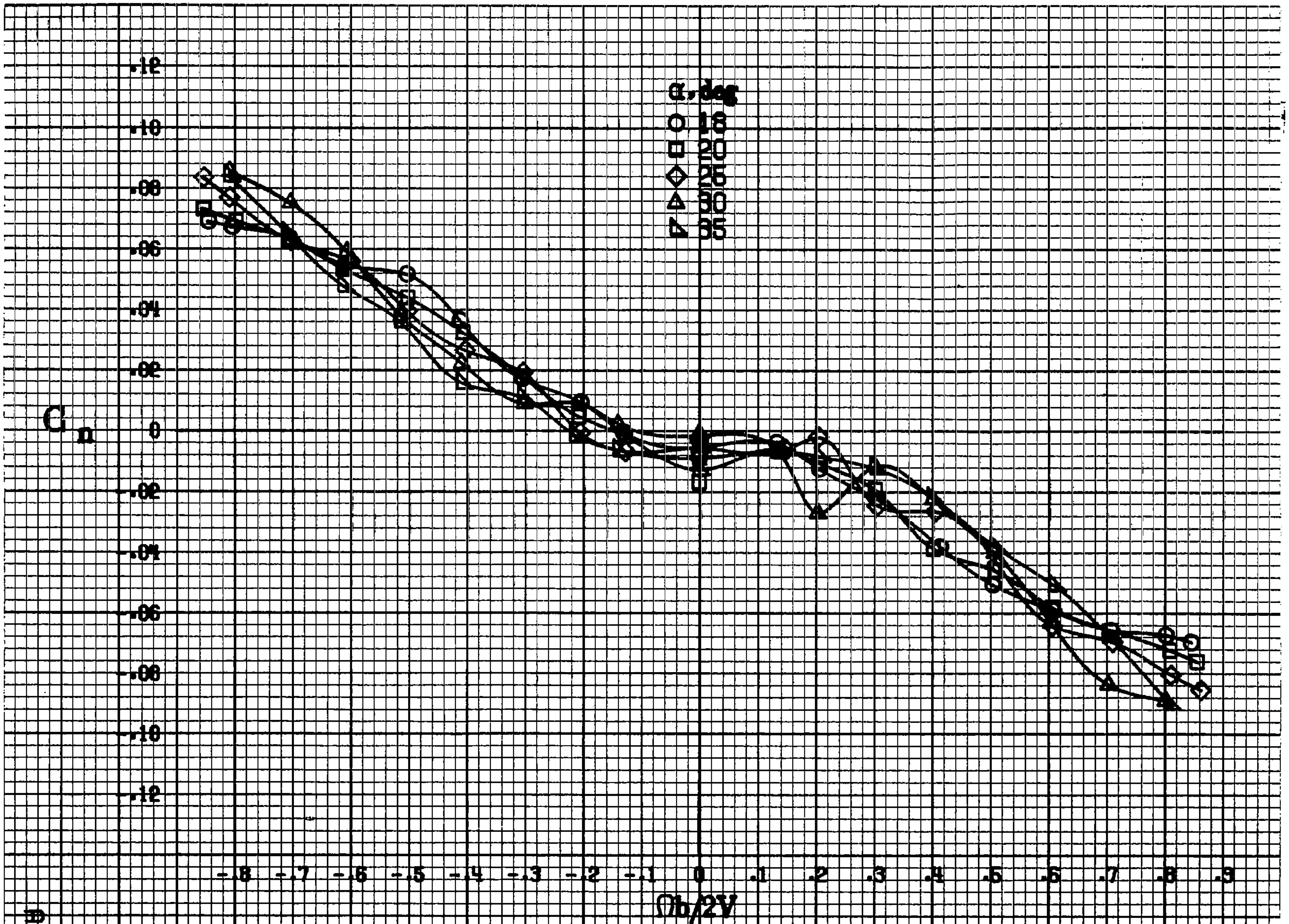

(b) α = 18 to 35 deg, SR = 182.9 cm (72 in).

Figure A49.-Continued.

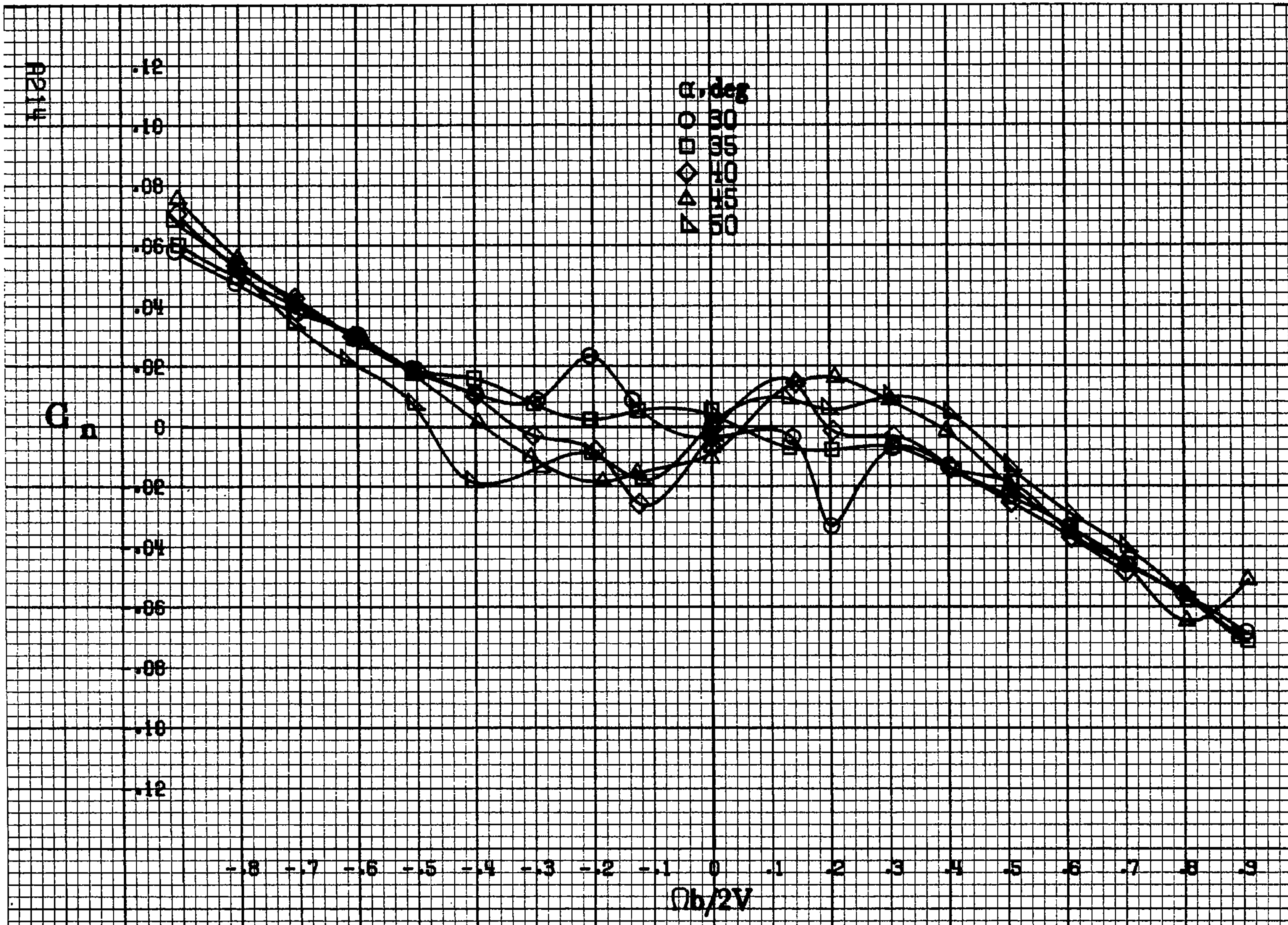

(c) α = 30 to 50 deg, SR = 0.

Figure A49.-Continued.

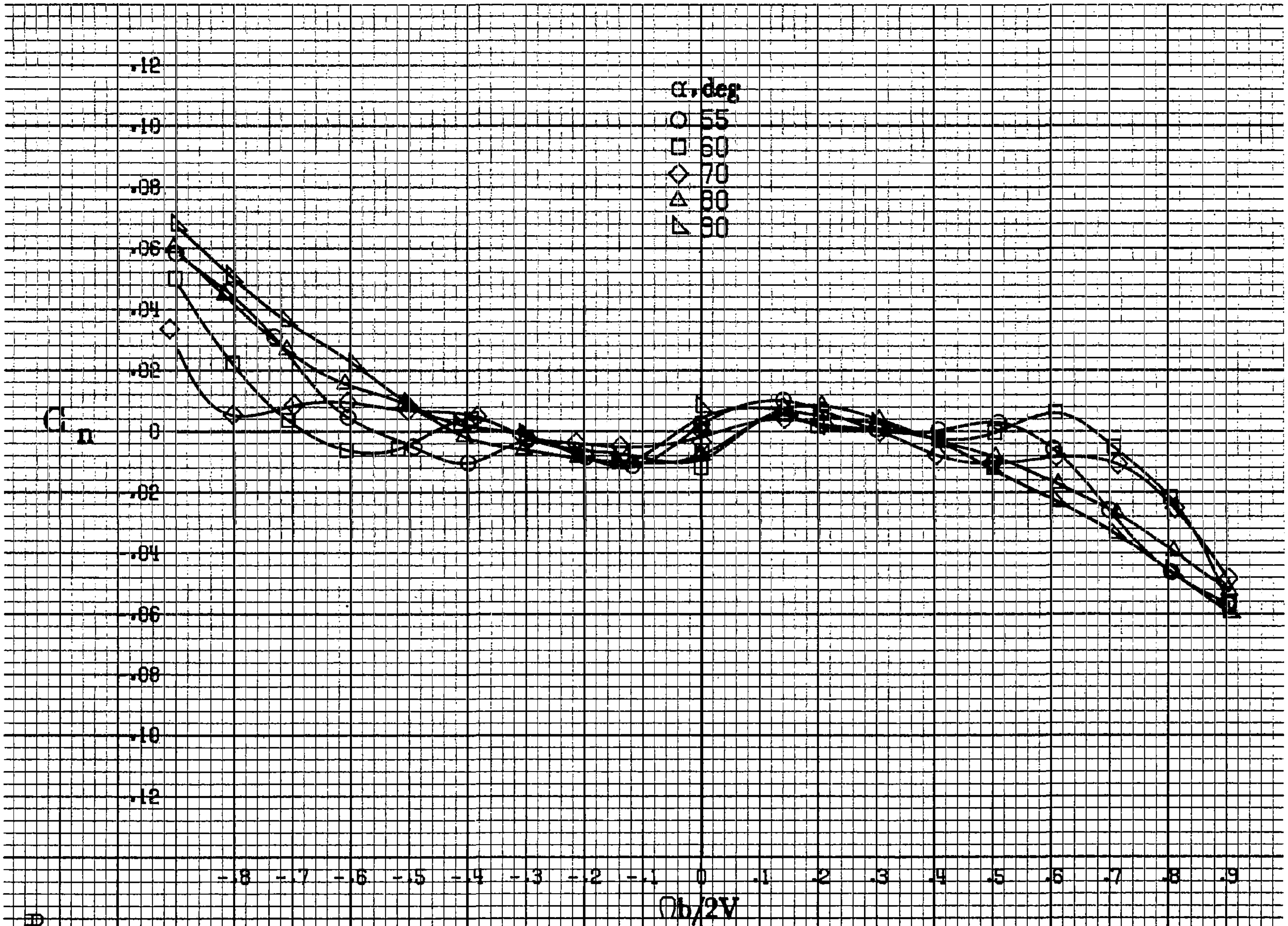

(d) α = 55 to 90 deg, SR = 0.

Figure A 49.-Concluded.

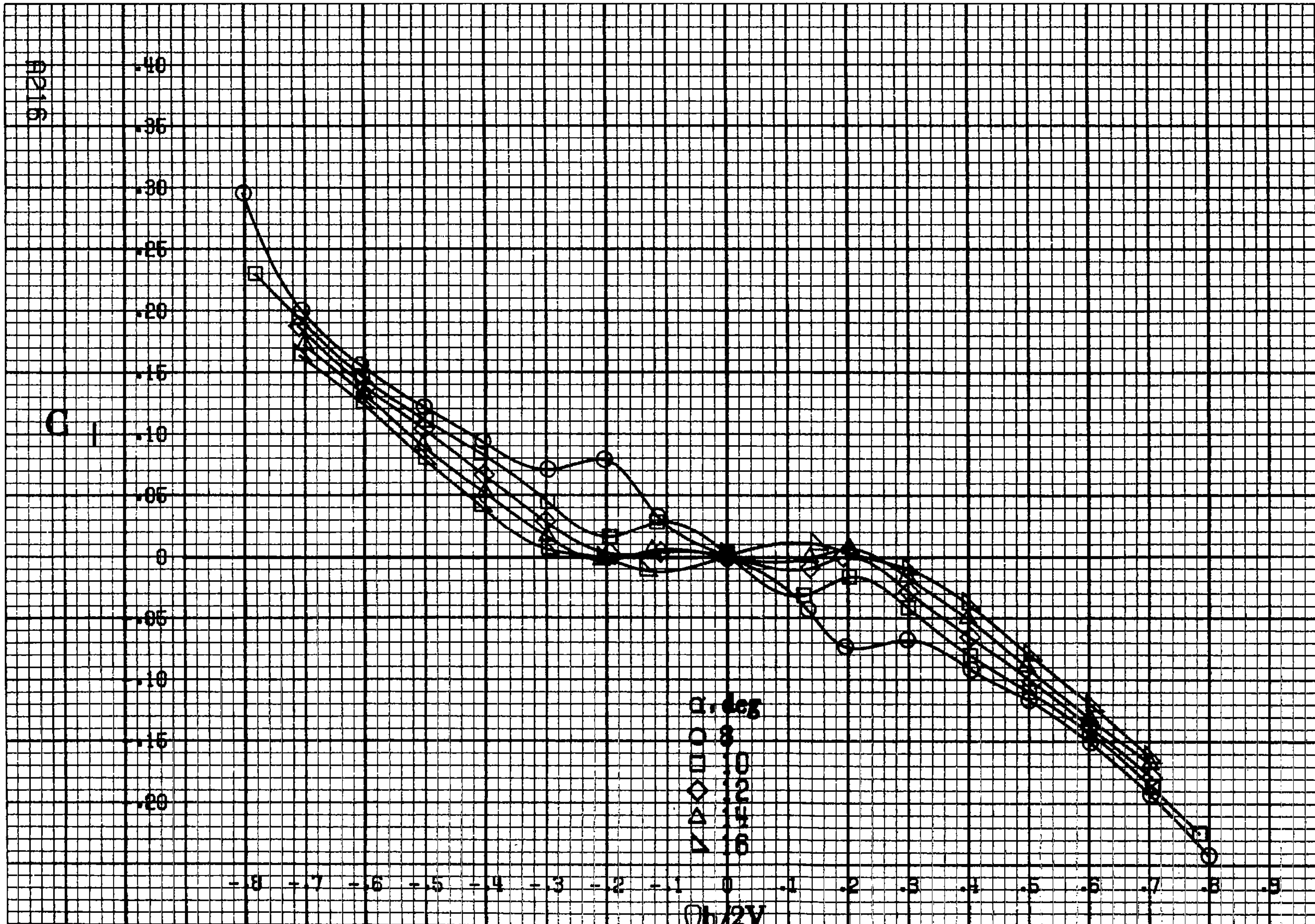

(a) α = 8 to 16 deg, SR = 182.9 cm (72 in).

Figure A50.- Effect of rotation rate and angle of attack on rolling-moment coefficient for outboard LE wing droop with large nose radius and inboard fairing. $\delta_e = 0°$, $\delta_a = 0°$, $\delta_r = 0°$, $\beta = 0°$.

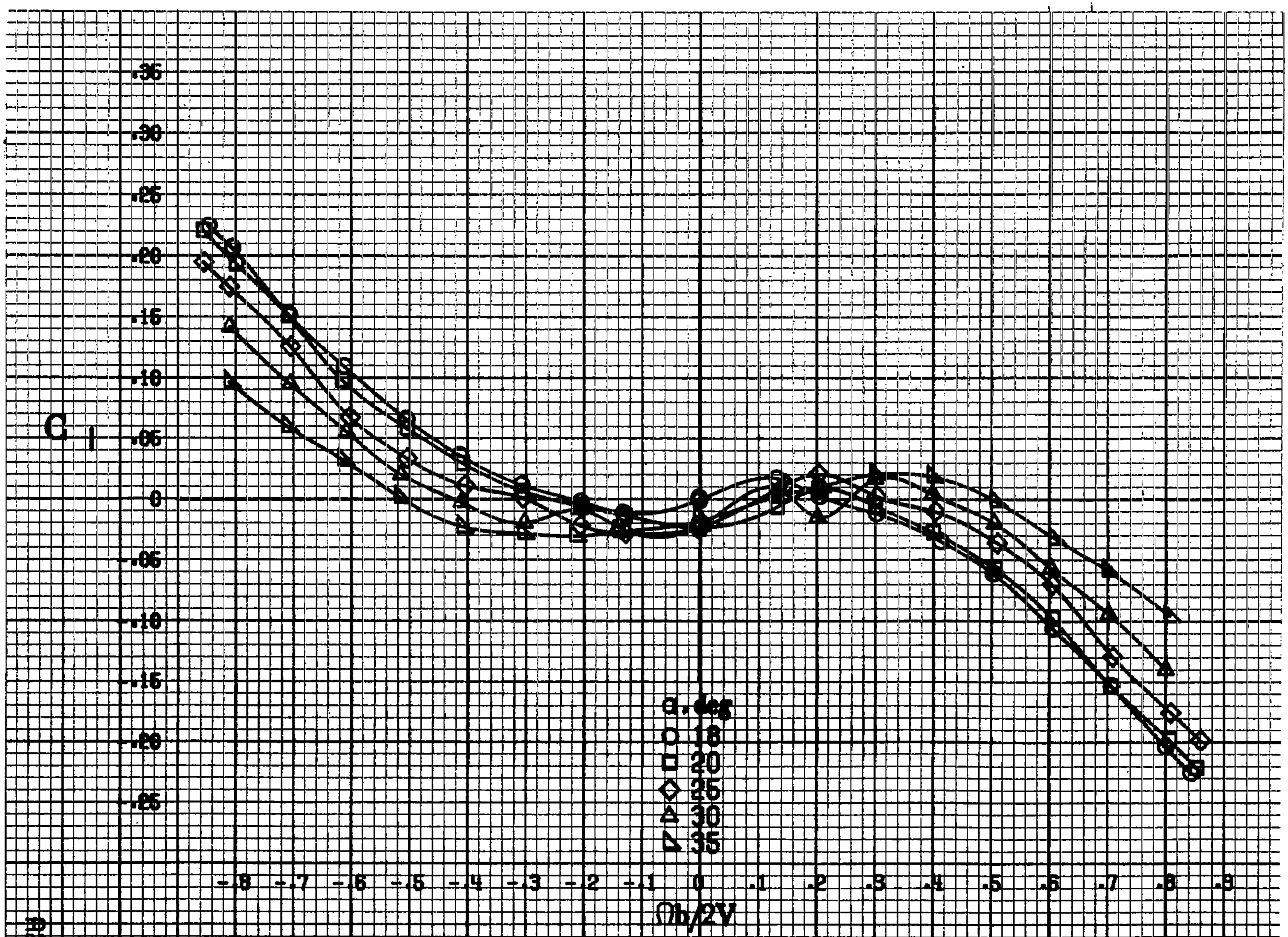

(b) α = 18 to 35 deg, SR = 182.9 cm (72 in).

Figure A50.-Continued.

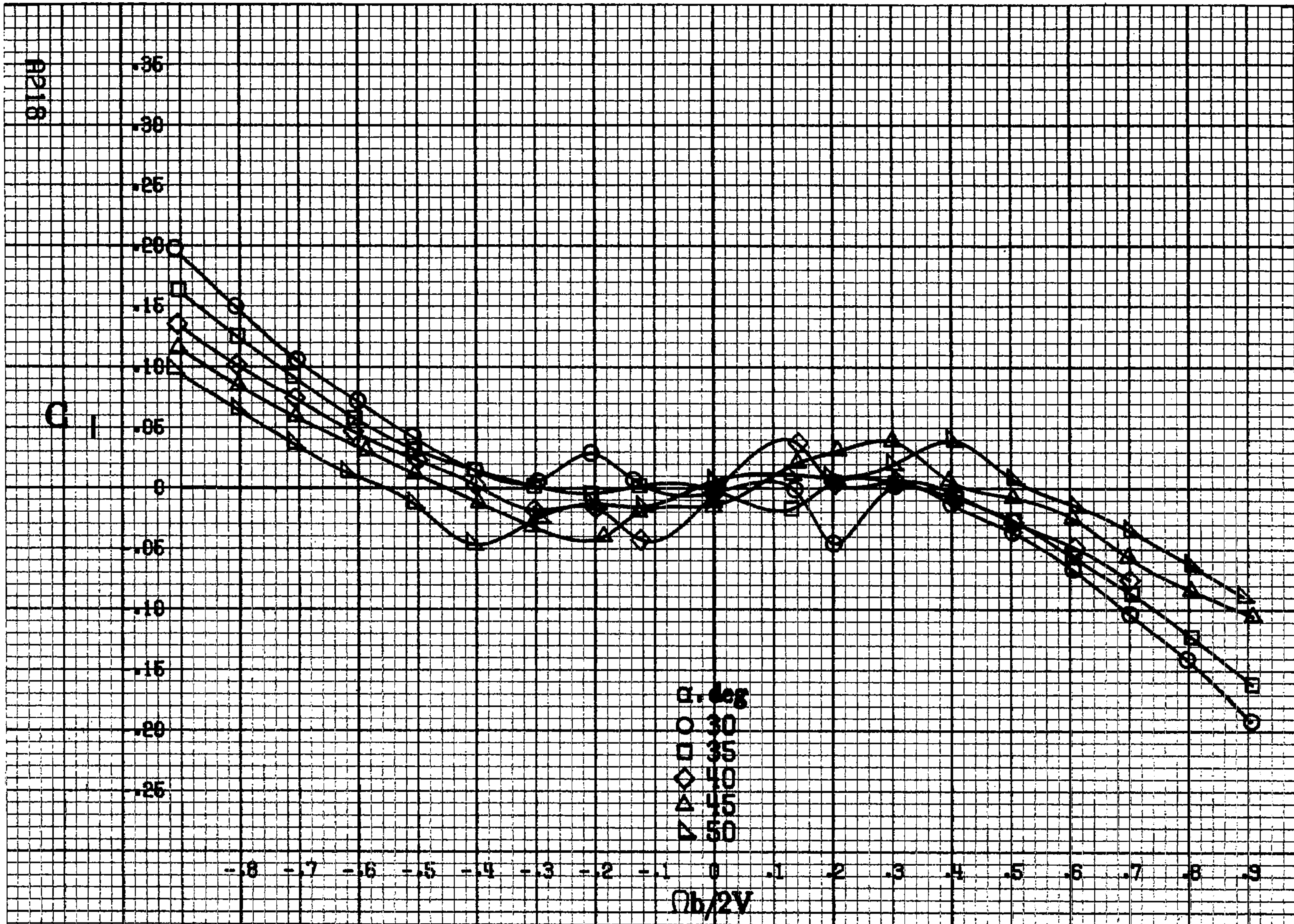

(c) α = 30 to 50 deg, SR = 0.

Figure A50.-Continued.

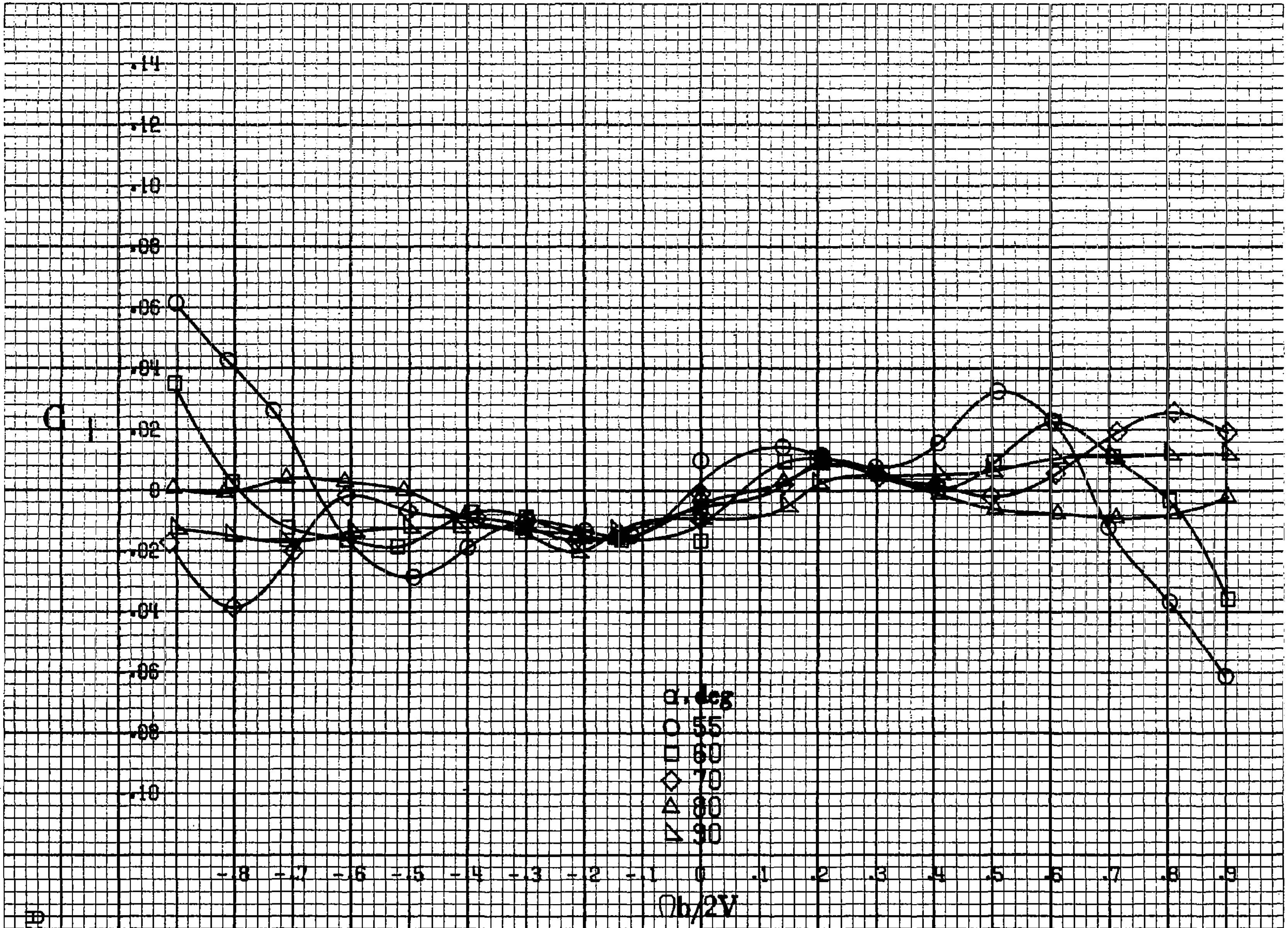

(d) α = 55 to 90 deg, SR = 0.

Figure A50.-Concluded.

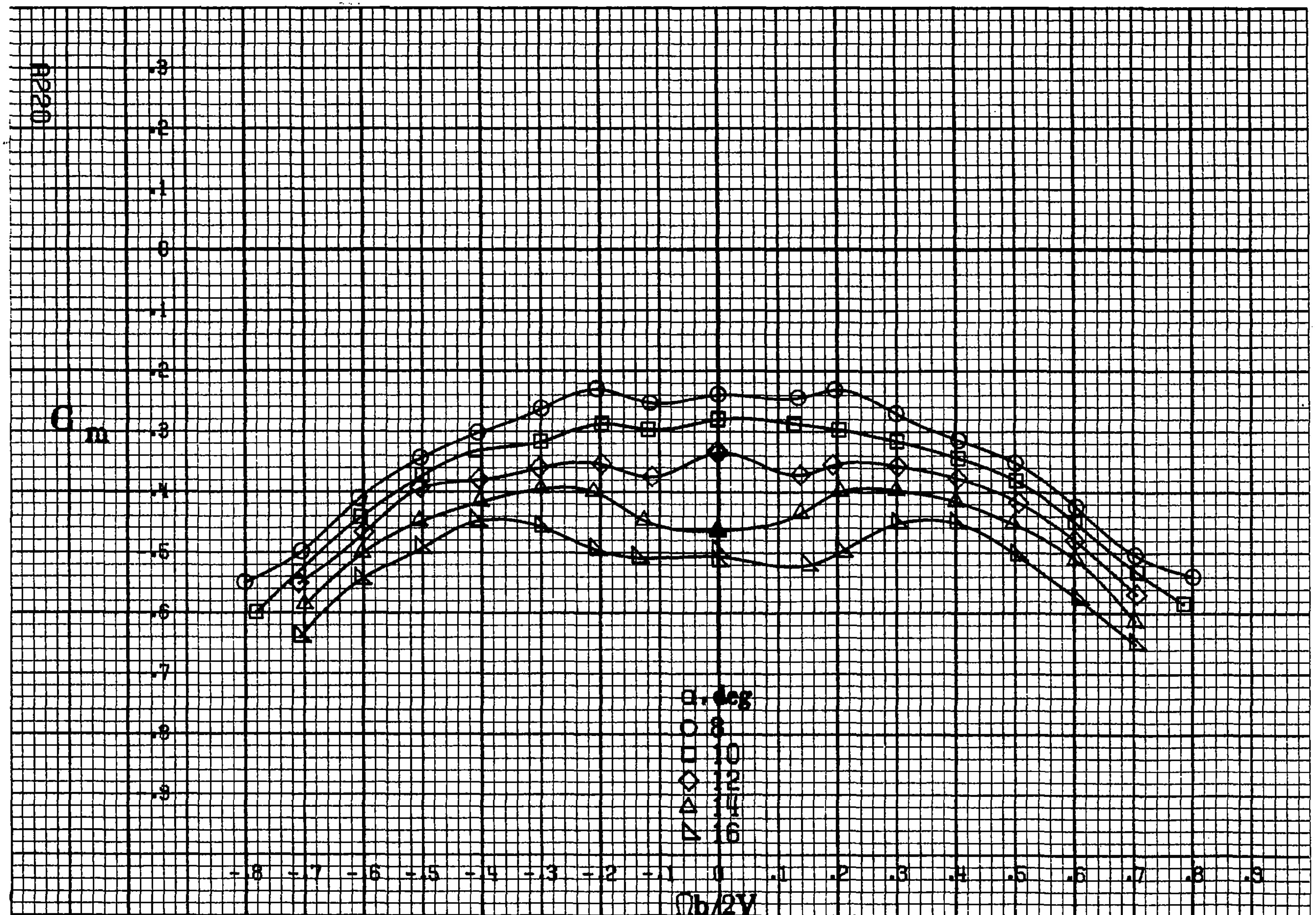

(a) $\alpha = 8$ to 16 deg, SR = 182.9 cm (72 in).

Figure A51.- Effect of rotation rate and angle of attack on pitching-moment coefficient for outboard LE wing droop with large nose radius and inboard fairing. $\delta_e = 0°$, $\delta_a = 0°$, $\delta_r = 0°$, $\beta = 0°$.

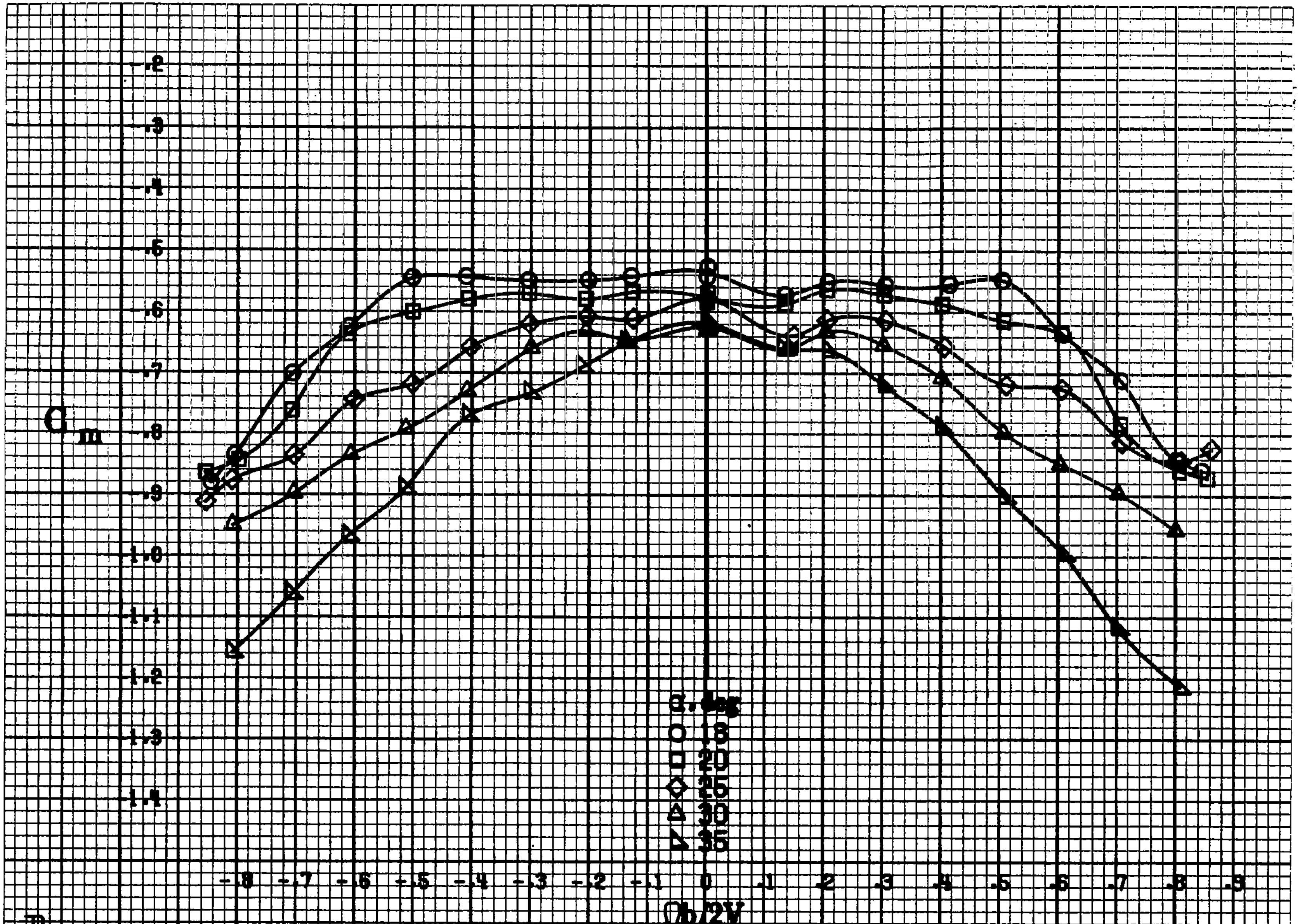

(b) α = 18 to 35 deg, SR = 182.9 cm (72 in).

Figure A51.-Continued.

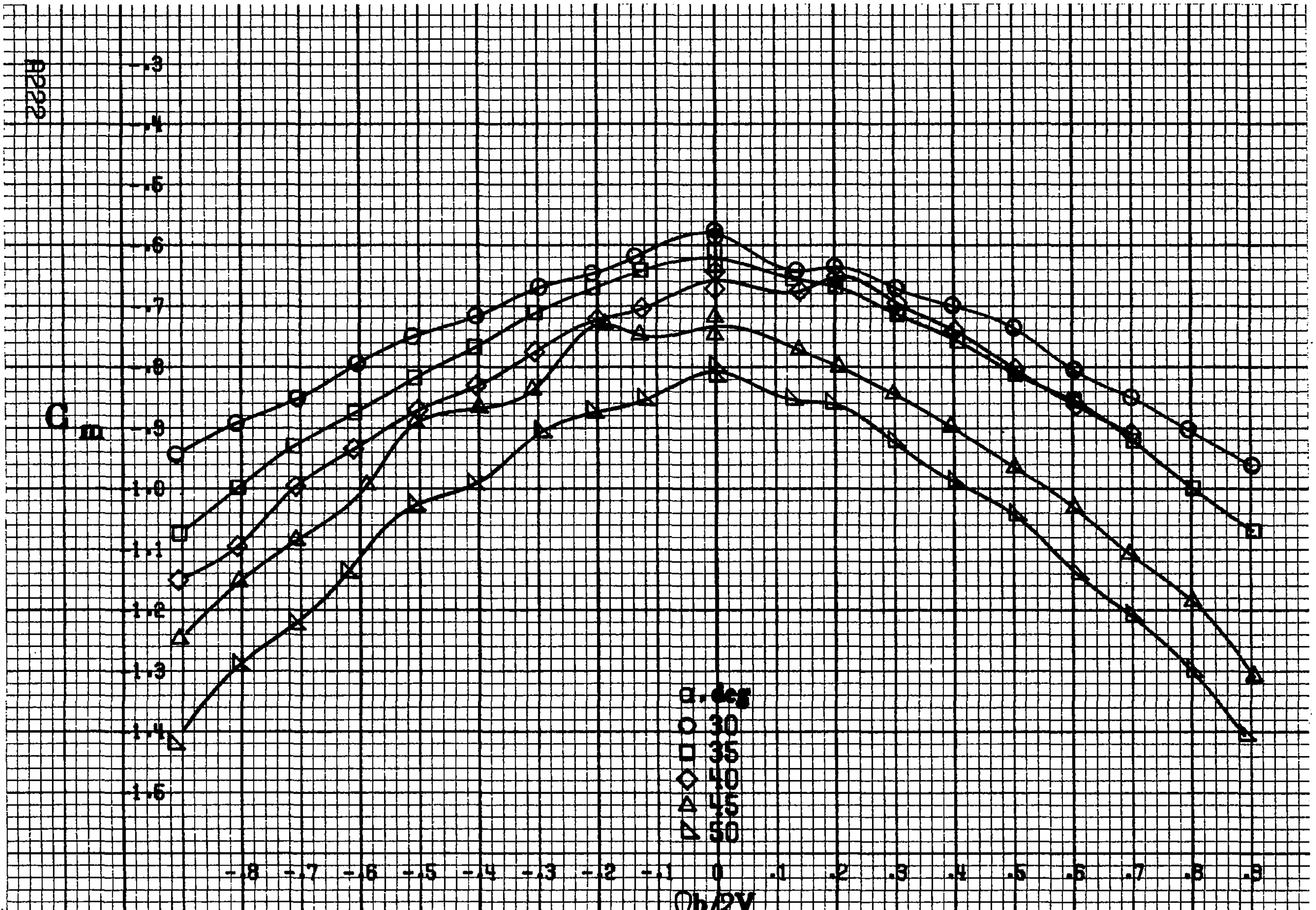

(c) α = 30 to 50 deg, SR = 0.

Figure A51.-Continued.

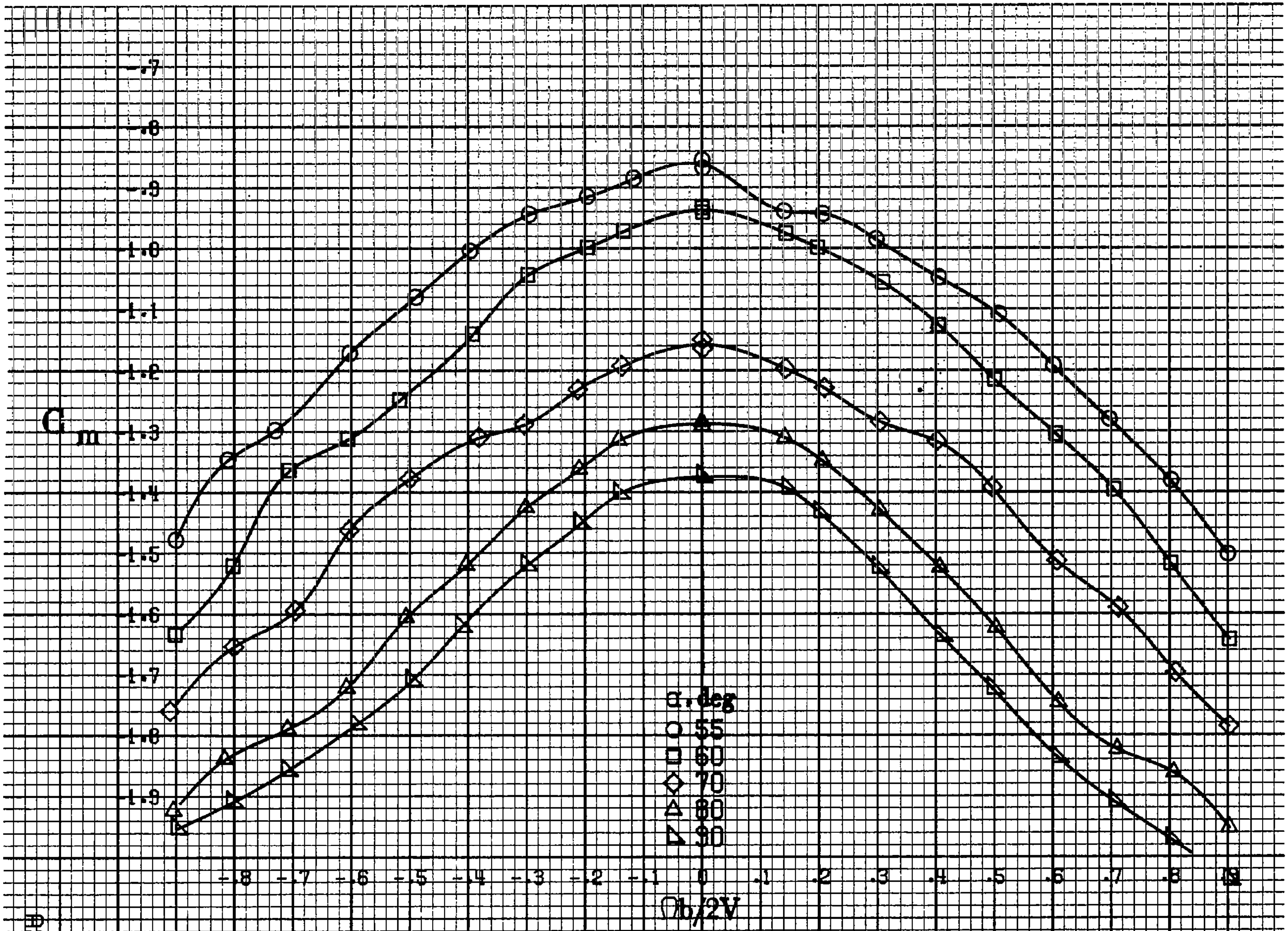

(d) α=55to90deg, SR=0.
Figure A51.-Concluded.

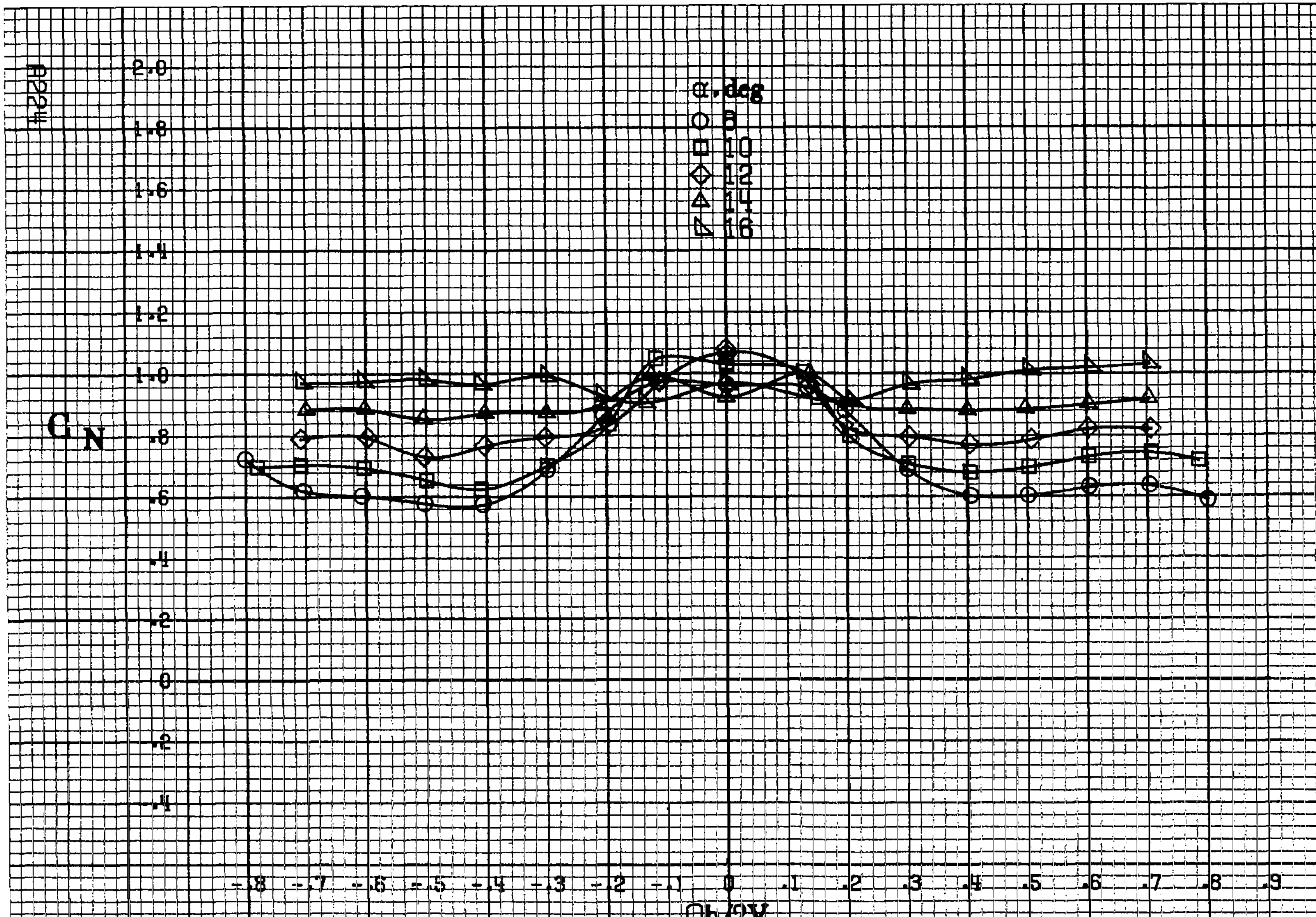

(a) $\alpha = 8$ to 16 deg, SR = 182.9 cm (72 in).

Figure A52.- Effect of rotation rate and angle of attack on normal-force coefficient for outboard LE wing droop with large nose radius and inboard fairing. $\delta_e = 0°$, $\delta_a = 0°$, $\delta_r = 0°$, $\beta = 0°$.

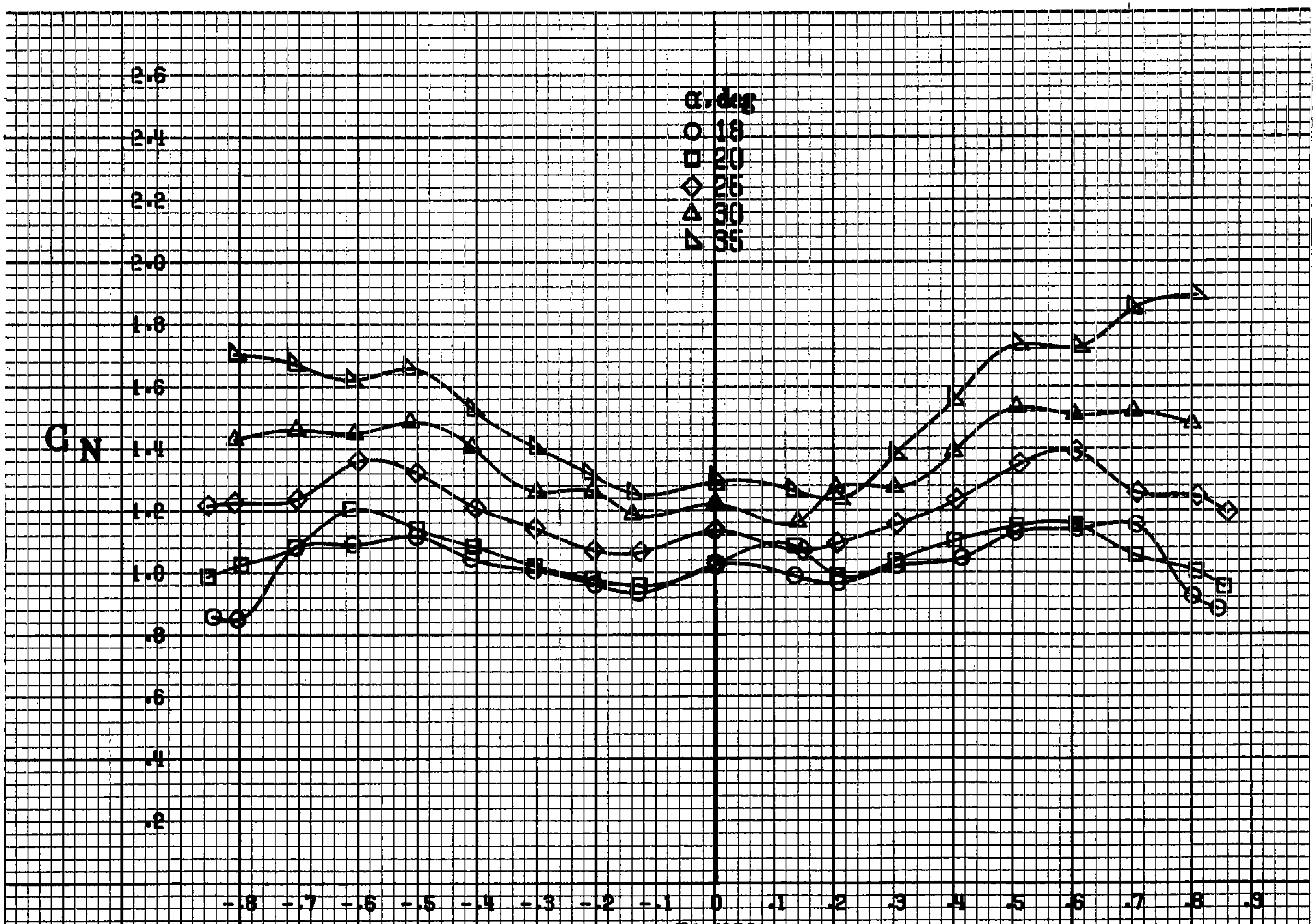

(b) α = 18 to 35 deg, SR = 182.9 cm (72 in).

Figure A52.–Continued.

A225

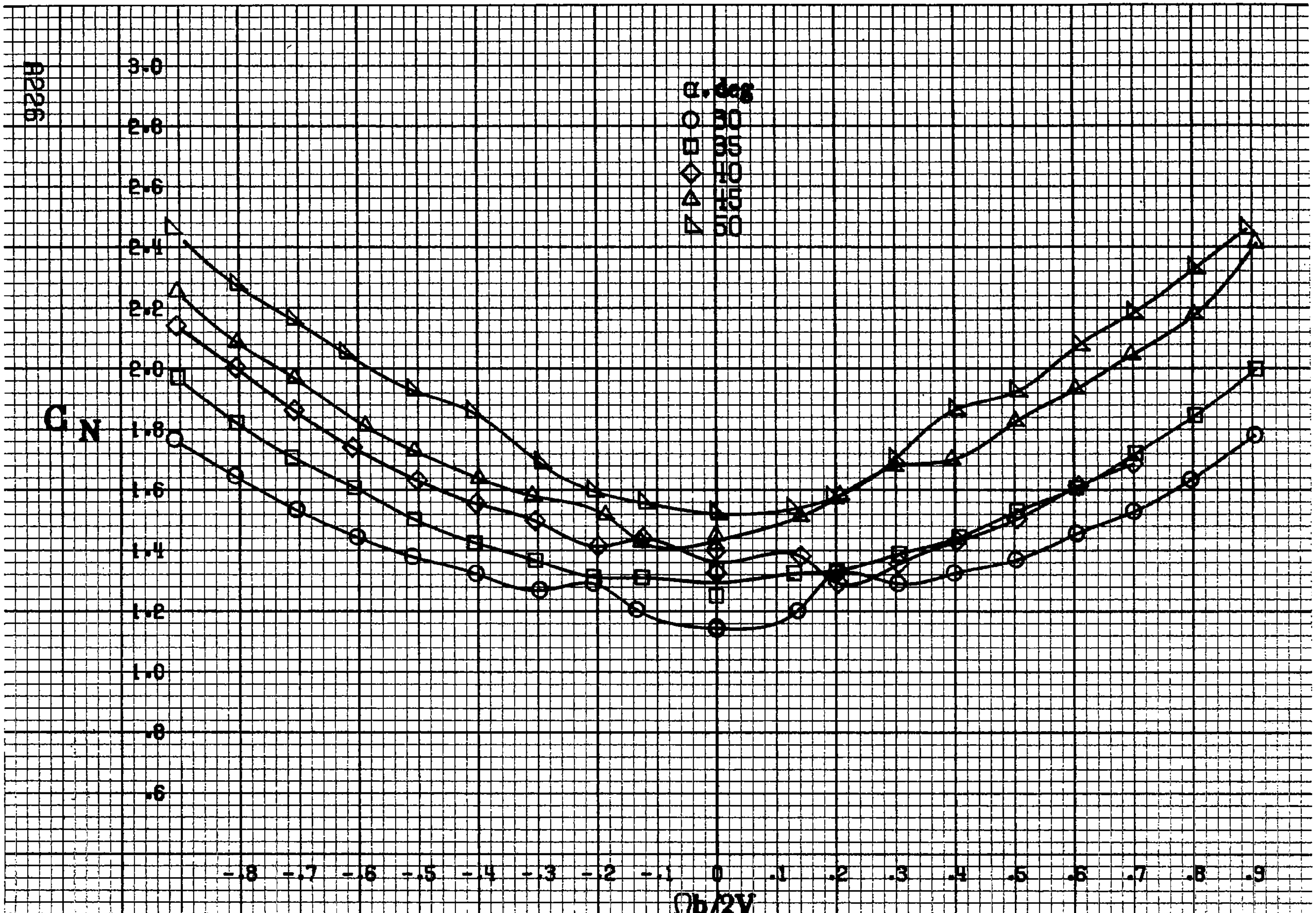

(c) α = 30 to 50 deg, SR = 0.

Figure A52.-Continued.

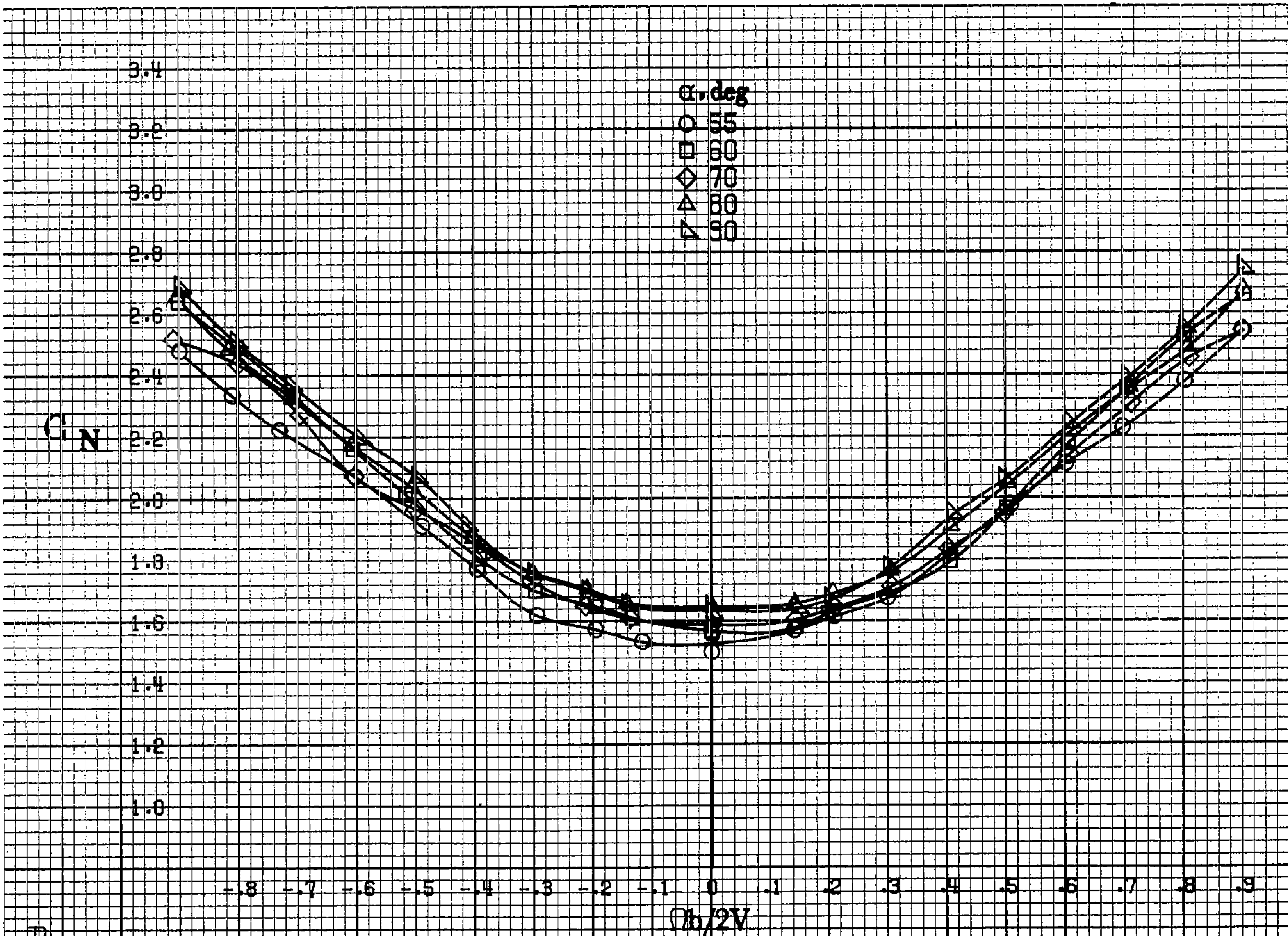

(d) β=55to90deg, SR=0.
Figure A52.-Concluded.

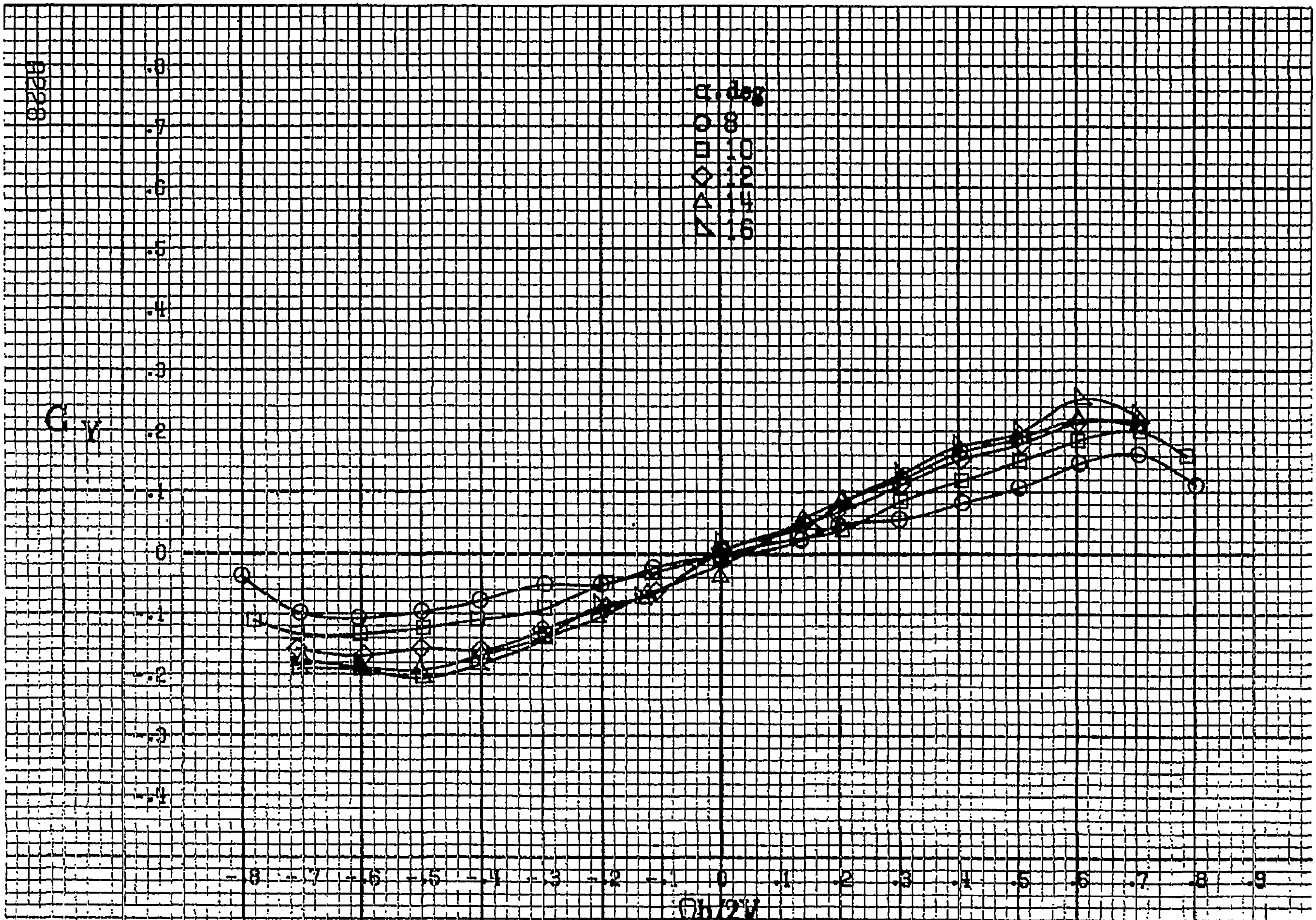

(a) $\alpha = 8$ to 16 deg, SR = 182.9 cm (72 in).

Figure A13.- Effect of rotation rate and angle of attack on side-force coefficient for outboard LE wing droop with large nose radius and inboard fairing. $\delta_h = 0°$, $\delta_a = 0°$, $\delta_r = 0°$, $\beta = 0°$.

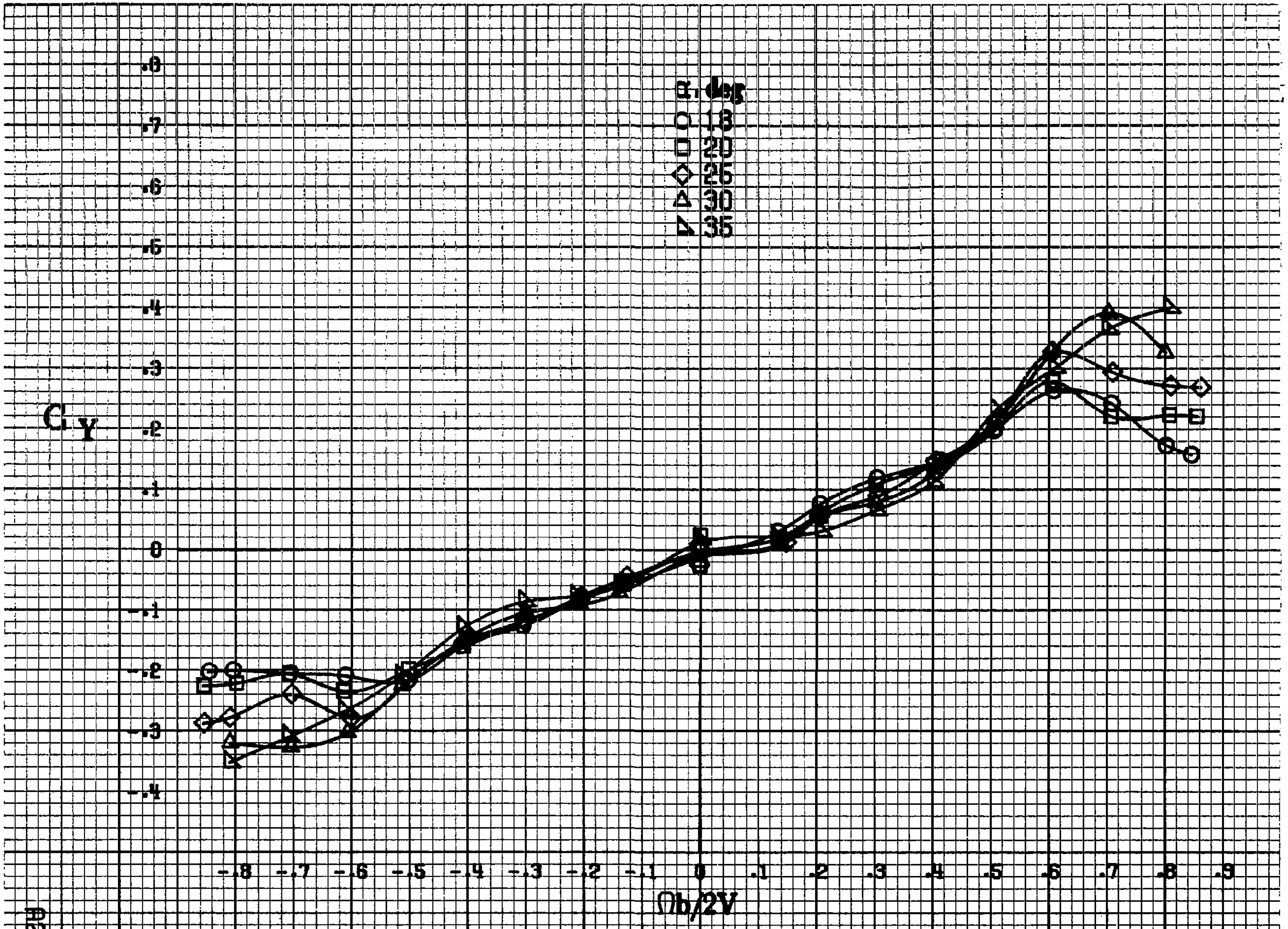

(b) α = 18 to 35 deg, SR = 182.9 cm (72 in).

Figure A58.-Continued.

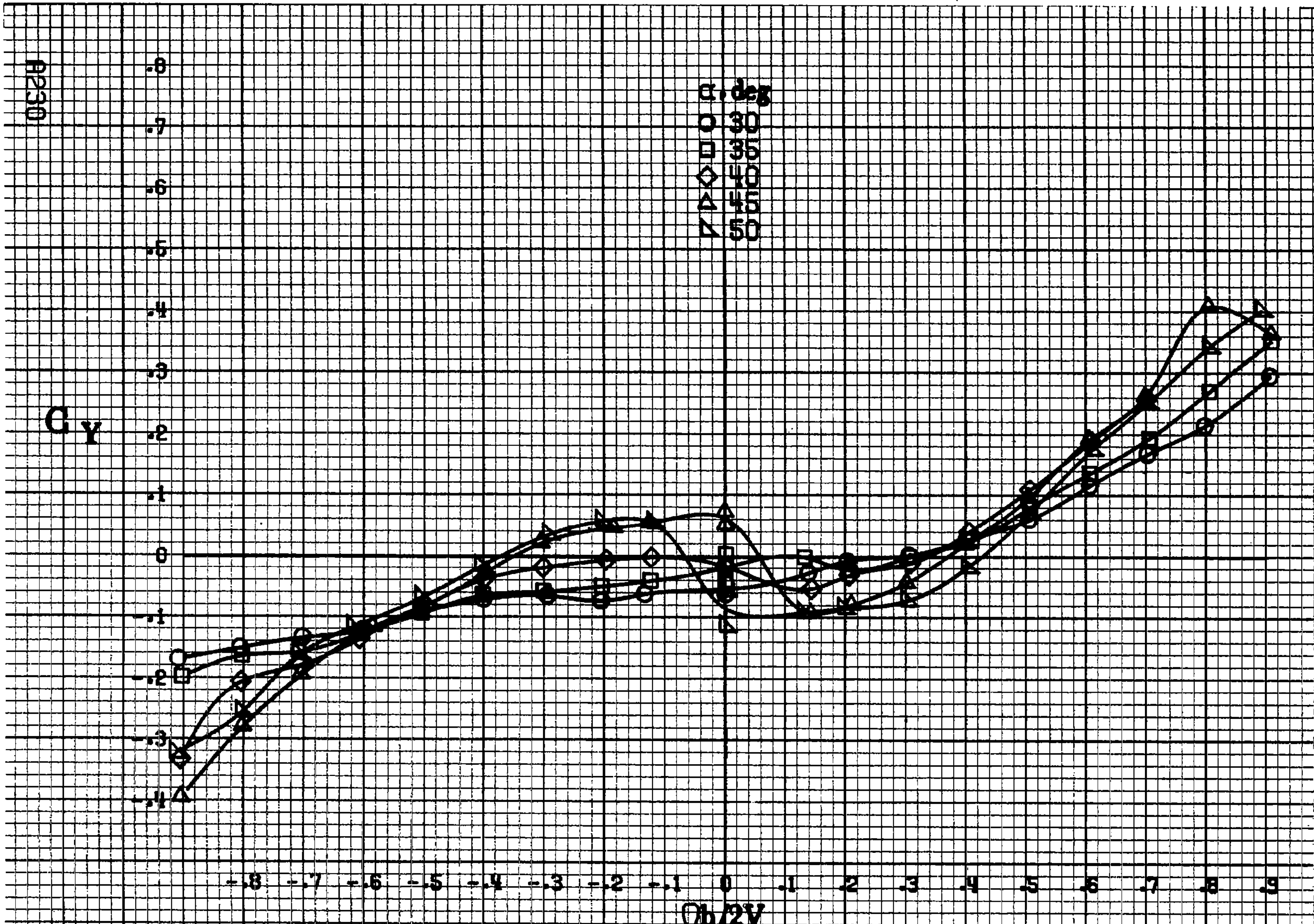

(c) α = 30 to 50 deg, SR = 0.

Figure A53.-Continued.

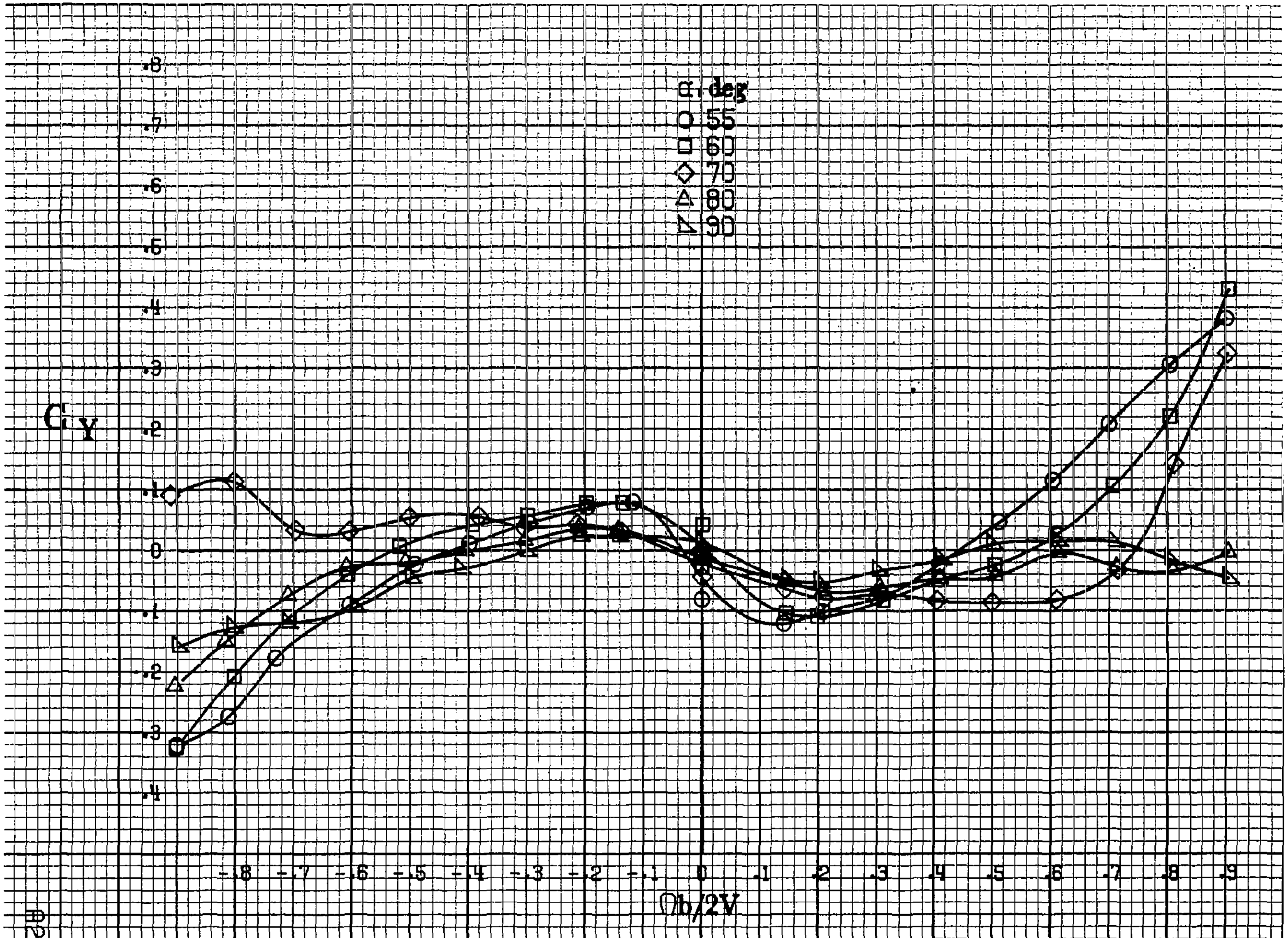

(d) α = 55 to 90 deg, SR = 0.
Figure A58.-Concluded.

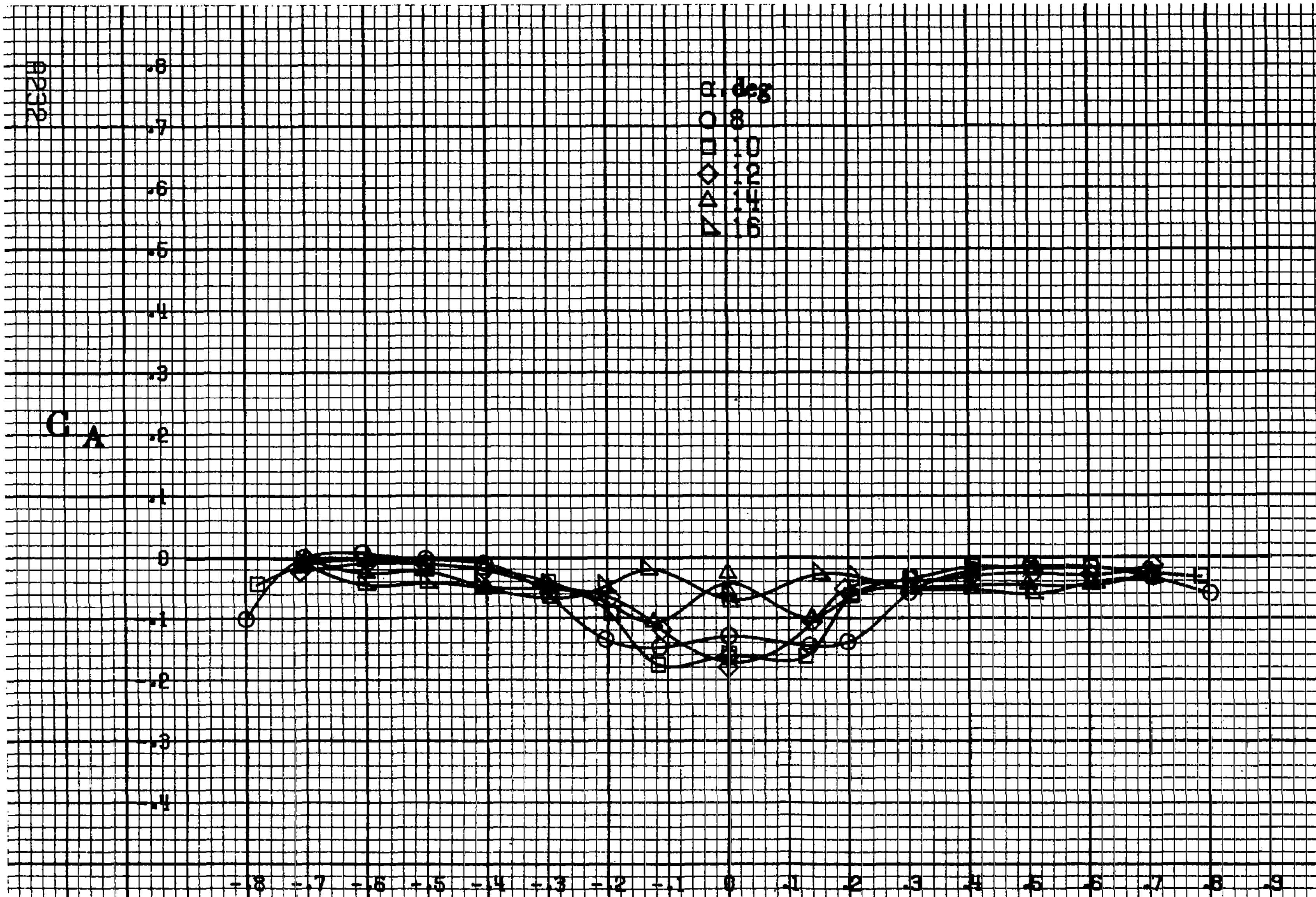

(a) $\alpha = 8$ to 16 deg, SR = 182.9 cm (72 in).

Figure A54.-Effect of rotation rate and angle of attack on axial-force coefficient for outboard LE wing droop with large nose radius and inboard fairing. $\delta_e = 0°$, $\delta_a = 0°$, $\delta_r = 0°$, $\beta = 0°$.

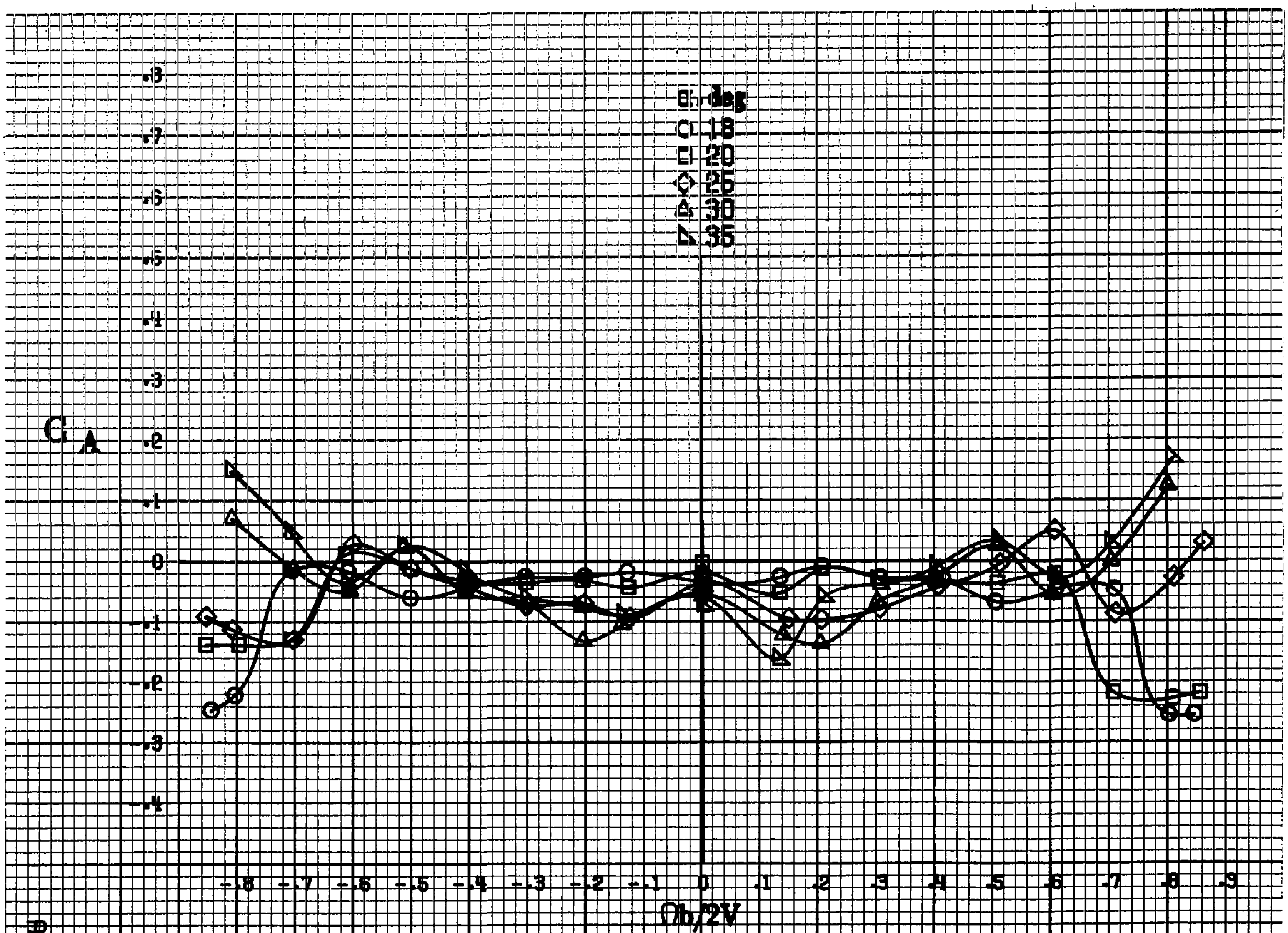

(h) α = 18to35deg, SR = 182.9cm (72in).
Figure A54.-Continued.

(c) α = 30 to 50 deg, SR = 0.

Figure A54.-Continued.

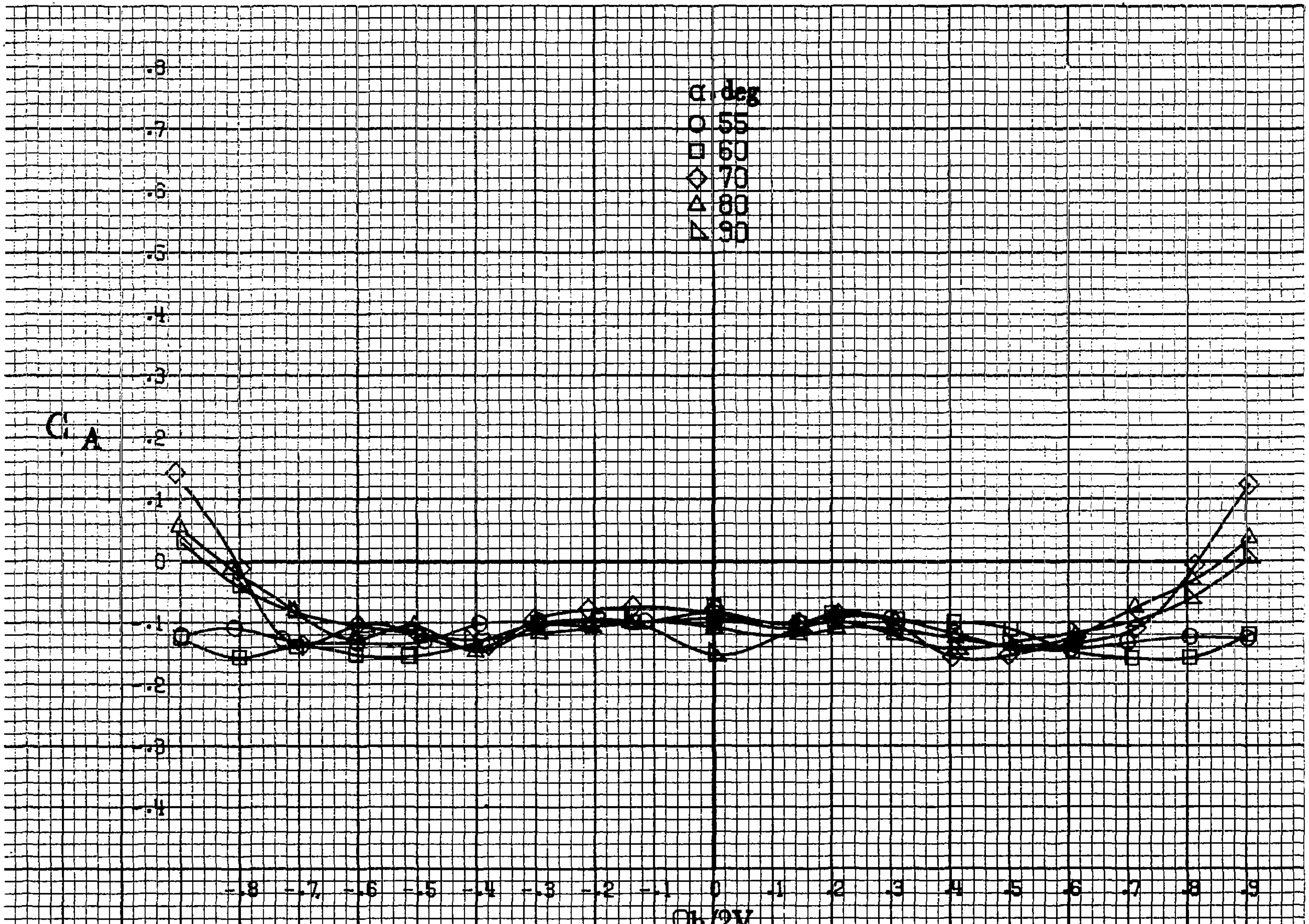

(d) α=55to90deg, SR=0.

Figure A54.-Concluded.

A235

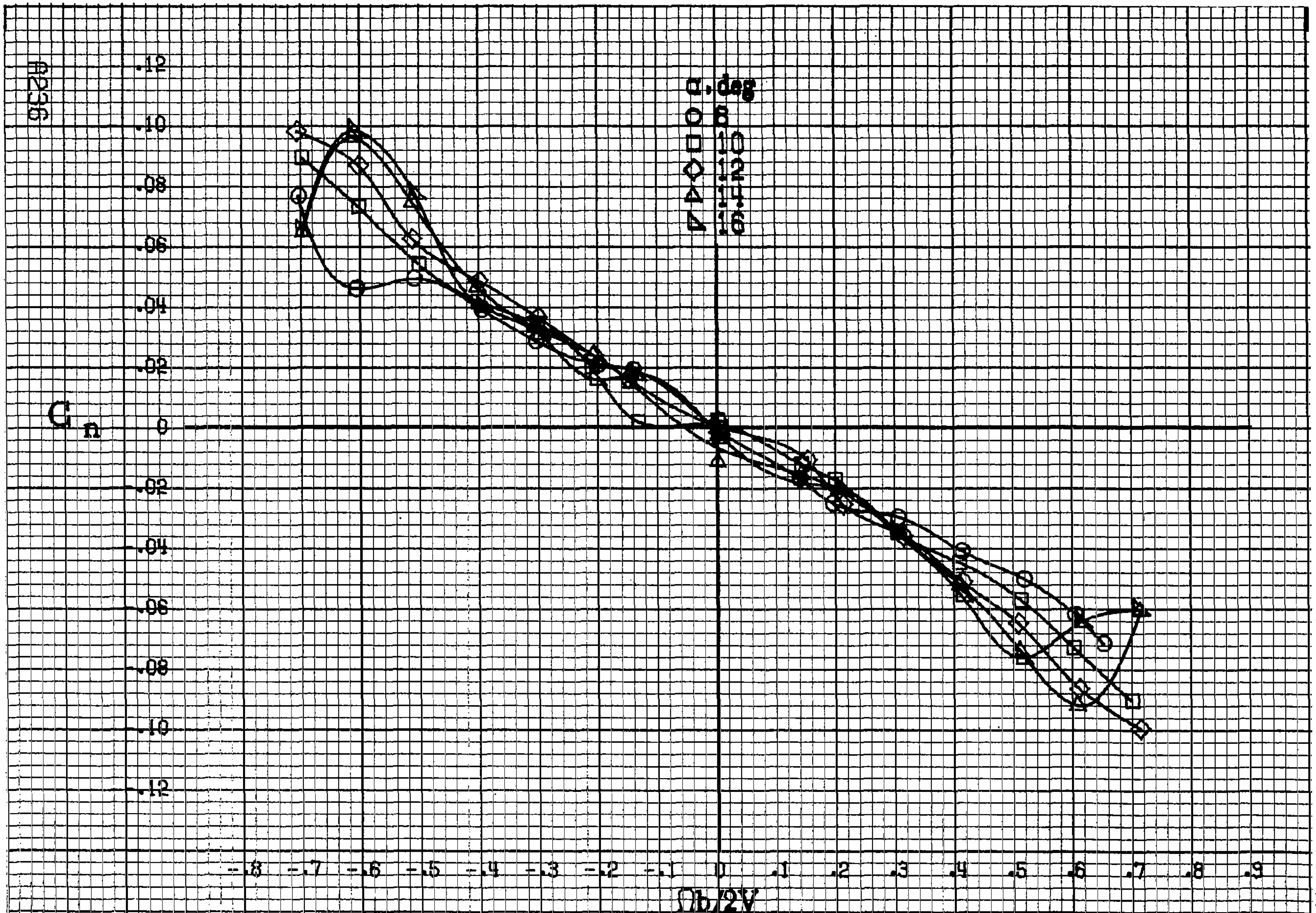

(a) $\alpha = 8$ to 16 deg, SR = 182.9 cm (72 in).

Figure A66.-Effect of rotation rate and angle of attack on yawing-moment coefficient for outboard LE wing droop with large nose radius. $\delta_a = 0°$, $\delta_s = 0°$, $\delta_r = 0°$. $\beta = 0°$.

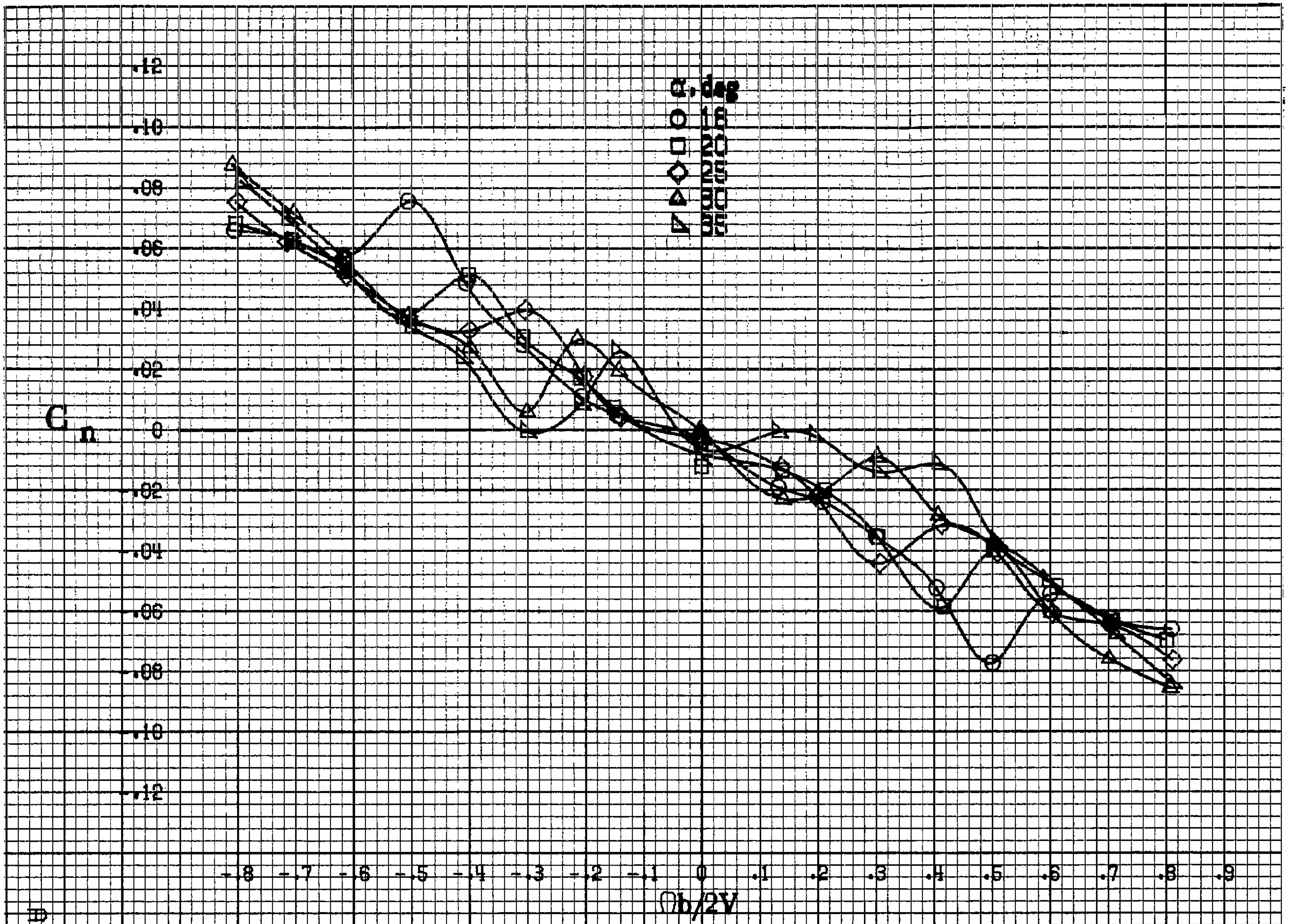

(b) α = 18 to 35 deg, SR = 182.9 cm (72 in).

Figure A55.-Continued.

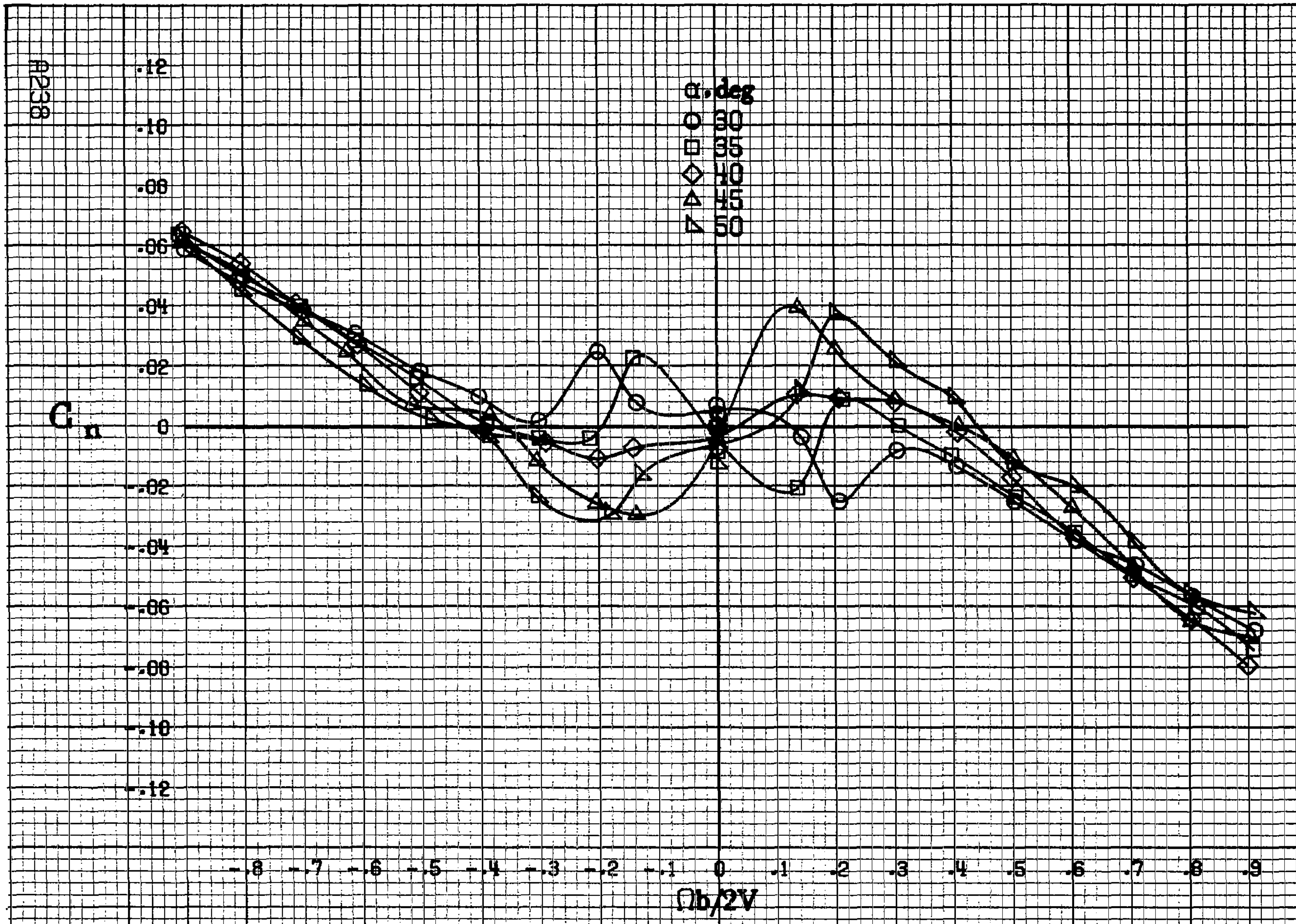

(c) α = 30 to 50 deg, SR = 0.
Figure A55.-Continued.

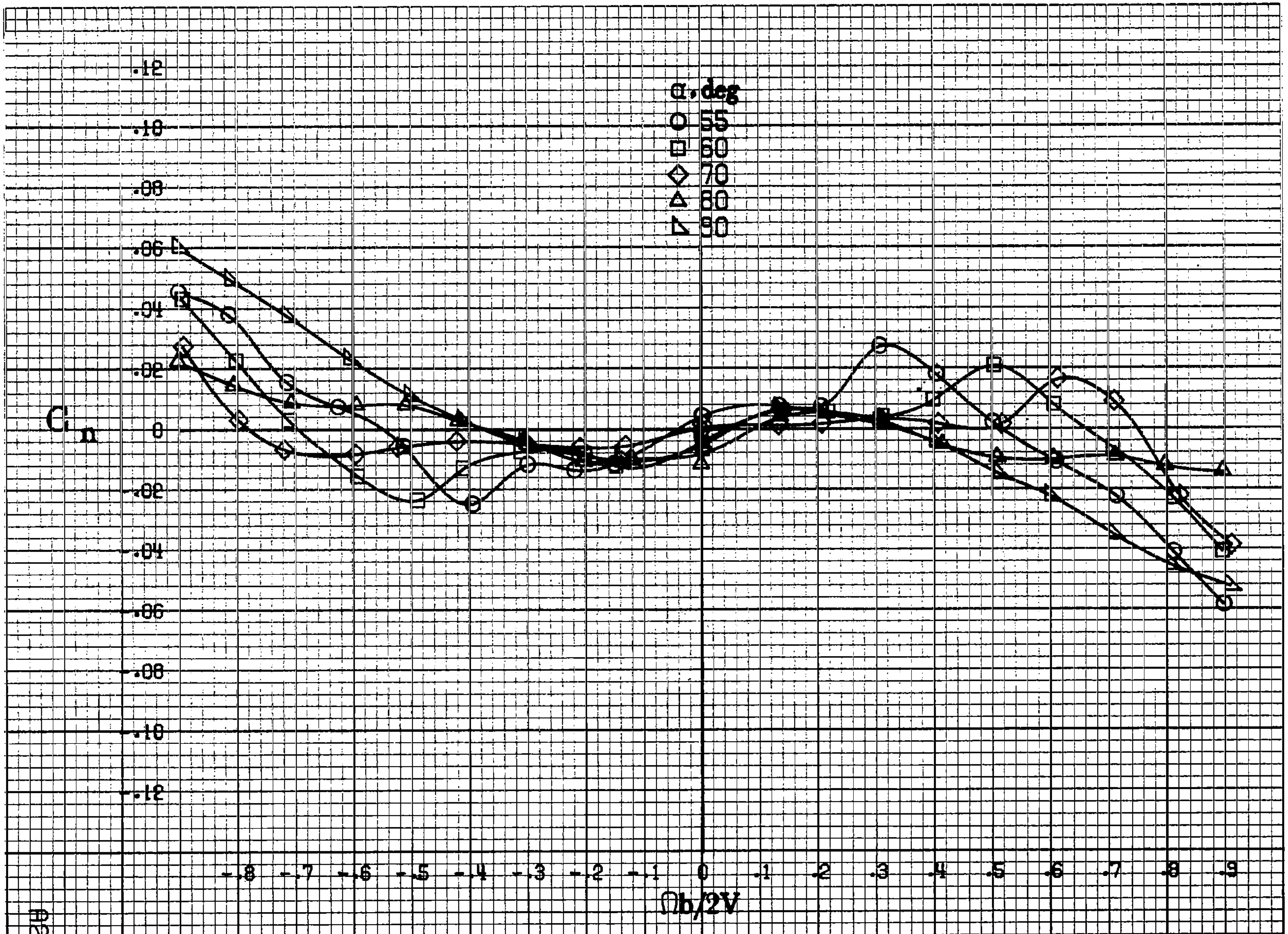

(d) α = 55 to 90 deg, SR = 0.

Figure A55.-Concluded.

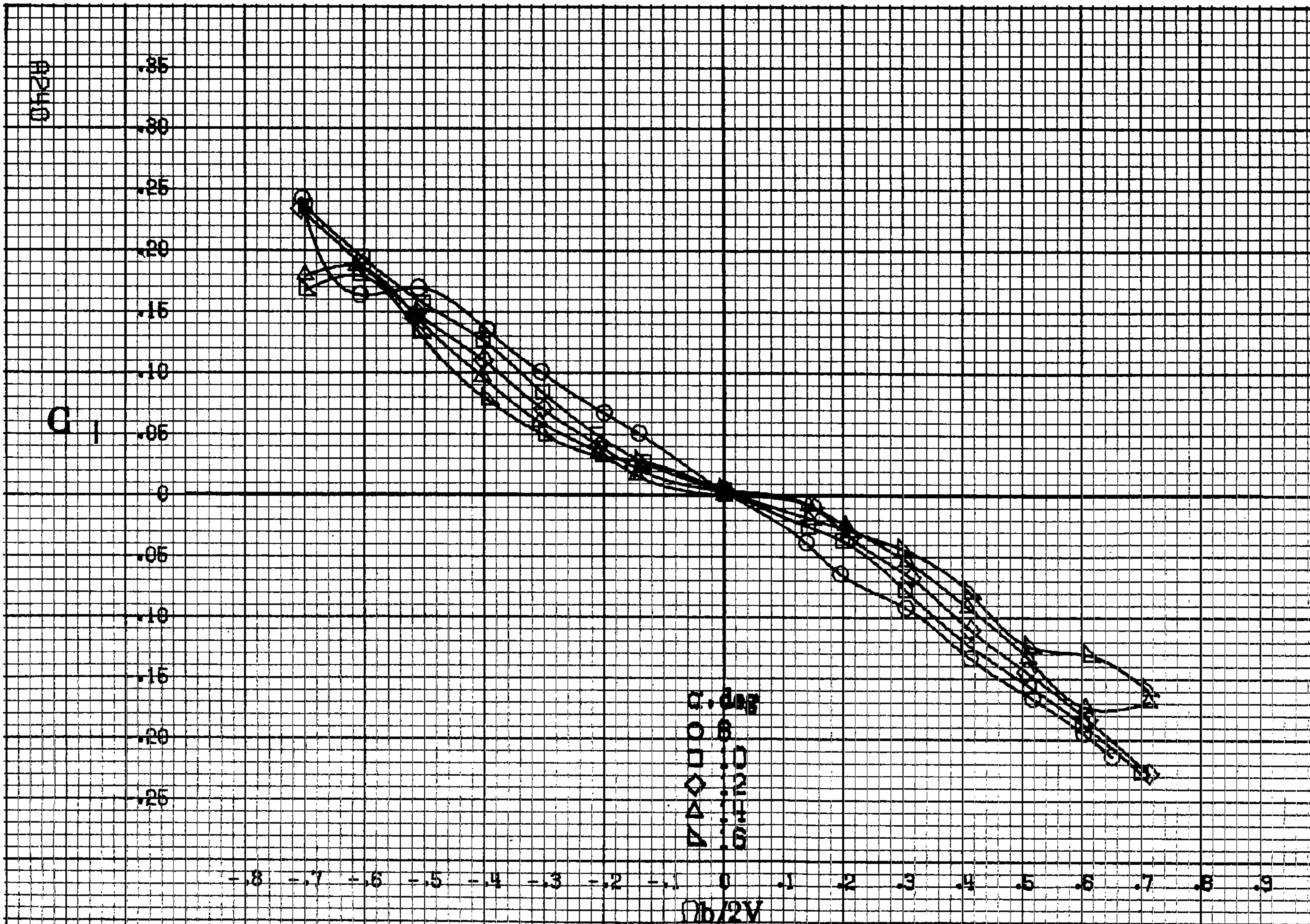

(a) $\alpha = 8$ to 16 deg, SR = 182.9 cm (72 in).

Figure A56.-Effect of rotation rate and angle of attack on rolling-moment coefficient for outboard LE wing droop with large nose radius. $\delta_e = 0°$, $\delta_a = 0°$, $\delta_r = 0°$, $\beta = 0°$.

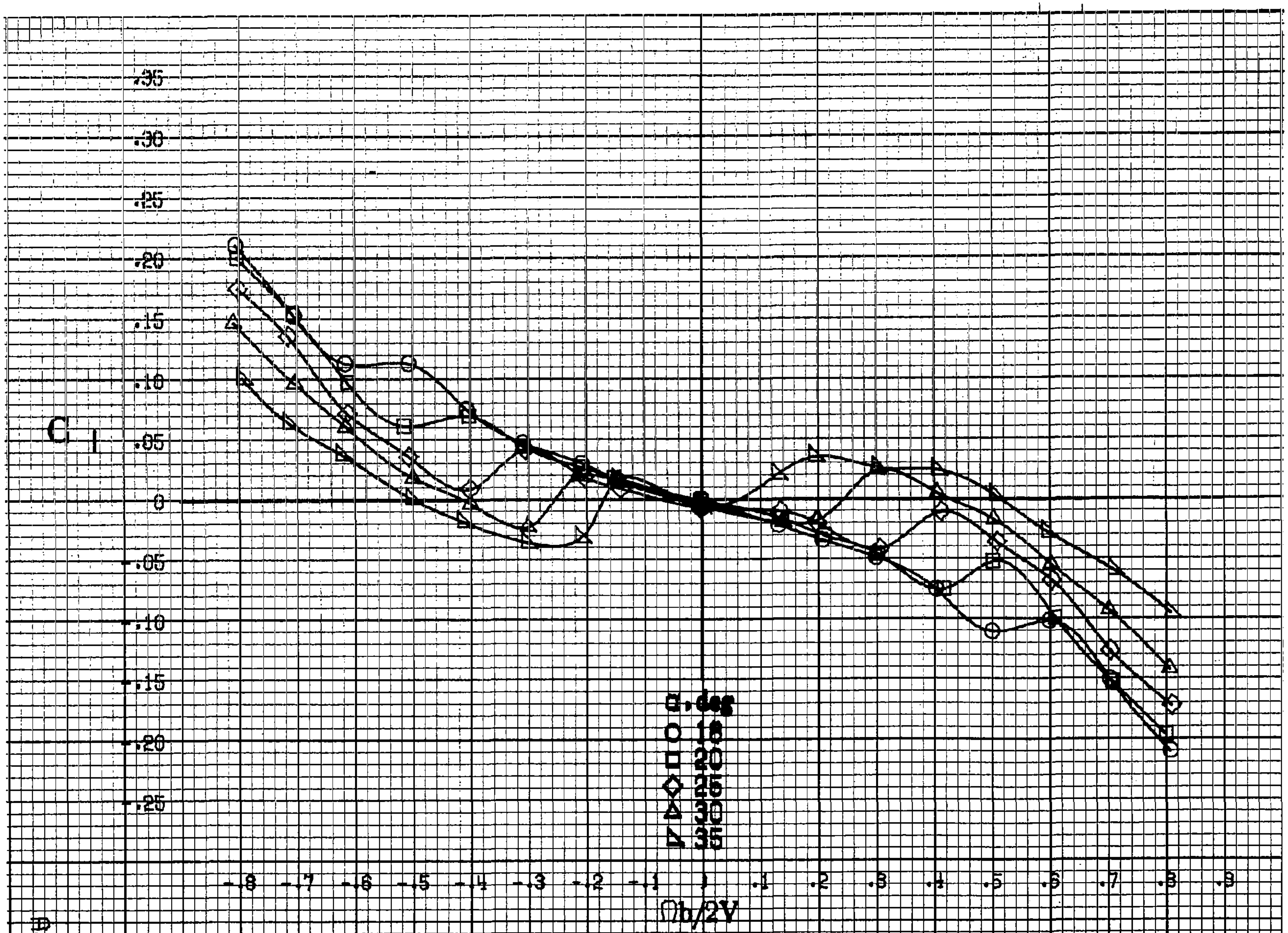

(b) α = 18 to 35 deg, SR = 182.9 cm (72 in).

Figure A56.-Continued.

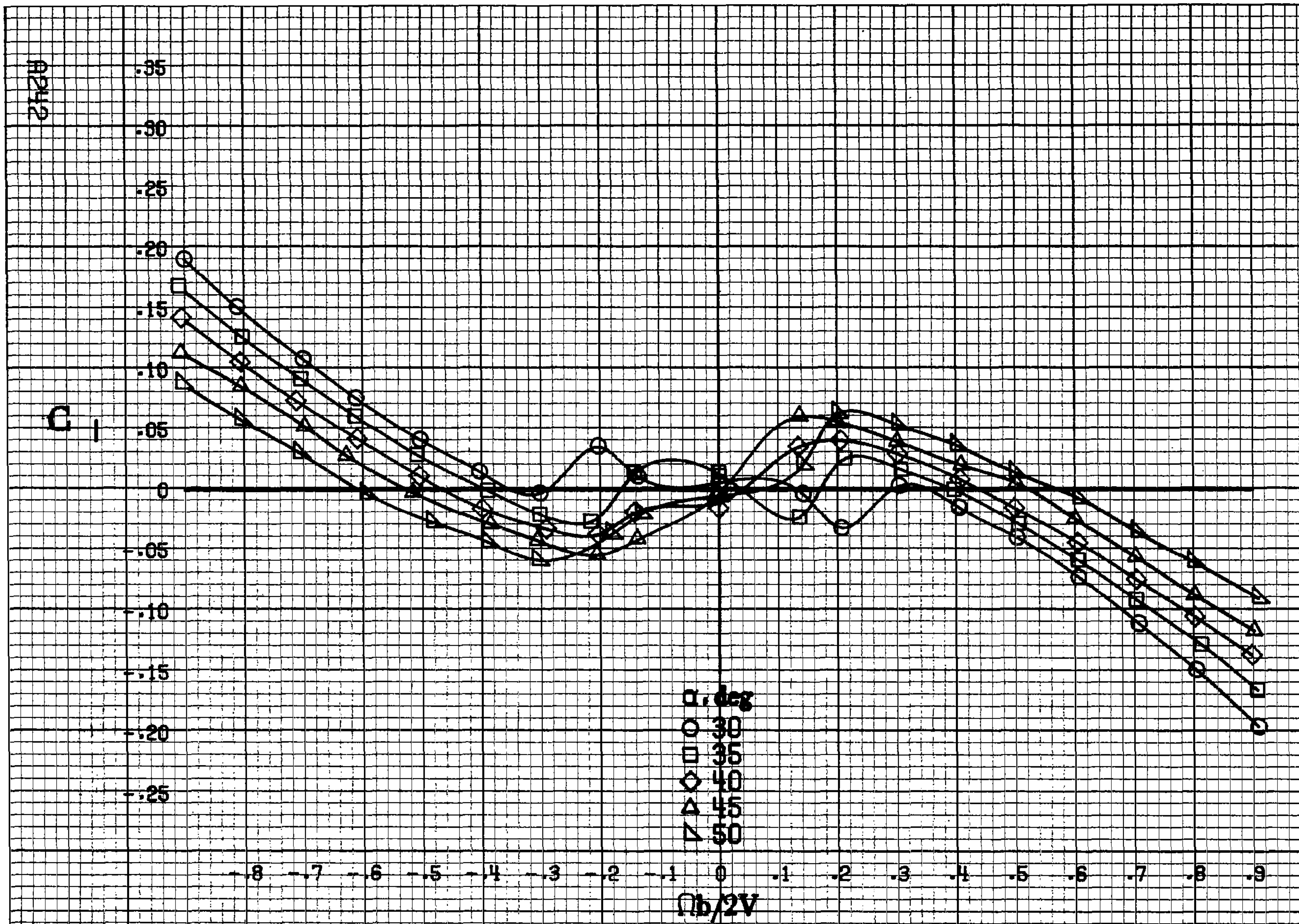

(c) α = 30 to 50 deg, SR = 0.

Figure A56.-Continued.

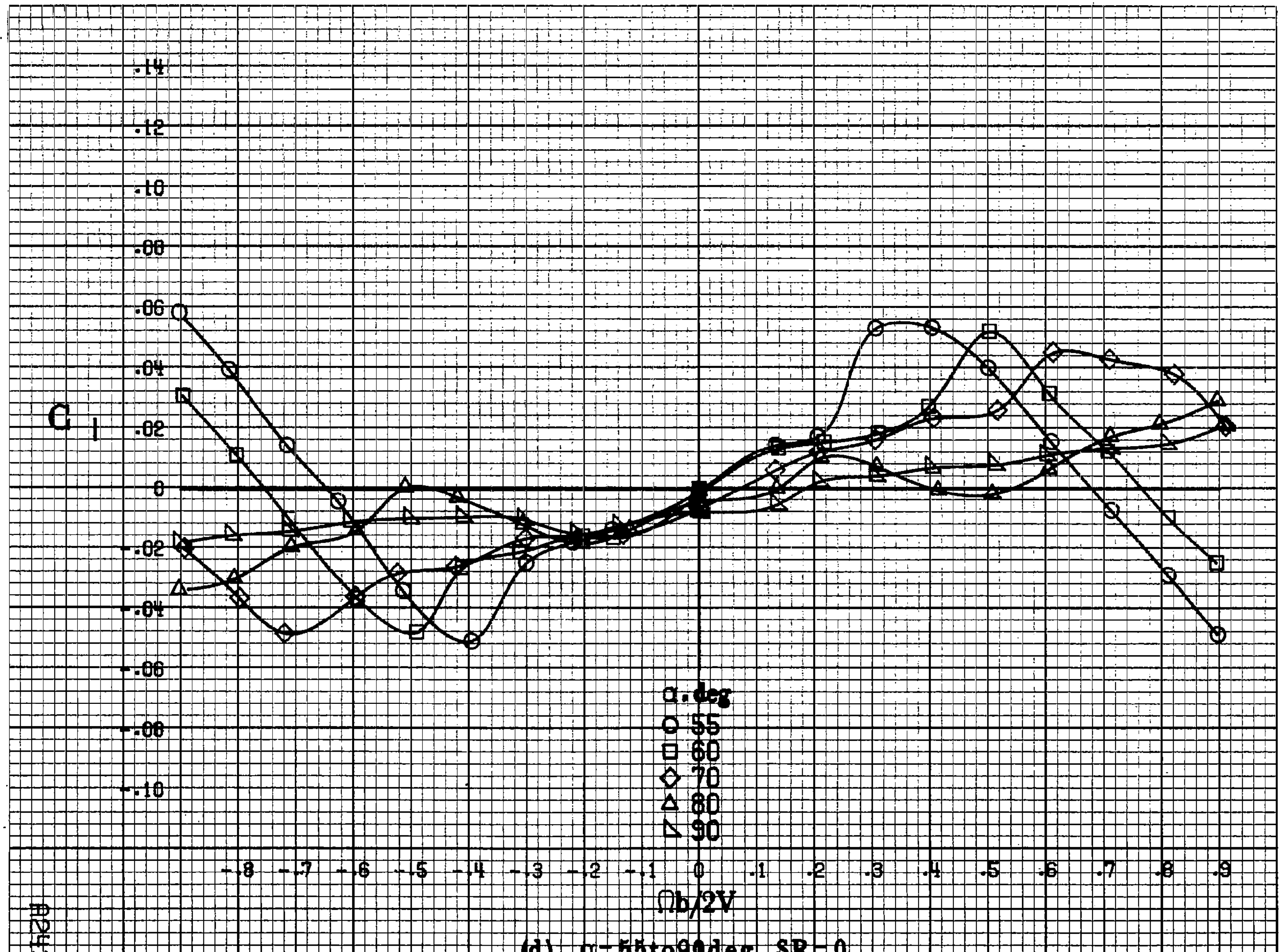

(d) α = 55 to 90 deg, SR = 0.

Figure A56.-Concluded.

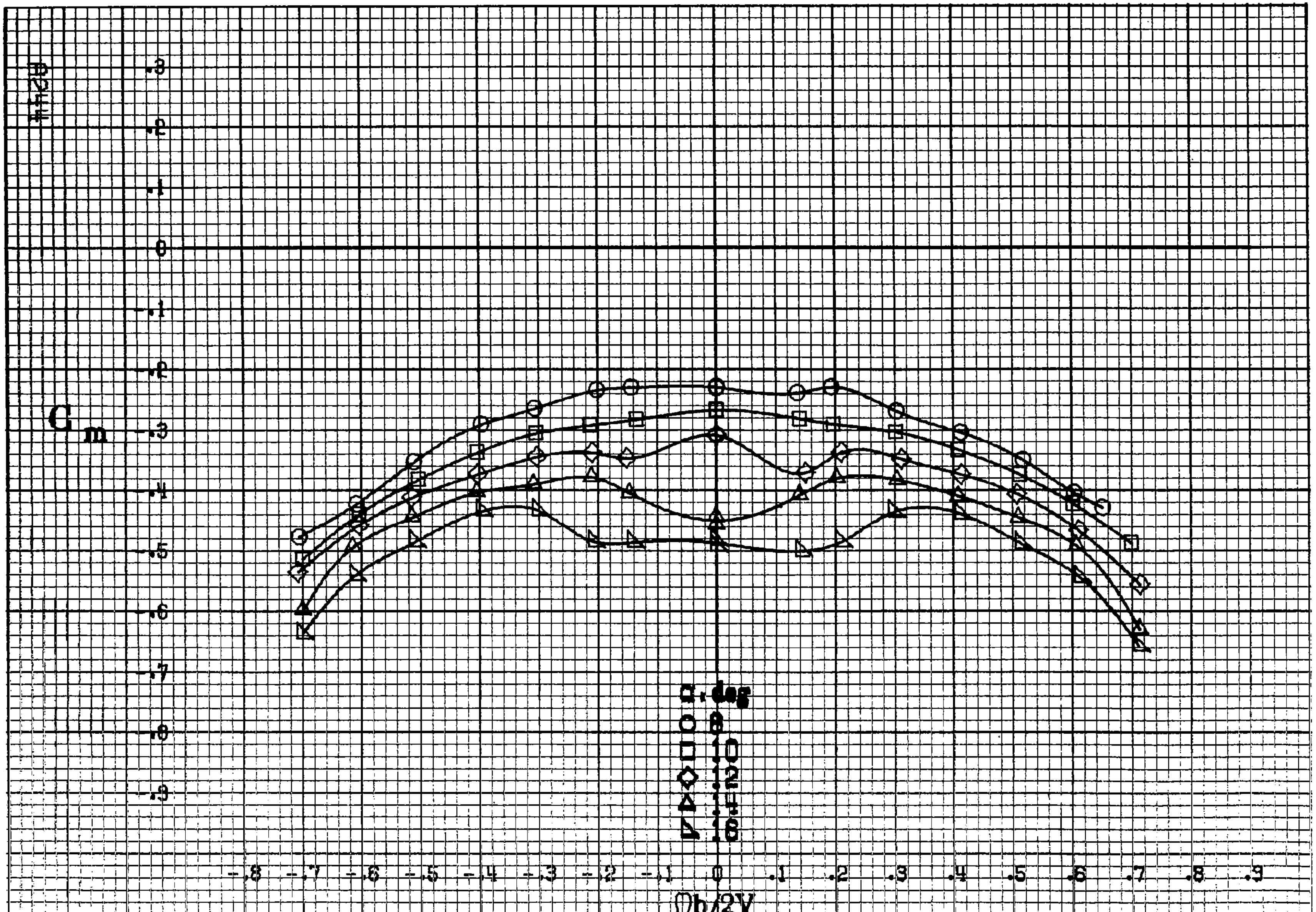

(a) $\alpha = 8$ to 16 deg, SR = 182.9cm (72in).

Figure A57.-Effect of rotation rate and angle of attack on pitching-moment coefficient for outboard LE wing droop with large nose radius. $\delta_e = 0°$, $\delta_a = 0°$, $\delta_r = 0°$, $\beta = 0°$.

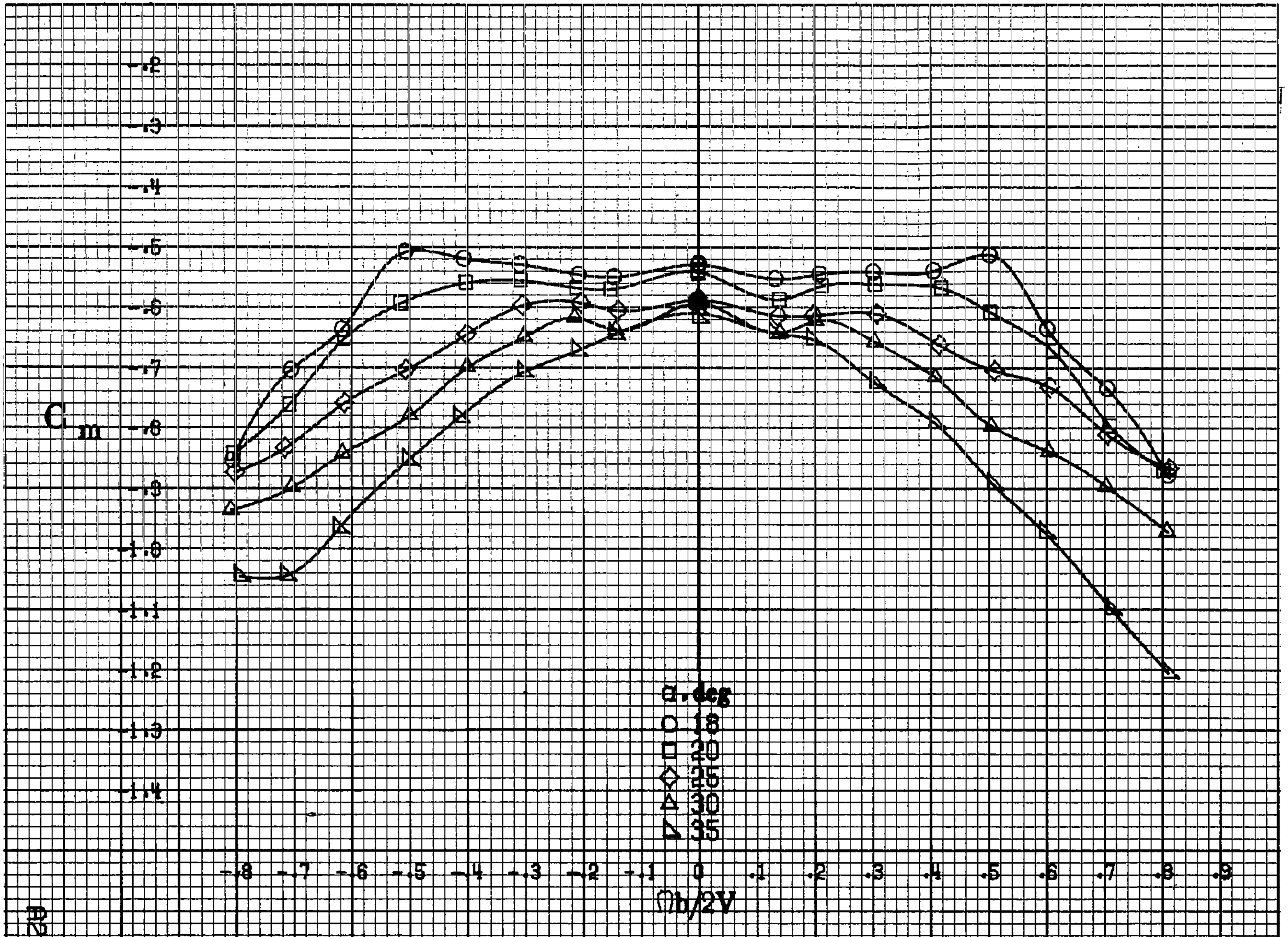

(b) α = 18 to 35 deg, SR = 182.9 cm (72 in).

Figure A57.-Continued.

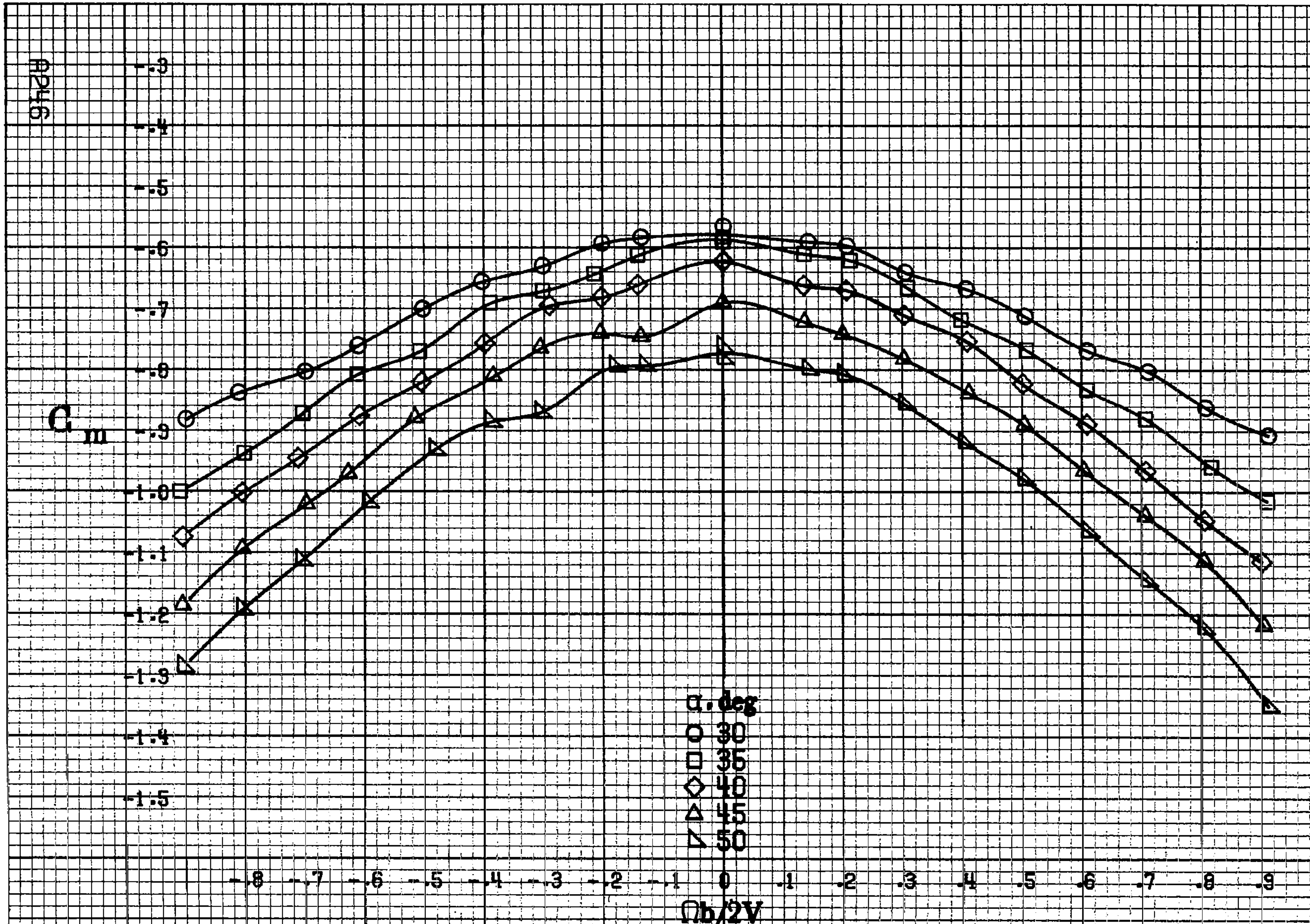

(c) α = 30 to 50 deg, SR = 0.

Figure A57.-Continued.

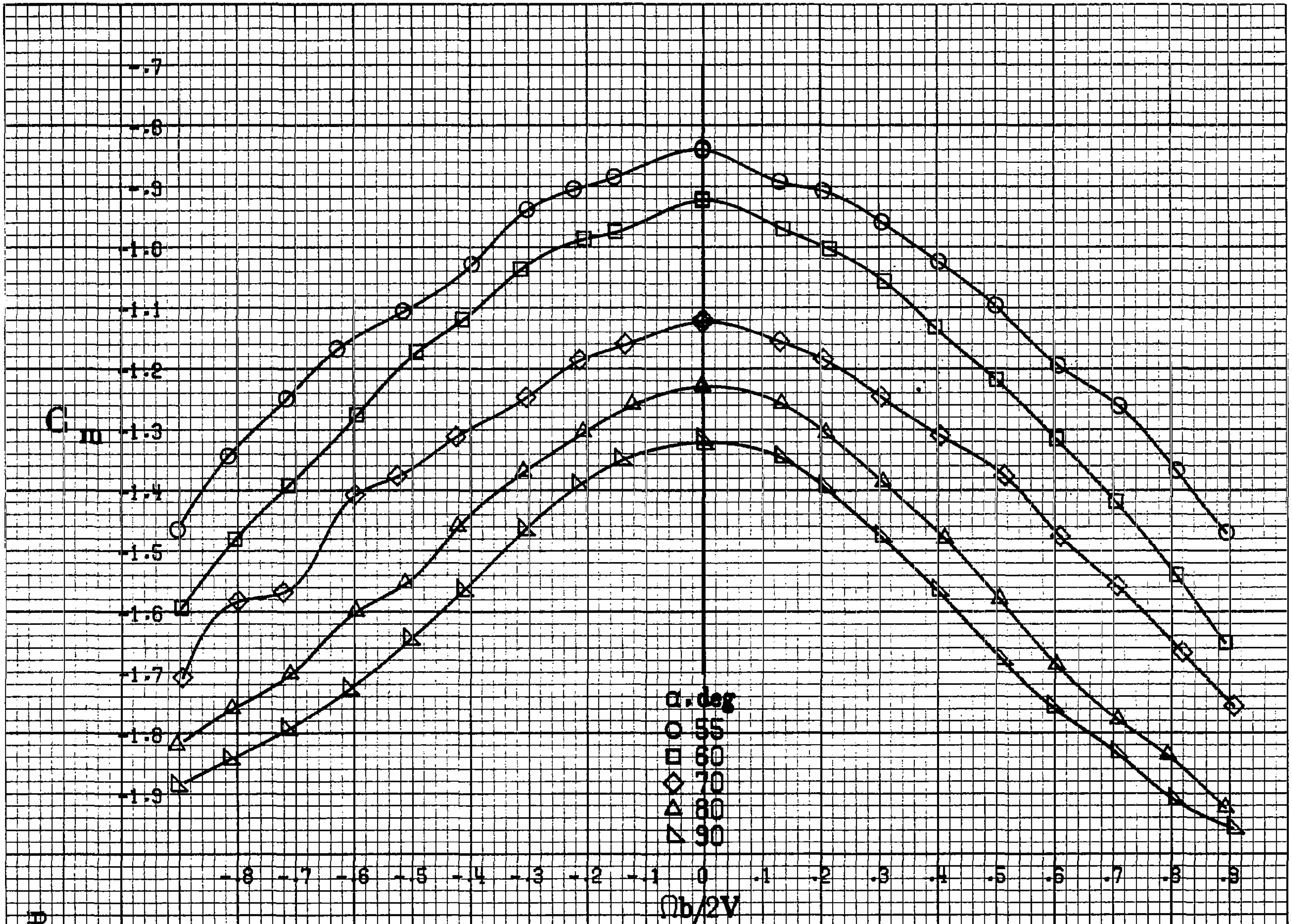

(d) α = 55 to 90 deg, SR = 0.

Figure A57.-Concluded.

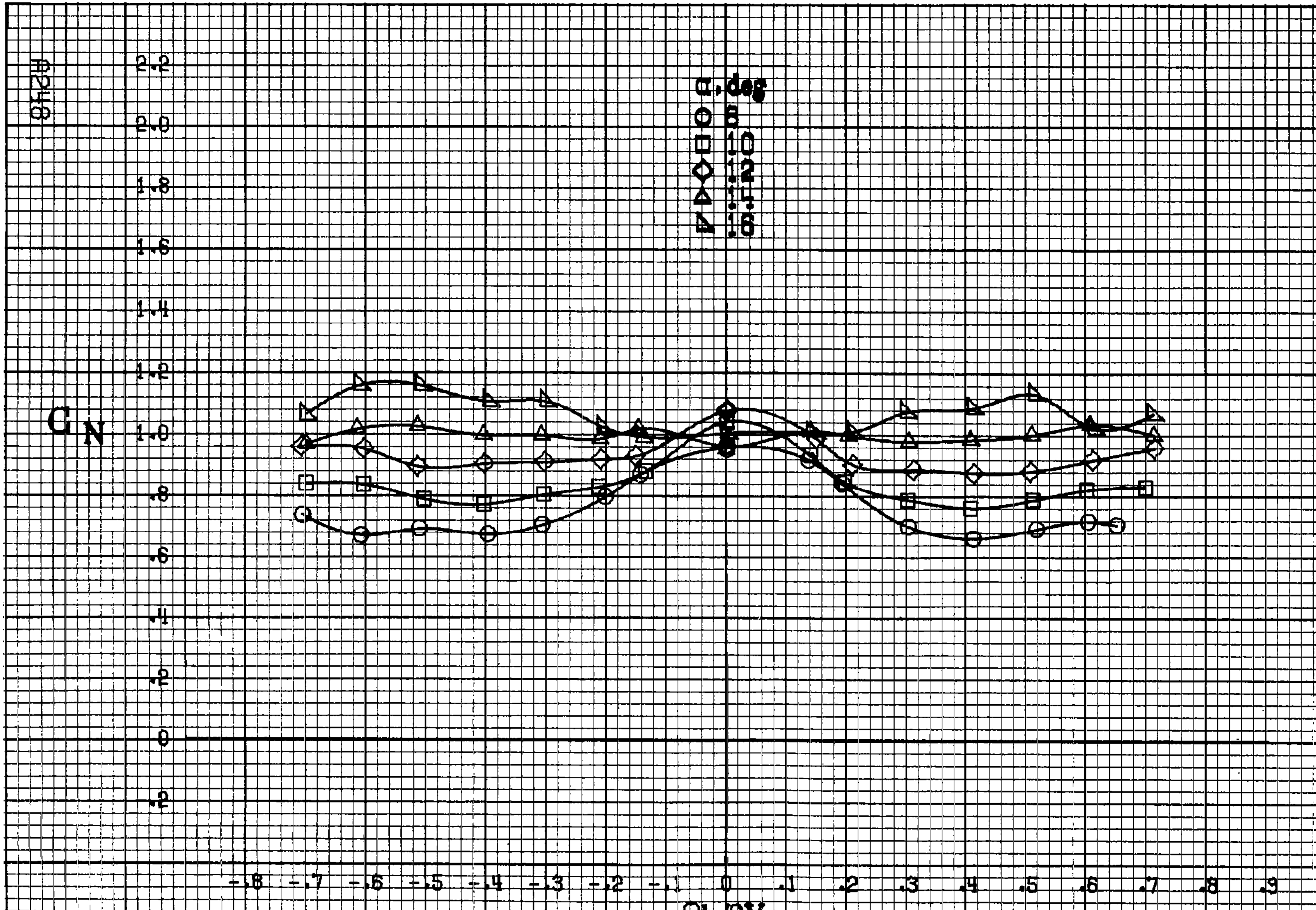

(a) $\alpha = 8$ to 16 deg, SR = 182.9 cm (72 in).

Figure A58.-Effect of rotation rate and angle of attack on normal-force coefficient for outboard LE wing droop with large nose radius. $\delta_e = 0°$, $\delta_a = 0°$, $\delta_r = 0°$, $\beta = 0°$.

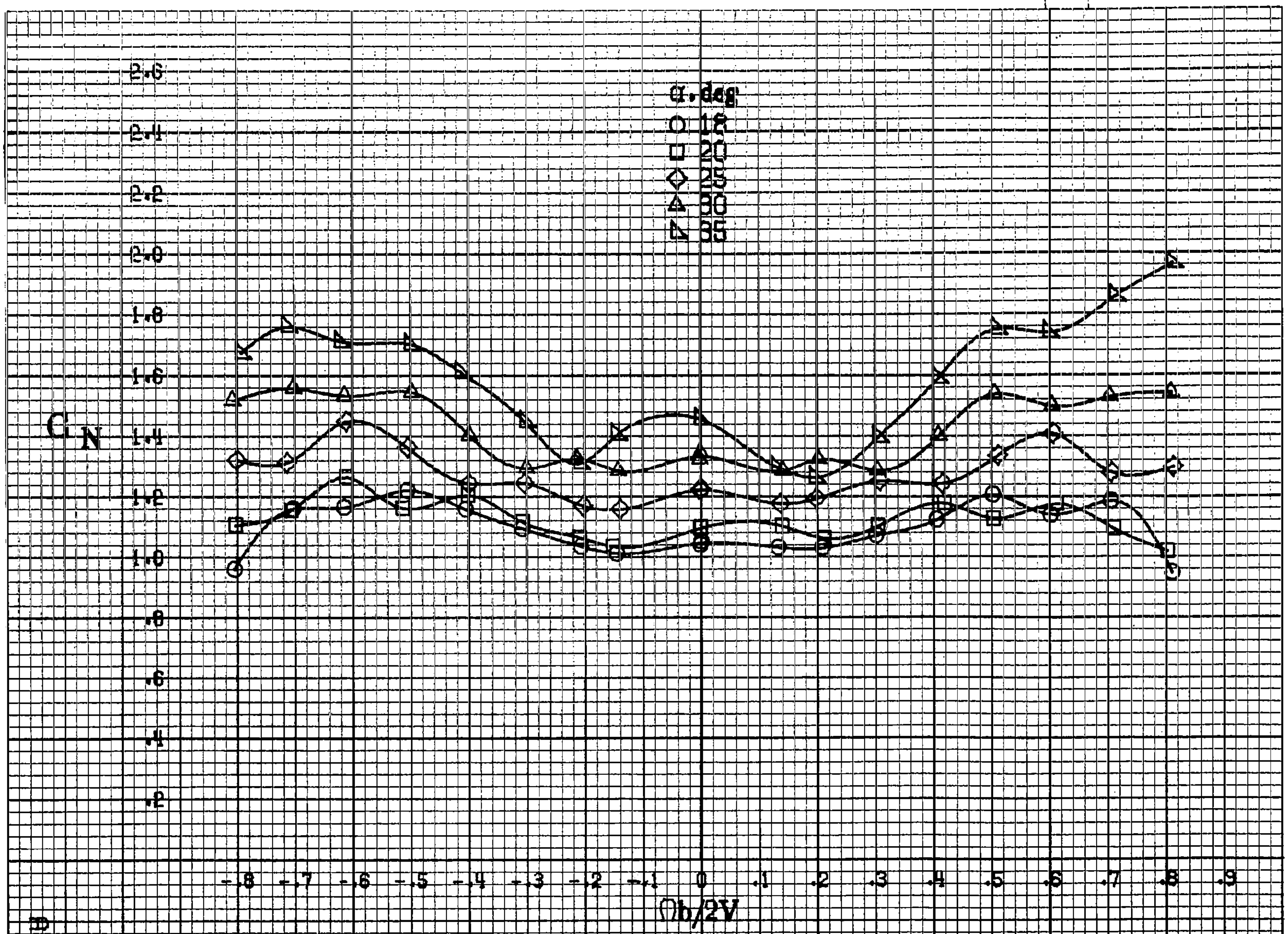

(b) α = 18 to 35 deg, SR = 182.9 cm (72 in).
Figure A58.-Continued.

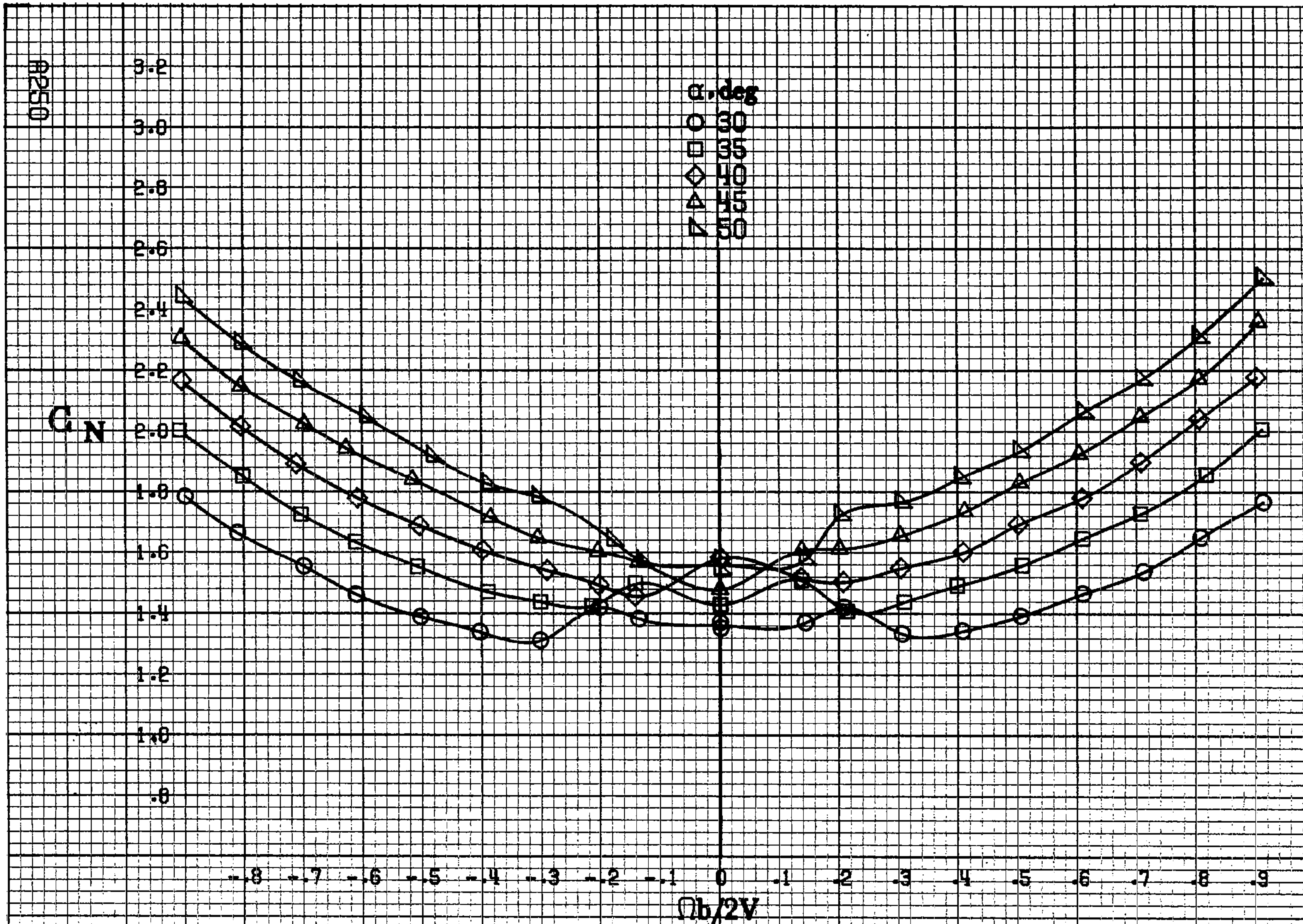

(c) α = 30to50deg, SR = 0.
Figure A58.-Continued.

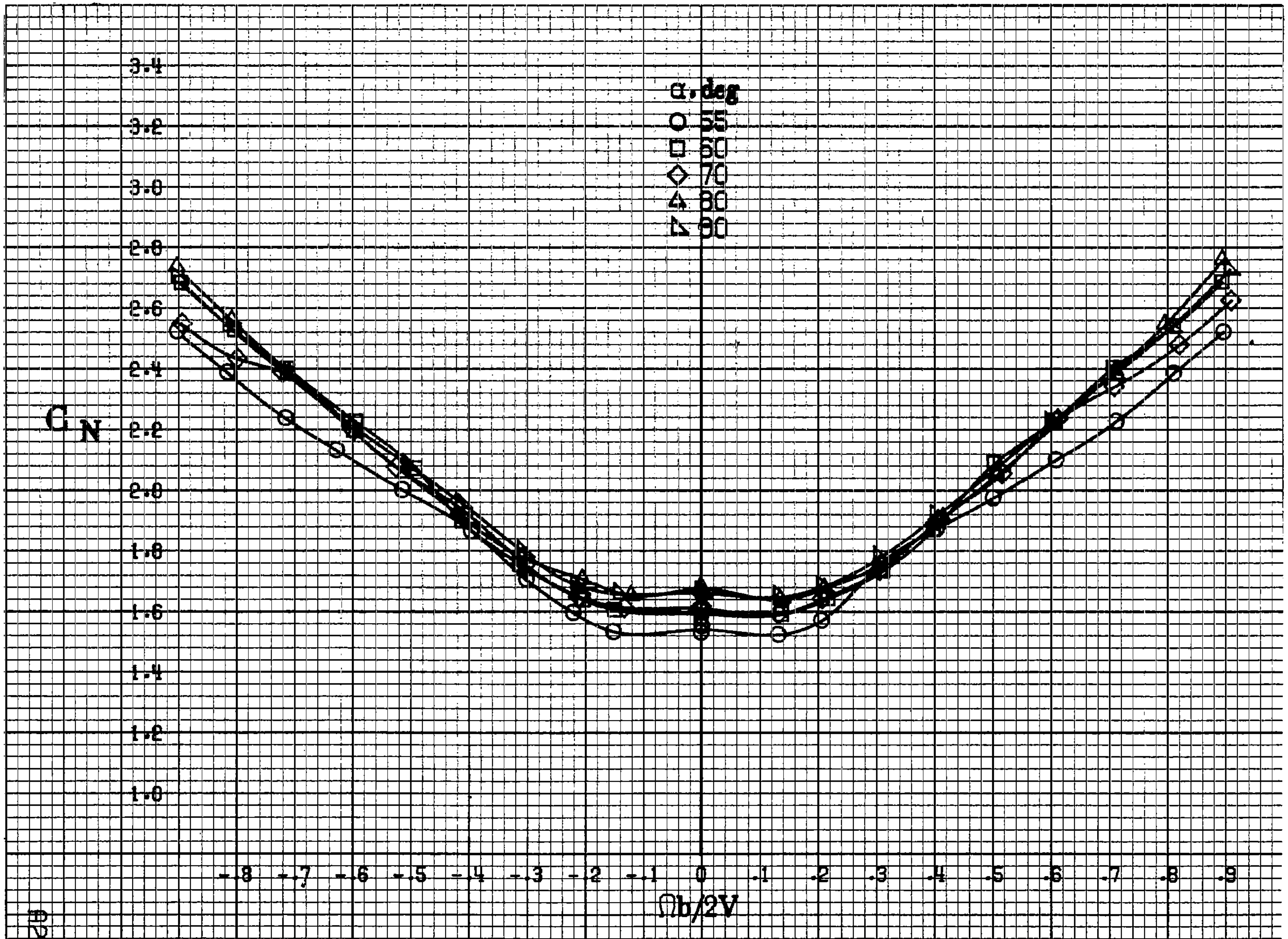

(d) α=55to90deg, SR=0.

Figure A58.-Concluded.

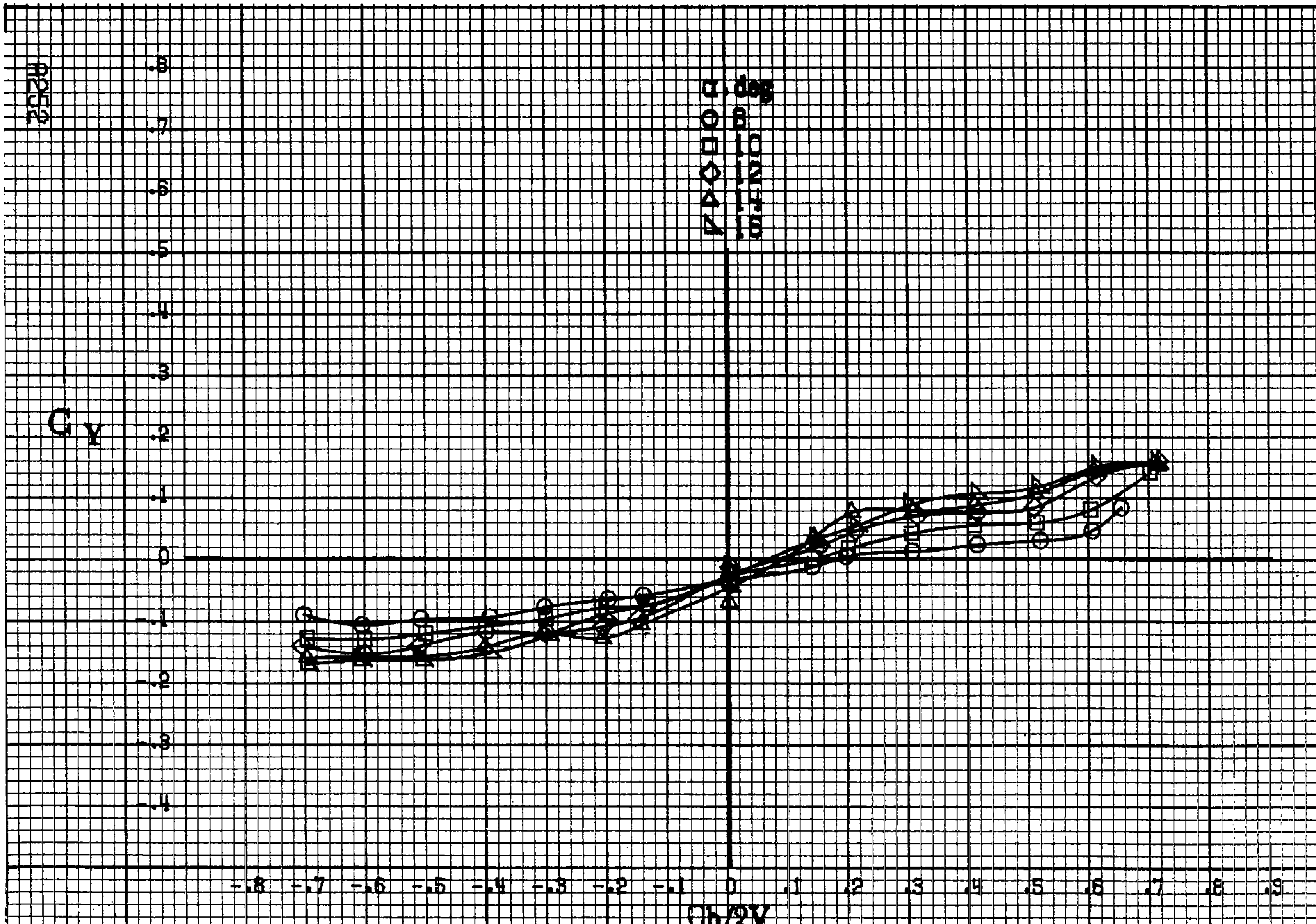

(a) $\alpha = 8$ to 16 deg, SR = 182.9 cm (72 in).

Figure A59.-Effect of rotation rate and angle of attack on side-force coefficient for outboard LE wing droop with large nose radius. $\delta_e = 0°$, $\delta_a = 0°$, $\delta_r = 0°$. $\beta = 0°$.

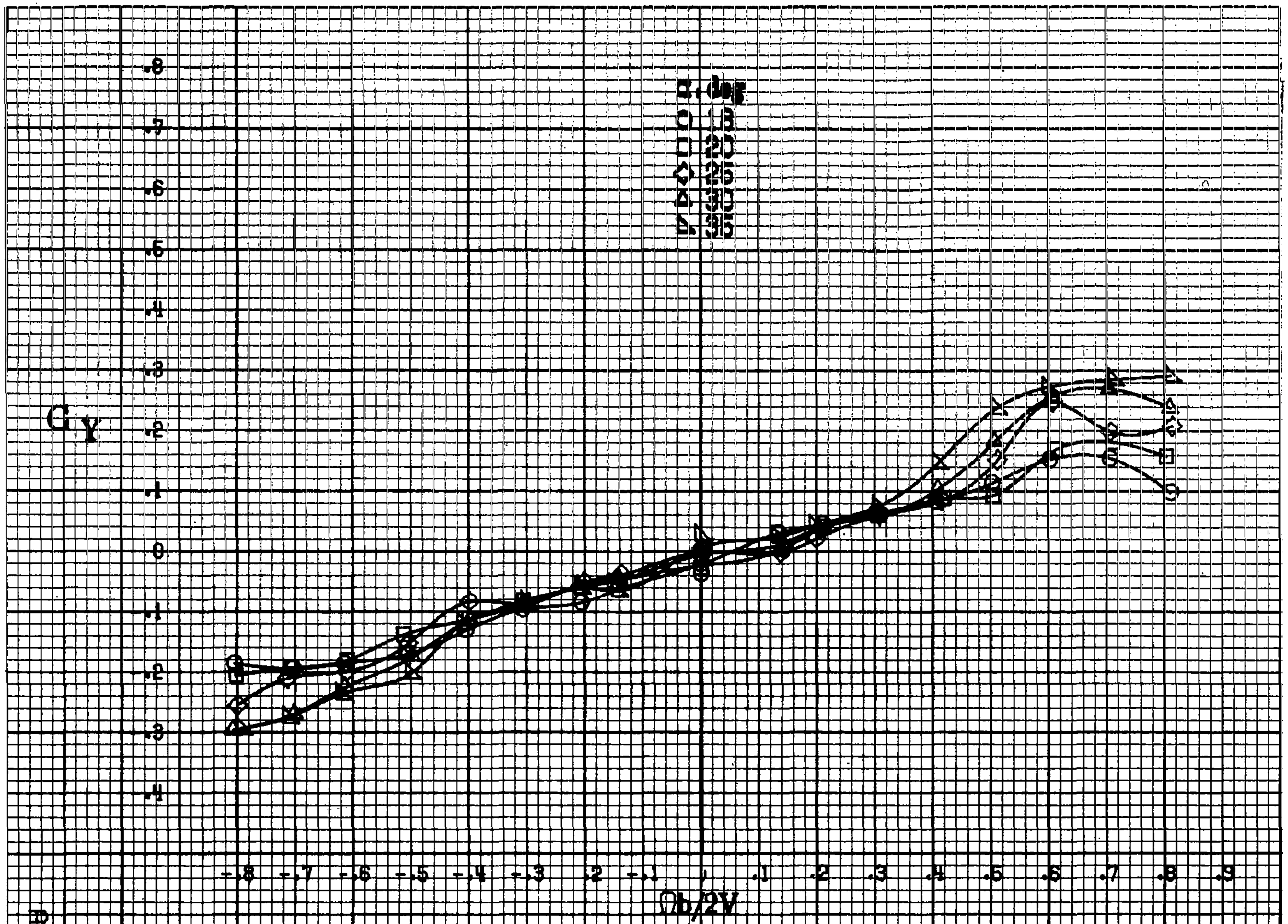

(b) α = 18 to 35 deg, SR = 182.9 cm (72 in).

Figure A59.-Continued.

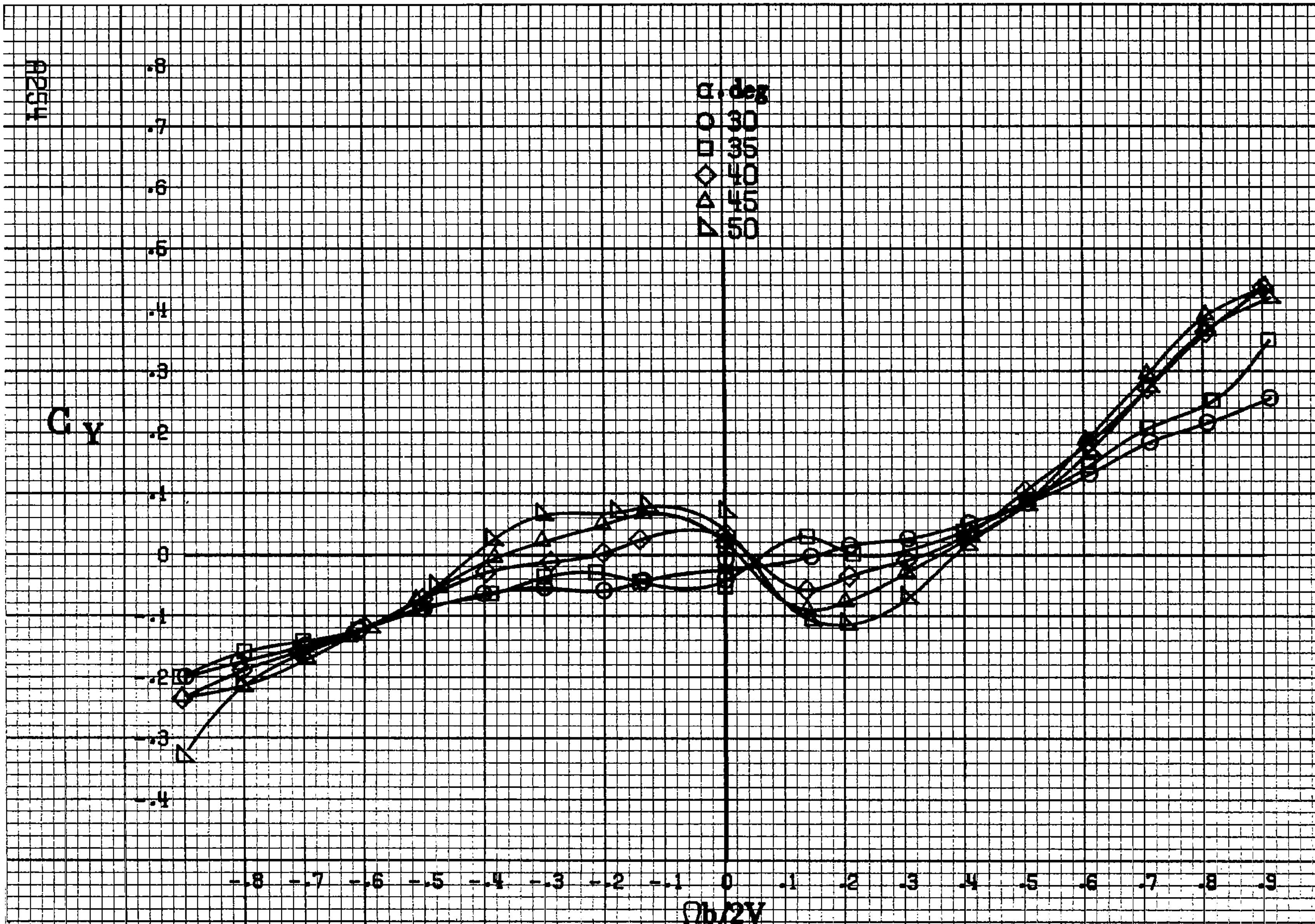

(c) α = 30 to 50 deg, SR = 0.
Figure A59.-Continued.

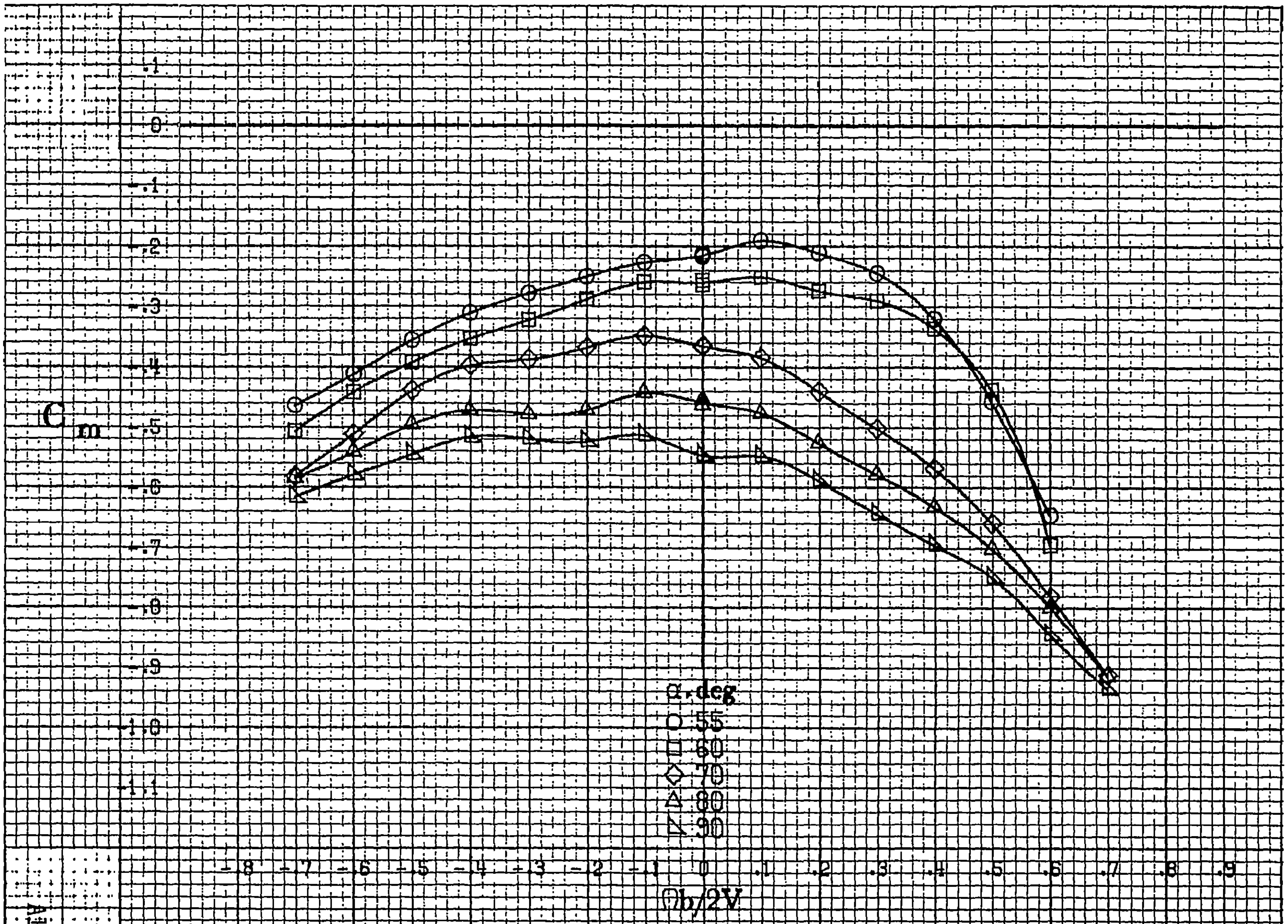

(d) α = 55 to 90 deg, SR = 0.

Figure A33.- Concluded.

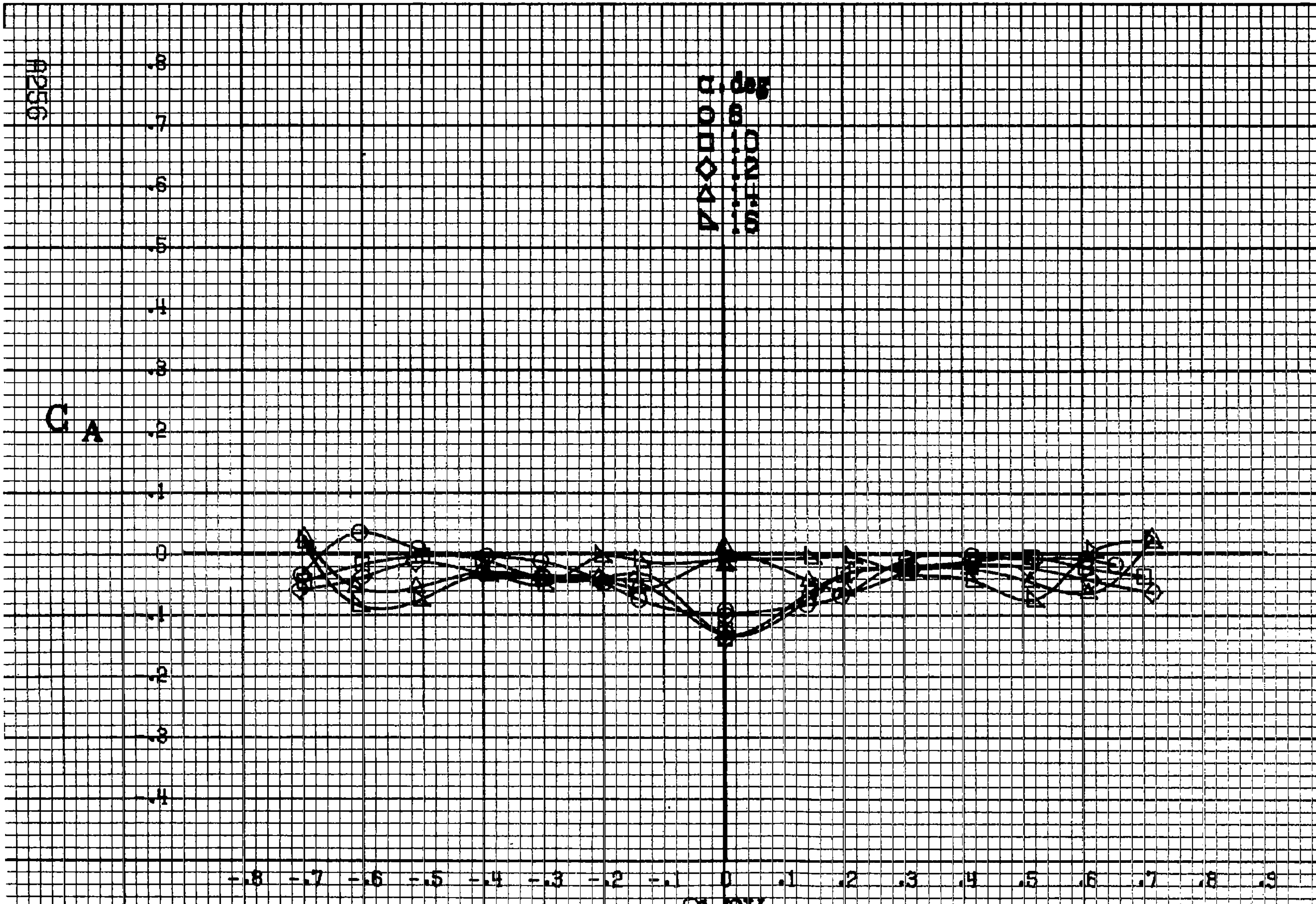

(a) α = 8 to 16 deg, SR = 182.9 cm (72 in).

Figure A60.-Effect of rotation rate and angle of attack on axial-force coefficient for outboard LE wing droop with large nose radius. $\delta_e = 0°$, $\delta_a = 0°$, $\delta_r = 0°$, $\beta = 0°$.

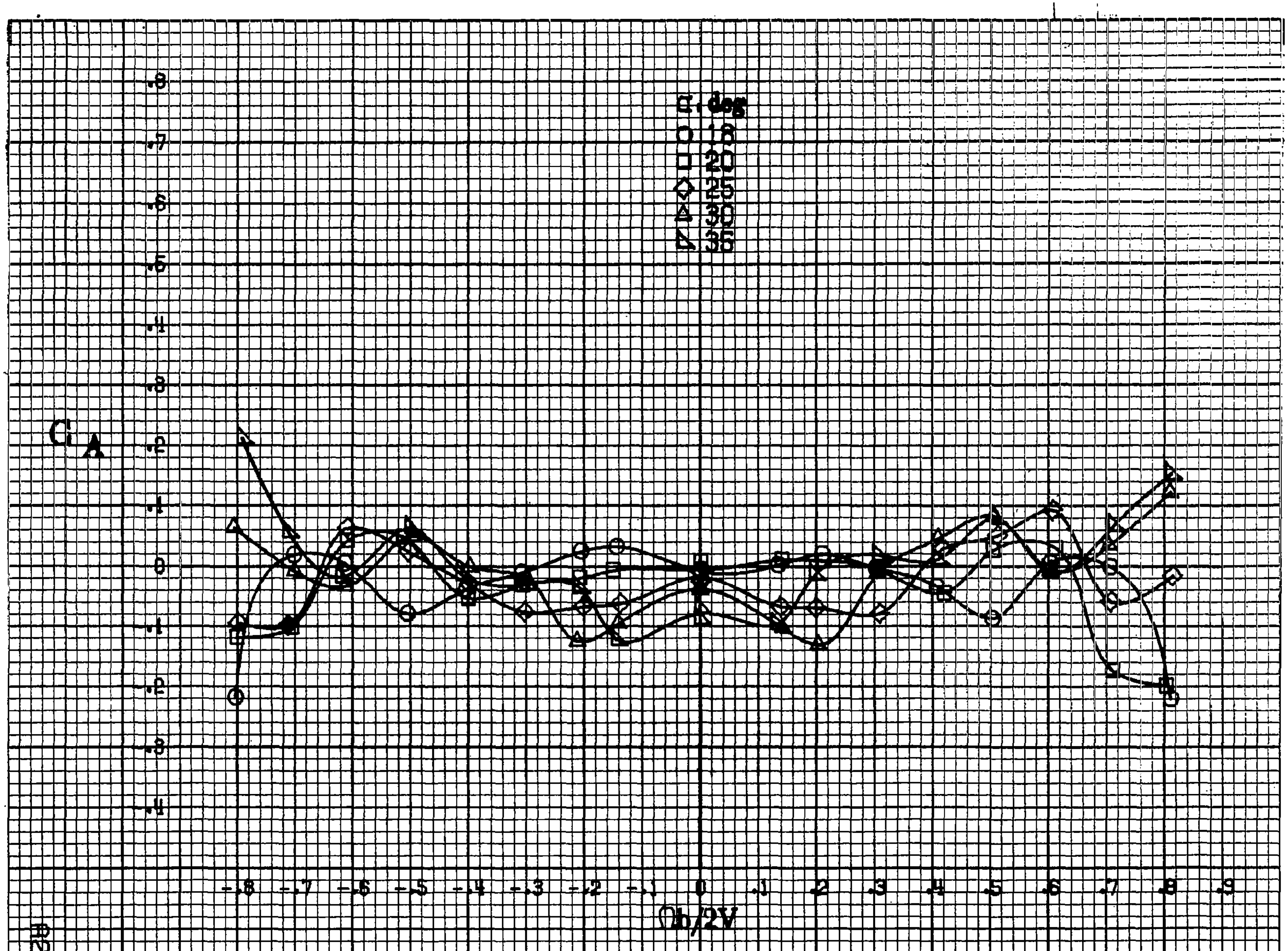

(b) α = 18 to 35 deg, SR = 182.9 cm (72 in).

Figure A60.–Continued.

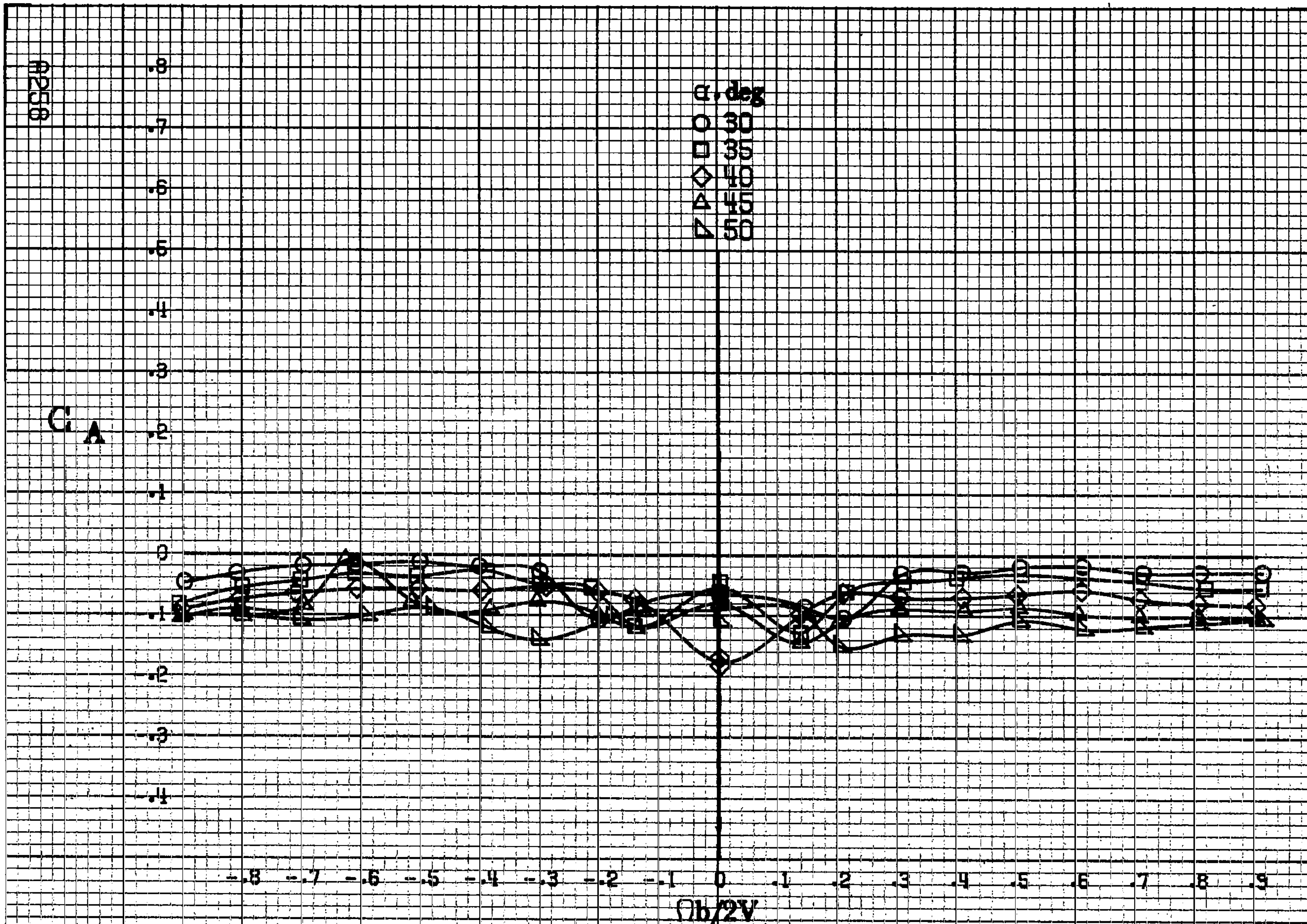

(c) α = 30 to 50 deg, SR = 0.

Figure A60.-Continued.

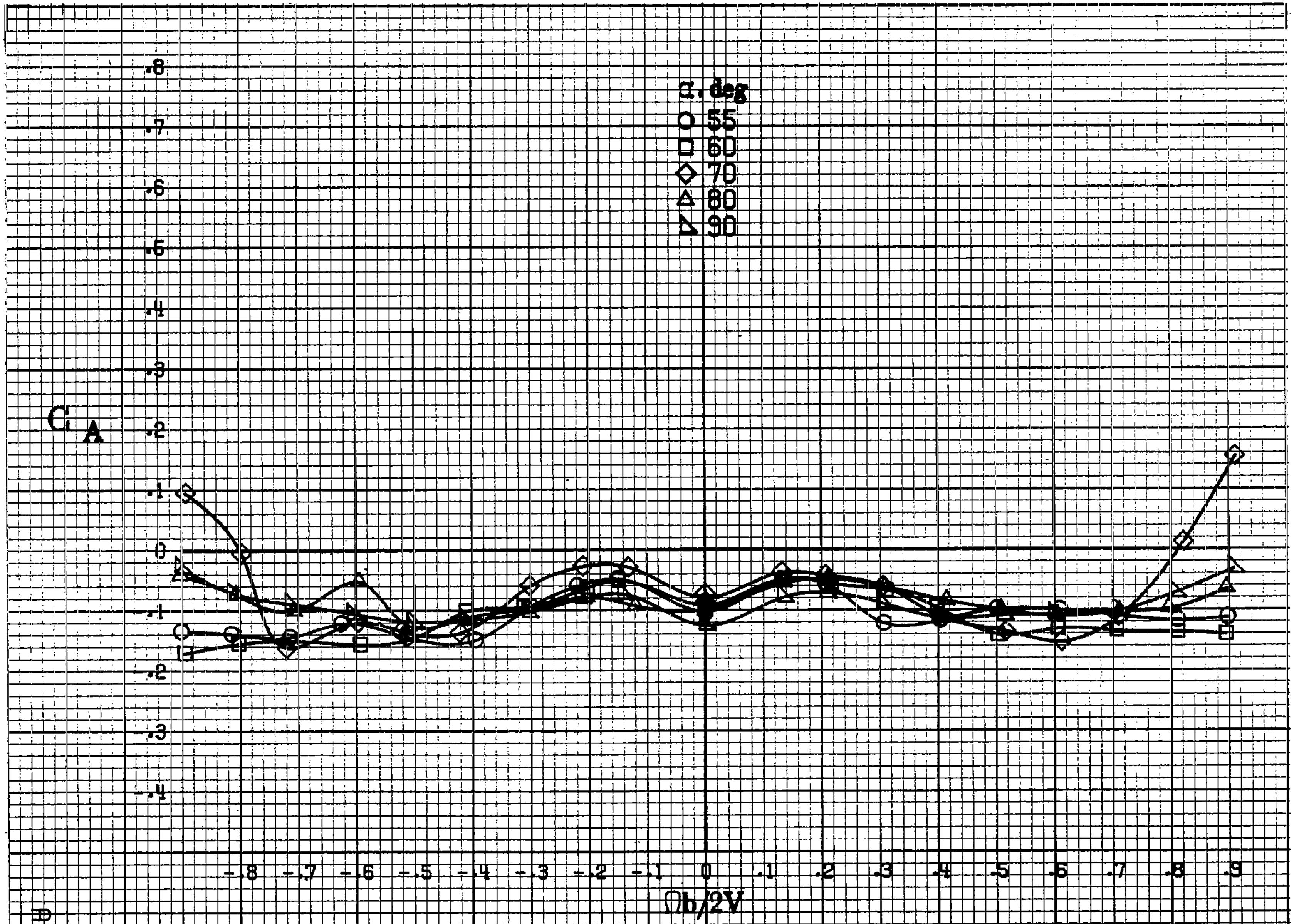

(d) α = 55 to 90 deg, SR = 0.

Figure A60.-Concluded.

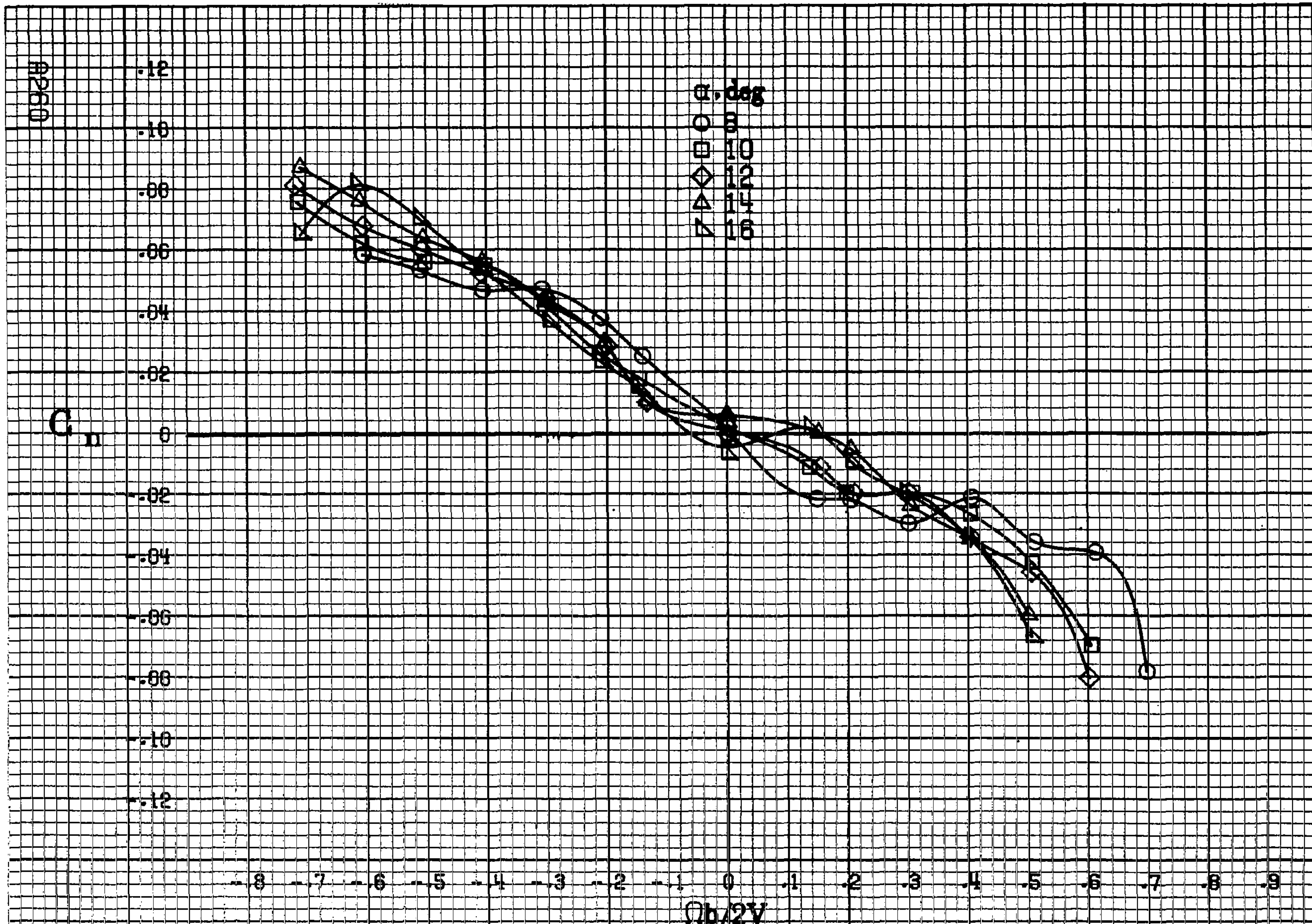

(a) α = 8 to 16 deg, SR = 182.9 cm (72 in.).

Figure A61.- Effect of rotation rate and angle of attack on yawing-moment coefficient for outboard LE wing droop with large nose radius. $\delta_e = 0°$, $\delta_a = 0°$, $\delta_r = 0°$, $\beta = 10°$.

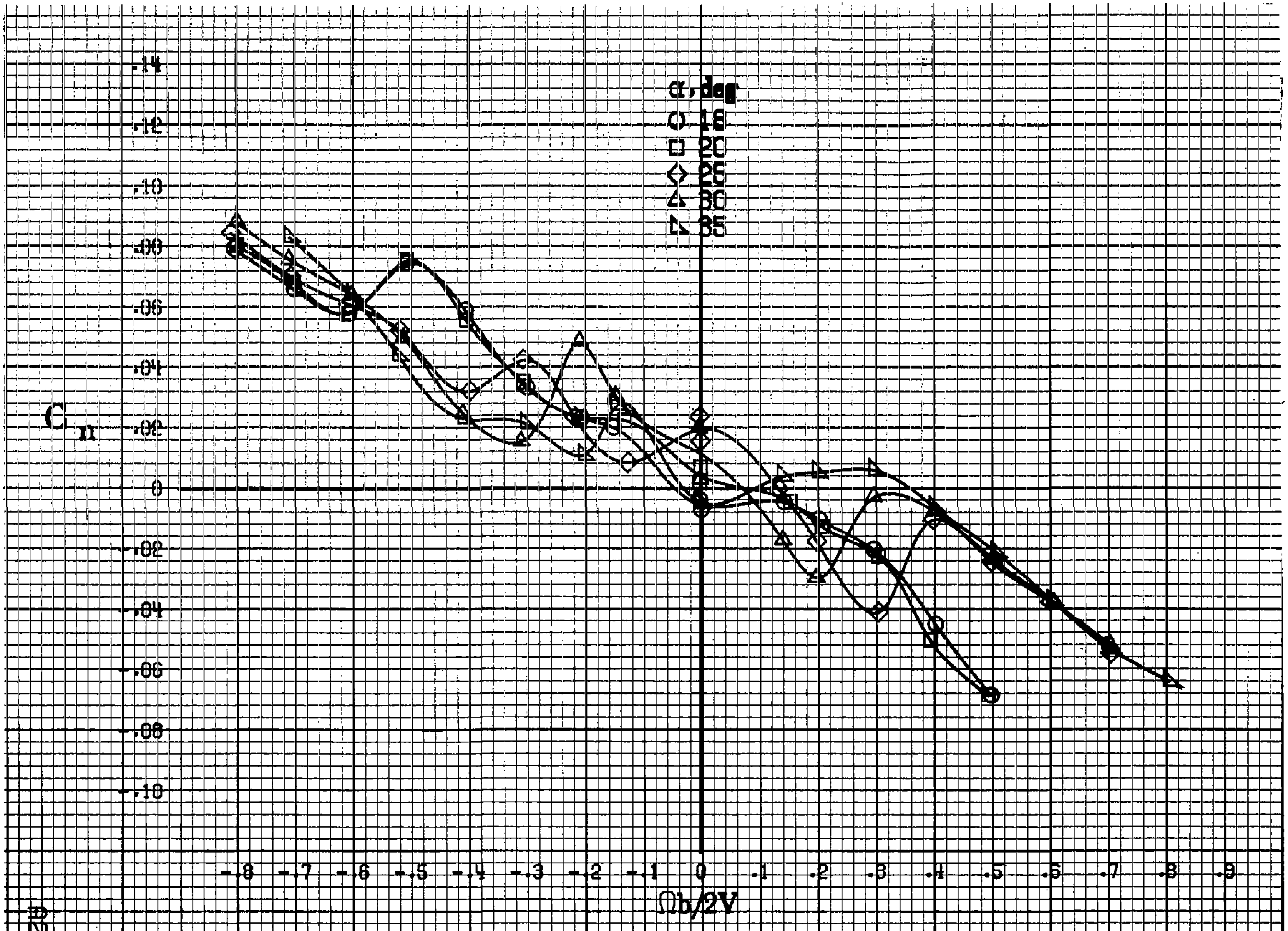

(b) α = 18 to 35 deg, SR = 182.9 cm (72 in).

Figure A61.- Continued.

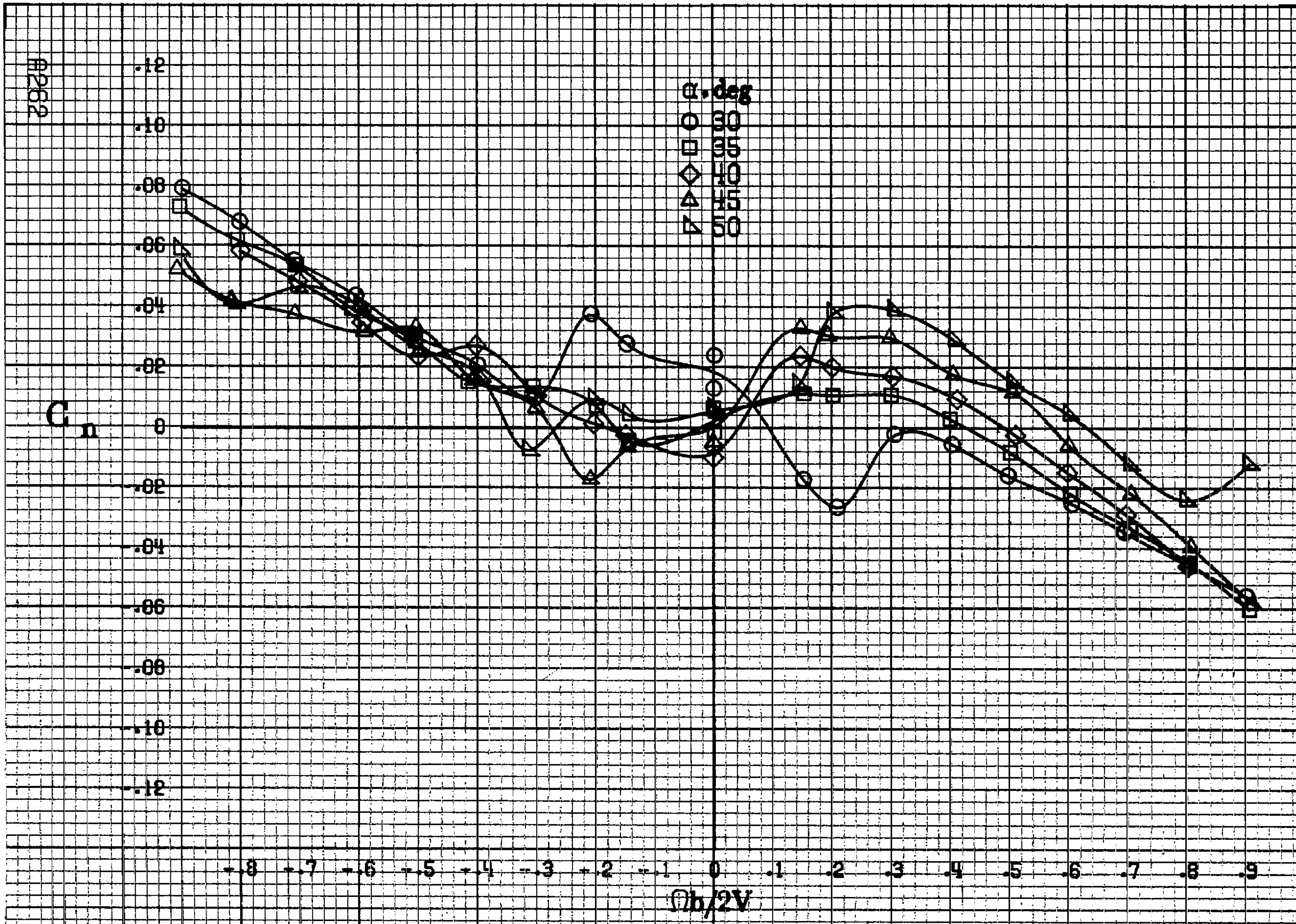

(c) α = 30 to 50 deg, SR = 0.

Figure A61.-Continued.

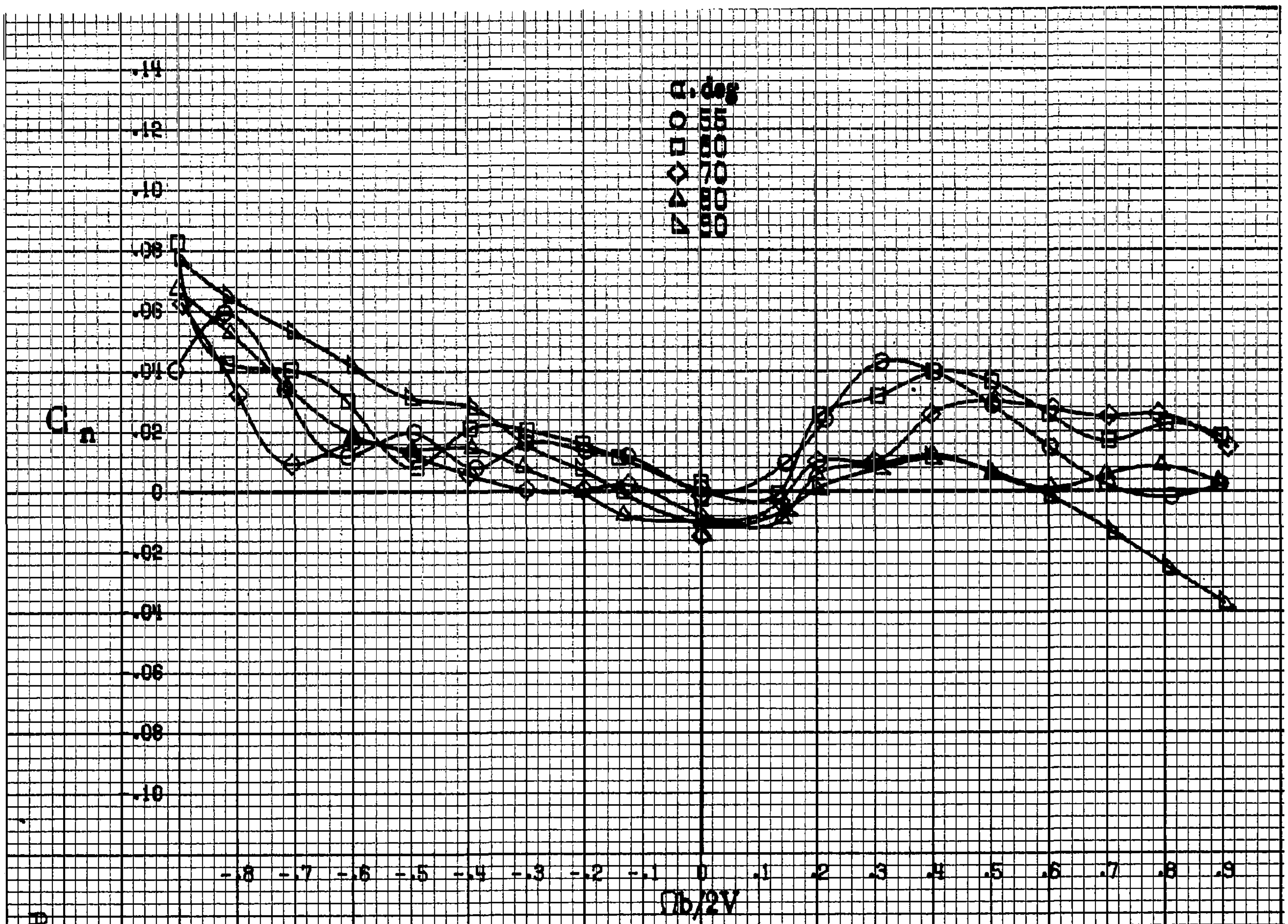

(d) α = 55 to 90 deg, SR = 0.

Figure A61.-Concluded.

A263

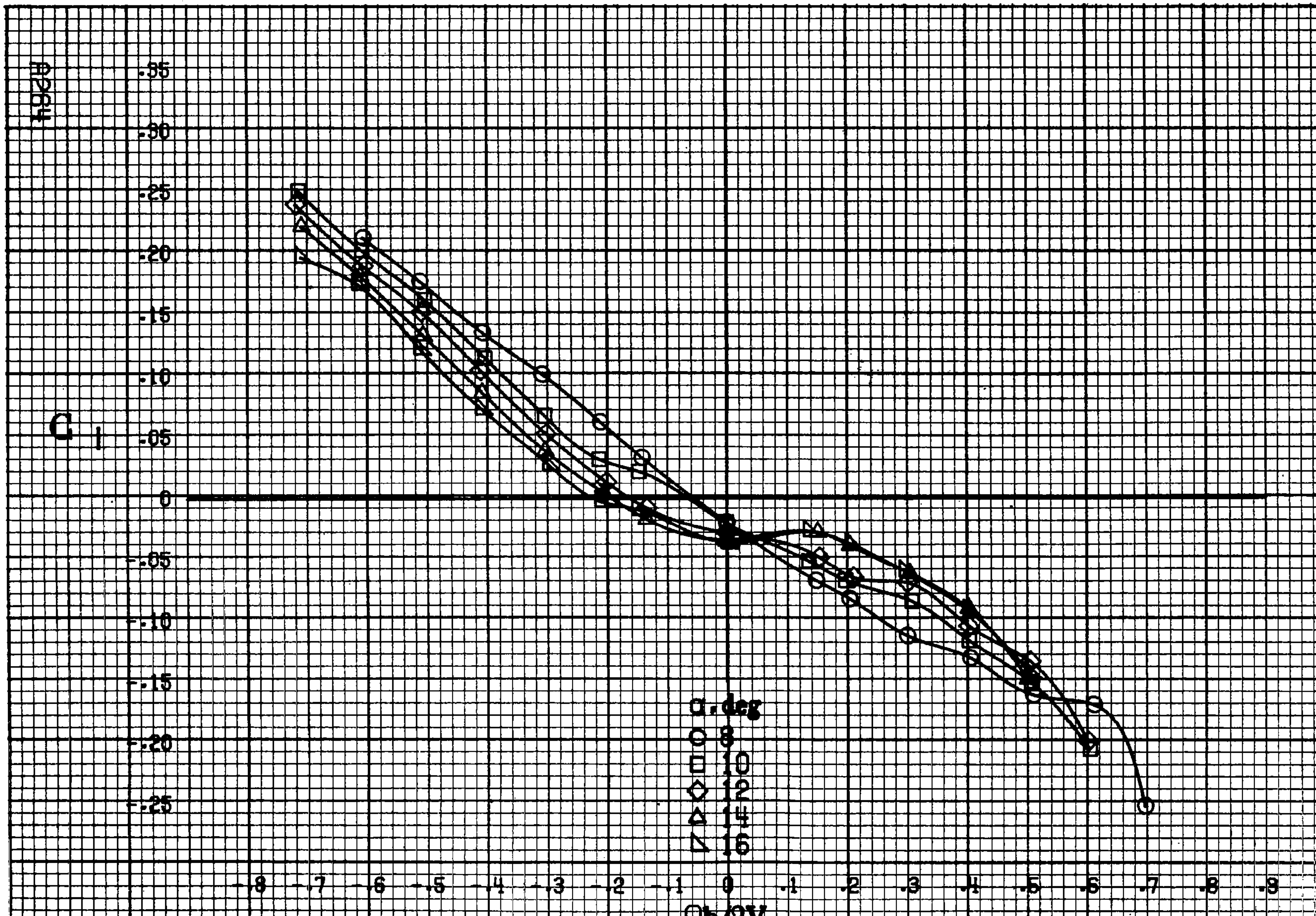

(a) α = 8 to 16 deg, SR = 182.9 cm (72 in).

Figure A62.- Effect of rotation rate and angle of attack on rolling-moment coefficient for outboard LE wing droop with large nose radius. $\delta_e = 0°$, $\delta_a = 0°$, $\delta_r = 0°$, $\beta = 10°$.

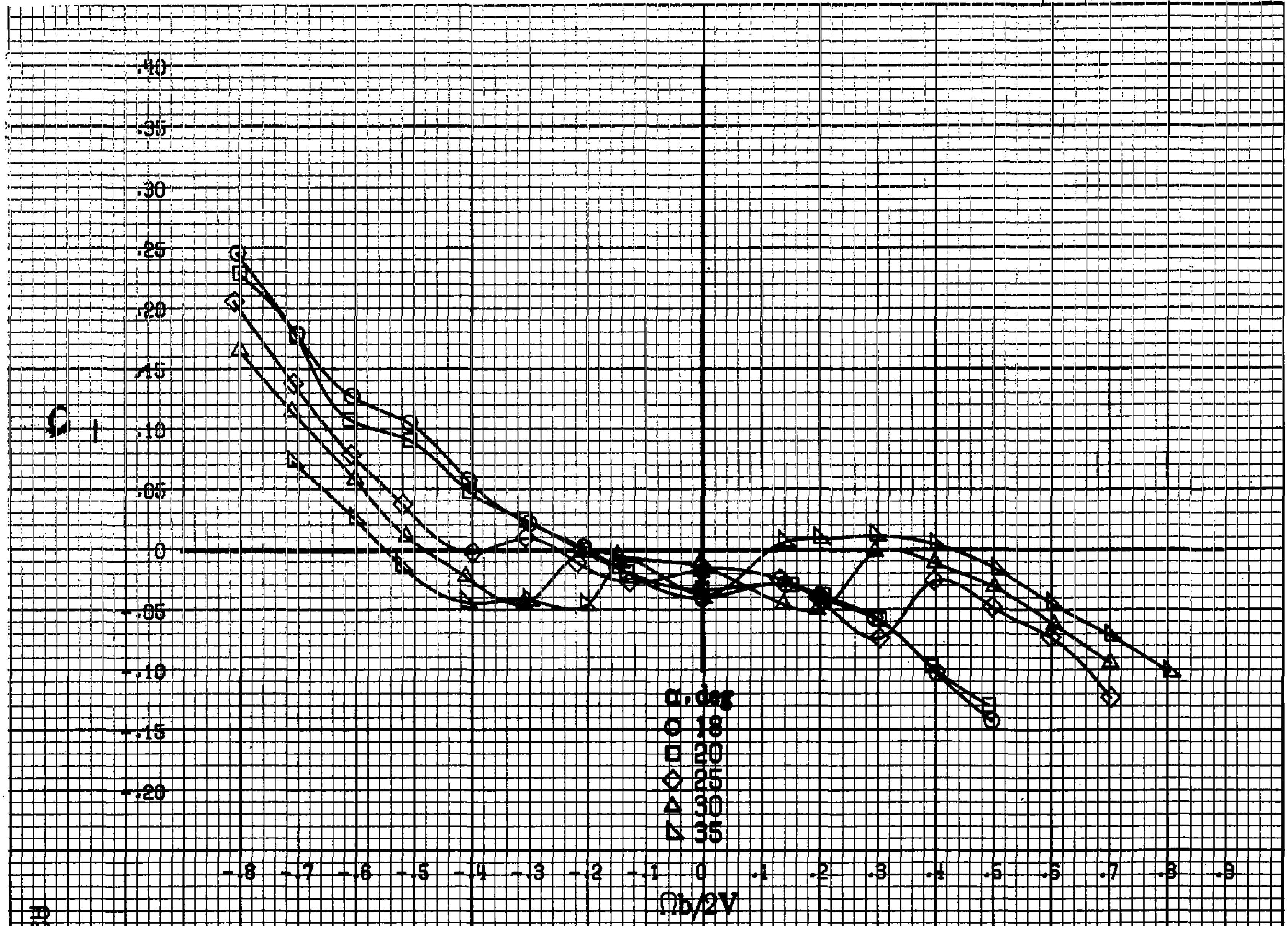

(b) α = 18to35deg, SR = 182.9cm (72in).

Figure A62.-Continued.

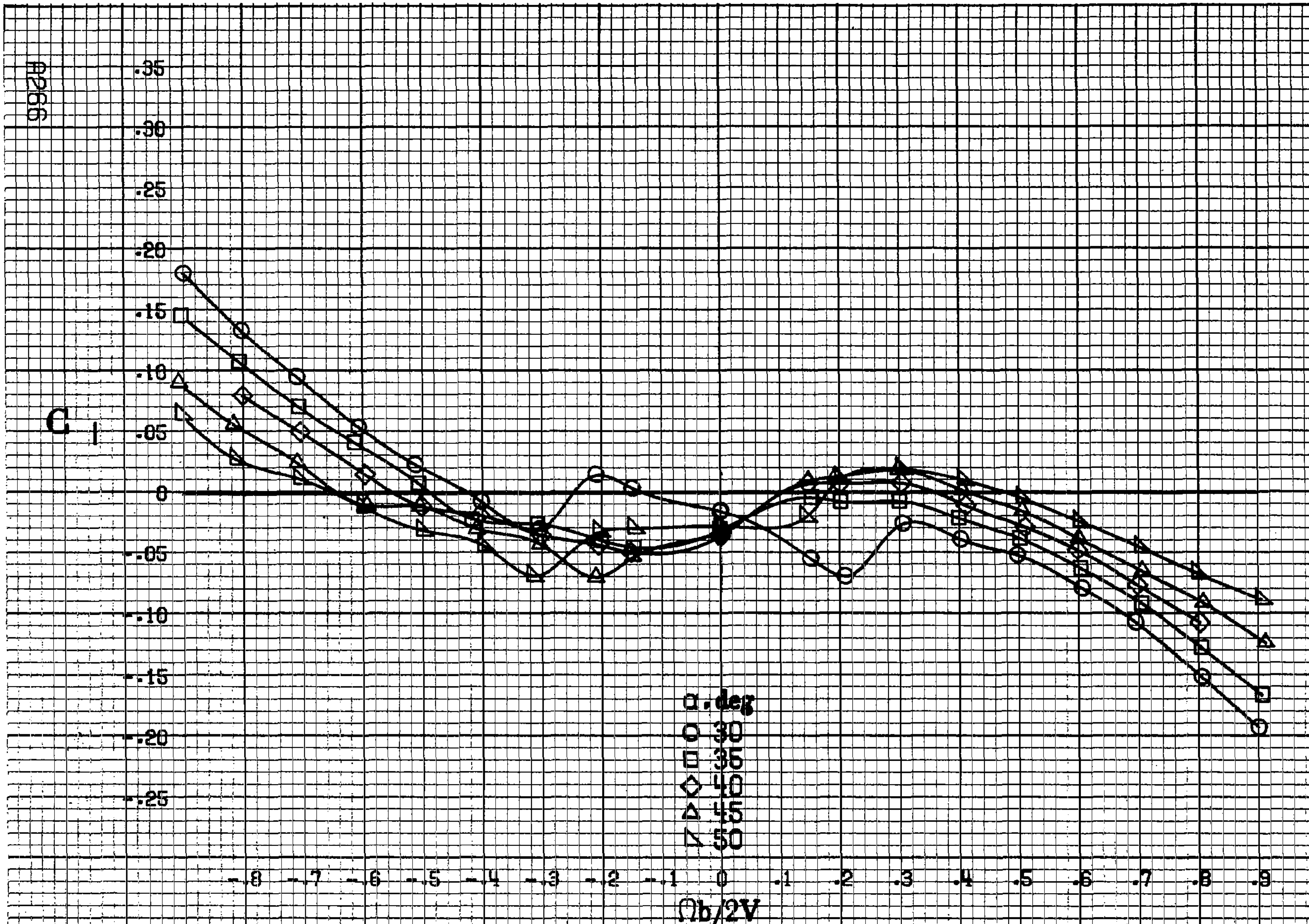

(c) $\alpha = 30$ to 50 deg, SR = 0.

Figure A62.-Continued.

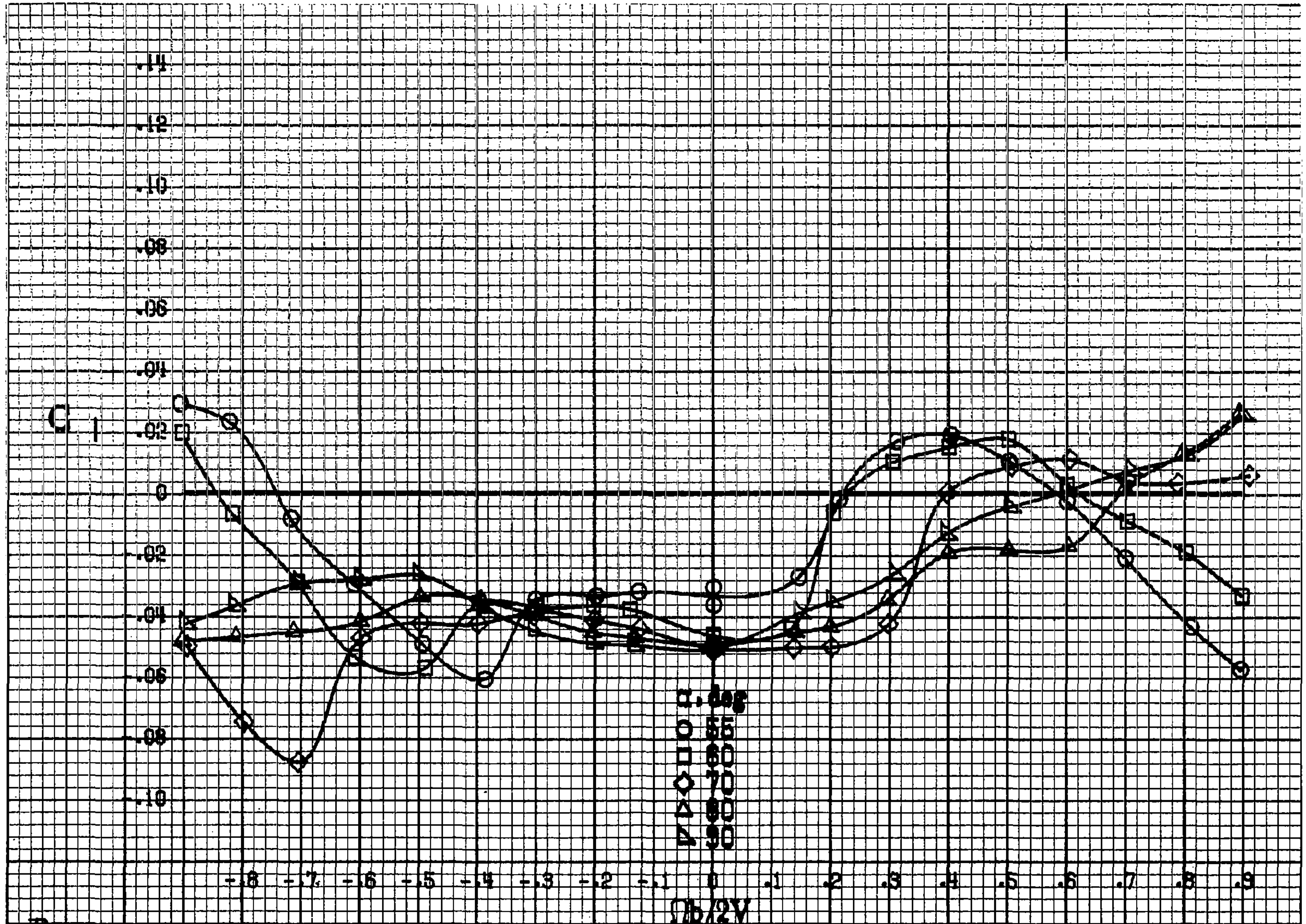

(d) α = 55 to 90 deg, SR = 0.

Figure A62.-Concluded.

A267

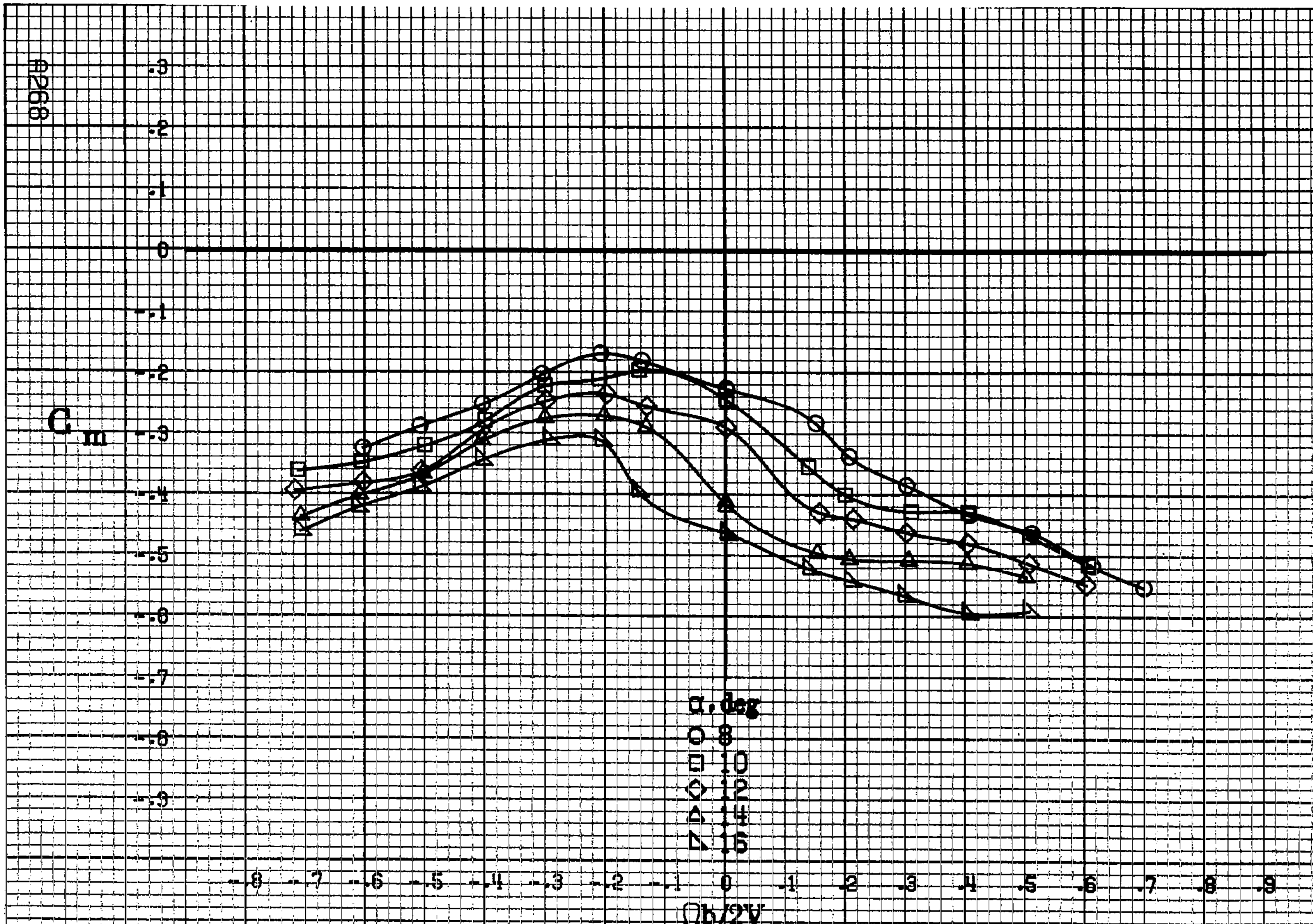

(a) $\alpha = 8$ to 16 deg, SR = 182.9 cm (72 in).

Figure A63.- Effect of rotation rate and angle of attack on pitching-moment coefficient for outboard LE wing droop with large nose radius. $\delta_e = 0°$, $\delta_a = 0°$, $\delta_r = 0°$, $\beta = 10°$.

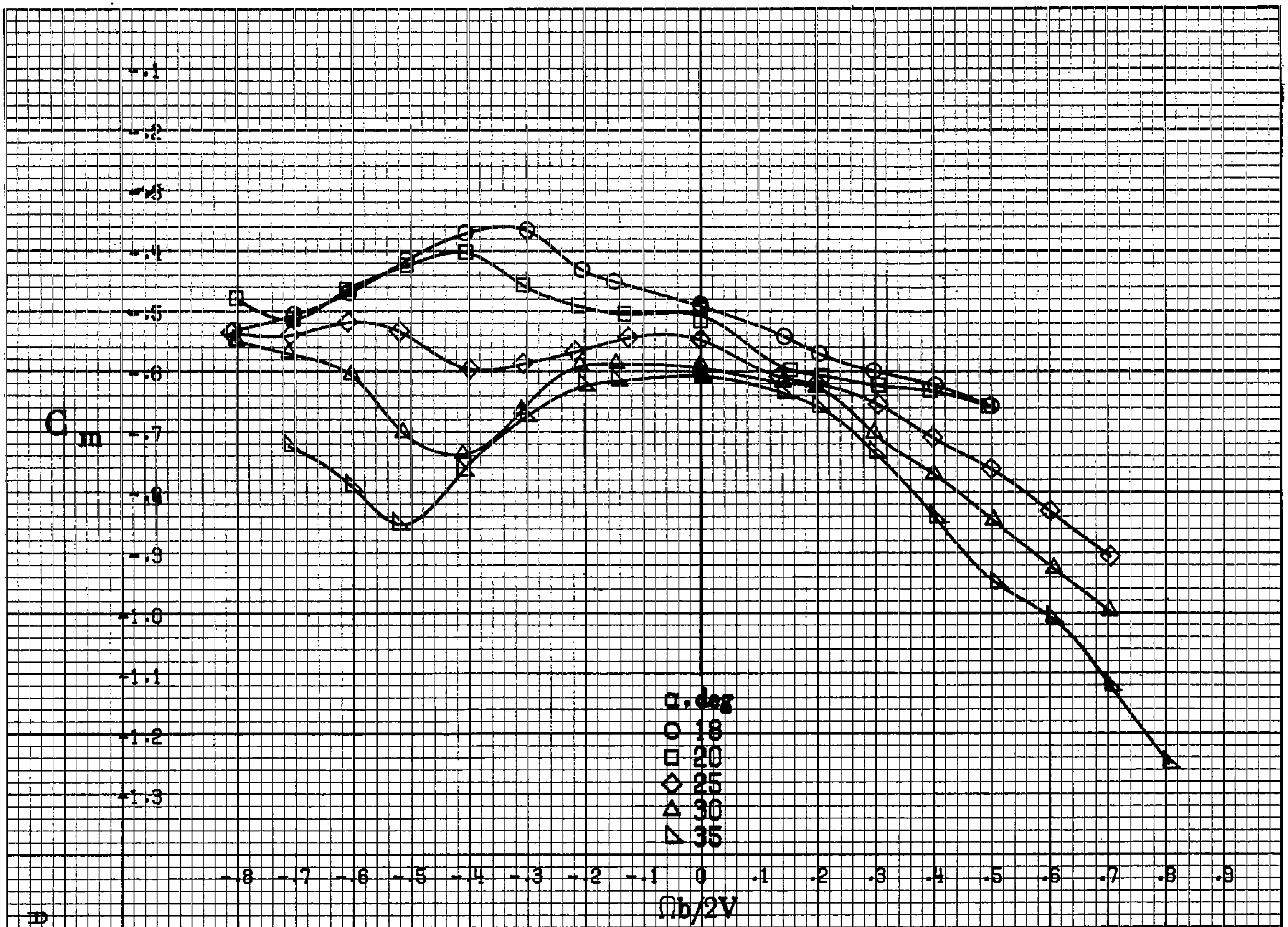

(b) α = 18 to 35 deg, SR = 182.9 cm (72 in).

Figure A63.-Continued.

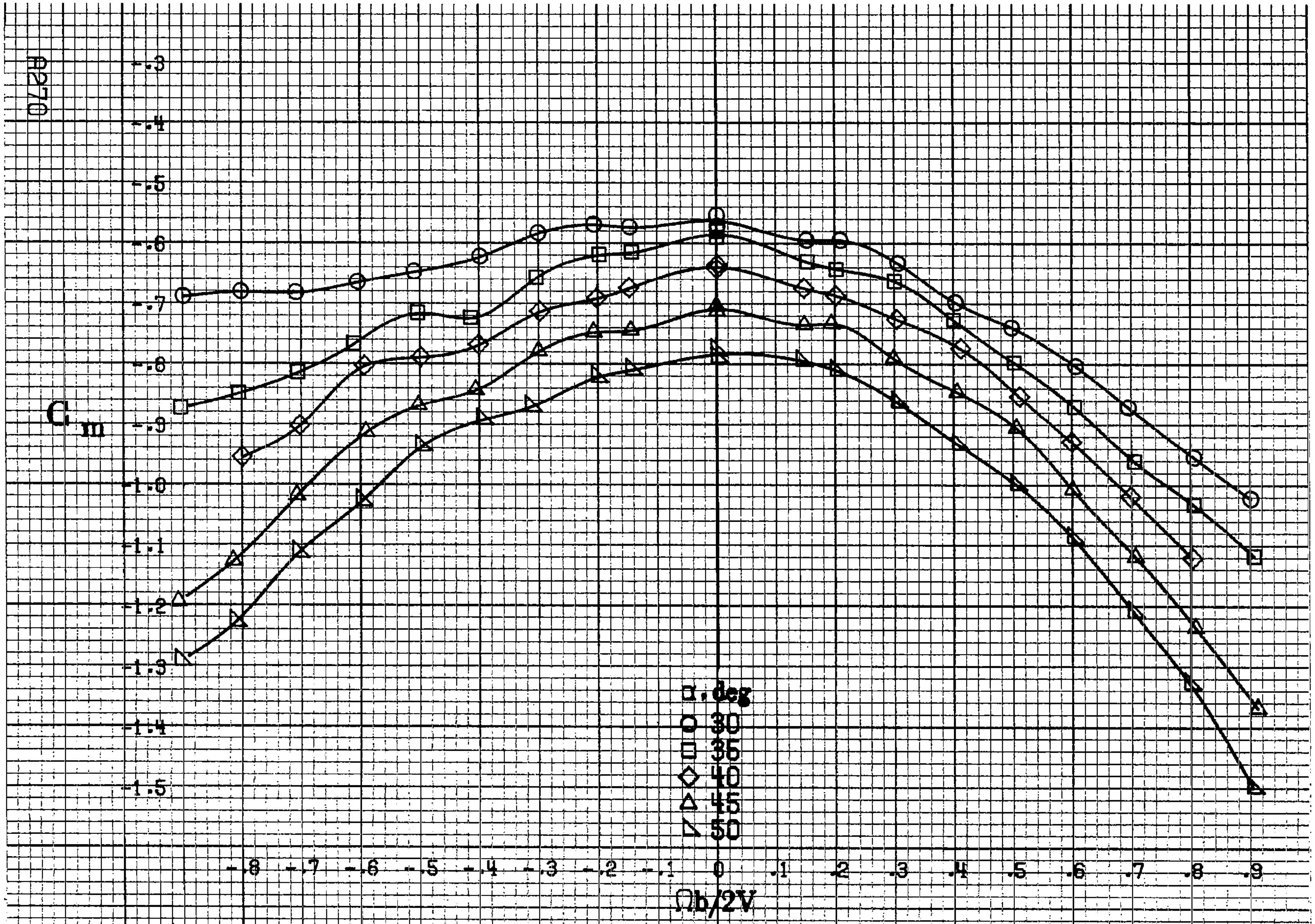

(c) α = 30 to 50 deg, SR = 0.

Figure A63.-Continued.

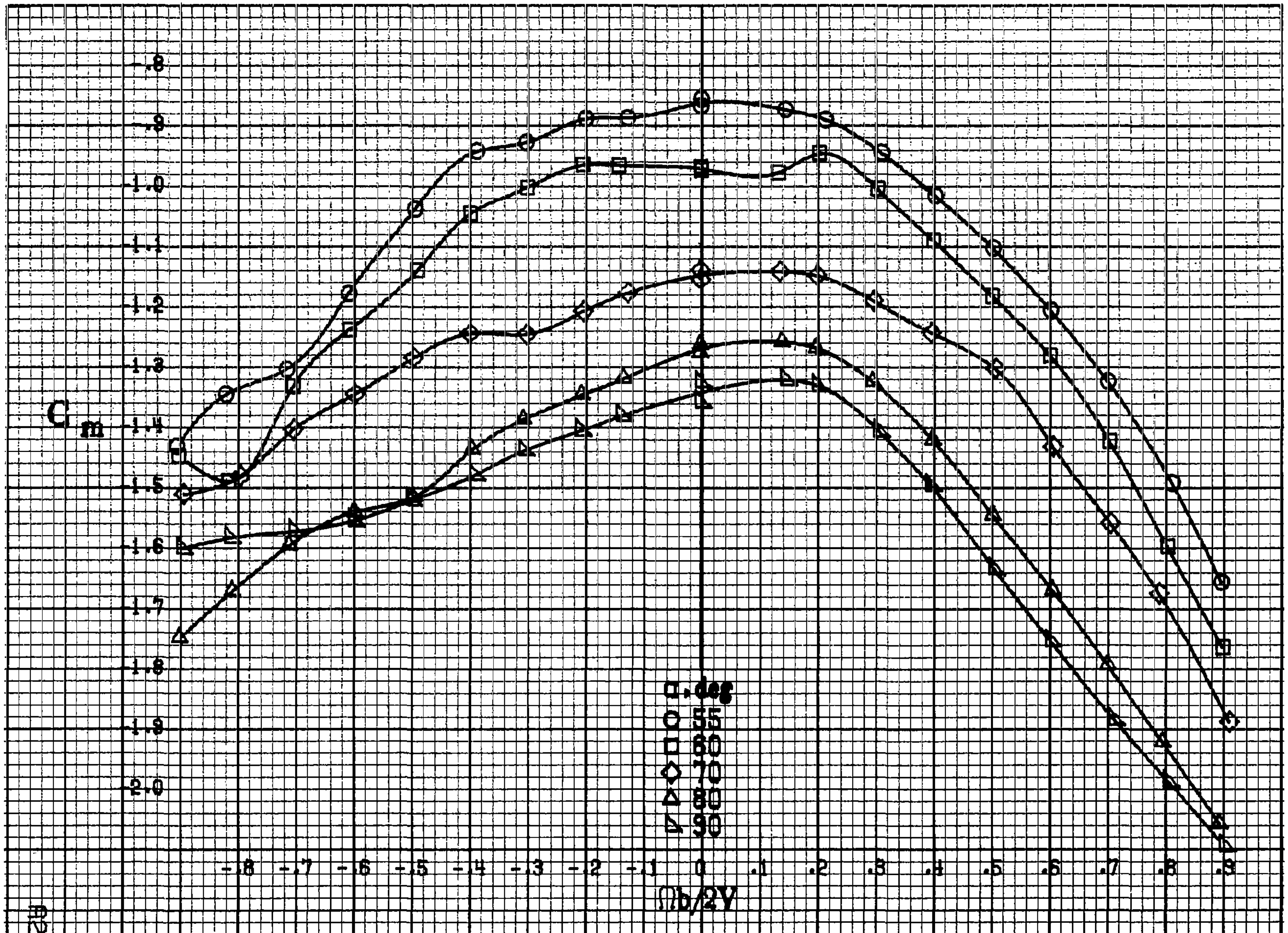

(d) α = 55 to 90 deg, δ_R = 0.

Figure A68.-Concluded.

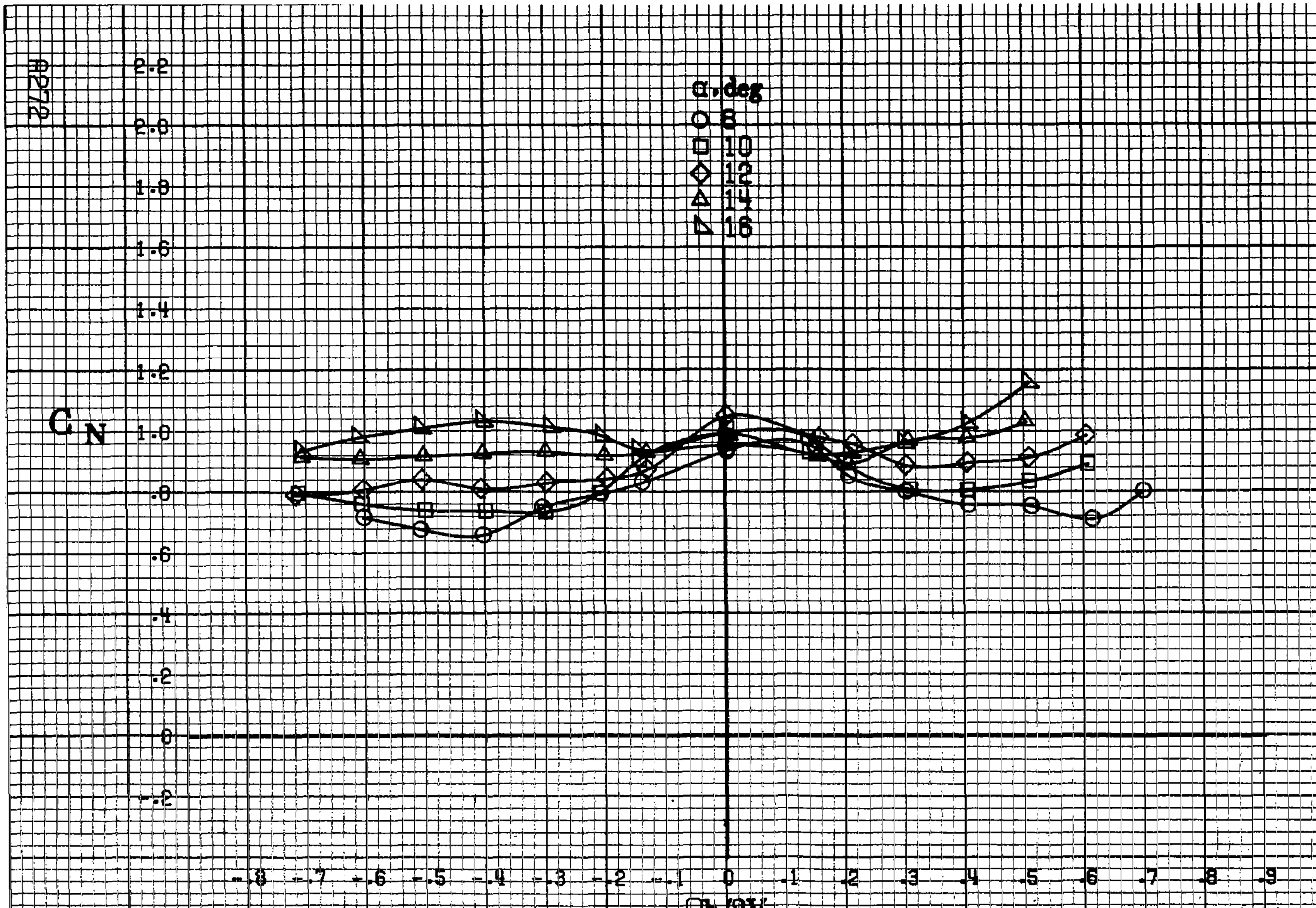

(a) $\alpha = 8$ to 16 deg, SR = 182.9 cm (72 in).

Figure A64.- Effect of rotation rate and angle of attack on normal-force coefficient for outboard LE wing droop with large nose radius. $\delta_e = 0°$, $\delta_a = 0°$, $\delta_r = 0°$. $\beta = 10°$.

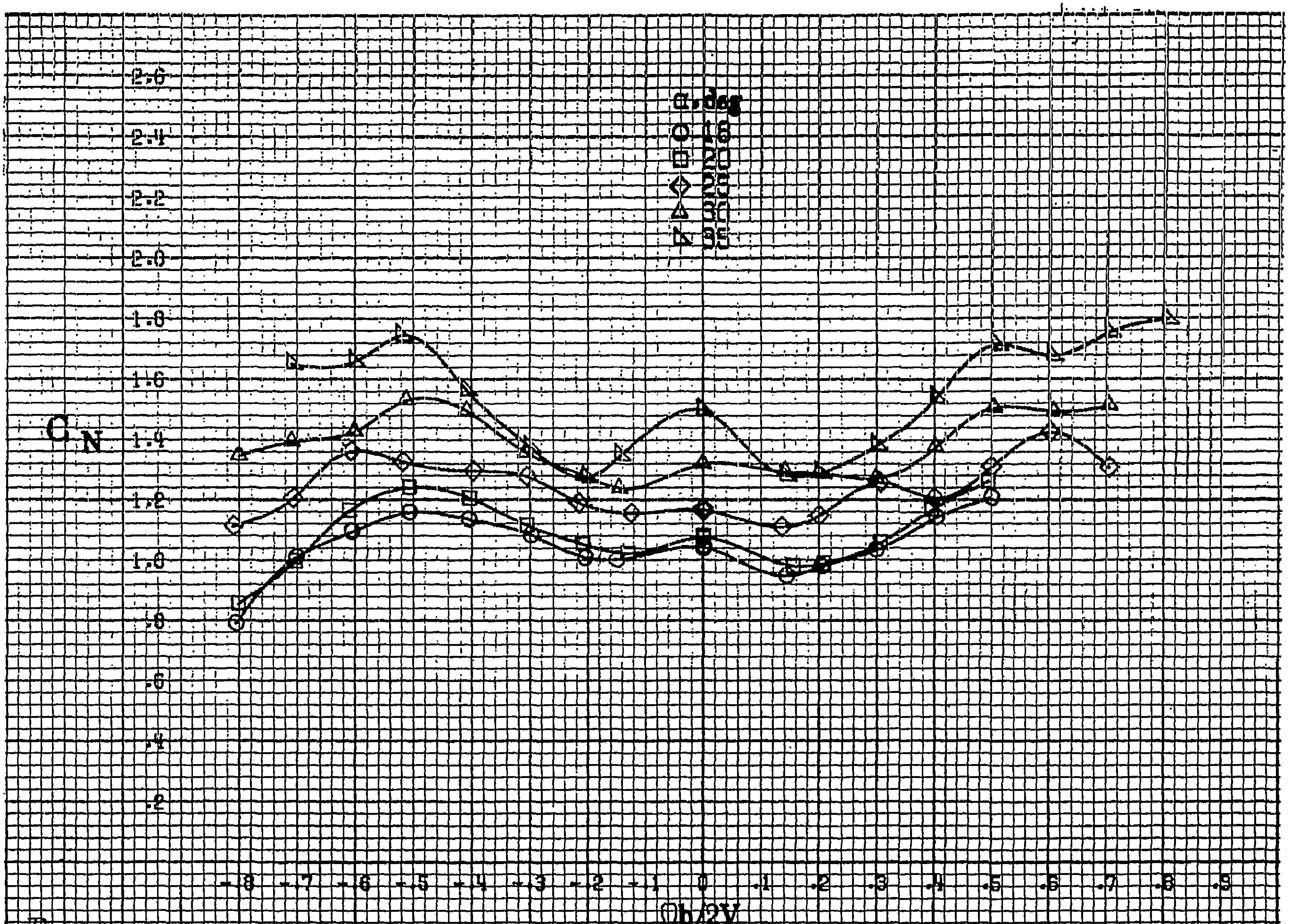

(b) α = 18 to 35 deg, SR = 182.9 cm (72 in).

Figure A64.-Continued.

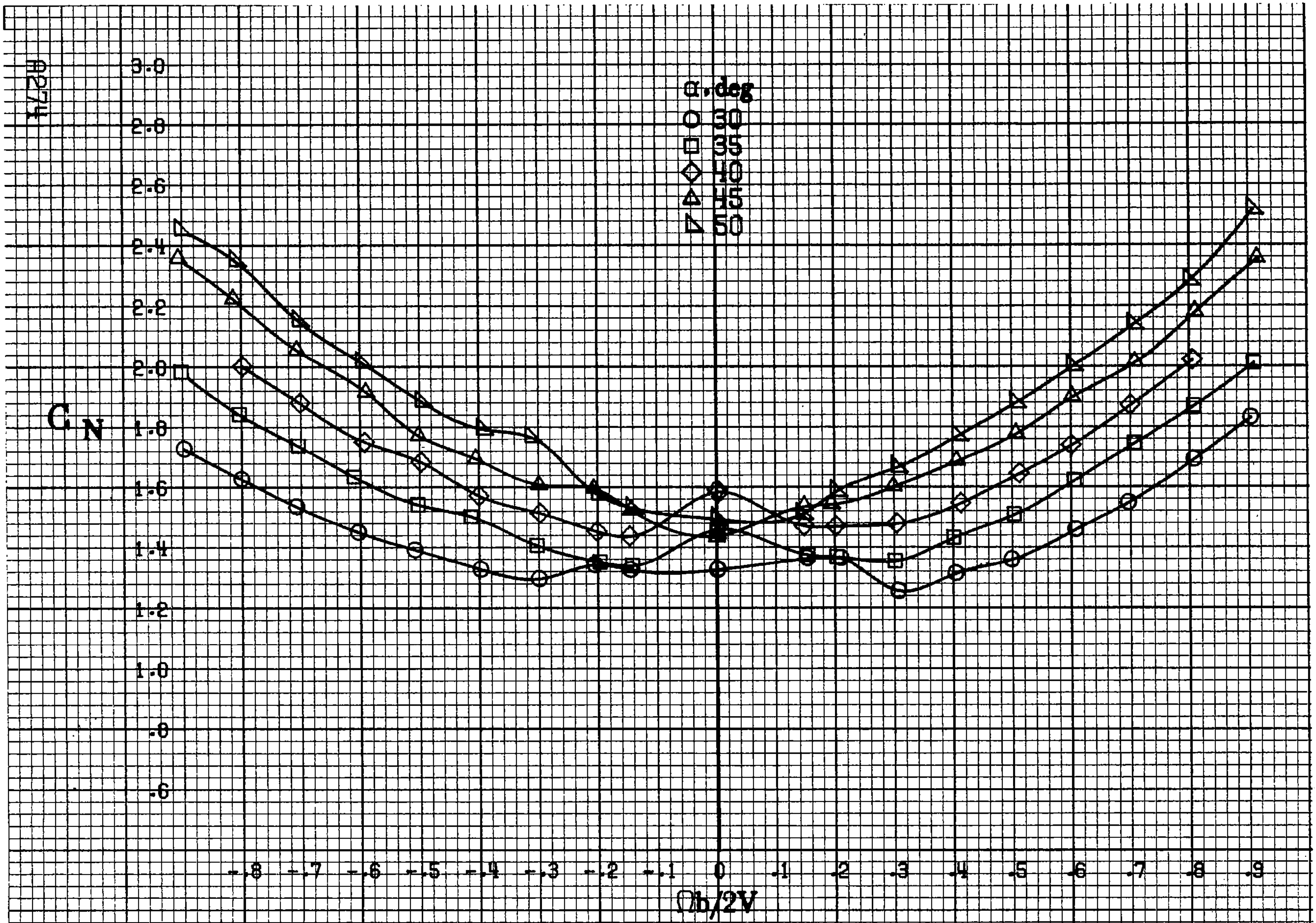

(c) α = 30 to 50 deg, SR = 0.

Figure A54.-Continued.

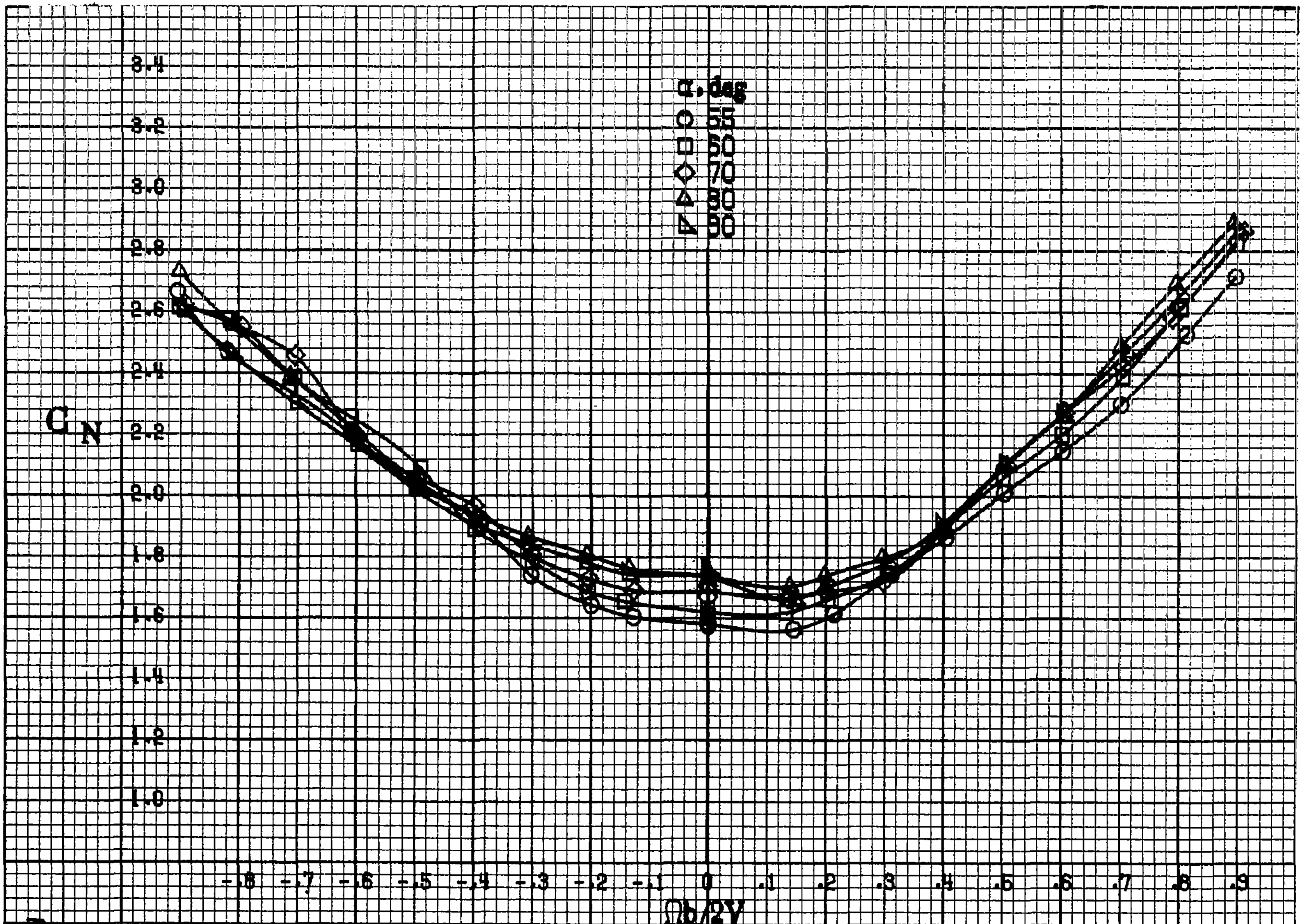

(d) α = 55 to 90 deg, SR = 0.

Figure A64.-Concluded.

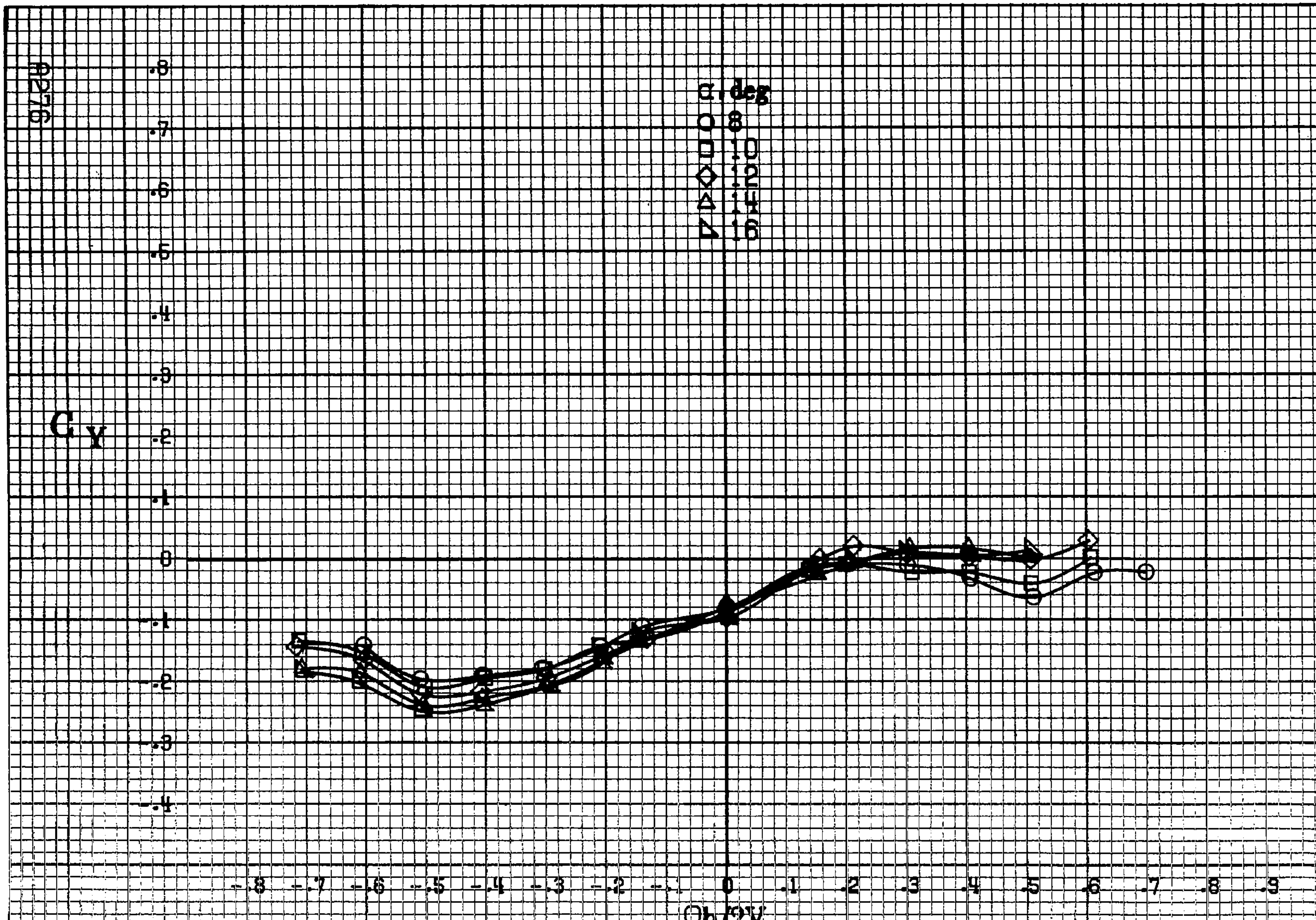

(a) α = 8 to 16 deg, SR = 182.9 cm (72 in.).

Figure A66.- Effect of rotation rate and angle of attack on side-force coefficient for outboard LE wing droop with large nose radius. $\delta_a = 0°$, $\delta_e = 0°$, $\delta_r = 0°$. $\beta = 10°$.

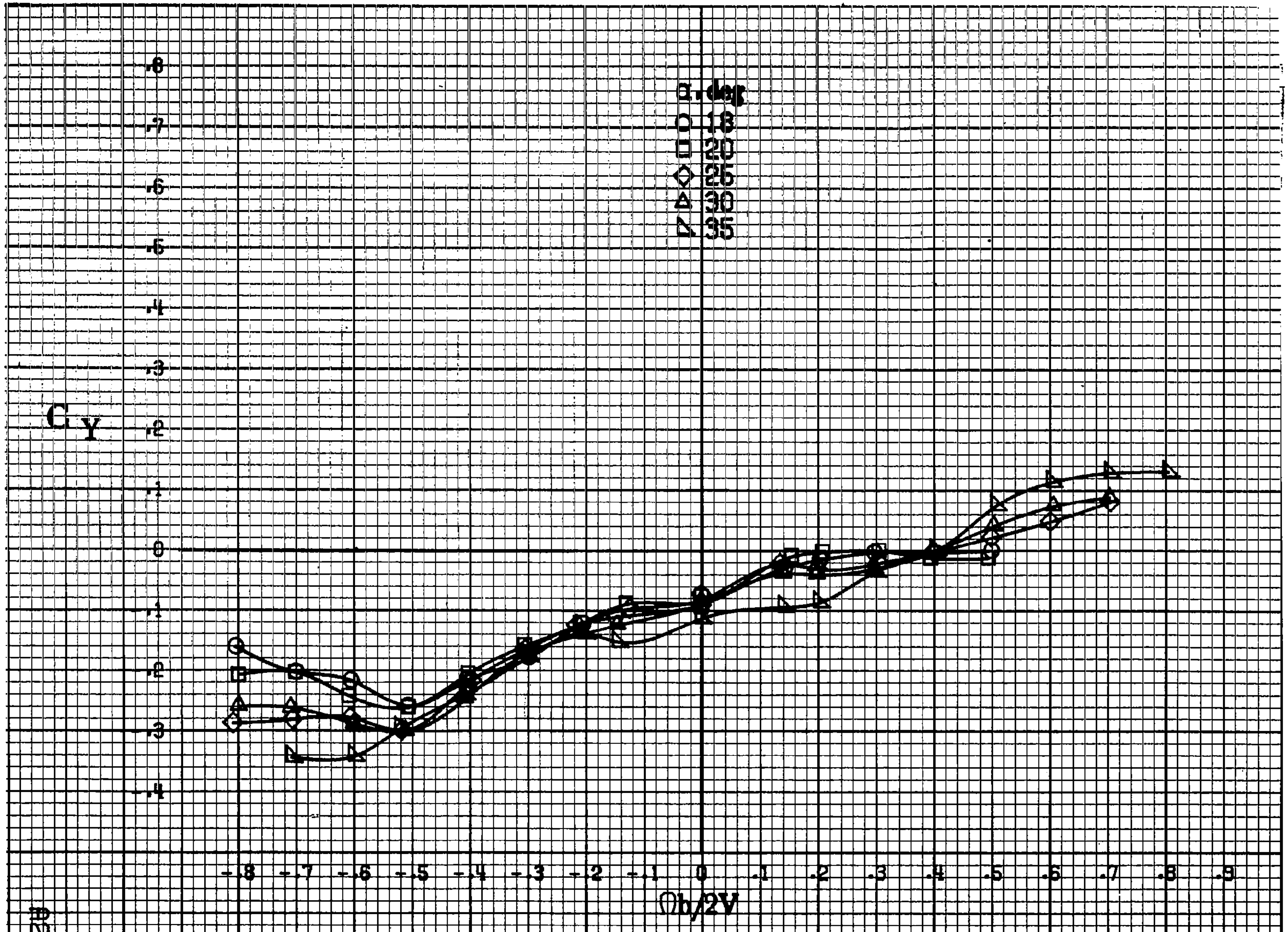

(b) α = 18 to 35 deg, SR = 182.9 cm (72 in).

Figure A65.-Continued.

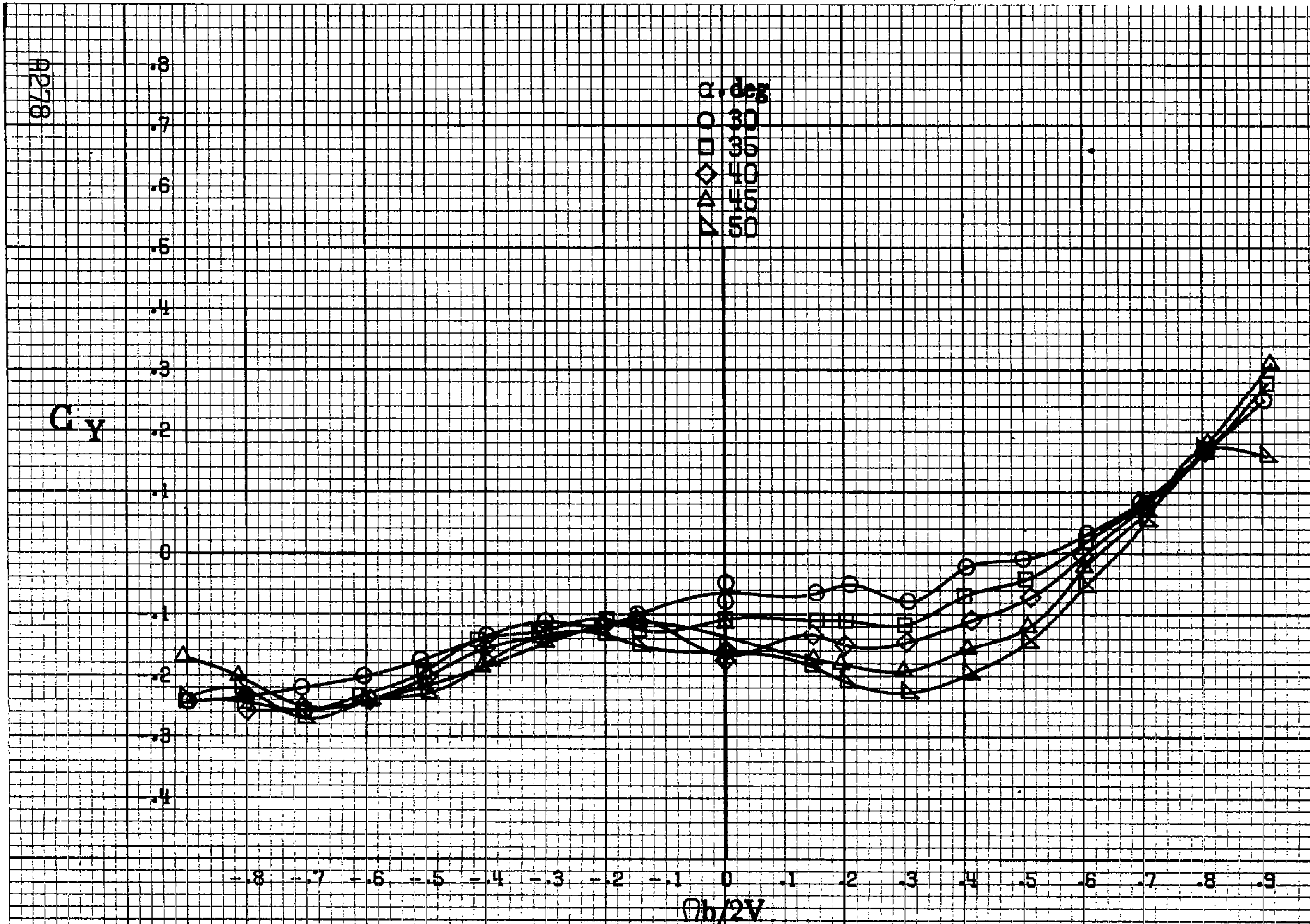

(c) α= 30to50deg, SR= 0.
Figure A65.-Continued.

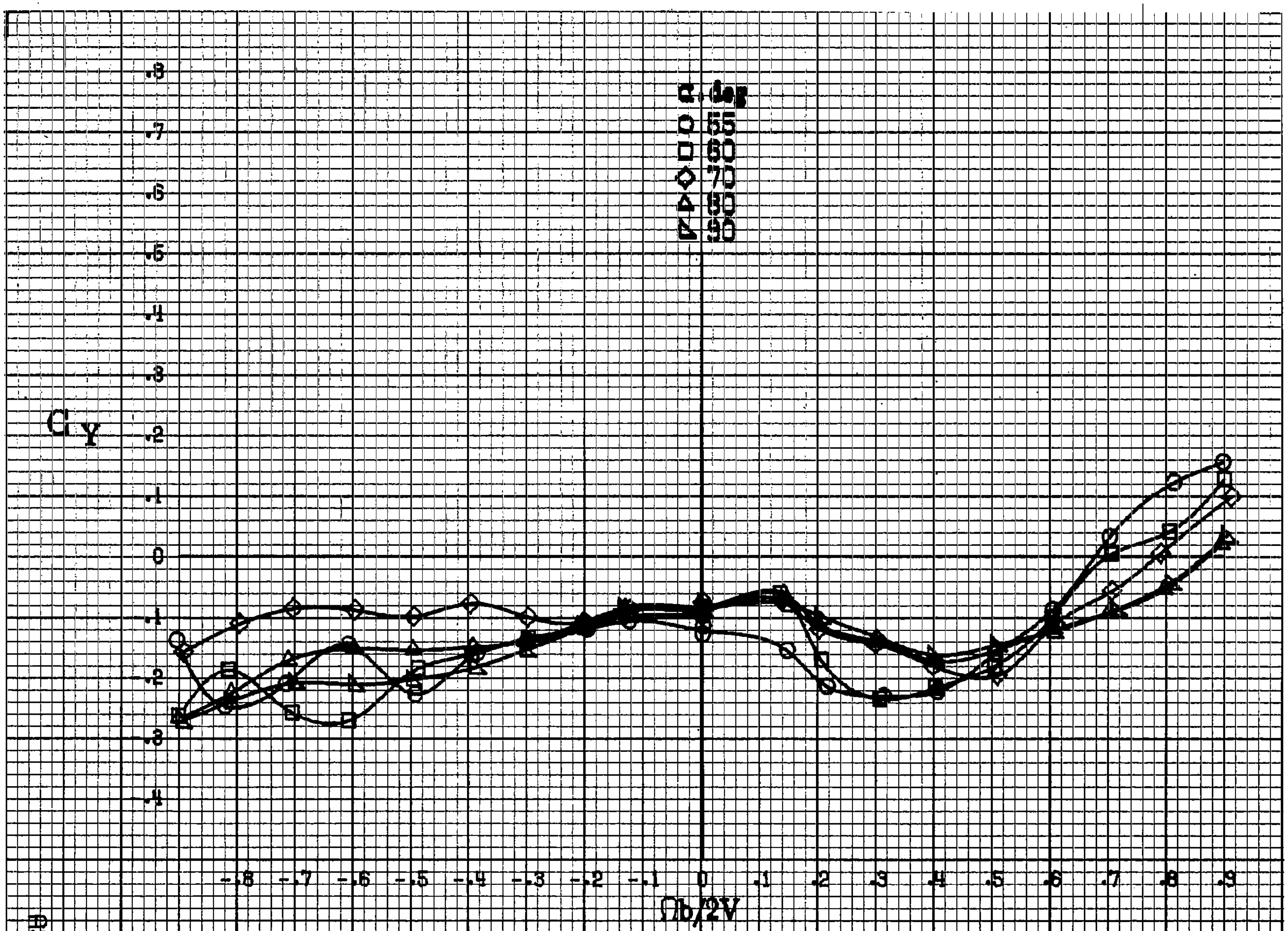

(d) α = 55 to 90 deg, SR = 0.

Figure A 66.-Concluded.

A279

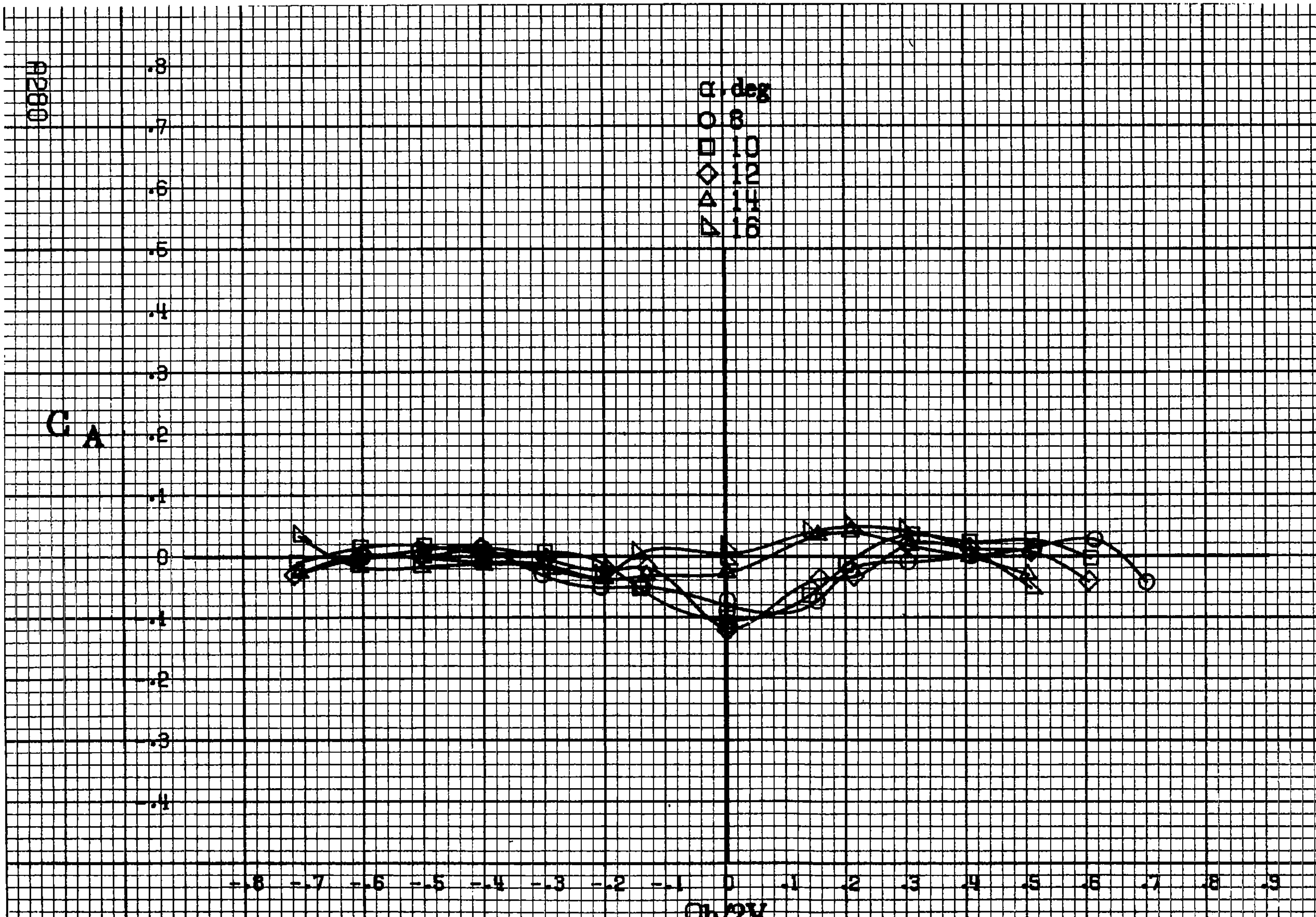

(a) α = 8 to 16 deg, SR = 182.9 cm (72 in).

Figure A66.-Effect of rotation rate and angle of attack on axial-force coefficient for outboard LE wing droop with large nose radius. $\delta_a = 0°$, $\delta_s = 0°$, $\delta_r = 0°$. $\beta = 10°$.

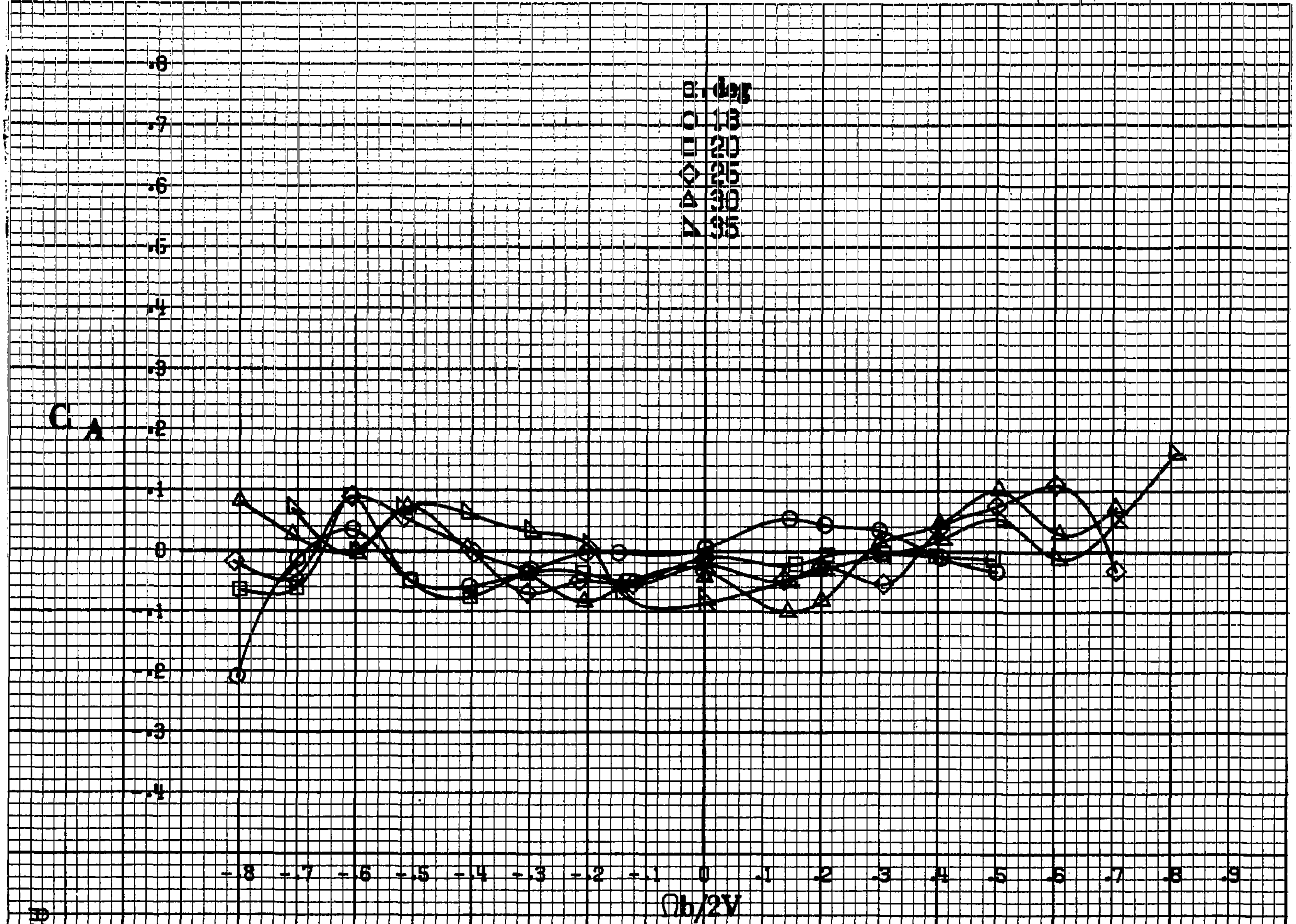

(b) α = 18 to 35 deg, SR = 182.9 cm (72 in).

Figure A66.- Continued.

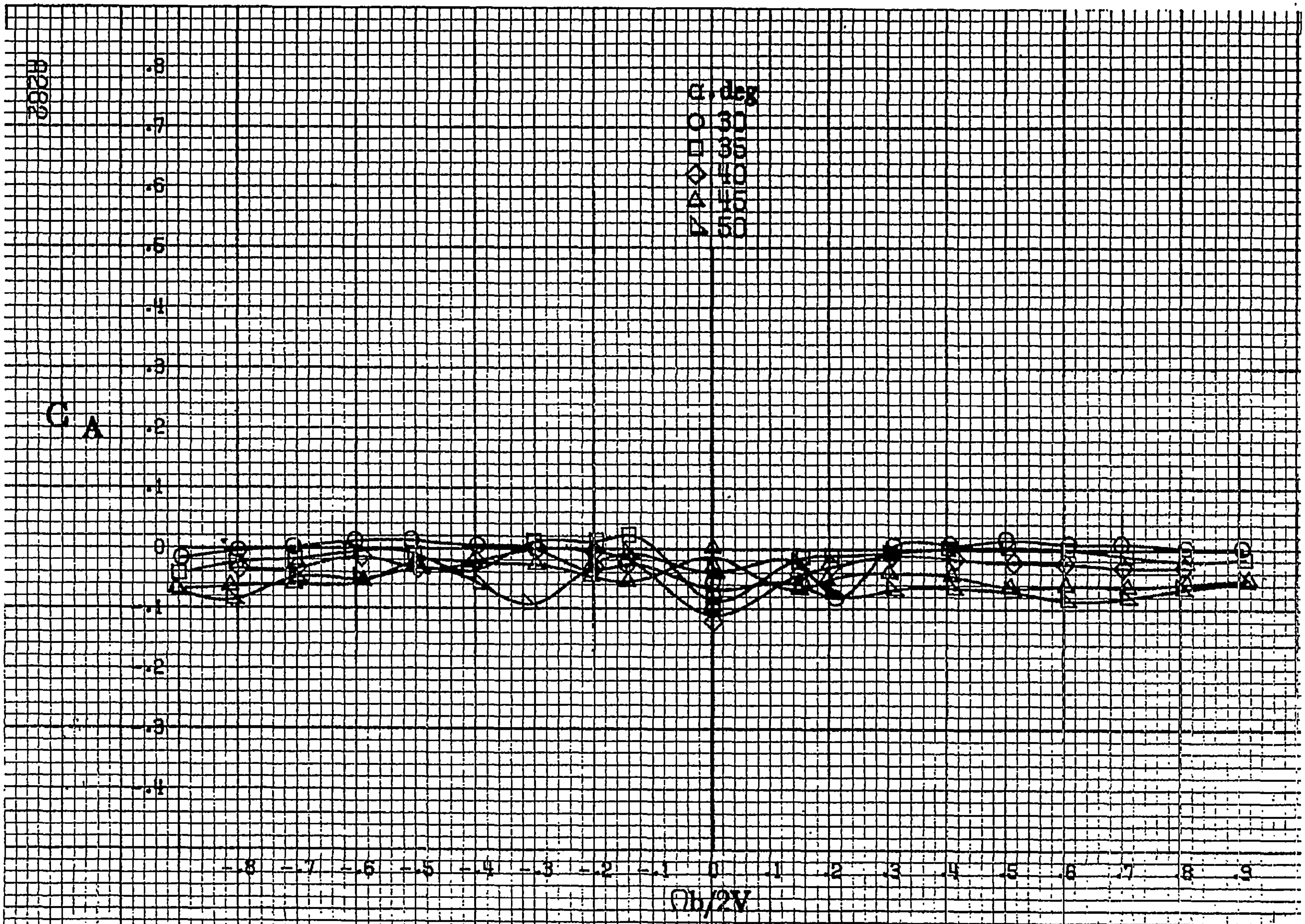

(c) α=30to50deg, SR=0.
Figure A66.-Continued.

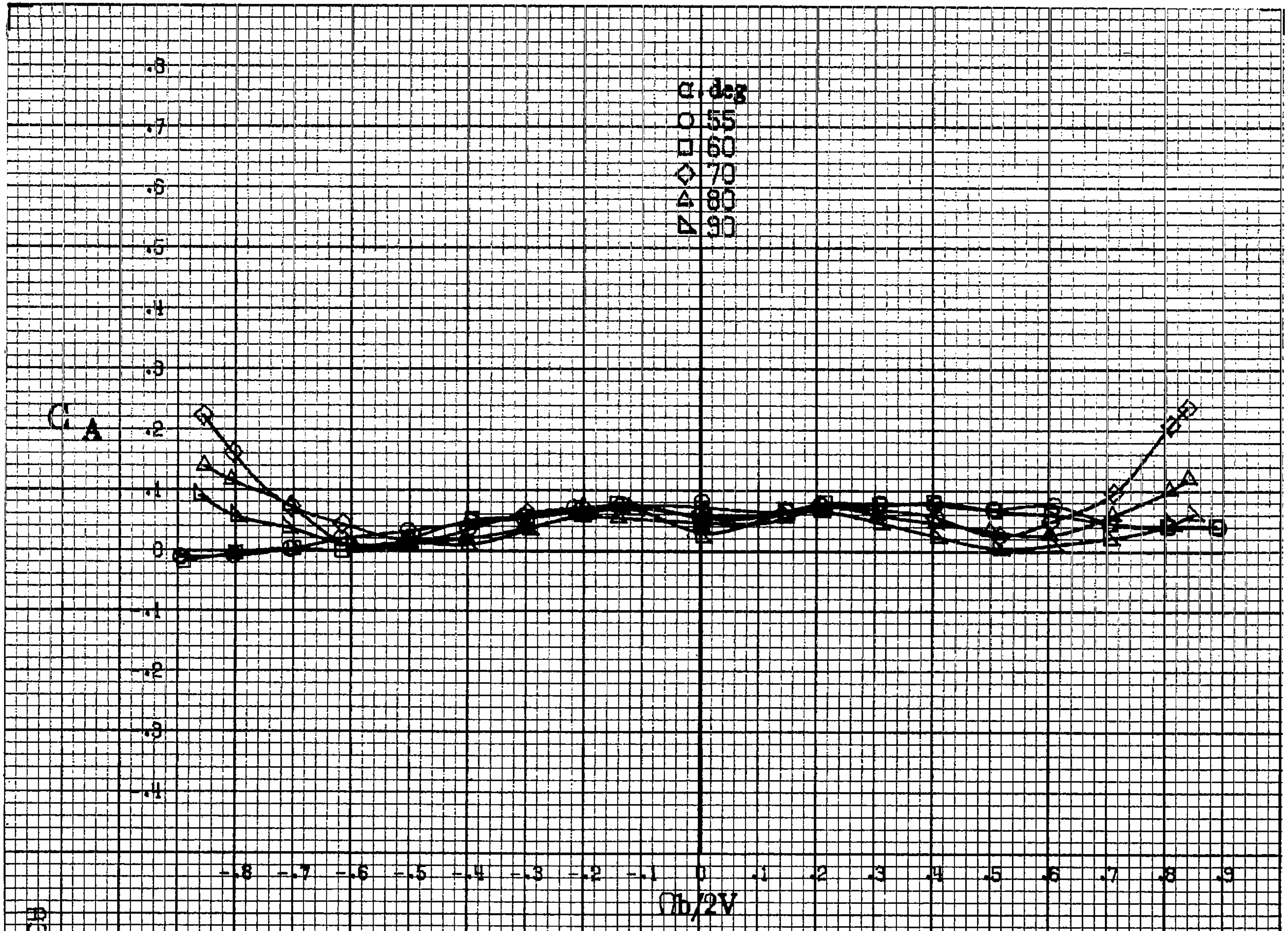

(d) α = 55 to 90 deg, SR = 0.
Figure A90.-Concluded.

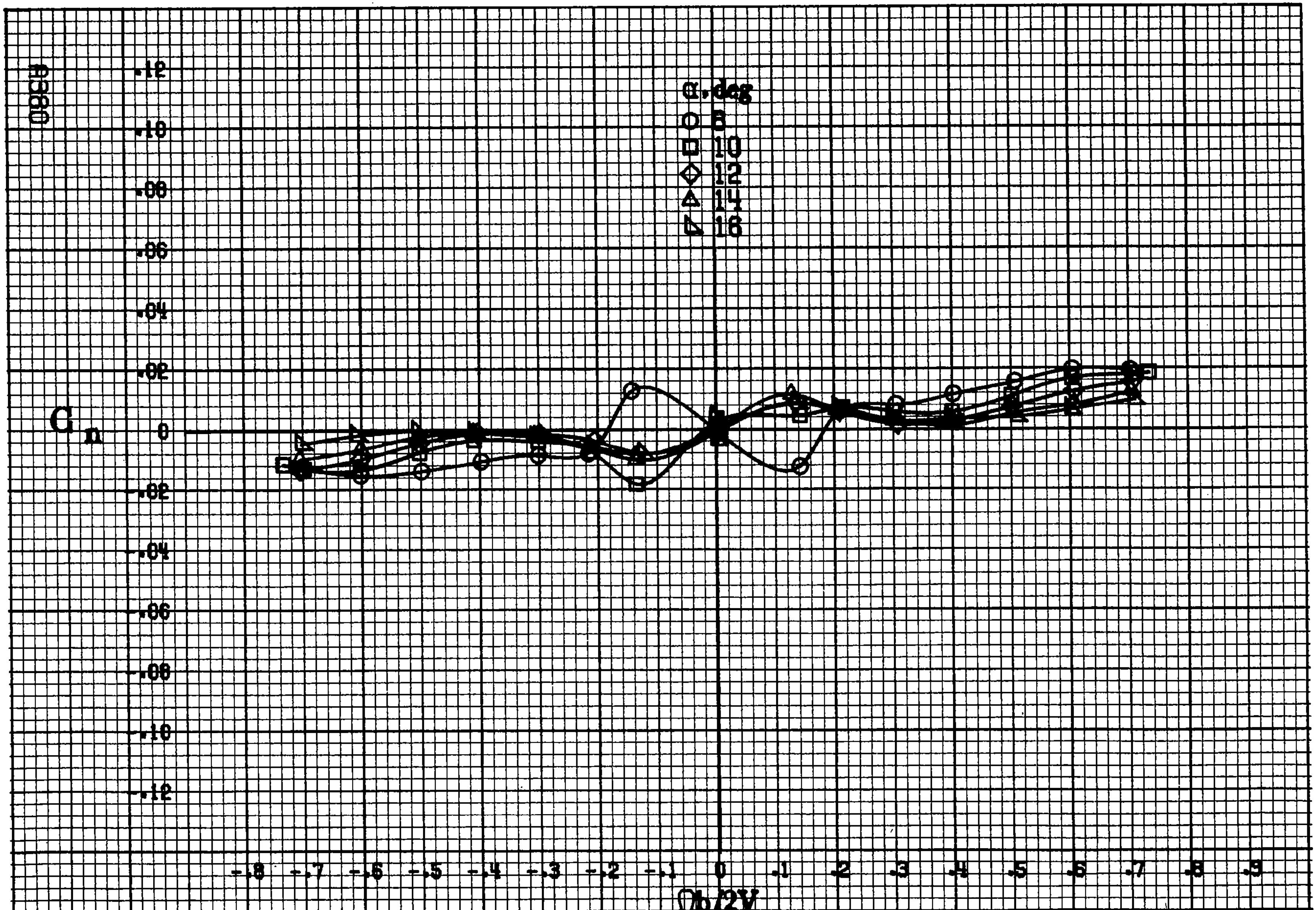

(a) $\alpha = 8$ to 16 deg, SR = 182.9 cm (72 in).

Figure A91.-Effect of rotation rate and angle of attack on yawing-moment coefficient for vertical tail off configuration. $\delta_e = 0°$, $\delta_a = 0°$, $\delta_r = 0°$, $\beta = 0°$.

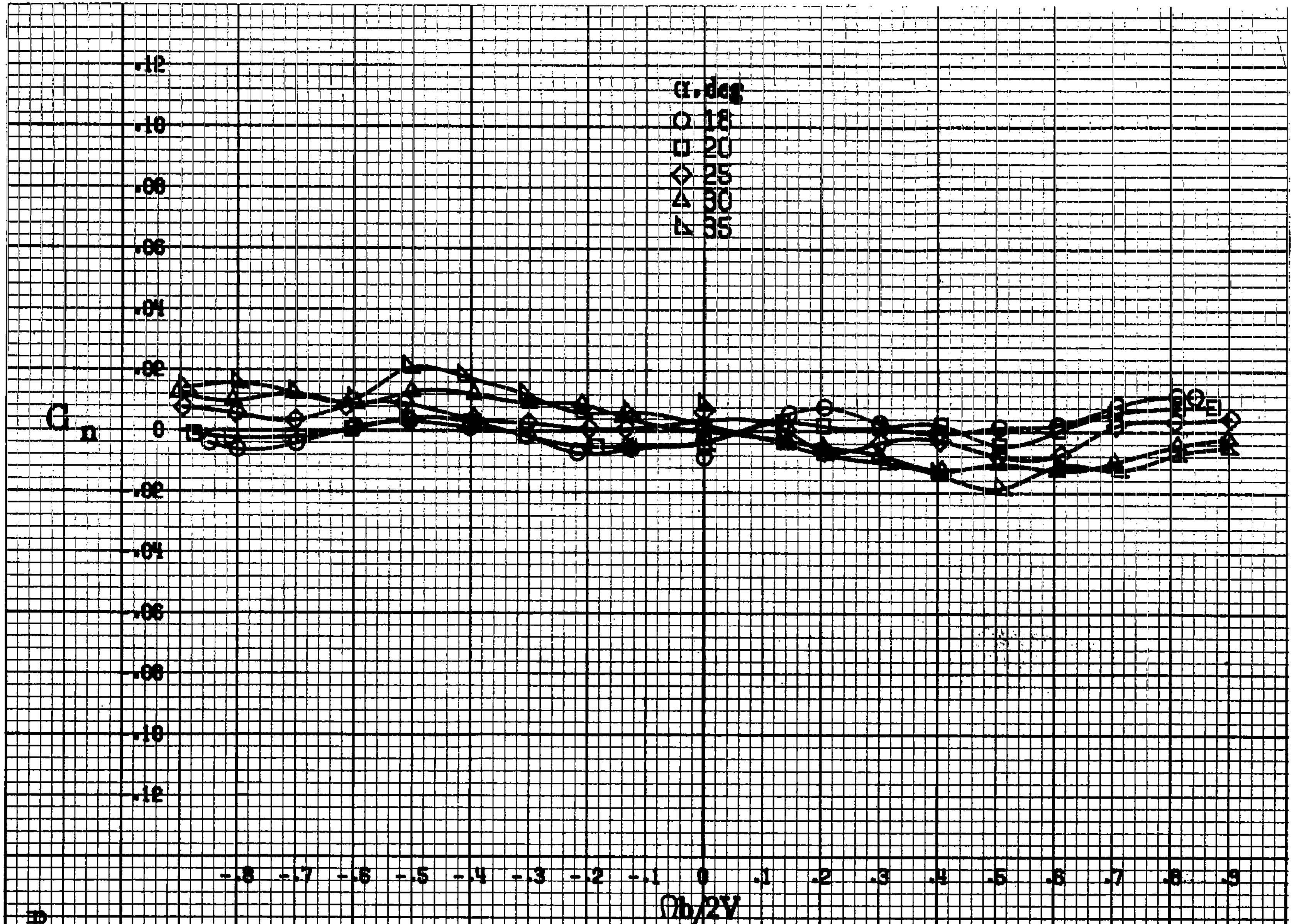

(b) α = 18 to 35 deg, SR = 182.9 cm (72 in).

Figure A91.-Continued.

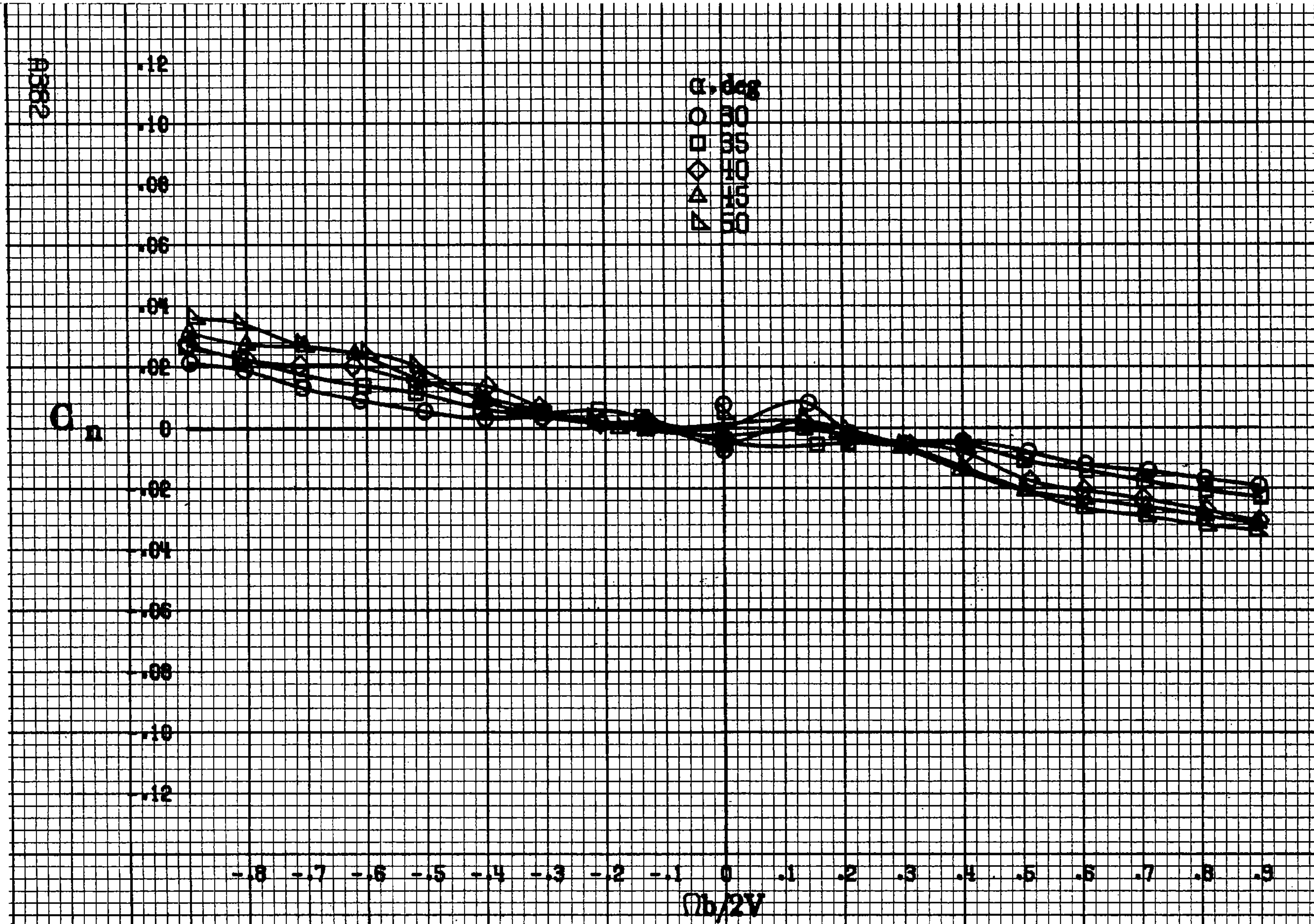

(c) α = 30 to 50 deg, SR = 0.

Figure A91.-Continued.

(d) α = 55 to 90 deg, SR = 0.

Figure A91.-Concluded.

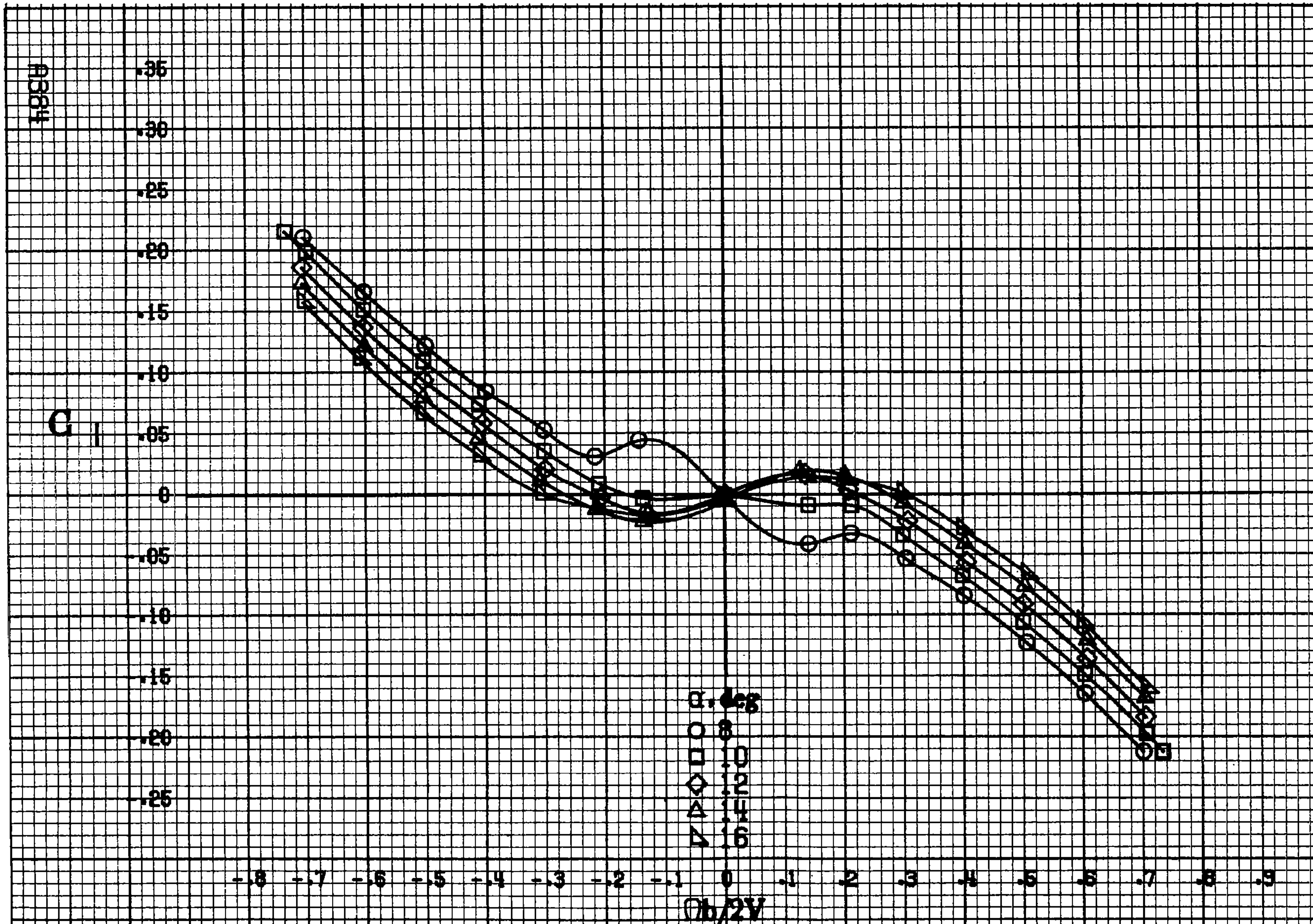

(a) α = 8 to 16 deg, SR = 182.9 cm (72 in).

Figure A92.- Effect of rotation rate and angle of attack on rolling-moment coefficient for vertical tail off configuration. $\delta_e = 0°$, $\delta_a = 0°$, $\delta_r = 0°$, $\beta = 0°$.

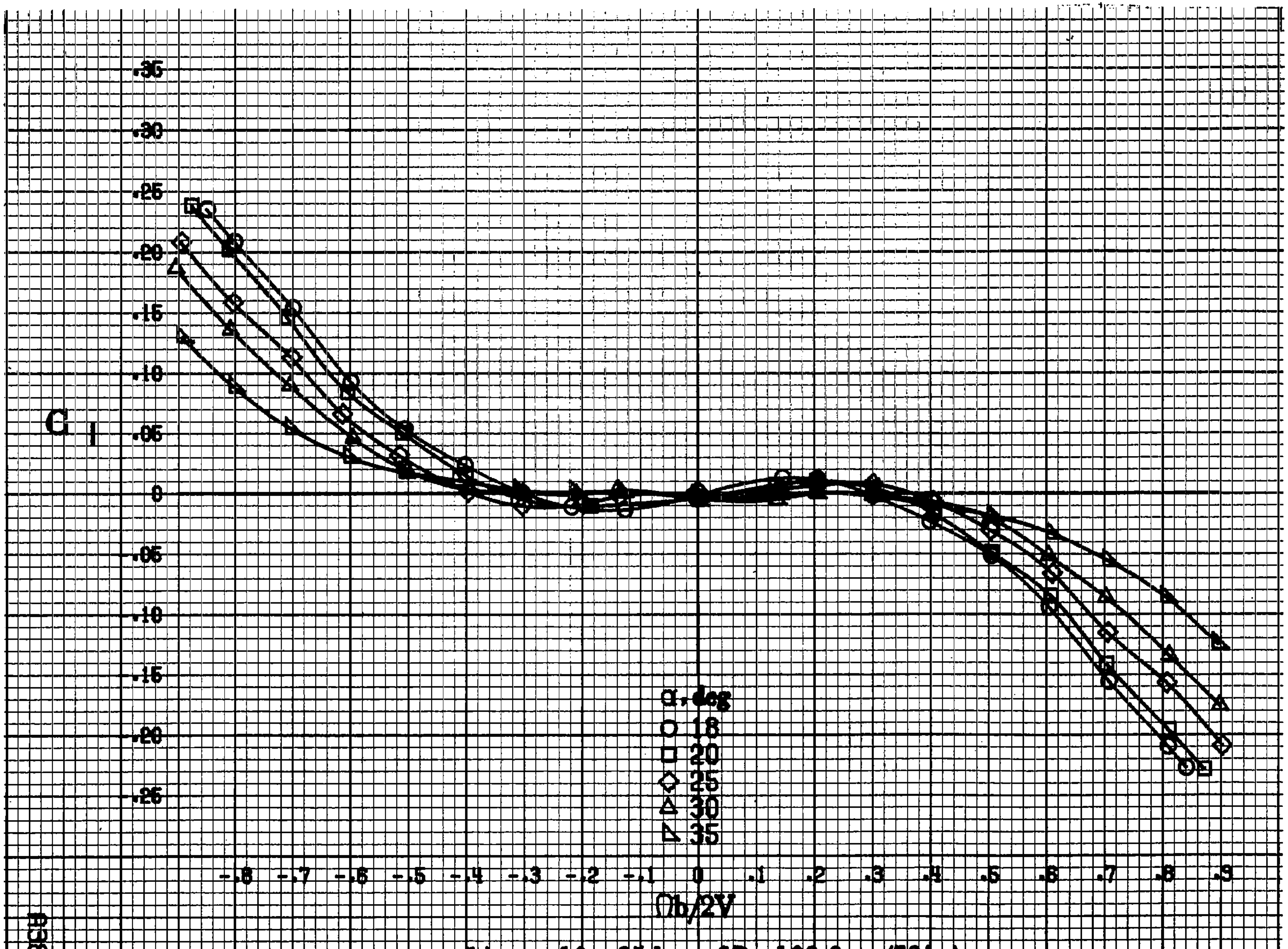

(b) α = 18 to 35 deg, SR = 182.9 cm (72 in).

Figure A92.-Continued.

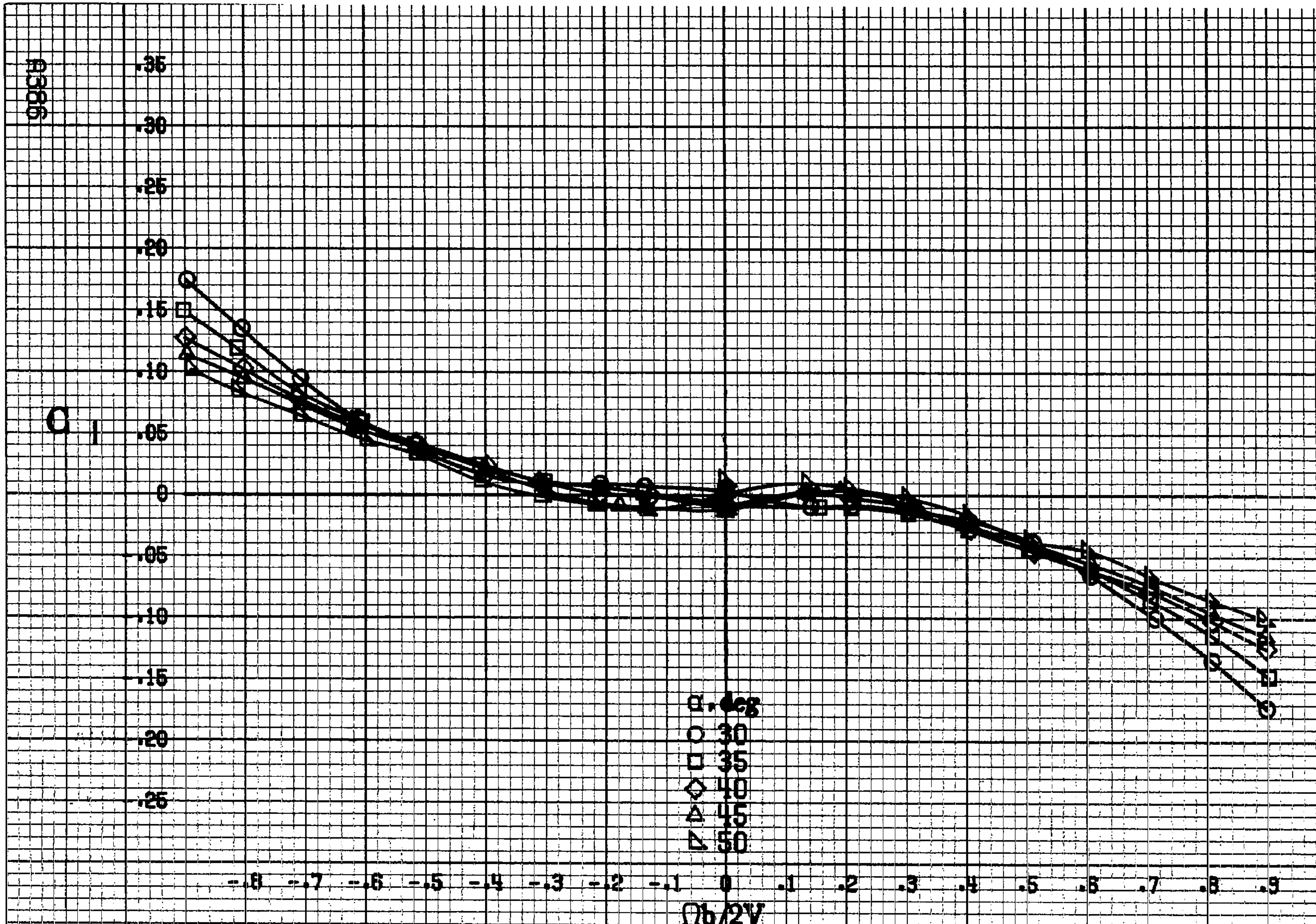

(c) α = 30 to 50 deg, SR = 0.

Figure A92.-Continued.

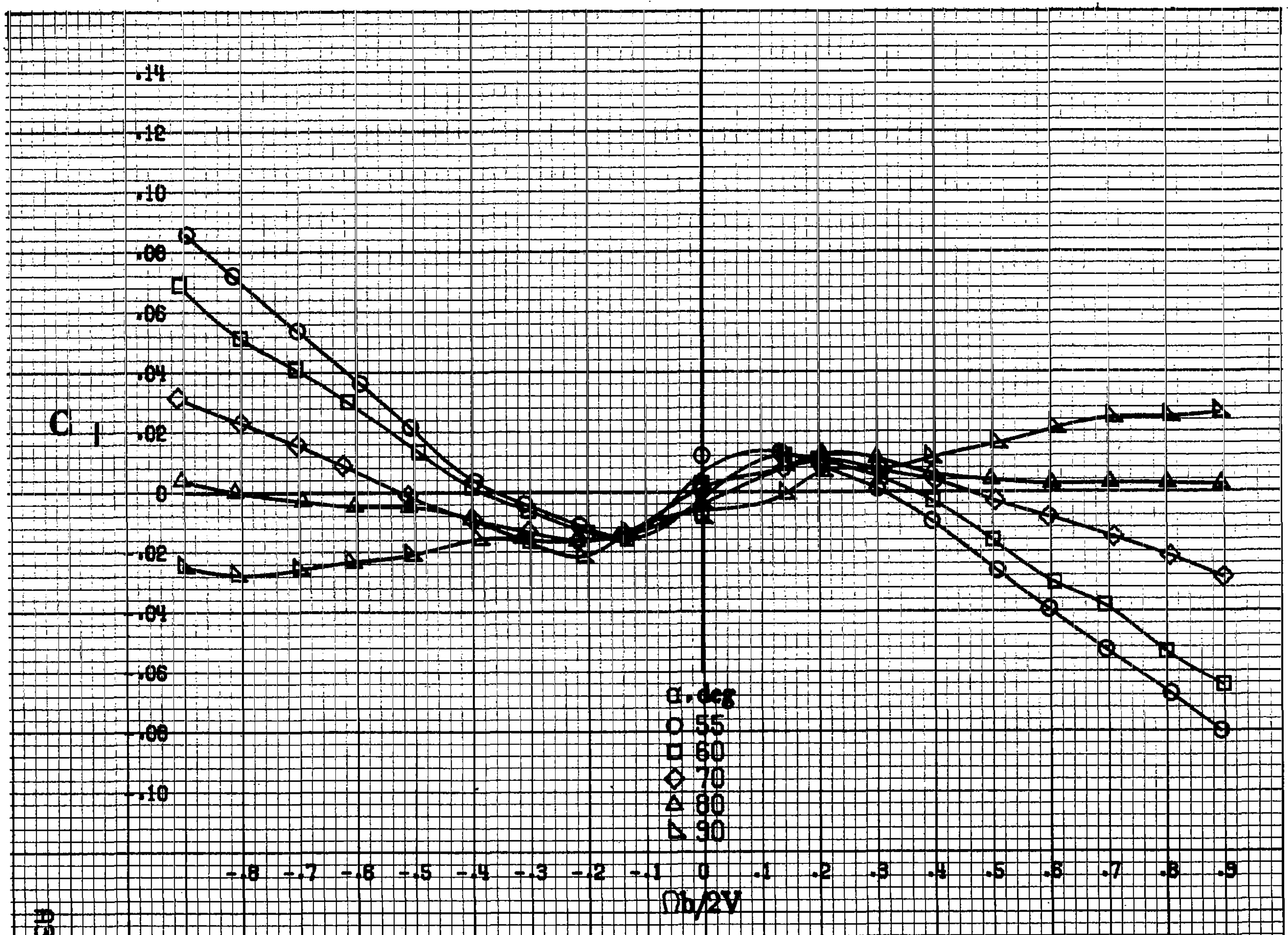

(d) α = 55 to 90 deg, SR = 0.

Figure A92.-Concluded.

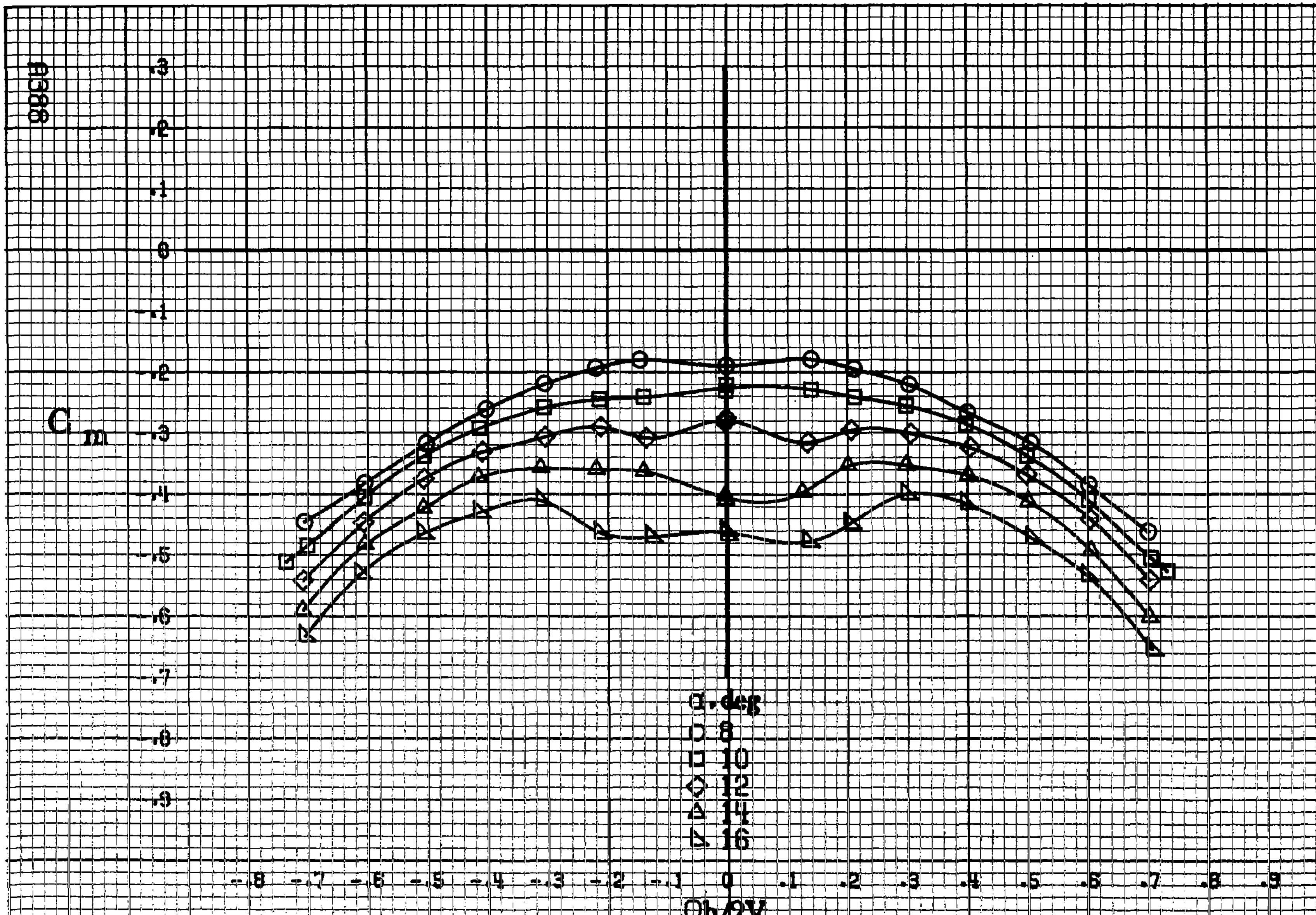

(a) $\alpha = 8$ to 16 deg, SR = 182.9 cm (72 in).

Figure A93.-Effect of rotation rate and angle of attack on pitching-moment coefficient for vertical tail off configuration. $\delta_e = 0°$, $\delta_a = 0°$, $\delta_r = 0°$, $\beta = 0°$.

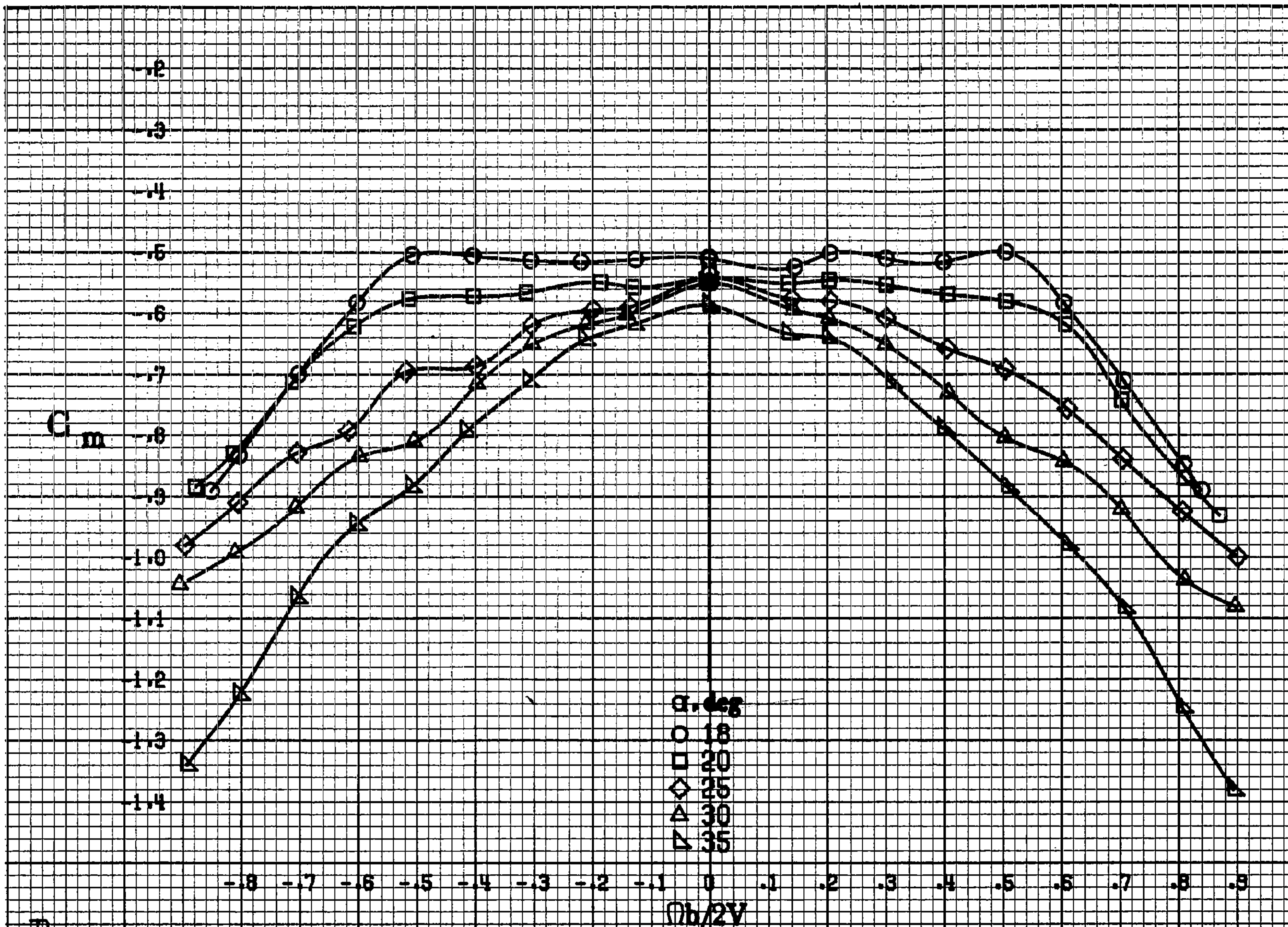

(b) α = 18 to 35 deg, SR = 182.9 cm (72 in).

Figure A98.-Continued.

A390

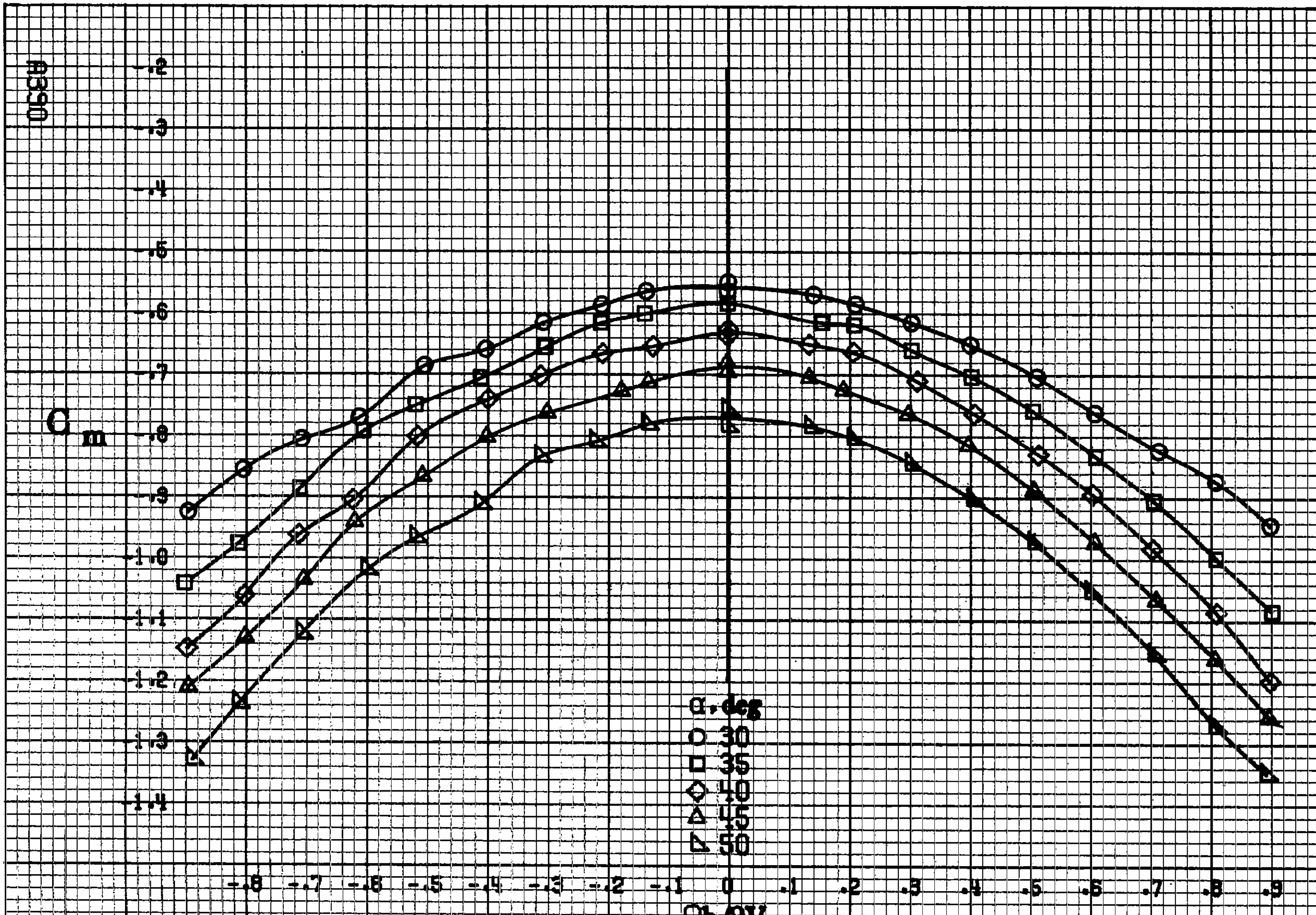

(c) α = 30 to 50 deg, SR = 0.

Figure A98.-Continued.

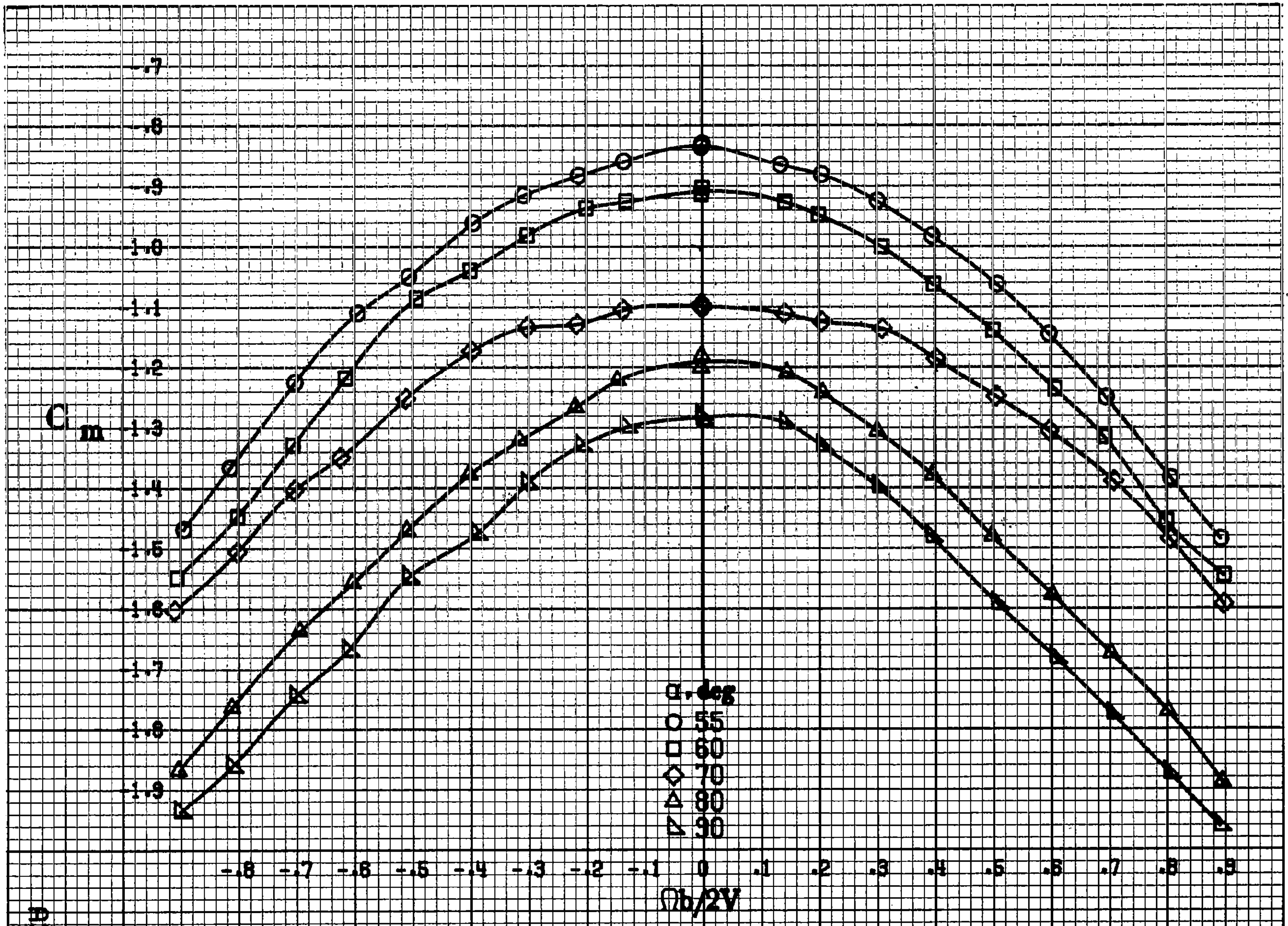

(d) α = 55 to 90 deg, SR = 0.

Figure A93.-Concluded.

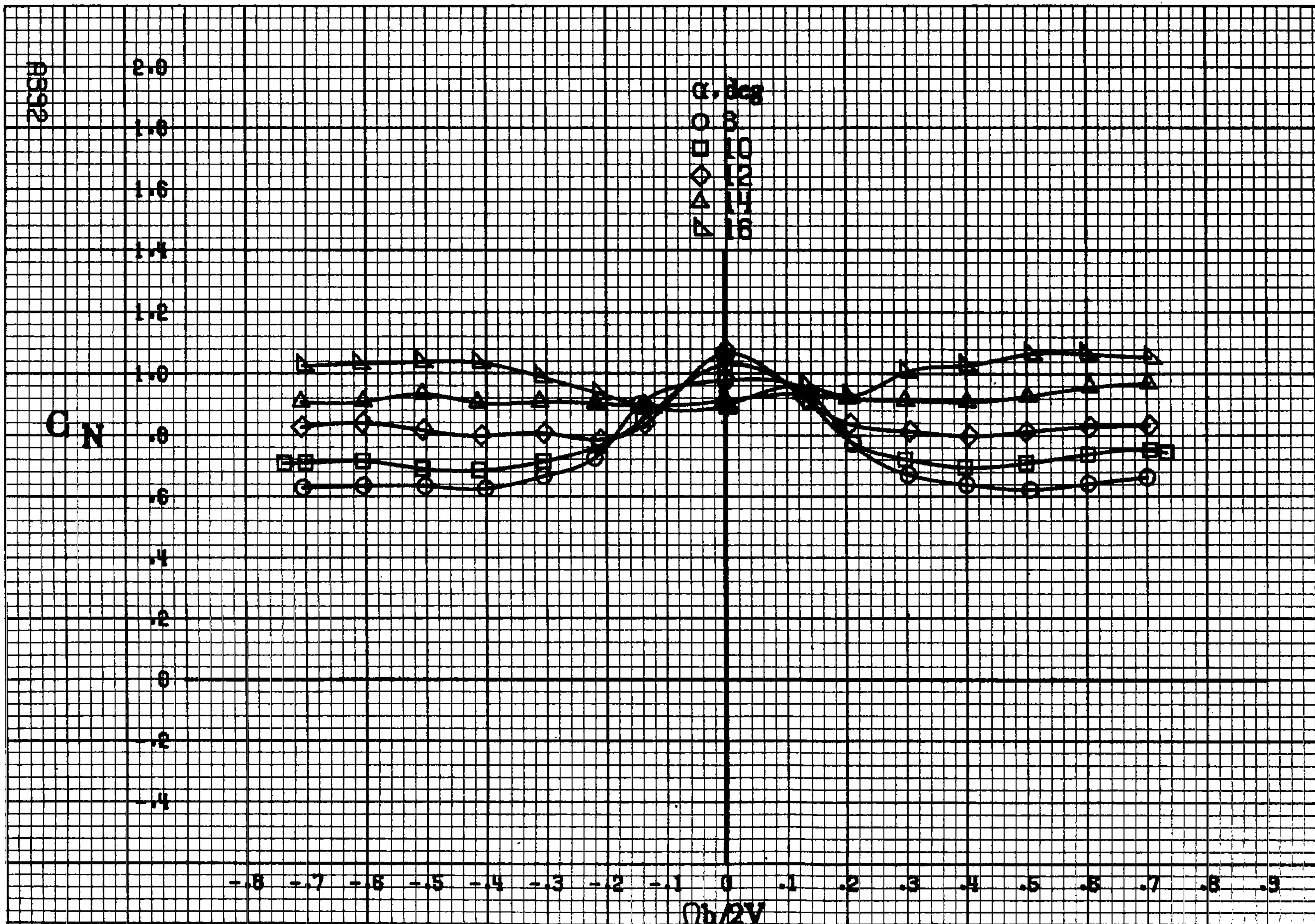

(a) α = 8 to 16 deg, SR = 182.9 cm (72 in.).

Figure A94.- Effect of rotation rate and angle of attack on normal-force coefficient for vertical tail off configuration. $\delta_e = 0°$, $\delta_a = 0°$, $\delta_r = 0°$, $\theta = 0°$.

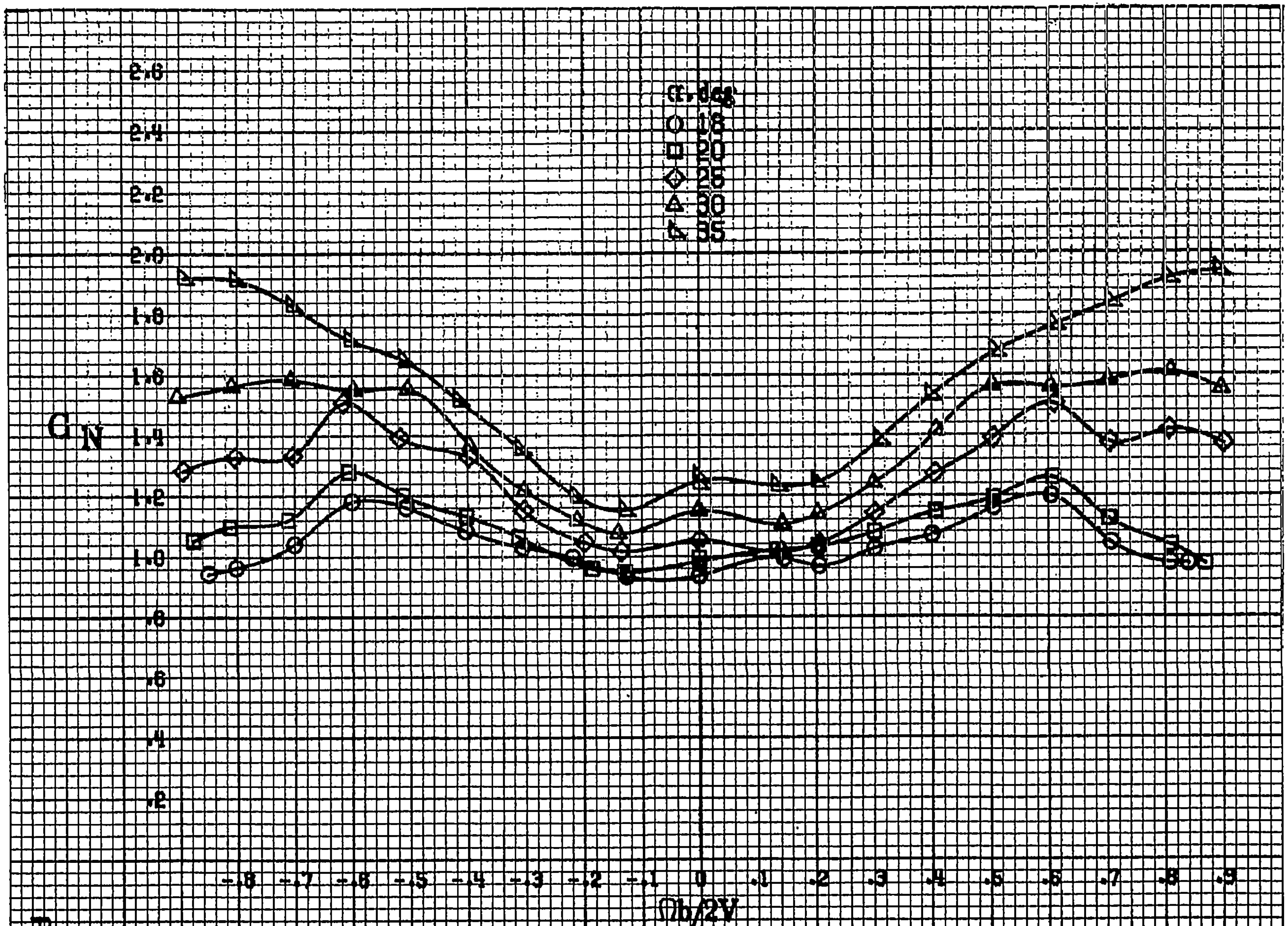

(b) α = 18 to 35 deg, SR = 182.9 cm (72 in).

Figure A94.-Continued.

A333

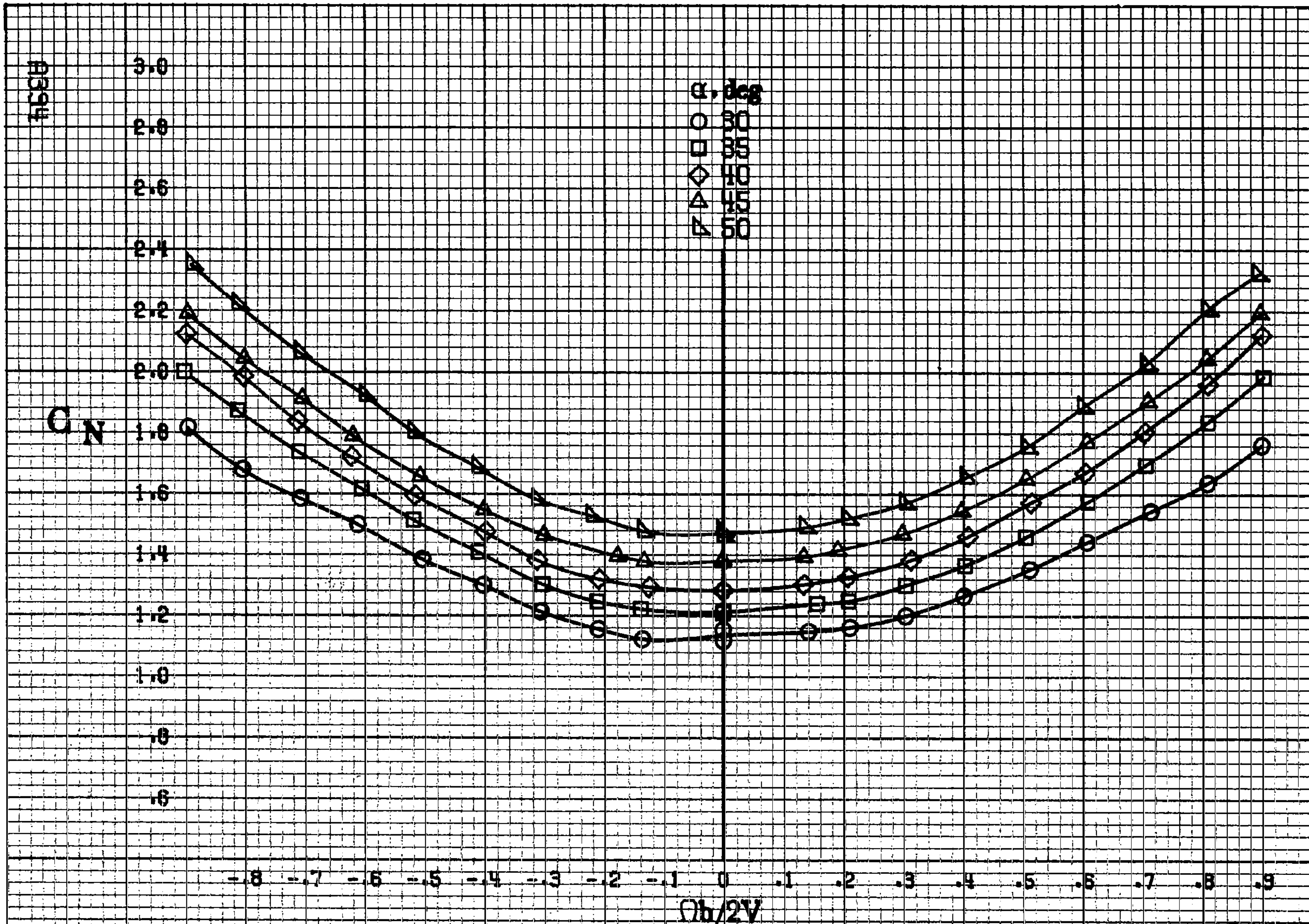

(c) $\alpha = 30$ to 50 deg, SR = 0.

Figure A94.- Continued.

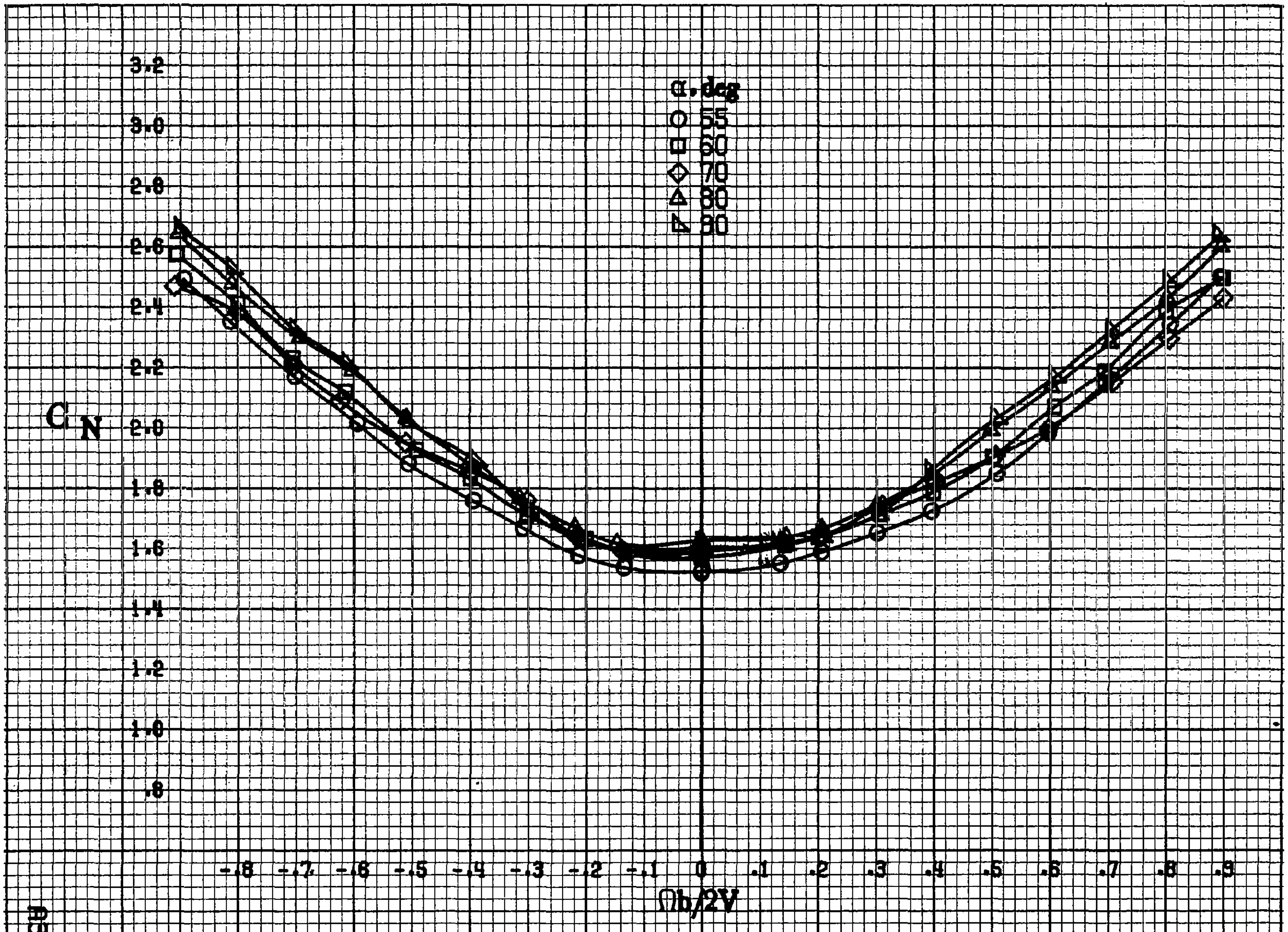

(d) α=55 to 90 deg, SR=0.

Figure A94.-Concluded.

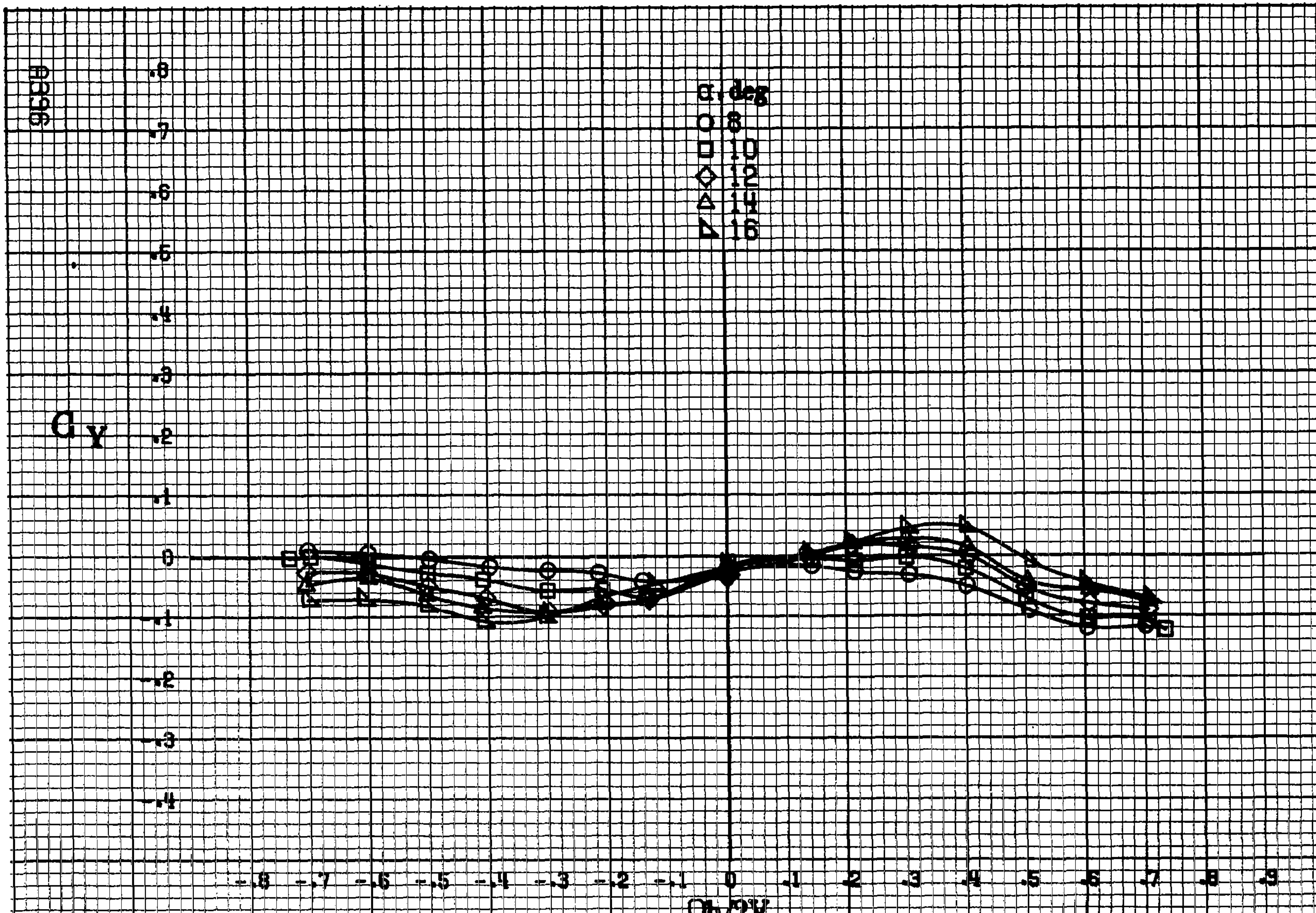

(a) $\alpha = 8$ to 16 deg, SR = 182.9 cm (72 in.).

Figure A96.- Effect of rotation rate and angle of attack on side-force coefficient for vertical tail off configuration. $\delta_e = 0°$, $\delta_a = 0°$, $\delta_r = 0°$, $\beta = 0°$.

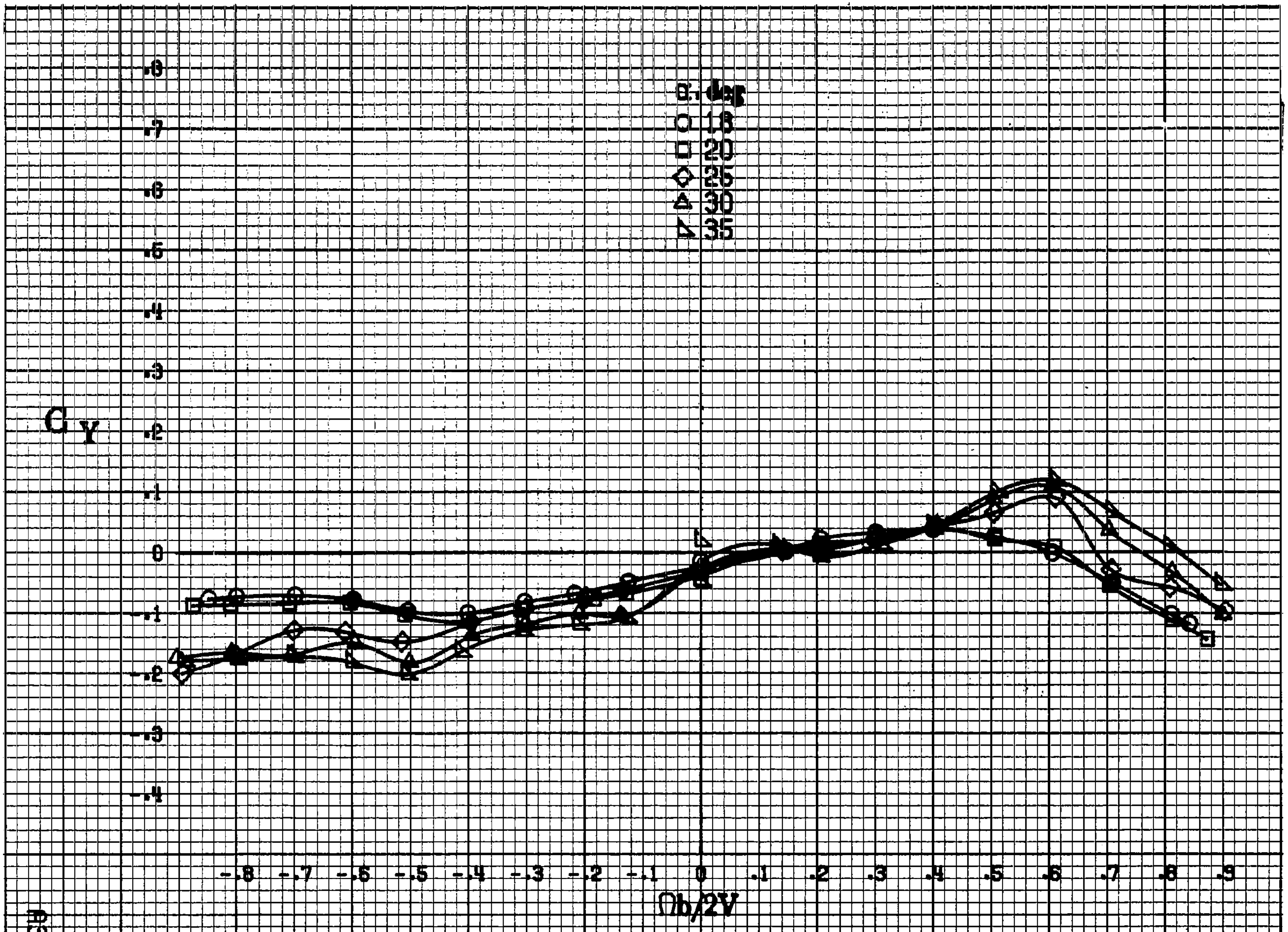

(b) α = 18 to 35 deg, SR = 182.9 cm (72 in).

Figure A95.-Continued.

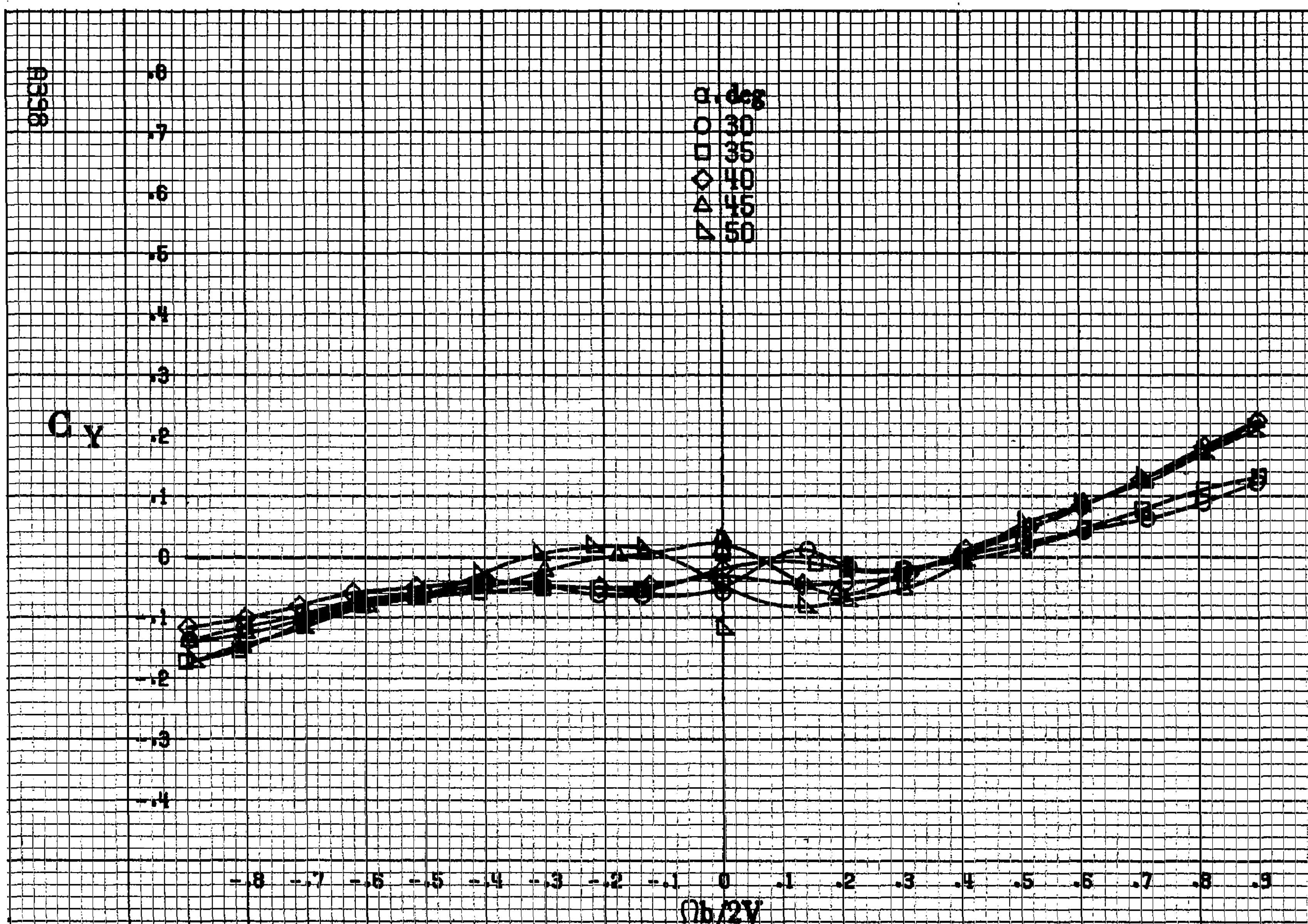

(c) α = 30 to 50 deg, SR = 0.
Figure A95.-Continued.

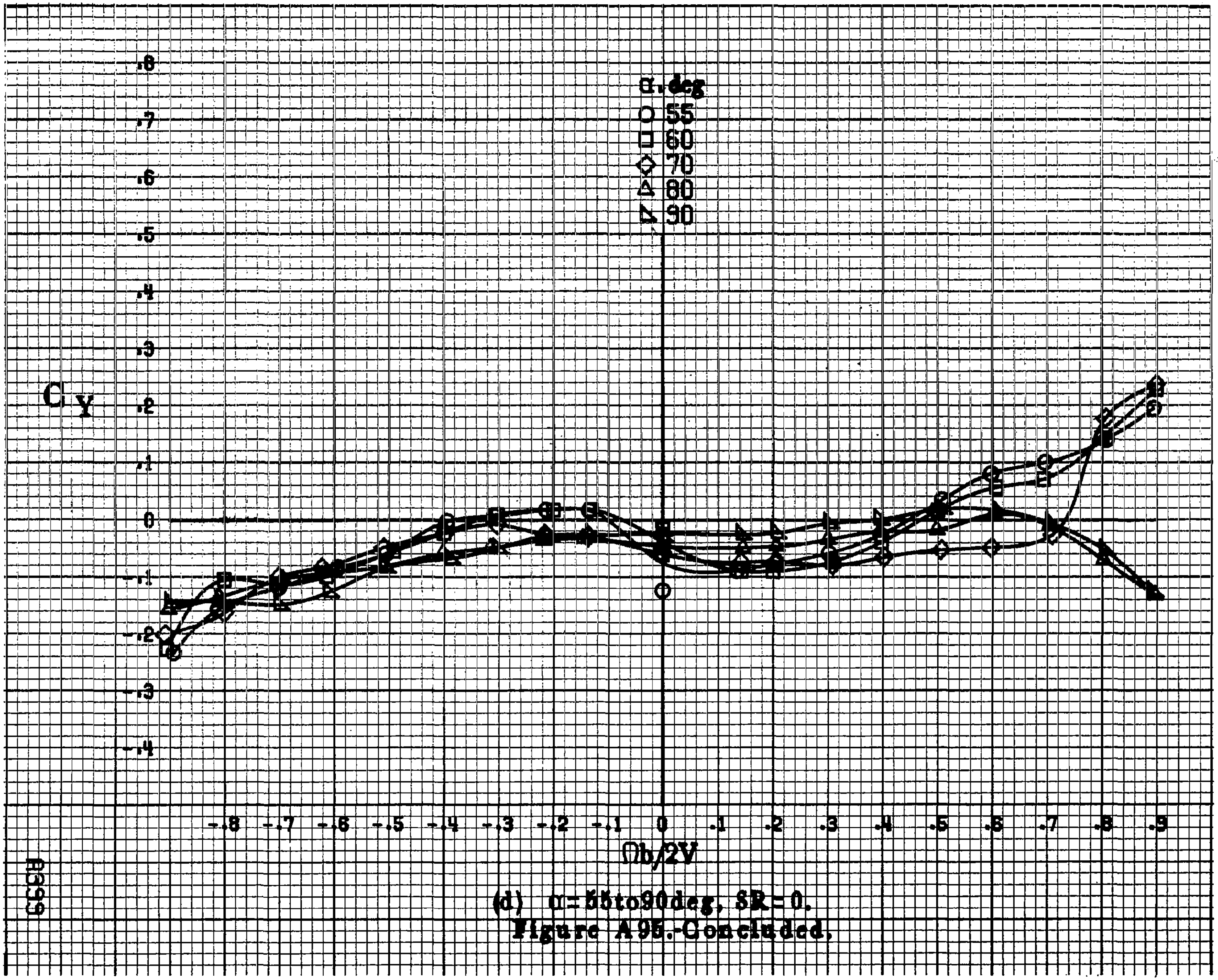

(d) α = 55 to 90 deg, SR = 0.
Figure A95.-Concluded.

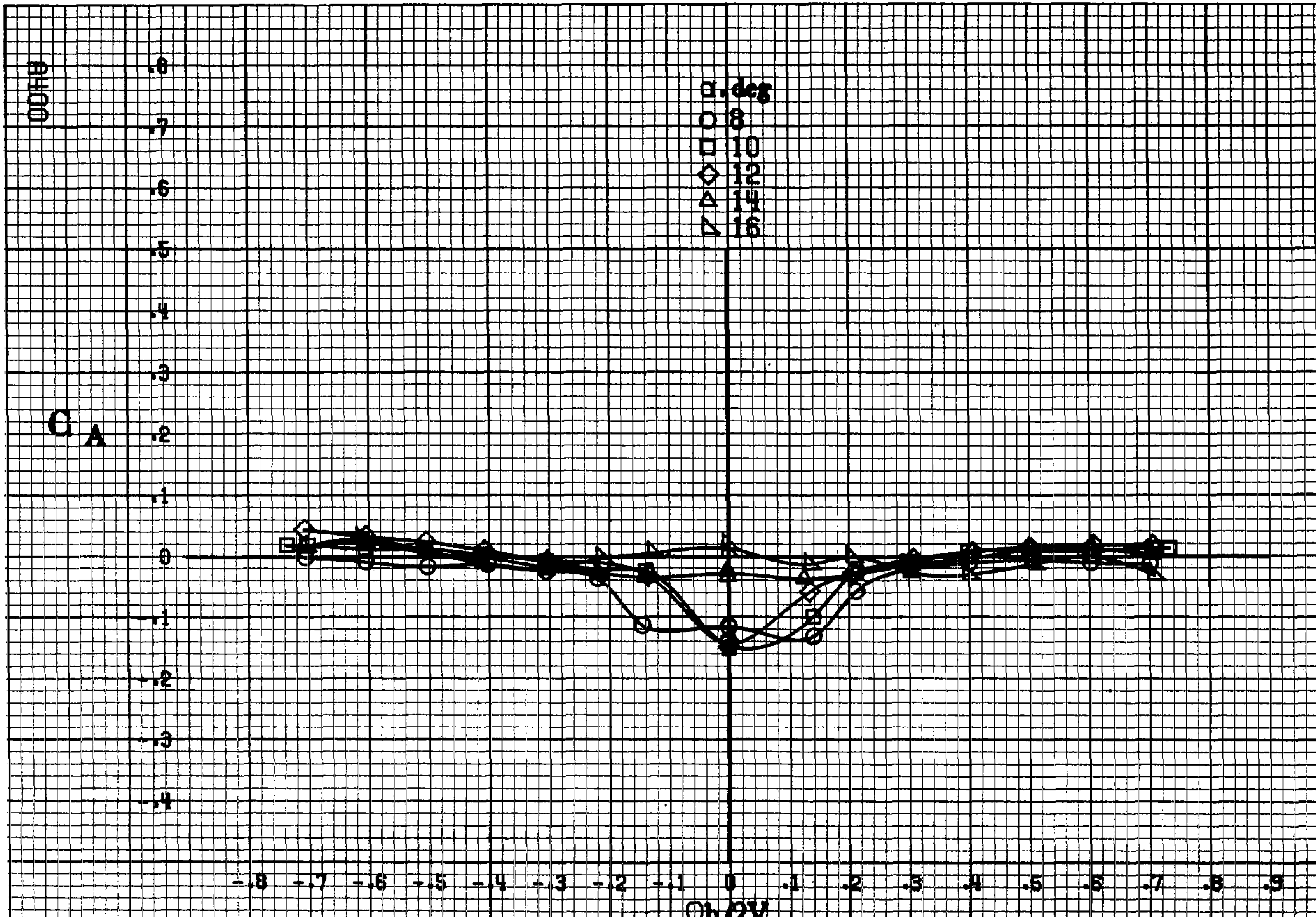

(a) $\alpha = 8$ to 16 deg, SR = 182.9 cm (72 in).

Figure A96.- Effect of rotation rate and angle of attack on axial-force coefficient for vertical tail off configuration. $\delta_e = 0°$, $\delta_a = 0°$, $\delta_r = 0°$, $\beta = 0°$.

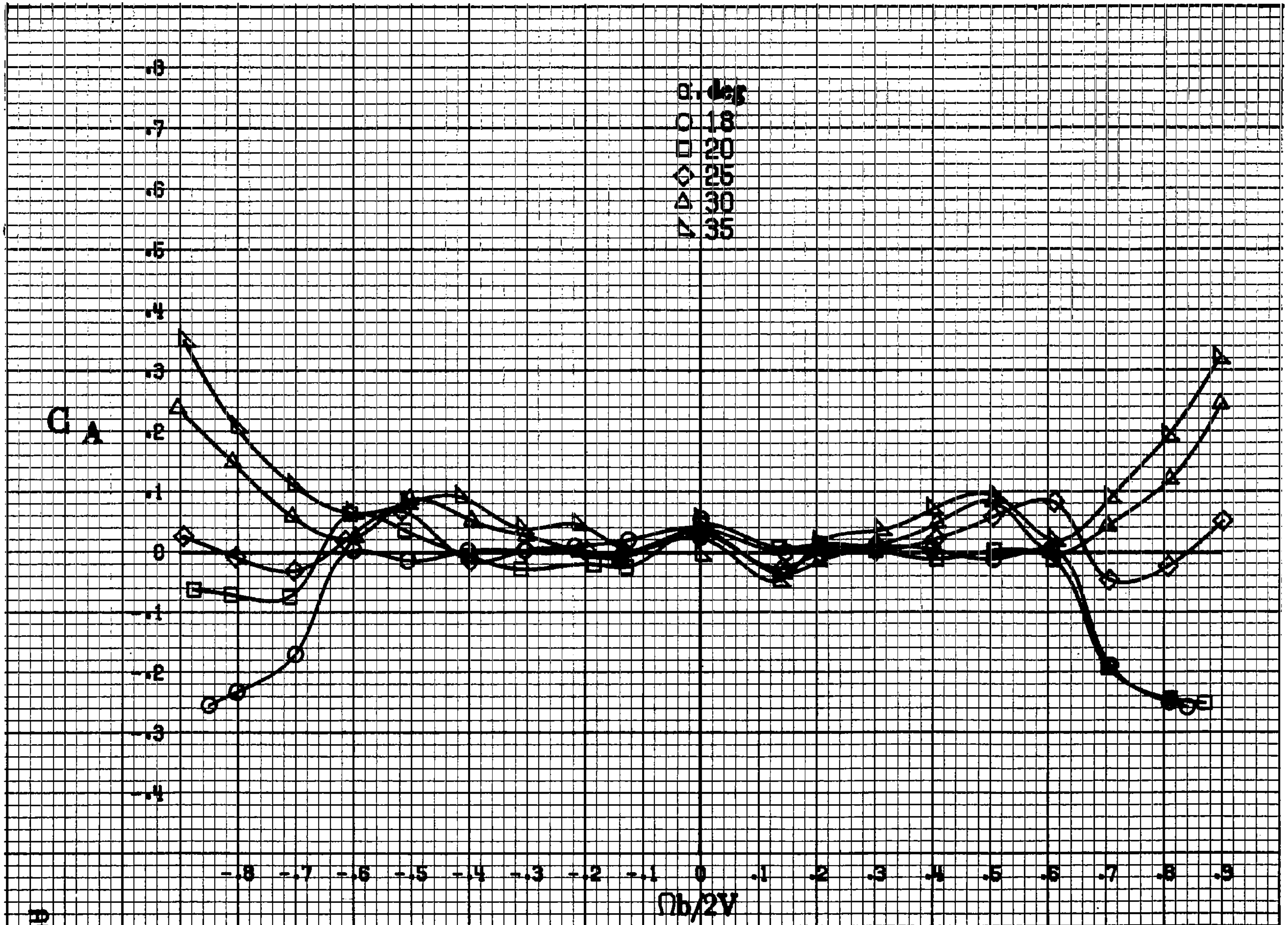

(b) α = 18 to 35 deg, SR = 182.9 cm (72 in).

Figure A96.-Continued.

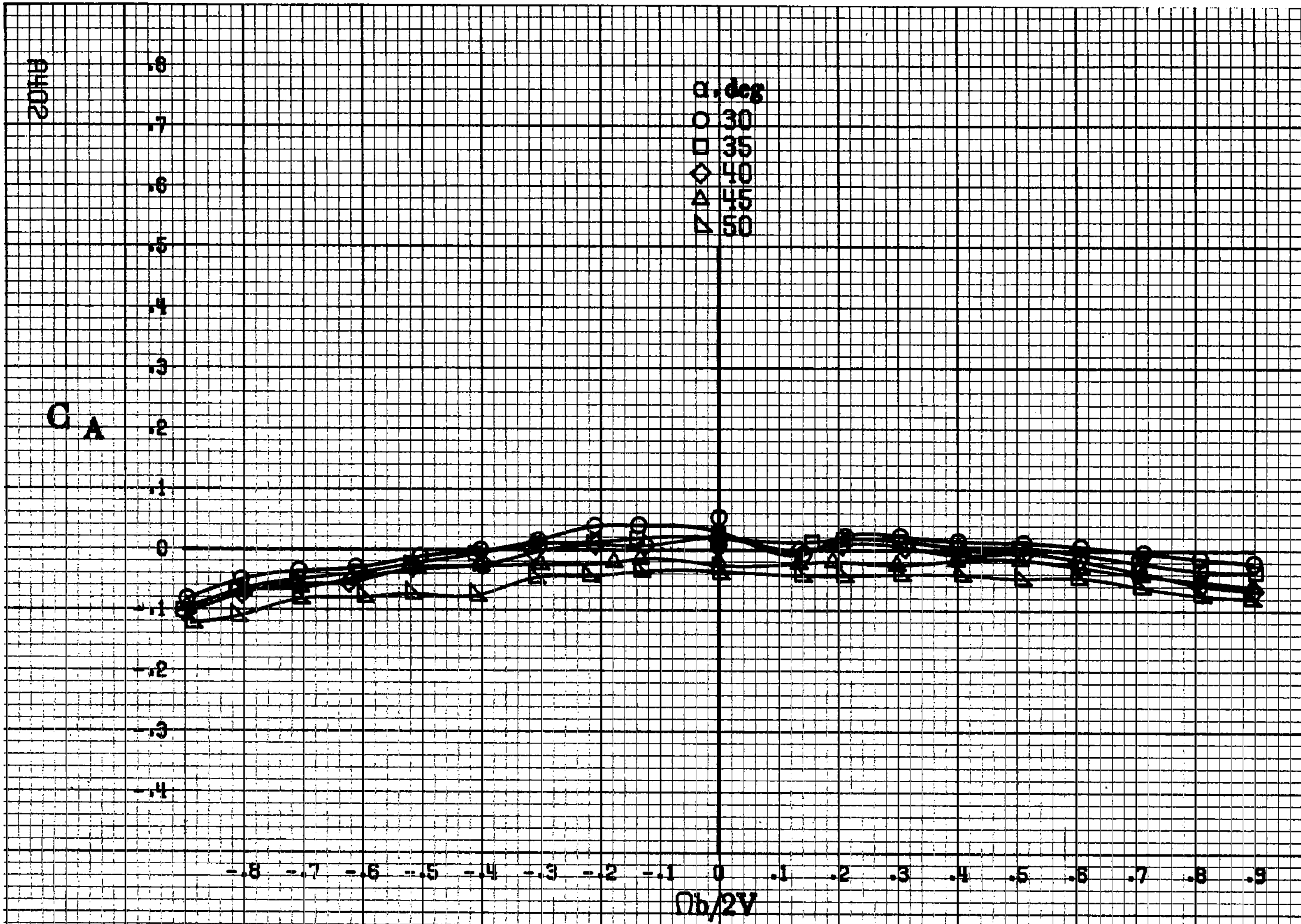

(c) α = 30 to 50 deg, SR = 0.
Figure A96.-Continued.

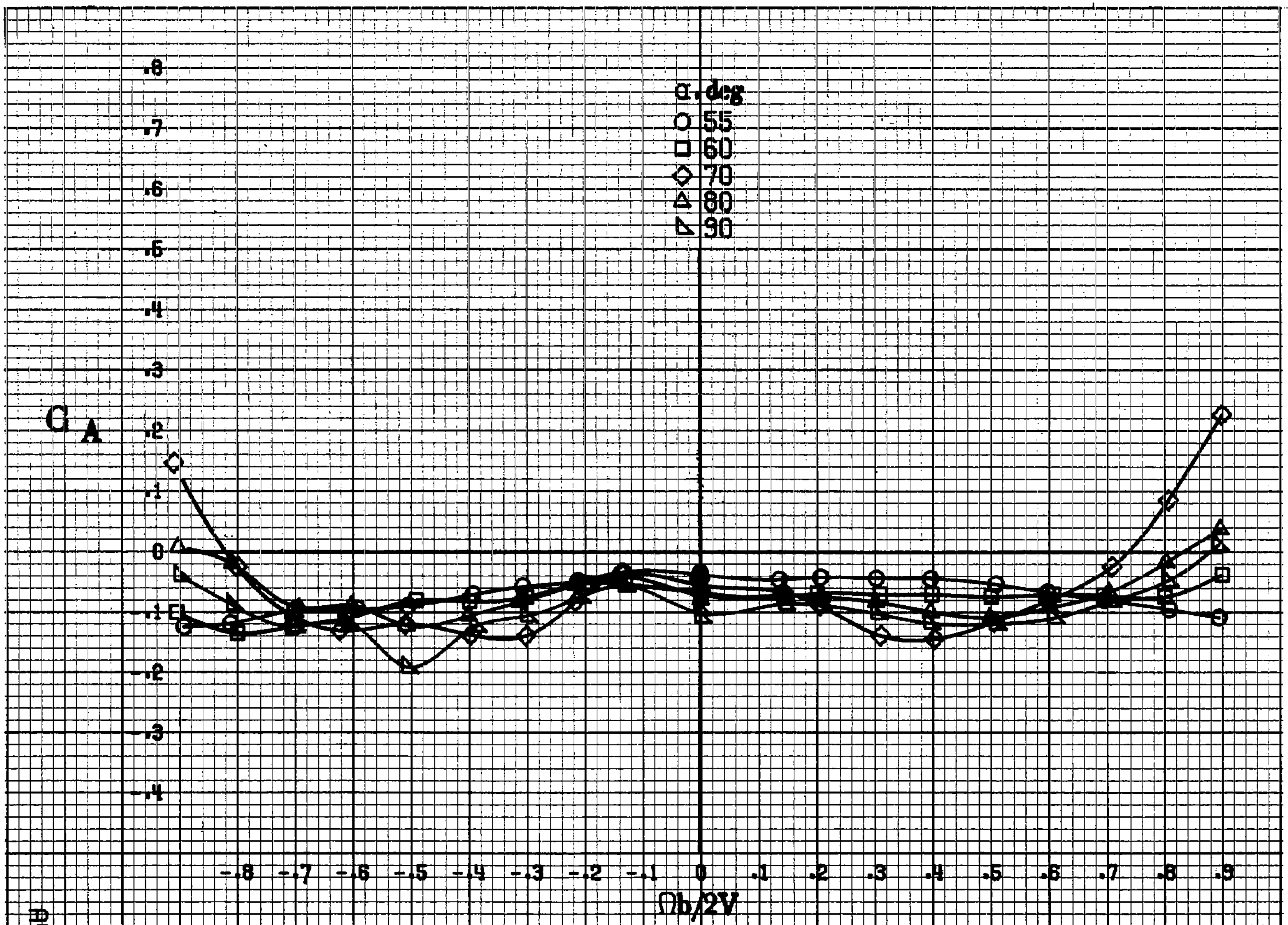

(d) α = 55 to 90 deg, SR = 0.

Figure A96.-Concluded.

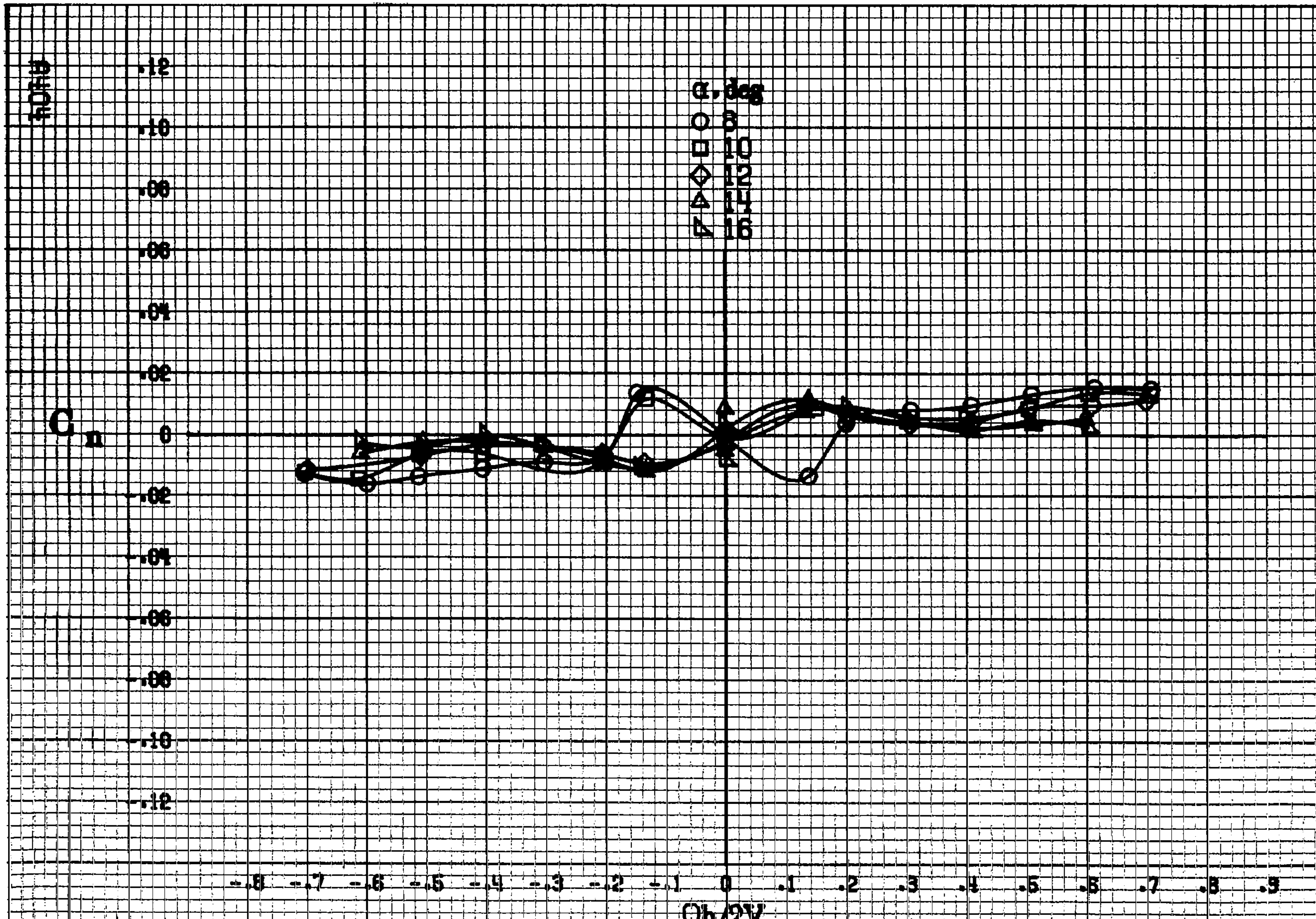

(a) α = 8 to 16 deg, SR = 182.9 cm (72 in).

Figure A97.-Effect of rotation rate and angle of attack on yawing-moment coefficient for horizontal and vertical tails off configuration. $\delta_e = 0°$, $\delta_a = 0°$, $\delta_r = 0°$, $\beta = 0°$.

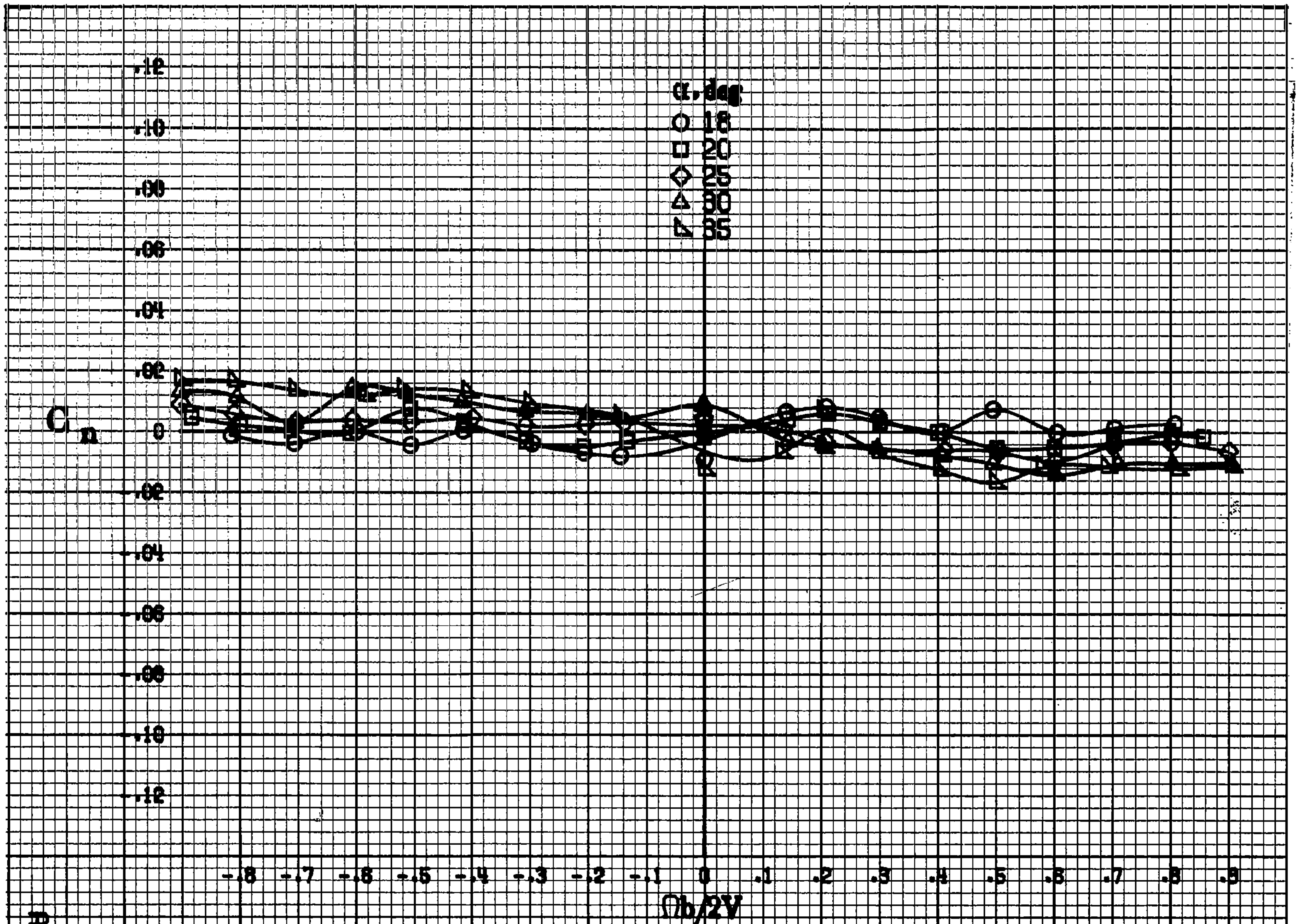

(b) α = 18 to 35 deg, SR = 182.9 cm (72 in).

Figure A97.-Continued.

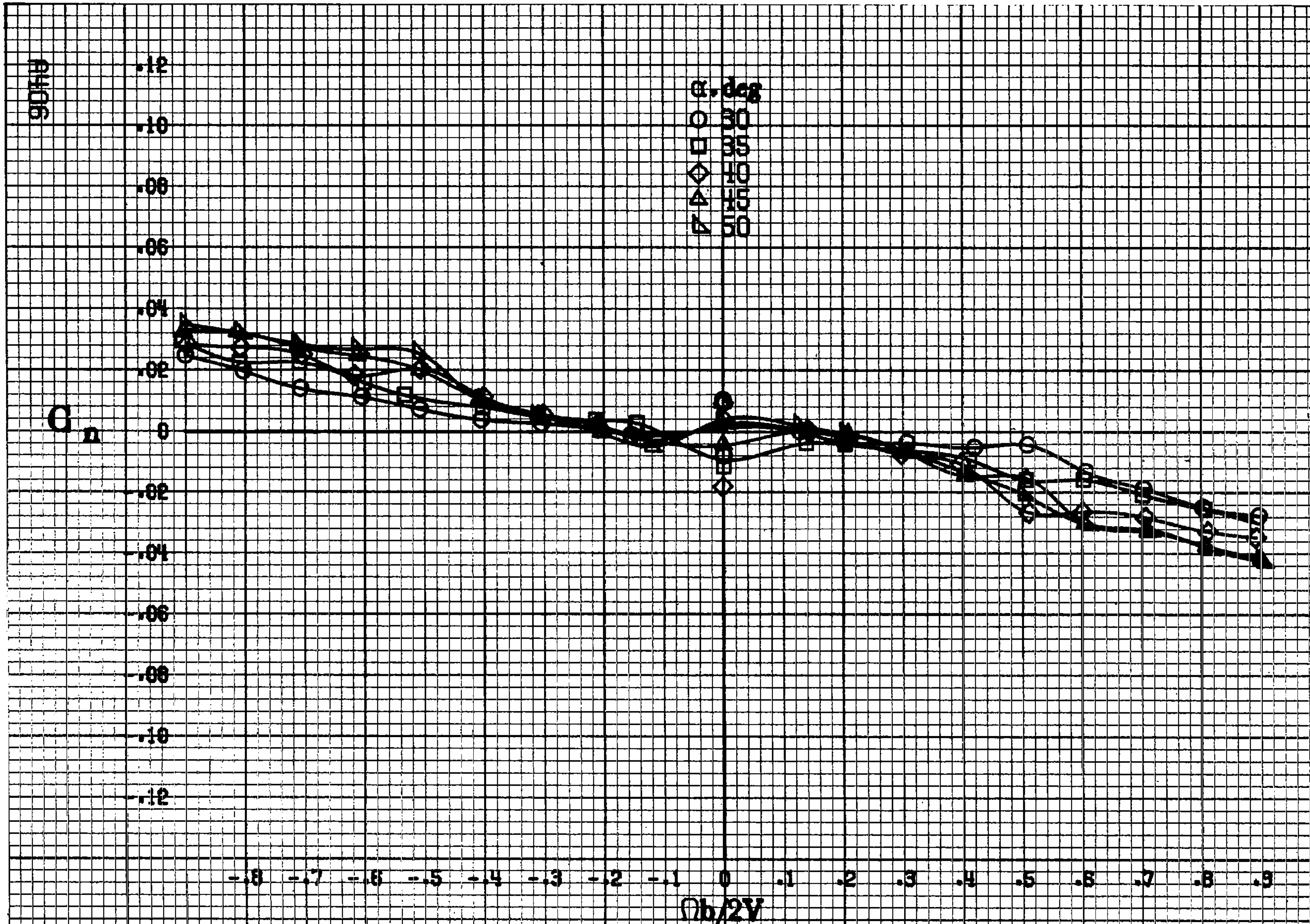

(c) $\alpha = 30$ to 50 deg, SR = 0.

Figure A97.-Continued.

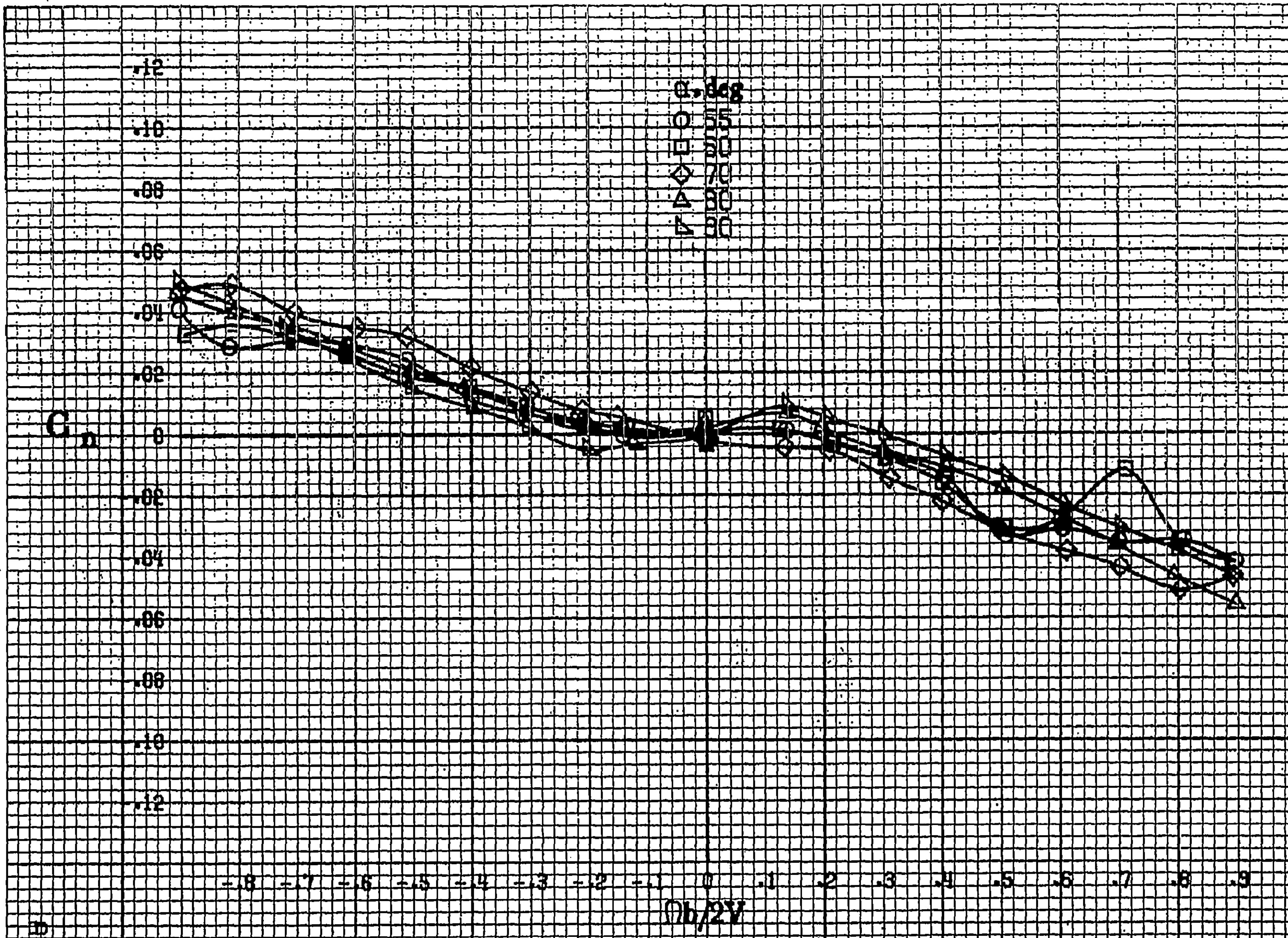

(d) α = 55 to 90 deg, SR = 0.

Figure A97.-Concluded.

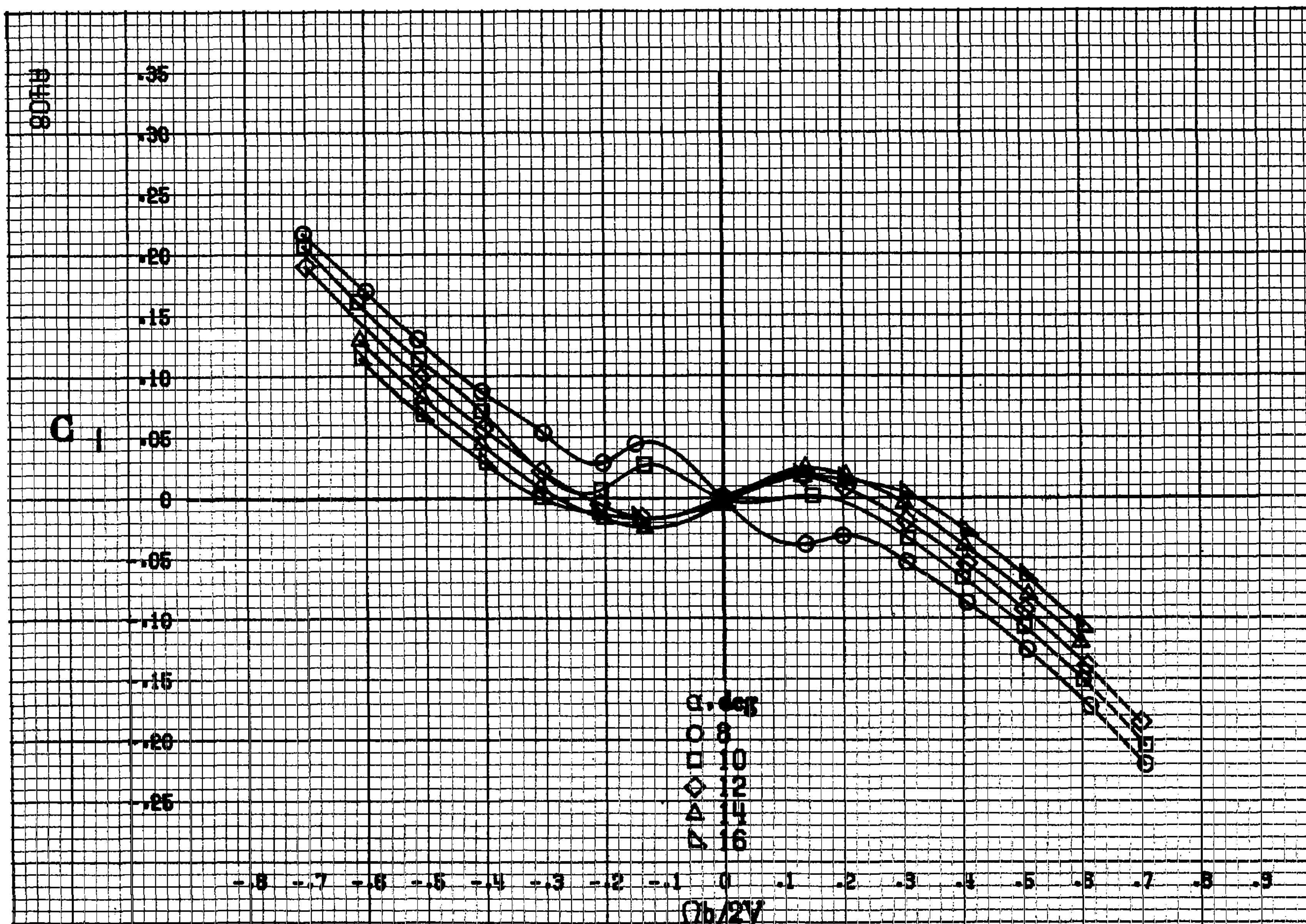

(a) α = 8 to 16 deg, SR = 182.9 cm (72 in).

Figure A98.- Effect of rotation rate and angle of attack on rolling-moment coefficient for horizontal and vertical tails off configuration. $\delta_r = 0°$, $\delta_a = 0°$, $\delta_e = 0°$, $\beta = 0°$.

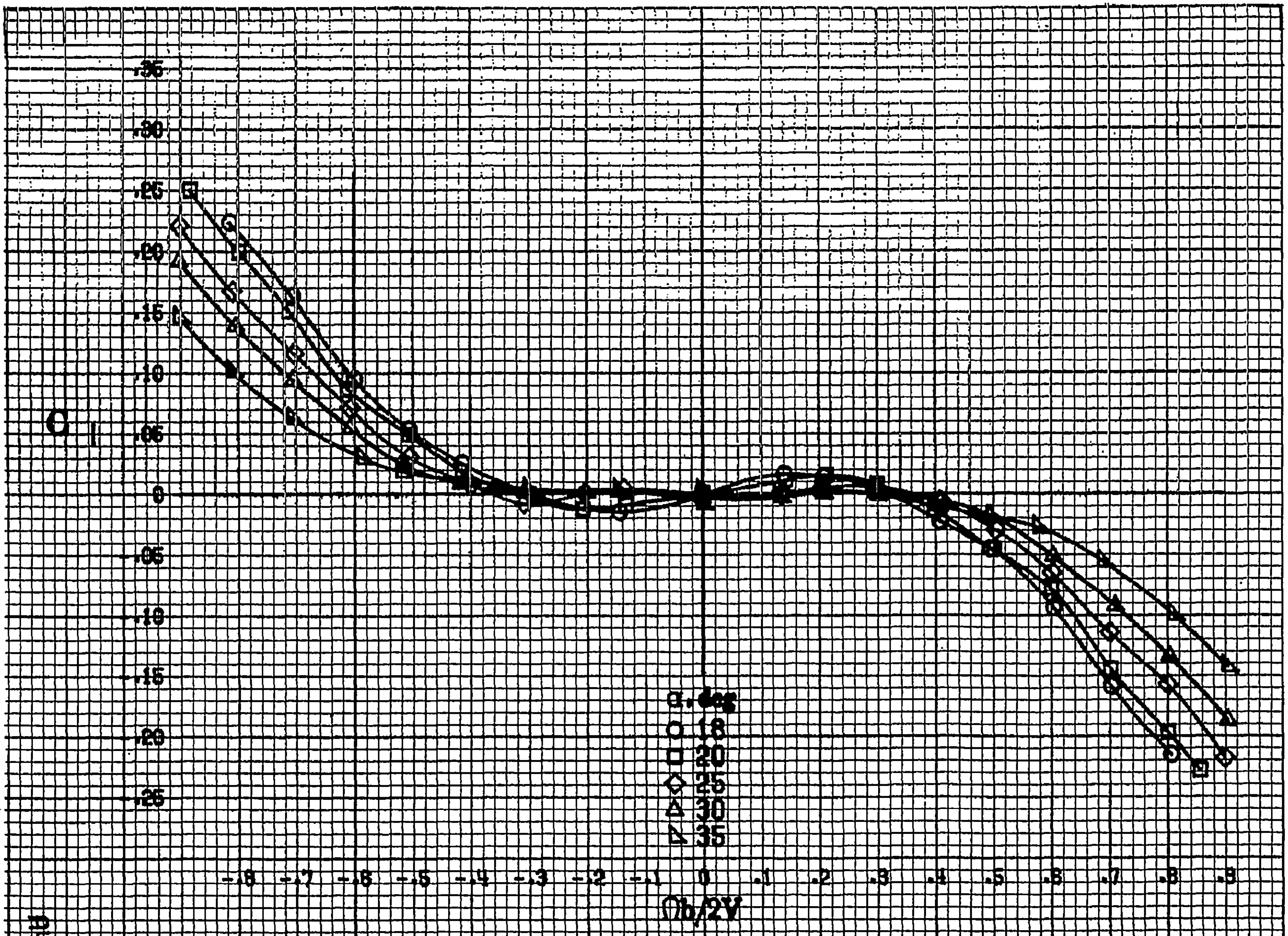

(b) α = 18 to 35 deg, SR = 182.9 cm (72 in).
Figure A98.-Continued.

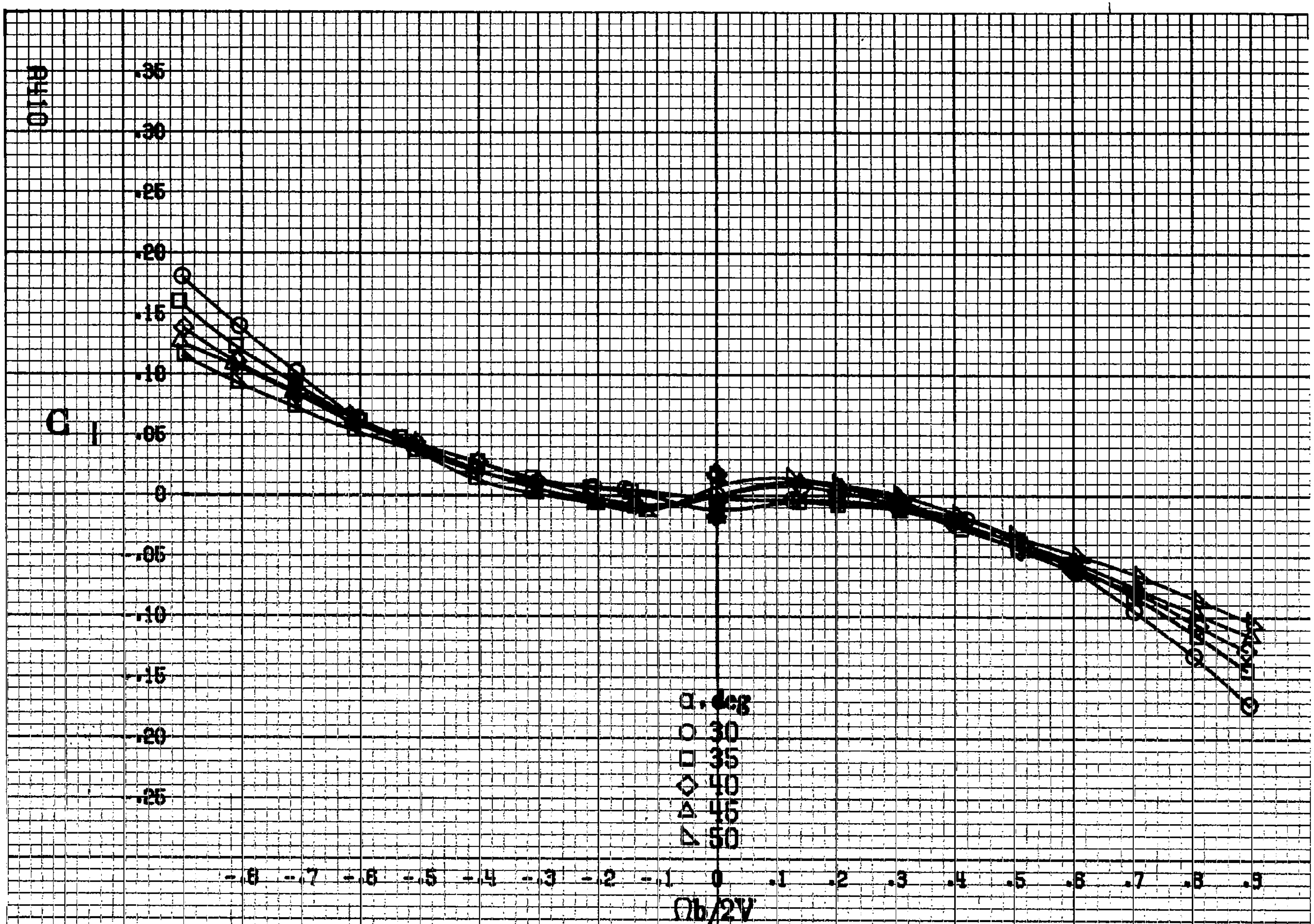

(c) α = 30 to 50 deg, SR = 0.

Figure A.98.-Continued.

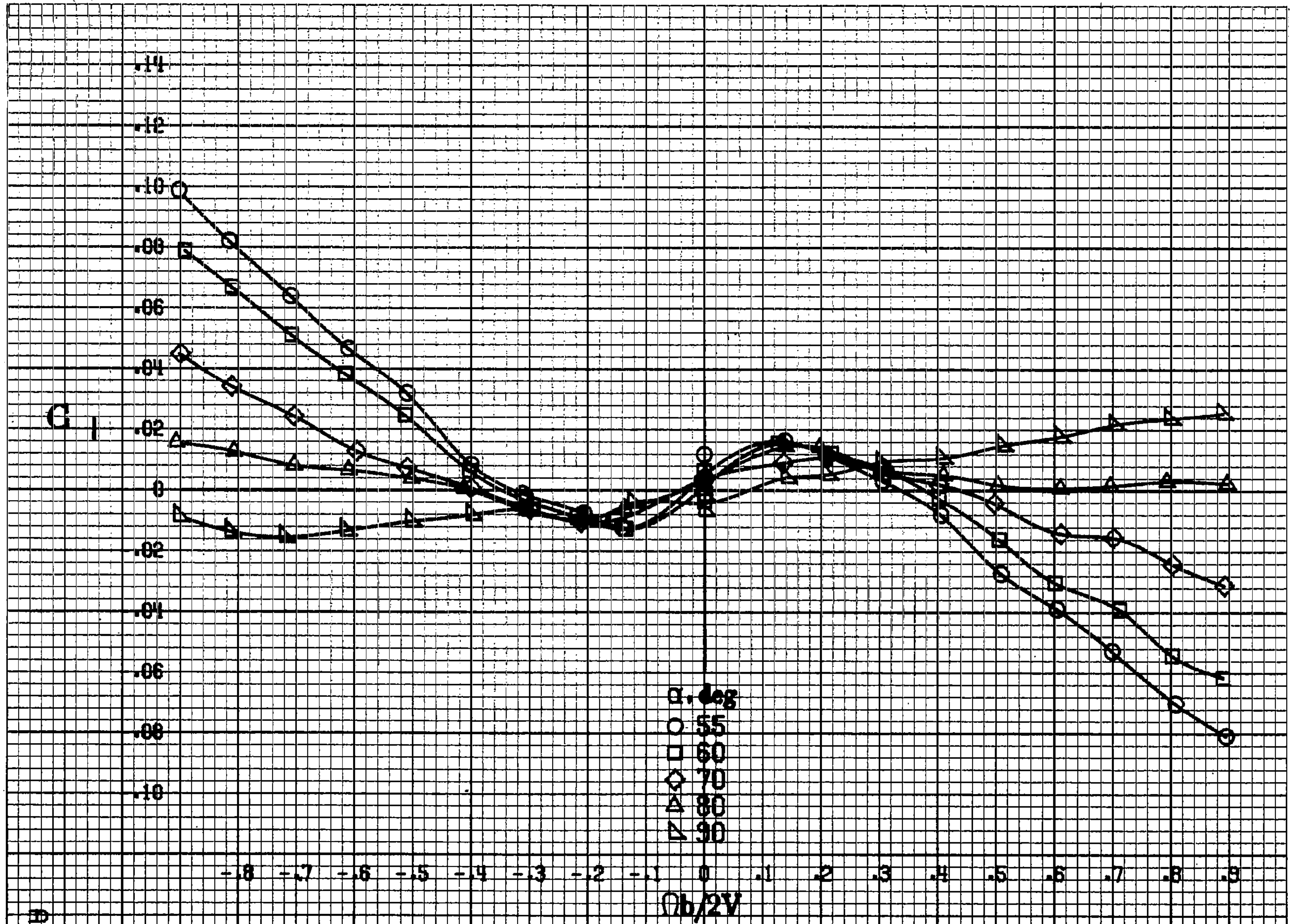

(d) α = 55 to 90 deg, SR = 0.
Figure A98.-Concluded.

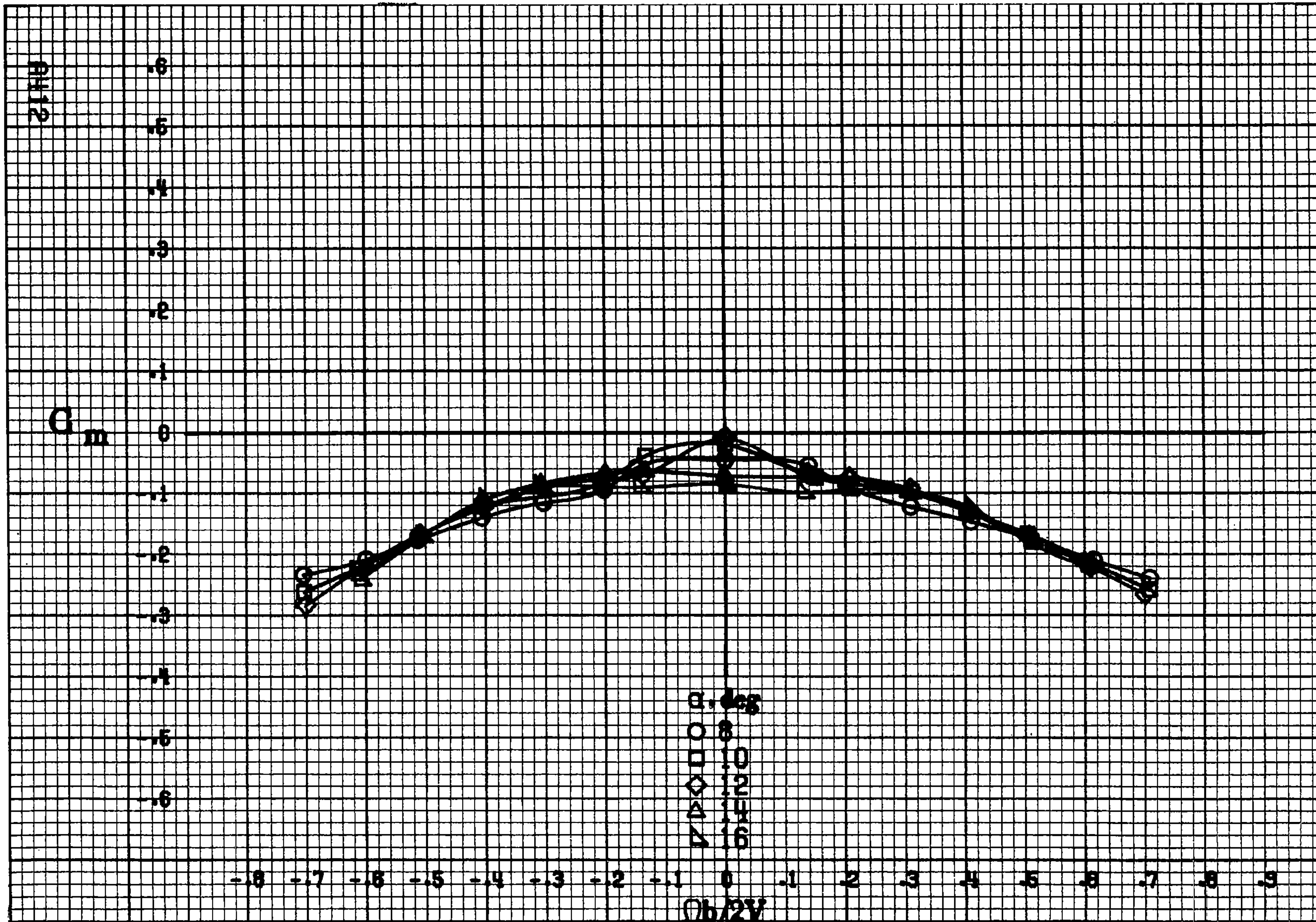

(a) $\alpha = 8$ to 16 deg, SR = 182.9 cm (72 in).

Figure A99.- Effect of rotation rate and angle of attack on pitching-moment coefficient for horizontal and vertical tails off configuration. $\delta_e = 0°$, $\delta_a = 0°$, $\delta_r = 0°$, $\beta = 0°$.

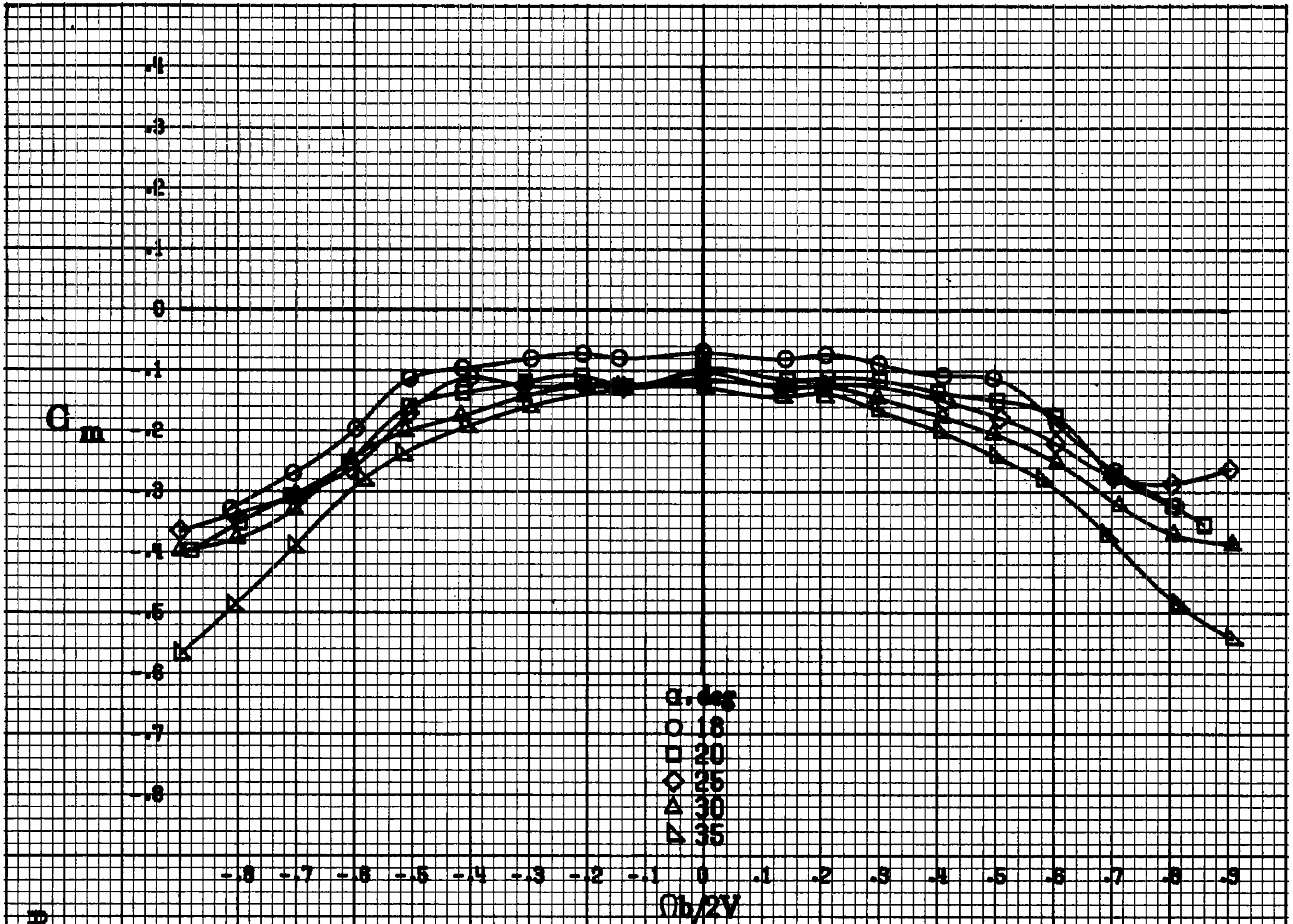

(b) α = 18 to 35 deg, SR = 182.9 cm (72 in).

Figure A99.-Continued.

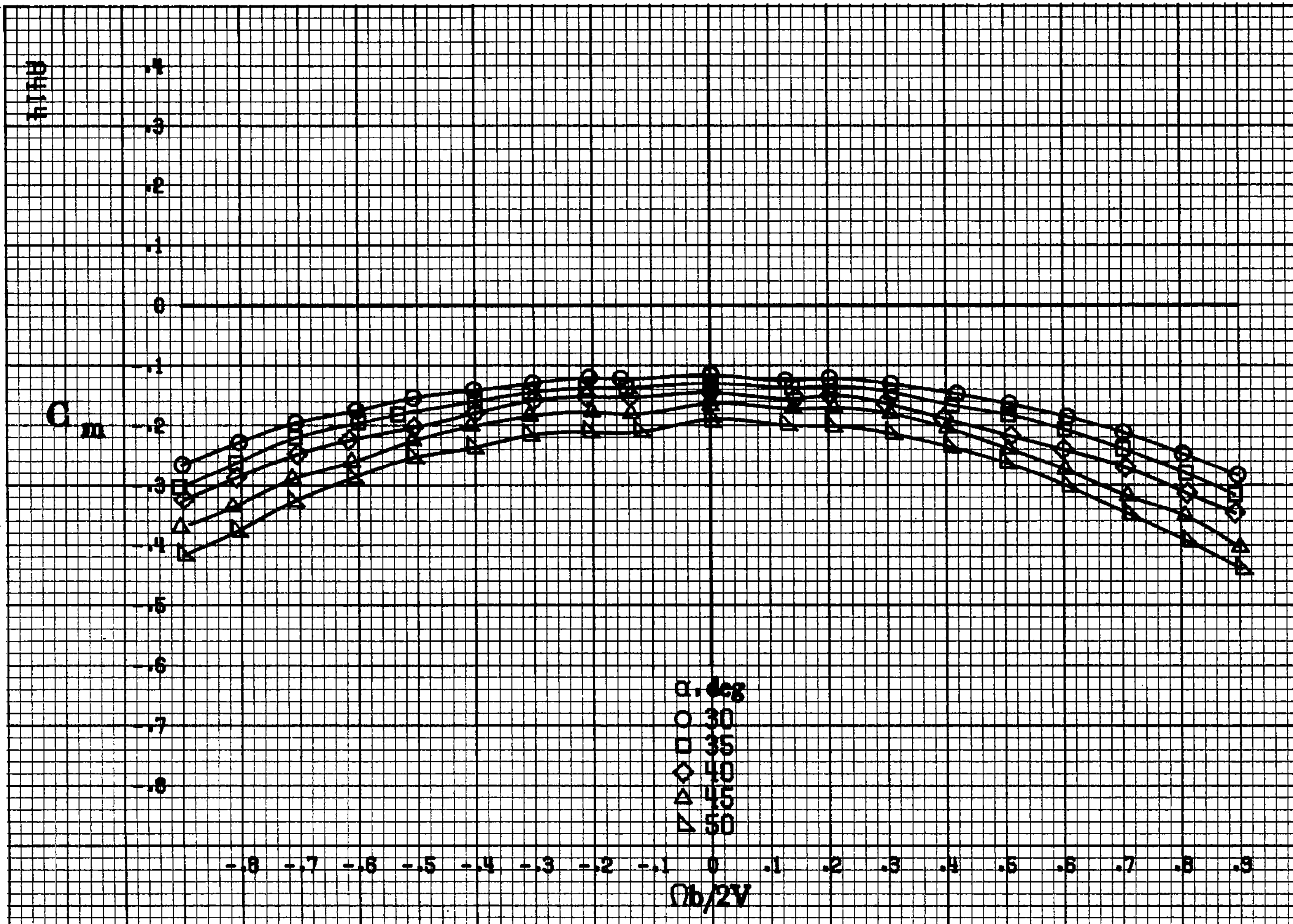

(c) α = 30 to 50 deg, SR = 0.

Figure A99.-Continued.

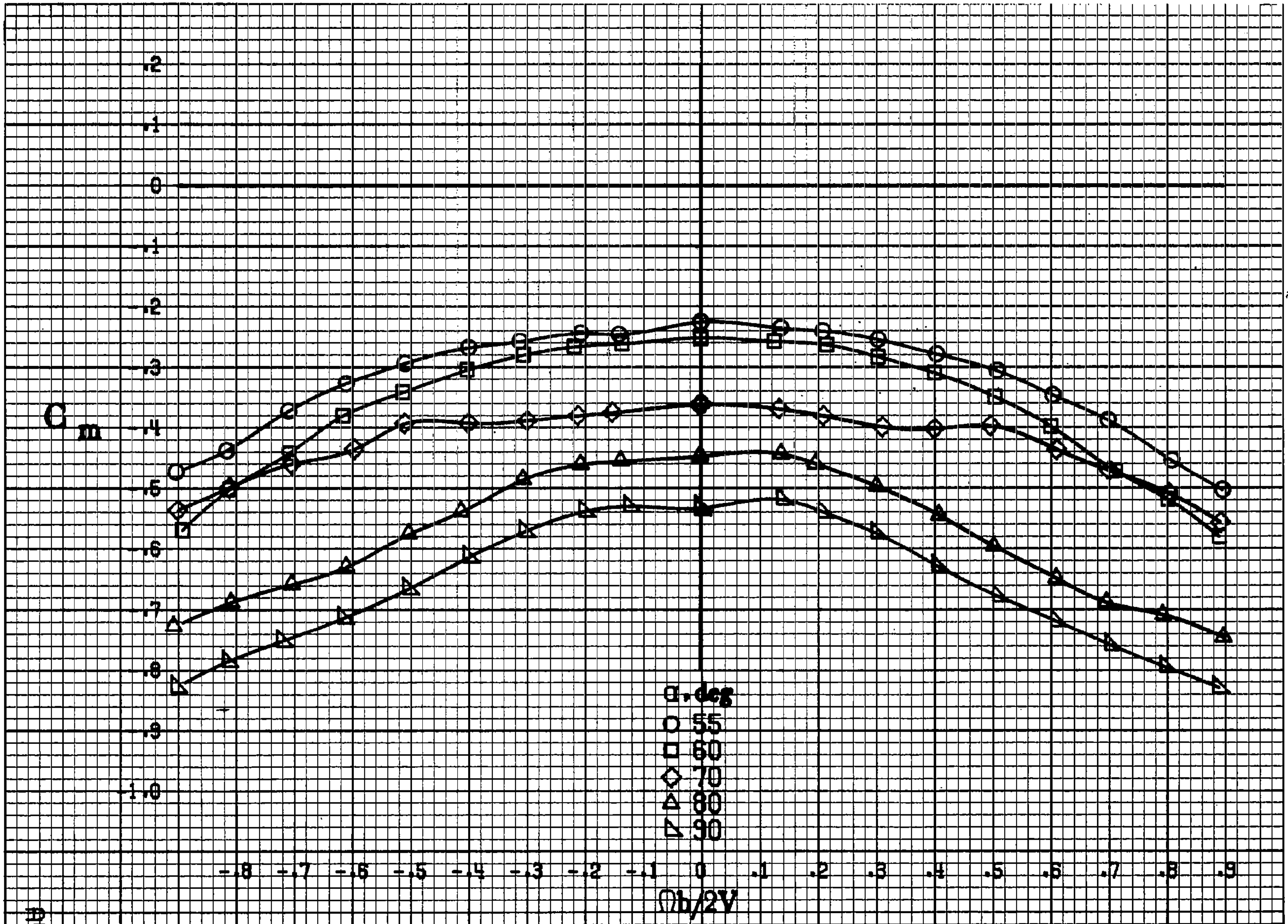

(d) α = 55 to 90 deg, SR = 0.
Figure A99.-Concluded.

A115

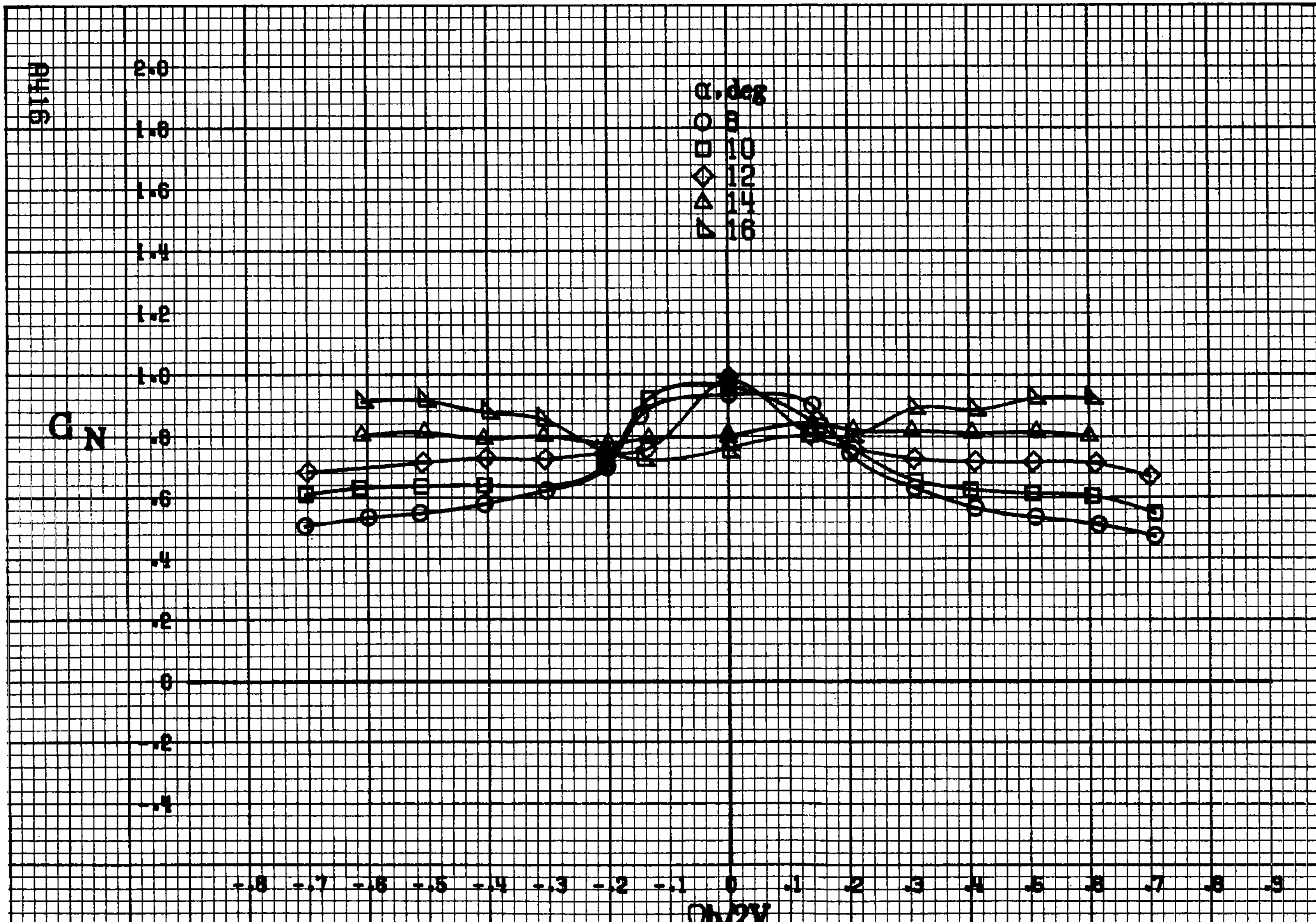

(a) α = 8 to 16 deg, SR = 182.9 cm (72 in).

Figure A100.- Effect of rotation rate and angle of attack on normal-force coefficient for horizontal and vertical tails off configuration. $\delta_e = 0°$, $\delta_a = 0°$, $\delta_r = 0°$, $\beta = 0°$.

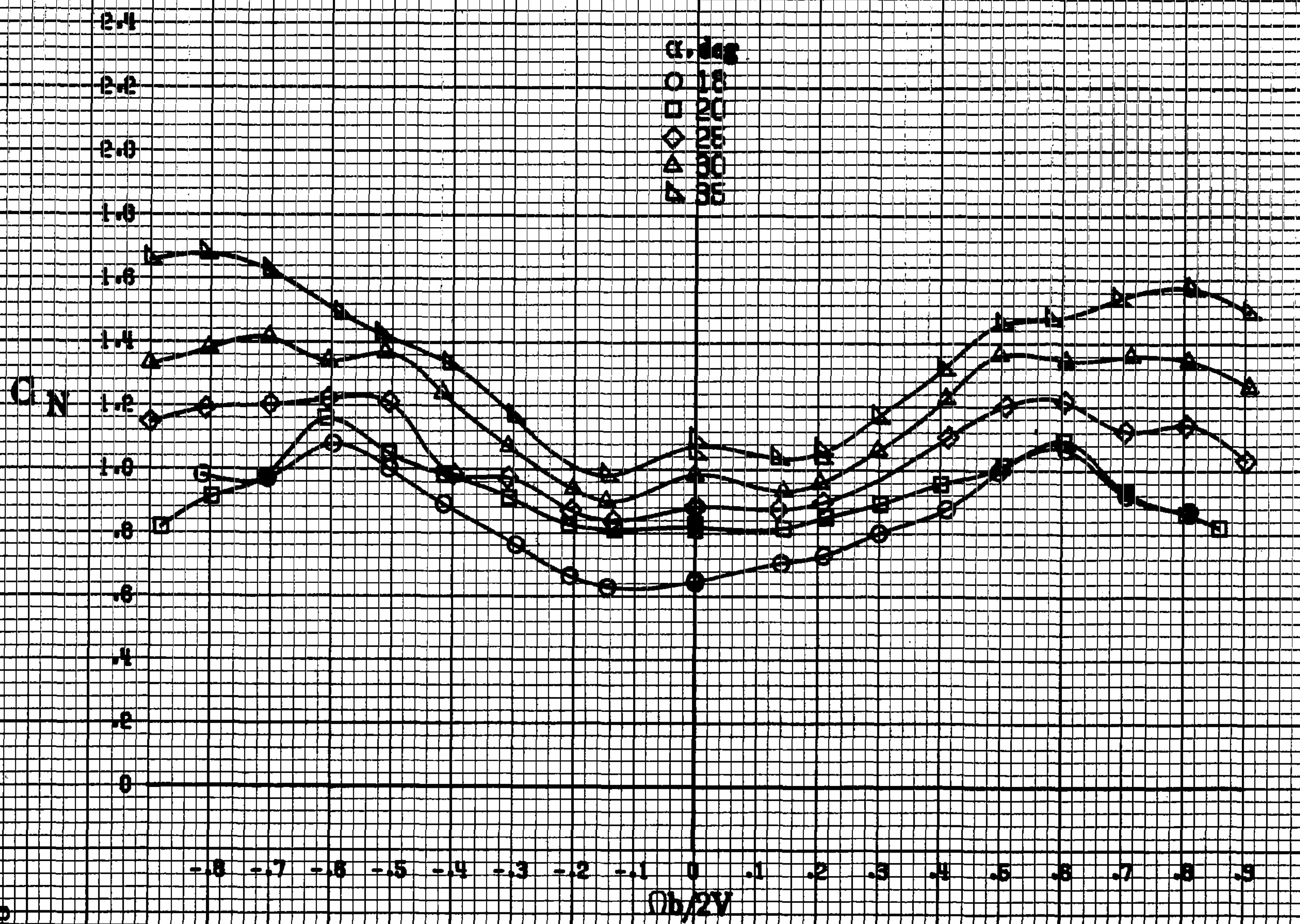

(b) α = 18 to 35 deg, SR = 182.9 cm (72 in).

Figure A100.-Continued.

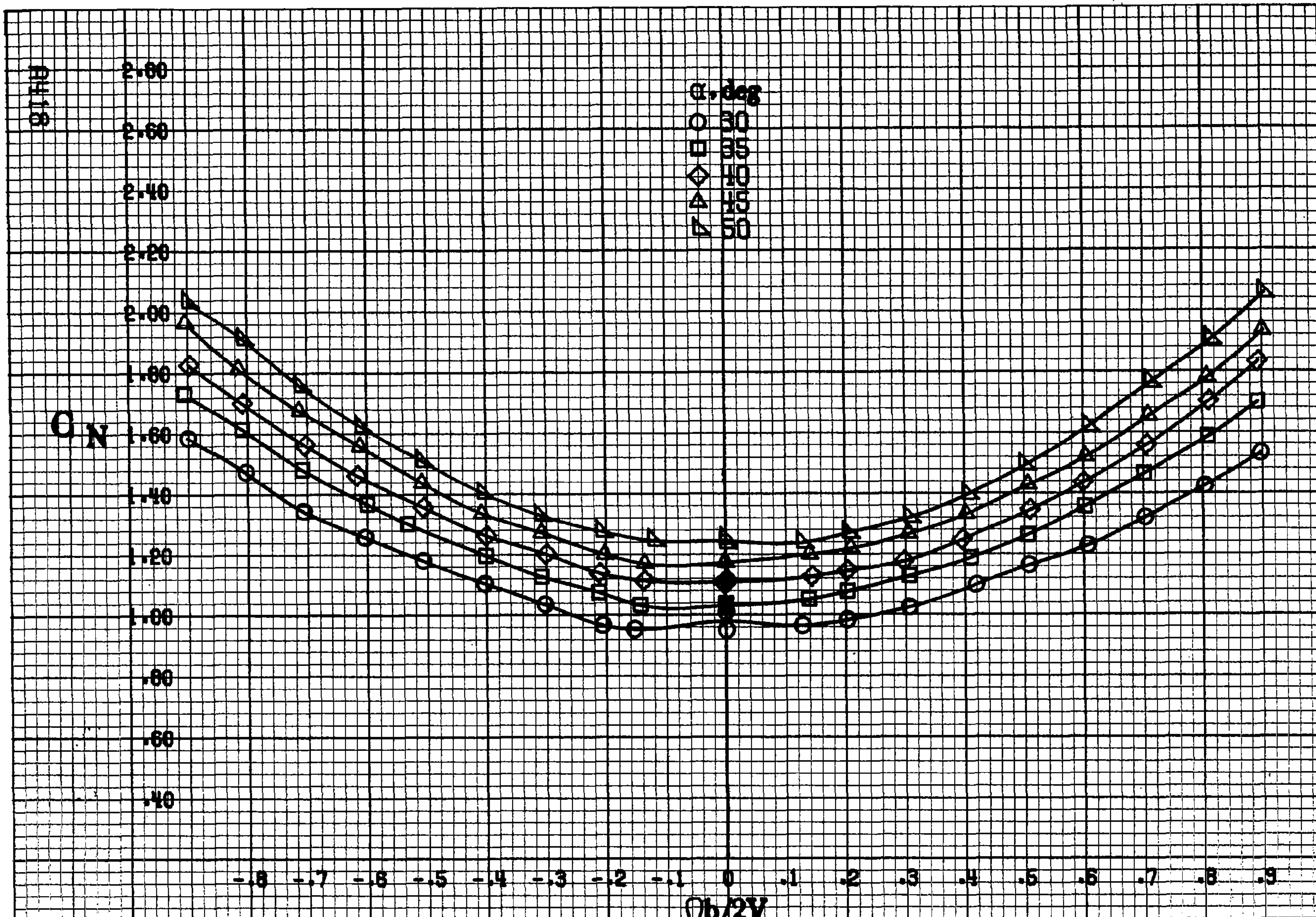

(c) α = 30 to 50 deg, SR = 0.
Figure A100.-Continued.

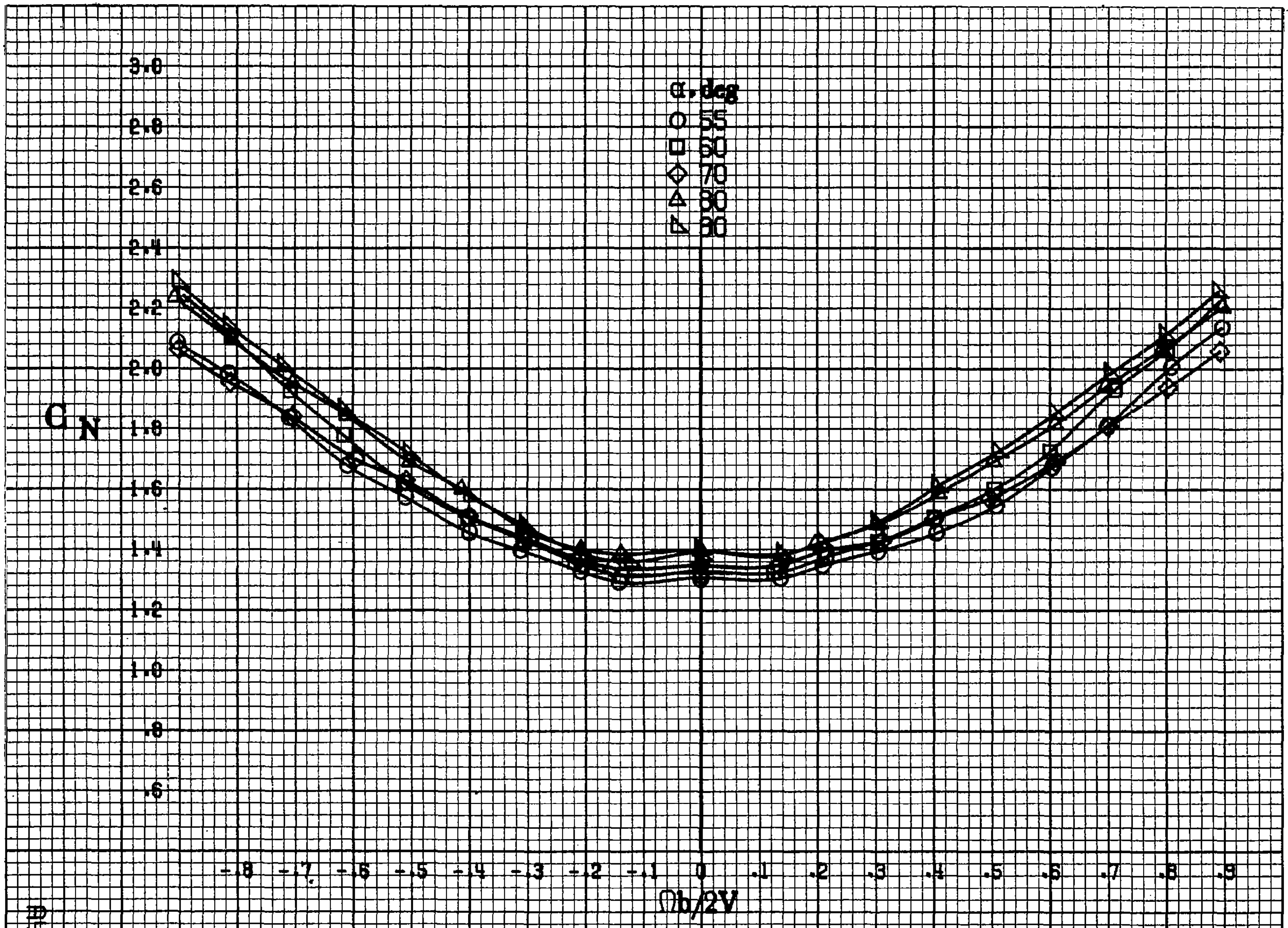

(d) α = 55 to 90 deg, SR = 0.

Figure A100.-Concluded.

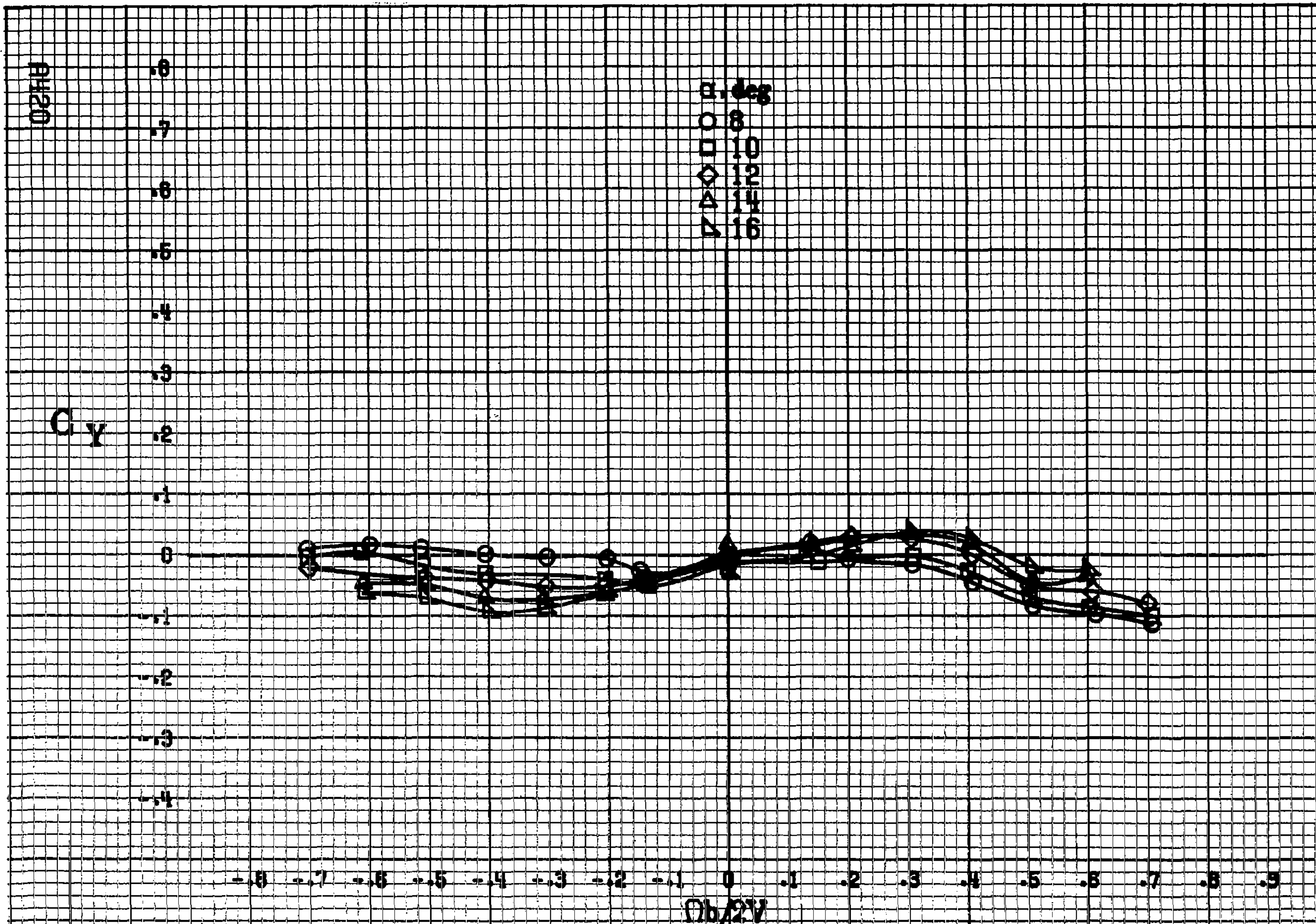

(a) α = 8 to 16 deg, SR = 182.9 cm (72 in).

Figure A101.-Effect of rotation rate and angle of attack on side-force coefficient for horizontal and vertical tails off configuration. $\delta_e = 0^\circ$, $\delta_a = 0^\circ$, $\delta_r = 0^\circ$. $\beta = 0^\circ$.

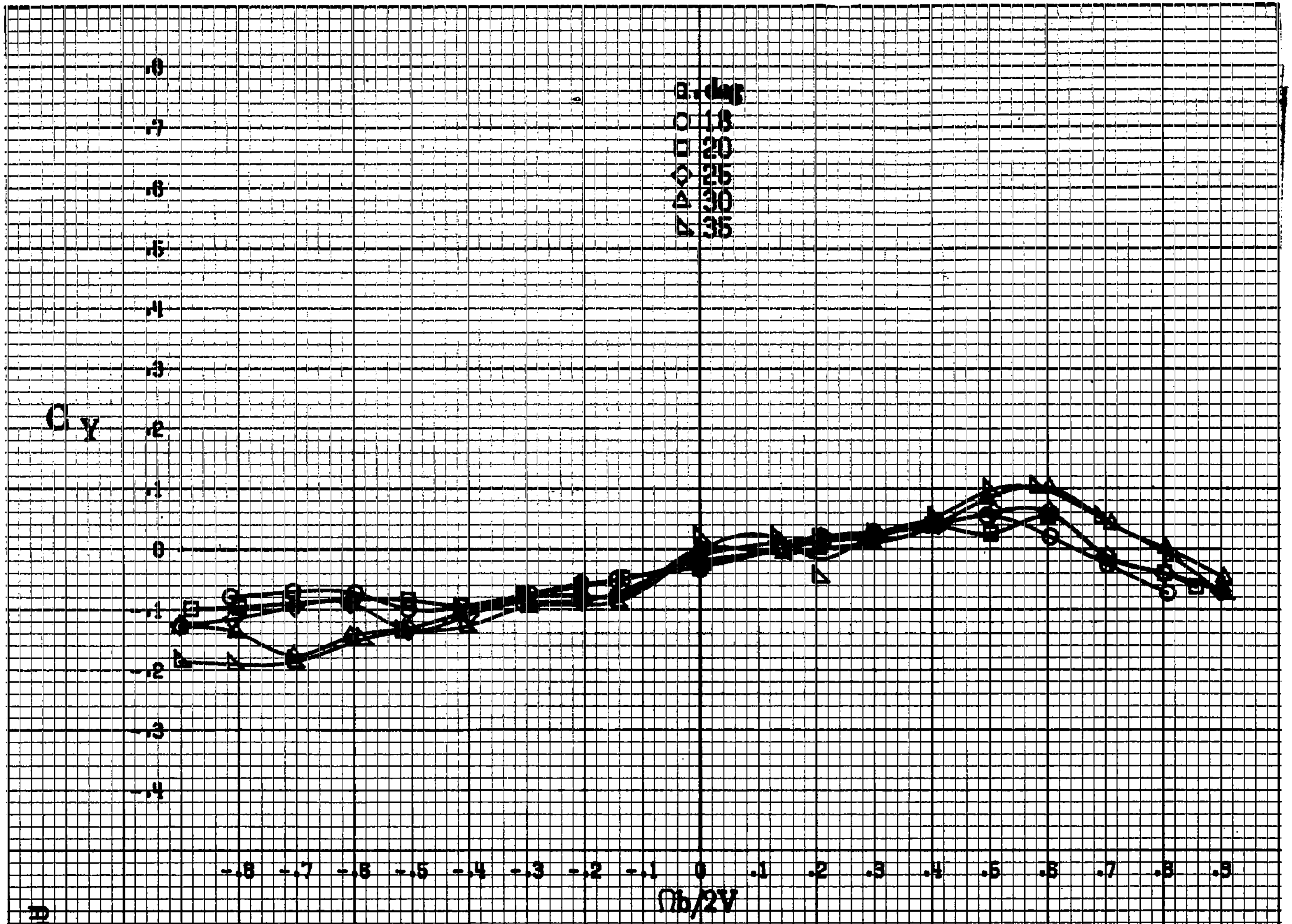

(b) α = 18 to 35 deg, SR = 182.9 cm (72 in).
Figure A101.-Continued.

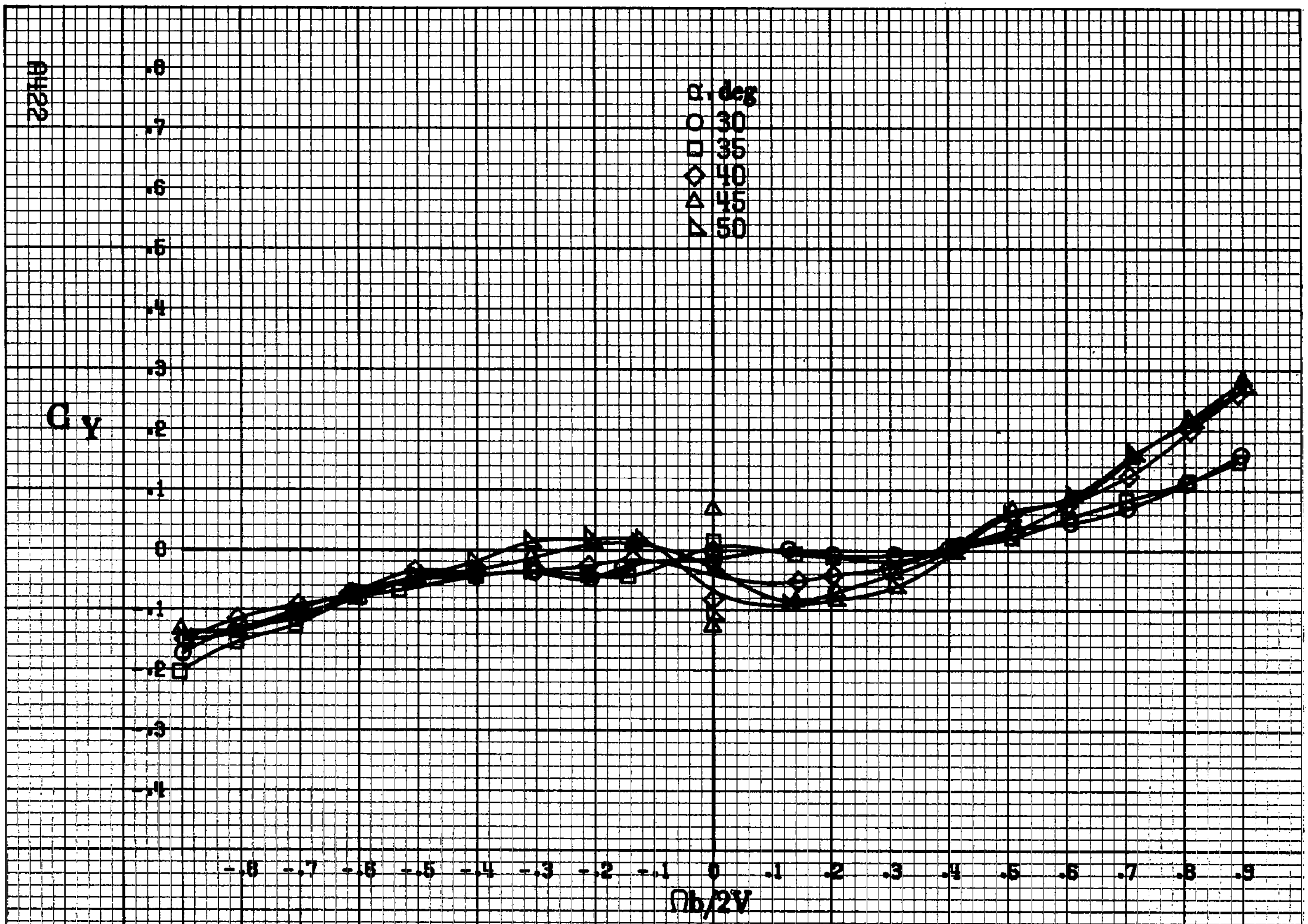

(c) α = 30 to 50 deg, δR = 0.

Figure A101.-Continued.

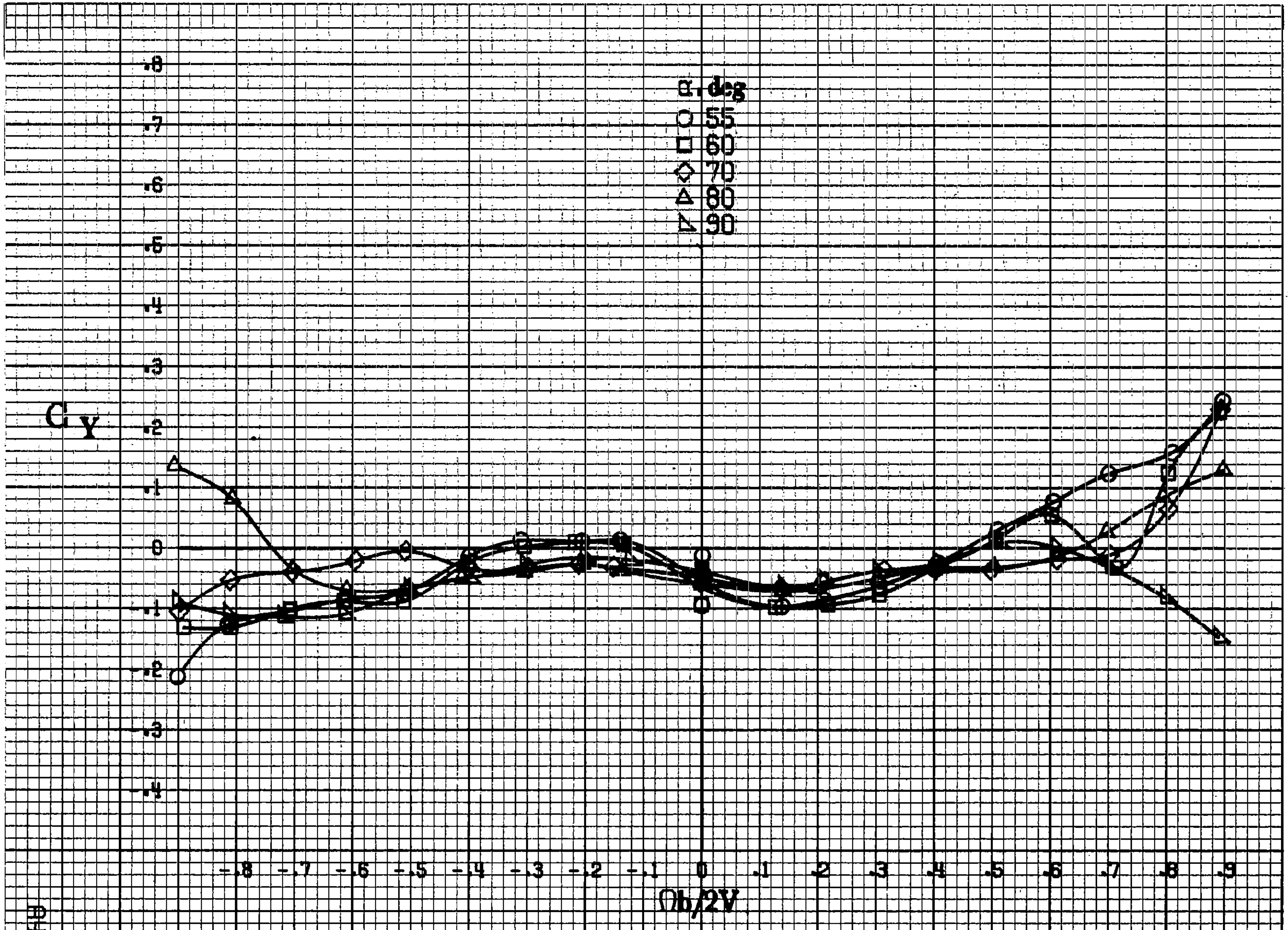

(d) α = 55to90deg, SR = 0.
Figure A101.-Concluded.

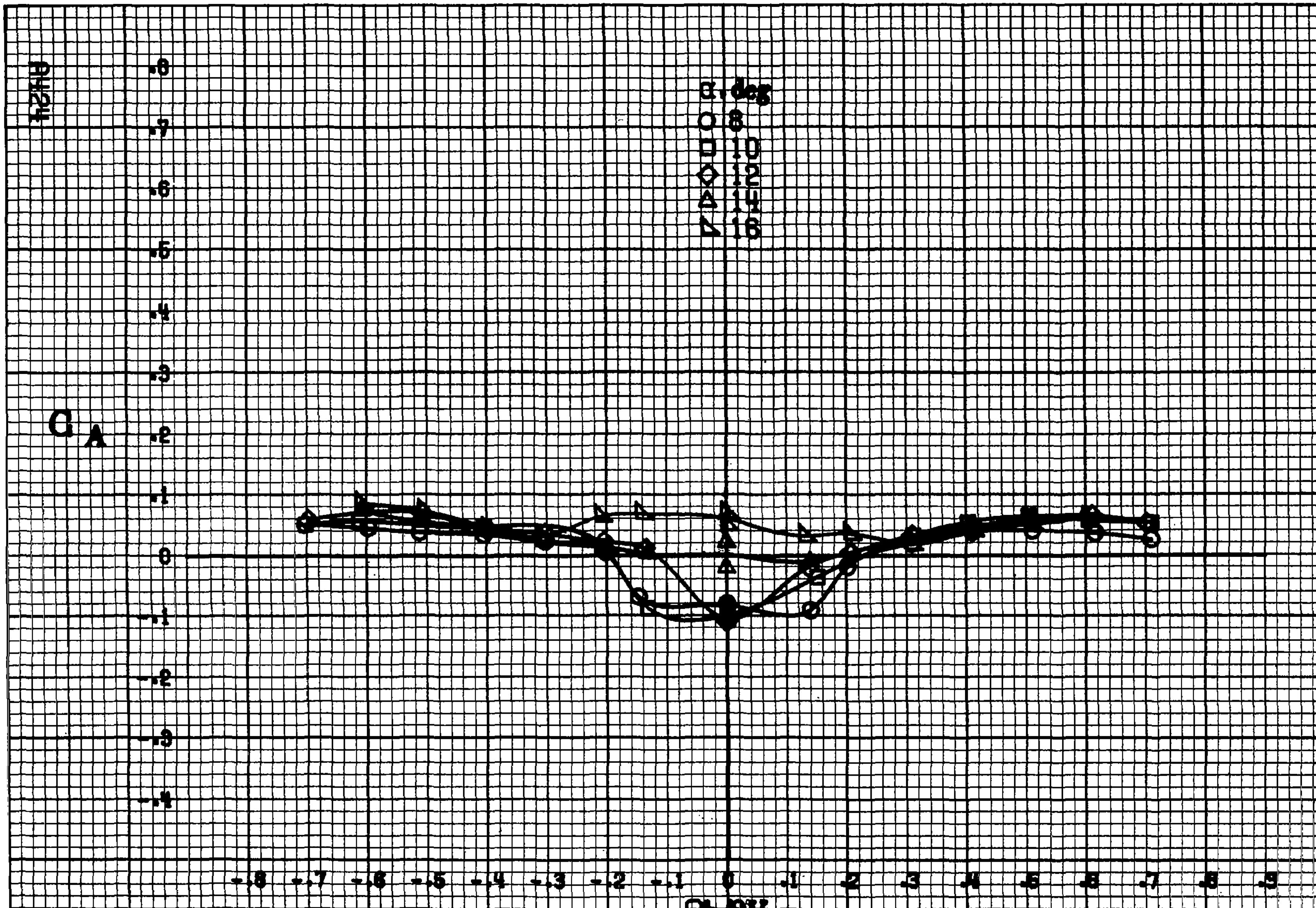

(a) α = 8 to 16 deg, SR = 182.9 cm (72 in).

Figure A102.-Effect of rotation rate and angle of attack on axial-force coefficient for horizontal and vertical tails off configuration. $\delta_e = 0°$, $\delta_a = 0°$, $\delta_r = 0°$, $\beta = 0°$.

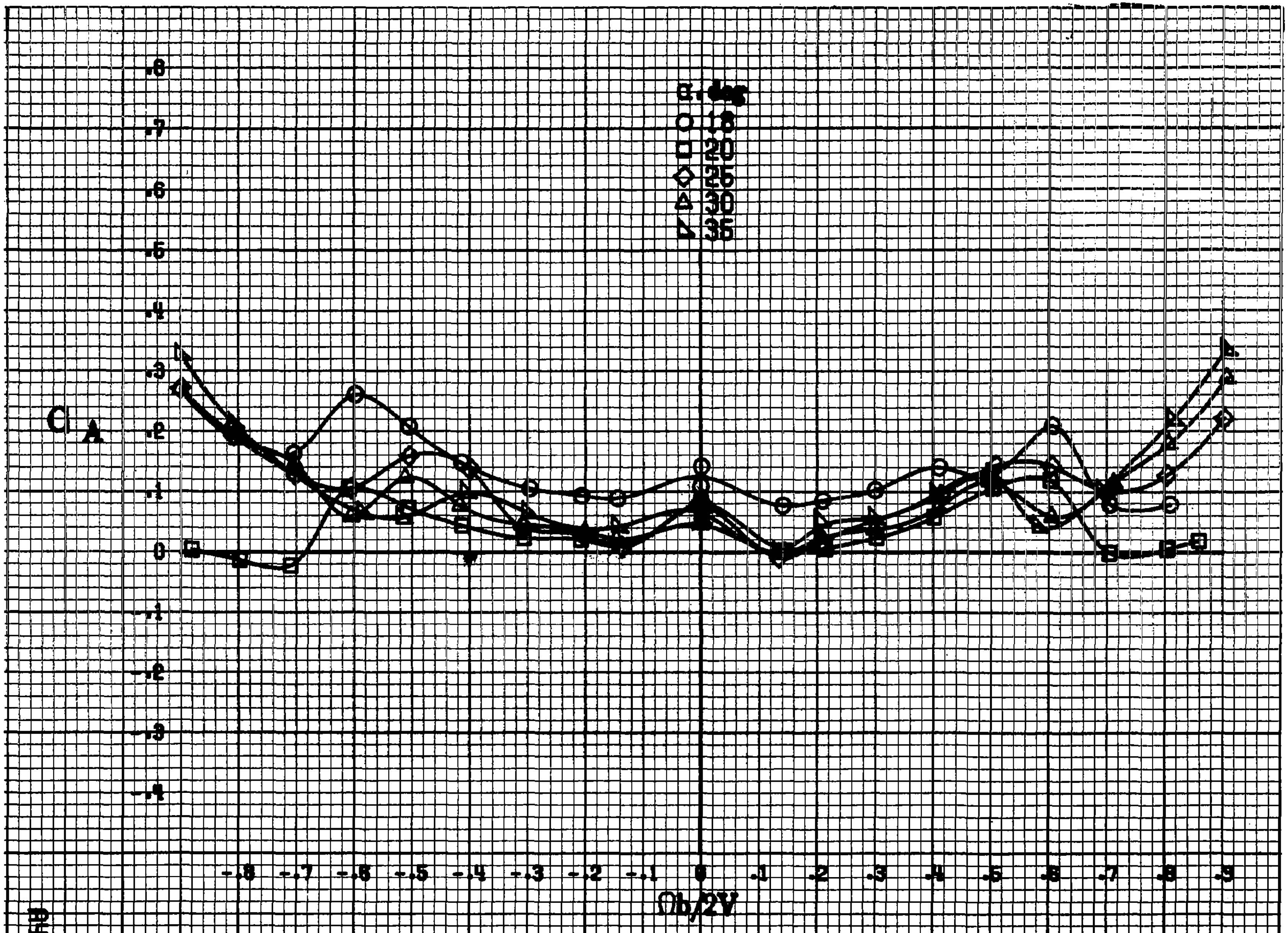

(b) α = 18 to 35 deg, SR = 182.9 cm (72 in).

Figure A102.–Continued.

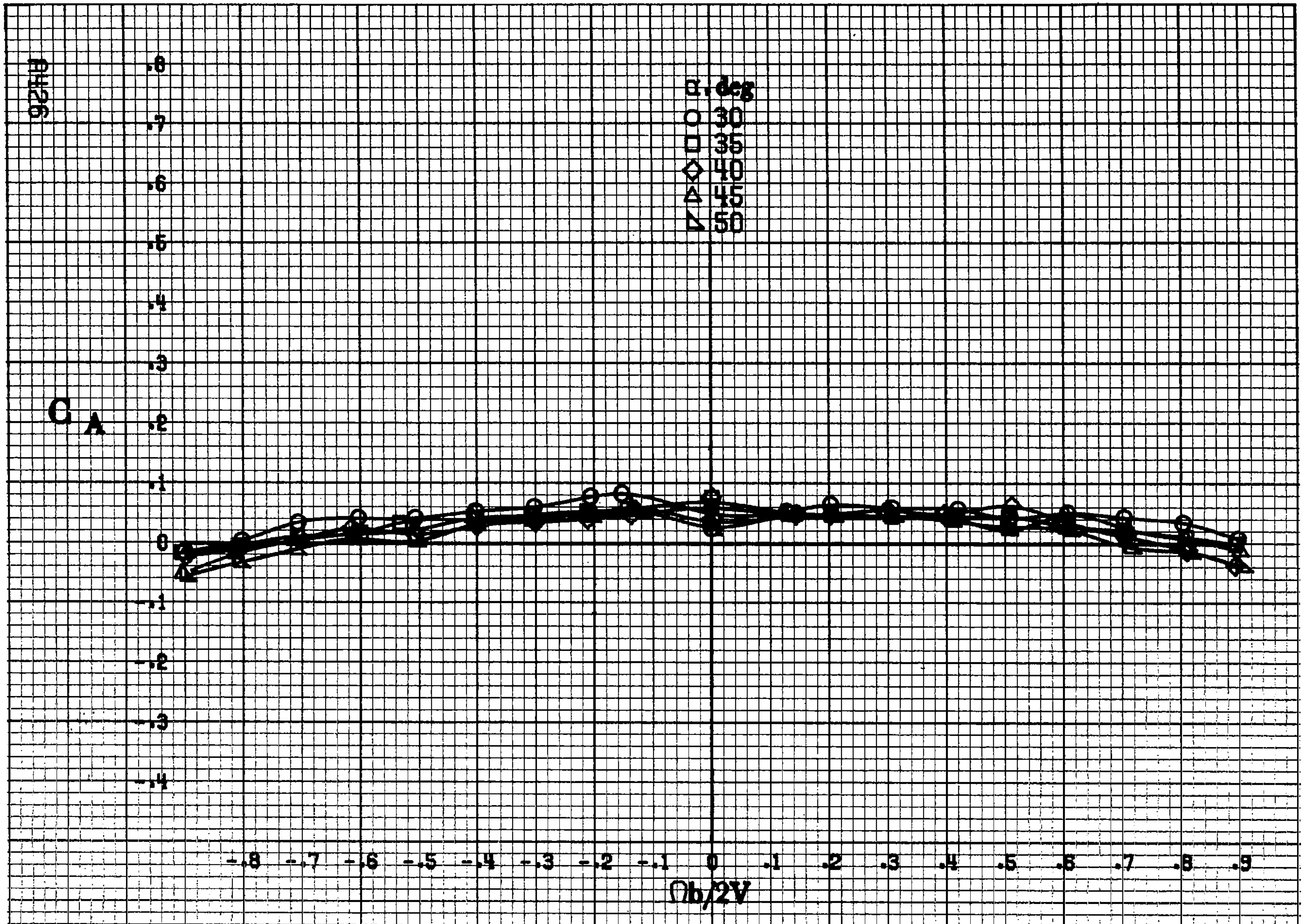

(c) α = 30 to 50 deg, SR = 0.

Figure A102.-Continued.

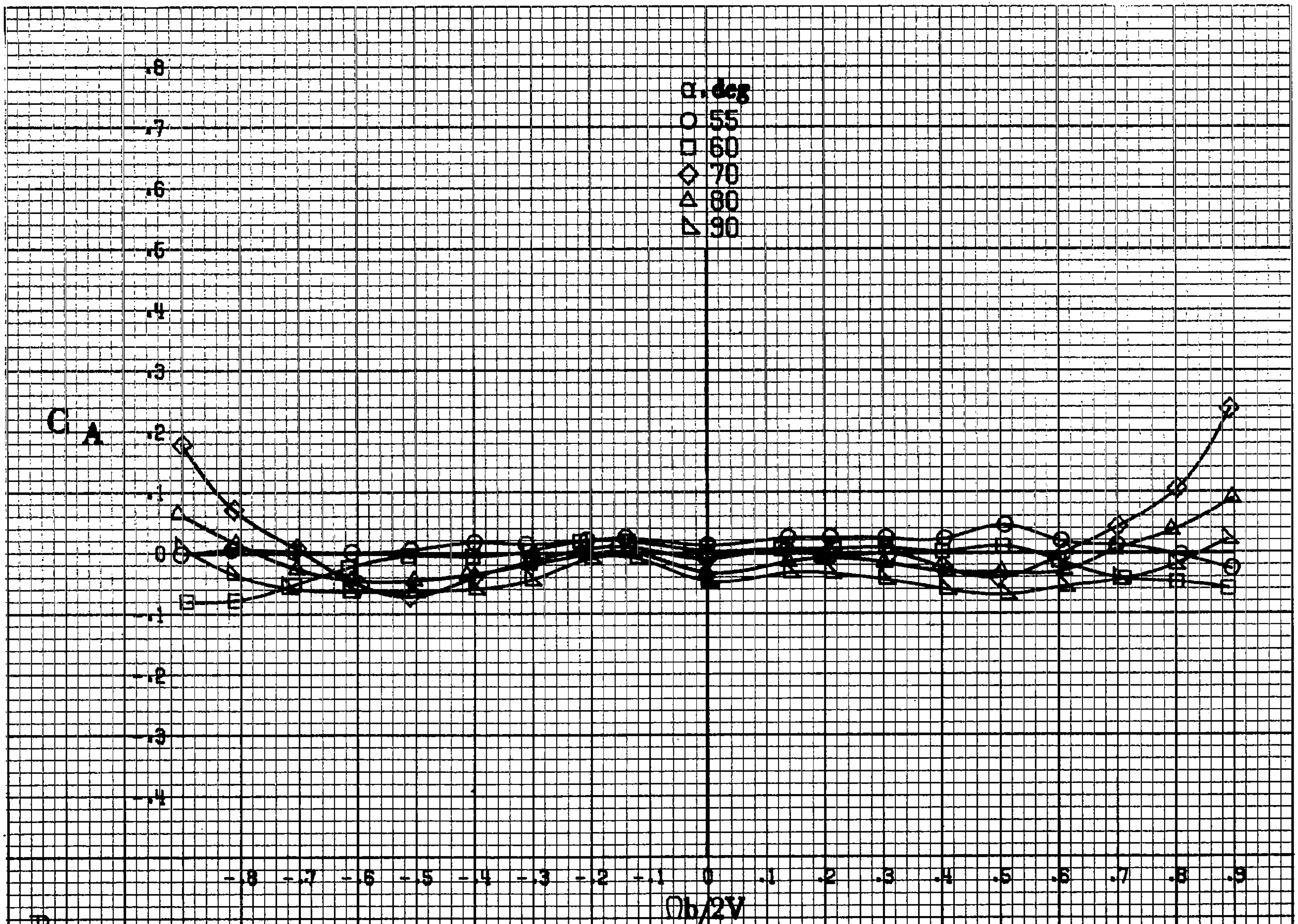

(d) α=55to90deg, SR=0.

Figure A102.-Concluded.

A427

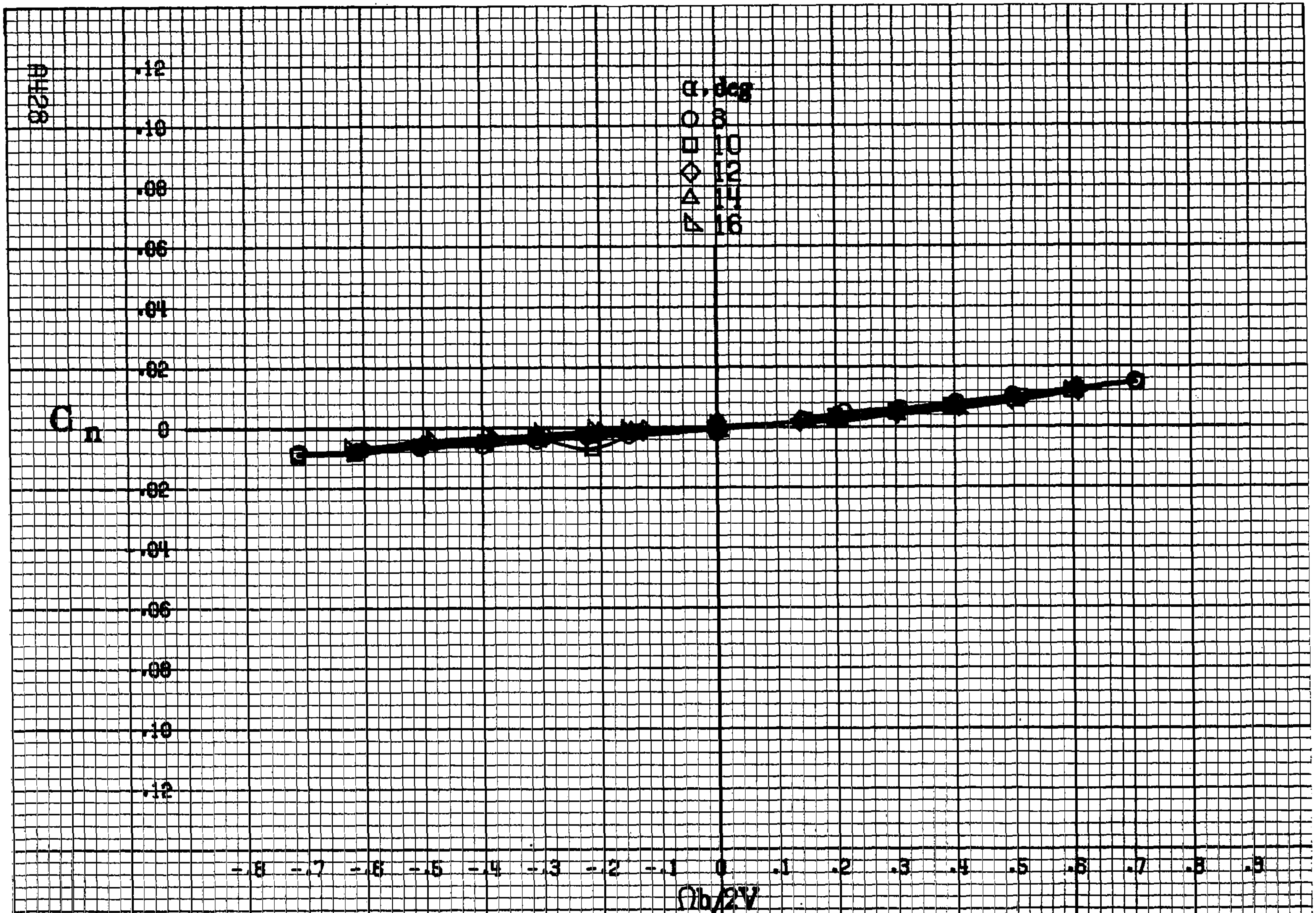

(a) $\alpha = 8$ to 16 deg, SR = 182.9 cm (72 in).

Figure A103.- Effect of rotation rate and angle of attack on yawing-moment coefficient for body alone configuration. $\delta_a = 0°$, $\delta_e = 0°$, $\delta_r = 0°$. $\beta = 0°$.

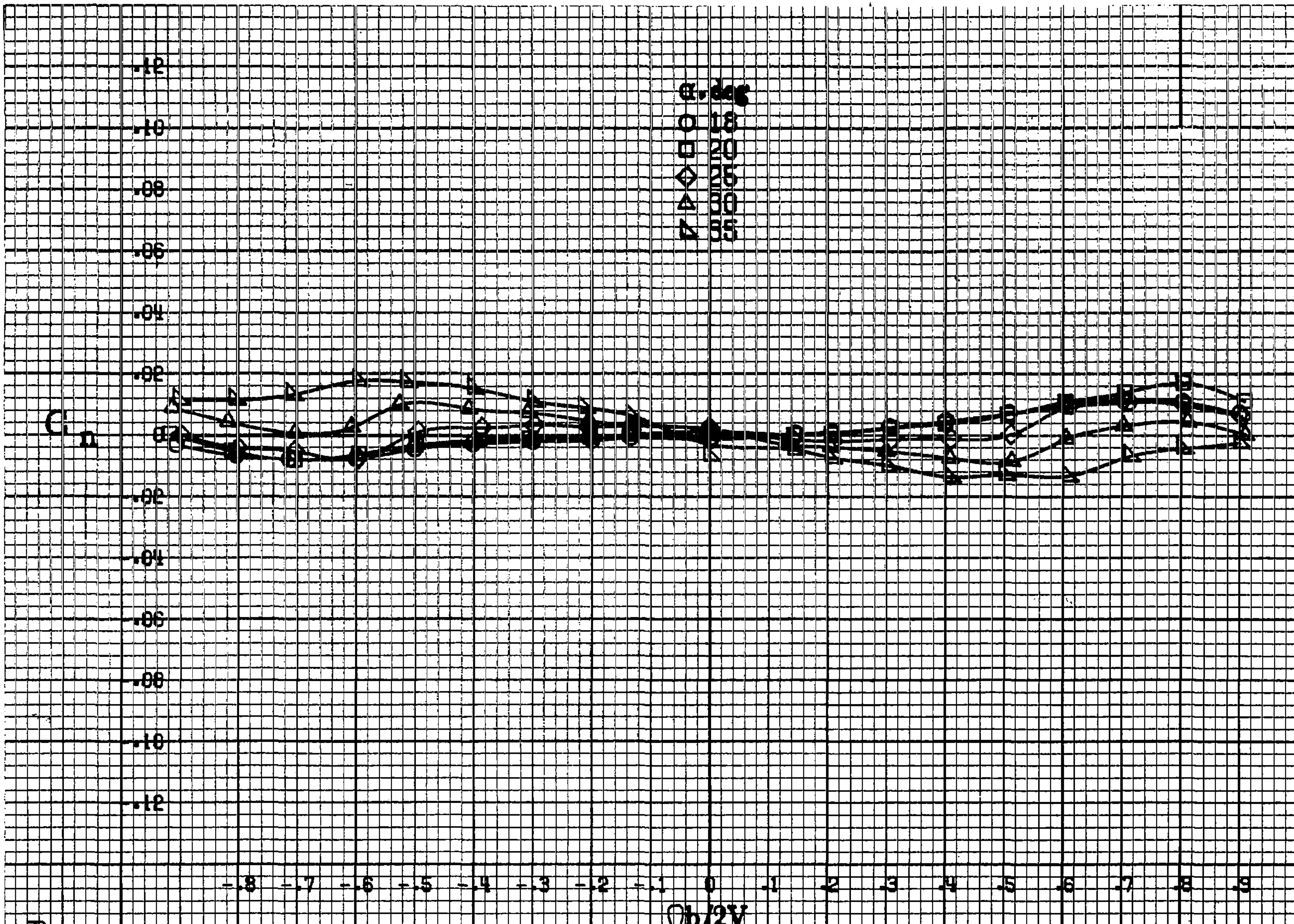

(b) α = 18 to 35 deg, SR = 182.9 cm (72 in).

Figure A108.-Continued.

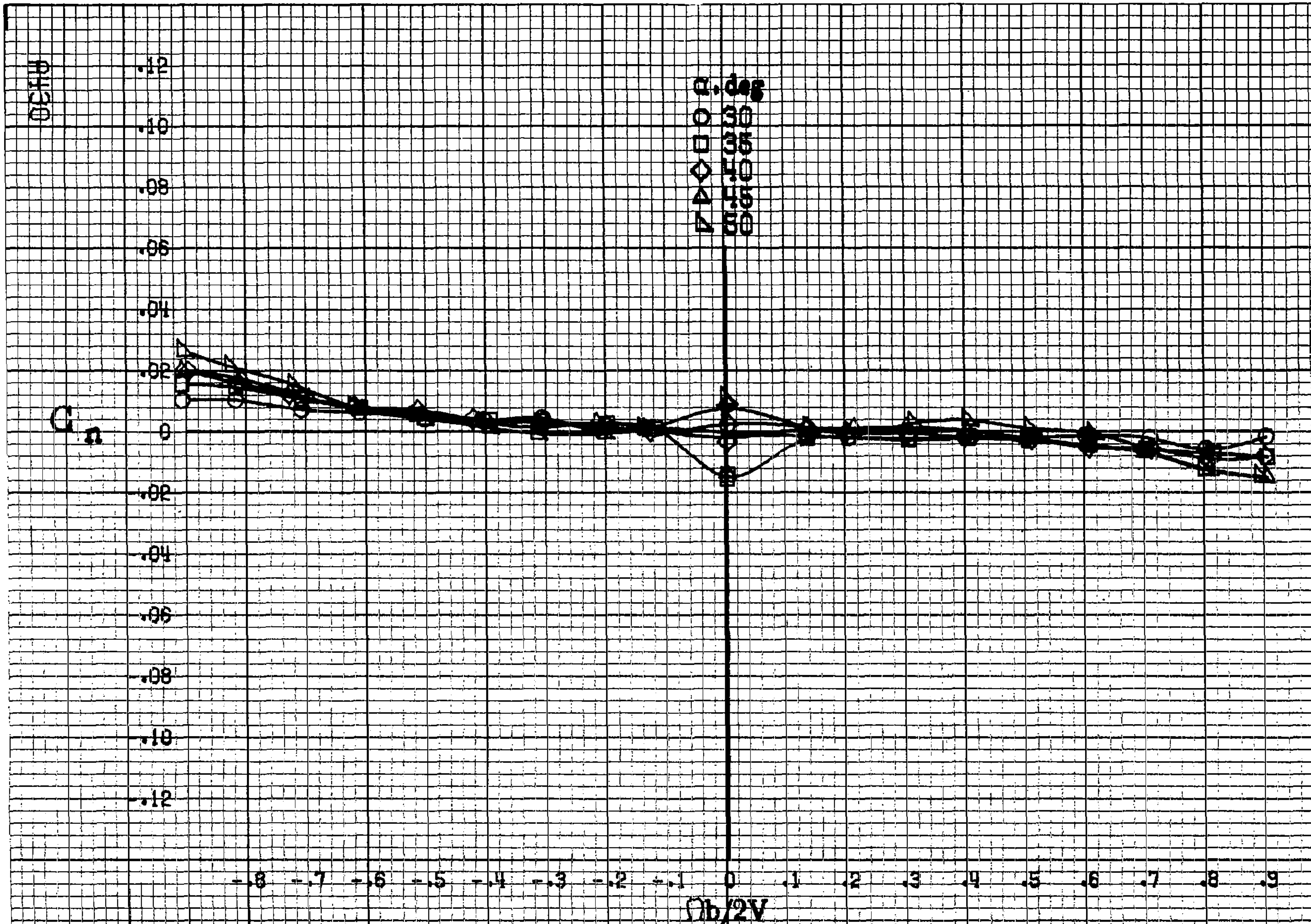

(c) α = 30 to 50 deg, SR = 0.

Figure A108. Continued.

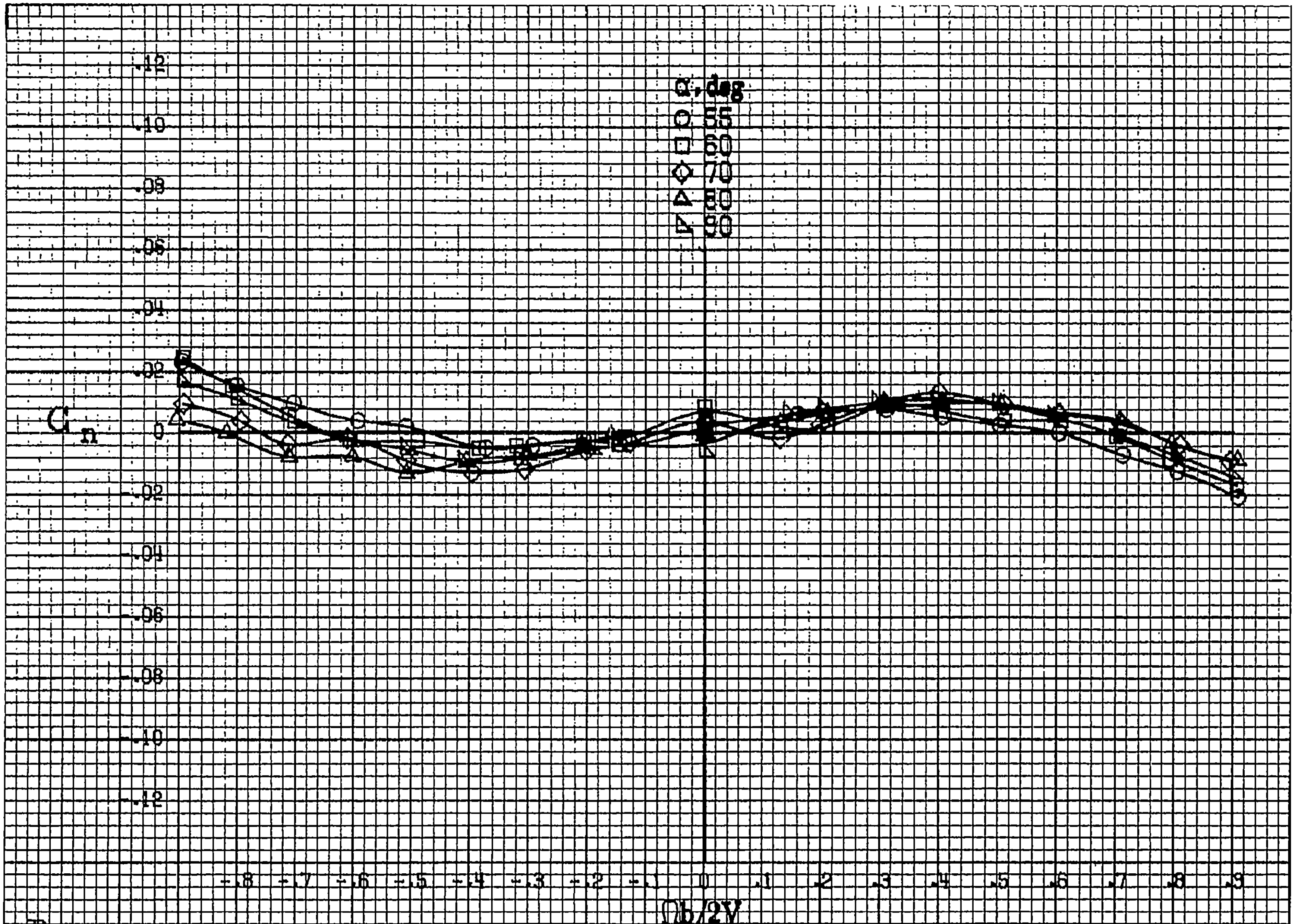

(d) α = 55 to 90 deg, SR = 0.
Figure A108.-Concluded.

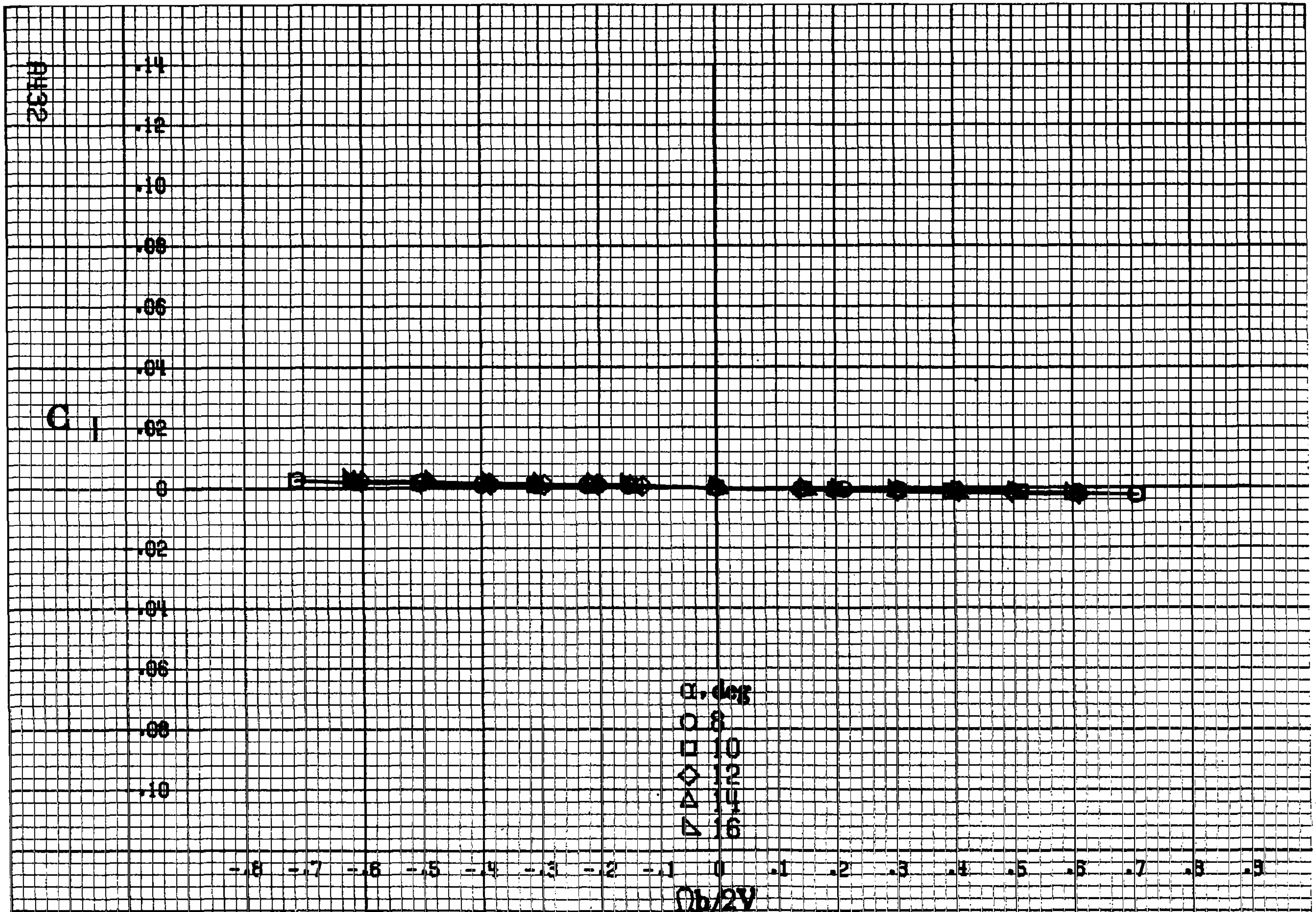

(a) α = 8 to 16 deg, SR = 182.9 cm (72 in).

Figure A104.-Effect of rotation rate and angle of attack on rolling-moment coefficient for body alone configuration, $\delta_e = 0°$, $\delta_a = 0°$, $\delta_r = 0°$, $\beta = 0°$.

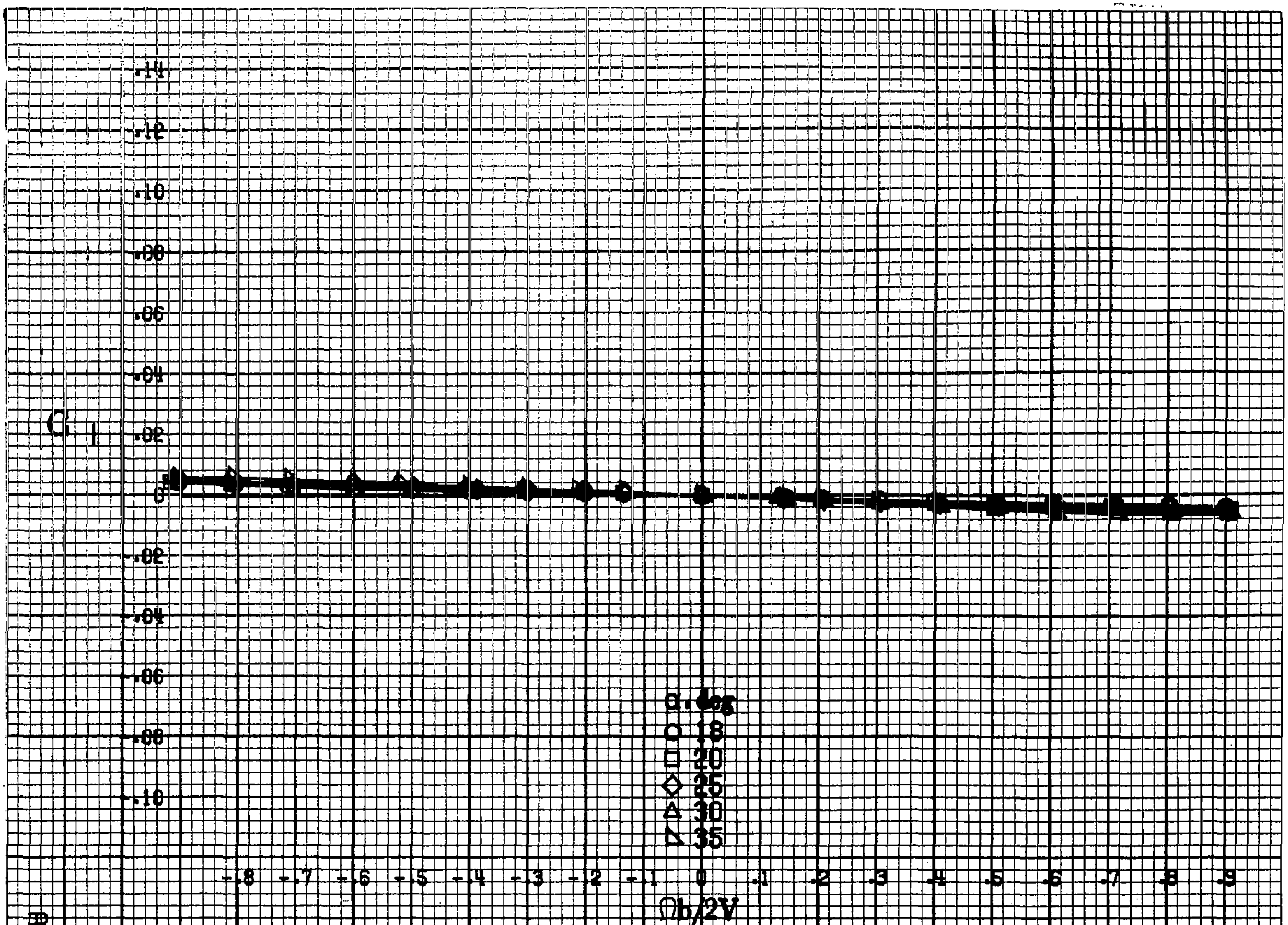

(b) α = 18 to 35 deg, SR = 182.9 cm (72 in).

Figure A104.-Continued.

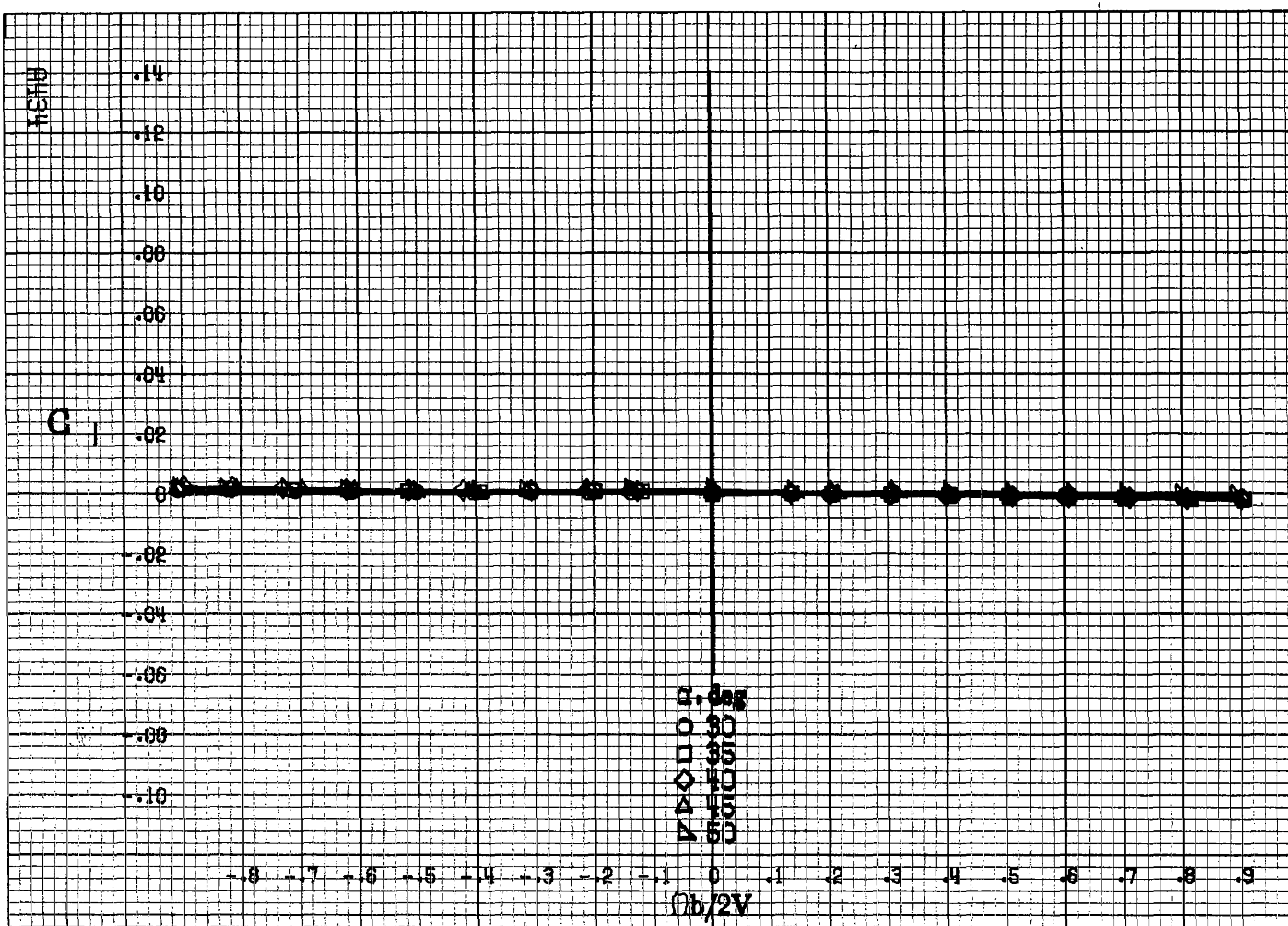

(c) α = 30 to 50 deg, SR = 0.

Figure A104. Continued.

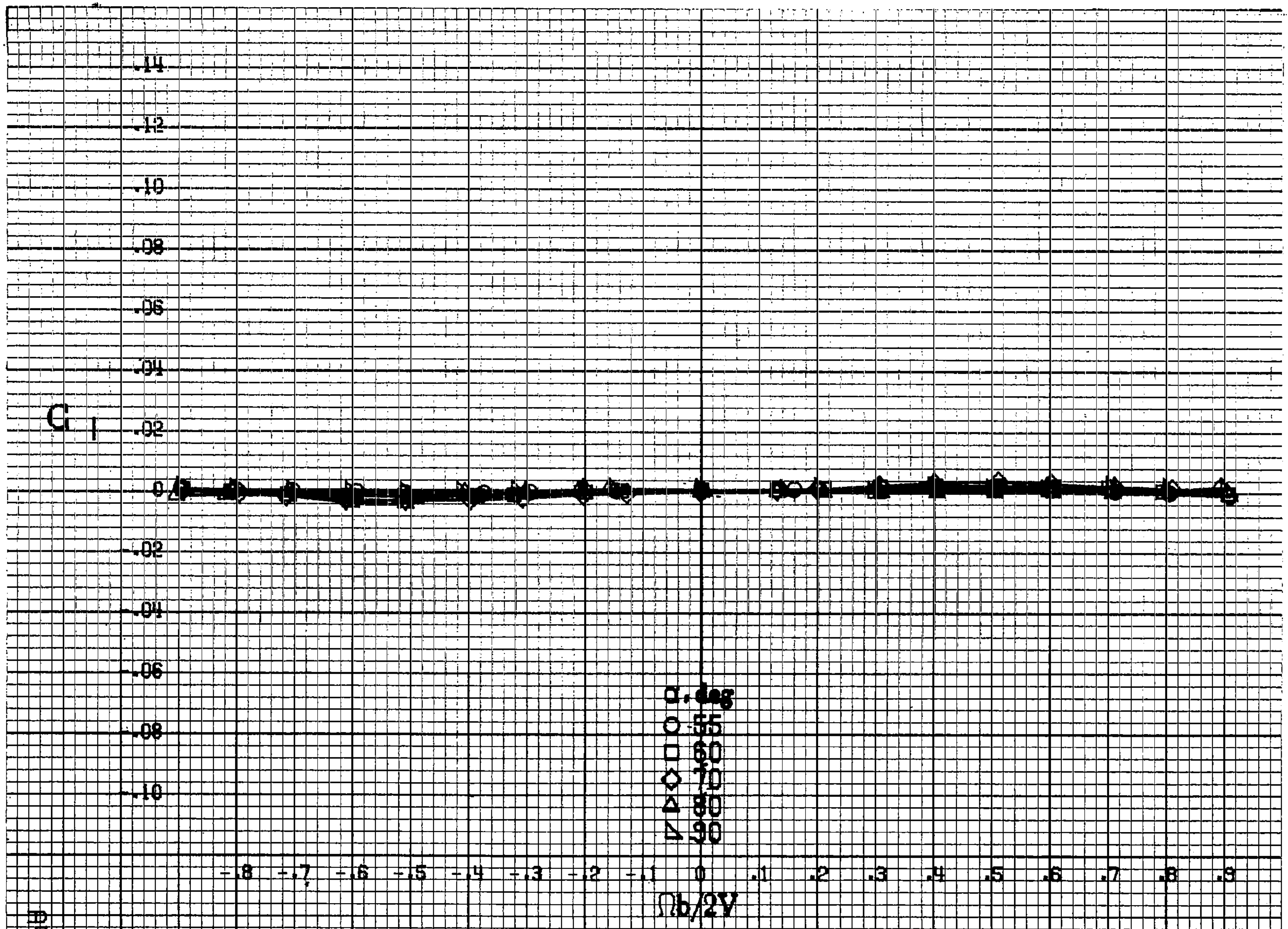

(d) $\alpha = 55$ to 90 deg, SR = 0.

Figure A104.-Concluded.

(a) $\alpha = 8$ to 16 deg, SR = 182.9 cm (72 in).

Figure A105.-Effect of rotation rate and angle of attack on pitching-moment coefficient for body alone configuration. $\delta_e = 0°$, $\delta_a = 0°$, $\delta_r = 0°$, $\beta = 0°$.

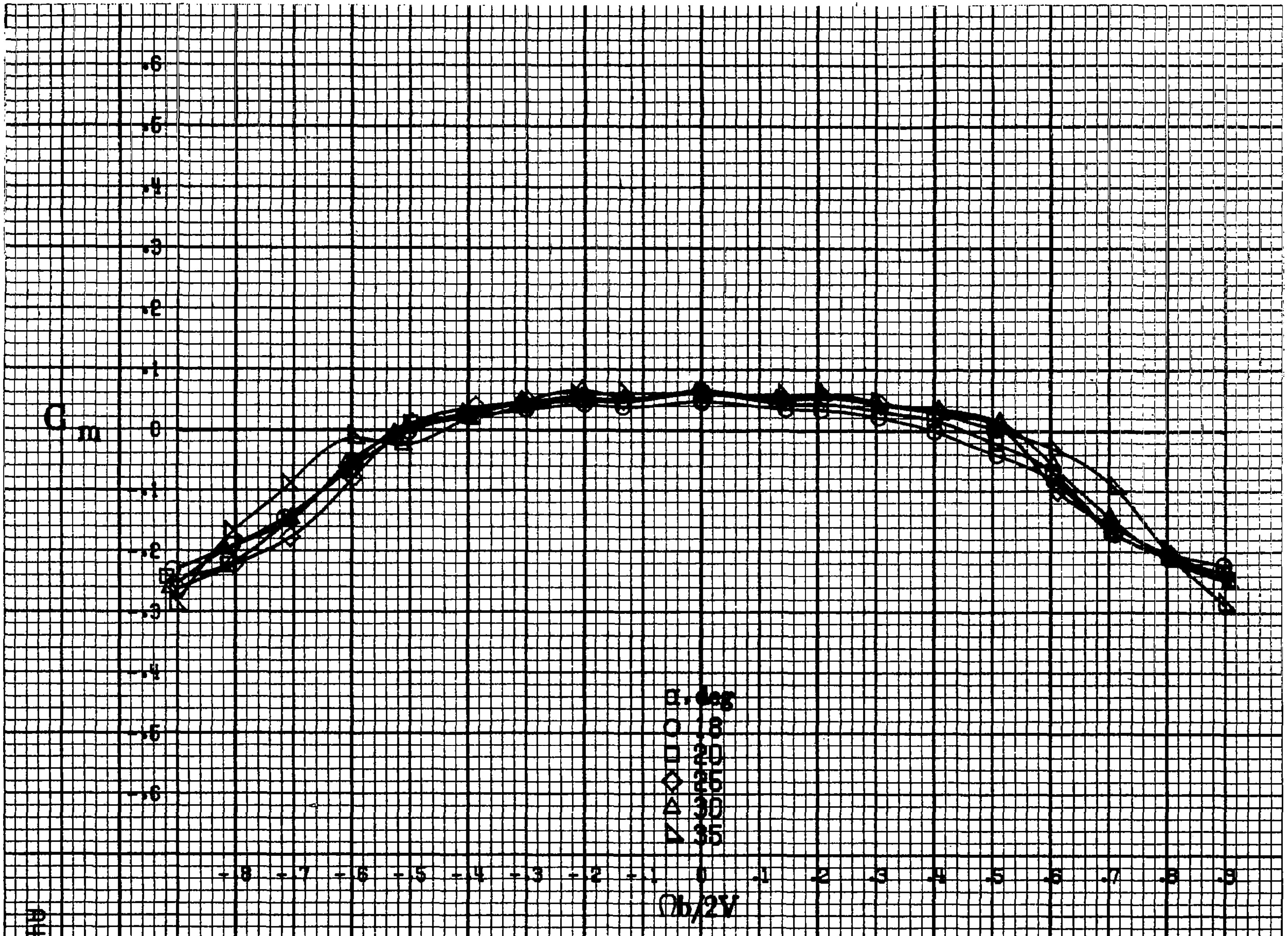

(b) α = 18 to 35 deg, SR = 182.9 cm (72 in).

Figure A105.-Continued.

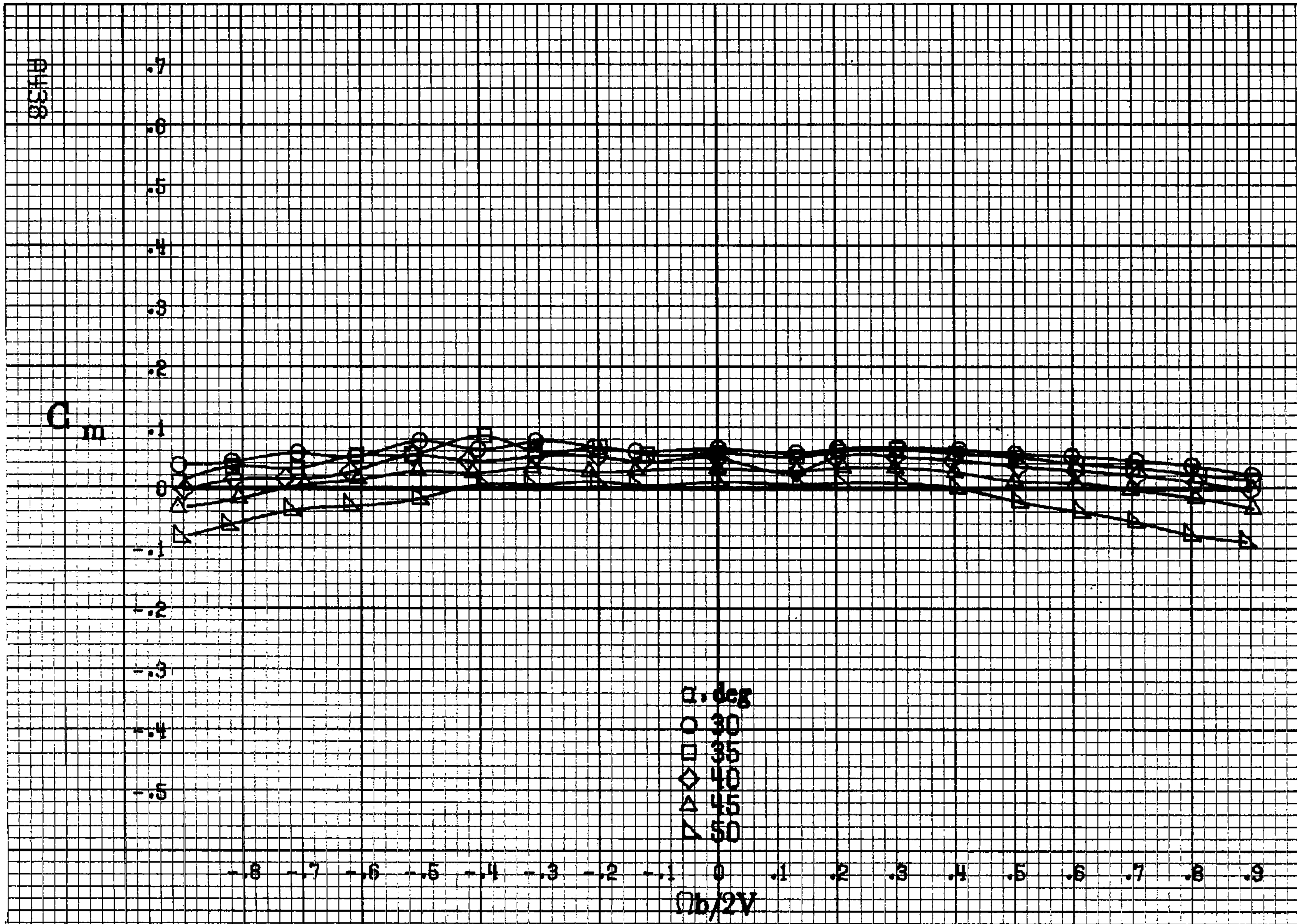

(c) α = 30 to 50 deg, SR = 0.

Figure A105.-Continued.

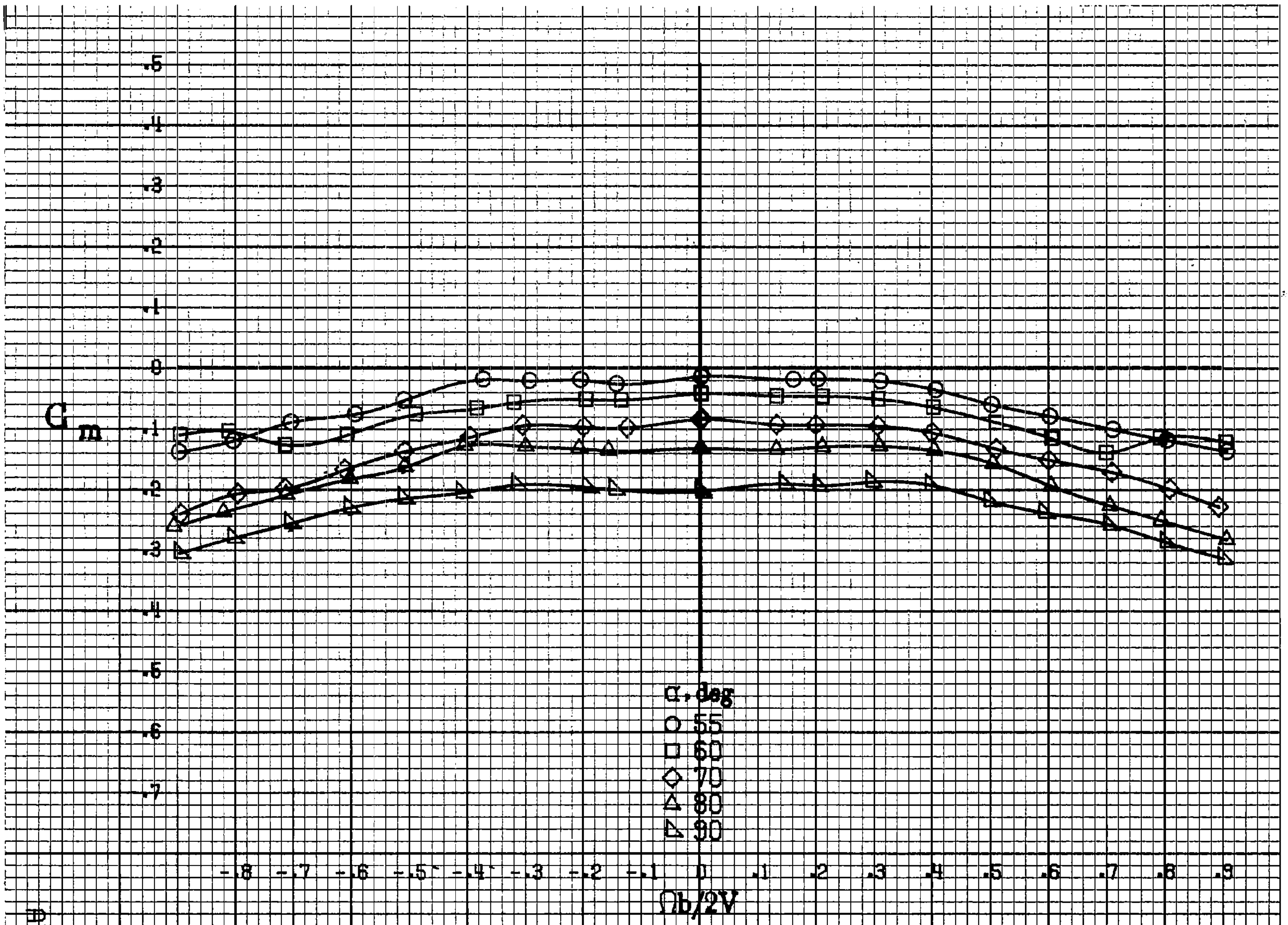

(d) α = 55 to 90 deg, SR = 0.

Figure A105.-Concluded.

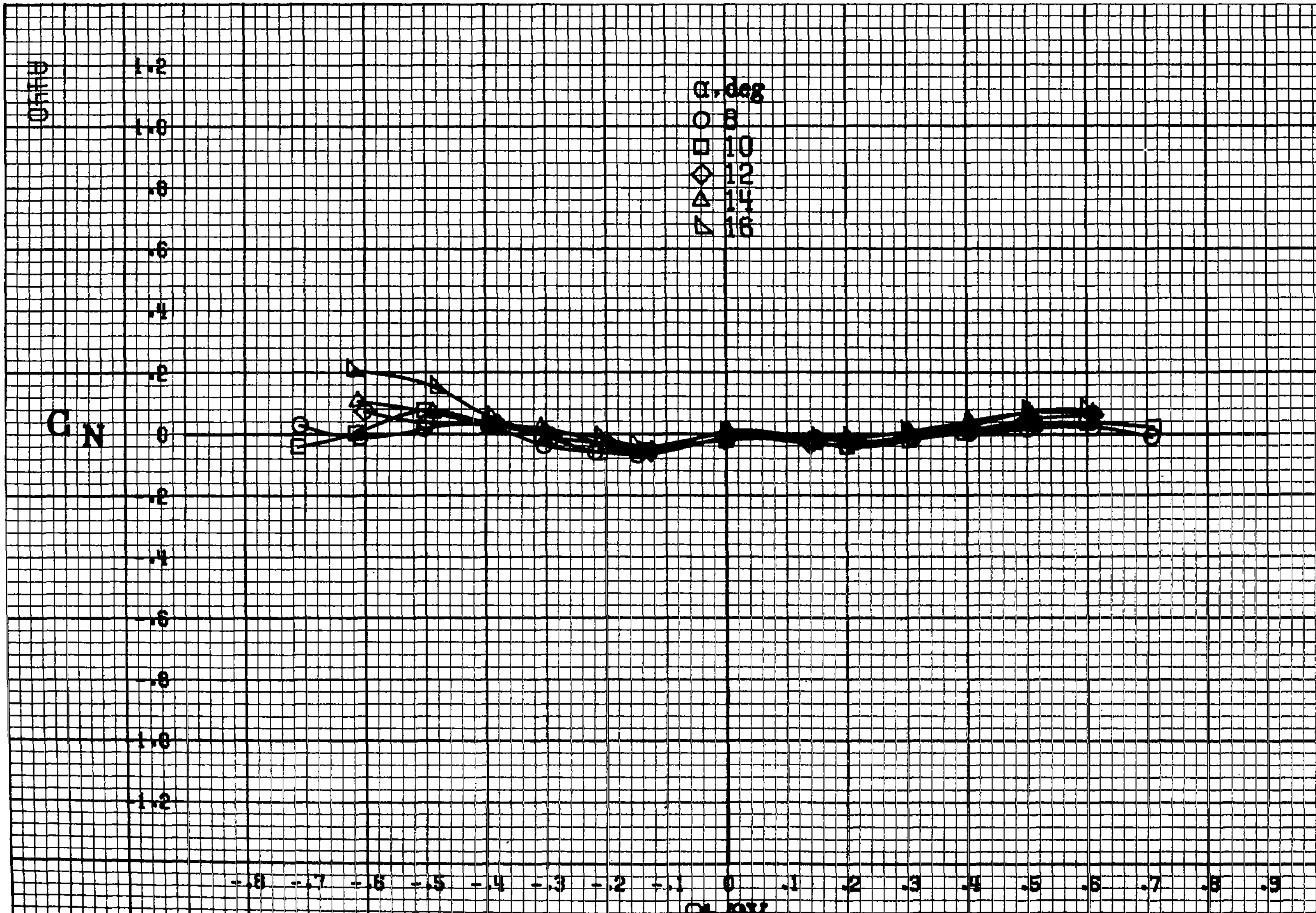

(a) $\alpha = 8$ to 16 deg, SR = 182.9 cm (72 in).

Figure A106.- Effect of rotation rate and angle of attack on normal-force coefficient for body alone configuration. $\delta_e = 0°$, $\delta_a = 0°$, $\delta_r = 0°$, $\beta = 0°$.

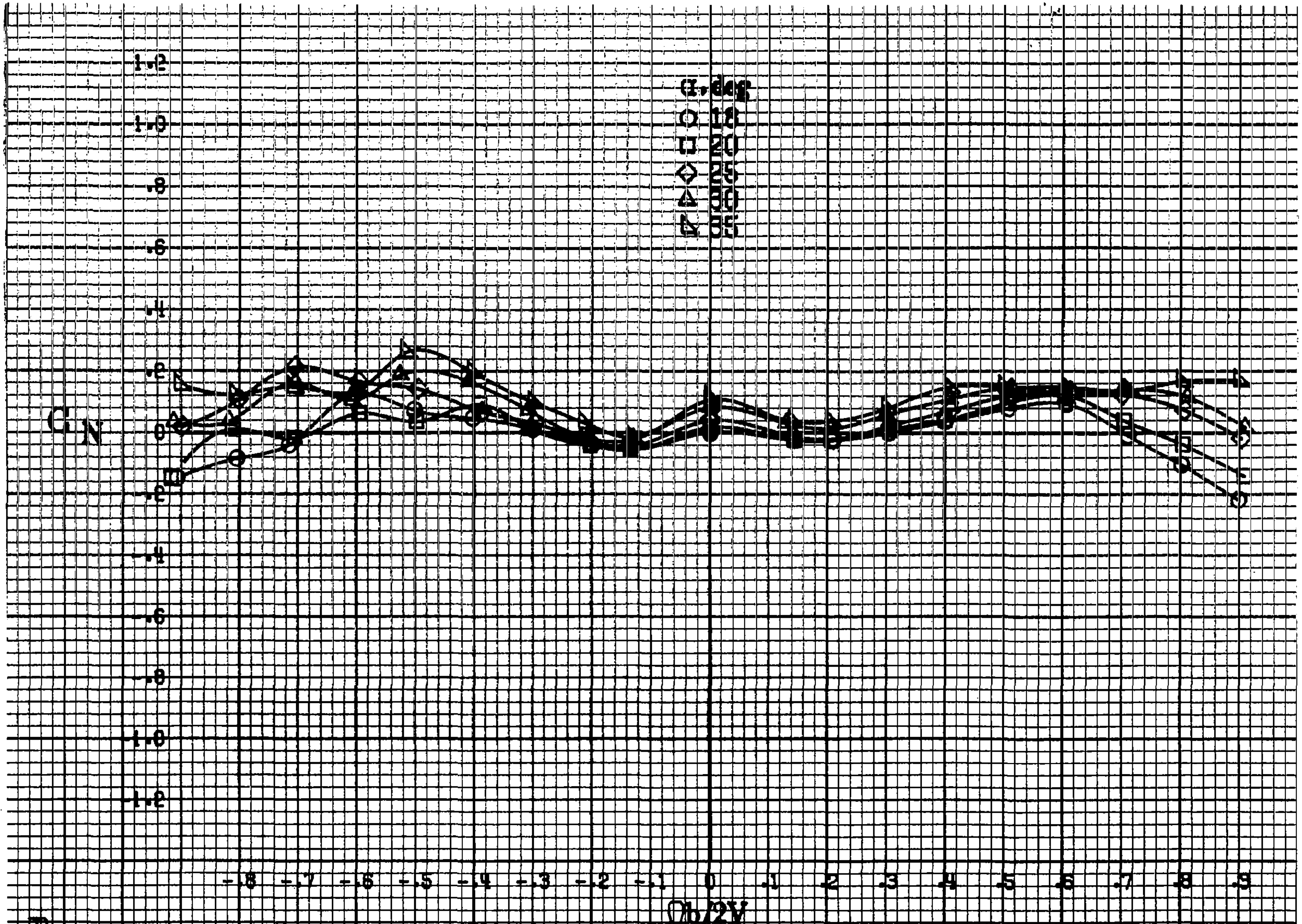

(b) α = 18 to 35 deg, SR = 182.9 cm (72 in).

Figure A106.- Continued.

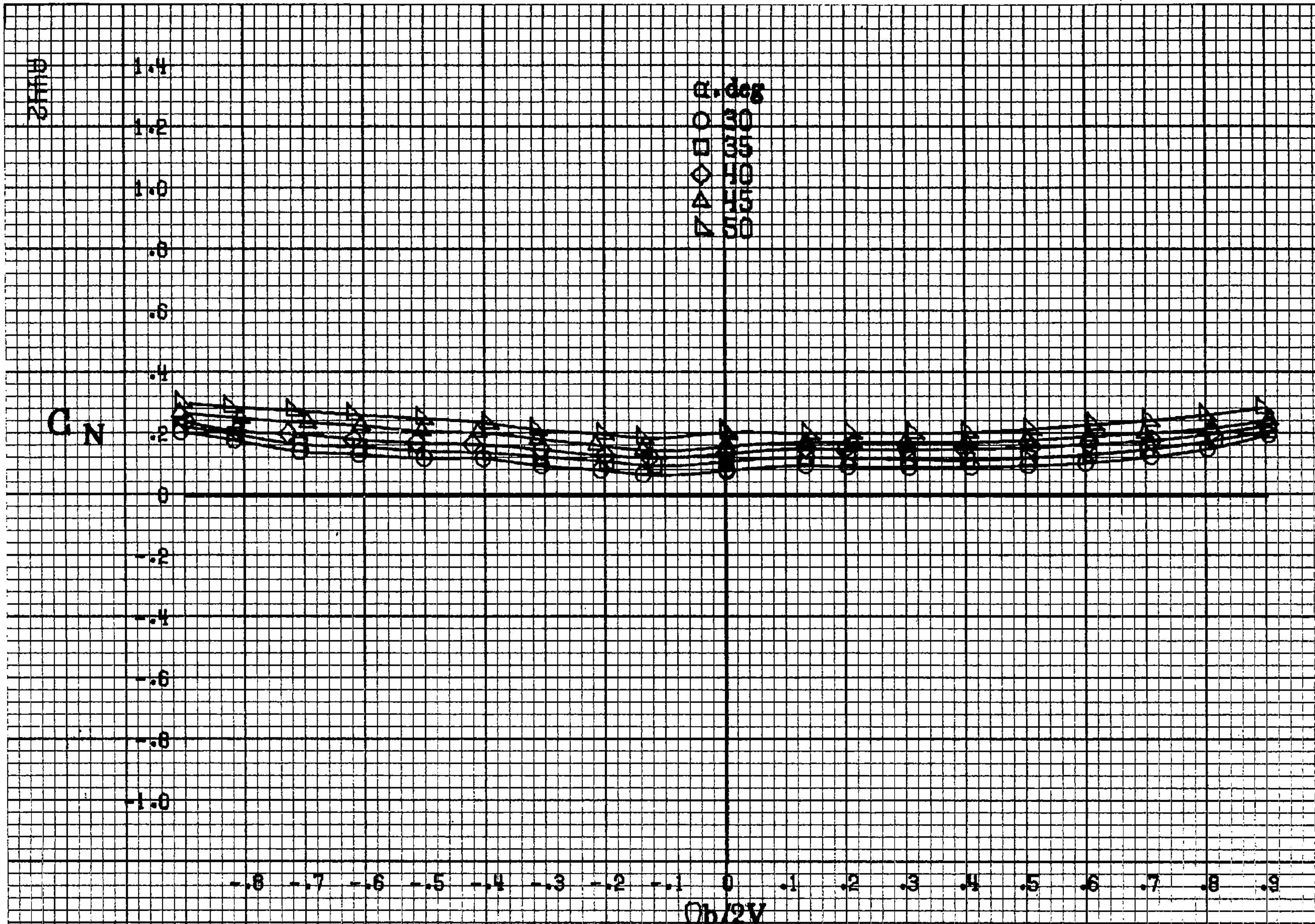

(c) α = 30 to 50 deg, SR = 0.

Figure A106.-Continued.

(d) α = 55 to 90 deg, SR = 0.

Figure A82.-Concluded.

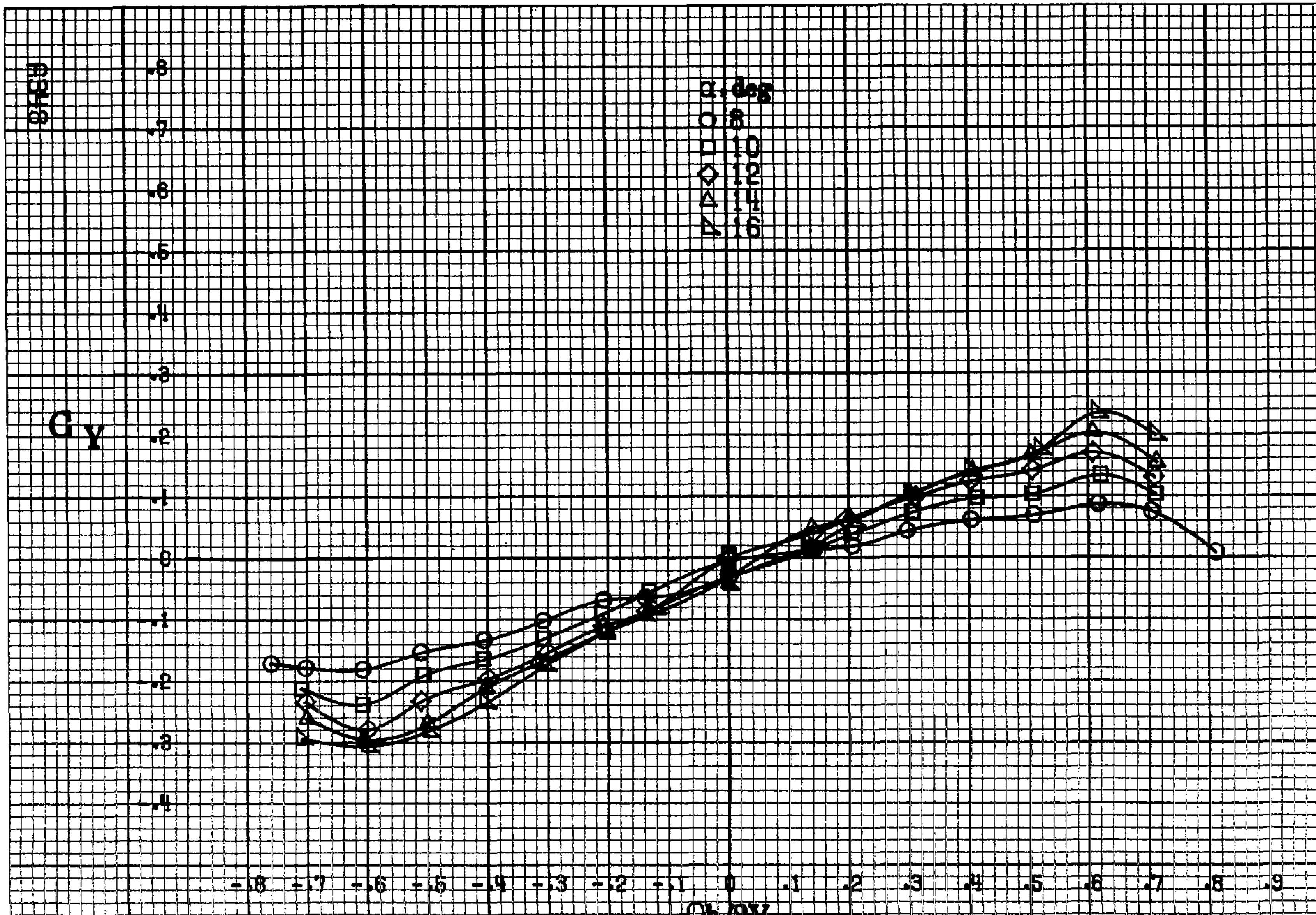

(a) α = 8 to 16 deg, SR = 182.9 cm (72 in).

Figure A88.- Effect of rotation rate and angle of attack on side-force coefficient for configuration having cowl strakes, ventral and tail fillets. $\delta_a = 0°$, $\delta_e = 0°$, $\delta_r = 0°$, $\beta = 0°$.

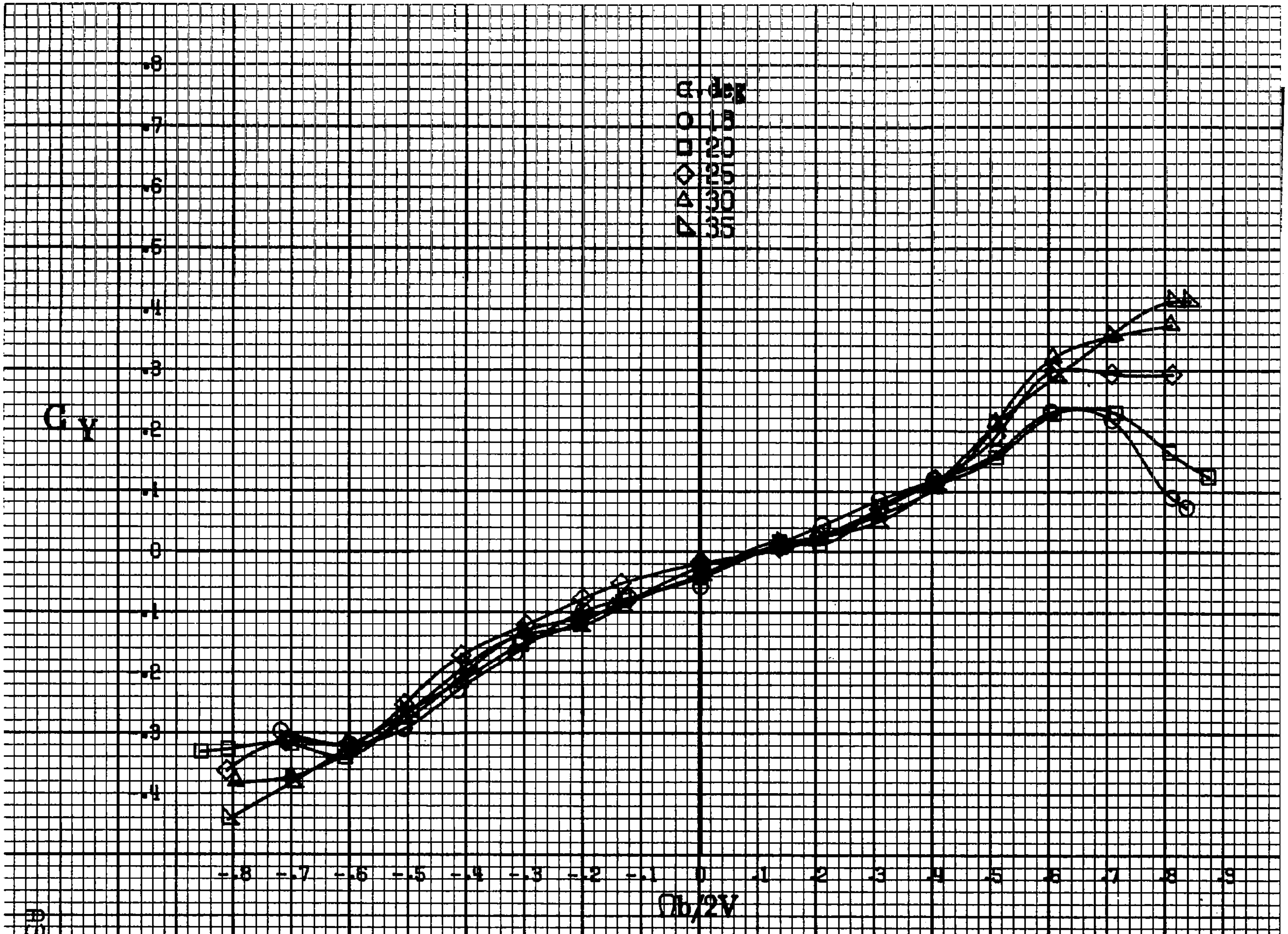

(b) α = 18 to 35 deg, SR = 182.9 cm (72 in).
Figure A88.-Continued.

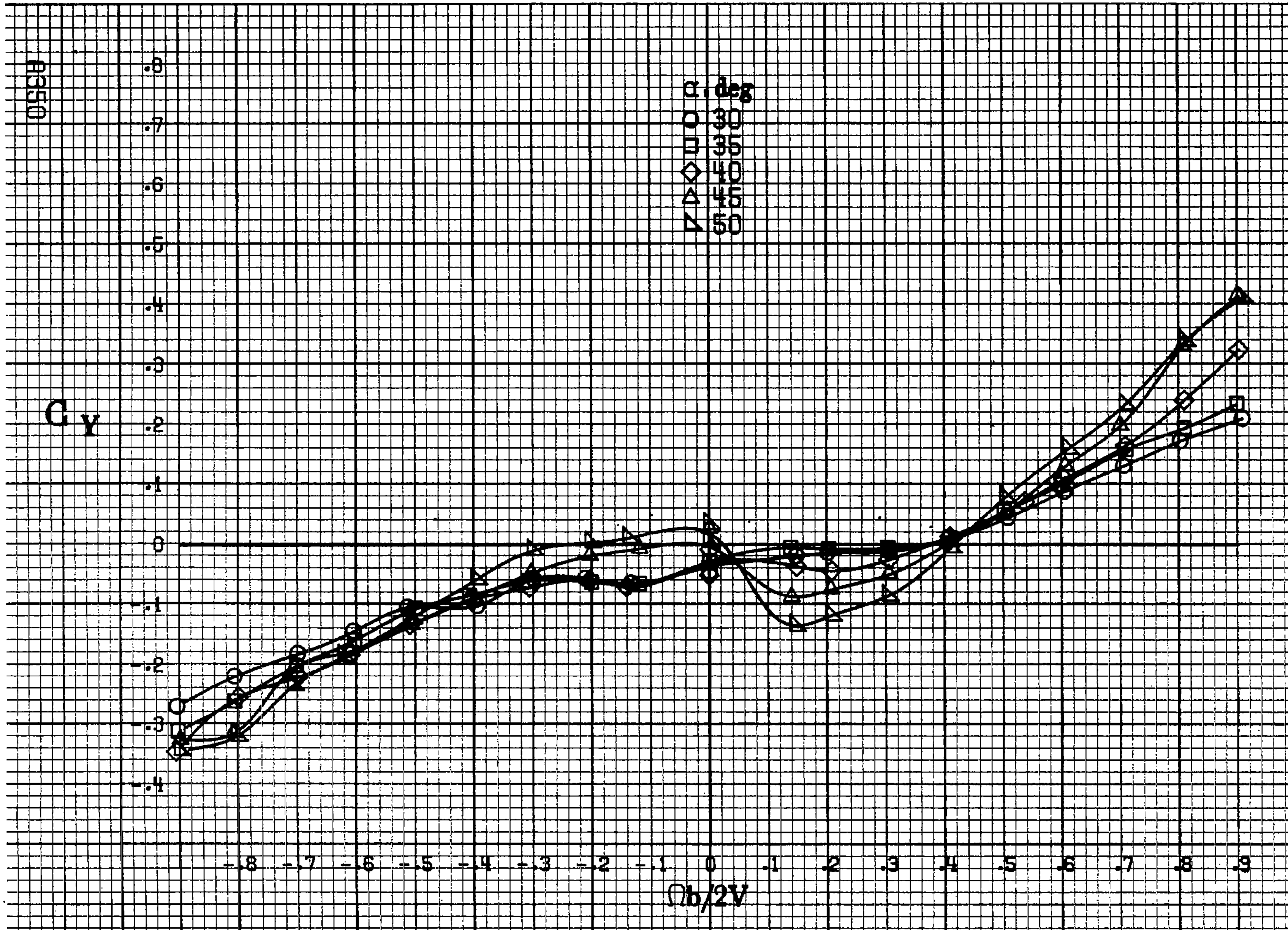

(c) α = 30to50deg, SR = 0.
Figure A83.-Continued.

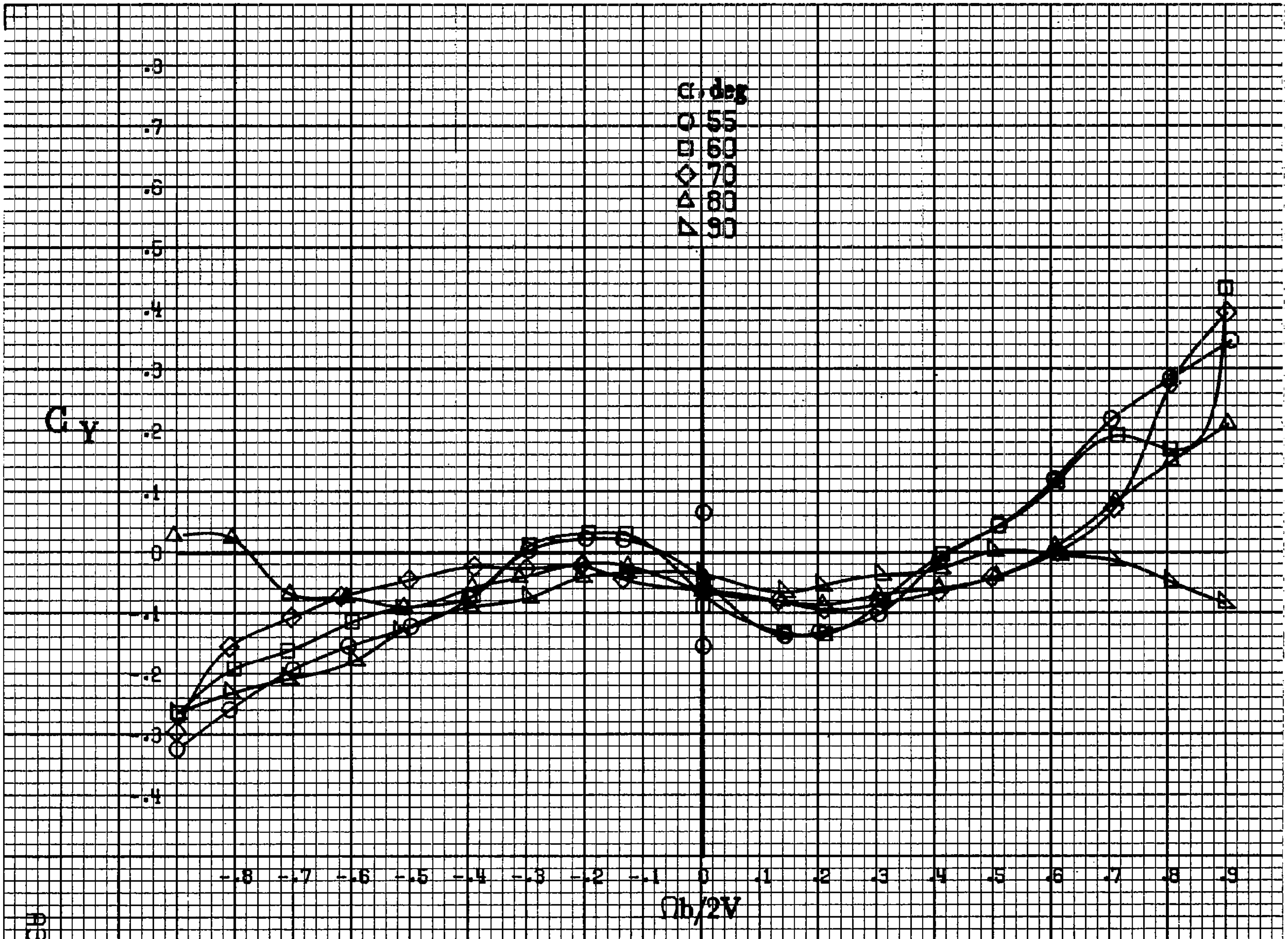

(d) α = 55 to 90 deg, SR = 0.

Figure A83.-Concluded.

A351

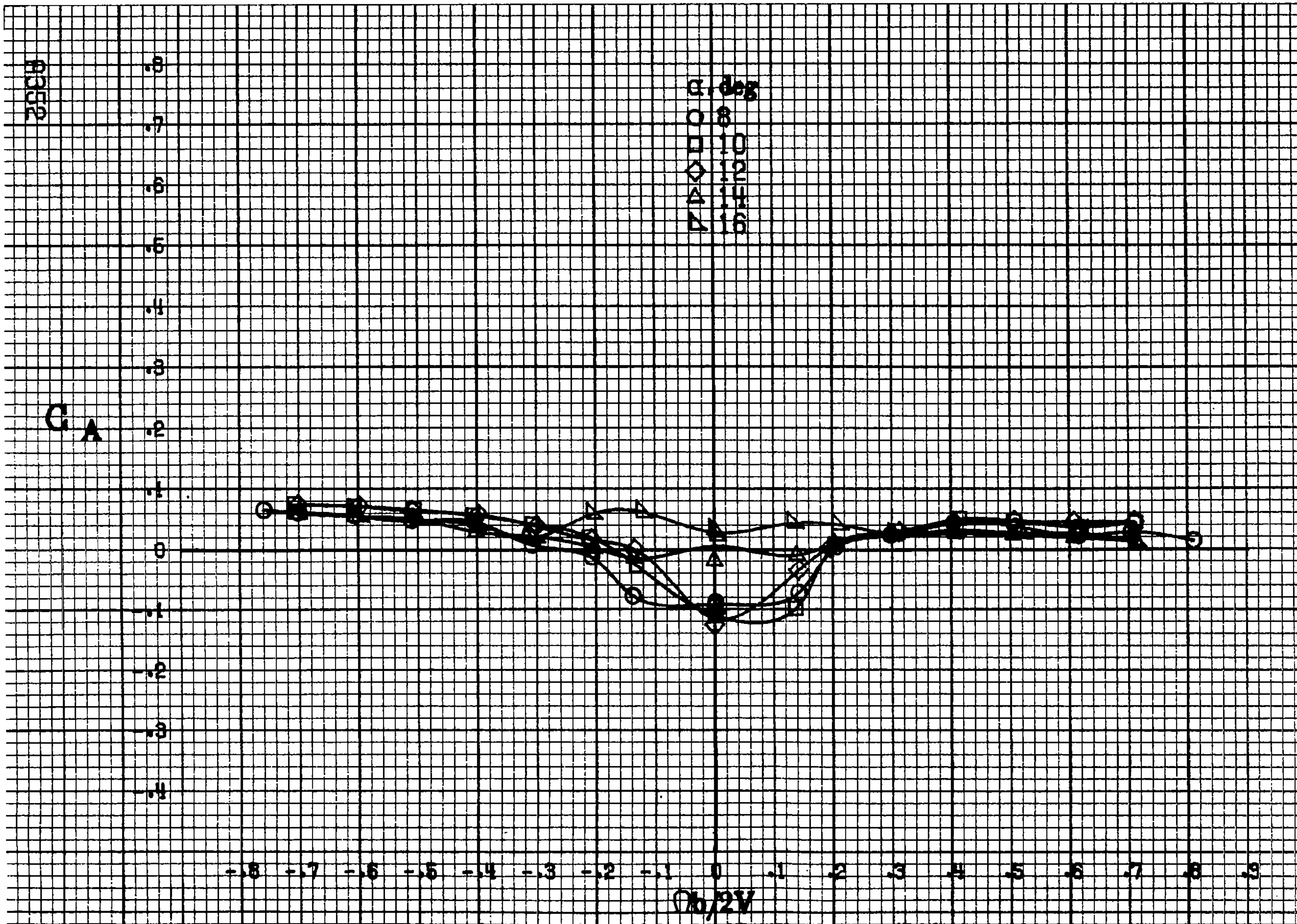

(a) α = 8 to 16 deg, SR = 182.9 cm (72 in).

Figure A34.- Effect of rotation rate and angle of attack on axial-force coefficient for configuration having cowl strakes, ventral and tail fillets. $\delta_e = 0°$, $\delta_a = 0°$, $\delta_r = 0°$, $\beta = 0°$.

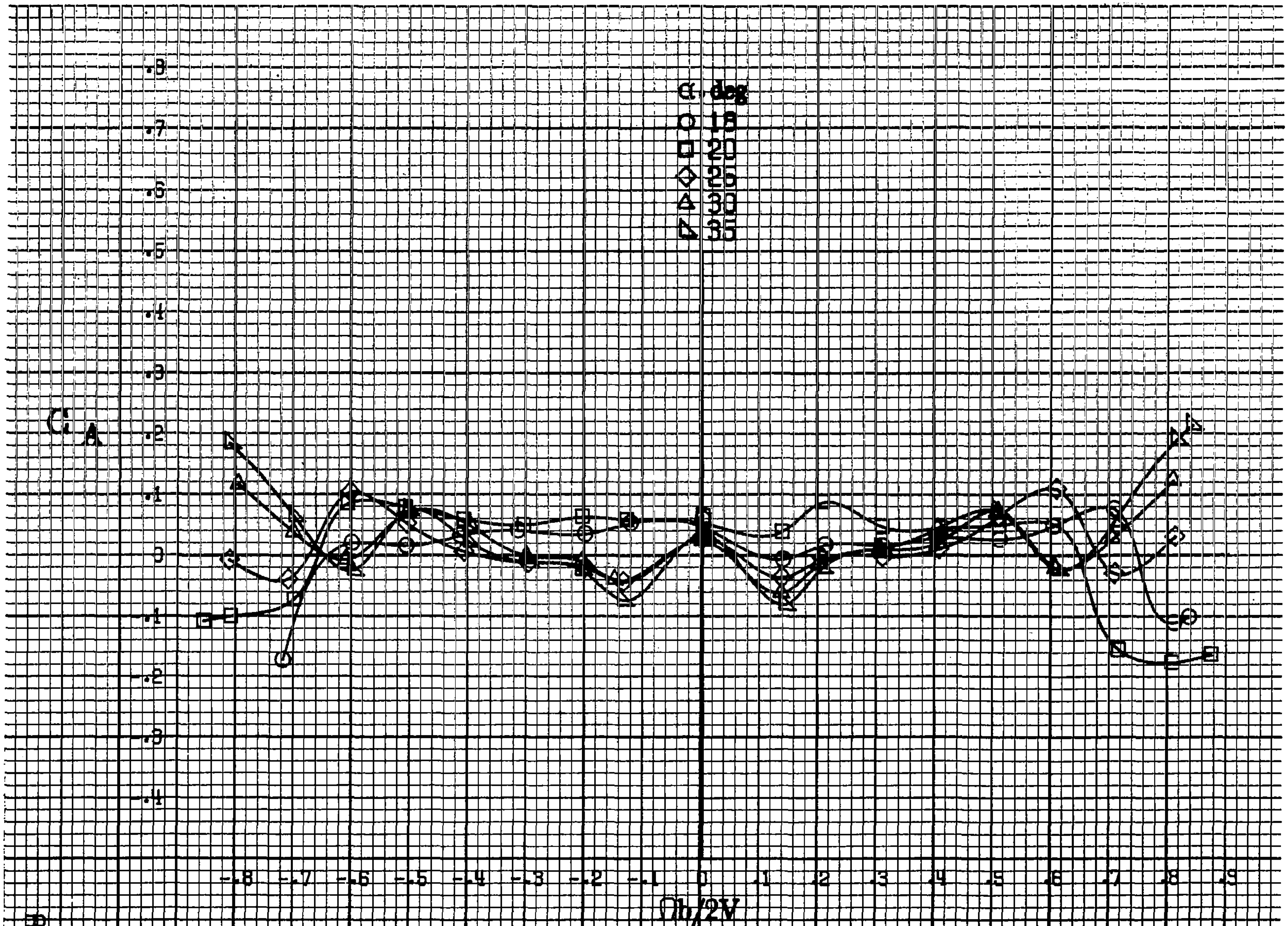

(b) α = 18 to 35 deg, SR = 182.9 cm (72 in).

Figure A84.- Continued.

(c) α = 30 to 50 deg, SR = 0.
Figure A84.-Continued.

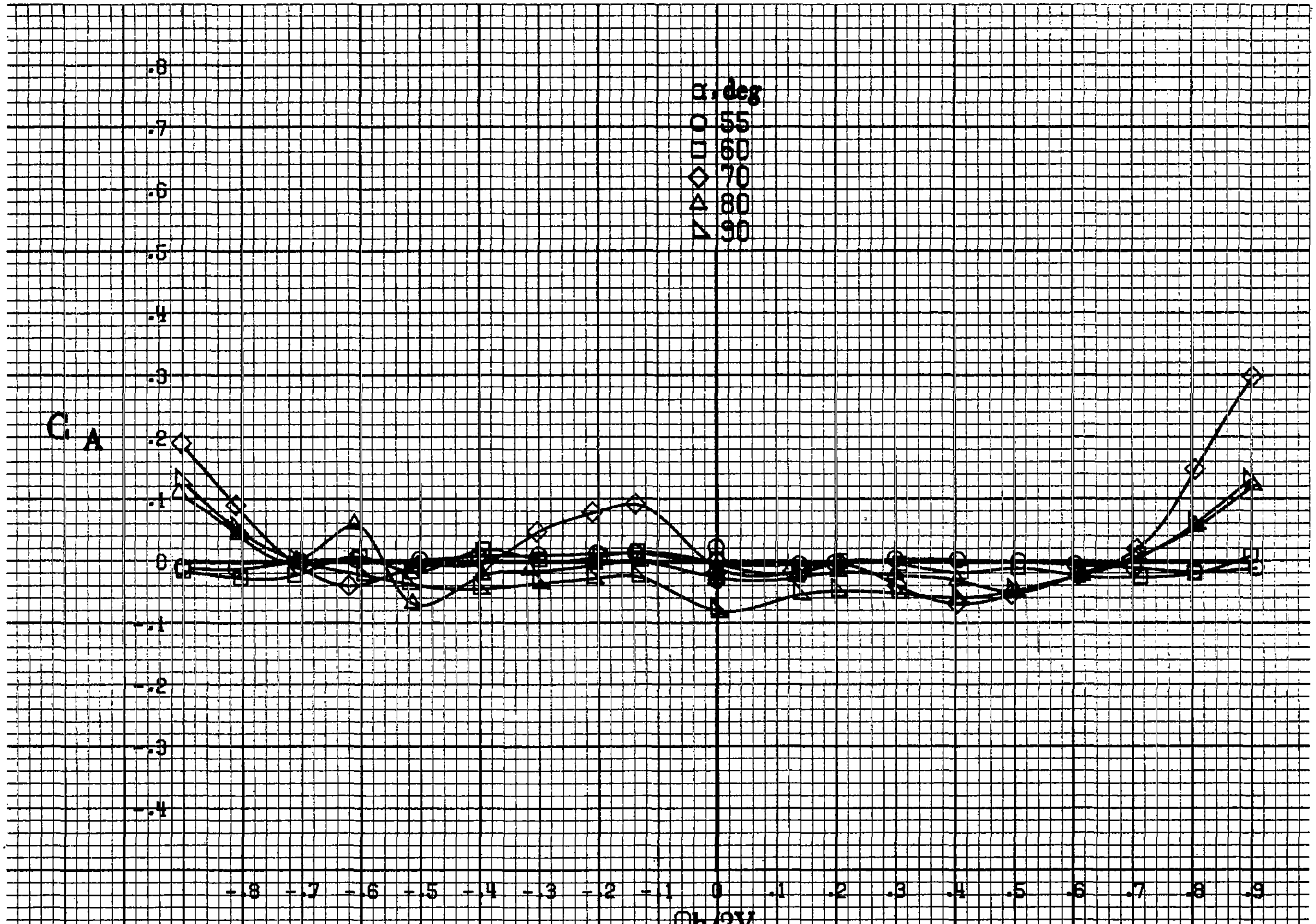

(d) α=55to90deg, SR=0.

Figure A84.-Concluded.

A355

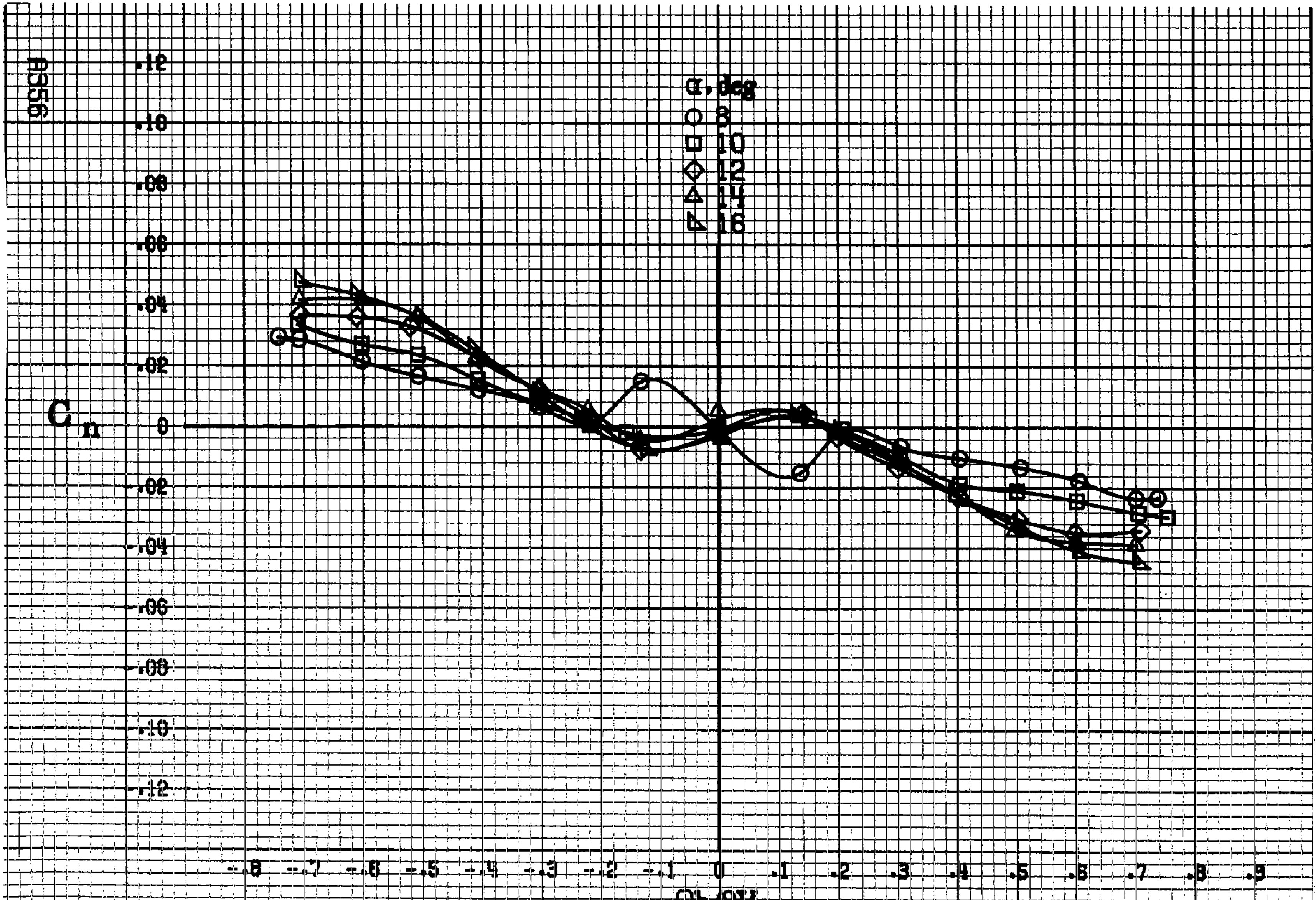

(a) α = 8 to 16 deg, SR = 182.9 cm (72 in).

Figure A85.- Effect of rotation rate and angle of attack on yawing-moment coefficient for horizontal tail off configuration. $\delta_e = 0°$, $\delta_a = 0°$, $\delta_r = 0°$, $\beta = 0°$.

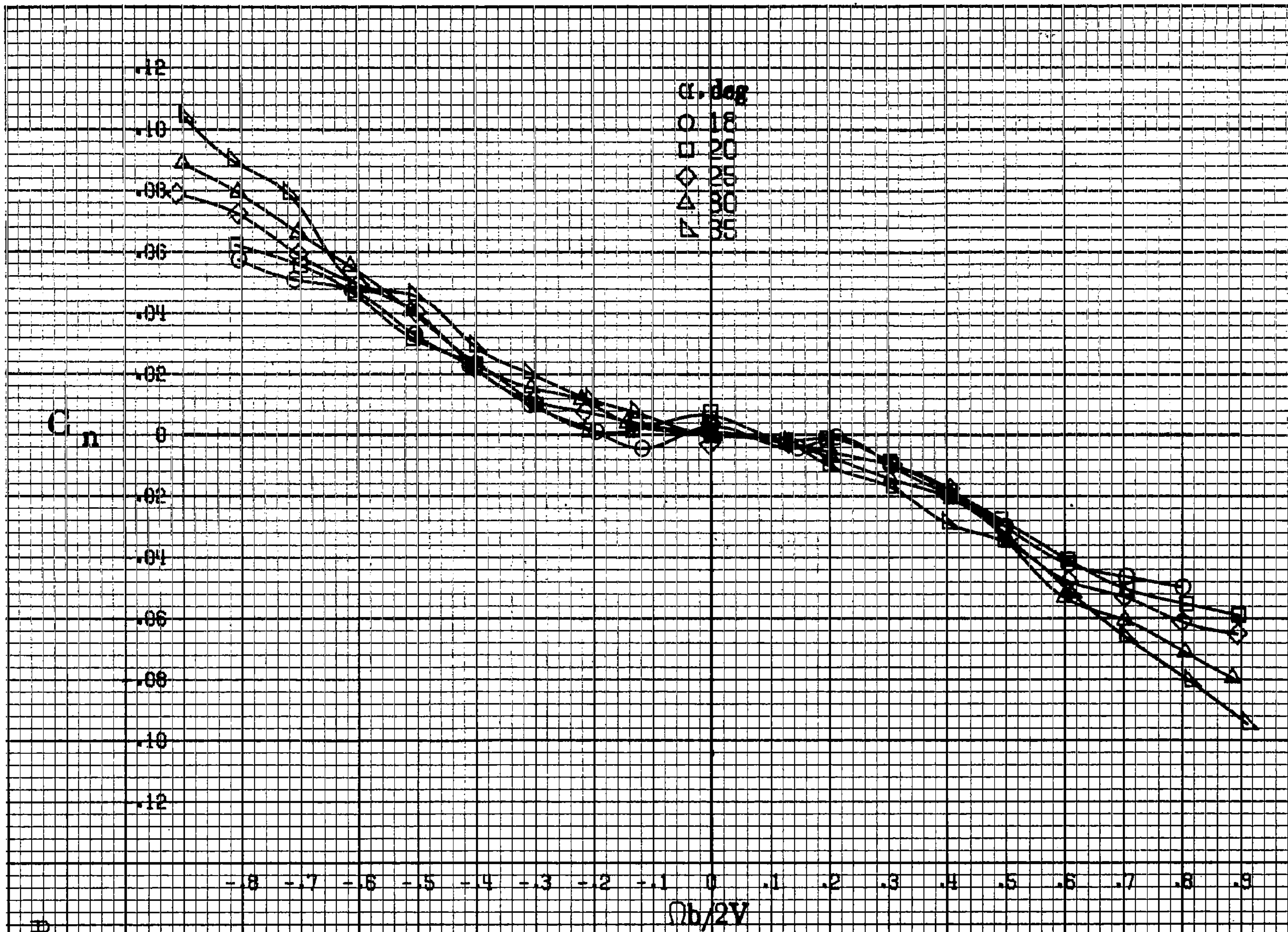

(b) α = 18 to 35 deg, SR = 182.9 cm (72 in).

Figure A85.-Continued.

A357

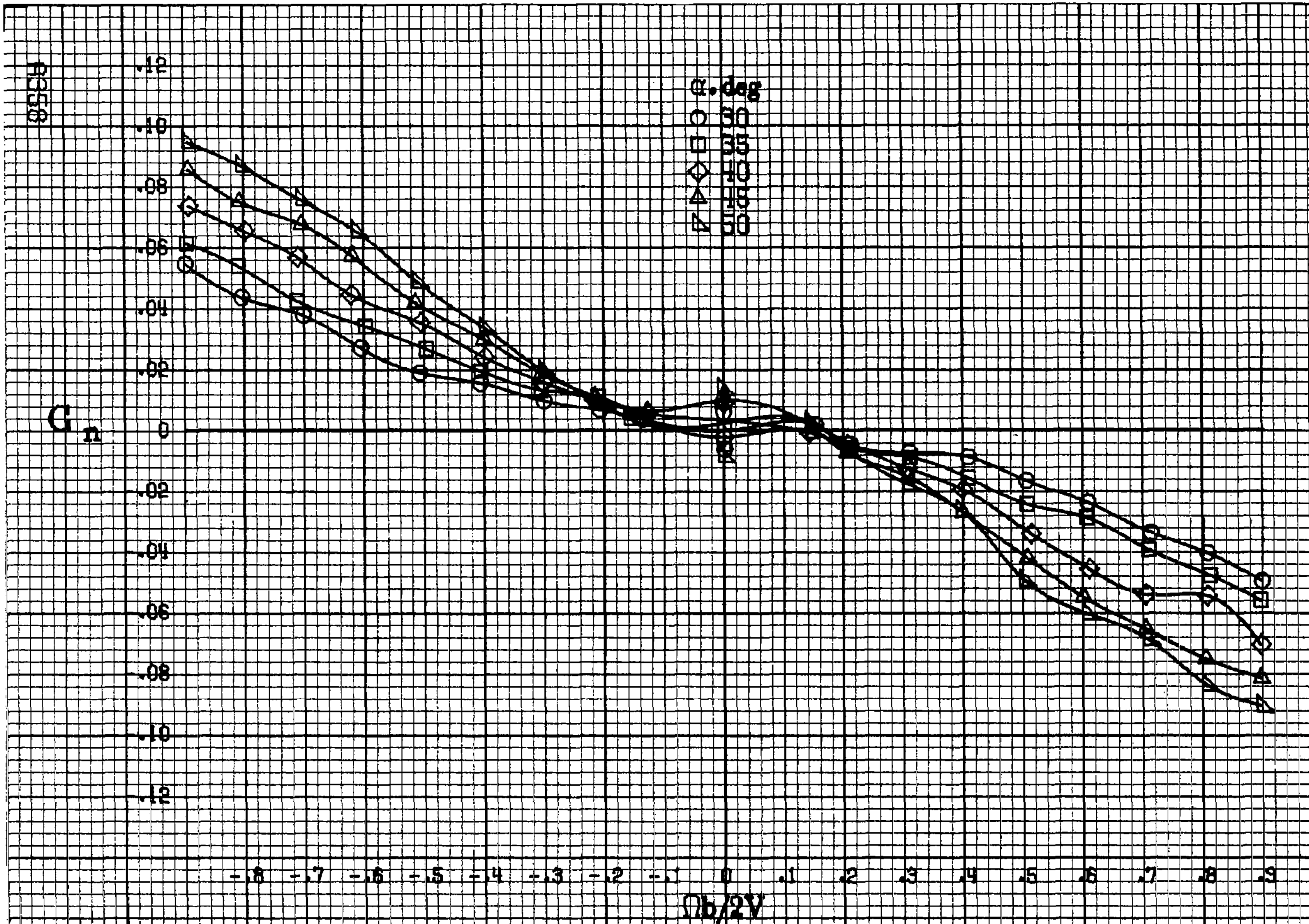

(c) α = 30 to 50 deg, SR = 0.

Figure A85.-Continued.

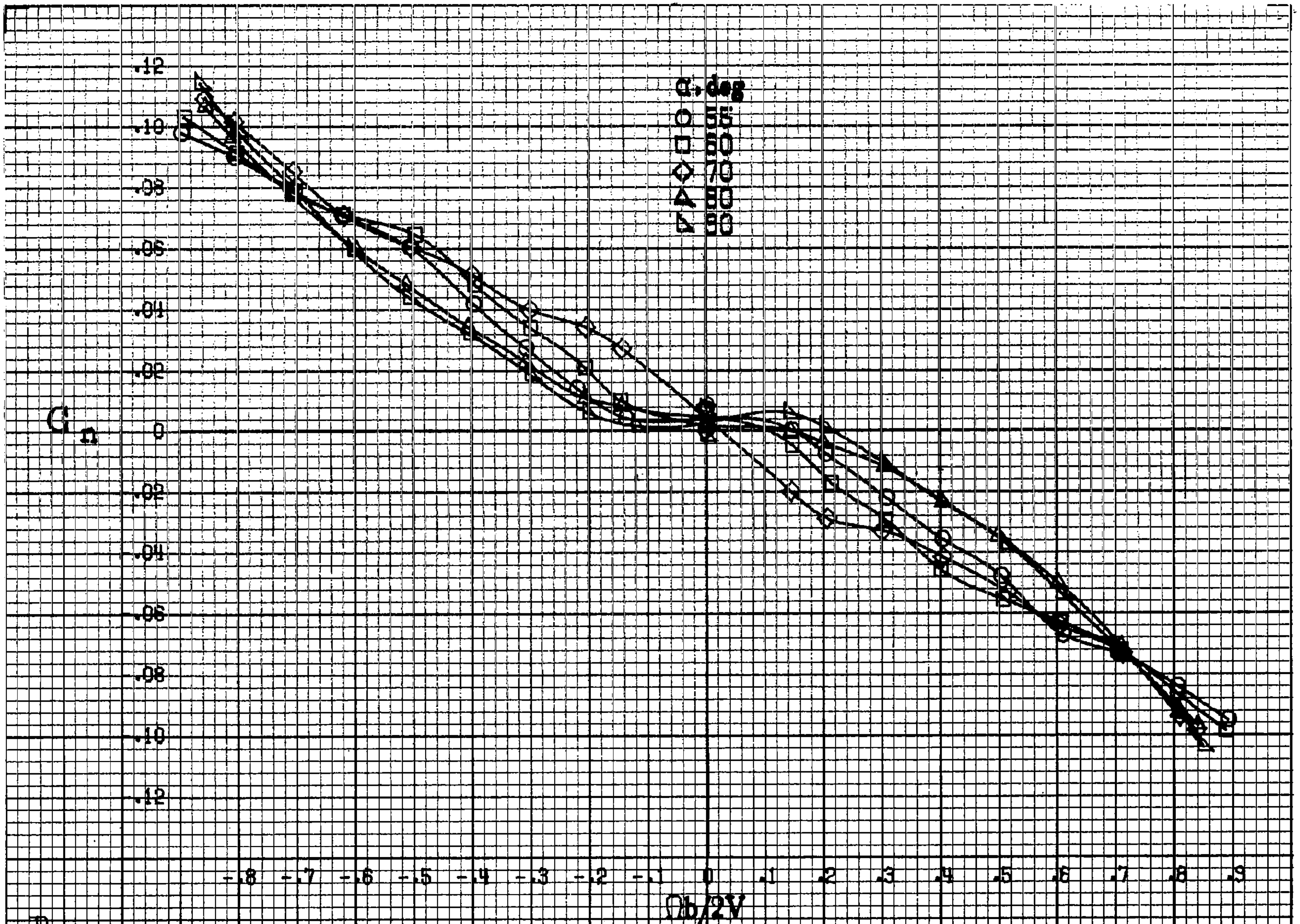

(d) α = 55 to 90 deg, SR = 0.

Figure A85.-Concluded.

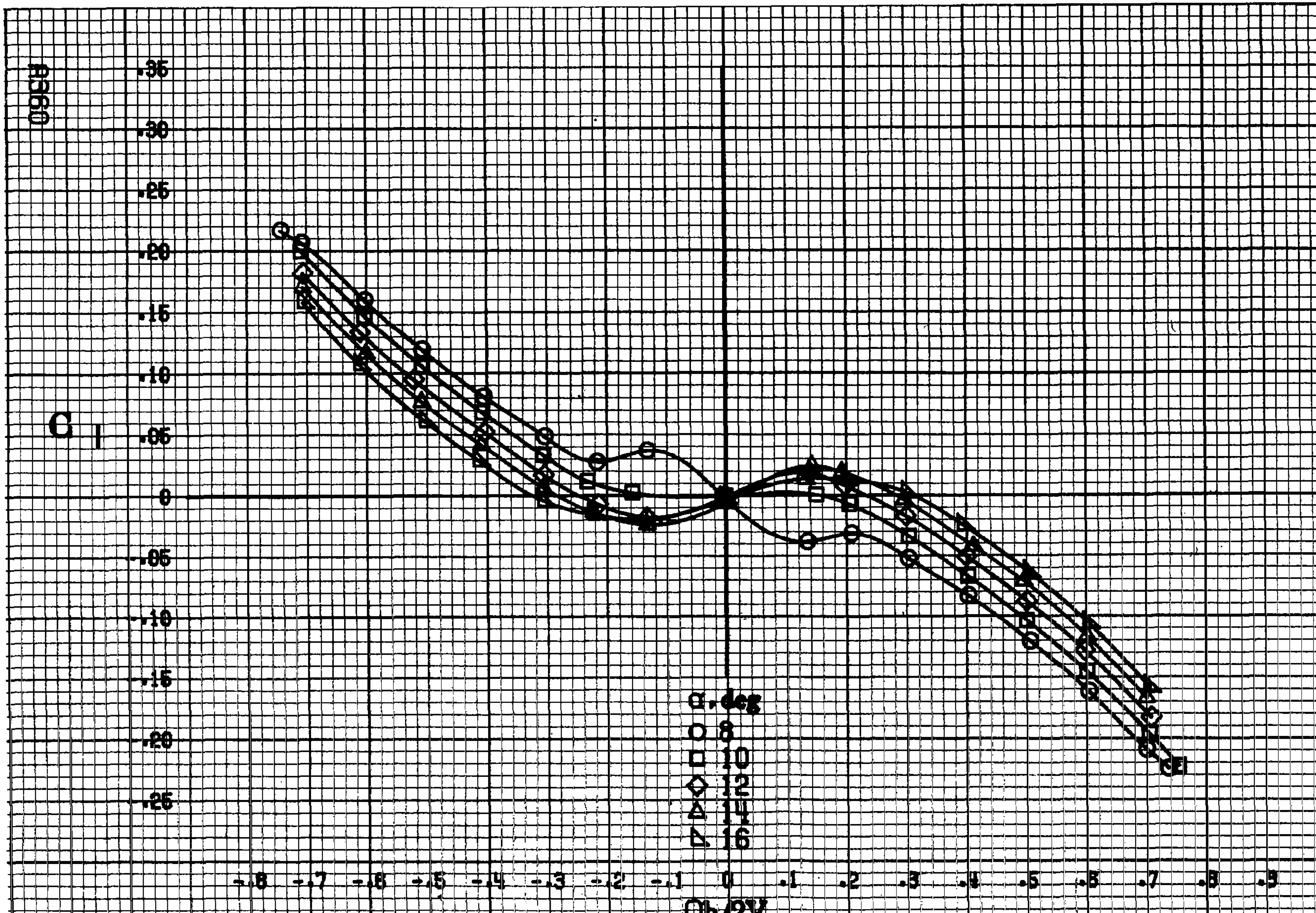

(a) α = 8 to 16 deg, SR = 182.9 cm (72 in).

Figure A86.- Effect of rotation rate and angle of attack on rolling-moment coefficient for horizontal tail off configuration. $\delta_e = 0°$, $\delta_a = 0°$, $\delta_r = 0°$, $\beta = 0°$.

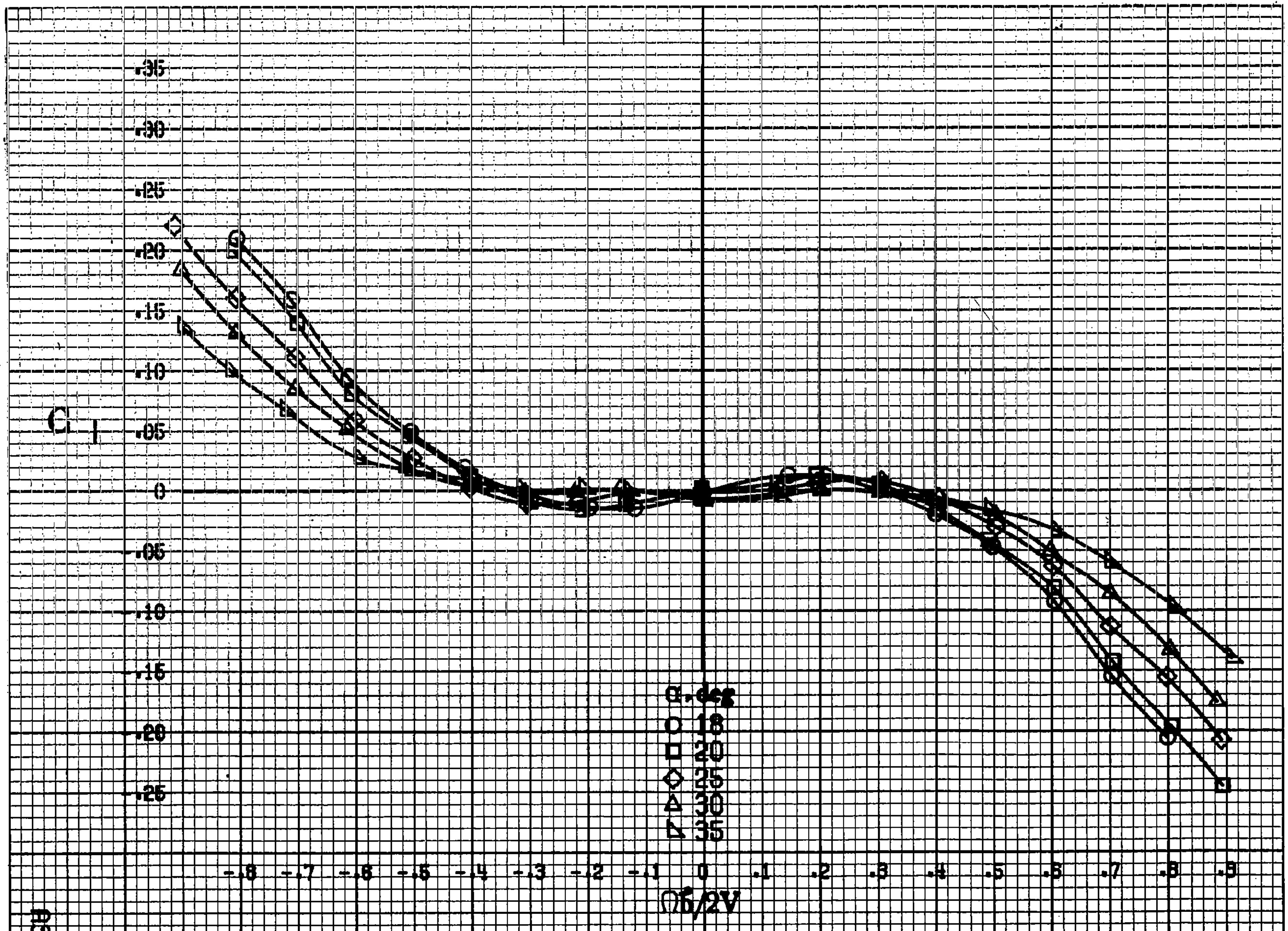

(b) α = 18 to 35 deg, SR = 182.9 cm (72 in).
Figure A86.-Continued.

A361

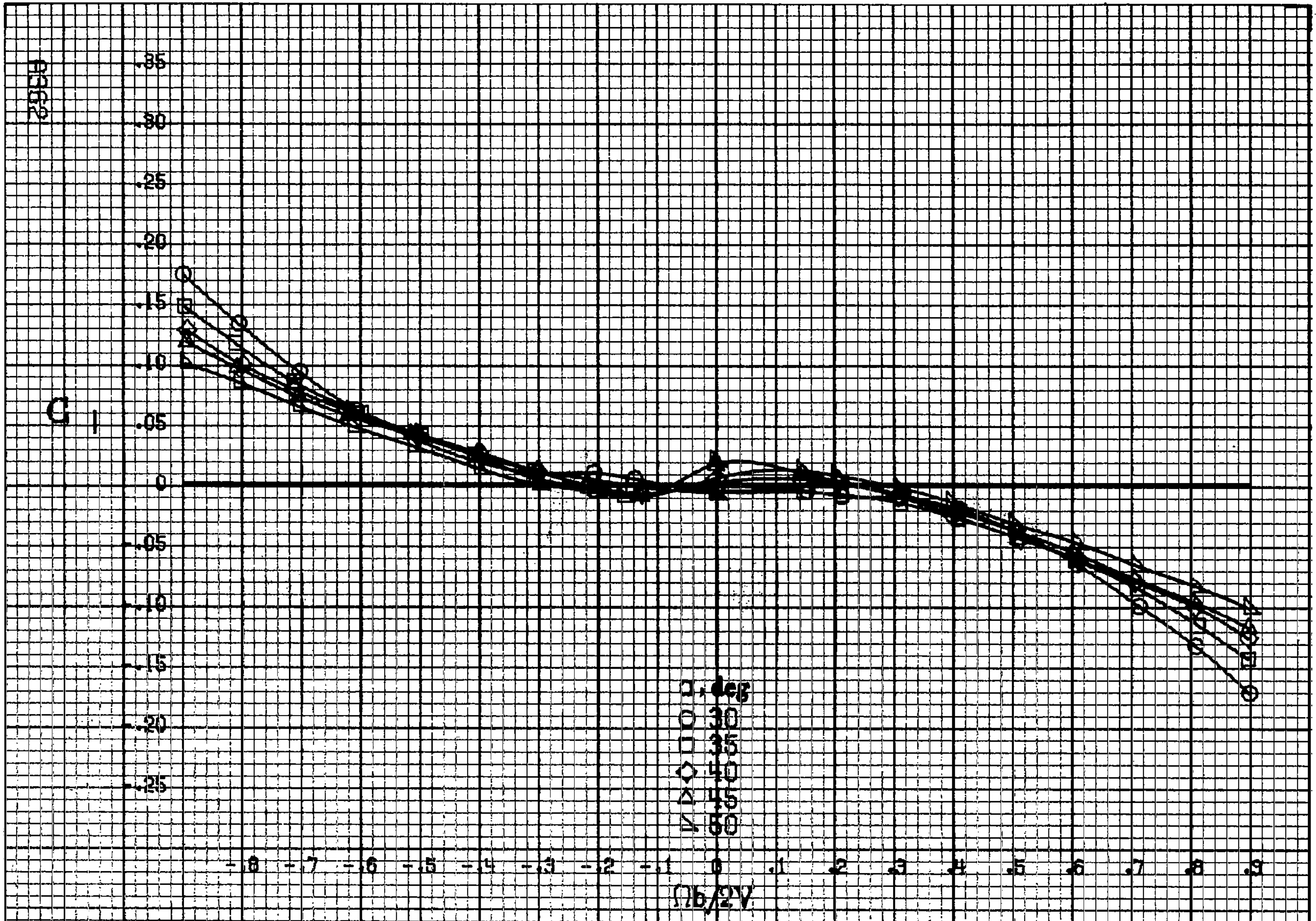

(c) α = 30 to 50 deg, SR = 0.
Figure A36.-Continued.

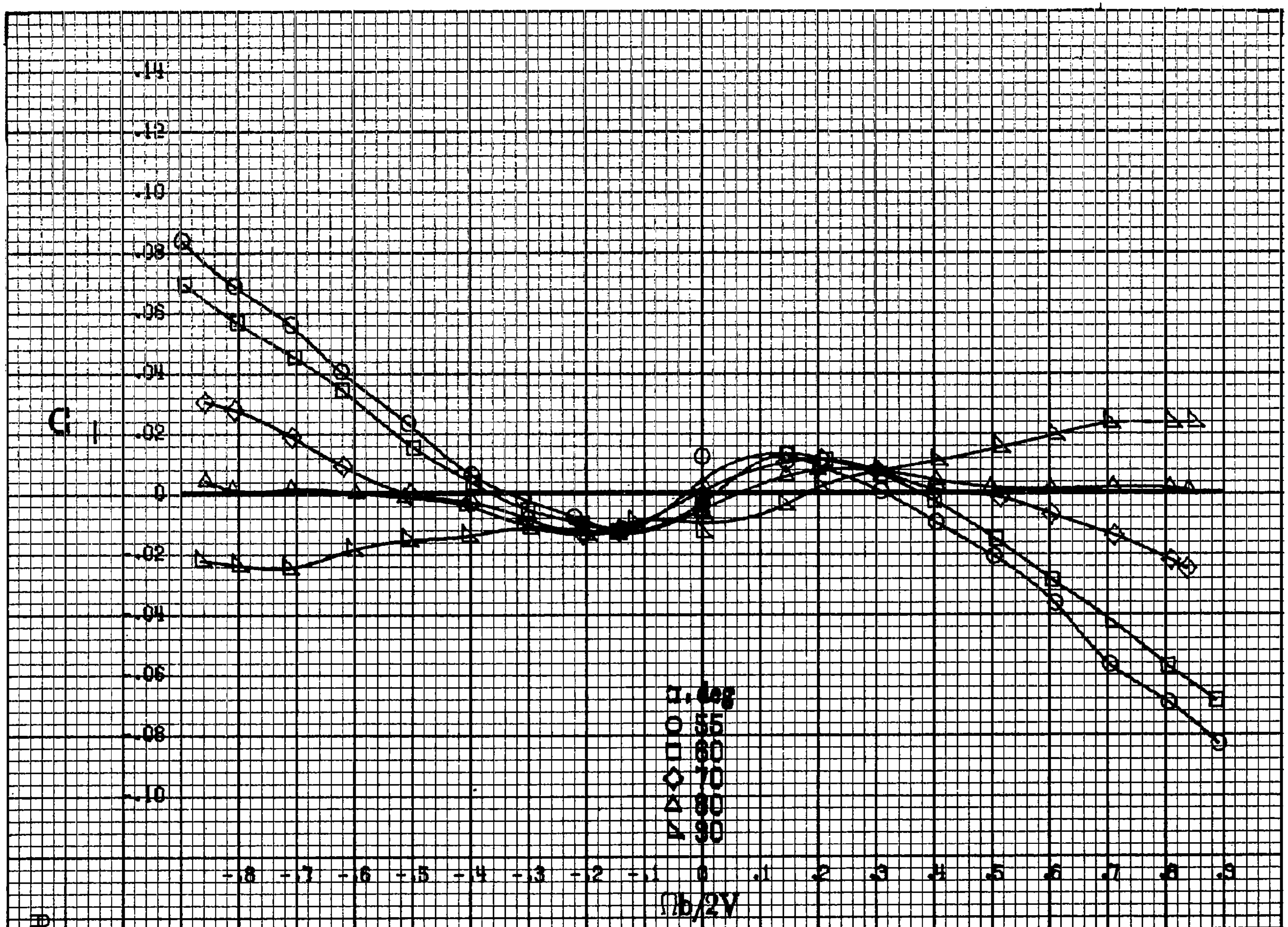

(d) α = 55 to 90 deg, SR = 0.
Figure A86.-Concluded.

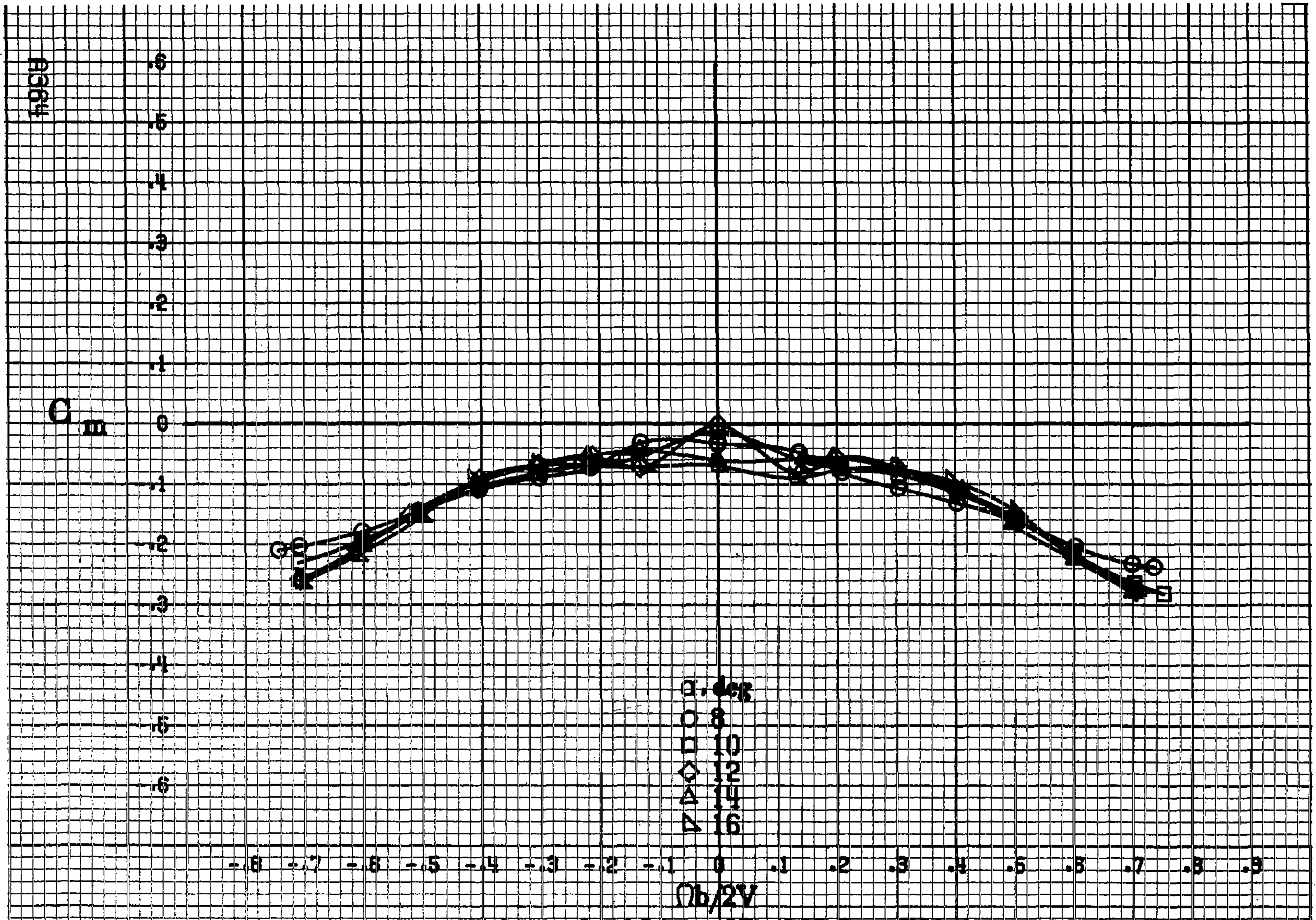

(a) $\alpha = 8$ to 16 deg, SR = 182.9 cm (72 in).

Figure A87.-Effect of rotation rate and angle of attack on pitching-moment coefficient for horizontal tail off configuration. $\delta_e = 0°$, $\delta_a = 0°$, $\delta_r = 0°$, $\beta = 0°$.

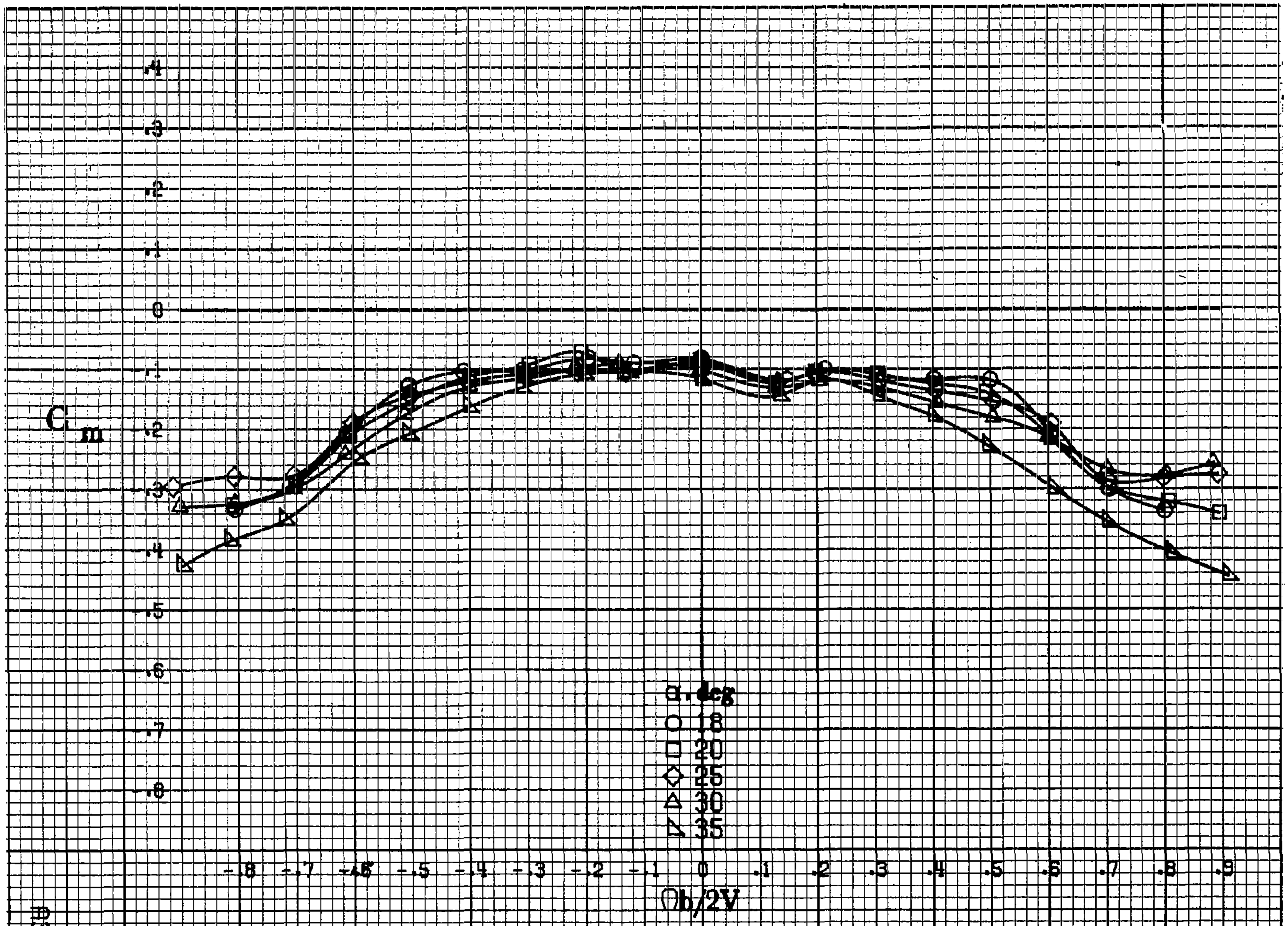

(b) α = 18 to 35 deg, SR = 182.9 cm (72 in).

Figure A87.-Continued.

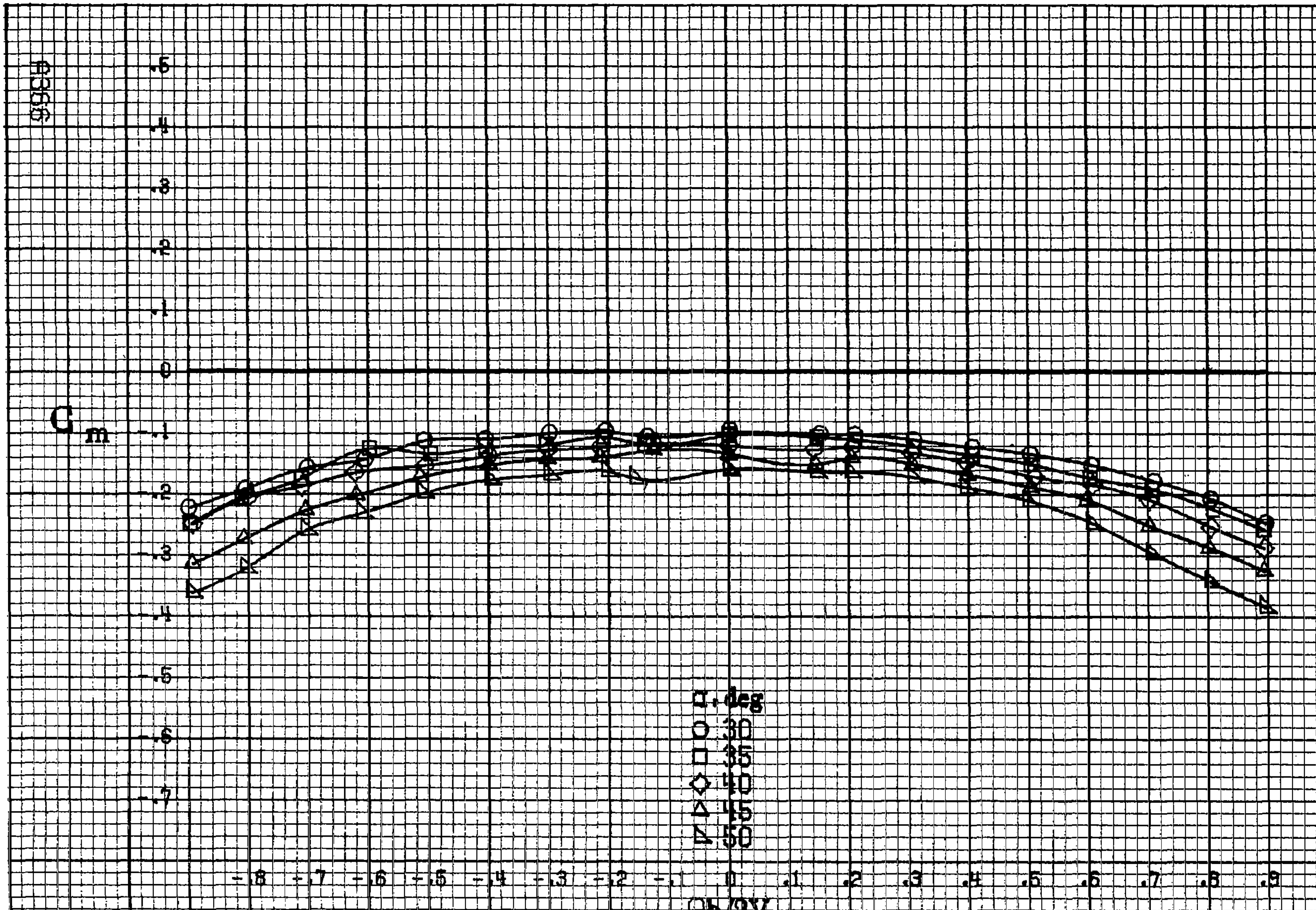

(c) α = 30 to 50 deg, SR = 0.

Figure A87.-Continued.

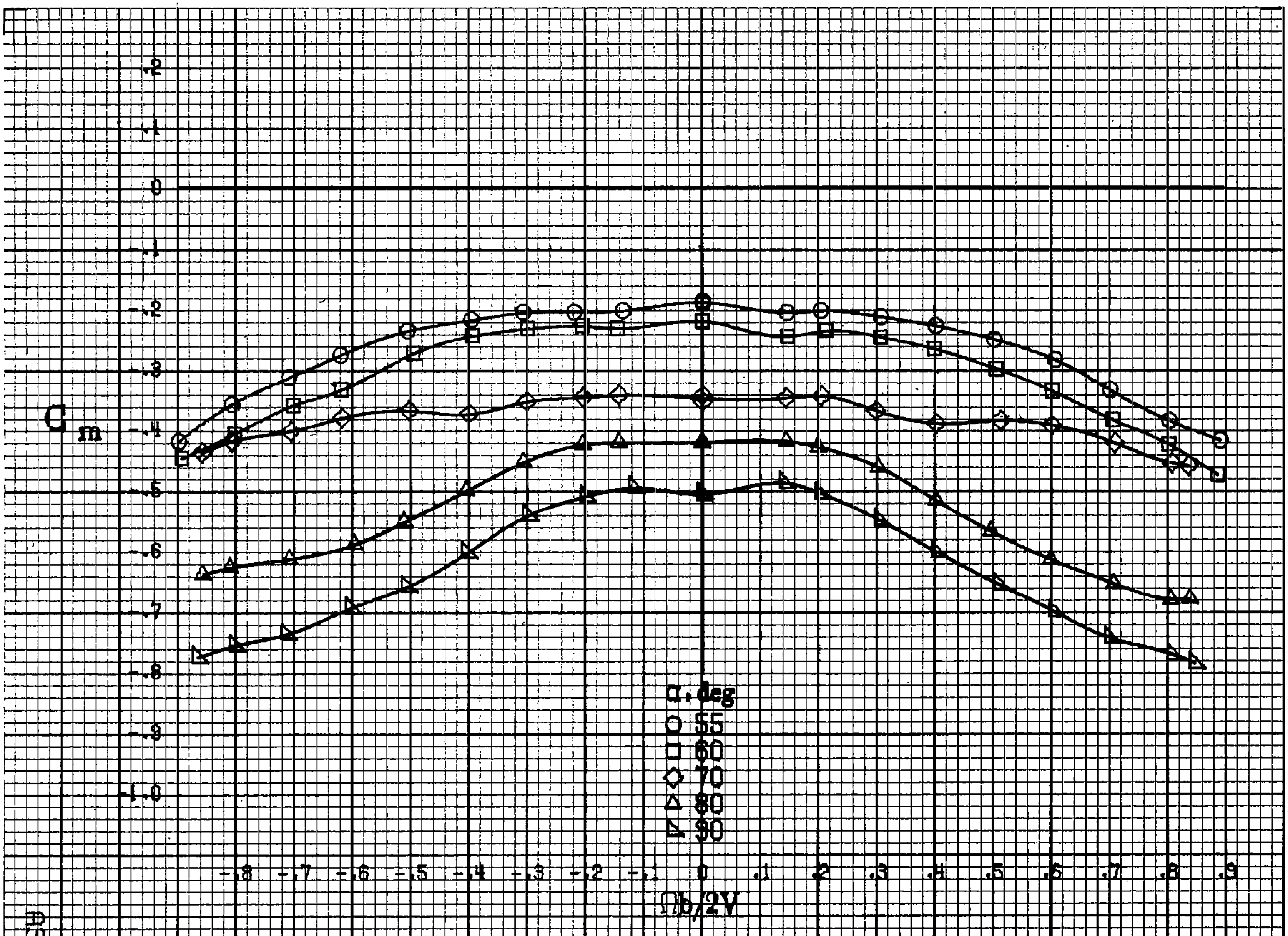

(d) α = 55 to 90 deg, SR = 0.

Figure A87.- Concluded.

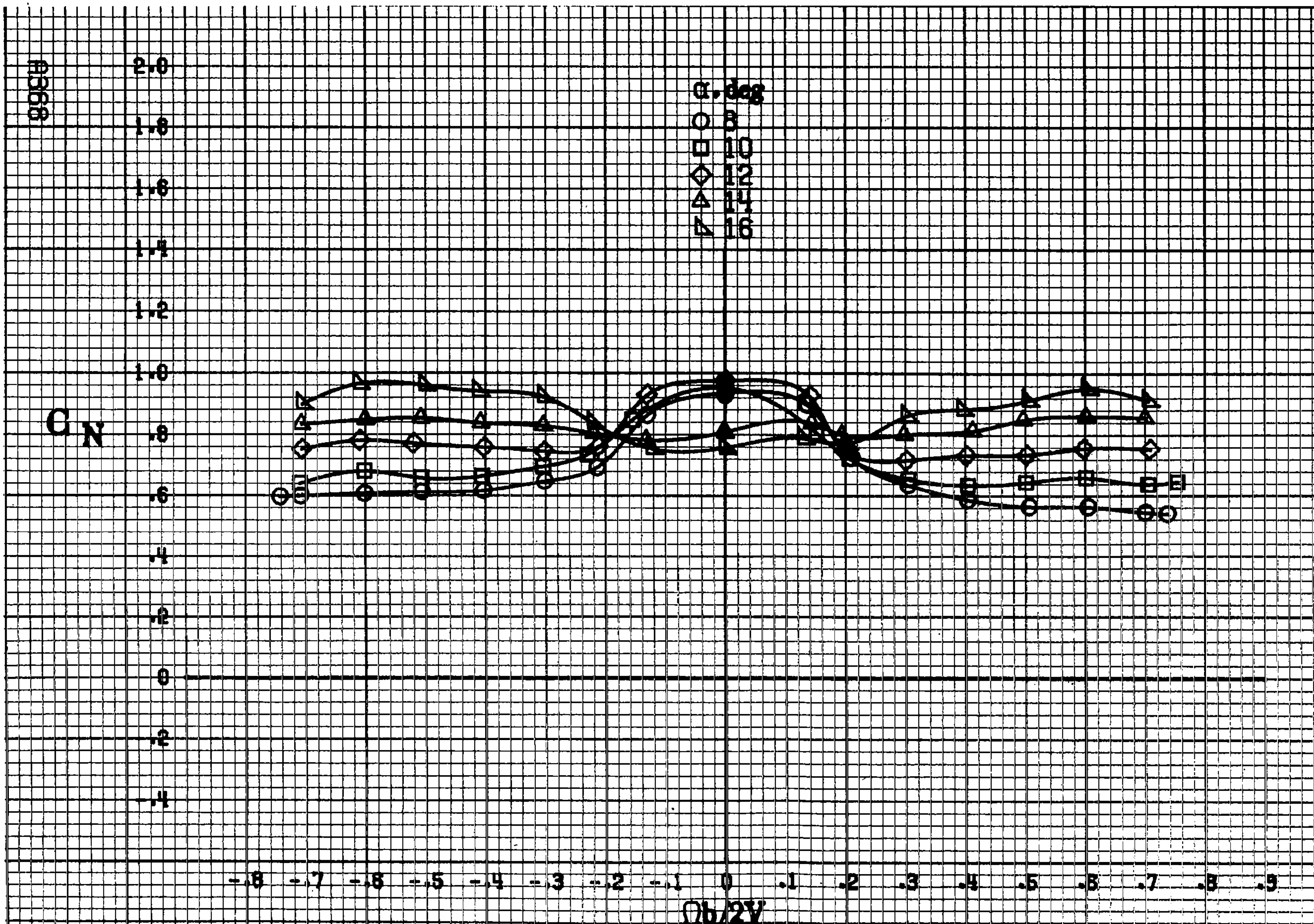

(a) $\alpha = 8$ to 16 deg, SR = 182.9 cm (72 in.).

Figure A88.- Effect of rotation rate and angle of attack on normal-force coefficient for horizontal tail off configuration. $\delta_e = 0°$, $\delta_a = 0°$, $\delta_r = 0°$, $\beta = 0°$.

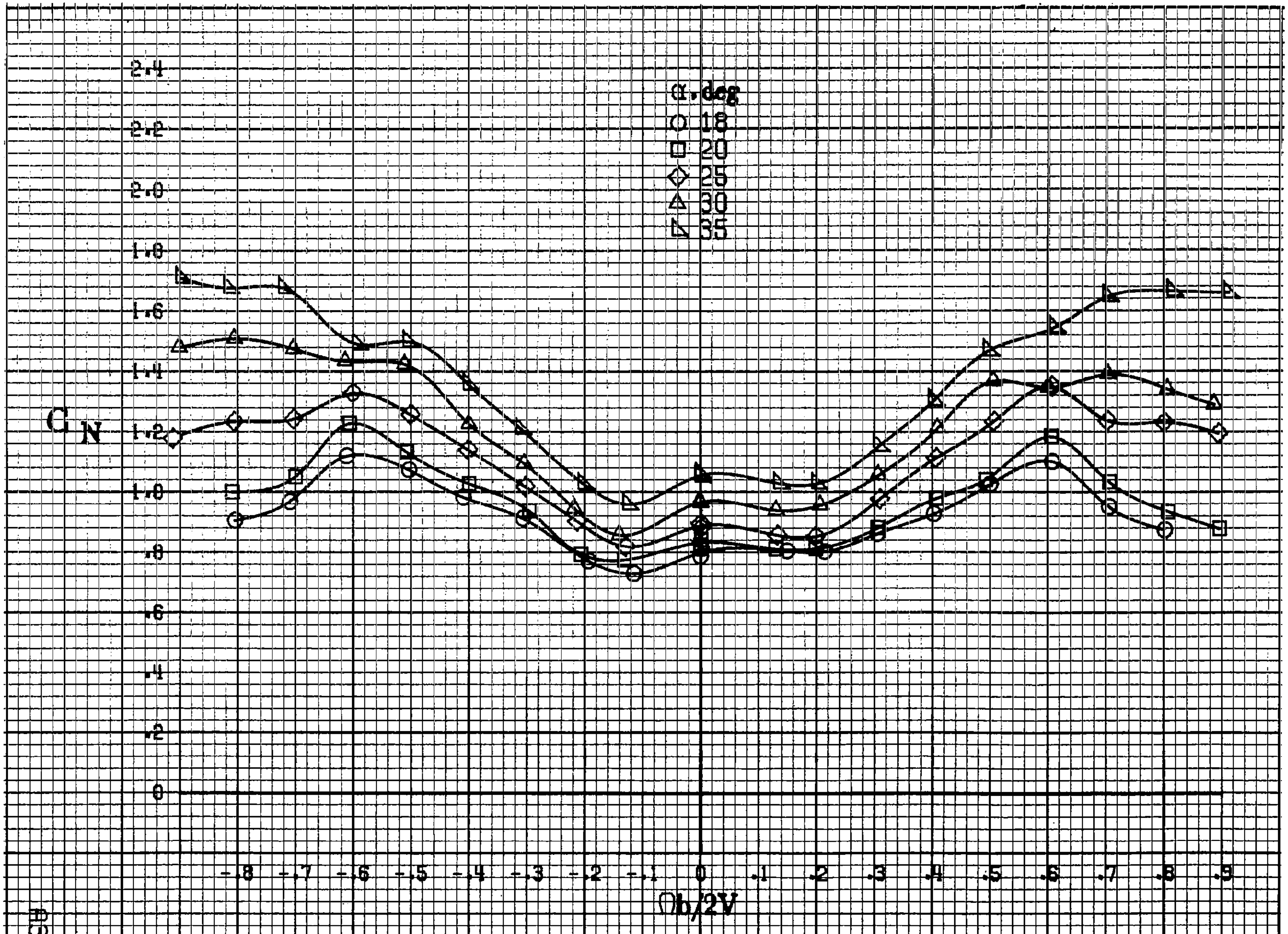

(b) α = 18 to 35 deg, SR = 182.9 cm (72 in).

Figure A88.-Continued.

A369

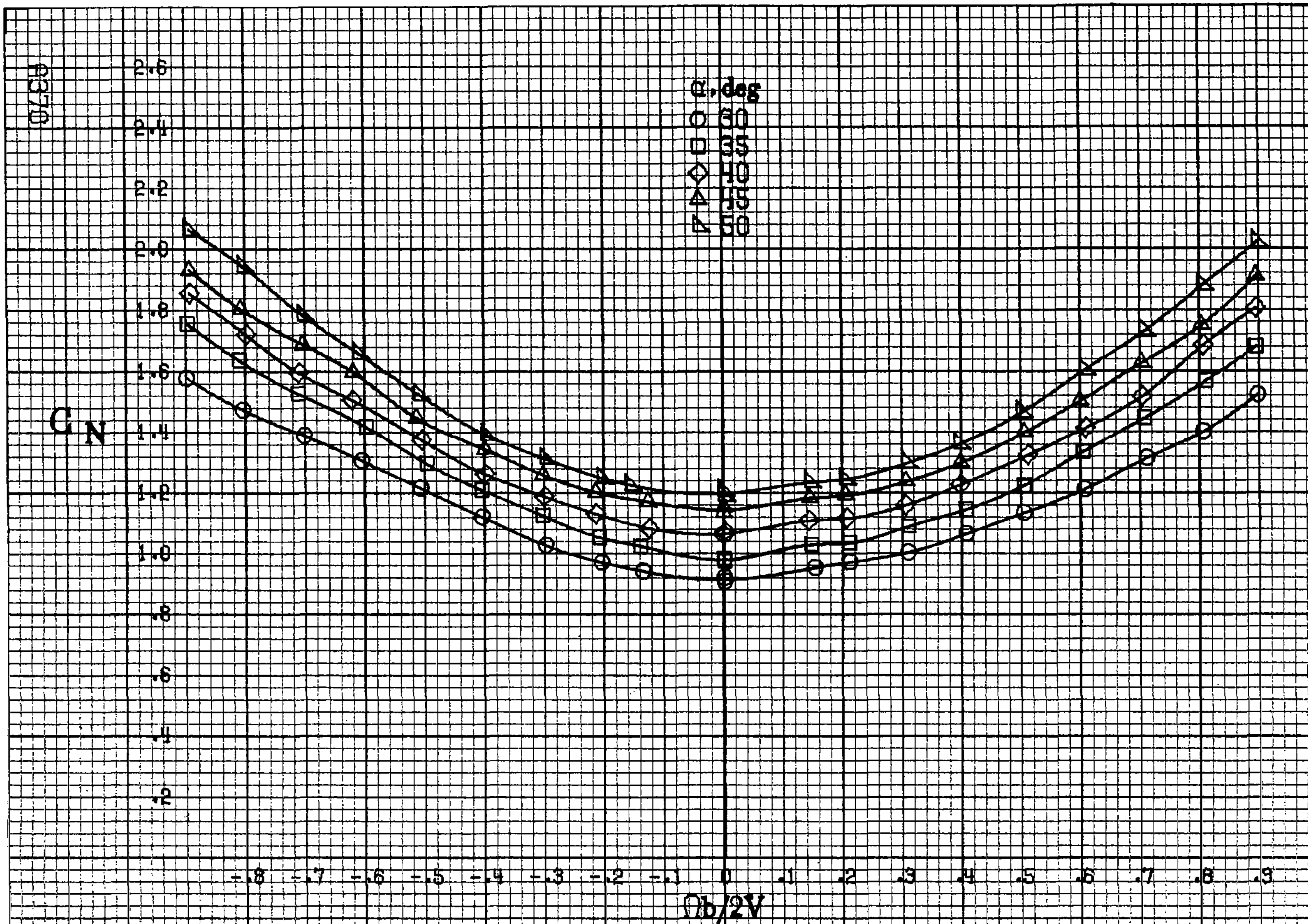

(c) α=30to50deg, SR=0.
Figure A88.-Continued.

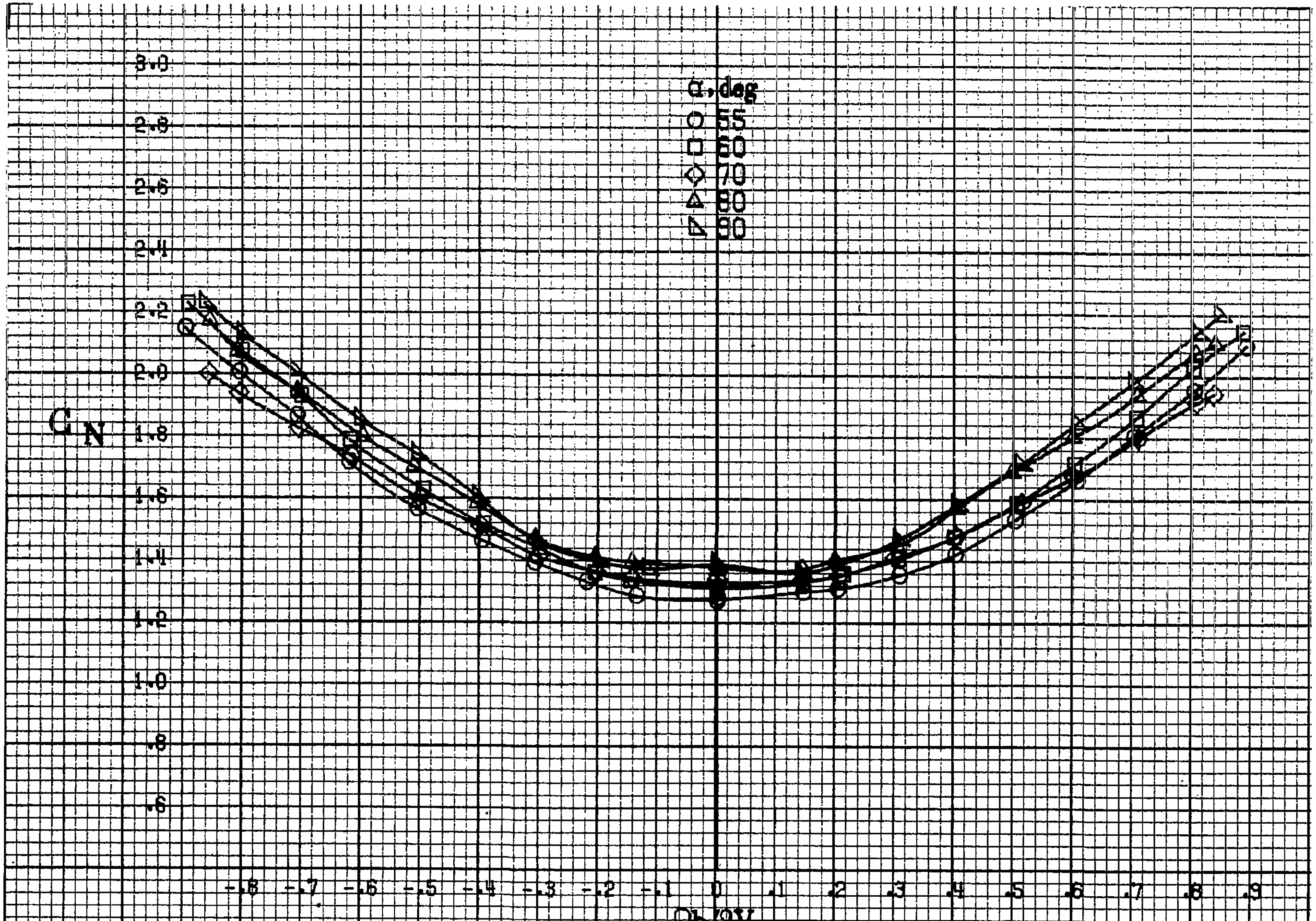

(d) α = 55 to 90 deg, SR = 0.

Figure A88.-Concluded.

A371

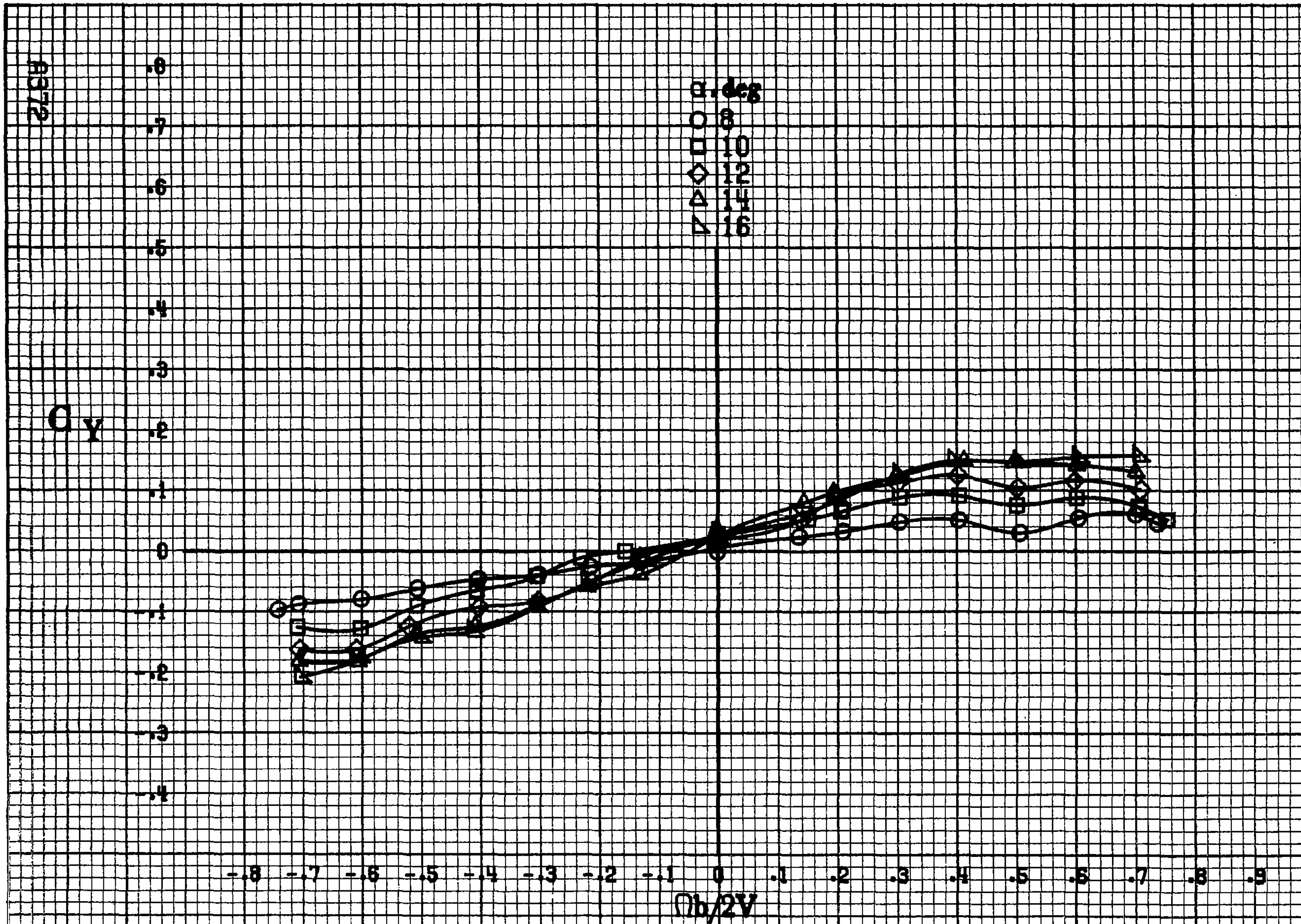

(a) $\alpha = 8$ to 16 deg, SR = 182.9 cm (72 in).

Figure A89.-Effect of rotation rate and angle of attack on side-force coefficient for horizontal tail off configuration. $\delta_e = 0°$, $\delta_a = 0°$, $\delta_r = 0°$, $\beta = 0°$.

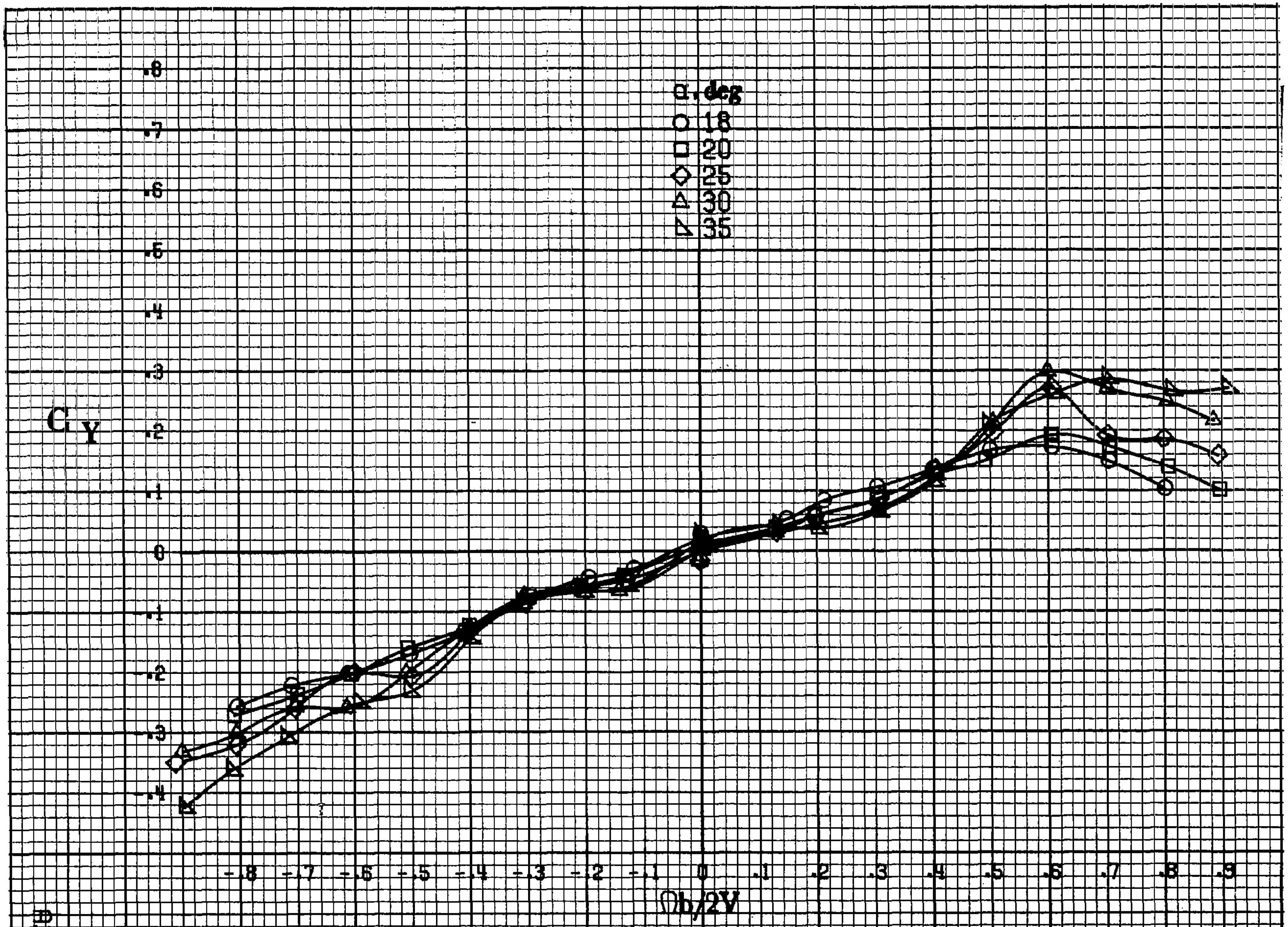

(b) α = 18 to 35 deg, SR = 182.9 cm (72 in).

Figure A89.- Continued.

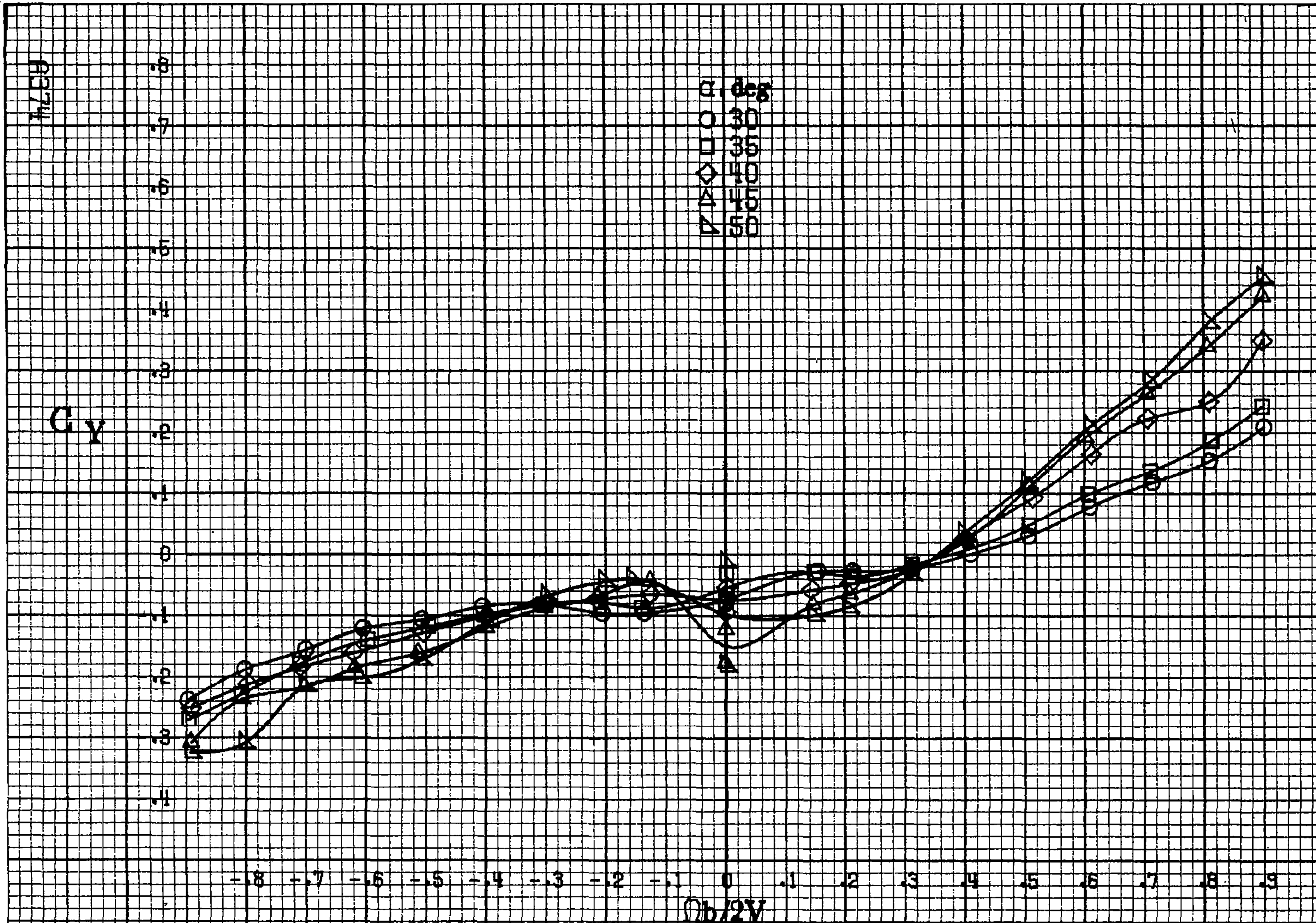

(c) α = 30 to 50 deg, SR = 0.

Figure A89.-Continued.

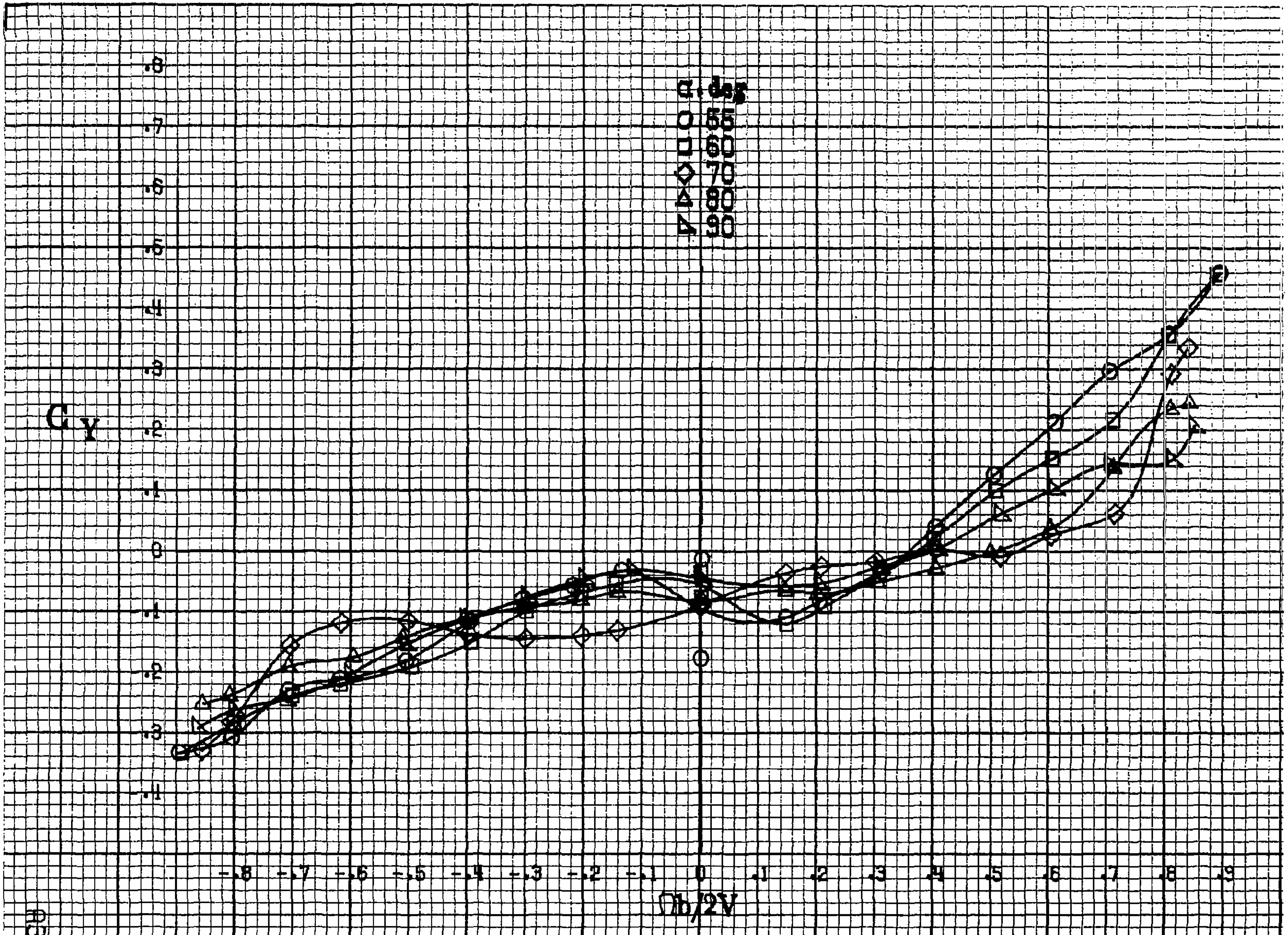

(d) α = 55 to 90 deg, SR = 0.
Figure A89.-Concluded.

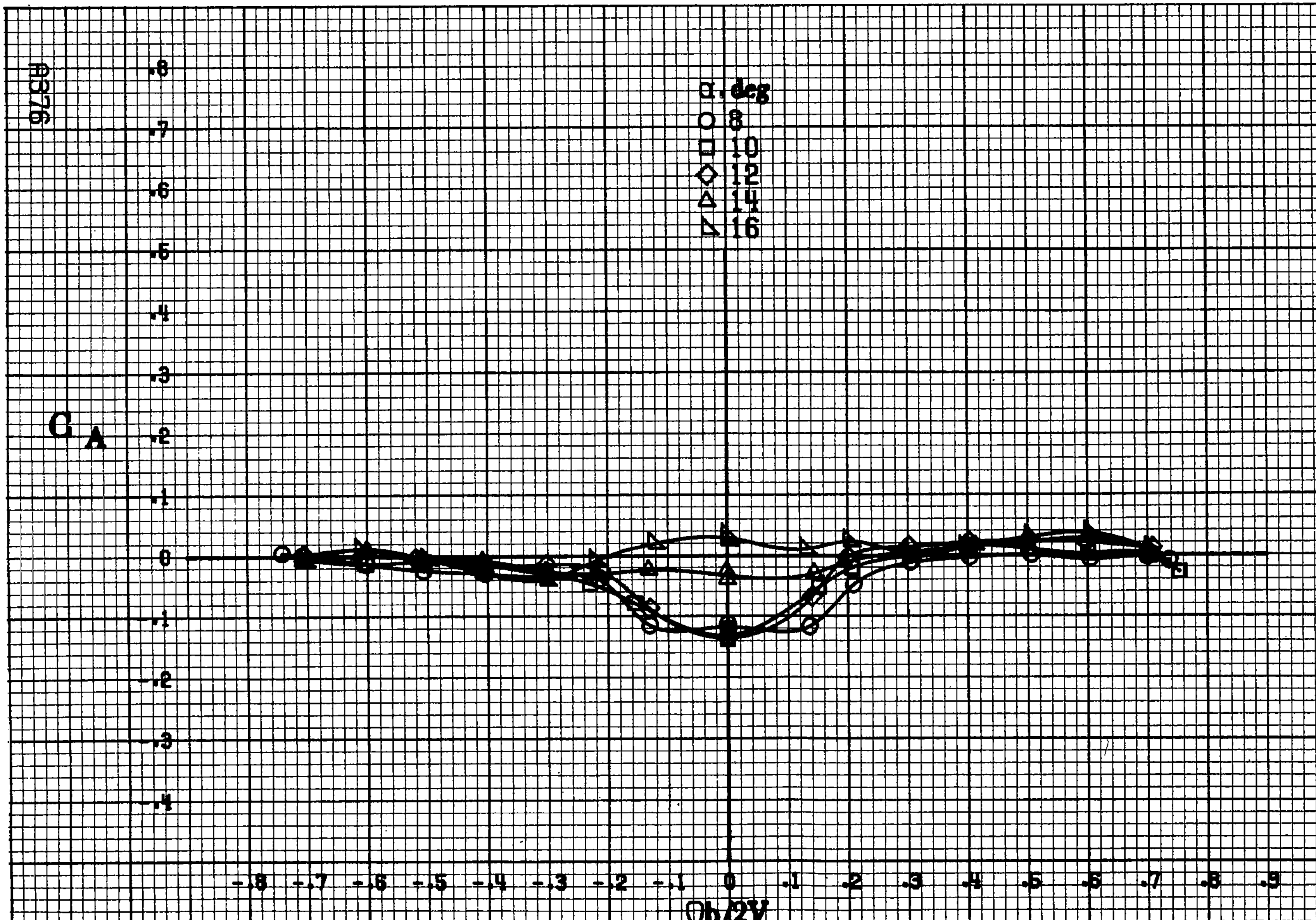

(a) α = 8 to 16 deg, SR = 182.9 cm (72 in).

Figure A90.- Effect of rotation rate and angle of attack on axial-force coefficient for horizontal tail off configuration. $\delta_e = 0°$, $\delta_a = 0°$, $\delta_r = 0°$, $\beta = 0°$.

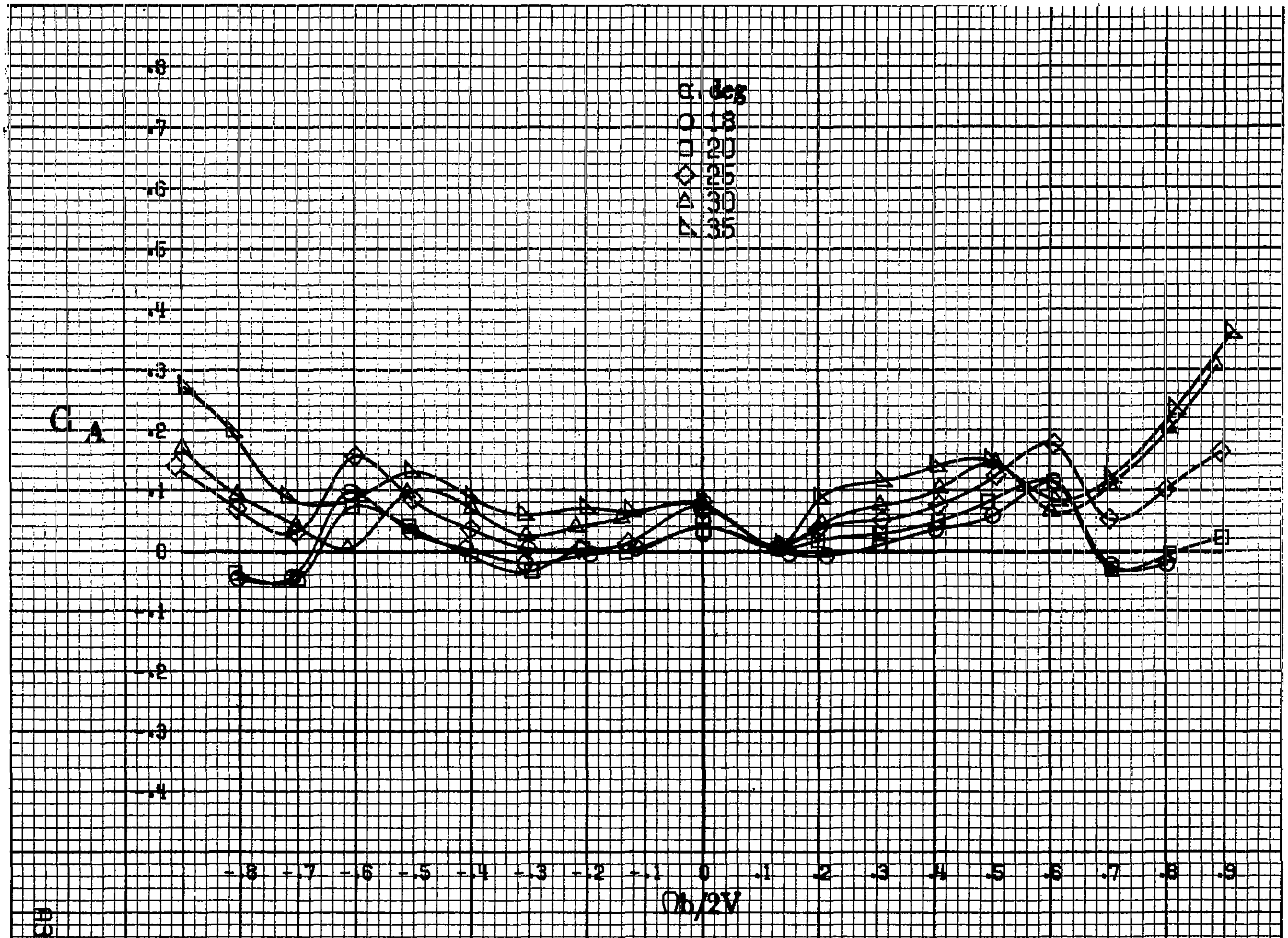

(b) α = 18 to 35 deg, SR = 182.9 cm (72 in).

Figure A90.-Continued.

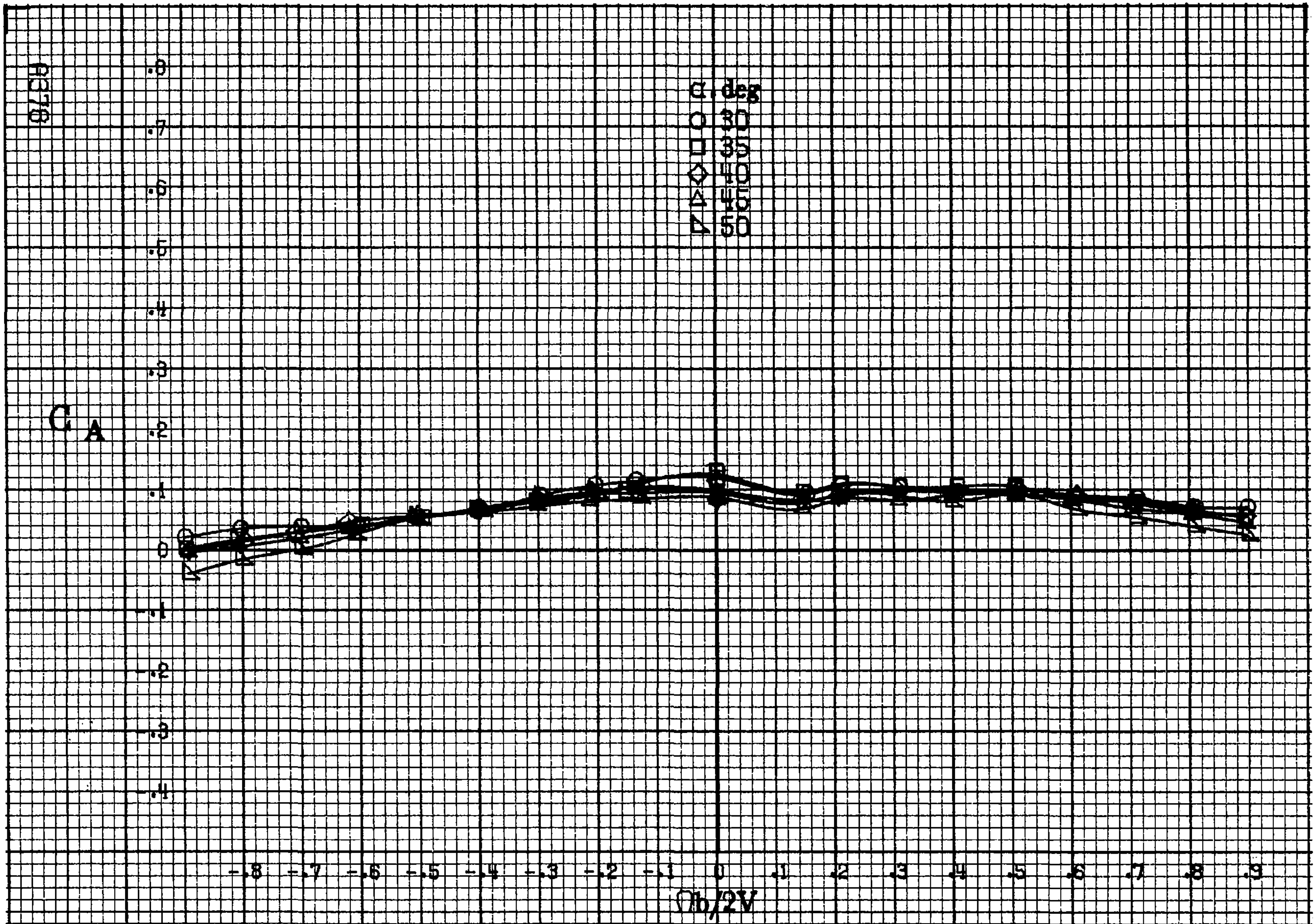

(c) α = 30 to 50 deg, SR = 0.

Figure A90.-Continued.

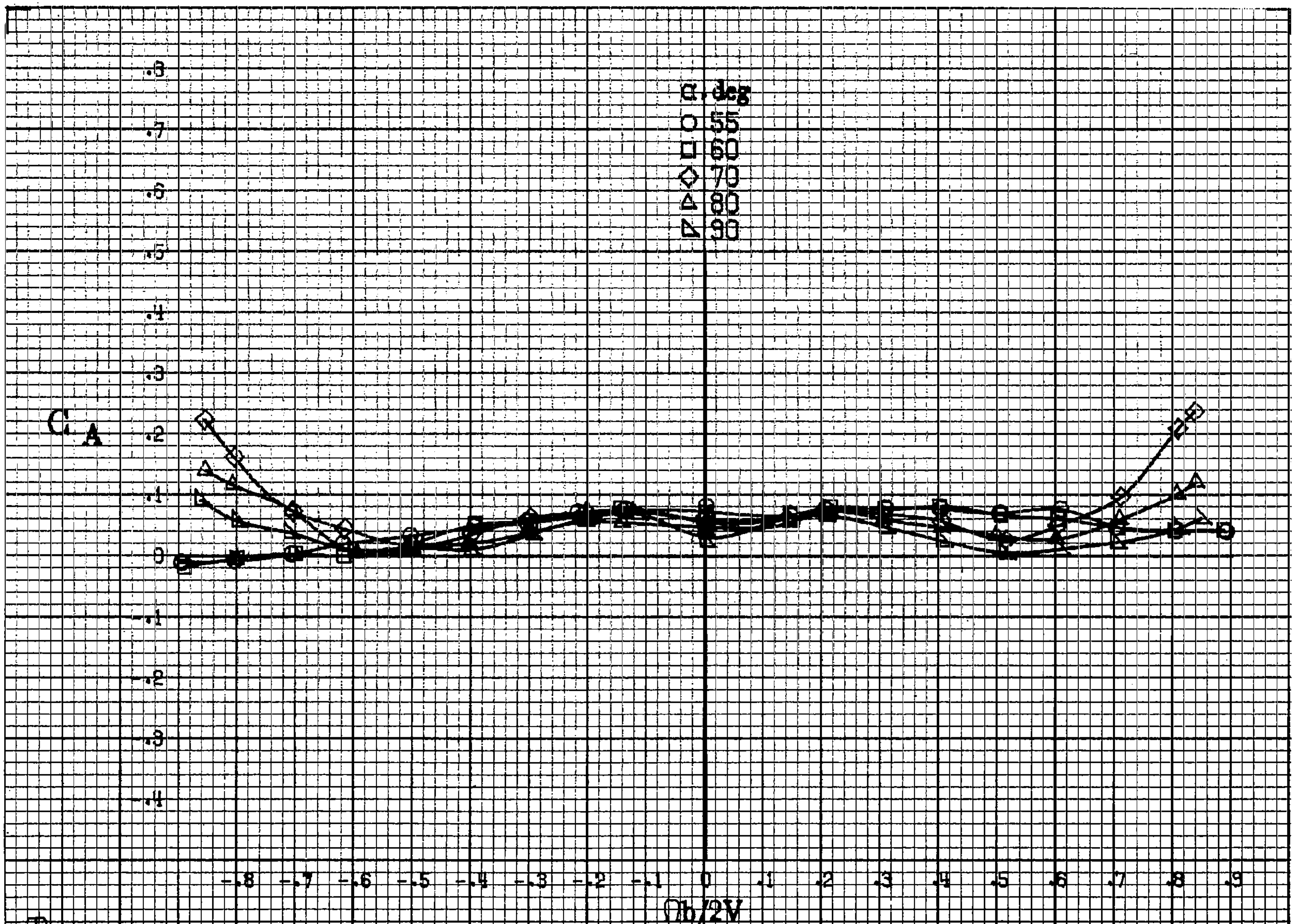

(d) α = 55 to 90 deg, SR = 0.

Figure A90.-Concluded.

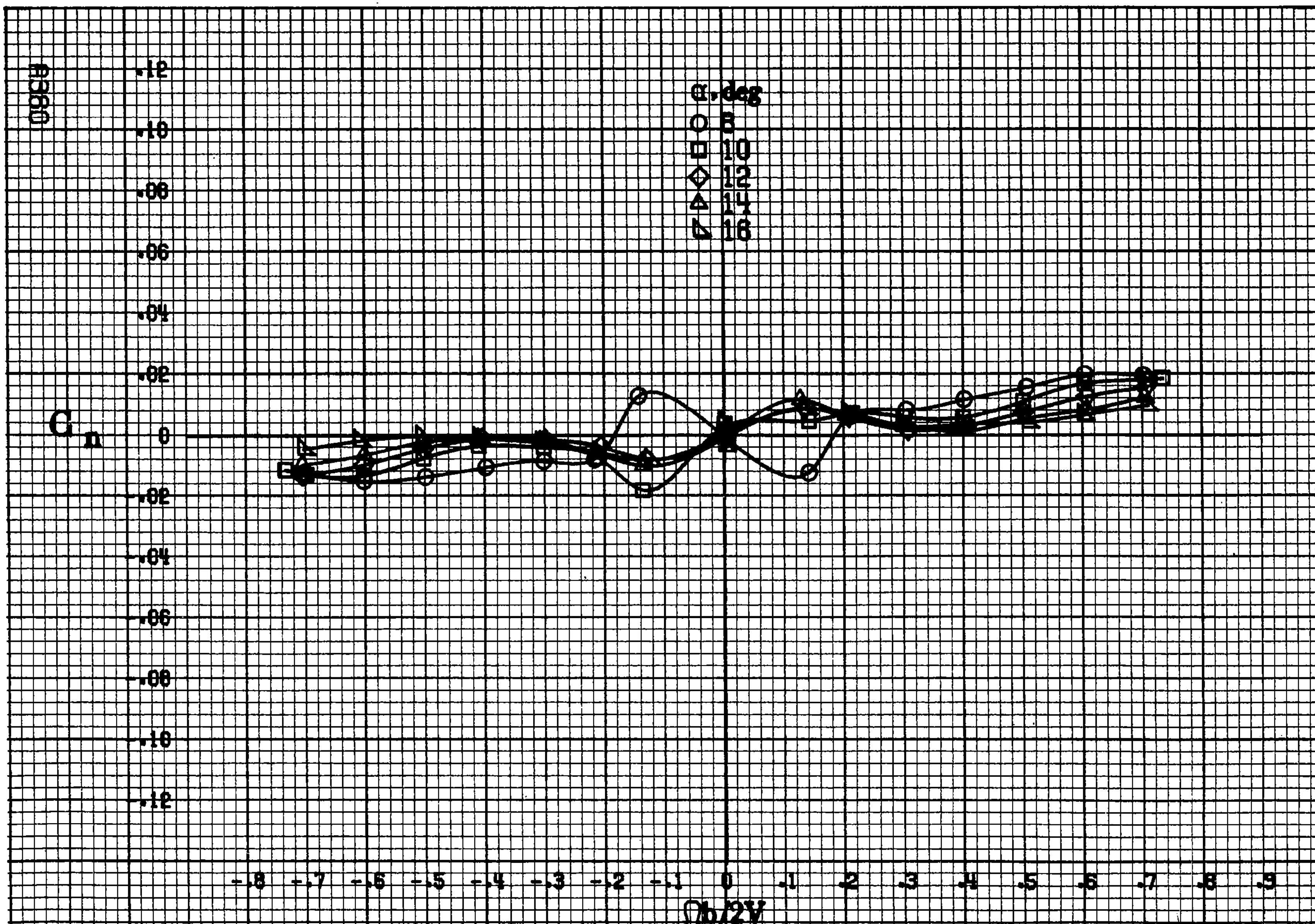

(a) $\alpha = 8$ to 16 deg, SR = 182.9 cm (72 in).

Figure A91.-Effect of rotation rate and angle of attack on yawing-moment coefficient for vertical tail off configuration. $\delta_e = 0°$, $\delta_a = 0°$, $\delta_r = 0°$, $\beta = 0°$.

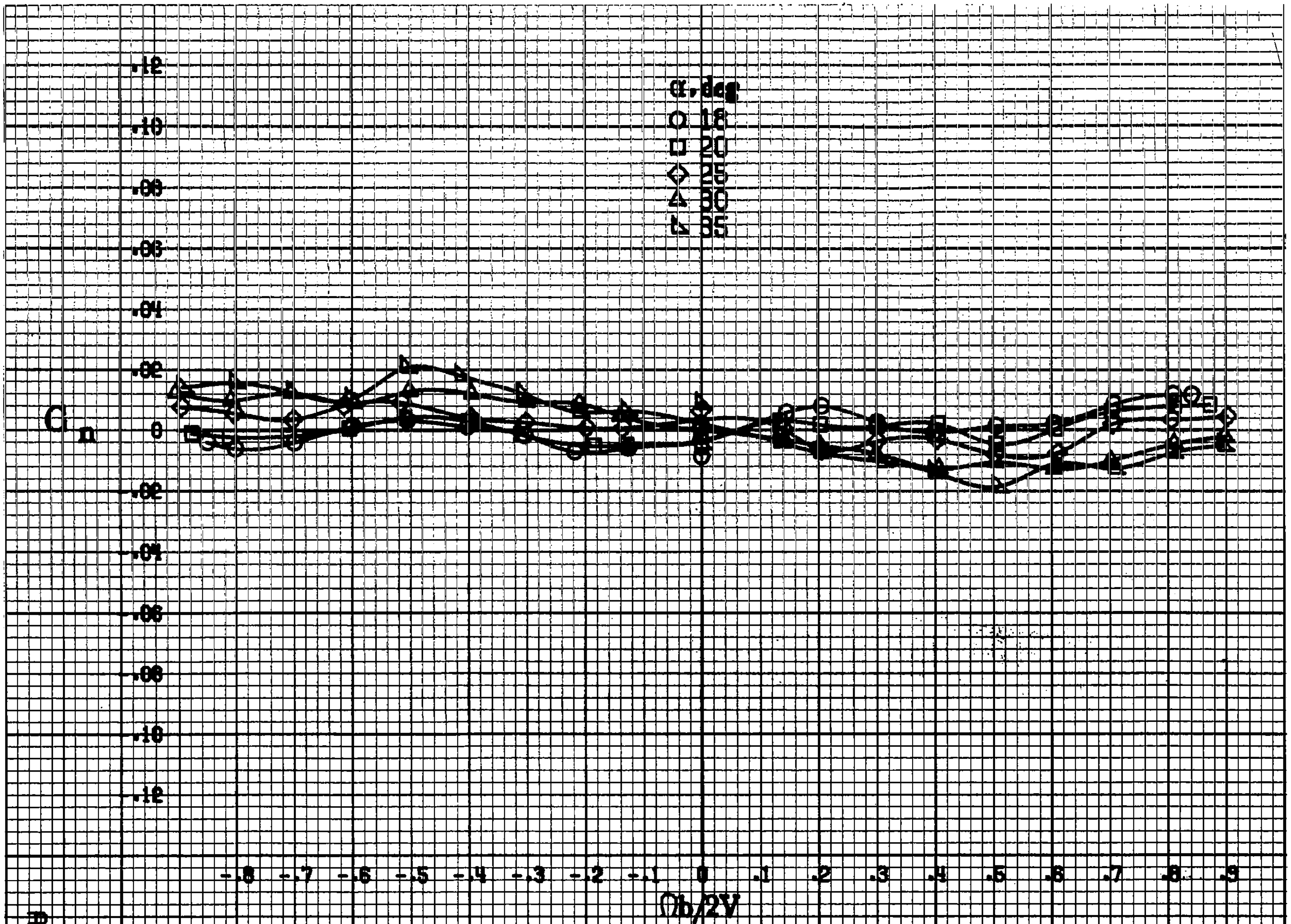

(b) α = 18 to 35 deg, SR = 182.9 cm (72 in).

Figure A91.-Continued.

A361

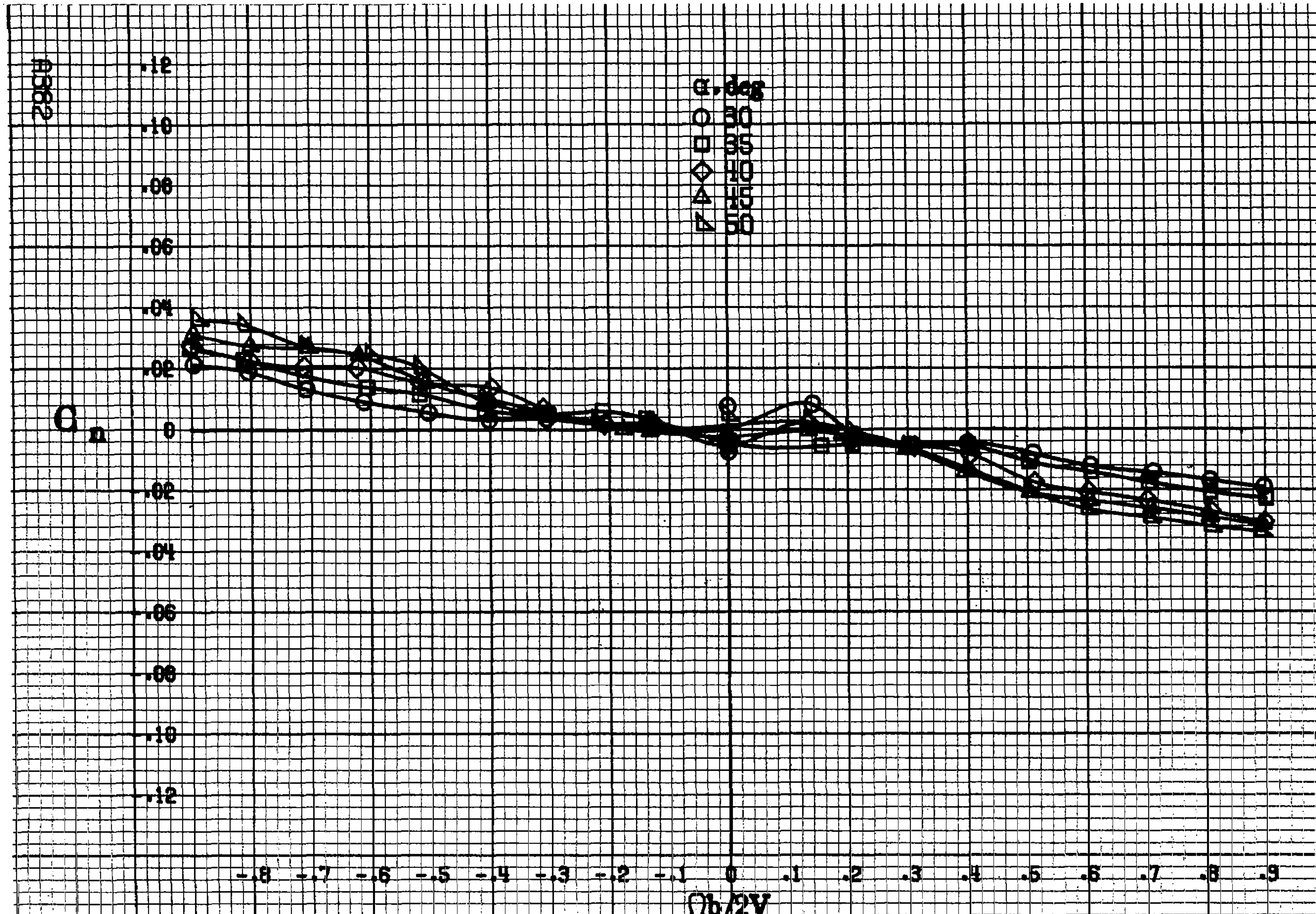

(c) $\alpha = 30$ to 50 deg, SR = 0.

Figure A91.-Continued.

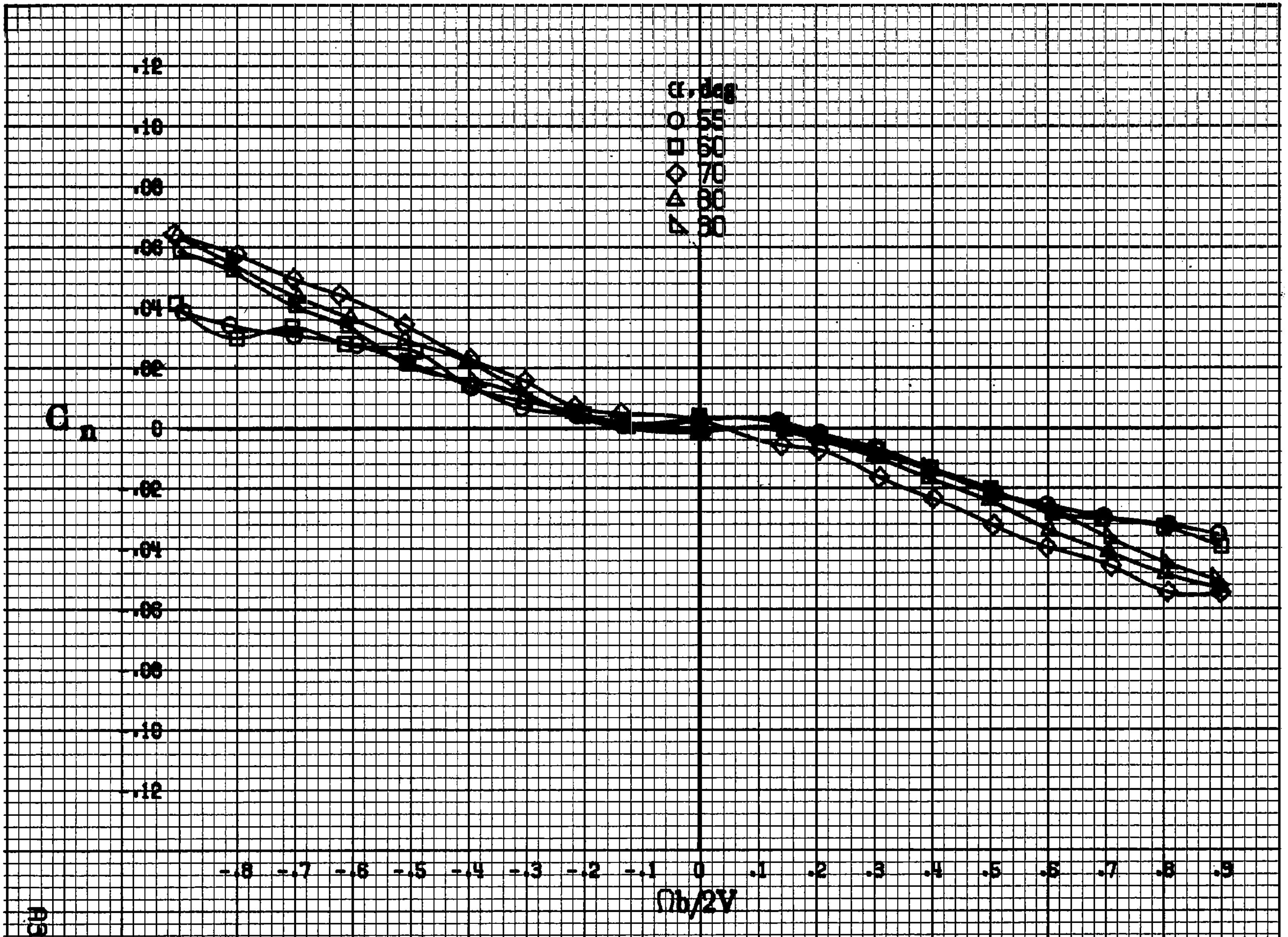

(d) $\alpha = 55$ to 90 deg, SR = 0.

Figure A91.-Concluded.

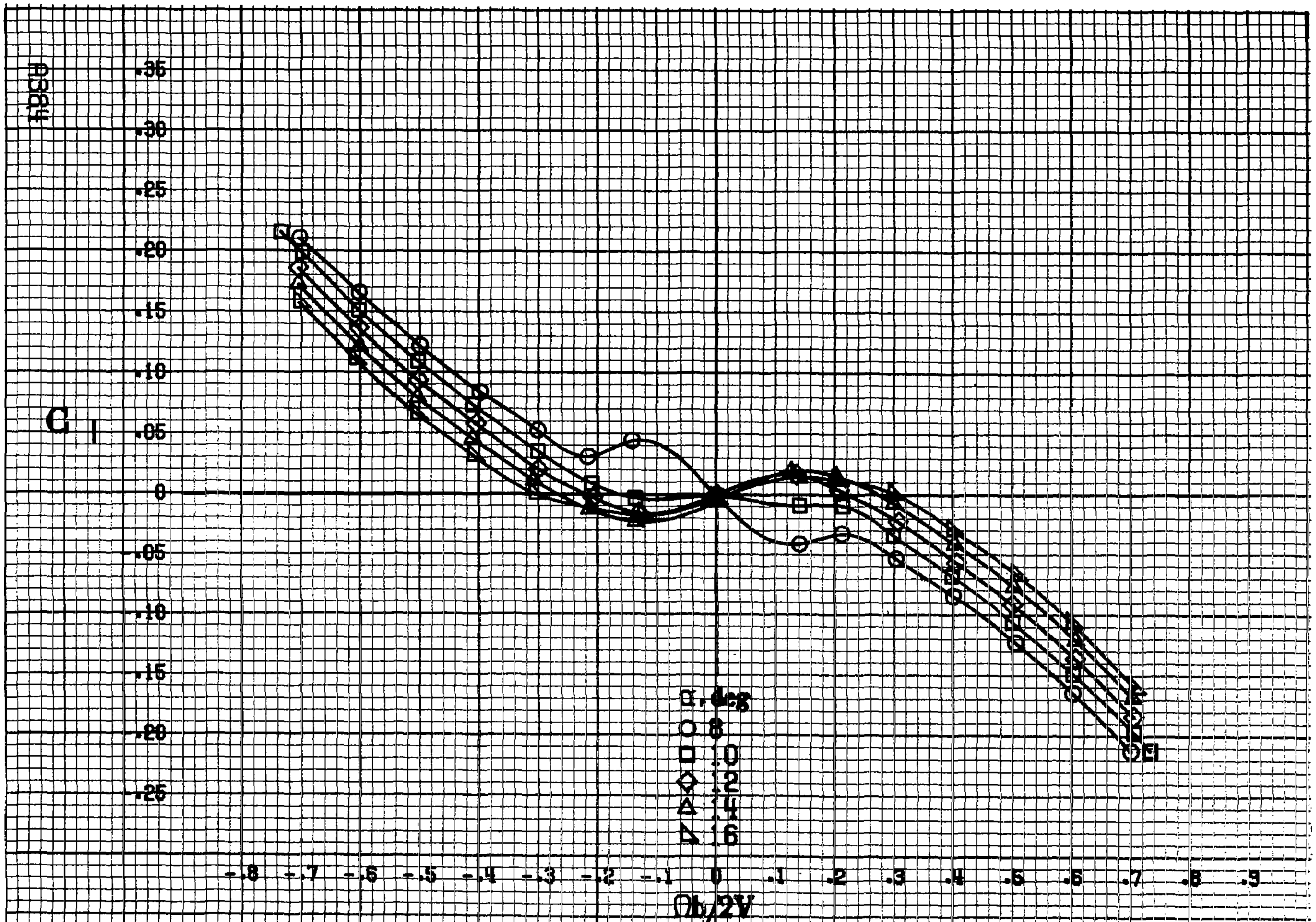

(a) α = 8 to 16 deg, SR = 182.9 cm (72 in.).

Figure A92. Effect of rotation rate and angle of attack on rolling-moment coefficient for vertical tail off configuration, $\delta_e = 0°$, $\delta_a = 0°$, $\delta_r = 0°$, $\beta = 0°$.

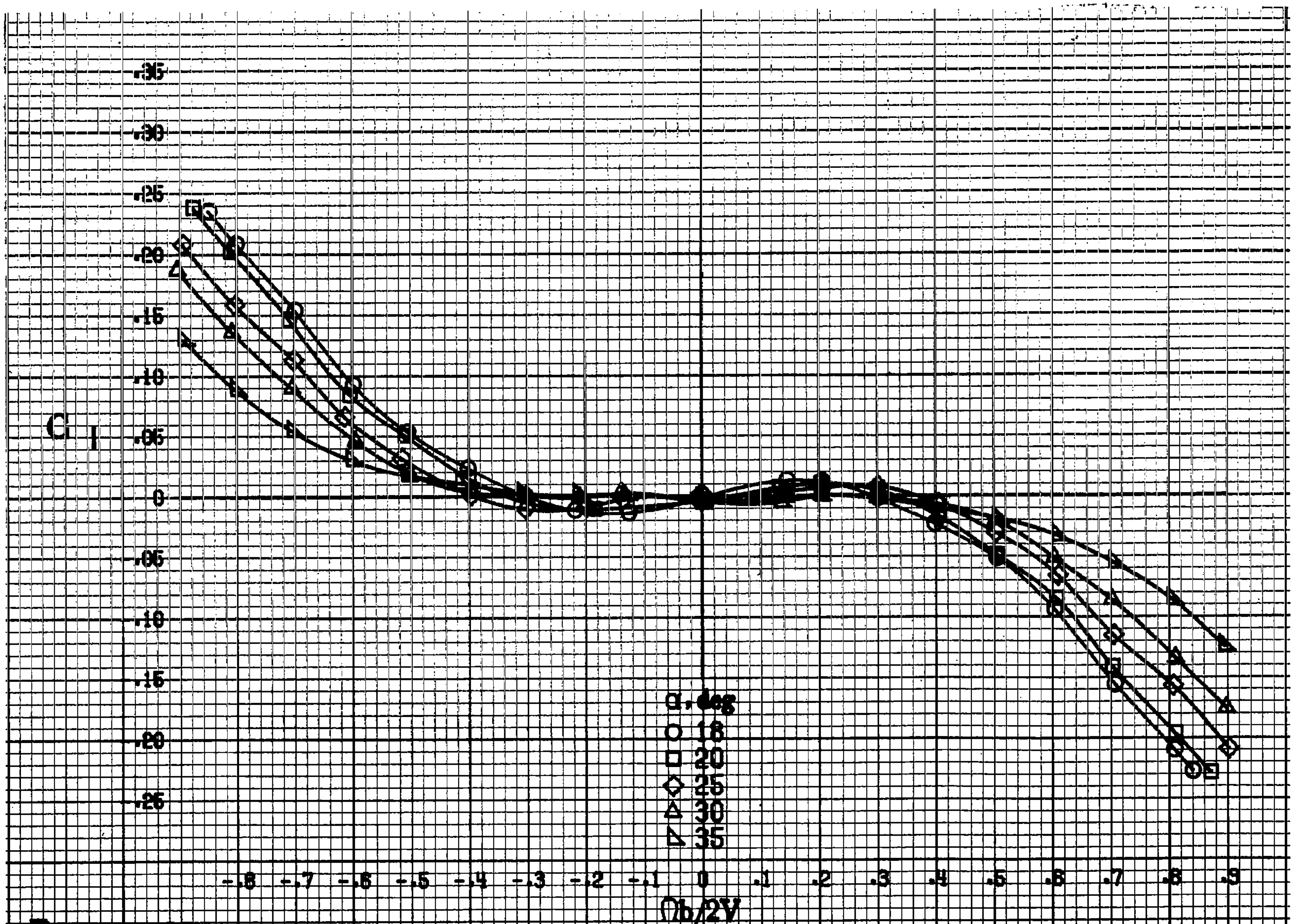

(b) α = 18 to 35 deg, SR = 182.9 cm (72 in).

Figure A92.-Continued.

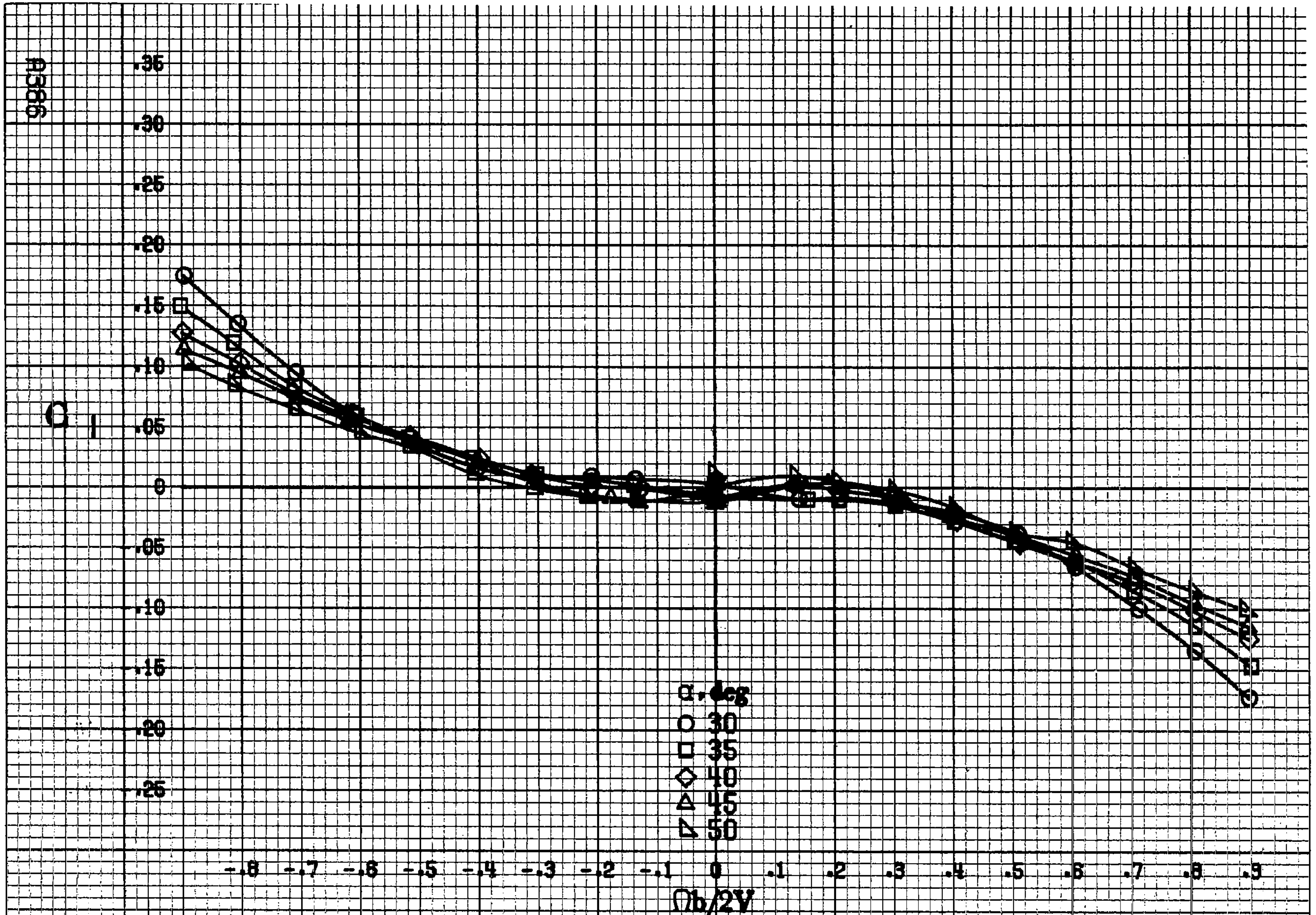

(c) α = 30 to 50 deg, SR = 0.
Figure A92.-Continued.

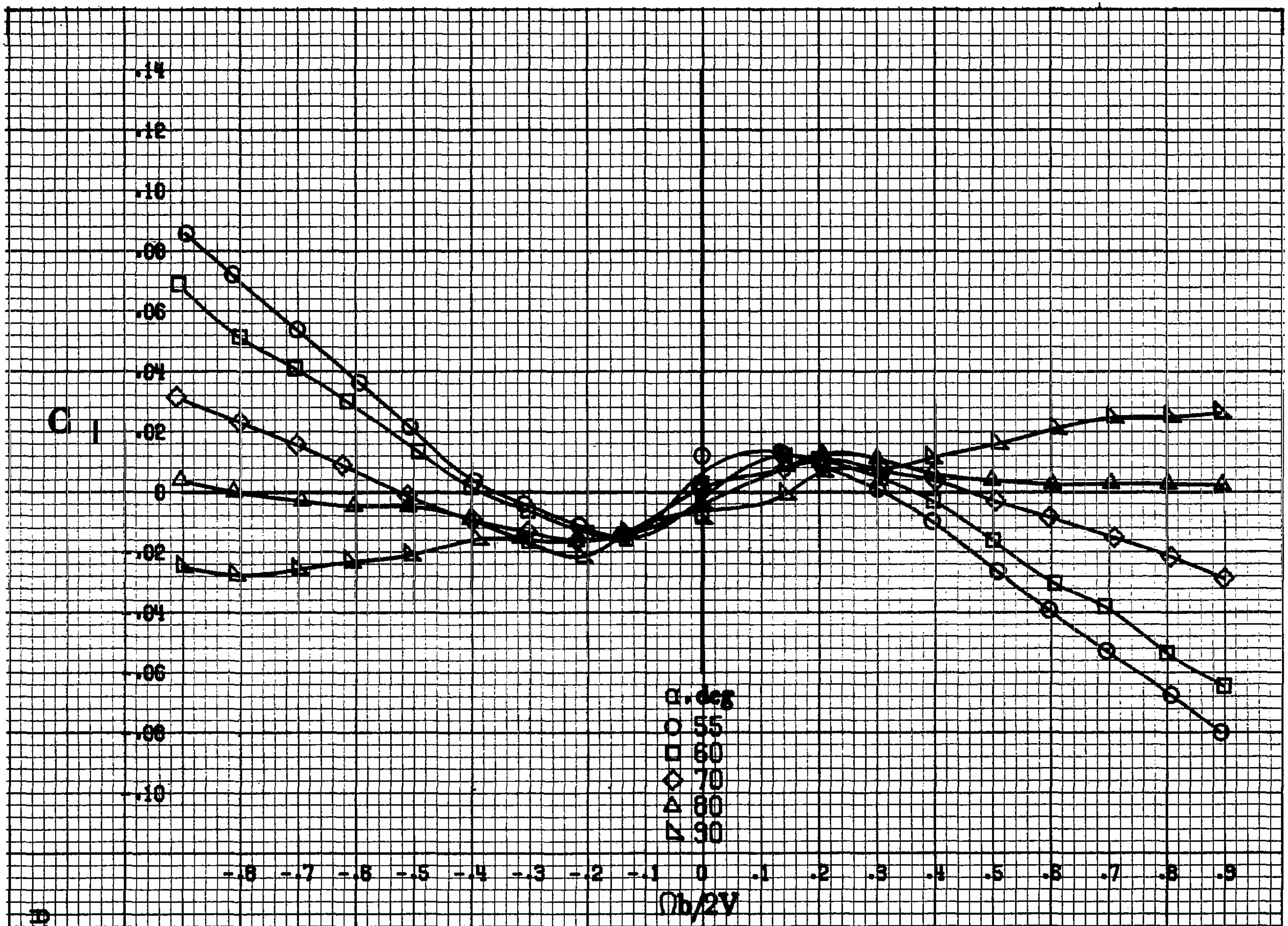

(d) α = 55 to 90 deg, SR = 0.
Figure A92.-Concluded.

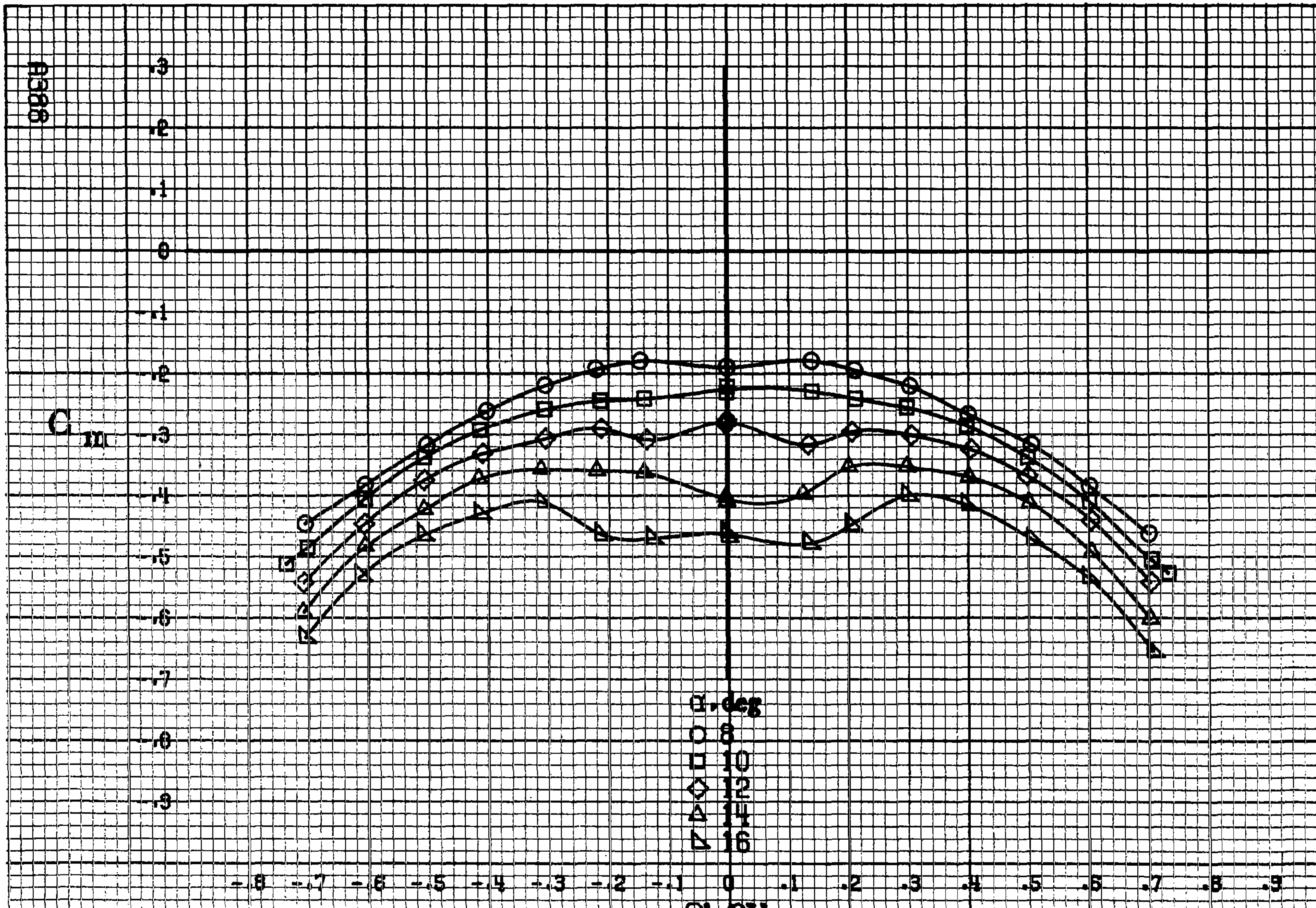

(a) $\alpha = 8$ to 16 deg, SR = 182.9 cm (72 in).

Figure A93.- Effect of rotation rate and angle of attack on pitching-moment coefficient for vertical tail off configuration. $\delta_e = 0°$, $\delta_a = 0°$, $\delta_r = 0°$, $\beta = 0°$.

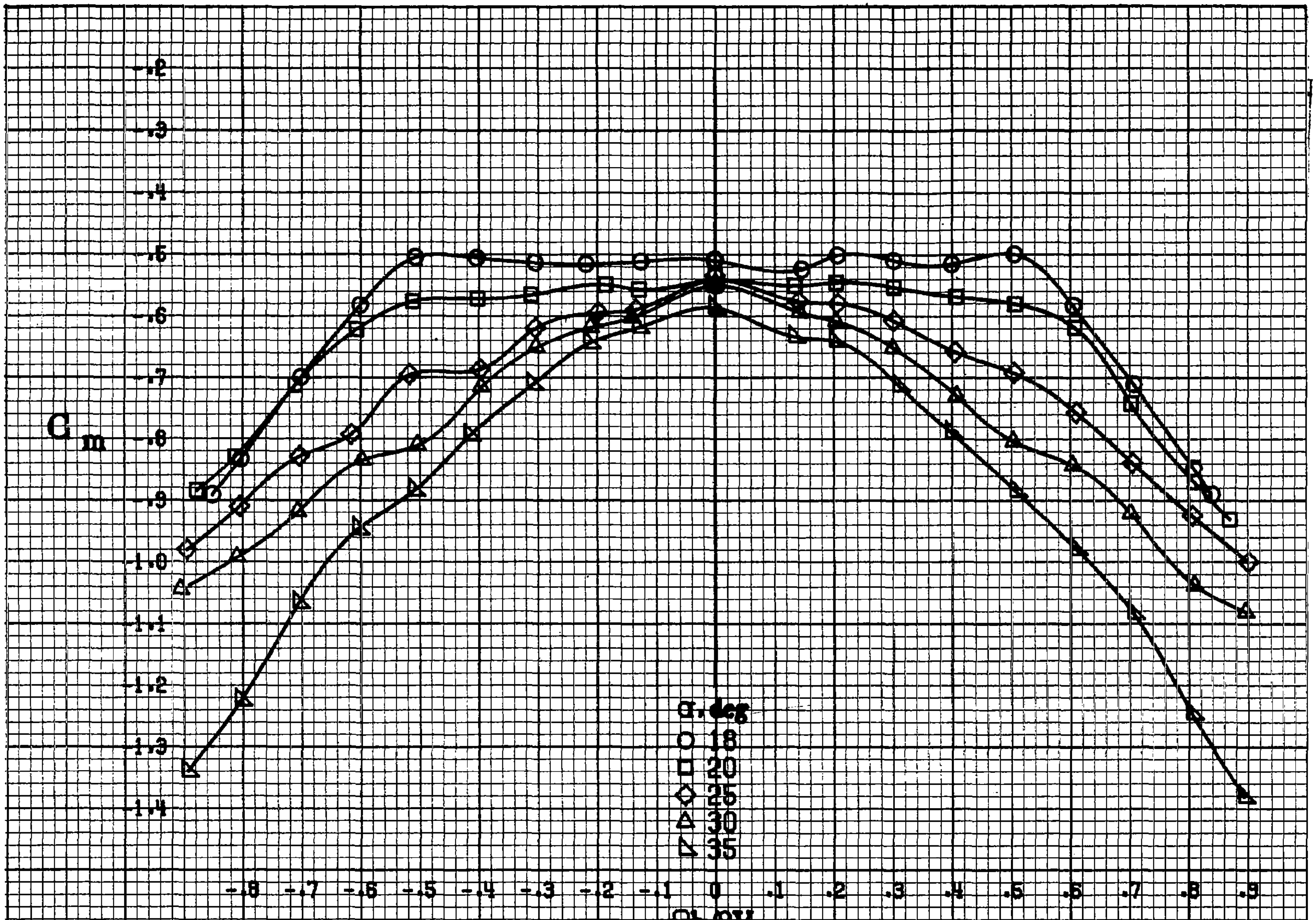

(b) α = 18 to 35 deg, SR = 182.9 cm (72 in).

Figure A98.-Continued.

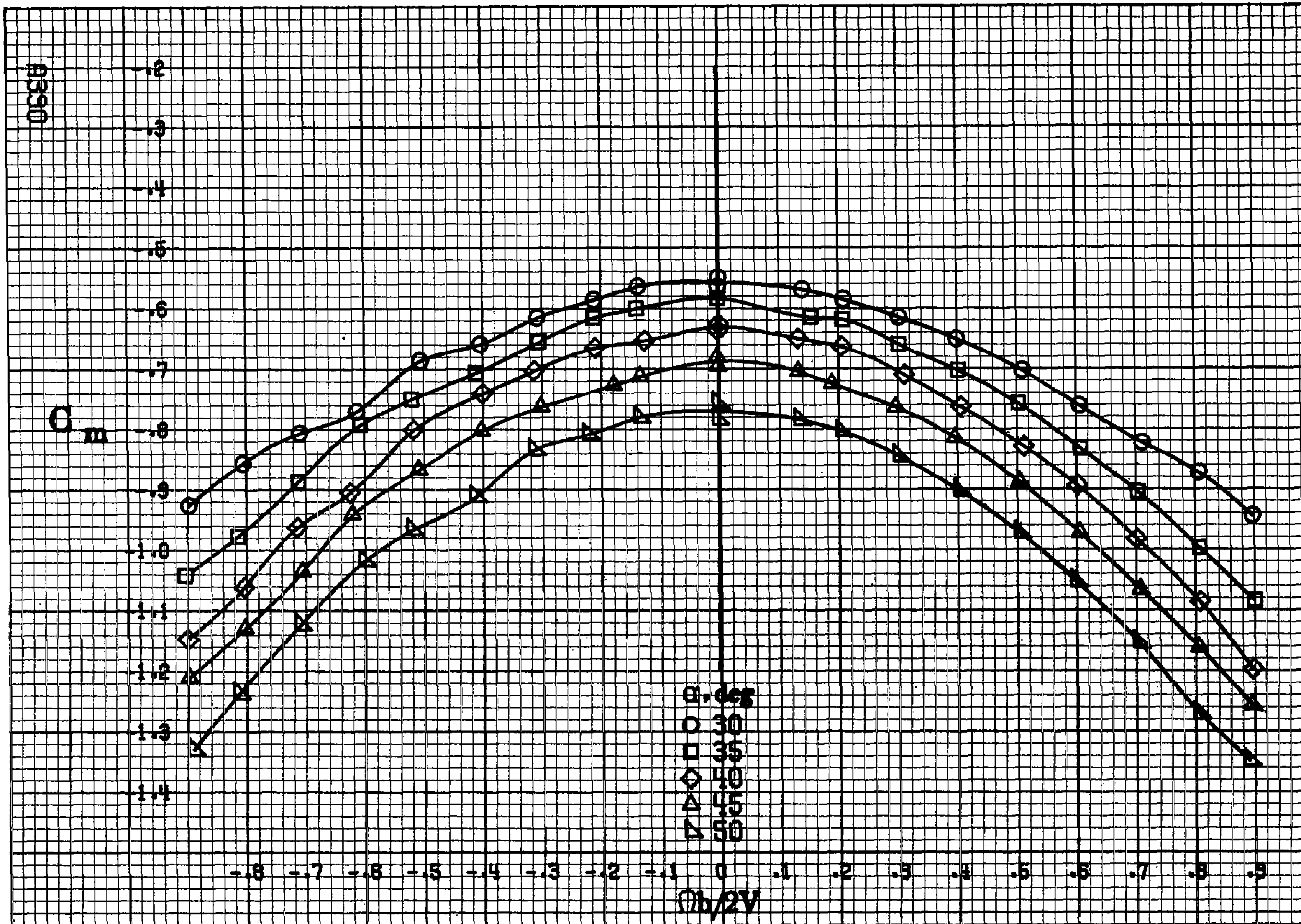

(c) α = 30 to 50 deg, SR = 0.
Figure A98.-Continued.

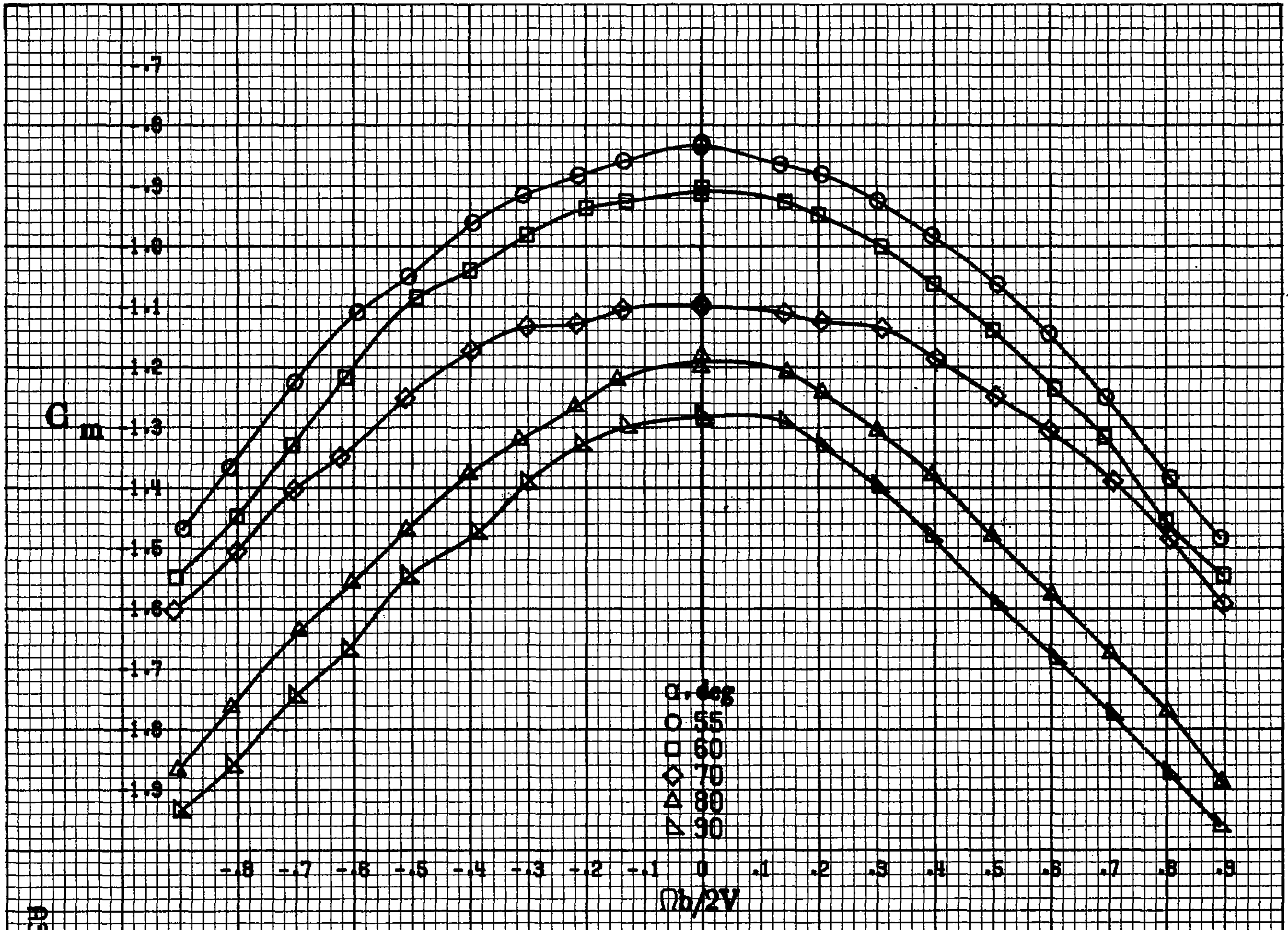

(d) α = 55 to 90 deg, SR = 0.

Figure A93.-Concluded.

A391

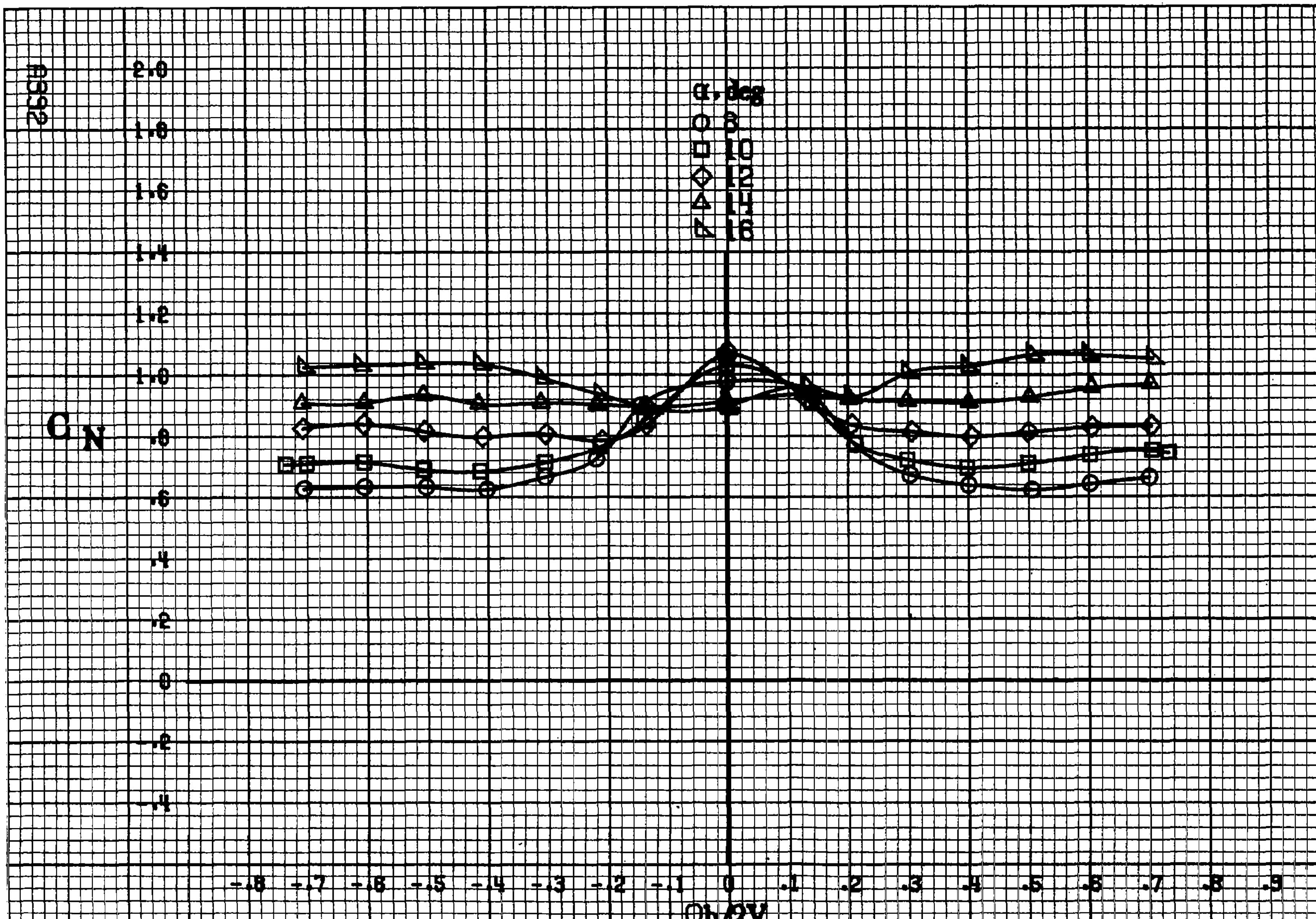

(a) α = 8 to 16 deg, SR = 182.9 cm (72 in).

Figure A94.-Effect of rotation rate and angle of attack on normal-force coefficient for vertical tail off configuration. $\delta_e = 0°$, $\delta_a = 0°$, $\delta_r = 0°$, $\beta = 0°$.

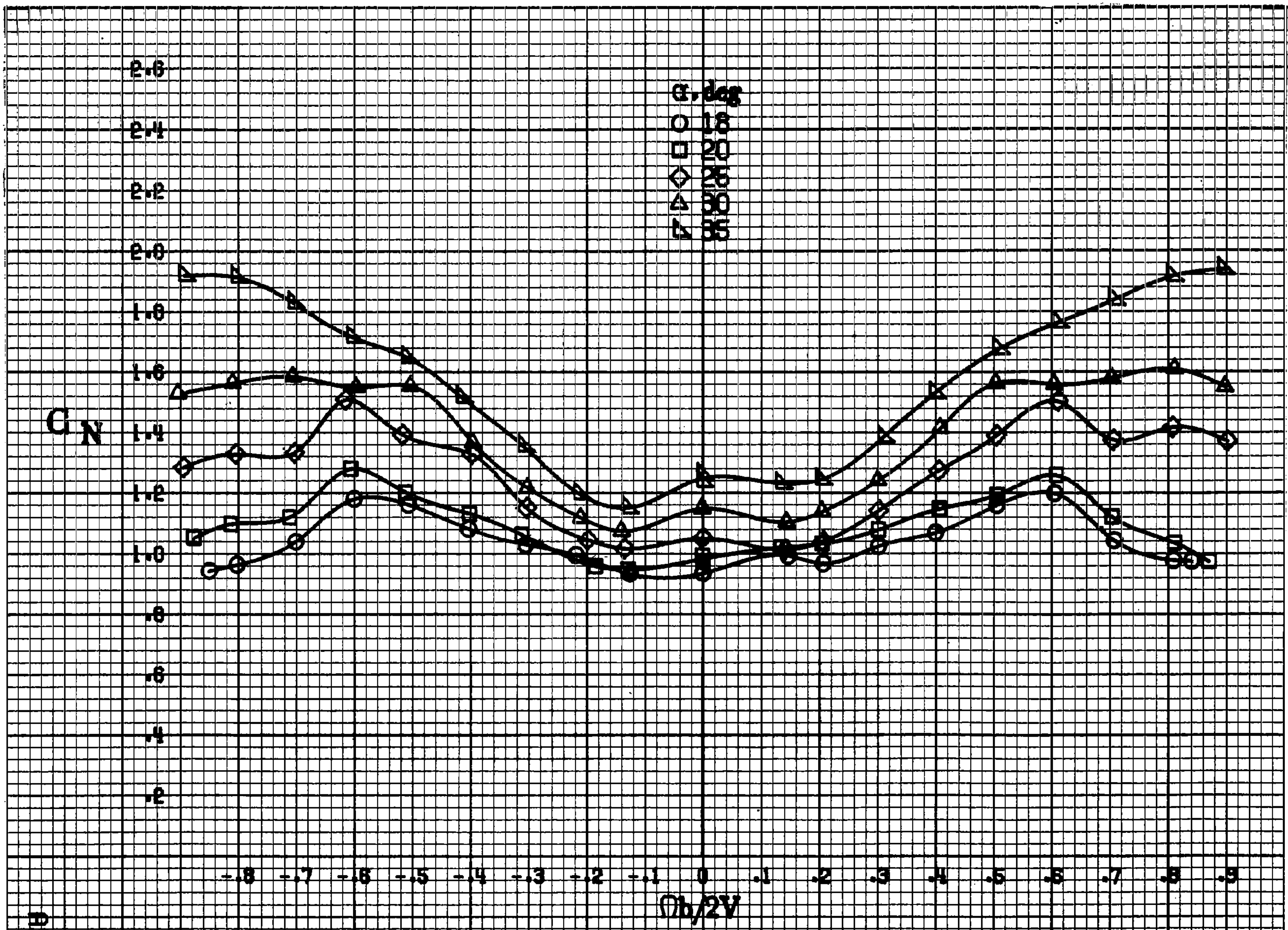

(b) α = 18 to 35 deg, SR = 182.9cm (72in).

Figure A94.-Continued.

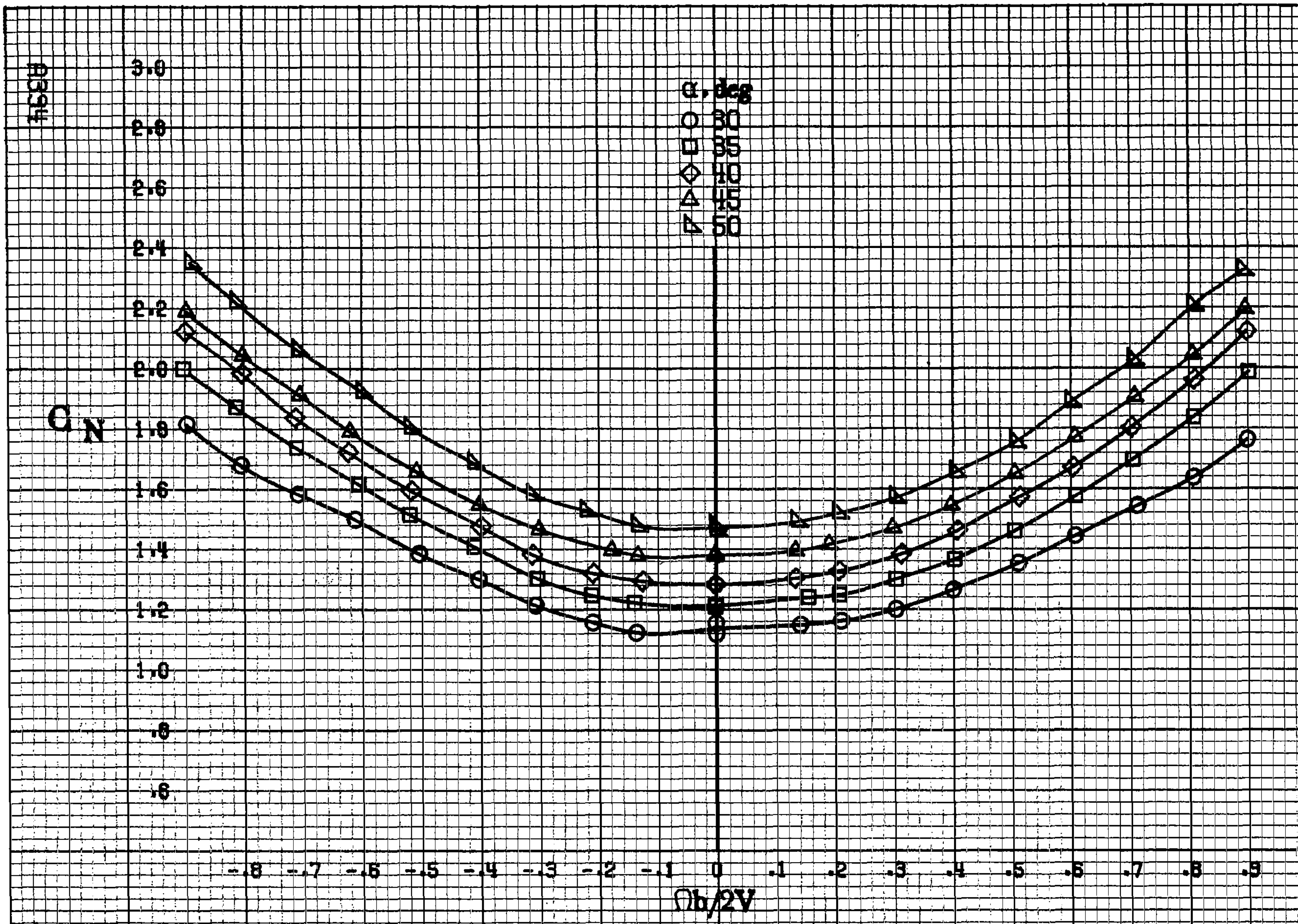

(c) α = 30 to 50 deg, SR = 0.

Figure A94.-Continued.

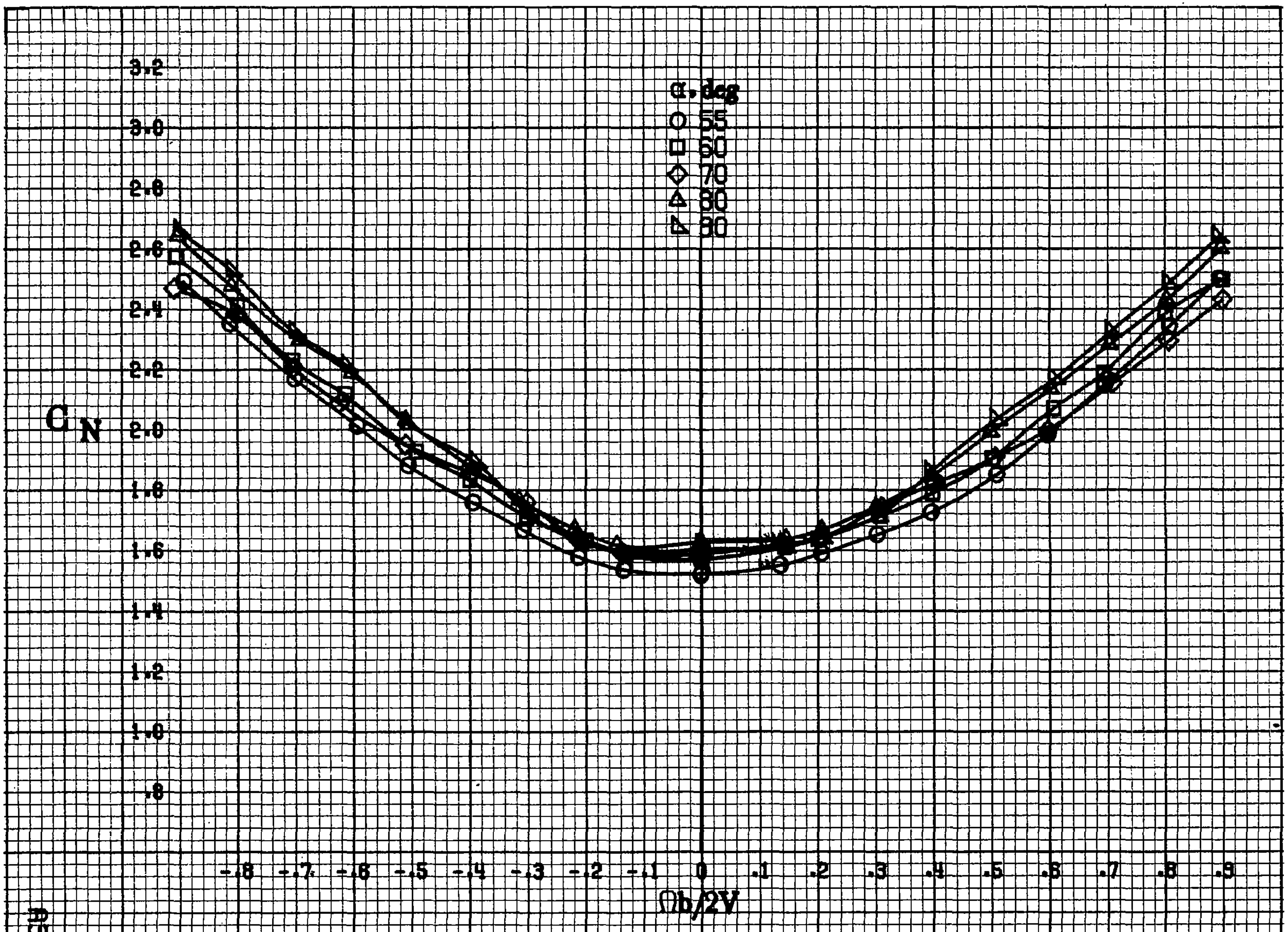

(d) α = 55 to 90 deg, SR = 0.

Figure A94.-Concluded.

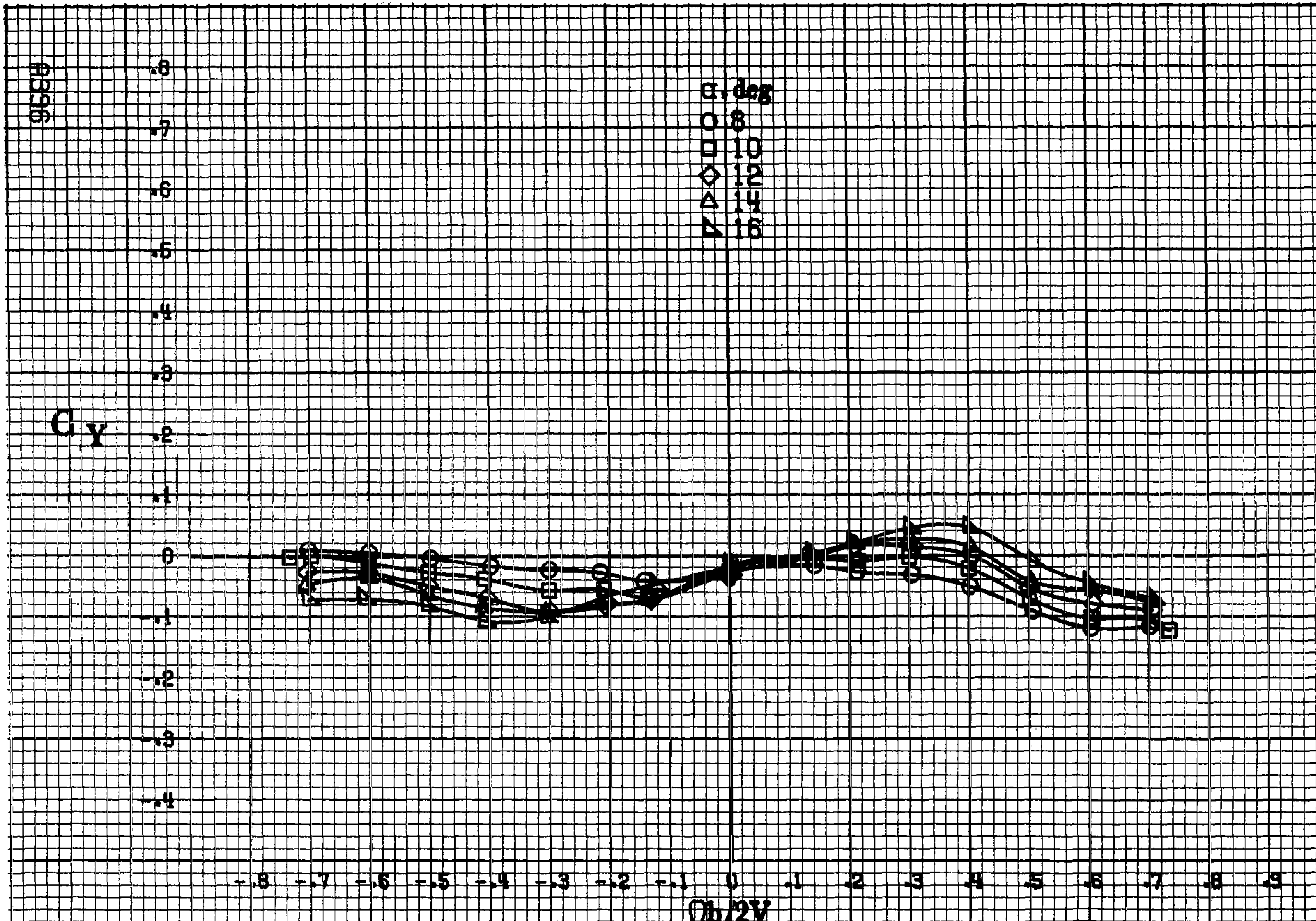

(a) α = 8 to 16 deg, SR = 182.9 cm (72 in).

Figure A96.- Effect of rotation rate and angle of attack on side-force coefficient for vertical tail off configuration. $\delta_e = 0°$, $\delta_a = 0°$, $\delta_r = 0°$, $\beta = 0°$.

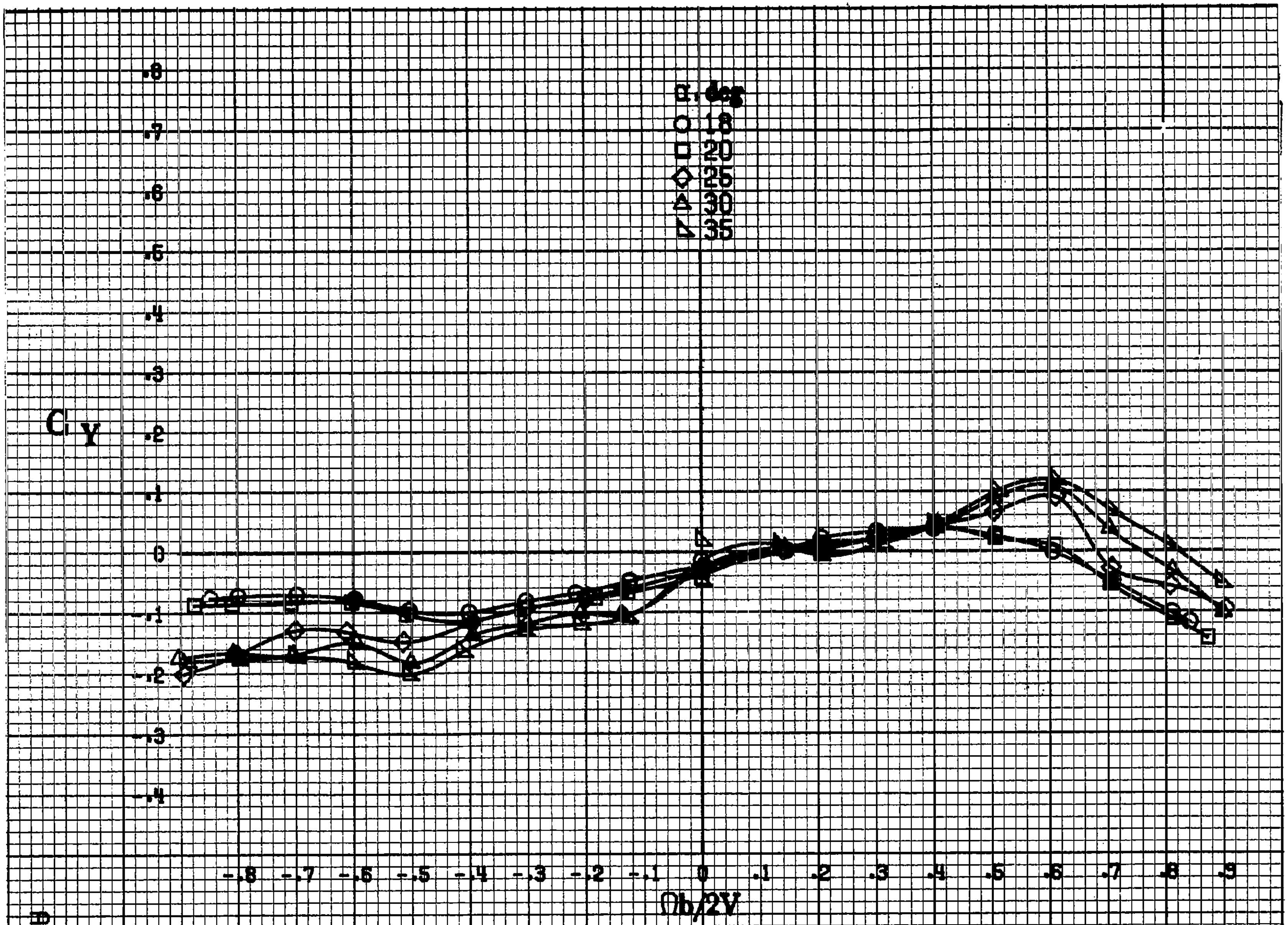

(b) α = 18 to 35 deg, SR = 182.9 cm (72 in).

Figure A96.-Continued.

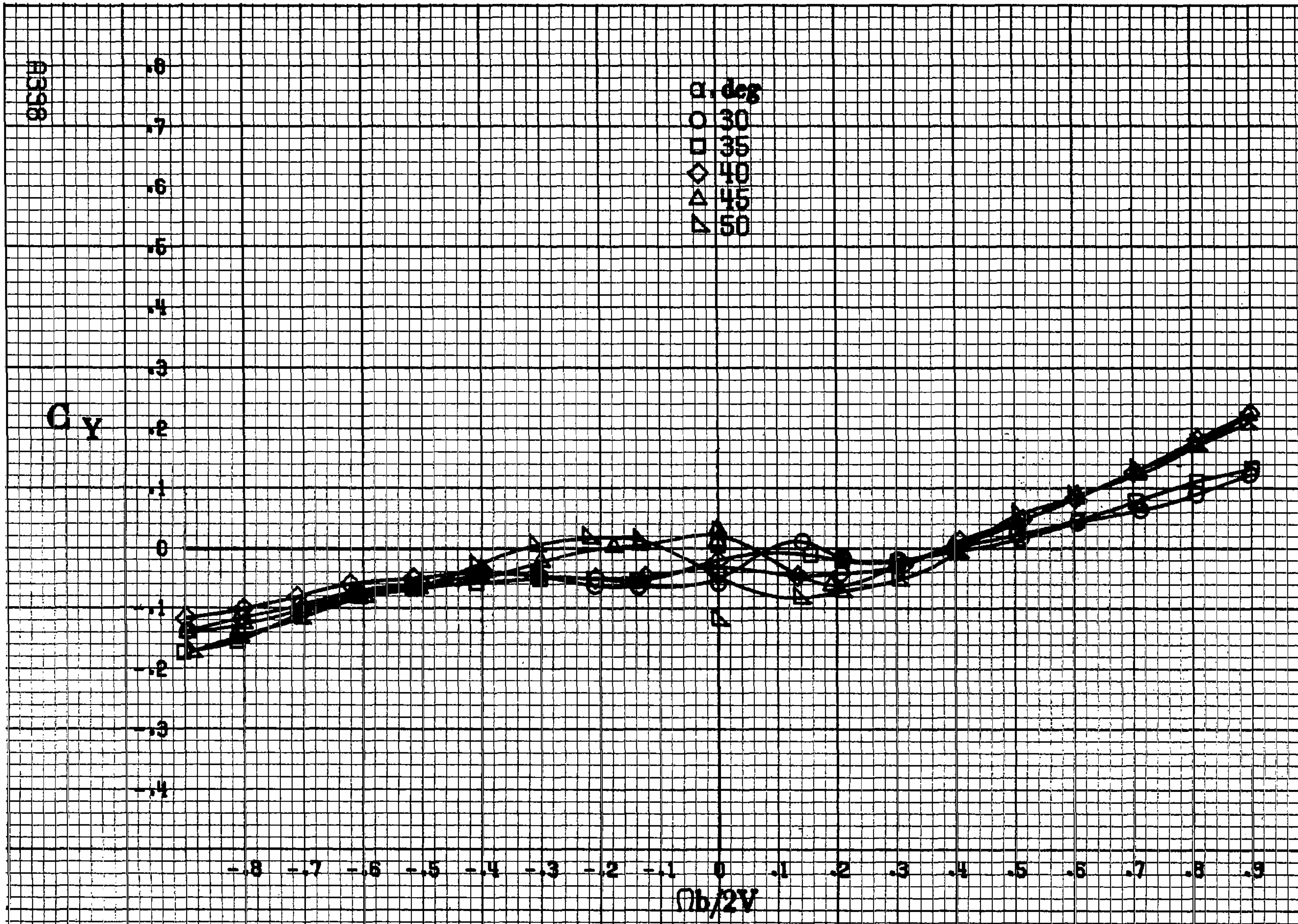

(c) α = 30 to 50 deg, SR = 0.

Figure A95.-Continued.

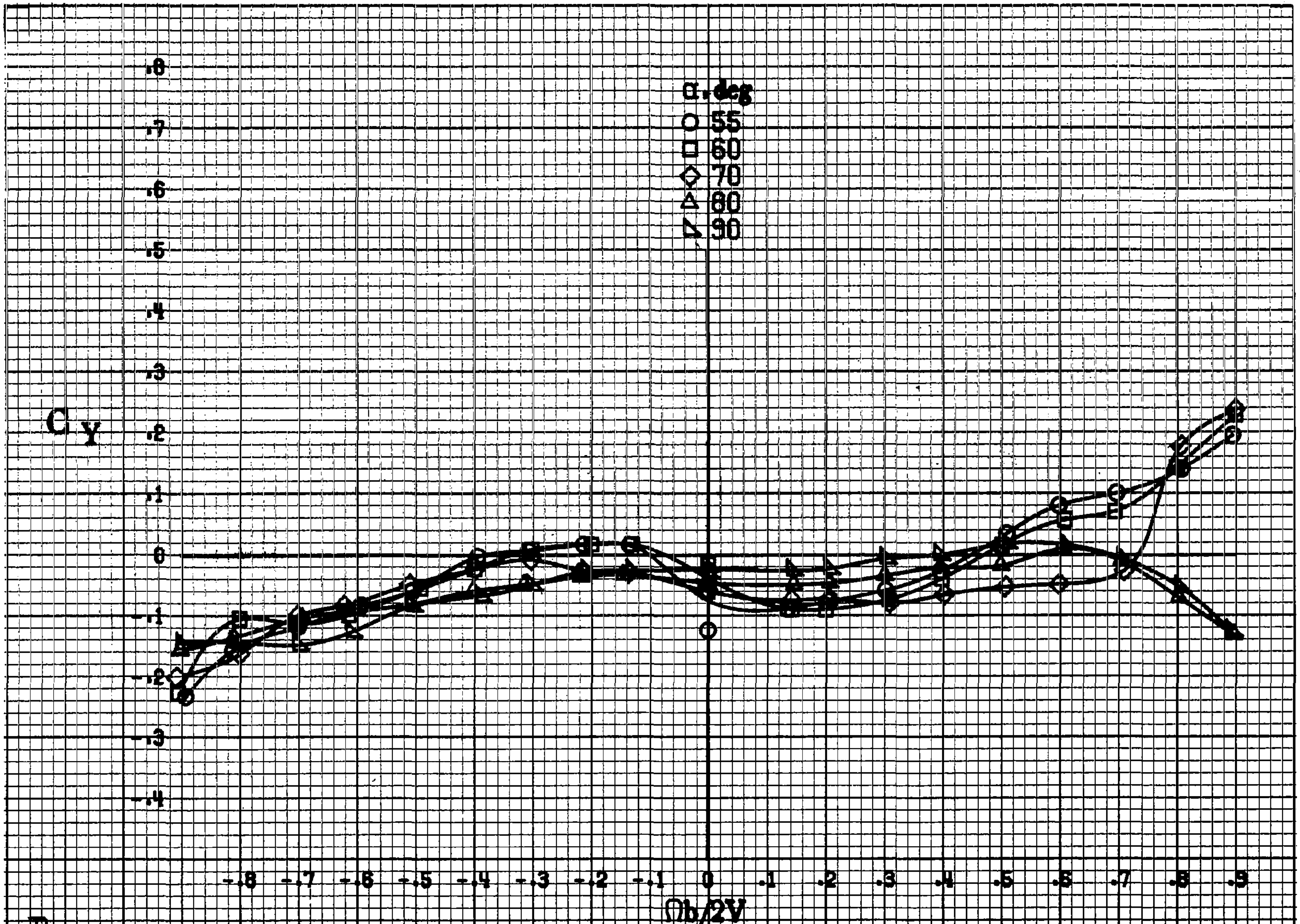

(d) α = 55 to 90 deg, δR = 0.

Figure A95.-Concluded.

(a) $\alpha = 8$ to 16 deg, SR = 182.9cm (72in).

Figure A96.- Effect of rotation rate and angle of attack on axial-force coefficient for vertical tail off configuration. $\delta_e = 0°$, $\delta_a = 0°$, $\delta_r = 0°$, $\beta = 0°$.

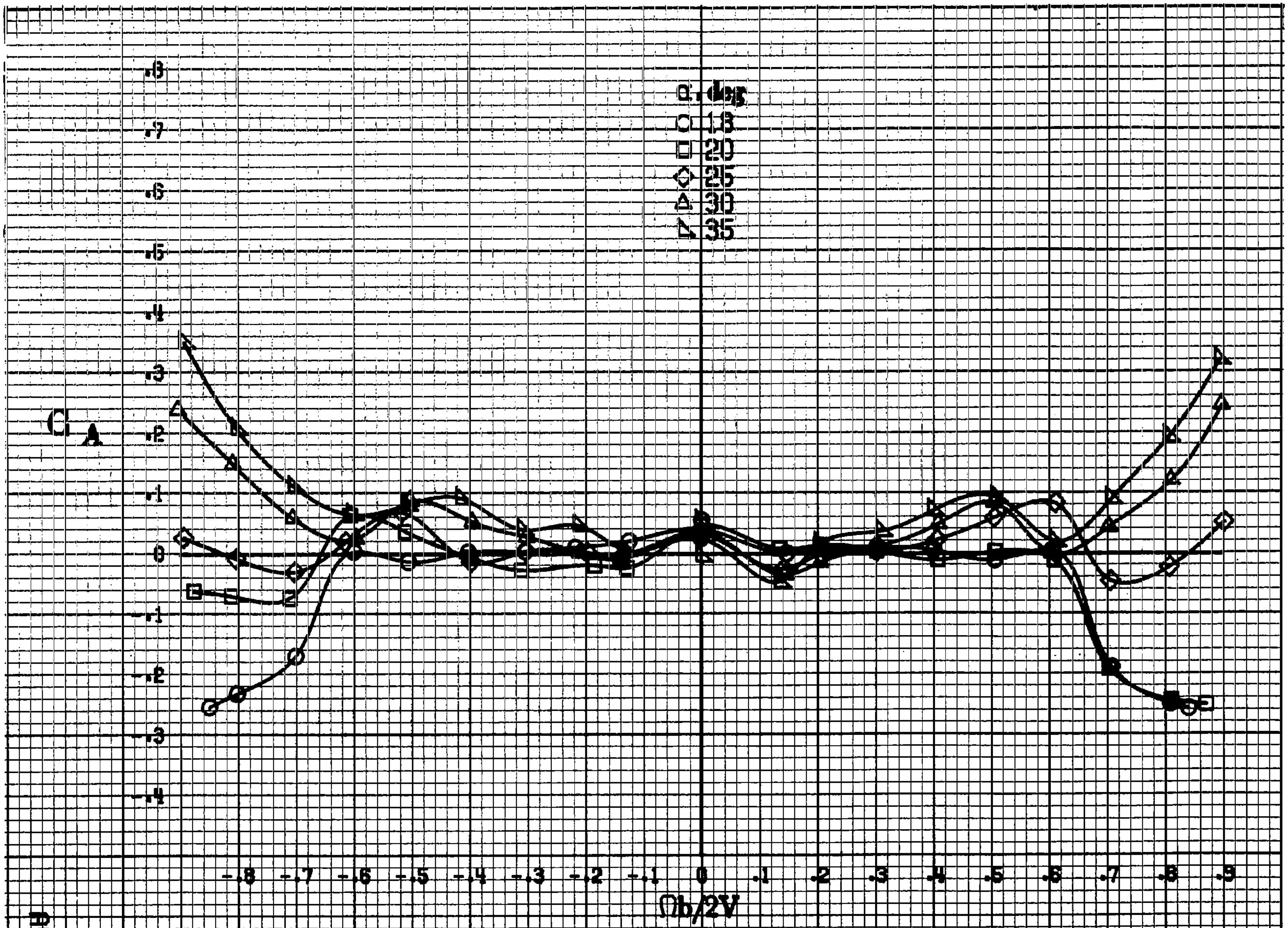

(b) α = 18 to 35 deg, SR = 182.9 cm (72 in).

Figure A96.-Continued.

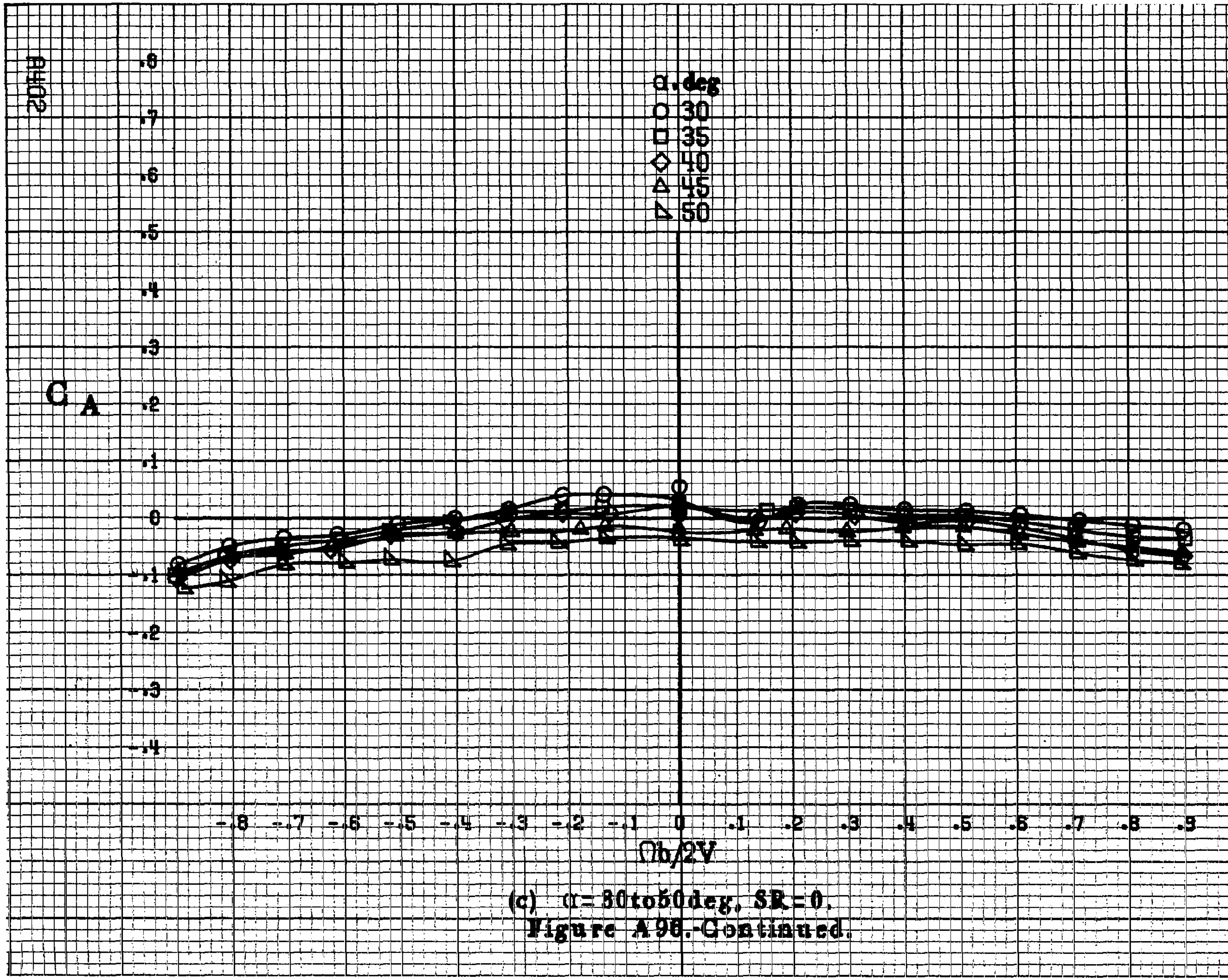

(c) $\alpha = 30$ to 50 deg, SR = 0.
Figure A96.-Continued.

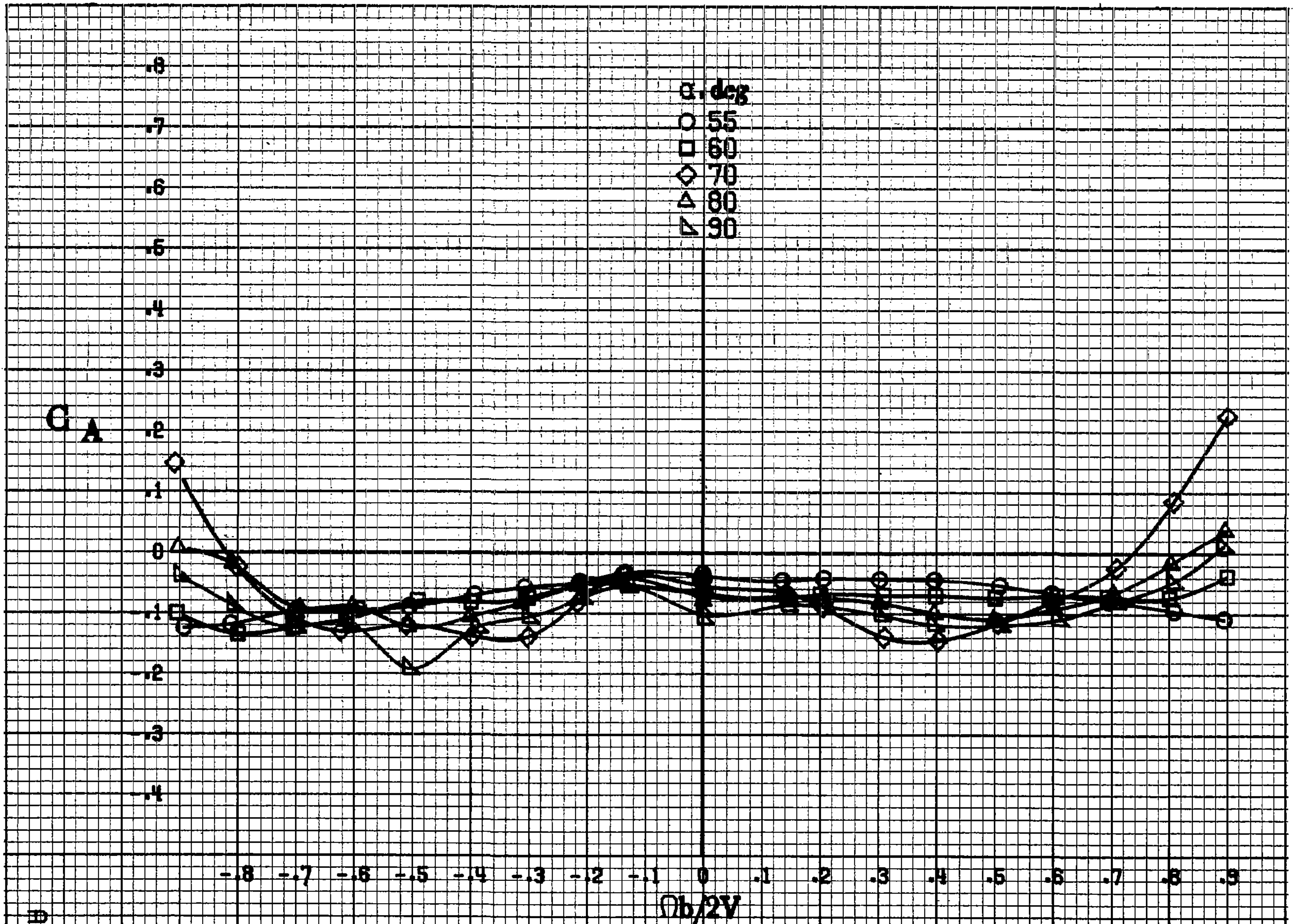

(d) α = 55 to 90 deg, SR = 0.

Figure A96.-Concluded.

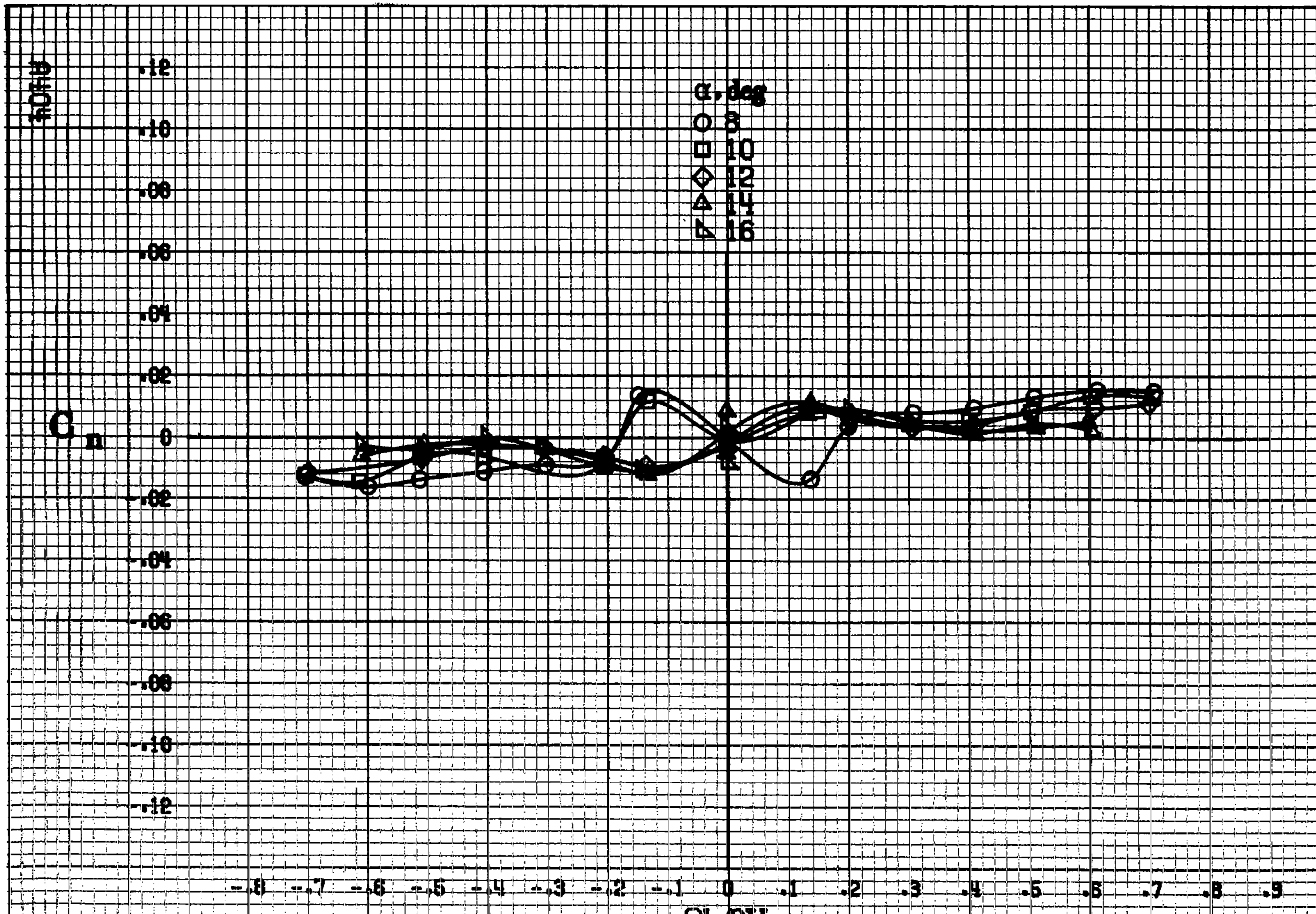

(a) α = 8 to 16 deg, SR = 182.9 cm (72 in).

Figure A97.- Effect of rotation rate and angle of attack on yawing-moment coefficient for horizontal and vertical tails off configuration. $\delta_e = 0°$, $\delta_a = 0°$, $\delta_r = 0°$, $\beta = 0°$.

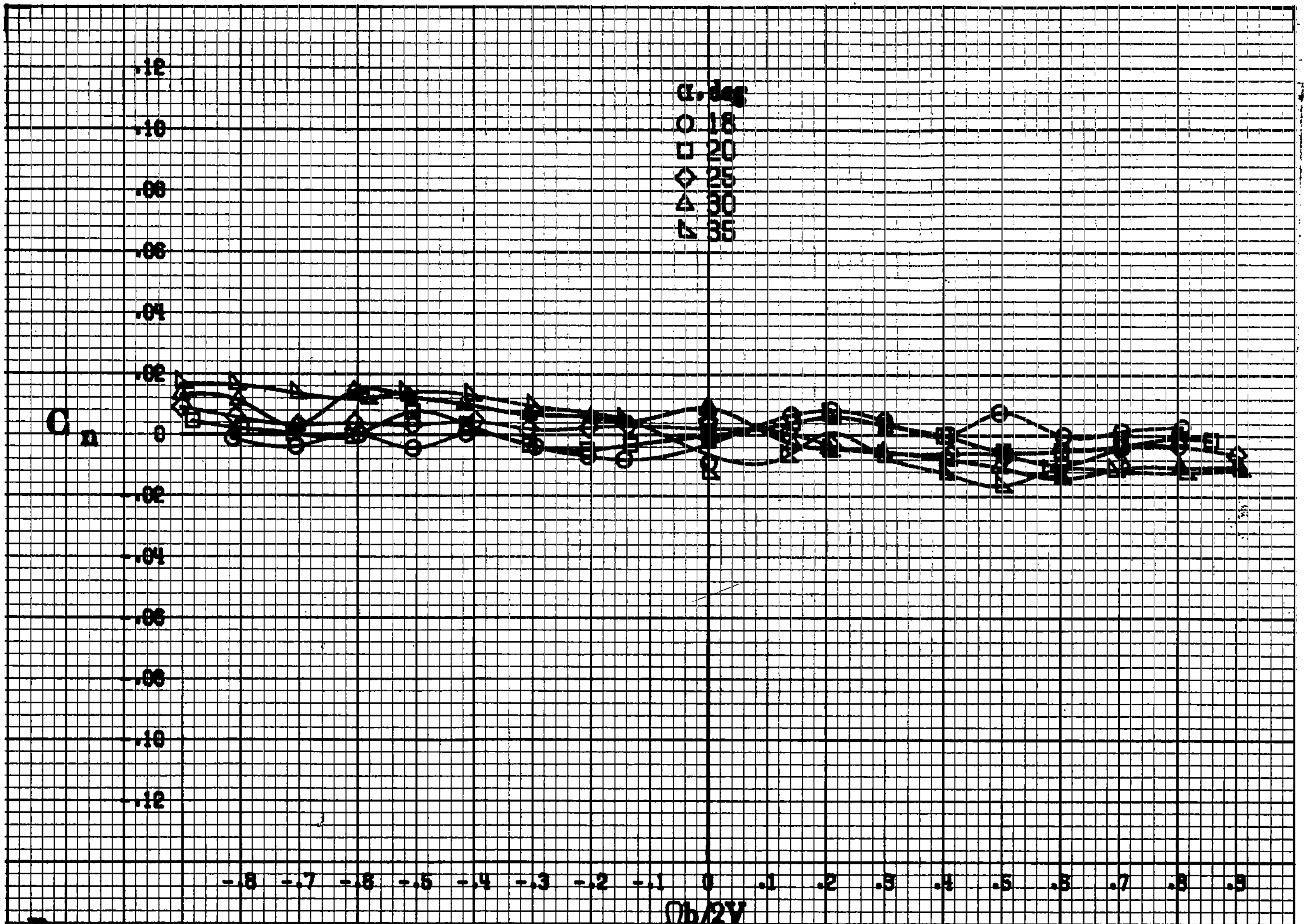

(b) α = 18 to 35 deg, SR = 182.9 cm (72 in).

Figure A97.-Continued.

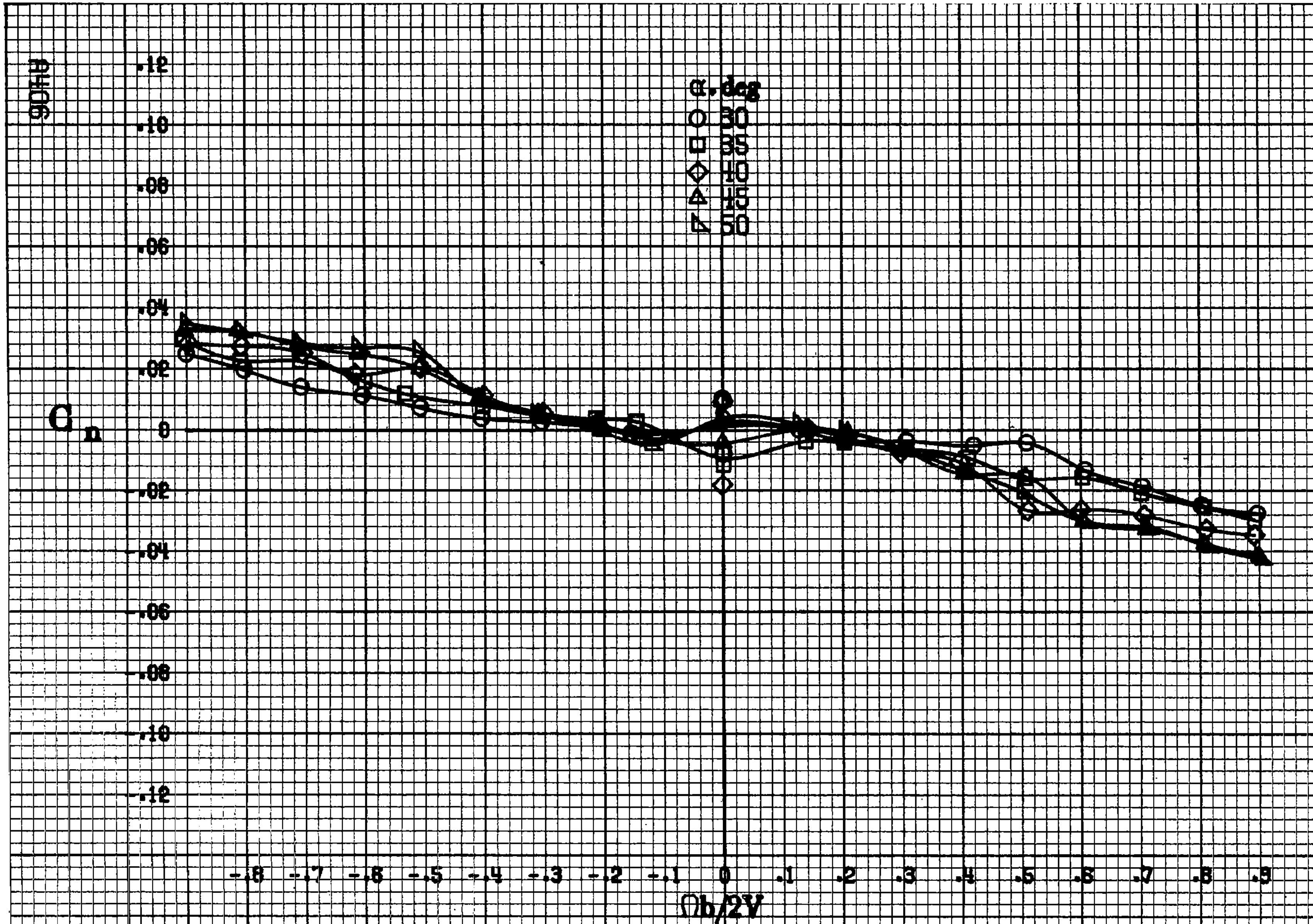

(c) α = 30 to 50 deg, SR = 0.

Figure A97.-Continued.

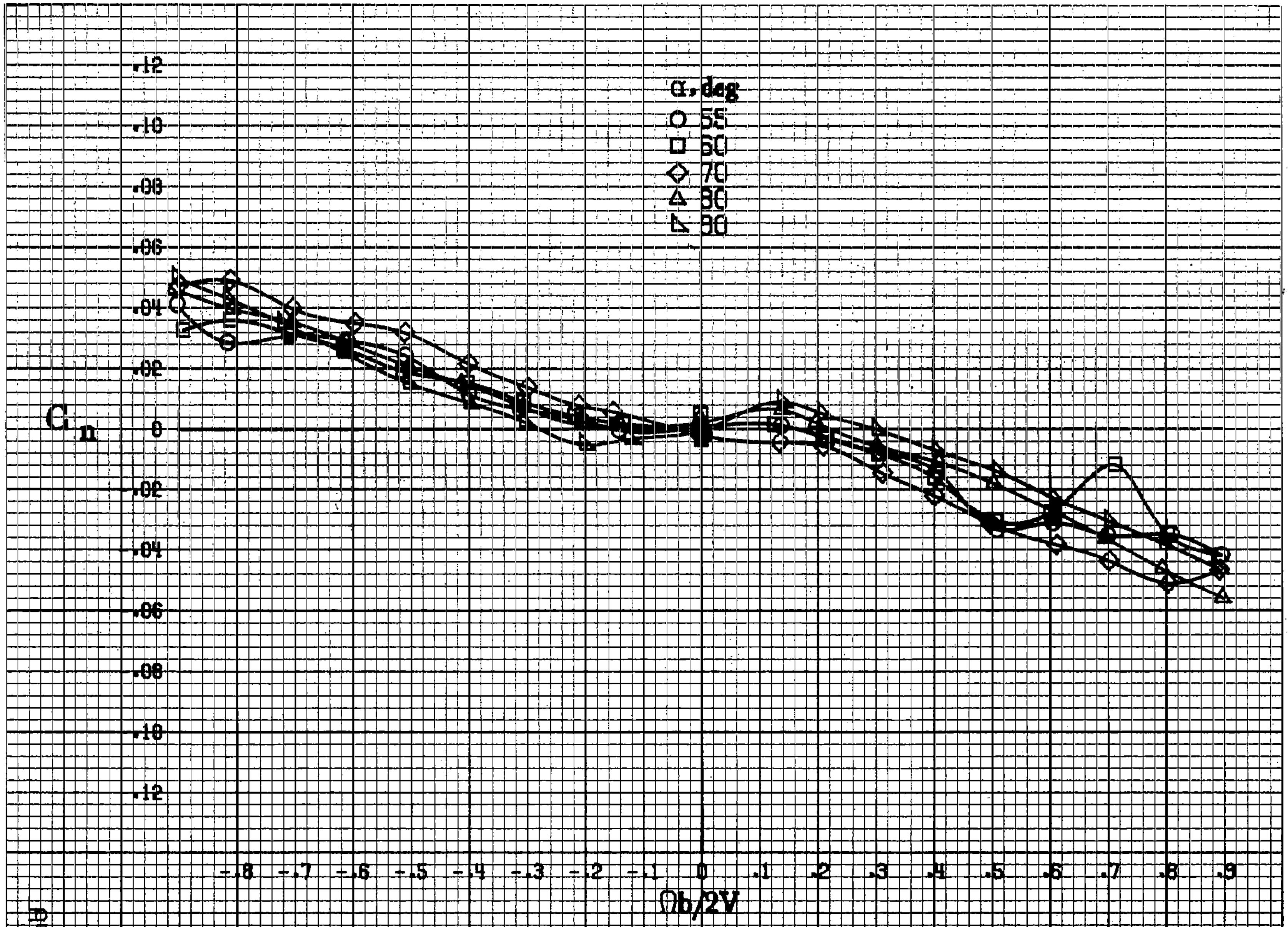

(d) α = 55 to 90 deg, SR = 0.

Figure A97.-Concluded.

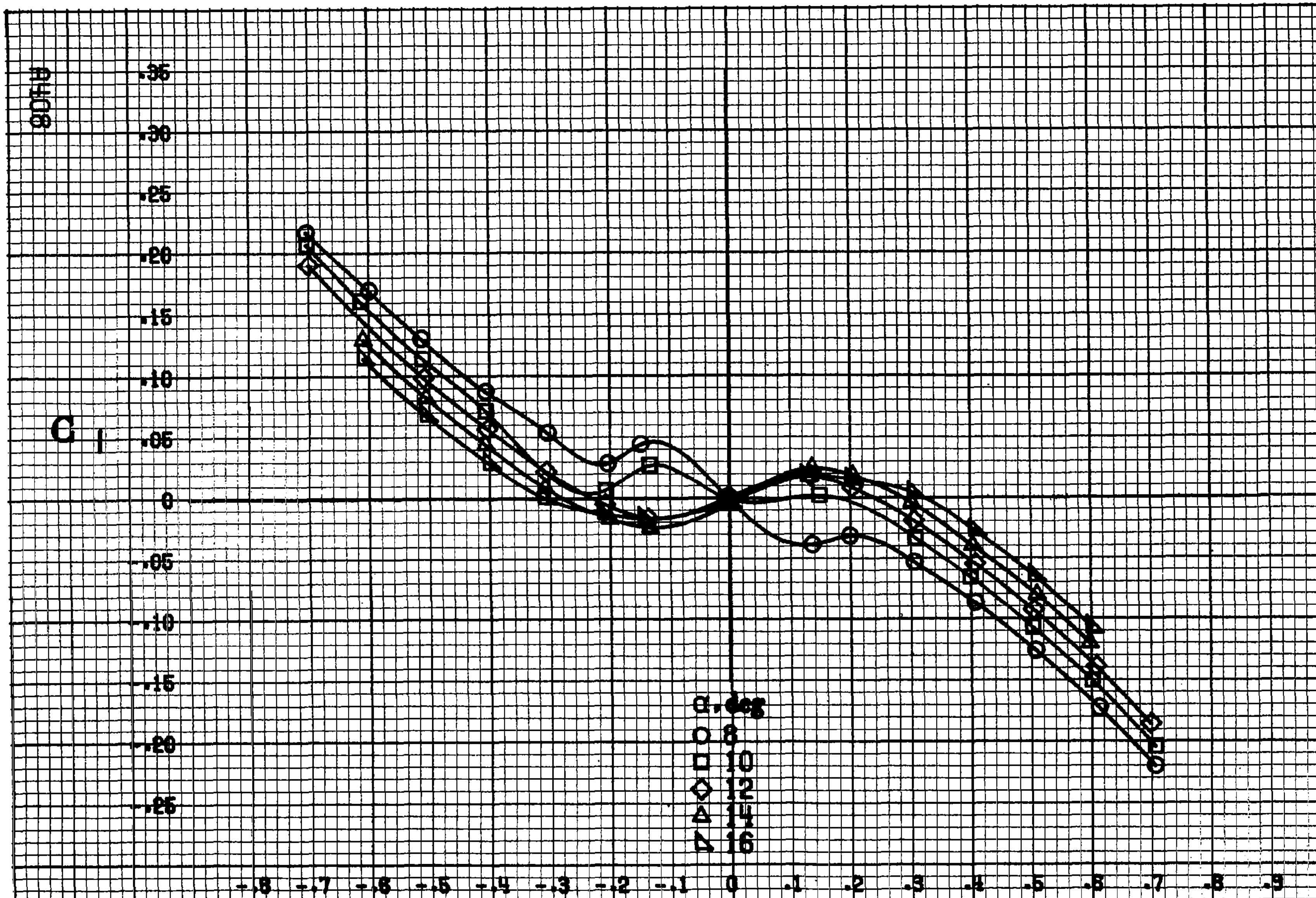

(a) α = 8 to 16 deg, SR = 182.9 cm (72 in).

Figure A98.- Effect of rotation rate and angle of attack on rolling-moment coefficient for horizontal and vertical tails off configuration. $\delta_e = 0°$, $\delta_a = 0°$, $\delta_r = 0°$, $\beta = 0°$.

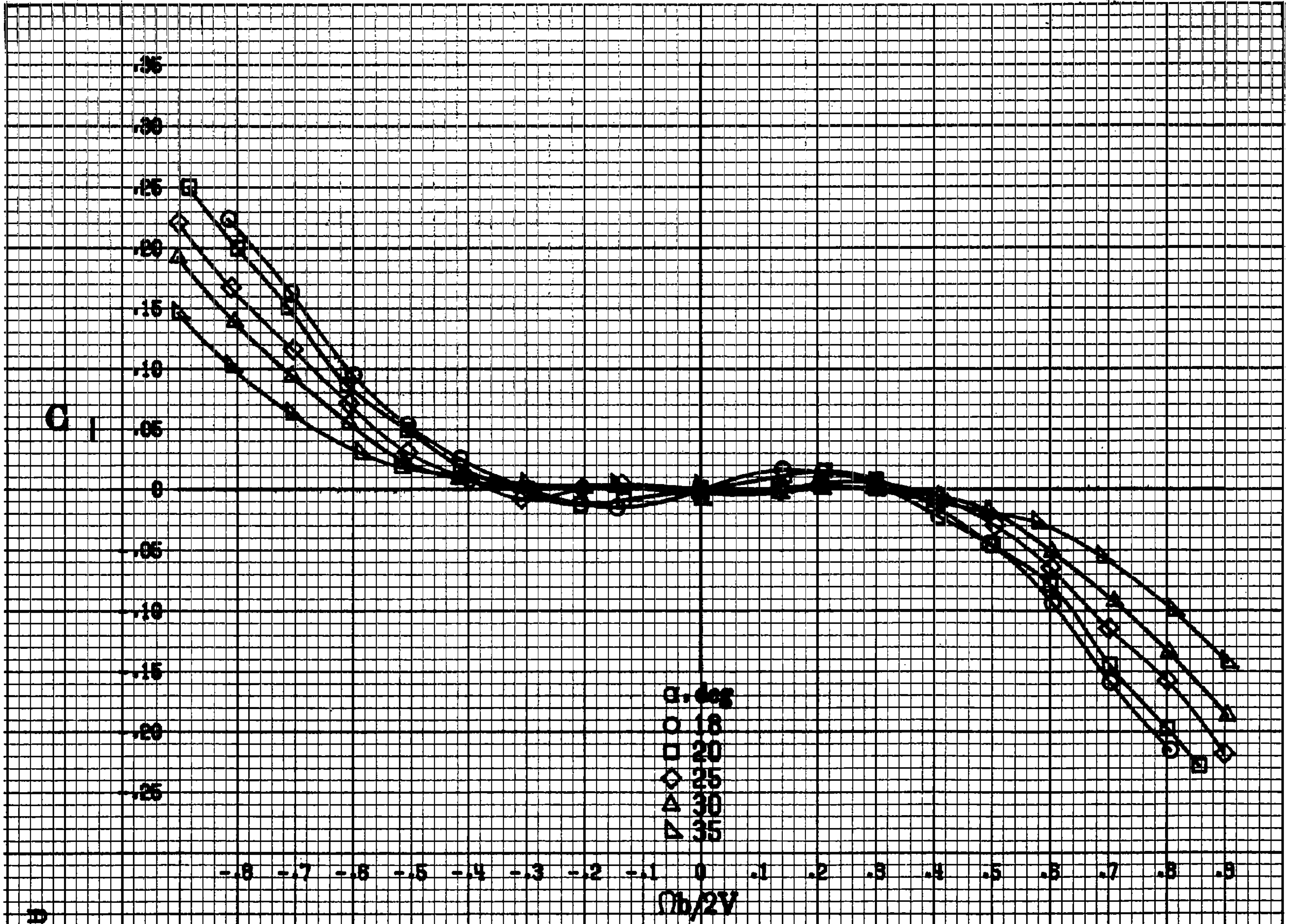

(b) α = 18 to 35 deg, SR = 182.9 cm (72 in).
Figure A98.-Continued.

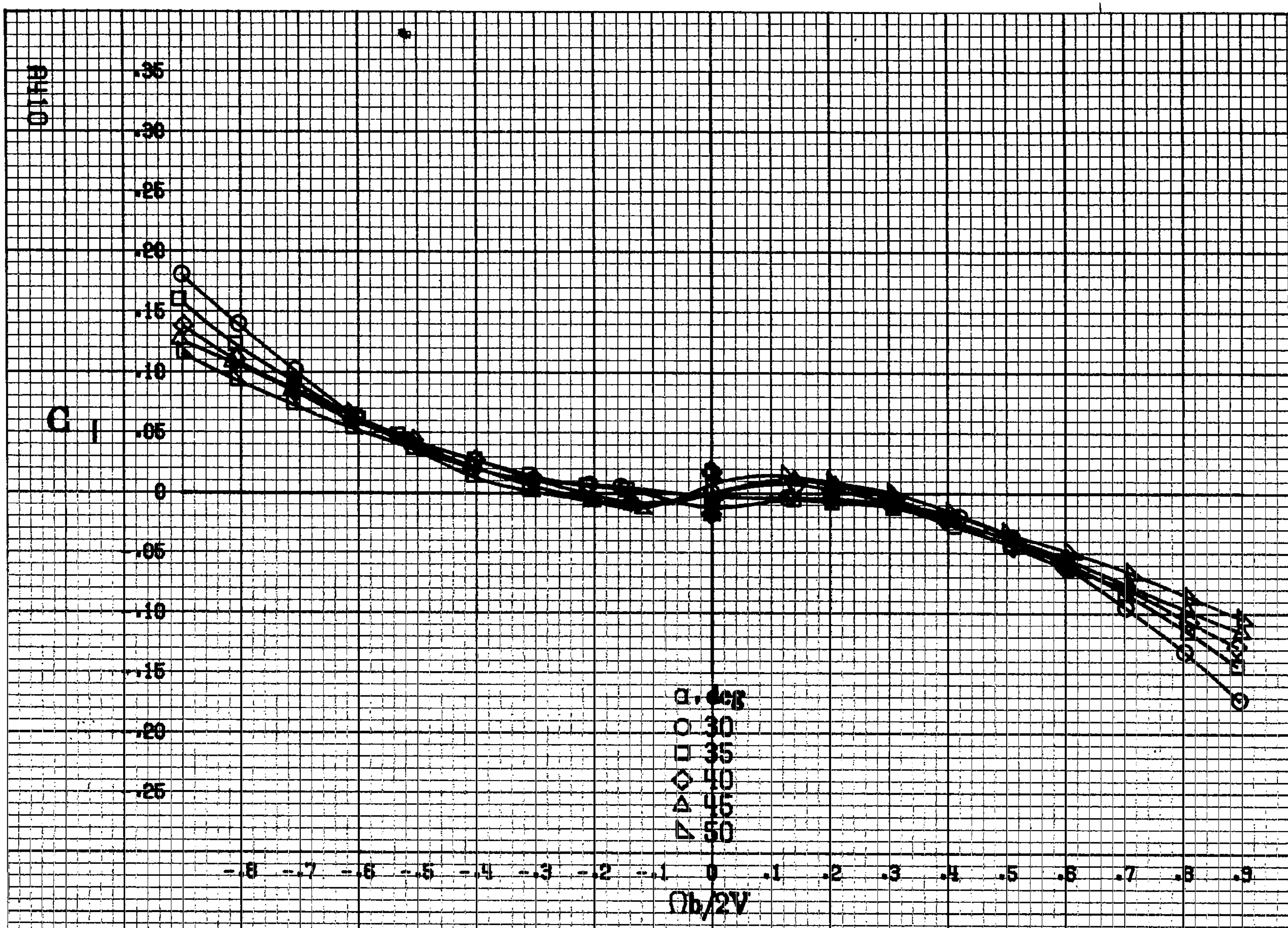

(c) α = 30 to 50 deg, SR = 0.

Figure A.98.-Continued.

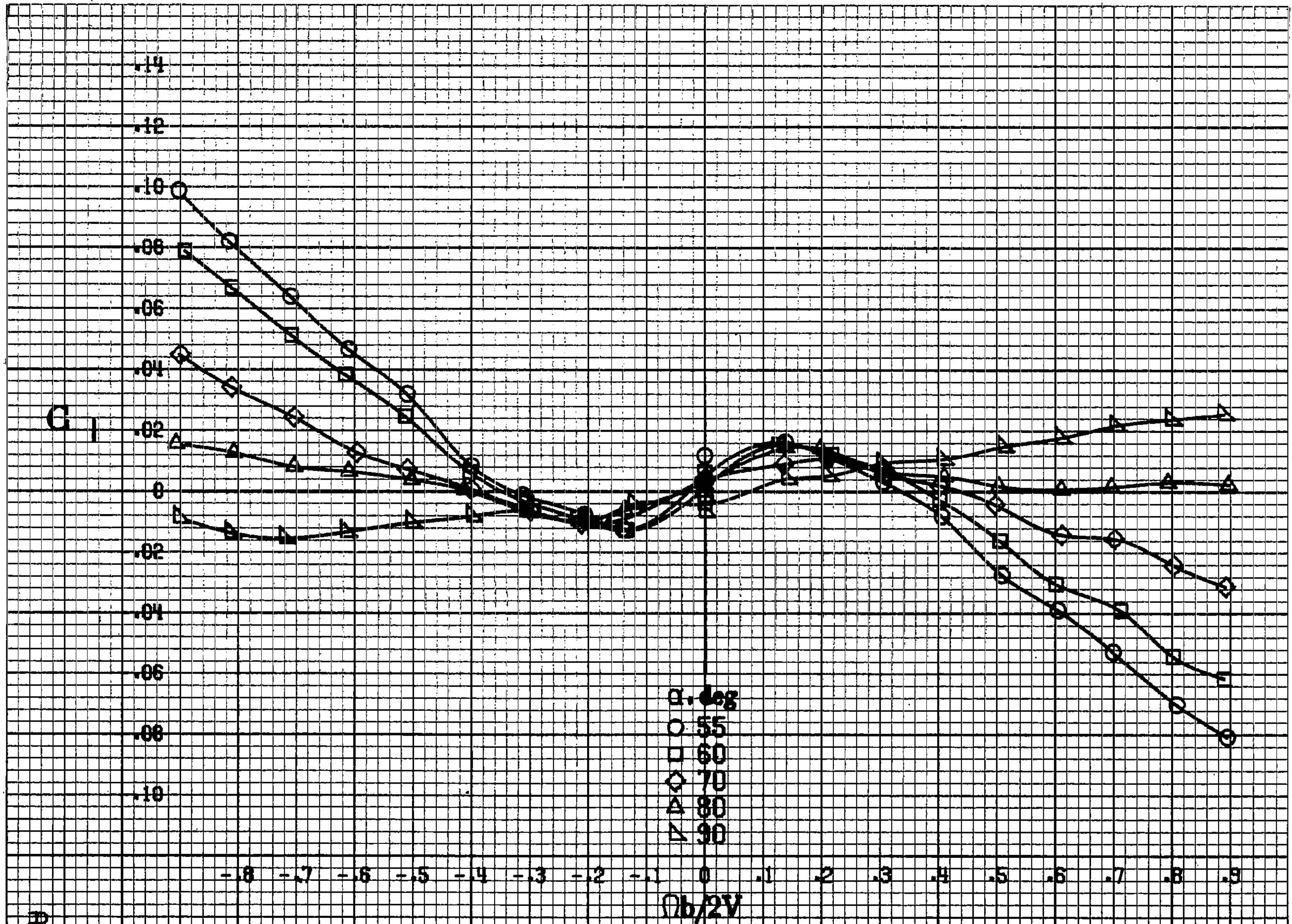

(d) $\alpha = 55$ to 90 deg, SR = 0.

Figure A98.-Concluded.

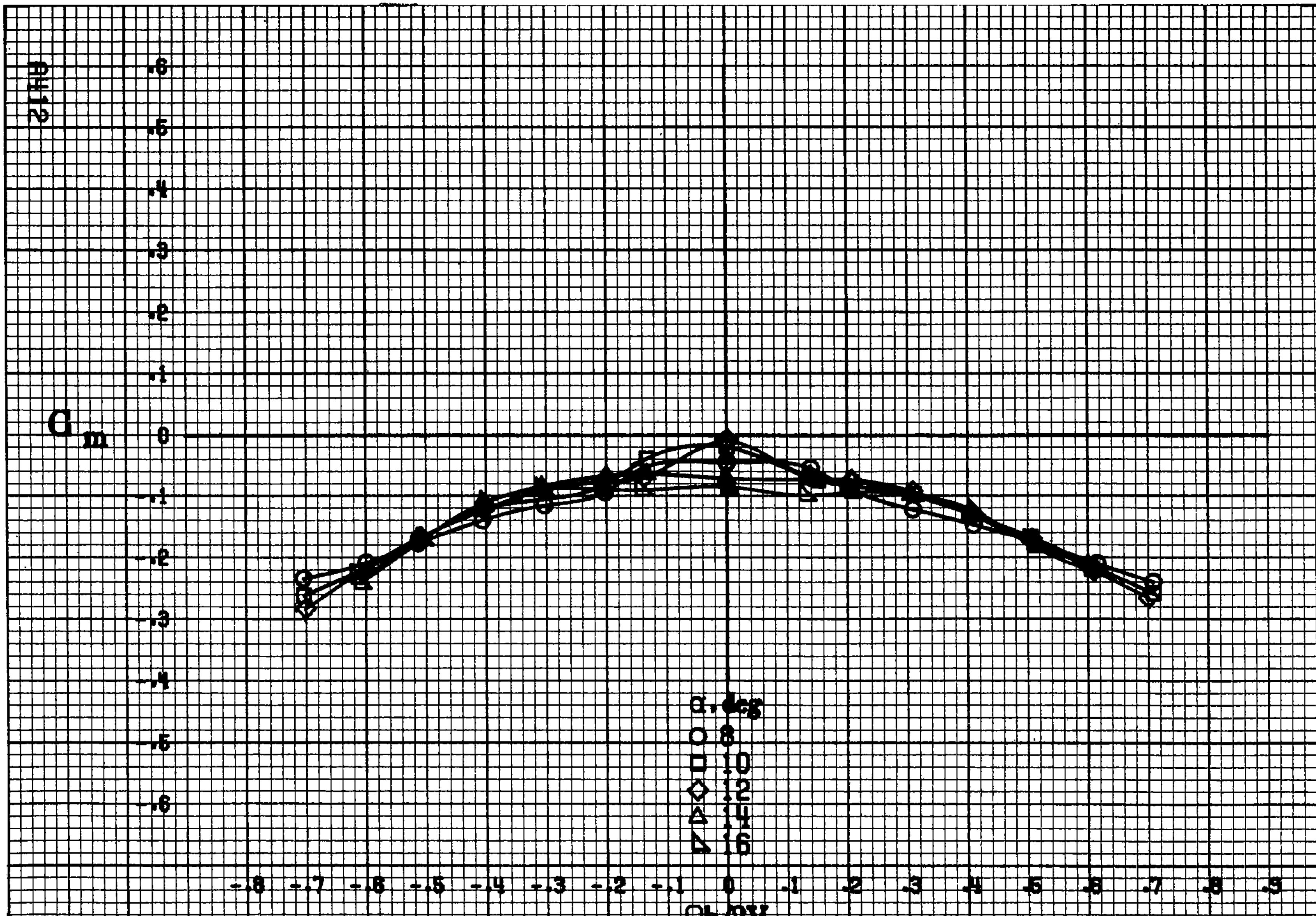

(a) $\alpha = 8$ to 16 deg, SR = 182.9 cm (72 in).

Figure A99.-Effect of rotation rate and angle of attack on pitching-moment coefficient for horizontal and vertical tails off configuration. $\delta_e = 0°$, $\delta_a = 0°$, $\delta_r = 0°$, $\beta = 0°$.

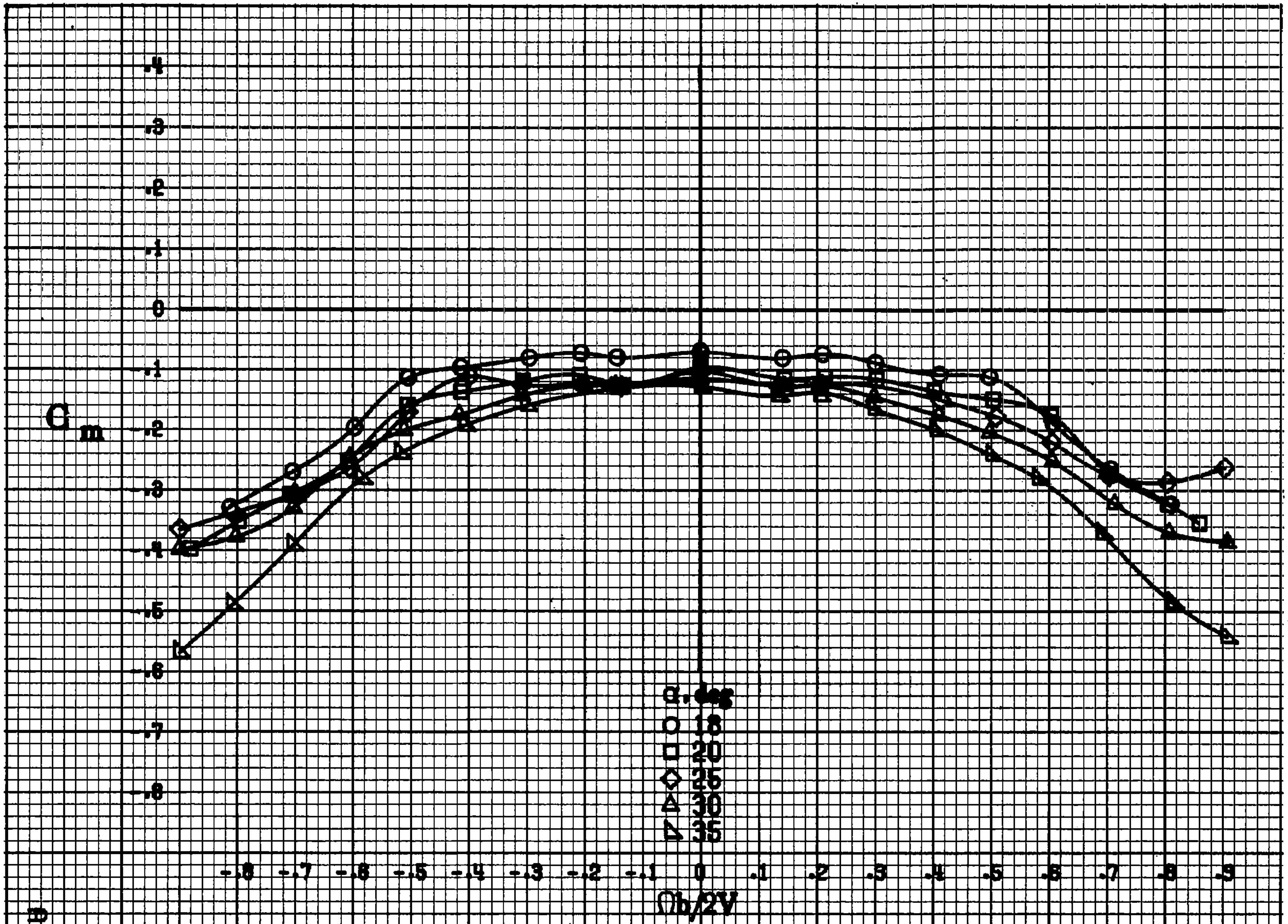

(b) α = 18 to 35 deg, SR = 182.9 cm (72 in).

Figure A99.-Continued.

A413

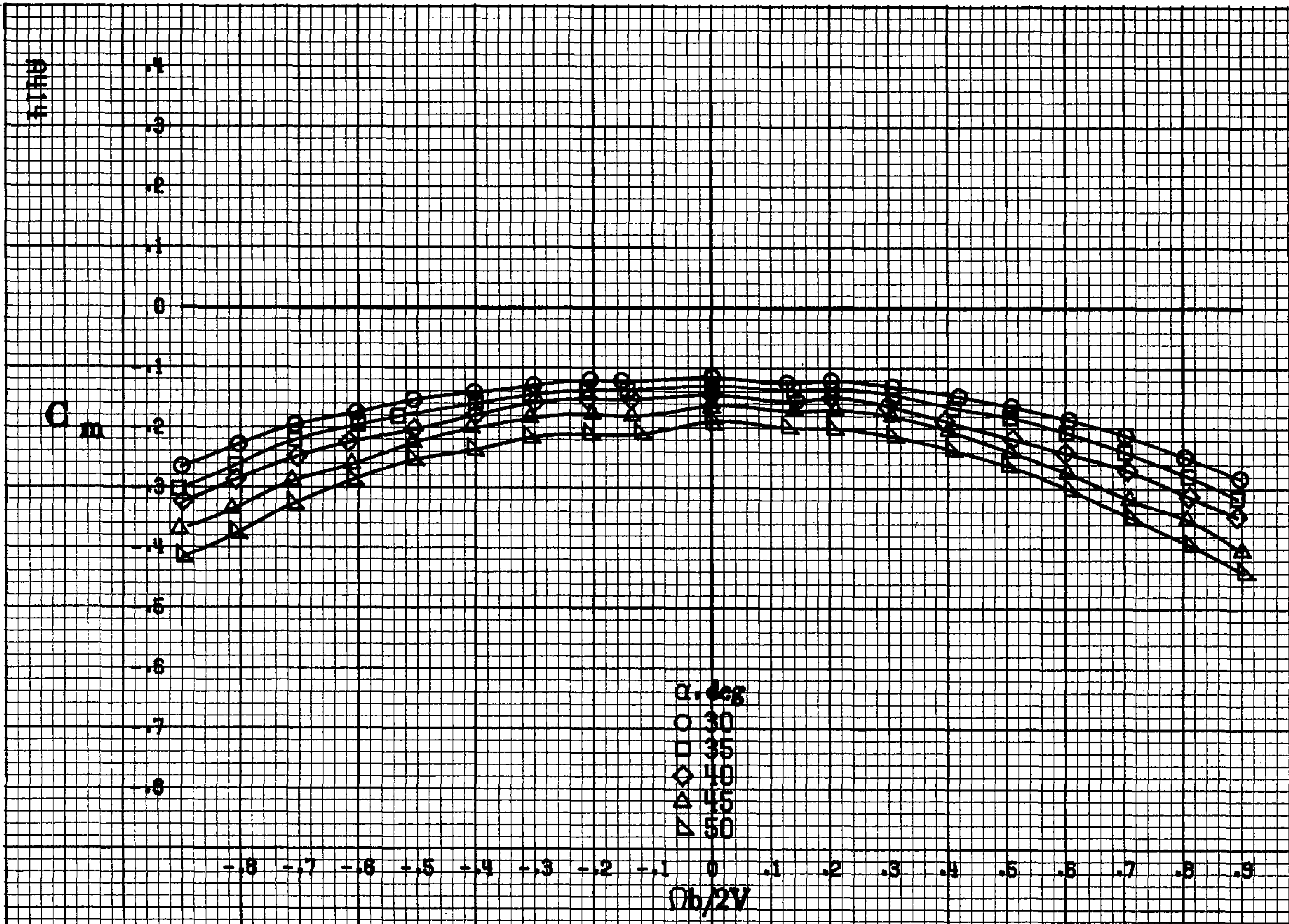

(c) α = 30 to 50 deg, SR = 0.

Figure A99.-Continued.

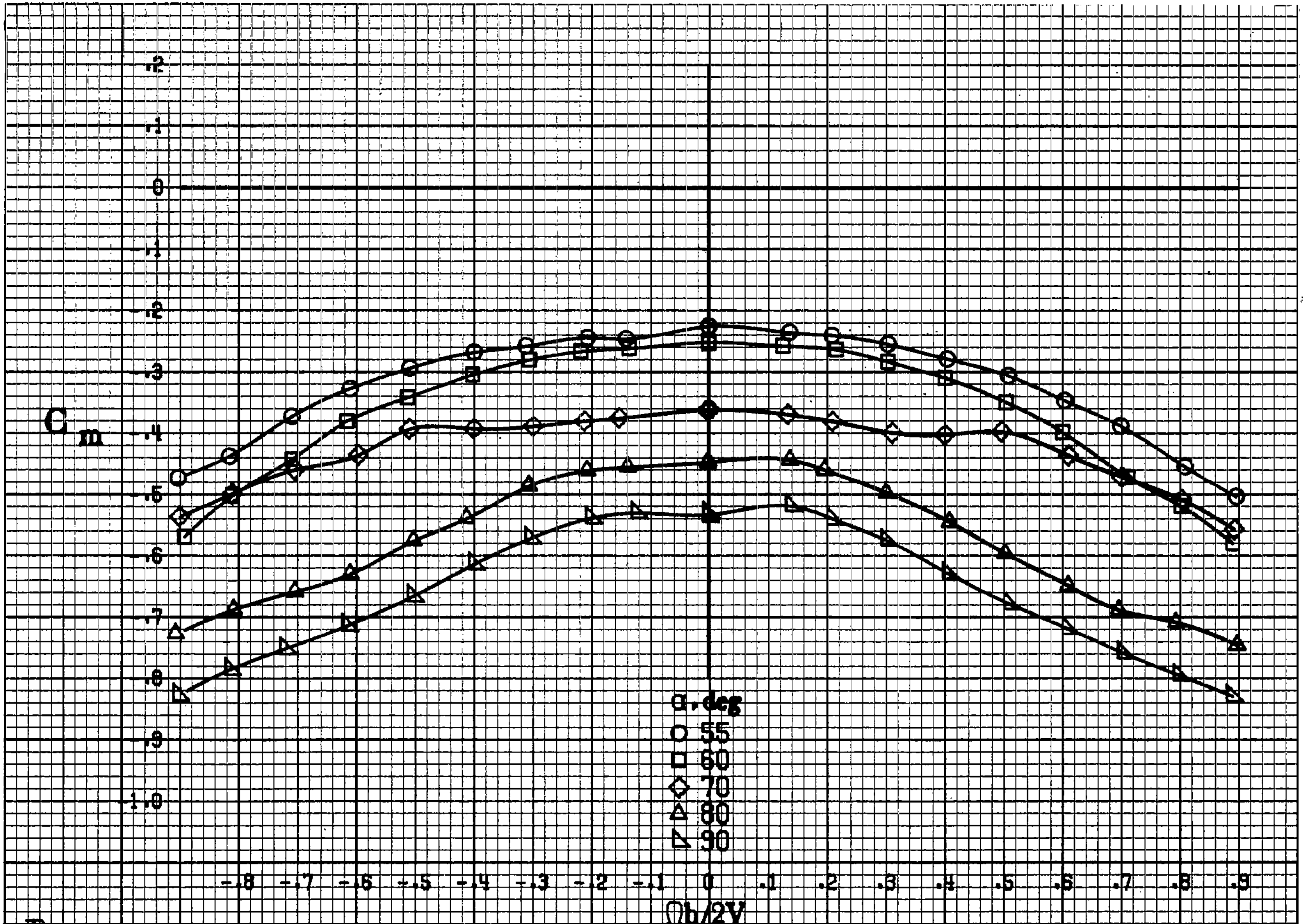

(d) α = 55 to 90 deg, SR = 0.

Figure A99.-Concluded.

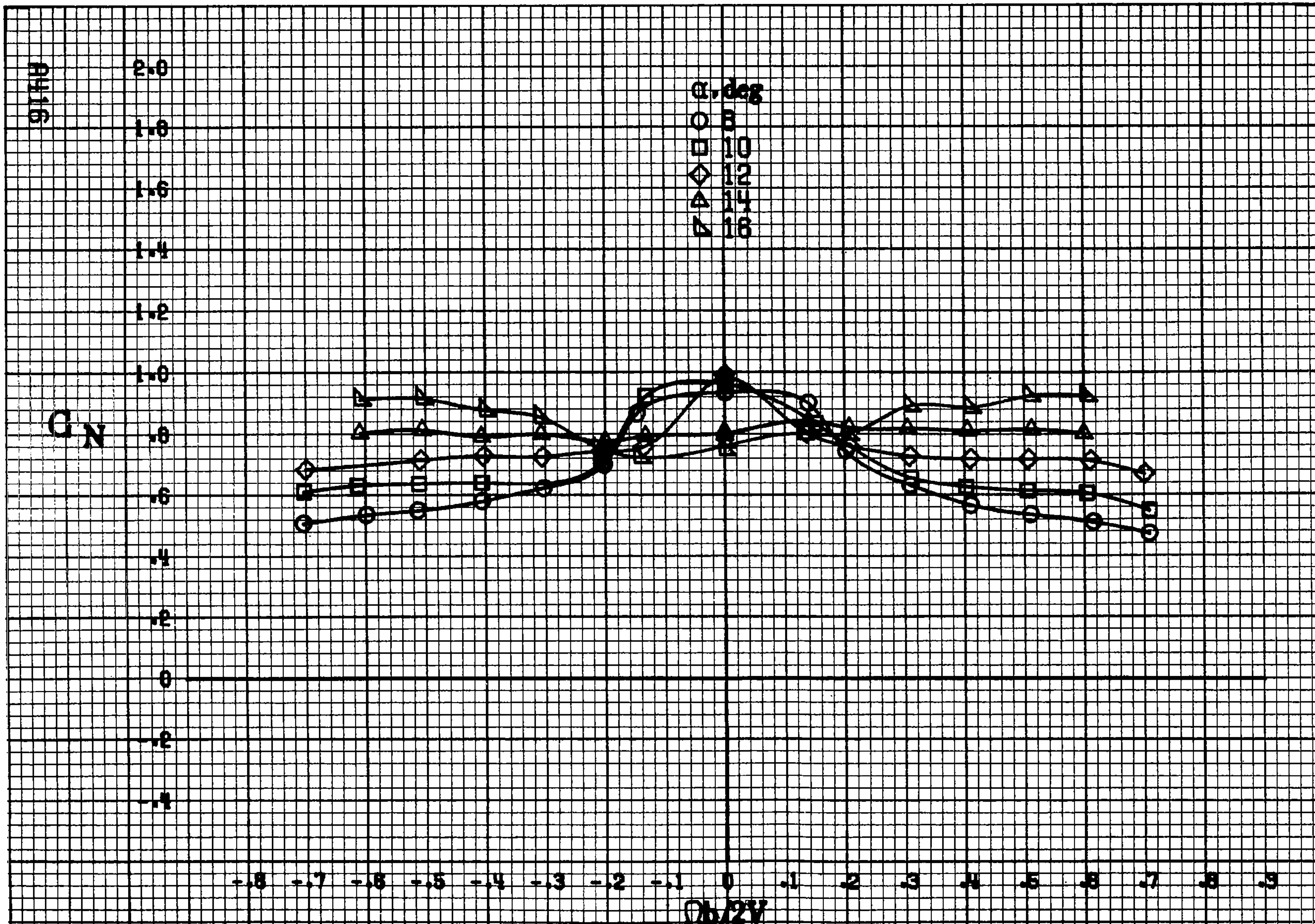

(a) α = 8 to 16 deg, SR = 182.9 cm (72 in).

Figure A100.-Effect of rotation rate and angle of attack on normal-force coefficient for horizontal and vertical tails off configuration. $\delta_e = 0°$, $\delta_a = 0°$, $\delta_r = 0°$, $\beta = 0°$.

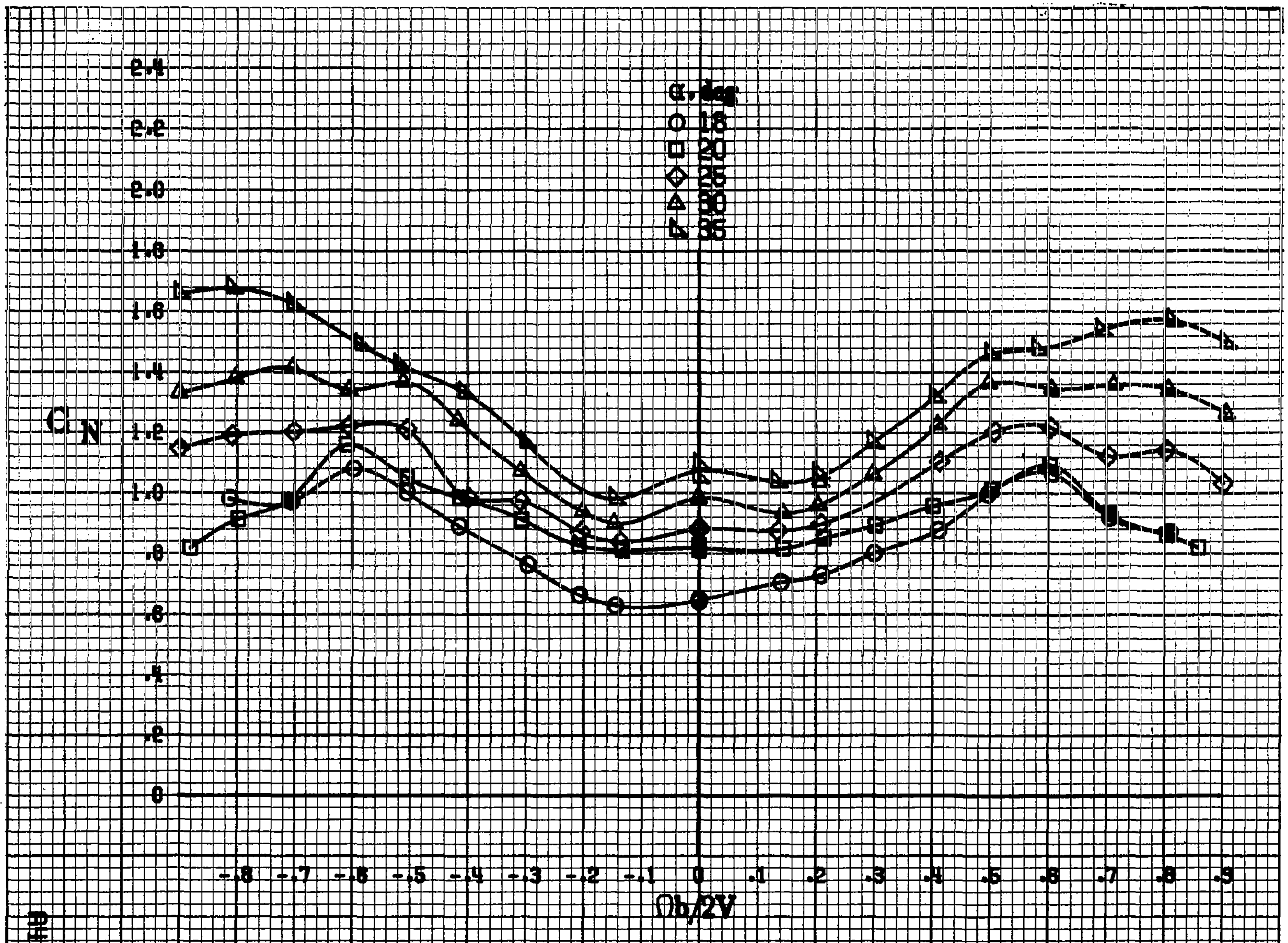

(b) α = 18 to 35 deg, SR = 182.9 cm (72 in).
Figure A100.-Continued.

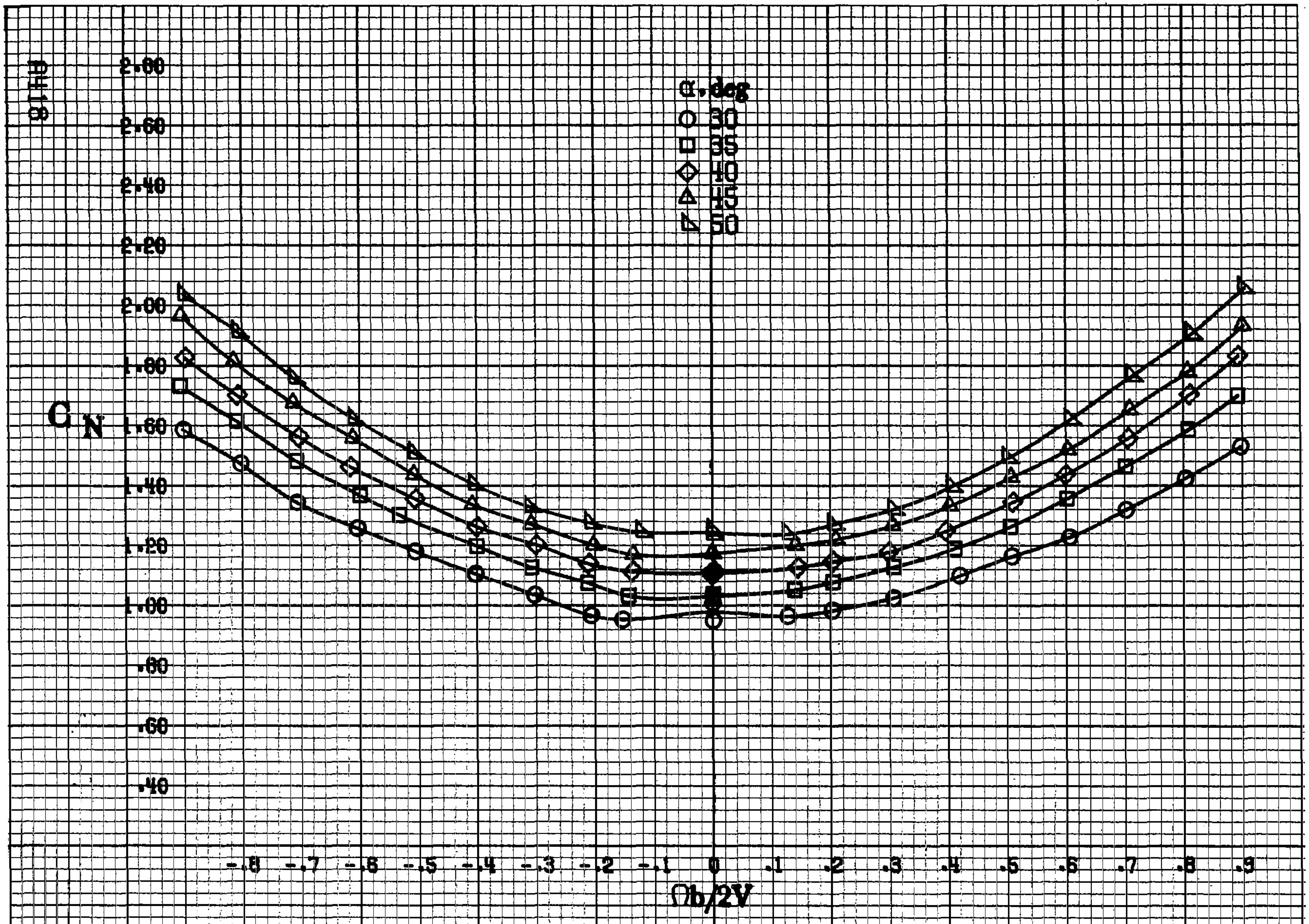

(c) α = 30 to 50 deg, SR = 0.

Figure A100.-Continued.

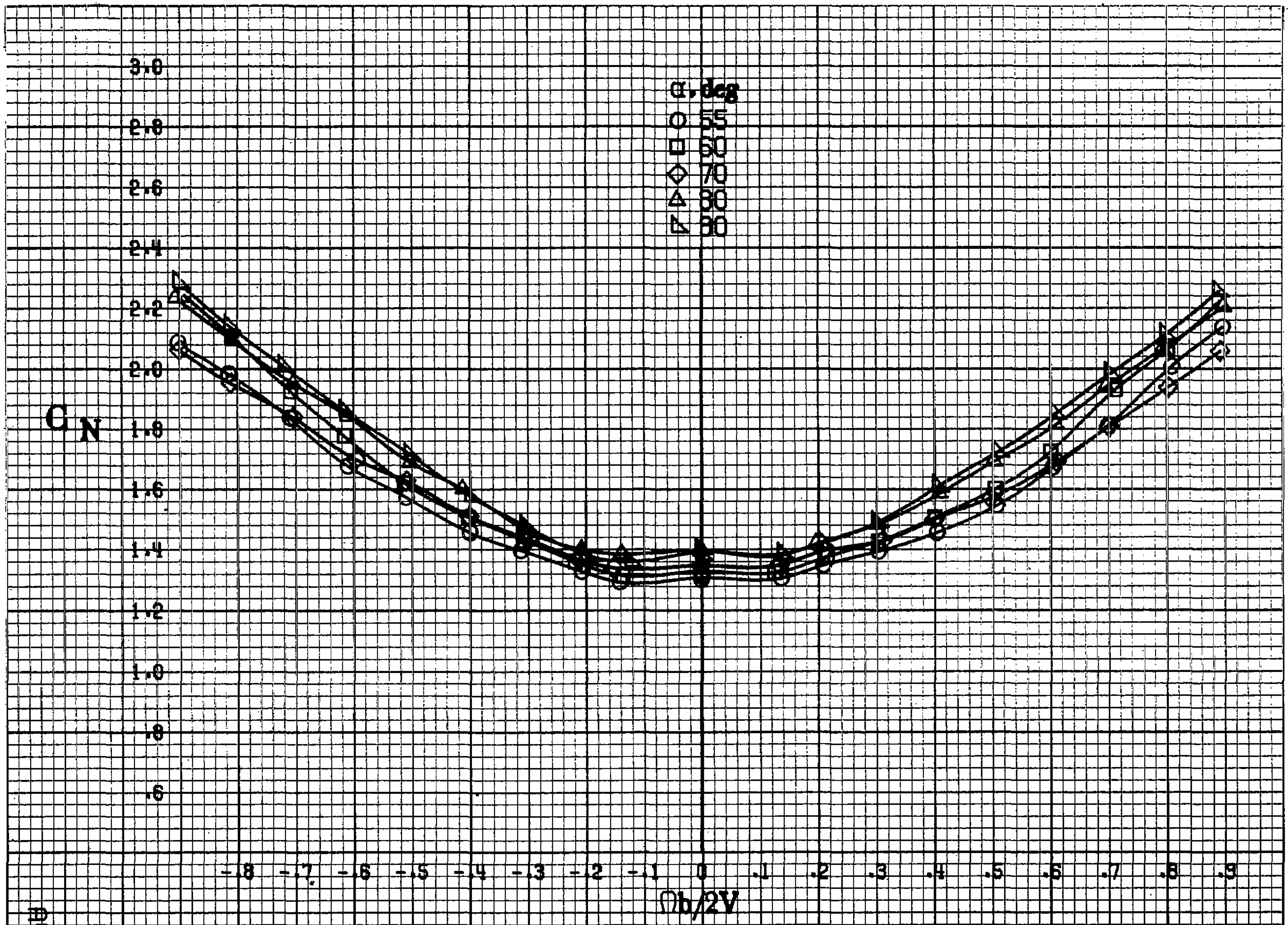

(d) α = 55 to 90 deg, SR = 0.

Figure A100.-Concluded.

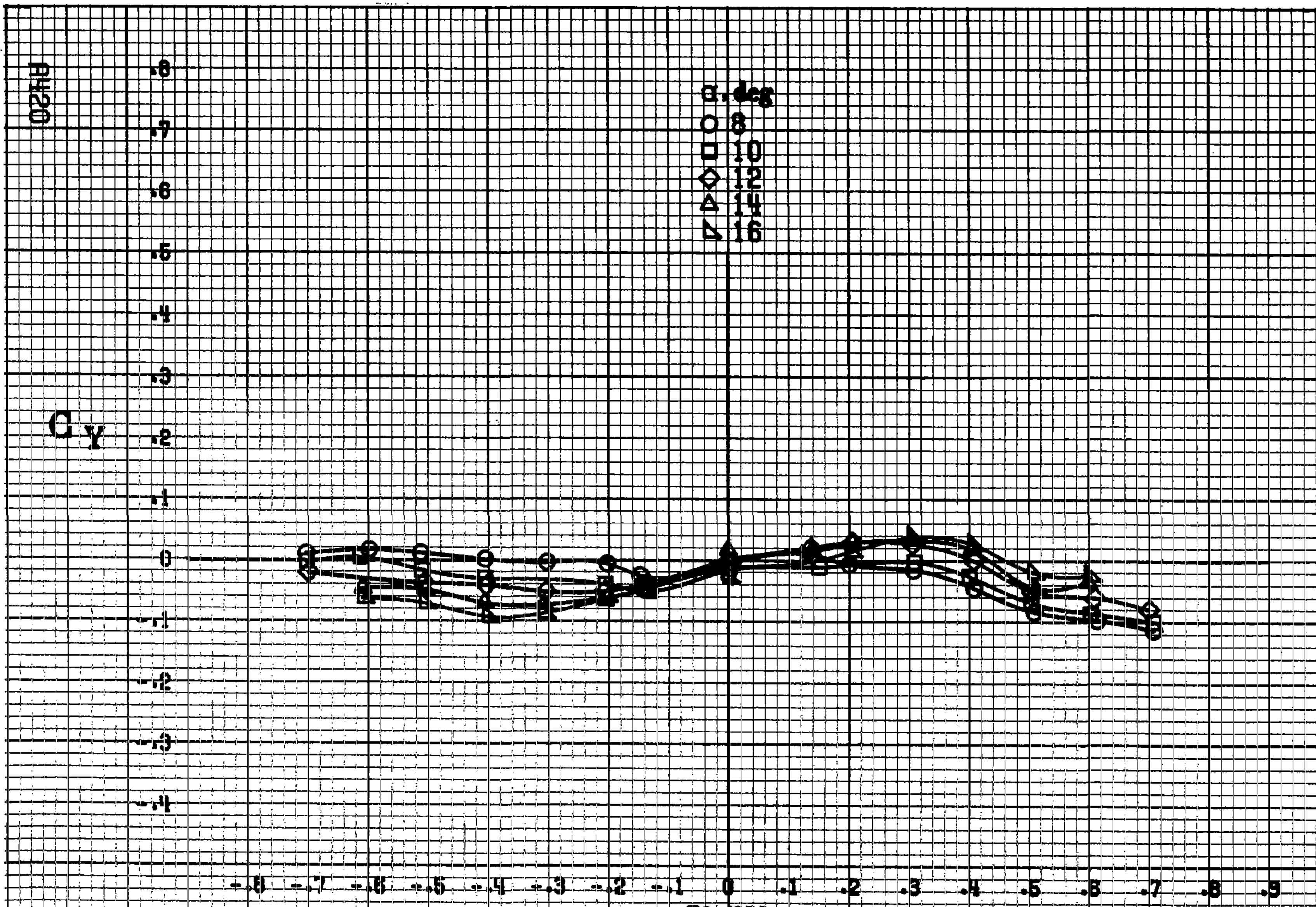

(a) α = 8 to 16 deg, SR = 182.9 cm (72 in.).

Figure A101.- Effect of rotation rate and angle of attack on side-force coefficient for horizontal and vertical tails off configuration. $\delta_e = 0°$, $\delta_a = 0°$, $\delta_r = 0°$, $\beta = 0°$.

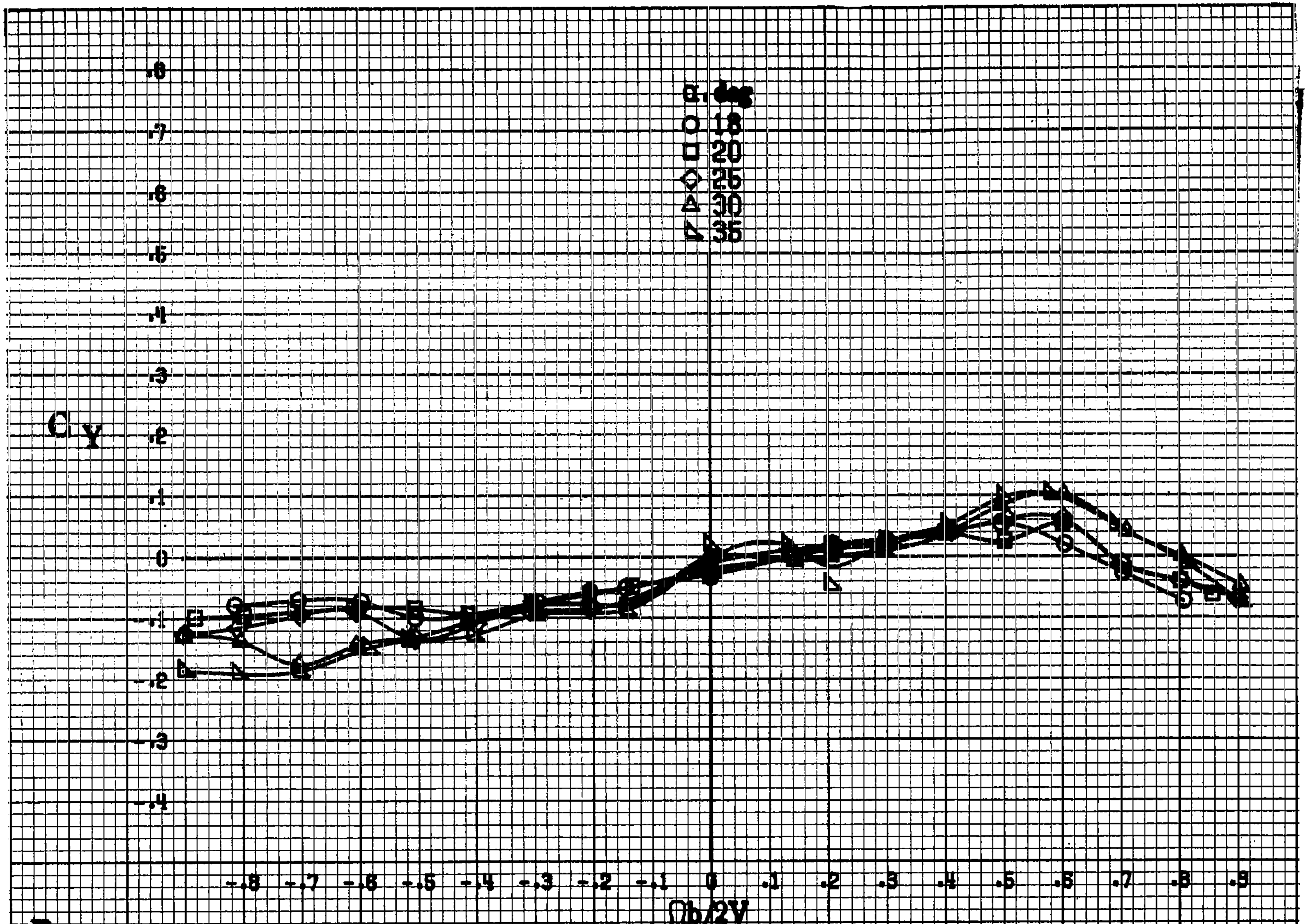

(b) α = 18 to 35 deg, SR = 182.9 cm (72 in).

Figure A101.-Continued.

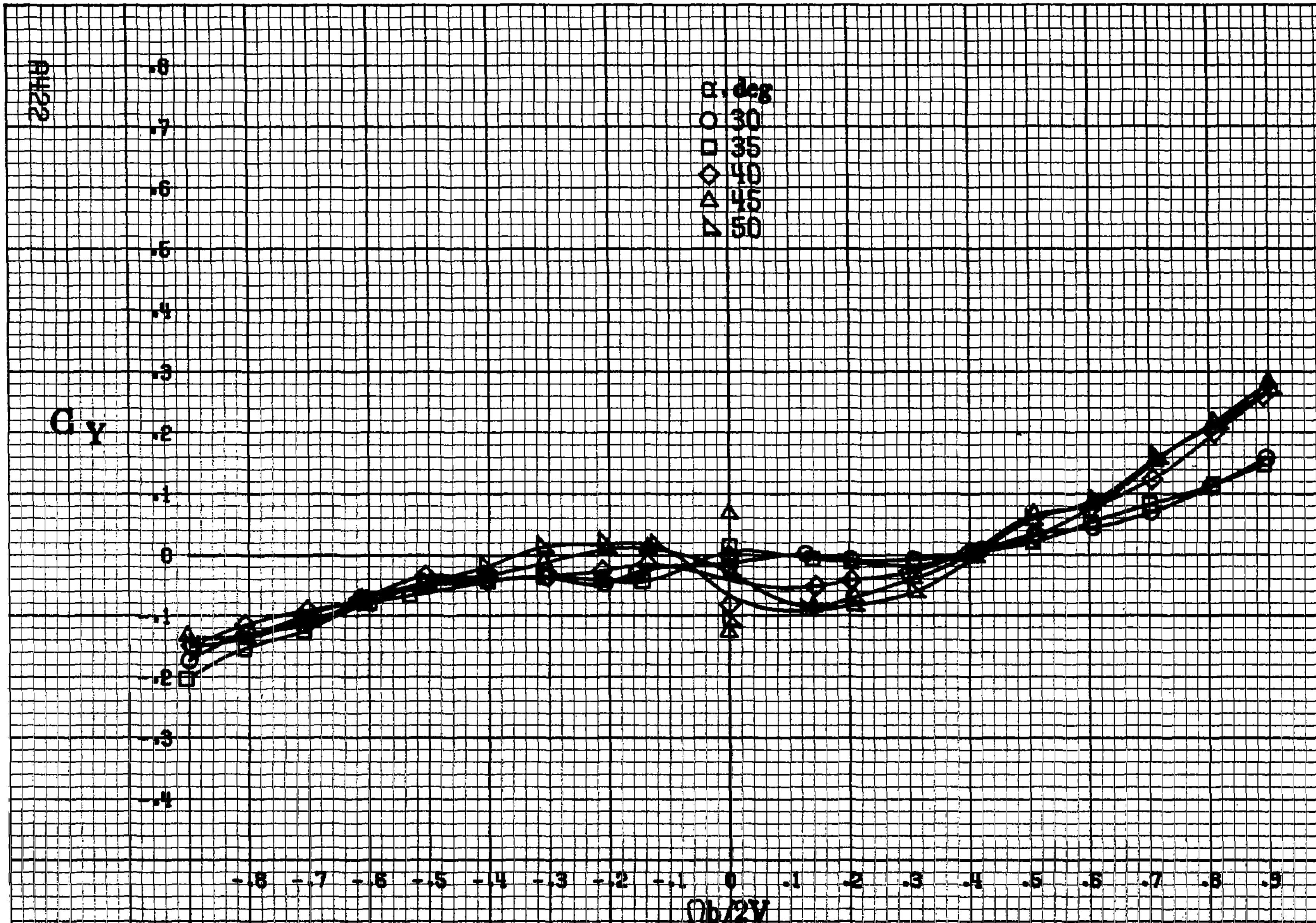

(c) α = 30 to 50 deg, SR = 0.

Figure A101.-Continued.

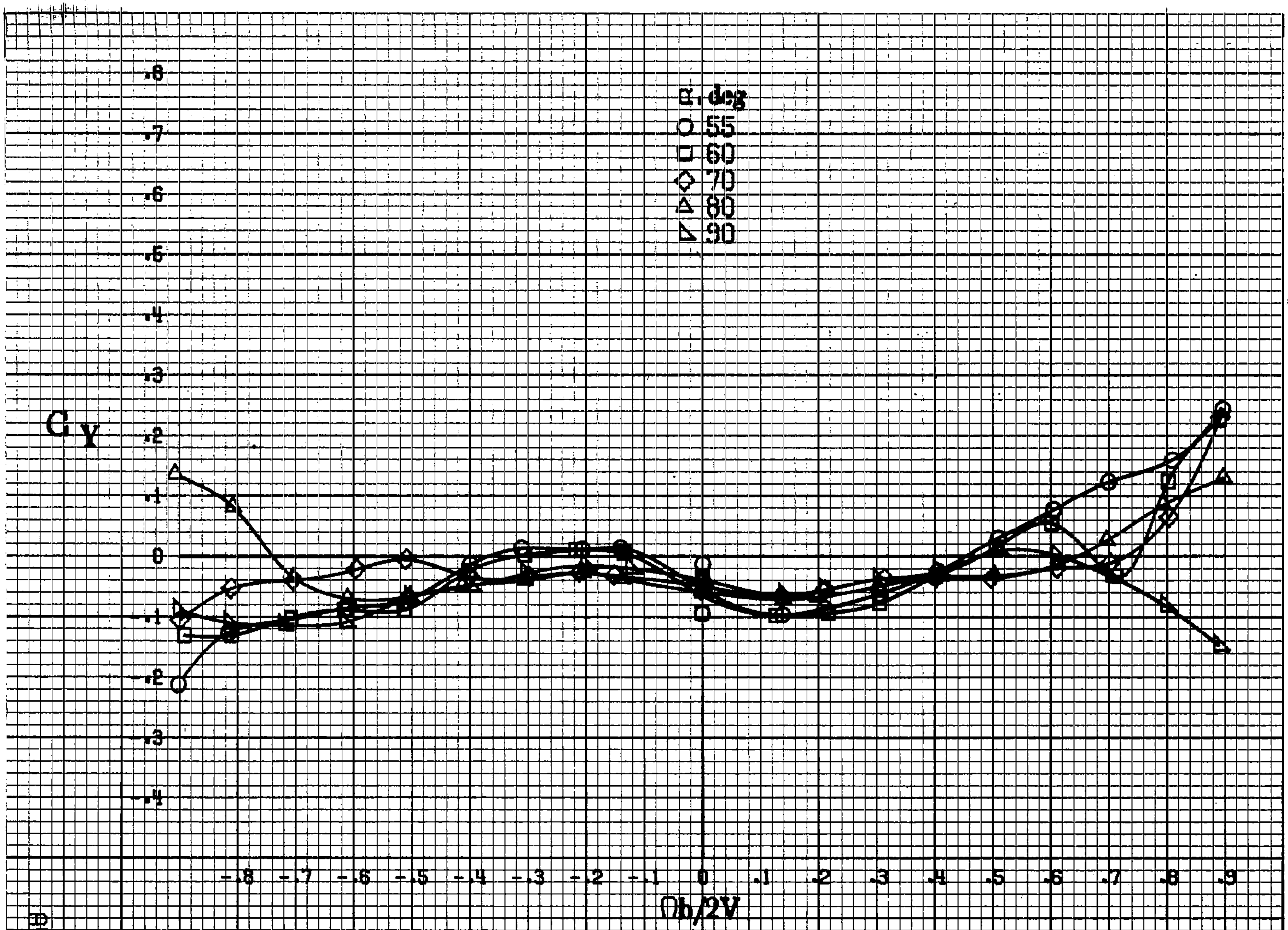

(d) $\alpha = 55$ to 90 deg, SR = 0.

Figure A101.-Concluded.

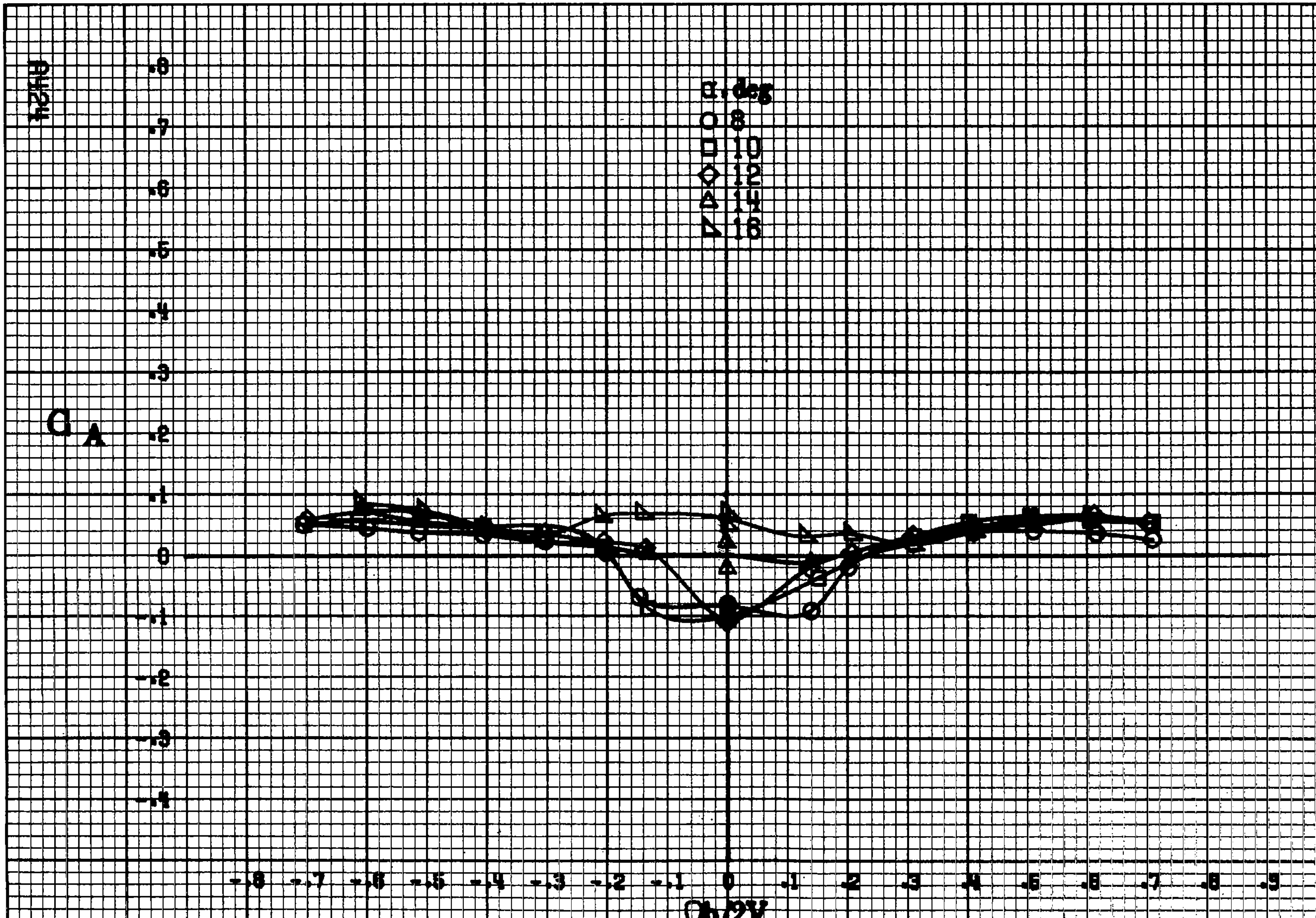

(a) α = 8 to 16 deg, SR = 182.9 cm (72 in).

Figure A102.-Effect of rotation rate and angle of attack on axial-force coefficient for horizontal and vertical tails off configuration. $\delta_e = 0°$, $\delta_a = 0°$, $\delta_r = 0°$, $\beta = 0°$.

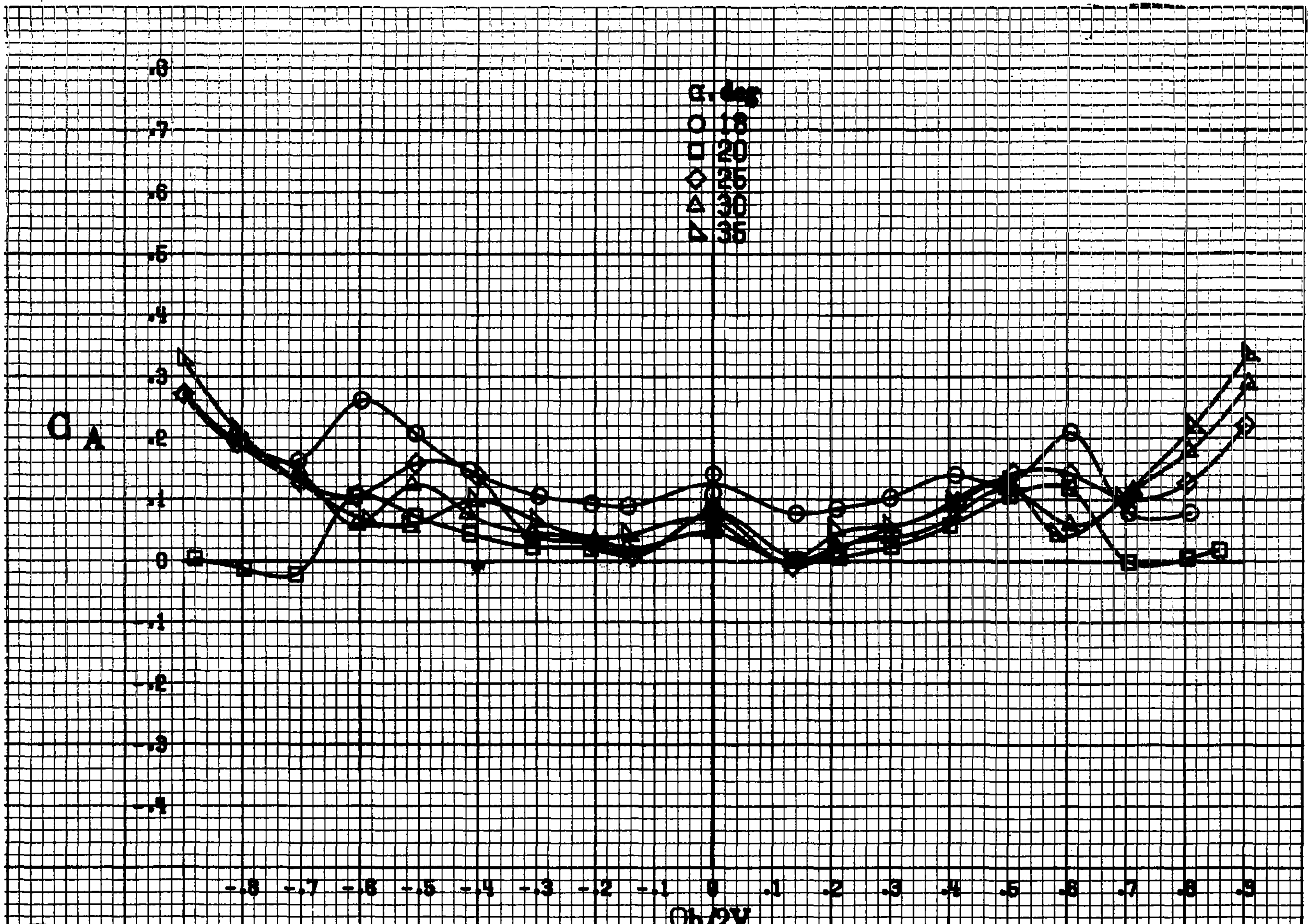

(b) α = 18 to 35 deg, SR = 182.9 cm (72 in).

Figure A102.-Continued.

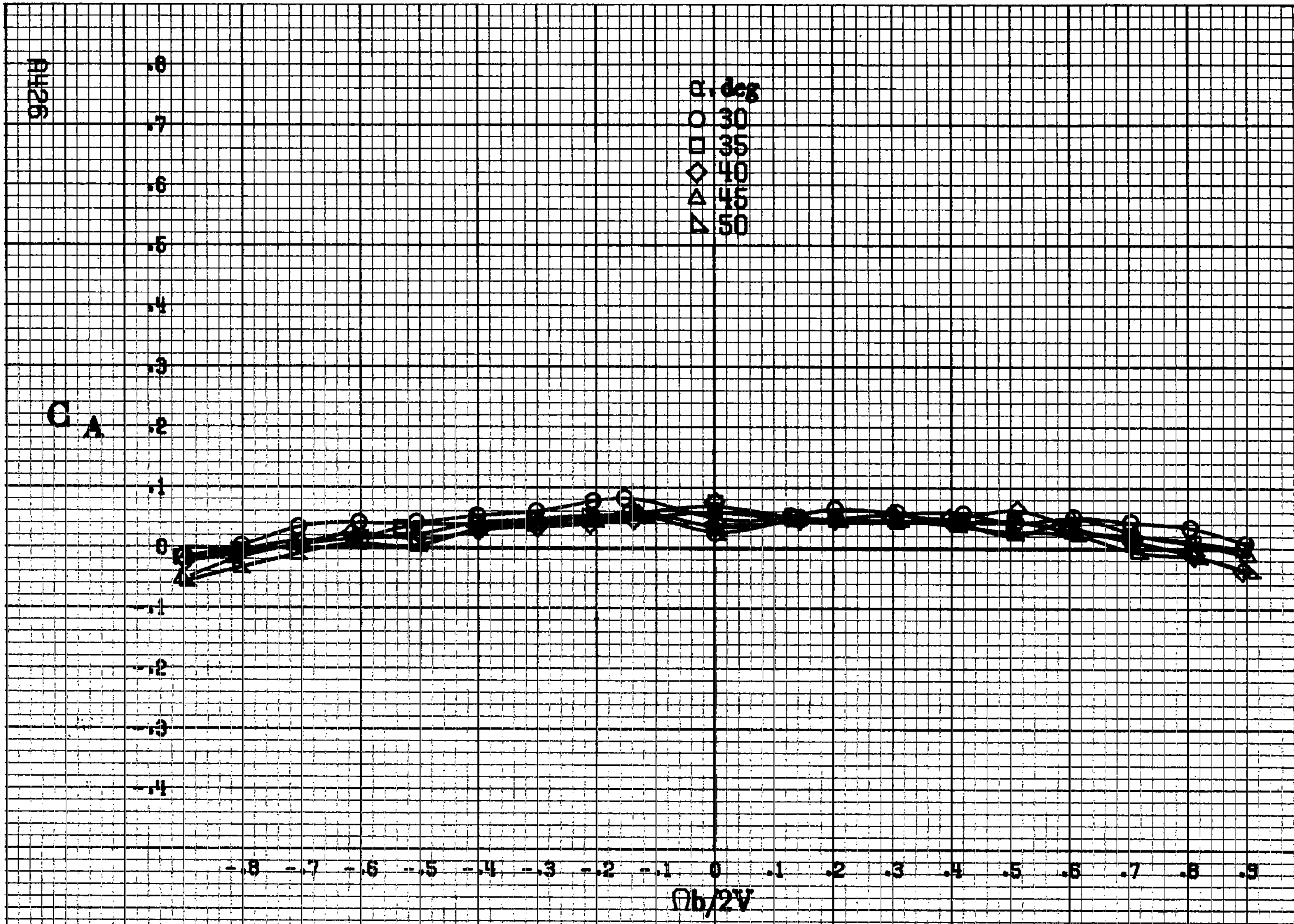

(c) α = 30 to 50 deg, SR = 0.

Figure A102.-Continued.

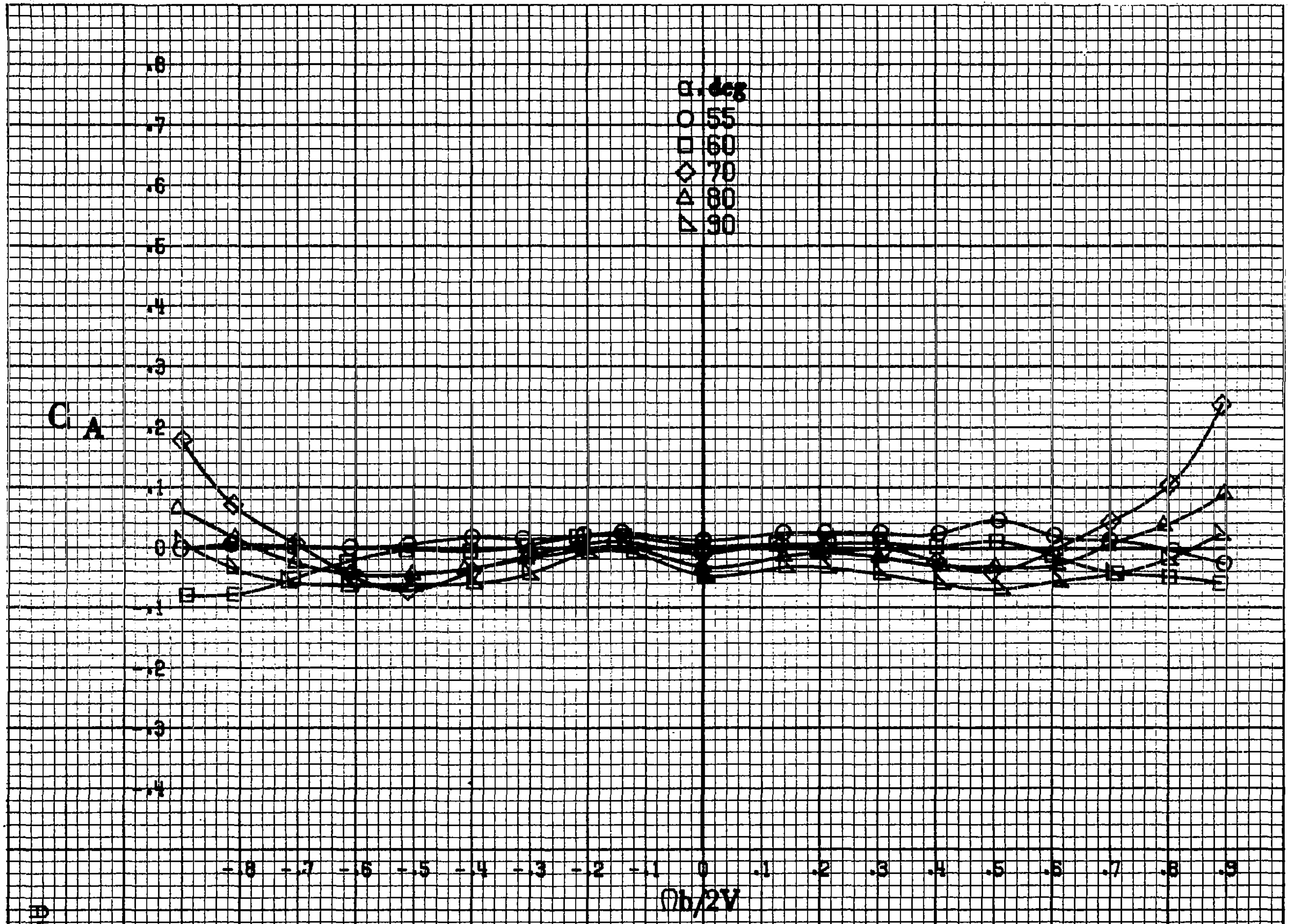

(d) $\alpha = 55$ to 90 deg, SR = 0.

Figure A102.-Concluded.

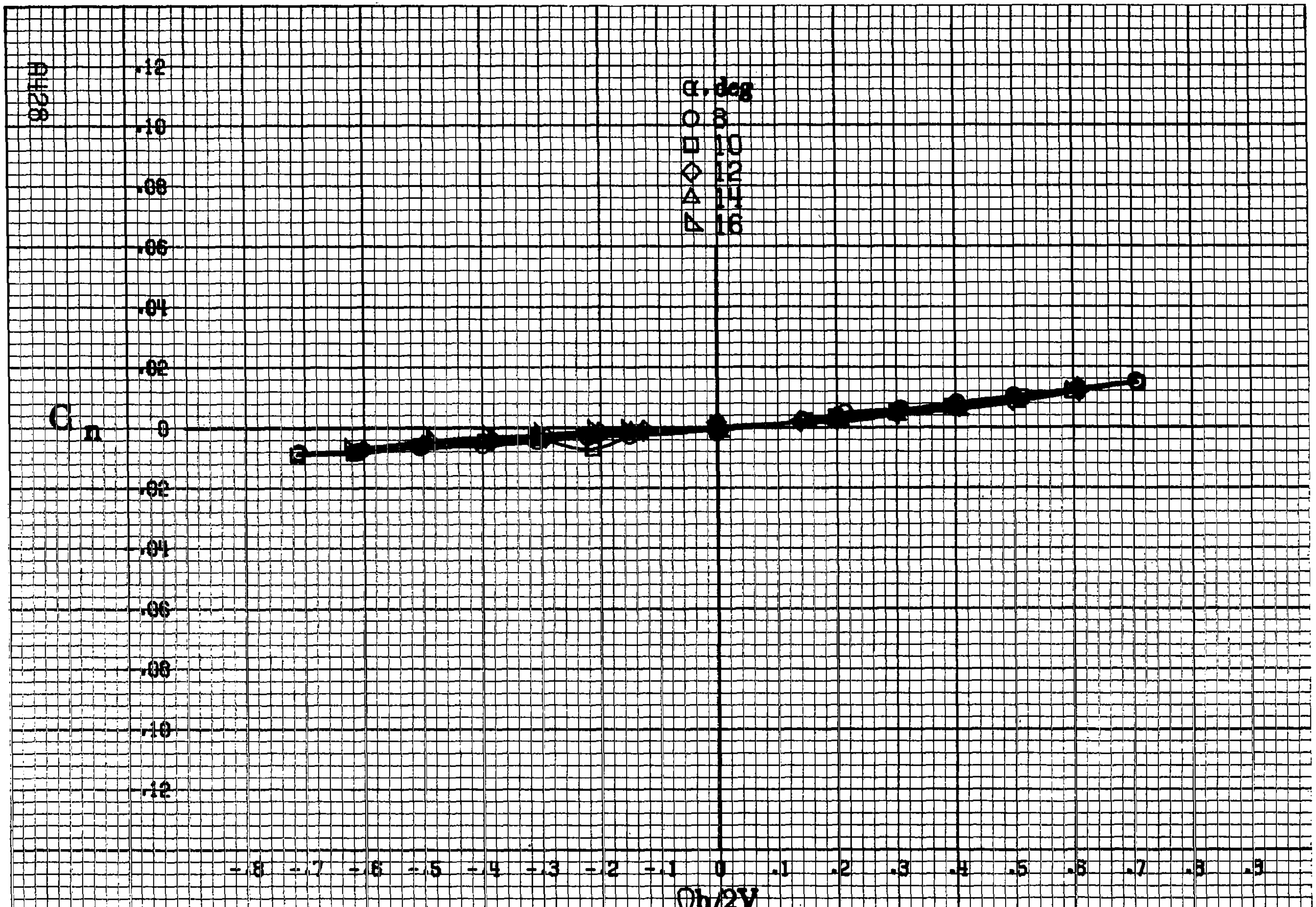

(a) $\alpha = 8$ to 16 deg, SR = 182.9 cm (72 in).

Figure A103.-Effect of rotation rate and angle of attack on yawing-moment coefficient for body alone configuration. $\delta_e = 0°$, $\delta_a = 0°$, $\delta_r = 0°$, $\beta = 0°$.

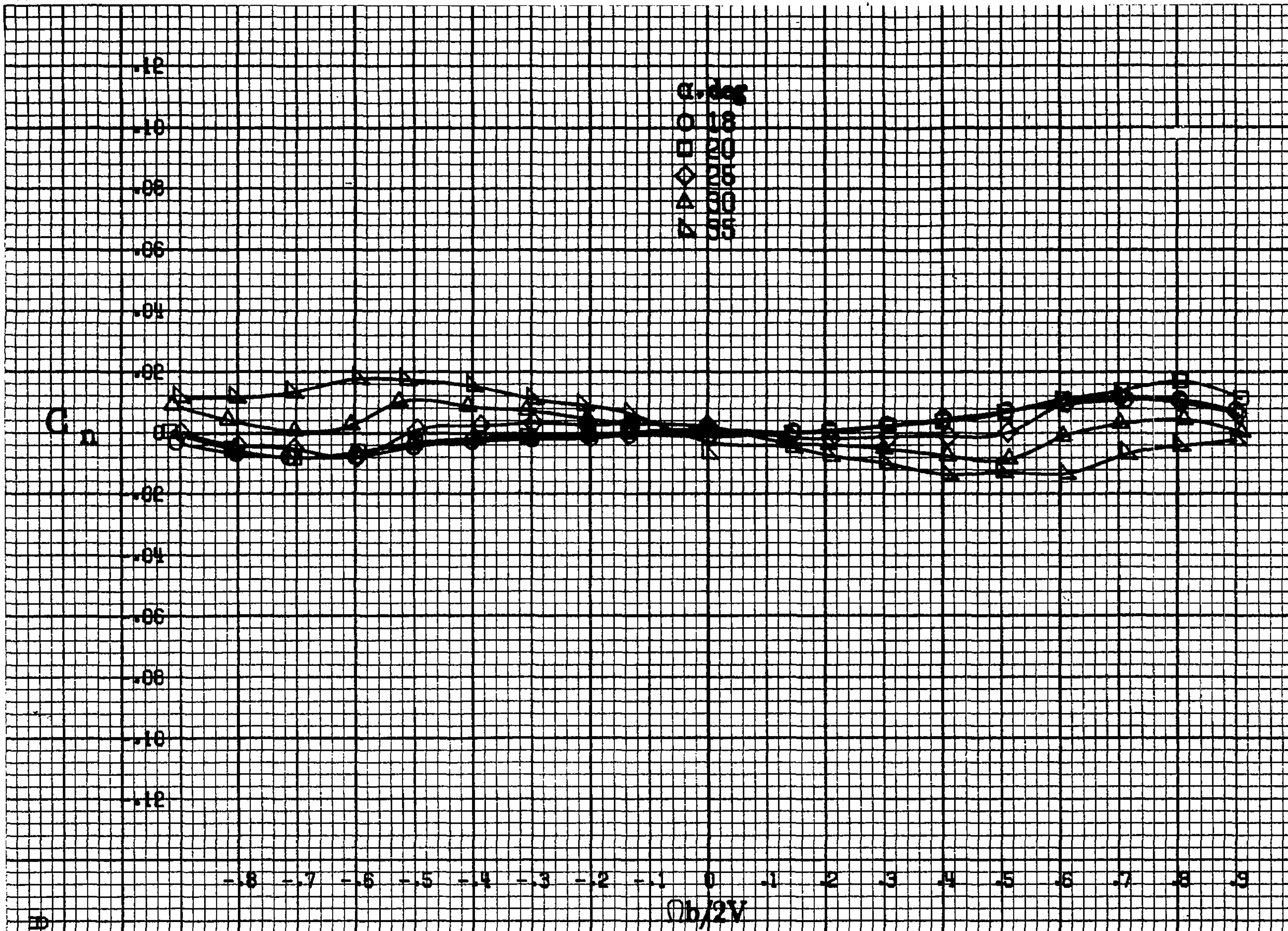

(b) α = 18 to 55 deg, SR = 182.9 cm (72 in).

Figure A108.-Continued.

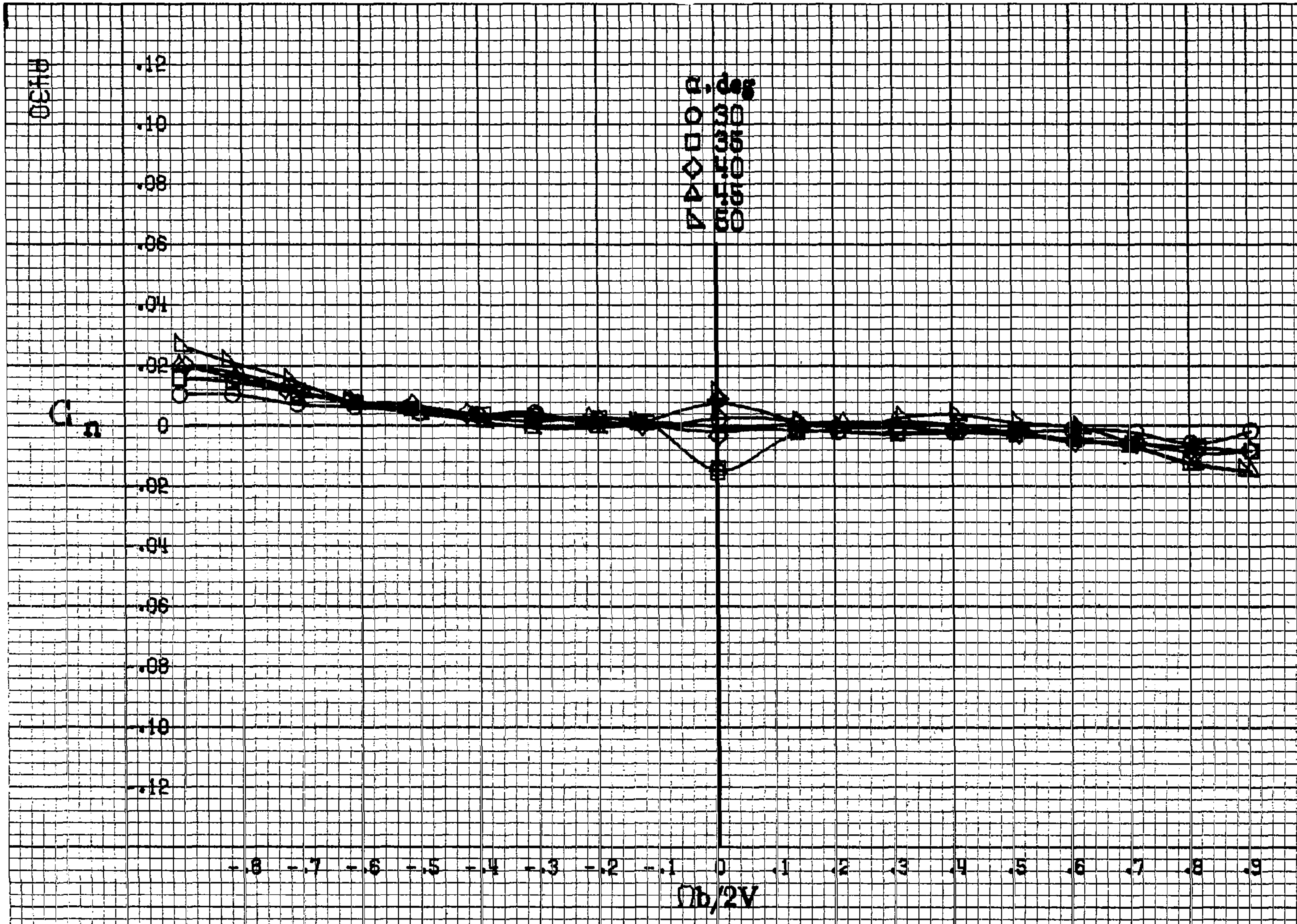

(c) α = 30 to 50 deg, SR = 0.

Figure A108.- Continued.

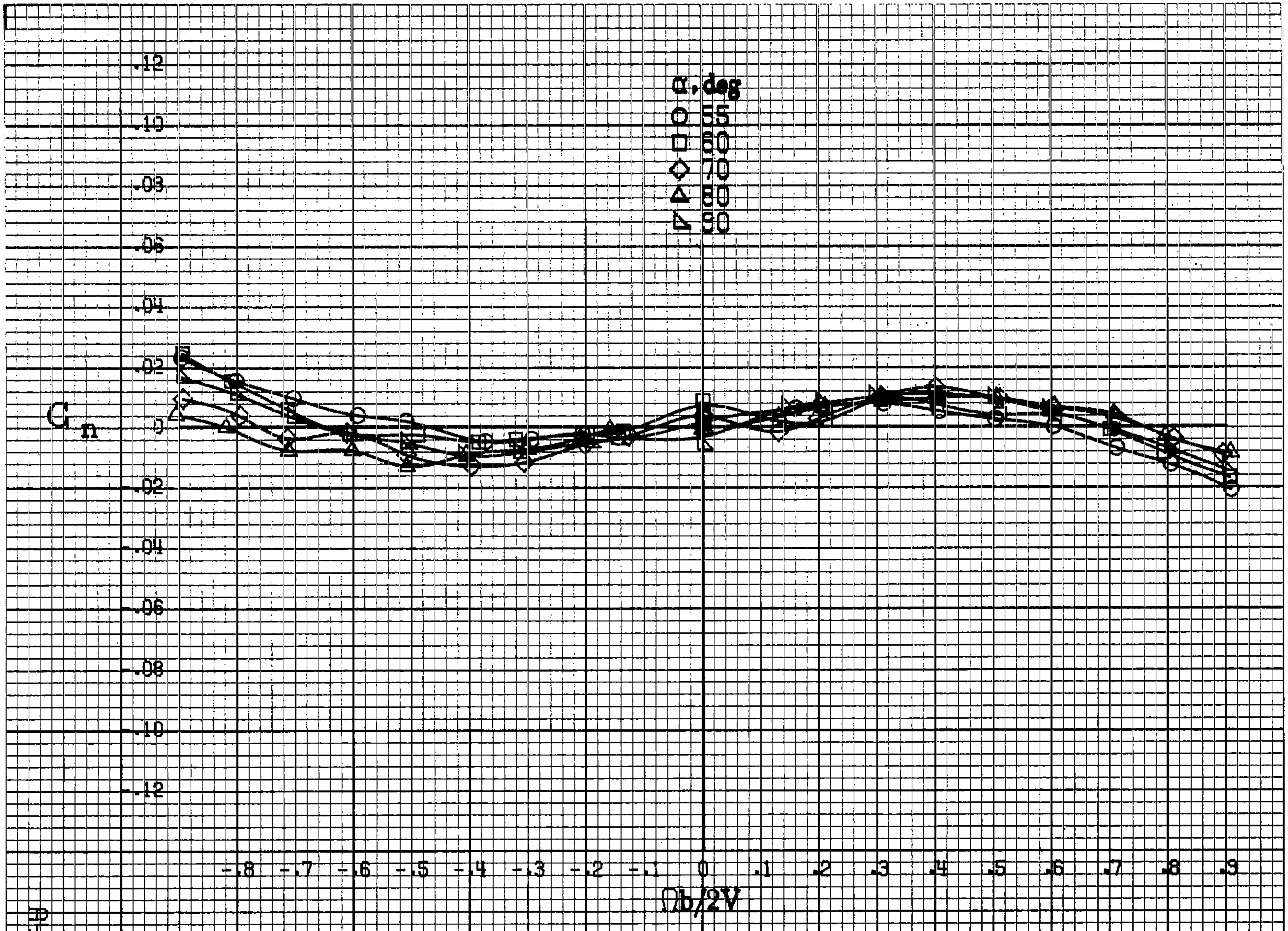

(d) α = 55 to 90 deg, SR = 0.

Figure A103. Concluded.

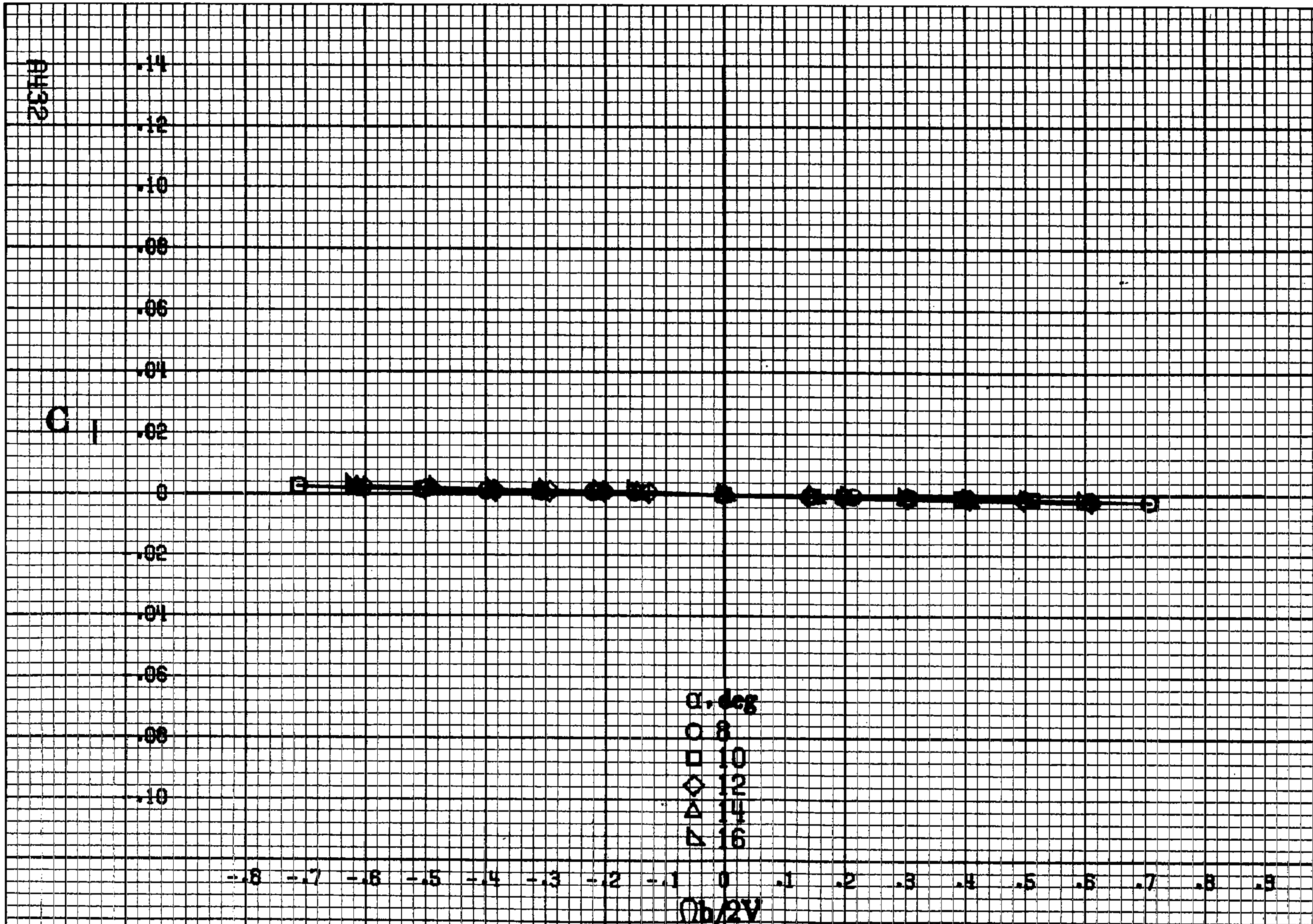

(a) α = 8 to 16 deg, SR = 182.9 cm (72 in).

Figure A104.- Effect of rotation rate and angle of attack on rolling-moment coefficient for body alone configuration. $\delta_e = 0°$, $\delta_a = 0°$, $\delta_r = 0°$, $\beta = 0°$.

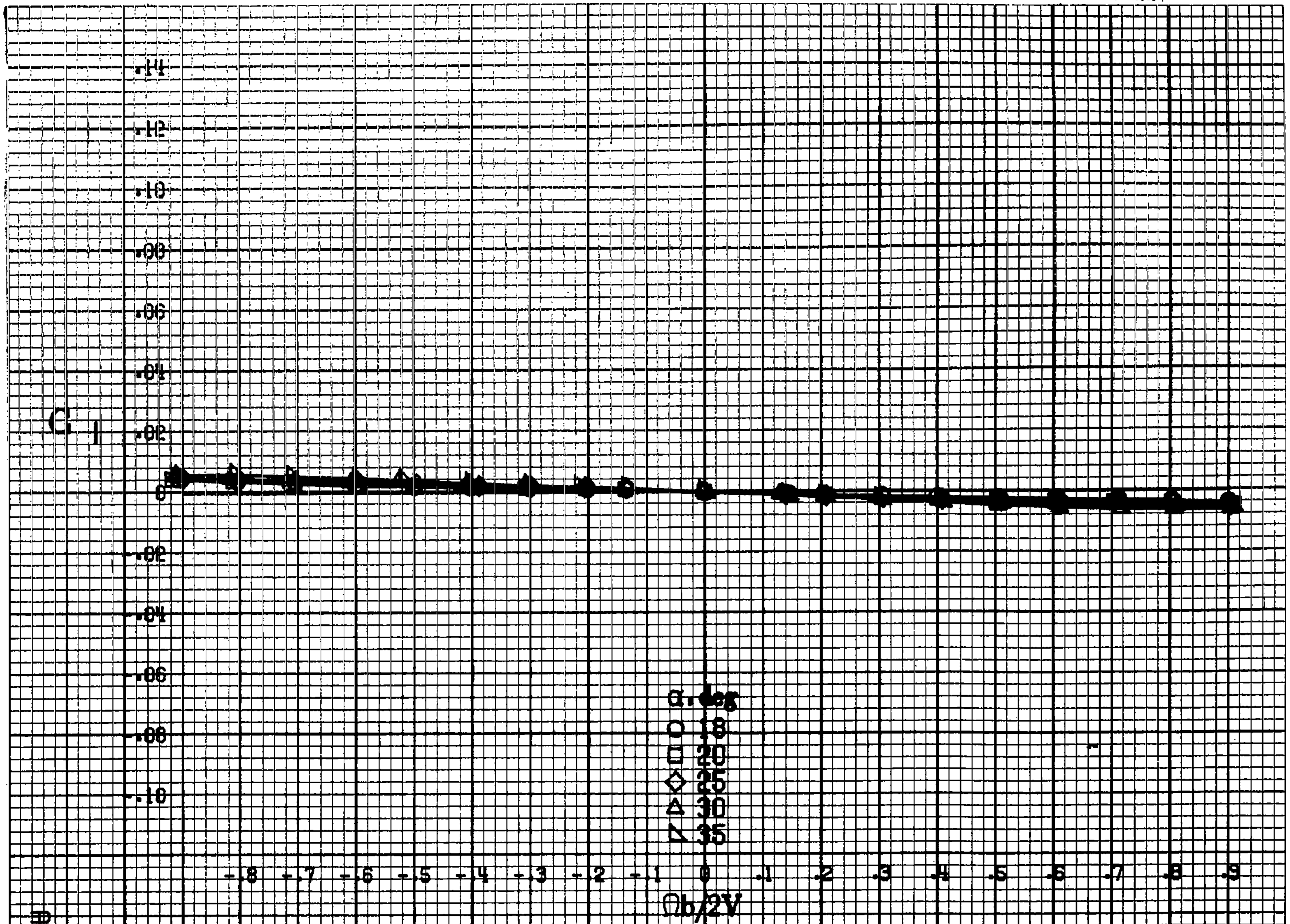

(b) α = 18 to 35 deg, SR = 182.9 cm (72 in).

Figure A104.-Continued.

A433

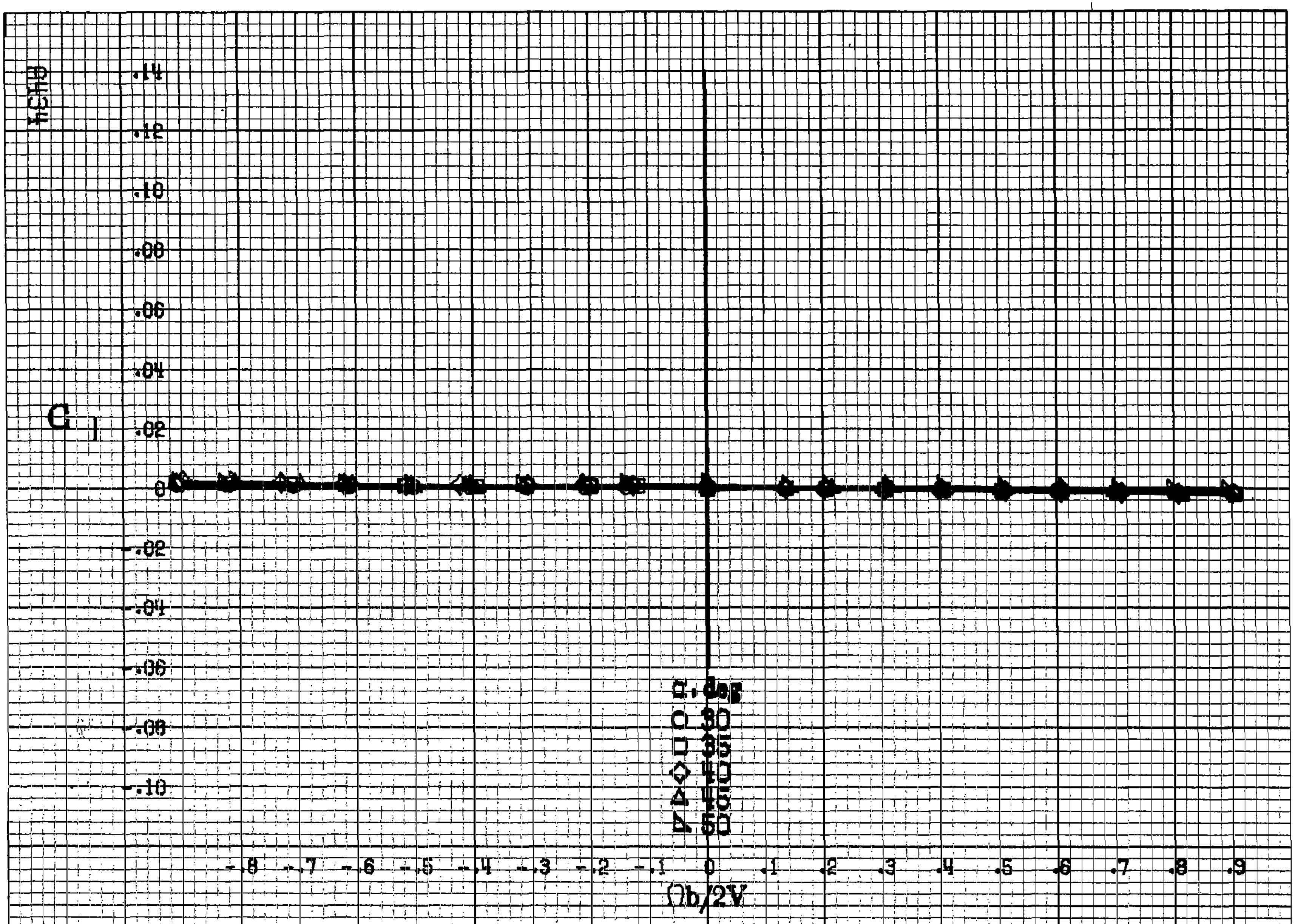

(c) α = 30 to 50 deg, SR = 0.

Figure A104. Continued.

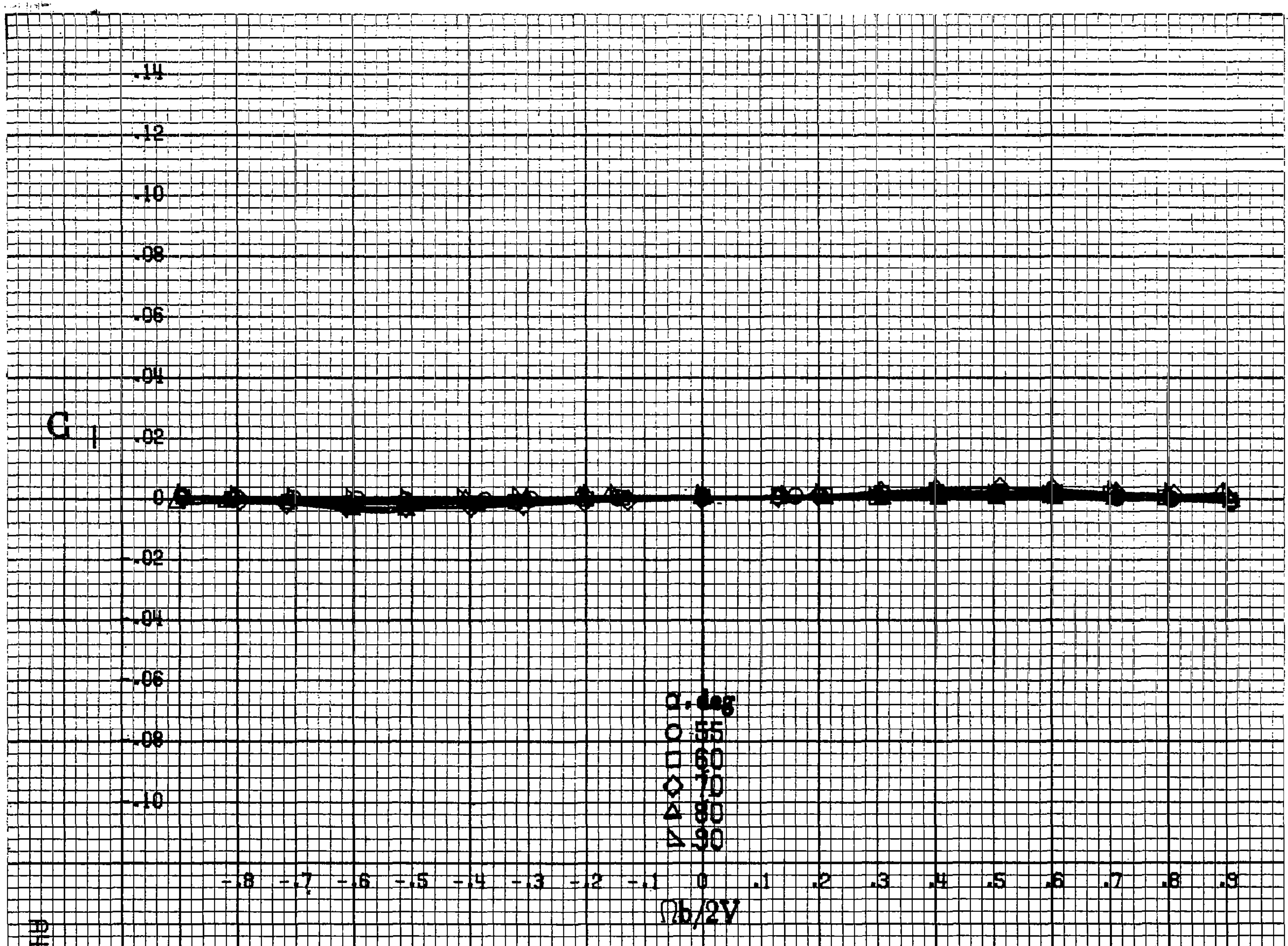

(d) α = 55 to 90 deg, SR = 0.

Figure A104.-Concluded.

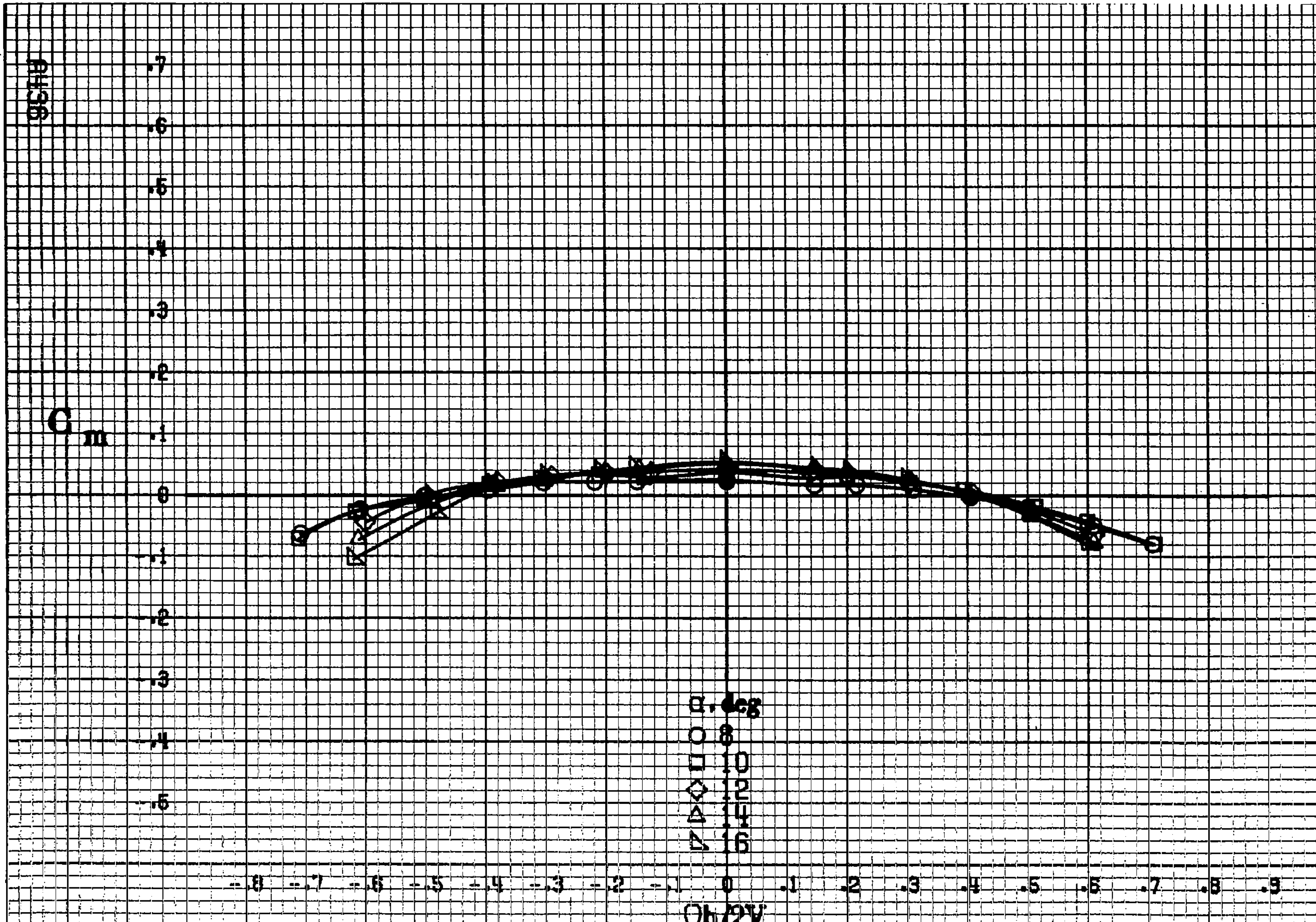

(a) α = 8 to 16 deg, SR = 182.9 cm (72 in).

Figure A105.-Effect of rotation rate and angle of attack on pitching-moment coefficient for body alone configuration. $\delta_e = 0°$, $\delta_a = 0°$, $\delta_r = 0°$, $\beta = 0°$.

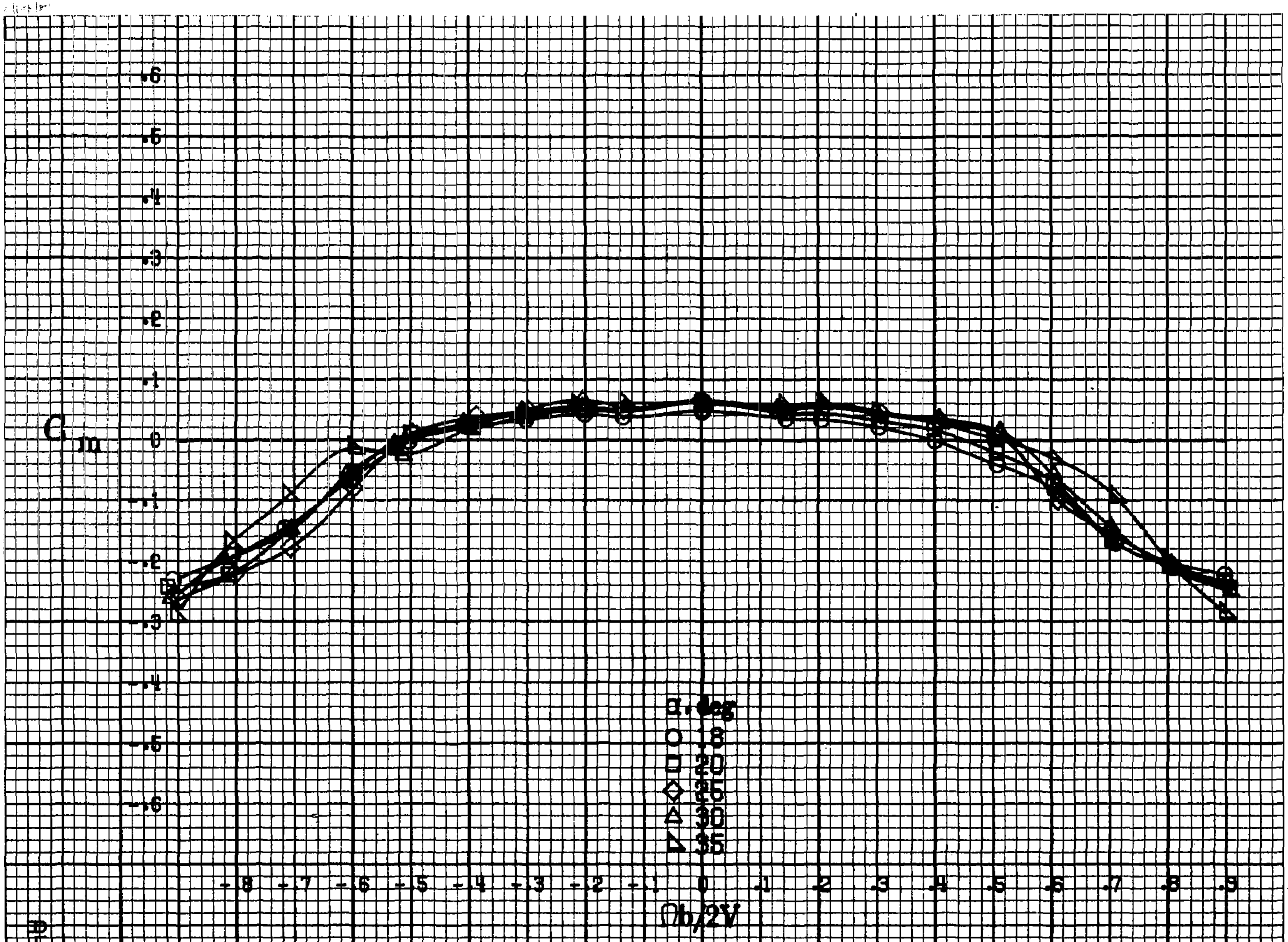

(b) α = 18 to 35 deg, SR = 182.9 cm (72 in).

Figure A105.-Continued.

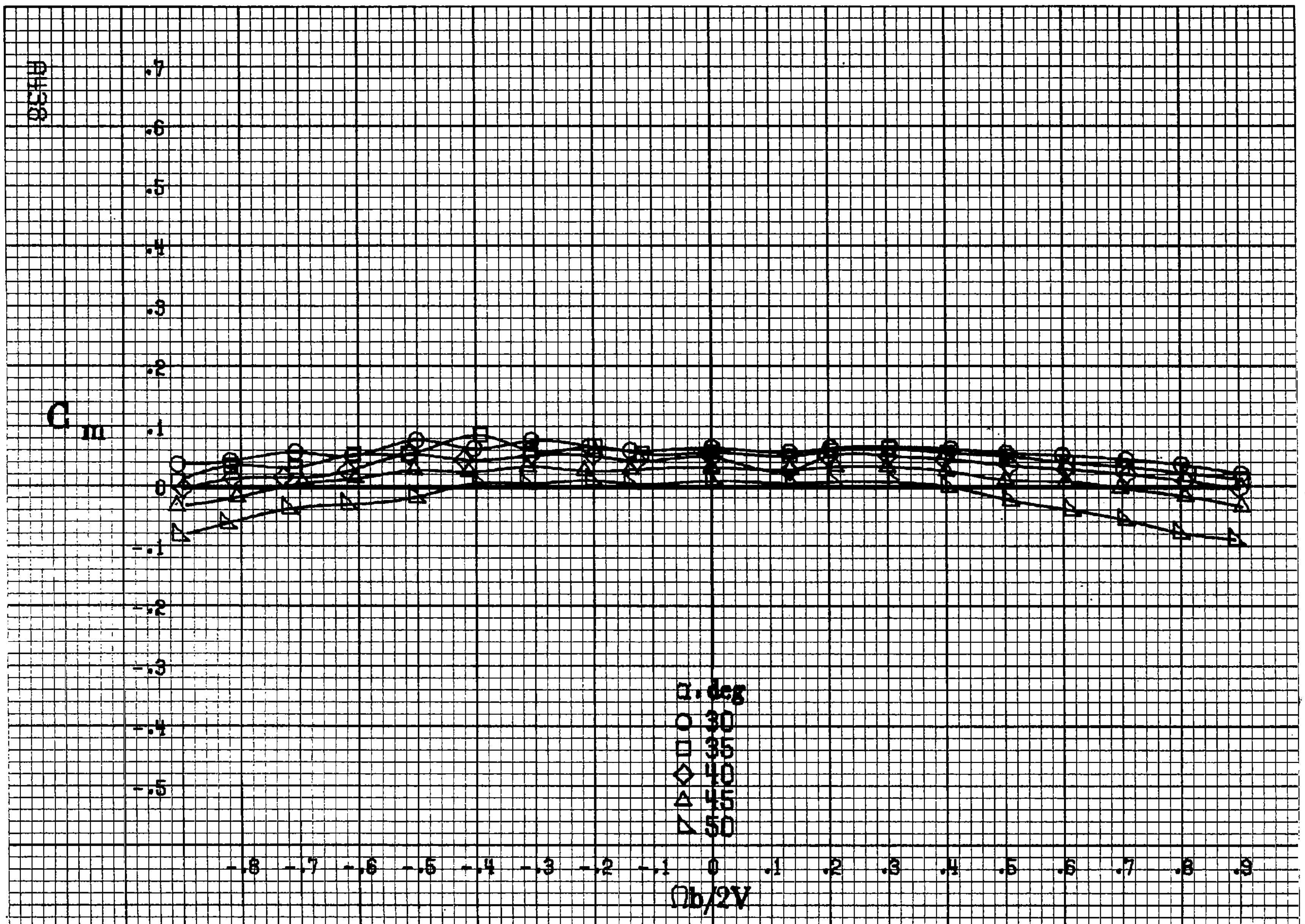

(c) α = 30 to 50 deg, SR = 0.

Figure A105.-Continued.

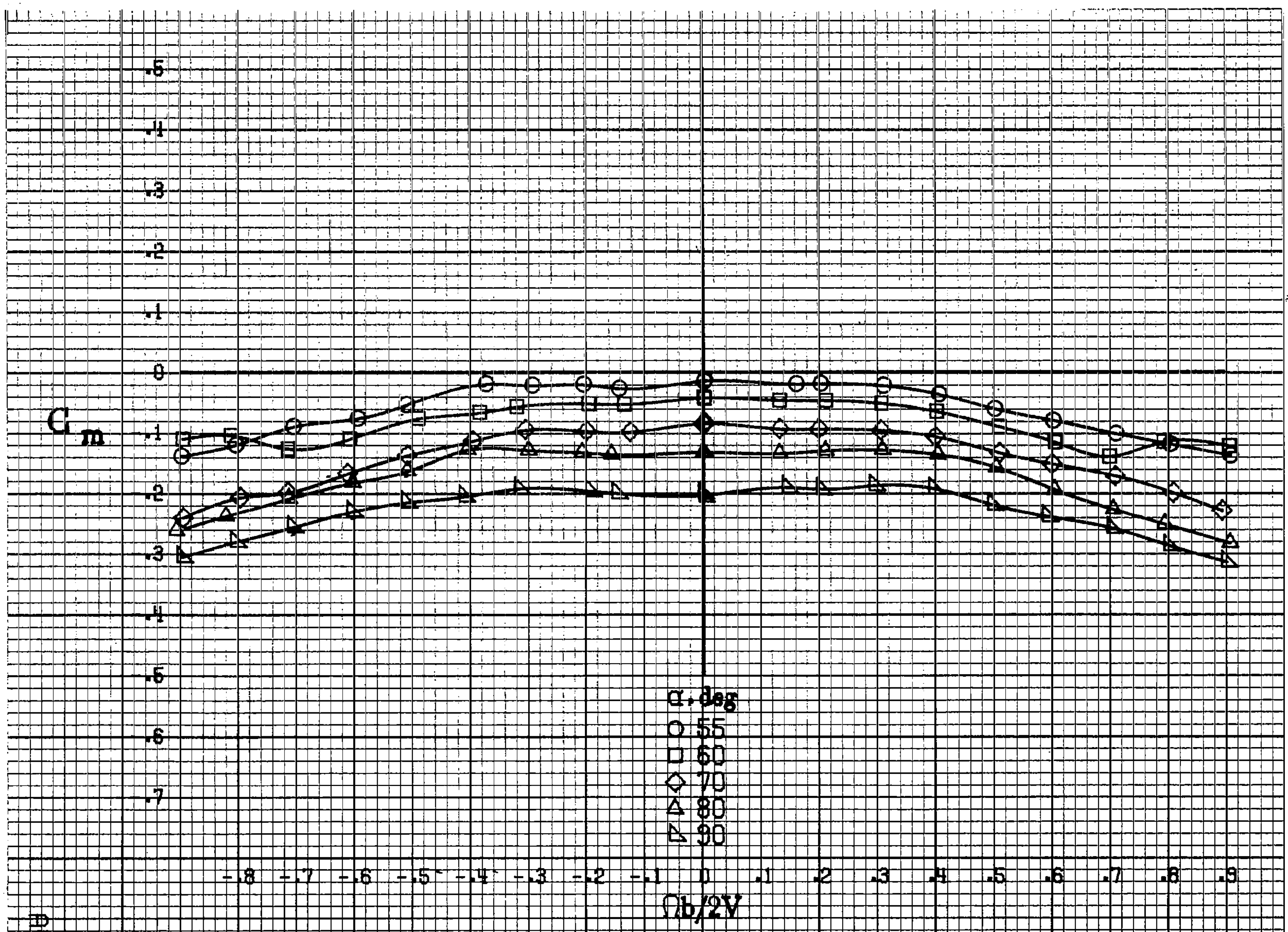

(d) α = 55 to 90 deg, SR = 0.

Figure A105.-Concluded.

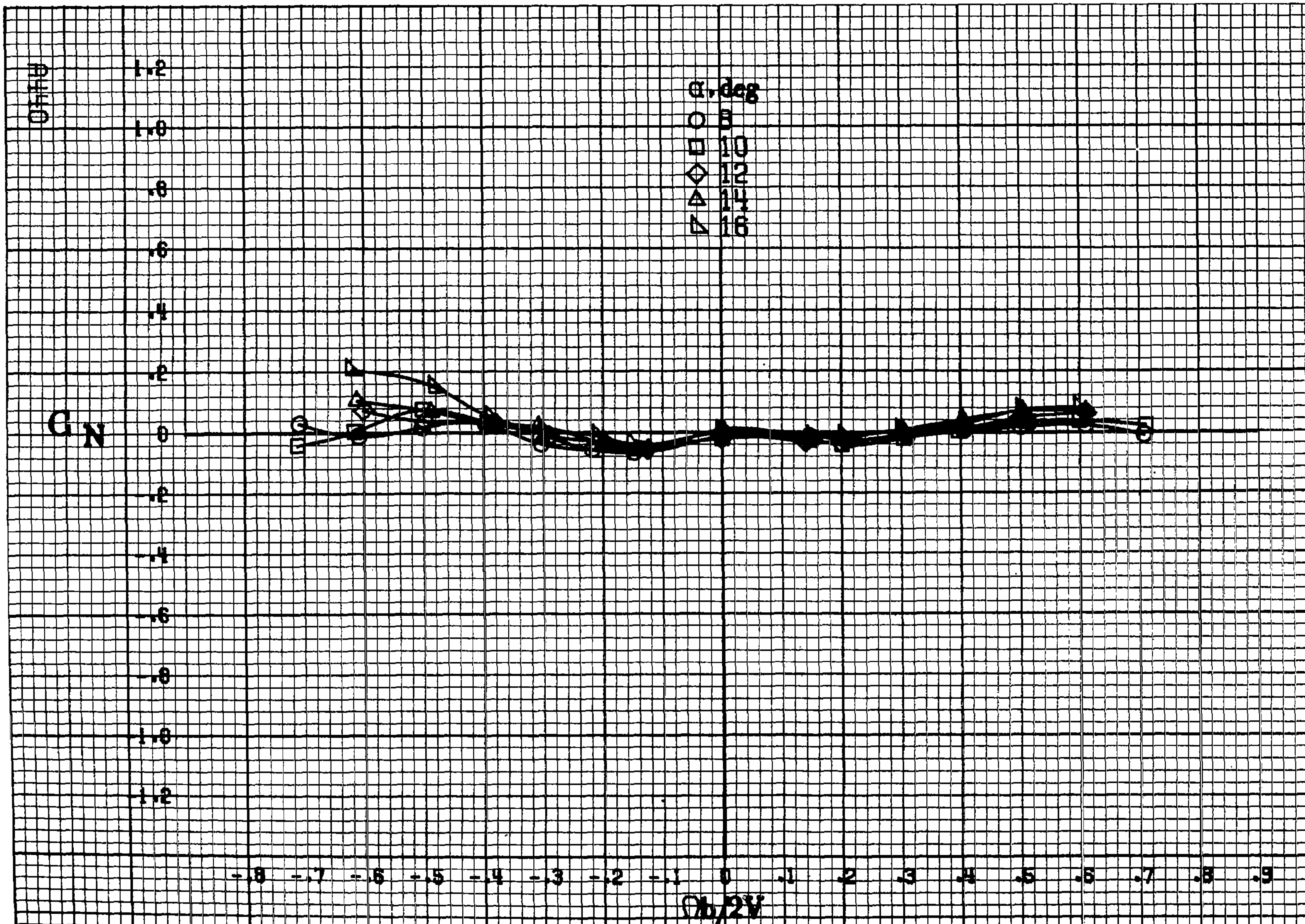

(a) $\alpha = 8$ to 16 deg, SR = 182.9 cm (72 in).

Figure A106.- Effect of rotation rate and angle of attack on normal-force coefficient for body alone configuration. $\delta_e = 0°$, $\delta_a = 0°$, $\delta_r = 0°$, $\beta = 0°$.

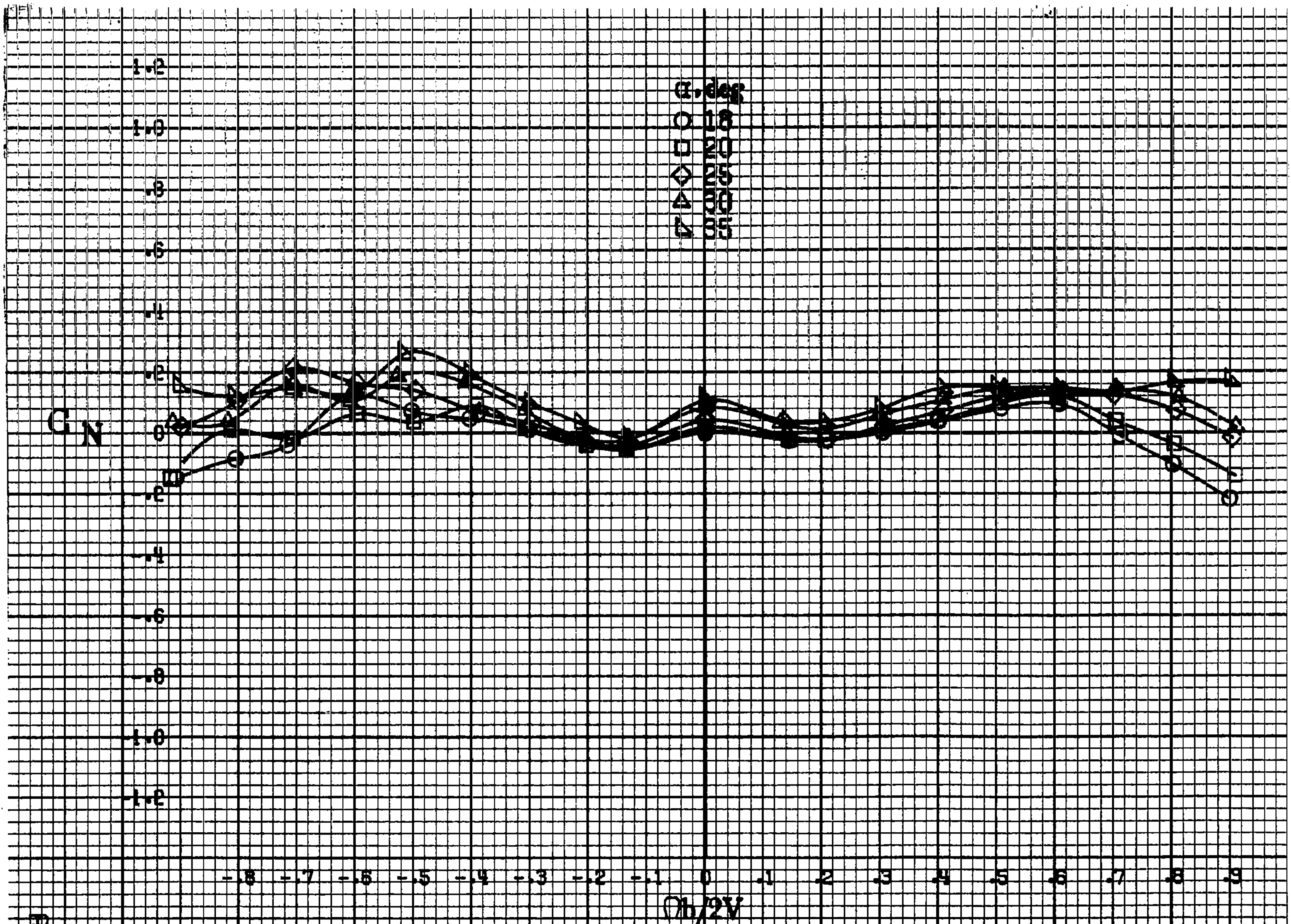

(b) α = 18 to 35 deg, SR = 182.9 cm (72 in).
Figure A106.-Continued.

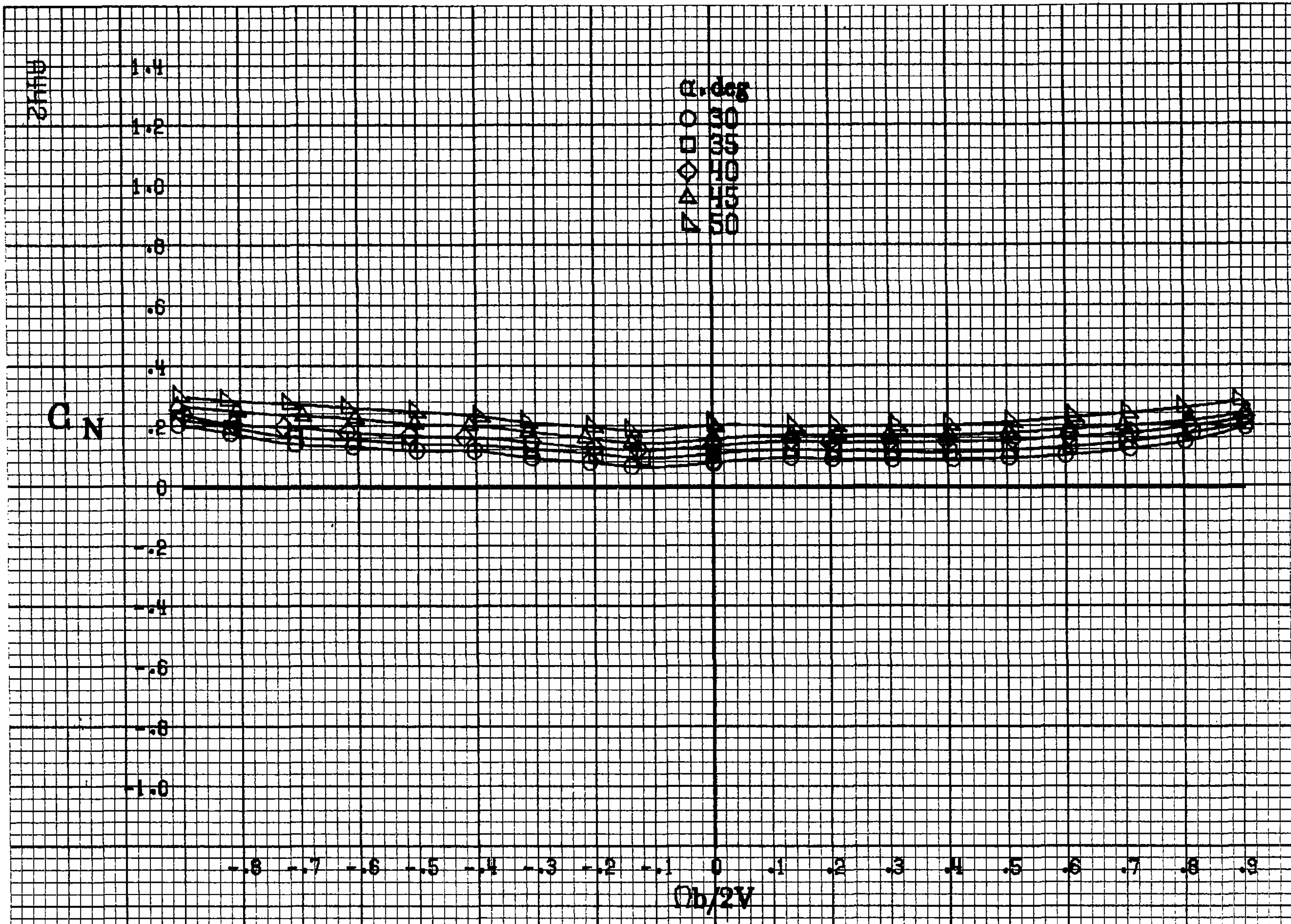

(c) α = 30 to 50 deg, SR = 0.

Figure A106.-Continued.

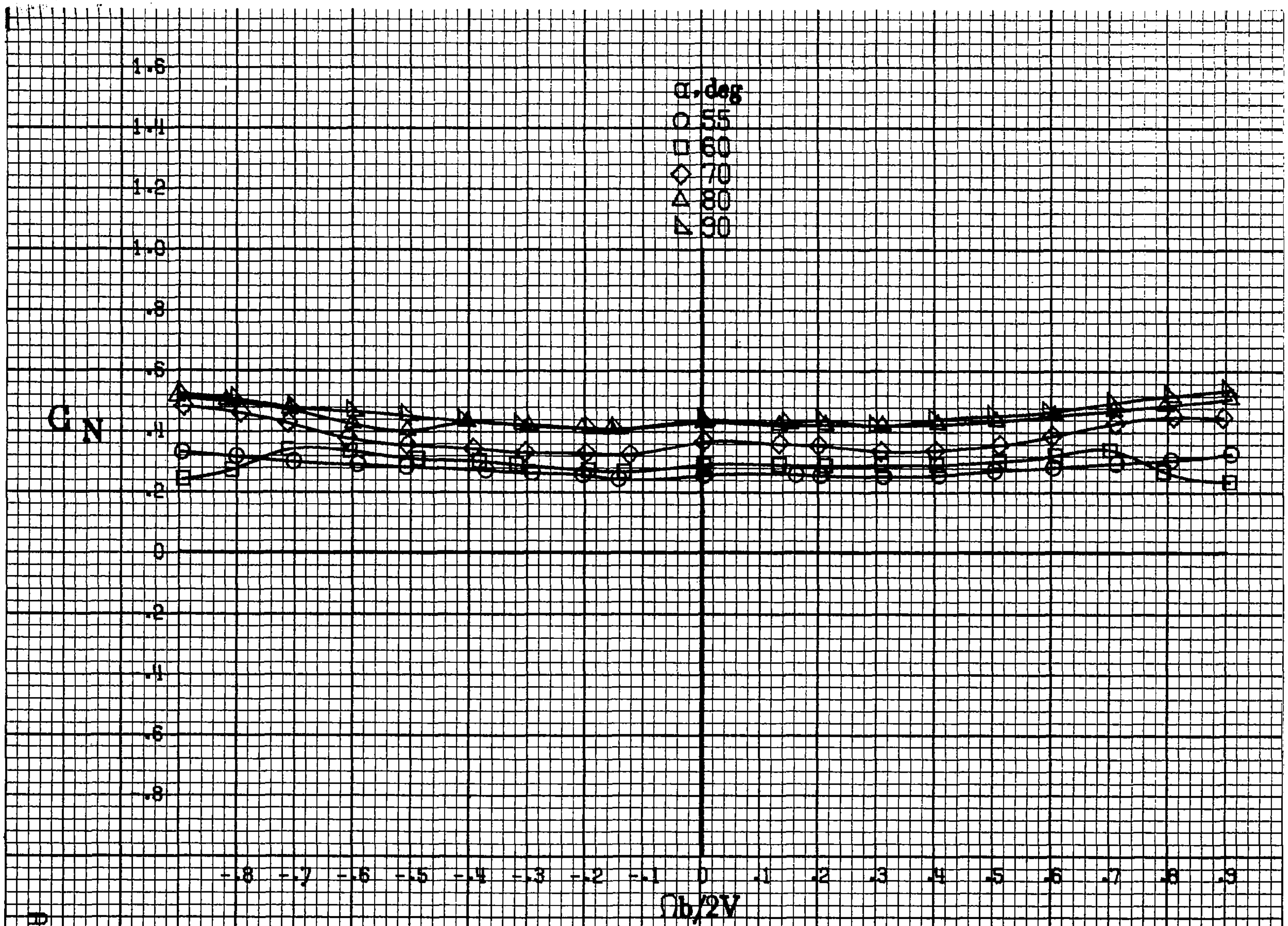

(d) α = 55 to 90 deg, SR = 0.
Figure A106. Concluded.

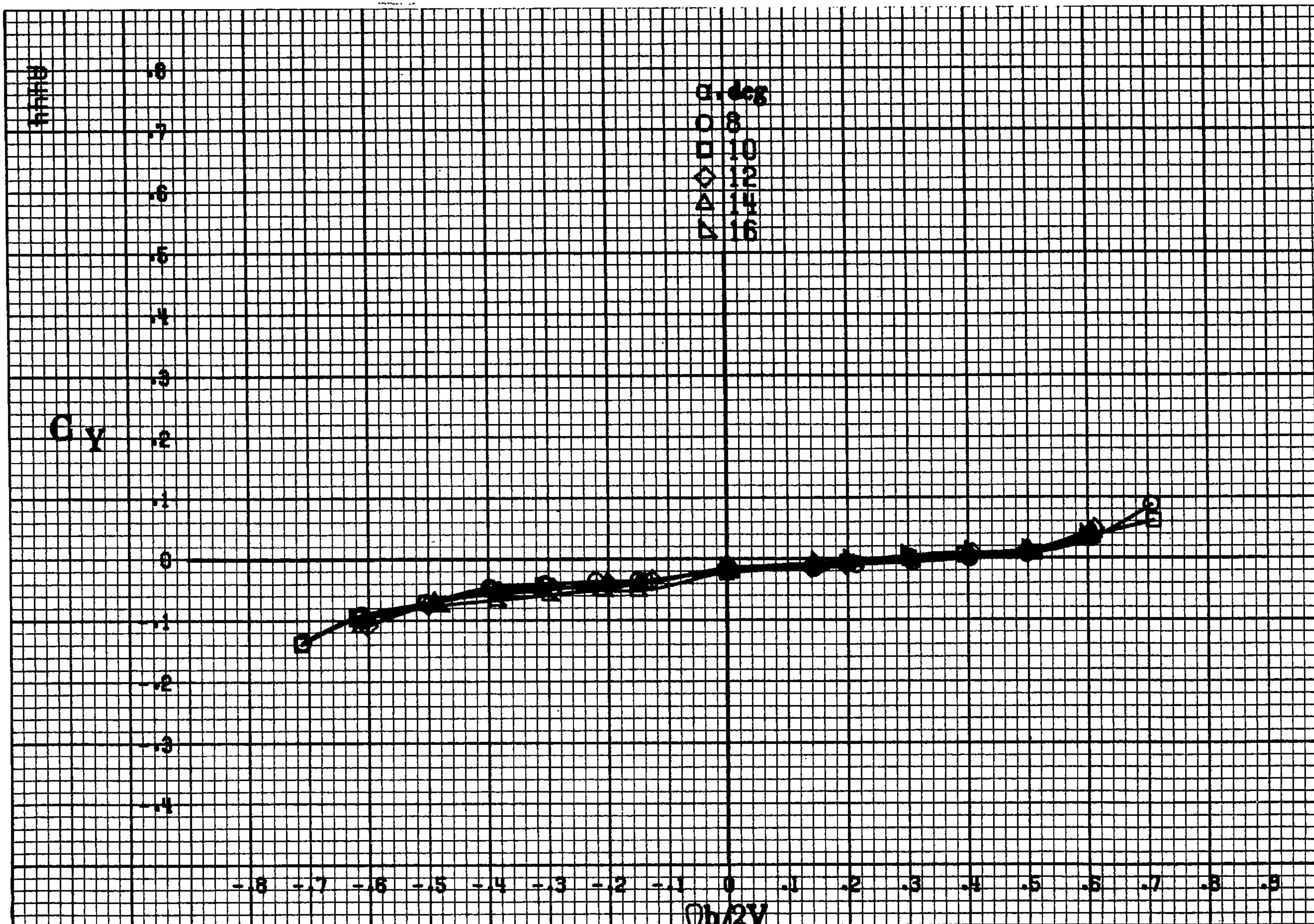

(a) $\alpha = 8$ to 16 deg, SR = 182.9 cm (72 in).

Figure A107.- Effect of rotation rate and angle of attack on side-force coefficient for body alone configuration. $\delta_e = 0°$, $\delta_a = 0°$, $\delta_r = 0°$, $\beta = 0°$.

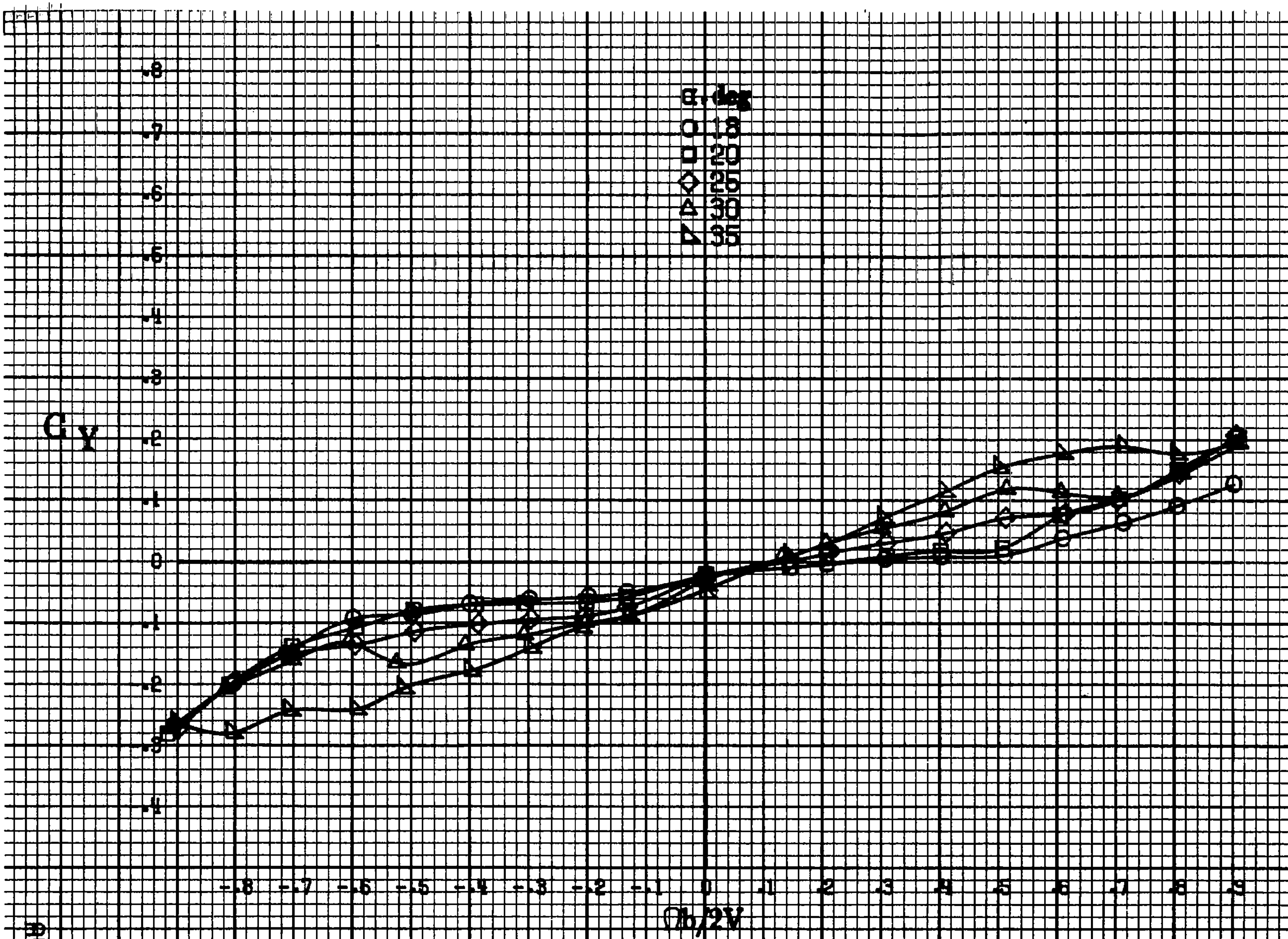

(b) α = 18 to 35 deg, SR = 182.9 cm (72 in).

Figure A107. Continued.

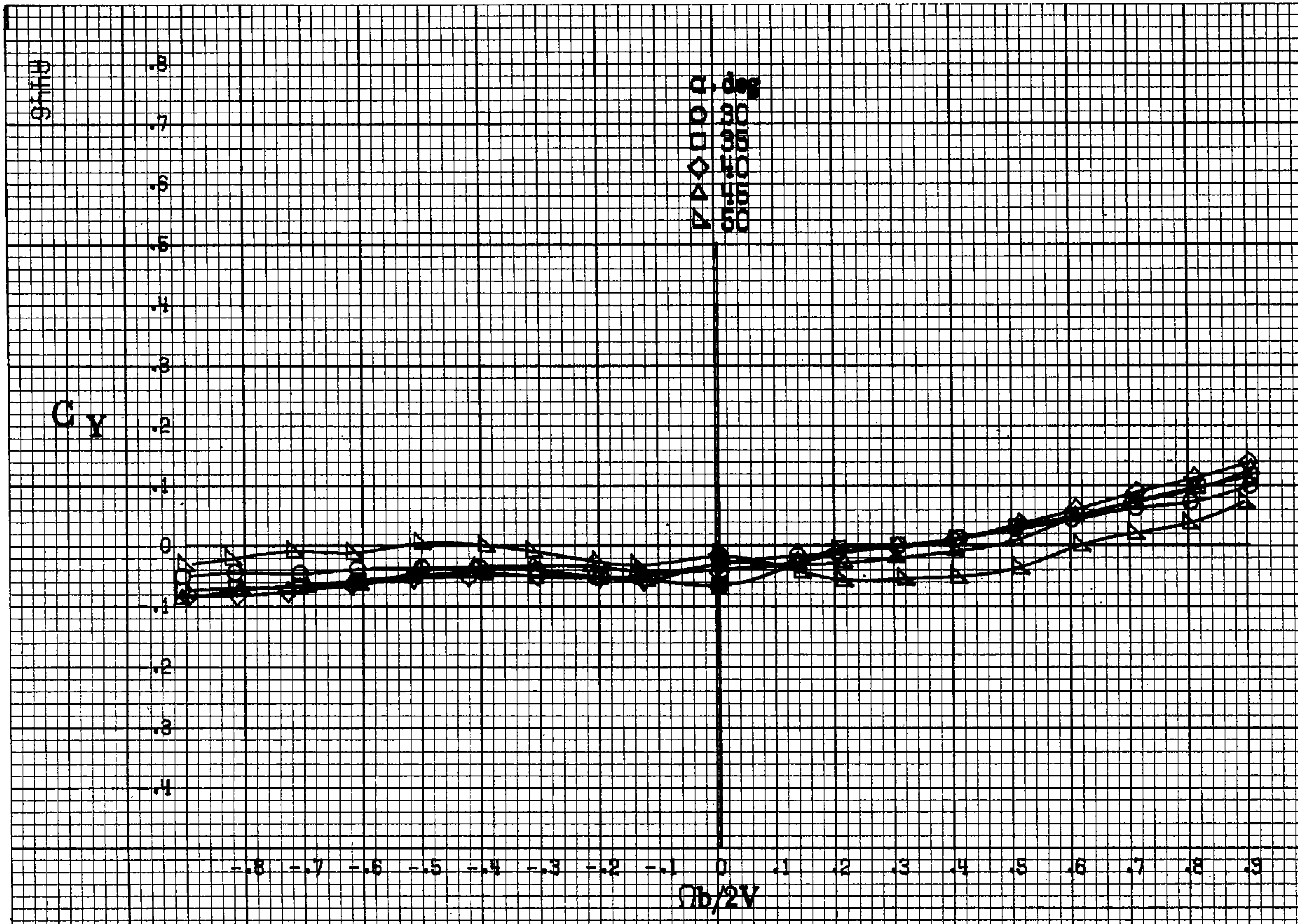

(c) α = 30 to 50 deg, SR = 0.

Figure A107. Continued.

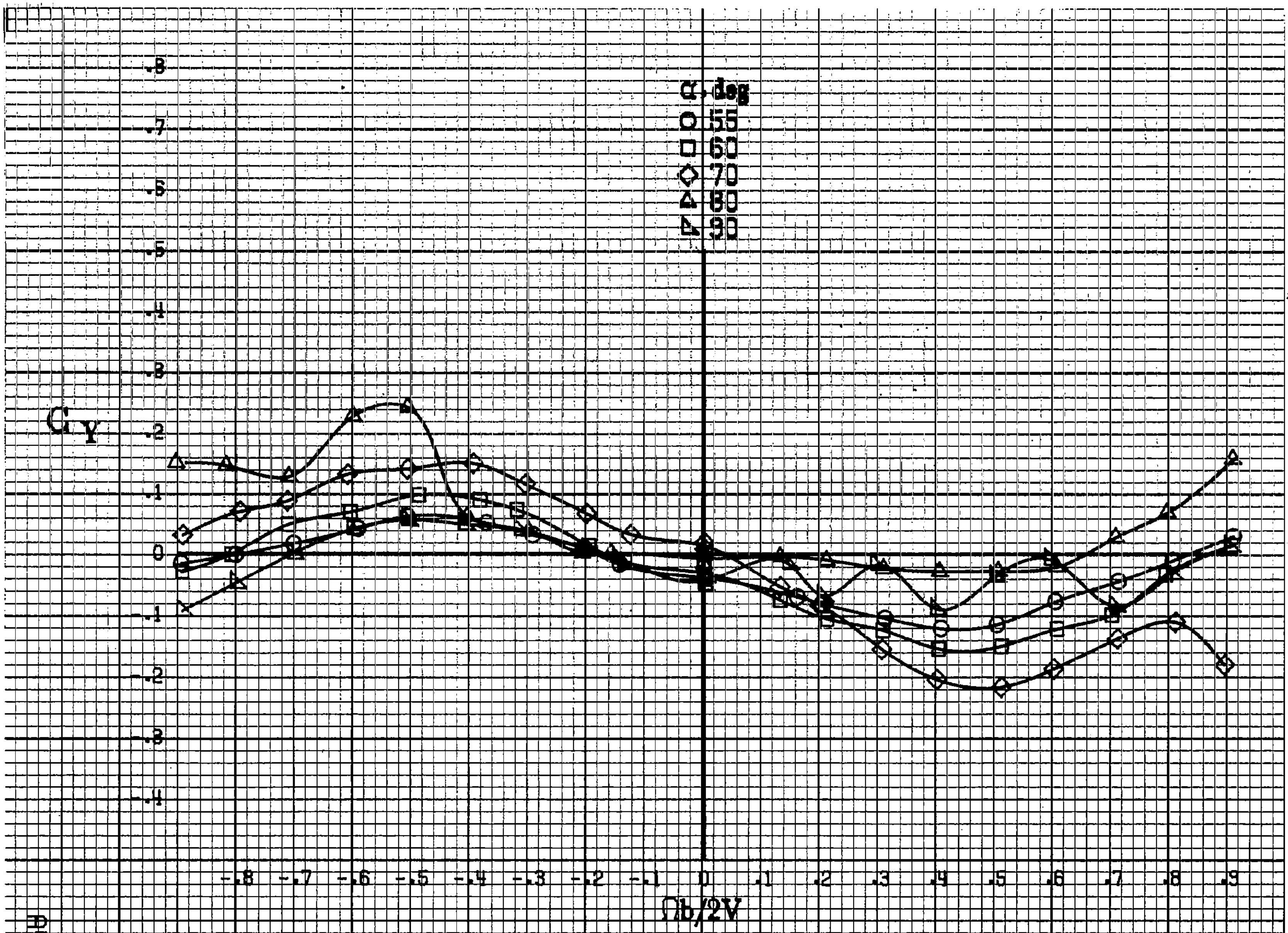

(d) α = 55to90deg, SR = 0.

Figure A107.-Concluded.

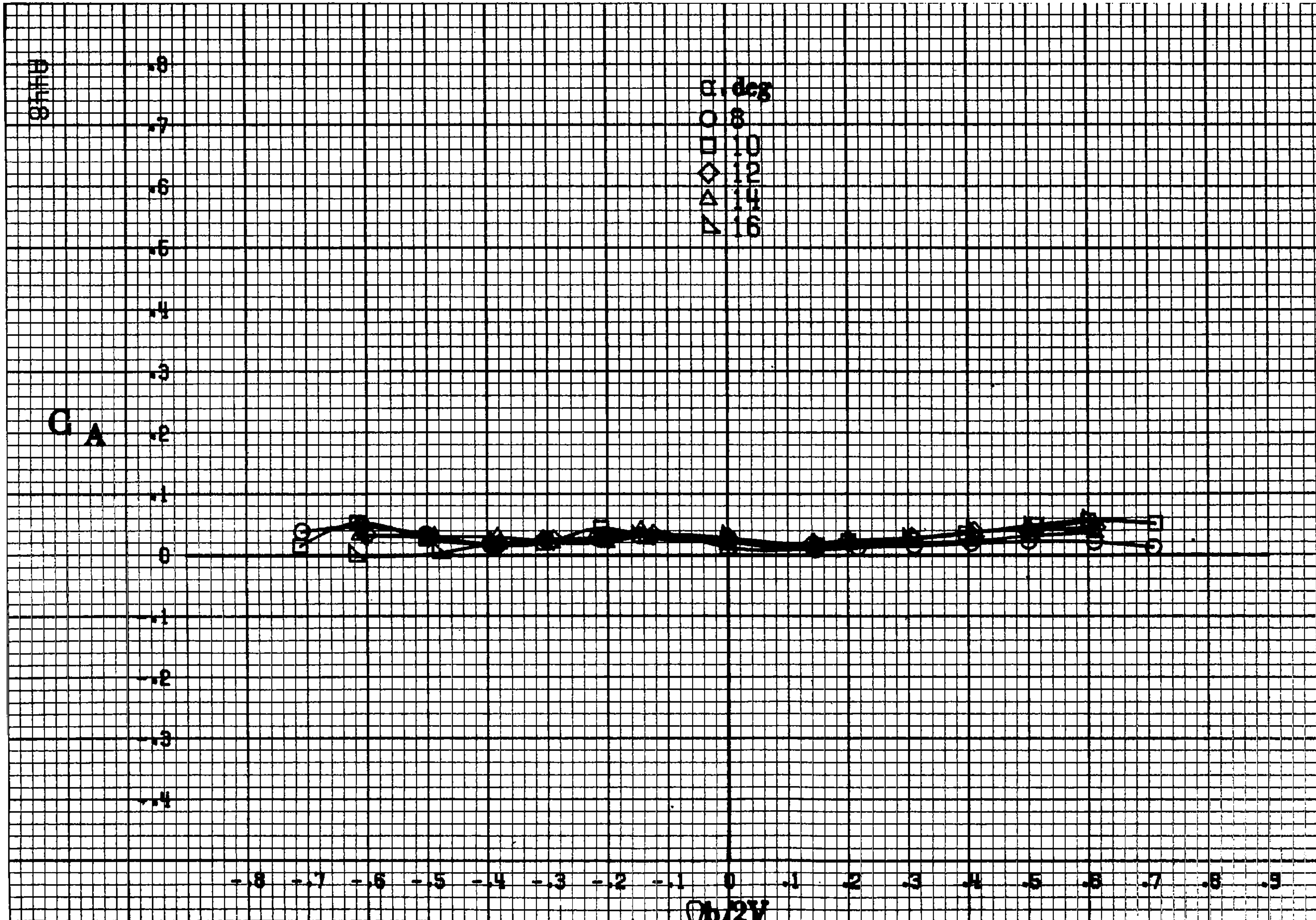

(a) α = 8 to 16 deg, SR = 182.9 cm (72 in).

Figure A108.-Effect of rotation rate and angle of attack on axial-force coefficient for body alone configuration. $\delta_e = 0°$, $\delta_a = 0°$, $\delta_r = 0°$, $\beta = 0°$.

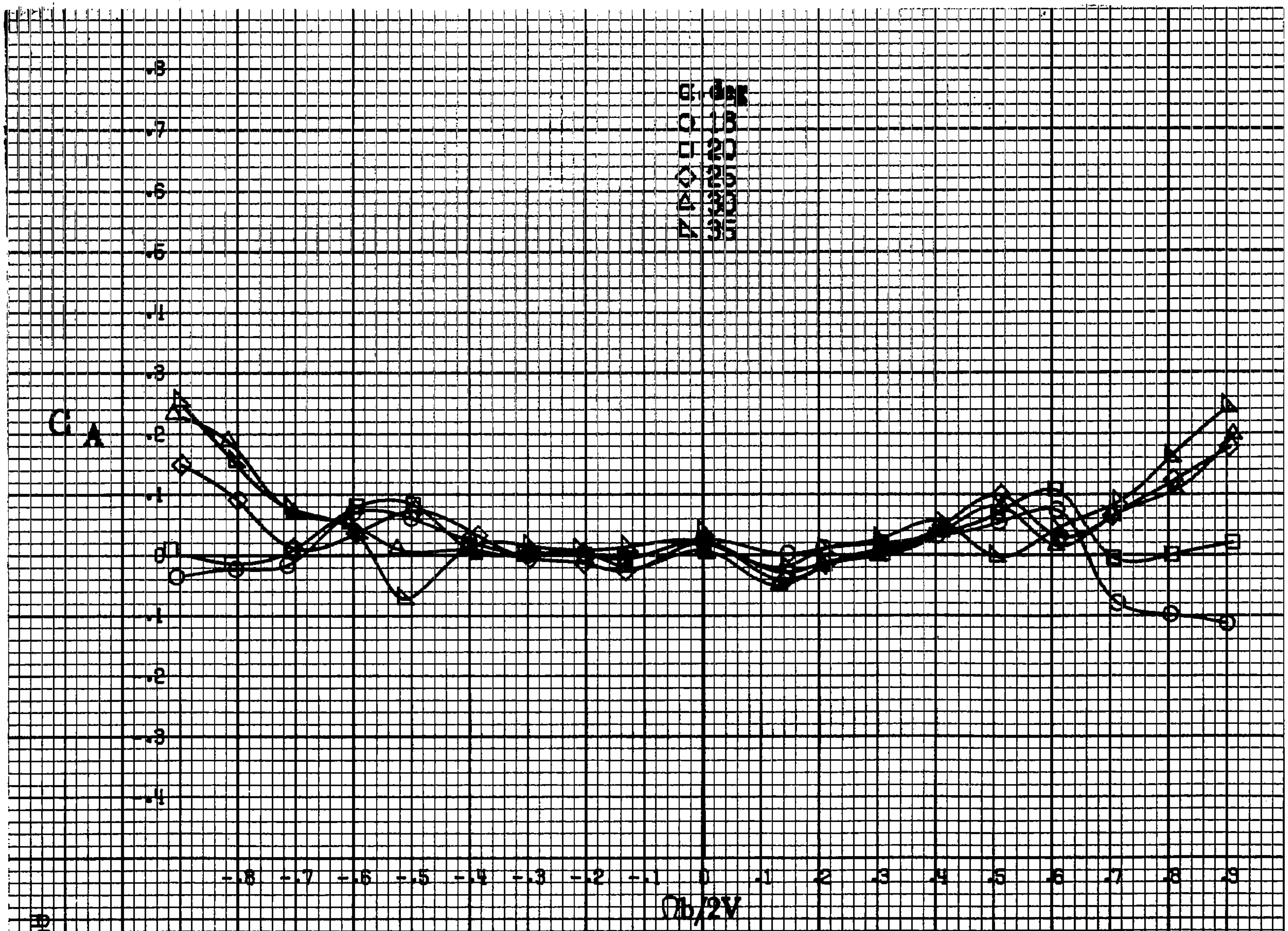

(b) α = 15 to 35 deg, SR = 182.9 cm (72 in).

Figure A108.-Continued.

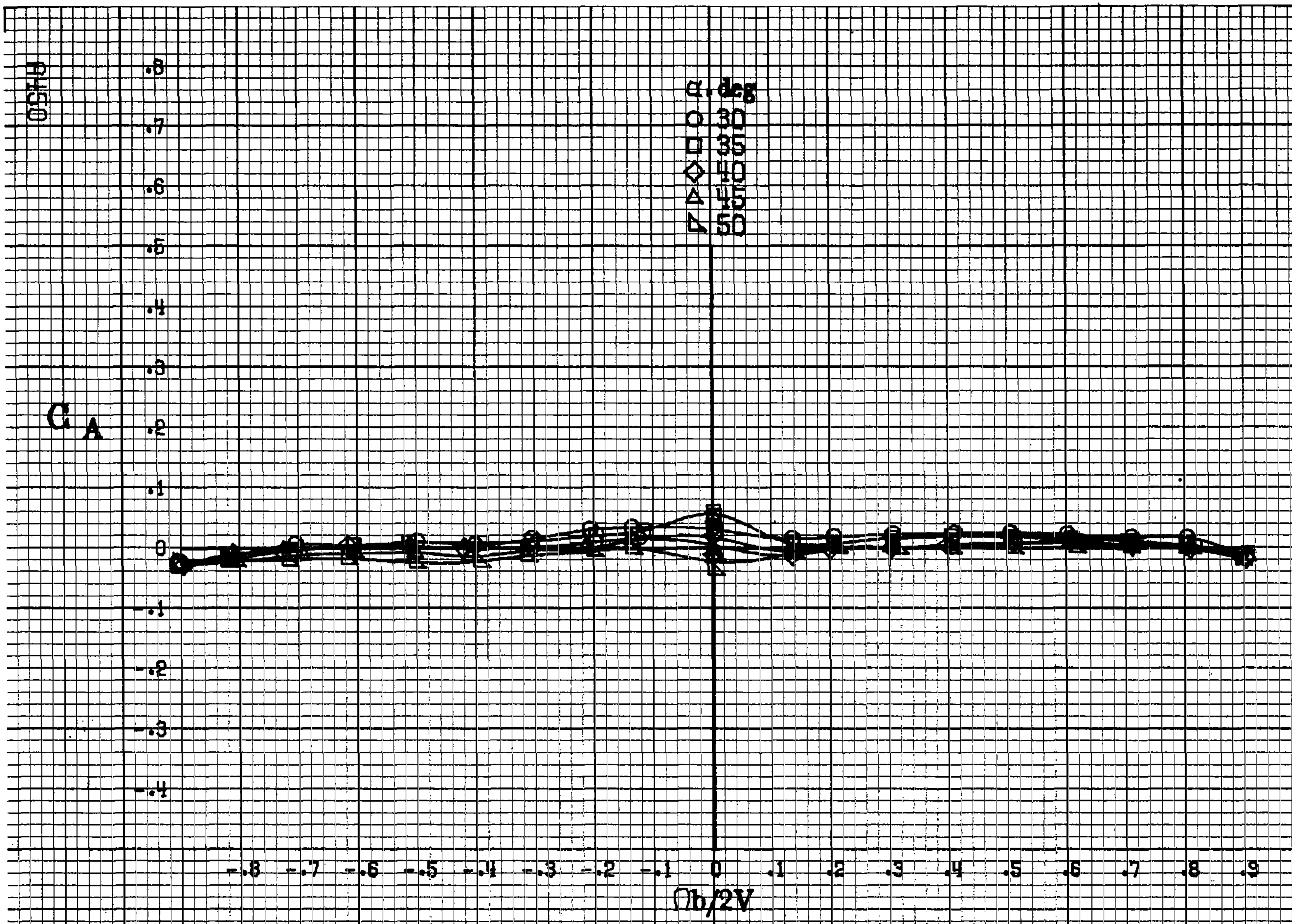

(c) α = 30 to 50 deg, δR = 0.

Figure A108.-Continued.

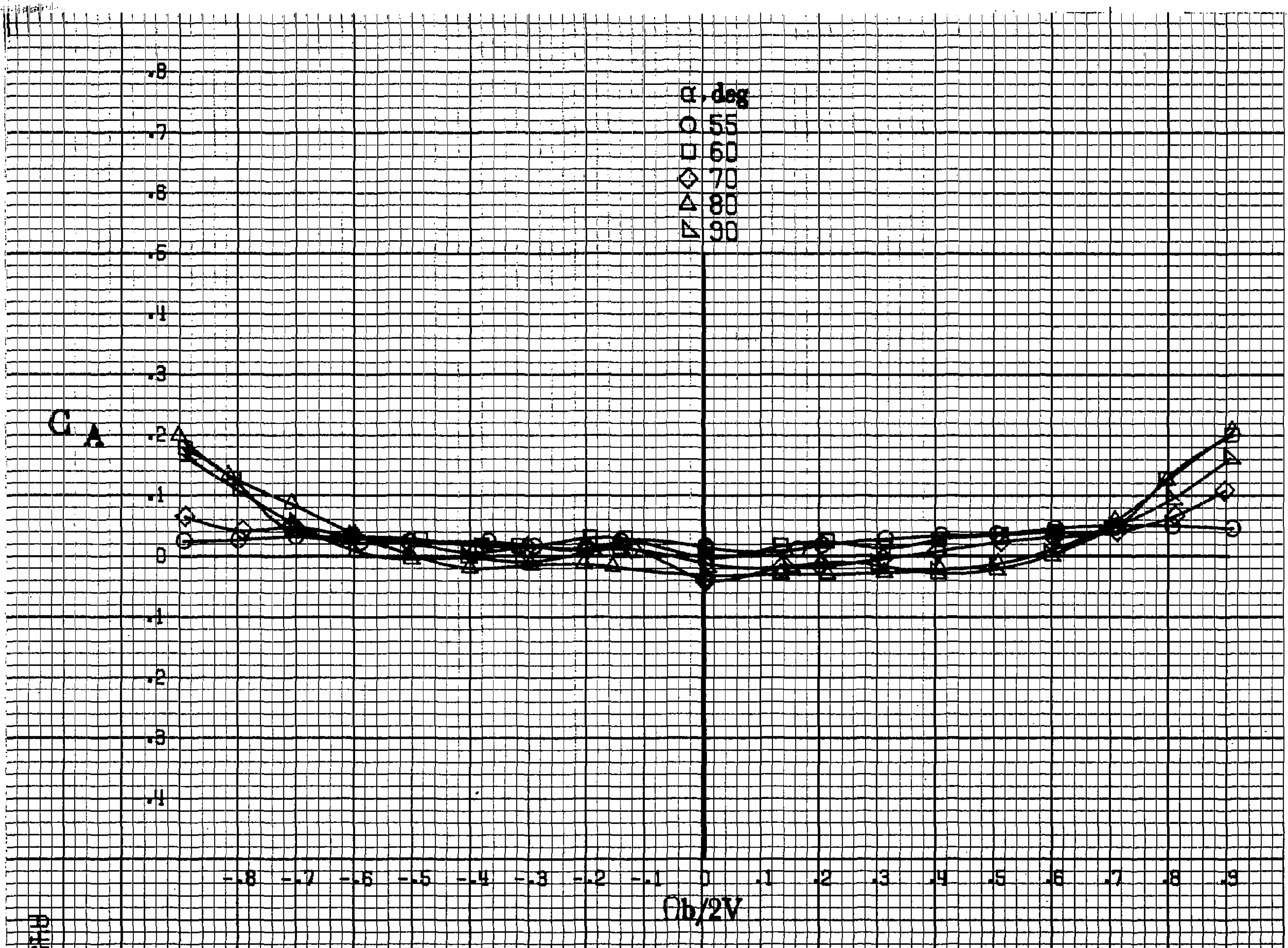

(d) α = 55 to 90 deg, SR = 0.
Figure A108.-Concluded.

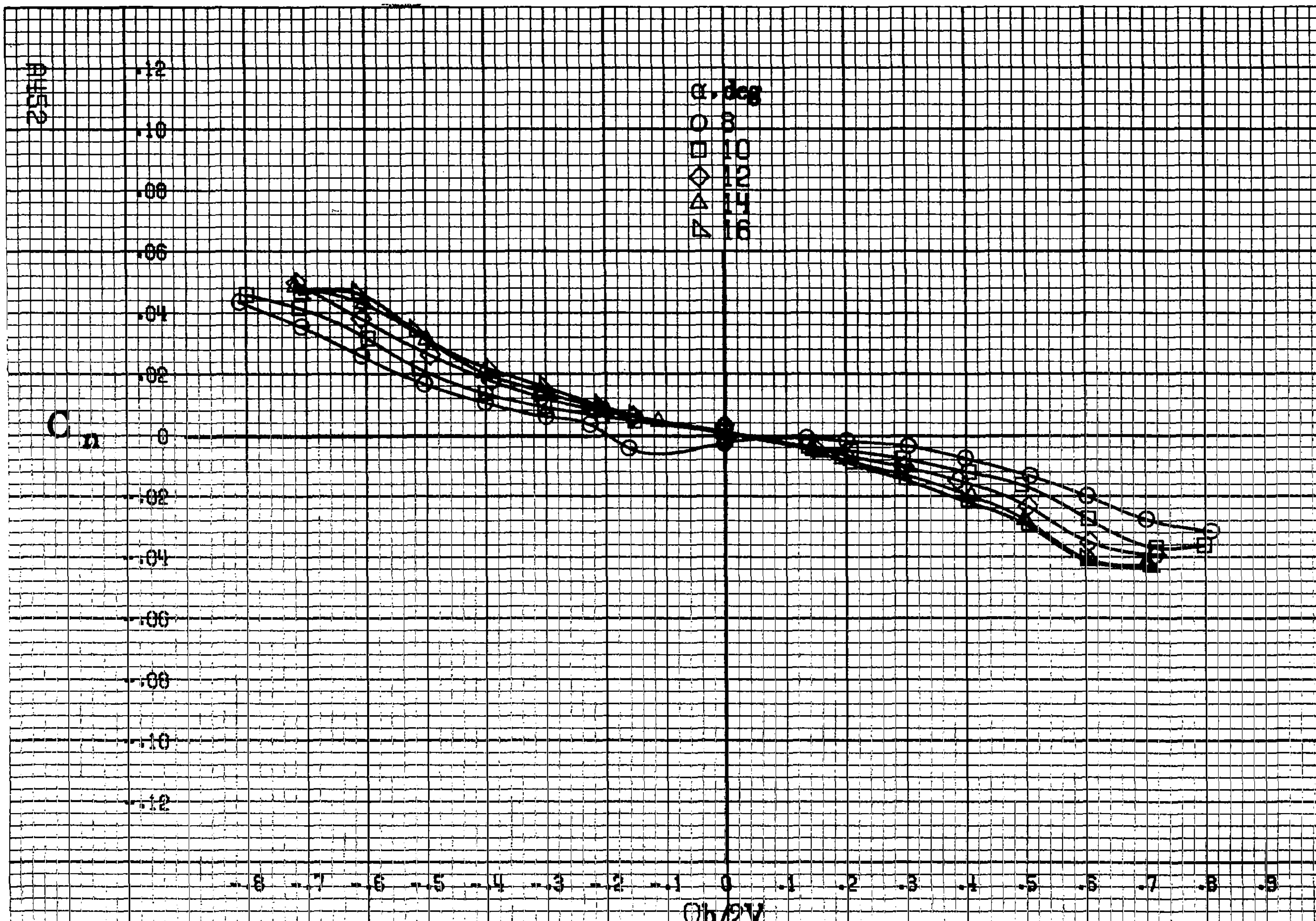

(a) $\alpha = 8$ to 16 deg, SR = 182.9 cm (72 in).

Figure A109.-Effect of rotation rate and angle of attack on yawing-moment coefficient for wing off configuration. $\delta_e = 0°$, $\delta_a = 0°$, $\delta_r = 0°$. $\beta = 0°$.

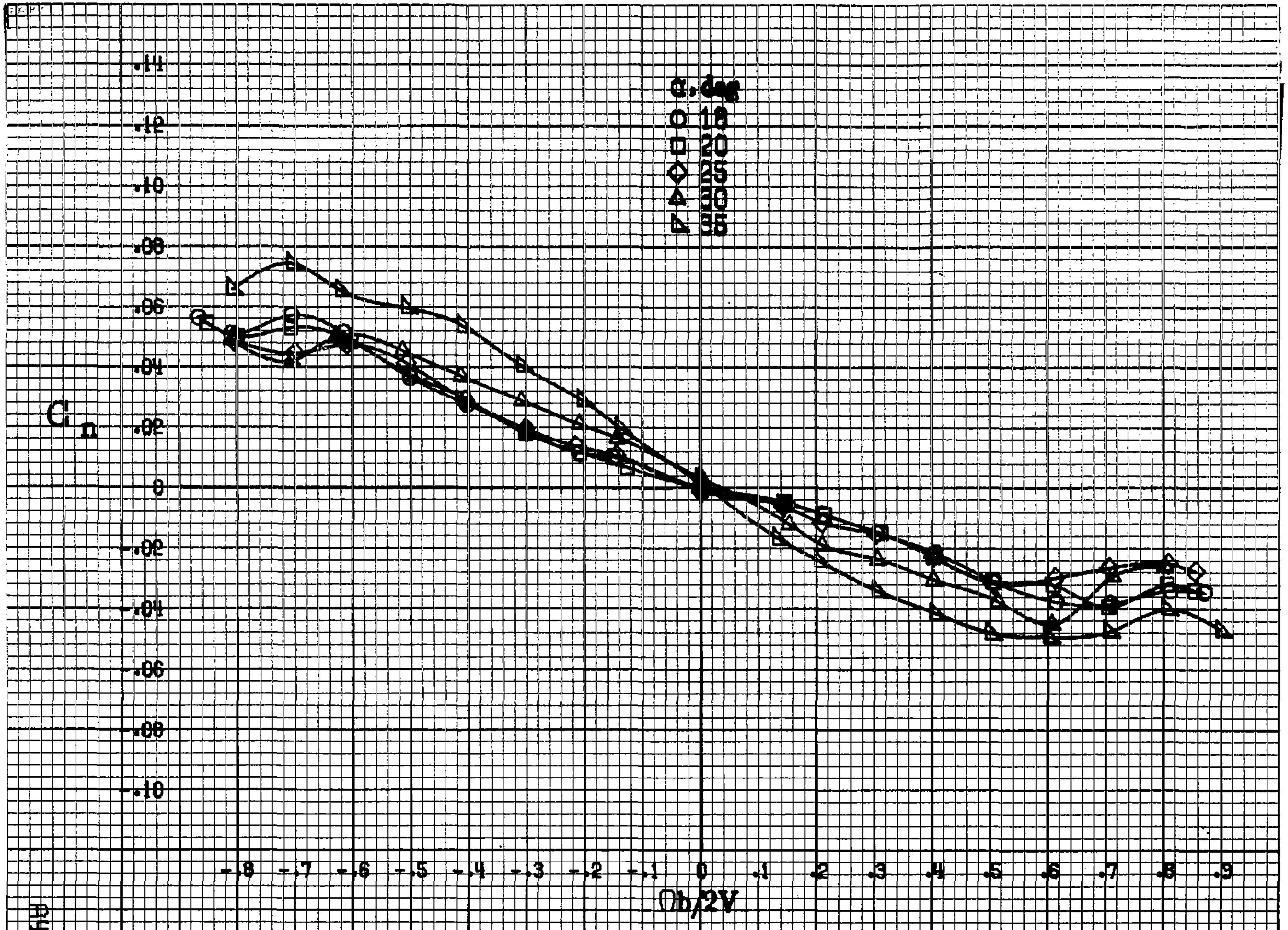

(b) α = 18 to 35 deg, SR = 182.9 cm (72 in).

Figure A109.-Continued.

A453

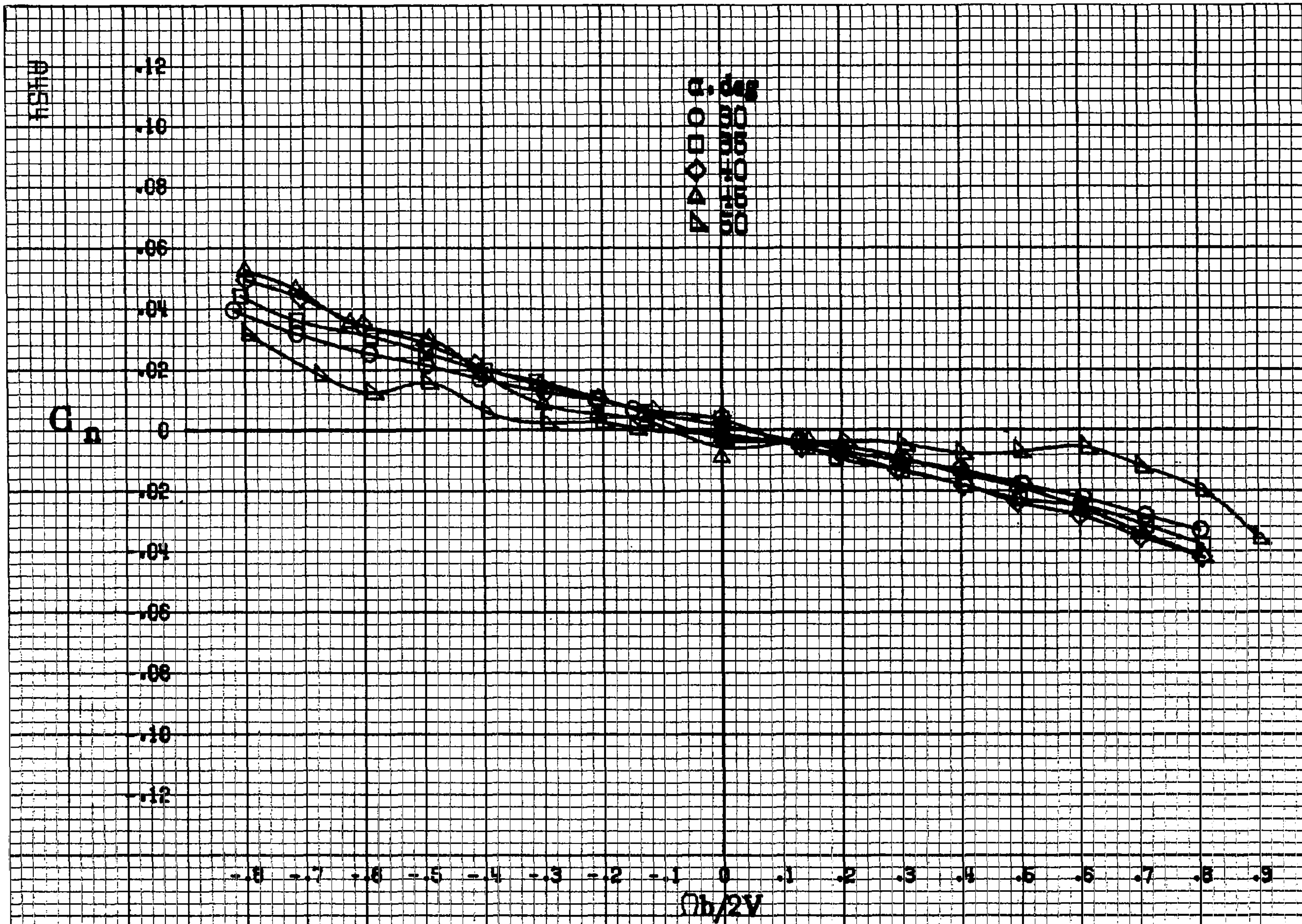

(c) α = 30 to 50 deg, δ_R = 0.

Figure A109.-Continued.

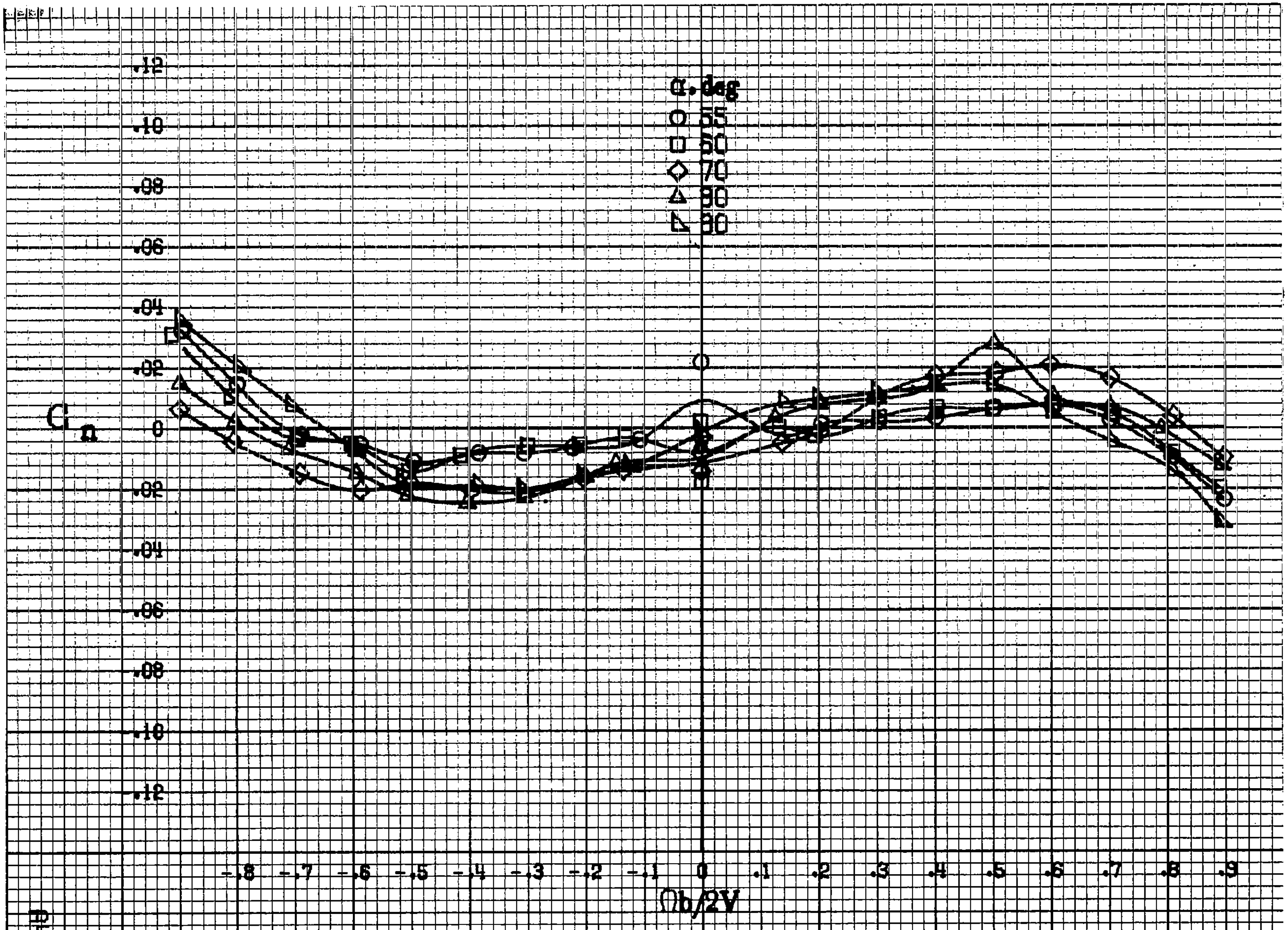

(d) α = 55 to 90 deg, SR = 0.
Figure A109.-Concluded.

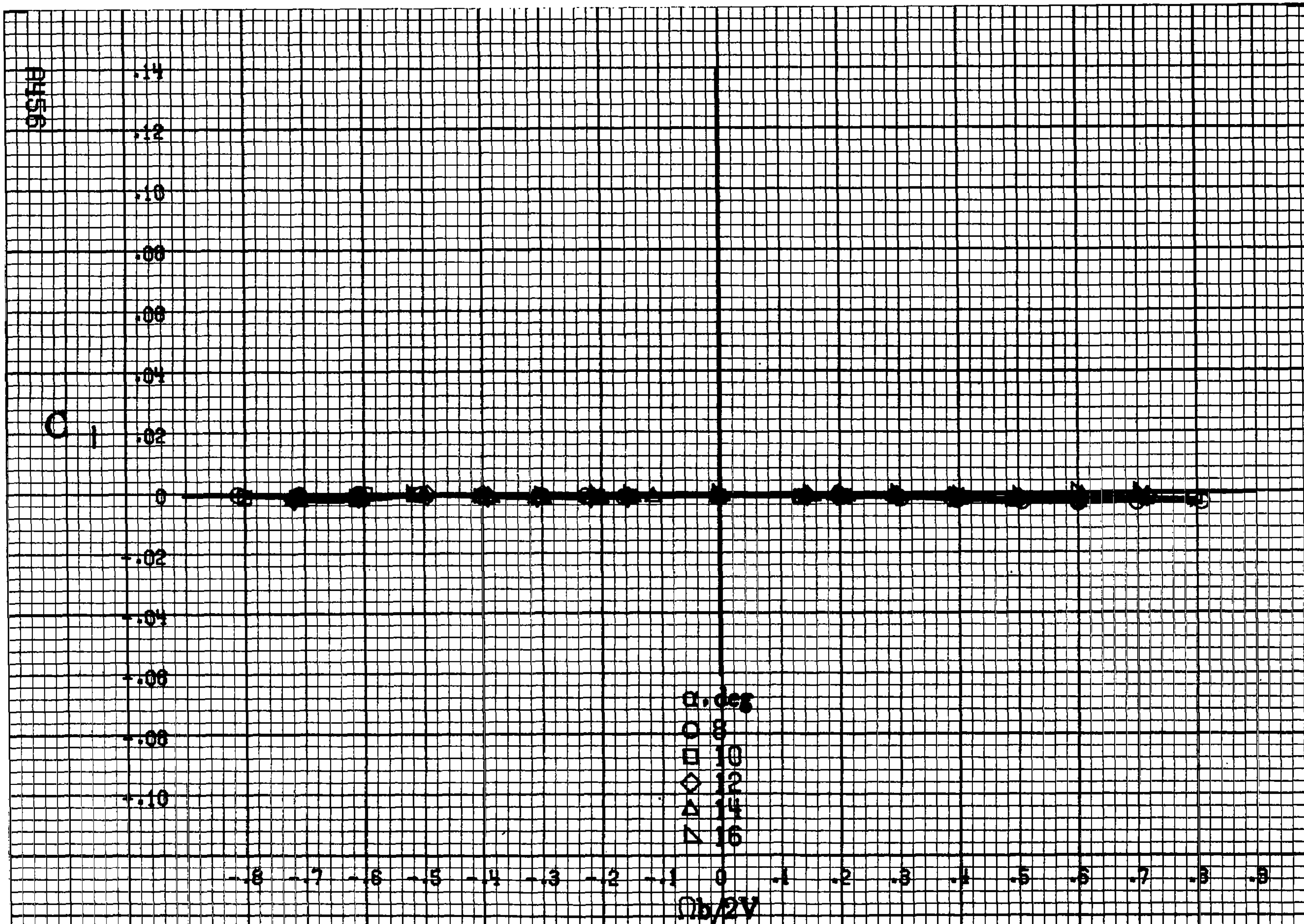

(a) $\alpha = 8$ to 16 deg. SR = 182.9cm (72in).

Figure A110.-Effect of rotation rate and angle of attack on rolling-moment coefficient for wing off configuration. $\delta_e = 0°$, $\delta_a = 0°$, $\delta_r = 0°$. $\beta = 0°$.

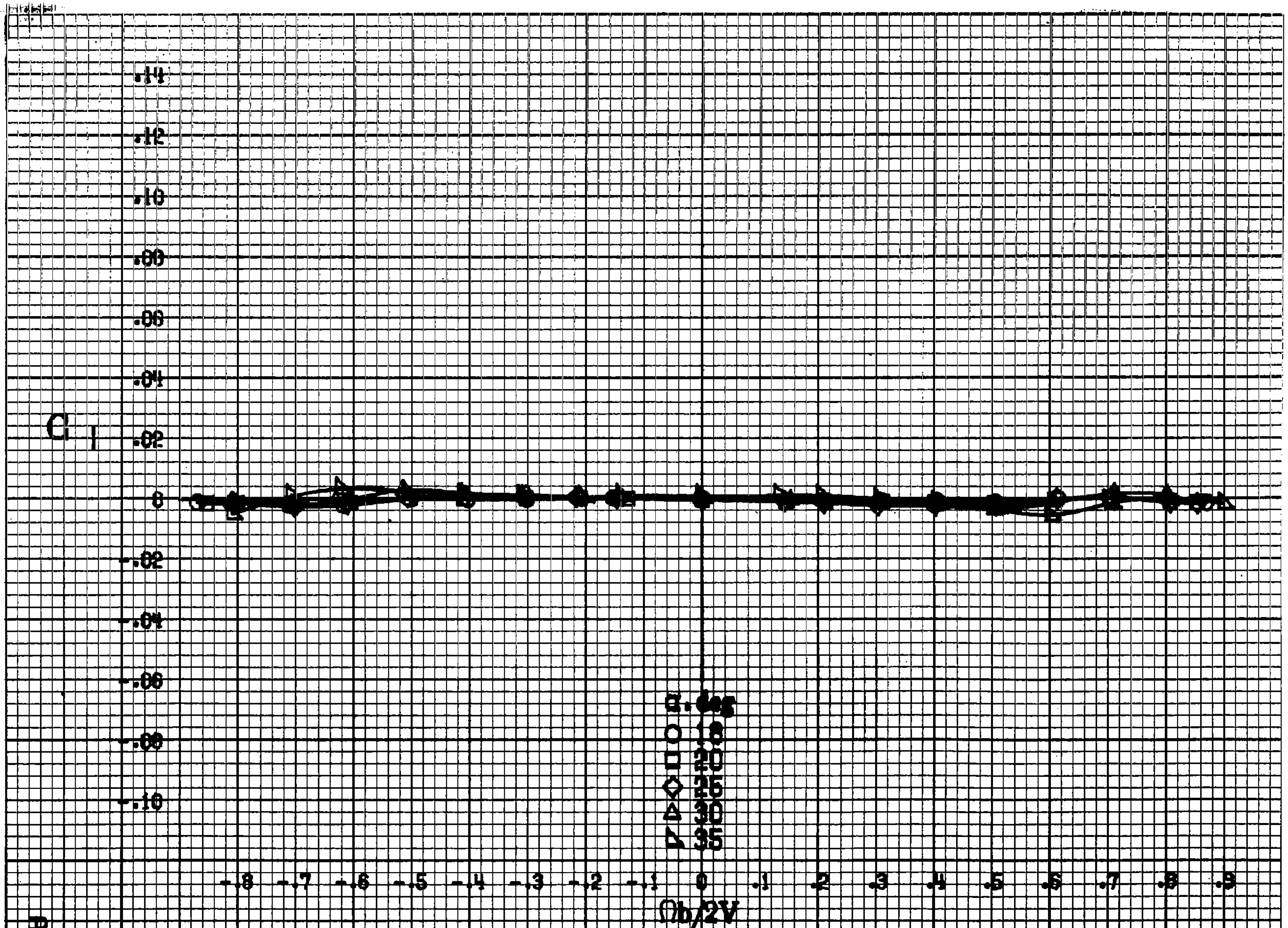

(b) α = 18 to 35 deg, δR = 182.9 cm (72 in).

Figure A110.-Continued.

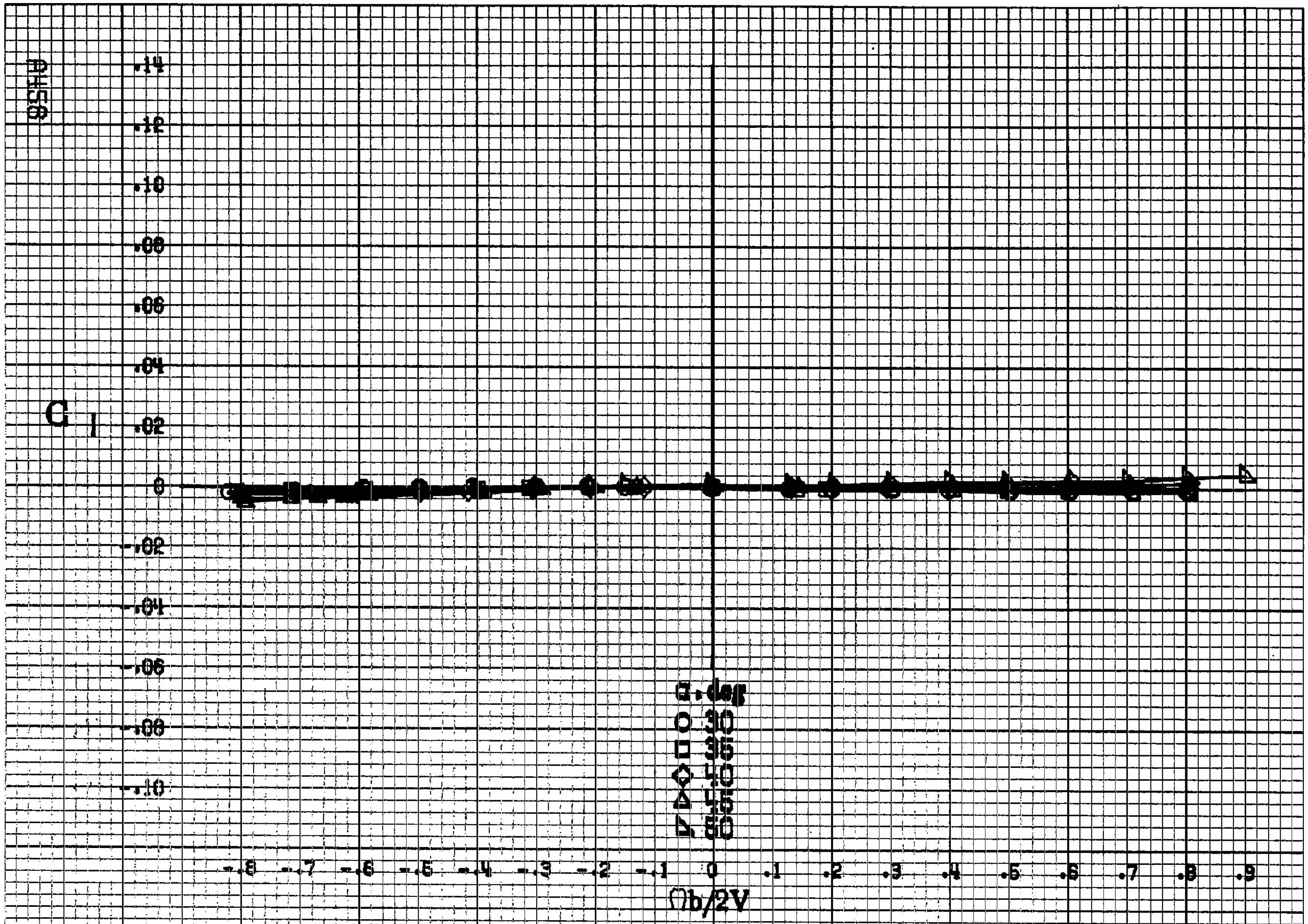

(c) α = 30 to 50 deg, SR = 0.

Figure A110.-Continued.

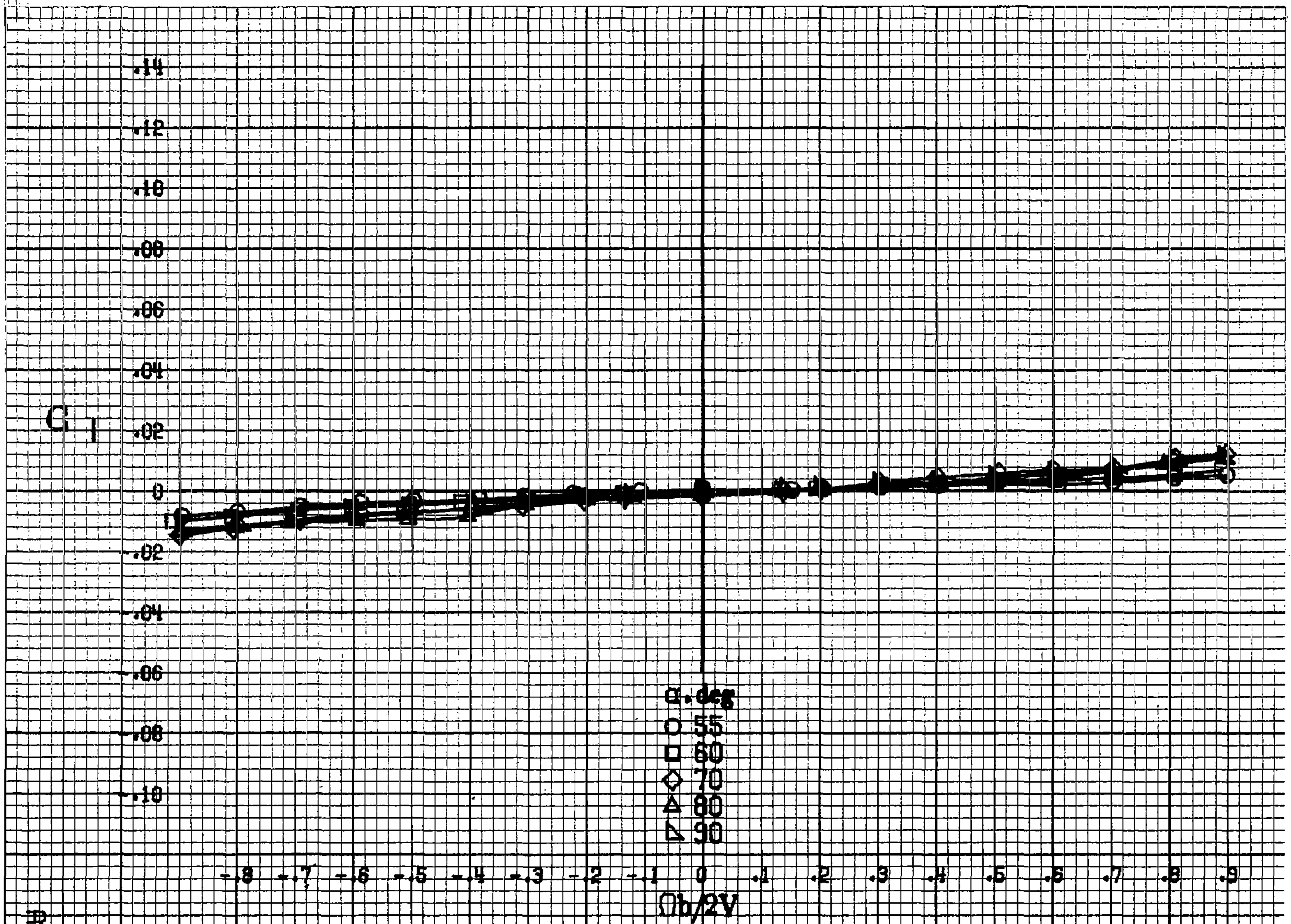

(d) $\alpha = 55$ to 90 deg, SR = 0.

Figure A110.–Concluded.

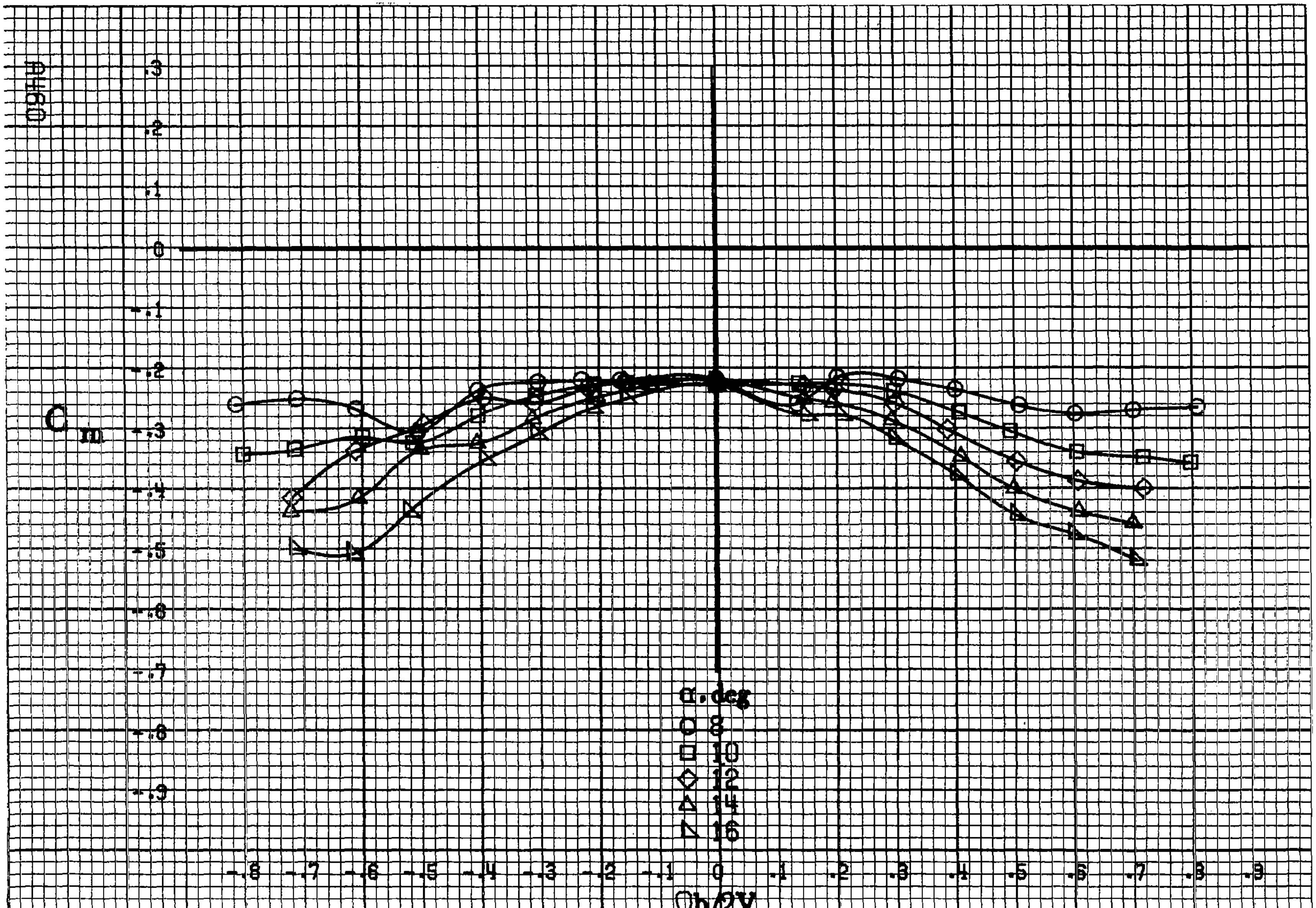

(a) $\alpha = 8$ to 16 deg, SR = 182.9cm (72in).

Figure A111.-Effect of rotation rate and angle of attack on pitching-moment coefficient for wing off configuration. $\delta_e = 0°$, $\delta_a = 0°$, $\delta_r = 0°$, $\beta = 0°$.

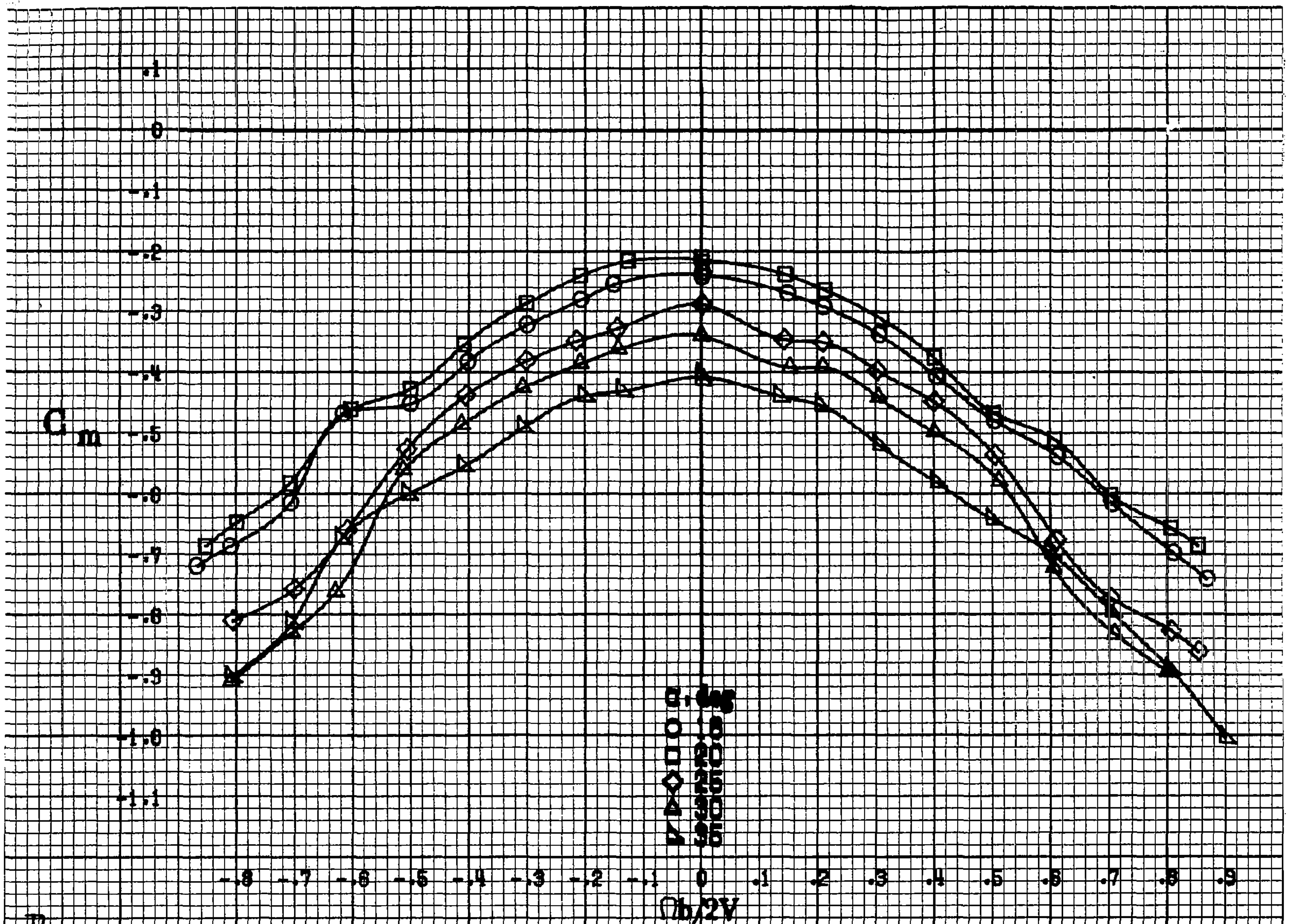

(b) α = 18 to 35 deg, SR = 182.9 cm (72 in).

Figure A111.-Continued.

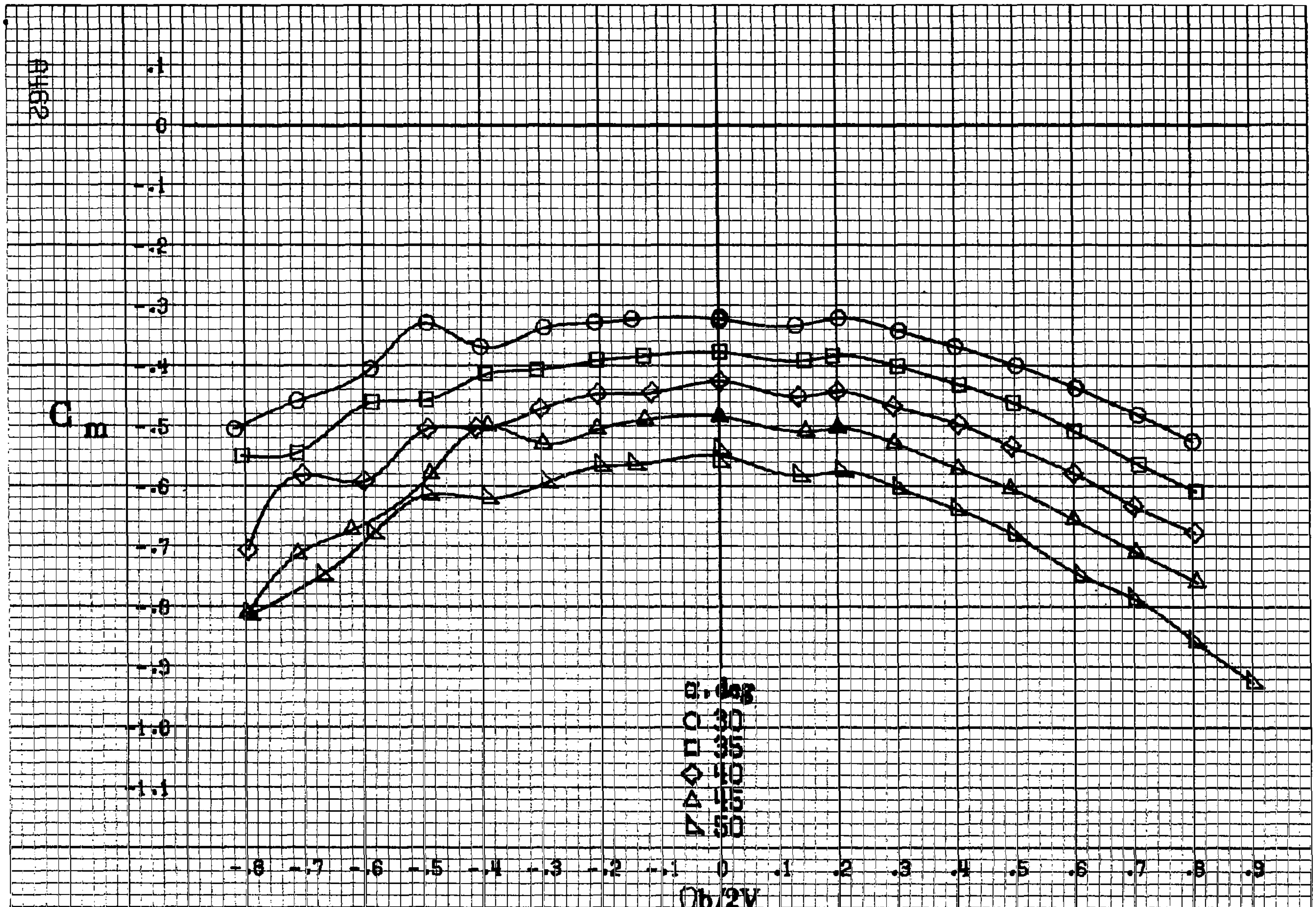

(c) α = 30 to 50 deg, SR = 0.

Figure A11.-Continued.

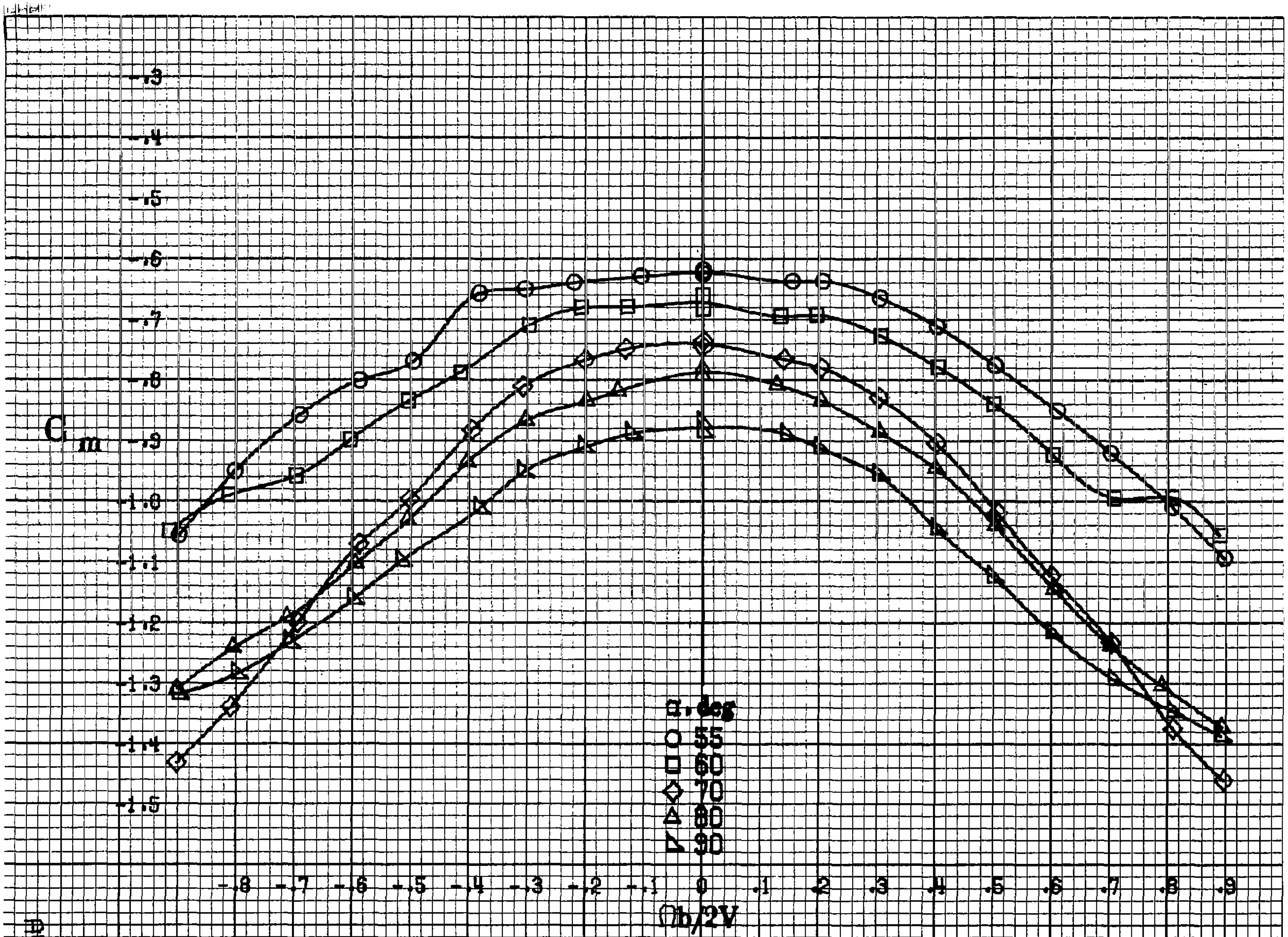

(d) α = 55 to 90 deg, SR = 0.

Figure A111.-Concluded.

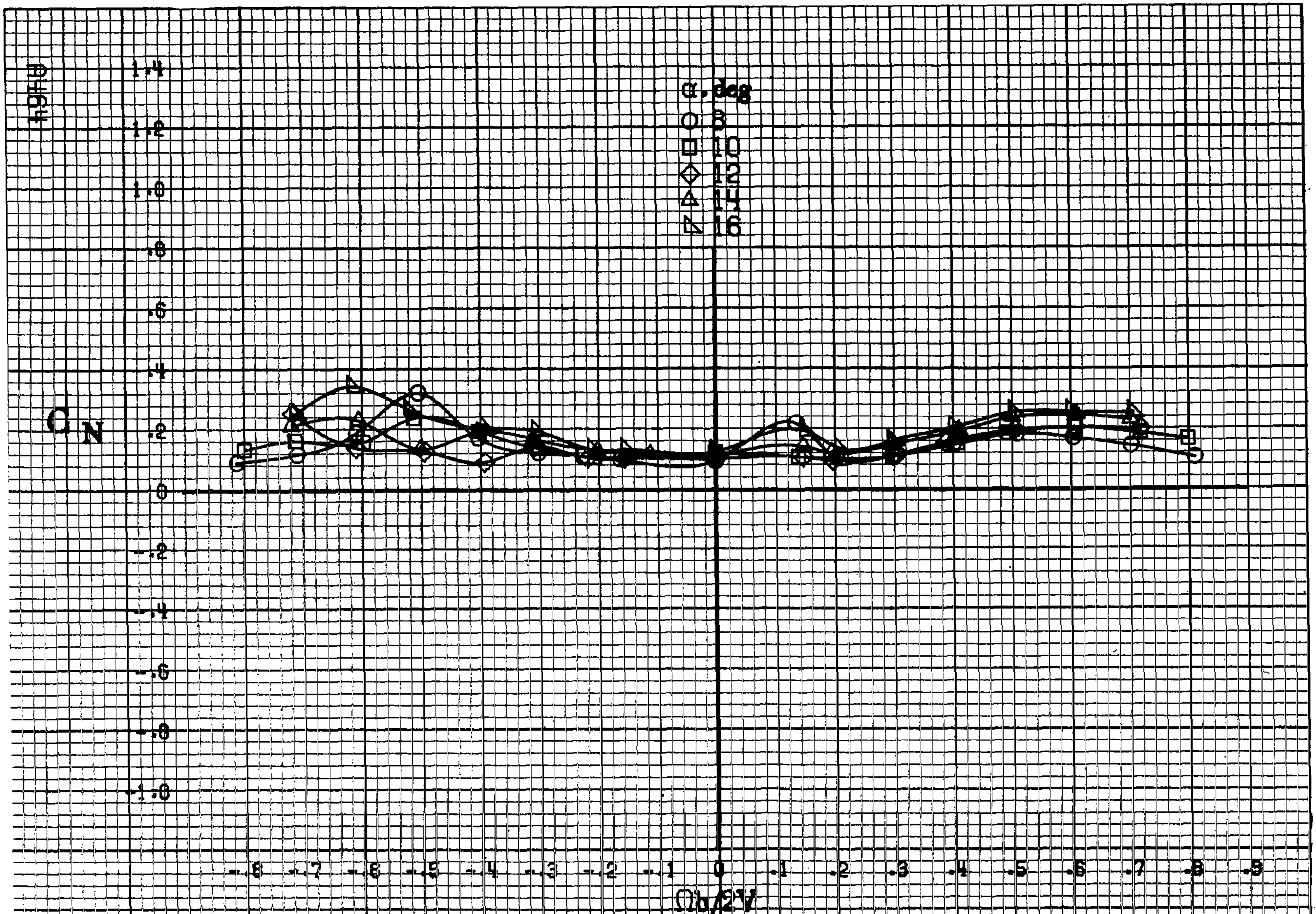

(a) $\alpha = 8$ to 16 deg, SR = 182.9 cm (72 in.).

Figure A112.- Effect of rotation rate and angle of attack on normal-force coefficient for wing off configuration. $\delta_e = 0°$, $\delta_a = 0°$, $\delta_r = 0°$. $\beta = 0°$.

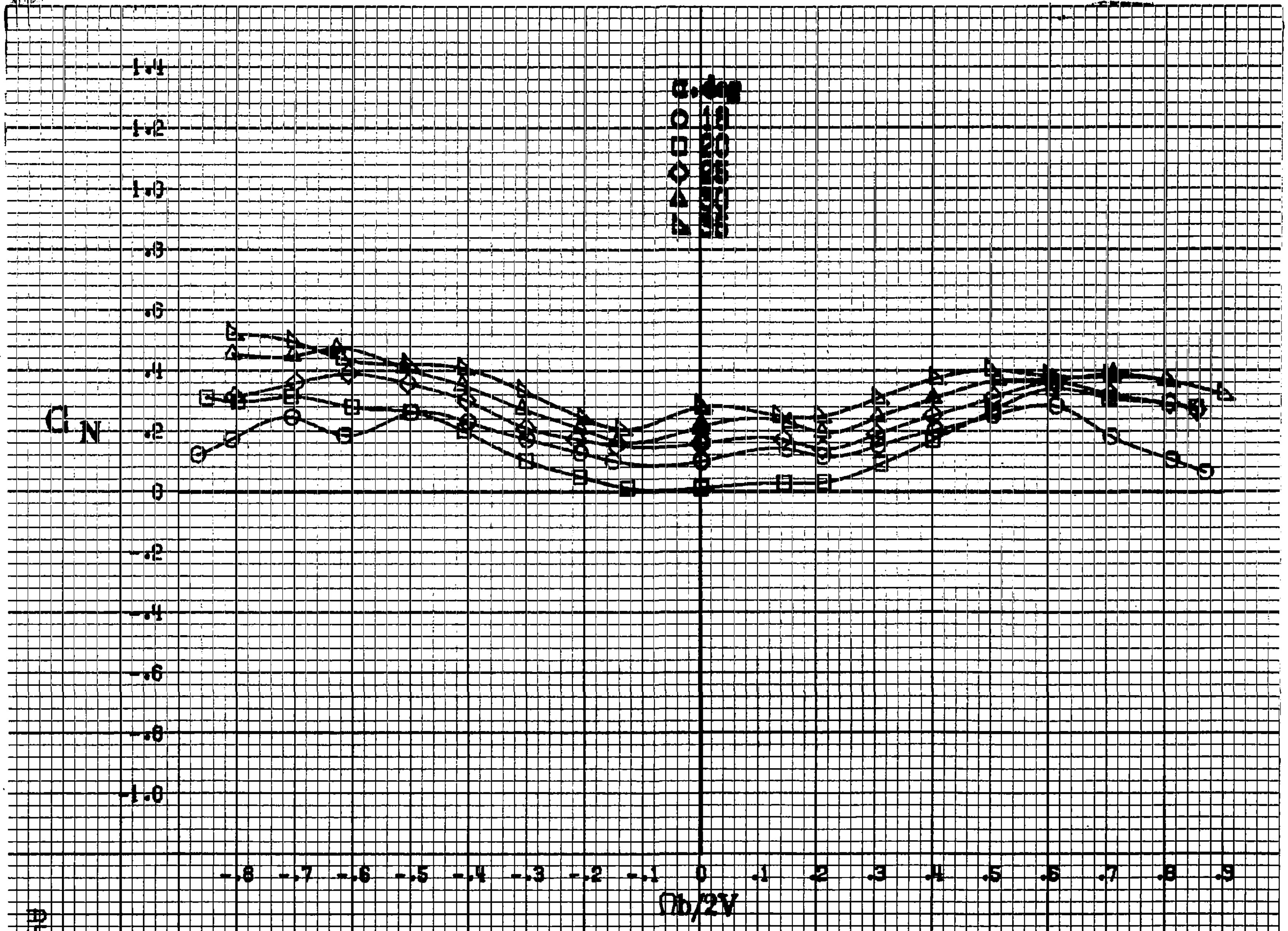

(b) α = 18 to 35 deg, SR = 182.9 cm (72 in).

Figure A112.- Continued.

A465

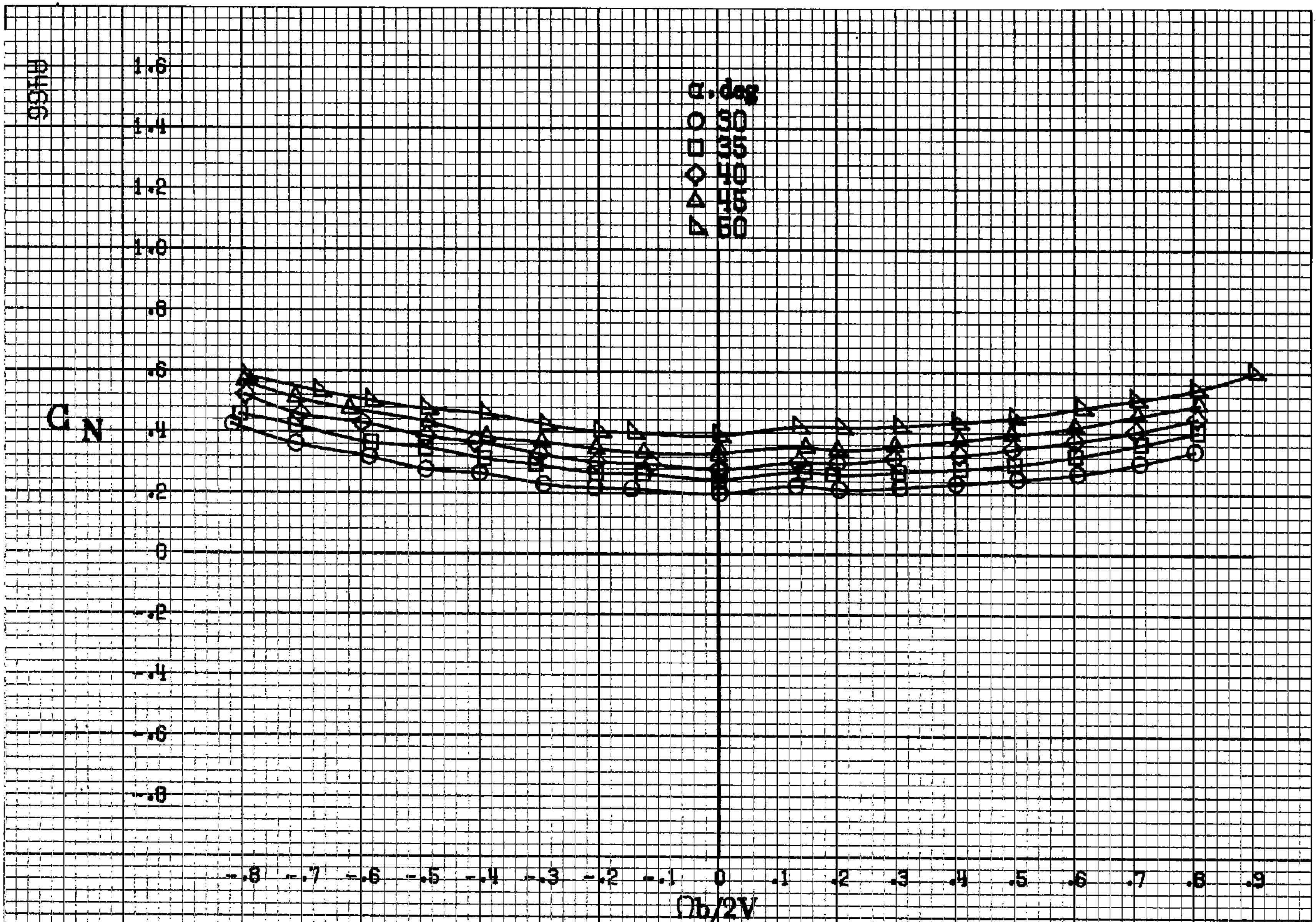

(c) α = 30 to 50 deg, SR = 0.

Figure A112.-Continued.

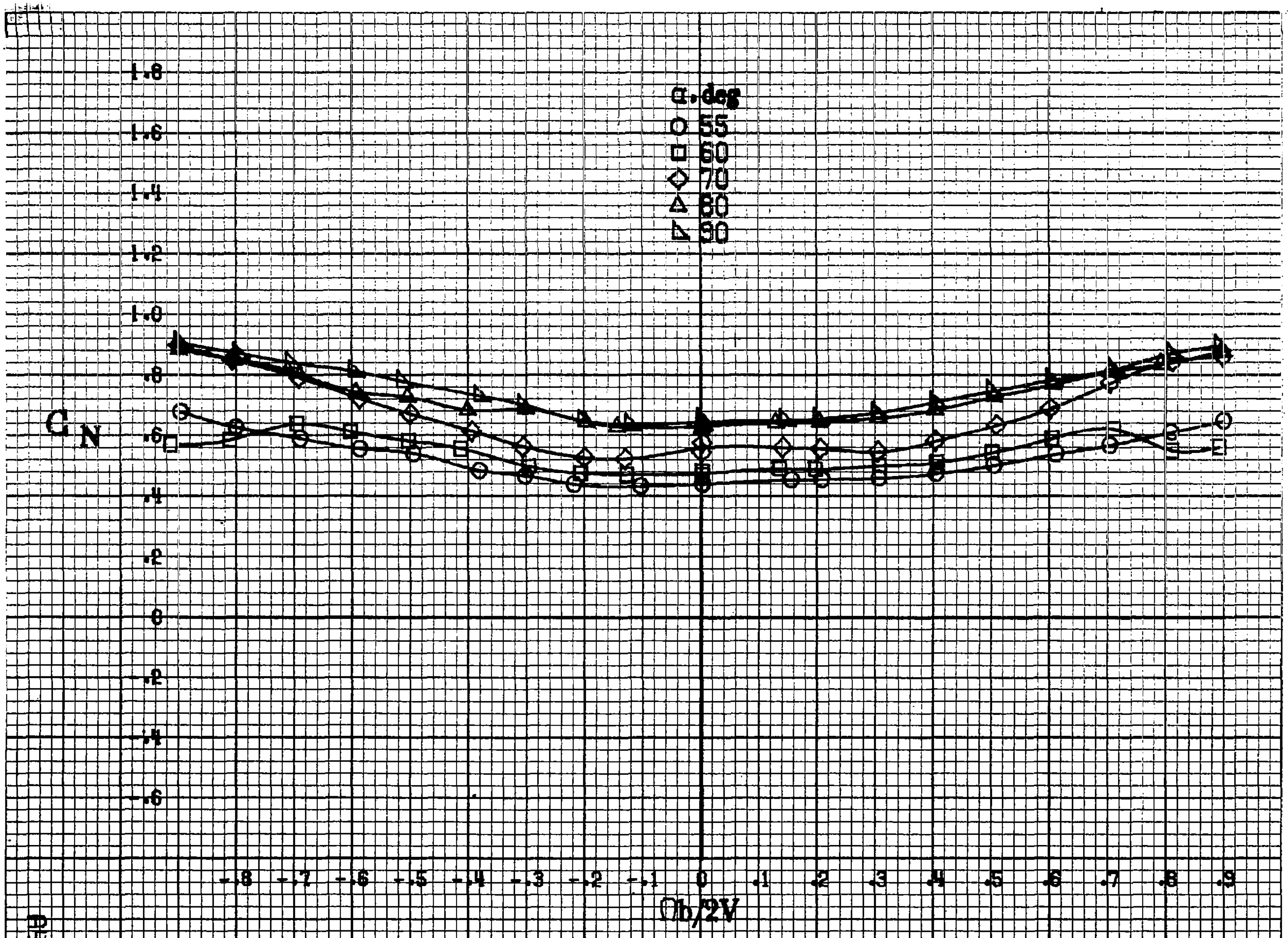

(d) α = 55 to 90 deg, SR = 0.

Figure A112.-Concluded.

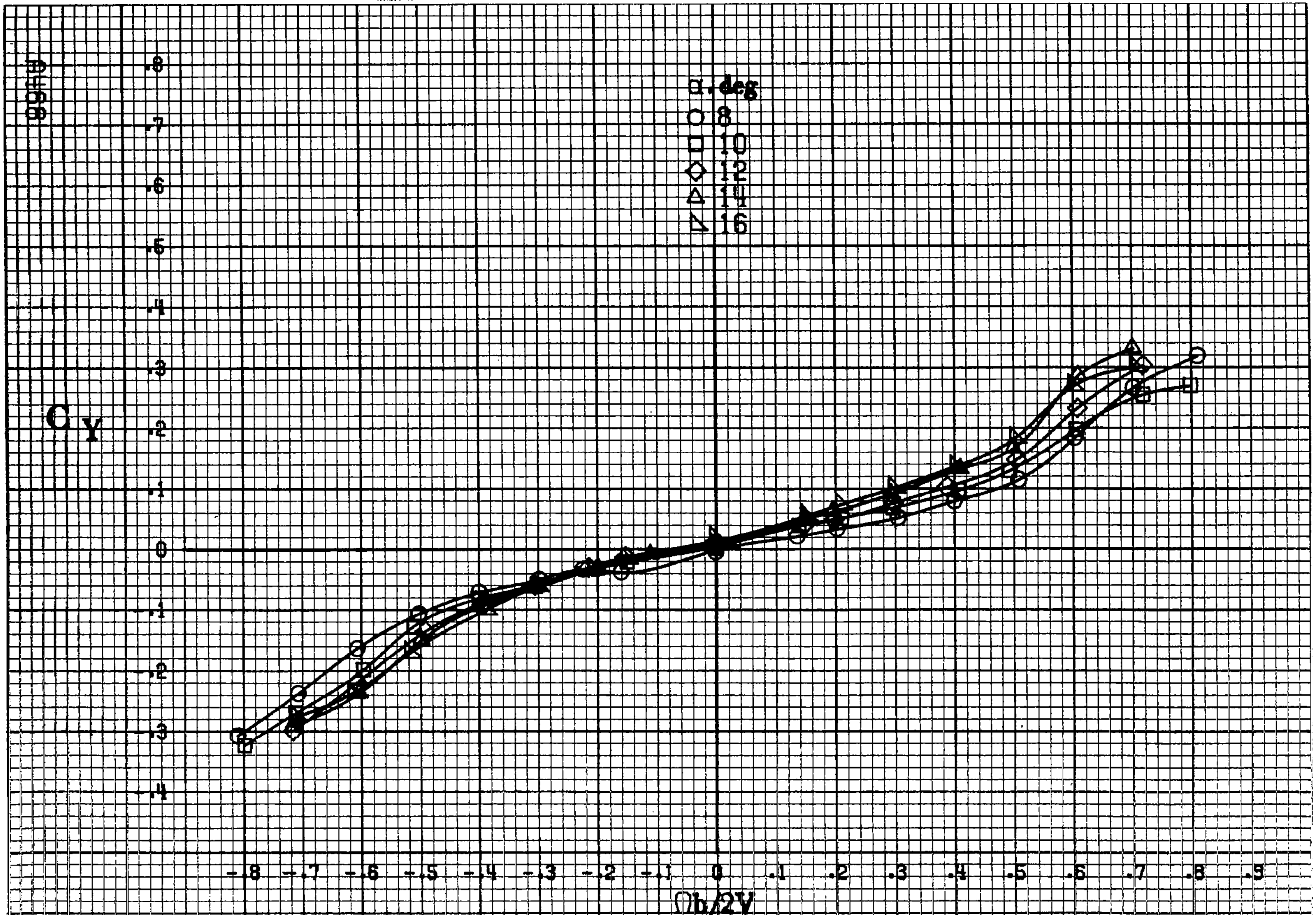

(a) $\alpha = 8$ to 16 deg, SR = 182.9cm (72in).

Figure A119.-Effect of rotation rate and angle of attack on side-force coefficient for wing off configuration. $\delta_e = 0°$, $\delta_a = 0°$, $\delta_r = 0°$, $\beta = 0°$.

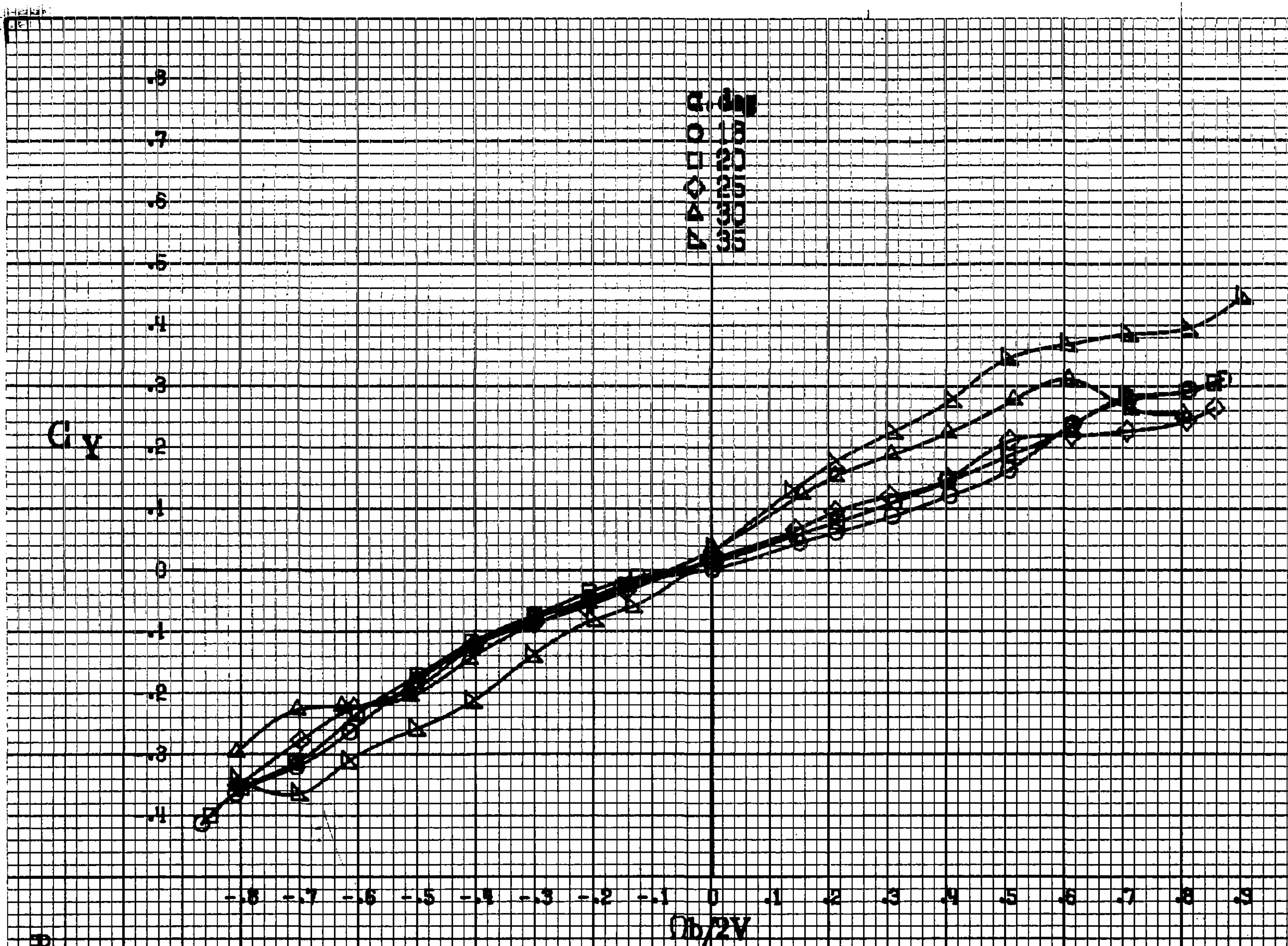

(b) α = 18 to 35 deg, SR = 182.9 cm (72 in).
Figure A118.-Continued.

A169

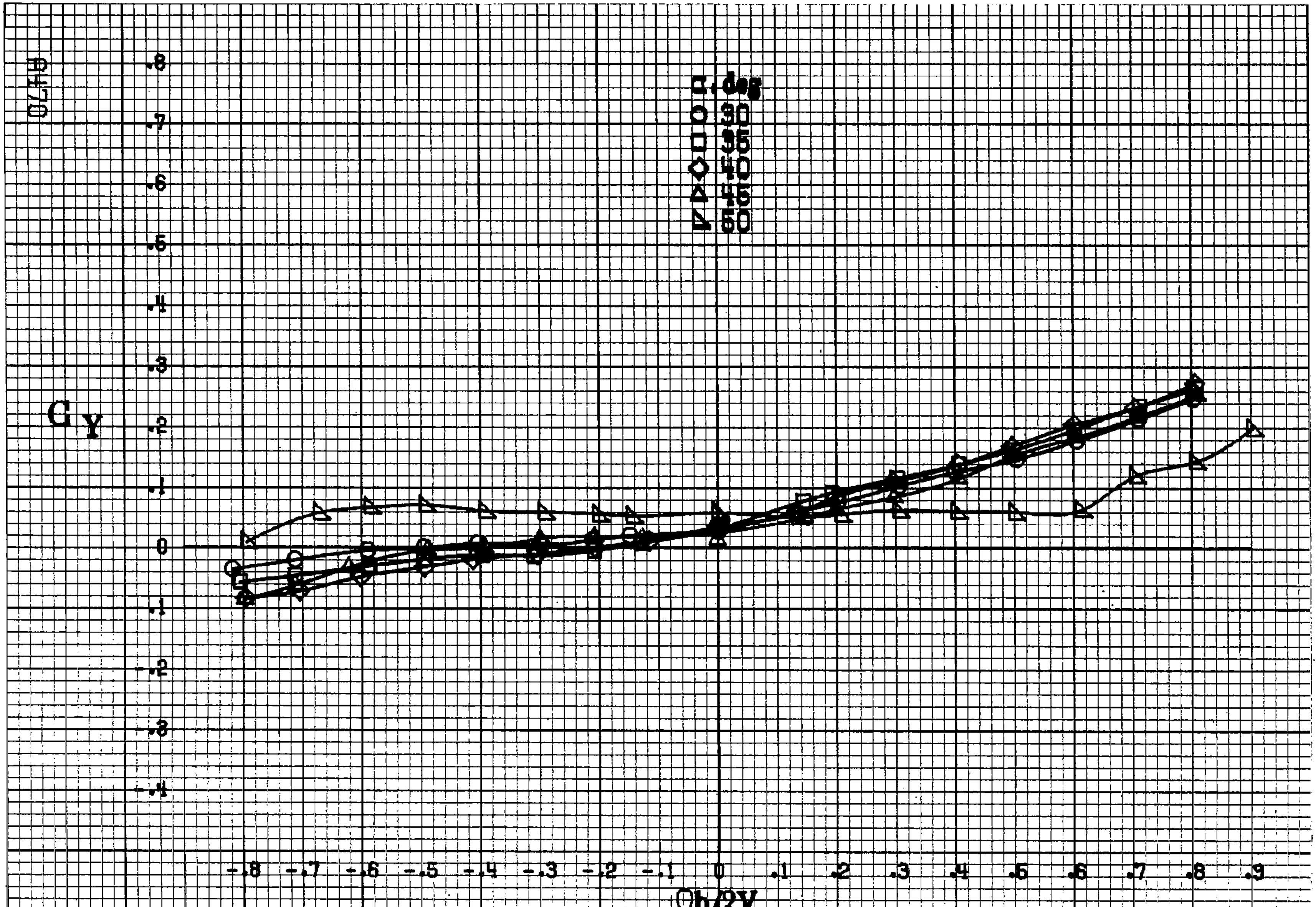

(c) α = 30 to 50 deg, SR = 0.

Figure A118.-Continued.

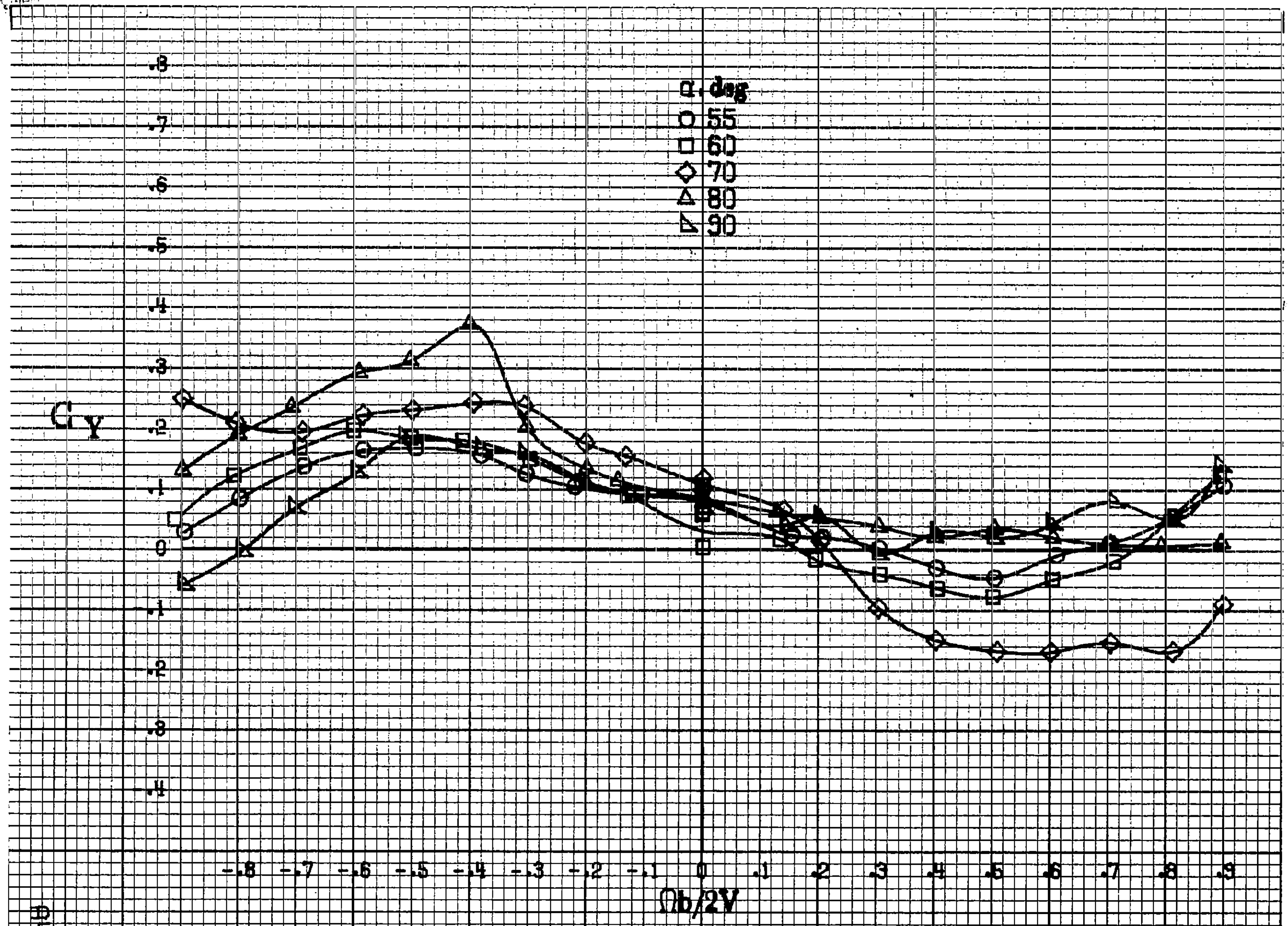

(d) α=55to90deg, SR=0.
Figure A118.-Concluded.

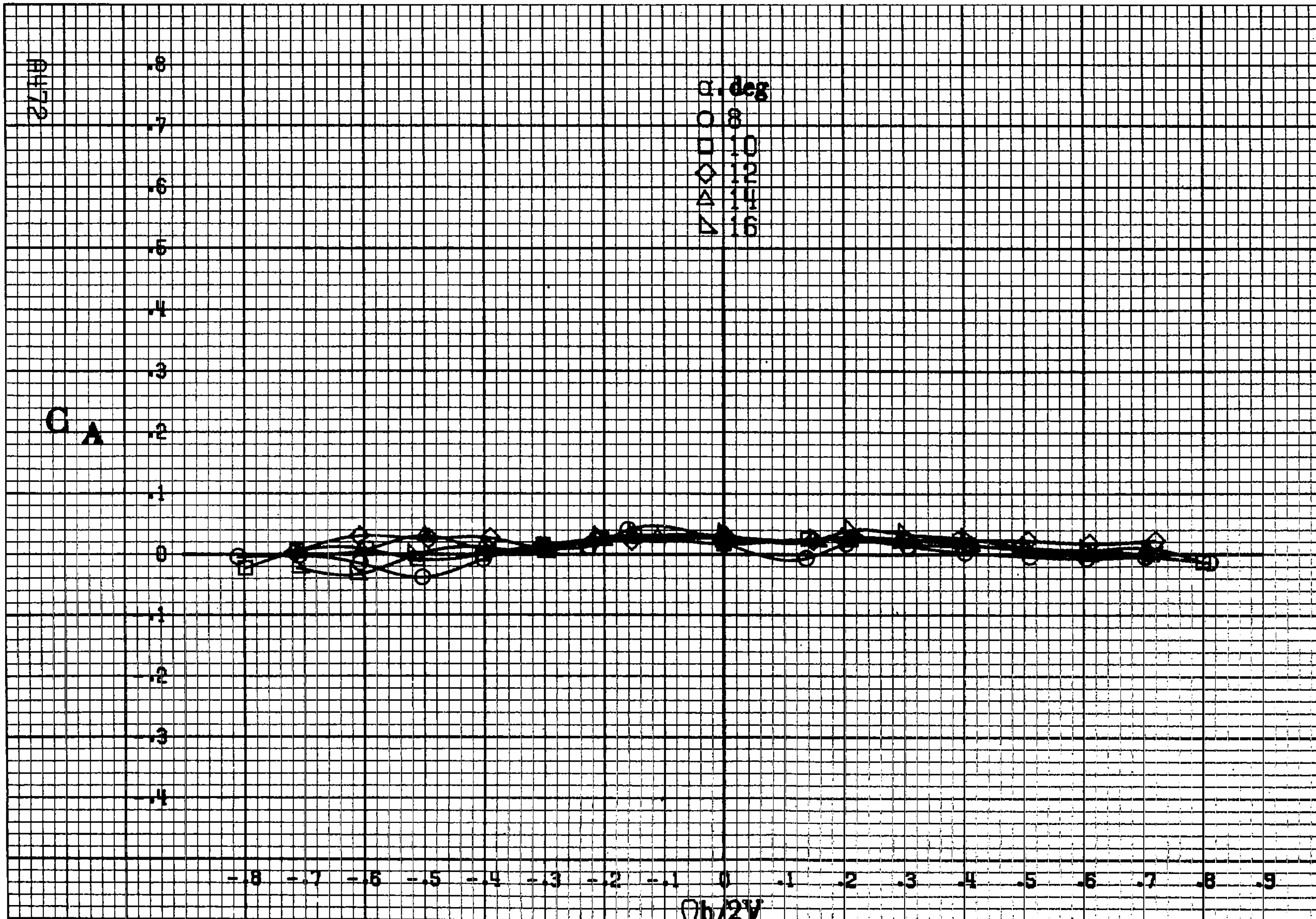

(a) $\alpha = 8$ to 16 deg, SR = 182.9 cm (72 in).

Figure A114.-Effect of rotation rate and angle of attack on axial-force coefficient for wing off configuration. $\delta_a = 0°$, $\delta_e = 0°$, $\delta_r = 0°$. $\beta = 0°$.

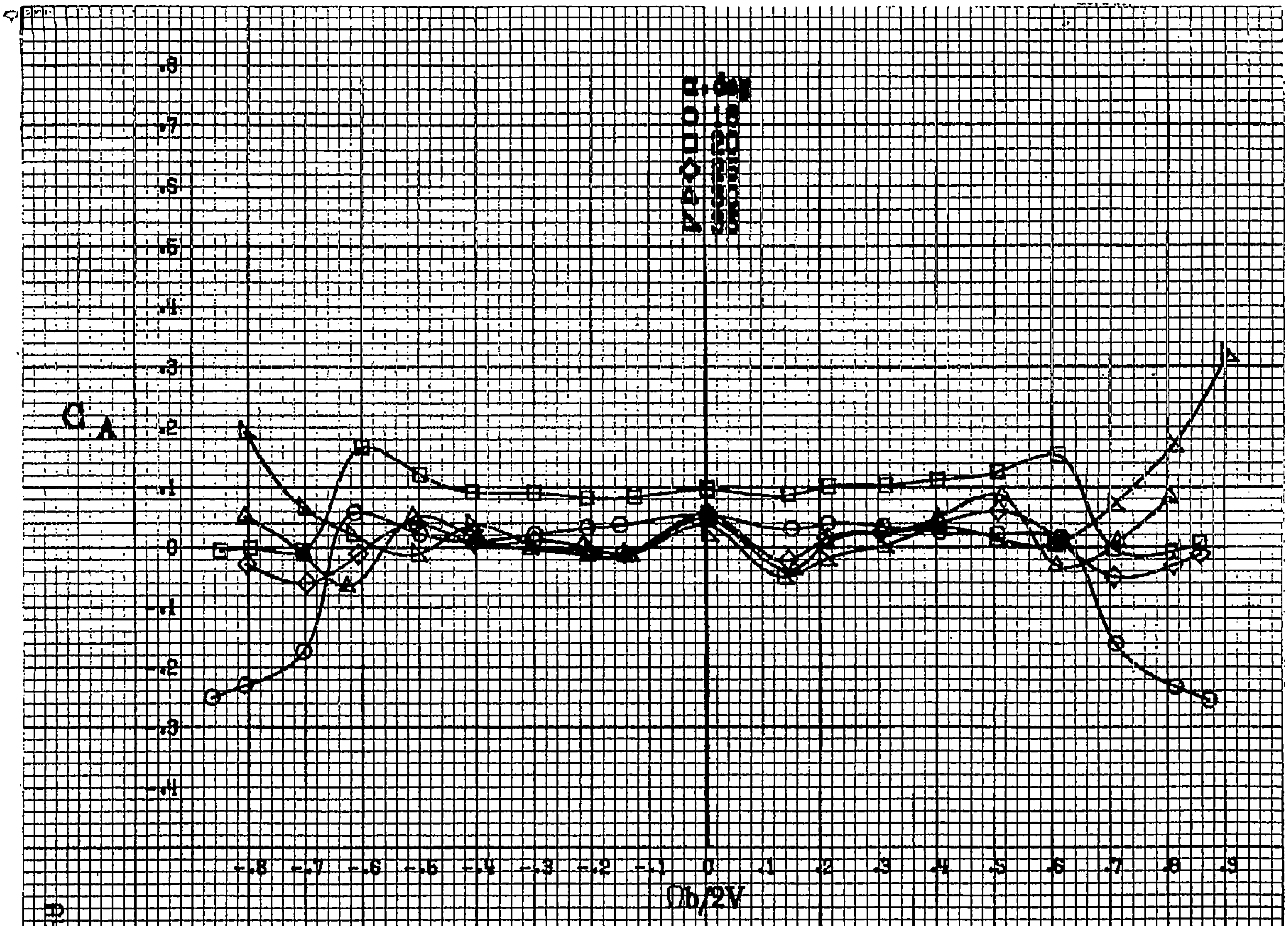

(b) α = 18 to 35 deg, SR = 182.9 cm (72 in).

Figure A114. Continued.

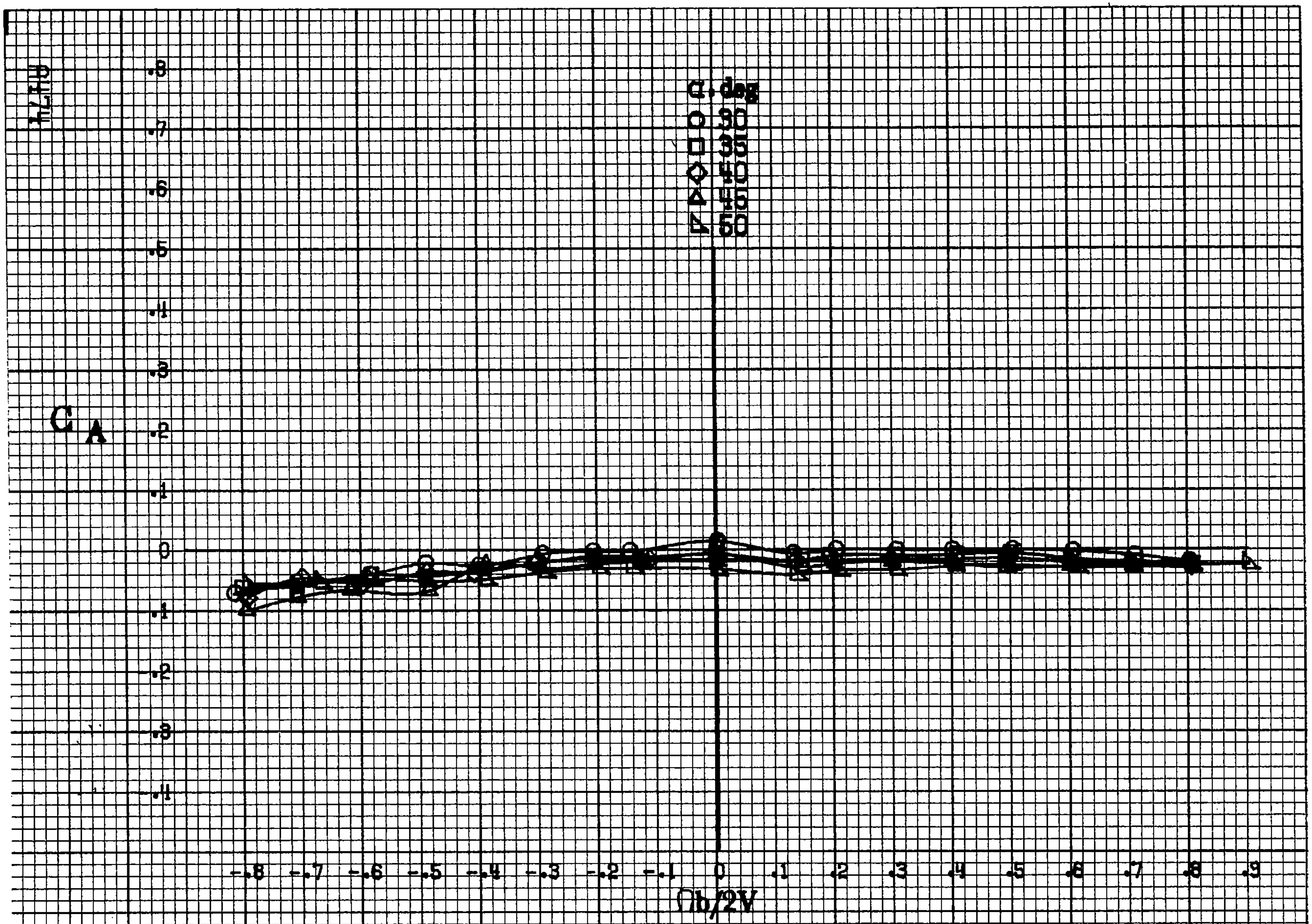

(c) α=30to50deg, SR=0.
Figure A114.-Continued.

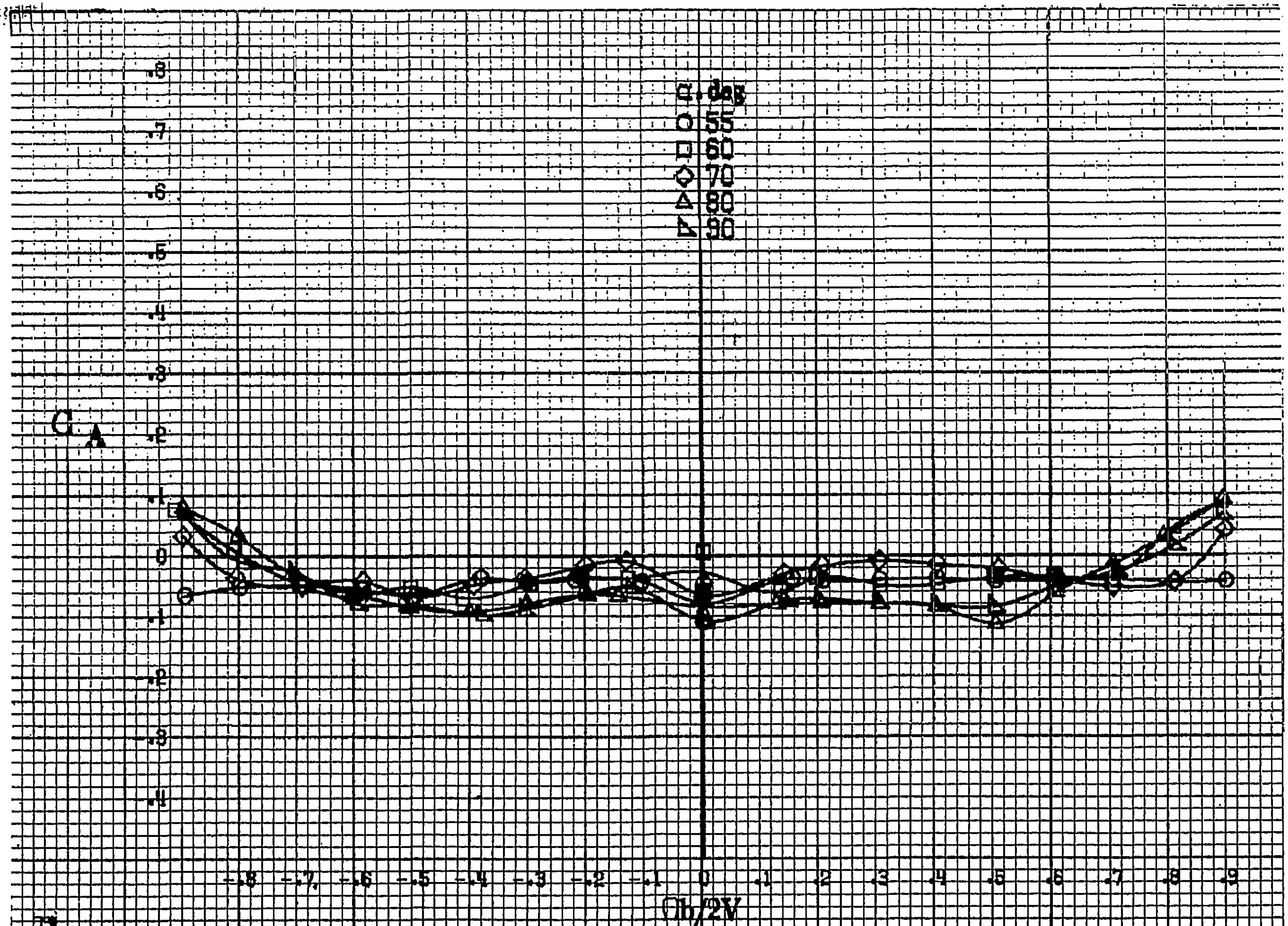

(d) α = 55 to 90 deg, SR = 0.

Figure A114. Concluded.

497

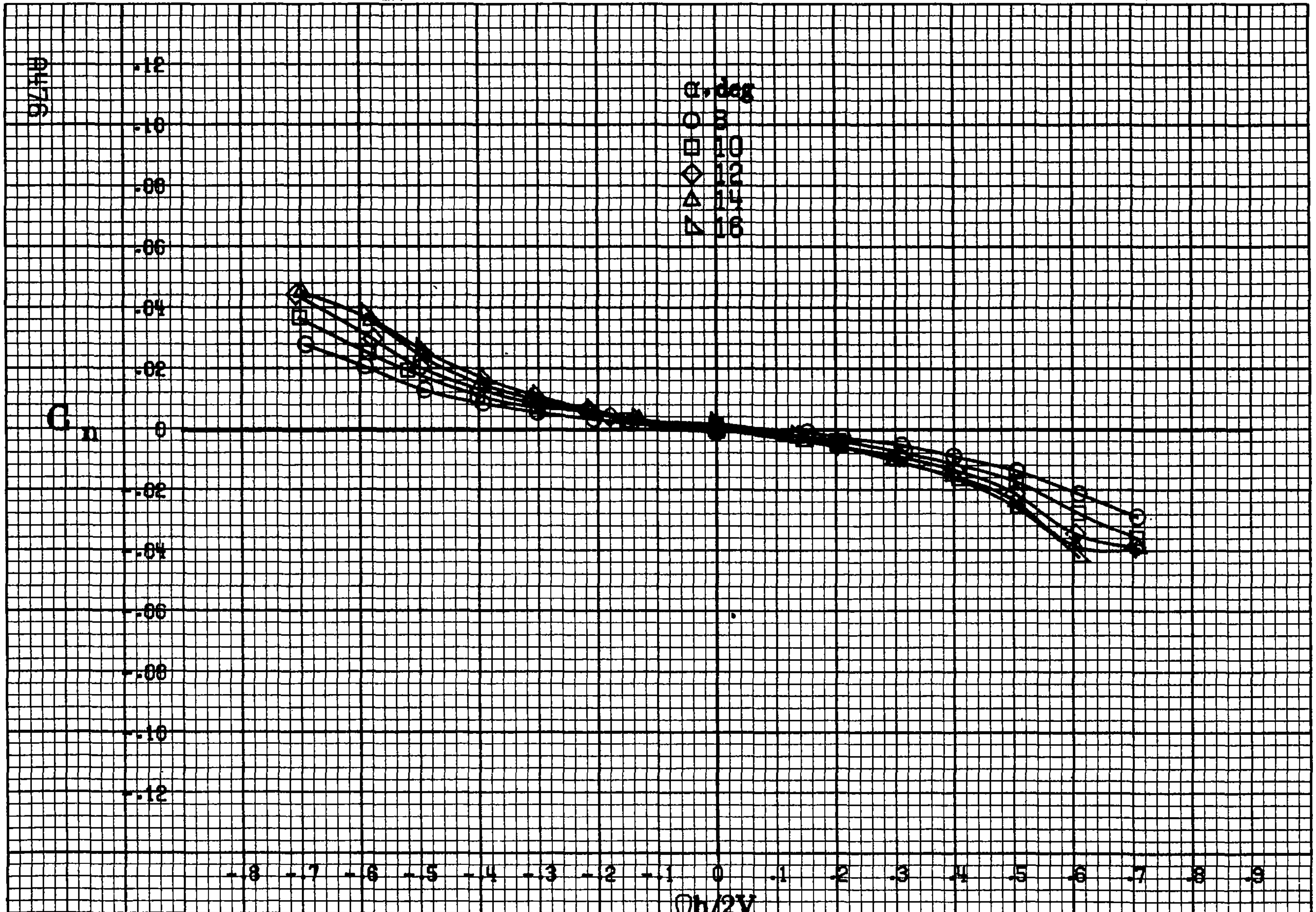

(a) α = 8 to 16 deg, SR = 182.9 cm (72 in).

Figure A115.-Effect of rotation rate and angle of attack on yawing-moment coefficient for wing and horizontal tail off configuration. $\delta_e = 0°$, $\delta_a = 0°$, $\delta_r = 0°$, $\beta = 0°$.

(b) α = 18 to 35 deg, SR = 182.9 cm (72 in).

Figure A115.-Continued.

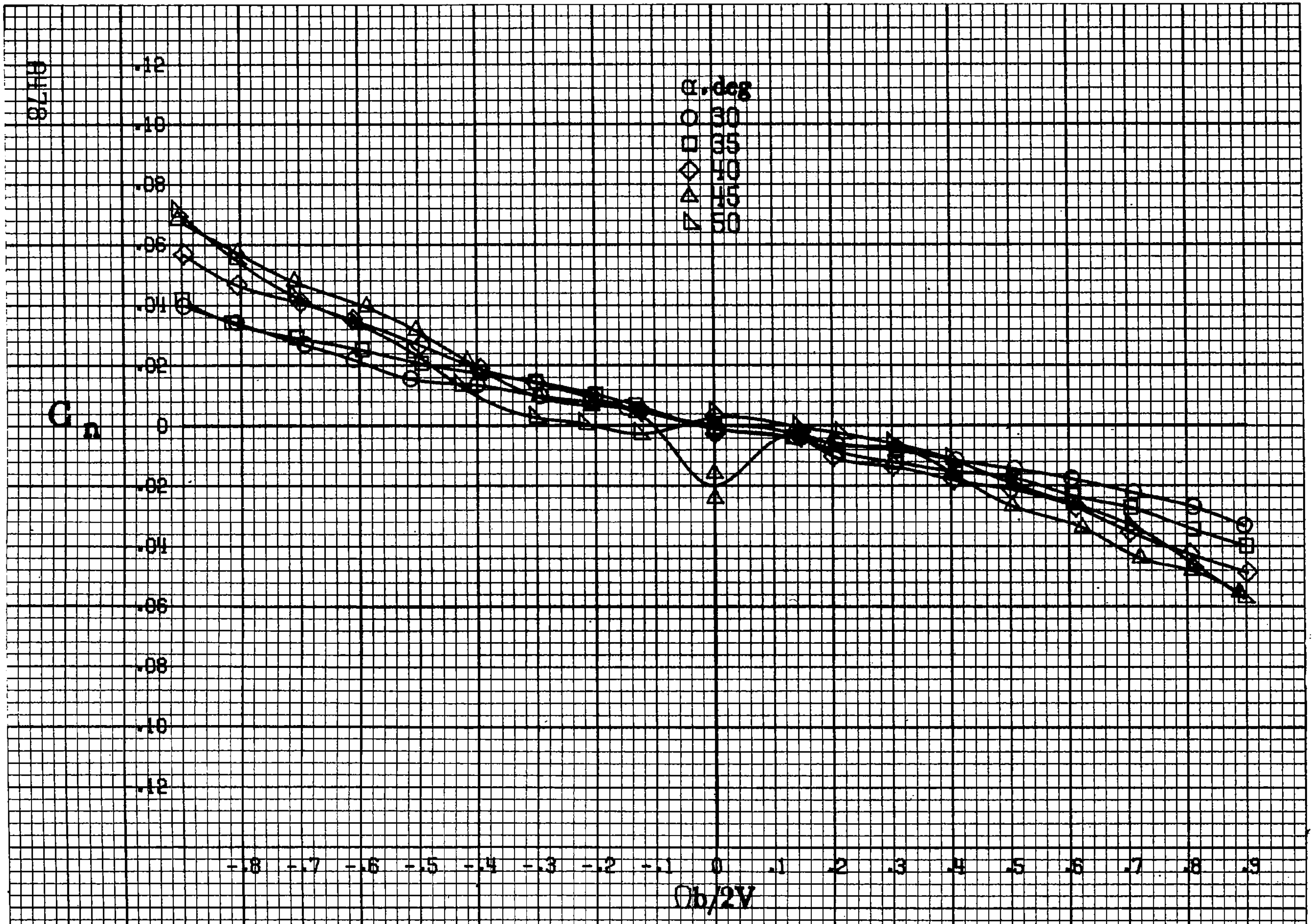

(c) α = 30 to 50 deg, SR = 0.

Figure A115.-Continued.

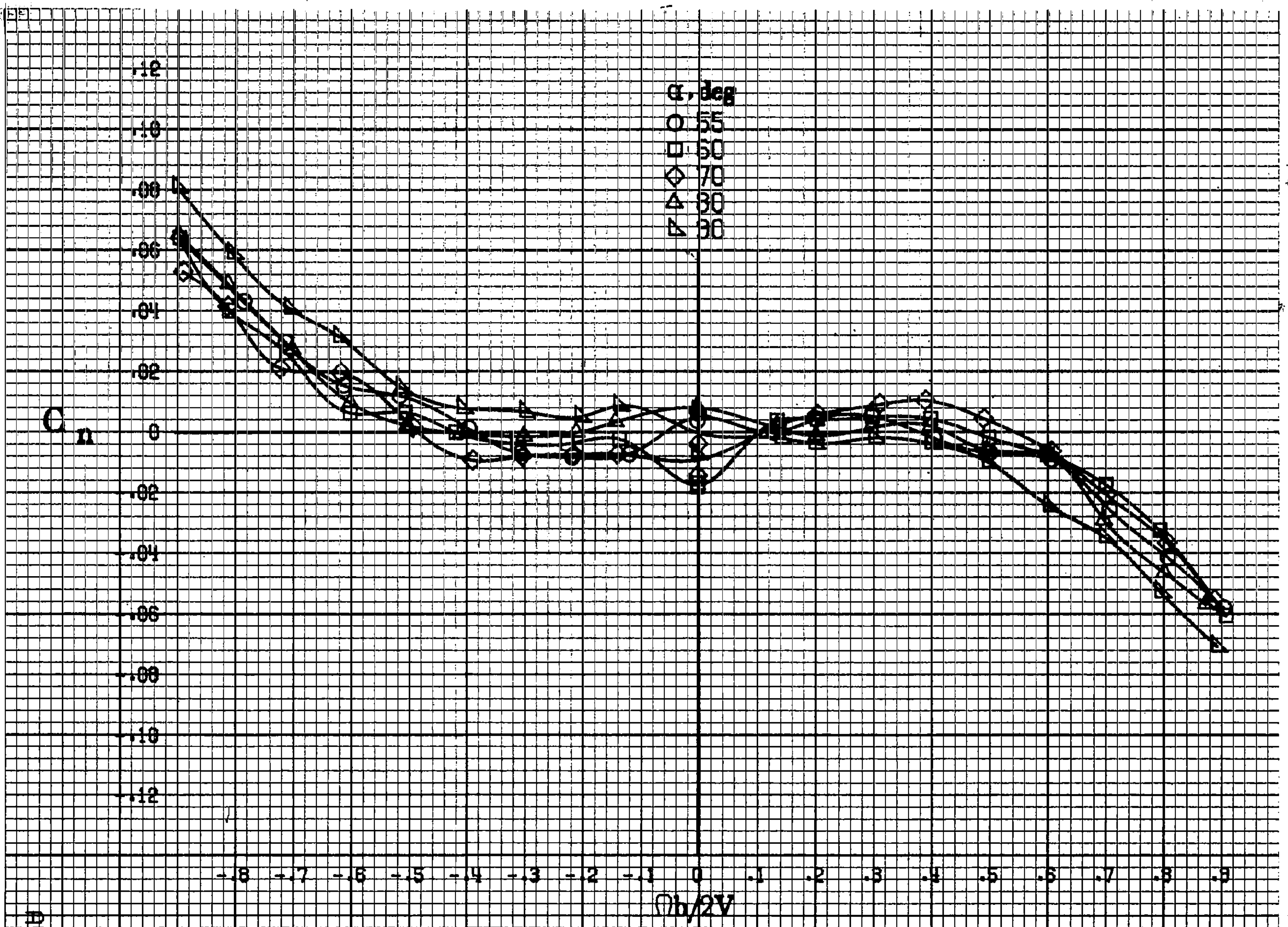

(d) α = 55 to 90 deg, SR = 0.

Figure A115.-Concluded.

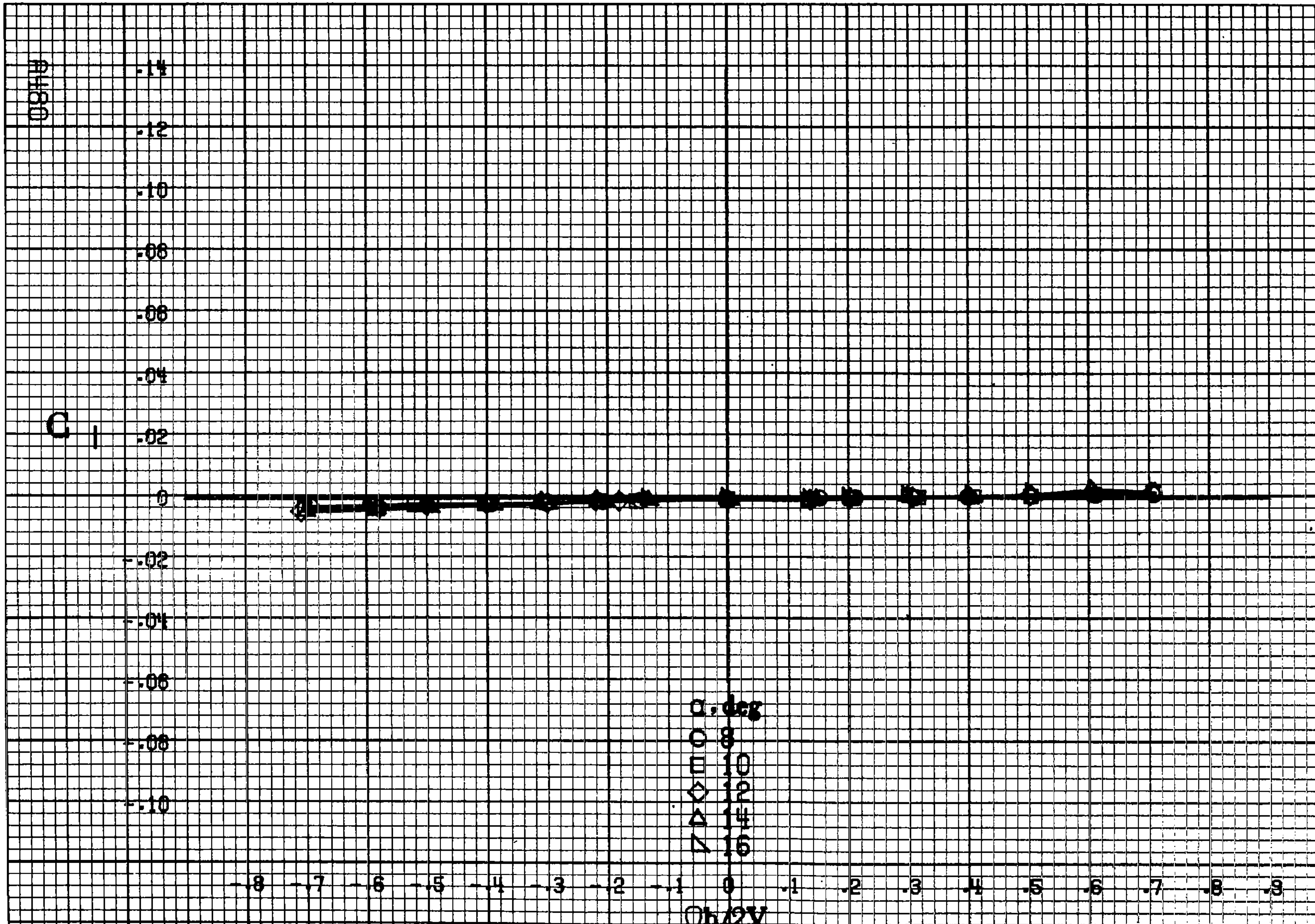

(a) α = 8 to 16 deg, SR = 182.9 cm (72 in).

Figure A116.- Effect of rotation rate and angle of attack on rolling-moment coefficient for wing and horizontal tail off configuration. $\delta_e = 0°$, $\delta_a = 0°$, $\delta_r = 0°$, $\beta = 0°$.

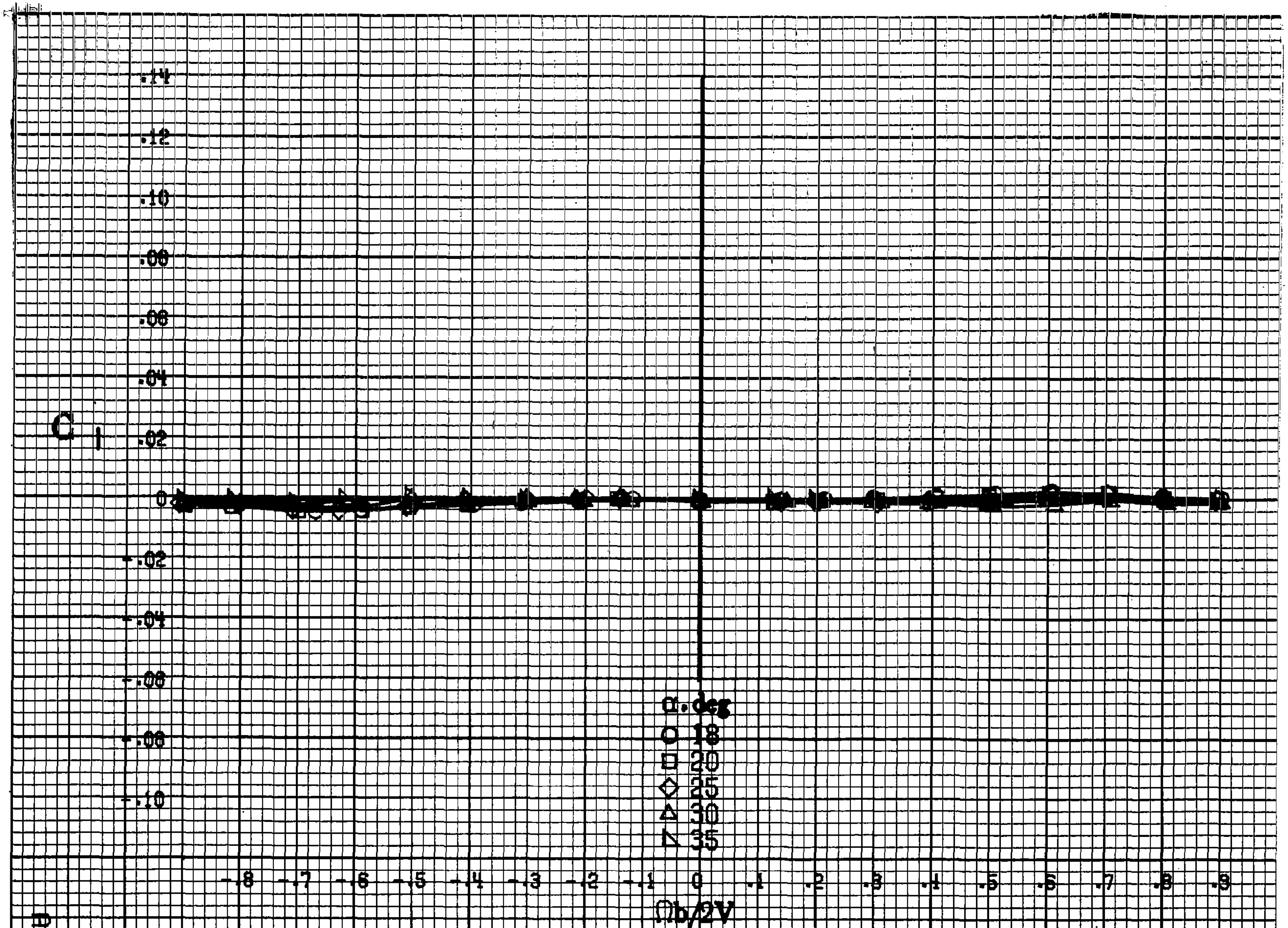

(b) α = 18 to 35 deg, SR = 182.9 cm (72 in).

Figure A116.-Continued.

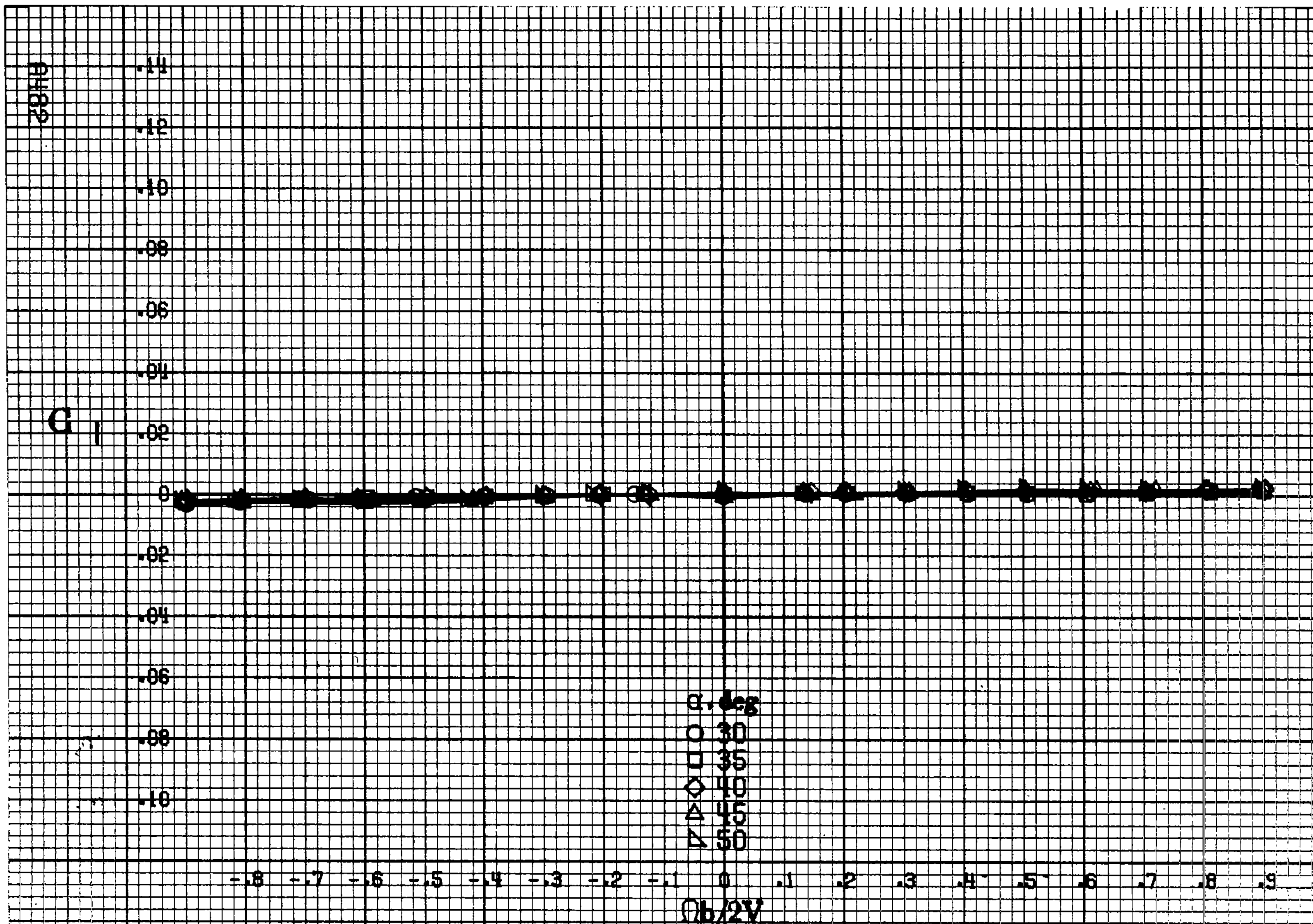

(c) α = 30 to 50 deg, SR = 0.
Figure A116.-Continued.

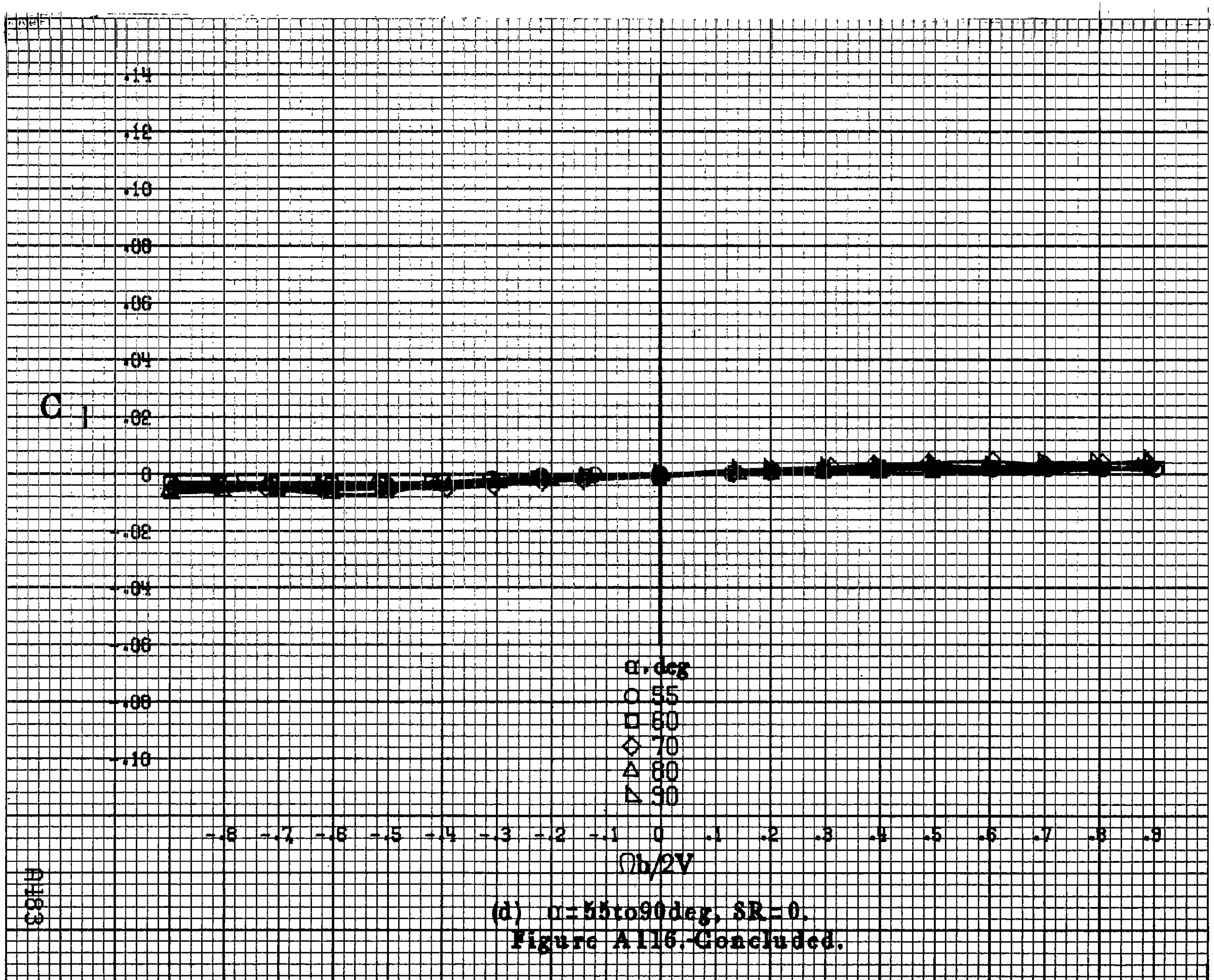

(d) α = 55 to 90 deg, SR = 0.
Figure A116.-Concluded.

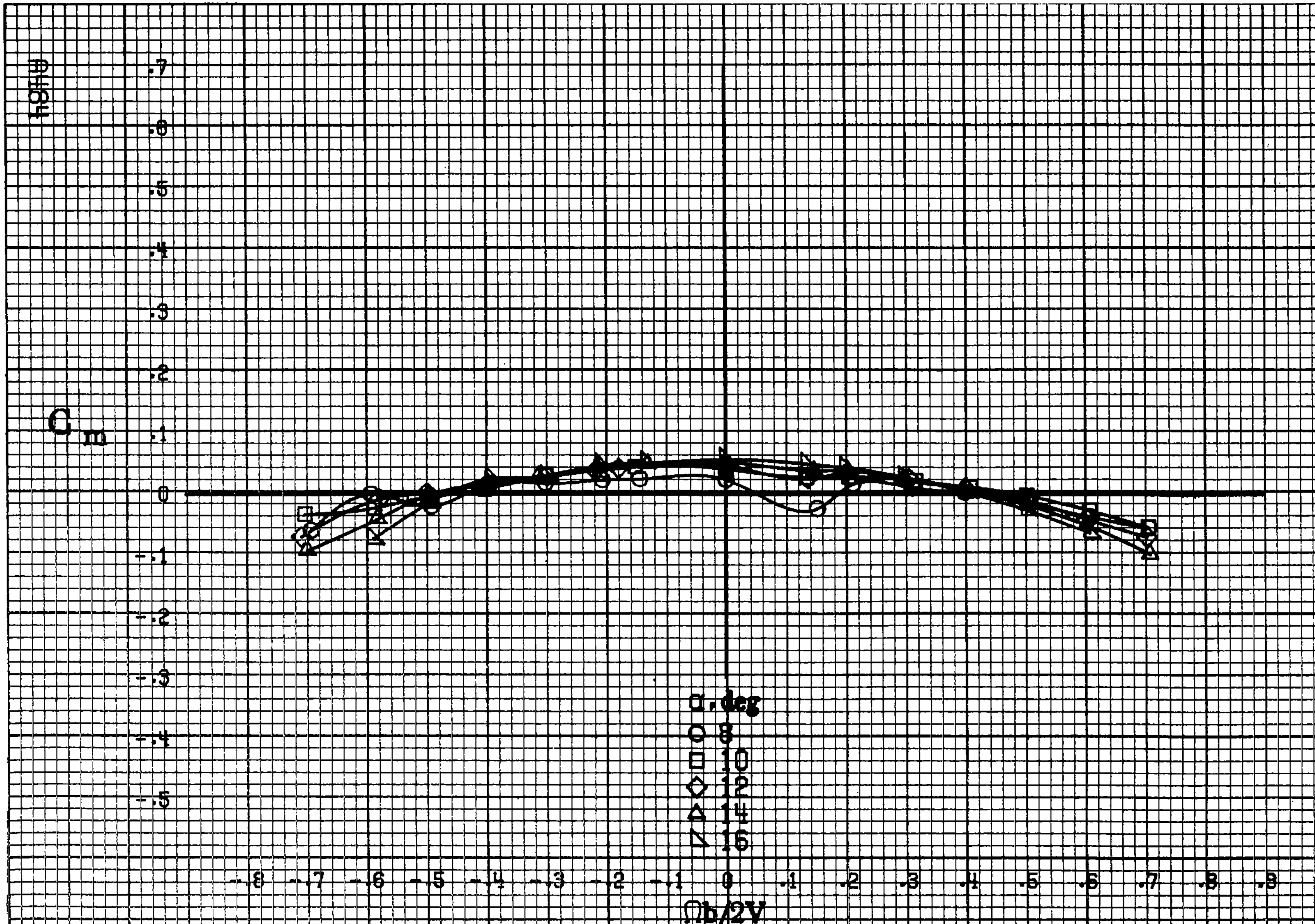

(a) $\alpha = 8$ to 16 deg, SR = 182.9cm (72in).

Figure A117.-Effect of rotation rate and angle of attack on pitching-moment coefficient for wing and horizontal tail off configuration. $\delta_e = 0°$, $\delta_a = 0°$, $\delta_r = 0°$, $\beta = 0°$.

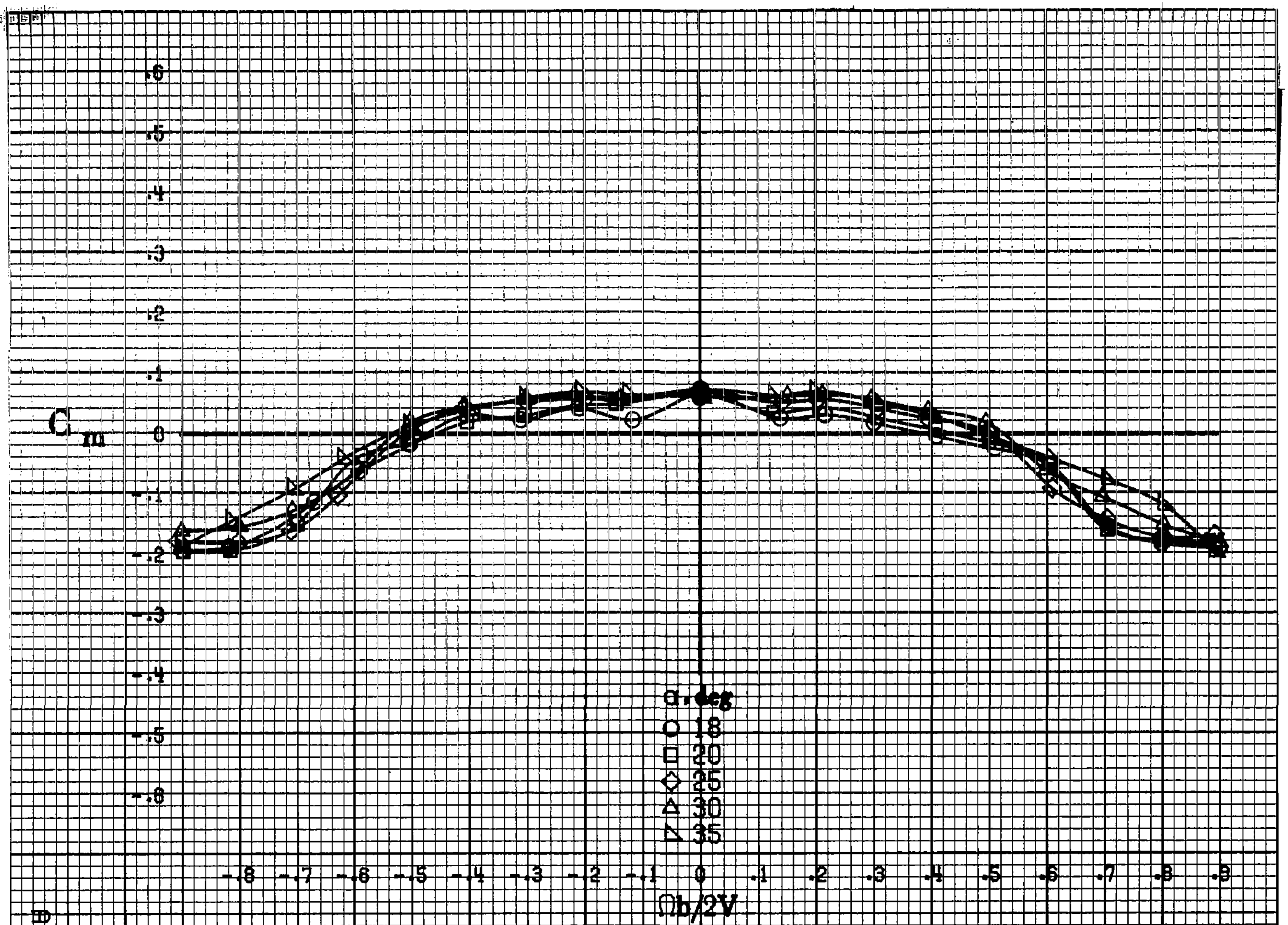

(b) α=18to35deg, SR=182.9cm(72in).
Figure A117.-Continued.

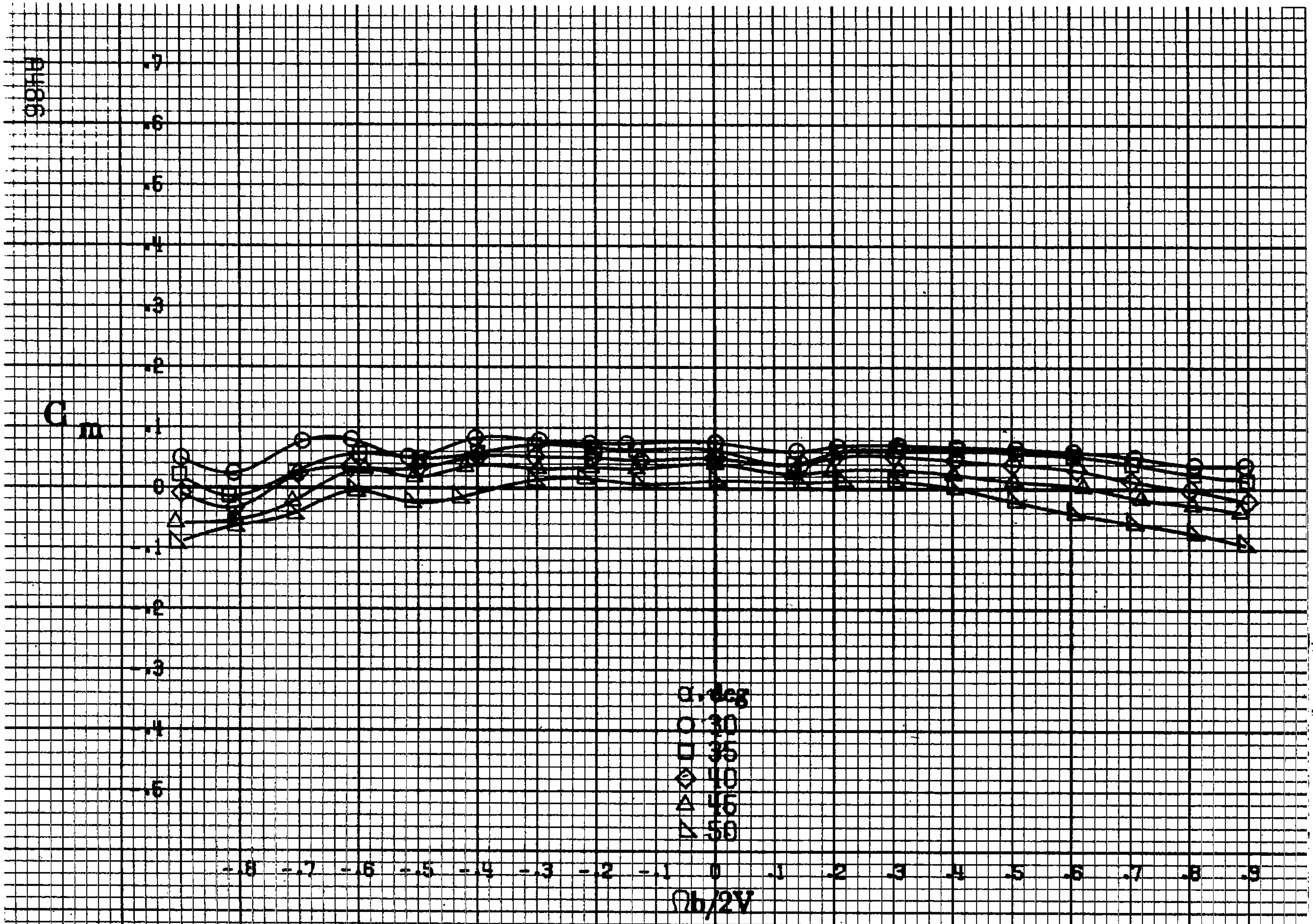

(c) α = 30 to 50 deg, SR = 0.

Figure A117. Continued.

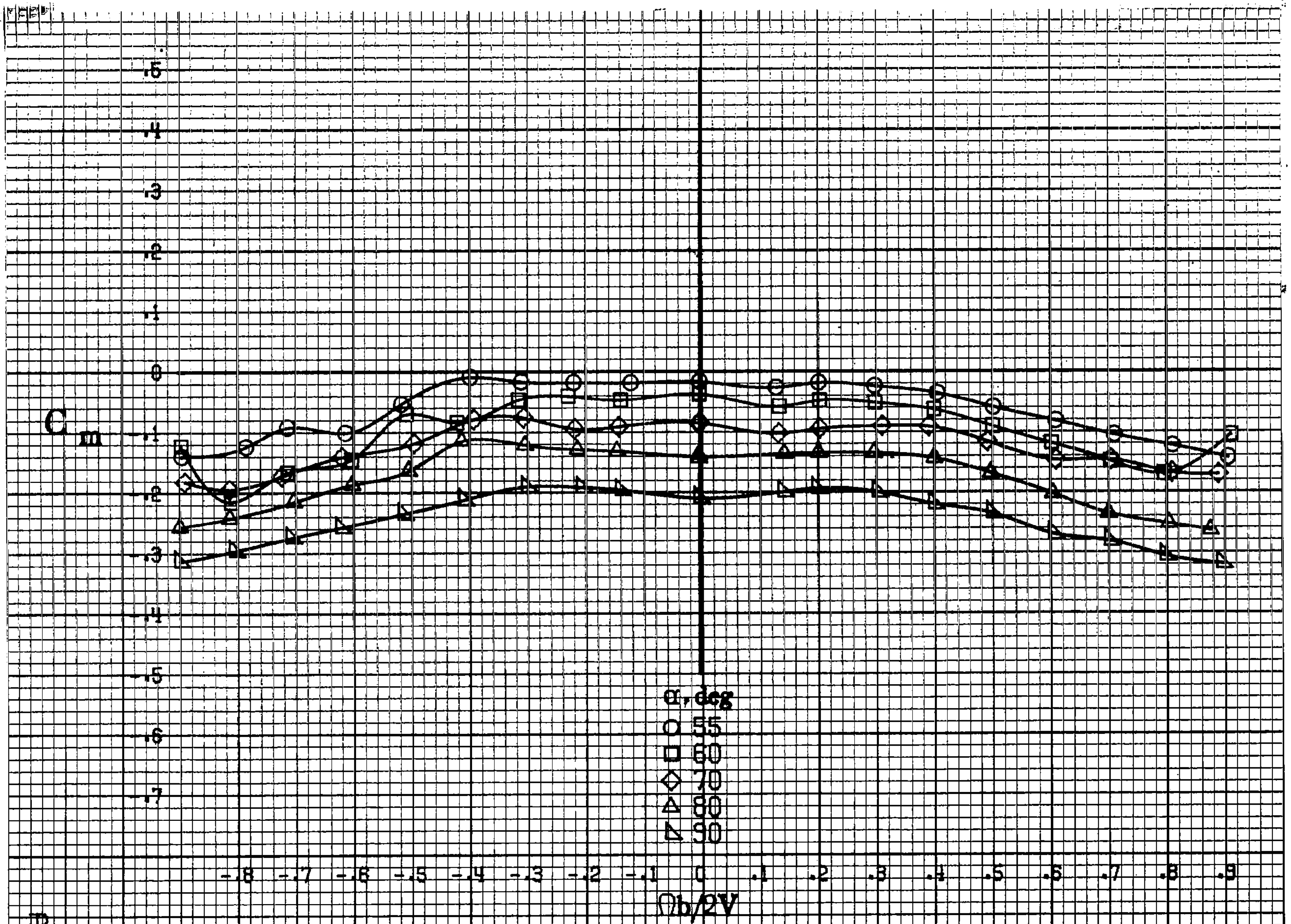

(d) α = 55 to 90 deg, SR = 0.

Figure A117.-Concluded.

A487

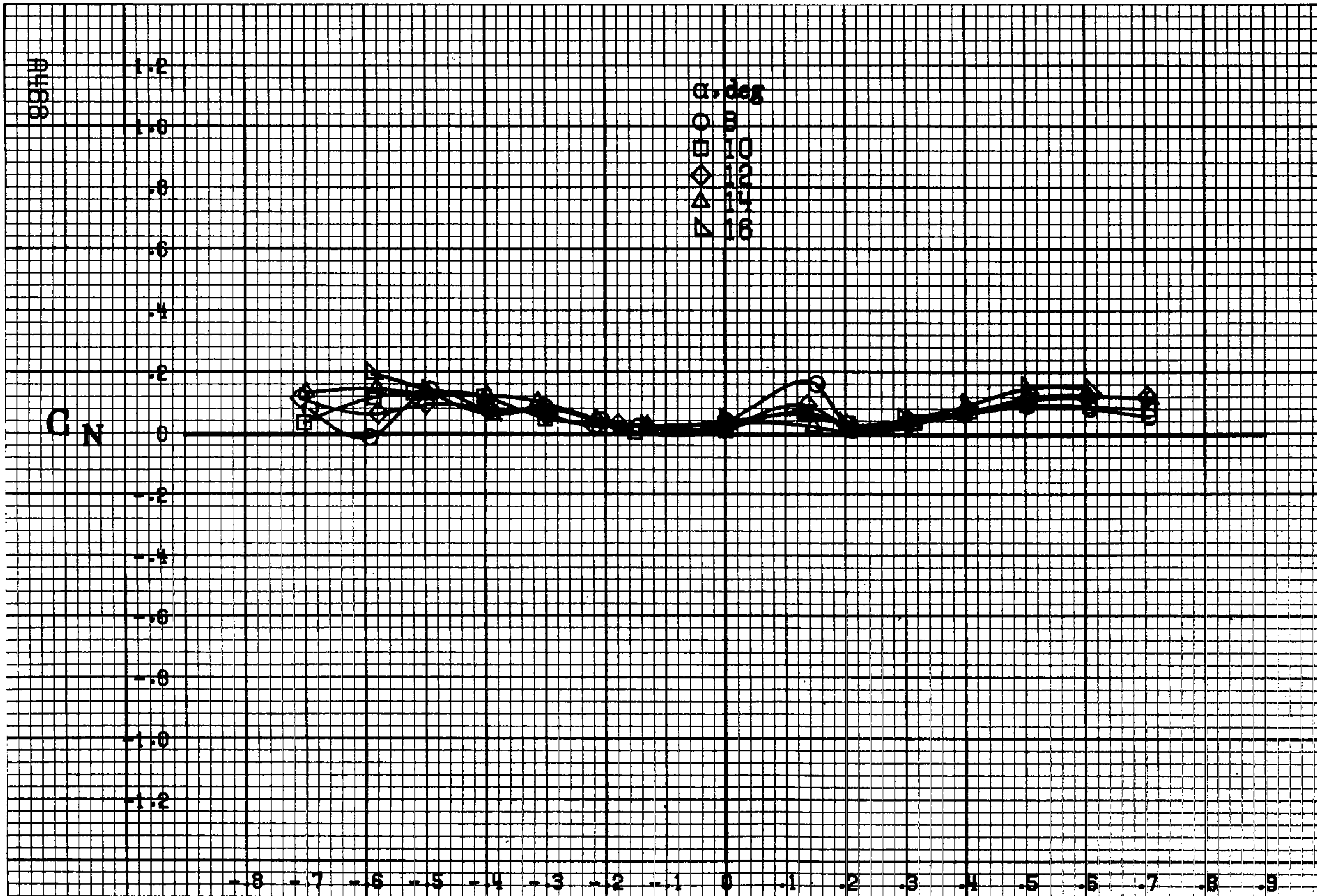

(a) $\alpha = 8$ to 16 deg, SR = 182.9 cm (72 in).

Figure A118.- Effect of rotation rate and angle of attack on normal-force coefficient for wing and horizontal tail off configuration. $\delta_a = 0°$, $\delta_e = 0°$, $\delta_r = 0°$, $\beta = 0°$.

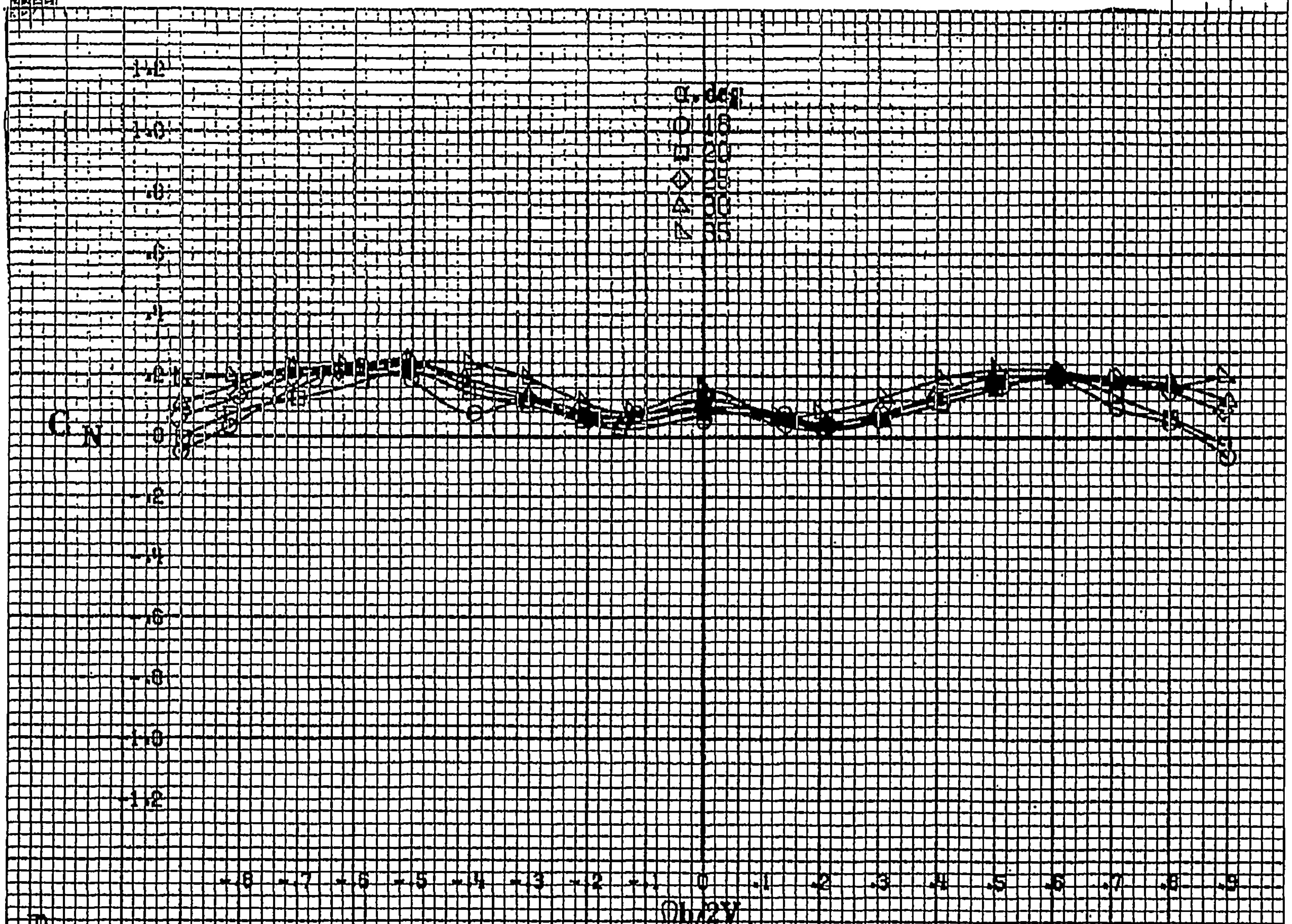

(b) α = 18 to 35 deg, SR = 182.9 cm (72 in).

Figure A118.-Continued.

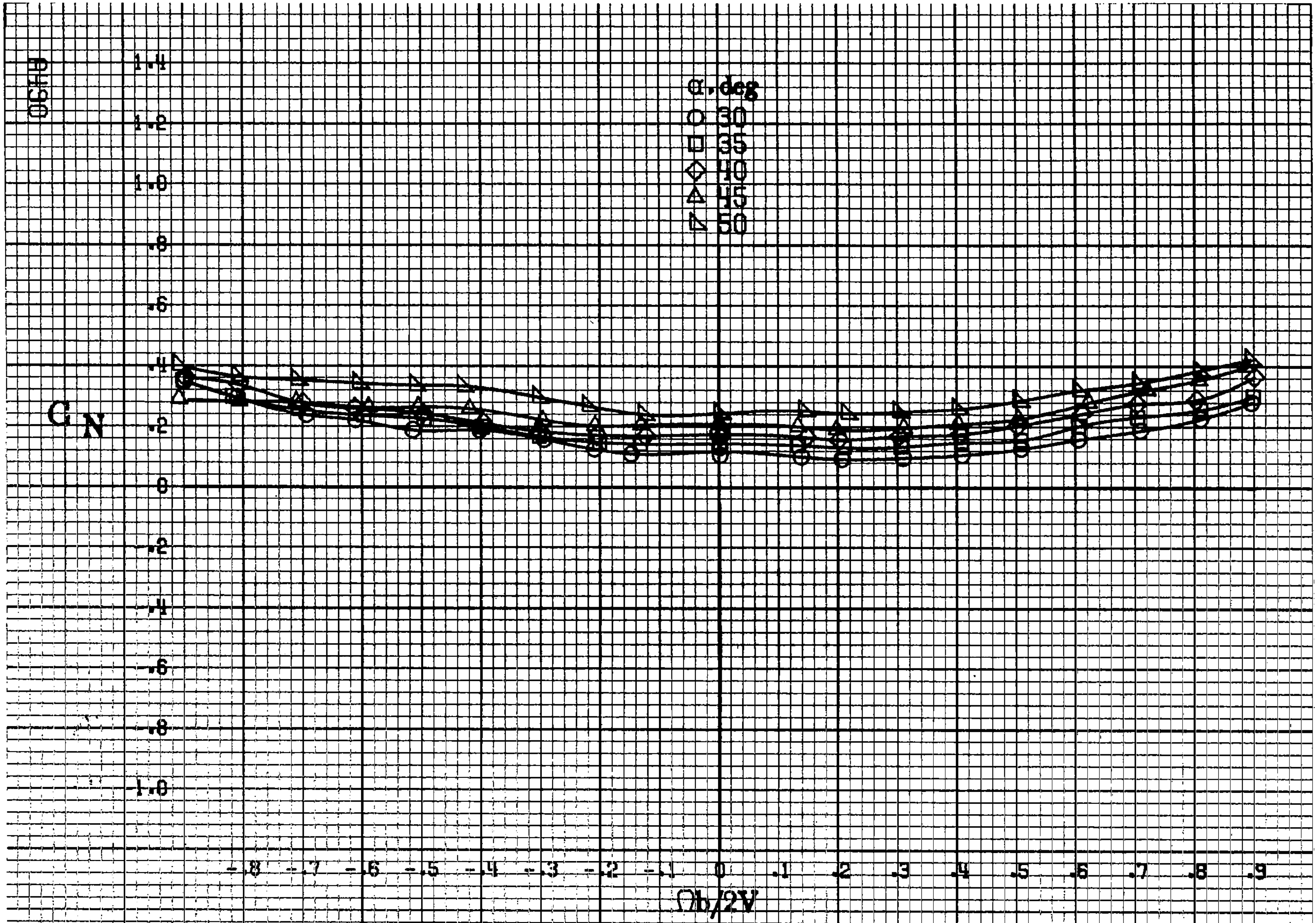

(c) α = 30 to 50 deg, SR = 0.

Figure A118.-Continued.

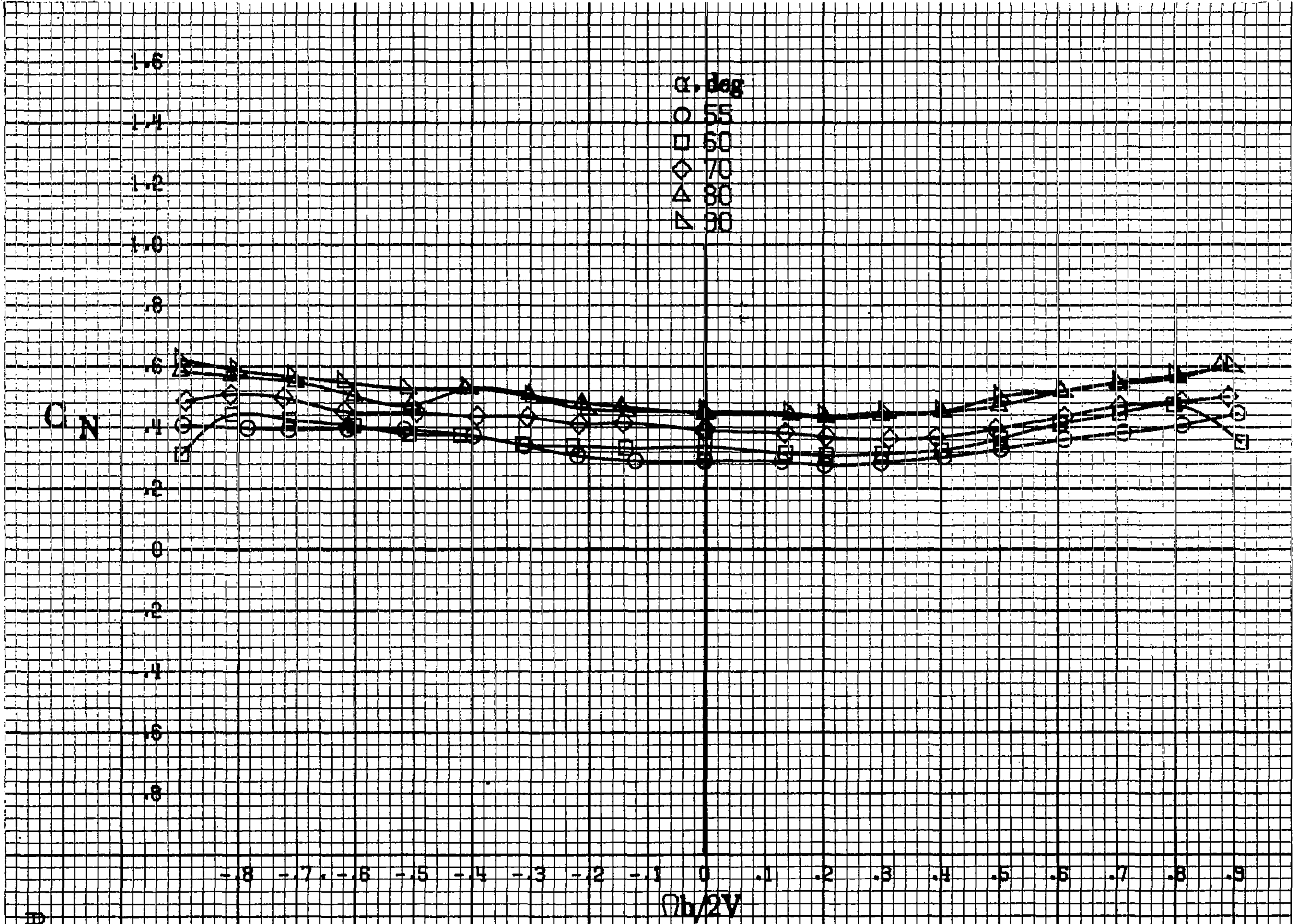

(d) α = 55 to 90 deg, SR = 0.

Figure A118.-Concluded.

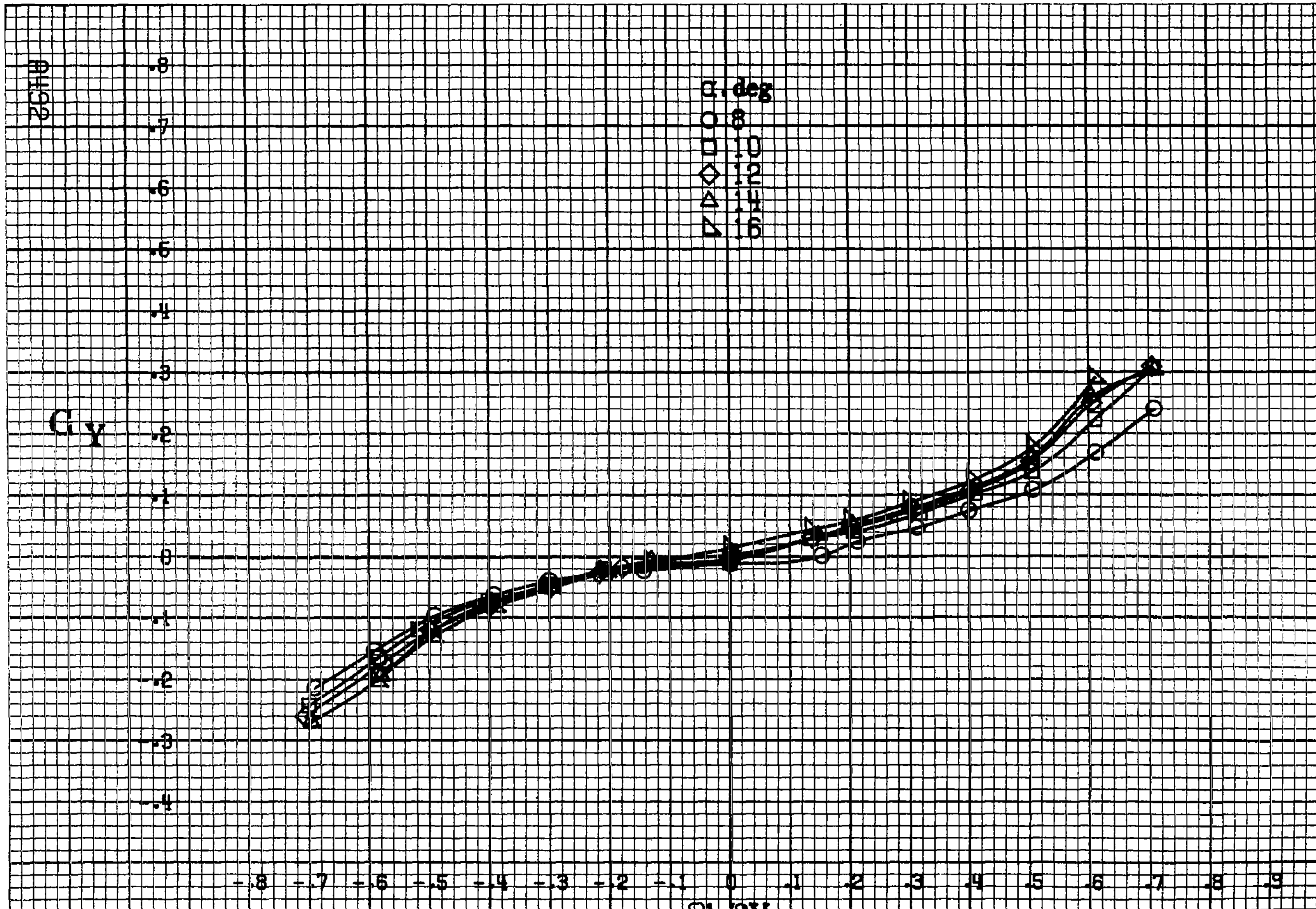

(a) α = 8 to 16 deg, SR = 182.9 cm (72 in).

Figure A119.-Effect of rotation rate and angle of attack on side-force coefficient for wing and horizontal tail off configuration. $\delta_e = 0°$, $\delta_a = 0°$, $\delta_r = 0°$, $\beta = 0°$.

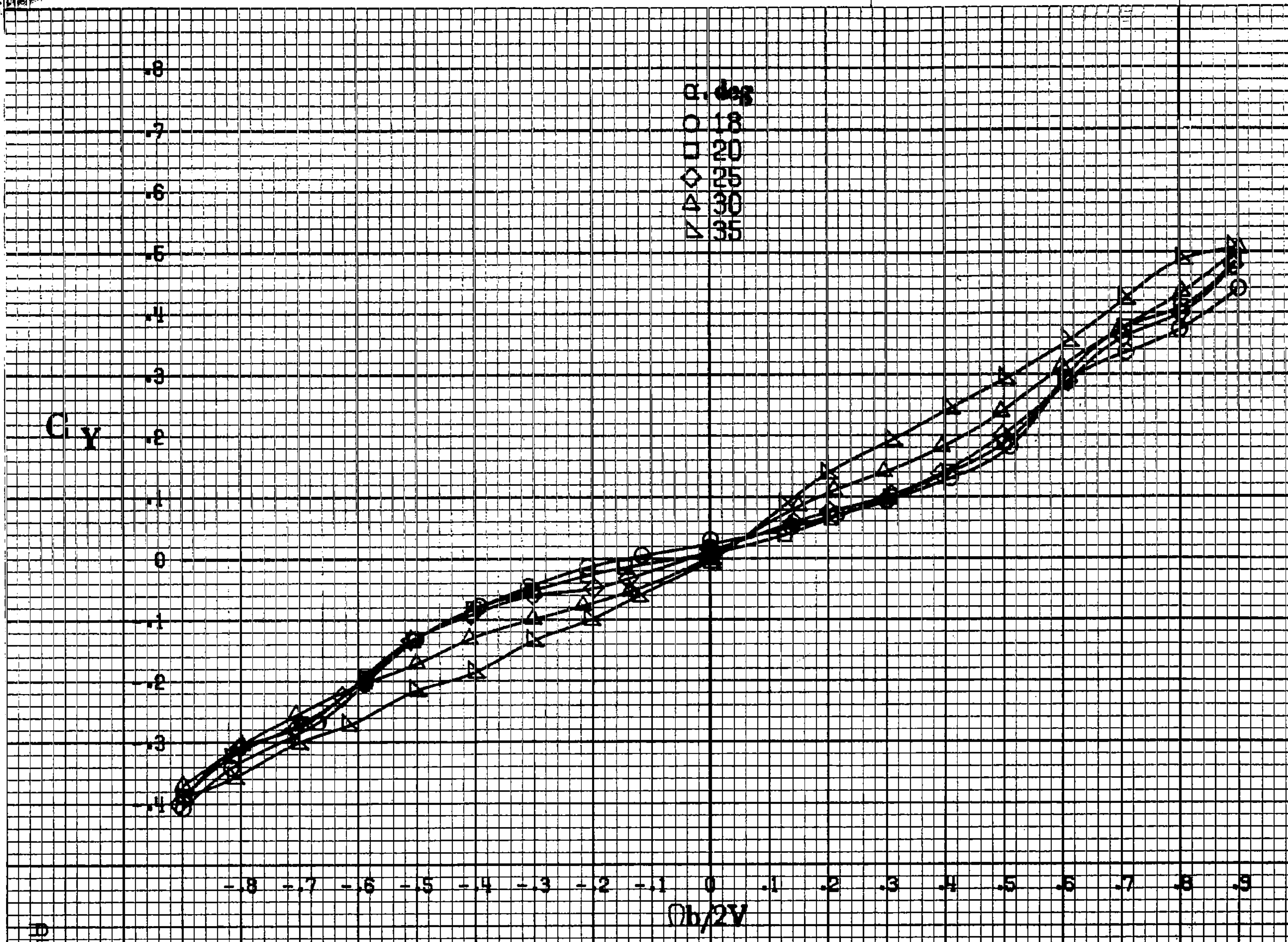

(b) α = 18 to 35 deg, SR = 182.9 cm (72 in).

Figure A119.-Continued.

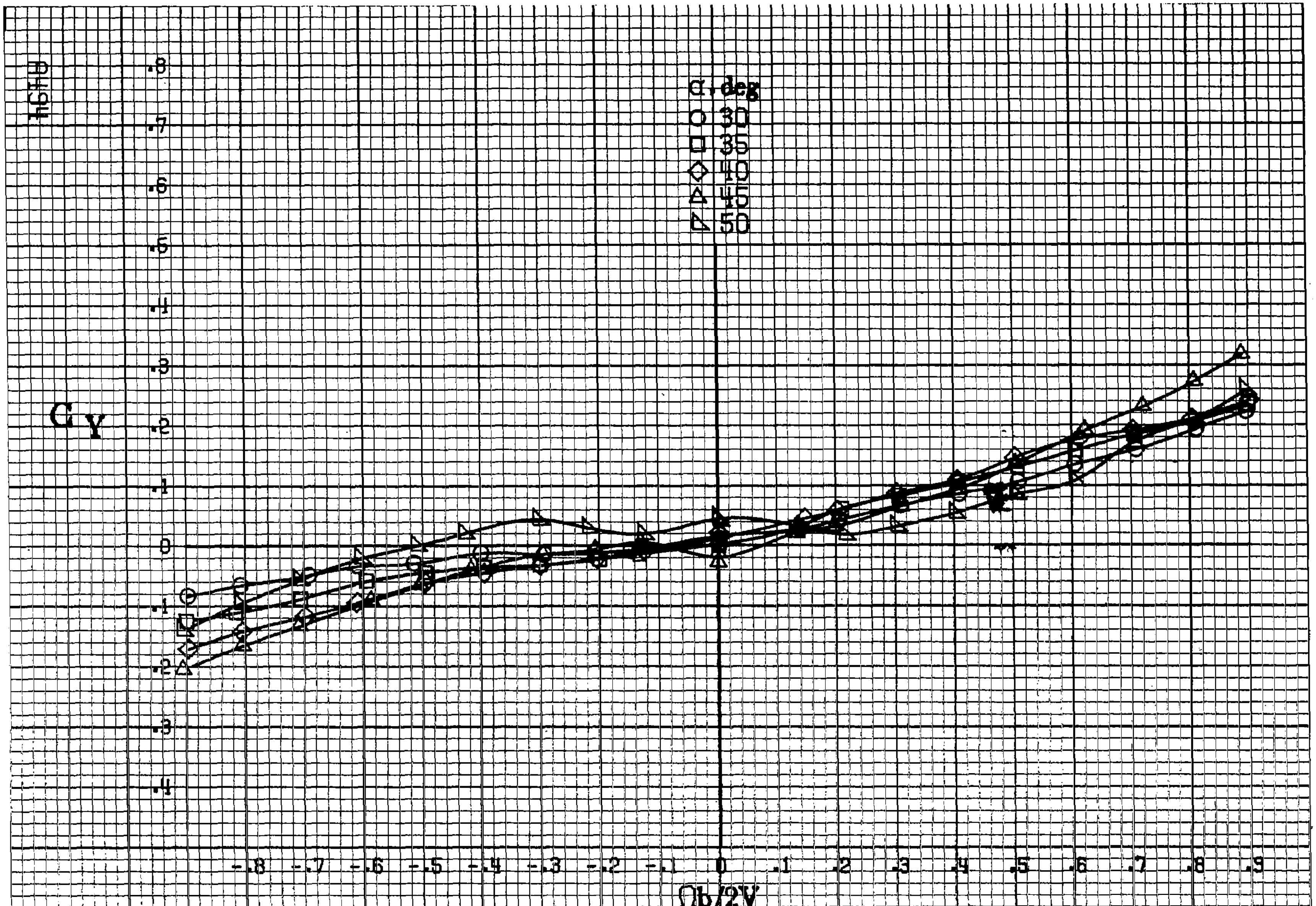

(c) α = 30 to 50 deg, SR = 0.

Figure A119.-Continued.

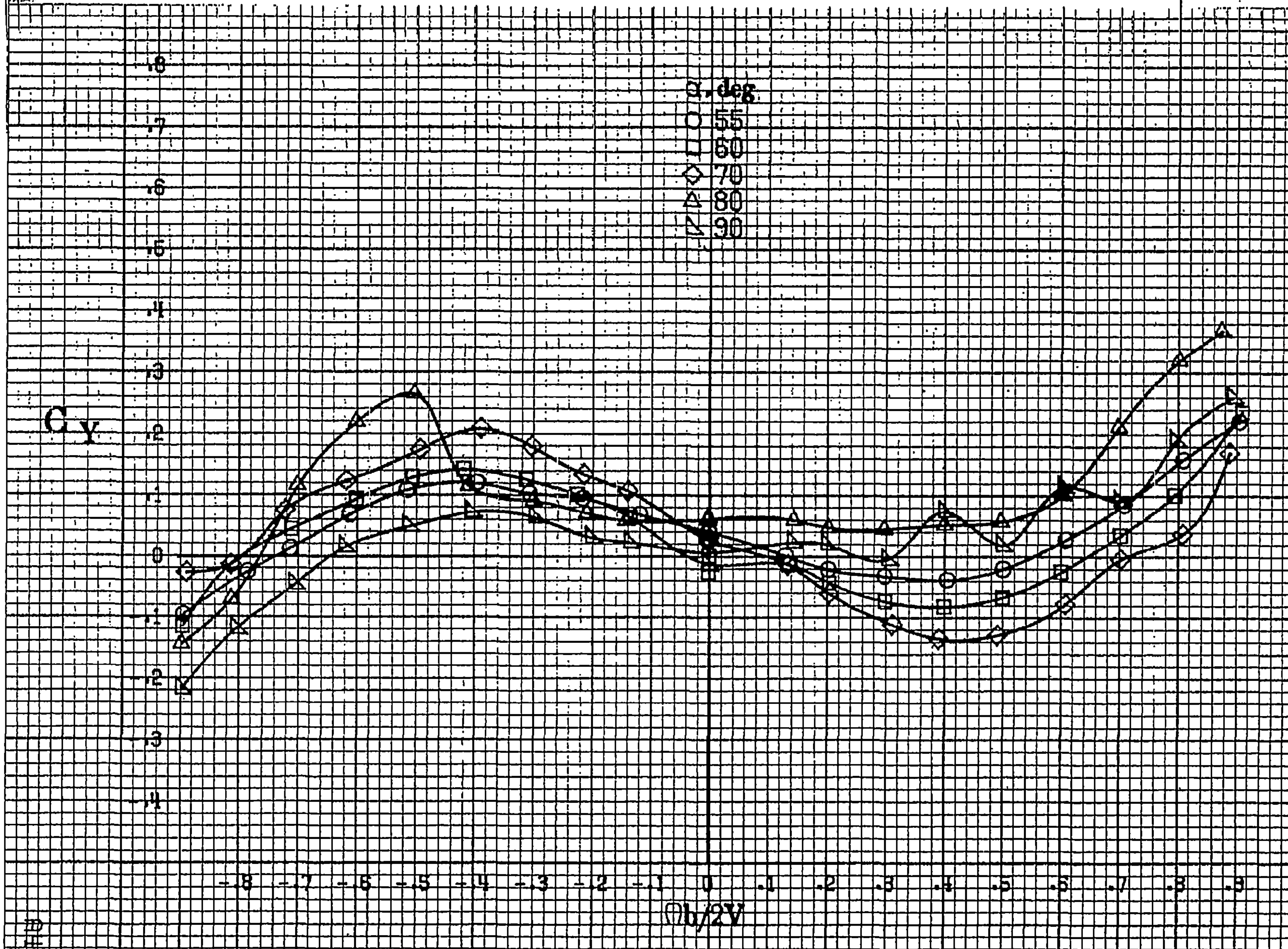

(d) α = 55 to 90 deg, SR = 0.

Figure A119.-Concluded.

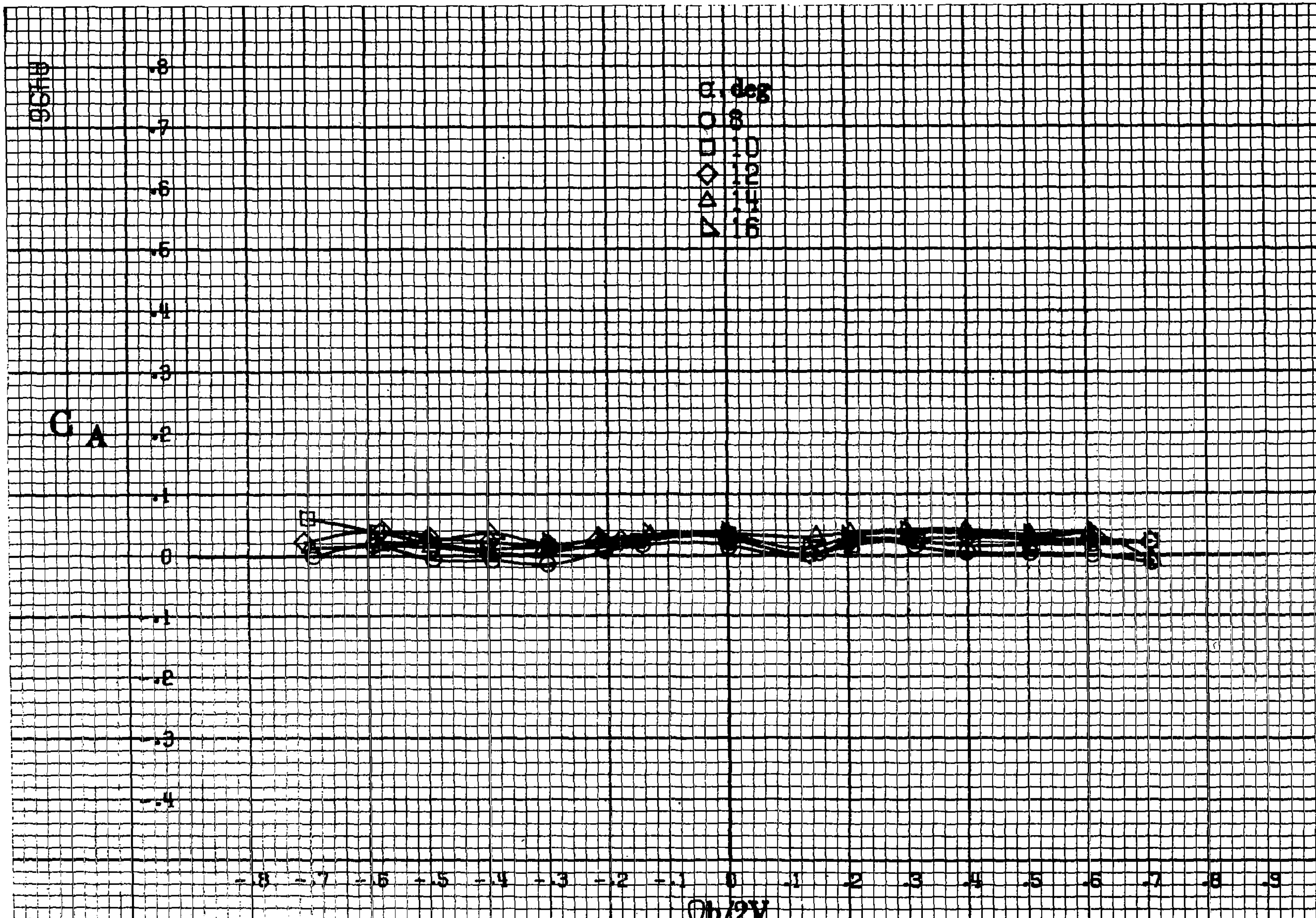

(a) $\alpha = 8$ to 16 deg, SR = 182.9 cm (72 in).

Figure A120.- Effect of rotation rate and angle of attack on axial-force coefficient for wing and horizontal tail off configuration. $\delta_e = 0°$, $\delta_a = 0°$, $\delta_r = 0°$, $\beta = 0°$.

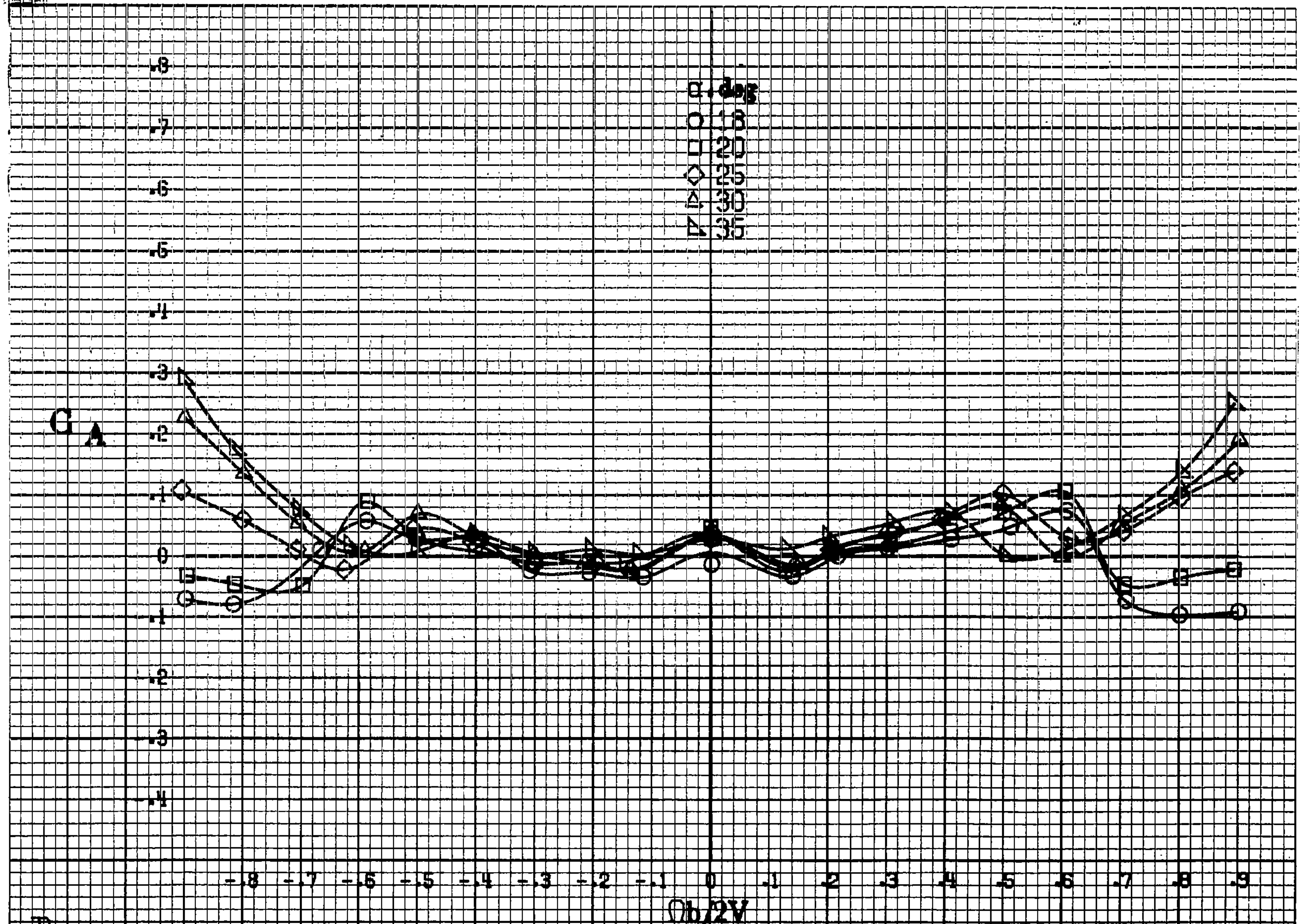

(b) α = 18 to 35 deg, SR = 182.9 cm (72 in).

Figure A120.- Continued.

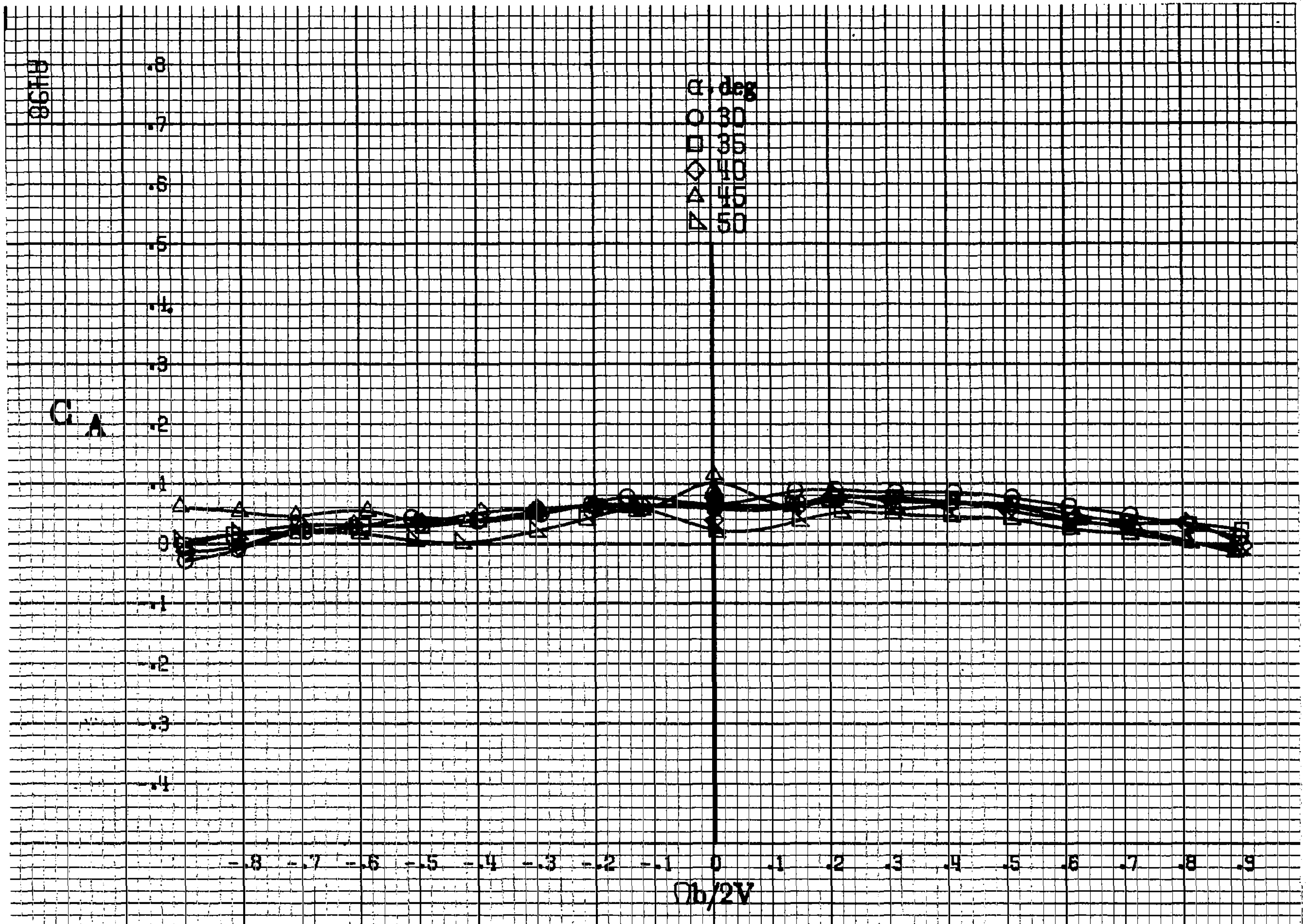

(c) α = 30 to 50 deg, SR = 0.

Figure A120. Continued.

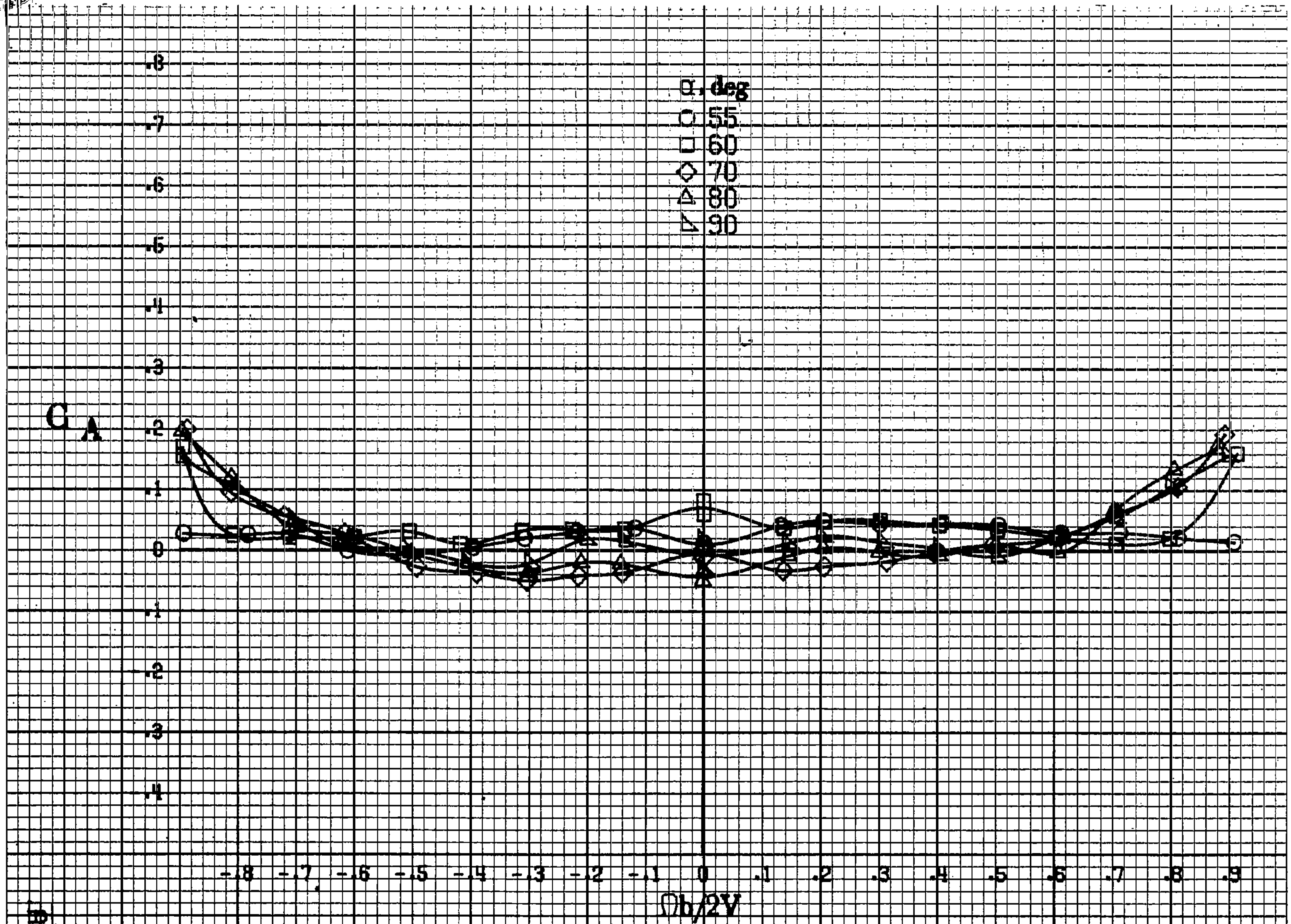

(d) $\alpha = 55$ to 90 deg, SR = 0.

Figure A120.-Concluded.

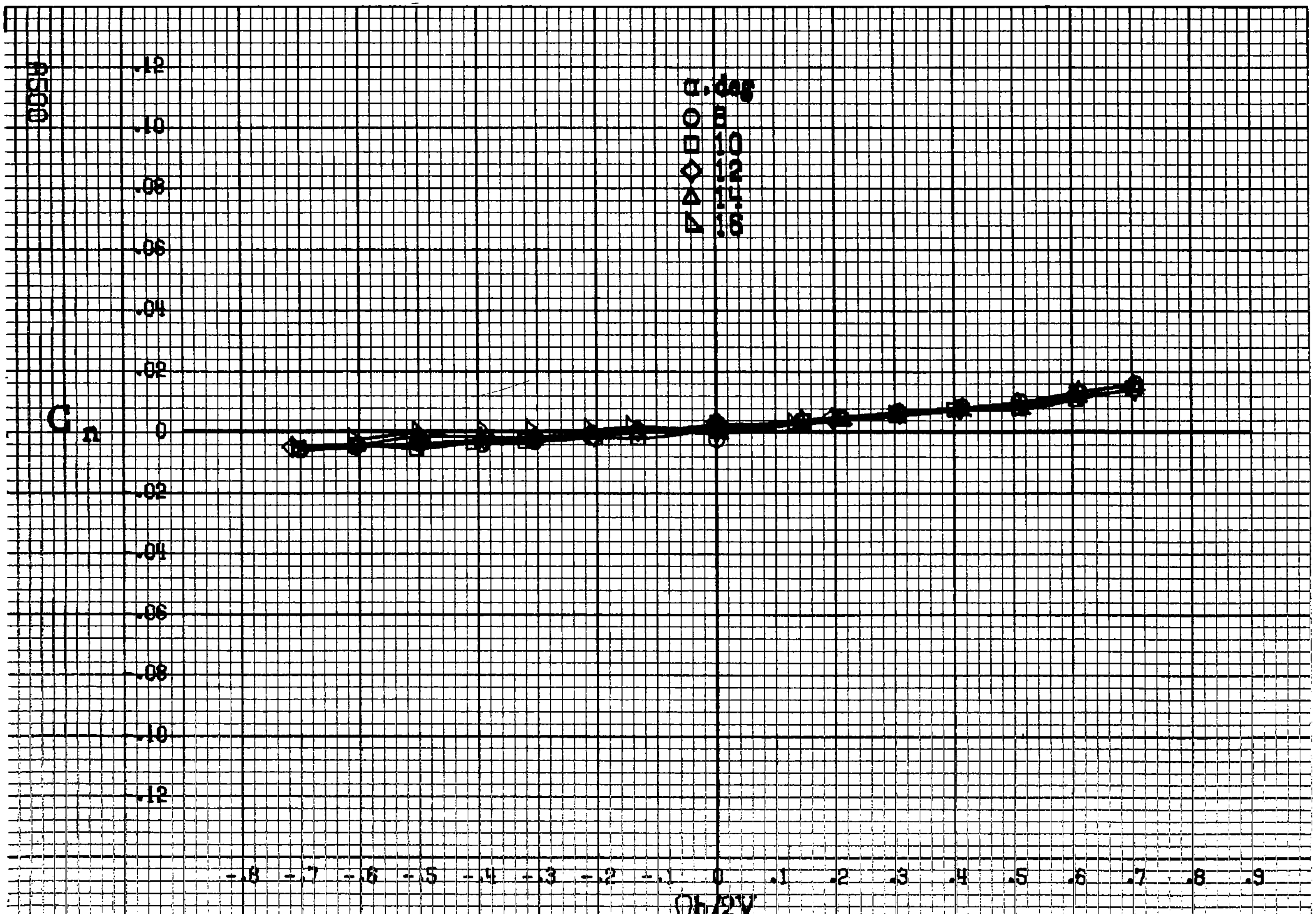

(a) $\alpha = 8$ to 16 deg, SR = 182.9 cm (72 in).

Figure A121.-Effect of rotation rate and angle of attack on yawing-moment coefficient for wing and vertical tail off configuration. $\delta_a = 0°$, $\delta_h = 0°$, $\delta_r = 0°$, $\beta = 0°$.

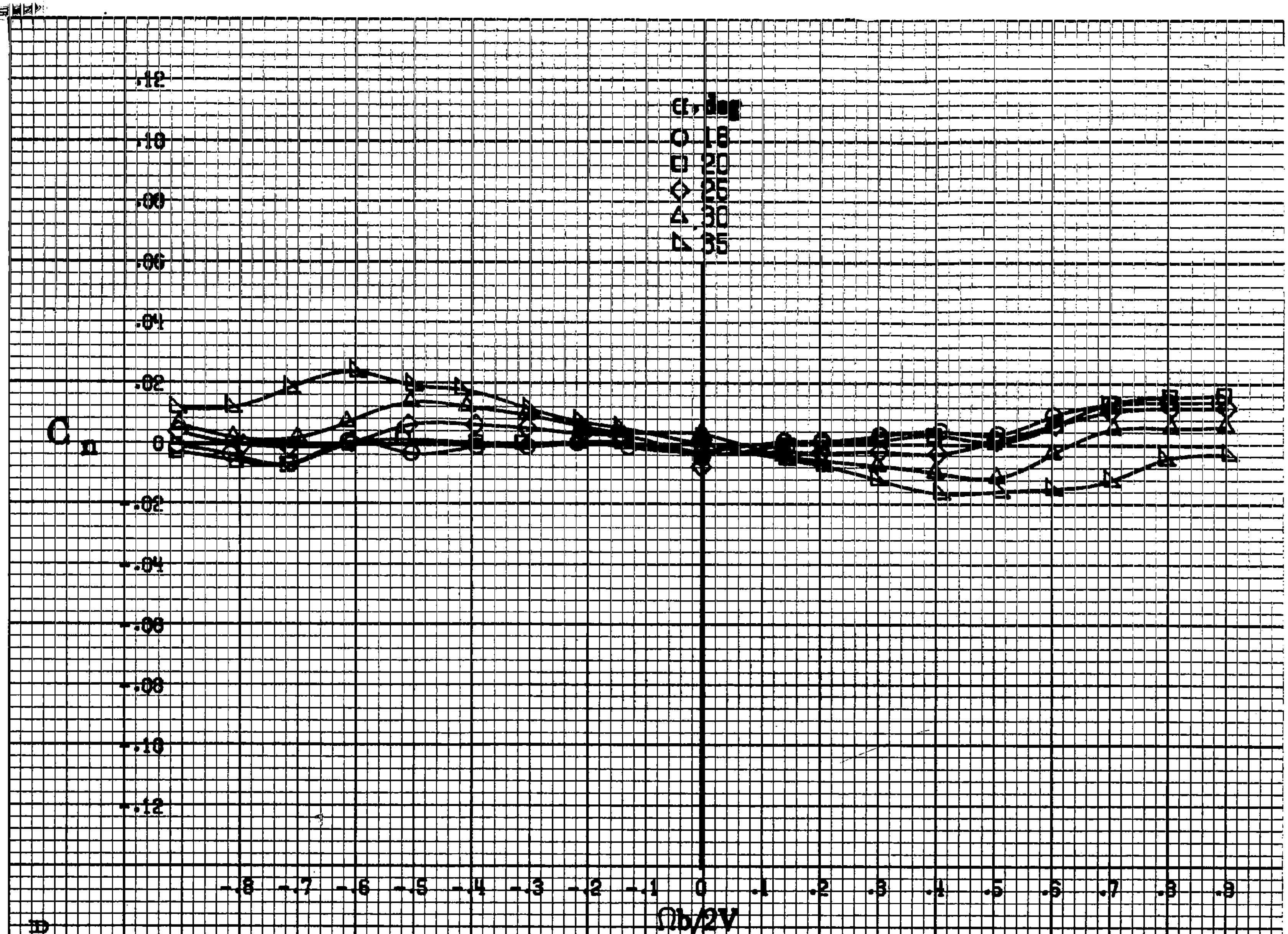

(b) α = 18 to 35 deg, SR = 182.9 cm (72 in).

Figure A121.-Continued.

A501

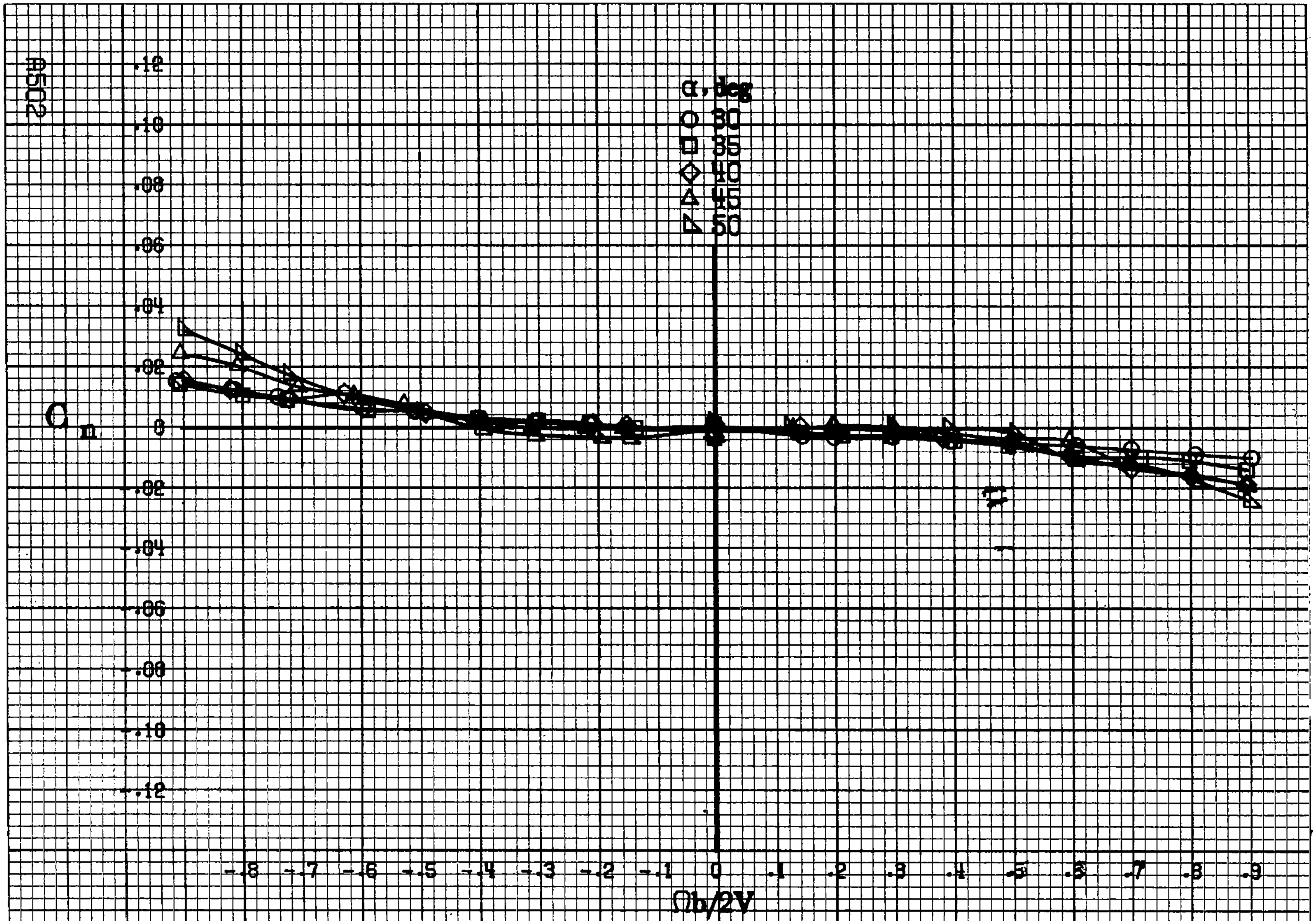

(c) α = 30 to 50 deg, SR = 0.

Figure A121.-Continued.

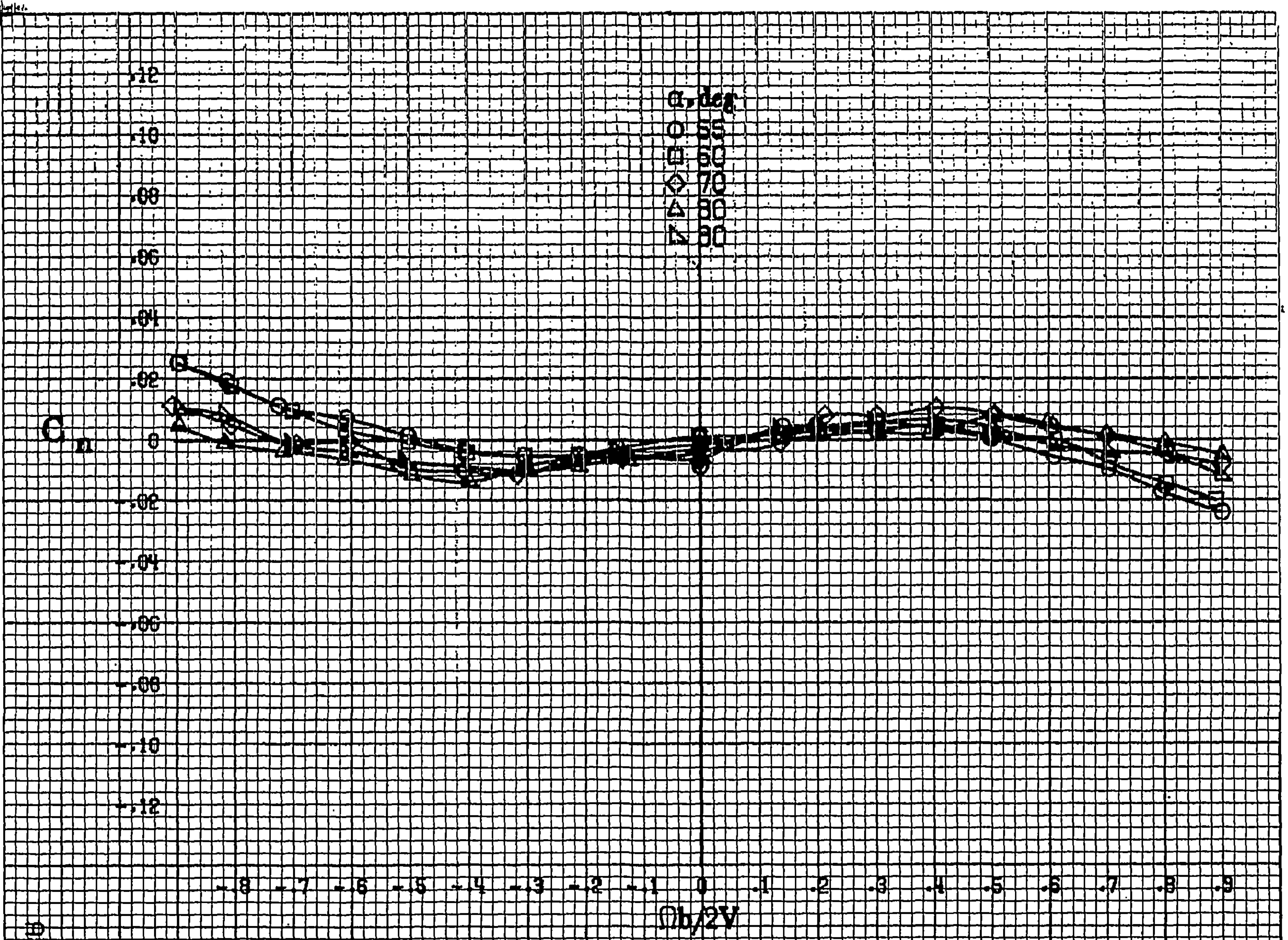

(d) α = 55 to 90 deg, SR = 0.

Figure A121.-Concluded.

A503

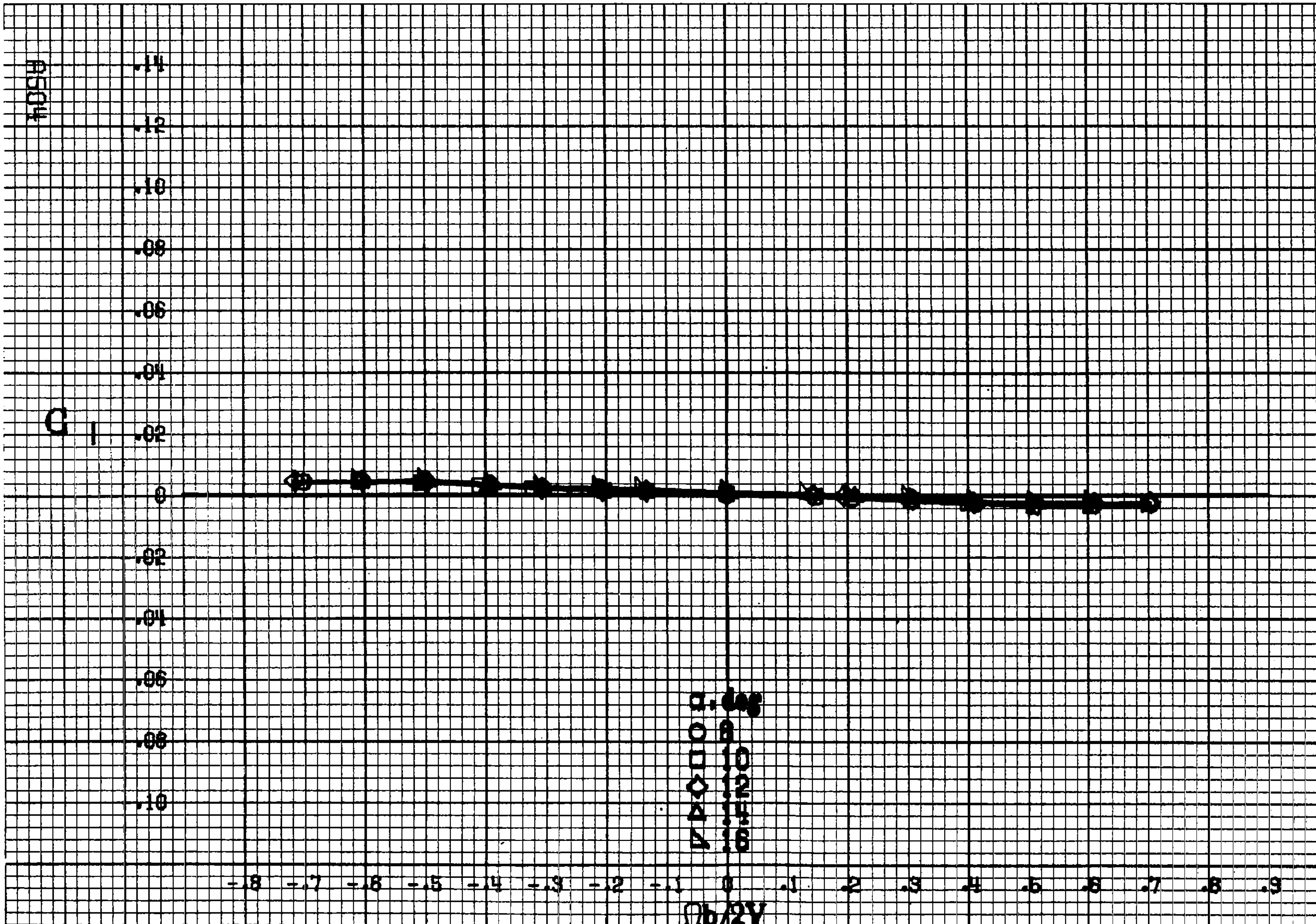

(a) $\alpha = 8$ to 16 deg, SR = 182.9 cm (72 in).

Figure A122.-Effect of rotation rate and angle of attack on rolling-moment coefficient for wing and vertical tail off configuration. $\delta_e = 0°$, $\delta_a = 0°$, $\delta_r = 0°$, $\beta = 0°$.

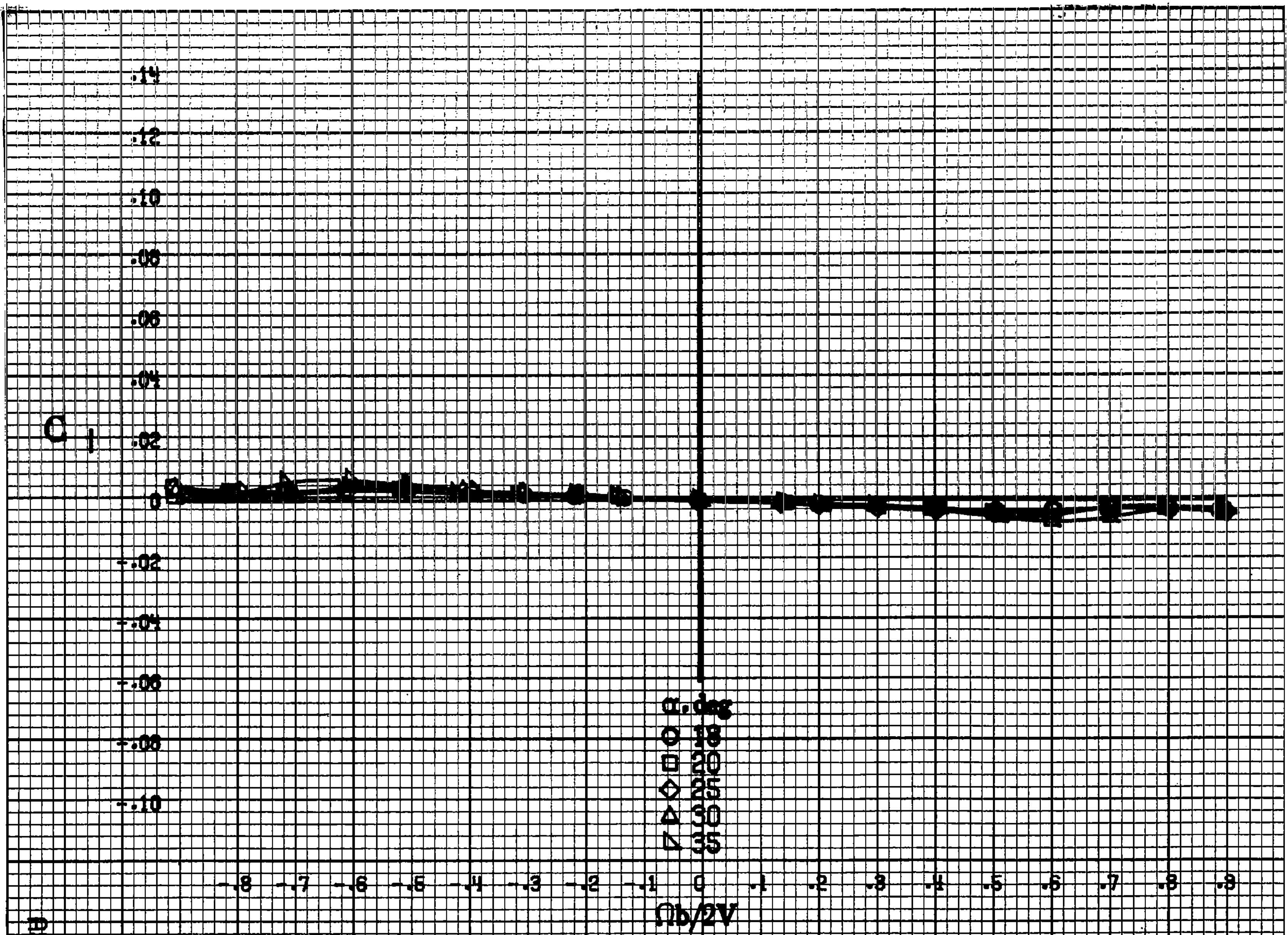

(b) $\alpha = 18$ to 35 deg, SR = 182.9 cm (72 in).

Figure A122.-Continued.

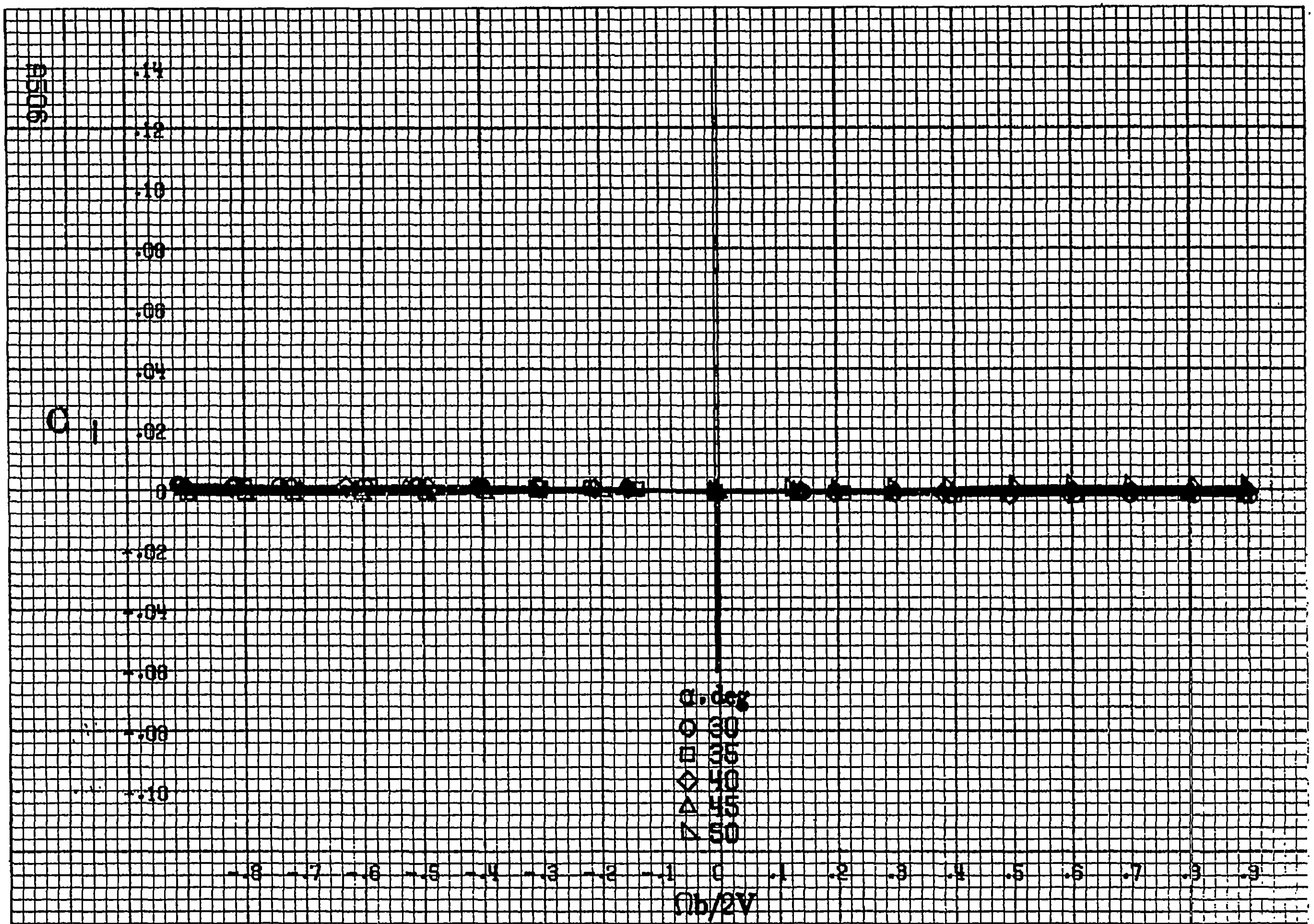

(c) α = 30 to 50 deg, SR = 0.
Figure A122.-Continued.

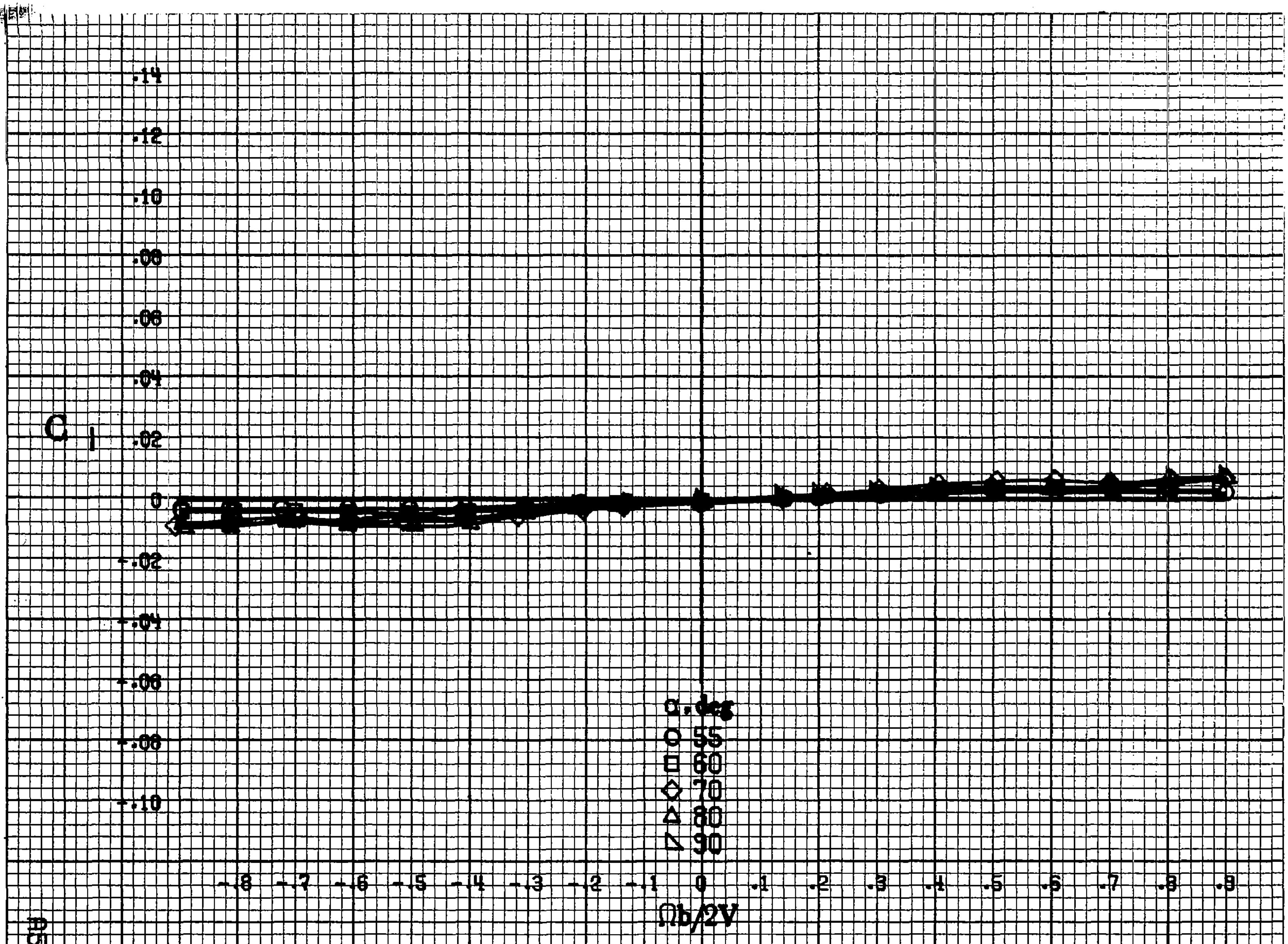

(d) α = 55 to 90 deg, SR = 0.

Figure A122.-Concluded.

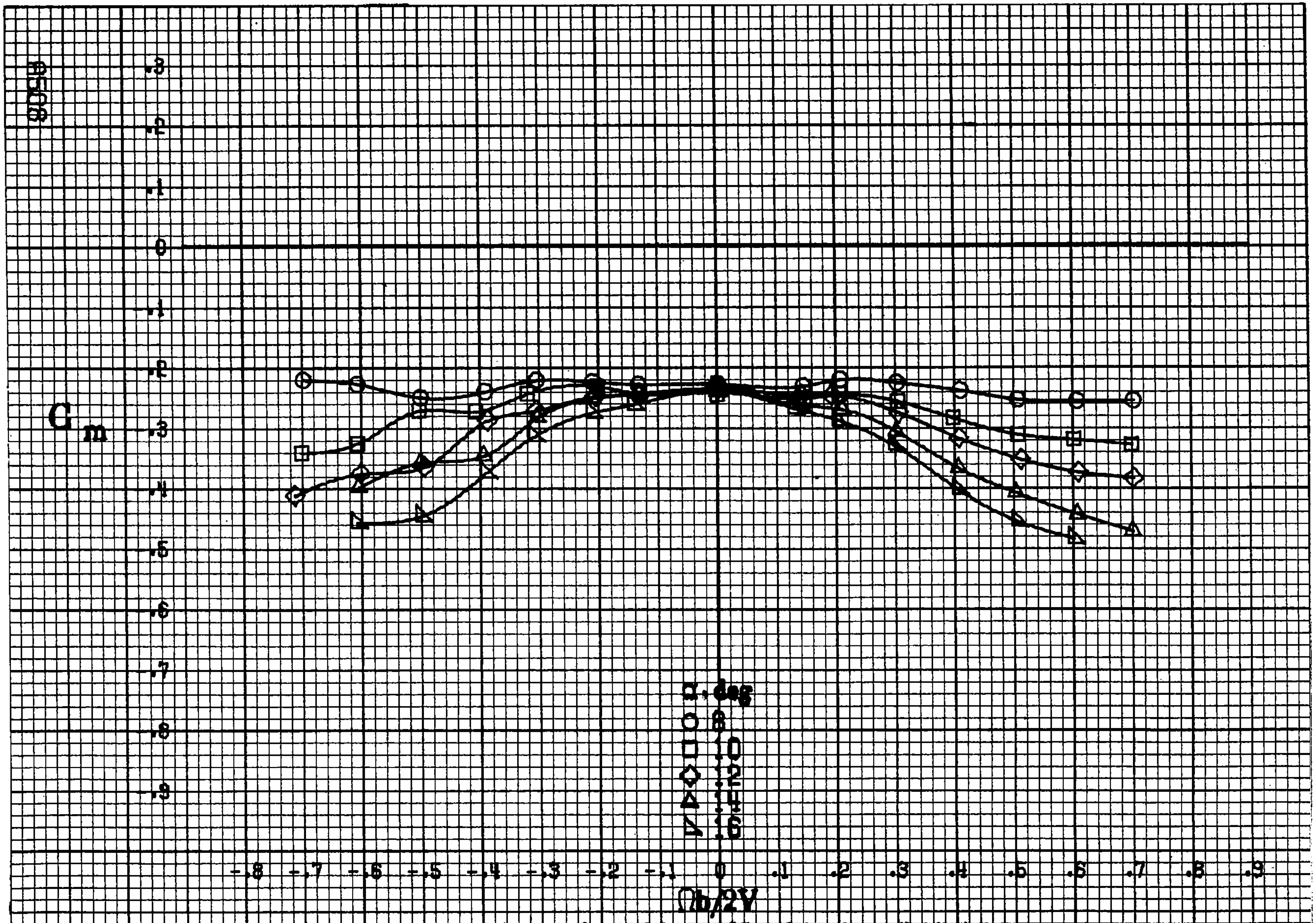

(a) α = 8 to 16 deg, SR = 182.9 cm (72 in).

Figure A128.- Effect of rotation rate and angle of attack on pitching-moment coefficient for wing and vertical tail off configuration. $\delta_e = 0°$, $\delta_a = 0°$, $\delta_r = 0°$, $\beta = 0°$.

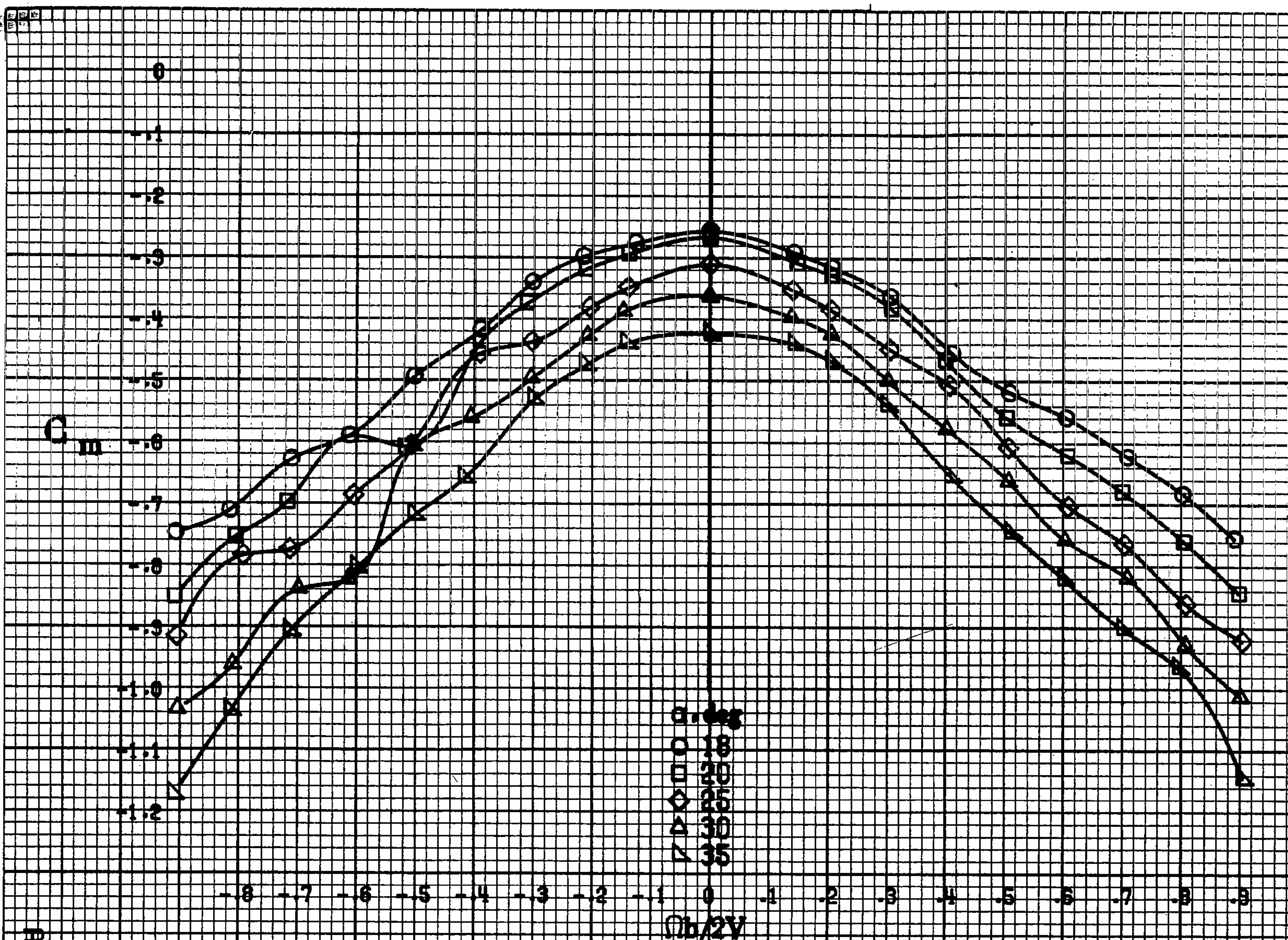

(b) α = 18 to 35 deg, SR = 182.9 cm (72 in).

Figure A123.-Continued.

A509

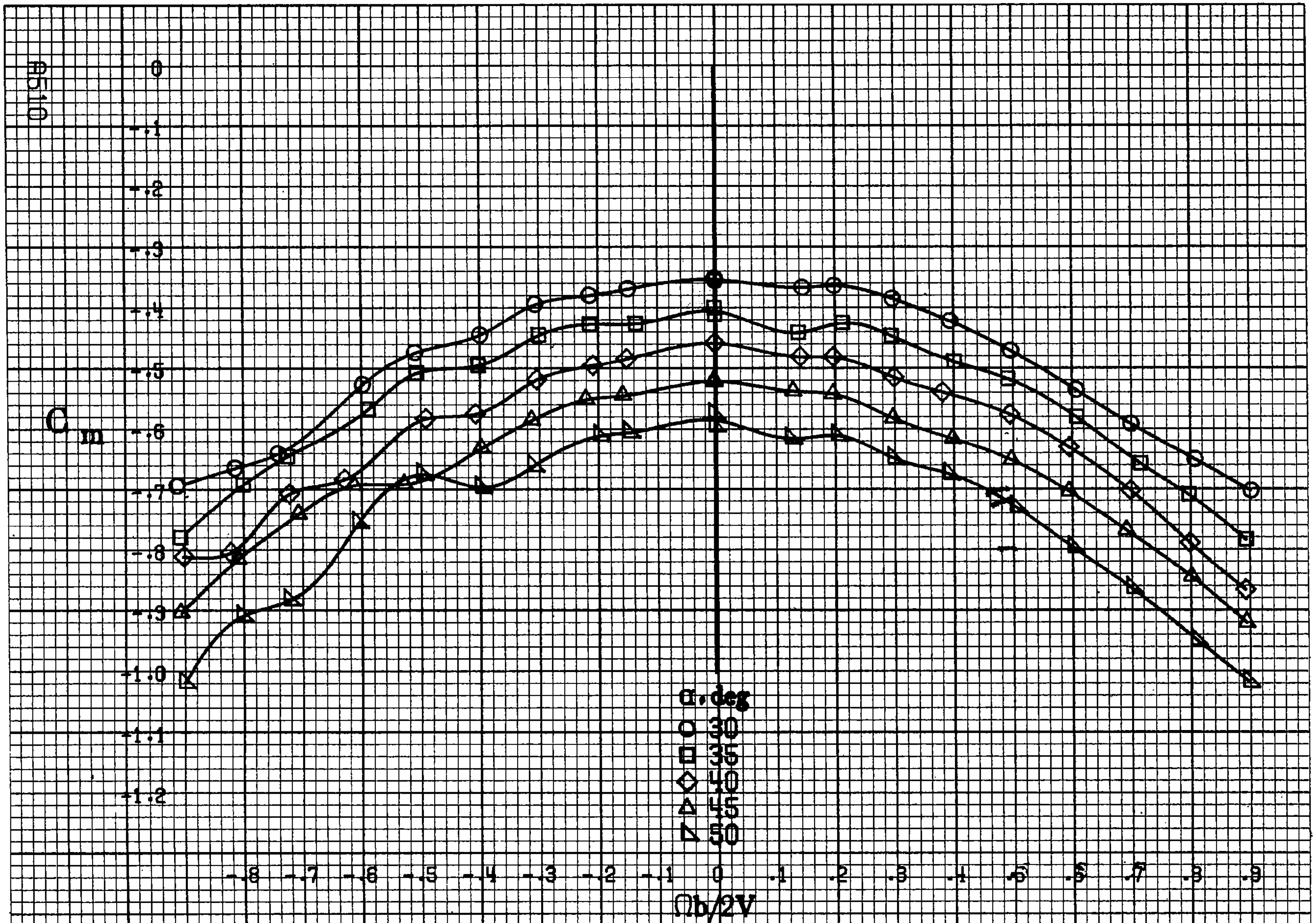

(c) α = 30 to 50 deg, SR = 0.
Figure A128.-Continued.

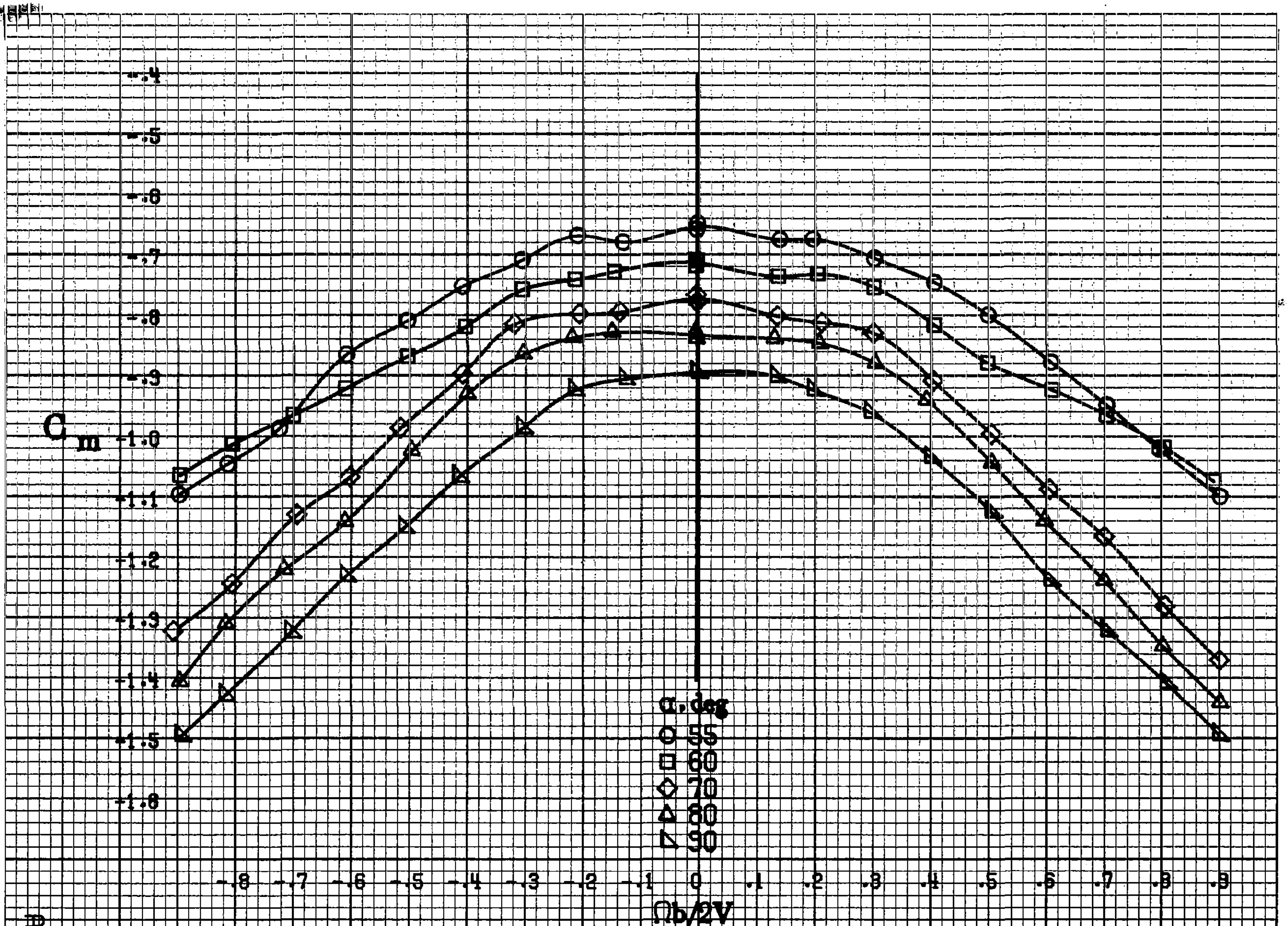

(d) α = 55 to 90 deg, SR = 0.

Figure A123.-Concluded.

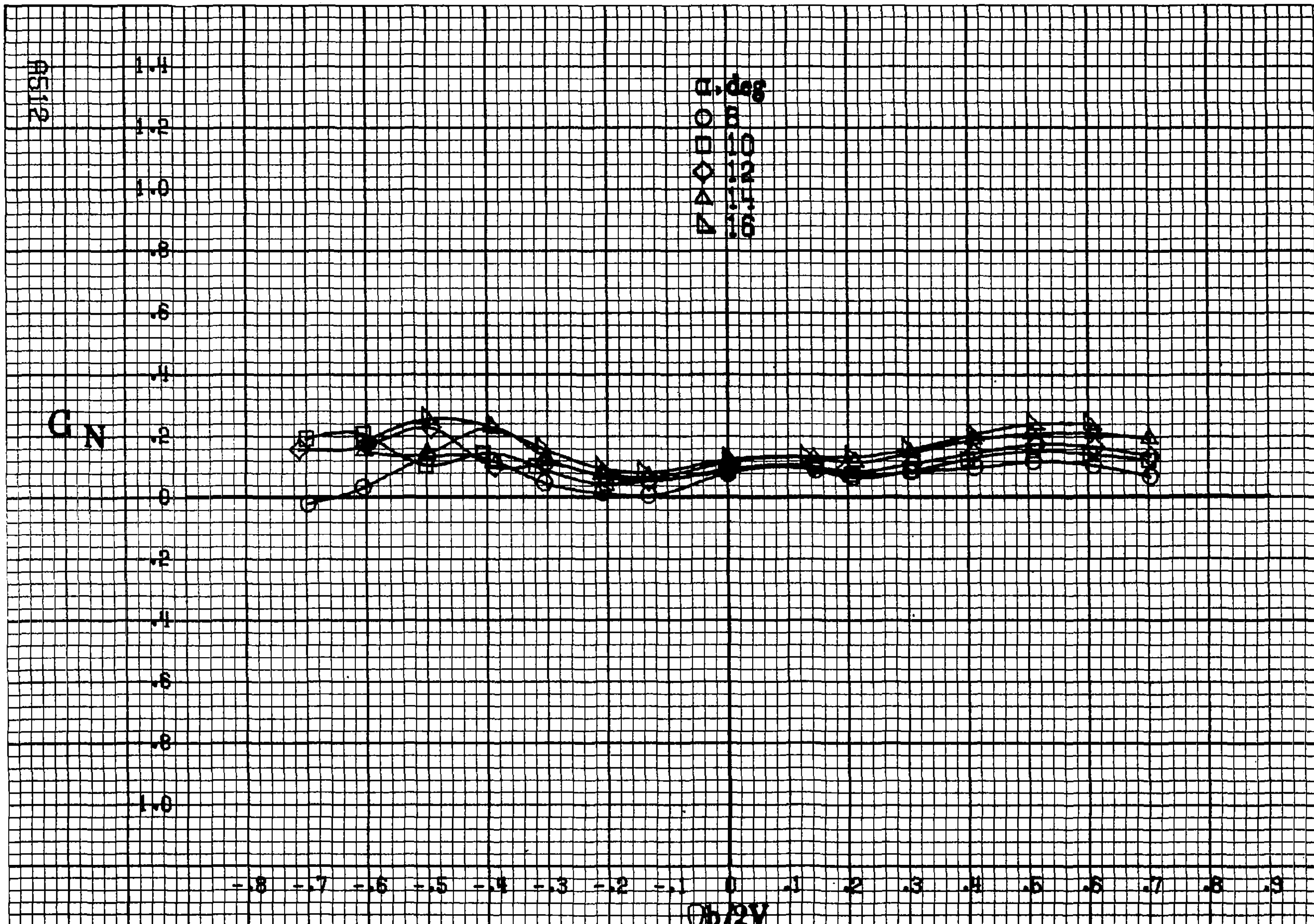

(a) $\alpha = 8$ to 16 deg, SR = 182.9 cm (72 in).

Figure A124.-Effect of rotation rate and angle of attack on normal-force coefficient for wing and vertical tail off configuration. $\delta_e = 0°$, $\delta_a = 0°$, $\delta_r = 0°$, $\beta = 0°$.

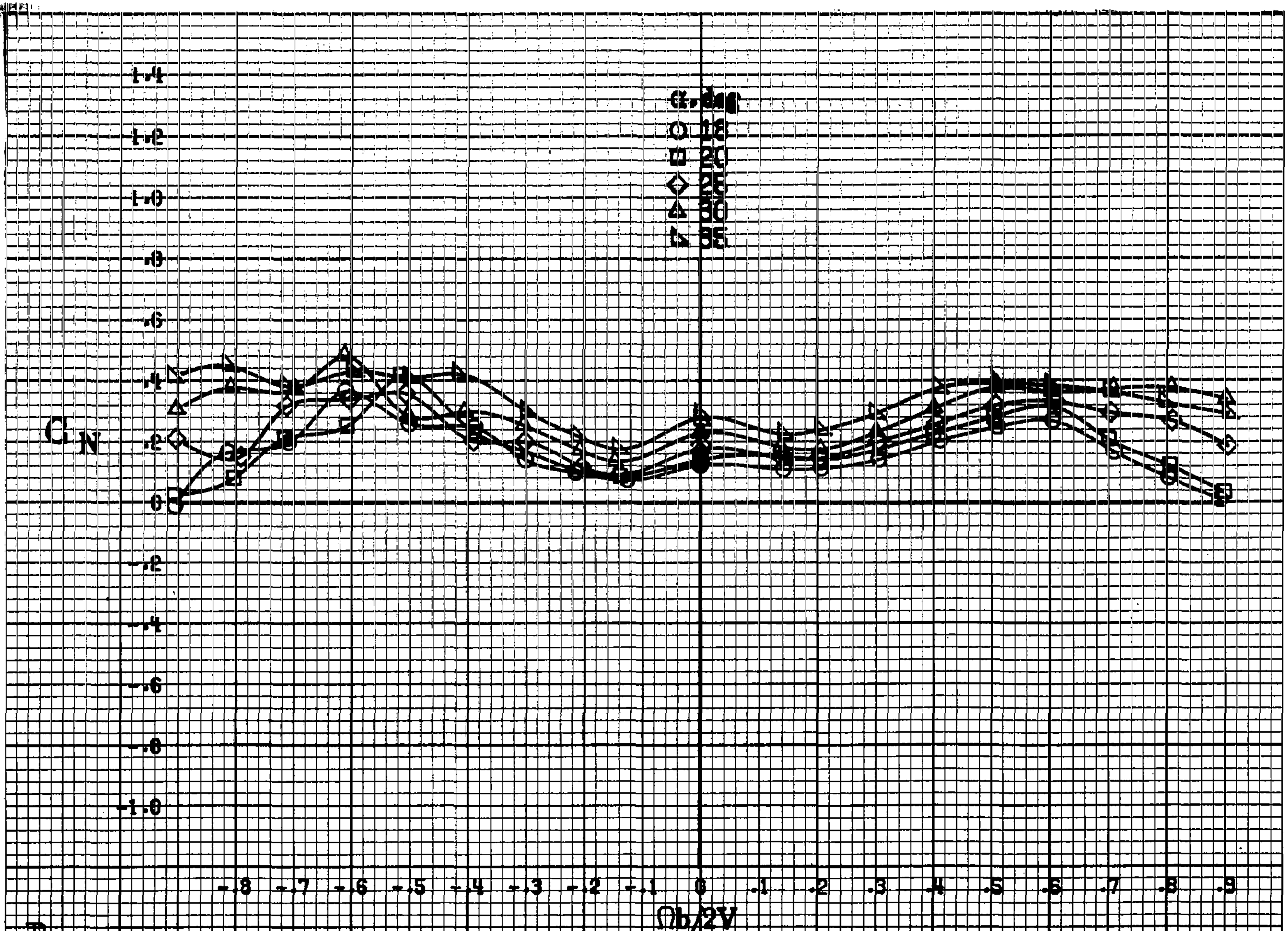

(b) α = 18 to 35 deg, SR = 182.9 cm (72 in).

Figure A124.- Continued.

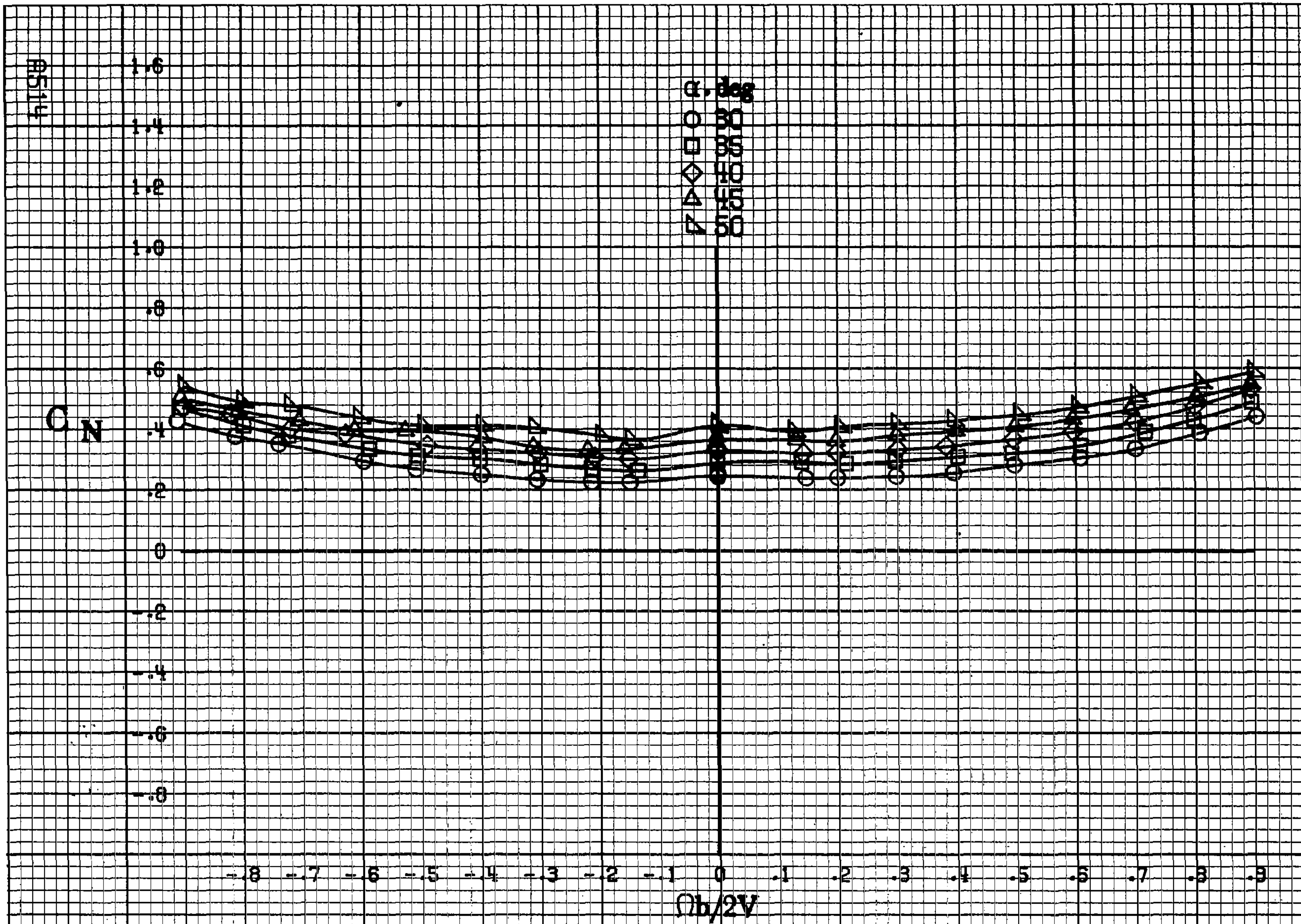

(c) α = 30 to 50 deg, SR = 0.

Figure A124.-Continued.

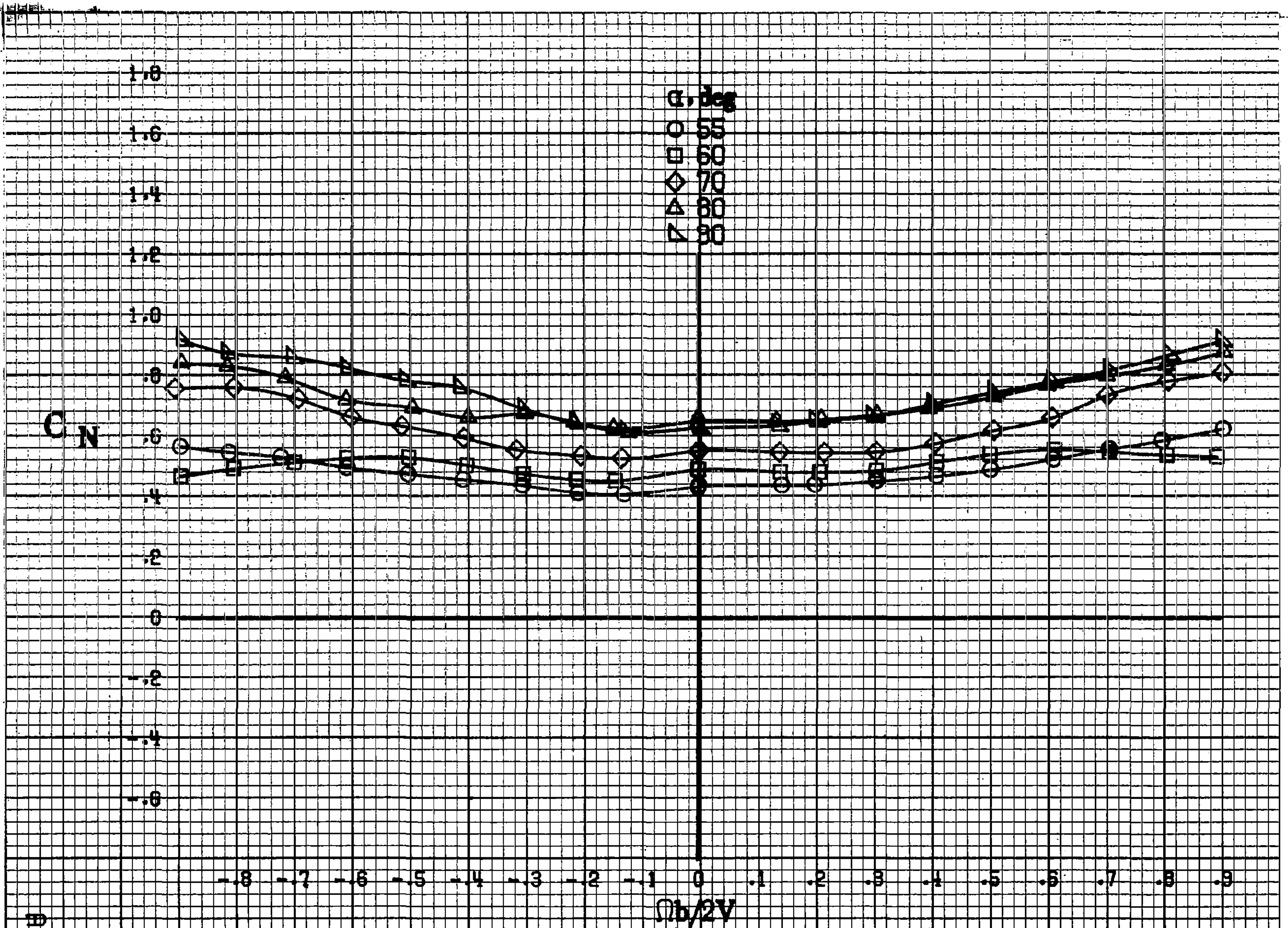

(d) α = 55 to 90 deg, SR = 0.

Figure A124.-Concluded.

A515

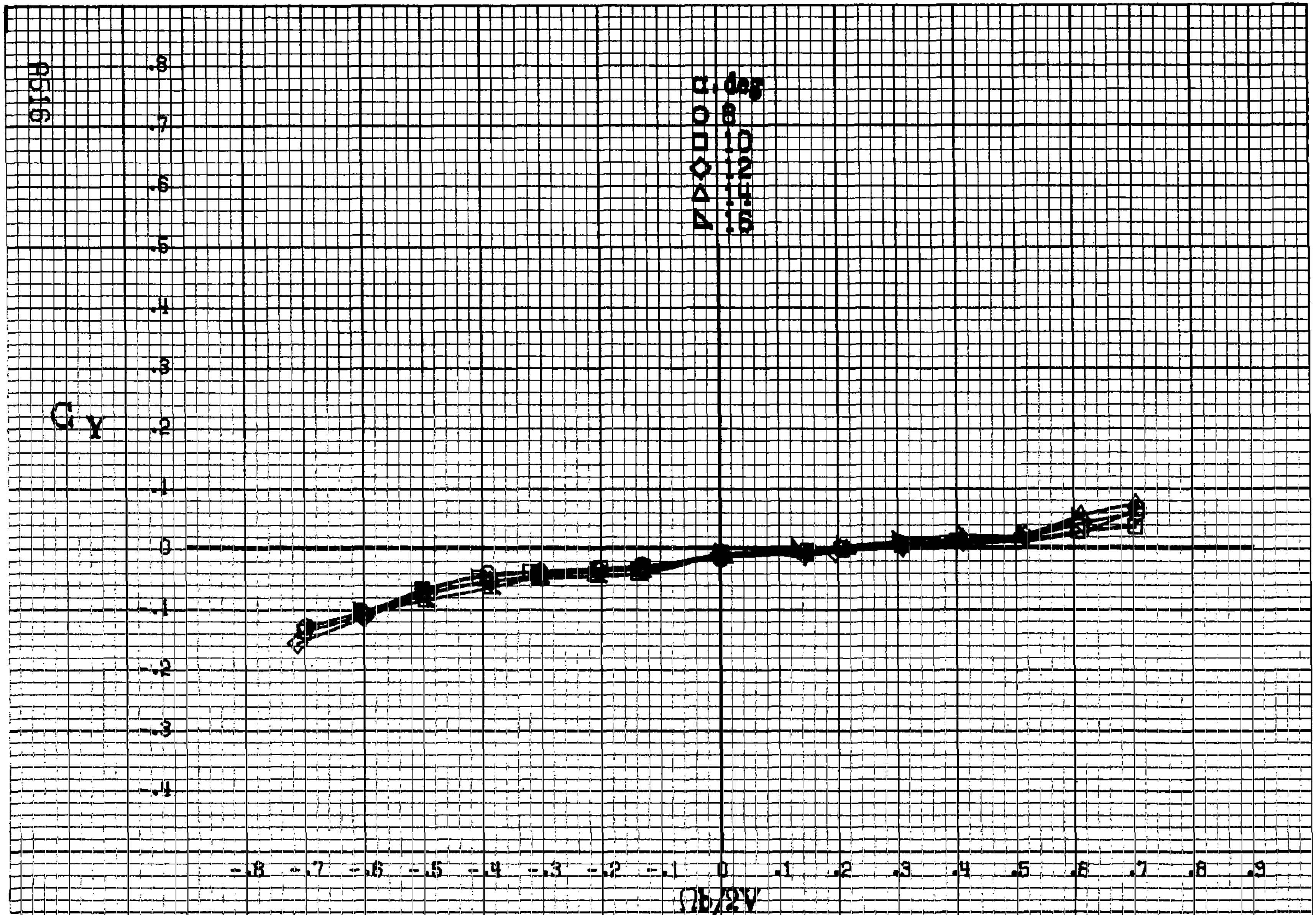

(a) α = 8 to 16 deg, SR = 182.9 cm (72 in).

Figure A125.- Effect of rotation rate and angle of attack on side-force coefficient for wing and vertical tail off configuration. $\delta_e = 0°$, $\delta_a = 0°$, $\delta_r = 0°$, $\beta = 0°$.

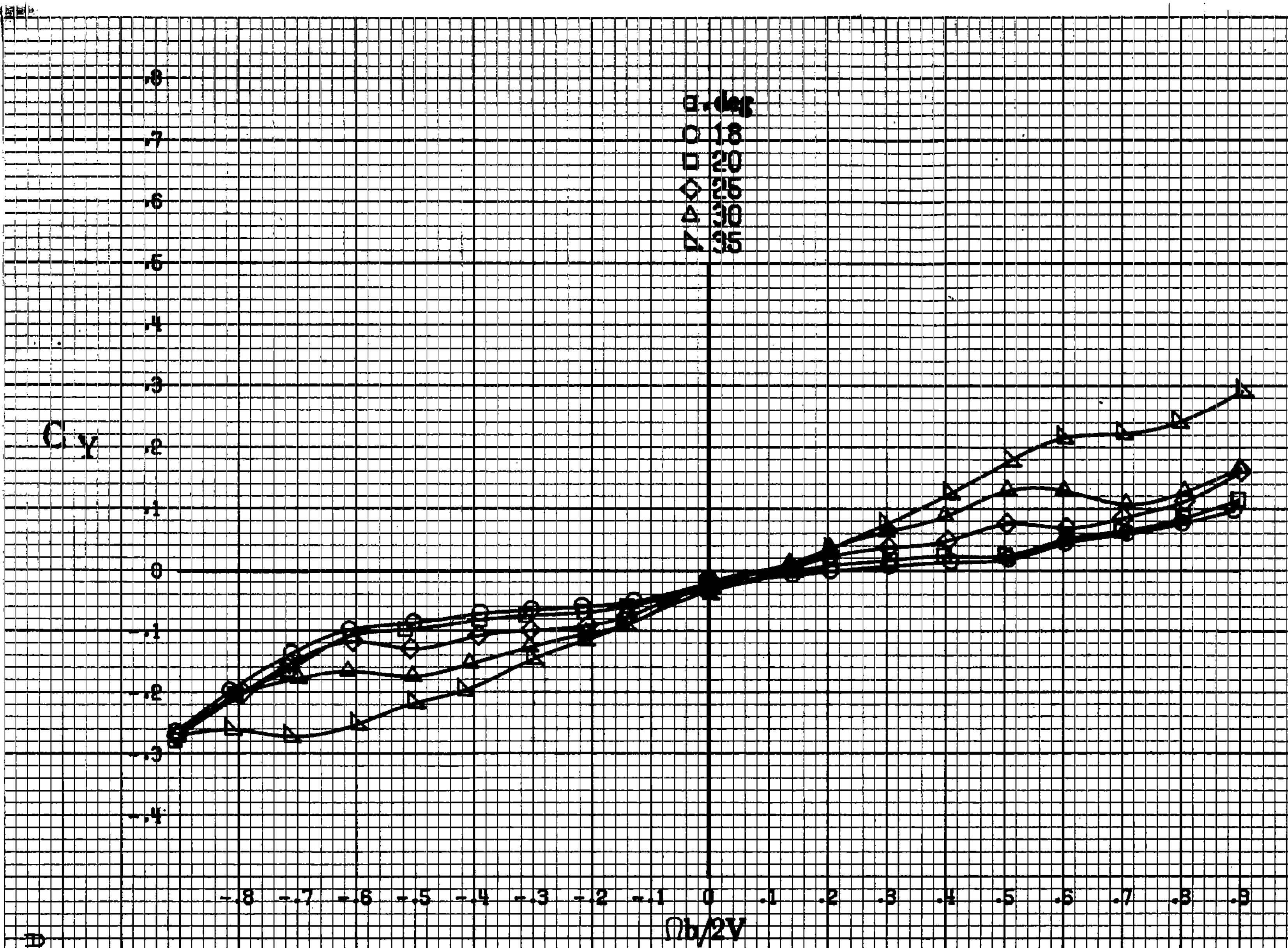

(b) α = 18 to 35 deg, SR = 182.9 cm (72 in).

Figure A125.-Continued.

A517

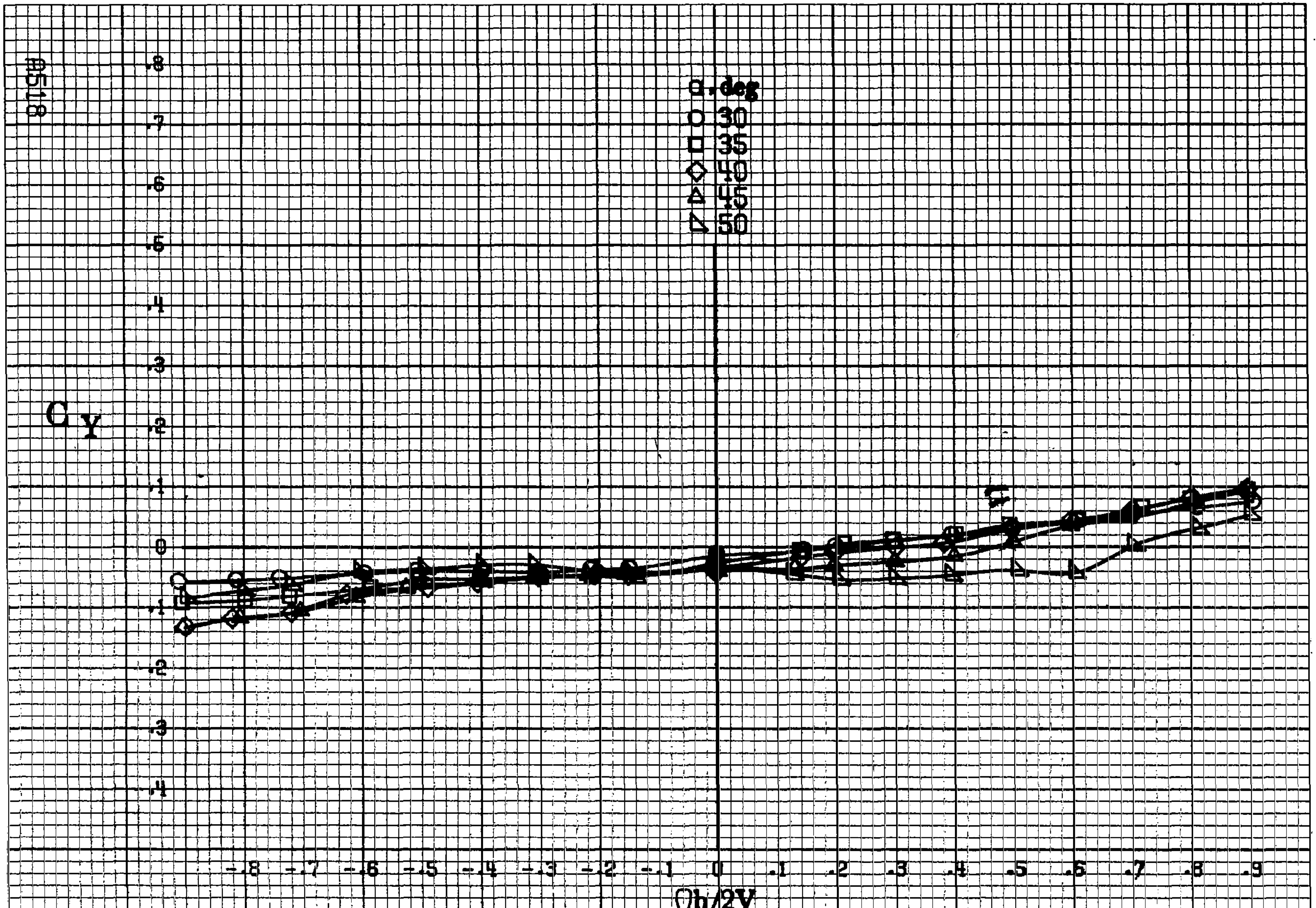

(c) α = 30 to 50 deg, SR = 0.

Figure A125.-Continued.

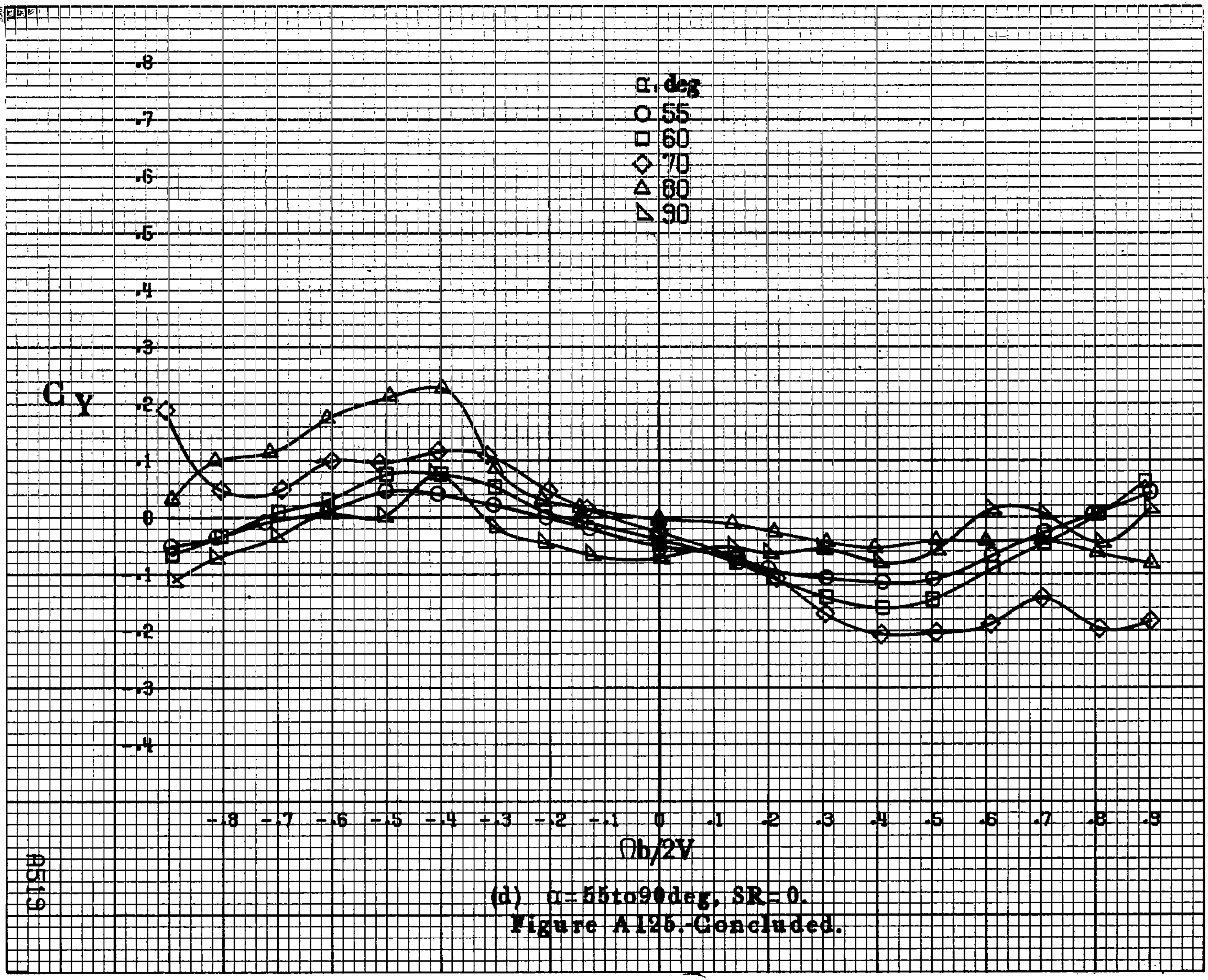

(d) α = 55 to 90 deg, SR = 0.

Figure A125.-Concluded.

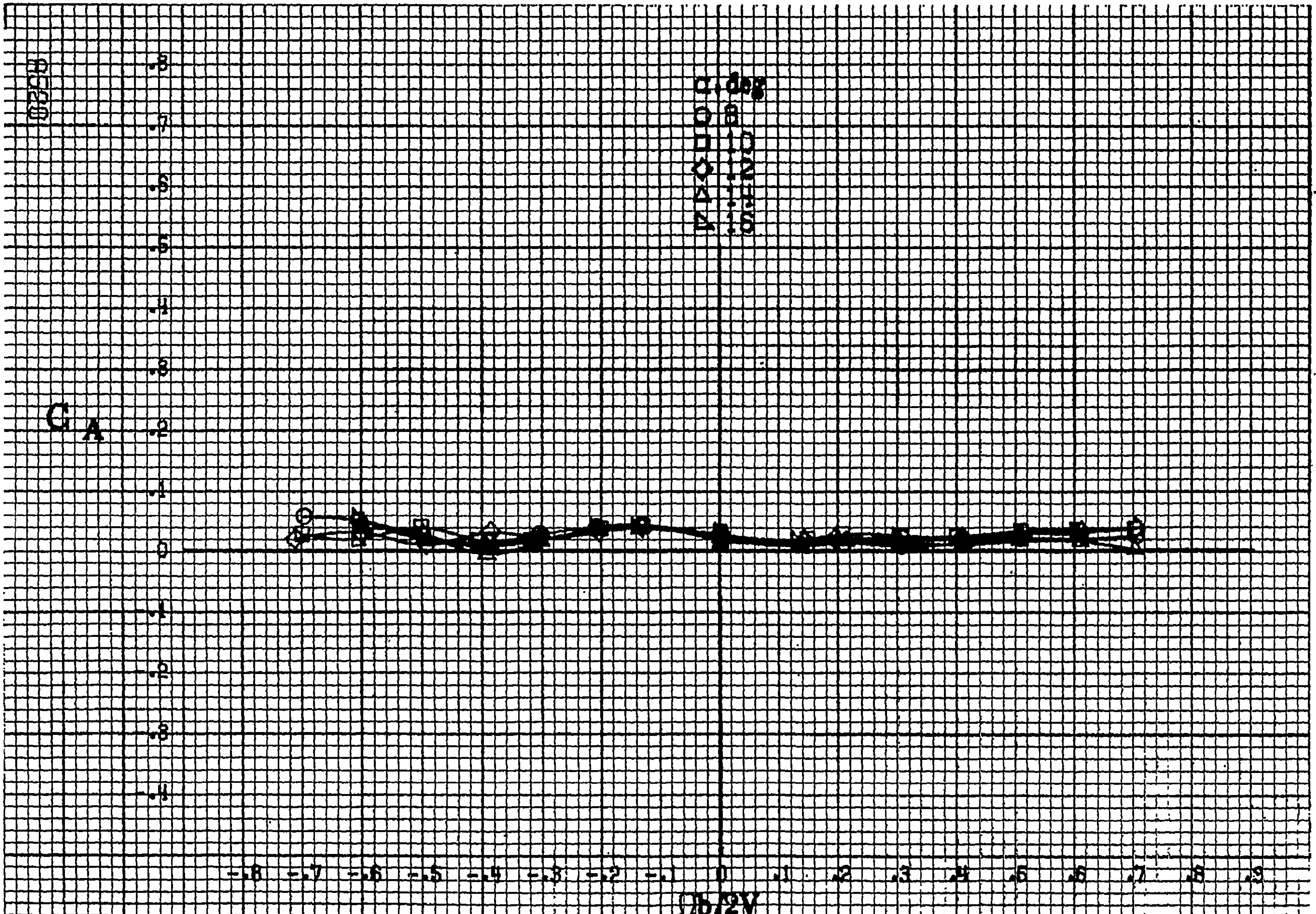

(a) $\alpha = 8$ to 16 deg, SR = 182.9 cm (72 in).

Figure A126.- Effect of rotation rate and angle of attack on axial-force coefficient for wing and vertical tail off configuration. $\delta_e = 0°$, $\delta_a = 0°$, $\delta_r = 0°$, $\beta = 0°$.

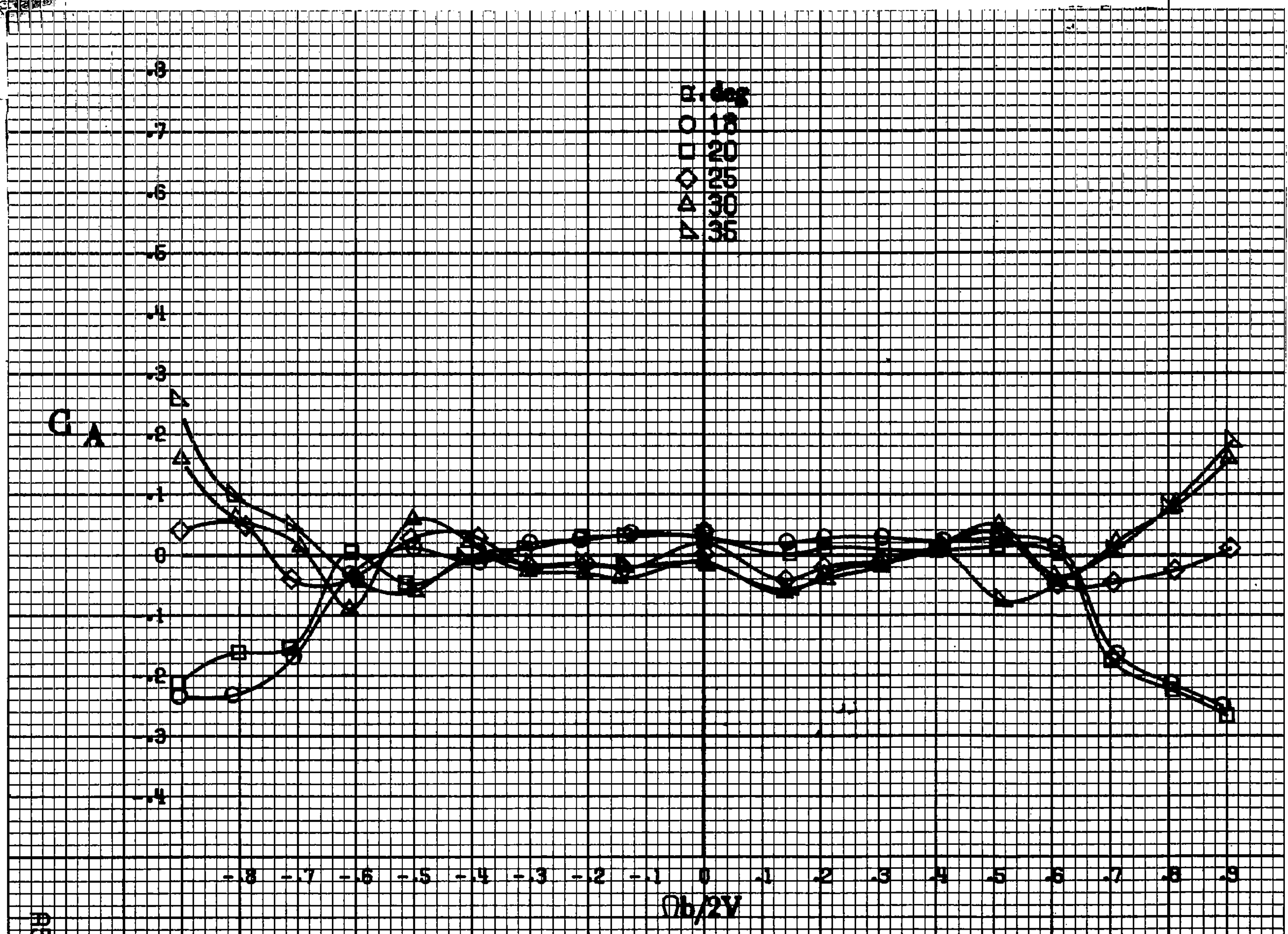

(b) α = 18 to 35 deg, SR = 182.9 cm (72 in).

Figure A126.-Continued.

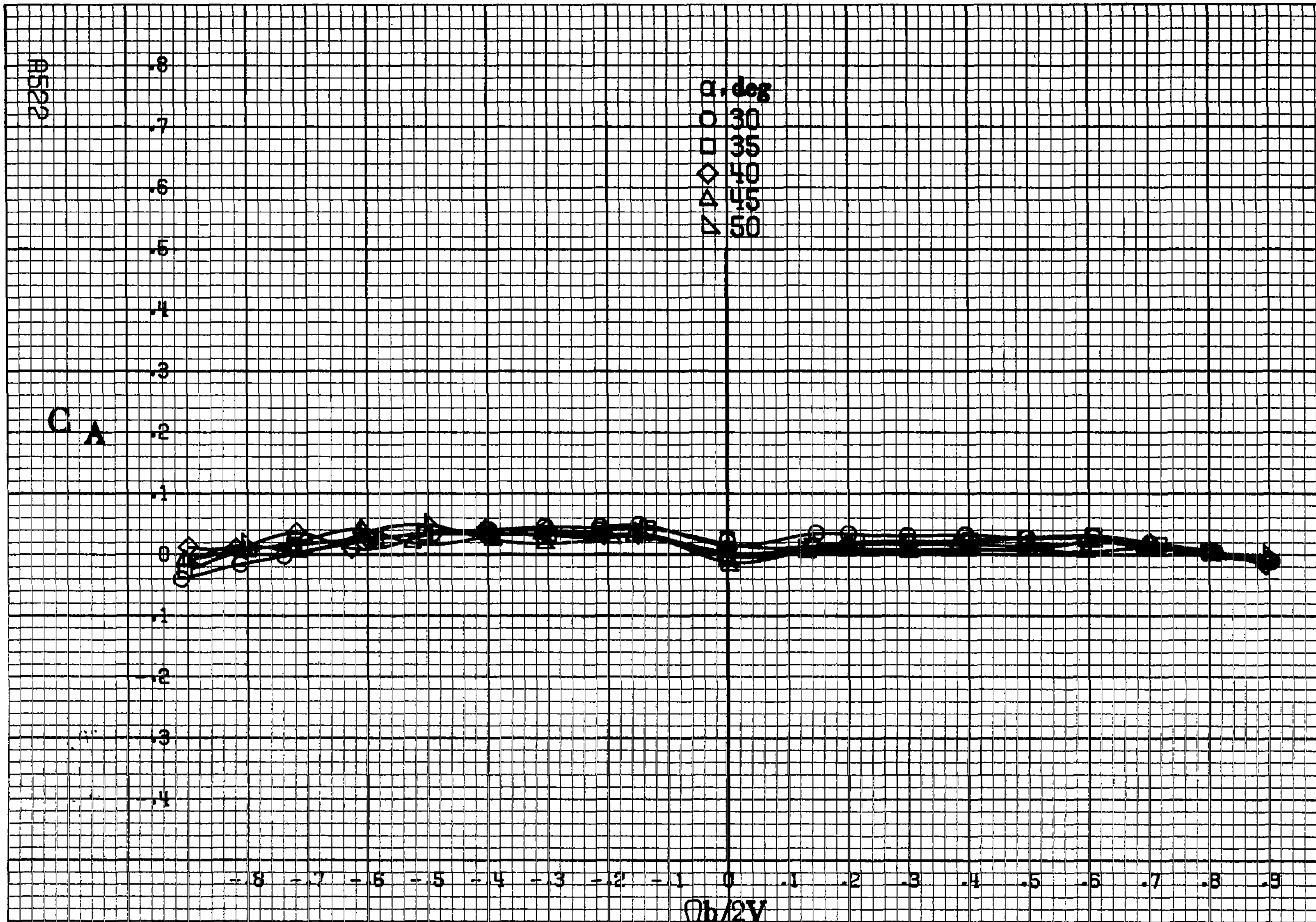

(c) α = 30 to 50 deg, SR = 0.

Figure A126.-Continued.

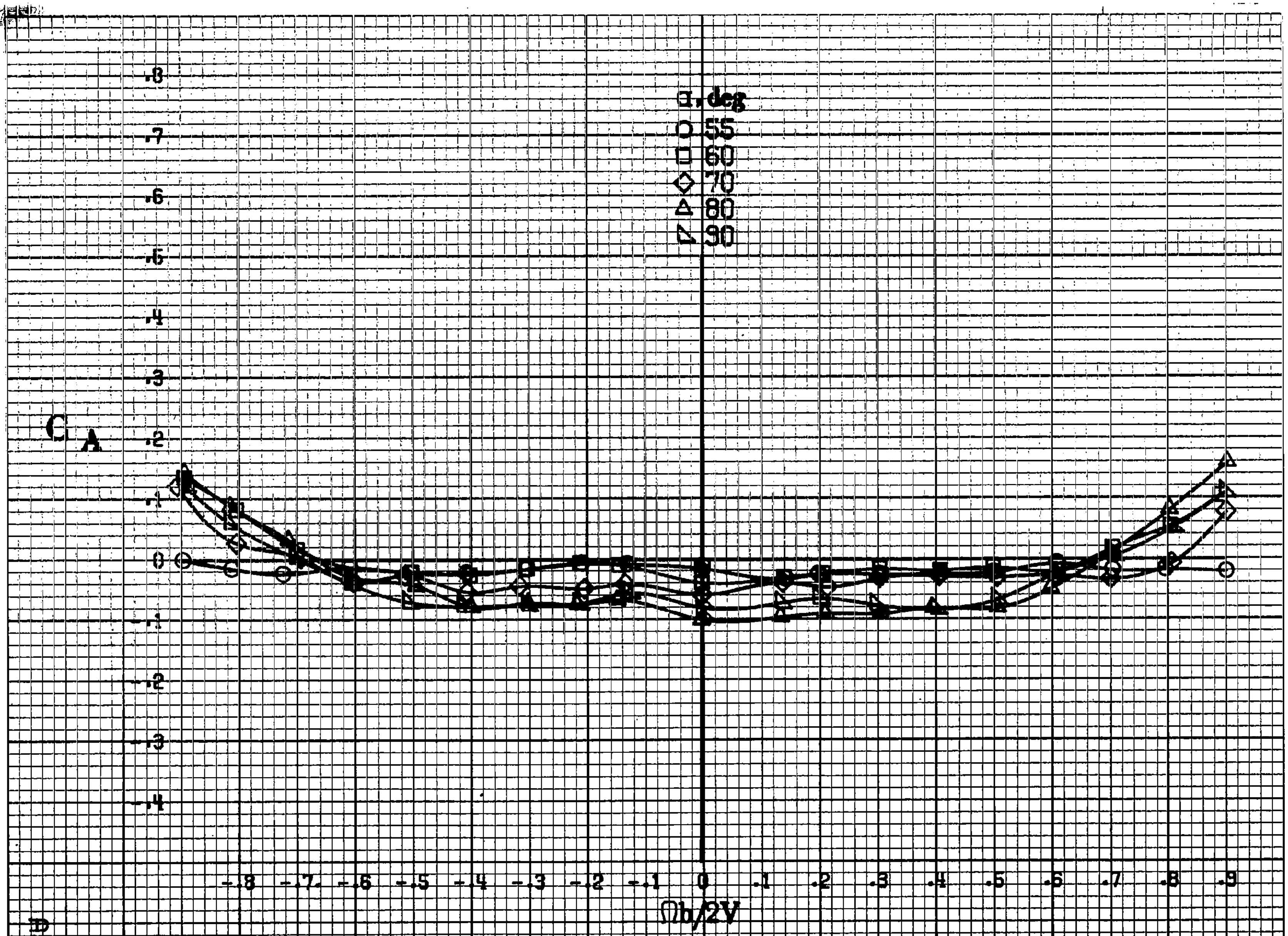

(d) α = 55 to 90 deg, SR = 0.

Figure A126.-Concluded.

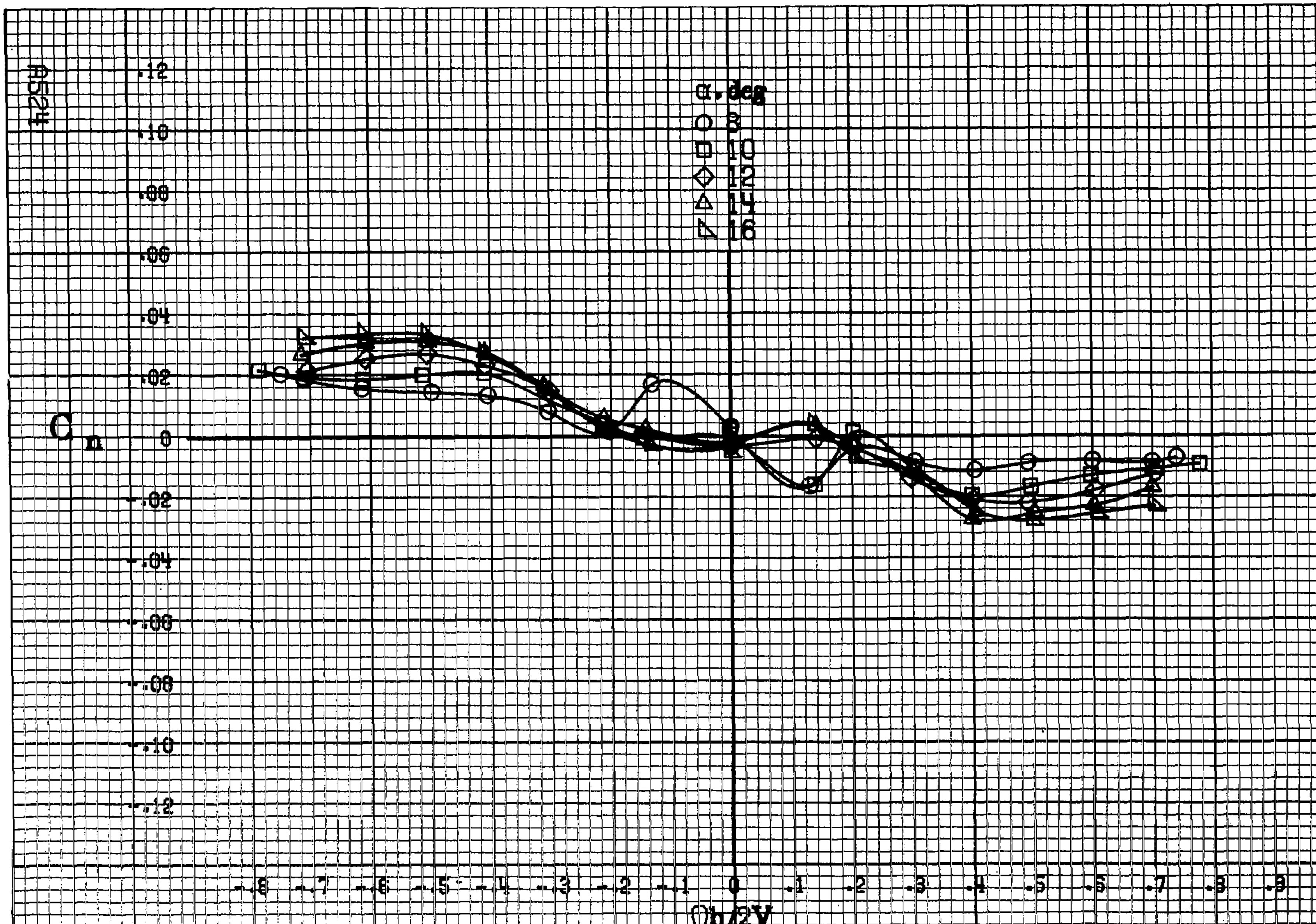

(a) $\alpha = 8$ to 16 deg, SR = 182.9 cm (72 in).

Figure A127.-Effect of rotation rate and angle of attack on yawing-moment coefficient for dorsal fin off configuration. $\delta_e = 0°$, $\delta_a = 0°$, $\delta_r = 0°$, $\beta = 0°$.

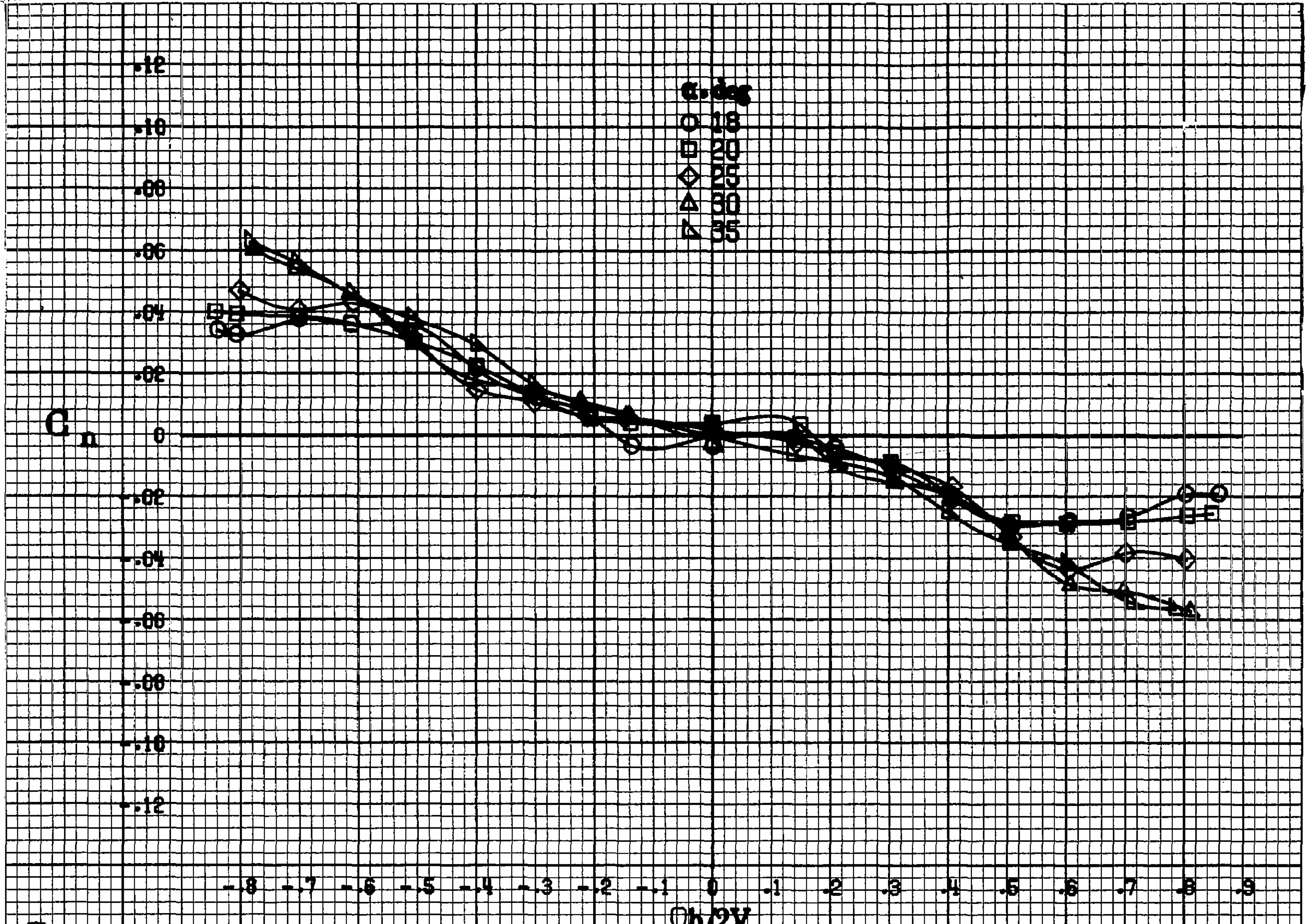

(b) α = 18 to 35 deg, SR = 182.9 cm (72 in).

Figure A127.-Continued.

A525

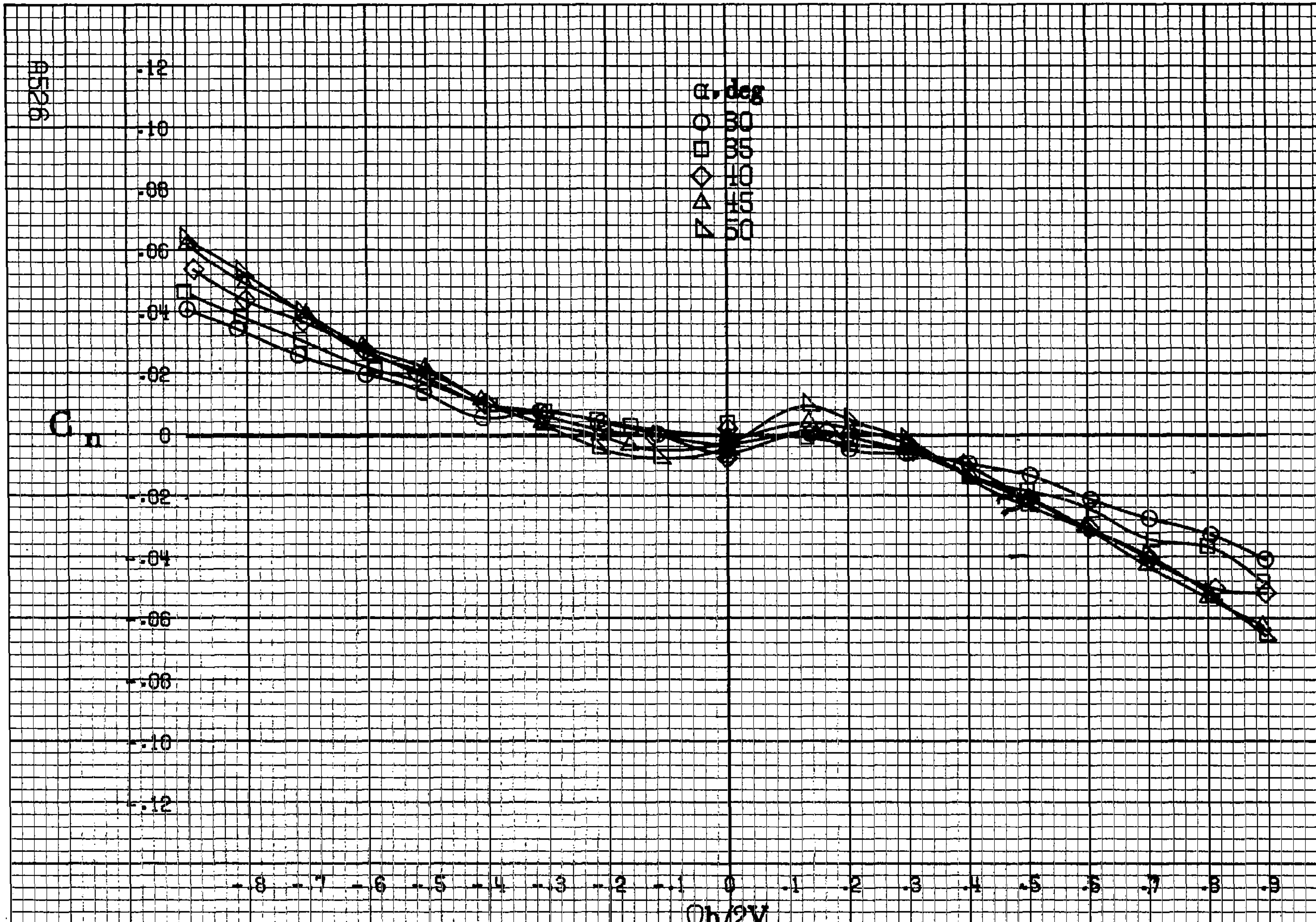

(c) $\alpha = 30$ to 50 deg, SR = 0.

Figure A127.-Continued.

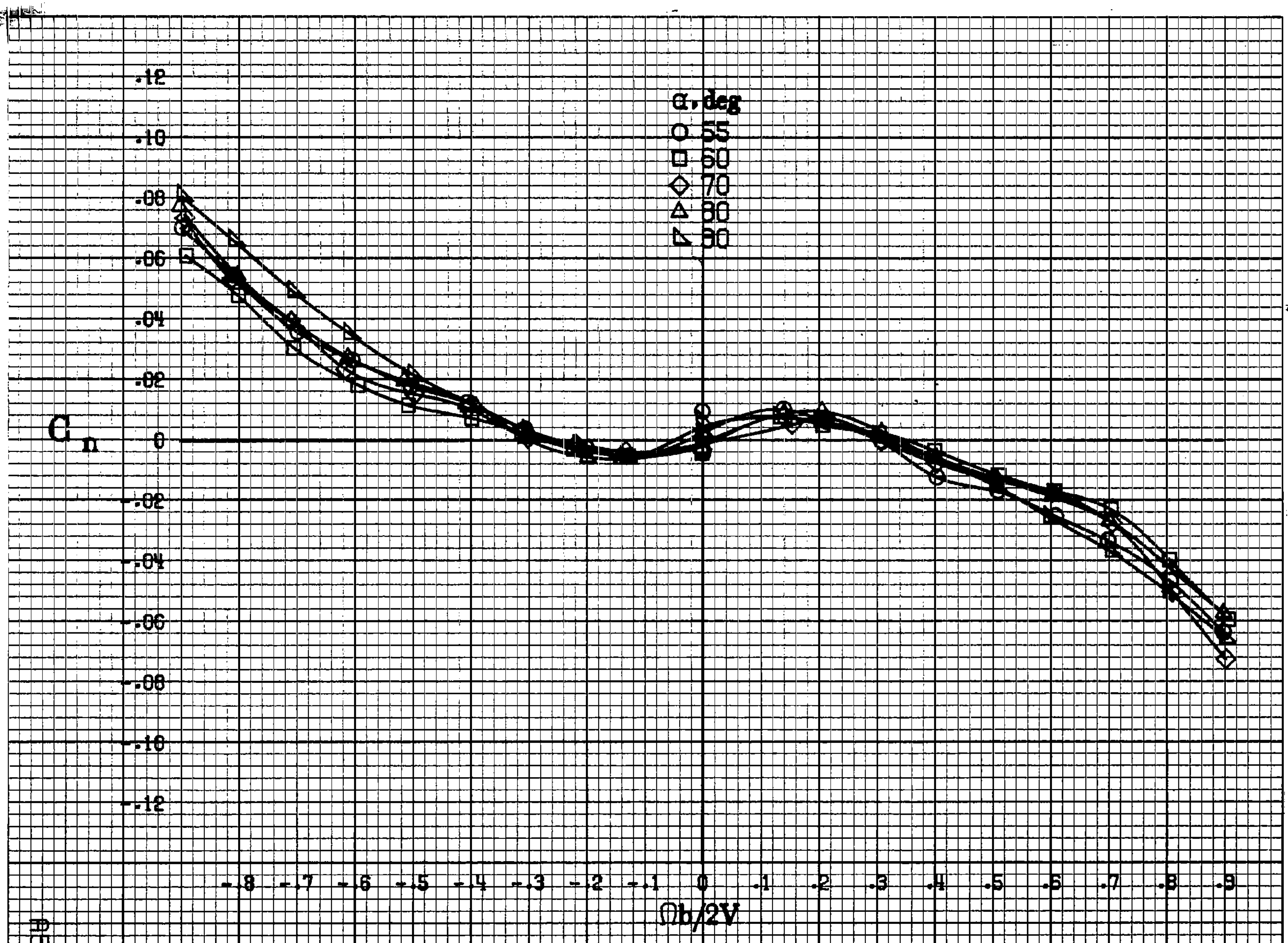

(d) α = 55 to 90 deg, SR = 0.

Figure A127.-Concluded.

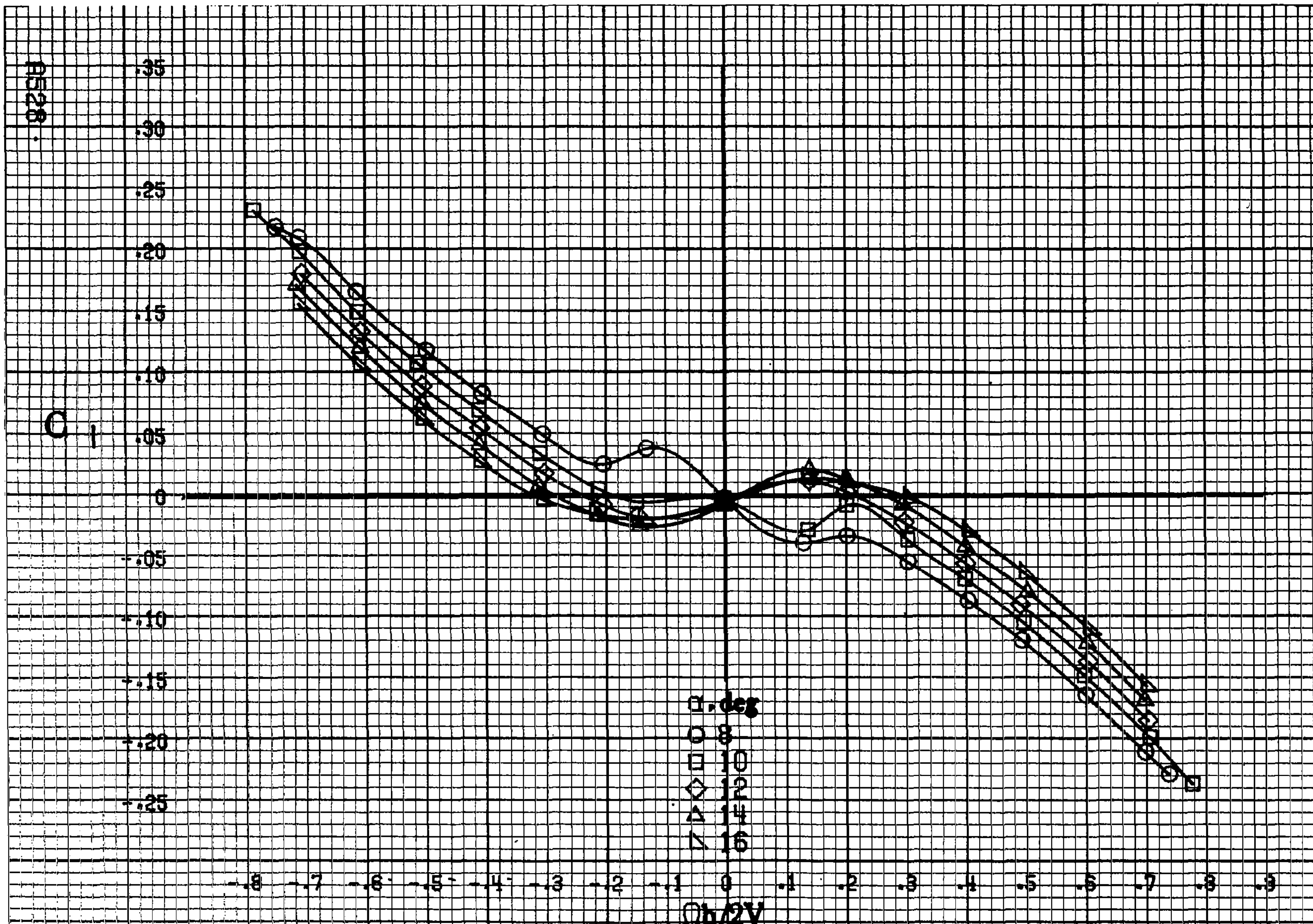

(a) $\alpha = 8$ to 16 deg, SR = 182.9 cm (72 in).

Figure A128.- Effect of rotation rate and angle of attack on rolling-moment coefficient for dorsal fin off configuration. $\delta_e = 0°$, $\delta_a = 0°$, $\delta_r = 0°$. $\beta = 0°$.

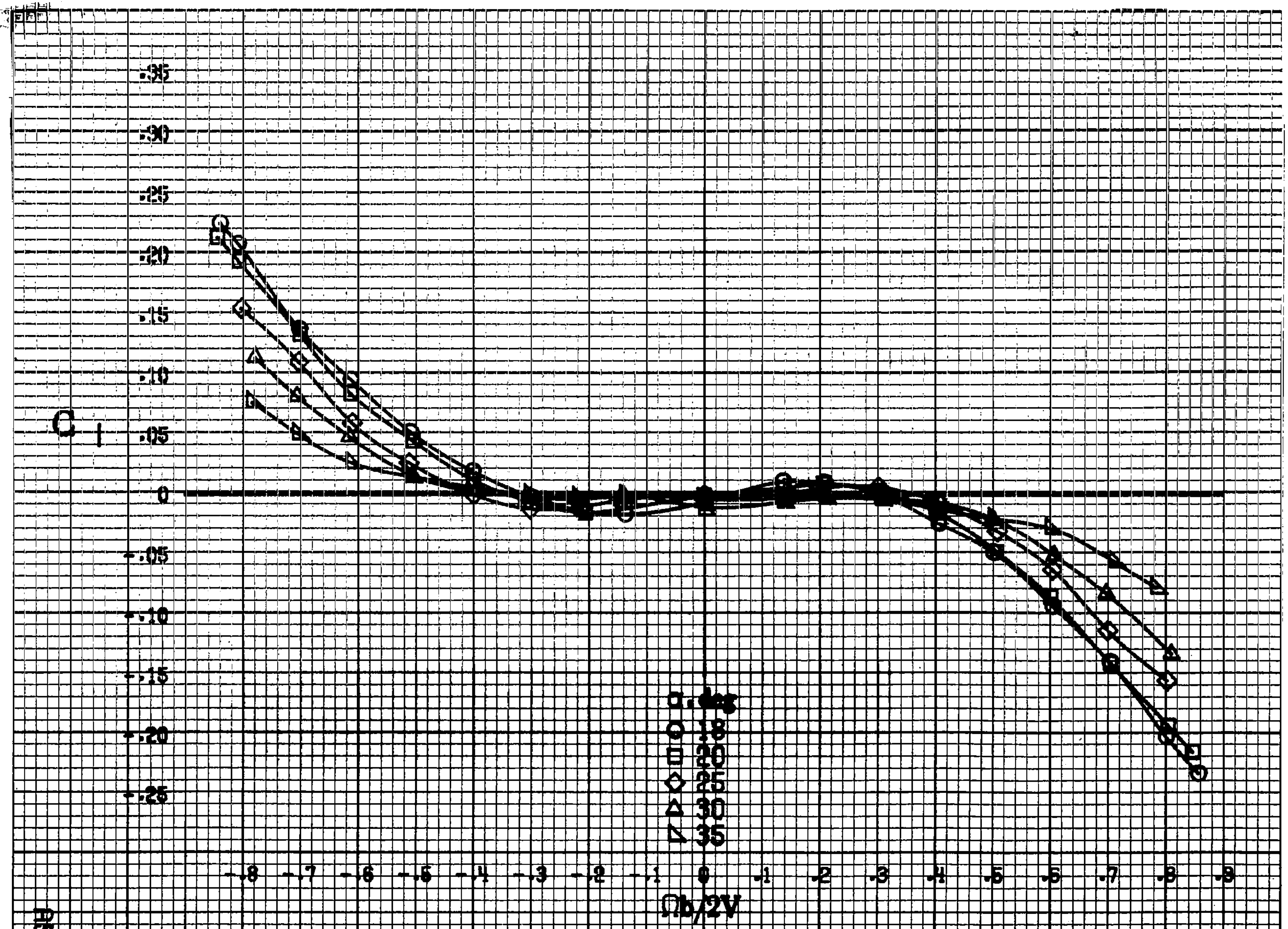

(b) α = 18 to 35 deg, SR = 182.9 cm (72 in).
Figure A128.-Continued.

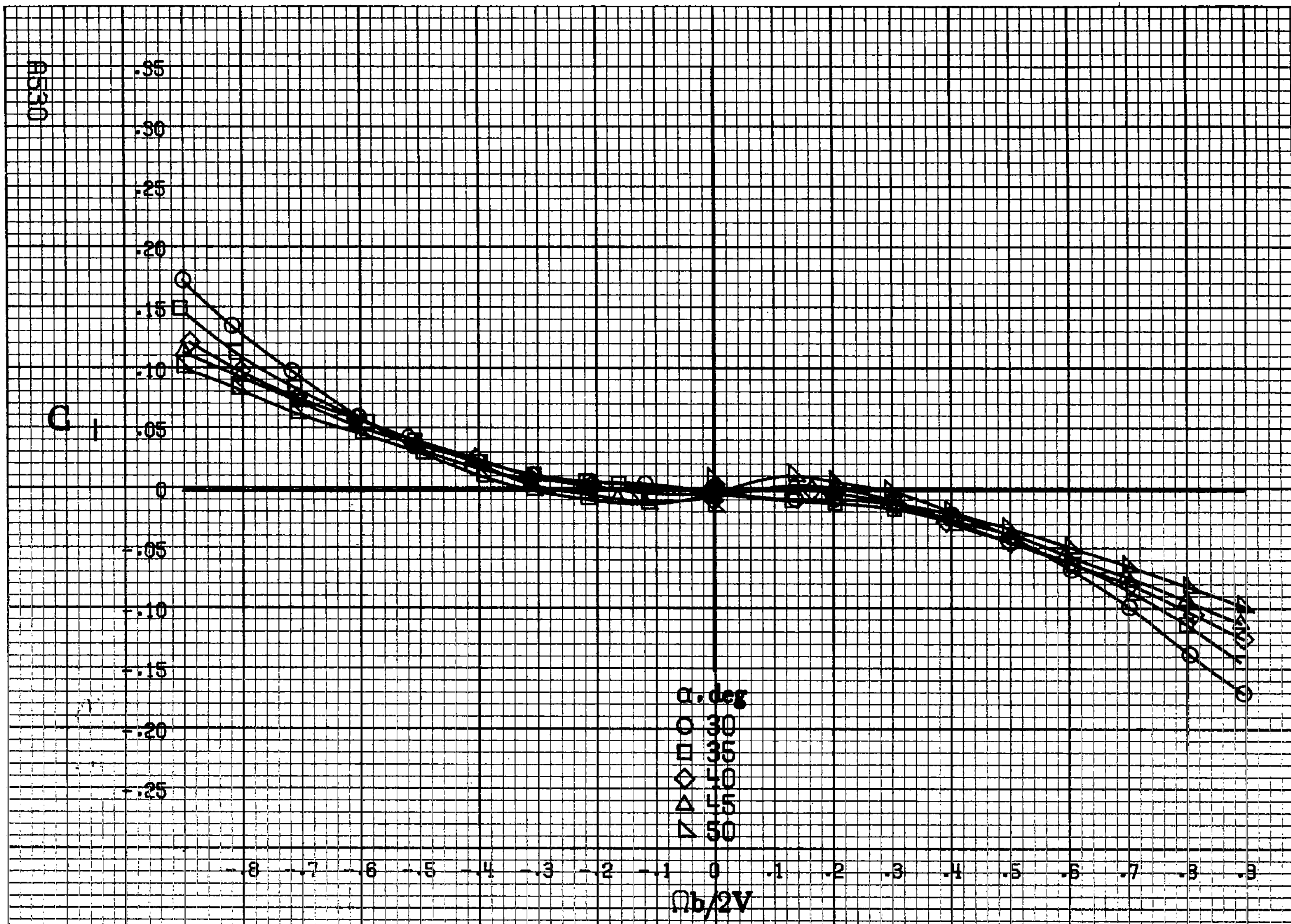

(c) α = 30 to 50 deg, SR = 0.

Figure A128.-Continued.

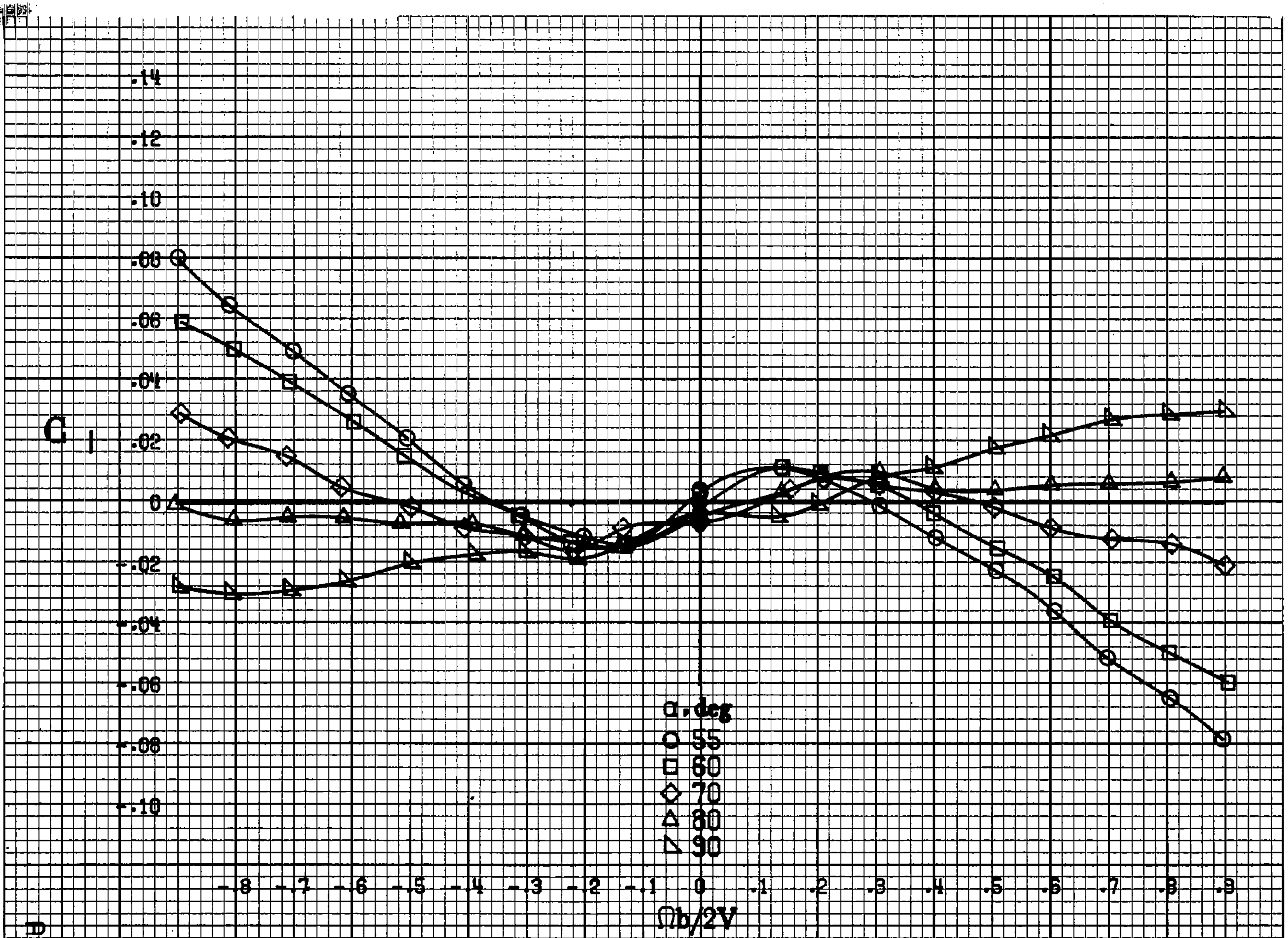

(d) α = 55 to 90 deg, SR = 0.

Figure A128.-Concluded.

A531

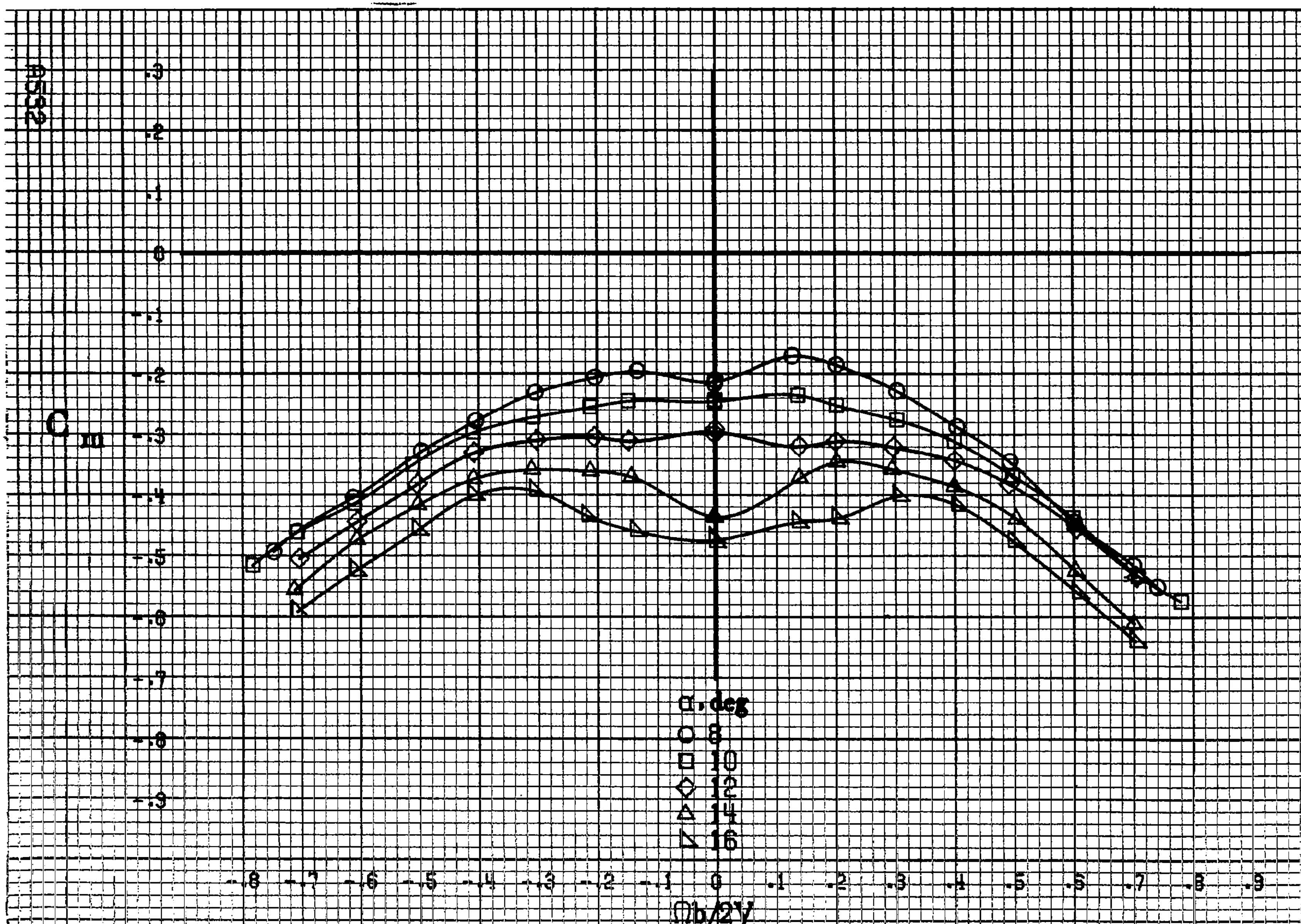

(a) α = 8 to 16 deg, SR = 182.9 cm (72 in).

Figure A129.-Effect of rotation rate and angle of attack on pitching-moment coefficient for dorsal fin off configuration. $\delta_a = 0°$, $\delta_e = 0°$, $\delta_r = 0°$, $\beta = 0°$.

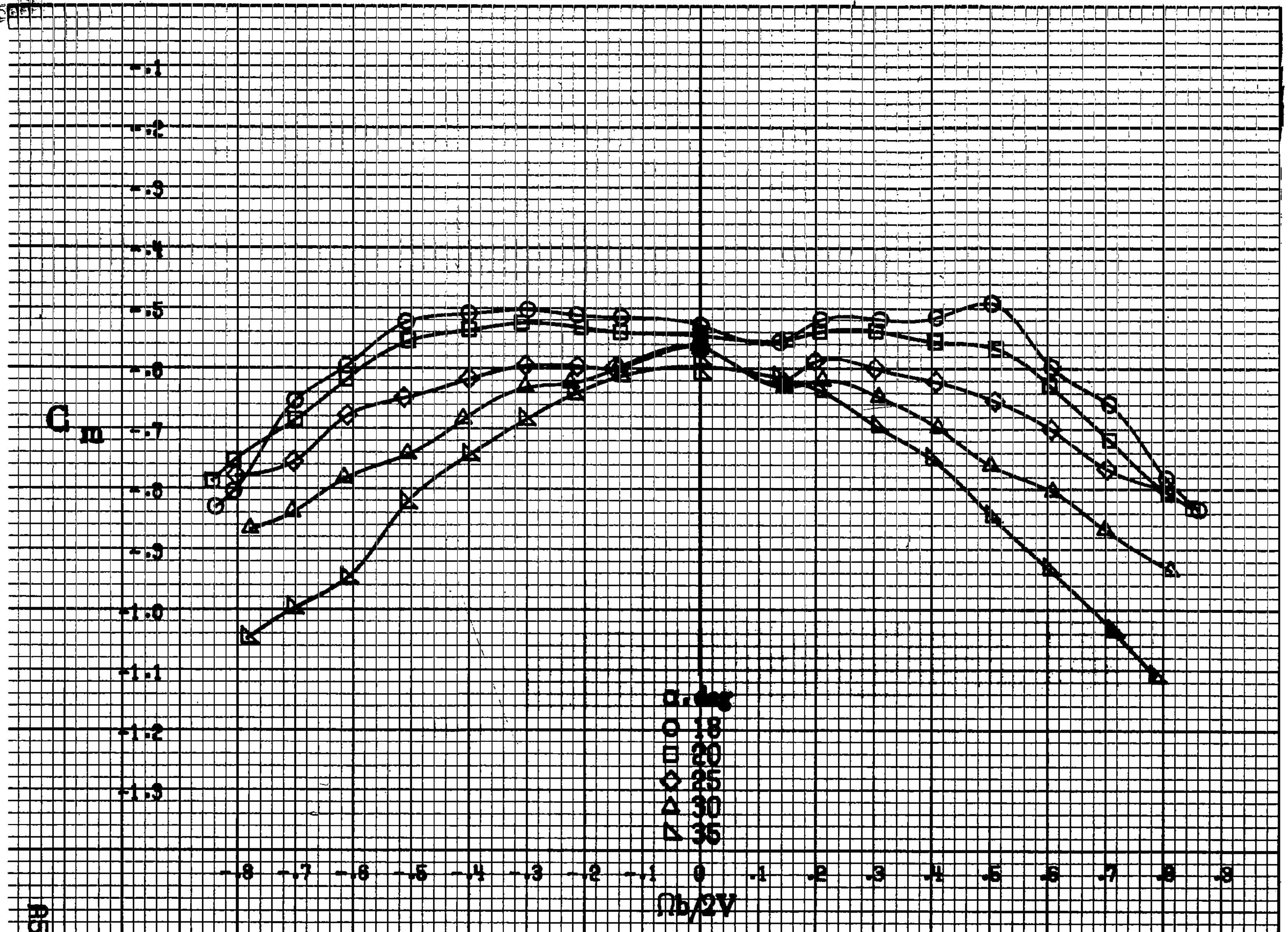

(b) α = 18 to 35 deg, SR = 182.9 cm (72 in).

Figure A129.-Continued.

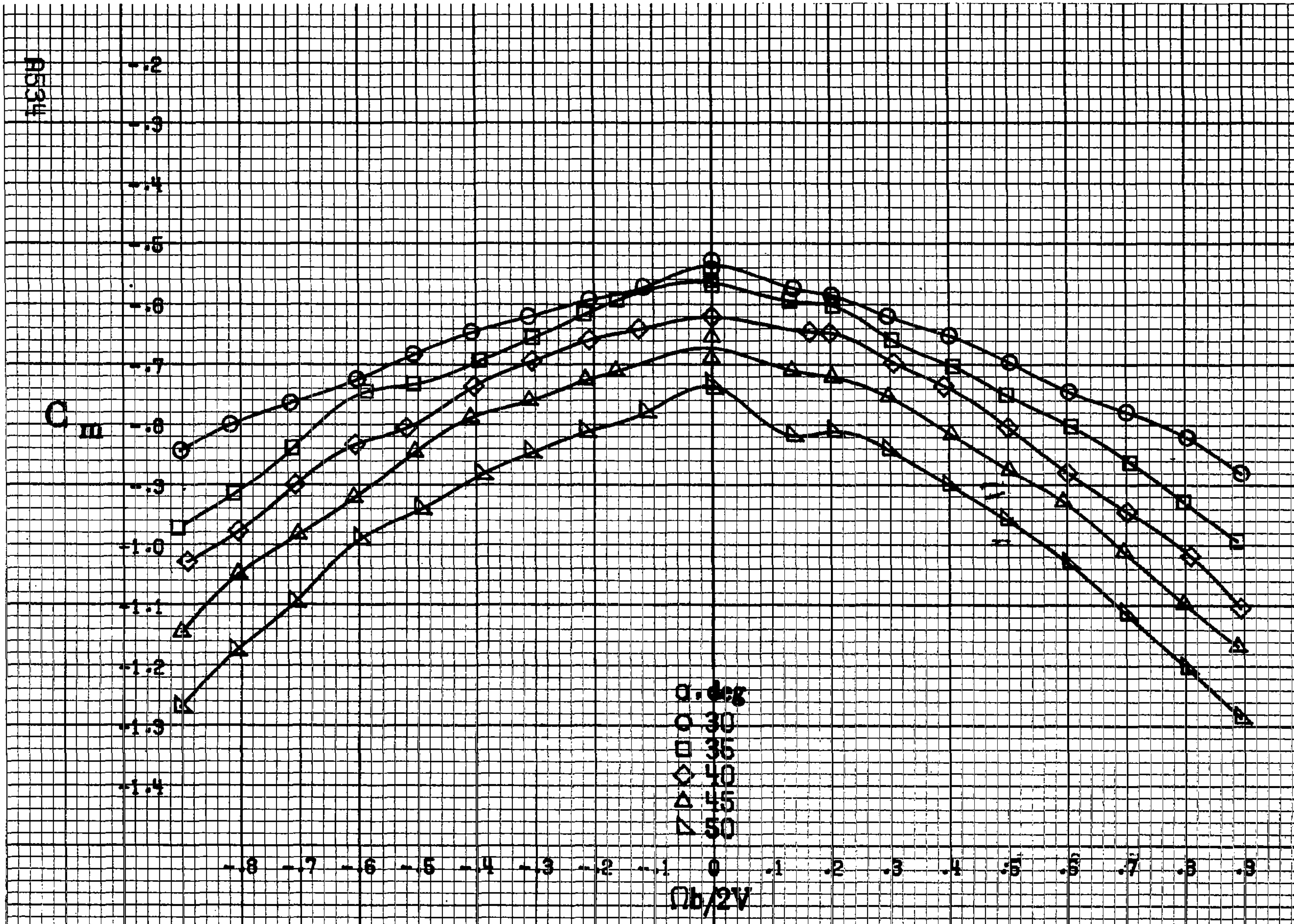

(c) α = 30 to 50 deg, SR = 0.

Figure A129.-Continued.

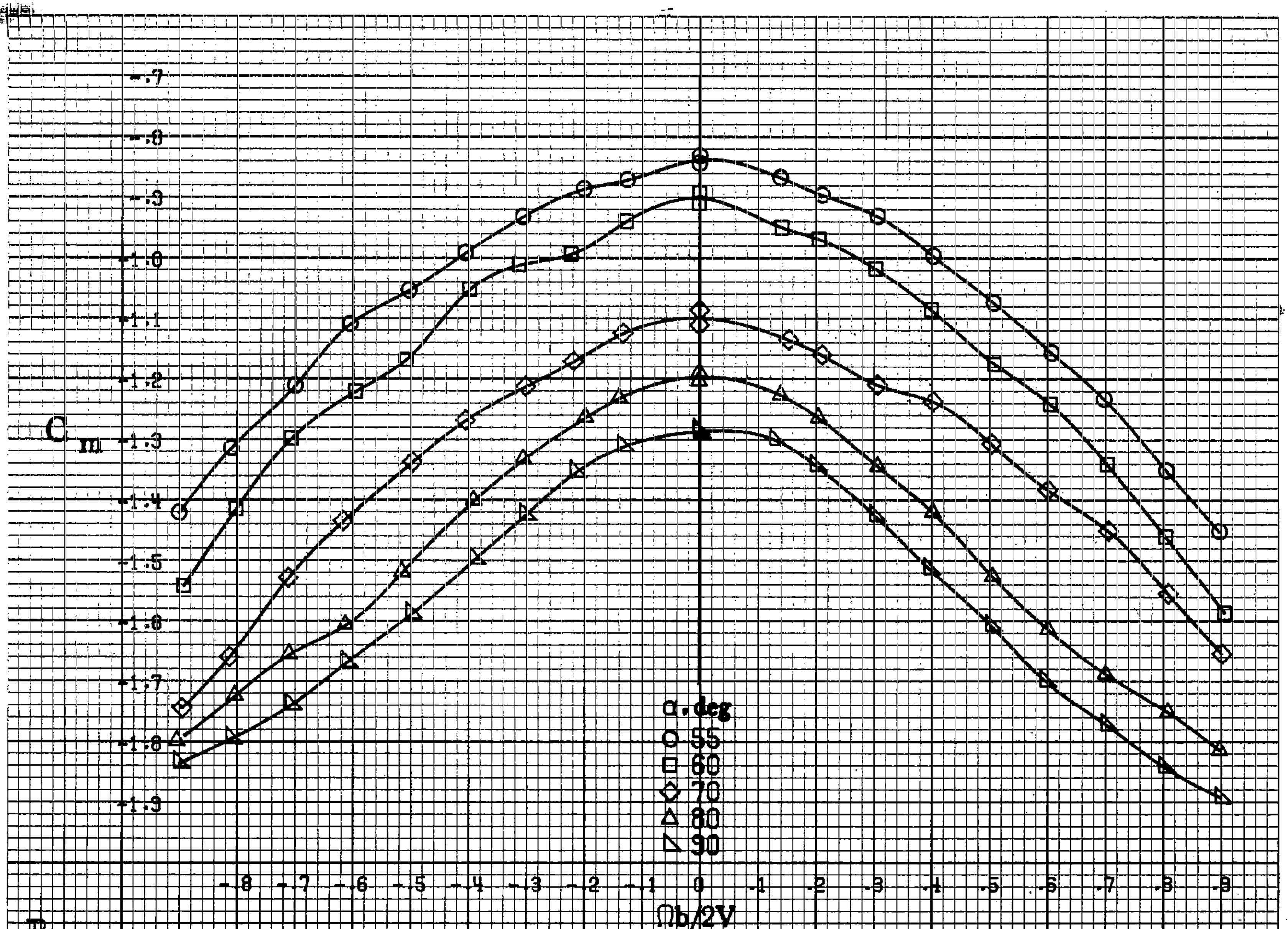

(d) $\alpha = 55$ to 90 deg, SR = 0.

Figure A129.-Concluded.

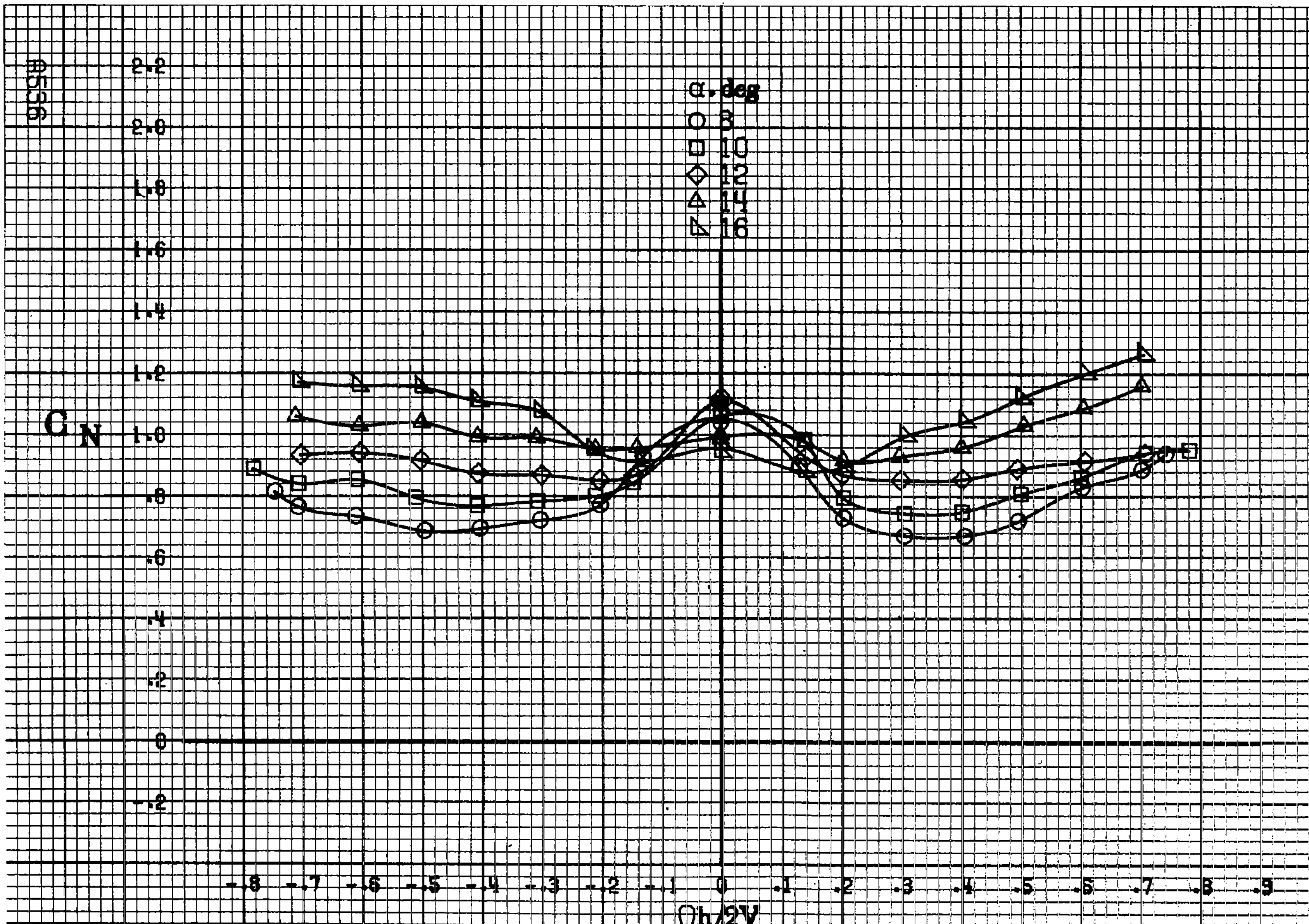

(a) α = 8 to 16 deg, SR = 182.9 cm (72 in).

Figure A180.-Effect of rotation rate and angle of attack on normal-force coefficient for dorsal fin off configuration. $\delta_e = 0^\circ$, $\delta_a = 0^\circ$, $\delta_r = 0^\circ$, $\beta = 0^\circ$.

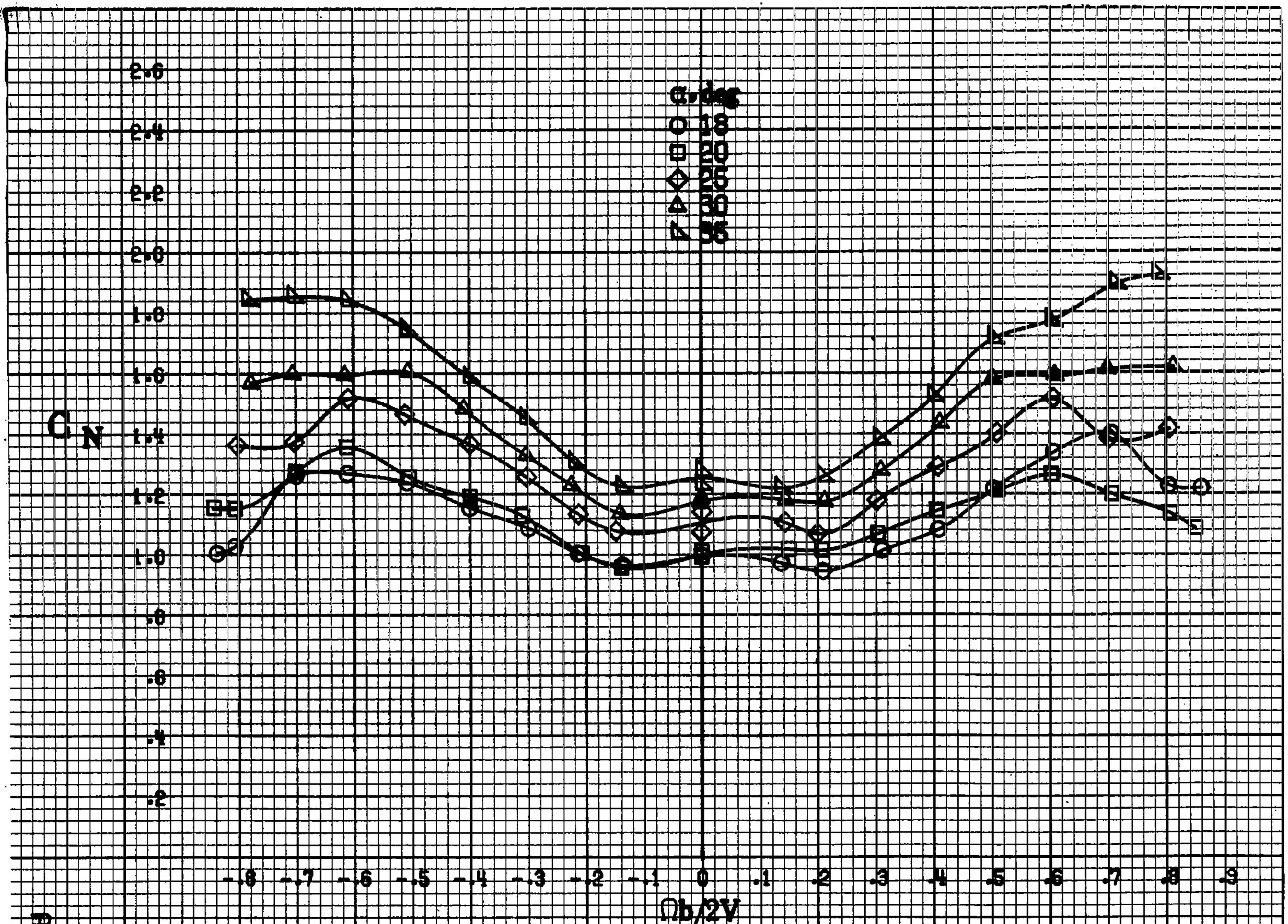

(b) α = 18 to 35 deg, SR = 182.9 cm (72 in).
Figure A130.-Continued.

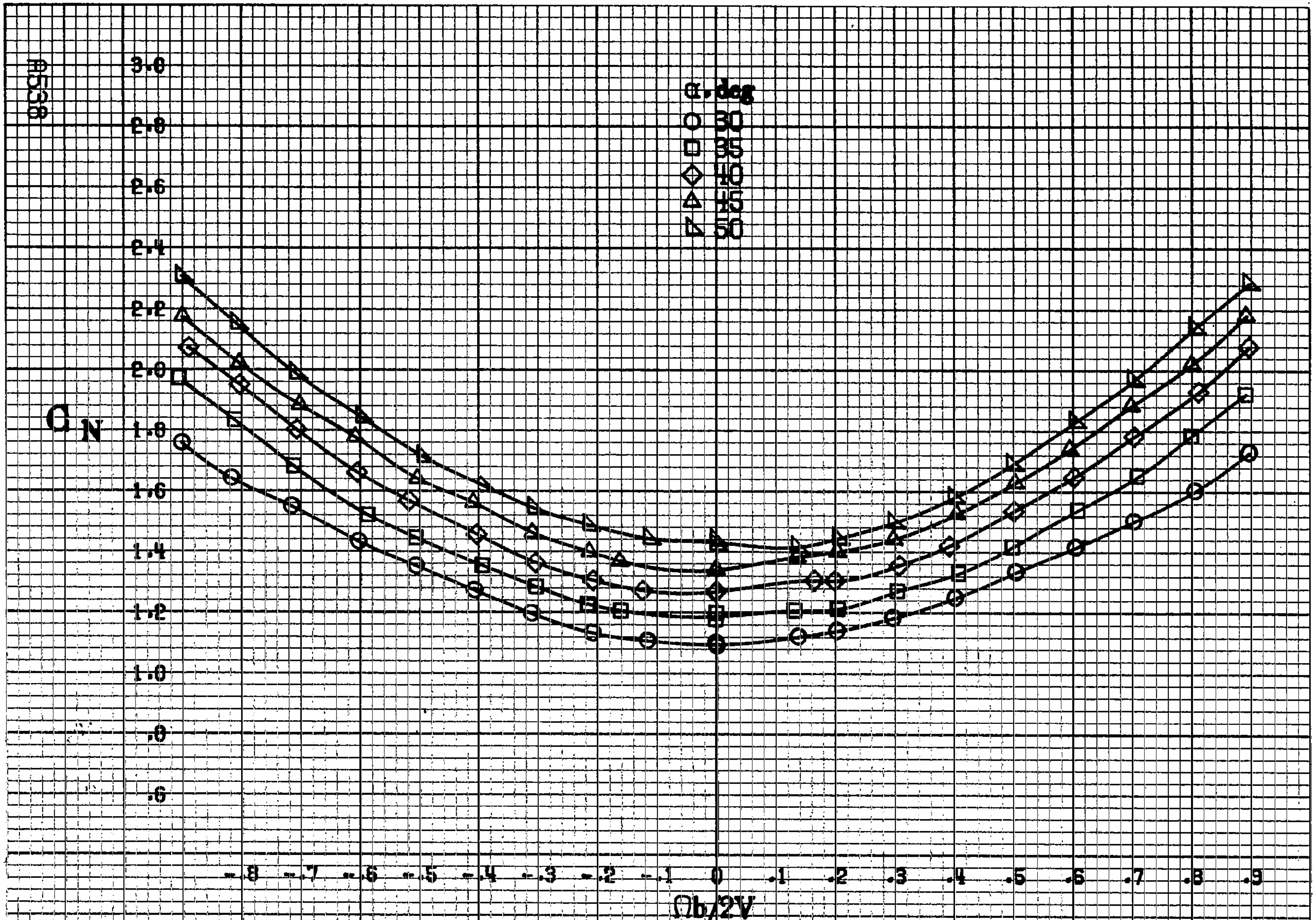

(c) α = 30 to 50 deg, δ_R = 0.

Figure A190.-Continued.

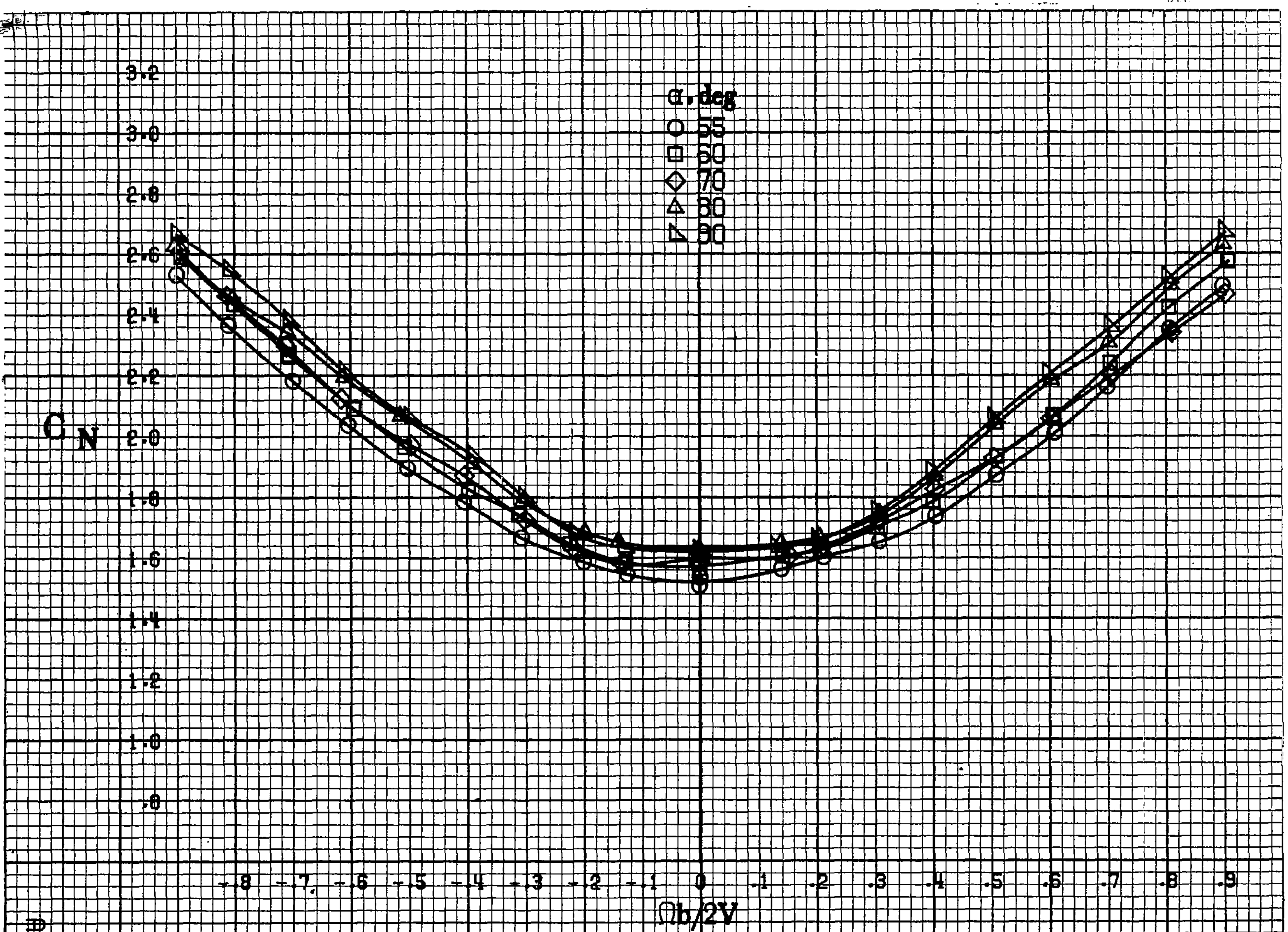

(d) α = 55 to 90 deg, SR = 0.

Figure A130.-Concluded.

A539

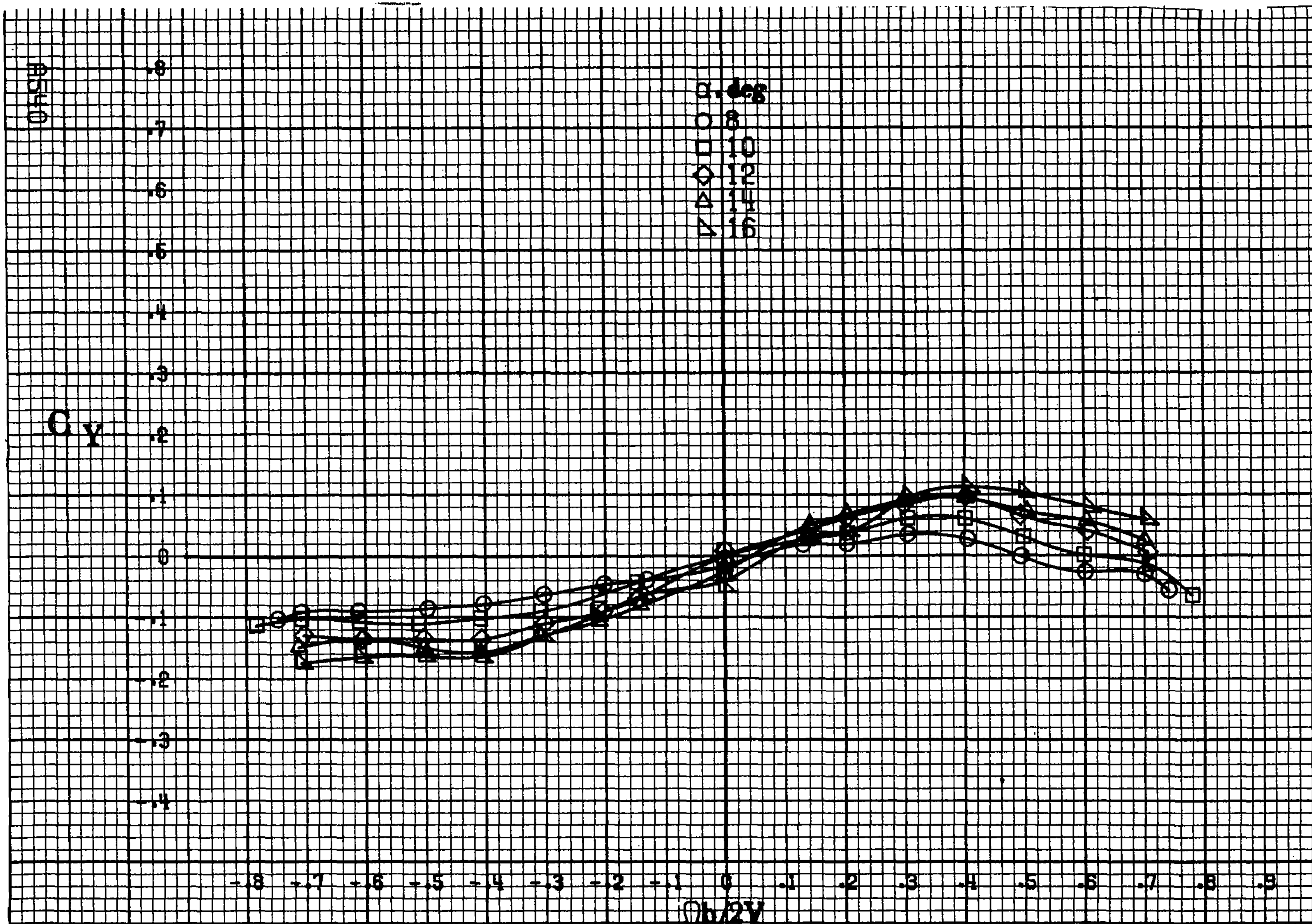

(a) α = 8 to 16 deg, SR = 182.9 cm (72 in).

Figure A131.-Effect of rotation rate and angle of attack on side-force coefficient for dorsal fin off configuration. $\delta_e = 0°$, $\delta_a = 0°$, $\delta_r = 0°$. $\beta = 0°$.

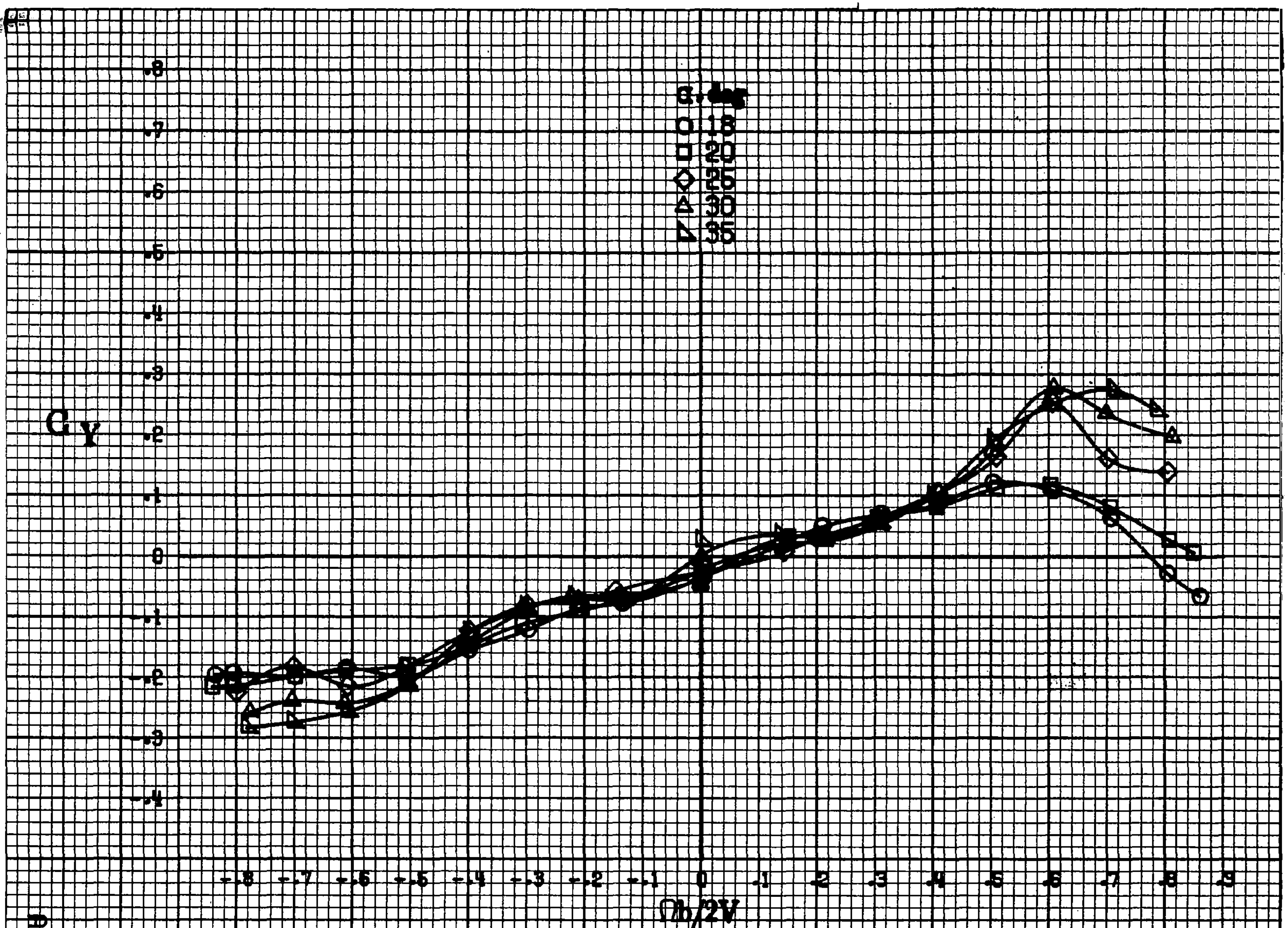

(b) α = 18 to 35 deg, SR = 182.9 cm (72 in).

Figure A191.-Continued.

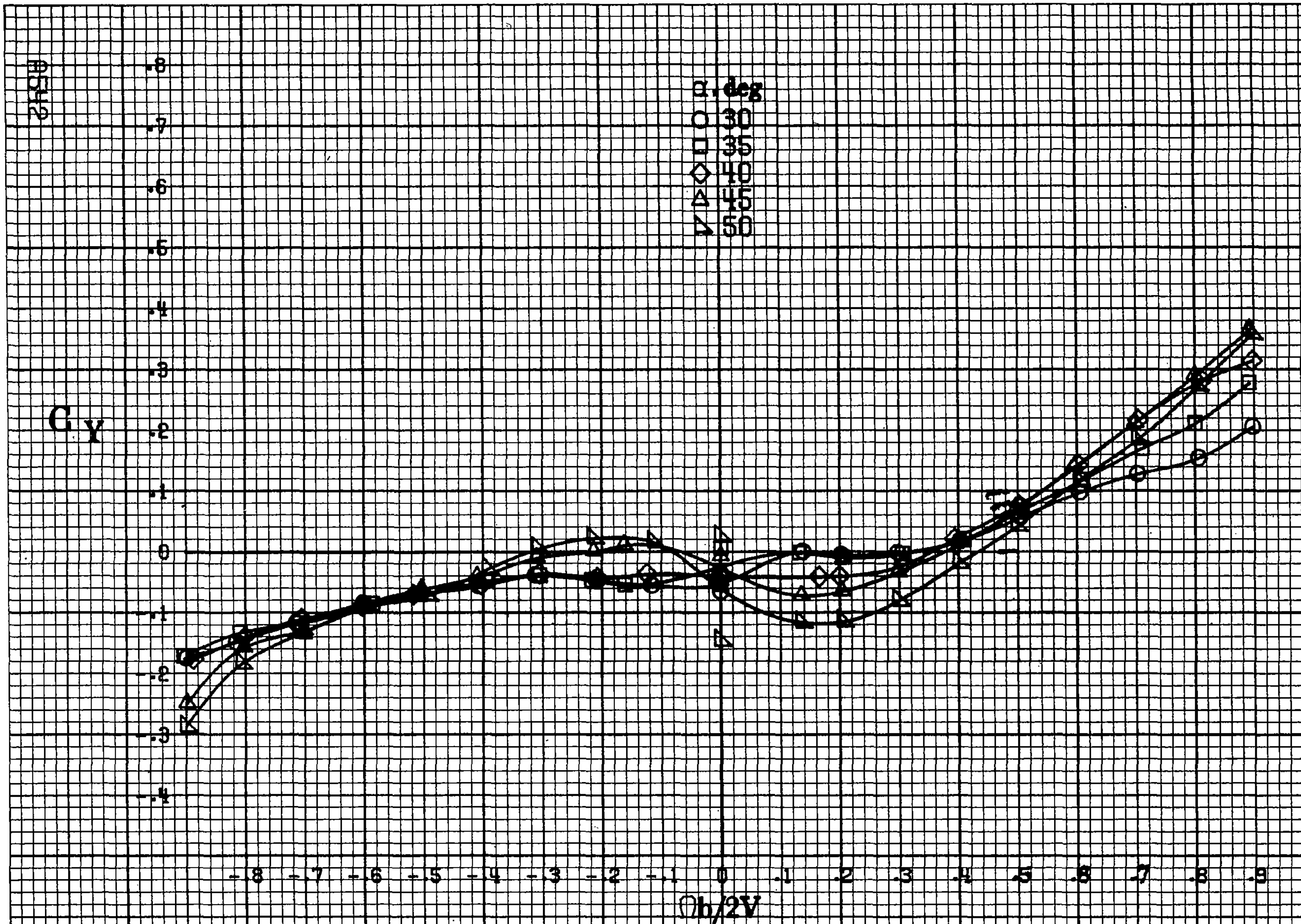

(c) α = 30 to 50 deg, SR = 0.

Figure A131.-Continued.

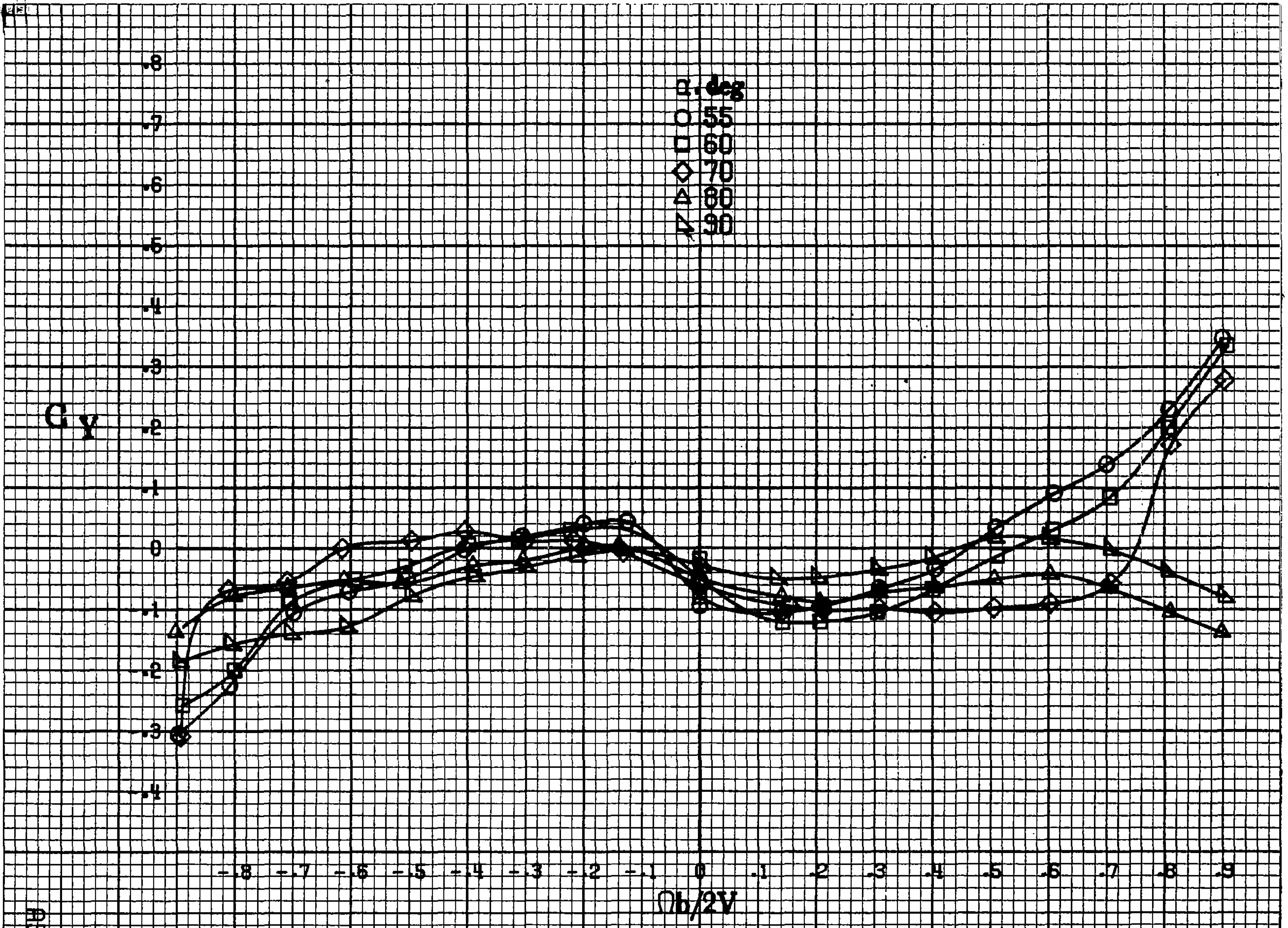

(d) α = 55 to 90 deg, SR = 0.

Figure A181.-Concluded.

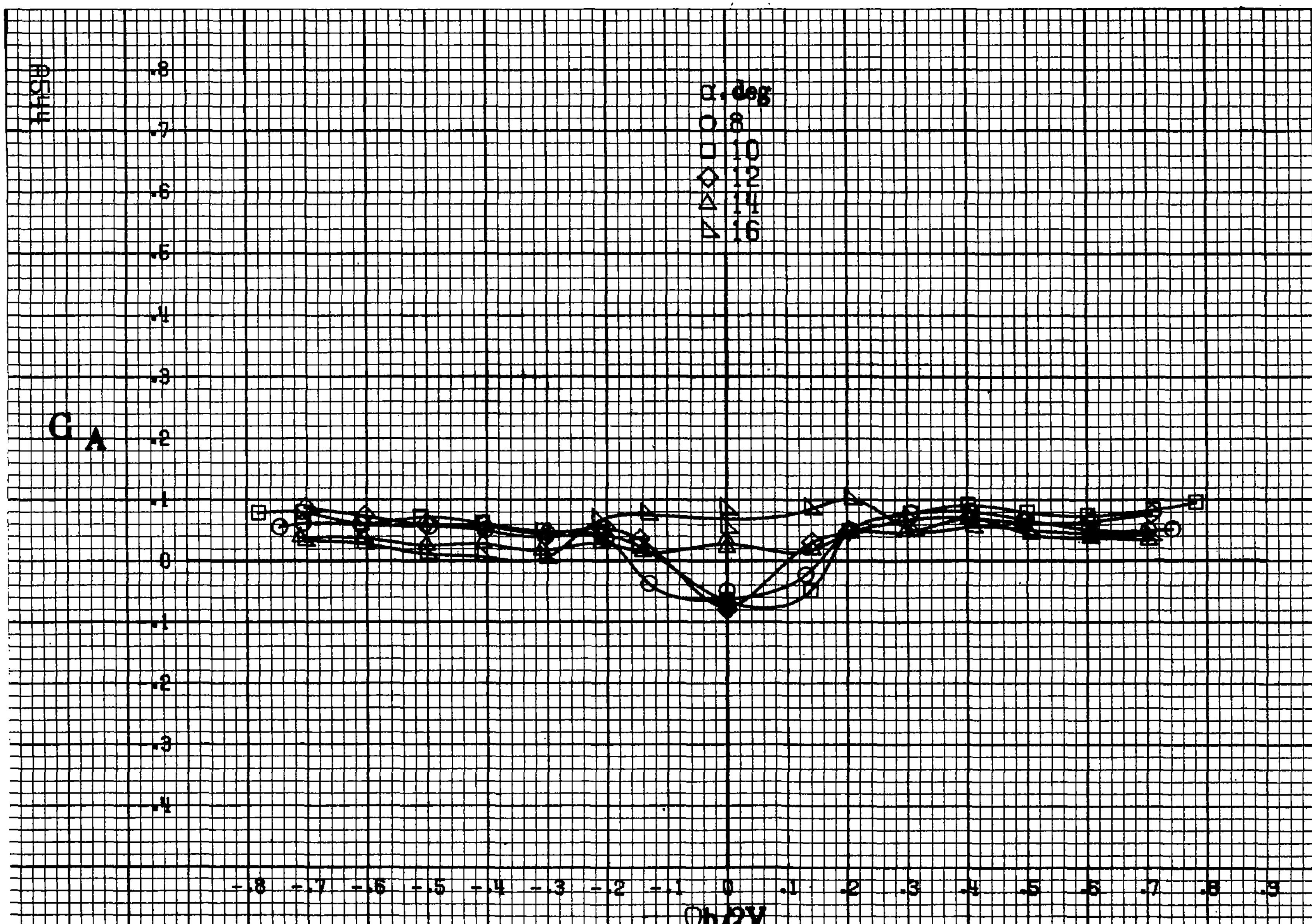

(a) α = 8 to 16 deg, SR = 182.9 cm (72 in).

Figure A132.-Effect of rotation rate and angle of attack on axial-force coefficient for dorsal fin off configuration. $\delta_e = 0°$, $\delta_a = 0°$, $\delta_r = 0°$, $\beta = 0°$.

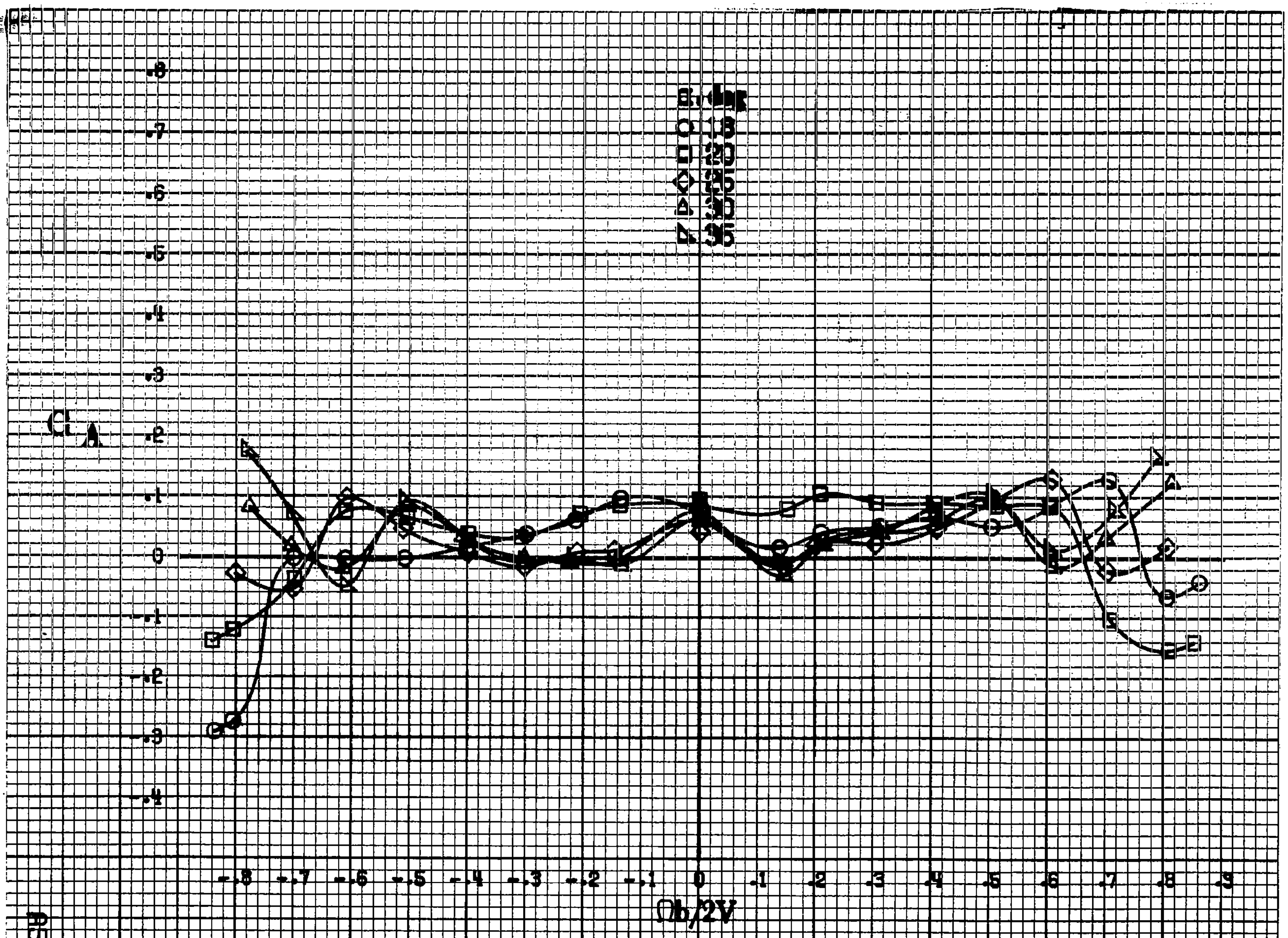

(b) α = 18 to 35 deg, SR = 182.9 cm (72 in).

Figure A192.-Continued.

A545

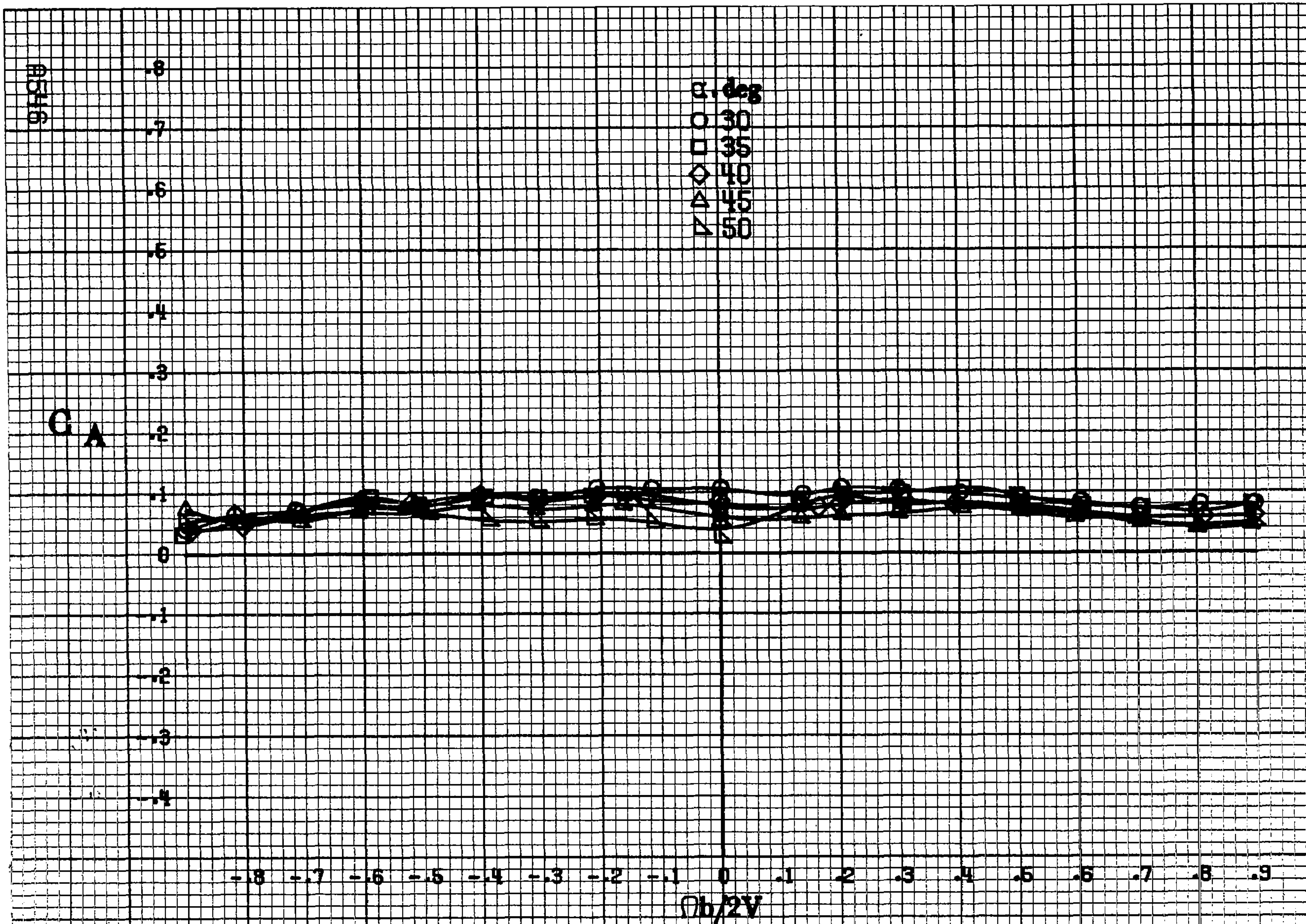

(c) α = 30 to 50 deg, SR = 0.

Figure A192.-Continued.

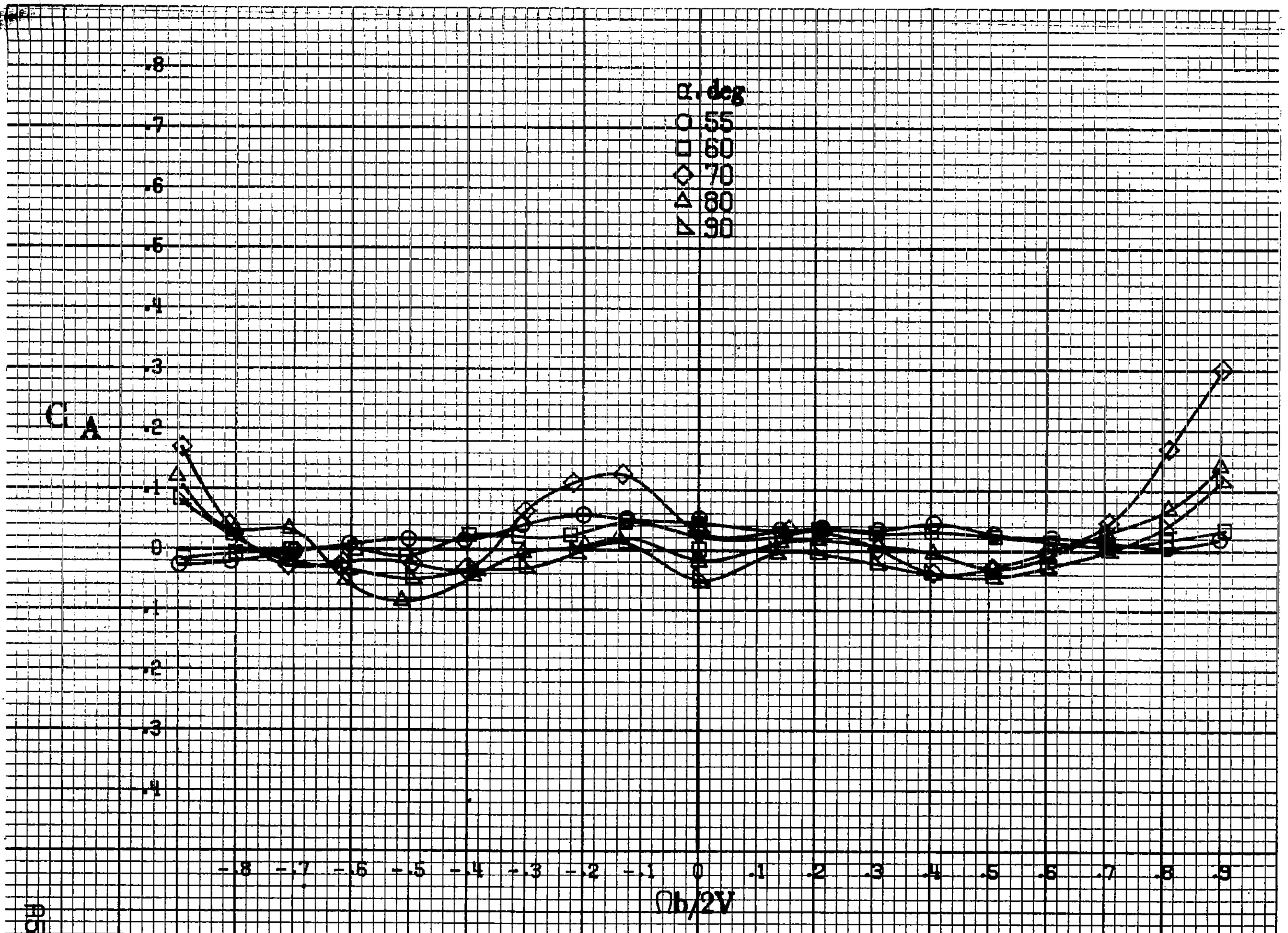

(d) α = 55 to 90 deg, SR = 0.

Figure A132.-Concluded.

(a) α = 8 to 16 deg, SR = 182.9 cm (72 in).

Figure A13?.-Effect of rotation rate and angle of attack on yawing-moment coefficient for T-tail configuration. $\delta_e = 0°$, $\delta_a = 0°$, $\delta_r = 0°$, $\beta = 0°$.

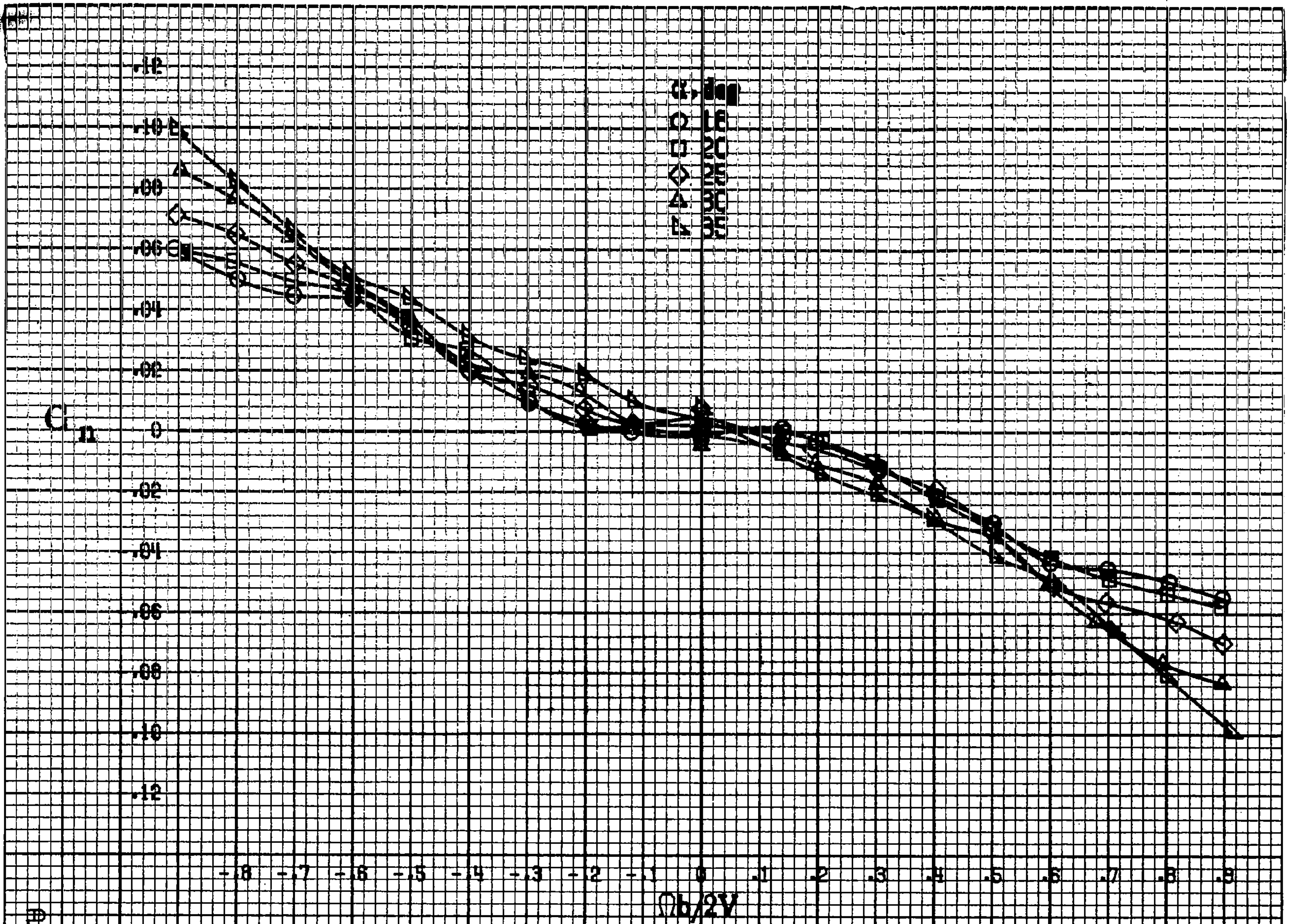

(b) α = 18 to 35 deg, SR = 182.9 cm (72 in).

Figure A138.-Continued.

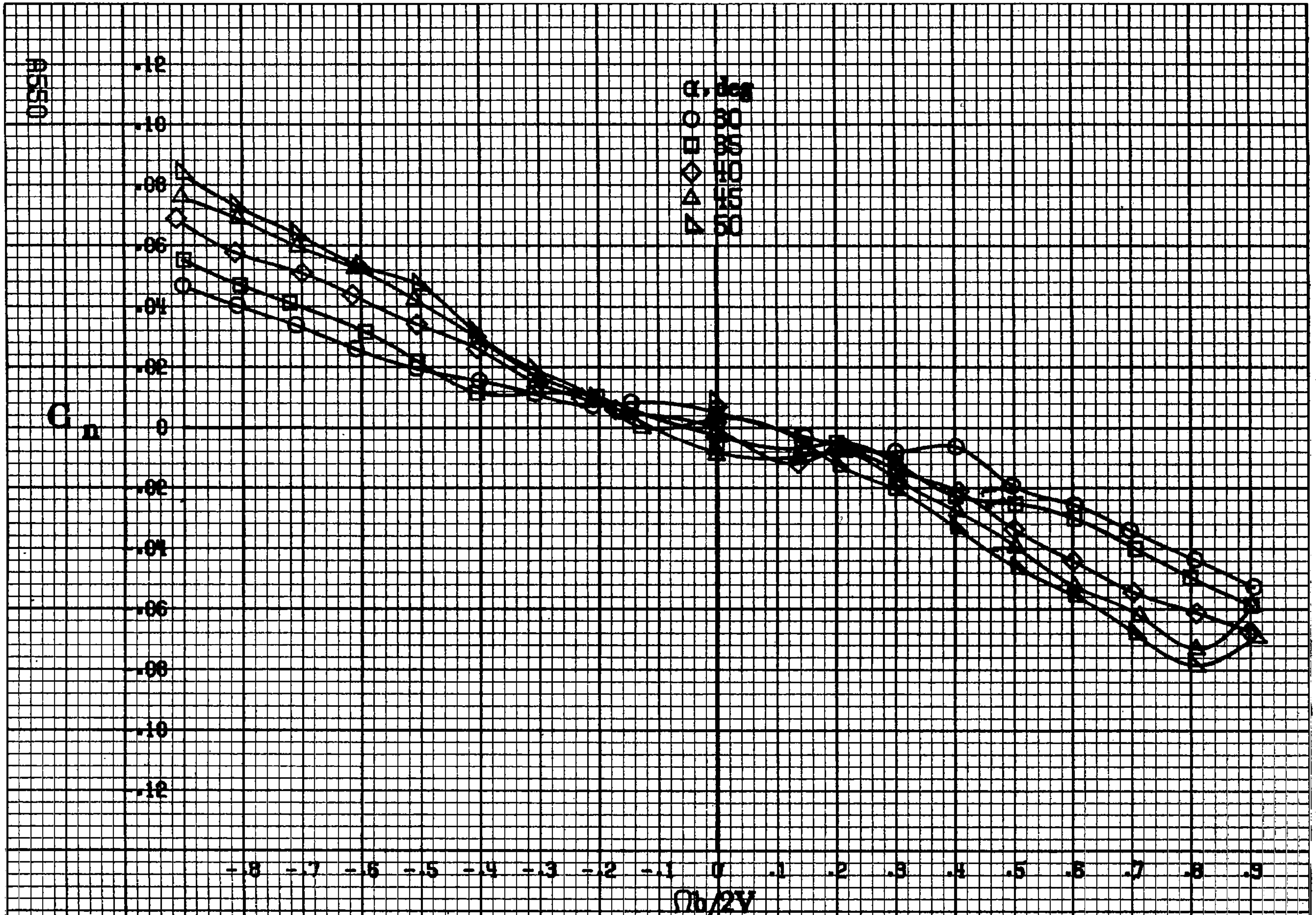

(c) $\alpha = 30$ to 50 deg, SR = 0.

Figure A188.-Continued.

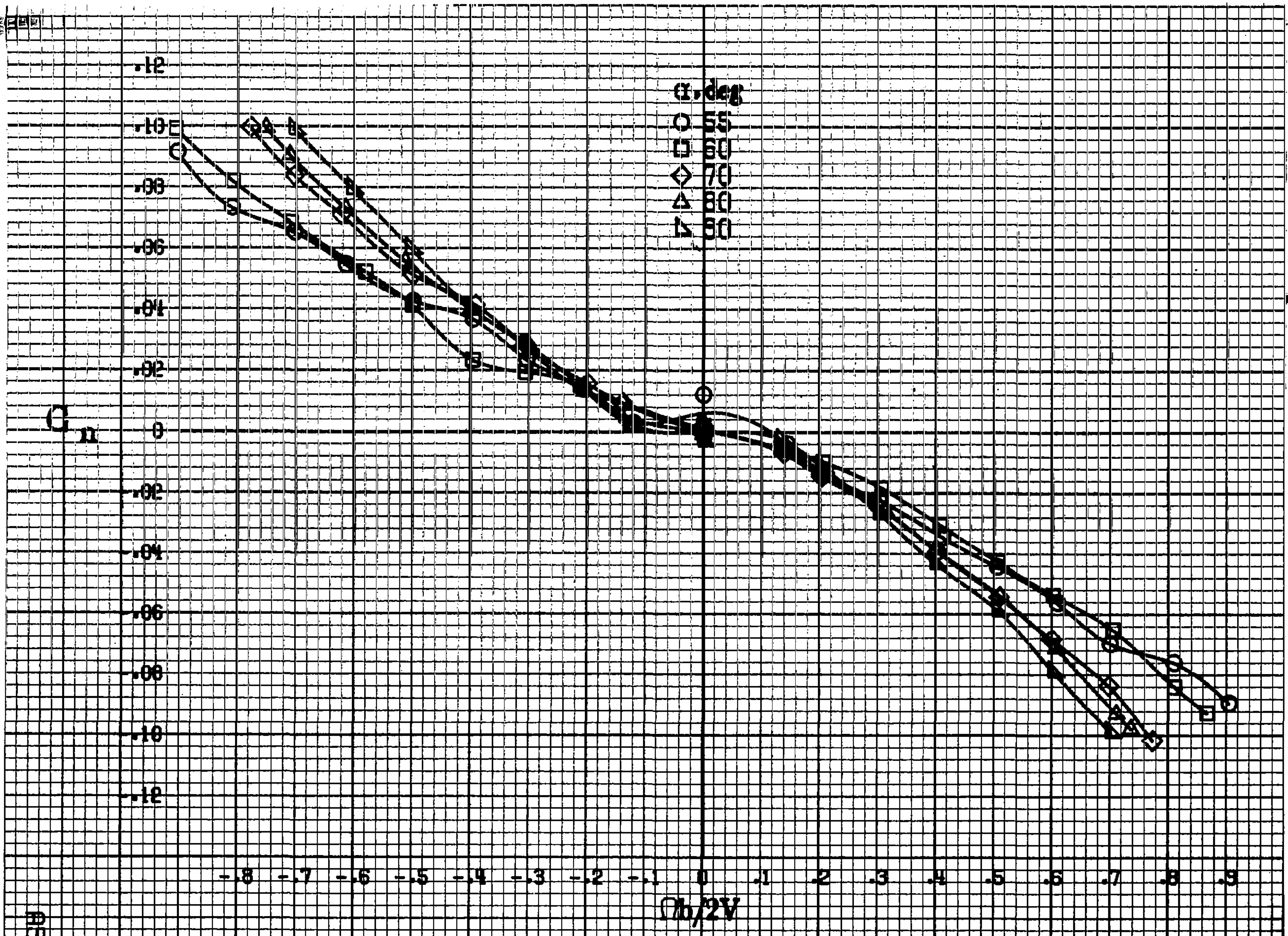

(d) α = 55 to 90 deg, SR = 0.

Figure A183.-Concluded.

A551

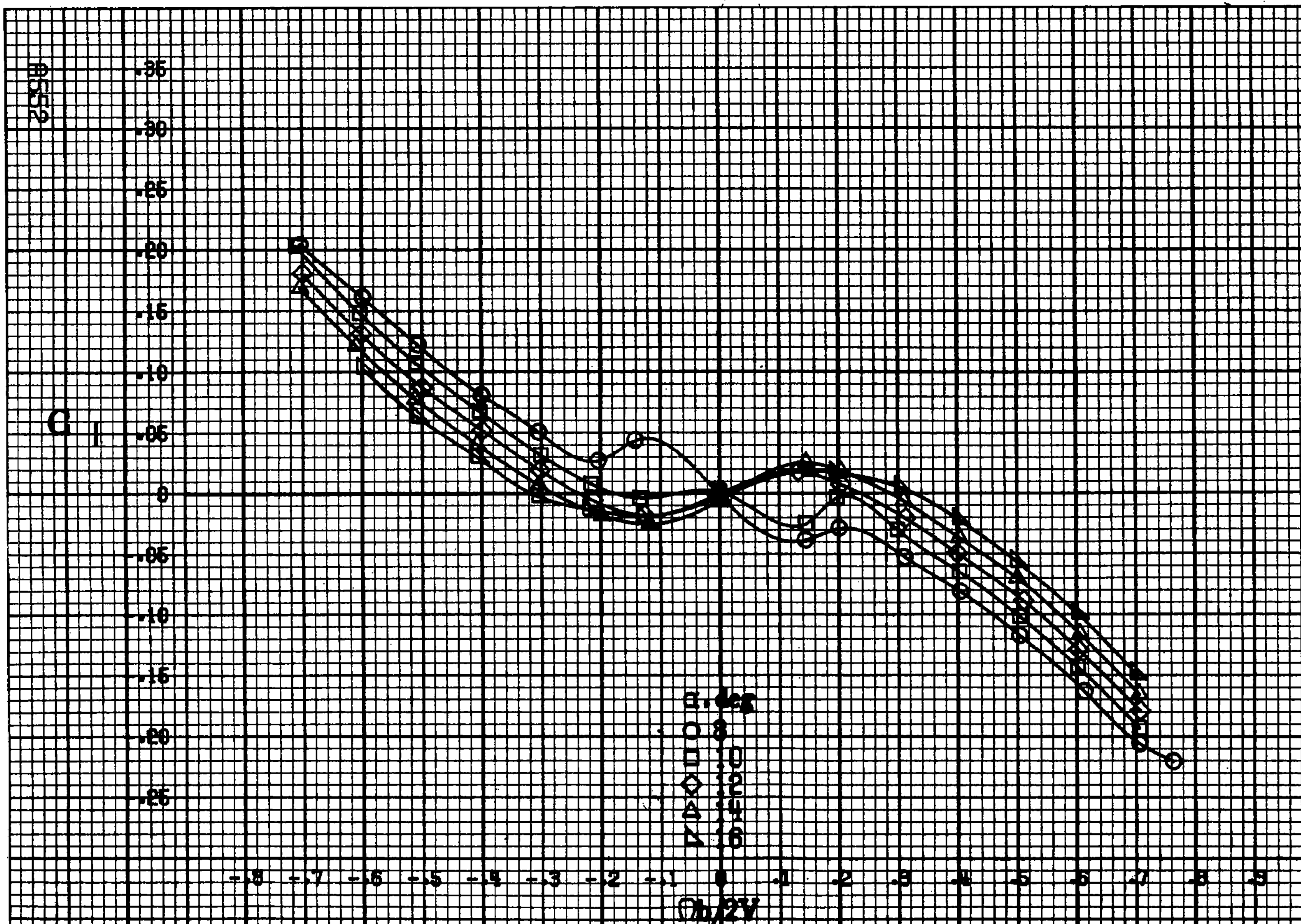

(a) $\alpha = 8$ to 16 deg, SR = 182.9 cm (72 in).

Figure A134.–Effect of rotation rate and angle of attack on rolling-moment coefficient for T-tail configuration. $\delta_e = 0°$, $\delta_a = 0°$, $\delta_r = 0°$, $\beta = 0°$.

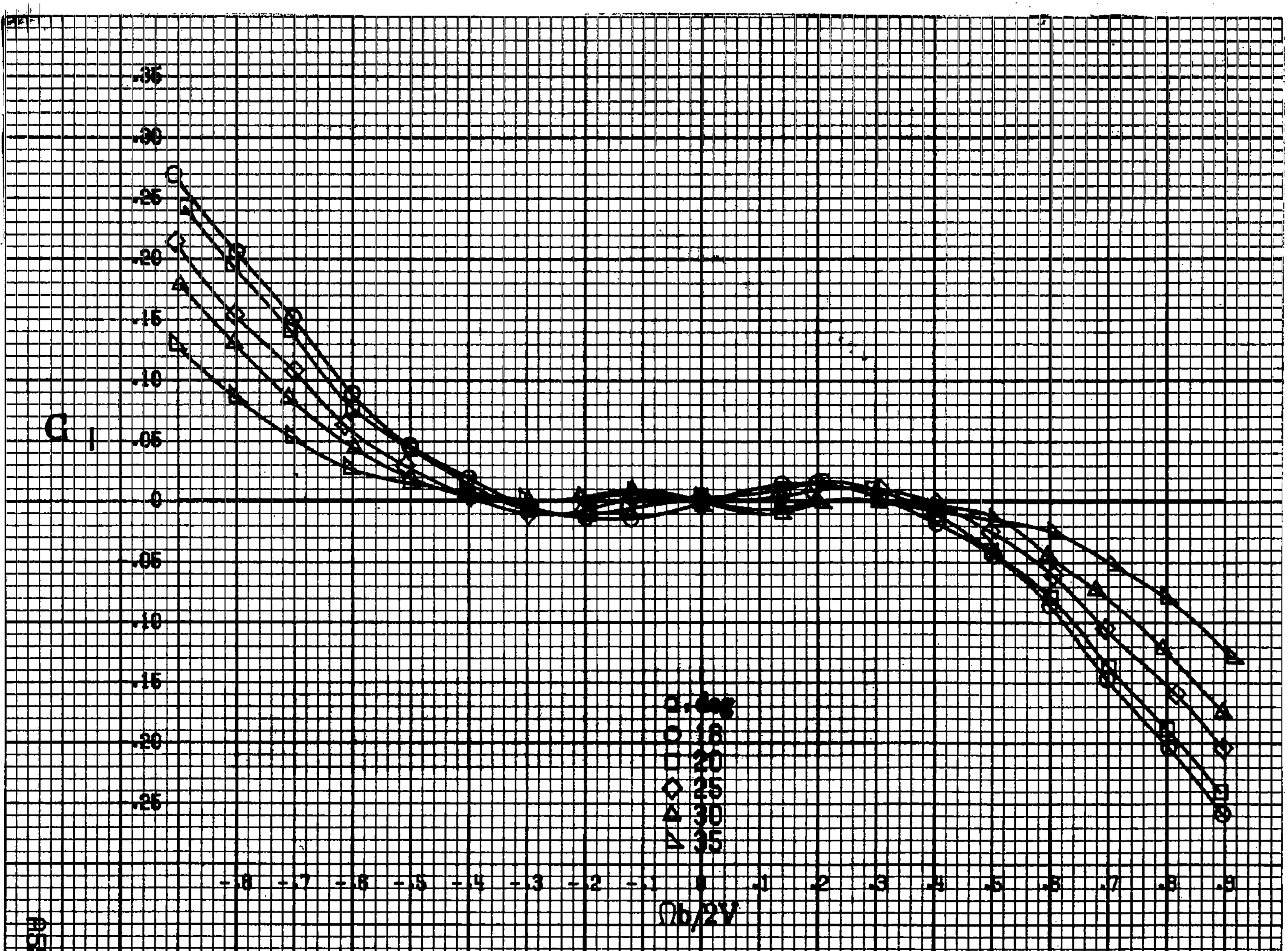

(b) α = 18 to 35 deg, SR = 182.9 cm (72 in).

Figure A134.-Continued.

A553

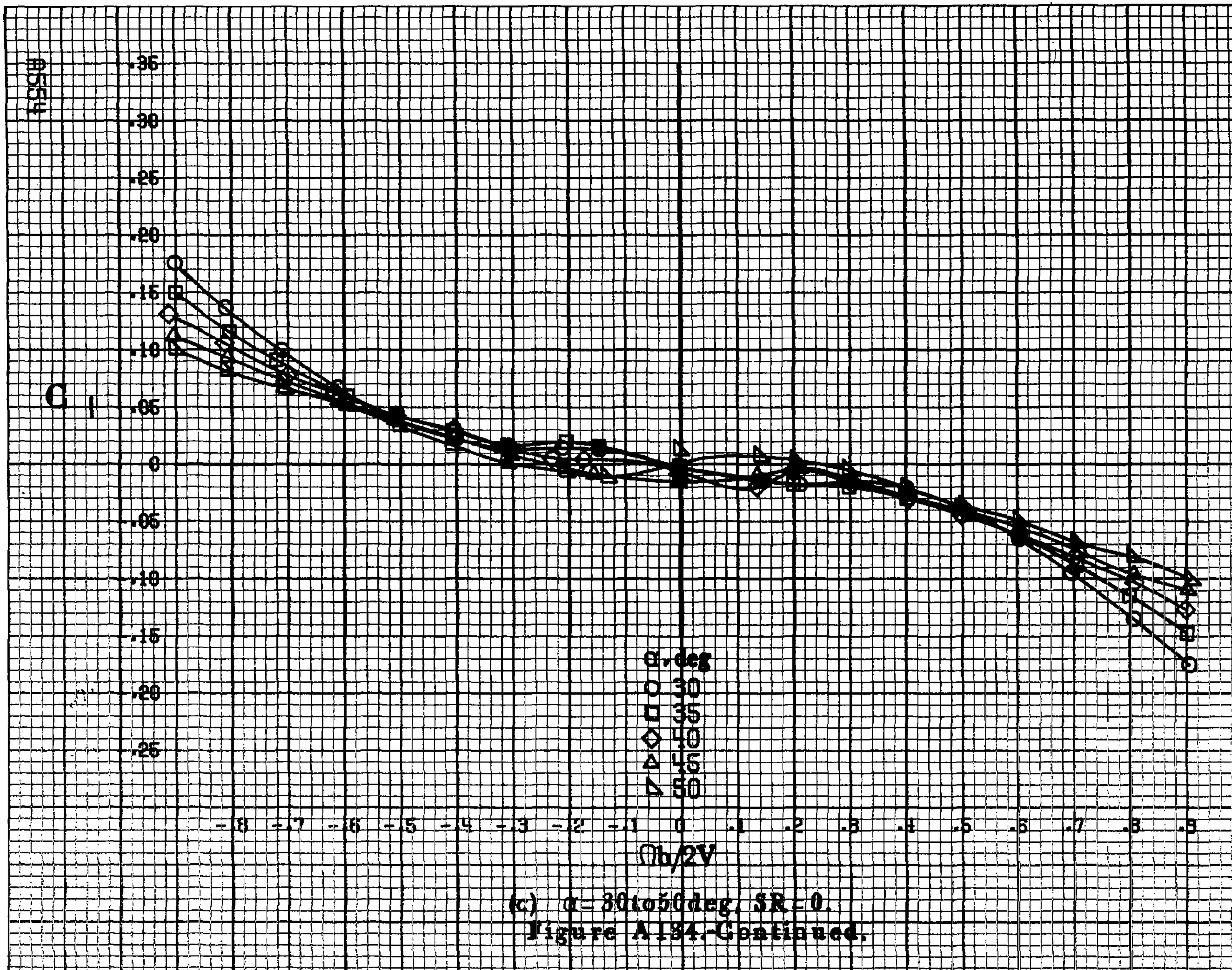

(c) $\alpha = 30$ to 50 deg, SR = 0.

Figure A134.-Continued.

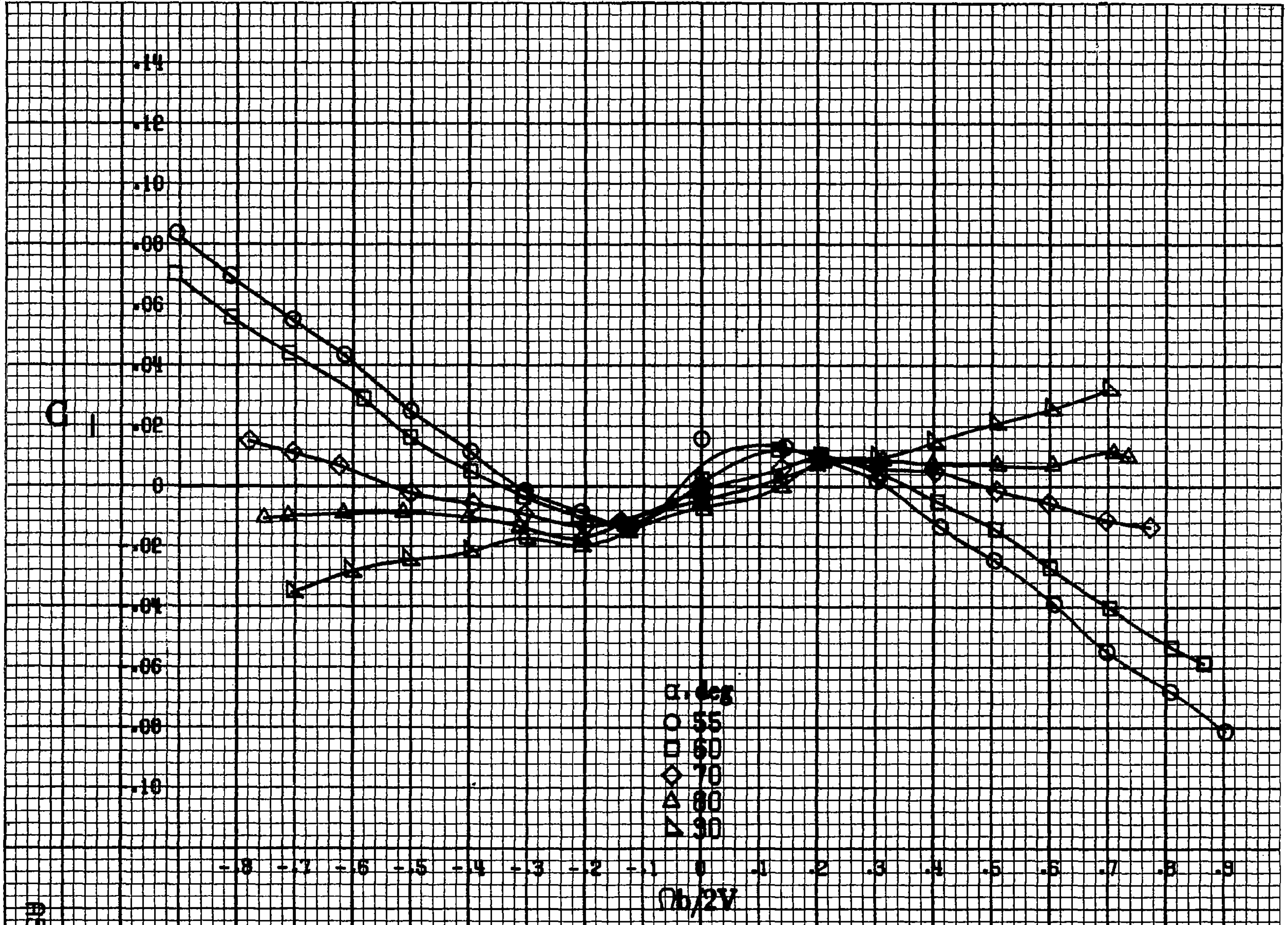

(d) α = 55 to 90 deg, SR = 0.

Figure A184.-Concluded.

A555

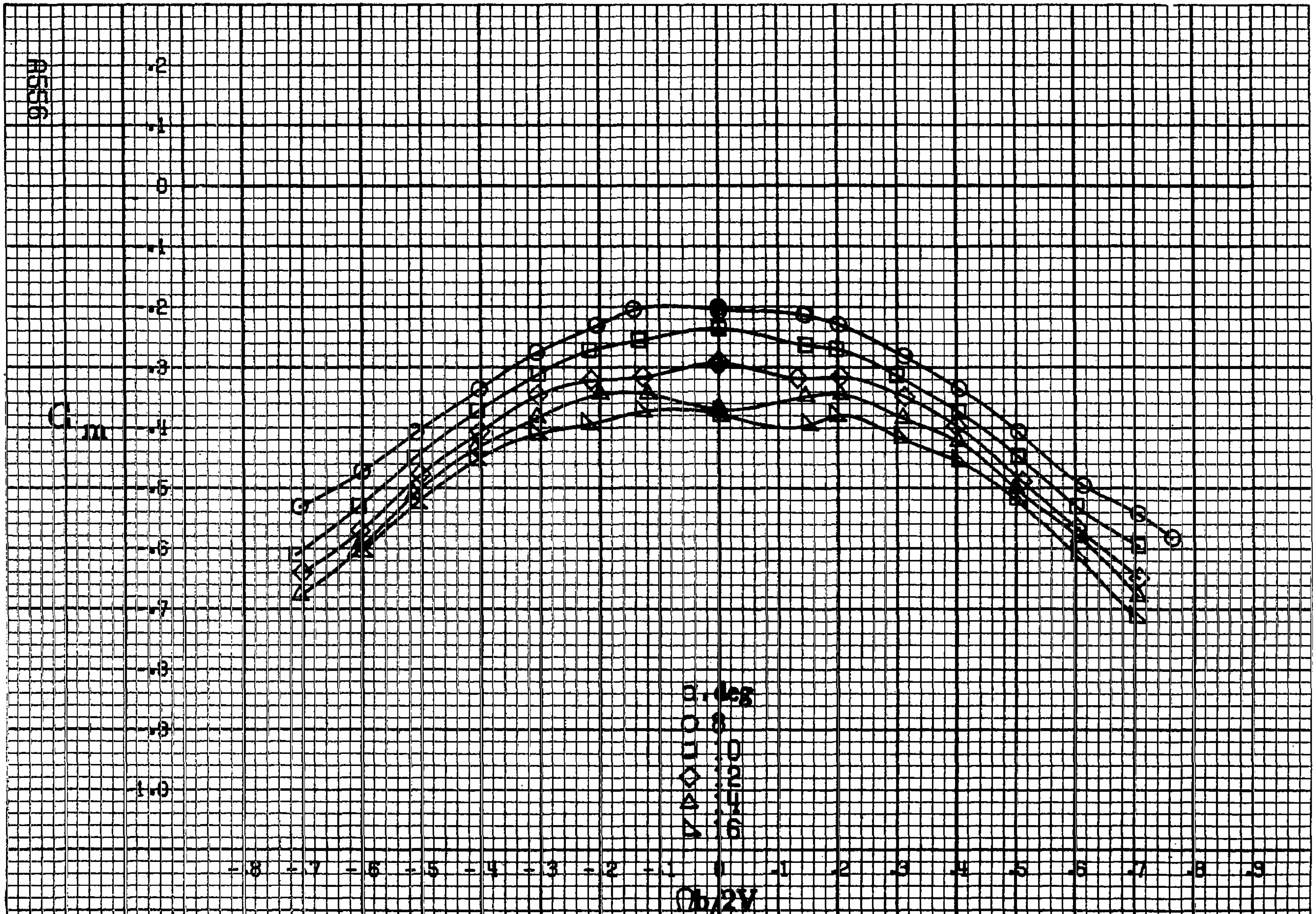

(a) $\alpha = 8$ to 16 deg, SR = 182.9 cm (72 in).

Figure A135.- Effect of rotation rate and angle of attack on pitching-moment coefficient for T-tail configuration. $\delta_e = 0°$, $\delta_a = 0°$, $\delta_r = 0°$, $\beta = 0°$.

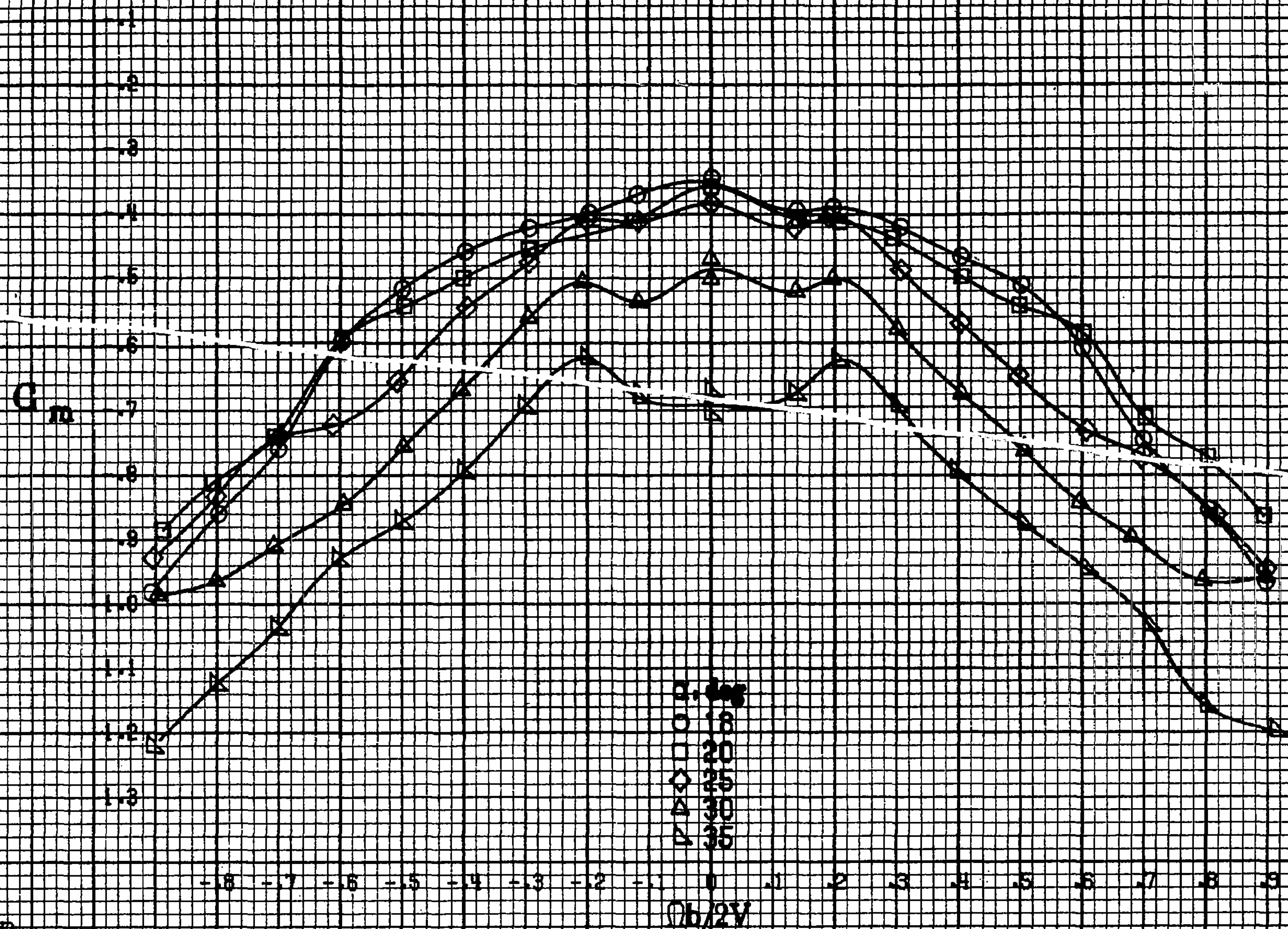

(b) α=18to35deg, SR=182.9cm(72in).
Figure A185.-Continued.

A557

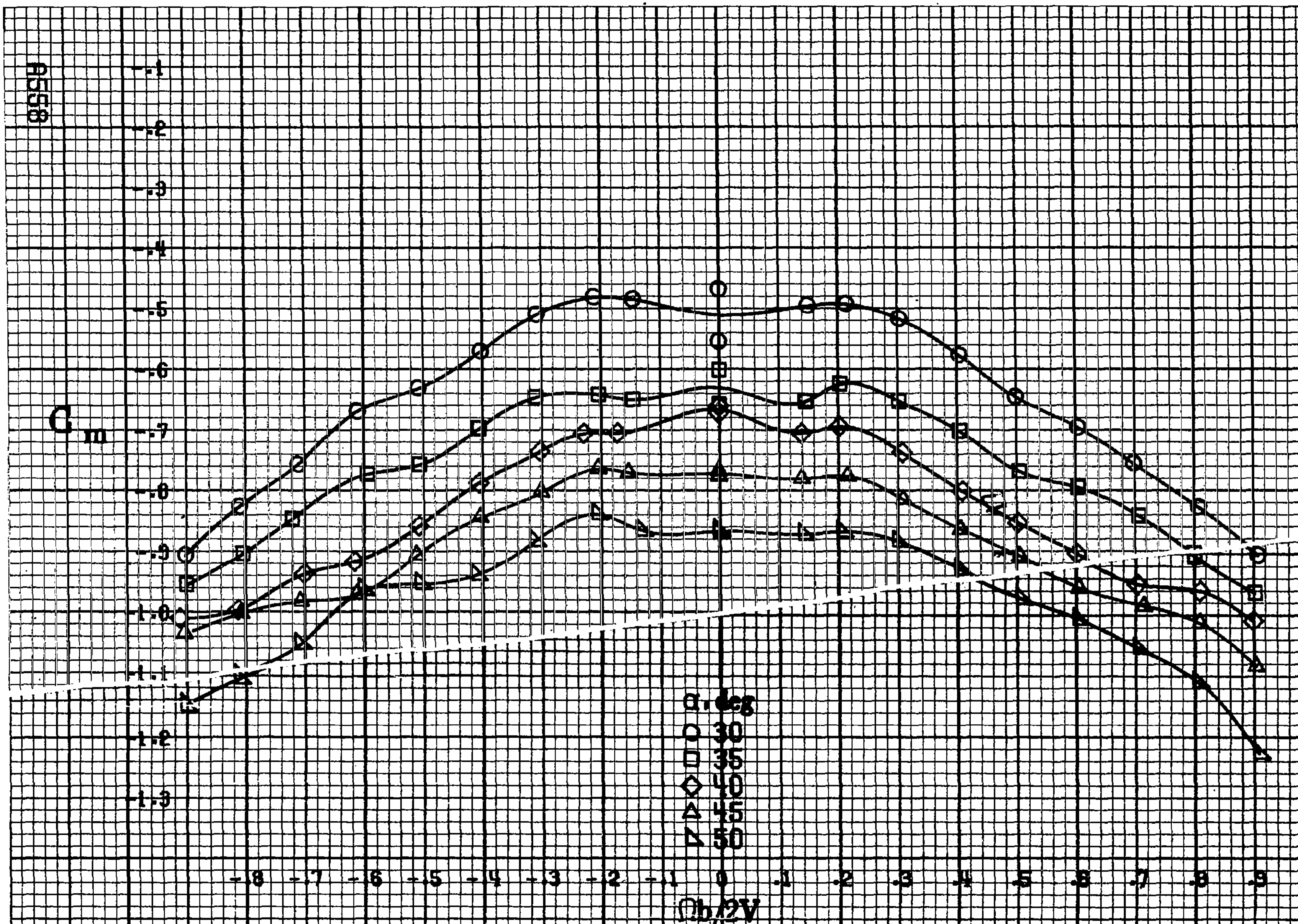

(c) α = 30 to 50 deg, SR = 0.

Figure A135.-Continued.

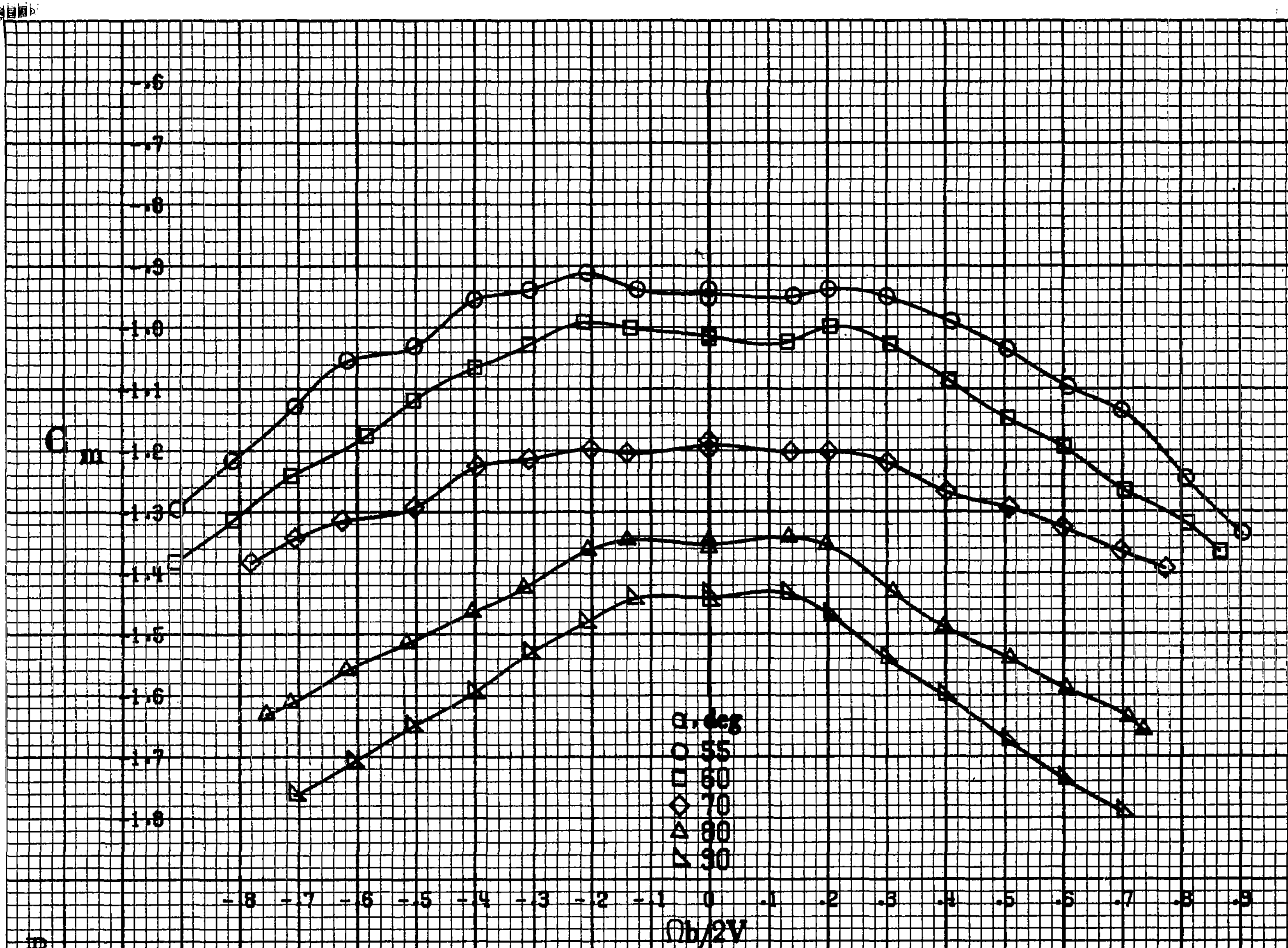

(d) α = 55to90deg, SR = 0.

Figure A185.-Concluded.

(a) $\alpha = 8$ to 16 deg, SR = 182.9 cm (72 in).

Figure A136.-Effect of rotation rate and angle of attack on normal-force coefficient for T-tail configuration. $\delta_e = 0°$, $\delta_a = 0°$, $\delta_r = 0°$, $\beta = 0°$.

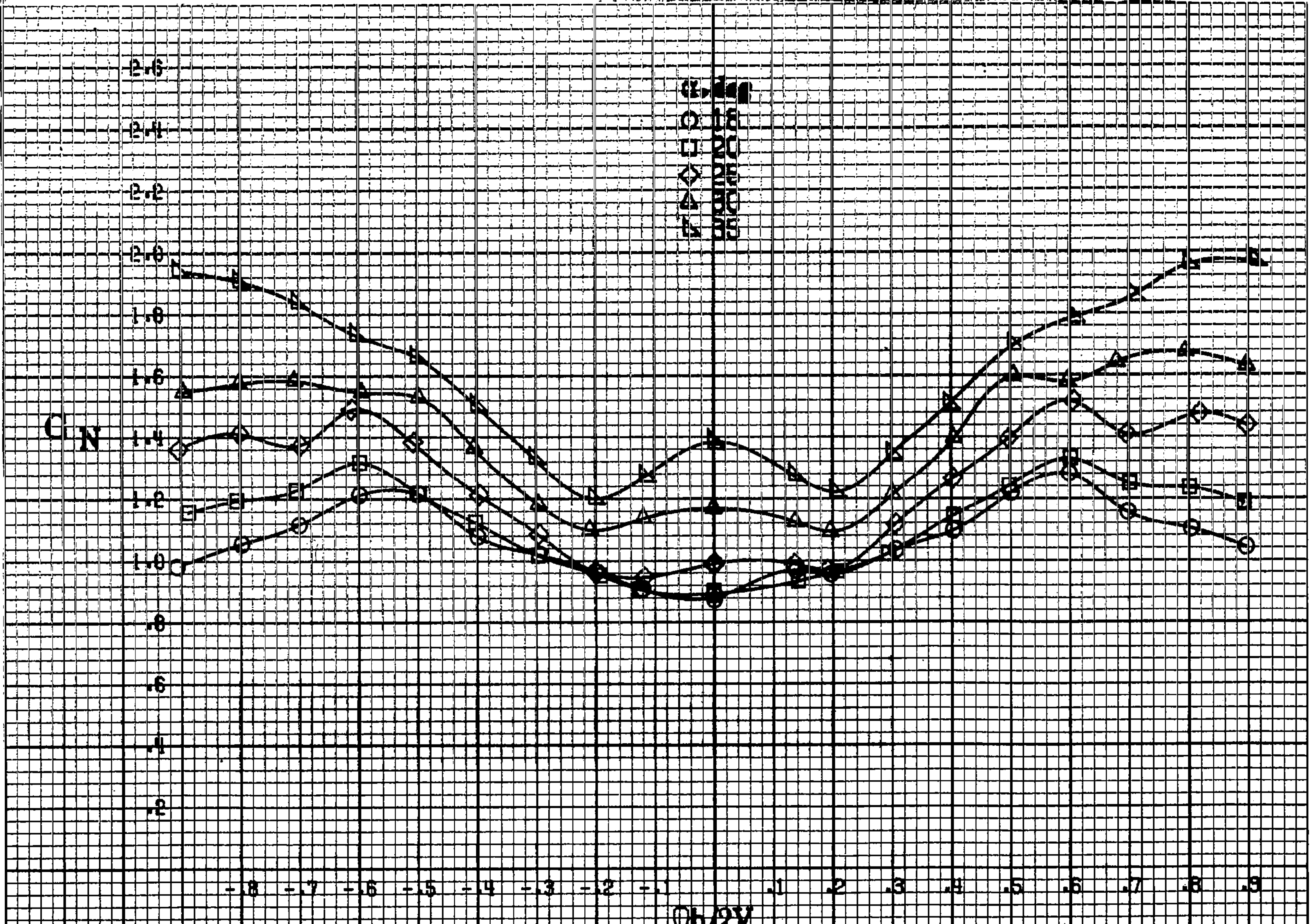

(b) α = 18 to 35 deg, SR = 182.9 cm (72 in).

Figure A186.-Continued.

A561

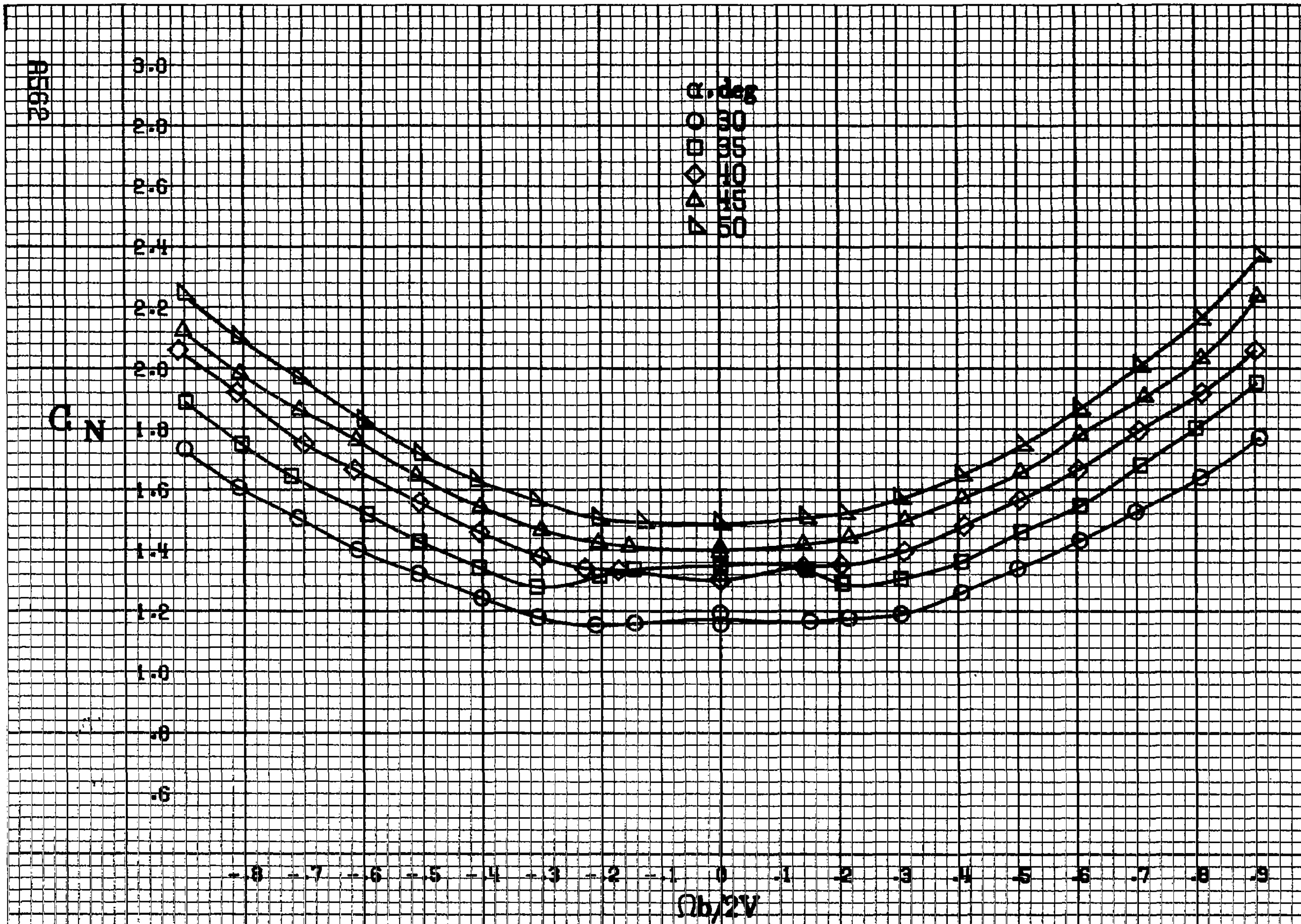

(c) α = 30 to 50 deg, SR = 0.

Figure A196.-Continued.

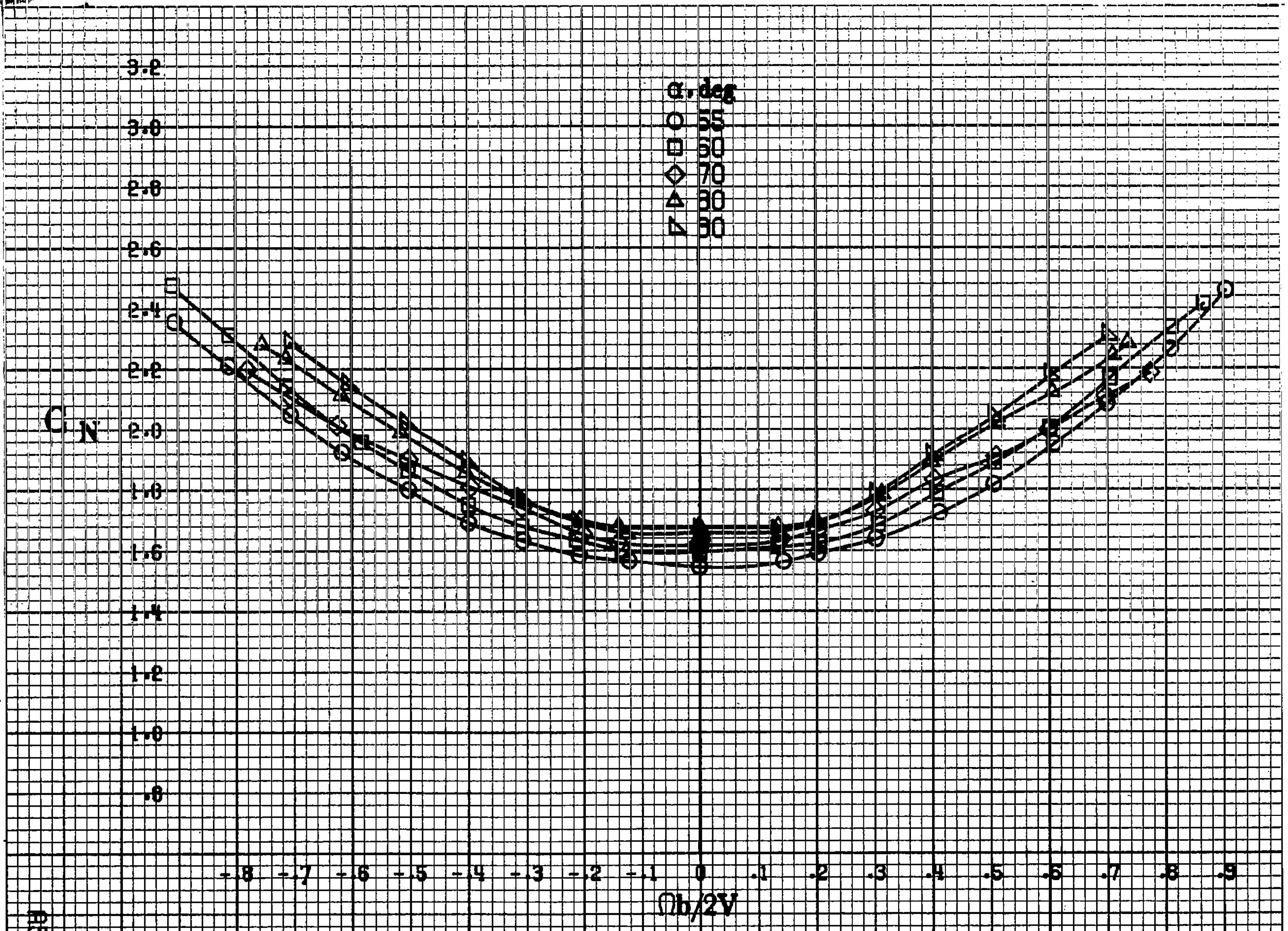

(d) α=55 to 90 deg, SR=0.

Figure A136.-Concluded.

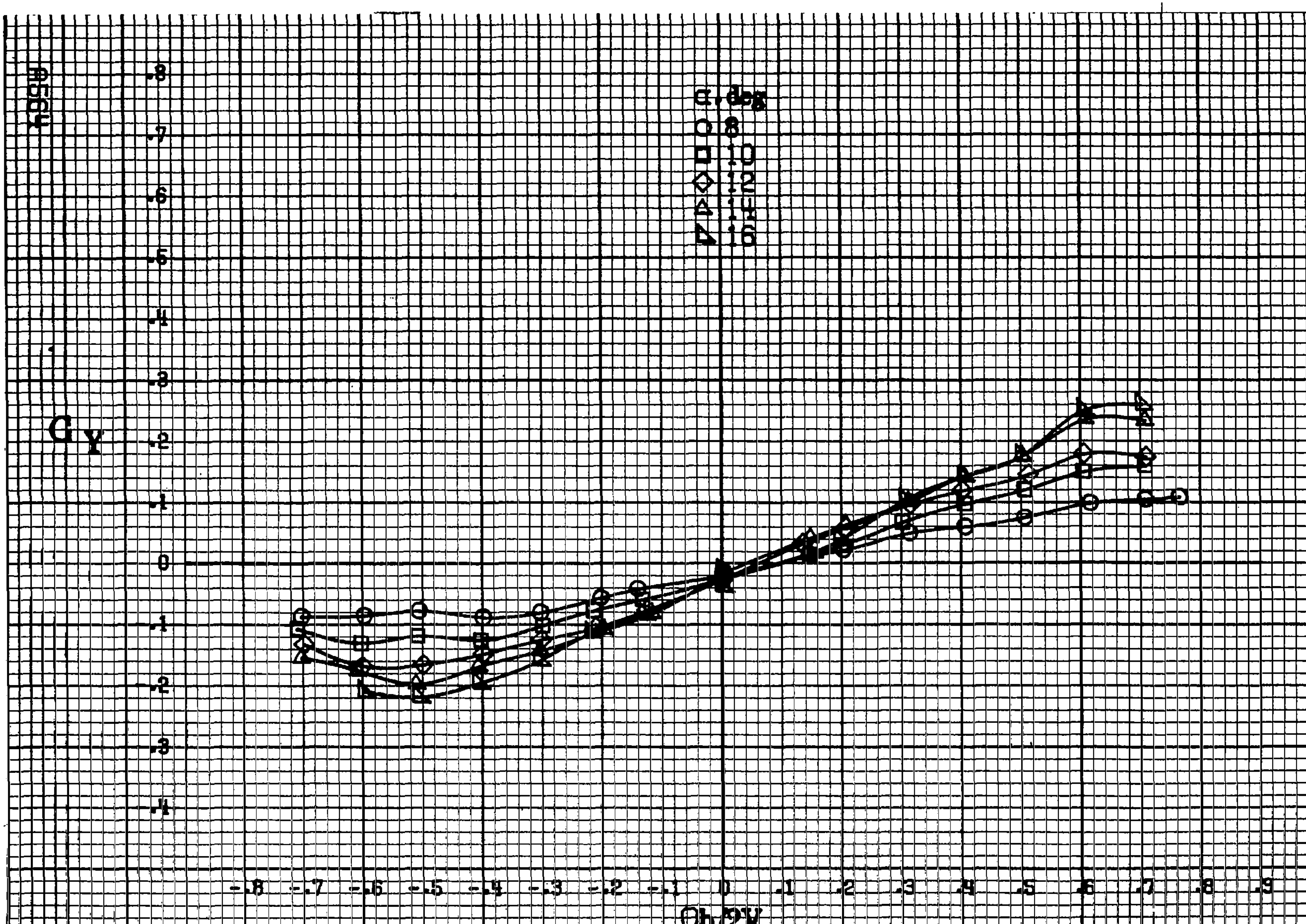

(a) α = 8 to 16 deg, SR = 182.9 cm (72 in).

Figure A137.- Effect of rotation rate and angle of attack on side-force coefficient for T-tail configuration. $\delta_e = 0°$, $\delta_a = 0°$, $\delta_r = 0°$, $\theta = 0°$.

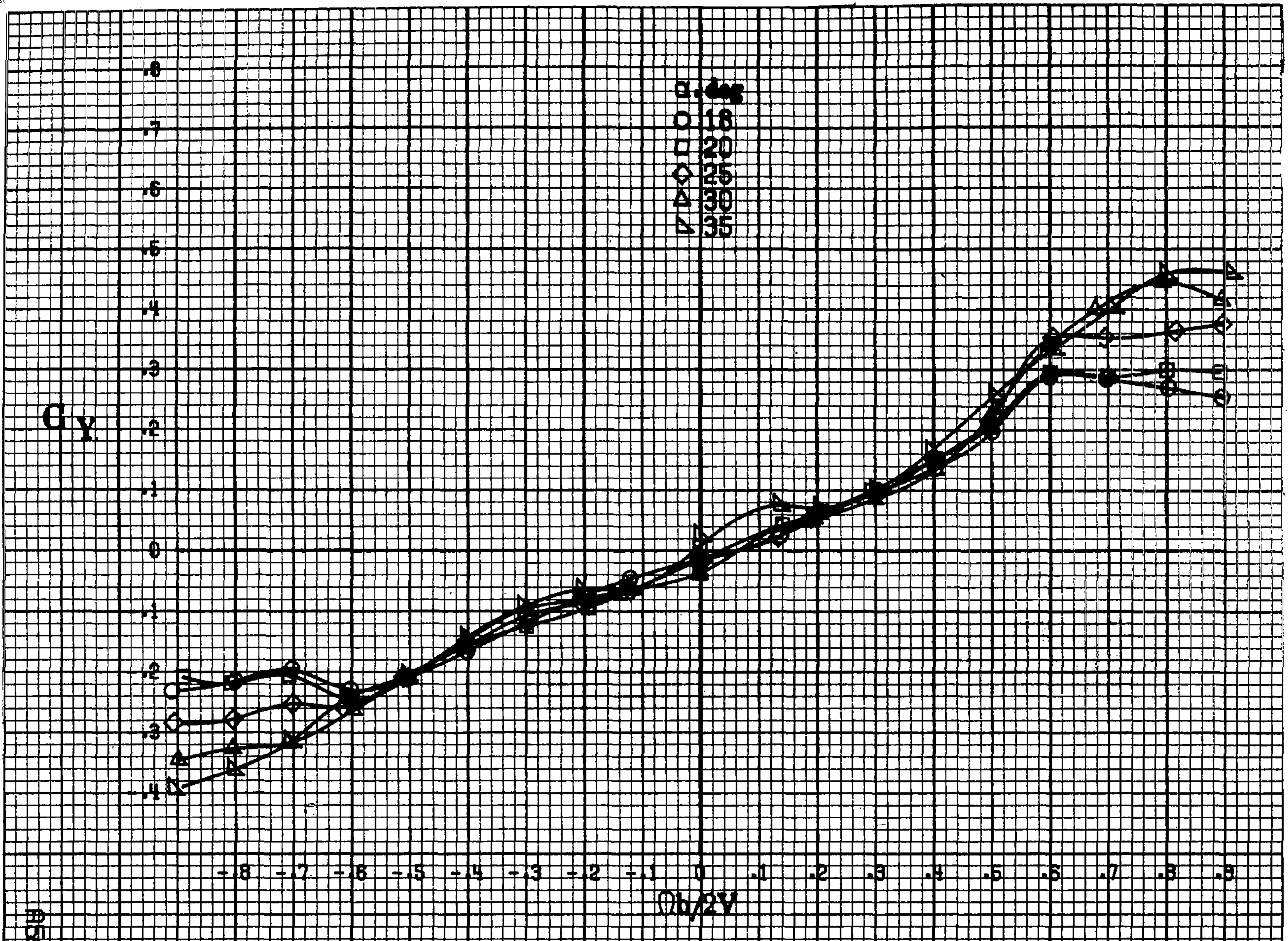

(b) α = 18 to 35 deg, SR = 182.9 cm (72 in).

Figure A187.- Continued.

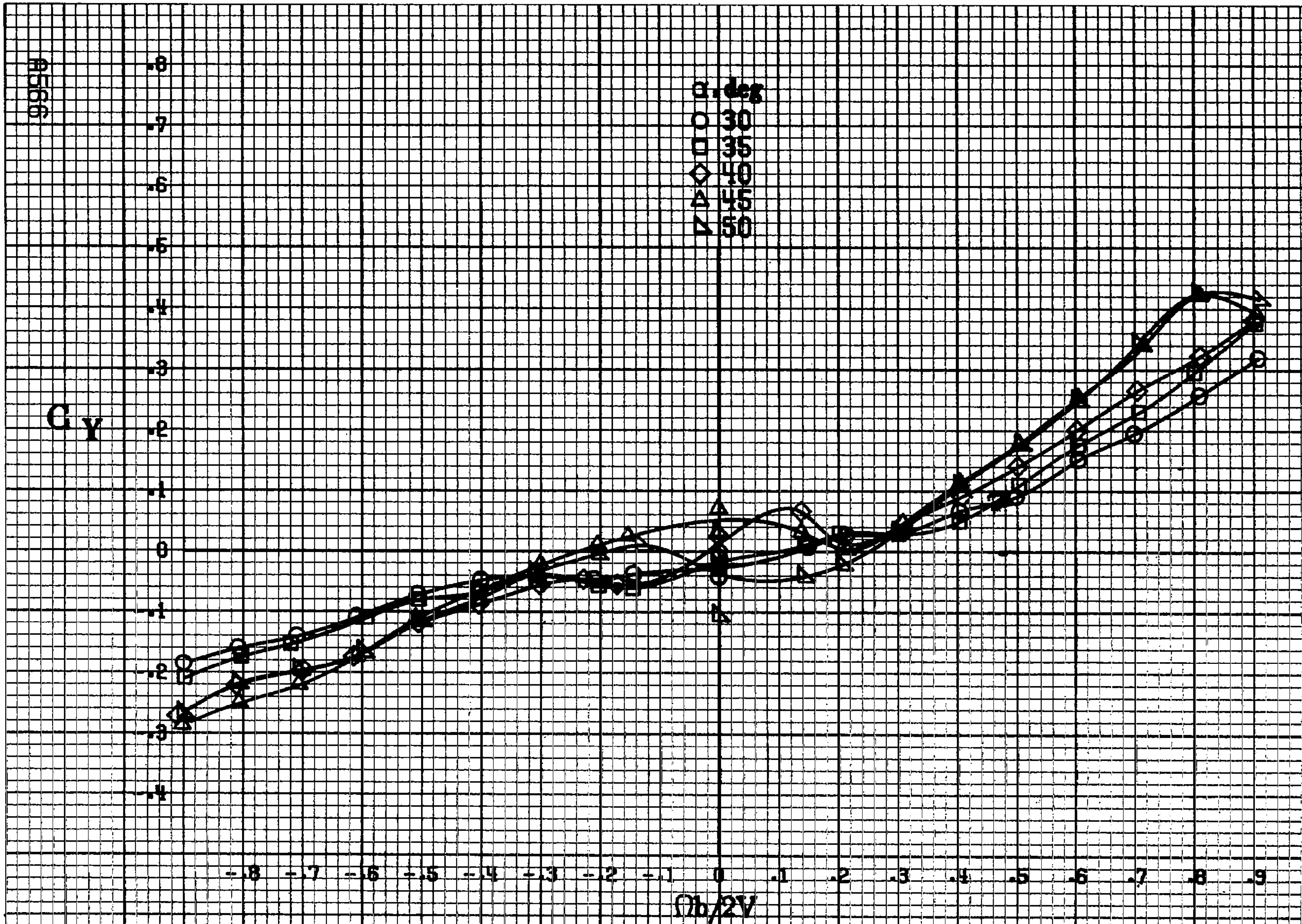

(c) α = 30 to 50 deg, SR = 0.
Figure A187.-Continued.

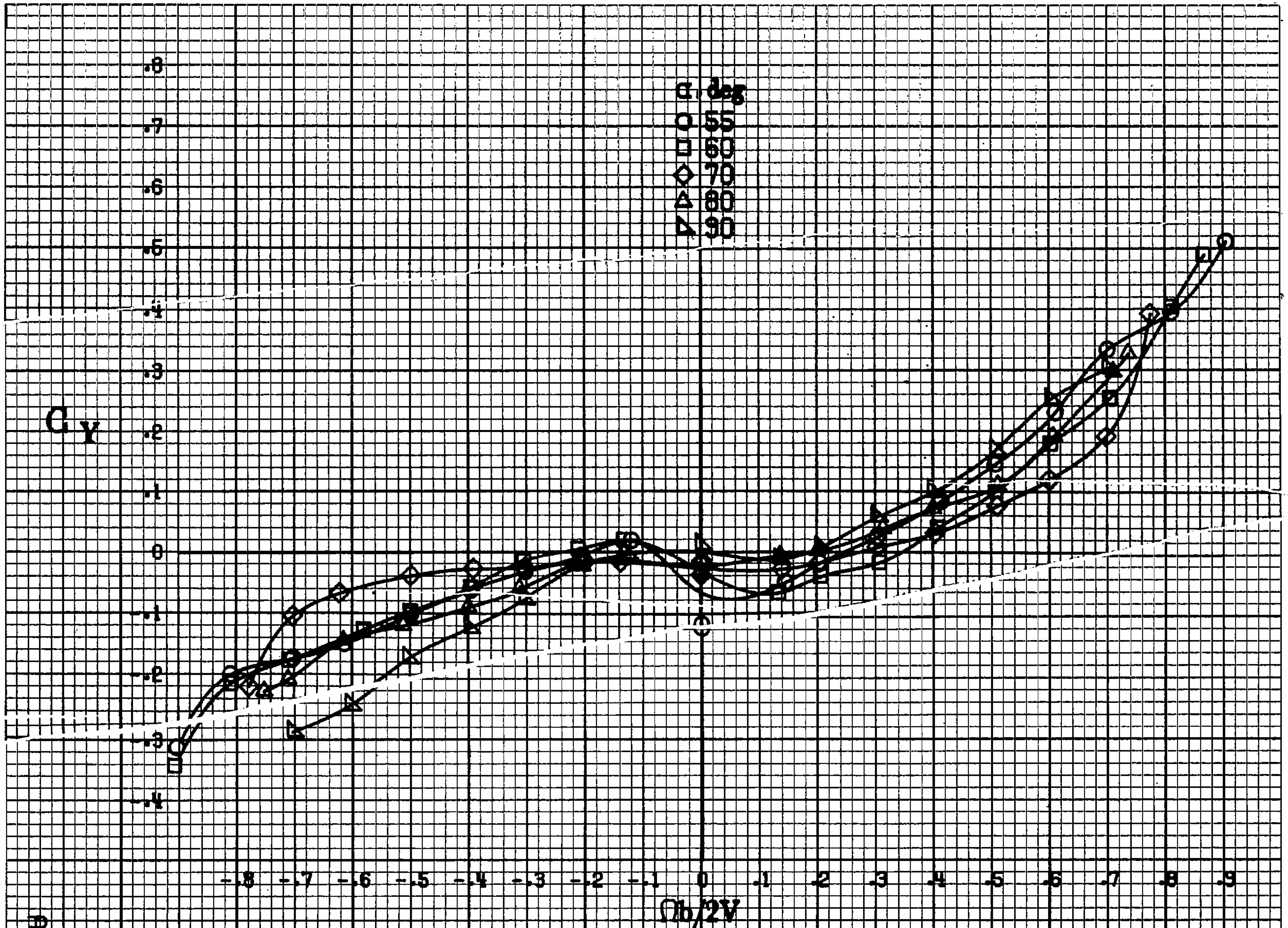

(d) α = 55 to 90 deg, SR = 0.
Figure A187.-Concluded.

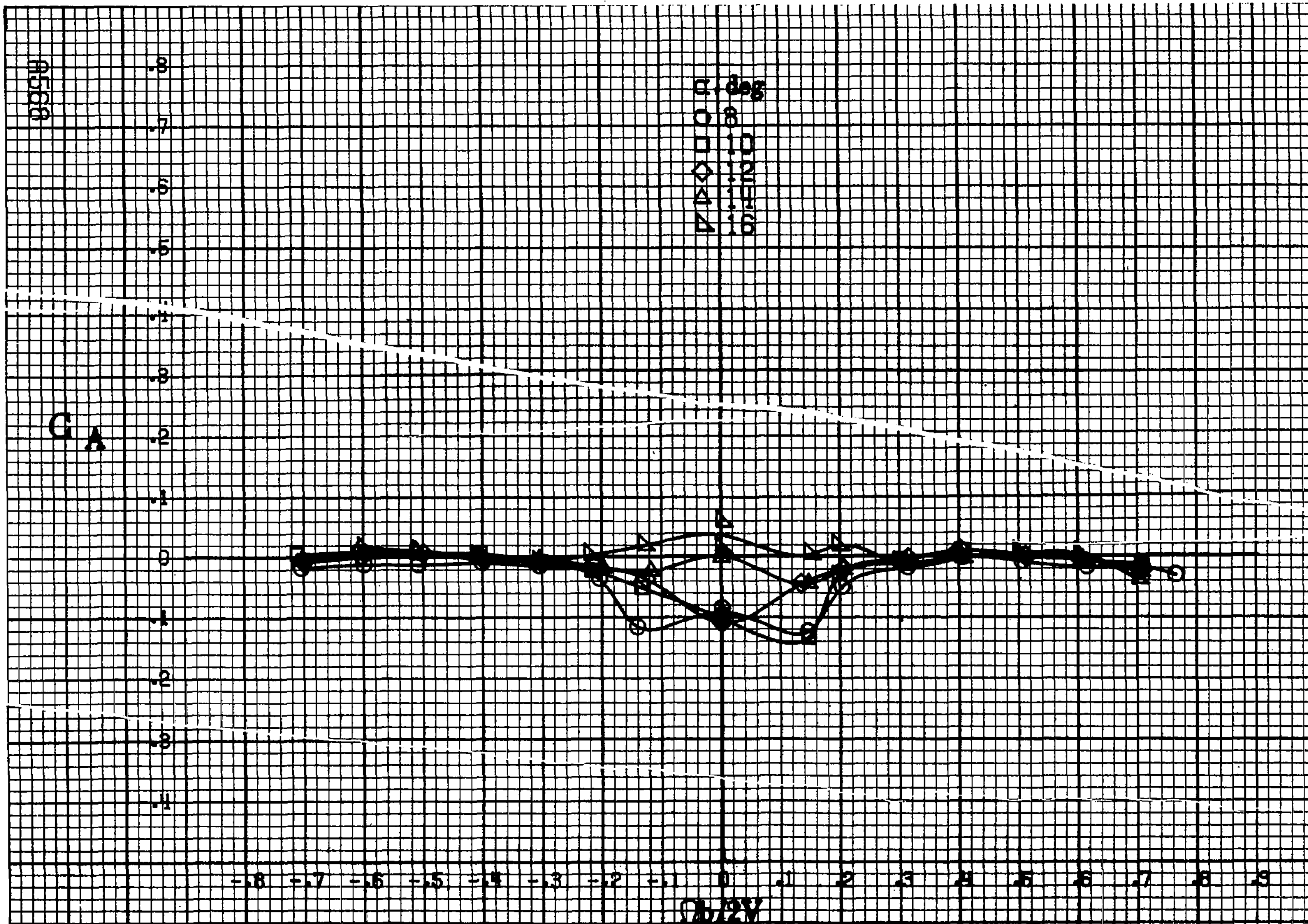

(a) α = 8 to 16 deg, SR = 182.9 cm (72 in).

Figure A138.-Effect of rotation rate and angle of attack on axial-force coefficient for T-tail configuration. $\delta_e = 0°$, $\delta_a = 0°$, $\delta_r = 0°$, $\beta = 0°$.

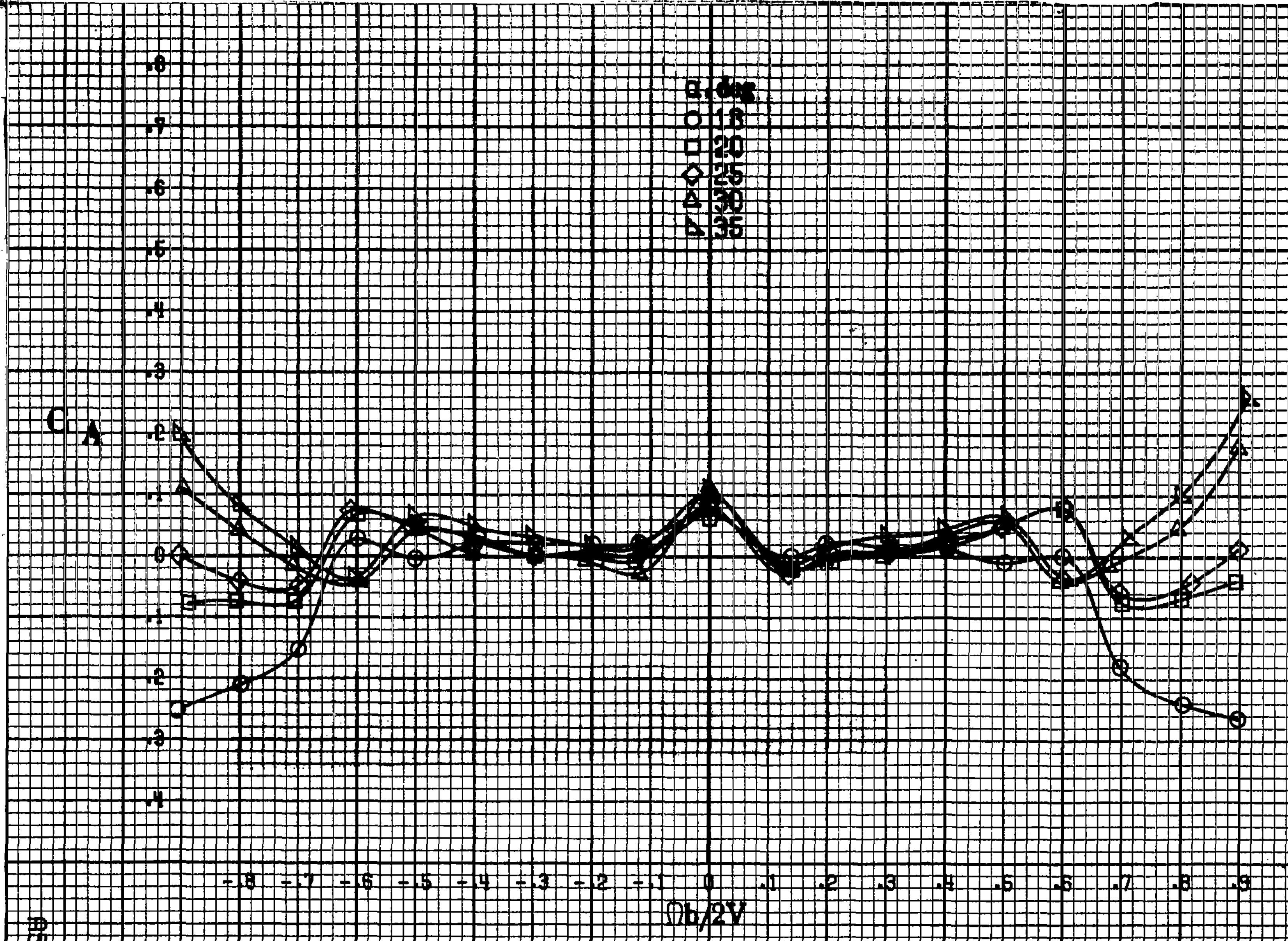

(b) α = 18 to 35 deg, SR = 182.9 cm (72 in).
Figure A138.-Continued.

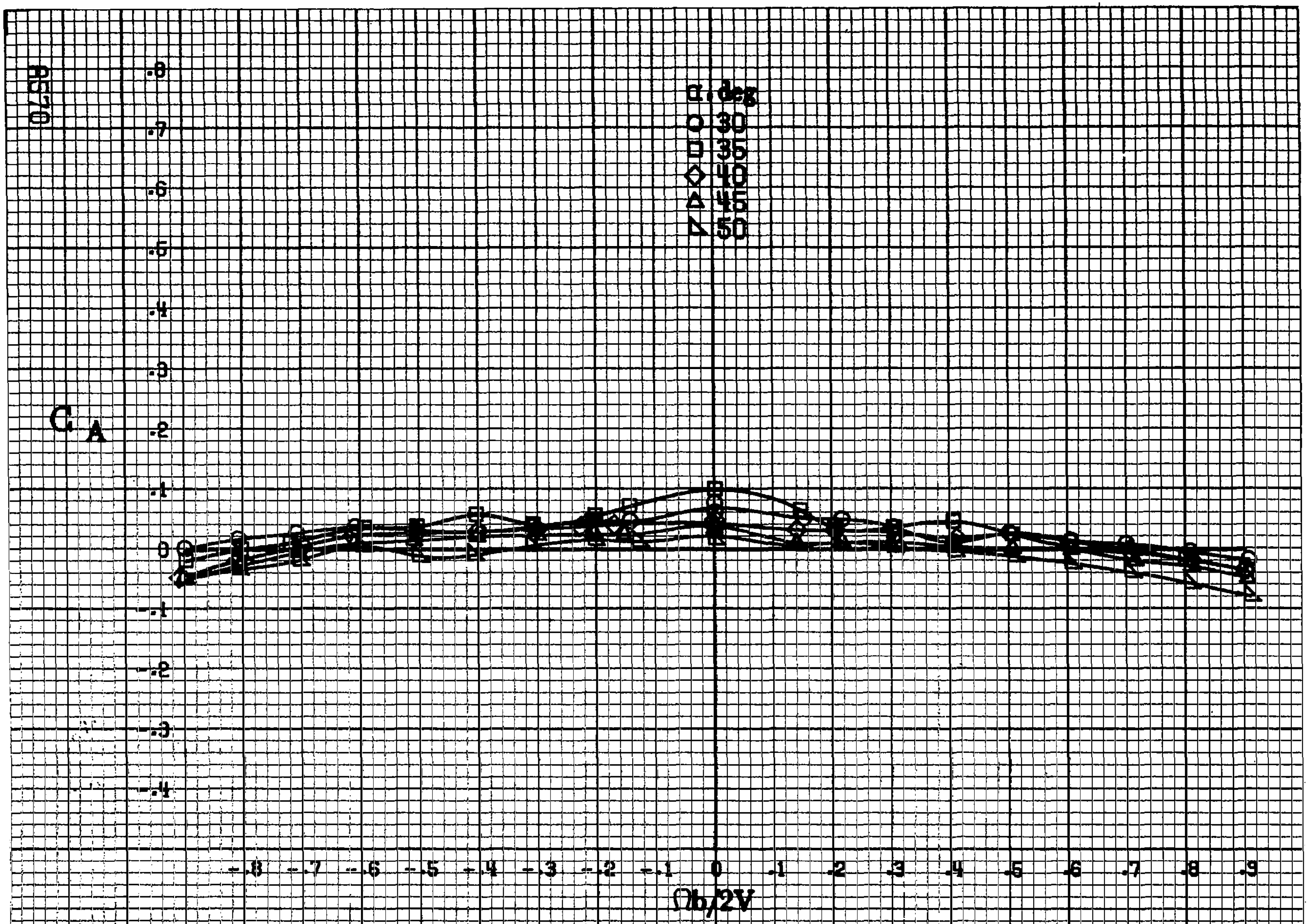

(c) α = 30 to 50 deg, SR = 0.

Figure A198.-Continued.

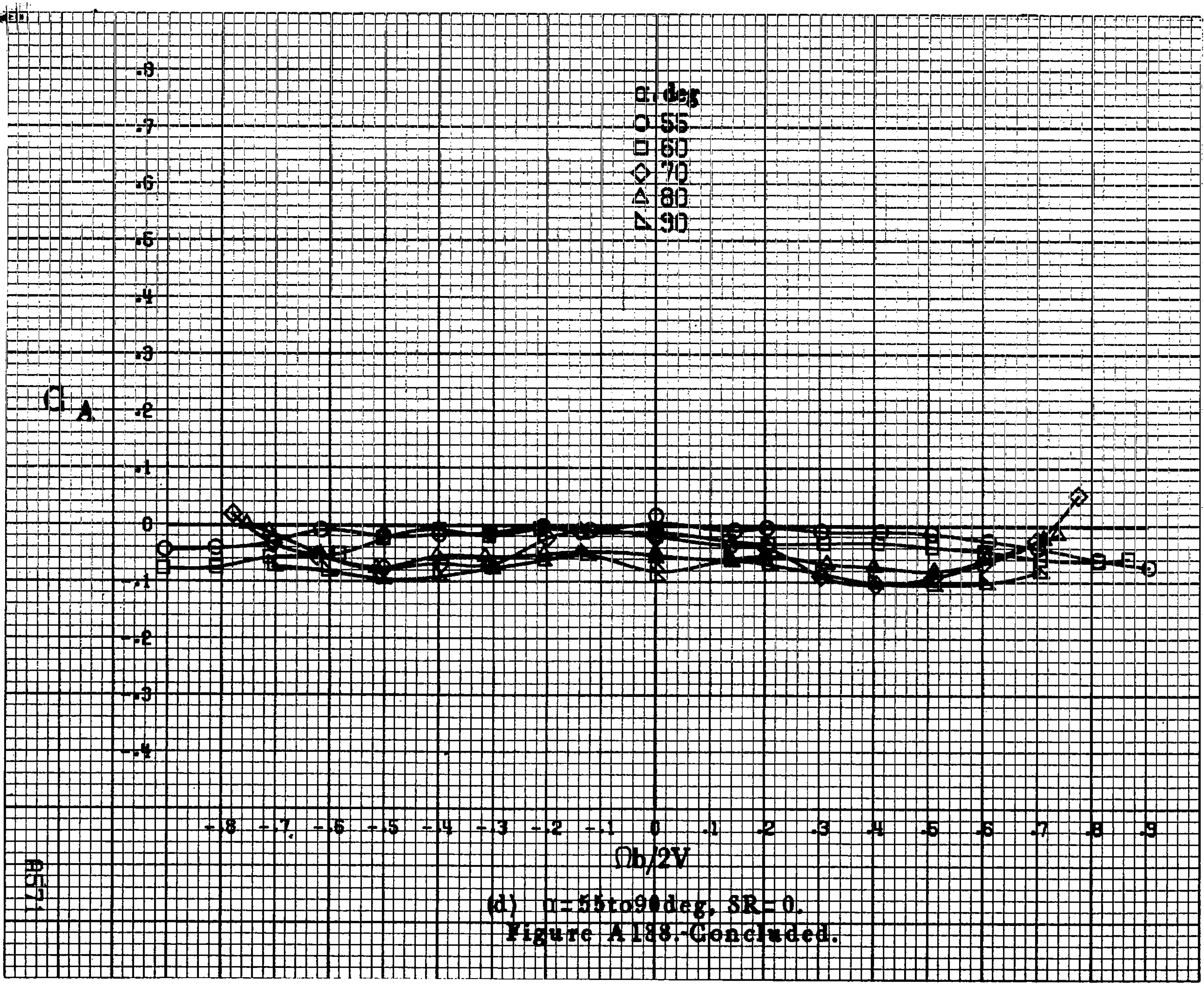

(d) α = 55 to 90 deg, SR = 0.

Figure A188.-Concluded.

A571

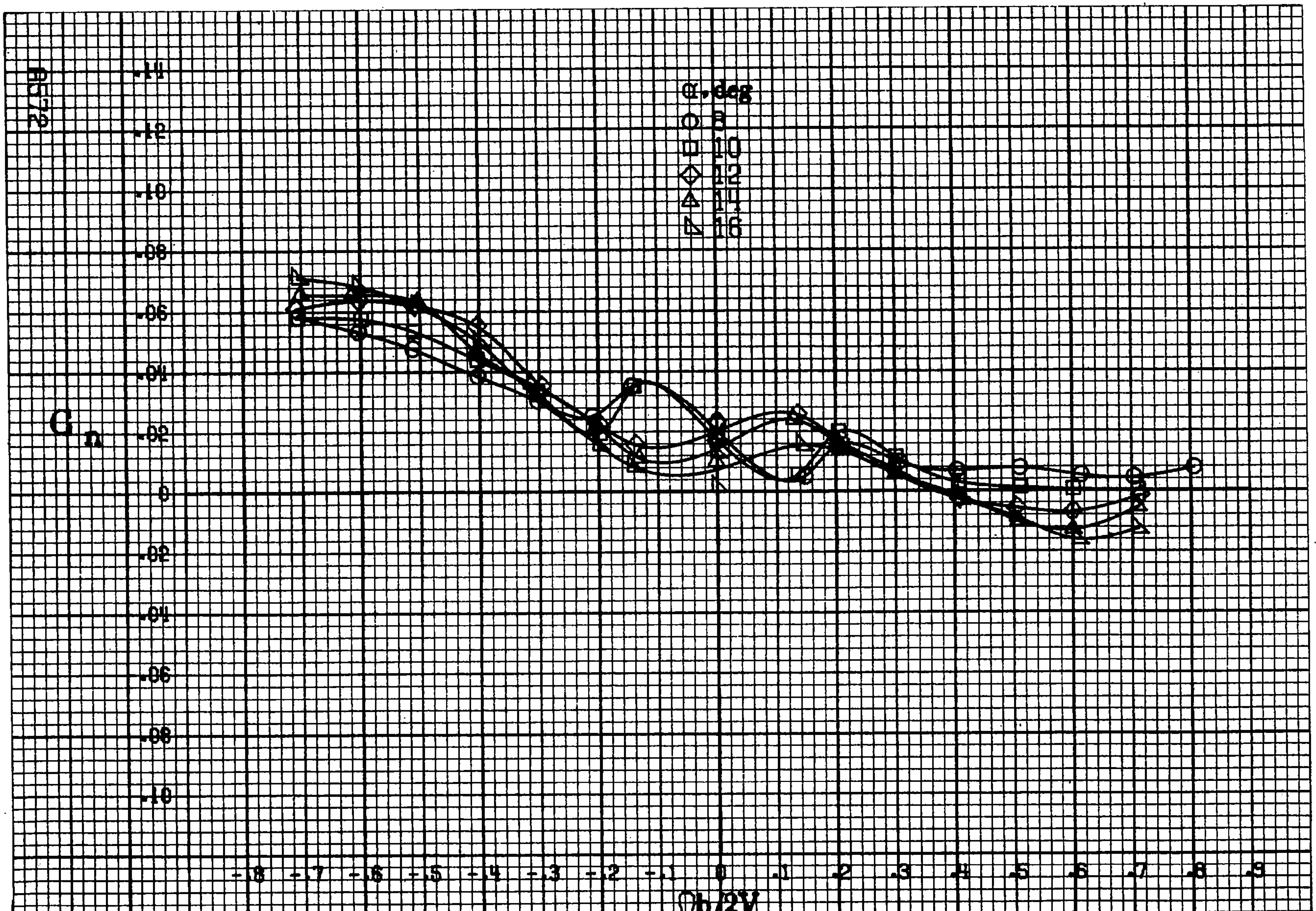

(a) α = 8 to 16 deg, SR = 182.9 cm (72 in).

Figure A139.- Effect of rotation rate and angle of attack on yawing-moment coefficient for T-tail configuration. $\delta_e = -15°$, $\delta_a = 0°$, $\delta_r = -25°$, $\beta = 0°$.

(b) α = 18 to 35 deg, SR = 182.9 cm (72 in).

Figure A189.-Continued.

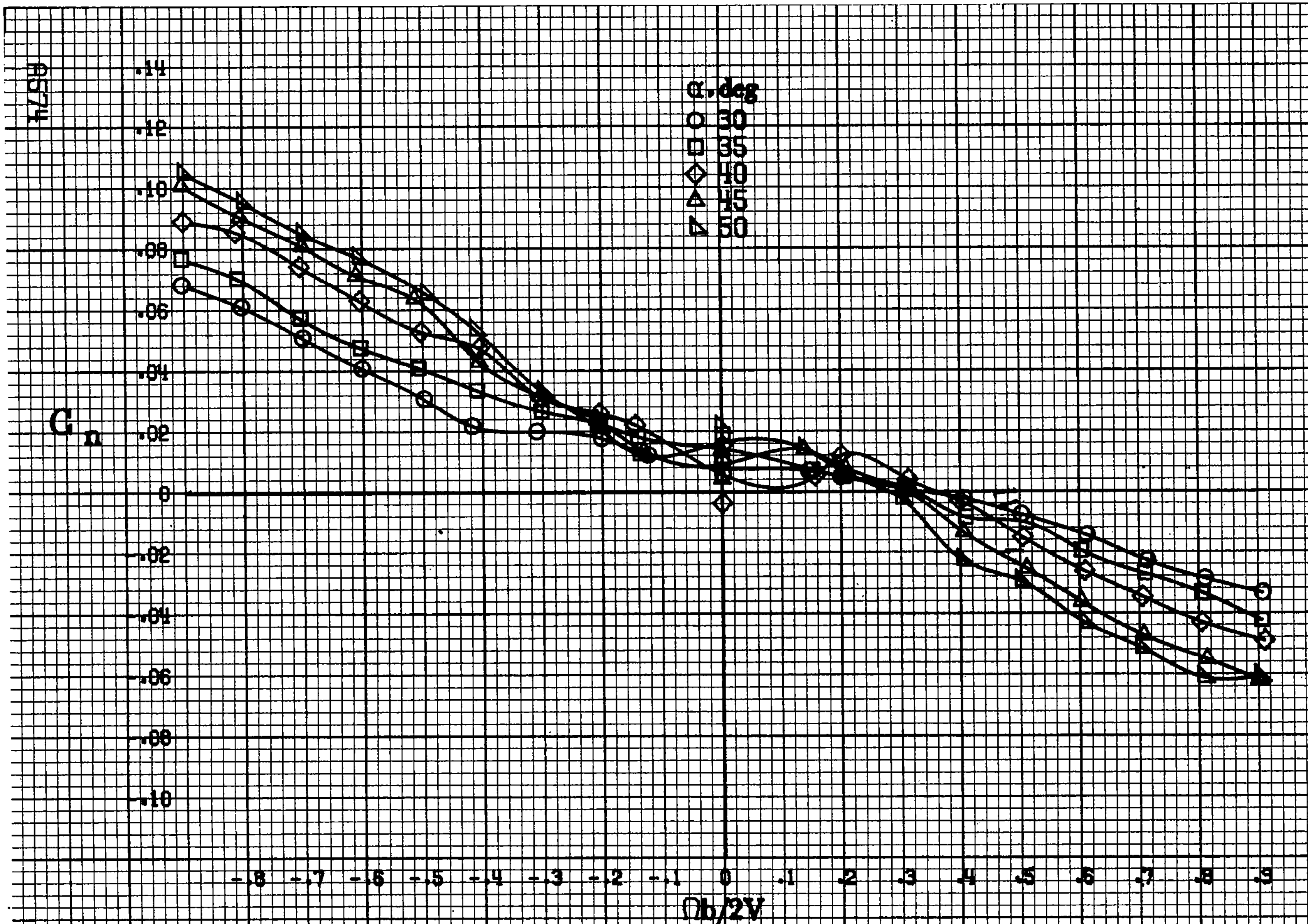

(c) α = 30 to 50 deg, SR = 0.

Figure A189.-Continued.

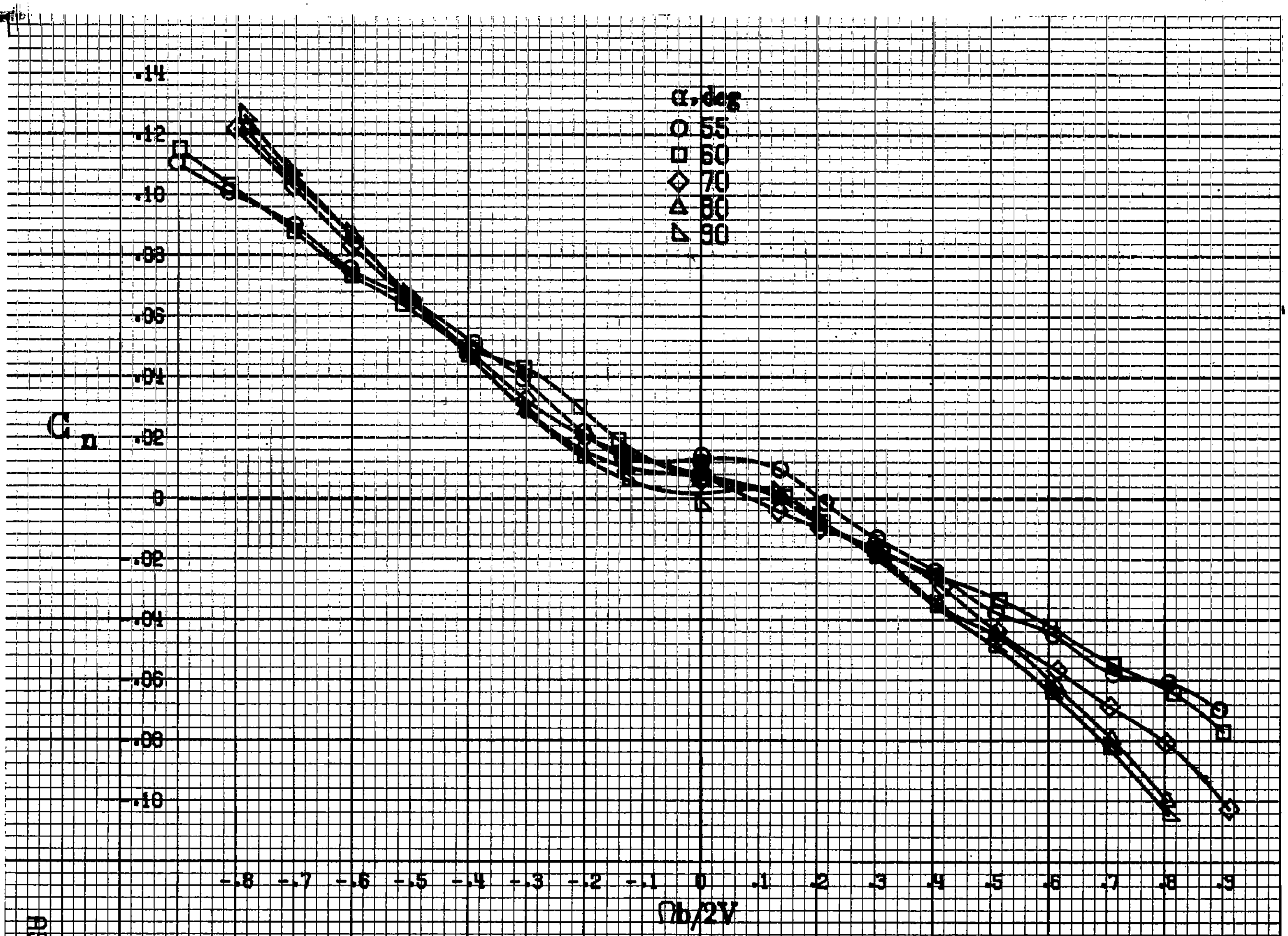

(d) $\alpha = 55$ to 90 deg, SR = 0.

Figure A199.-Concluded.

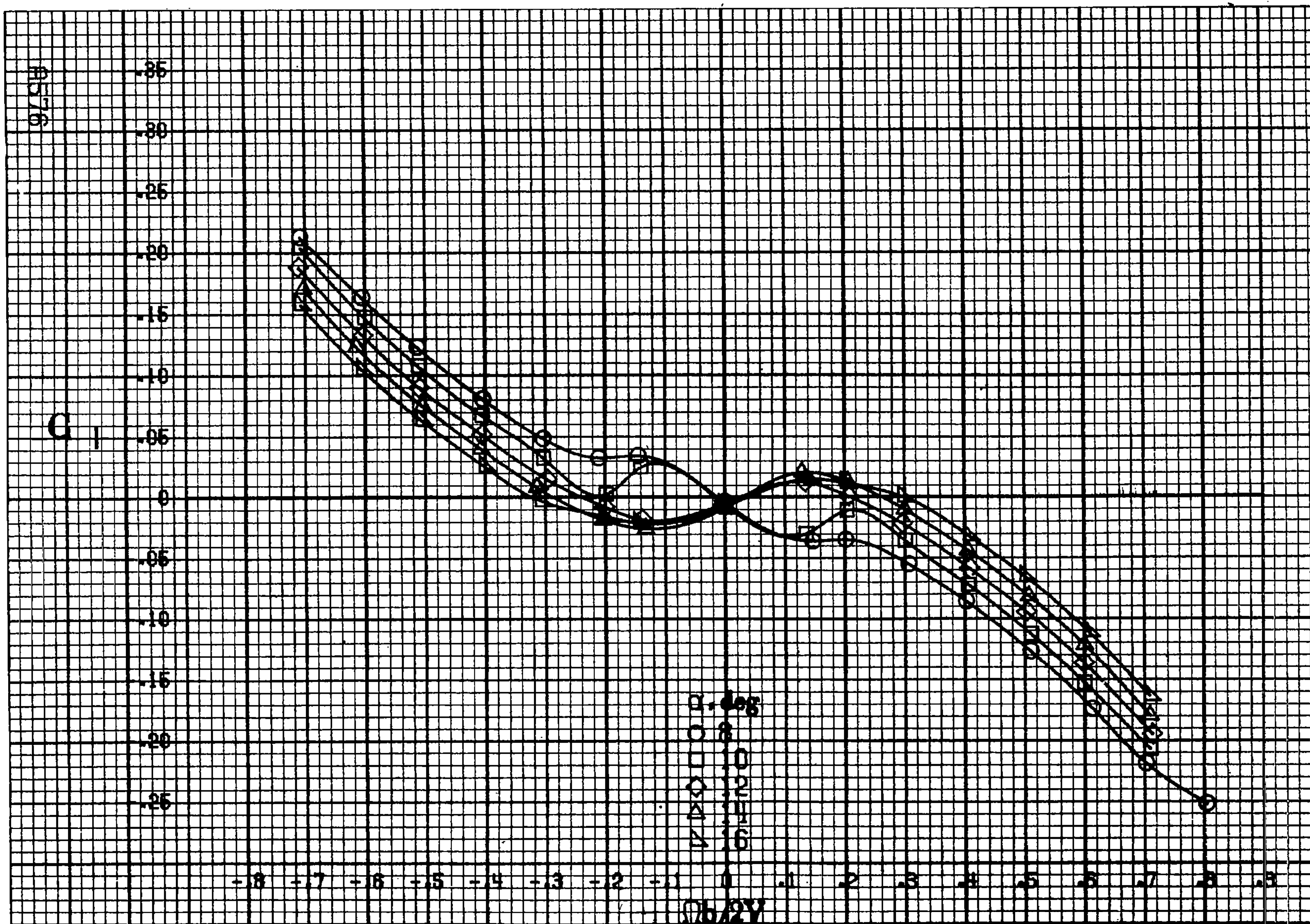

(c) α = 8 to 16 deg, SR = 182.9 cm (72 in).

Figure A140.-Effect of rotation rate and angle of attack on rolling-moment coefficient for T-tail configuration. $\delta_a = -15°$, $\delta_e = 0°$, $\delta_r = -25°$, $\beta = 0°$.

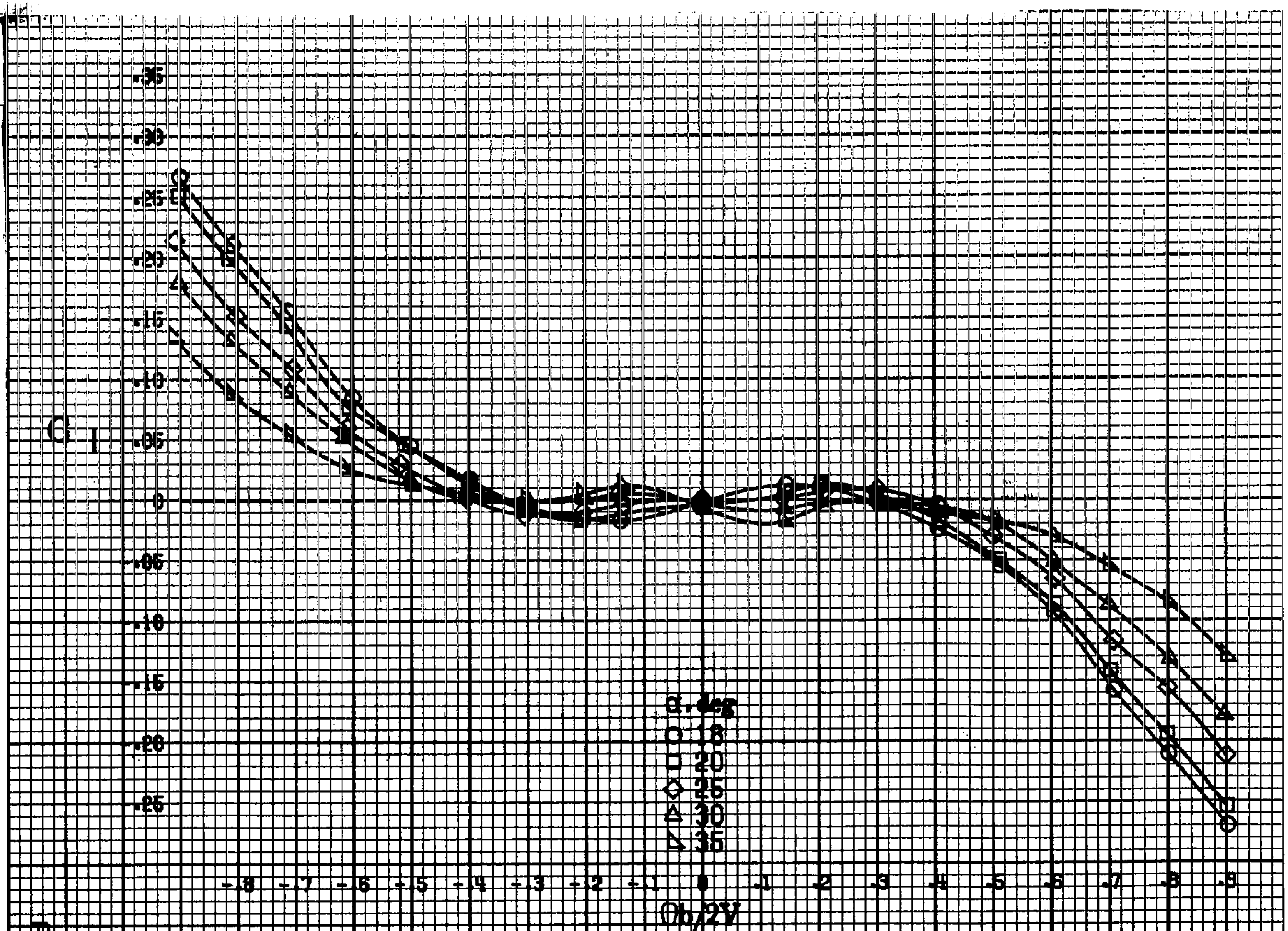

(b) α = 18 to 35 deg, SR = 182.9 cm (72 in).

Figure A140.- Continued.

A577

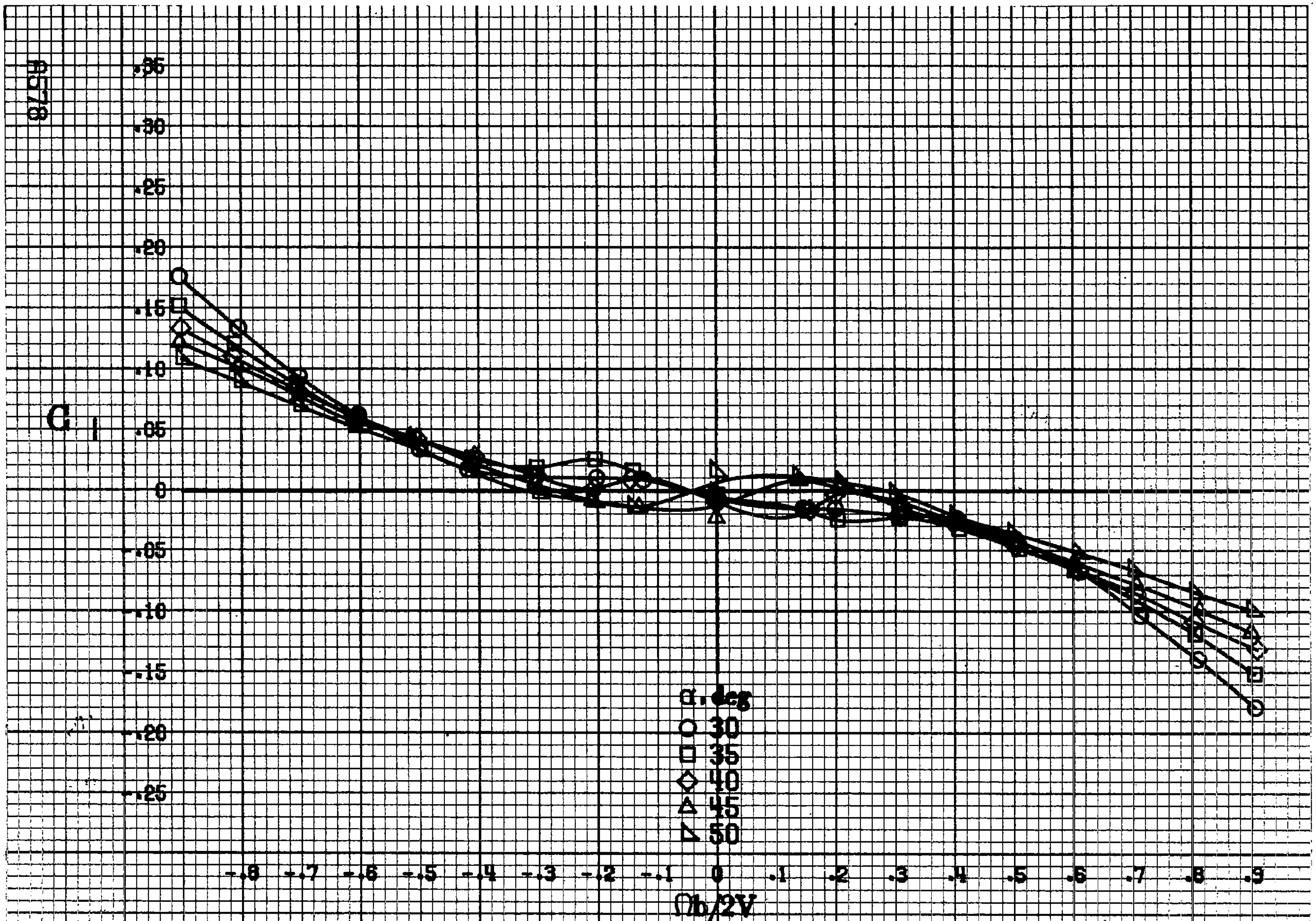

(c) α = 30 to 60 deg, SR = 0.

Figure A140.- Continued.

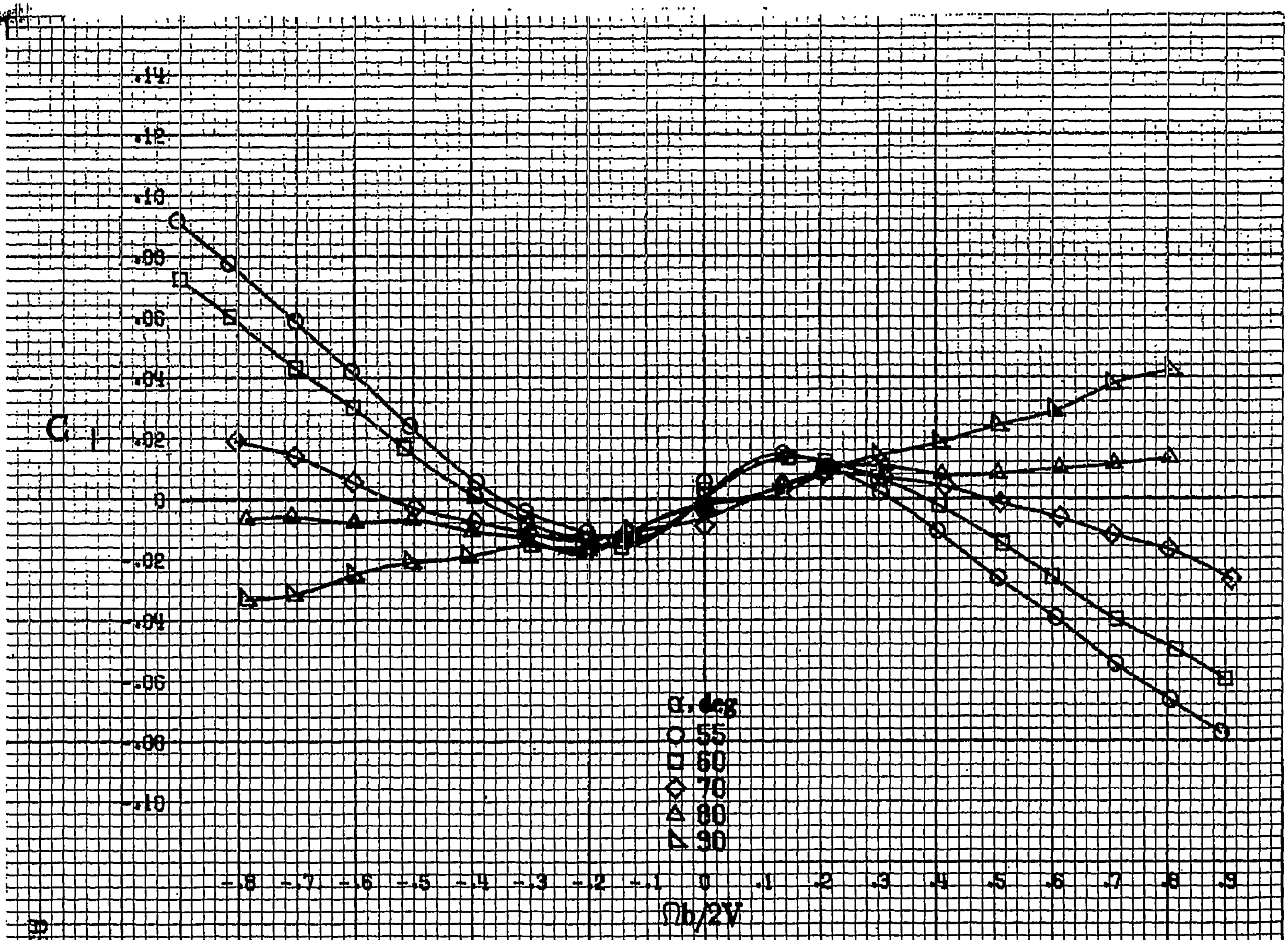

(d) α = 55 to 90 deg, SR = 0.
Figure A140.-Concluded.

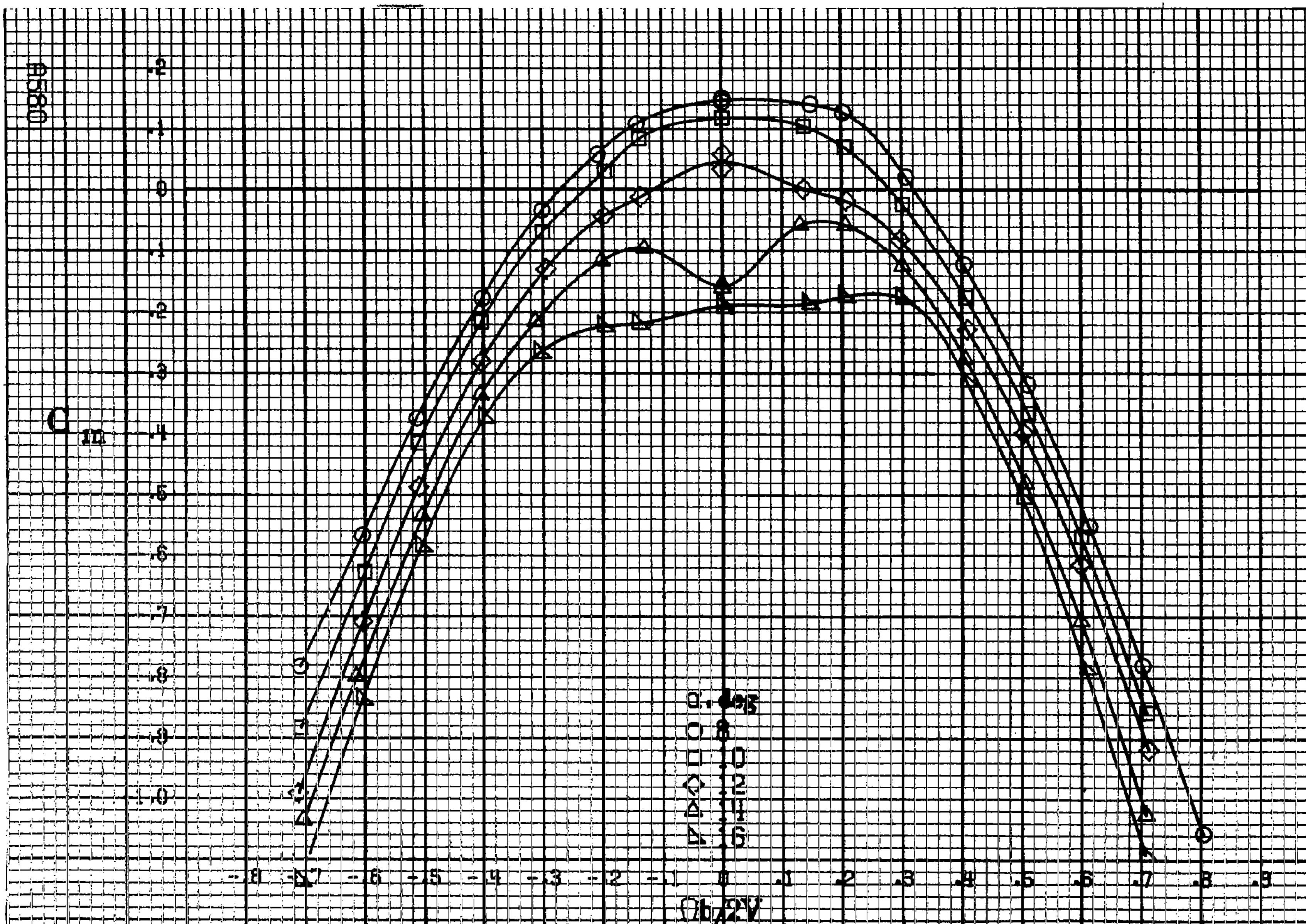

(a) $\alpha = 8$ to 16 deg, SR = 182.9 cm (72 in).

Figure A141.- Effect of rotation rate and angle of attack on pitching-moment coefficient for T-tail configuration. $\delta_e = -15°$, $\delta_a = 0°$, $\delta_r = -25°$, $\beta = 0°$.

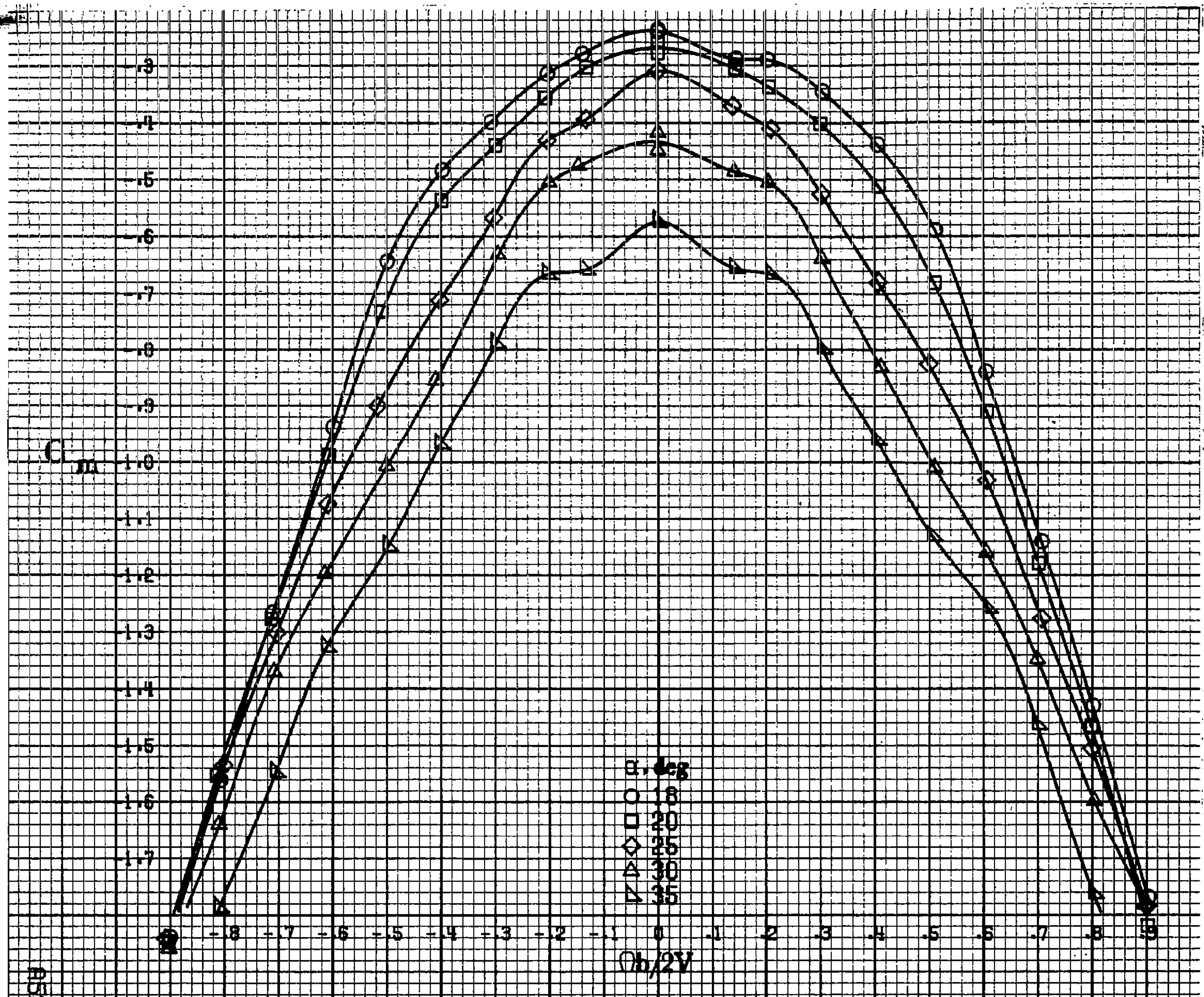

(b) α = 18 to 35 deg, SR = 182.9 cm (72 in).

Figure A141.-Continued.

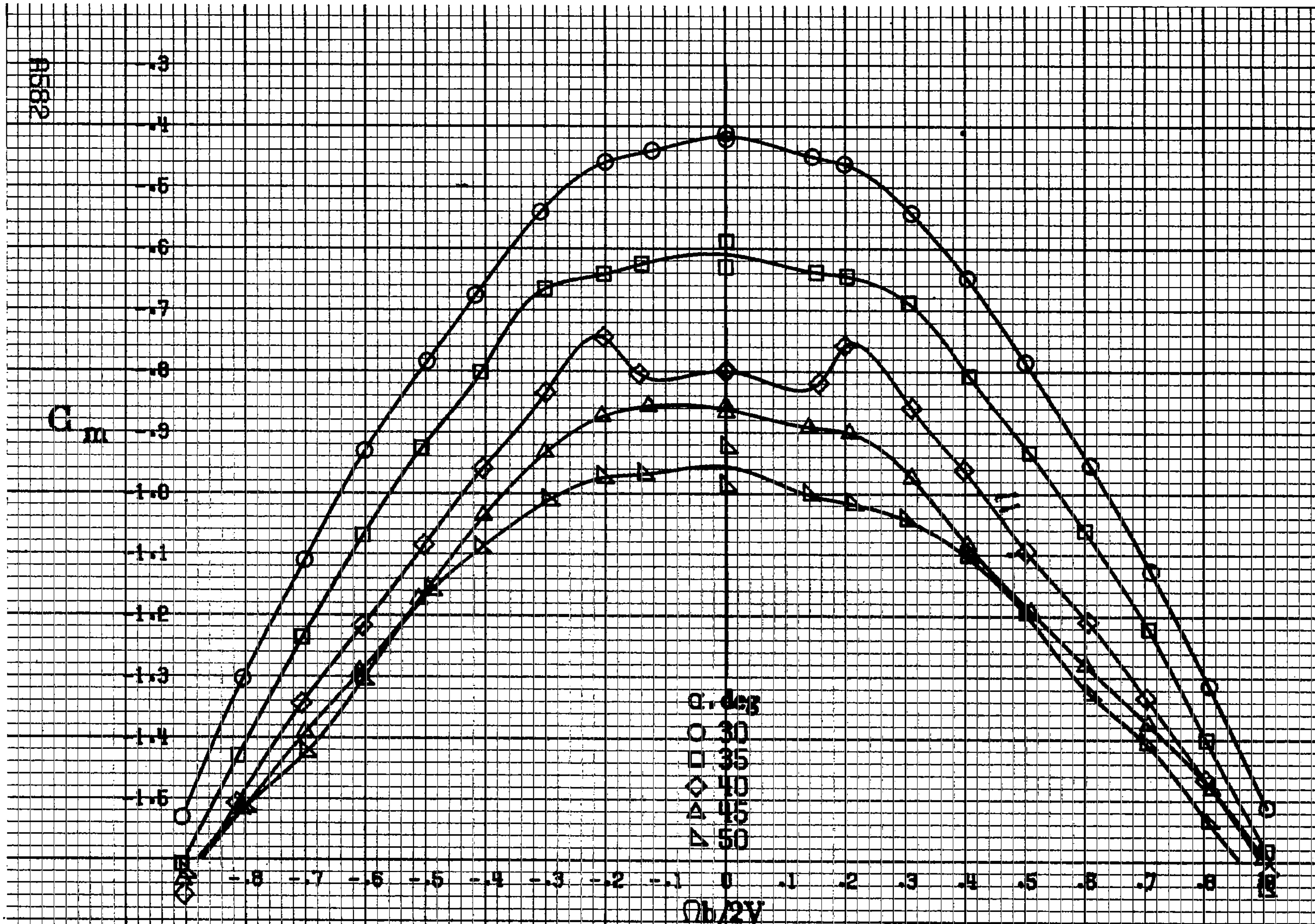

(c) α = 30 to 50 deg, SR = 0.

Figure A141.-Continued.

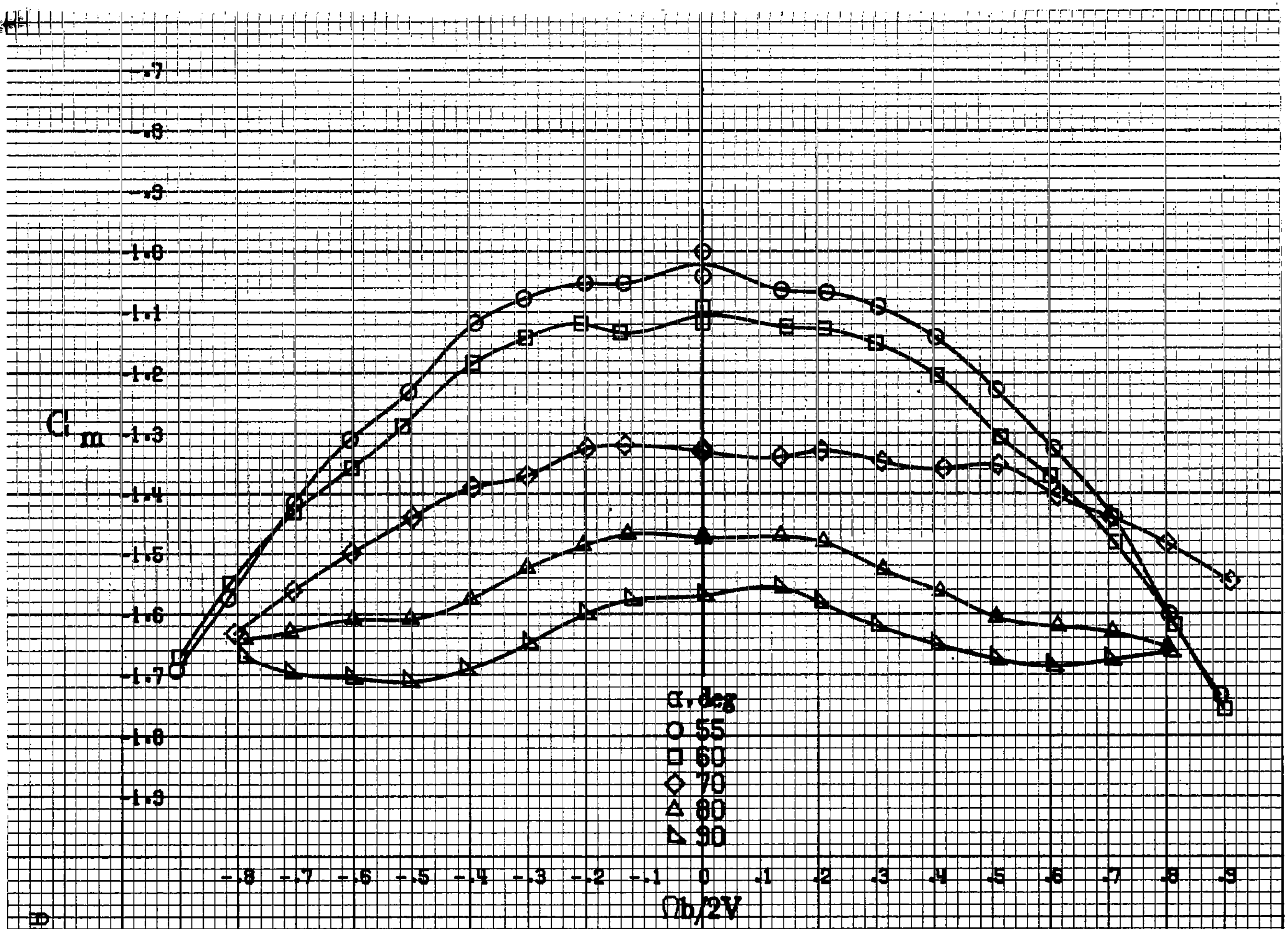

(d) α = 55 to 90 deg, SR = 0.

Figure A141.-Concluded.

(a) $\alpha = 8$ to 16 deg, SR = 182.9 cm (72 in).

Figure A142.- Effect of rotation rate and angle of attack on normal-force coefficient for T-tail configuration. $\delta_a = -15°$, $\delta_e = 0°$, $\delta_r = -25°$, $\beta = 0°$.

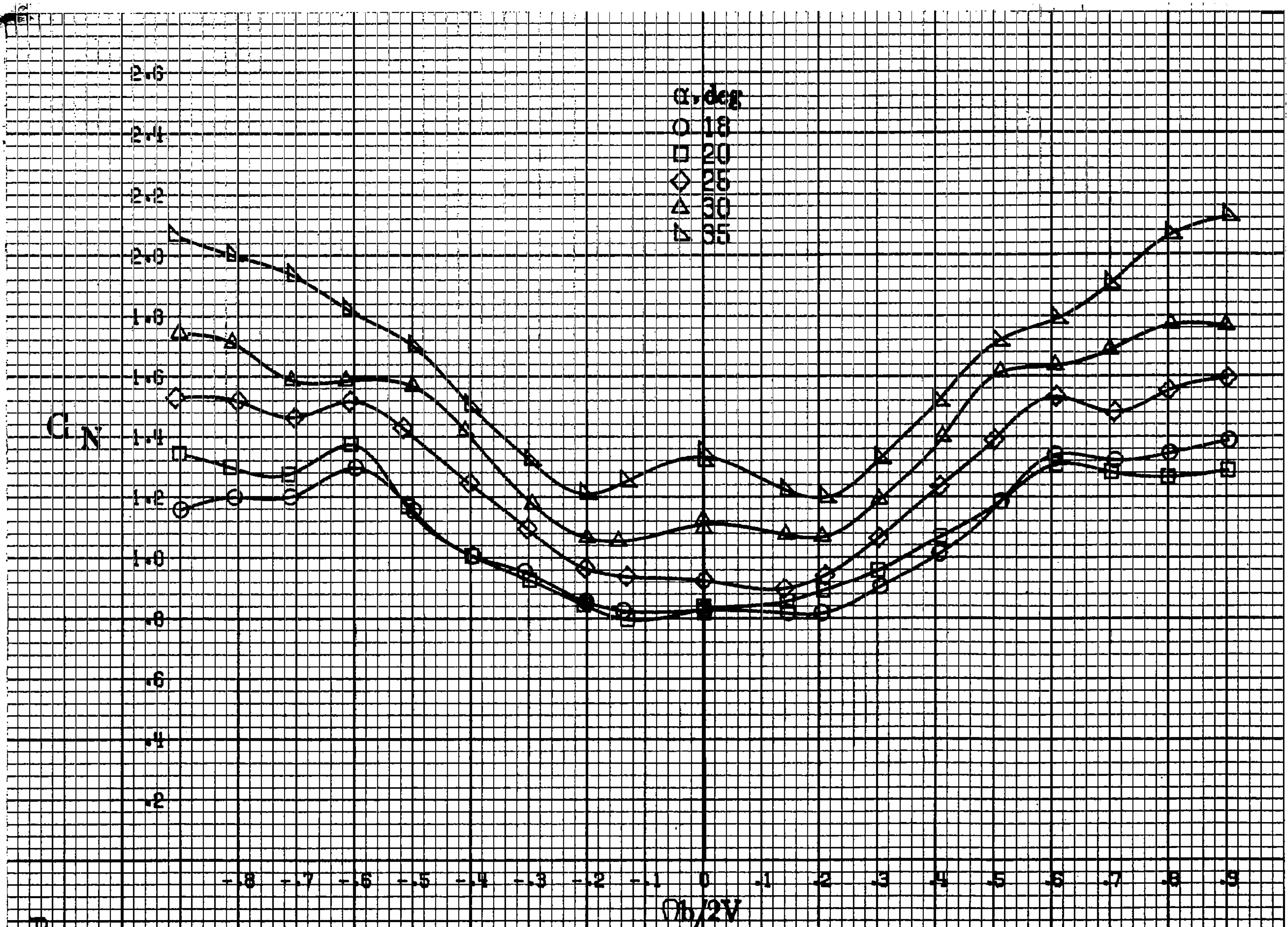

(b) α = 18 to 35 deg, SR = 182.9 cm (72 in).

Figure A142. Continued.

A585

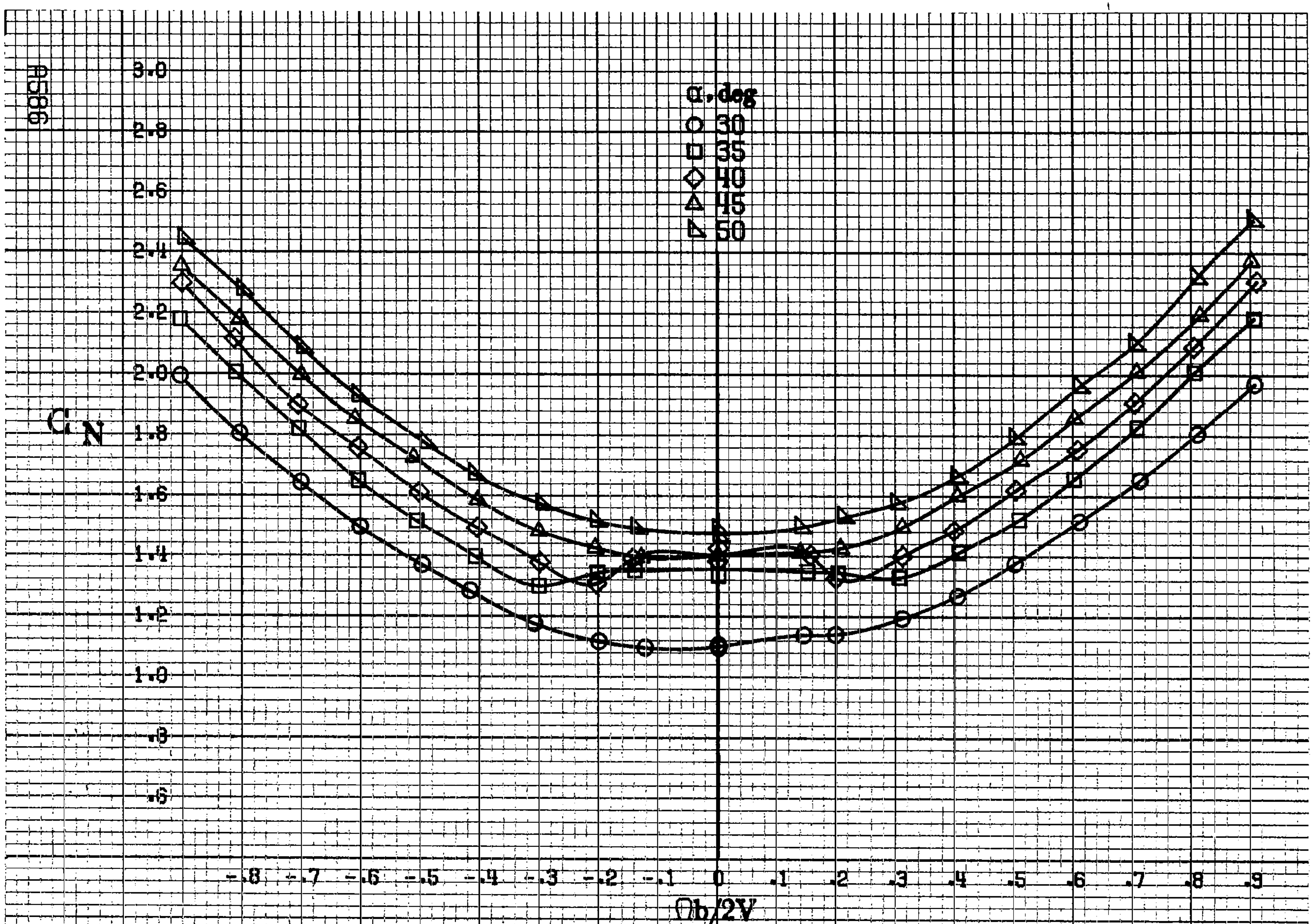

(c) α = 30 to 50 deg, SR = 0.

Figure A142.-Continued.

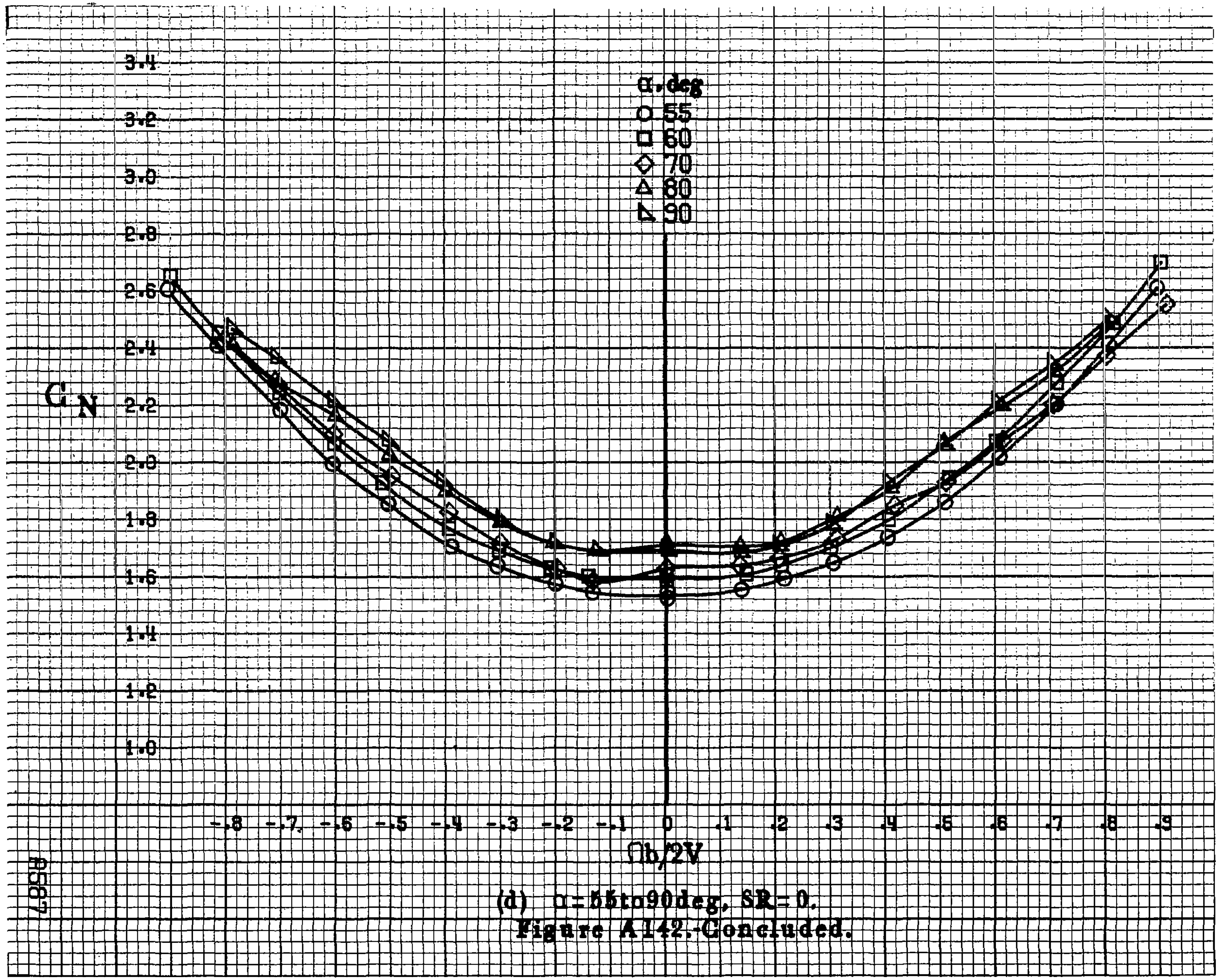

(d) α = 55 to 90 deg, SR = 0.

Figure A142.-Concluded.

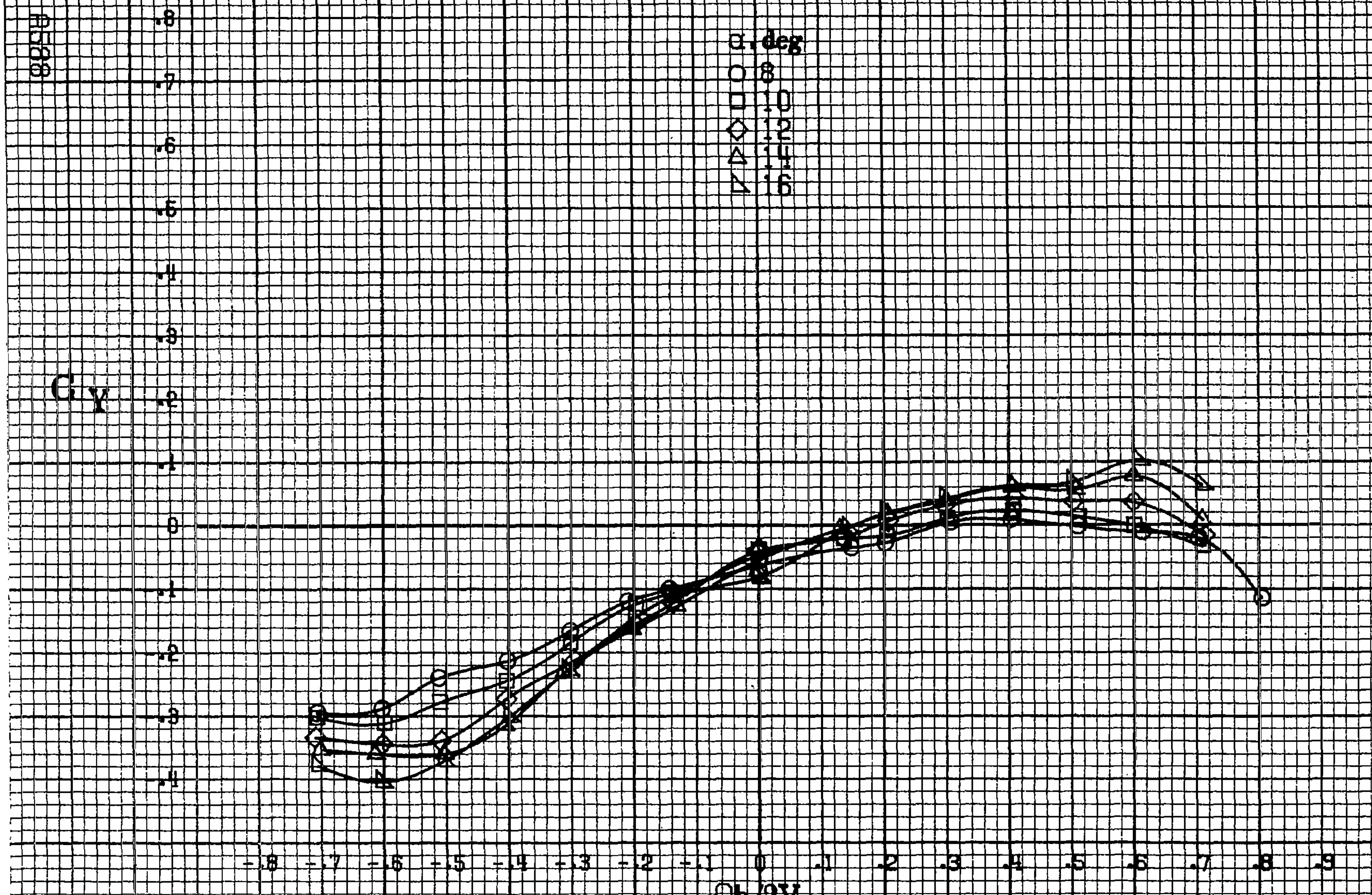

(a) $\alpha = 8$ to 16 deg, SR = 182.9 cm (72 in).

Figure A143.-Effect of rotation rate and angle of attack on side-force coefficient for T-tail configuration. $\delta_e = -15°$, $\delta_a = 0°$, $\delta_r = -25°$, $\beta = 0°$.

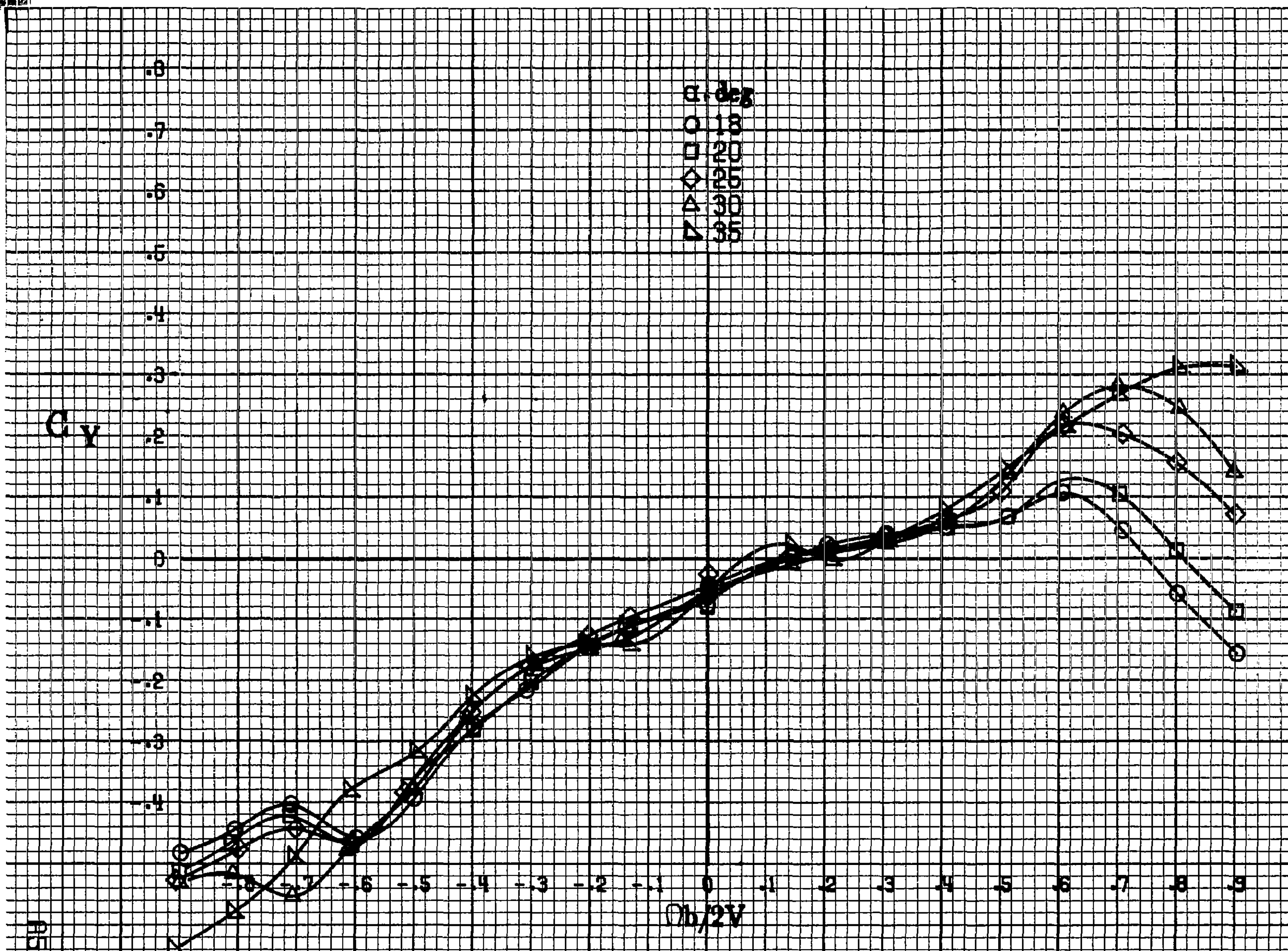

(b) α = 18 to 35 deg, SR = 182.9 cm (72 in).

Figure A143.-Continued.

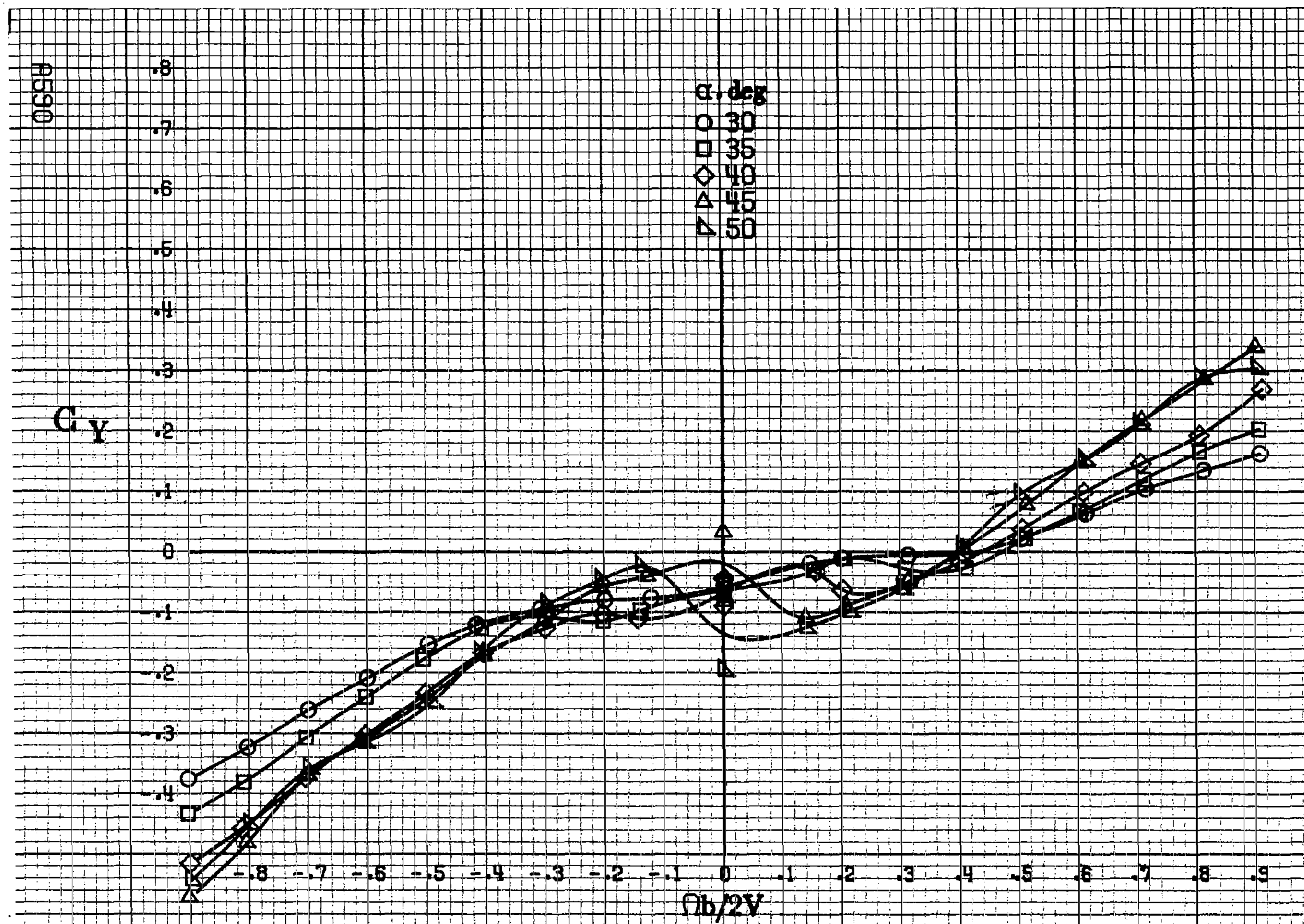

(c) α = 30to50deg, SR = 0.
Figure A143.-Continued.

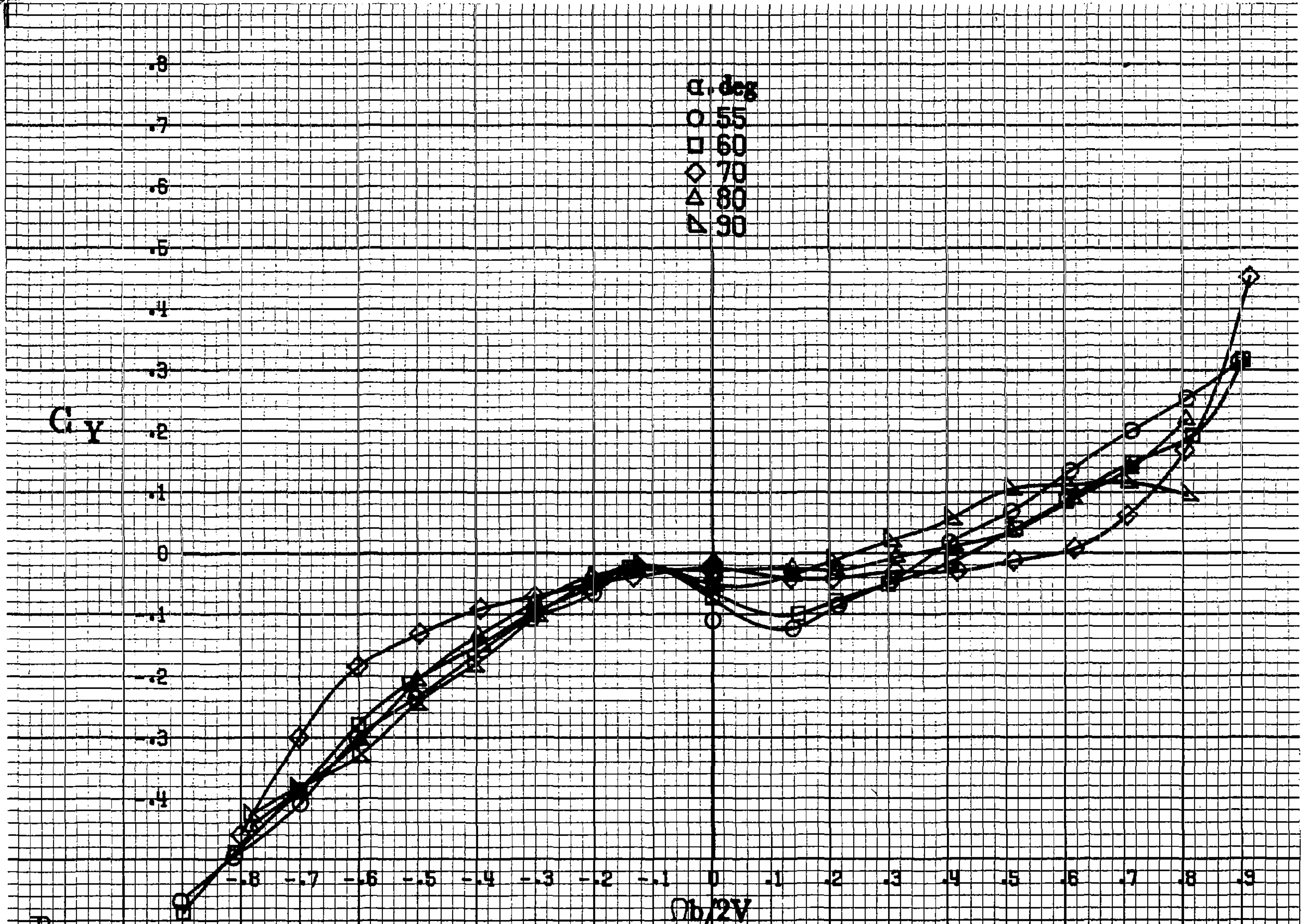

(d) α = 55 to 90 deg, SR = 0.

Figure A148.-Concluded.

A591

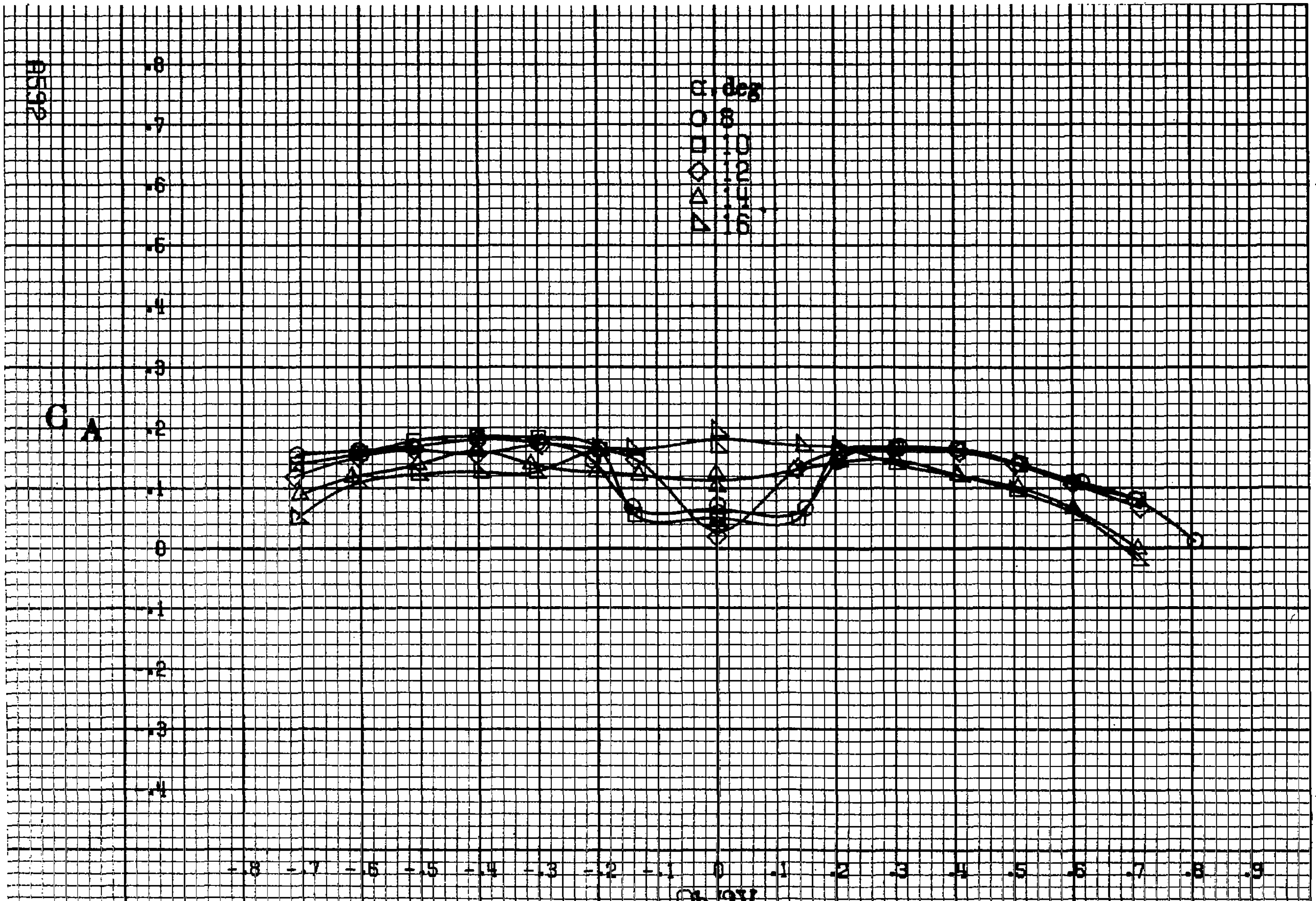

(a) α = 8 to 16 deg, SR = 182.9 cm (72 in).

Figure A144.- Effect of rotation rate and angle of attack on axial-force coefficient for T-tail configuration. $\delta_e = -15°$, $\delta_a = 0°$, $\delta_r = -25°$, $\beta = 0°$.

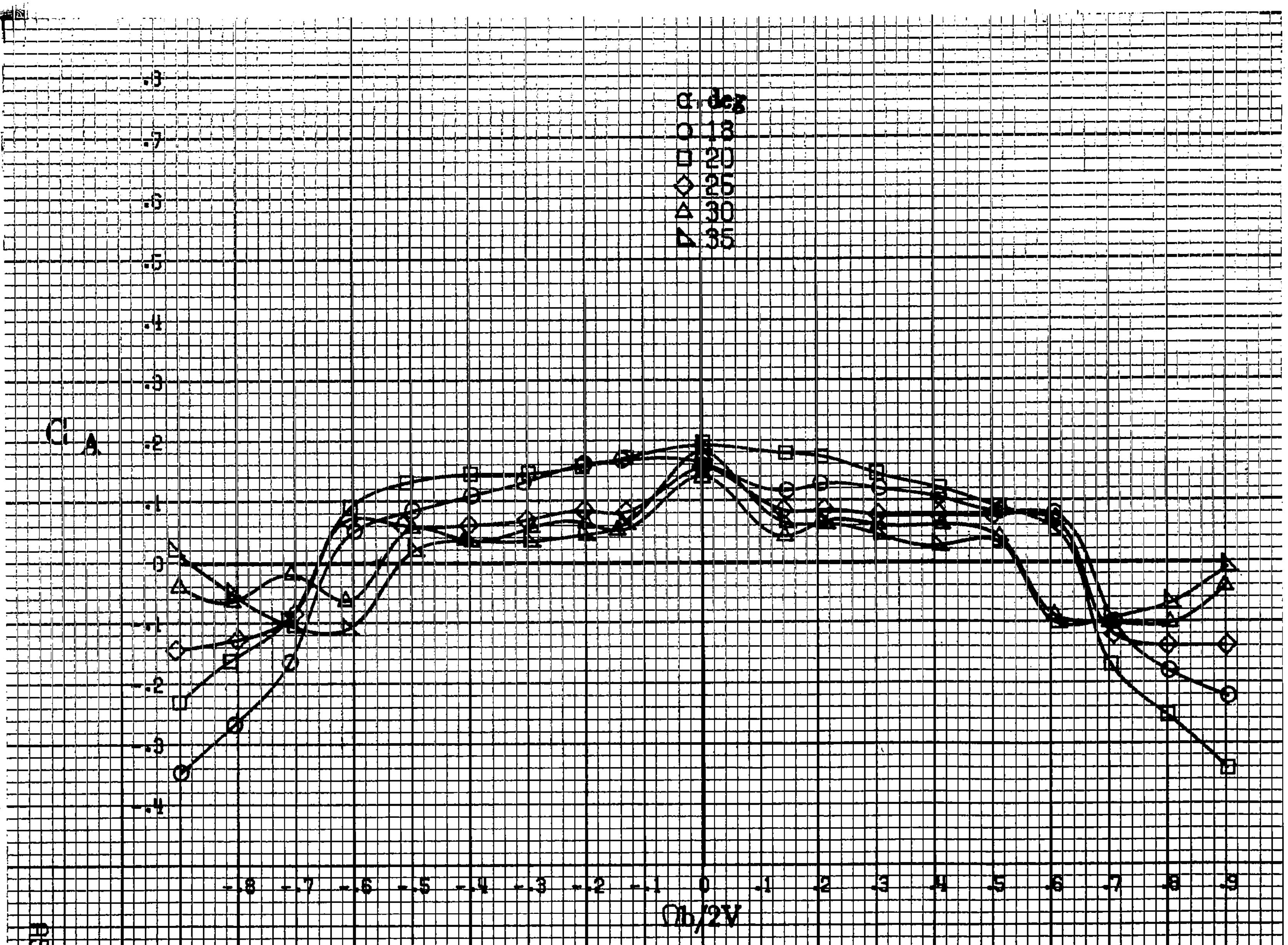

(b) α = 18 to 35 deg, SR = 182.9 cm (72 in).

Figure A144.-Continued.

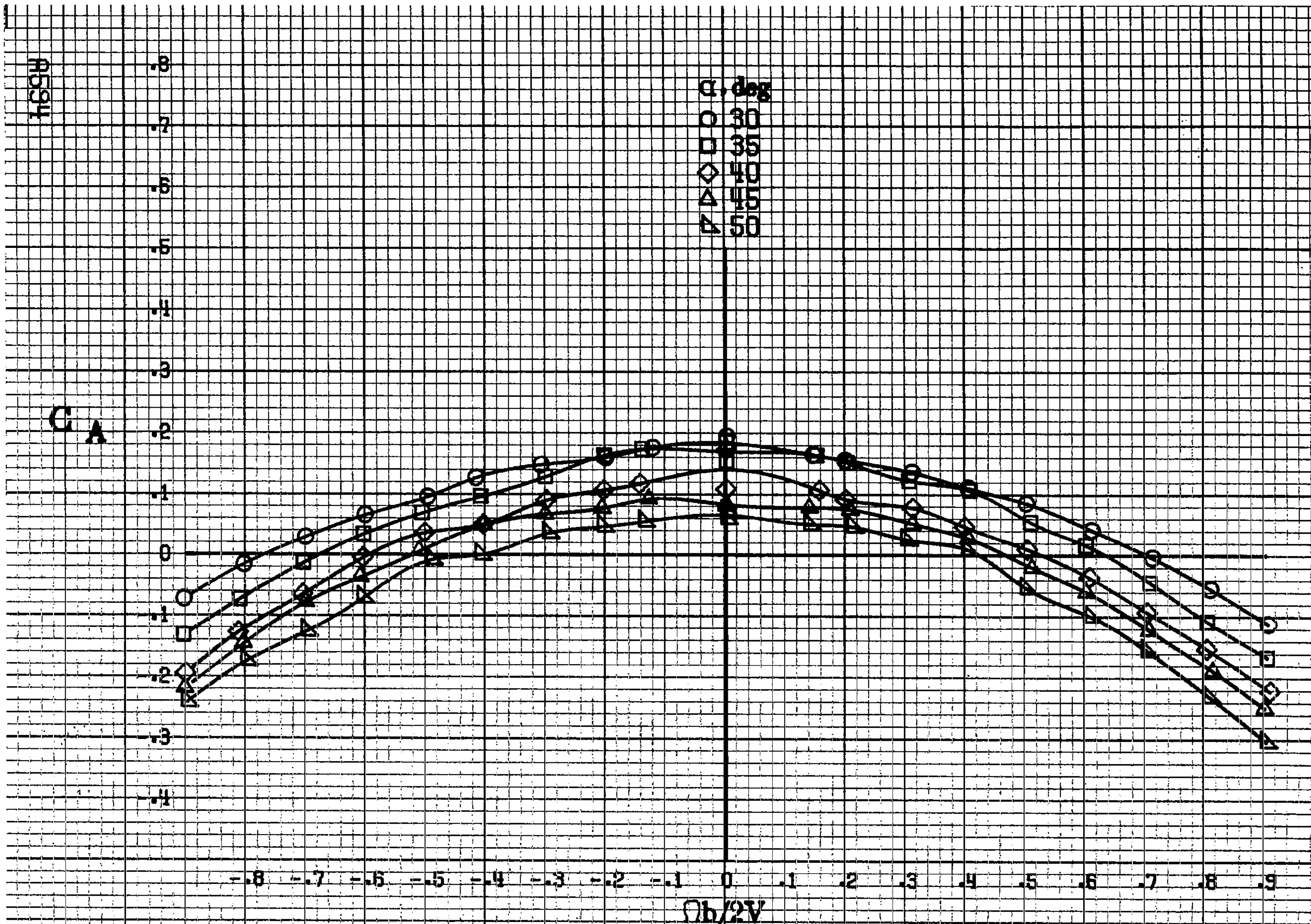

(c) α = 30 to 50 deg, SR = 0.

Figure A144.-Continued.

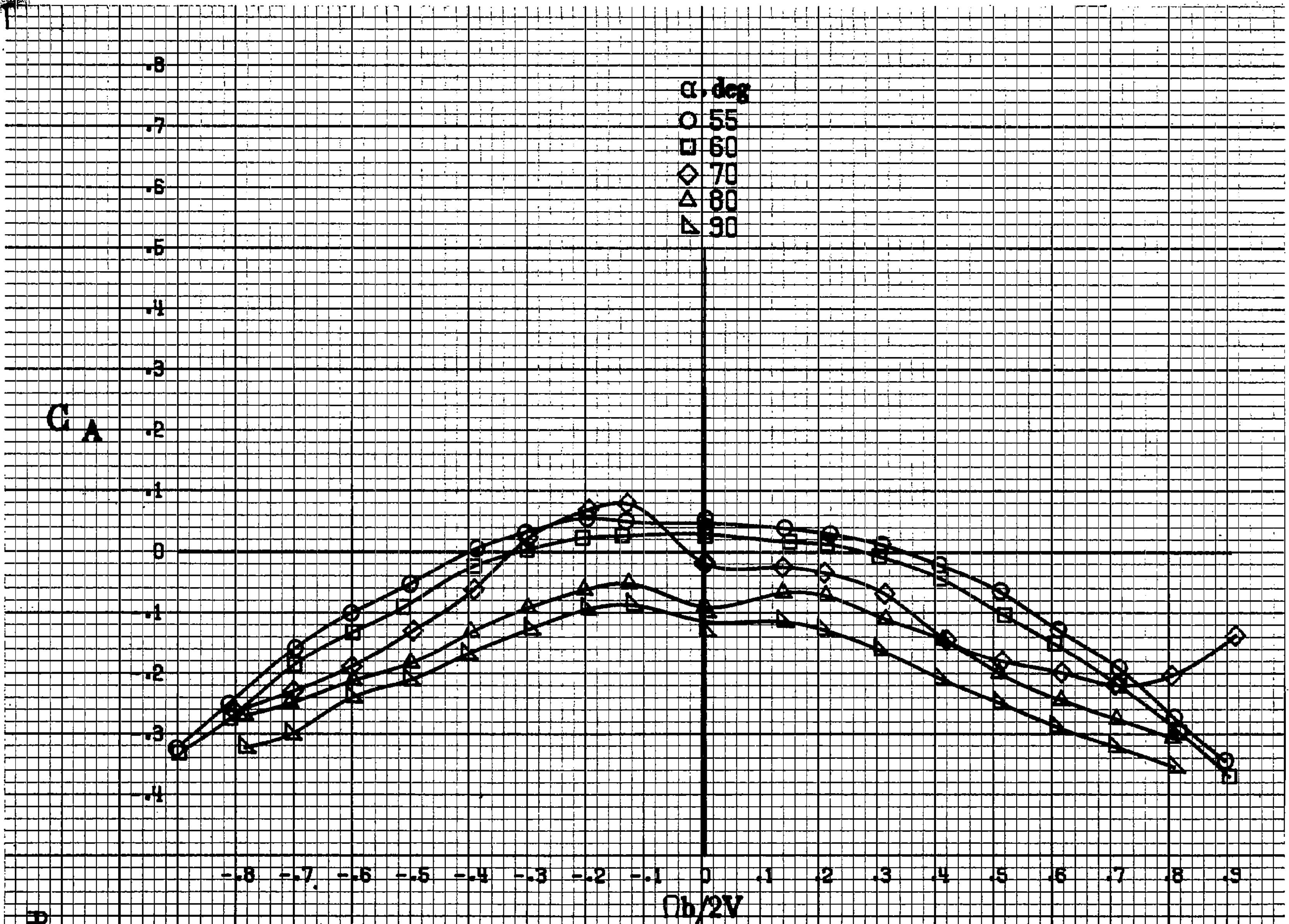

(d) α=55to90deg, SR=0.

Figure A144.-Concluded.

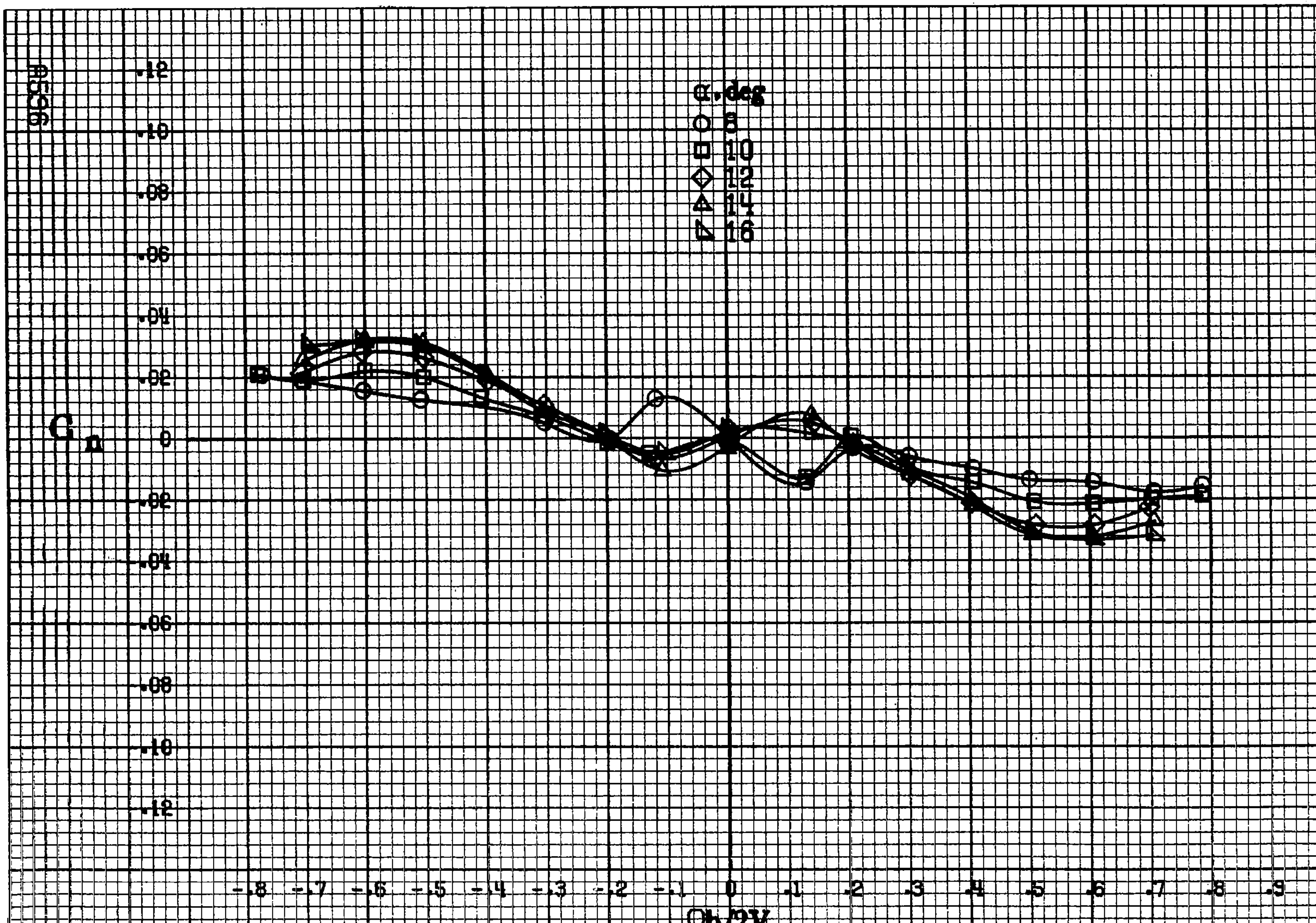

(a) α = 8 to 16 deg, SR = 182.9 cm (72 in).

Figure A145.-Effect of rotation rate and angle of attack on yawing-moment coefficient for no. 1 horizontal tail configuration. $\delta_e = 0°$, $\delta_a = 0°$, $\delta_r = 0°$, $\delta = 0°$.

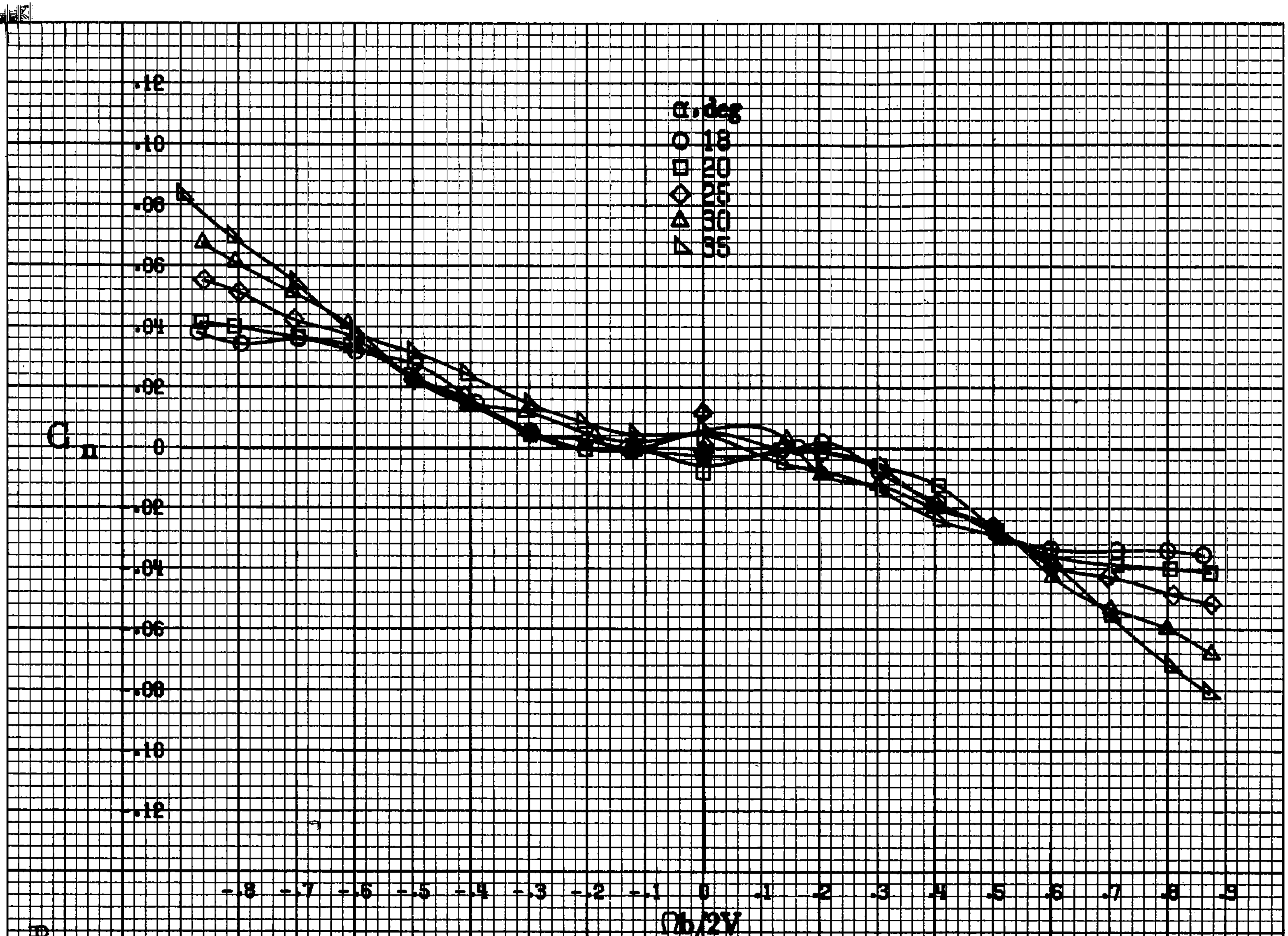

(b) α = 18 to 35 deg, SR = 182.9 cm (72 in).

Figure A145.-Continued.

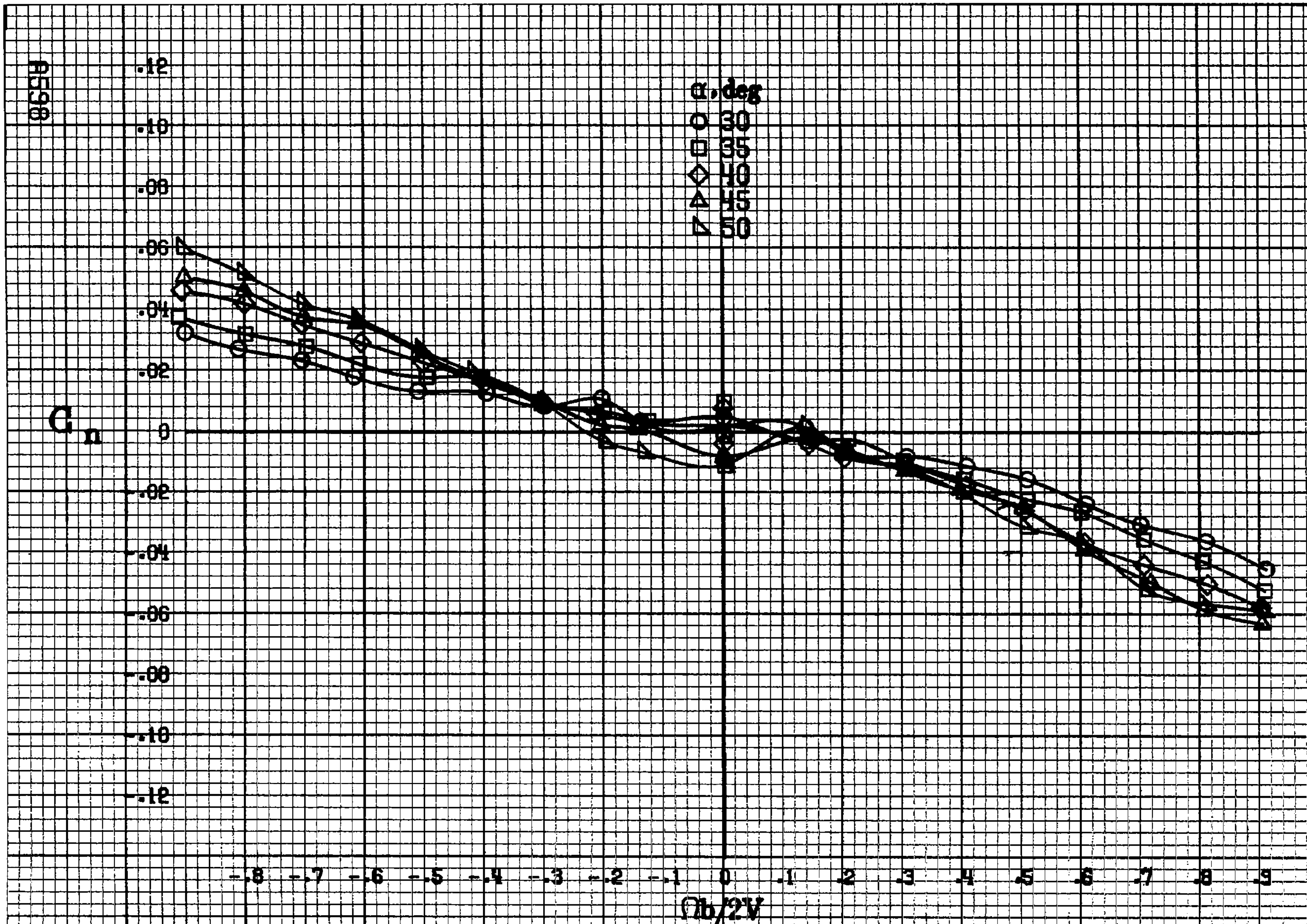

(c) α = 30 to 50 deg, SR = 0.

Figure A145.-Continued.

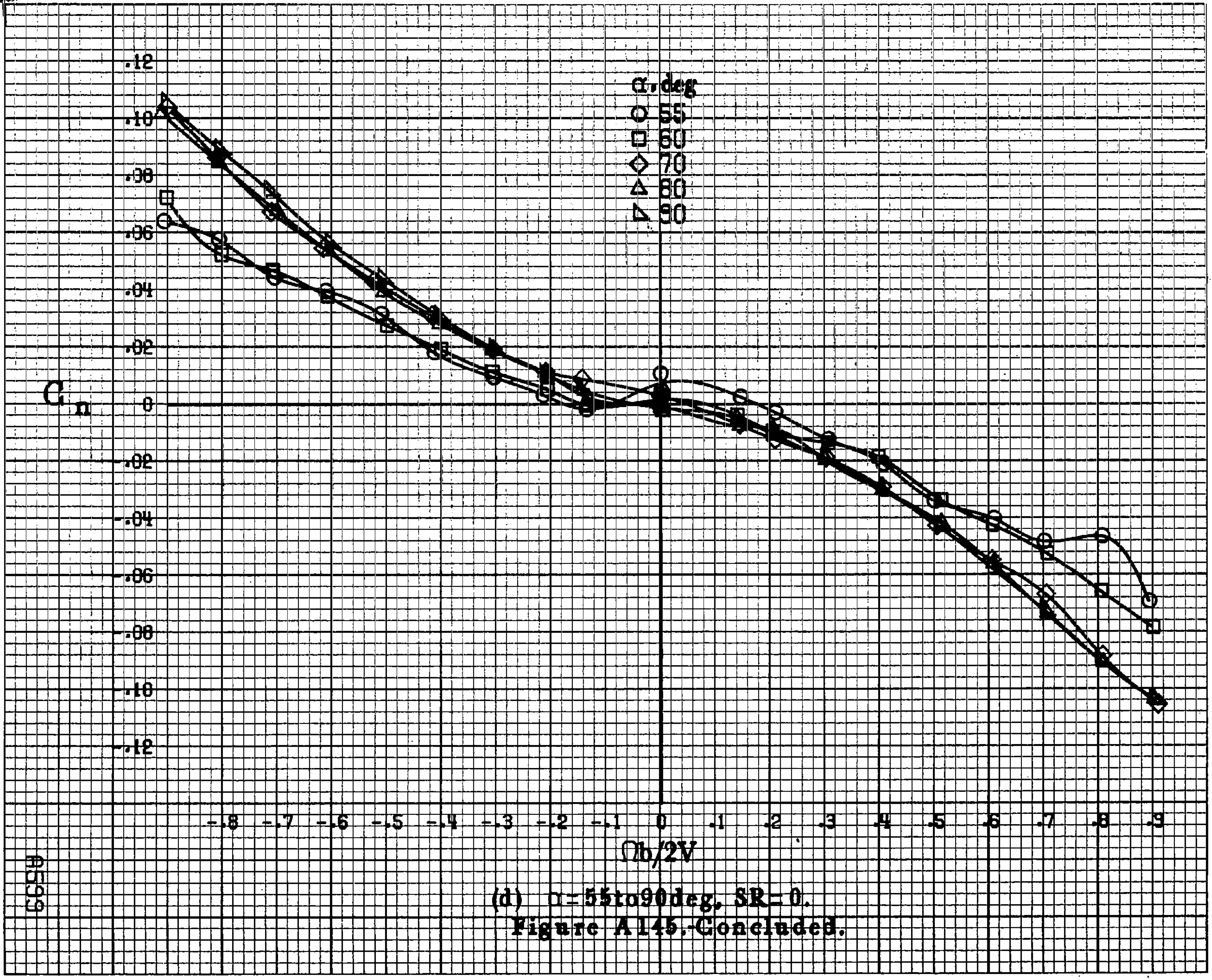

(d) α = 55 to 90 deg, SR = 0.

Figure A145.-Concluded.

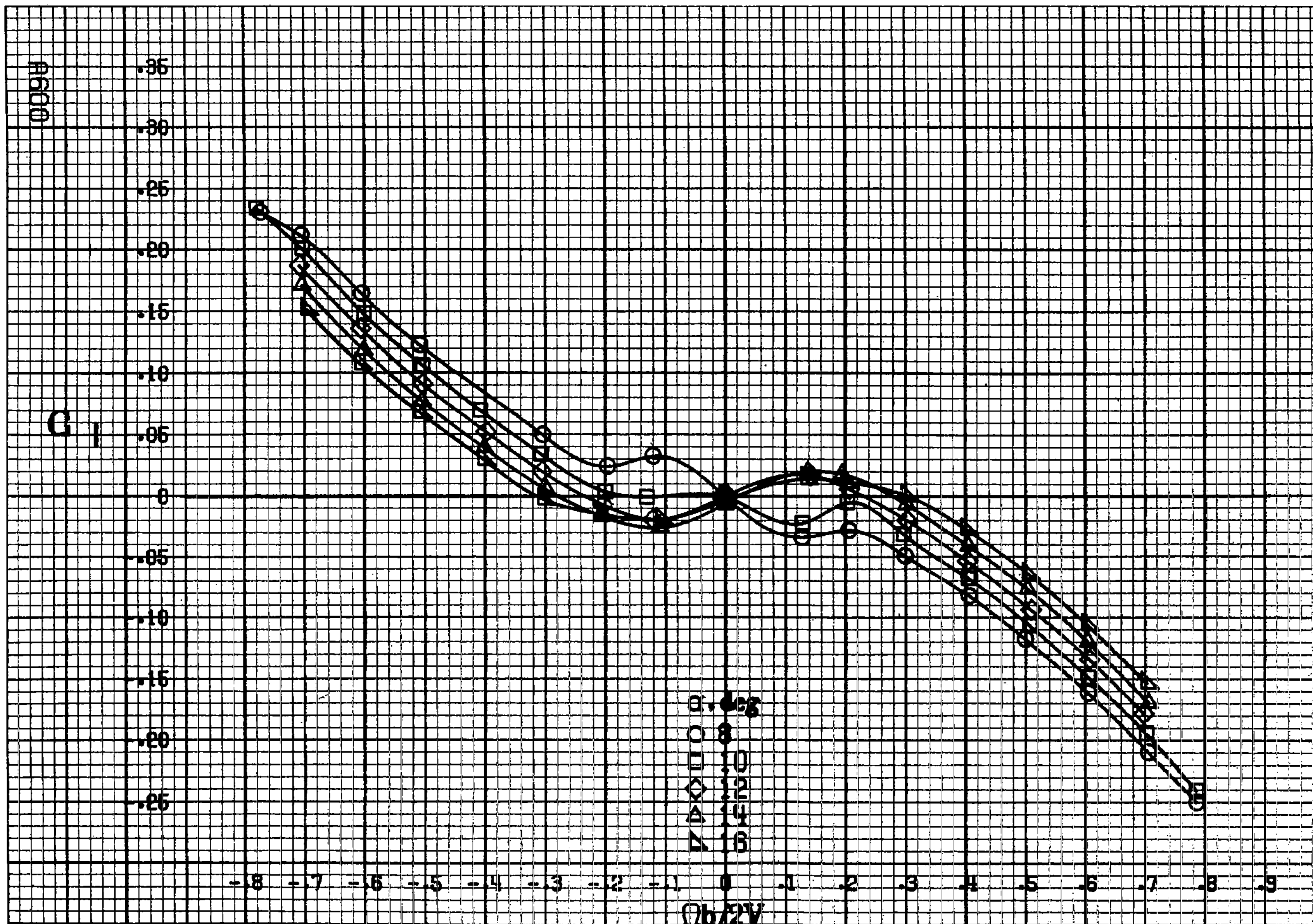

(a) α = 8 to 16 deg, SR = 182.9 cm (72 in).

Figure A146.-Effect of rotation rate and angle of attack on rolling-moment coefficient for no. 1 horizontal tail configuration. $\delta_e = 0°$, $\delta_a = 0°$, $\delta_r = 0°$, $\delta = 0°$.

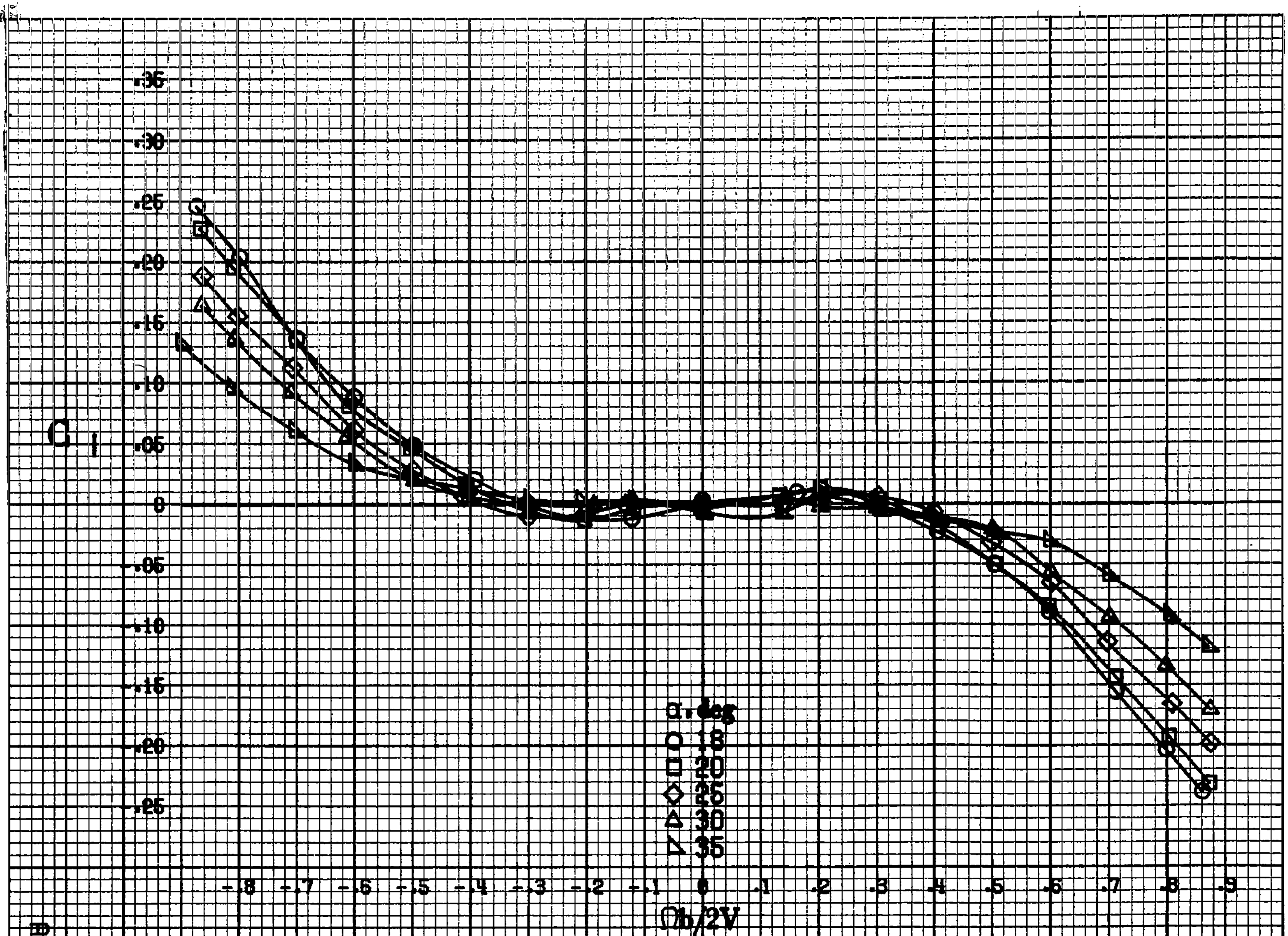

(b) α = 18 to 35 deg, SR = 182.9 cm (72 in).

Figure A146.-Continued.

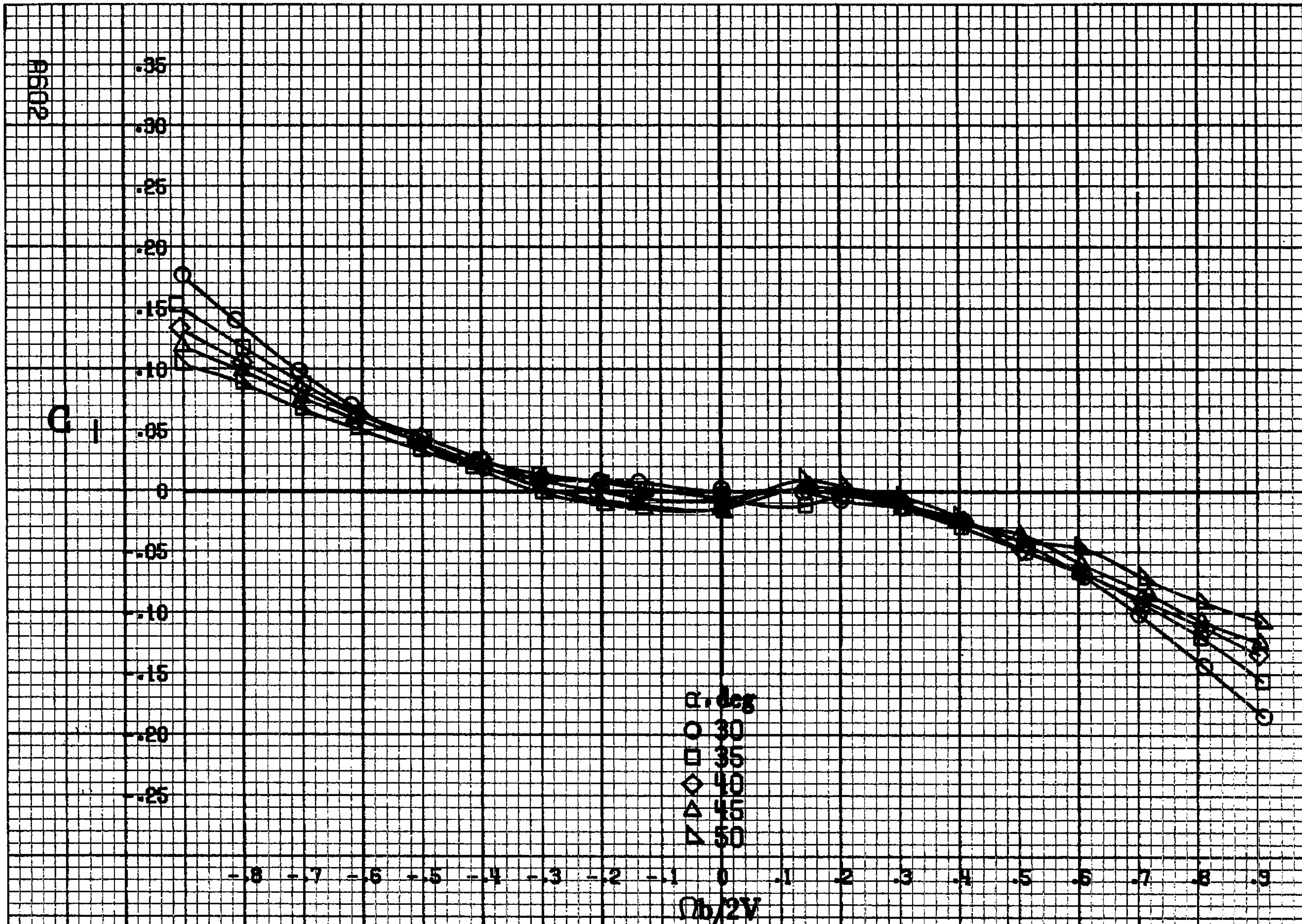

(c) α = 30 to 50 deg, SR = 0.

Figure A146.-Continued.

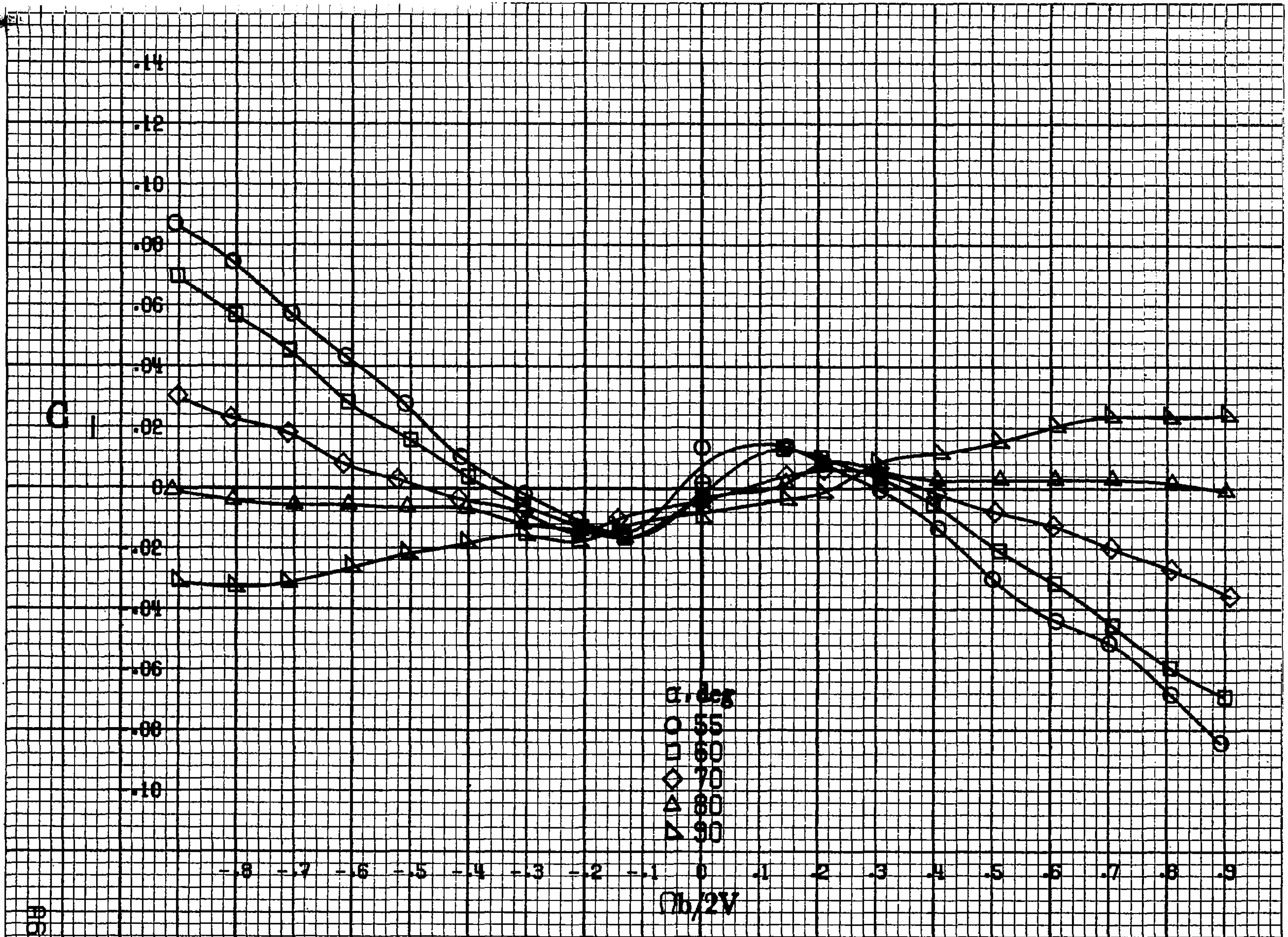

(d) α = 55 to 90 deg, SR = 0.
Figure A146.-Concluded.

A604

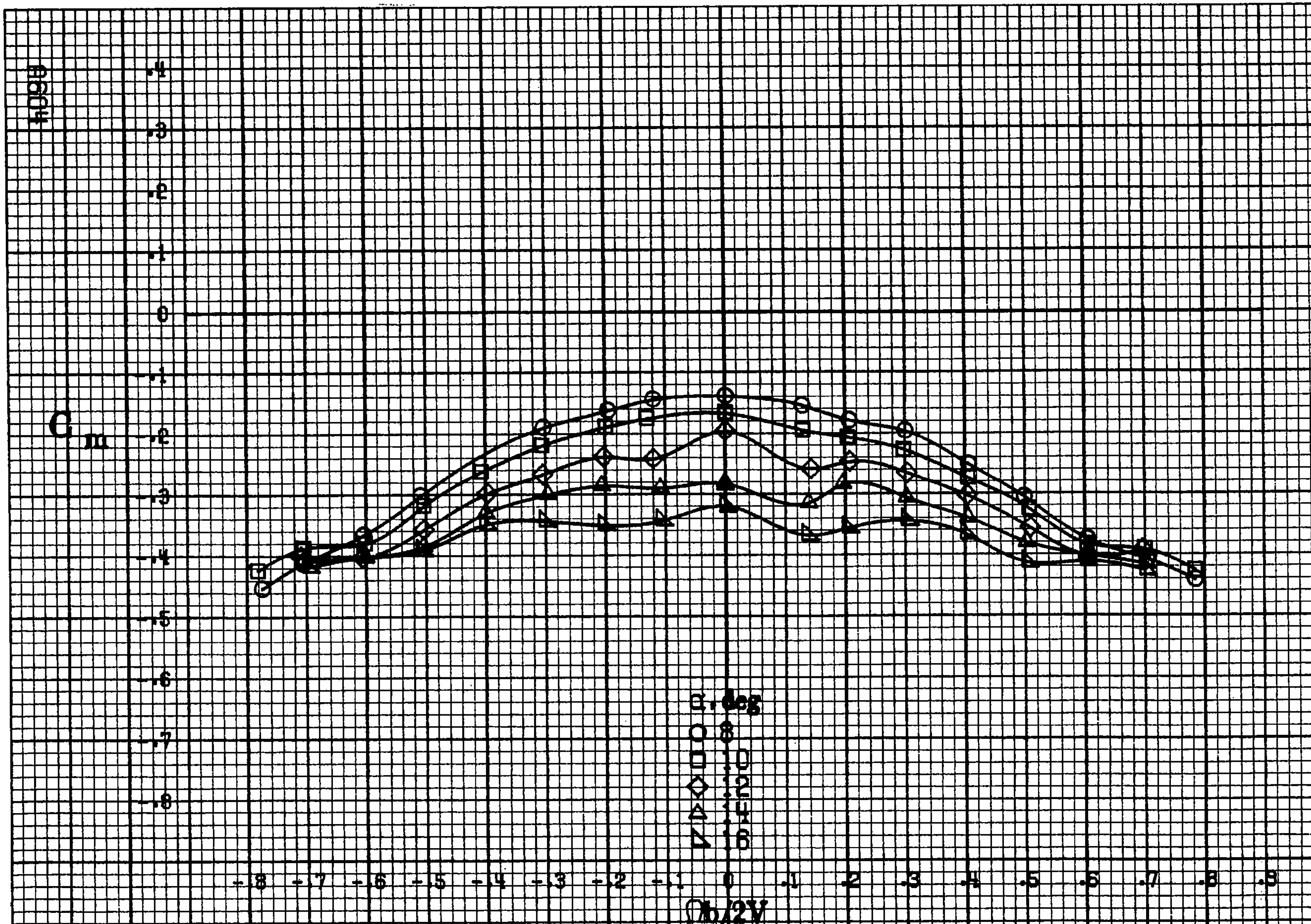

(a) $\alpha = 8$ to 16 deg, SR = 182.9 cm (72 in).

Figure A147.-Effect of rotation rate and angle of attack on pitching-moment coefficient for no. 1 horizontal tail configuration. $\delta_e = 0°$, $\delta_a = 0°$, $\delta_r = 0°$. $\delta = 0°$.

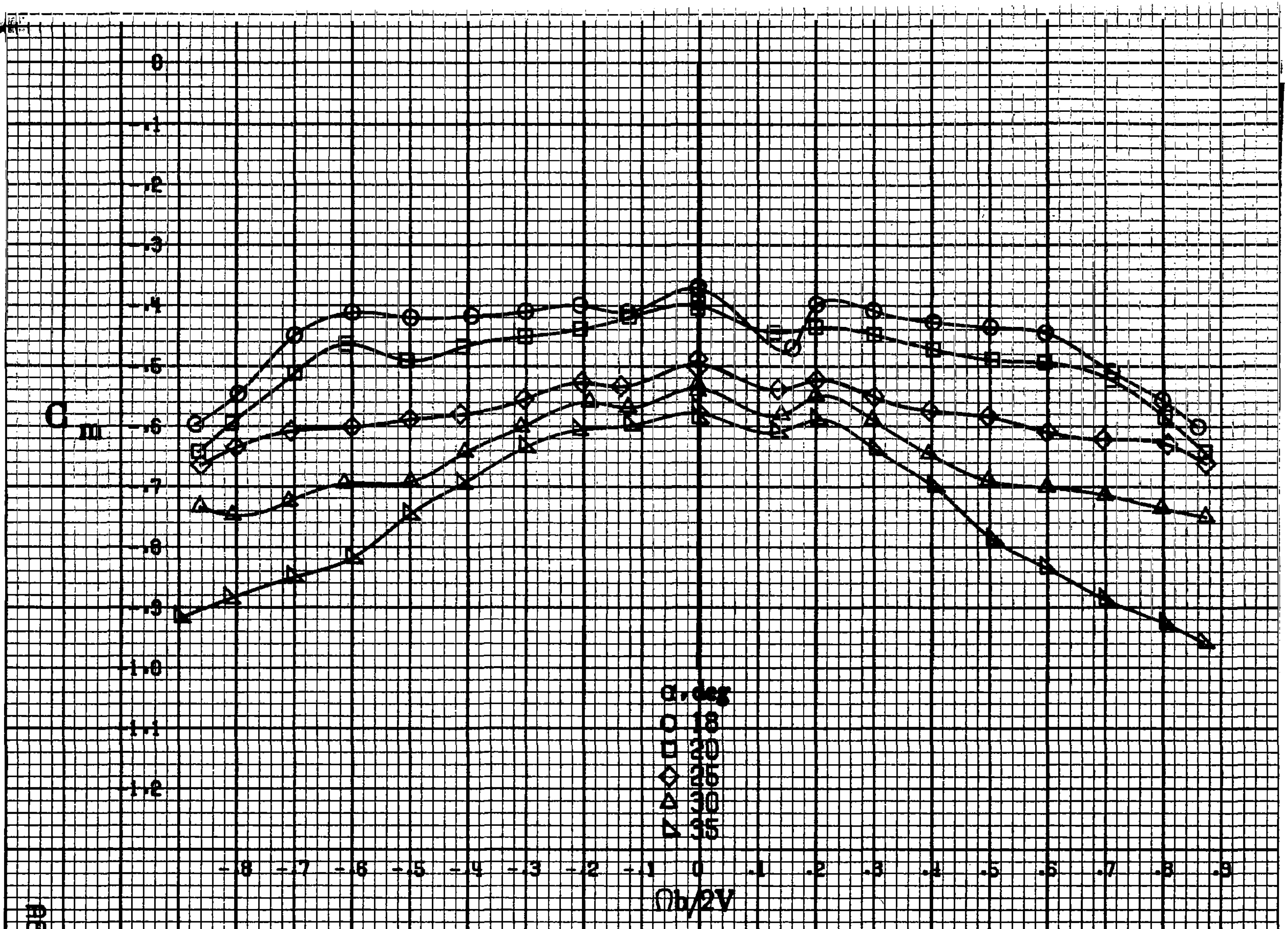

(b) α = 18 to 35 deg, SR = 182.9 cm (72 in).

Figure A147.-Continued.

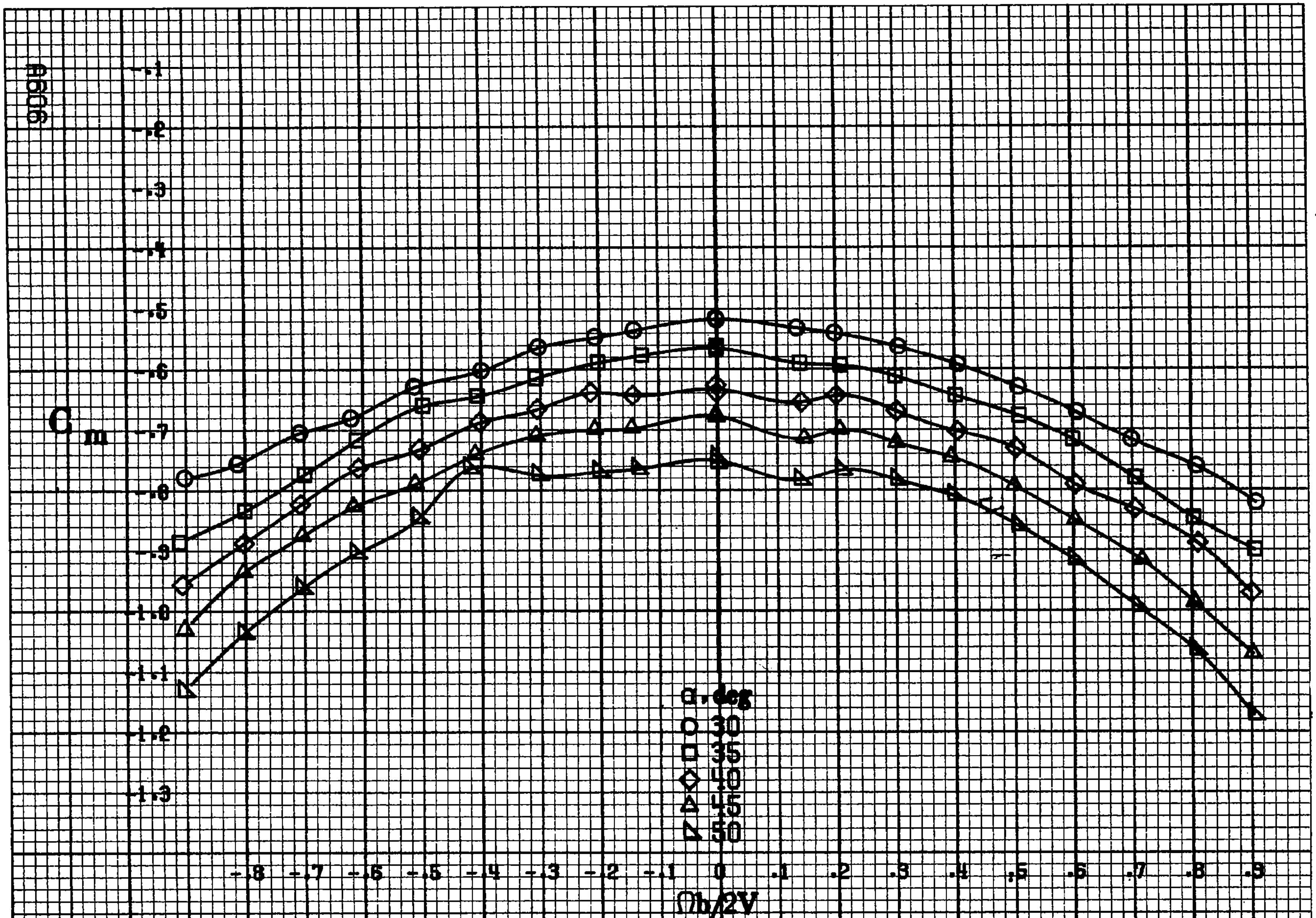

(c) α = 30to50deg, SR = 0.

Figure A147.-Continued.

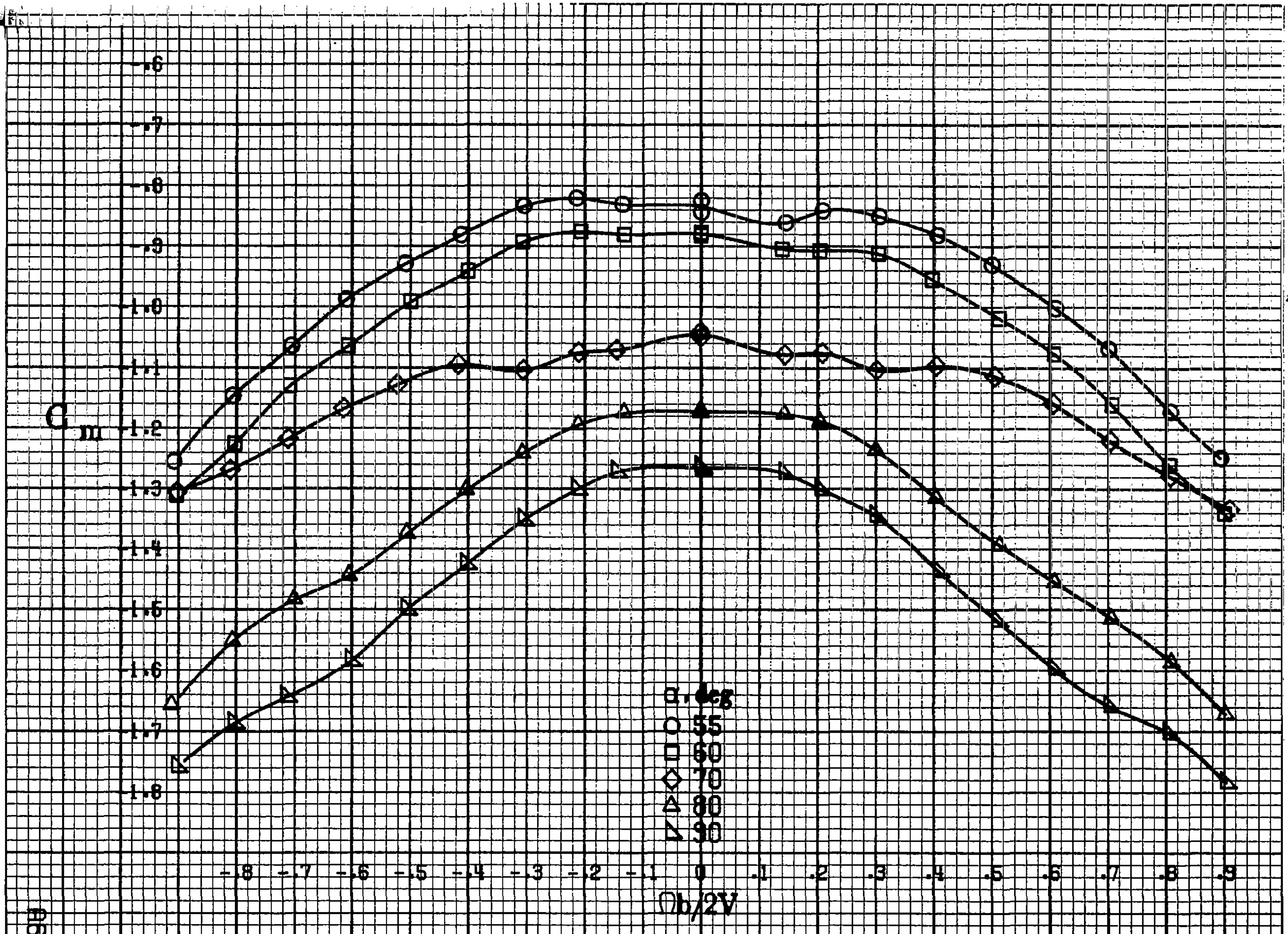

(d) α = 55 to 90 deg, SR = 0.

Figure A147.-Concluded.

A607

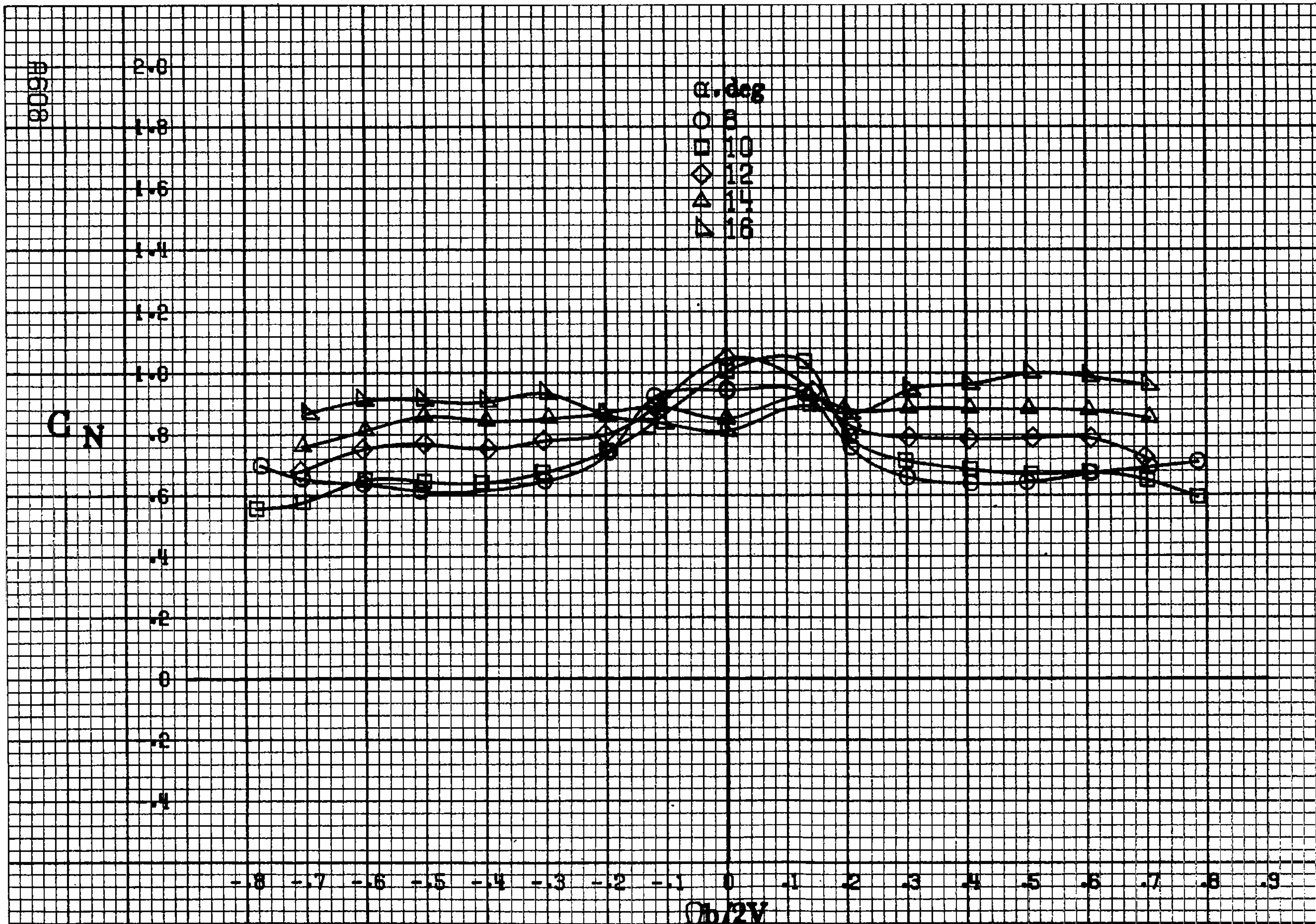

(a) $\alpha = 8$ to 16 deg, SR = 182.9 cm (72 in).

Figure A148.-Effect of rotation rate and angle of attack on normal-force coefficient for no. 1 horizontal tail configuration. $\delta_e = 0°$, $\delta_a = 0°$, $\delta_r = 0°$, $\delta = 0°$.

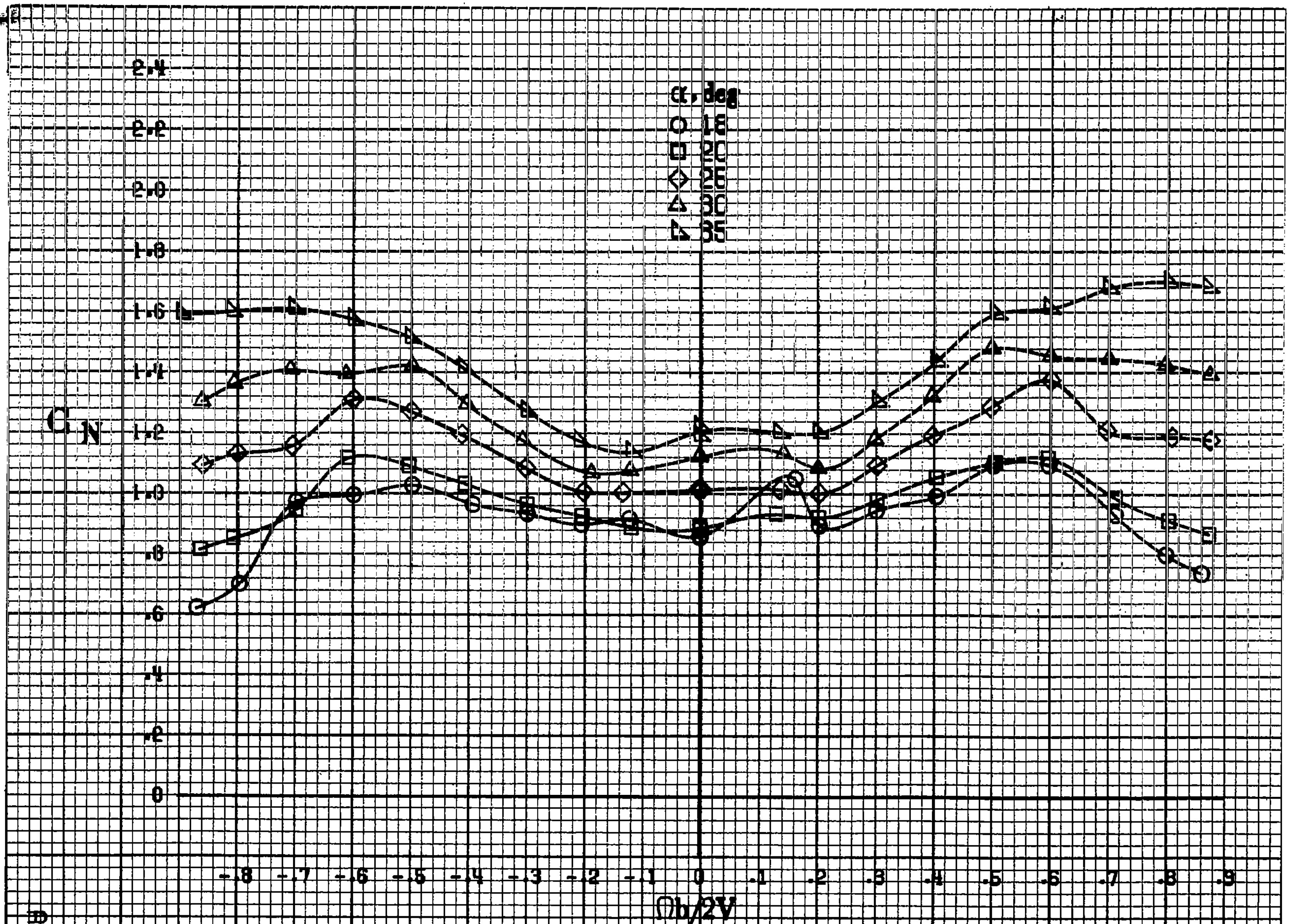

(b) α = 18 to 35 deg, SR = 182.9 cm (72 in).

Figure A148.-Continued.

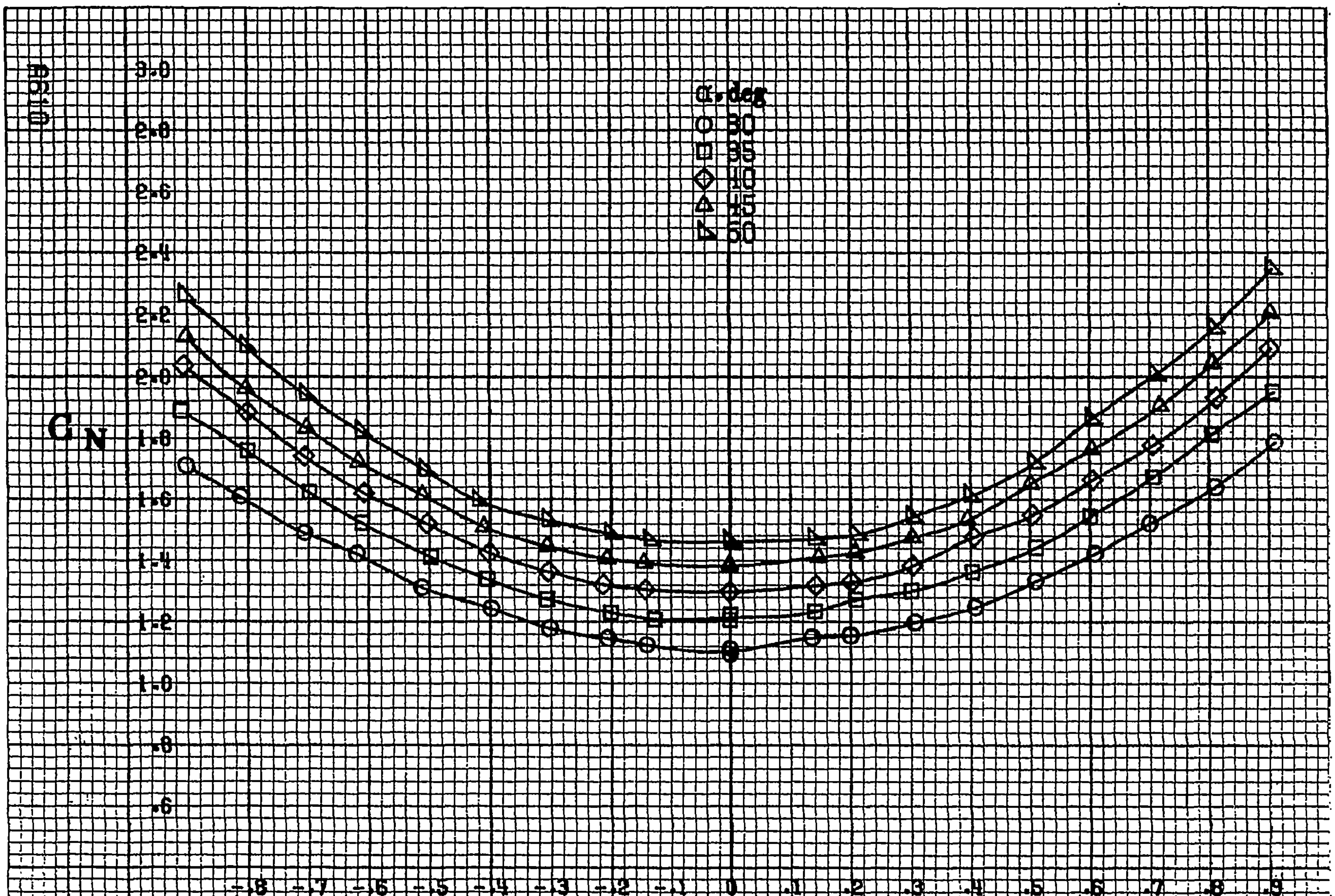

(c) α = 30 to 50 deg, SR = 0.

Figure A148.-Continued.

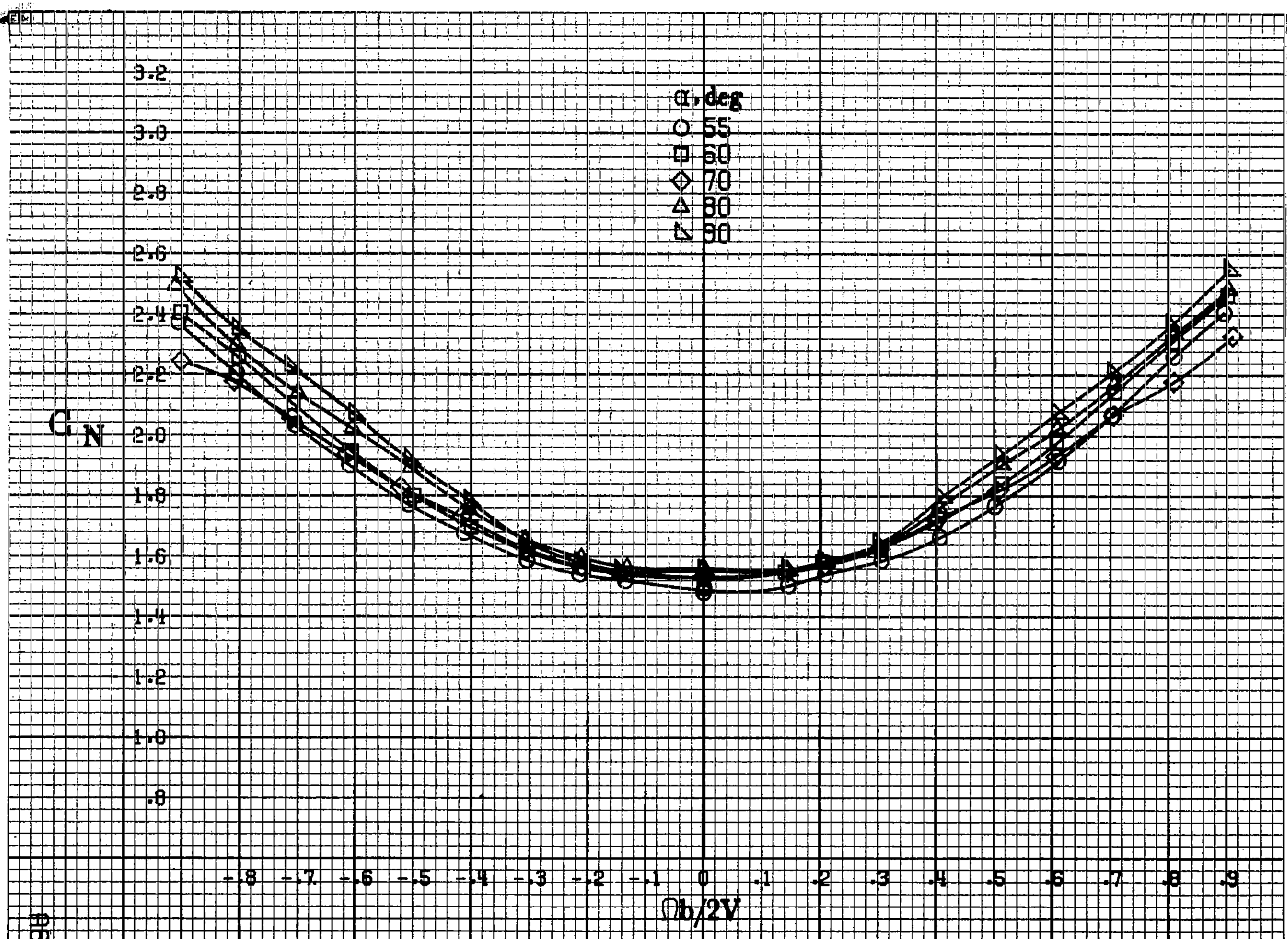

(d) α = 55 to 90 deg, SR = 0.

Figure A148.- Concluded.

A611

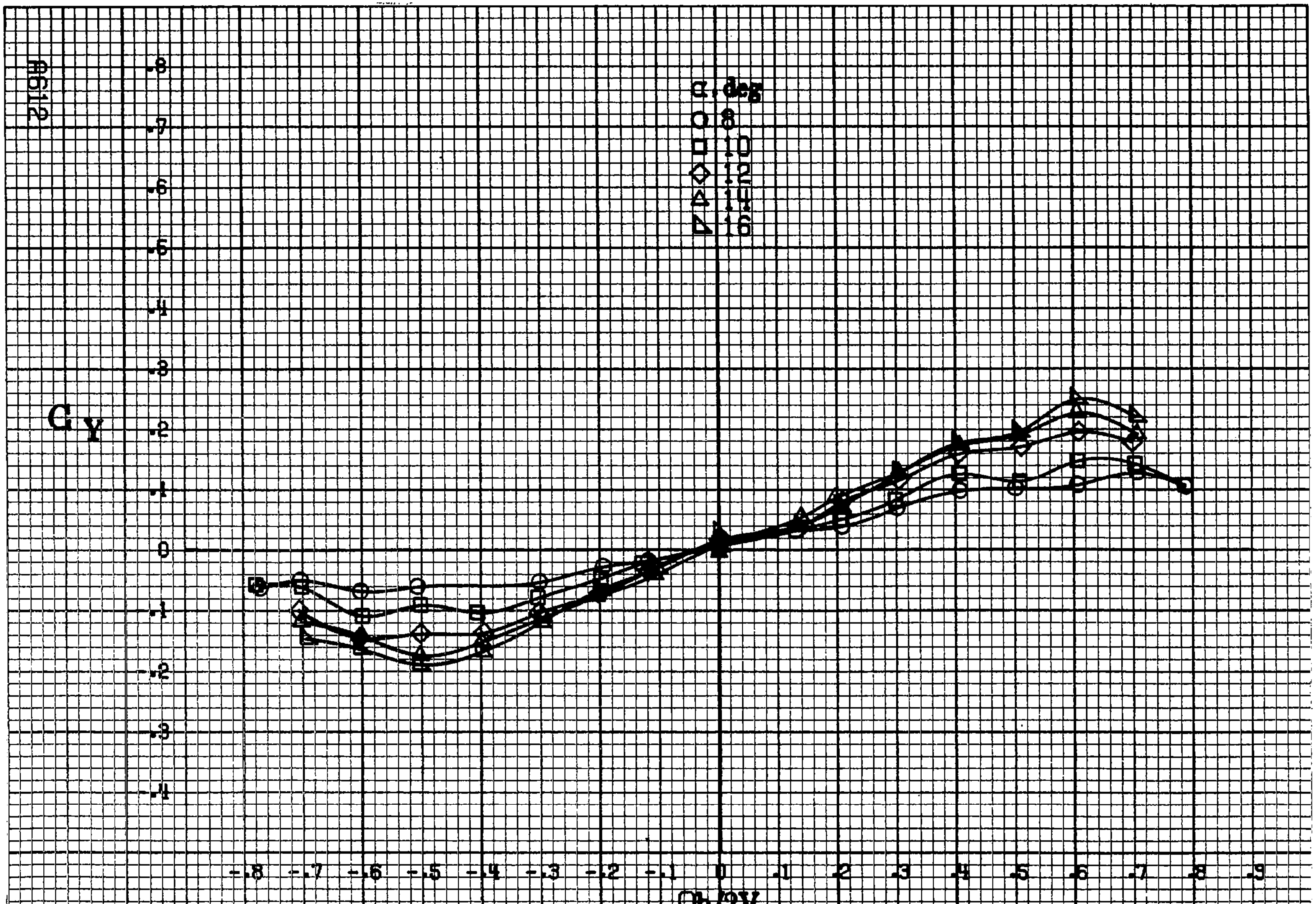

(a) α = 8 to 16 deg, SR = 182.9 cm (72 in).

Figure A149.- Effect of rotation rate and angle of attack on side-force coefficient for no. 1 horizontal tail configuration. $\delta_e = 0°$, $\delta_a = 0°$, $\delta_r = 0°$, $\beta = 0°$.

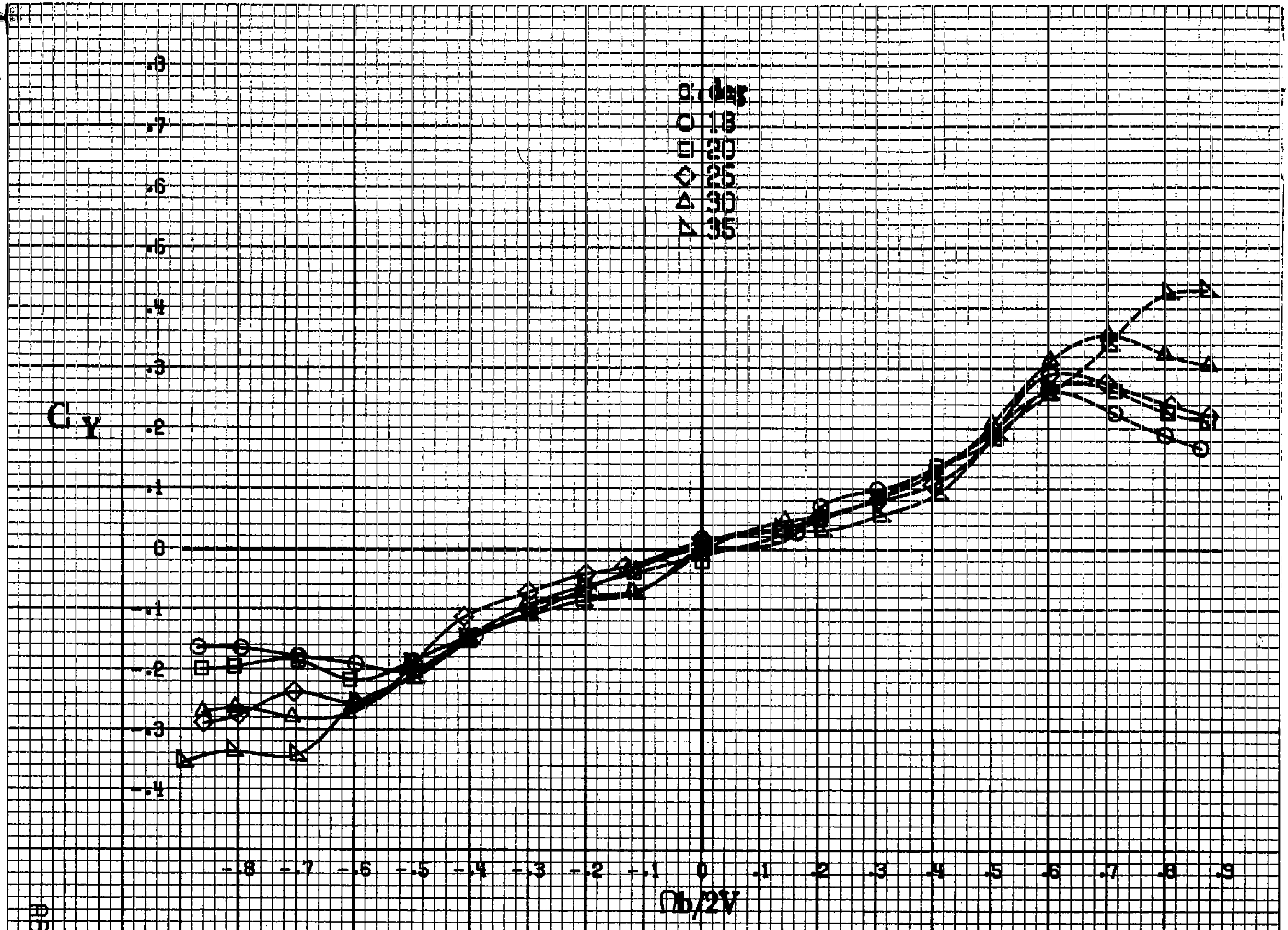

(b) α = 18 to 35 deg, SR = 182.9 cm (72 in).

Figure A149.-Continued.

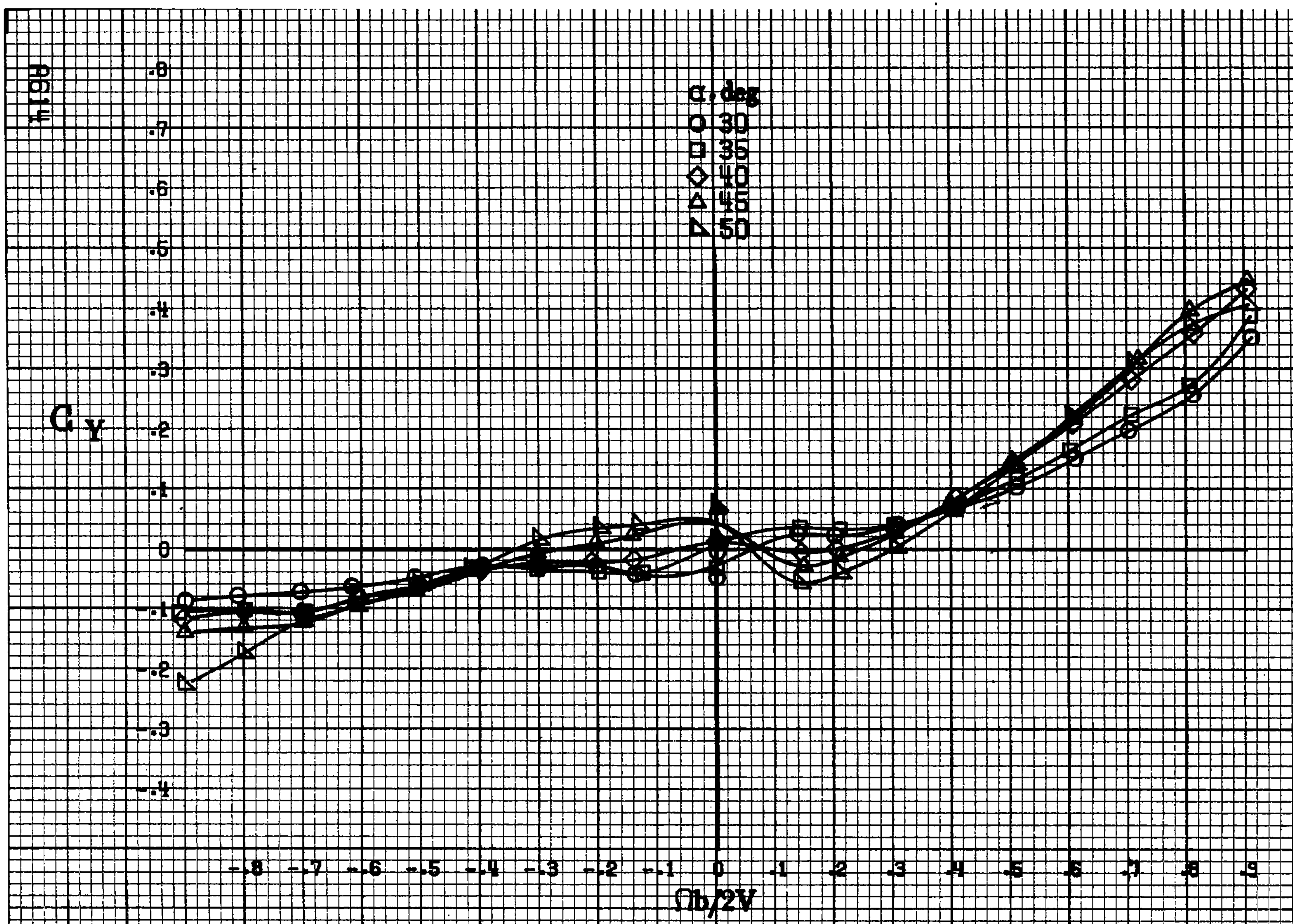

(c) α = 30 to 50 deg, SR = 0.

Figure A149.-Continued.

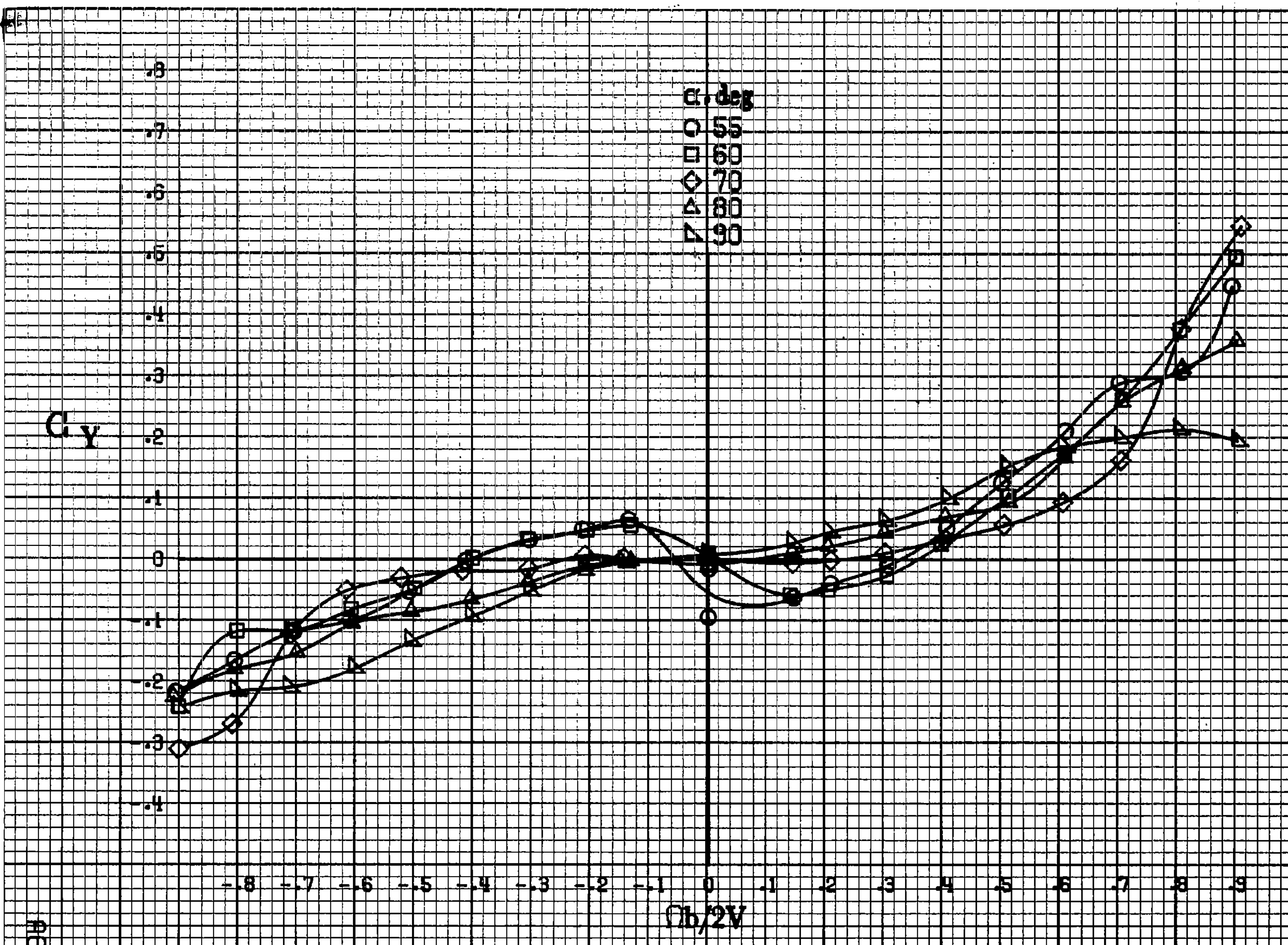

(d) α = 55 to 90 deg, SR = 0.

Figure A149.-Concluded.

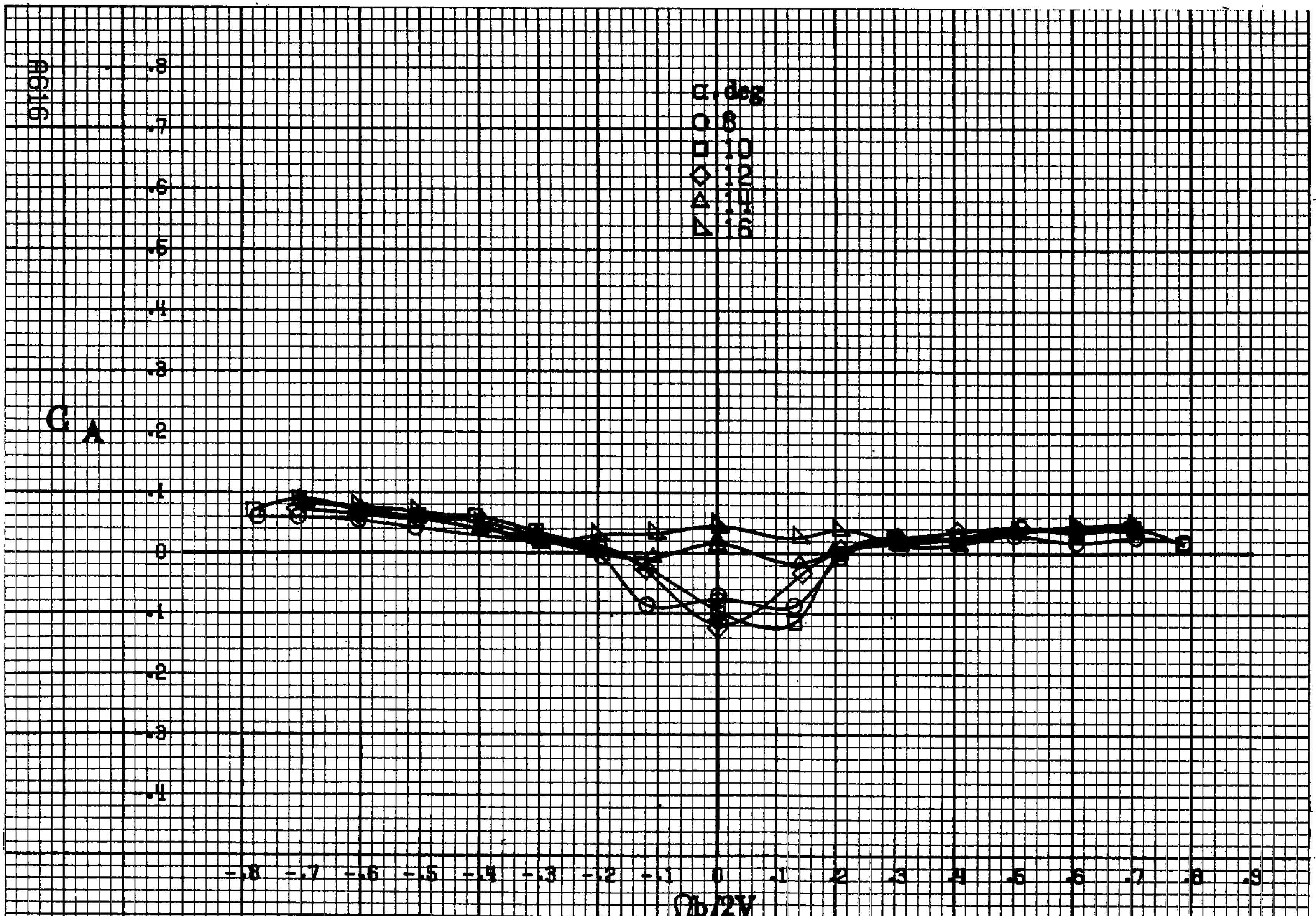

(a) $\alpha = 8$ to 16 deg, SR = 182.9 cm (72 in).

Figure A150.-Effect of rotation rate and angle of attack on axial-force coefficient for no. 1 horizontal tail configuration. $\delta_e = 0°$, $\delta_a = 0°$, $\delta_r = 0°$, $\beta = 0°$.

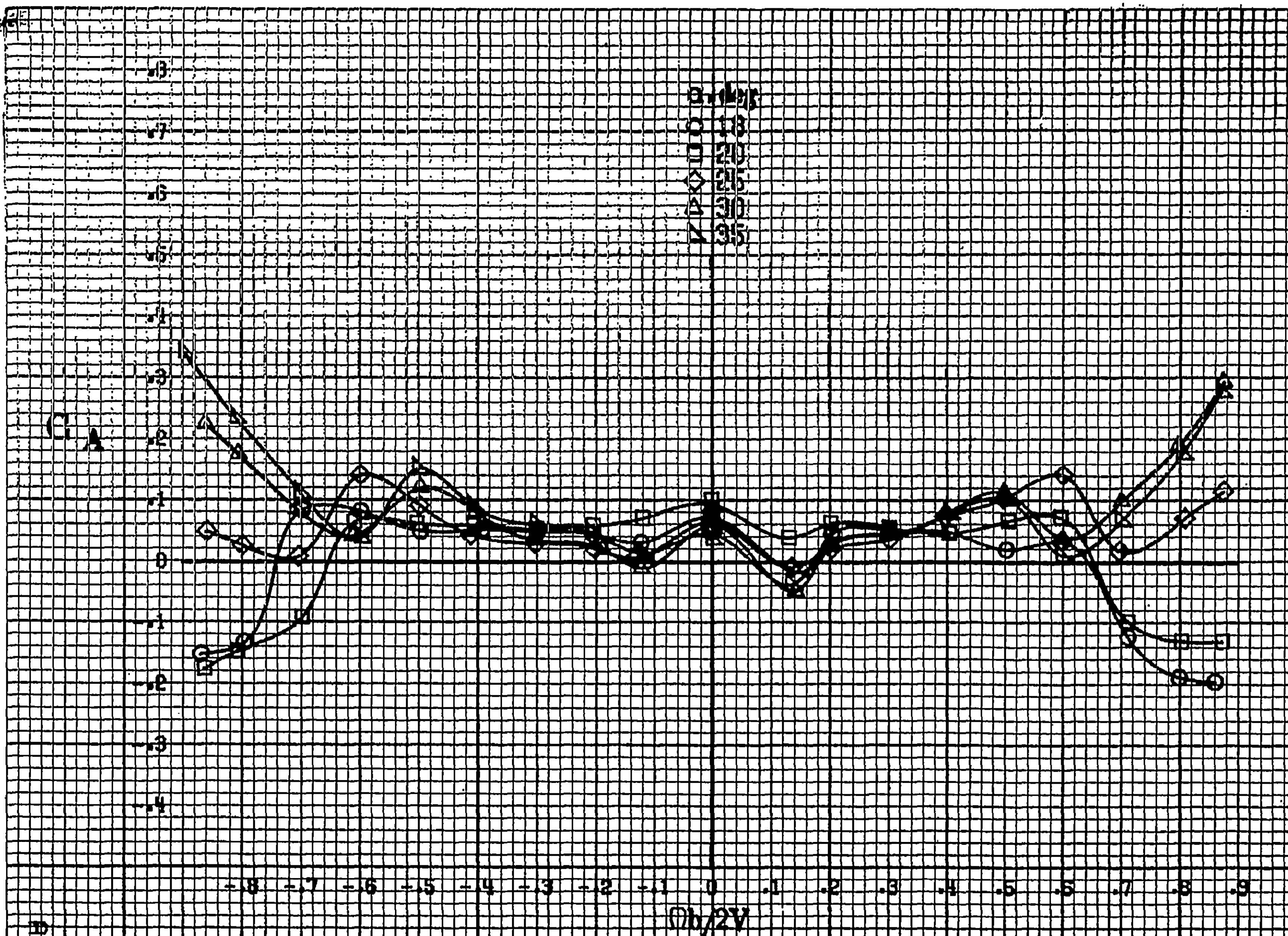

(b) α = 18 to 35 deg, SR = 182.9 cm (72 in)

Figure A150.-Continued.

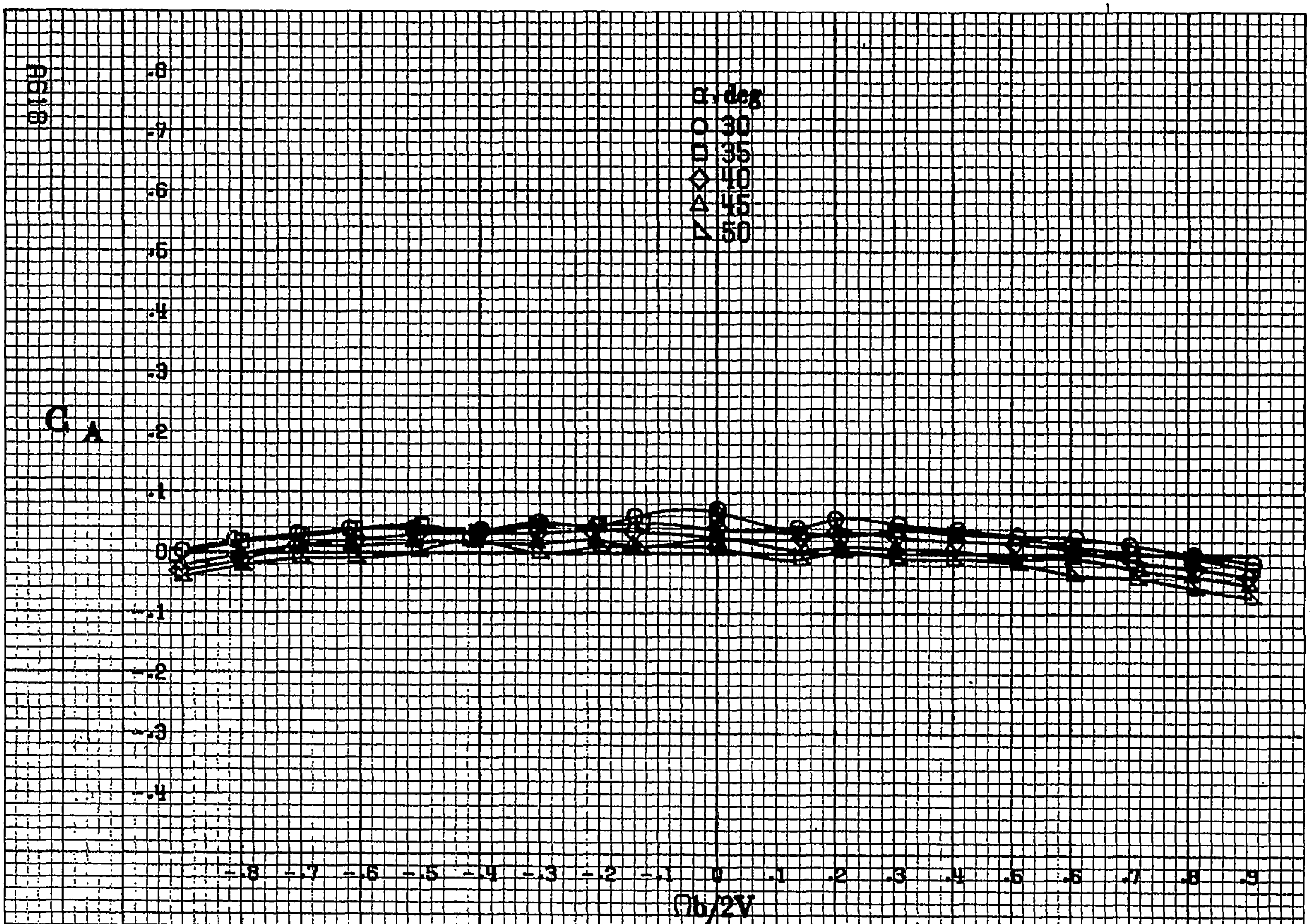

(c) α = 30 to 50 deg, SR = 0.

Figure A150.-Continued.

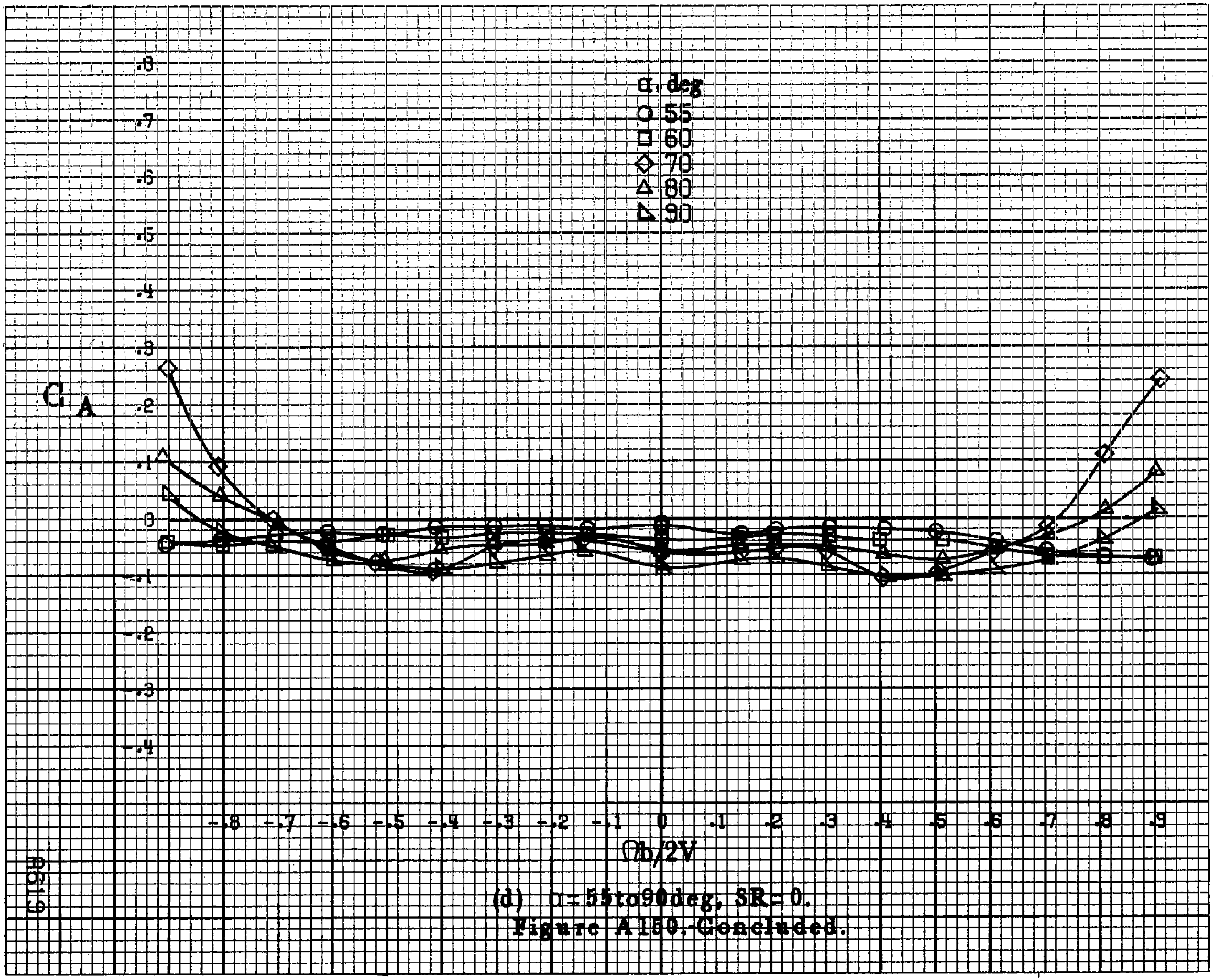

(d) α = 55 to 90 deg, SR = 0.

Figure A150.-Concluded.

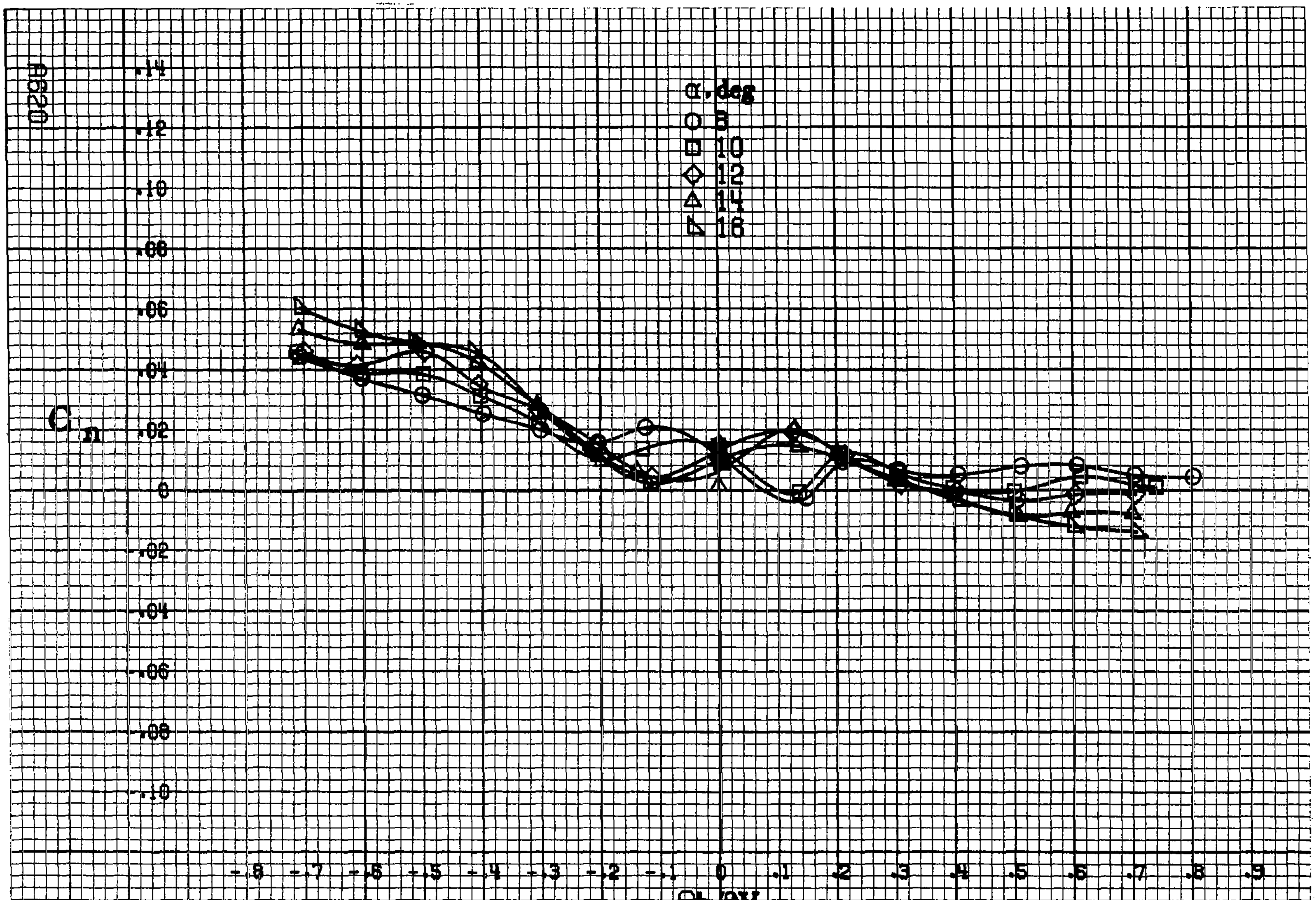

(a) $\alpha = 8$ to 16 deg, SR = 182.9 cm (72 in).

Figure A161.-Effect of rotation rate and angle of attack on yawing-moment coefficient for no. 1 horizontal tail configuration. $\delta_e = -15°$, $\delta_a = 0°$, $\delta_r = -25°$, $\beta = 0°$.

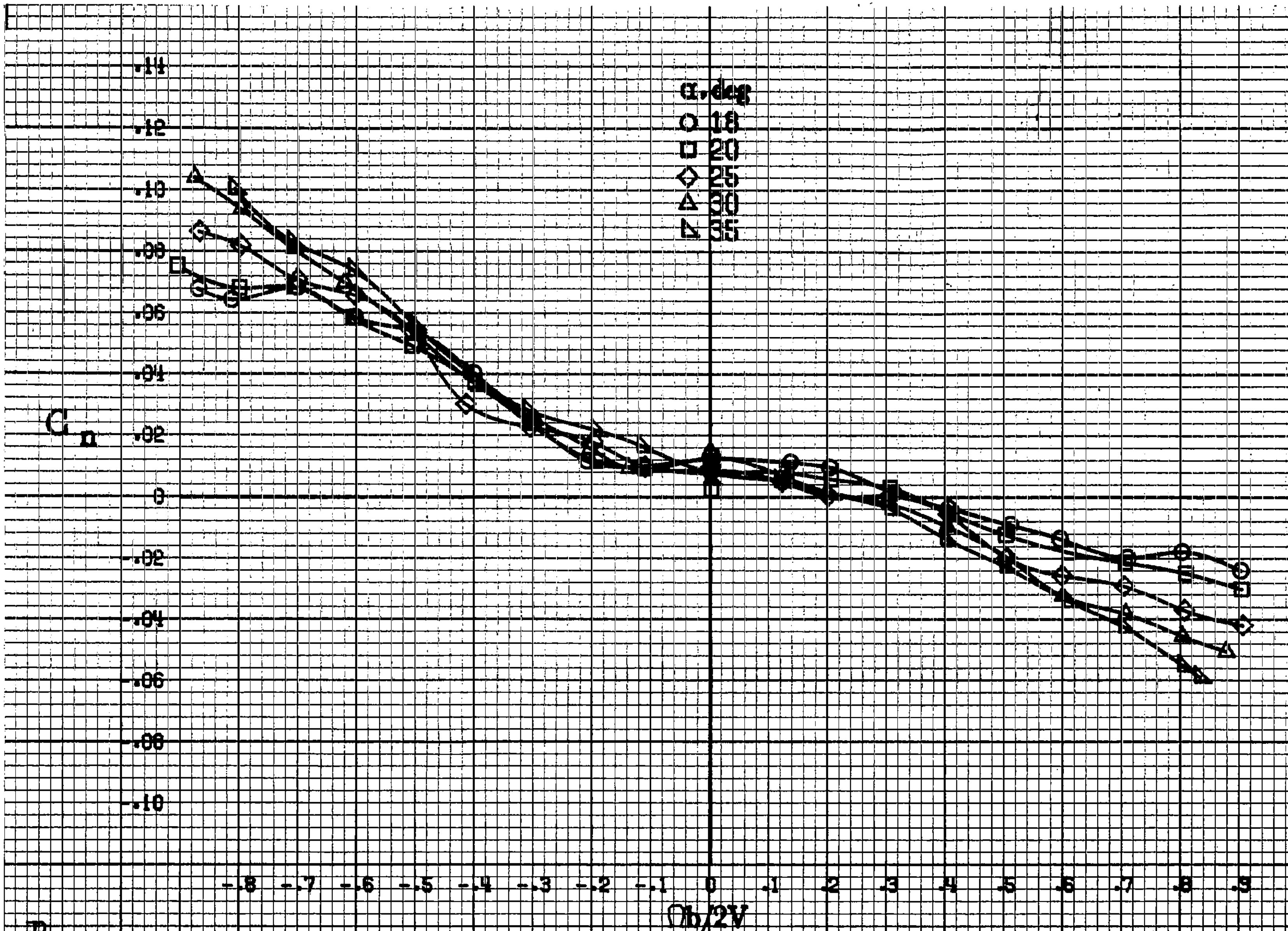

(b) α = 18 to 35 deg, SR = 182.9 cm (72 in).

Figure A151.- Continued.

A621

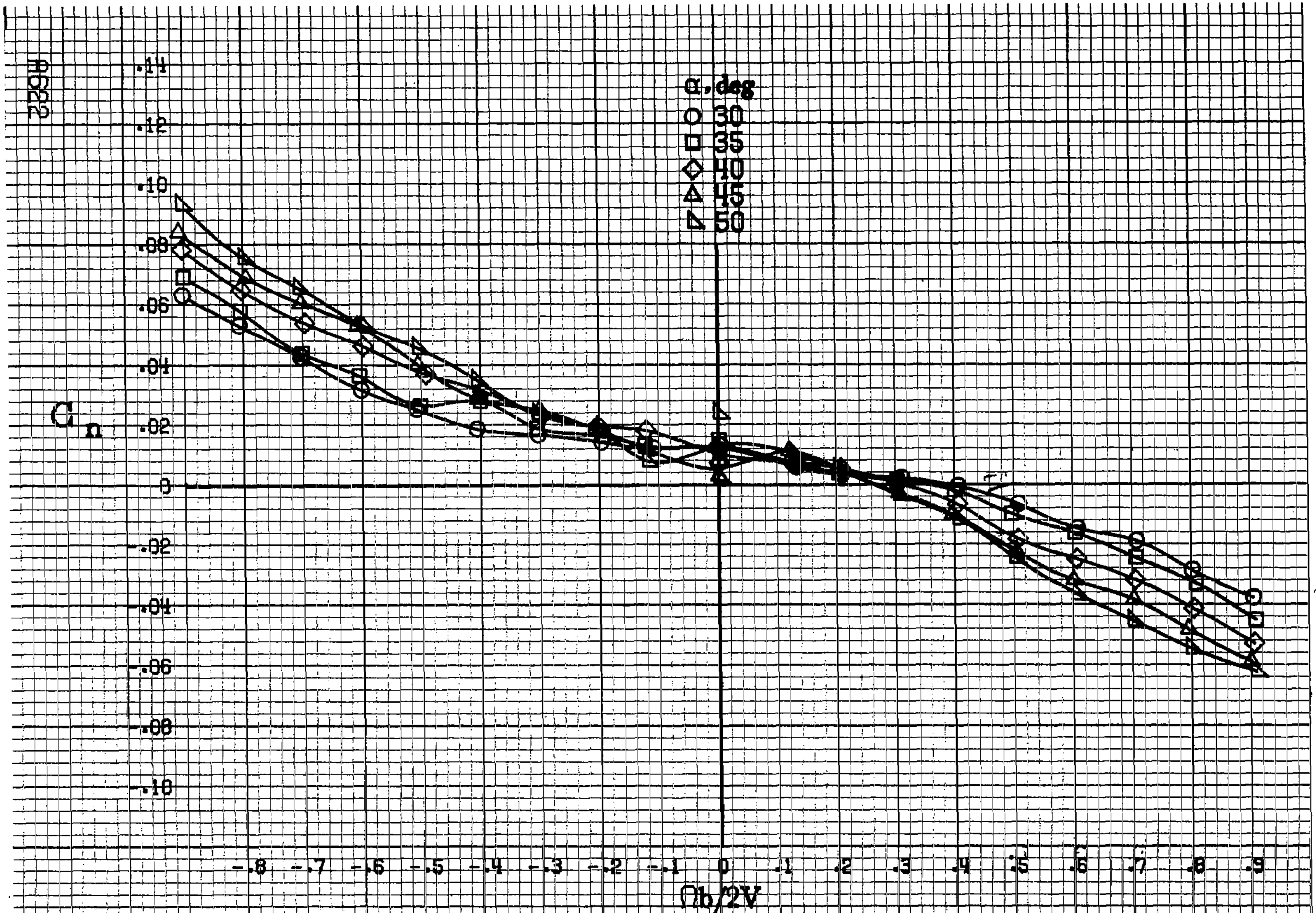

(c) α = 30 to 50 deg, SR = 0.
Figure A151.-Continued.

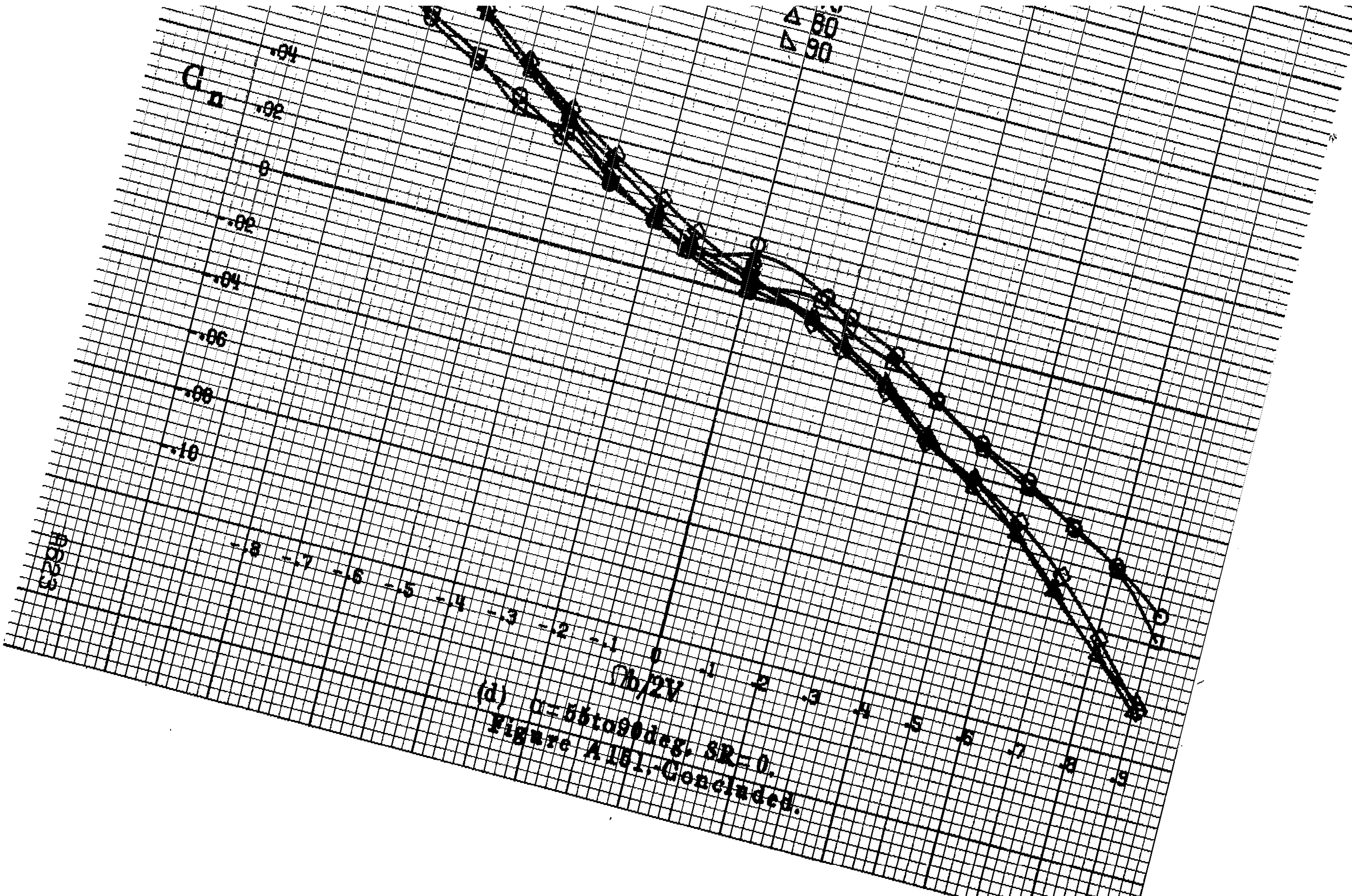

(d) α = 55 to 90 deg, SR = 0.

Figure A161.-Concluded.

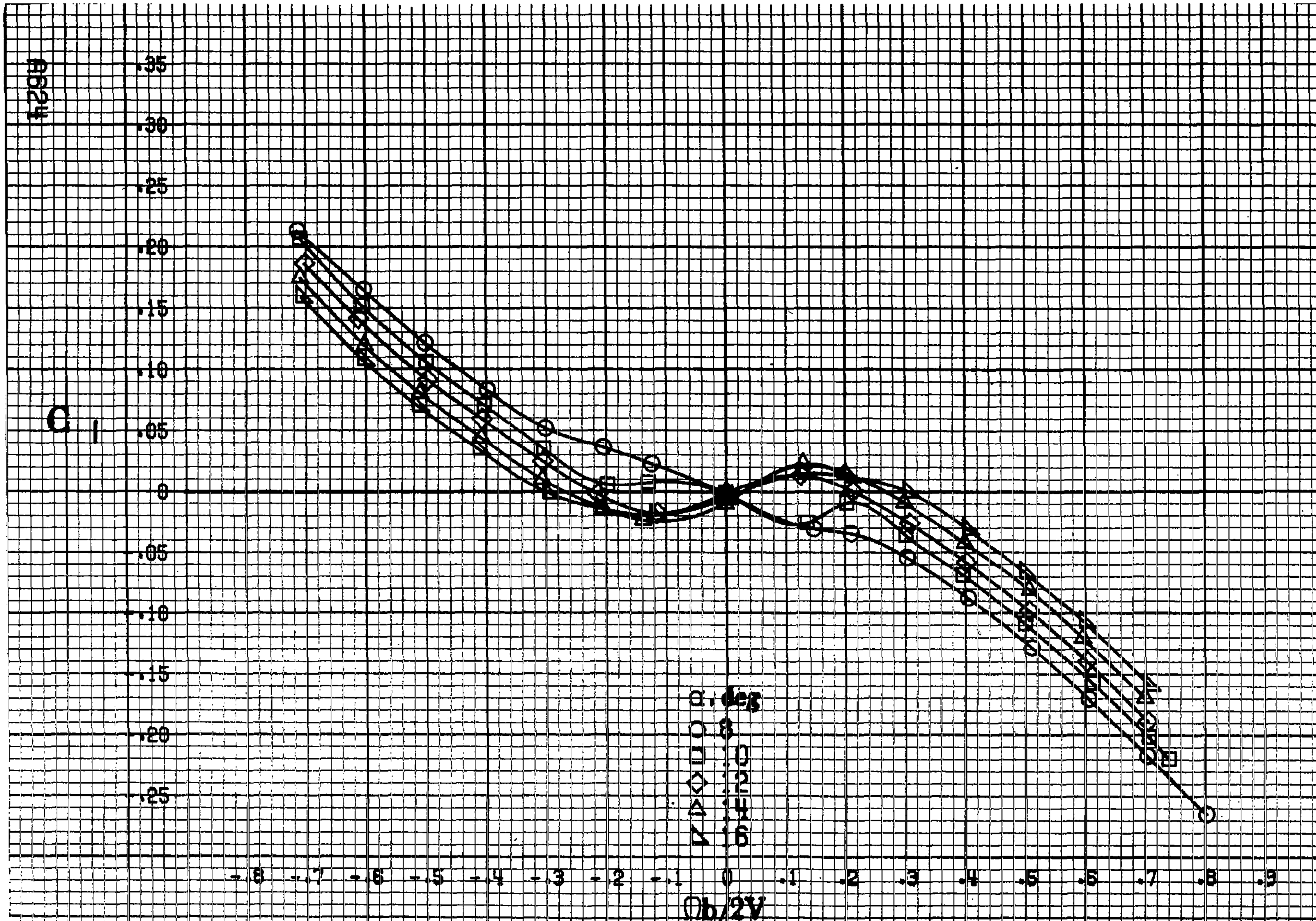

(a) α = 8 to 16 deg, SR = 182.9 cm (72 in).

Figure A152.- Effect of rotation rate and angle of attack on rolling-moment coefficient for no. 1 horizontal tail configuration. $\delta_e = -15°$, $\delta_a = 0°$, $\delta_r = -25°$, $\beta = 0°$.

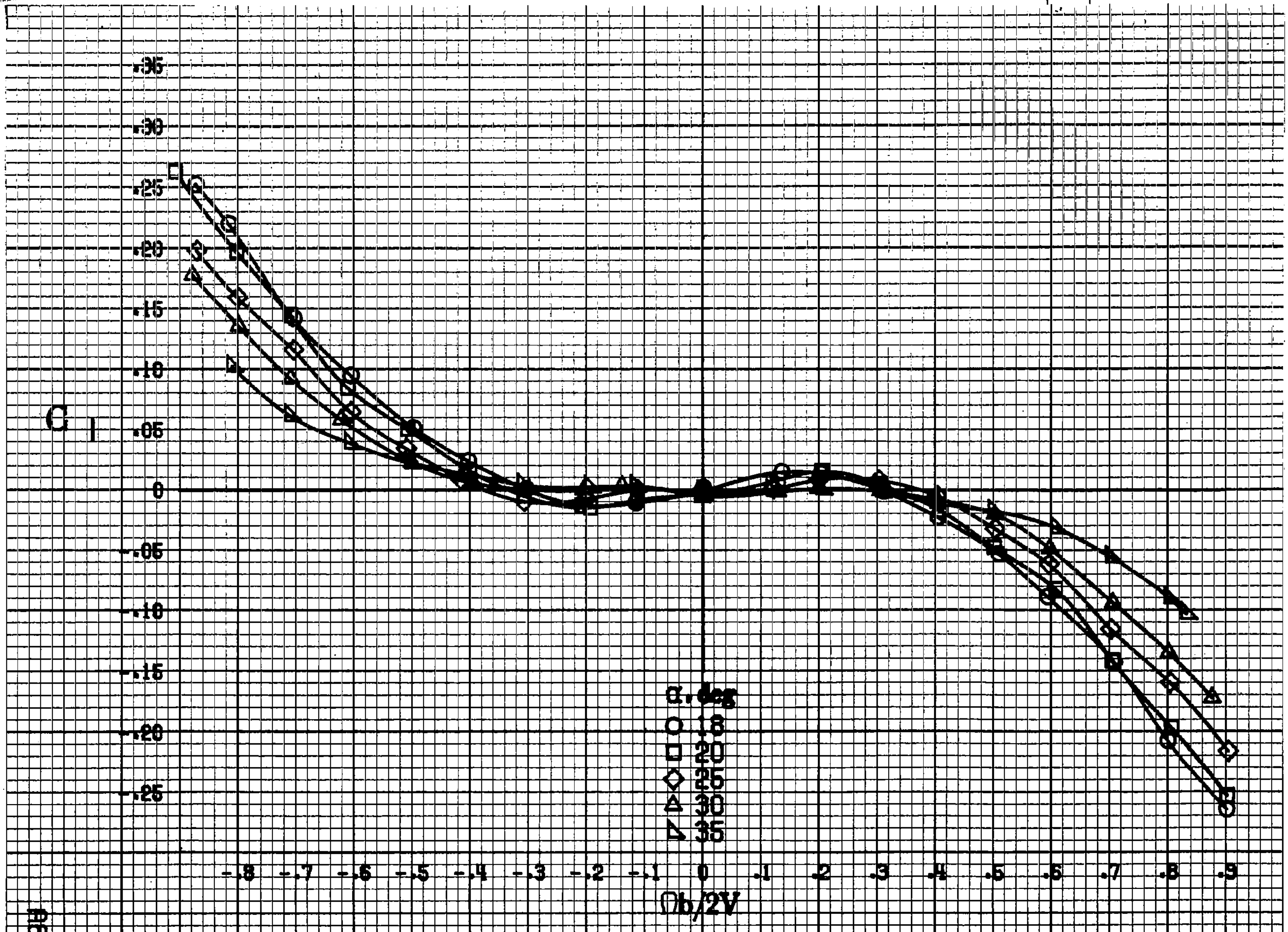

(b) α = 18 to 35 deg, SR = 182.9 cm (72 in).

Figure A152.-Continued.

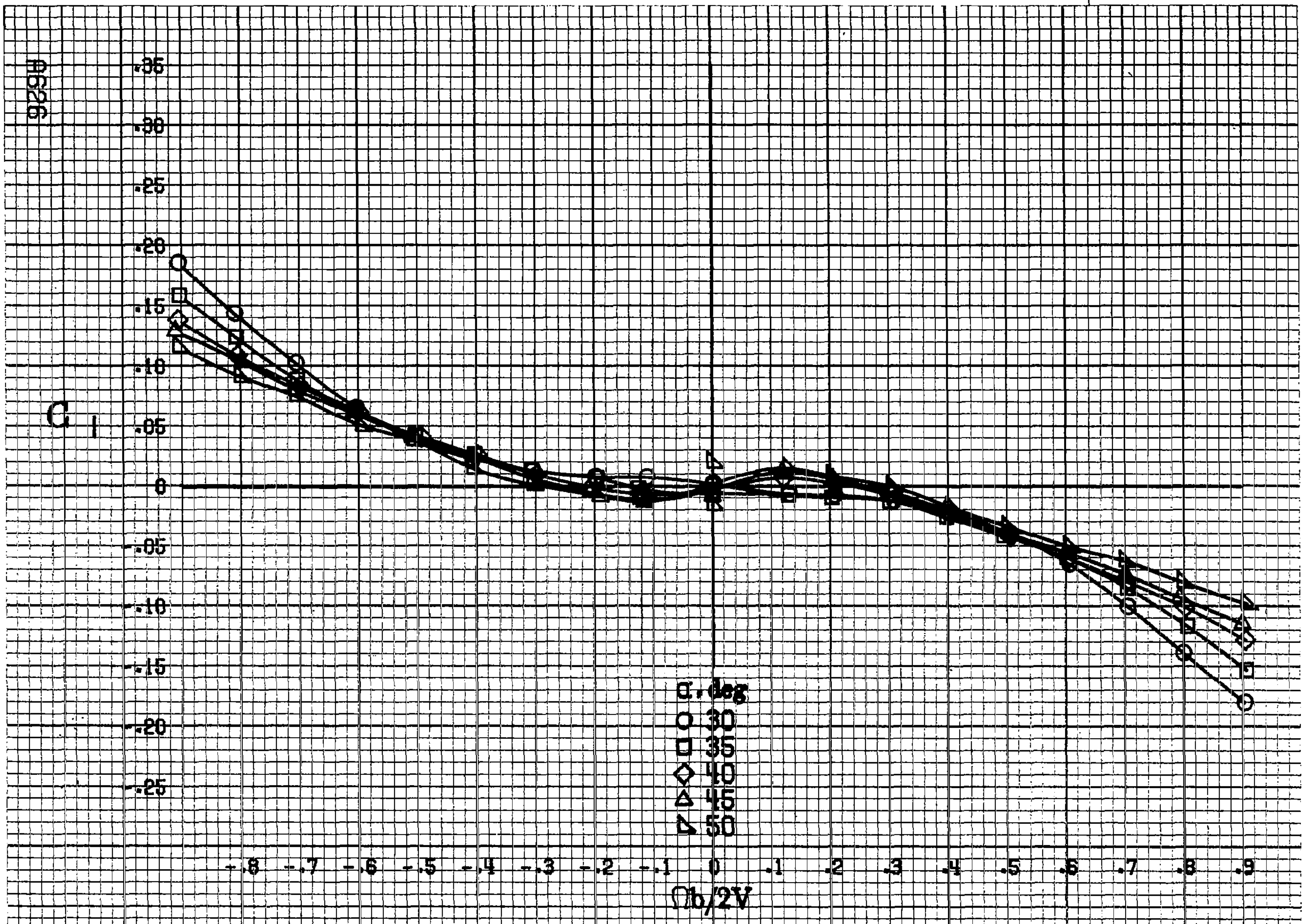

(c) $\alpha = 30$ to 50 deg, SR = 0.

Figure A152.-Continued.

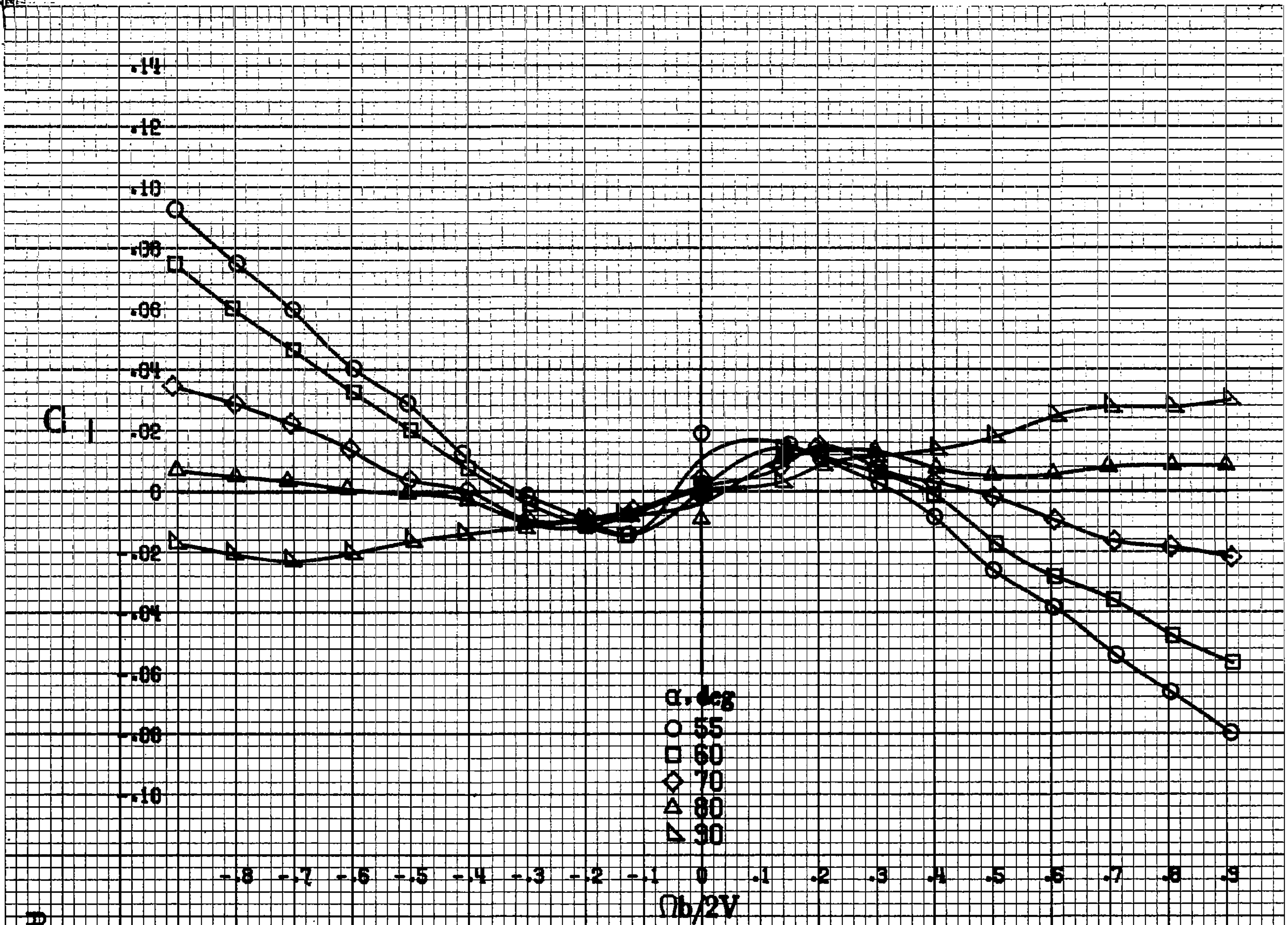

(d) α = 55 to 90 deg, SR = 0.
Figure A152.-Concluded.

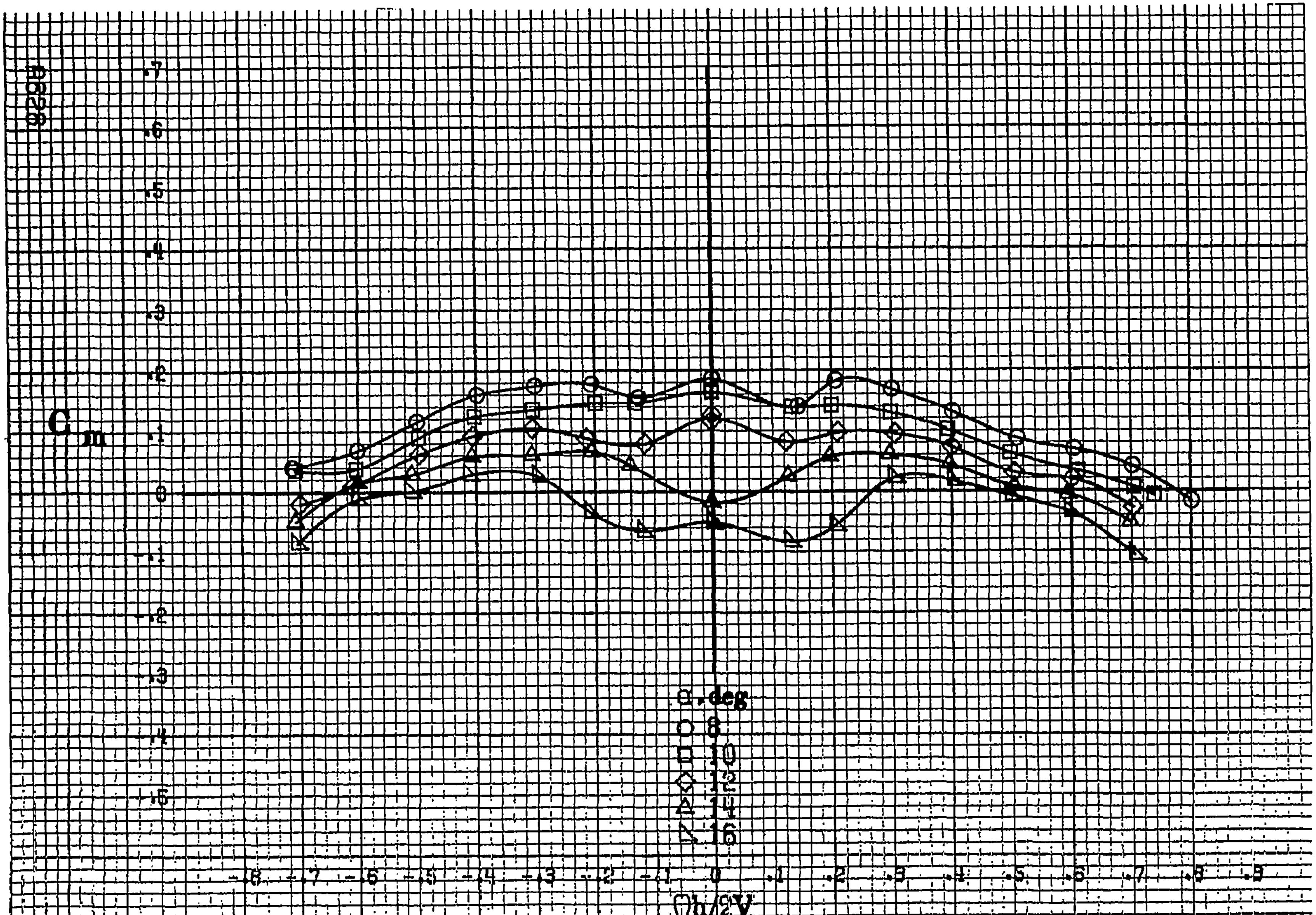

(a) $\alpha = 8$ to 16 deg, SR = 182.9 cm (72 in).

Figure A158.-Effect of rotation rate and angle of attack on pitching-moment coefficient for no. 1 horizontal tail configuration. $\delta_e = -15°$, $\delta_a = 0°$, $\delta_r = -25°$, $\beta = 0°$.

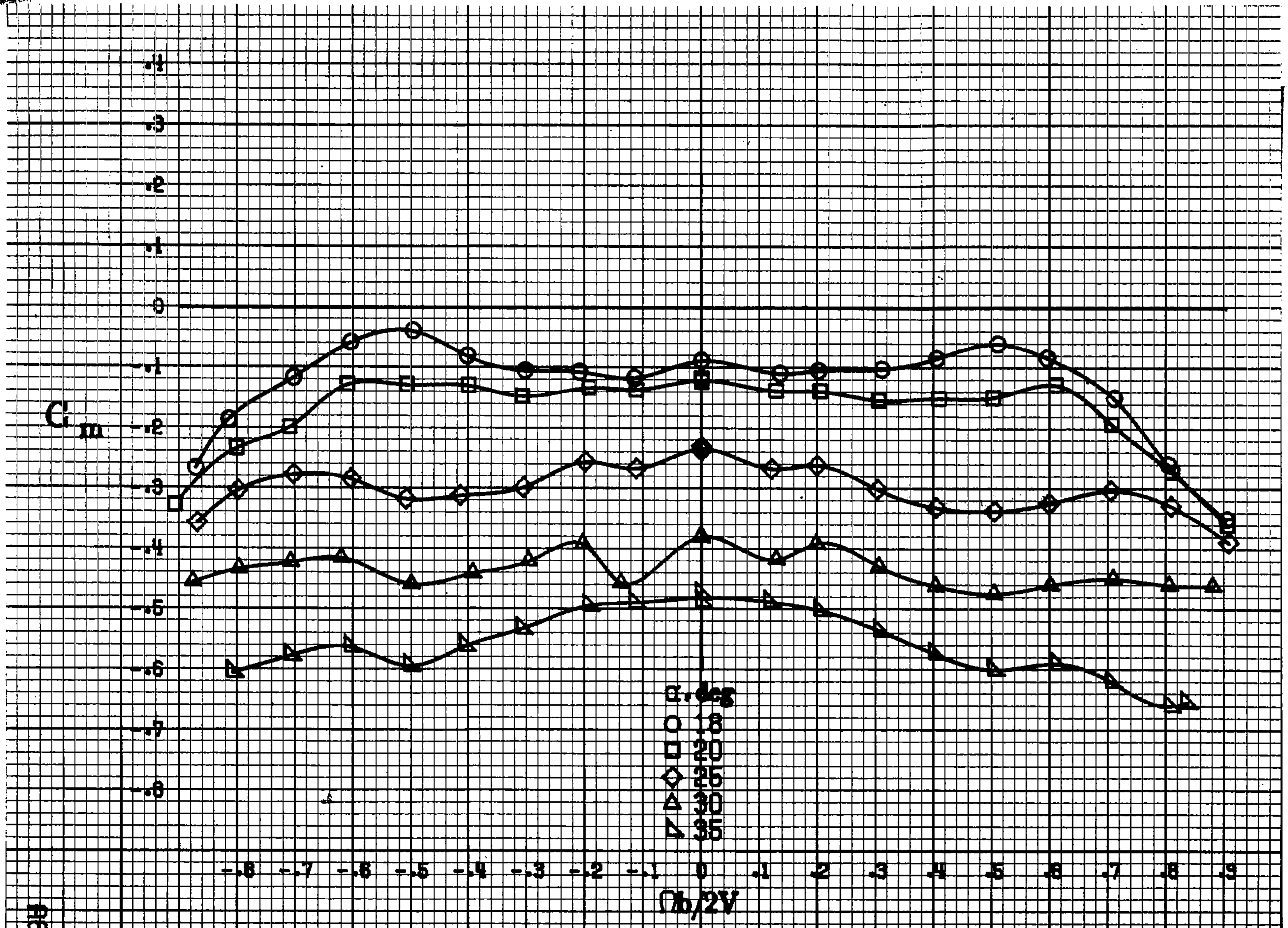

(b) α = 18 to 35 deg, SR = 182.9 cm (72 in).

Figure A 153.-Continued.

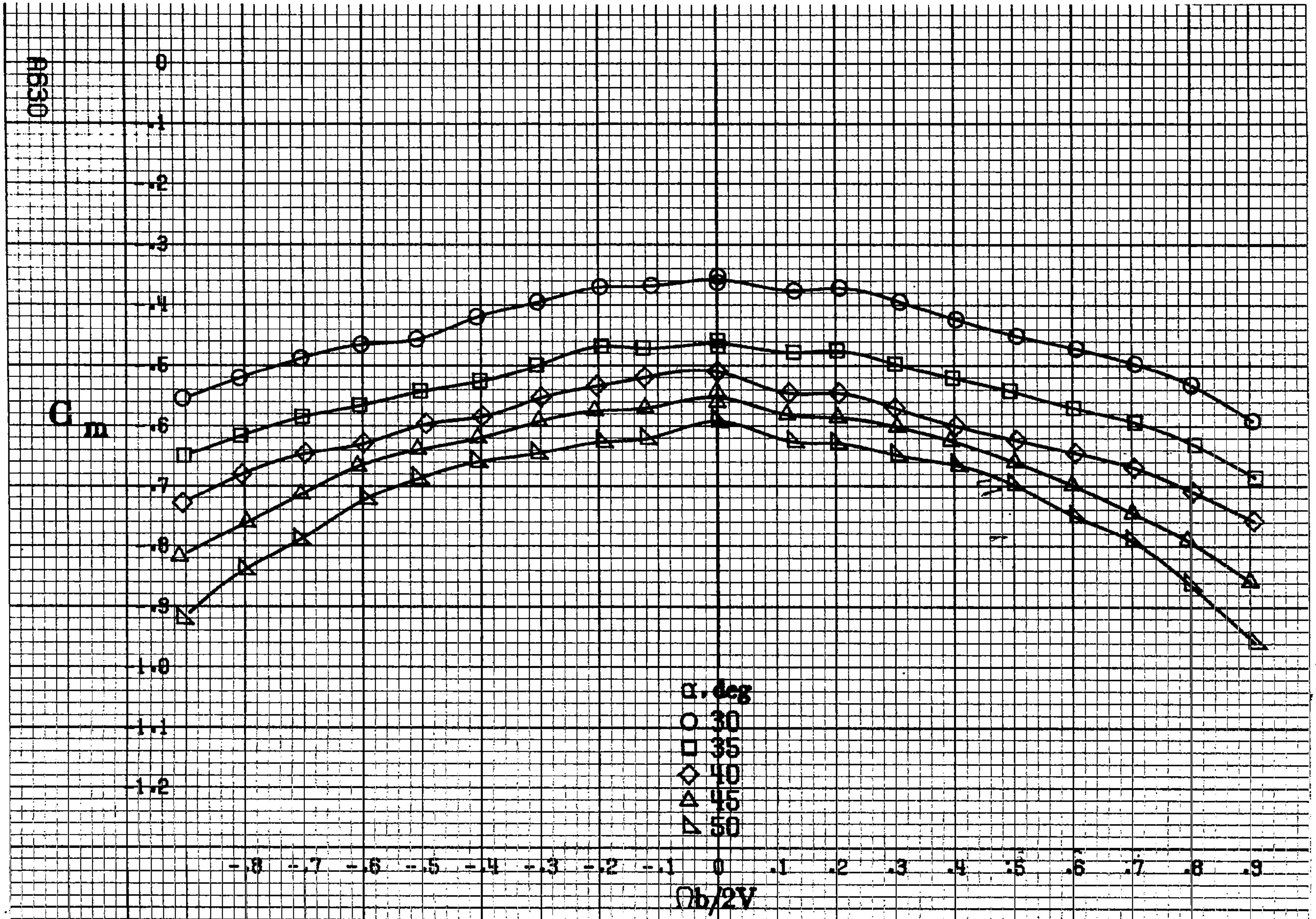

(c) α = 30 to 50 deg, SR = 0.

Figure A158.-Continued.

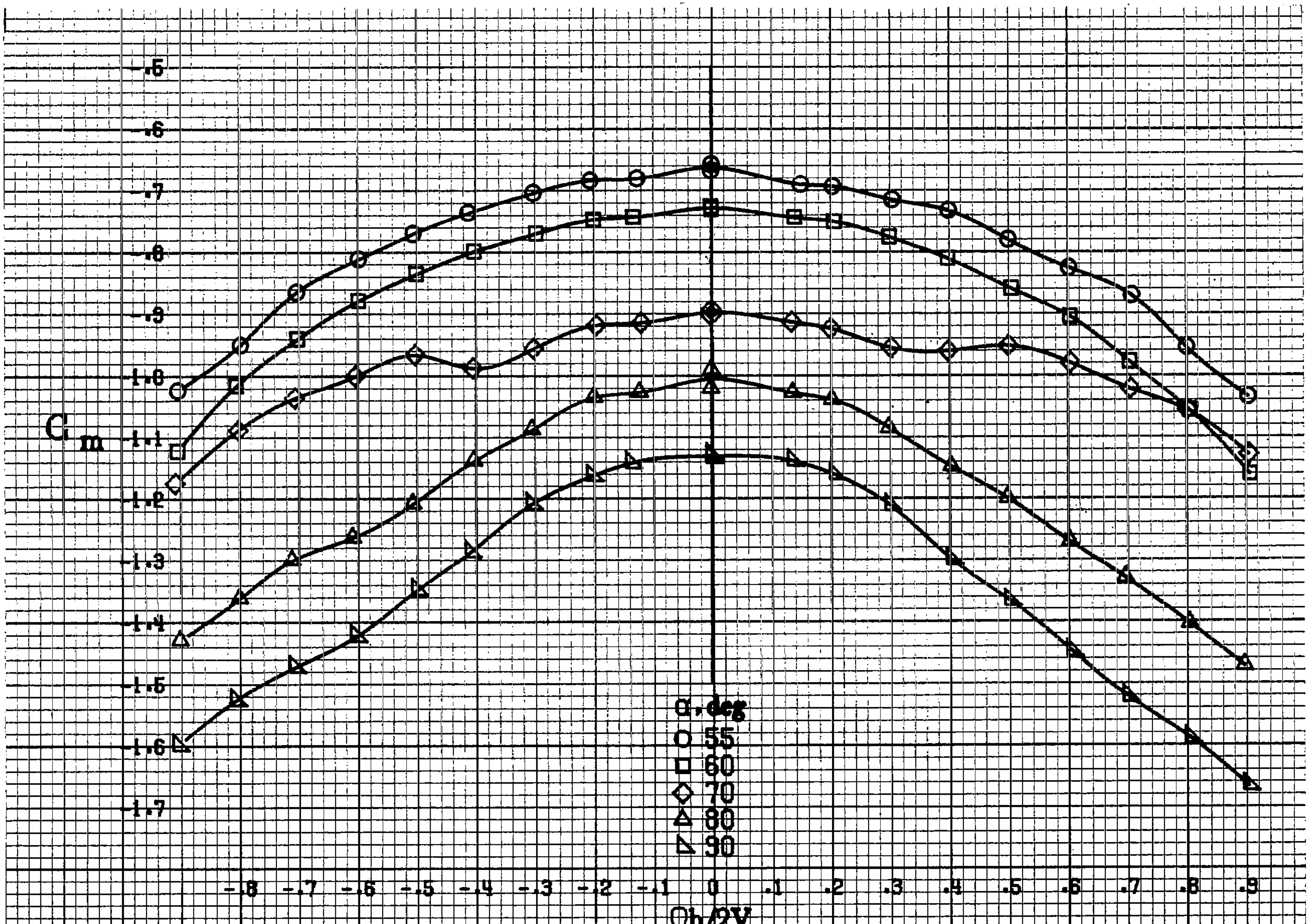

(d) α = 55 to 90 deg, SR = 0.

Figure A158.-Concluded.

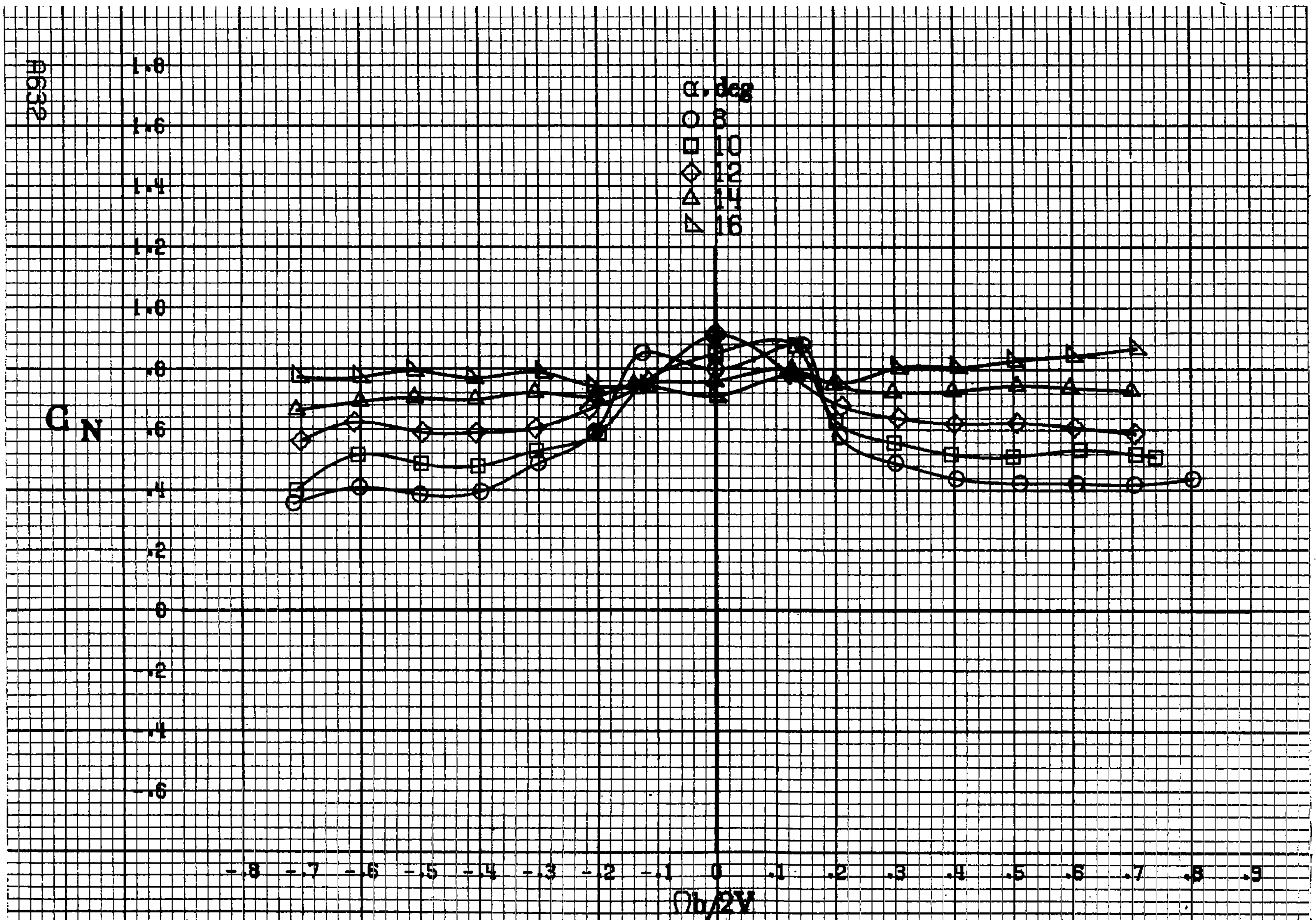

(a) α = 8 to 16 deg, SR = 182.9 cm (72 in).

Figure A154.- Effect of rotation rate and angle of attack on normal-force coefficient for no. 1 horizontal tail configuration. $\delta_e = -15°$, $\delta_a = 0°$, $\delta_r = -25°$, $\beta = 0°$.

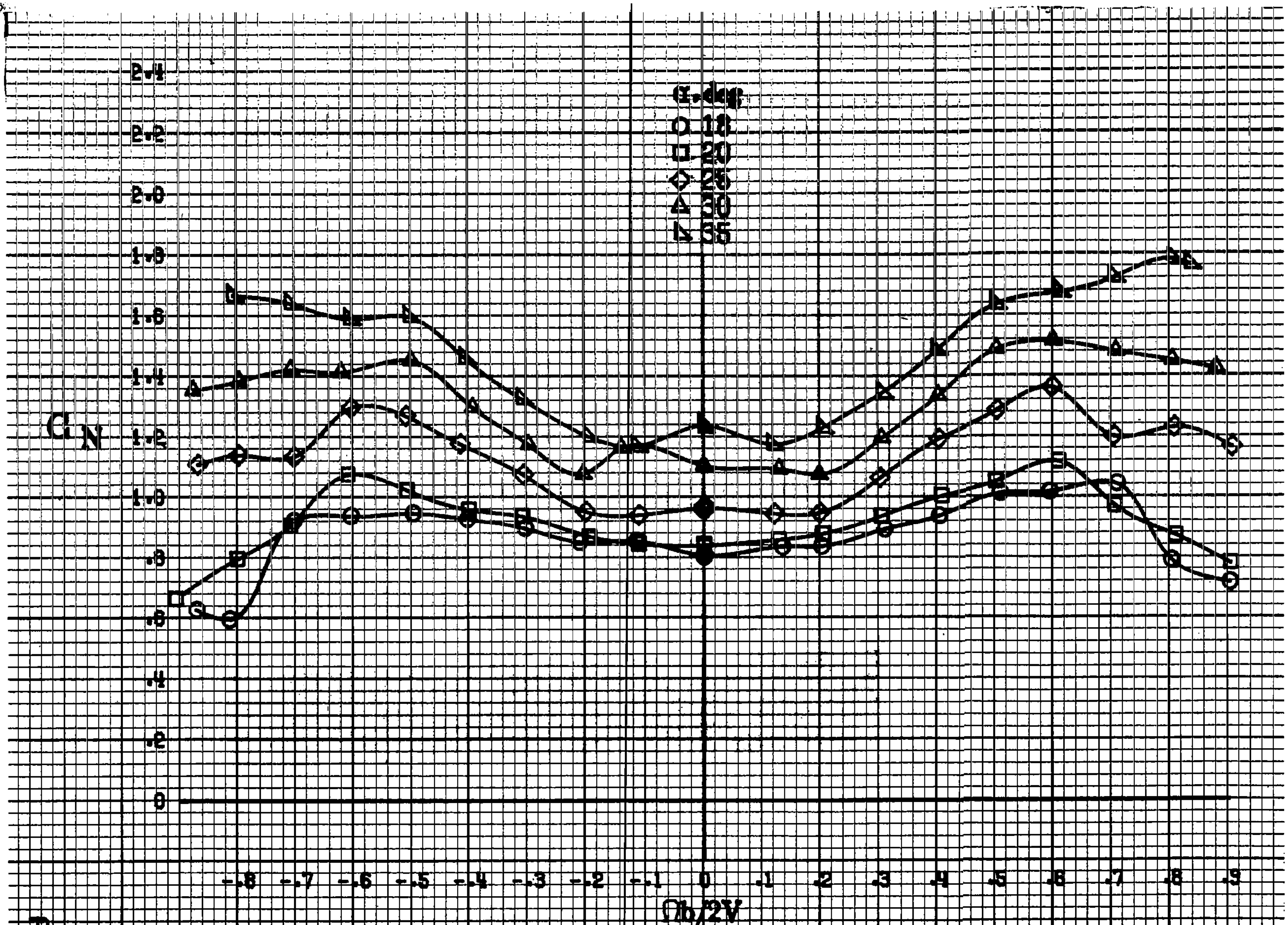

(b) α = 18 to 35 deg, SR = 182.9 cm (72 in).

Figure A154.-Continued.

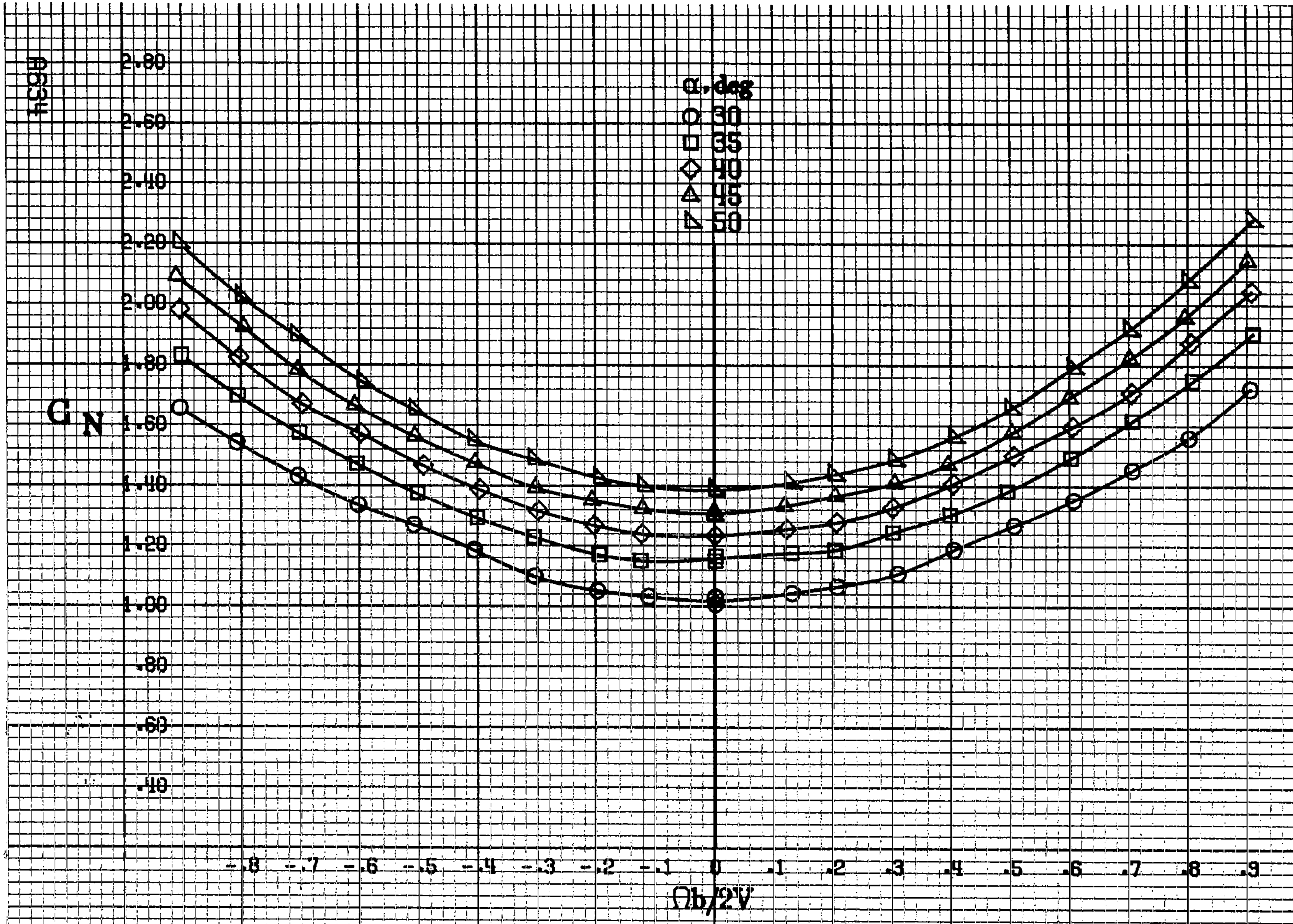

(c) α = 30 to 50 deg, SR = 0.

Figure A.154.-Continued.

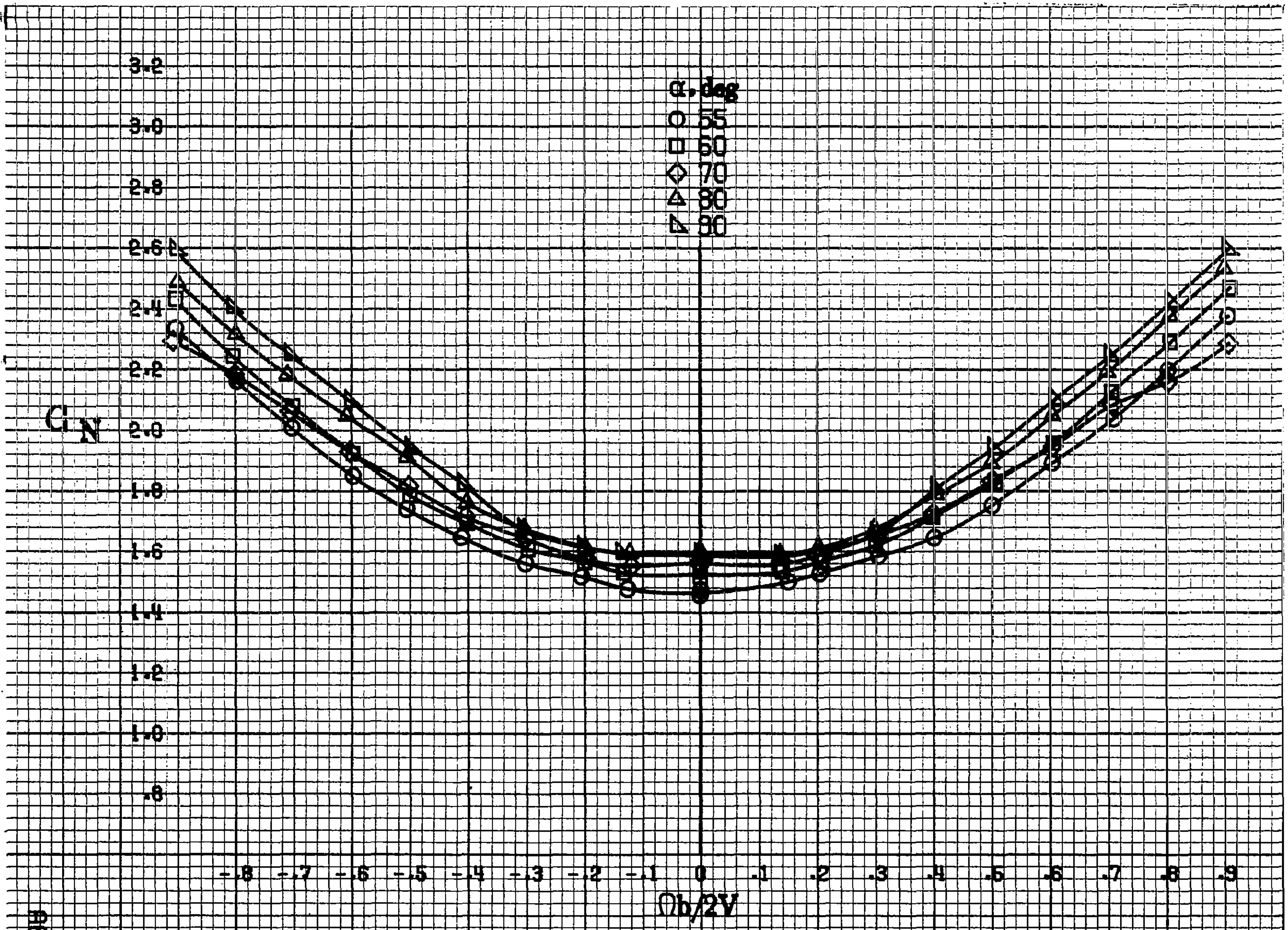

(d) α = 55 to 90 deg, SR = 0.

Figure A154.-Concluded.

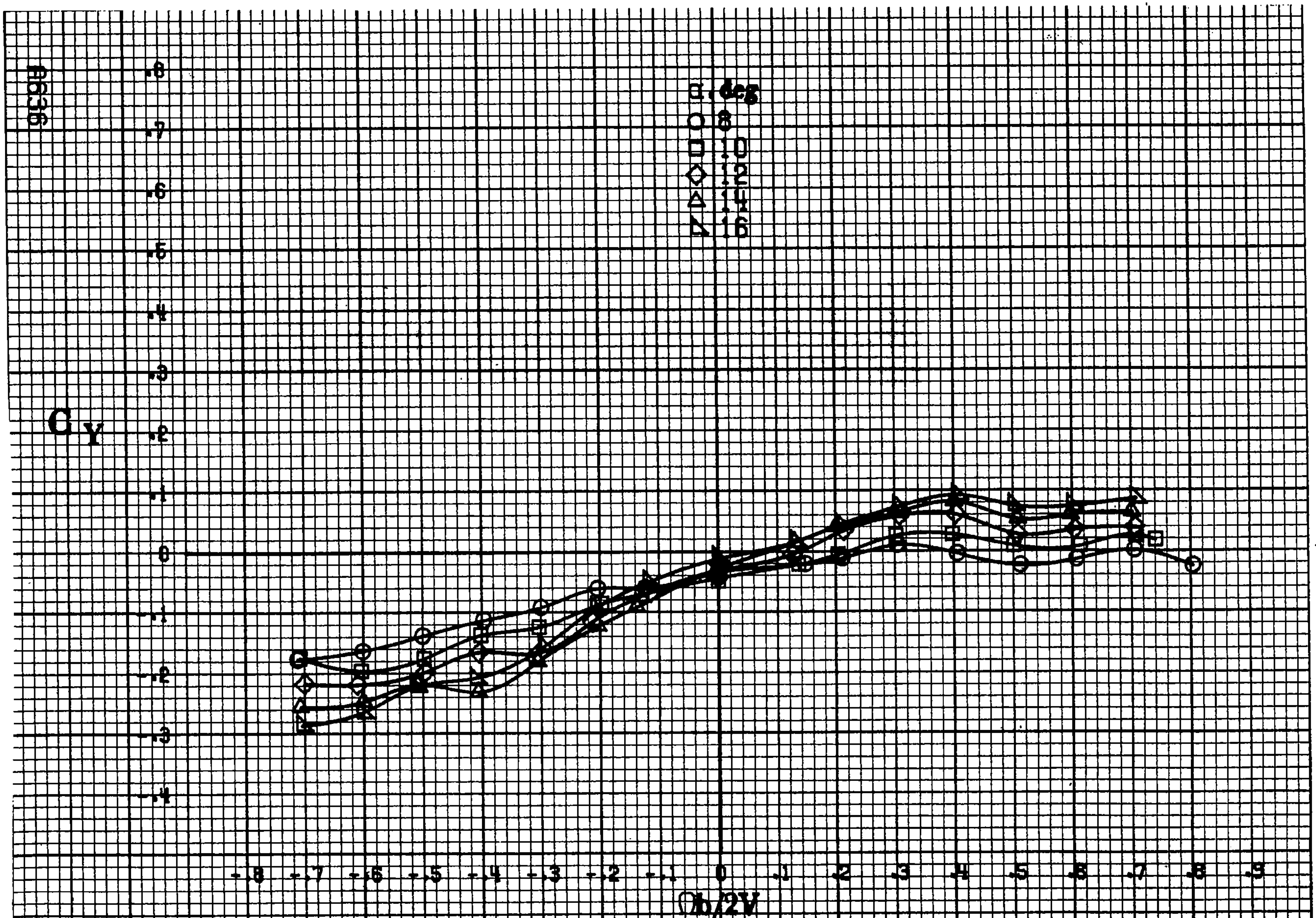

(a) $\alpha = 8$ to 16 deg, $SR = 182.9$ cm (72 in).

Figure A155.-Effect of rotation rate and angle of attack on side-force coefficient for no. 1 horizontal tail configuration. $\delta_e = -15°$, $\delta_a = 0°$, $\delta_r = -25°$, $\beta = 0°$.

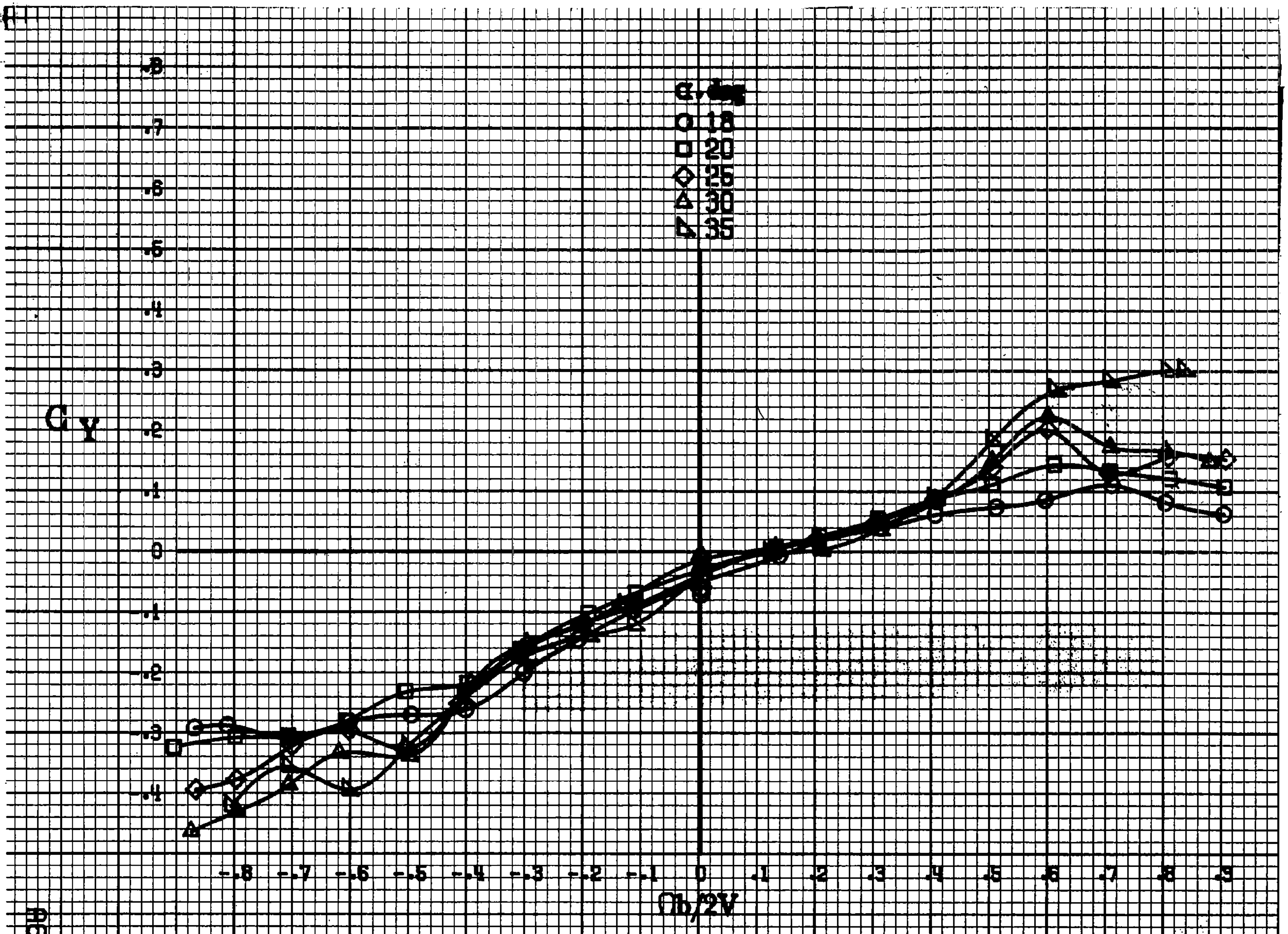

(b) α = 18 to 35 deg, SR = 182.9 cm (72 in).

Figure A155.-Continued.

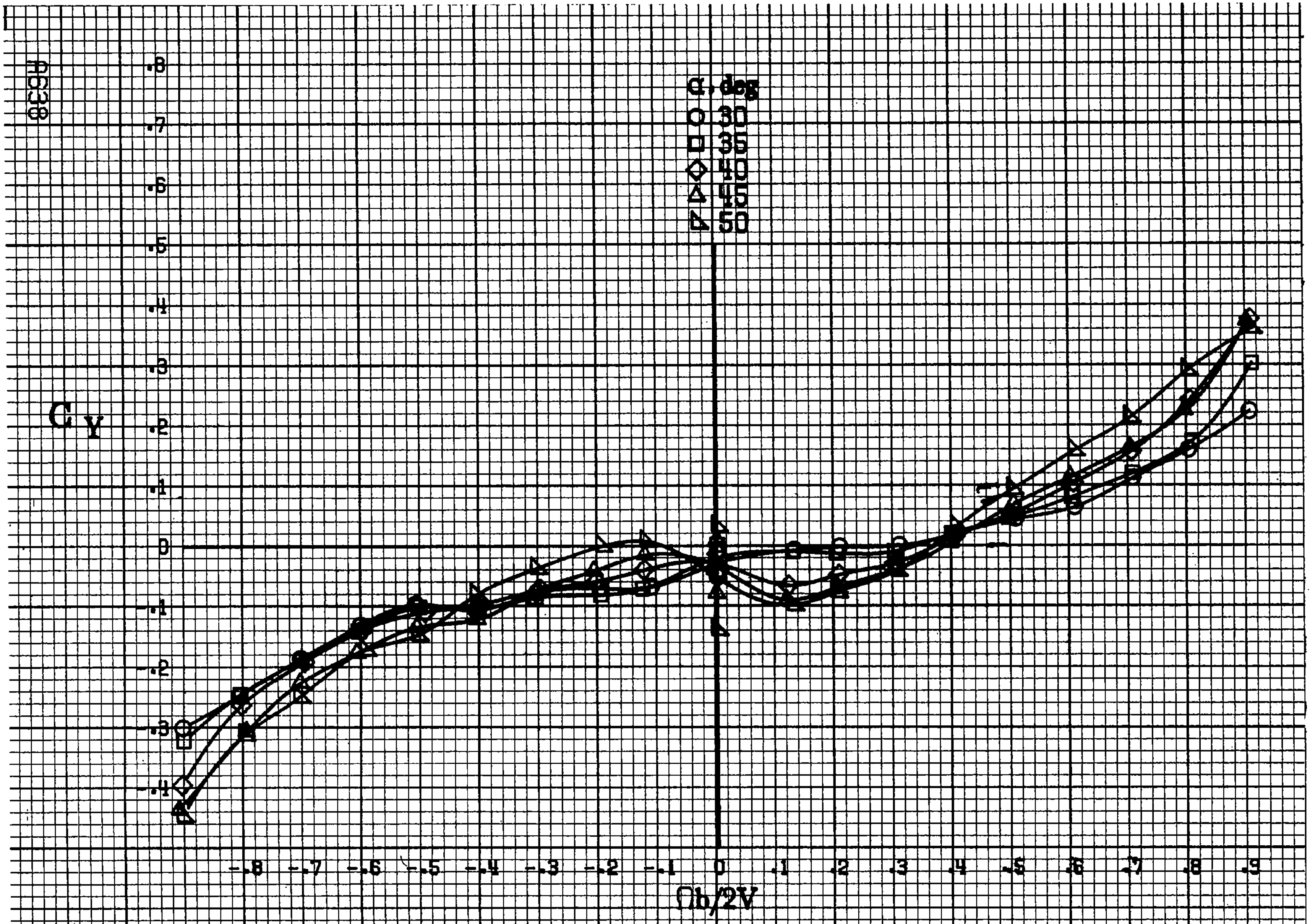

(c) α = 30 to 50 deg, SR = 0.
Figure A155.-Continued.

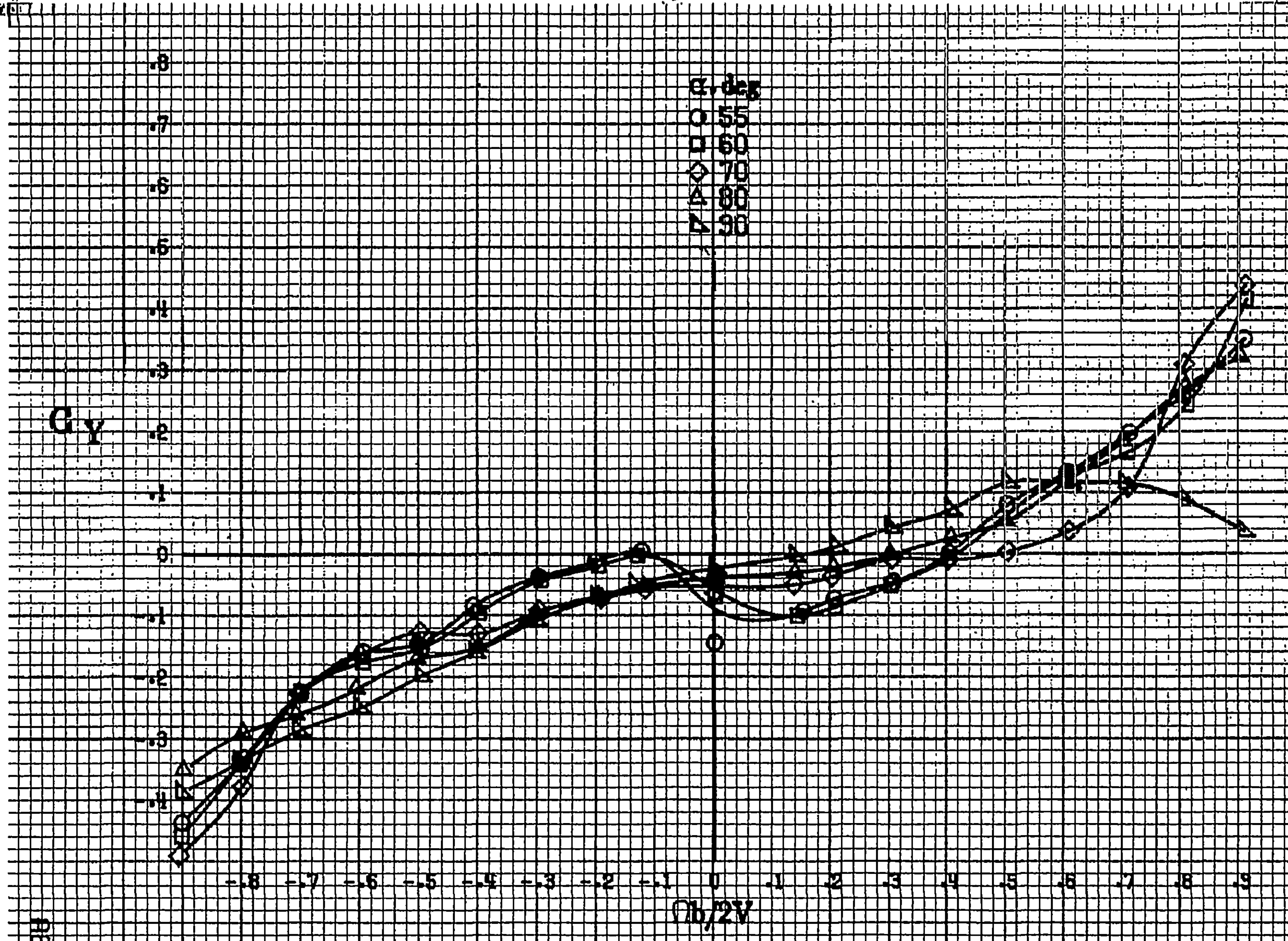

(d) α = 55 to 90 deg, SR = 0.
Figure A155. Concluded.

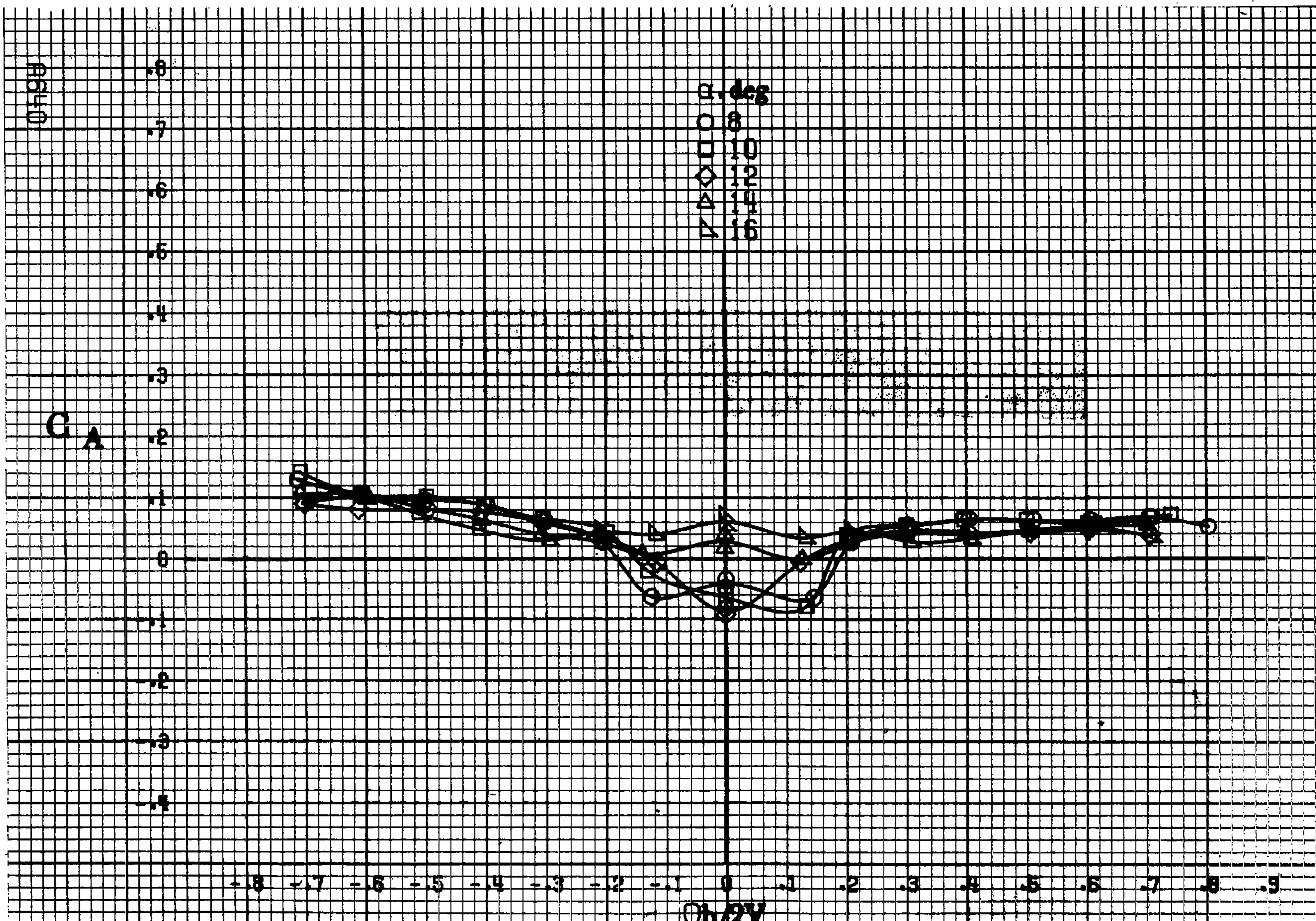

(a) α = 8 to 16 deg, SR = 182.9 cm (72 in).

Figure A156.-Effect of rotation rate and angle of attack on axial-force coefficient for no. 1 horizontal tail configuration. $\delta_e = -15°$, $\delta_a = 0°$, $\delta_r = -25°$, $\beta = 0°$.

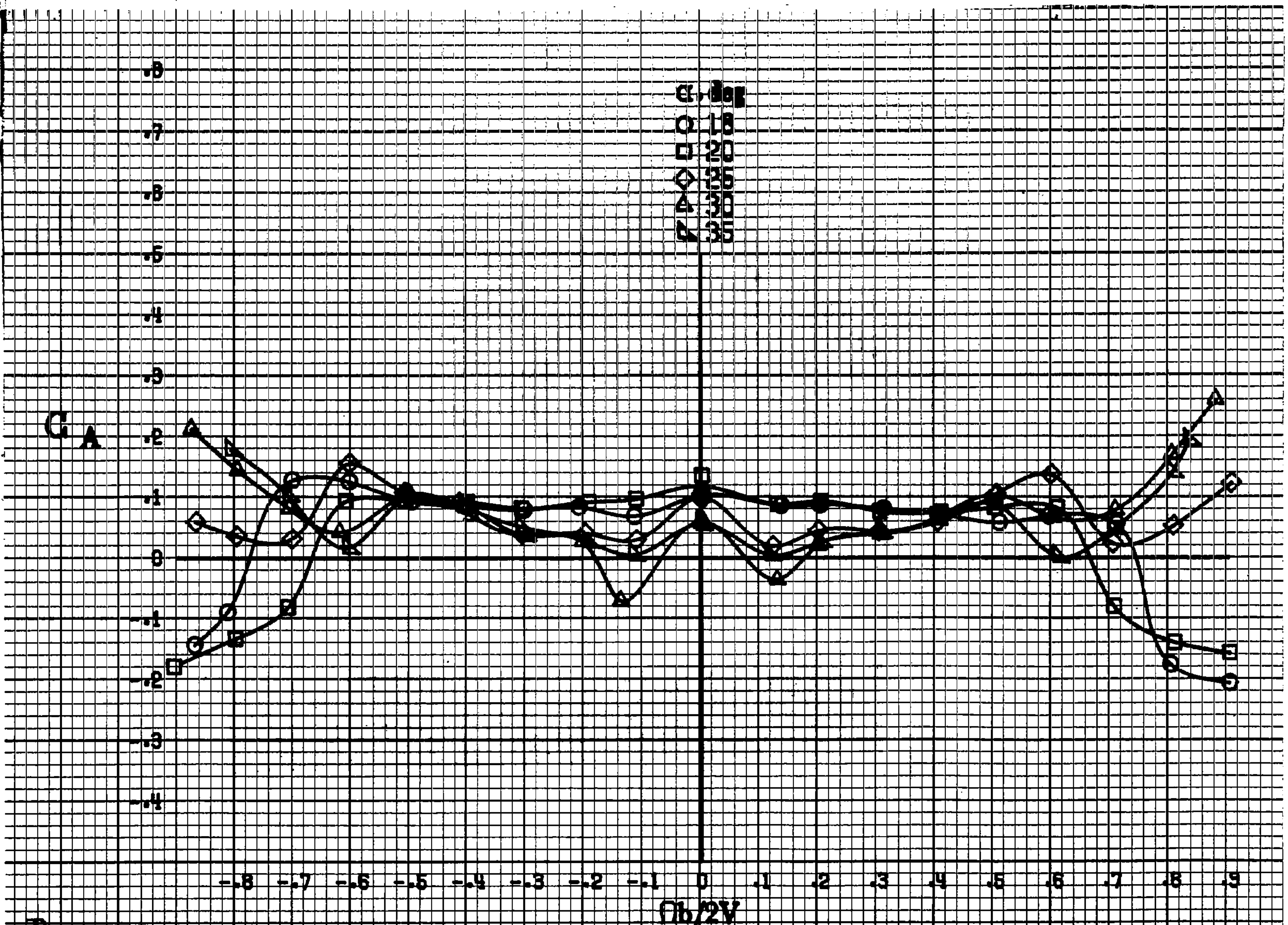

(b) α = 18 to 35 deg, SR = 182.9 cm (72 in).

Figure A156.-Continued.

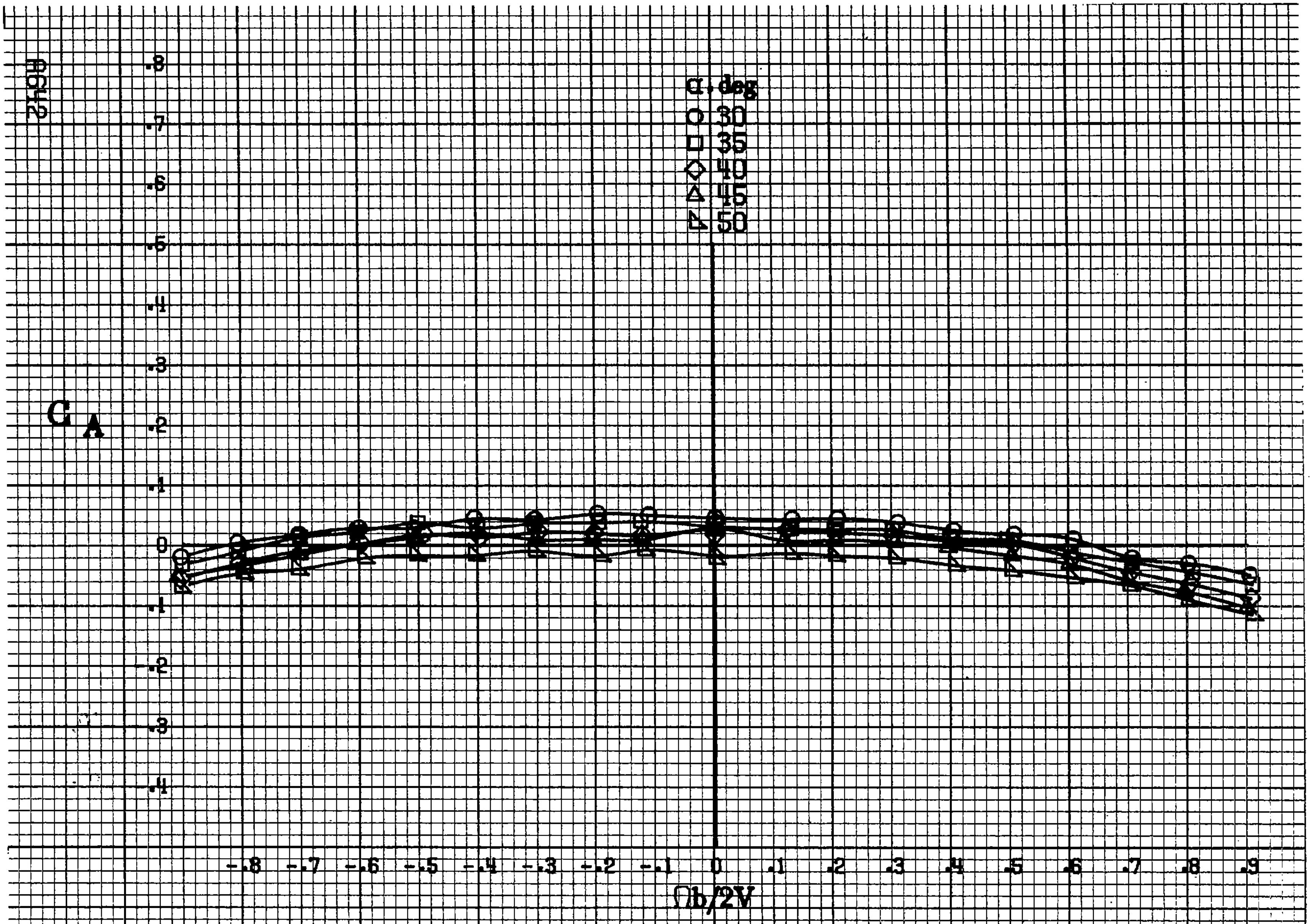

(c) α = 30 to 50 deg, SR = 0.
Figure A156.-Continued.

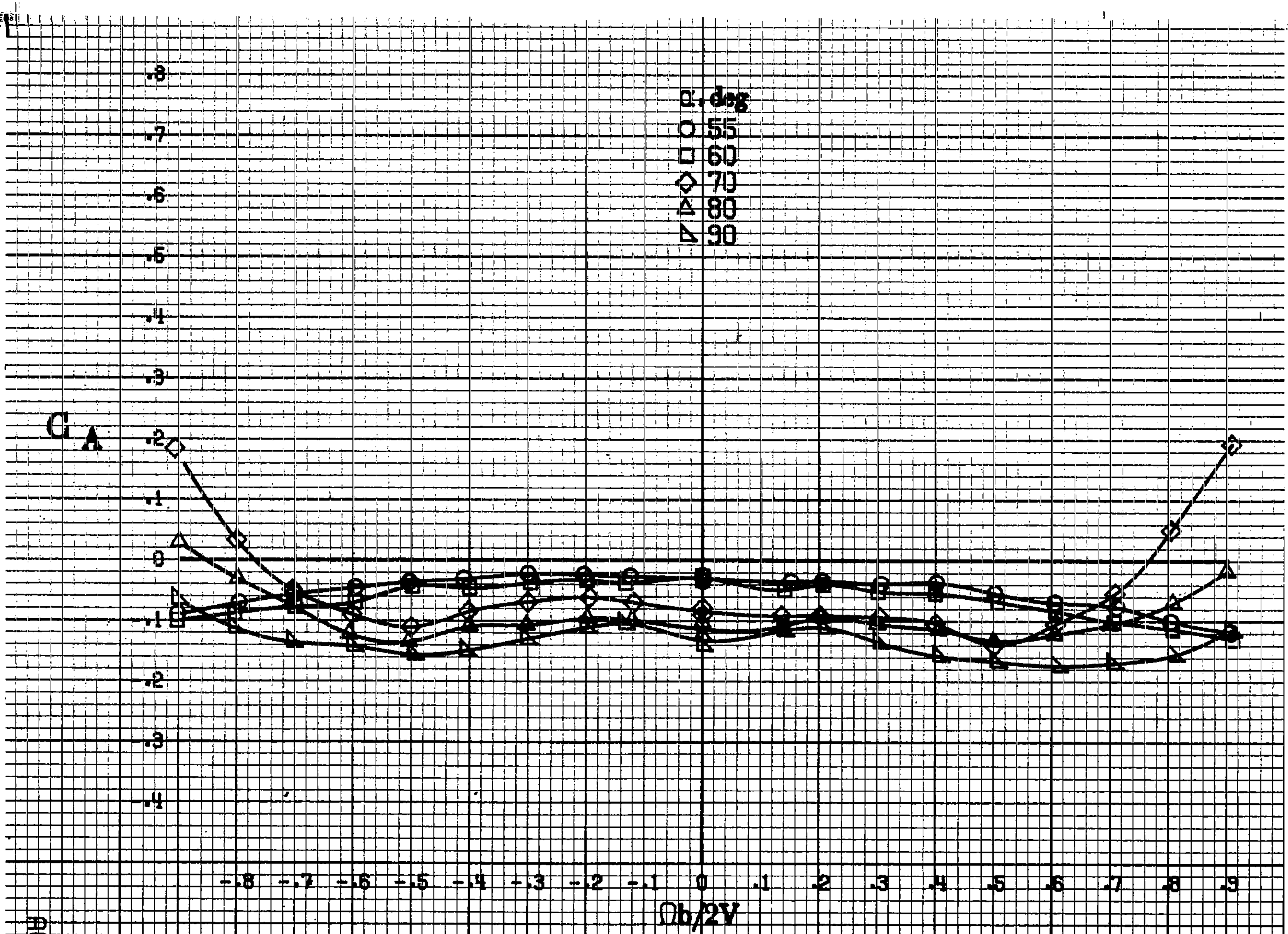

(d) α=55to90deg, SR=0.
Figure A156.-Concluded.

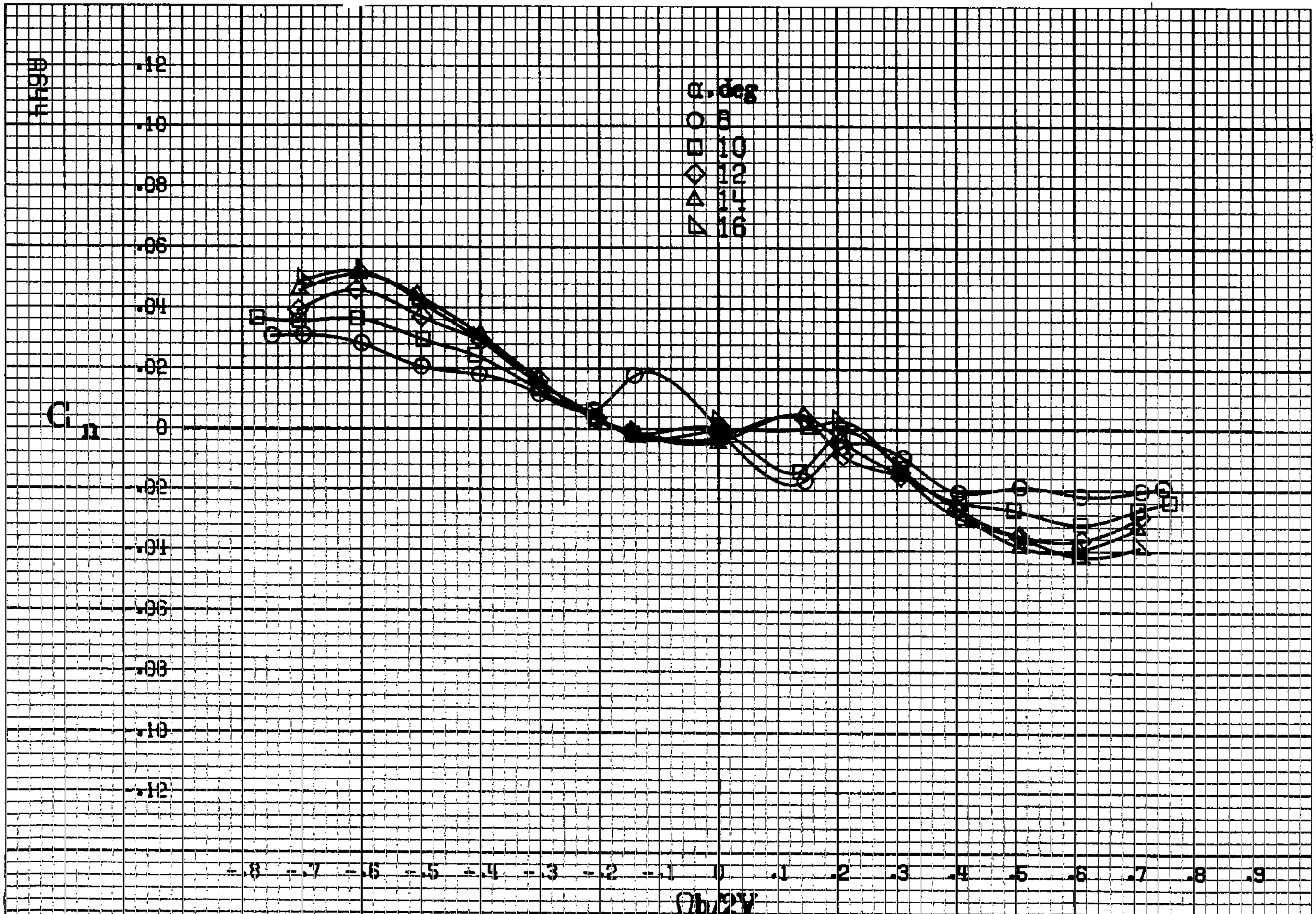

(a) α = 8 to 16 deg, SR = 182.9 cm (72 in).

Figure A157.-Effect of rotation rate and angle of attack on yawing-moment coefficient for configuration having cowl strakes, tail fillets and emergency spin chute installation. $\delta_e = 0°$, $\delta_a = 0°$, $\delta_r = 0°$, $\beta = 0°$.

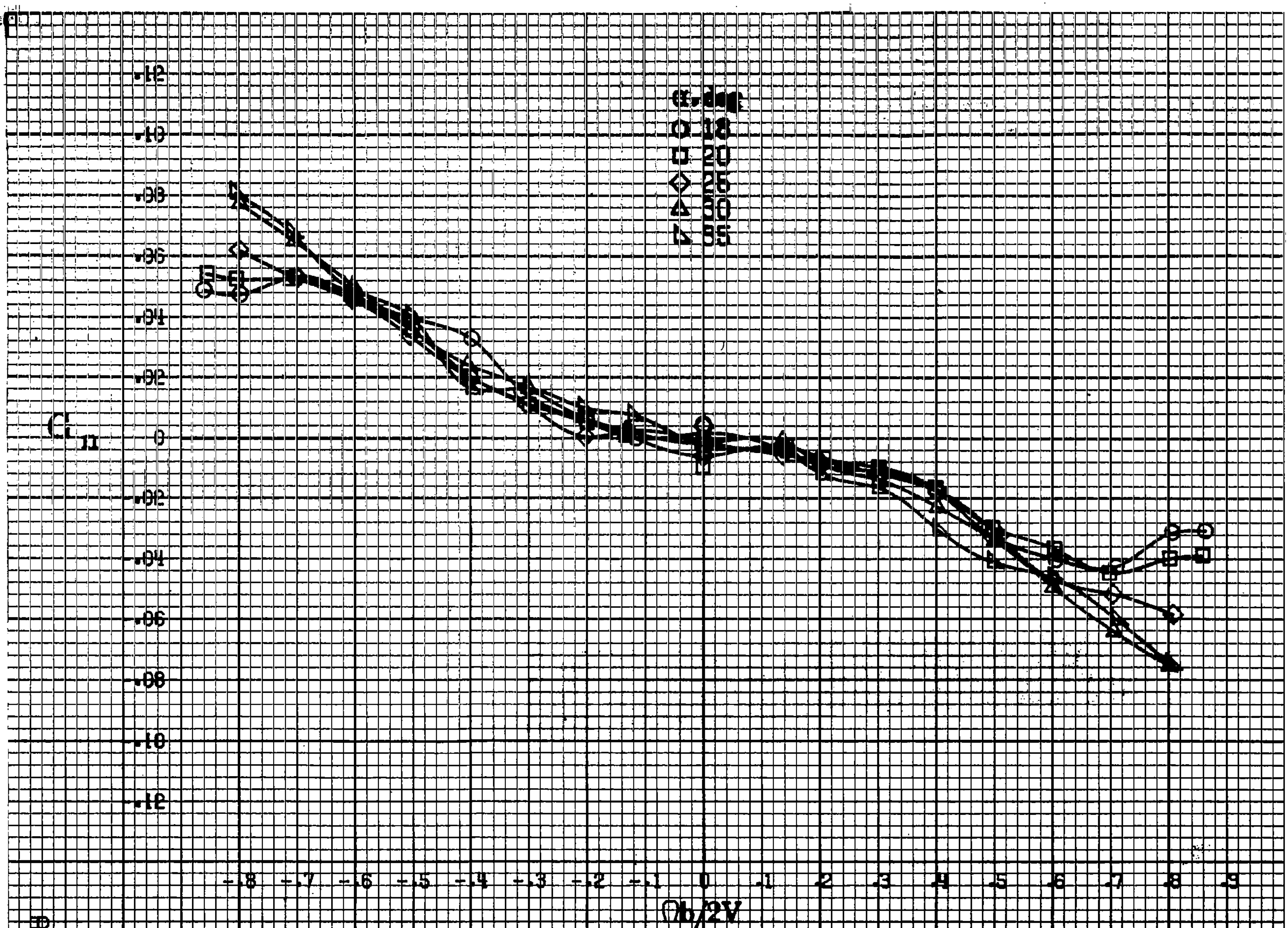

(b) α = 18 to 35 deg, SR = 182.9 cm (72 in).

Figure A157.-Continued.

A645

(c) α = 30 to 50 deg, SR = 0.

Figure A157. Continued.

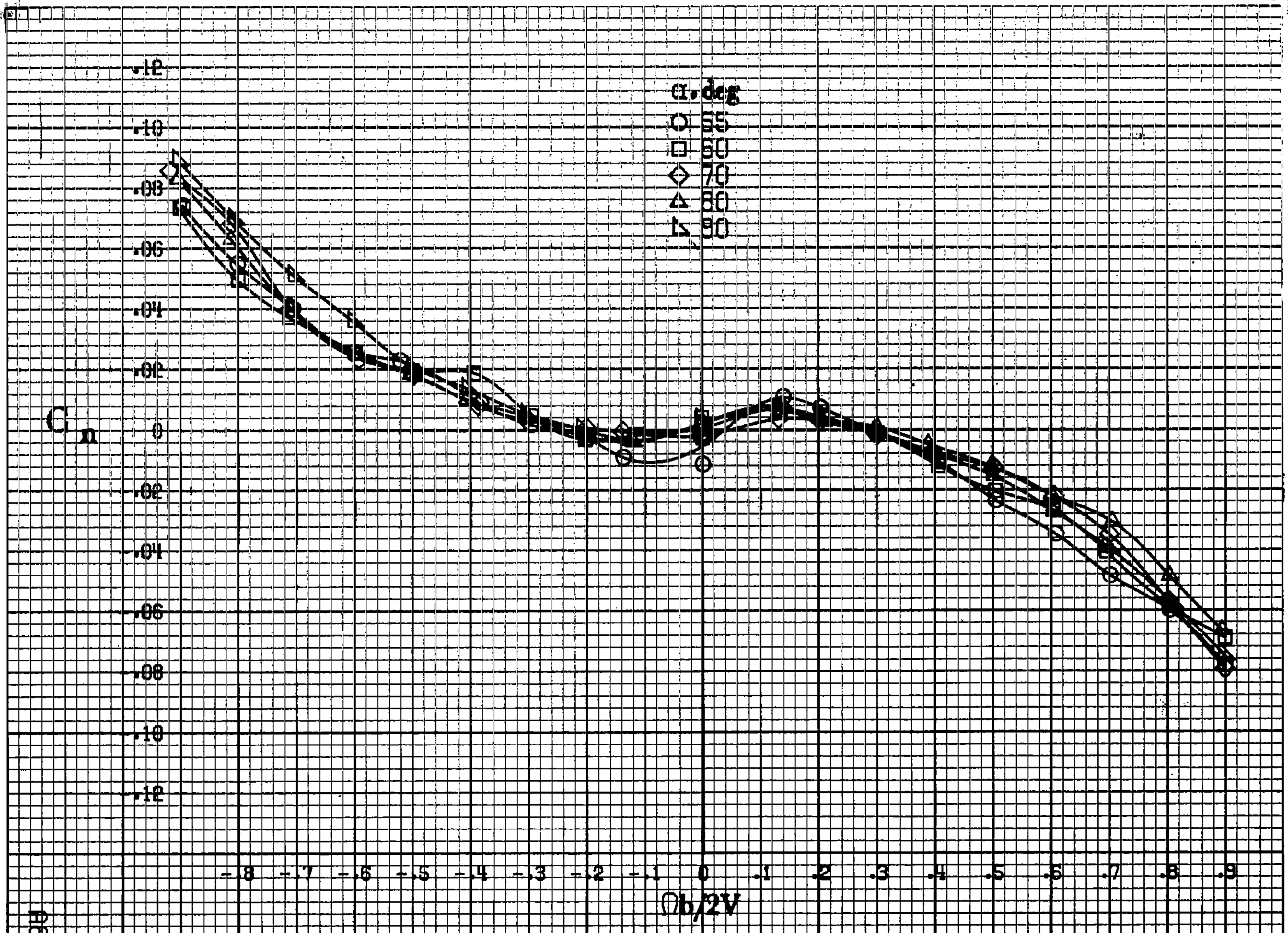

(d) α=55to90deg, SR=0.

Figure A157.-Concluded.

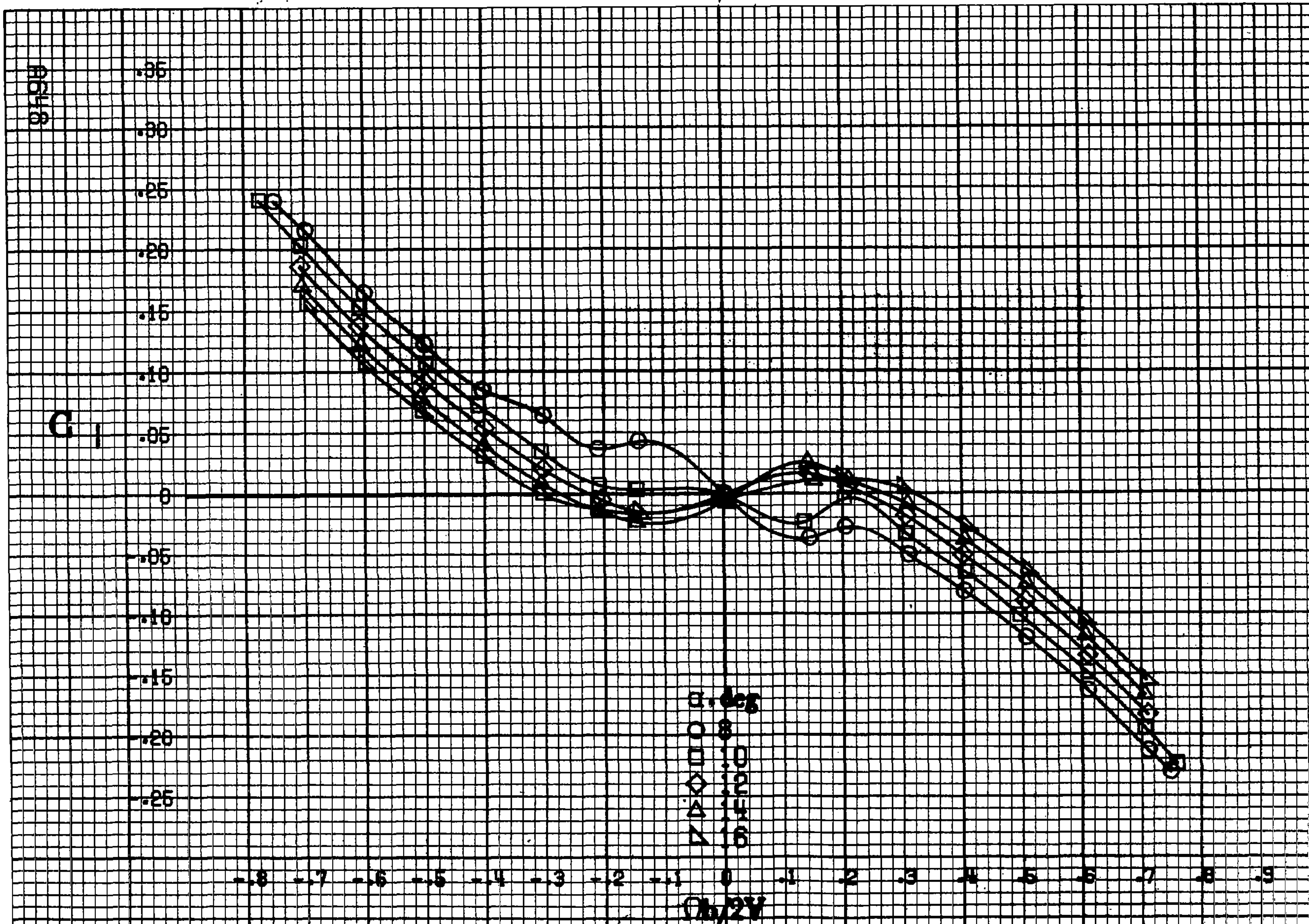

(e) $\alpha = 8$ to 16 deg, SR = 182.9 cm (72 in).

Figure A158.-Effect of rotation rate and angle of attack on rolling-moment coefficient for configuration having cowl strakes, tail fillets and emergency spin chute installation. $\delta_e = 0°$, $\delta_a = 0°$, $\delta_r = 0°$, $\beta = 0°$.

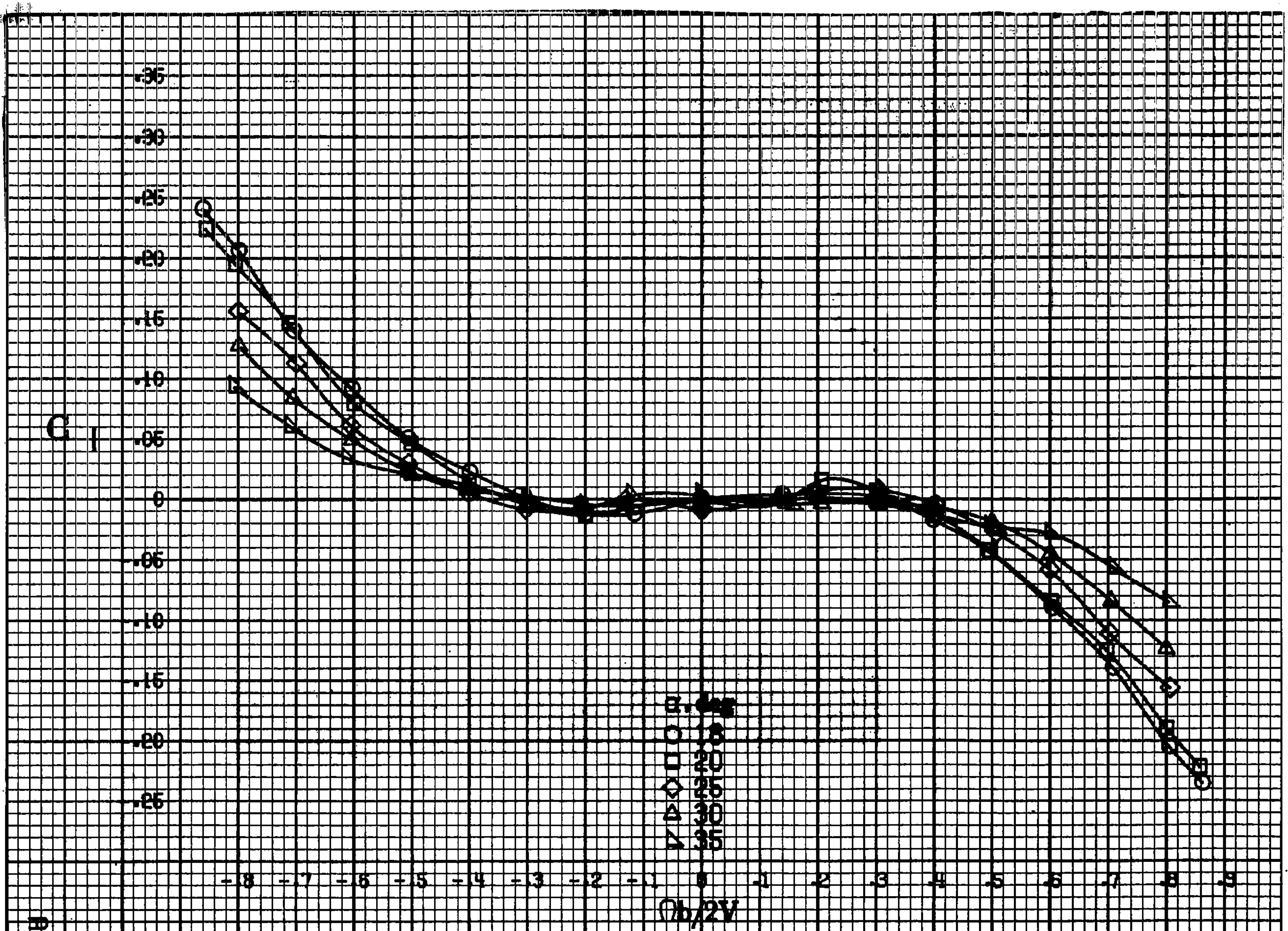

(b) α = 15 to 35 deg, SR = 182.9 cm (72 in).

Figure A158.-Continued.

A649

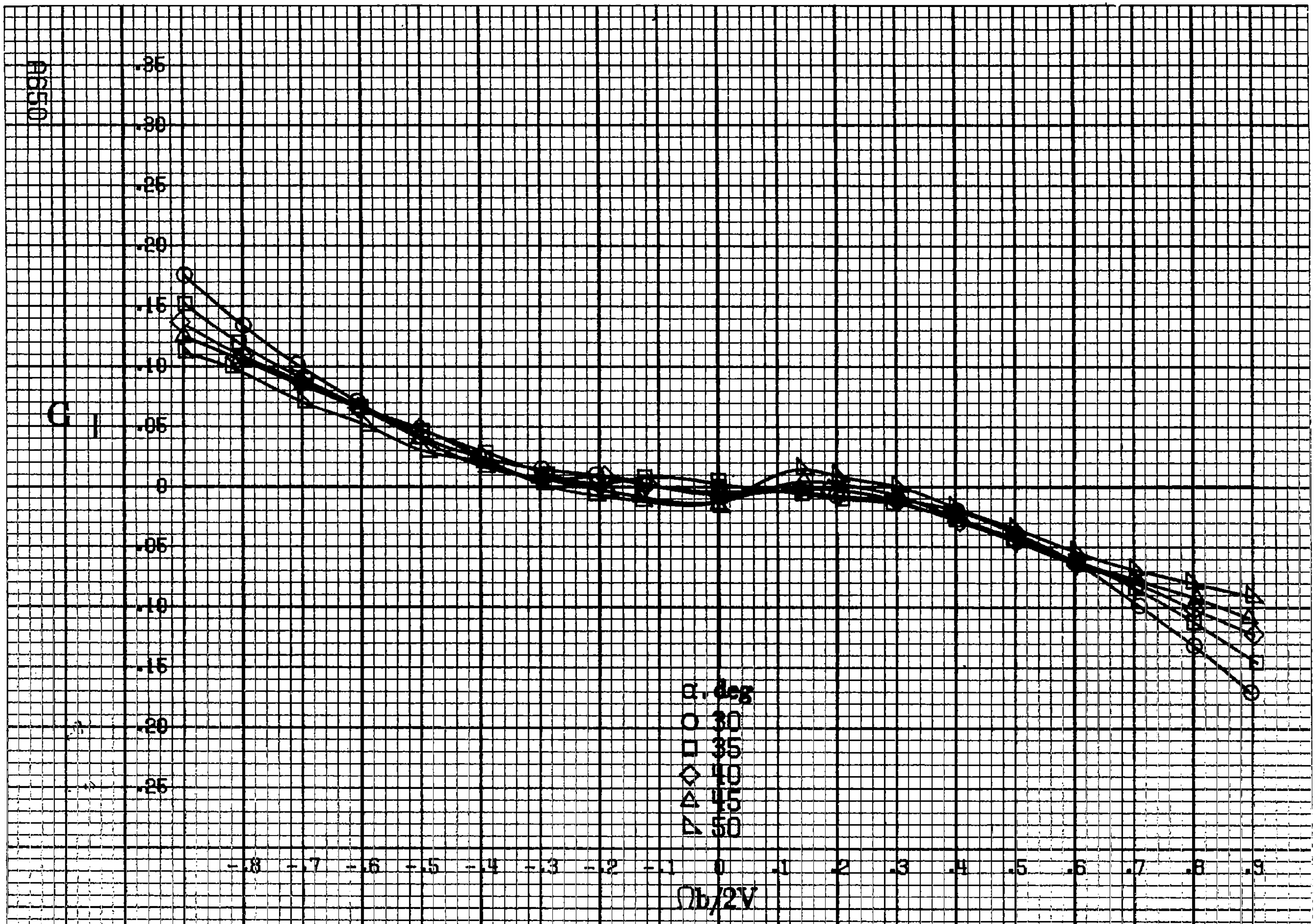

(c) α = 30 to 50 deg, SR = 0.

Figure A158. Continued.

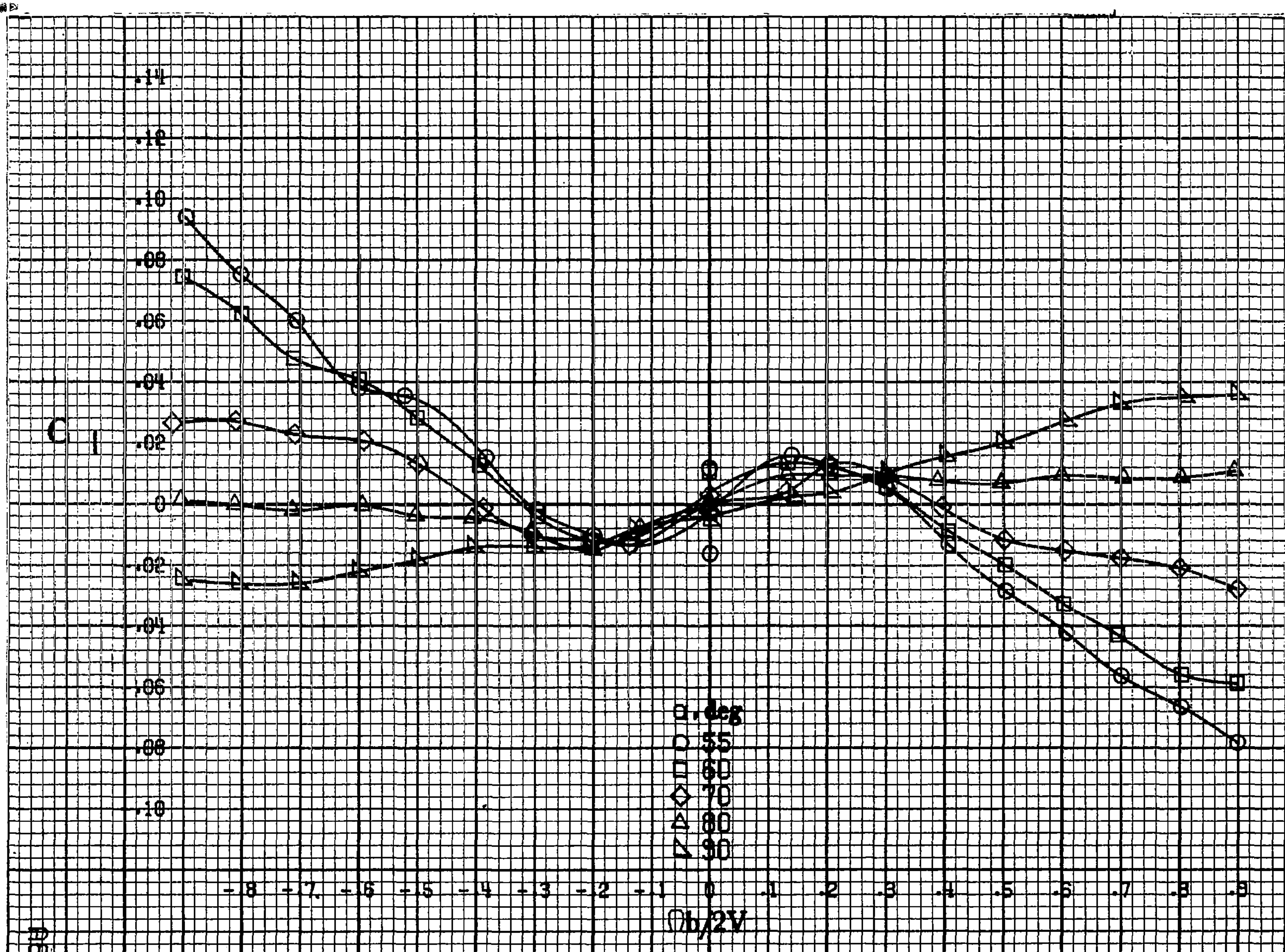

(d) α = 55 to 90 deg, SR = 0.

Figure A158.-Concluded.

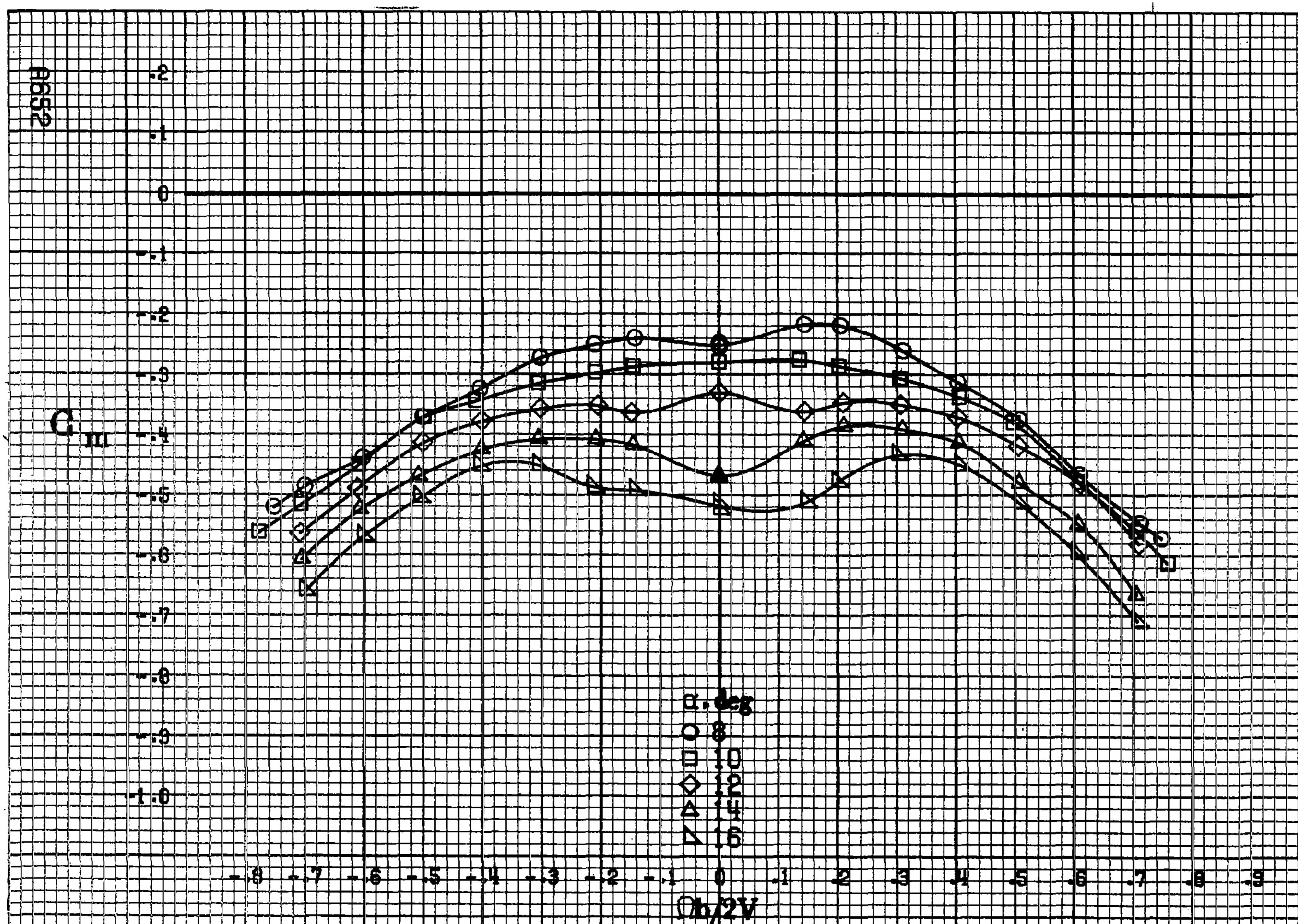

(a) α = 8 to 16 deg, SR = 182.9 cm (72 in).

Figure A159.-Effect of rotation rate and angle of attack on pitching-moment coefficient for configuration having cowl strakes, tail fillets and emergency spin chute installation. $\delta_e = 0°$, $\delta_a = 0°$, $\delta_r = 0°$, $\beta = 0°$.

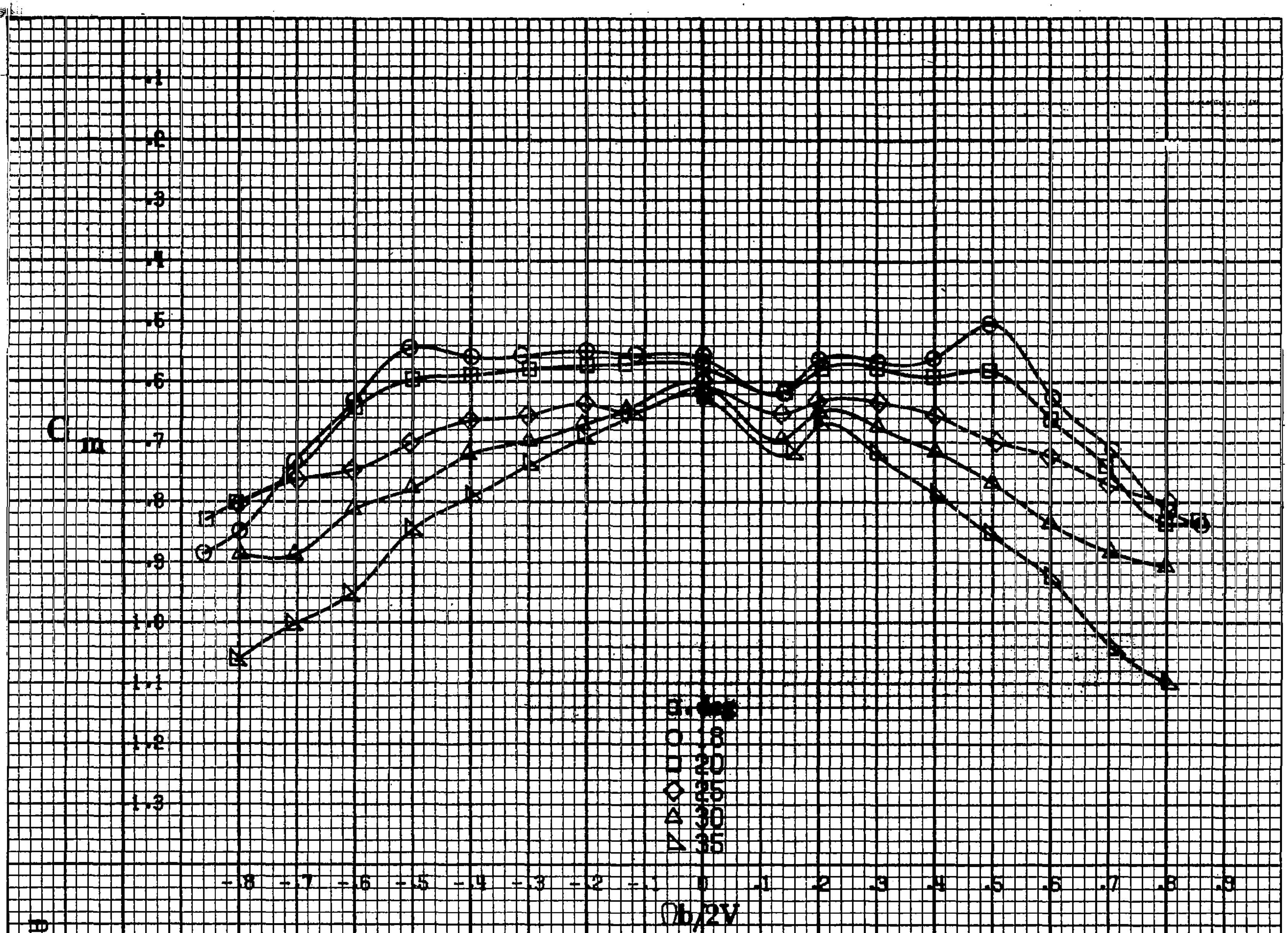

(b) α = 18 to 35 deg, SR = 182.9 cm (72 in).
Figure A159. Continued.

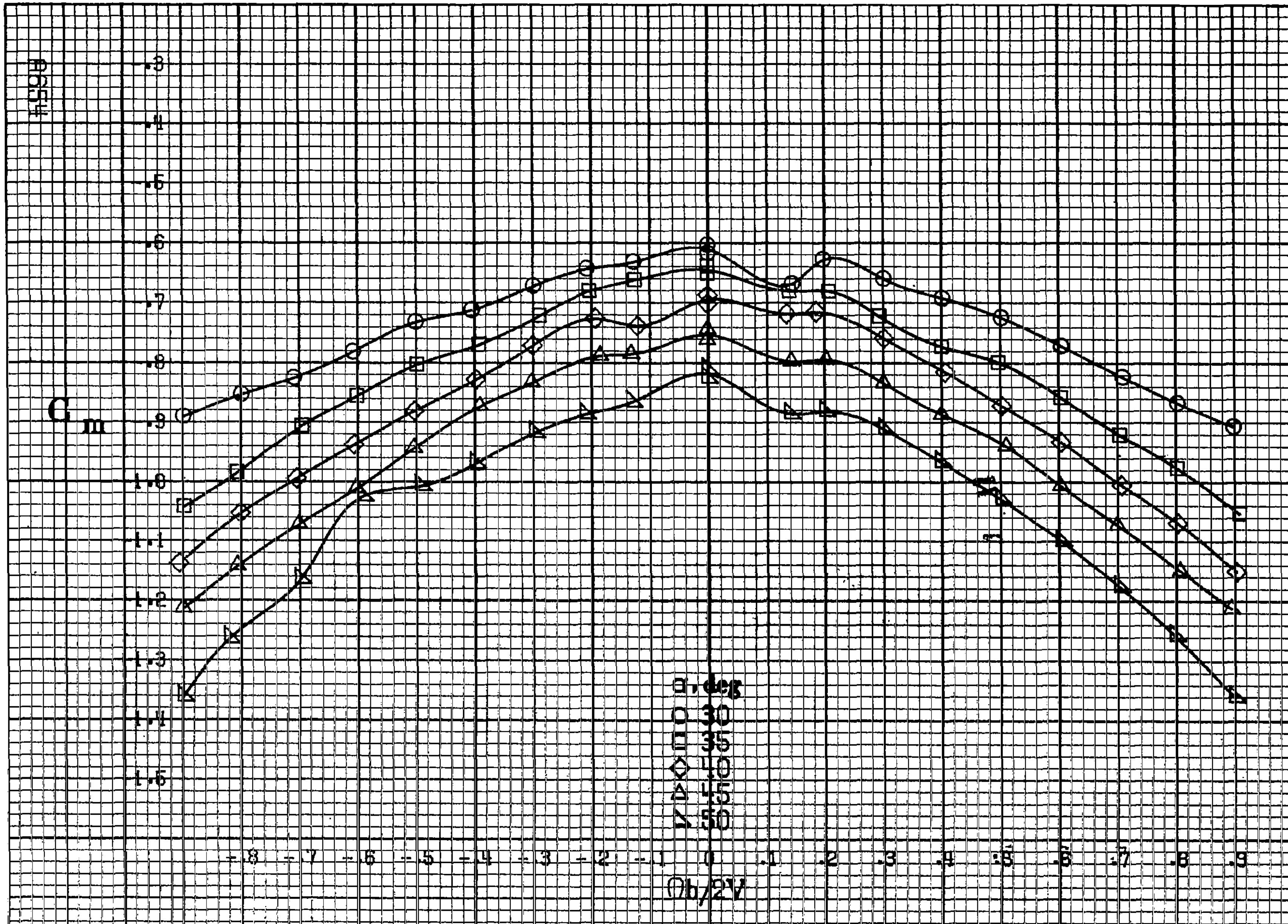

(c) α = 30 to 50 deg, SR = 0.

Figure A159.-Continued.

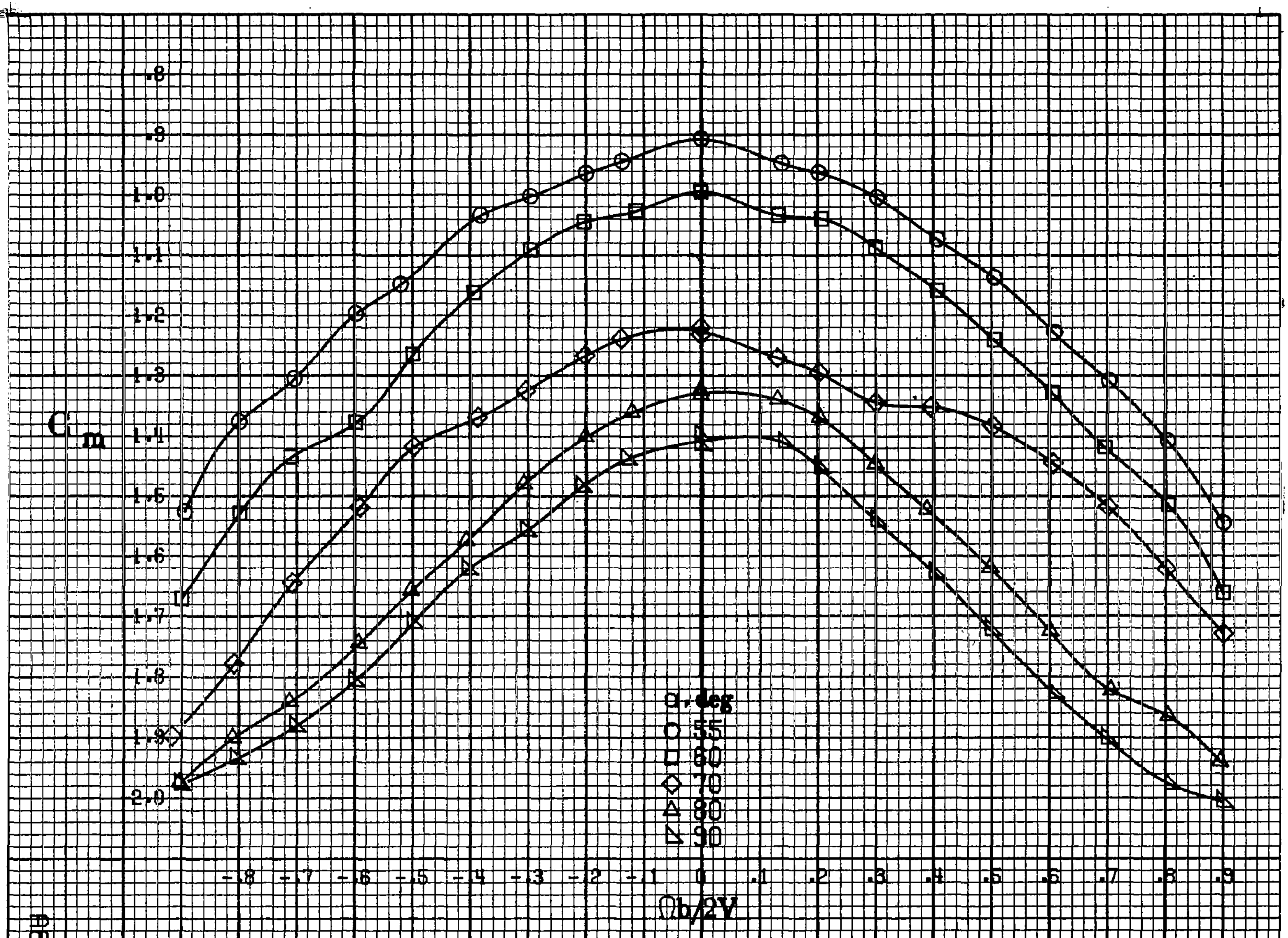

(d) α = 55 to 90 deg, SR = 0.

Figure A159.-Concluded.

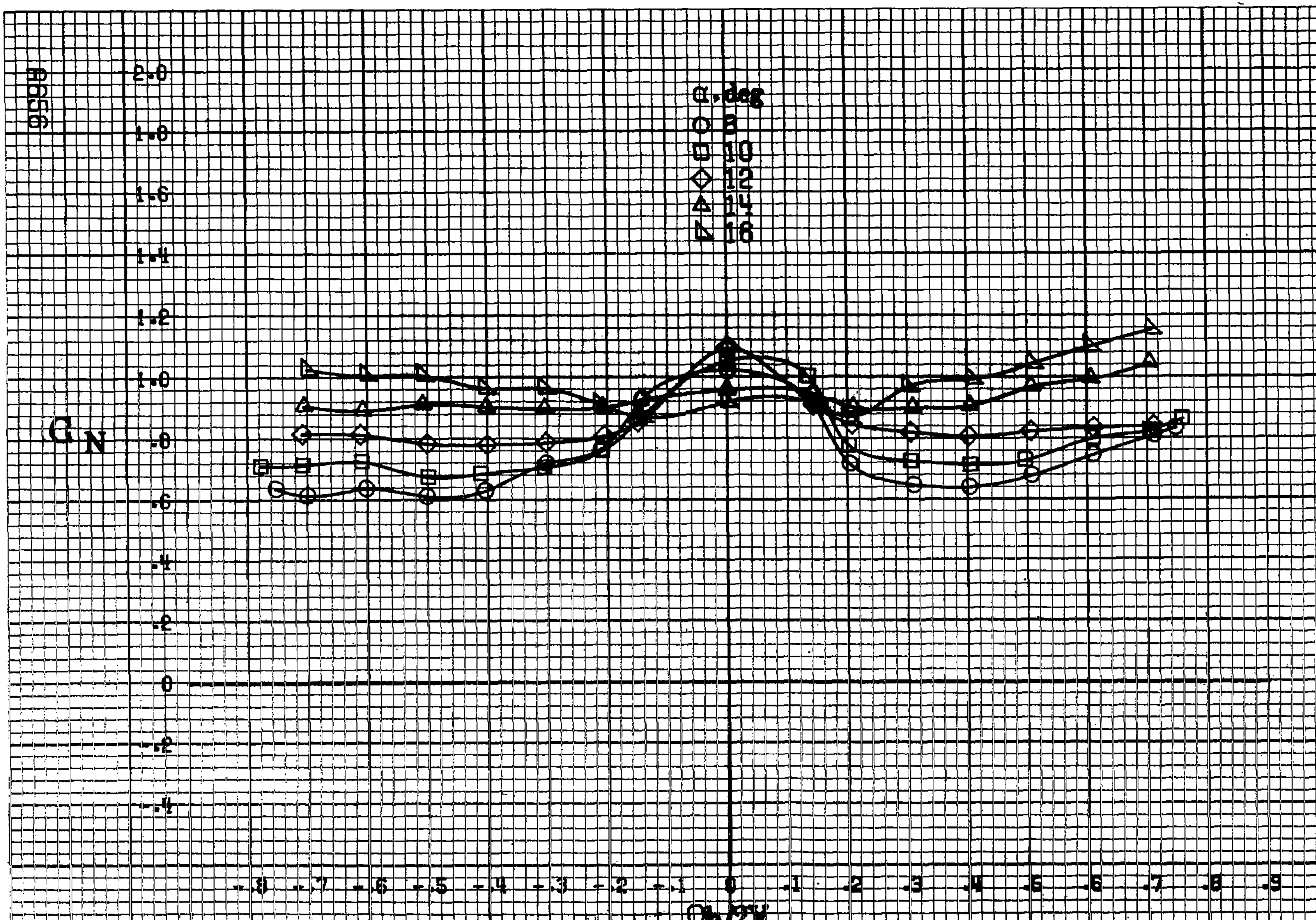

(a) $\alpha = 8$ to 16 deg, $SR = 182.9$ cm (72 in).

Figure A160.-Effect of rotation rate and angle of attack on normal-force coefficient for configuration having cowl strakes, tail fillets and emergency spin chute installation. $\delta_e = 0°$, $\delta_a = 0°$, $\delta_r = 0°$, $\beta = 0°$.

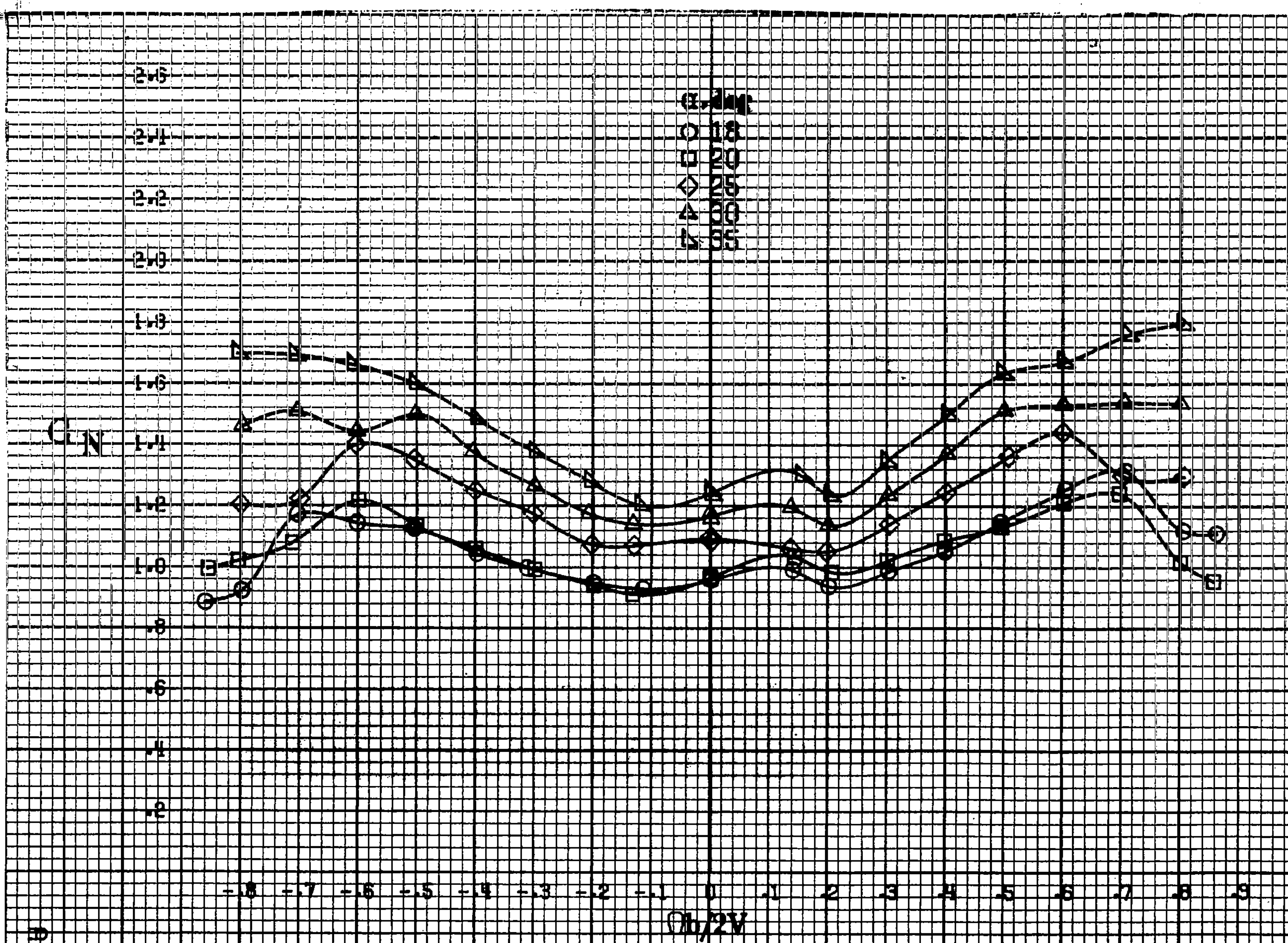

(b) α = 18 to 35 deg, SR = 182.9 cm (72 in).

Figure A160. Continued.

A657

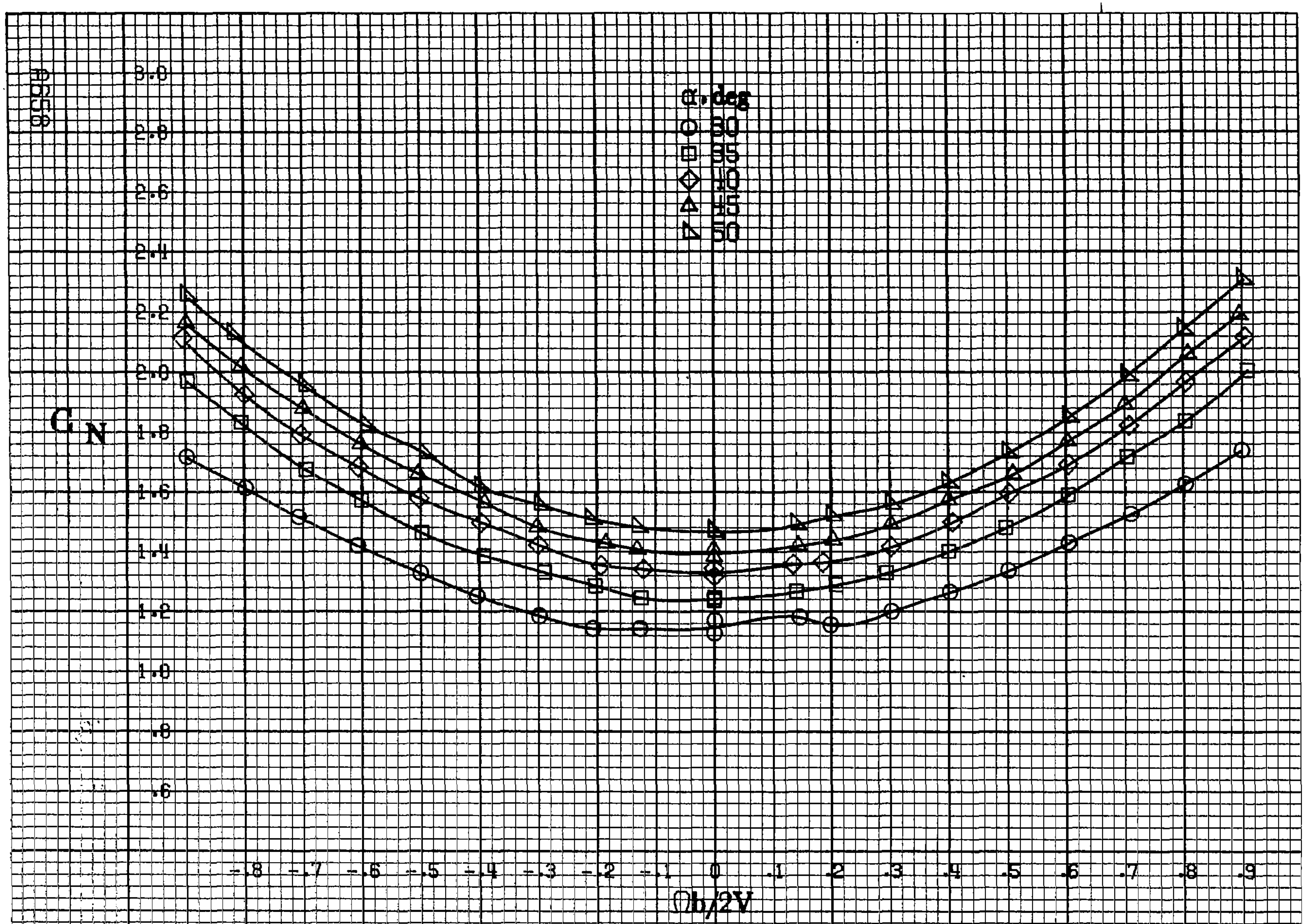

(c) α = 30 to 50 deg, δR = 0.
Figure A160.-Continued.

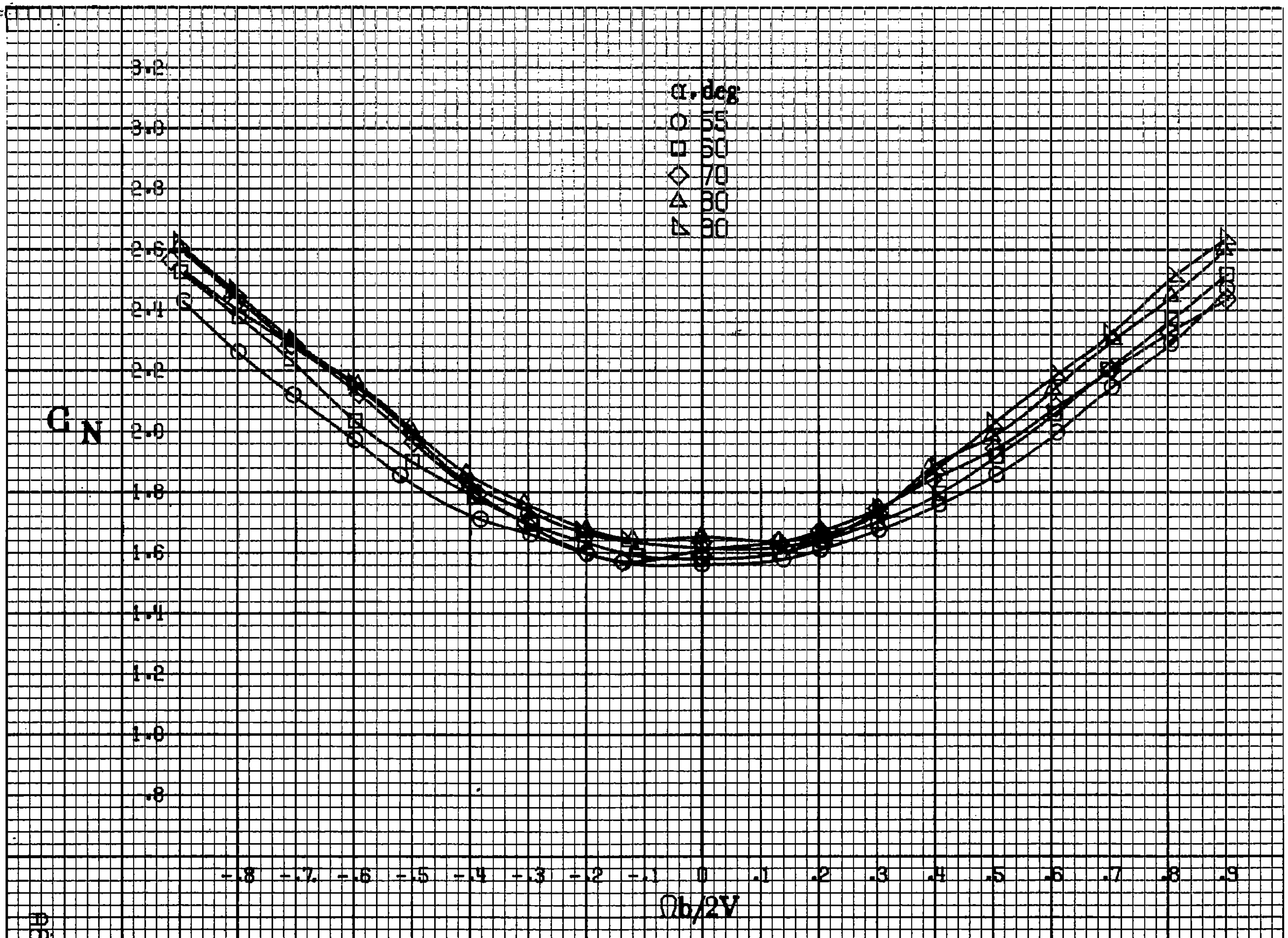

(d) α = 55 to 90 deg, SR = 0.
Figure A160.-Concluded.

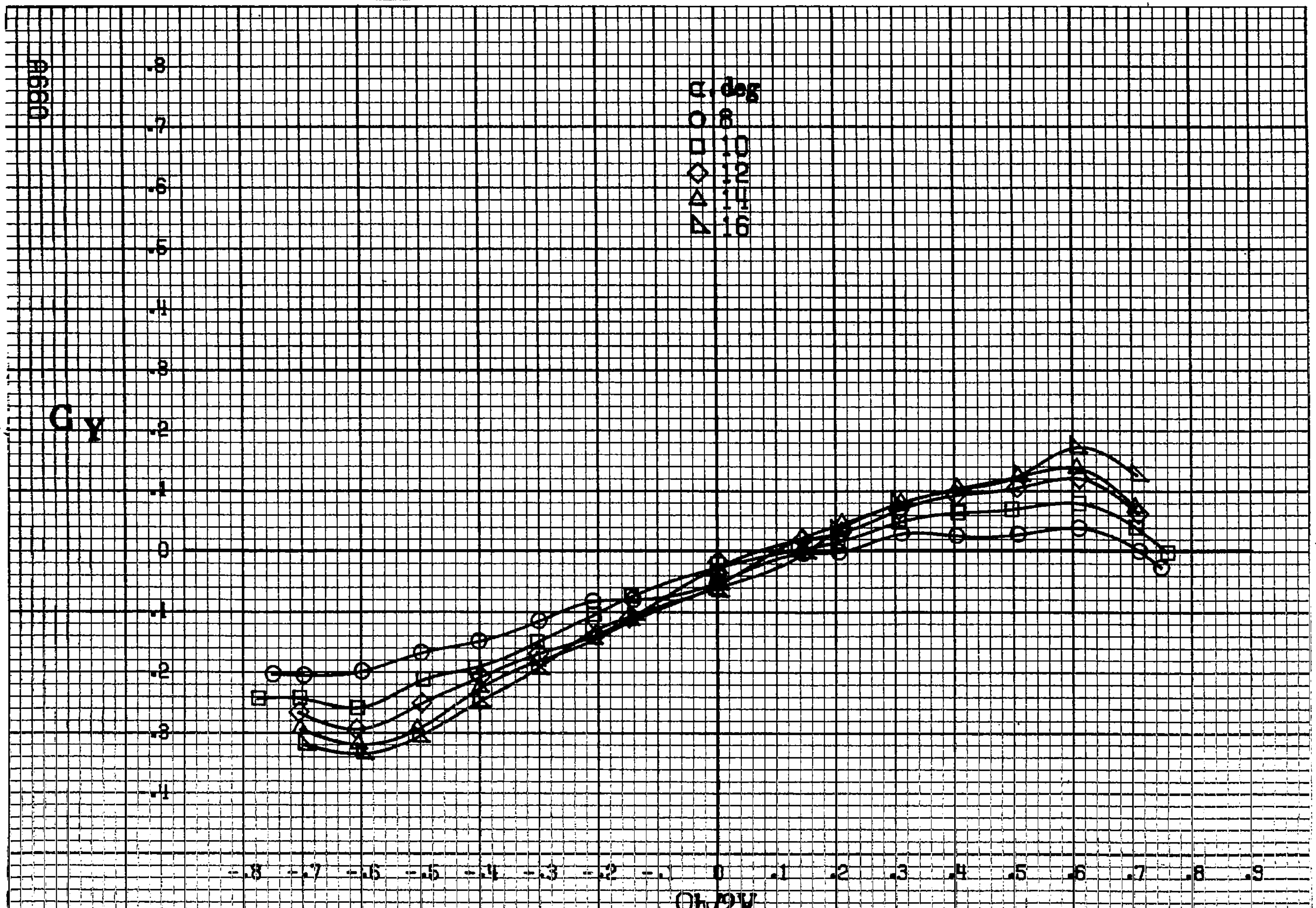

(a) α = 8 to 16 deg, SR = 182.9 cm (72 in).

Figure A161.-Effect of rotation rate and angle of attack on side-force coefficient for configuration having cowl strakes, tail fillets and emergency spin chute installation. $\delta_e = 0°$, $\delta_a = 0°$, $\delta_r = 0°$. $\beta = 0°$.

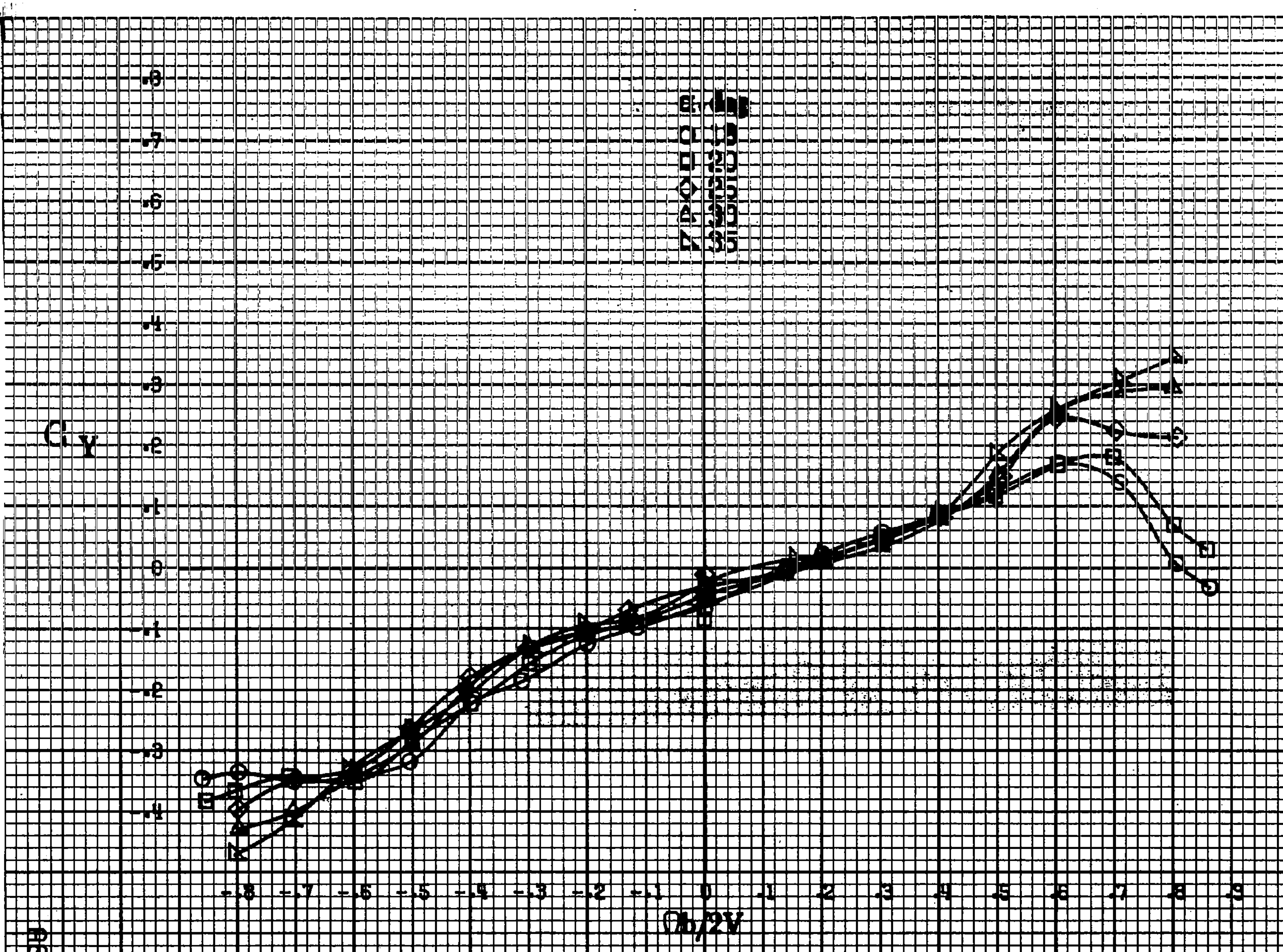

(b) Ω = 18 to 36 deg, SR = 182.9 cm (72 in).

Figure A161.-Continued.

A661

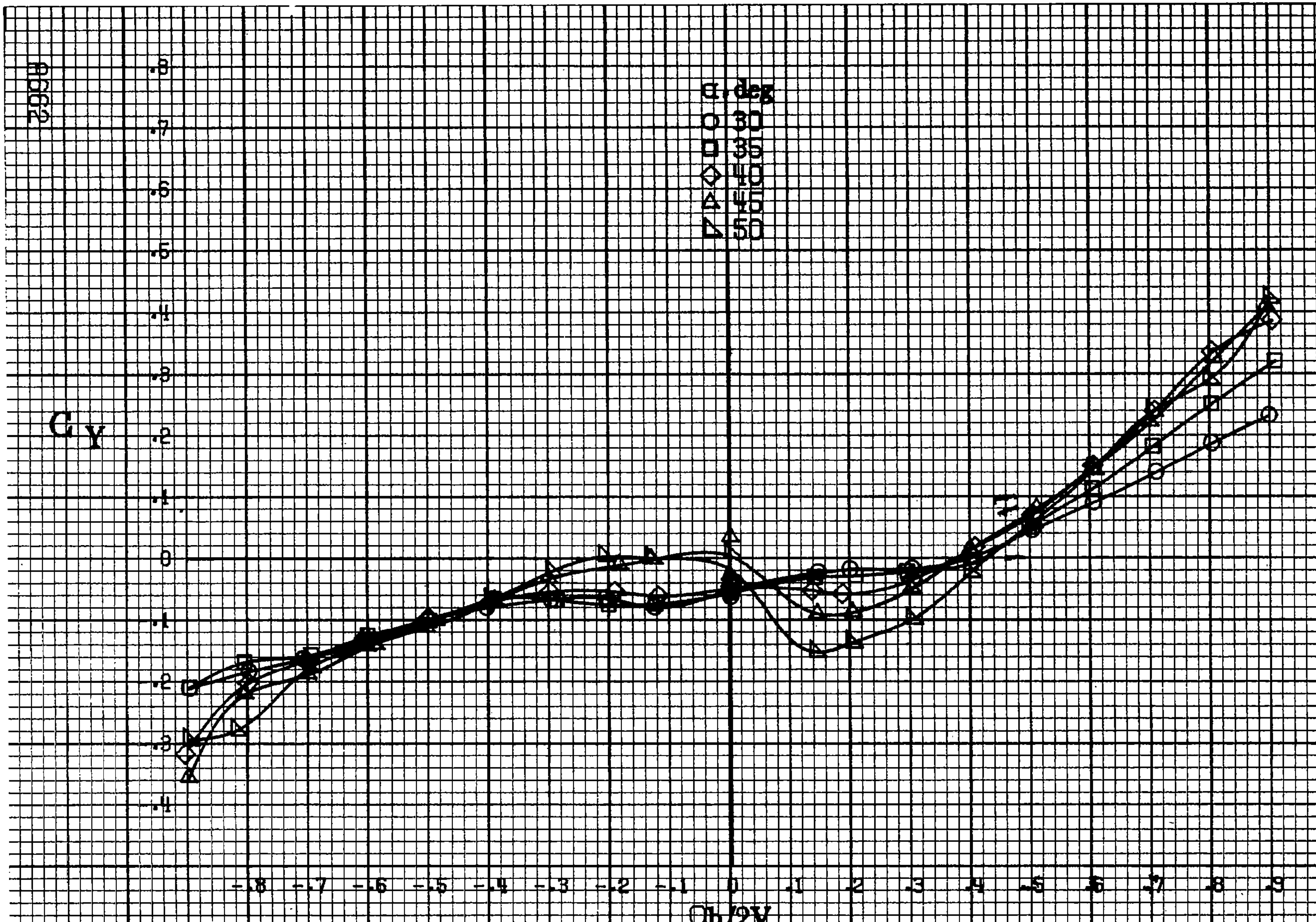

(c) α = 30 to 50 deg, SR = 0.

Figure A161.-Continued.

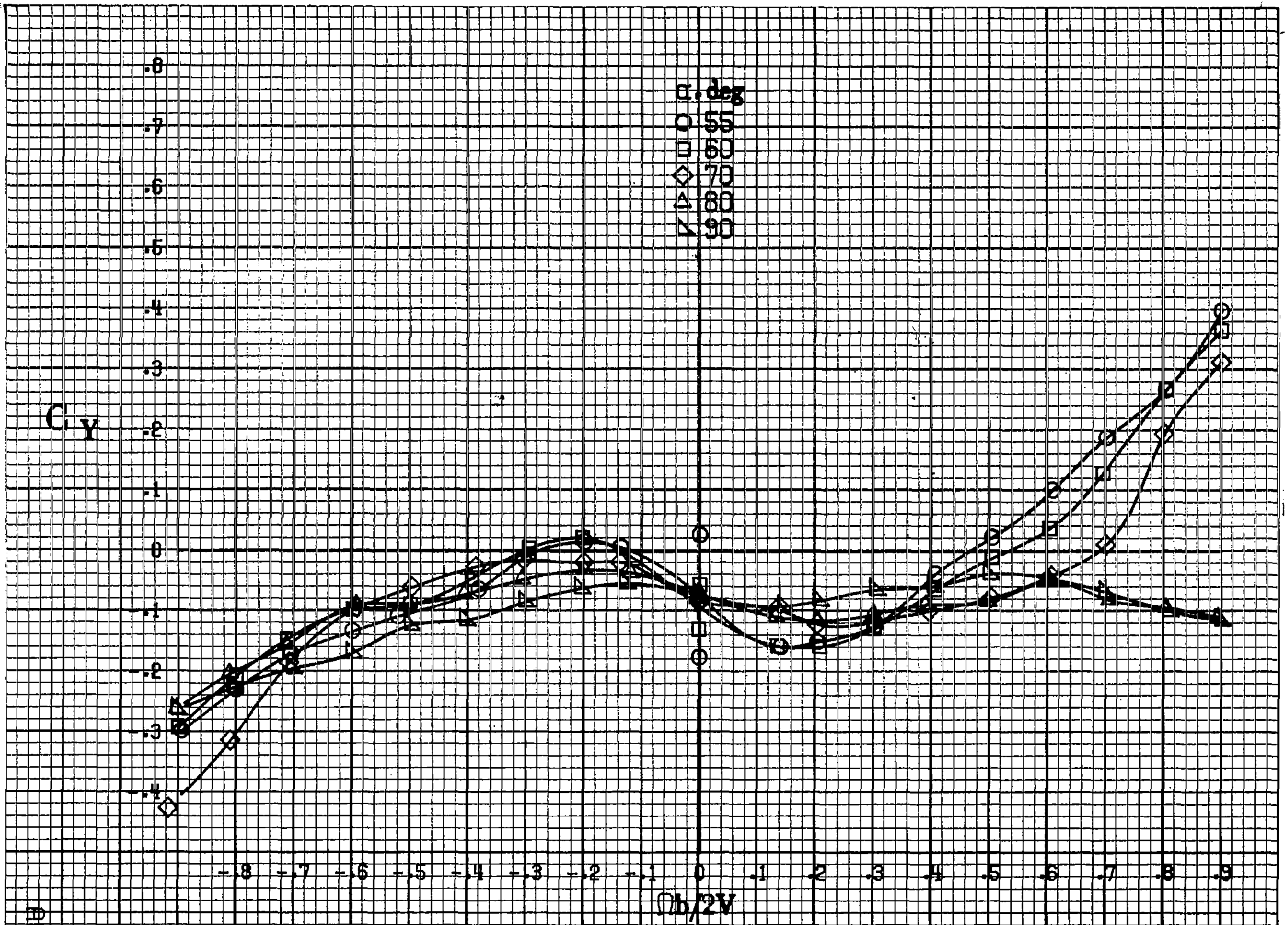

(d) α = 55 to 90 deg, SR = 0.

Figure A161. Concluded.

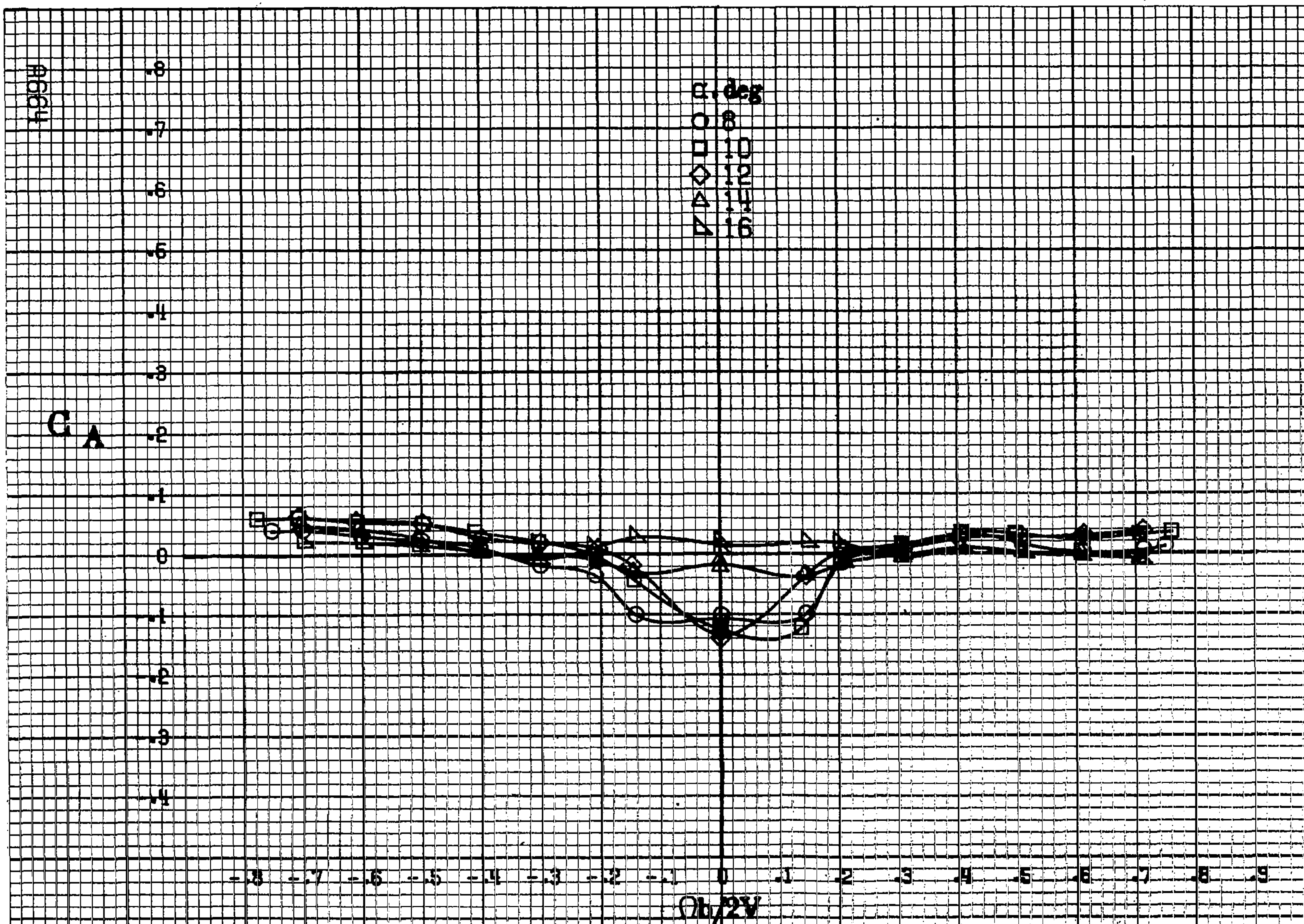

(a) $\alpha = 8$ to 16 deg, SR = 182.9 cm (72 in).

Figure A182.- Effect of rotation rate and angle of attack on axial-force coefficient for configuration having cowl strakes, tail fillets and emergency spin chute installation. $\delta_e = 0°$, $\delta_a = 0°$, $\delta_r = 0°$, $\beta = 0°$.

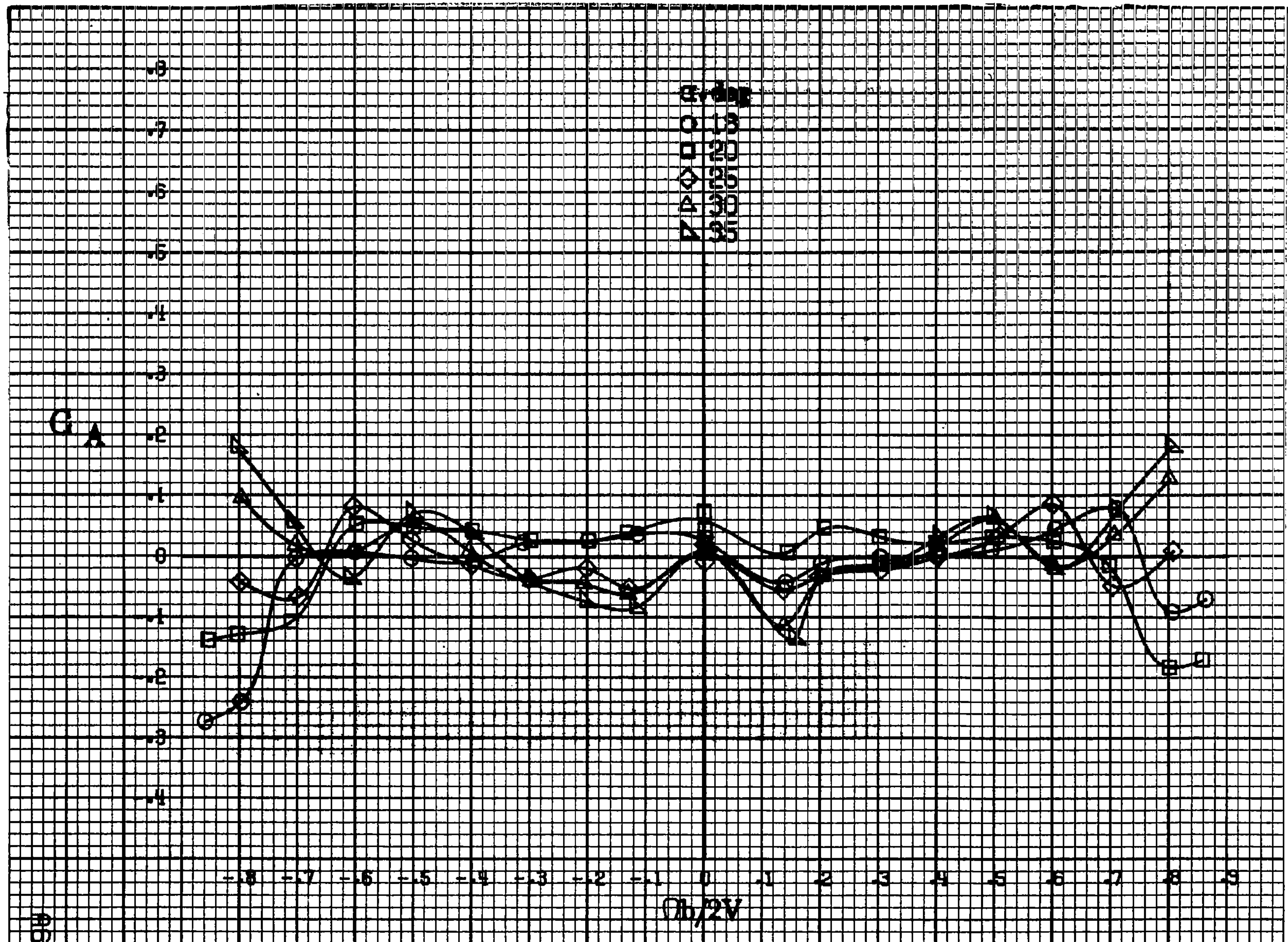

(b) α = 18 to 35 deg, SR = 182.9 cm (72 in).

Figure A162.-Continued.

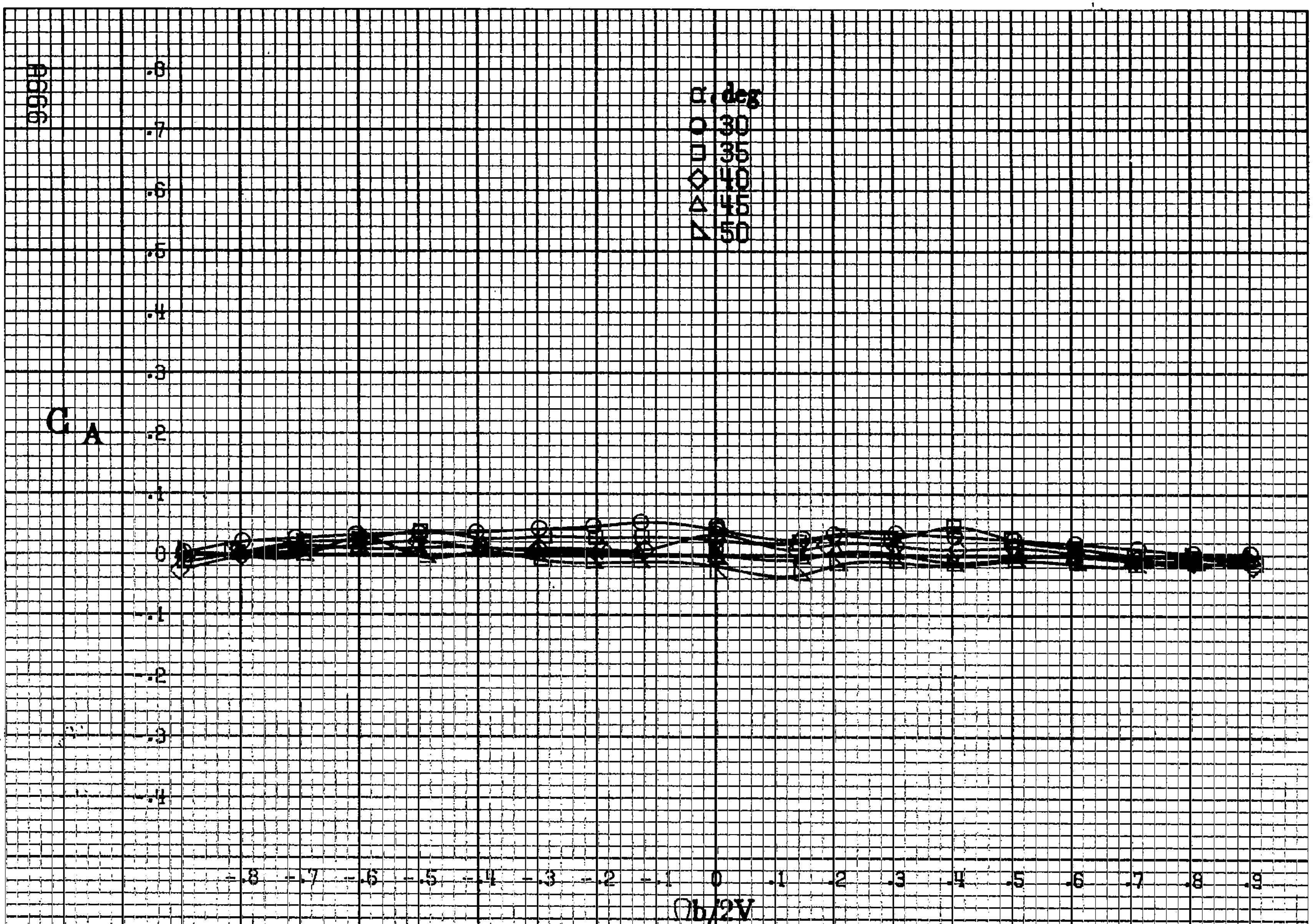

(c) α = 30 to 50 deg, SR = 0.

Figure A162. Continued.

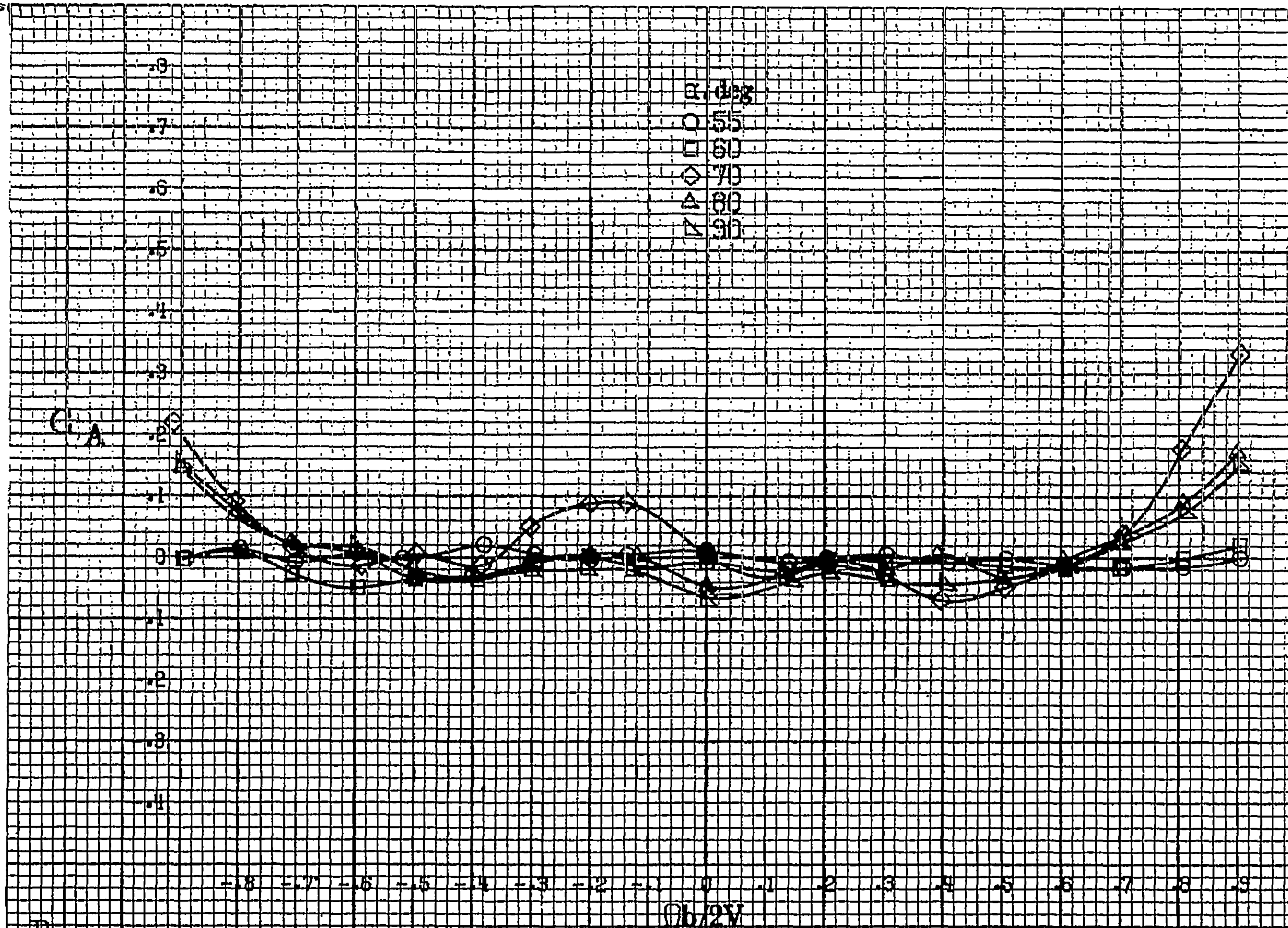

(d) α = 55 to 90 deg, SR = 0.

Figure A102. Concluded.

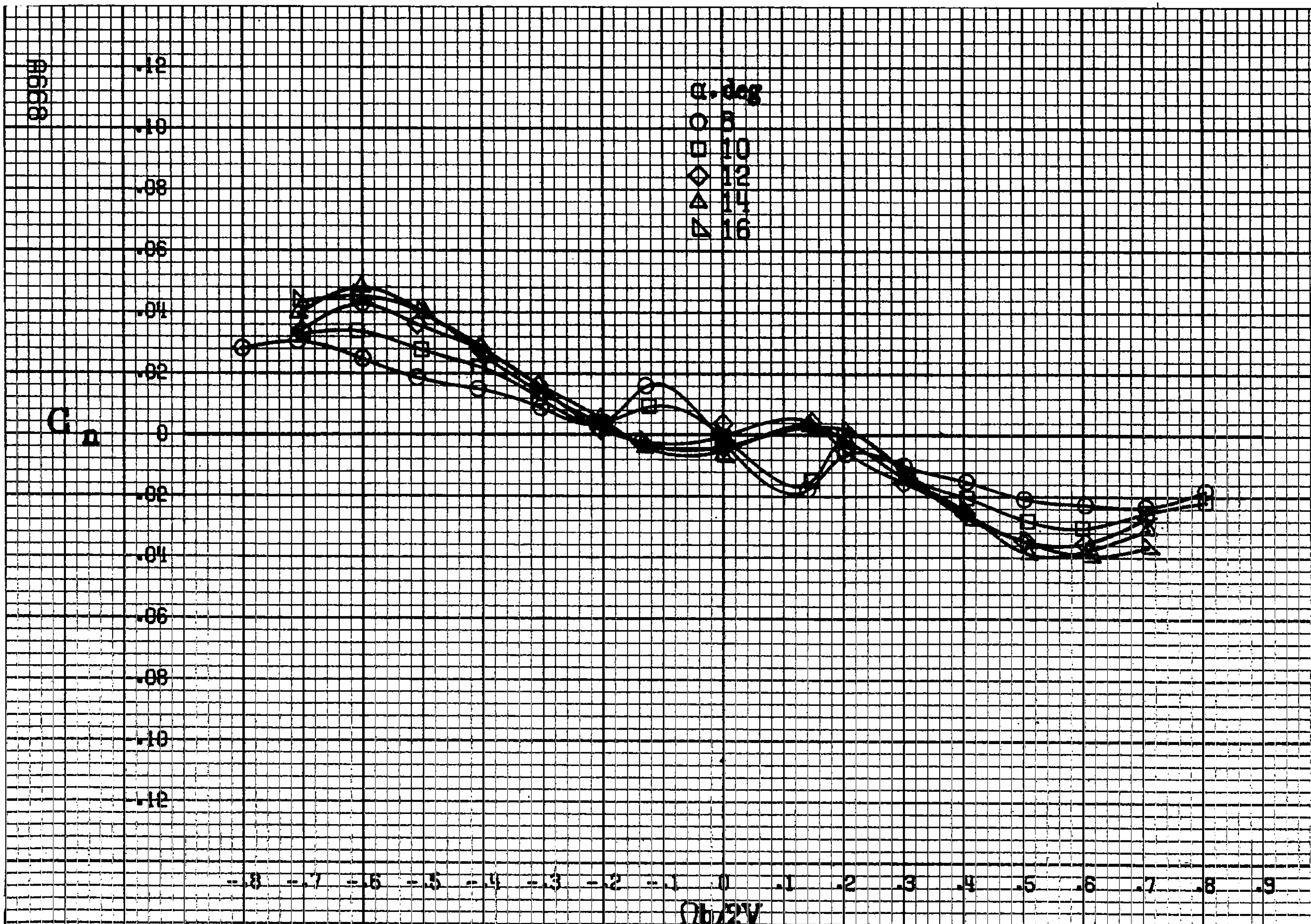

(a) $\alpha = 8$ to 16 deg, SR = 182.9 cm (72 in).

Figure A-183.-Effect of rotation rate and angle of attack on yawing-moment coefficient for configuration having cowl strakes and tail fillets. $\delta_e = 0°$, $\delta_a = 0°$, $\delta_r = 0°$, $\beta = 0°$.

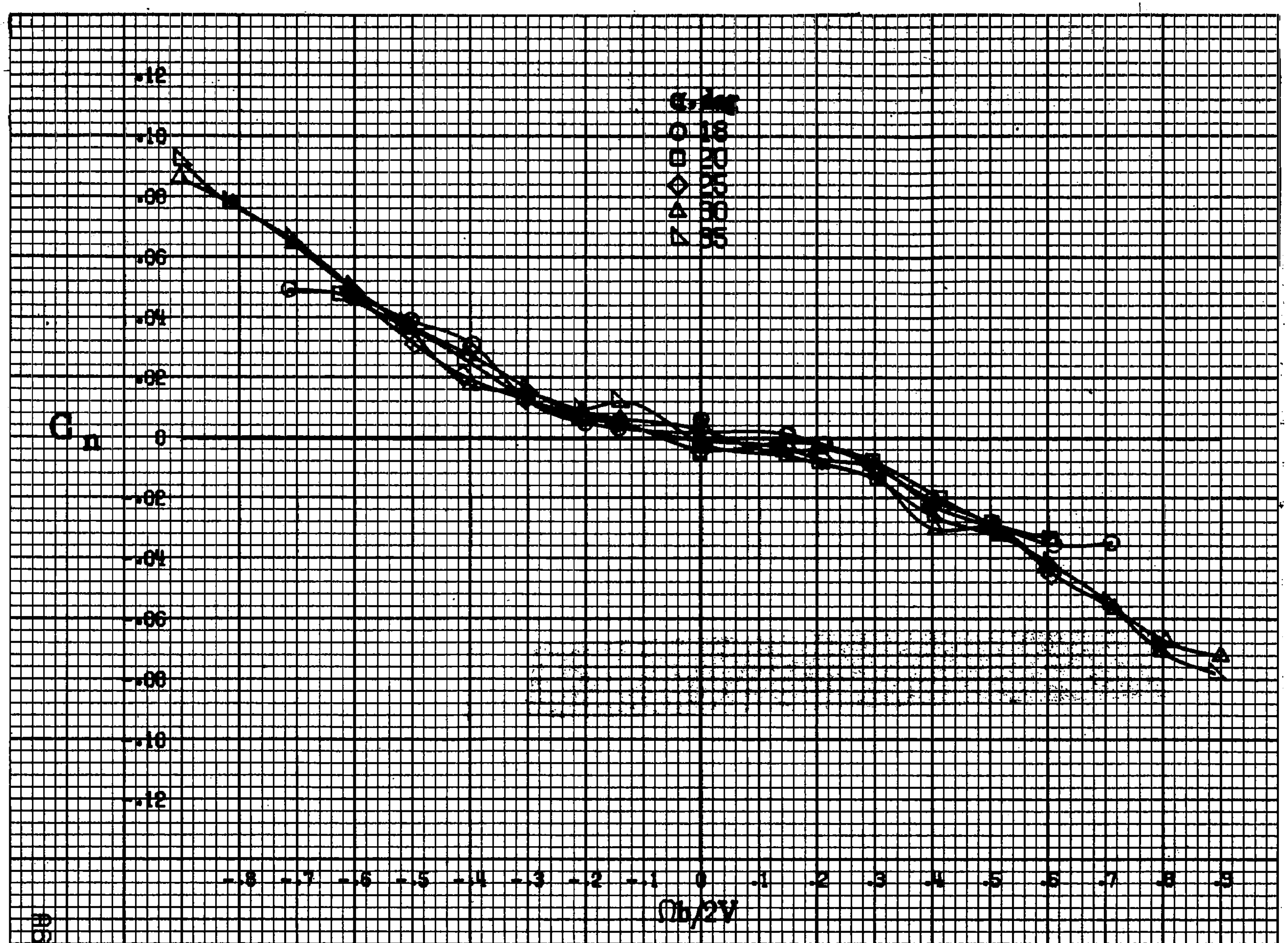

(b) α = 18 to 35 deg, SR = 182.9 cm (72 in).

Figure A163.- Continued.

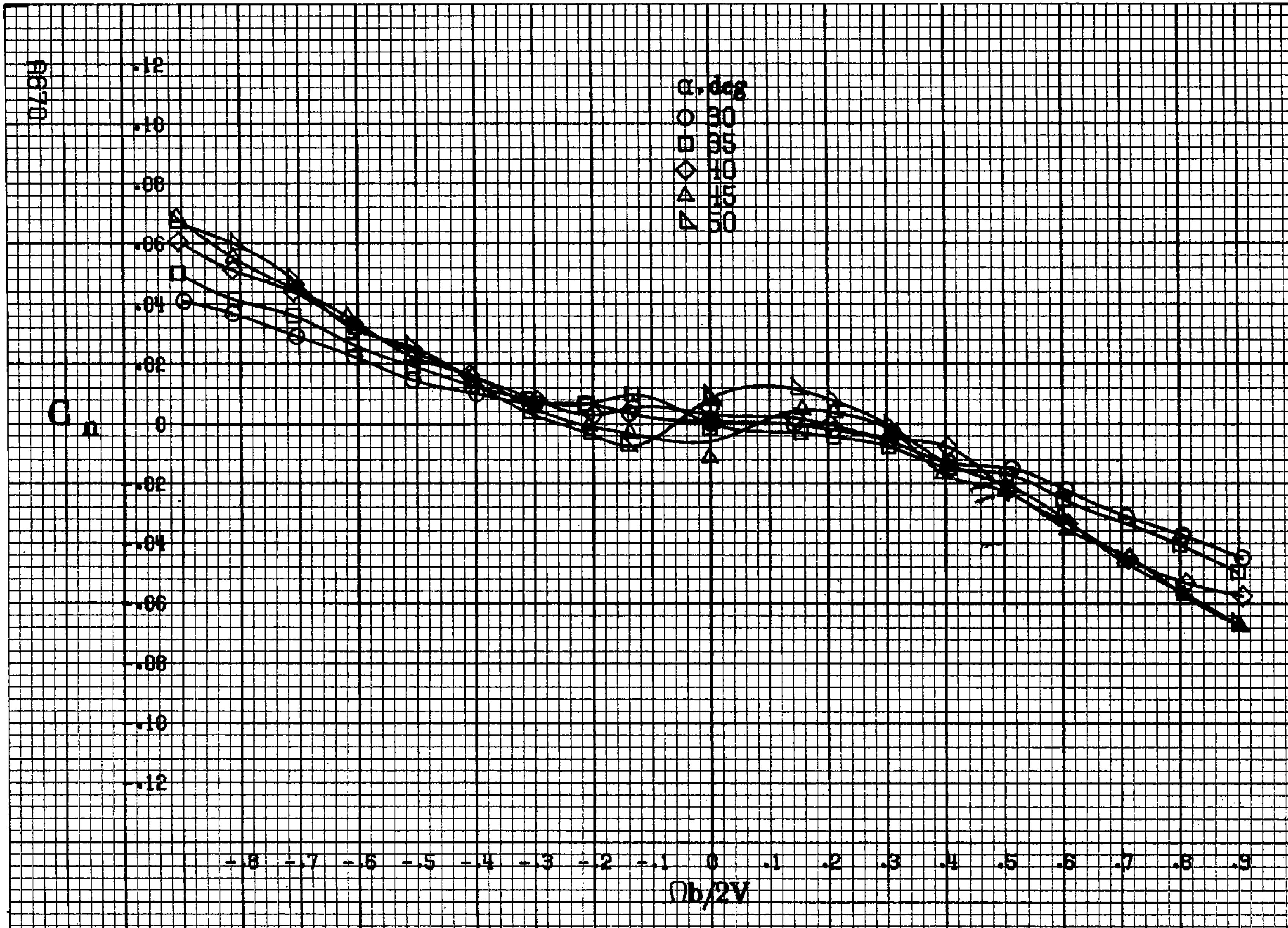

(c) α = 30 to 50 deg, SR = 0.
Figure A163.-Continued.

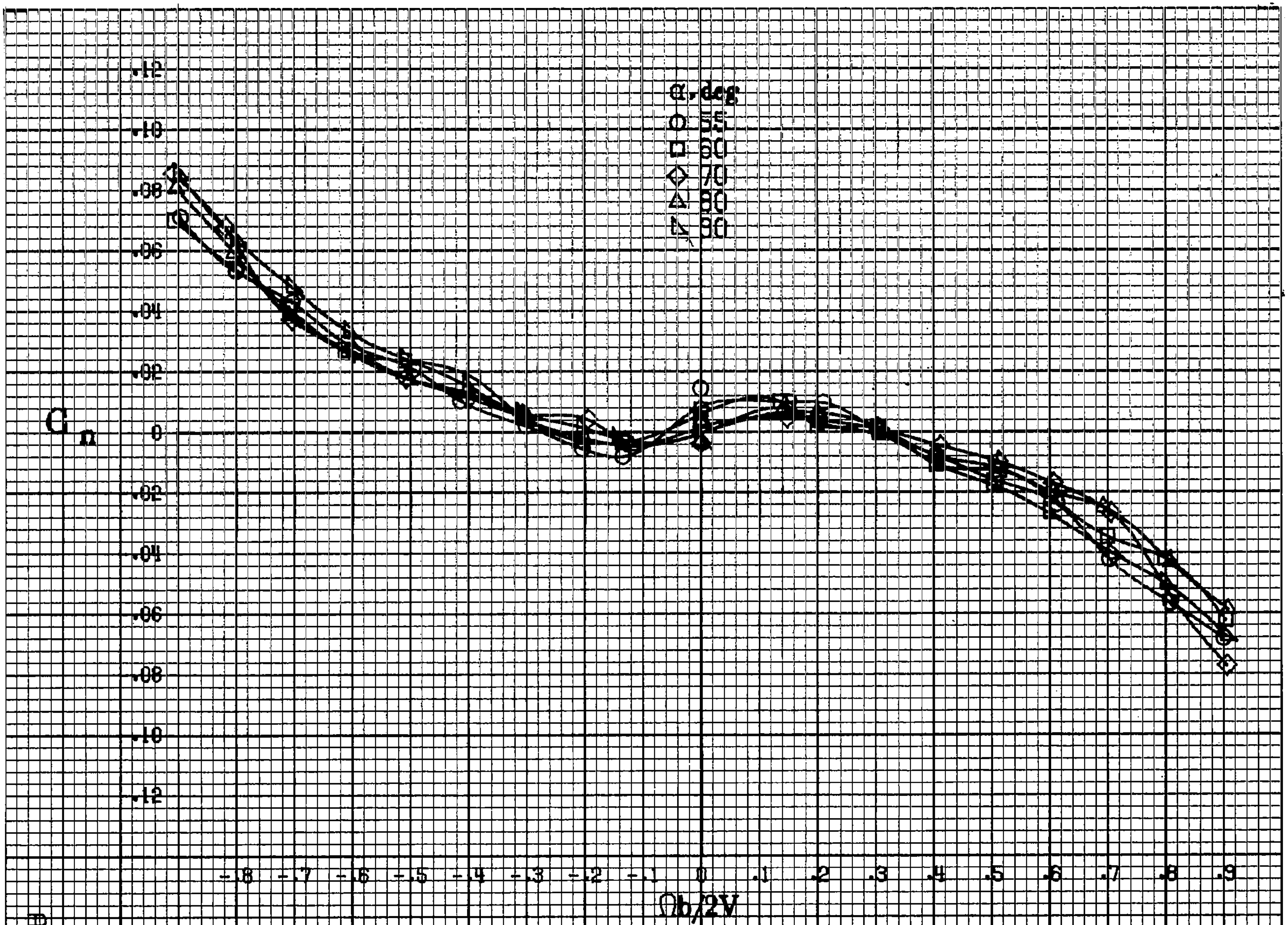

(d) α = 55 to 90 deg, SR = 0.
Figure A163.-Concluded.

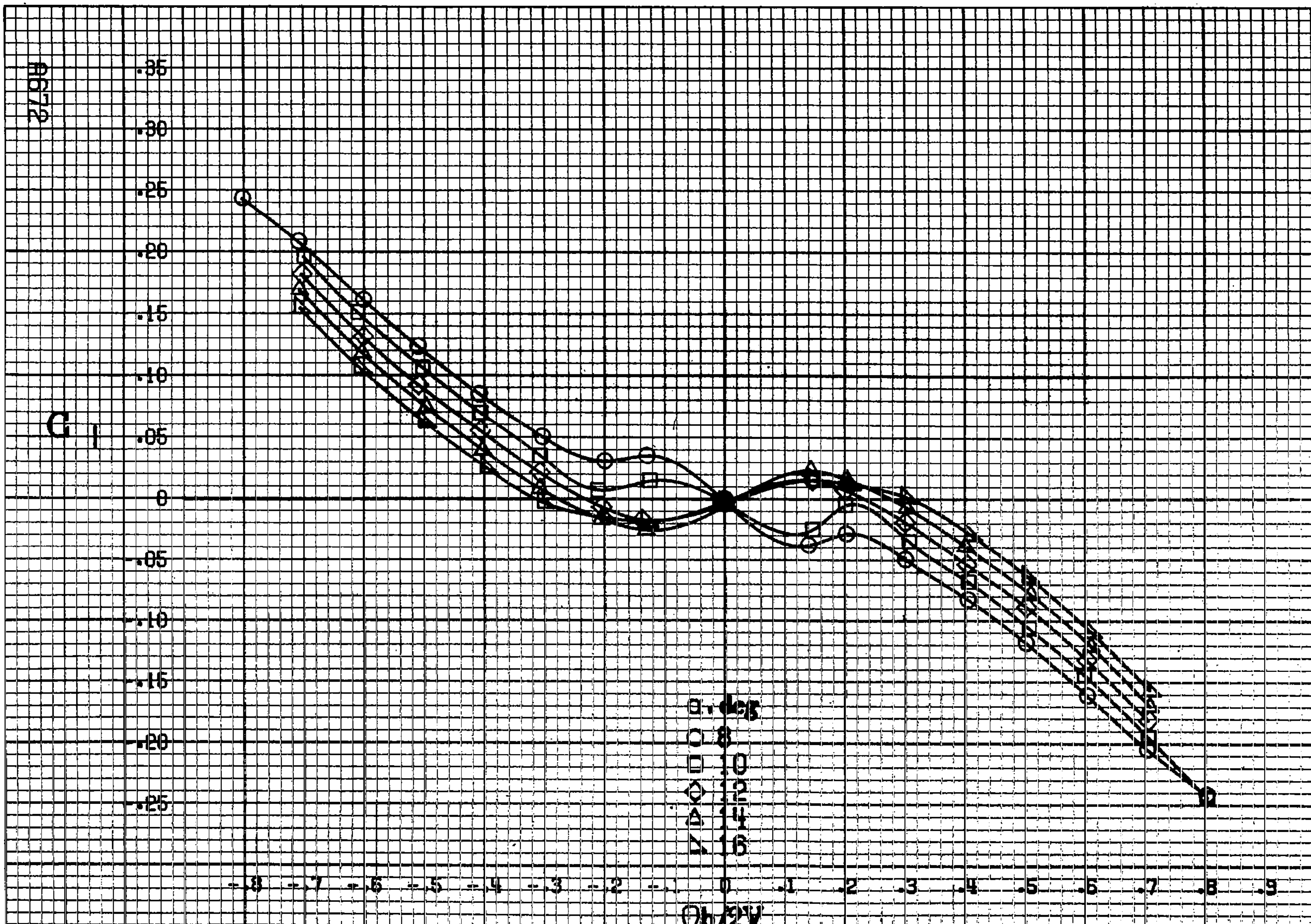

(a) $\alpha = 8$ to 16 deg, SR = 182.9 cm (72 in).

Figure A184.-Effect of rotation rate and angle of attack on rolling-moment coefficient for configuration having canard strakes and tail fillets. $\delta_s = 0°$, $\delta_a = 0°$, $\delta_r = 0°$, $\beta = 0°$.

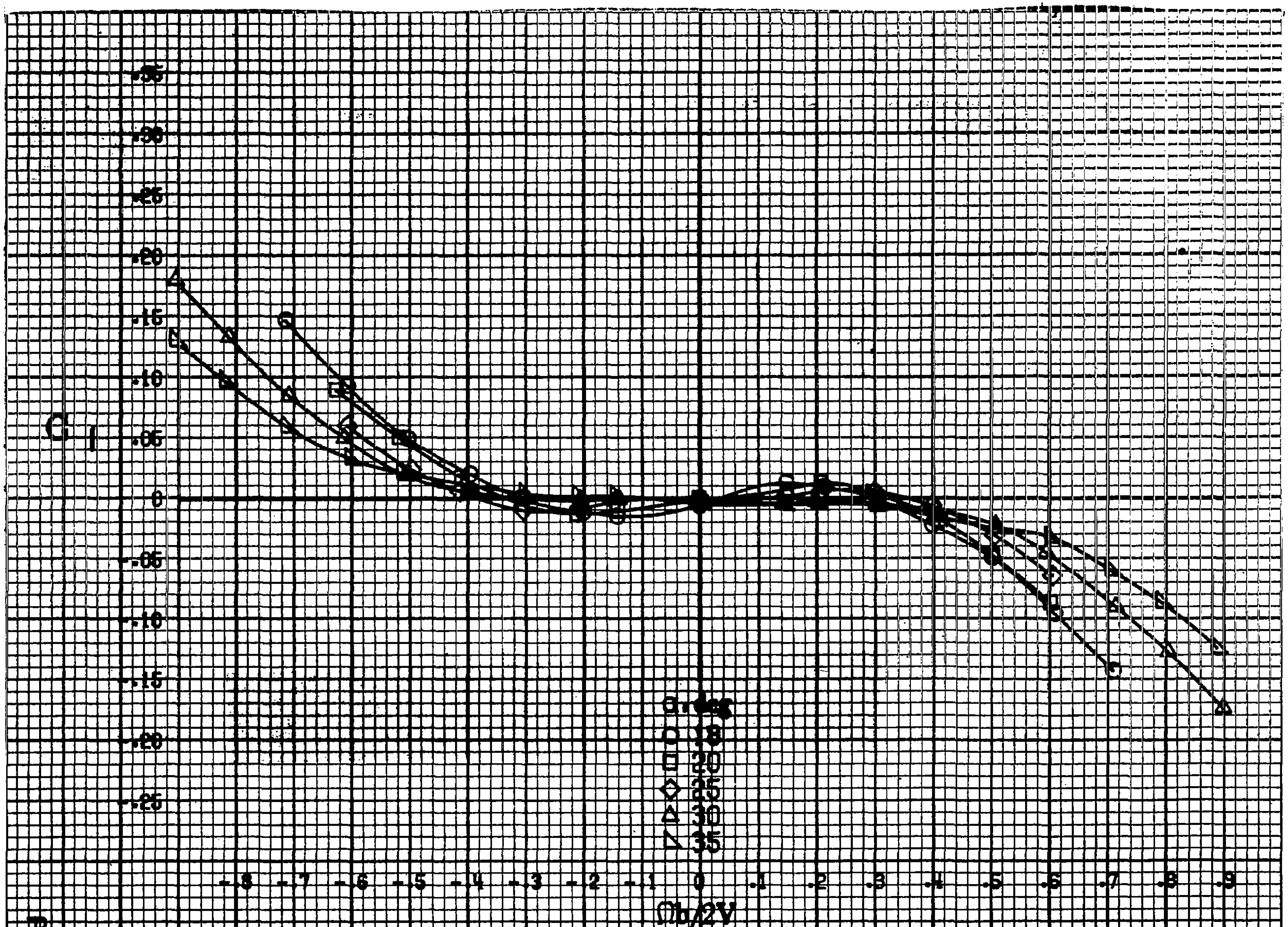

(b) α = 18 to 35 deg, SR = 182.9 cm (72 in).

Figure A104.-Continued.

A6579

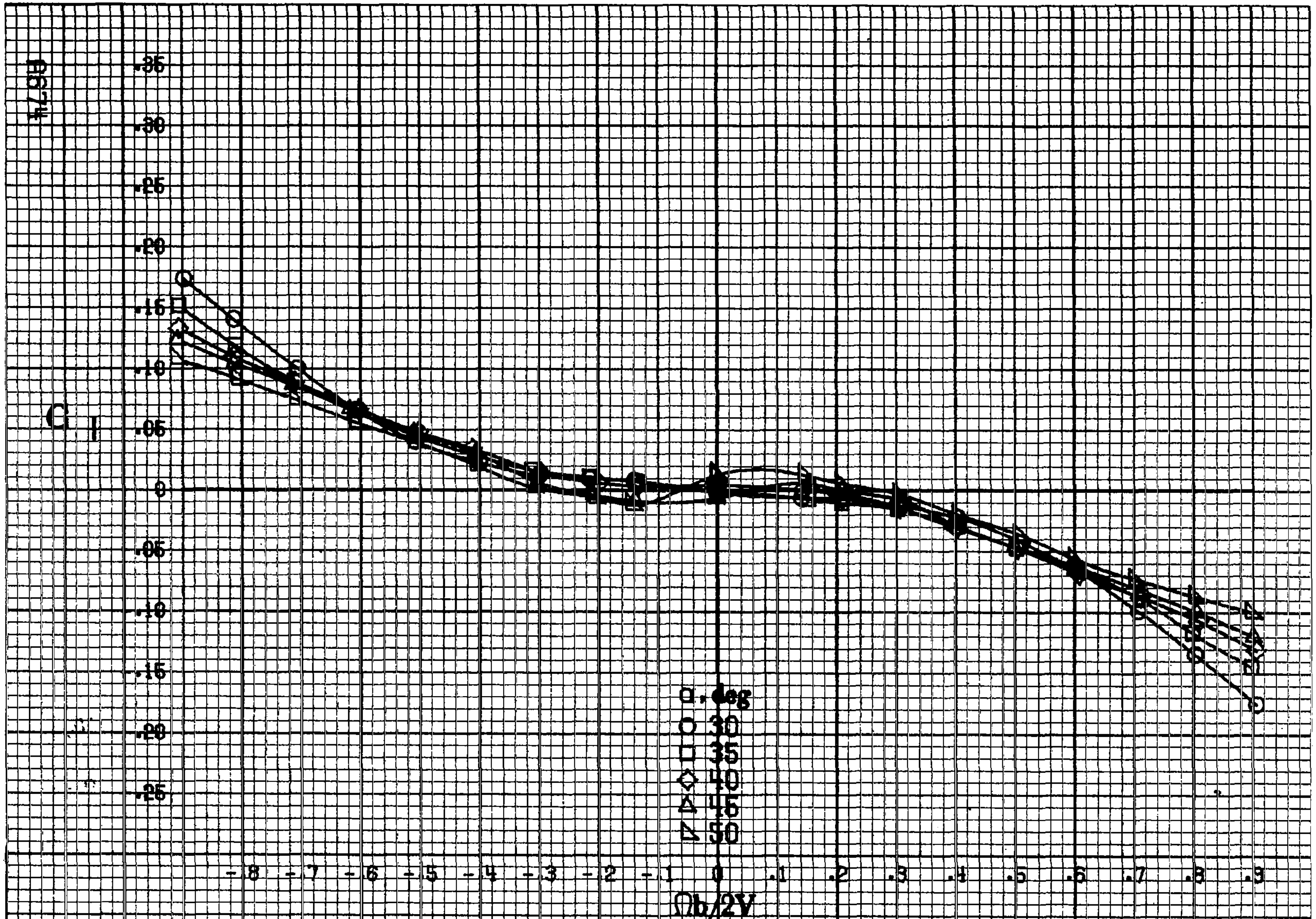

(c) α = 30 to 50 deg, SR = 0.

Figure A104.-Continued.

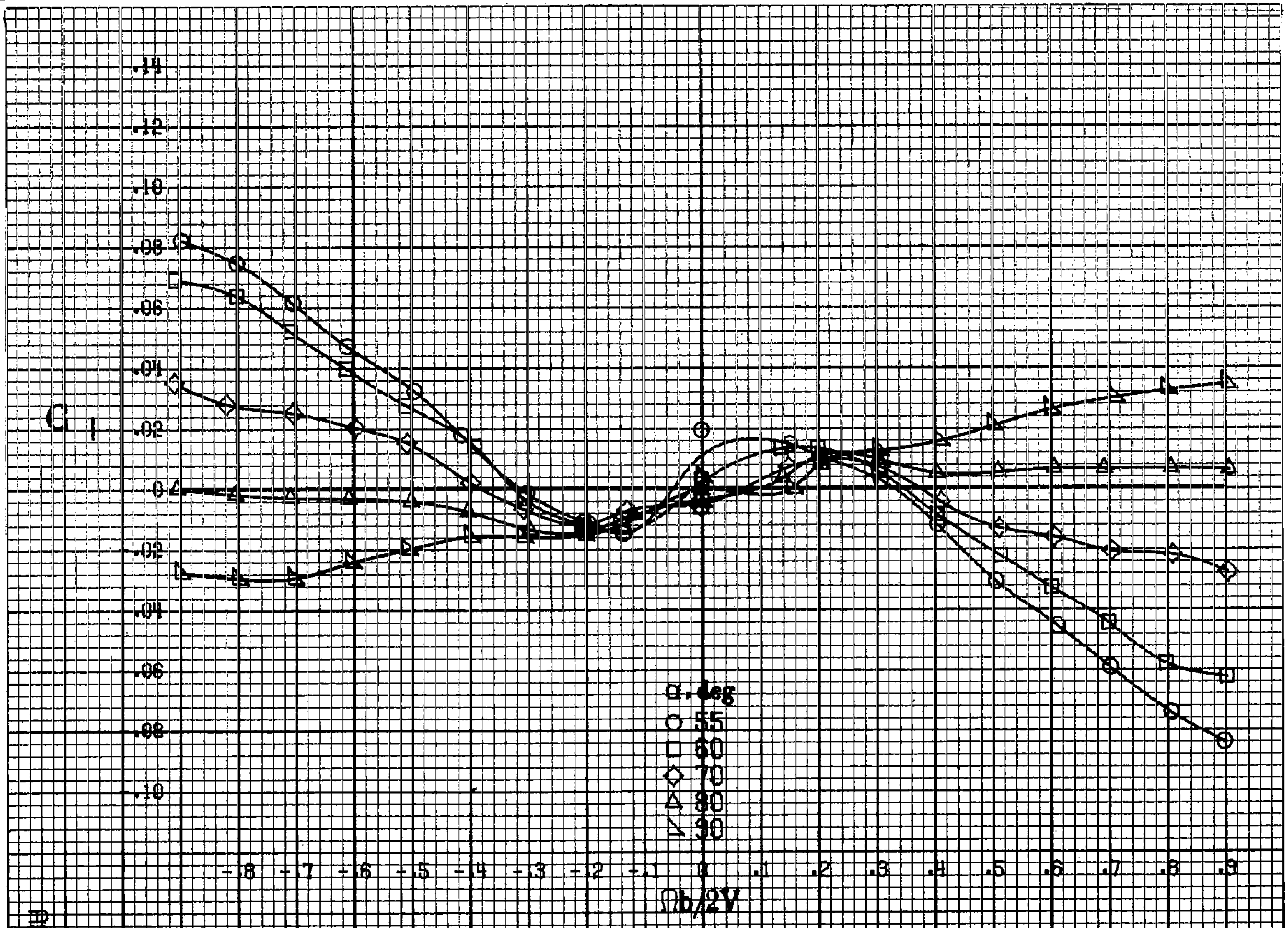

(d) α = 55 to 90 deg, SR = 0.

Figure A164.-Concluded.

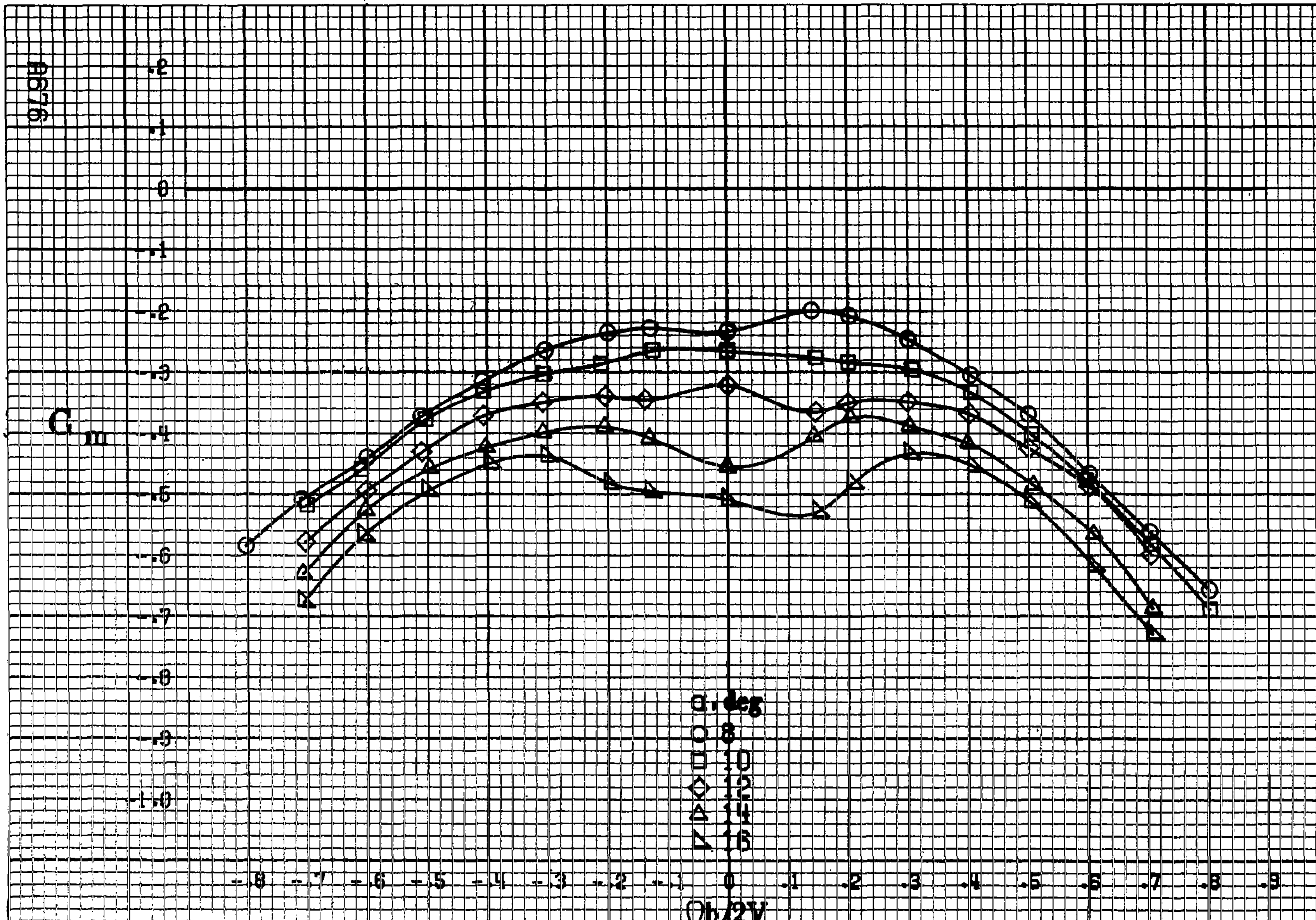

(a) α = 8 to 16 deg, SR = 182.9 cm (72 in).

Figure A185.- Effect of rotation rate and angle of attack on pitching-moment coefficient for configuration having cowl strakes and tail fillets. $\delta_e = 0°$, $\delta_a = 0°$, $\delta_r = 0°$, $\beta = 0°$.

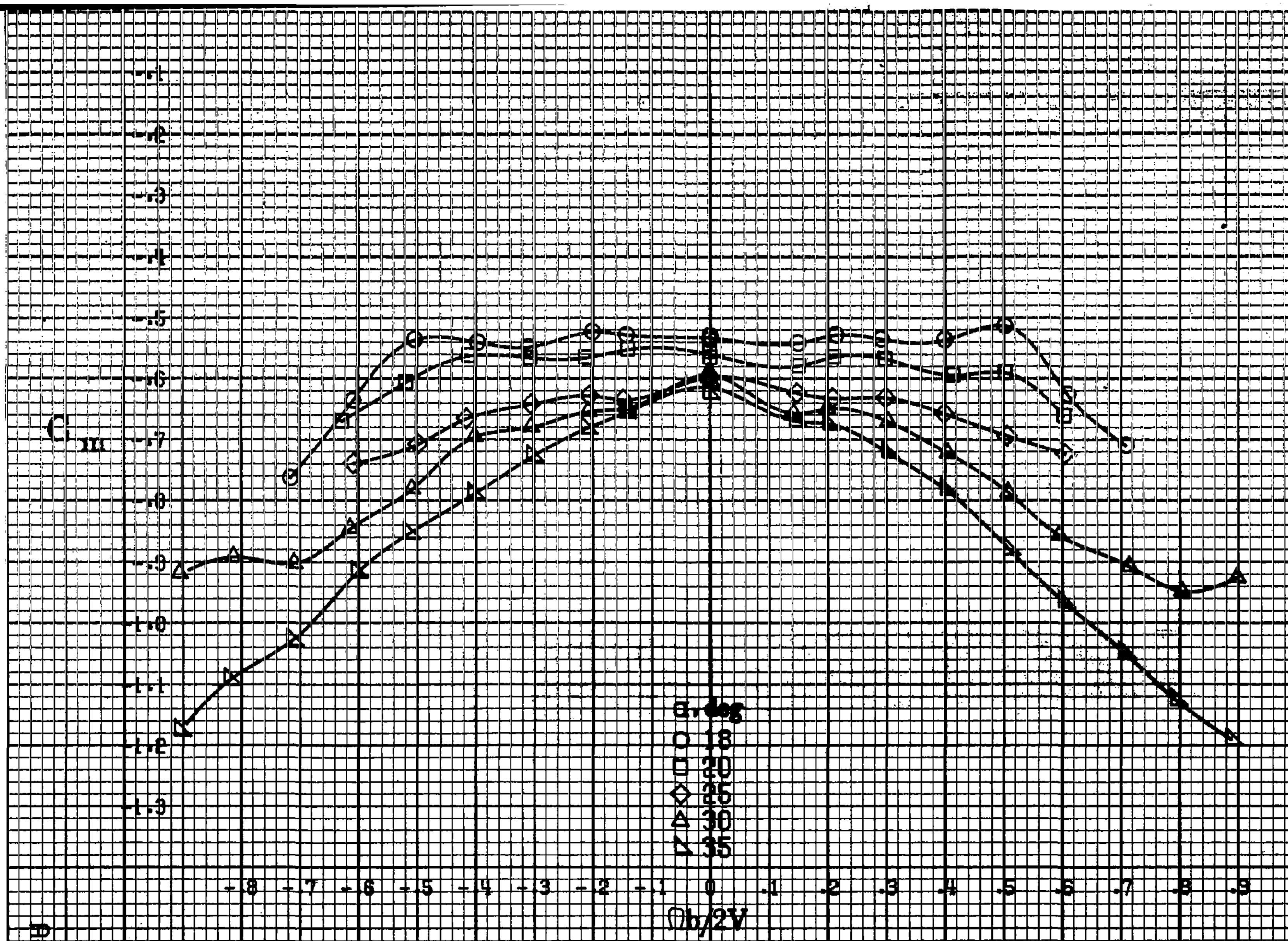

(b) α = 18 to 35 deg, SR = 182.9 cm (72 in).

Figure A166.-Continued.

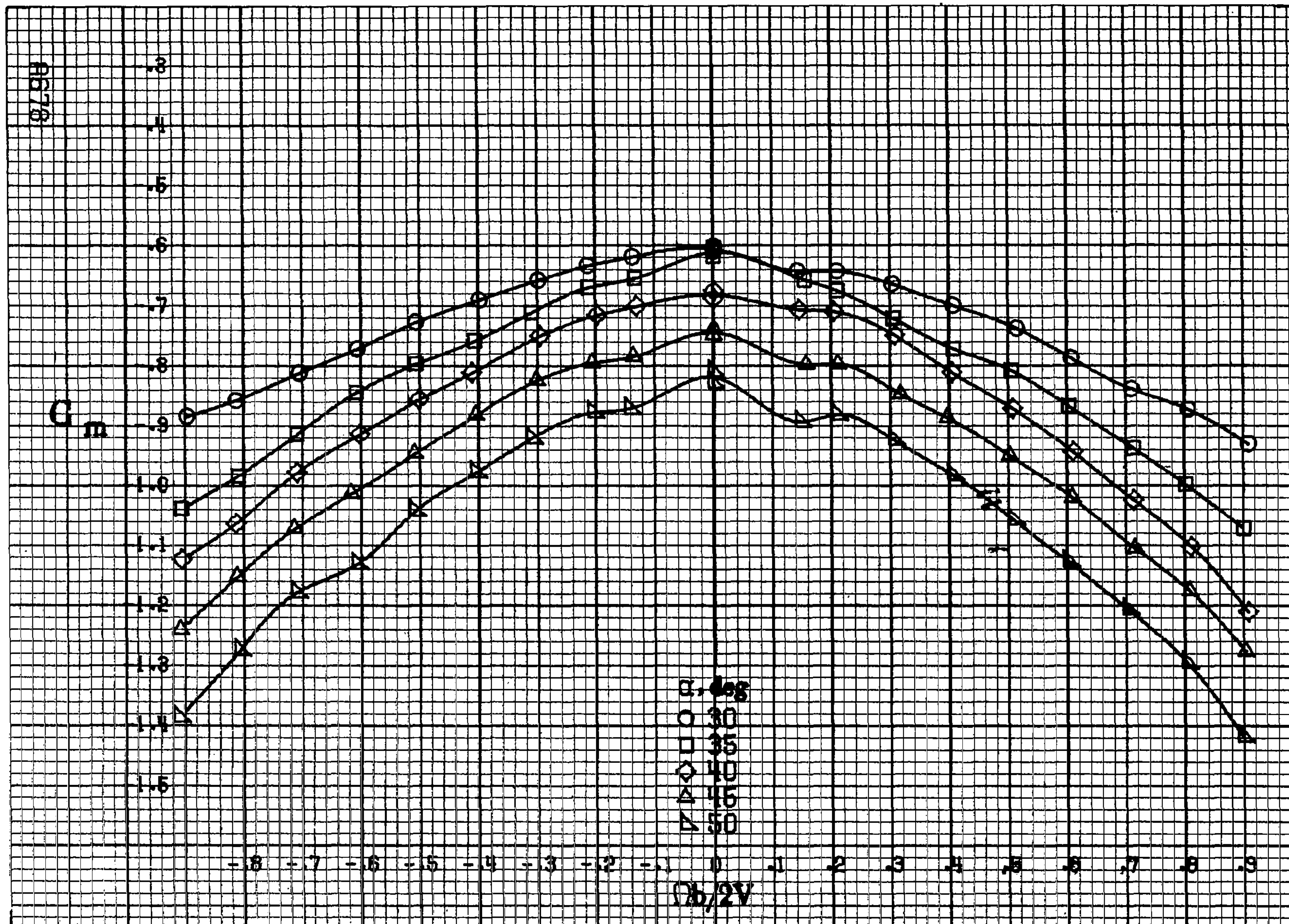

(c) α = 30 to 50 deg, SR = 0.

Figure A165.-Continued.

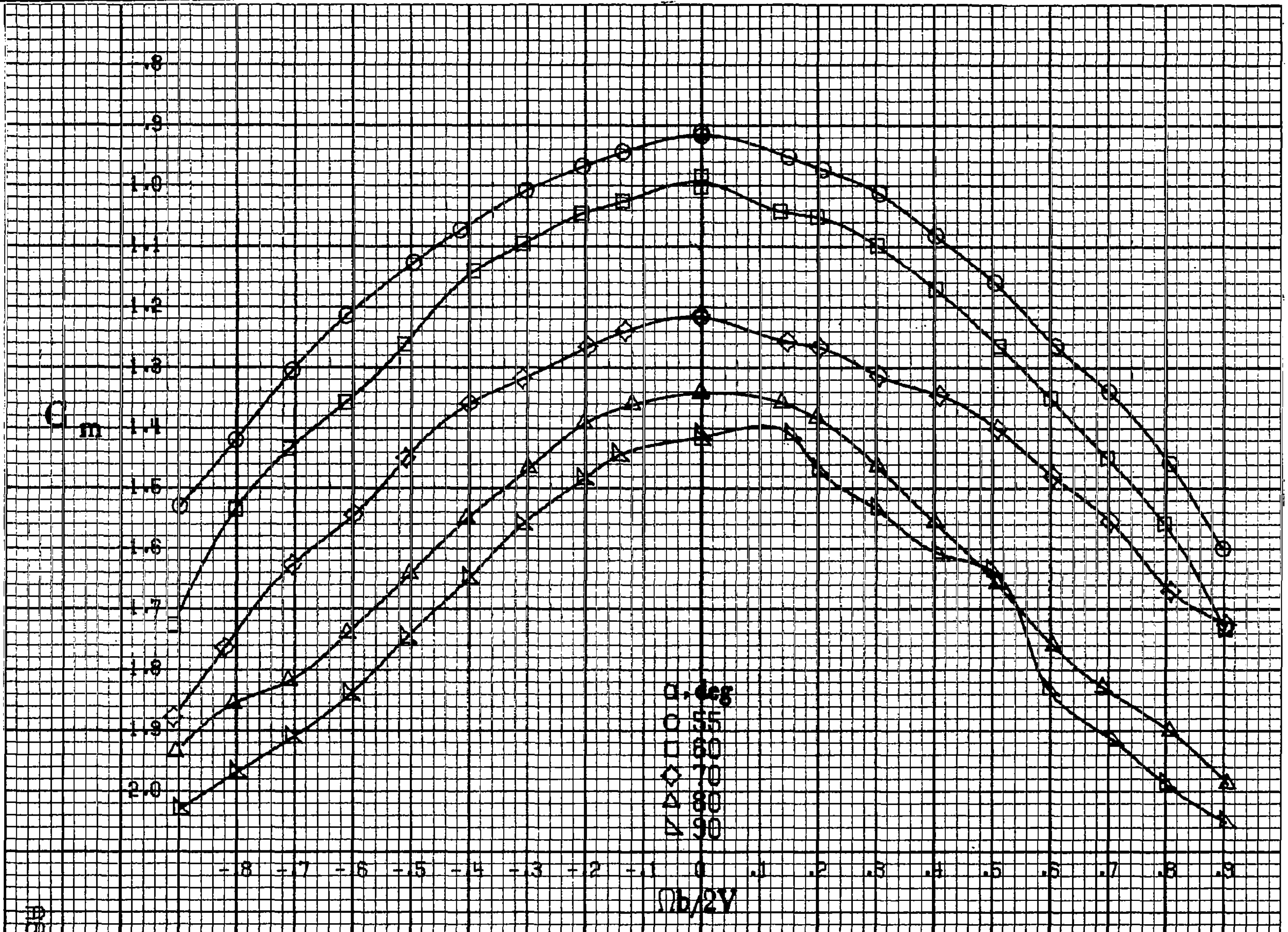

(d) α = 55 to 90 deg, SR = 0.

Figure A165.-Concluded.

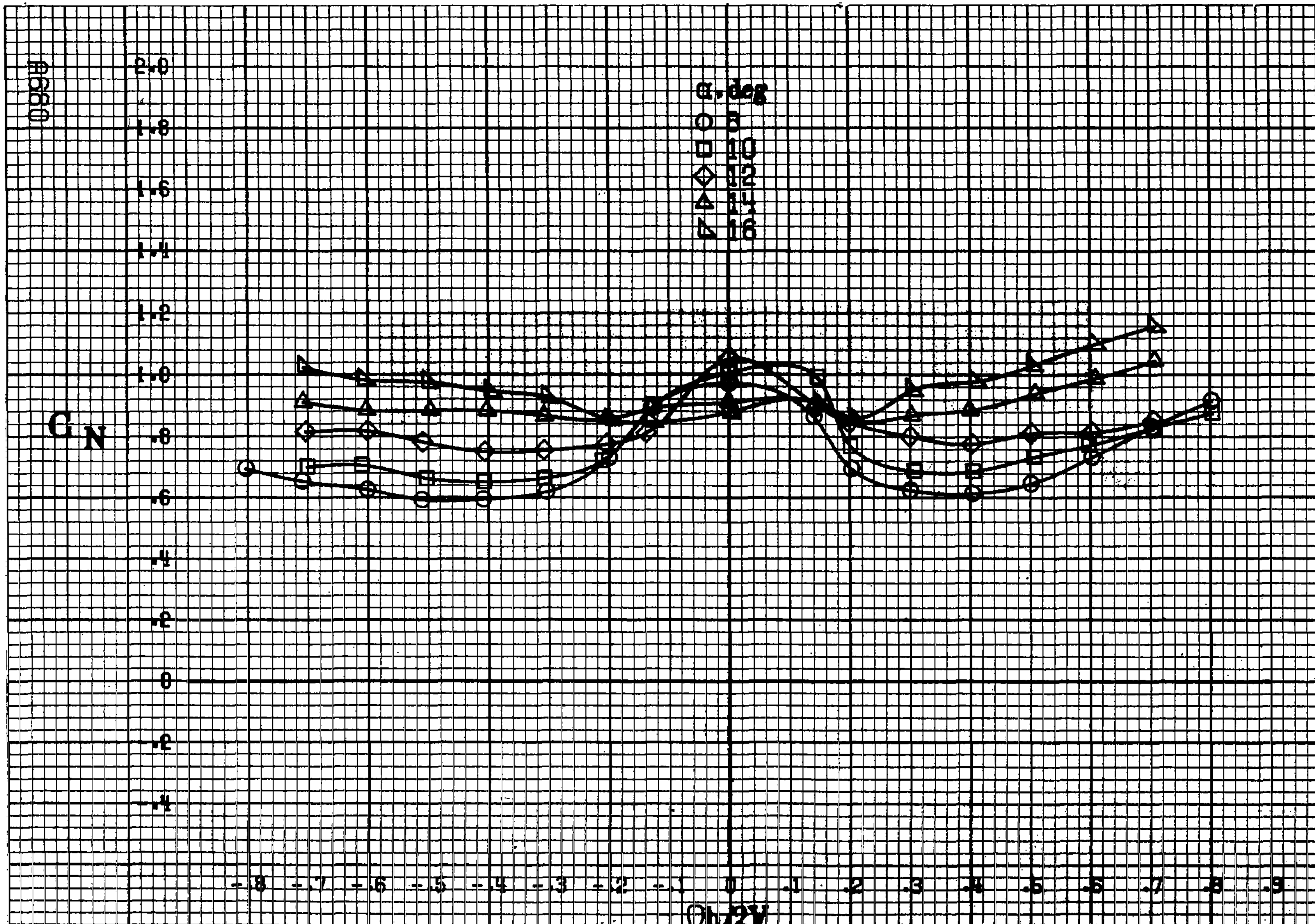

(a) α = 8 to 16 deg, SR = 182.9 cm (72 in).

Figure A166.- Effect of rotation rate and angle of attack on normal-force coefficient for configuration having cowl strakes and tail fillets. $\delta_e = 0°$, $\delta_a = 0°$, $\delta_r = 0°$, $\beta = 0°$.

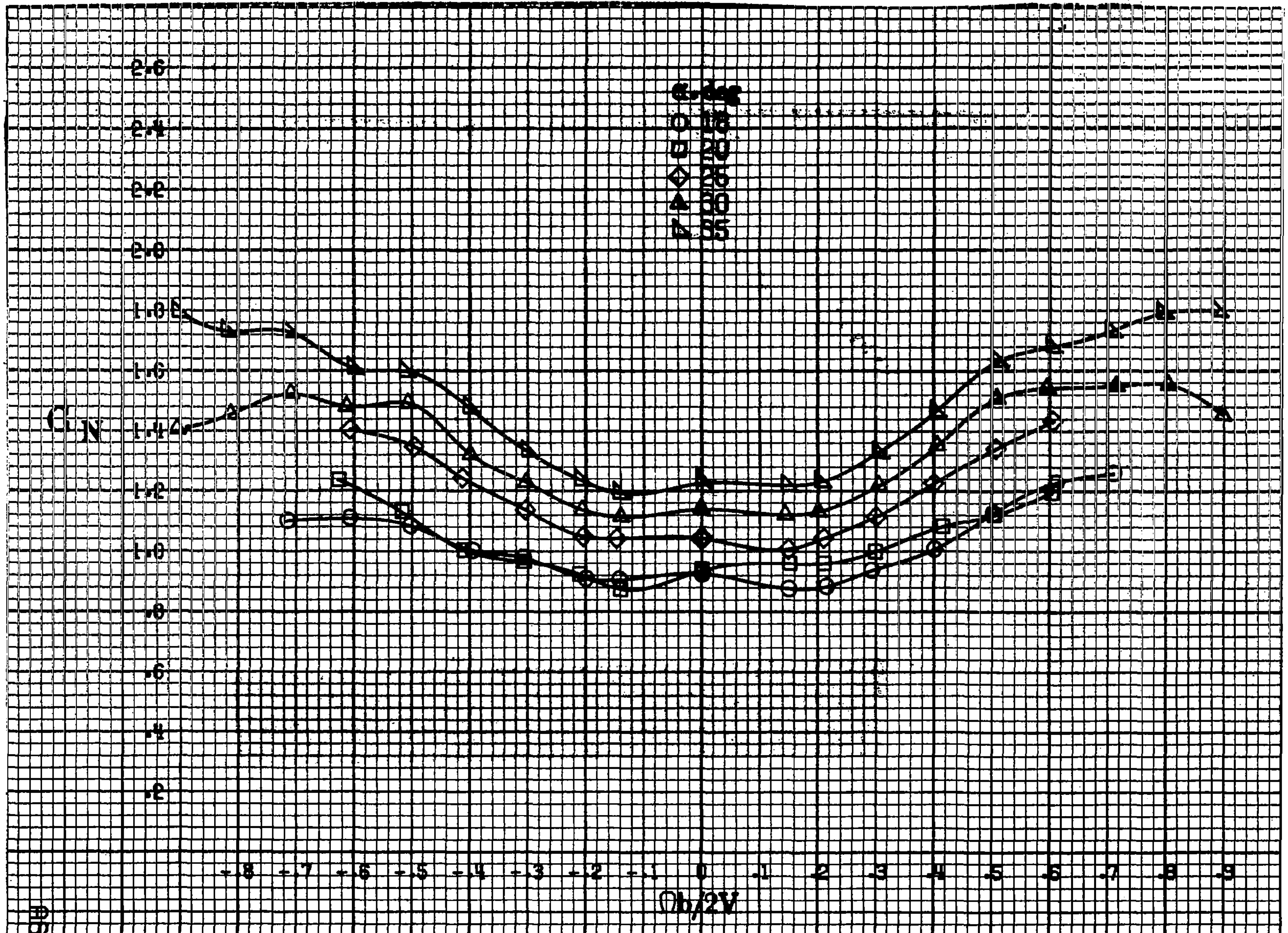

(b) α = 18 to 35 deg, SR = 182.9 cm (72 in).

Figure A166.-Continued.

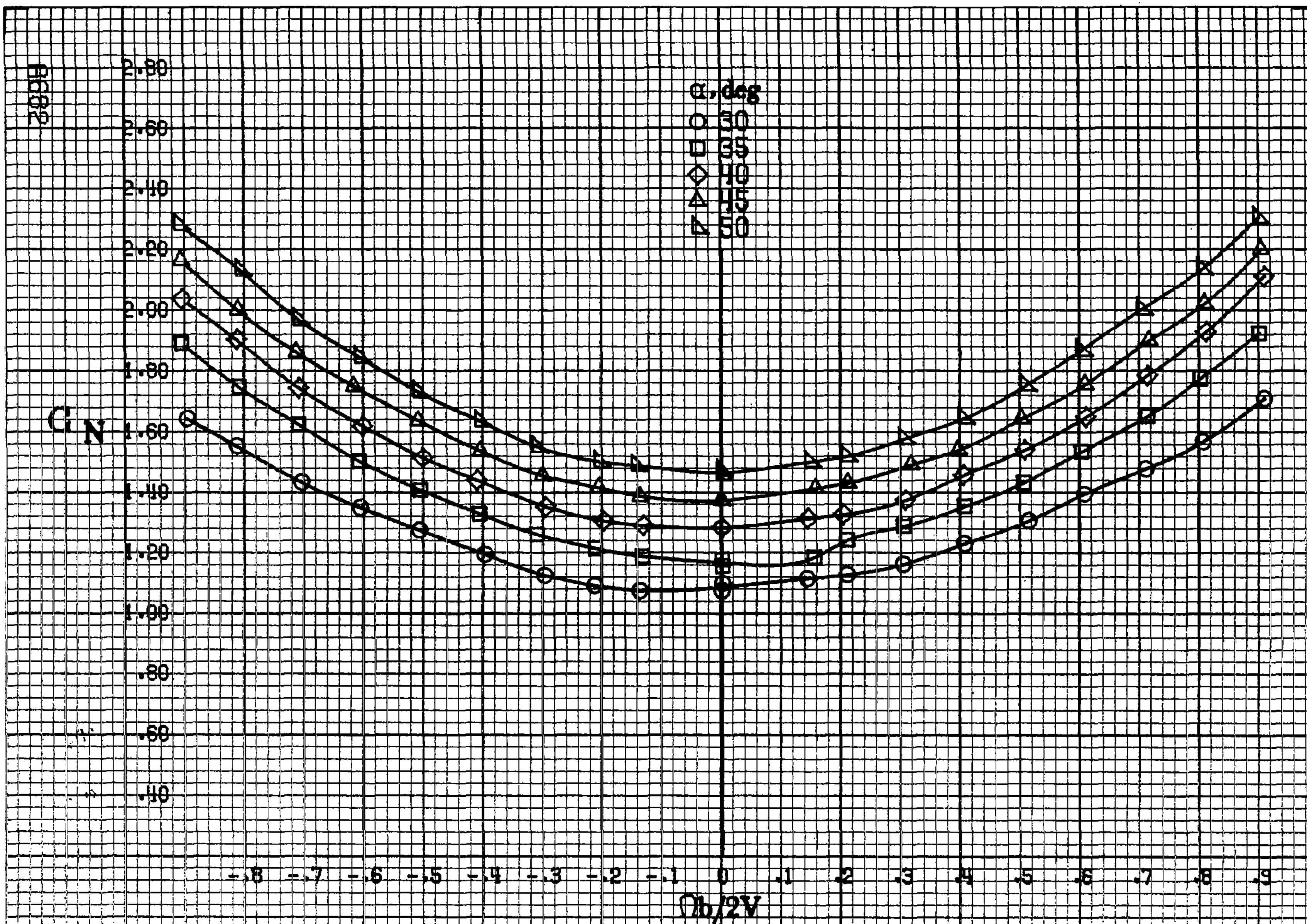

(c) α = 30 to 50 deg, SR = 0.
Figure A166.-Continued.

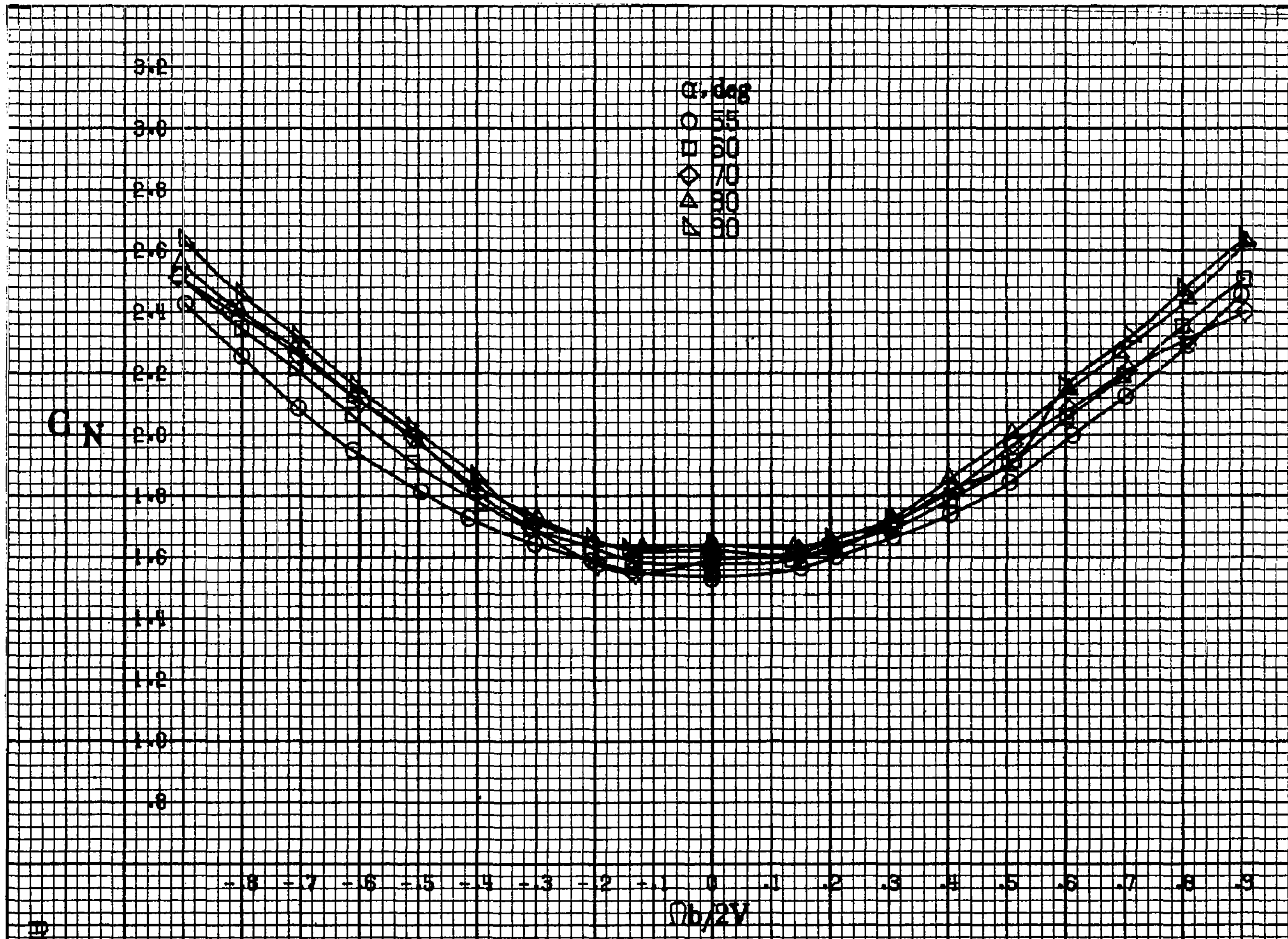

(d) α = 55 to 90 deg, SR = 0.

Figure A166. Concluded.

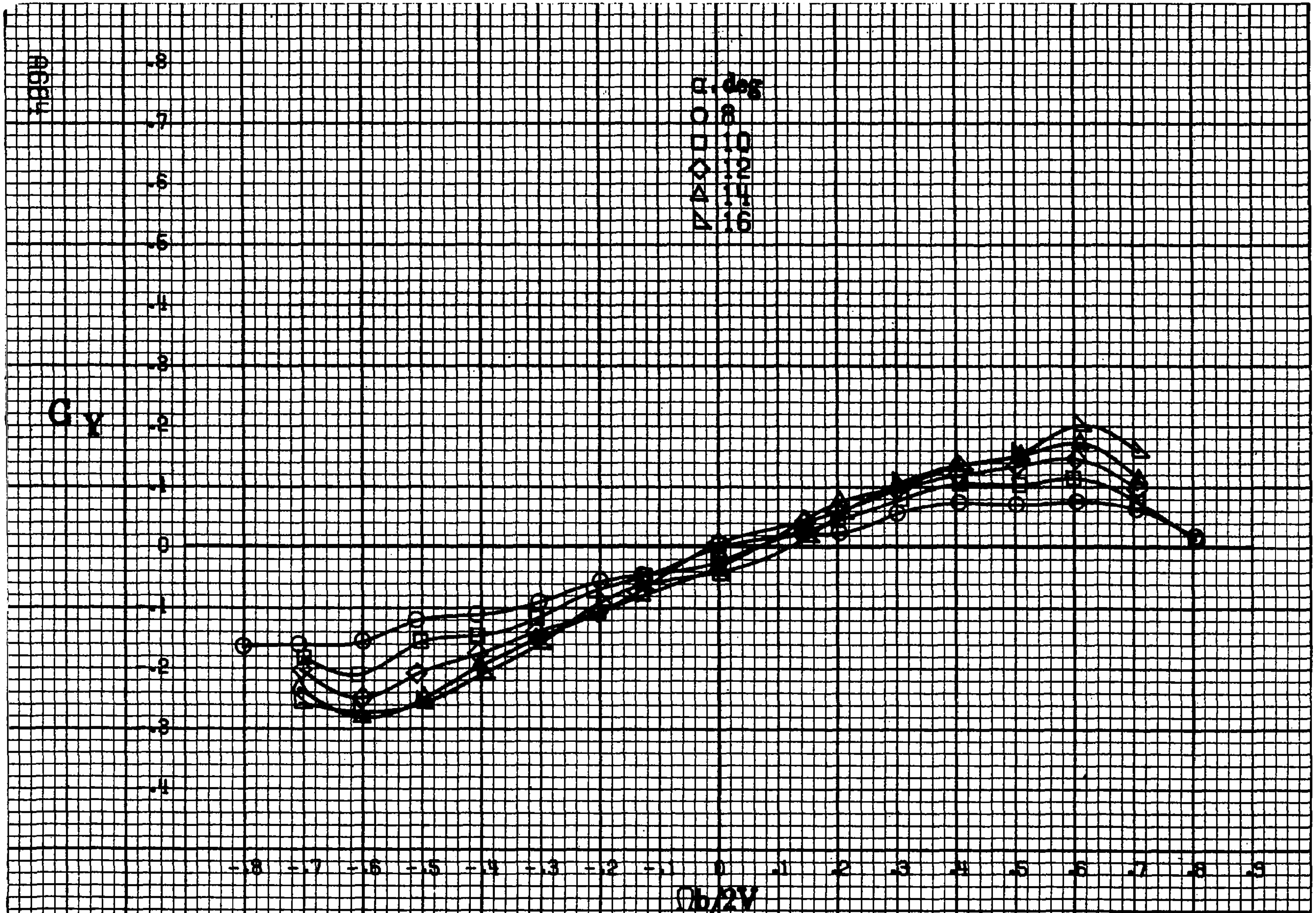

(a) α = 8 to 16 deg, SR = 182.9 cm (72 in).

Figure A167.- Effect of rotation rate and angle of attack on side-force coefficient for configuration having cowl strakes and tail fillets. $\delta_e = 0°$, $\delta_a = 0°$, $\delta_r = 0°$, $\beta = 0°$.

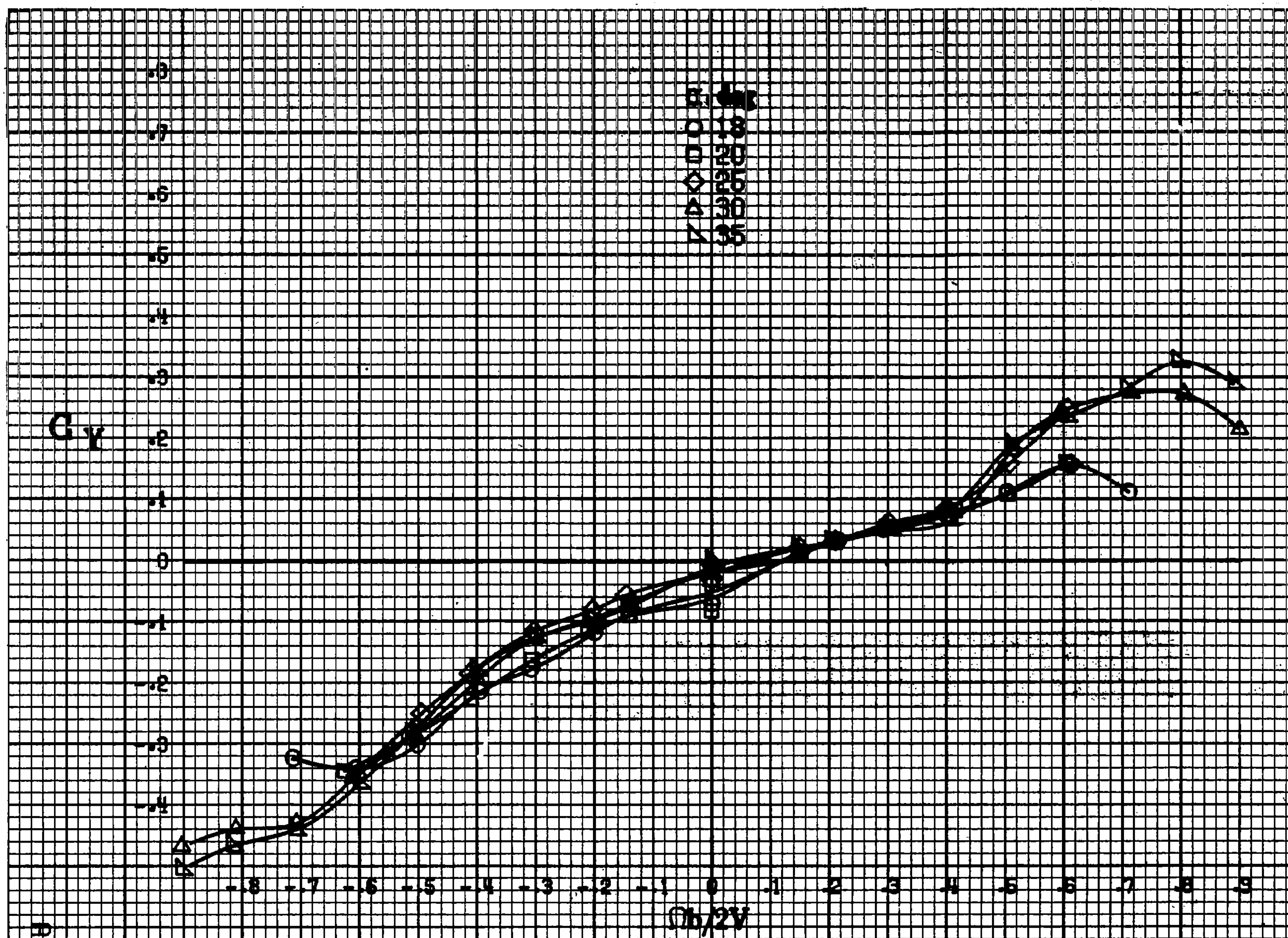

(b) α = 18 to 35 deg, SR = 182.9 cm (72 in).
Figure A167.-Continued.

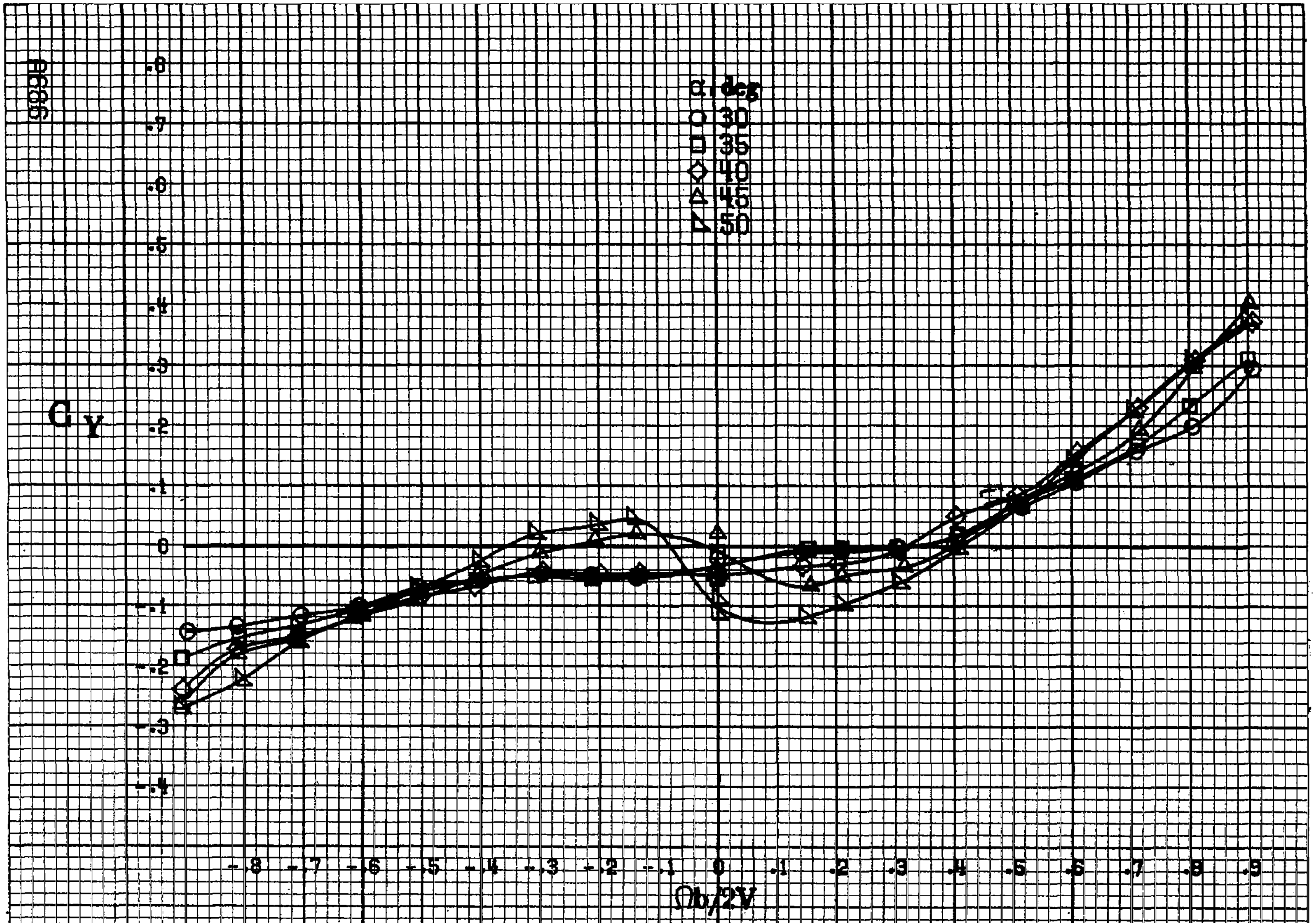

(c) α = 30 to 50 deg, δR = 0.

Figure A167.- Continued.

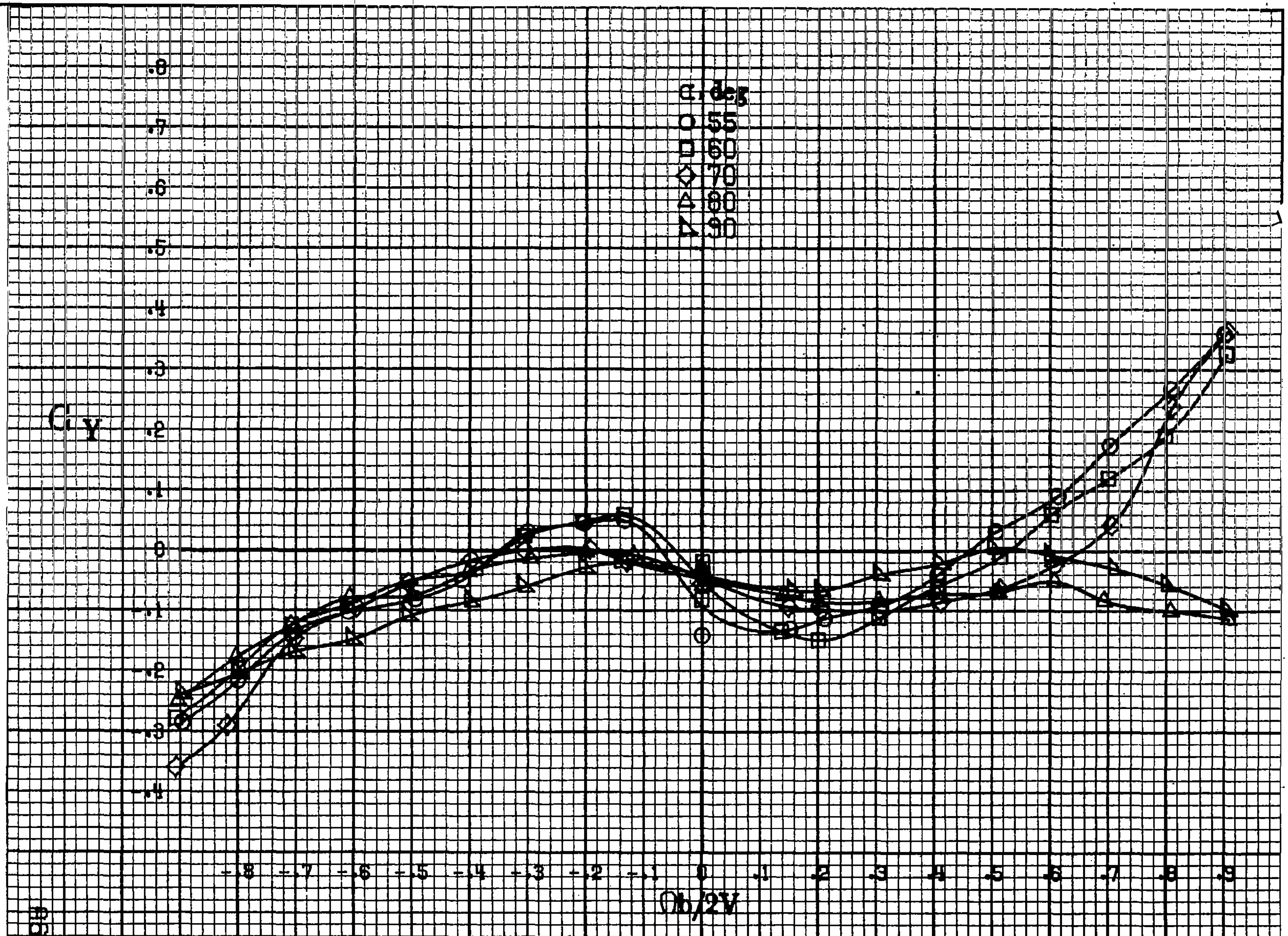

(d) α = 55 to 90 deg, SR = 0.

Figure A167.-Concluded.

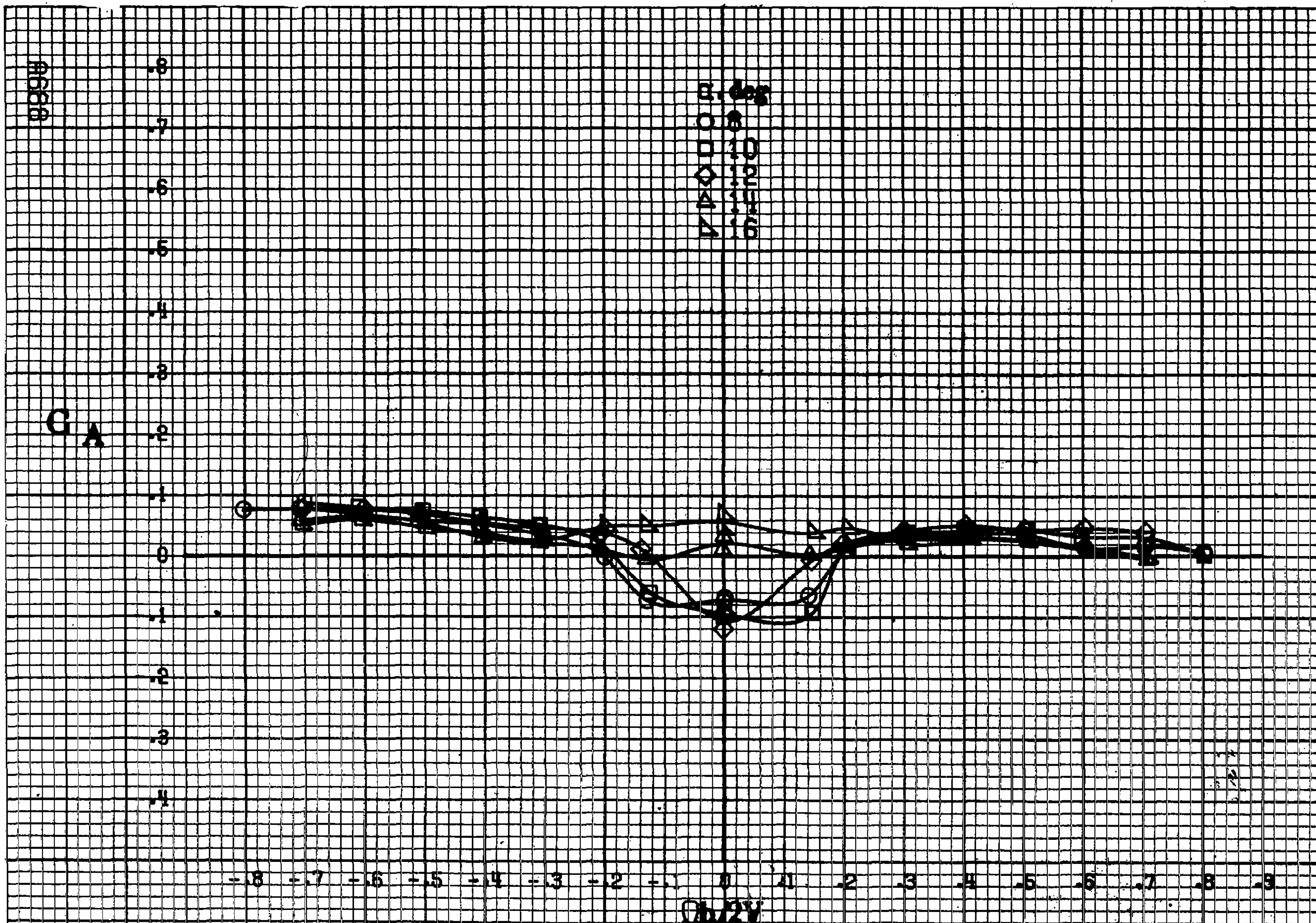

(a) α = 8 to 16 deg, SR = 182.9 cm (72 in).

Figure A168.- Effect of rotation rate and angle of attack on axial-force coefficient for configuration having cowl strakes and tail fillets. $\delta_a = 0°$, $\delta_e = 0°$, $\delta_r = 0°$, $\beta = 0°$.

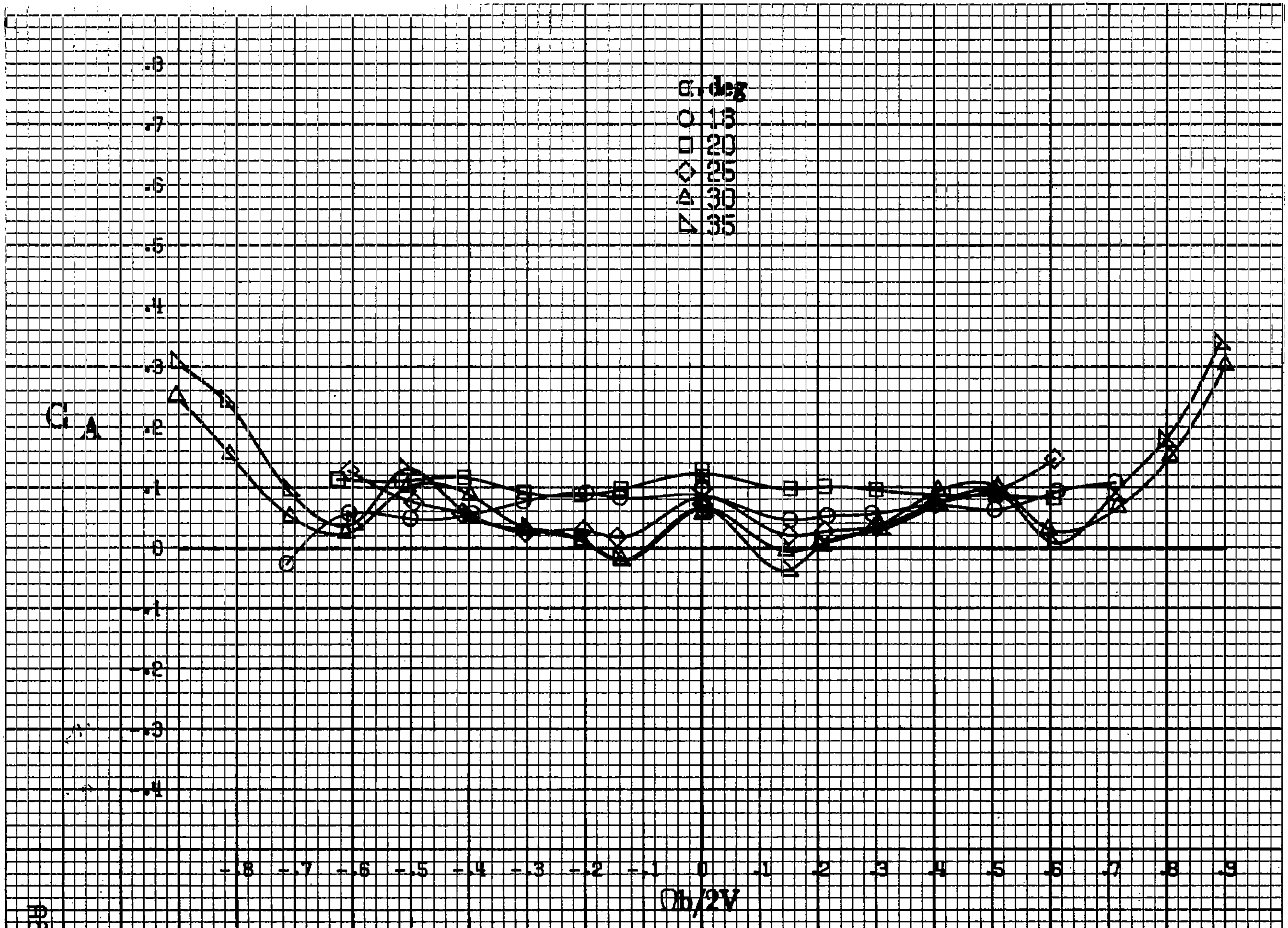

(b) α = 18 to 35 deg, SR = 182.9 cm (72 in).

Figure A168.- Continued.

(c) α = 30 to 50 deg, SR = 0.

Figure A168.-Continued.

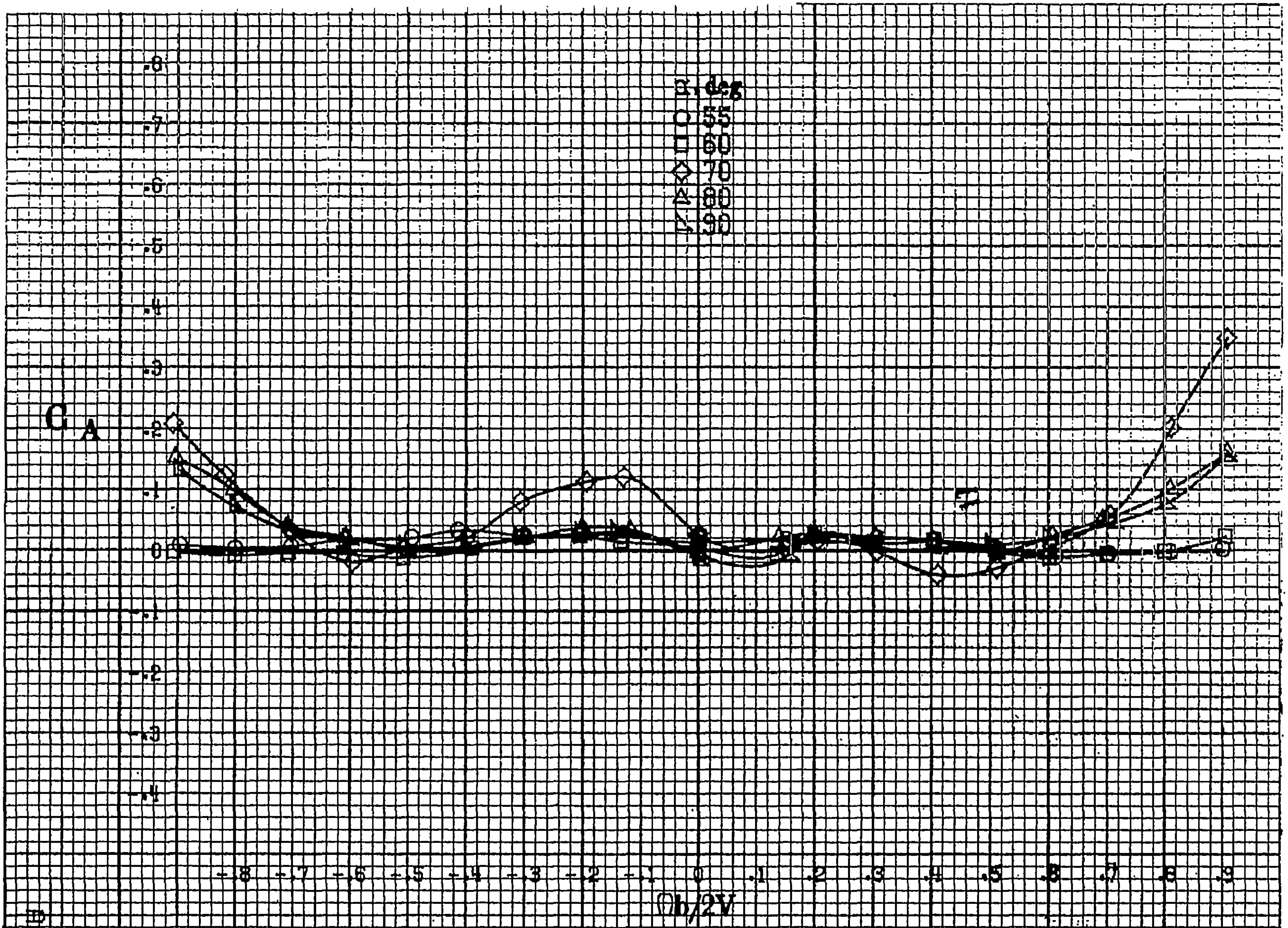

(d) η=55 to 90 deg, SR=0.

Figure A168.-Concluded.

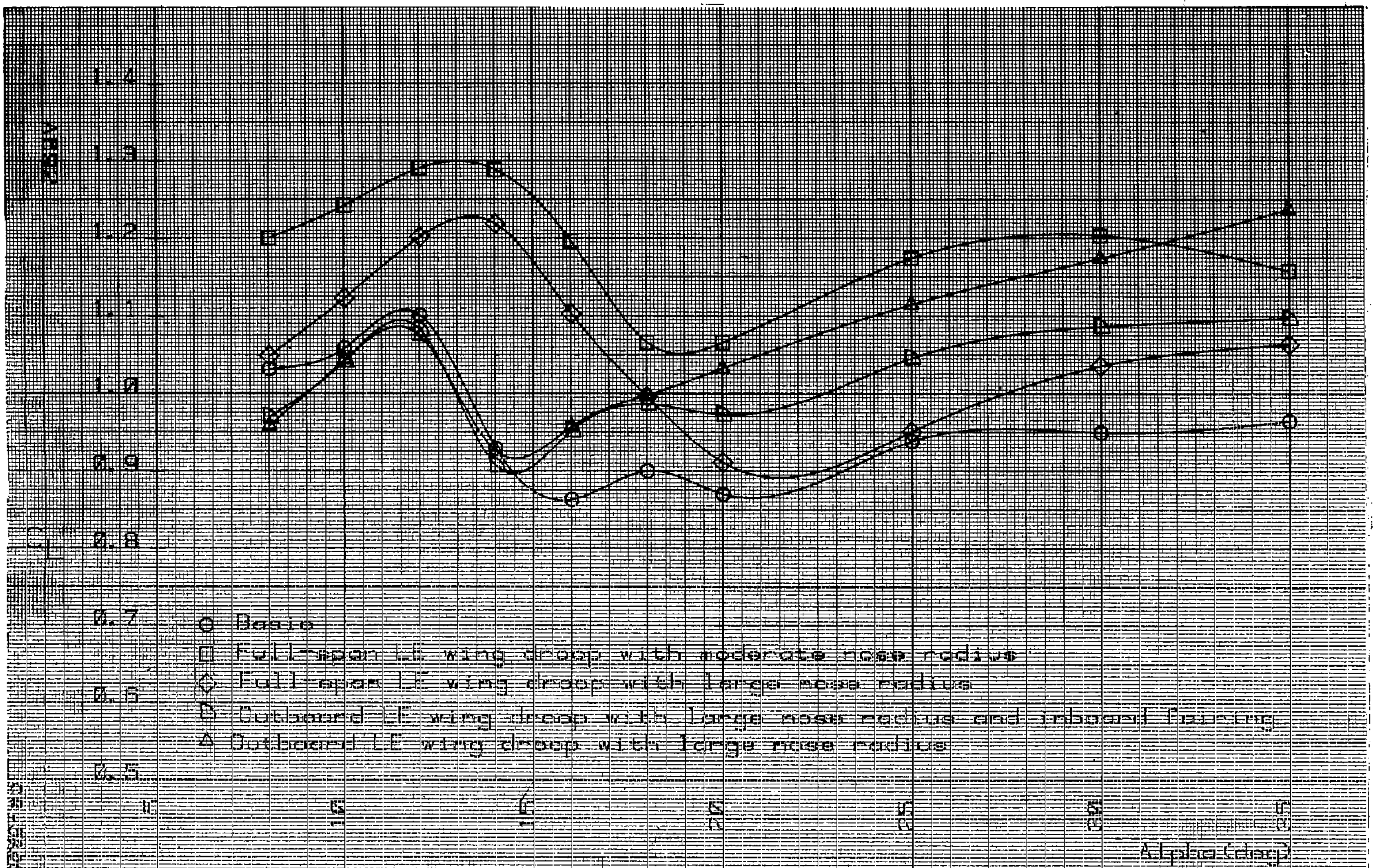

Figure A155. – Lift coefficient as a function of angle of attack for various wing LE devices.

1. Report No.	2. Government Accession No.	3. Recipient's Catalog No.
NASA CR-3200		
4. Title and Subtitle Rotary Balance Data for a Typical Single-Engine General Aviation Design for an Angle-of-Attack Range of 8° to 90°. I - Low-Wing Model C.		5. Report Date October 1980 6. Performing Organization Code
7. Author(s) William J. Mulcay Robert A. Rose		8. Performing Organization Report No.
9. Performing Organization Name and Address Bihrle Applied Research, Inc. 400 Jericho Turnpike Jericho, New York 11753		10. Work Unit No. 505-10-13-06 11. Contract or Grant No. NAS1-14849, Task 35
12. Sponsoring Agency Name and Address National Aeronautics and Space Administration Washington, DC 20546		13. Type of Report and Period Covered Contractor Report 14. Sponsoring Agency Code

15. Supplementary Notes

Langley Technical Monitor: James S. Bowman, Jr.

Topical report

16. Abstract

Aerodynamic characteristics obtained in a helical flow environment utilizing a rotary balance located in the Langley spin tunnel are presented in plotted form for a 1/6-scale, single-engine, low-wing, general aviation model (model C). The configurations tested included the basic airplane and control deflections, wing leading edge and fuselage modification devices, tail designs and airplane components. Data are presented without analysis for an angle-of-attack range of 8° to 90° and clockwise and counter-clockwise rotations covering an $\frac{\Omega b}{2V}$ range from 0 to .9.

17. Key Words (Suggested by Author(s))	18. Distribution Statement
General Aviation Spinning Rotary Balance High angle-of-attack wind tunnel data	Unclassified - Unlimited Subject Category 02

19. Security Classif. (of this report)	20. Security Classif. (of this page)	21. No. of Pages	22. Price
Unclassified	Unclassified	712	A99

N-305

For sale by the National Technical Information Service, Springfield, Virginia 22161

☆U.S. GOVERNMENT PRINTING OFFICE: 1980 635-050/5 1-3